Adrián Páramo Blázquez

PhD THESIS

2019

PhD THESIS

THE APPENDICULAR SKELETON VARIABILITY OF THE SAUROPODA TITANOSAURIA FROM THE UPPER CRETACEOUS OF LO HUECO (CUENCA, SPAIN)

Adrián Páramo Blázquez

2019

UNIVERSIDAD AUTÓNOMA
DE MADRID
FACULTAD DE CIENCIAS
DEPARTAMENTO DE BIOLOGÍA

The appendicular skeleton variability of the Sauropoda Titanosauria from the Upper Cretaceous of Lo Hueco (Cuenca, Spain)

Adrián Páramo Blázquez

Director: José Luis Sanz

Co-director: Francisco Ortega Coloma

TESIS DOCTORAL

Memoria presentada para la obtención del título de Doctor en Biología por la Universidad Autónoma de Madrid, Facultad de Ciencias. Esta tesis fue realizada gracias a la Ayuda para Contratos Predoctorales para la Formación de Doctores BES-2013-065509 - Ministerio de Economía y Competitividad. Esta beca doctoral está asociada al Proyecto de Investigación CGL2012-35199 - Ministerio de Economía y Competitividad.

OCTUBRE 2019

"The mystery of life isn't a problem to solve, but a reality to experience"

Reverend Mother Gaius Helen Mohiam to Paul Atreides
(*Dune*)

RESUMEN

En este volumen se presentan nuevos datos acerca del esqueleto apendicular de los titanosaurios del yacimiento Campano-Maastrichtiense de Lo Hueco (Cuenca, España). En este yacimiento se ha recuperado una muestra abundante de restos referidos a saurópodos titanosaurios, con varios ejemplares en conexión y decenas de ejemplares aislados. En esta muestra se identifica una elevada variabilidad morfológica en cada tipo de elemento apendicular y la presencia de ejemplares de pequeño tamaño.

Hasta ahora solo se ha descrito en el yacimiento una forma exclusiva de titanosaurio, *Lohuecotitan pandafilandi*. No obstante, los estudios de los abundantes restos encontrados en el yacimiento habían permitido identificar dos morfotipos principales de dientes, dos tipos de basicraneos de titanosaurio, tres posibles morfotipos identificados en el esqueleto axial correspondiente a las vértebras dorsales, y cuatro morfotipos en el estudio de las vértebras caudales.

En el presente estudio se explora la elevada variabilidad encontrada en la muestra de restos apendiculares. Para ello se utilizan una serie de técnicas analíticas relacionadas con el *machine learning* y la morfometría geométrica en 3D con el objetivo de identificar posibles morfotipos que ayuden a explicar esta variabilidad. Se desarrolla un flujo de trabajo de digitalización del ejemplar en 3D, proceso de restauración virtual en caso de ser ejemplares fragmentarios, y su posterior análisis estadístico. Mediante estas técnicas se determina la presencia de dos morfotipos principales. A partir de esta identificación, se procede a la cuantificación de la variabilidad intraespecífica en cada uno de ellos, así como la determinación de posibles secuencias ontogenéticas y la variabilidad debida a cambios durante el crecimiento del esqueleto apendicular de los titanosaurios.

Algunos indicios apuntan a la que los dos morfotipos identificados en el yacimiento pertenecerían a dos gremios distintos que tendrían dos estrategias tróficas distintas. En el presente trabajo se discuten las posibles implicaciones en las diferencias morfológicas observadas entre ambos morfotipos principales. Se realiza un modelo aproximado con el que relacionar la morfología general de las extremidades en neosaurópodos con estos dos tipos de gremios y se relacionan los dos morfotipos principales con dos estrategias tróficas congruentes con los datos del estudio de material craneal.

La variabilidad intraespecífica observada en cada morfotipo permite determinar sus implicaciones en la codificación de caracteres morfológicos apendiculares. En este trabajo se han identificado varias secuencias ontogenéticas relativas a cada tipo de elemento analizado. Se describe en detalle por primera vez las secuencias de transformaciones ontogenéticas en estos titanosaurios, así como el estadio y tiempo relativo en que se producen dichos cambios y sus implicaciones en las codificaciones de caracteres morfológicos.

ABSTRACT

In the current dissertation a revision of new data of the appendicular skeleton of the Campanian-Maastrichtian fossil site of Lo Hueco (Cuenca, Spain) is presented. This fossil site have yielded an abundant sample of specimens referable to titanosaur sauropods, with several individuals partially articulated and tens of isolated specimens. There has been identified a high morphological variability in each appendicular element and the presence of several small-sized specimens in this sample.

Until now, a single titanosaur exclusive form have been described, *Lohuecotitan pandafilandi*. However, the study of abundant isolated specimens from the fossil site have allowed to identify two main teeth morphotypes, two types of braincase, three morphotypes identified in the axial skeleton of the dorsal region, and four morphotypes among the caudal vertebrae.

The current study explores the high variability found in the sample of appendicular elements. For this matter, a series of analytical techniques related with modern machine learning and 3D geometric morphometrics are used with the objective of identifying the probable morphotypes that help explain the morphological variance. A 3D digitizing workflow of the specimens of study is herein proposed, with a new proposal for virtual restoration of fragmentary elements and its incorporation to statistical analyses. Using these techniques it has been identified two main appendicular morphotypes. Based on this morphotypes, the intraspecific variability has been quantified in each of them, the ontogenetic sequences have been identified and the variability related to transformations during titanosaur ontogenetic development.

Previous studies indicates that two titanosaur morphotype from Lo Hueco could have been pertain to two different guilds with two different types of feeding niche exploitation. In the current study, the implications of several morphological differences between both main morphotypes are discussed under the hypothesis of differences in the ecomorphological specialization. A statistical proxy model was created to test the relationships between main appendicular morphology with ecomorphological specialization related with the height of the feeding envelope among neosauropods. The results allow relating the two main morphotypes with two different feeding niche exploitation strategies congruent with previous analyses in the cranial material.

The observed intraspecific variability in each morphotype allows determining its impact on morphological character scoring. In the current dissertation it has been identified the presence of several ontogenetic sequences in each morphotype. The ontogenetic sequences have been comprehensively described for first time in this group, as well as the ontogenetic stage and relative time estimation of the morphological character changes with implications for character scorings.

INDEX

AGRADECIMIENTOS

Llegado este momento, uno debe reflexionar sobre todos los momentos en estos 6 años de trabajo y las personas que han hecho posible o han contribuido en este viaje.

En primer lugar, he de agradecer la labor de mis directores, J.L. Sanz y F. Ortega, sin quienes no hubiese podido realizar el presente proyecto de tesis. Desde el planteamiento de un proyecto de investigación, las tutorías, consejos y revisiones que han permitido elaborar este proyecto de investigación a lo largo de estos años. A F. Ortega además querría agradecerle haber permitido asistir a las numerosas excavaciones en el Jurásico portugués y Cretácico español, así como participar en los diversos proyectos de investigación del Grupo de Biología Evolutiva. A J.L. Sanz agradecerle la oportunidad de ser profesor universitario, aunque de momento haya sido de manera temporal, aprendí a valorar este aspecto de la profesión de distinta forma.

Esta tesis no hubiese podido ser realizada sin la inestimable ayuda en el muestreo, preparación, localización de elmentos en plano e incontables horas de trabajo de F. Marcos-Fernández. Nieve, llueva o haya una tormenta de polvo (seguramente proveniente del laboratorio de preparación), nunca ha impedido que todo fósil sea procesado. Por todos estos años de aprendizaje y apoyo. Junto a la labor de de los miembros pasados y actuales de Conservación GBE, sin ningún orden particular: A. Elvira, S. Santiandreu, J.N. Torres, M. Onrubia (proveedora de memes), S. Bartolomé, S. López, E. Fernández, I. Martínez-Fernández, E. Navarro, y algunos más que seguro me dejaré por el camino. También me gustaría agradecer la labor de todas las promociones de "Metodología de la Conservación y Restauración del Patrimonio Arqueológico" del Grado de Conservación y Restauración del Patrimonio Cultural de la UCM en estos últimos años, que han permitido preparar gran parte del material de Lo Hueco.

Tampoco hubiése podido terminar el muestreo de esta tesis sin el esfuerzo de los sucesivos Talleres de Empleo de Restauración Paleontológica de Cuenca. Desde 2013-2014, la labor de sus alumnos y personal han permitido la preparación de buena parte de los restos aquí analizados.

A I. Narváez, "*Chicho*", tutor en excavaciones, edición de imágen y maquetación que ha permitido evolucionar y mejorar en todos esos aspectos. Tutor en buen proceder en el tapeo, y compañero de viajes a la nave de Lo Hueco así como taréas varias en las que hubo que *pringar* irremediablemente, con una carcajada desafiante a la tarea más difícil que hubiese que acometer. Siempre dispuesto a ayudar.

A F. Escaso, por todo lo mismo que a Chicho pero sin los memes. Valioso instructor y a quien agradezco todos sus comentarios y aportaciones al presente proyecto de tesis. Intentaremos que esto esté a la altura del último empujón.

A P. Escaso, el editor más joven que ha contribuido a la realización de esta tesis. Todo cuellilargo de la maqueta fue corregido al tamaño adecuado.

También ha sido posible realizar esta tesis a los comentarios de P.Mocho, todos ellos valiosos y de la profesionalidad y determinación que le caracteriza. Aunque entrasen en conflicto con observaciones de formato de F. Escaso. Por los incontables viajes también a la nave. Así como los viajes por Europa a su lado y a aprender apreciar mejor el café.

No hubiese sido lo mismo en este largo viaje sin compañeros de despacho y desventuras, C. de Miguel Chaves, gran científico, mejor cantante, largas horas de trabajo productivo a su lado.

A. Suárez, nos hemos conocido poco pero estaba allí en momentos clave, puesto que organizar un congreso es difícil. A A. Serrano, con quien aguantar directores, largas charlas científicas sobre modelos de probabilidad basadas en dados de 6 caras, y un excelente investigador. Les deseo lo mejor a él y la dra. M.Sanz. A D. Vidal, compañero de mi primer congreso internacional y con quien desarrollamos el procolo de digitalización actual. Los momentos junto a E. Cuesta, quien tiene una memoria inigualable y siempre atenta hasta el último detalle, era el cerebro que a veces (me) faltaba a la hora del papeleo y horario de conferencias en la UAM. Sin tu ayuda algunas veces hubiese estado muy perdido. A E. Manzanero, algo caótico a veces, pero encomiable curiosidad por el paleoarte. También la inestimable labor de M. Martín-Jiménez, allá donde haga falta para lo que haga falta. Sin tu apoyo logístico no hubiése podido terminar algunos de los interminables muestreo en este y otros proyectos. Sin olvidar a A. Pérez-García, por comentarios, momentos de distensión y la ayuda brindada todos estos años.

Un agradecimiento a A. de Celis. Llegó de los últimos pero estará entre los primeros sin duda. Al igual que A. Guerrero. Espero que se sus respectivas carreras en morfometría geométrica sean provechosas.

No podría olvidar a E. Malafaia, con quien he compartido congresos y proyectos portugueses, con modestia y un conocimiento inestimable, tu ayuda fue muy importante para los primeros pasos en algunos de los trabajos aquí presentados.

También me gustaría fuera del GBE la experiencia, comentarios y también los momentos de ocio y el apoyo de M. Aquilino, que bien sabe todo el esfuerzo que es necesario para sacar un trabajo contra viento y marea. Al igual que O. Herrero, su ayuda en algunos momentos, al igual que su apoyo, no serán olvidados.

Y también a compañeros de la UNED por todos los momentos juntos, I. Ozáez, R. Planelló, A. Belén.

A V. Díez-Díaz por esos breves momentos entre el final de su tesis y su partida a tierras alemanas. Así como inestimable ayuda en la organización del viaje a Argentina.

De la UAM y la organización del EJIP, así como viajes, congresos y labores varias cóm olvidar a F. Gascó, S. Pereira, S. Barrios recien doctorada y espero que sea provechoso, y C. Blanco a quien espero que pronto entregue también su proyecto.

Por último, al apoyo científico así como diversas conversaciones, por darme alojamiento y permitirme disfrutar de labor docente en Argentina, A. Arcucci. Y la acogida y los comentarios cientificos con R.A. Coria y R. Coria.

En un término más pesonal, quisiera dedicar un recuerdo especial a I. Herguedas, que siempre me ha acompañado y apoyado en toda esta historia. A quien debo bastantes momentos especiales, quien ha estado ahí con curiosidad para preguntar y esperar que le explicase cada nuevo descubrimiento. A quien espero enseñar todos los lugares visitados durane el transcurso de este proyecto. Gracias a tí por todos estos años.

A S. Amor, quien también ha brindado ese apoyo y a subir la moral incluso en los momentos más necesarios. El impulso necesario para seguir adelante.

A I. Díaz-Martínez, quien ayudó no solo de manera profesional si no también personal con total implicación durante mi viaje a Argentina. Le debo mucho por esos meses y deseo lo mejor. Al igual que P. Cruzado-Caballero, quien también fue de gran apoyo al cruzar los mares. A T. Pedernera, los momentos a uno y otro lado del océano y el apoyo mutuo han sido de gran ayuda. Le deseo una prolífica carrera científica.

Desearía también dedicar un agradecimiento a los comentarios científicos y discusiones con I. Cerda, I. Canale, L. Filippi, R. Lefebvre, I. Canudo, R. Royo-Torres, M. Moreno-Azanza, J. Claude, J. Cantalapiedra.

El acceso a las diversas colecciones muestreadas durante este proyecto de tesis fue posible gracias al personal del Museo de Paleontología de Castilla-La Mancha, a I. Cerda, C. Muñoz, R. Coria, R. Juárez-Valieri, I. Canale, L. Filippi, S.Devicenzi, B. González Riga, M. Reguero, A. Otero, M. Ezcurra, A. García-Forner, J. Le Loeuff, S. Chapman, X. Pereda, J.A. Ramírez.

Y muchos más investigadores que en este momento no podré recordar.

Así como un breve recordatorio a toda la gente que visita habitualmente StackOverflow, una mente enjambre incansable al servicio de todo el que necesite ayuda. Incontables comentarios han ayudado a que hoy conozca mejor el código y la realziación de esta tesis.

Este proyecto de tesis fue financiado también con el Proyecto CGL2015-68363-P - Ministerio de Economía y Competitivad. Los proyectos de la Junta de Comunidades de Castilla-La Mancha SBPLY/15/180601/000045, SBPLY/16/180801/000017 y SBPLY/17/ 180801/000063.

El acceso a colecciones fue posible gracias a la Ayuda para la Movilidad Predoctoral para la Realización de Estancias Breves en Centros de I+D 2016, EEBB-I-2016-11875 - Ministerio de Economía y Competitividad. Así como una beca Synthesys GB-TAF-6153.

CHAPTER I:

Introduction

I.1. THE TITANOSAUR SAUROPODS

The sauropods were a group of quadrupedal herbivorous dinosaurs characterized by their long neck and tails. They were among the largest terrestrial animals that have ever existed reaching multitoned body mass, some of them possibly surpassing 100 tonnes (estimation variable based in the applied method e.g. Mazzetta, Christiansen, & Fariña, 2004). They appeared in the Late Triassic, ~237-208.5 million years ago (m.y.a.), and were the predominant herbivorous group during the Jurassic (Upchurch, Barrett, & Dodson, 2004). The more derived clade of Sauropoda was the titanosaur sauropods. This group appeared at some time between the Upper Jurassic and the Early Cretaceous (~160-150 m.y. ;see D'Emic, 2012; Mannion *et al.*, 2019). They achieved global distribution (Cerda *et al.*, 2012) and were a diverse group of sauropod until the extinction event in the Late Cretaceous (66 m.y.; see its diversity in the Late Cretaceous of the Ibero-Armorican domain – Southern of modern France and the whole Iberian Peninsula, below). They presented a conservative body plan as all the sauropods, the common quadrupedal barrel-shaped body, small skull, long neck and tail, however, several differences can be observed between the titanosaurs and the non-titanosaur sauropods with especial relevance to the appendicular skeleton.

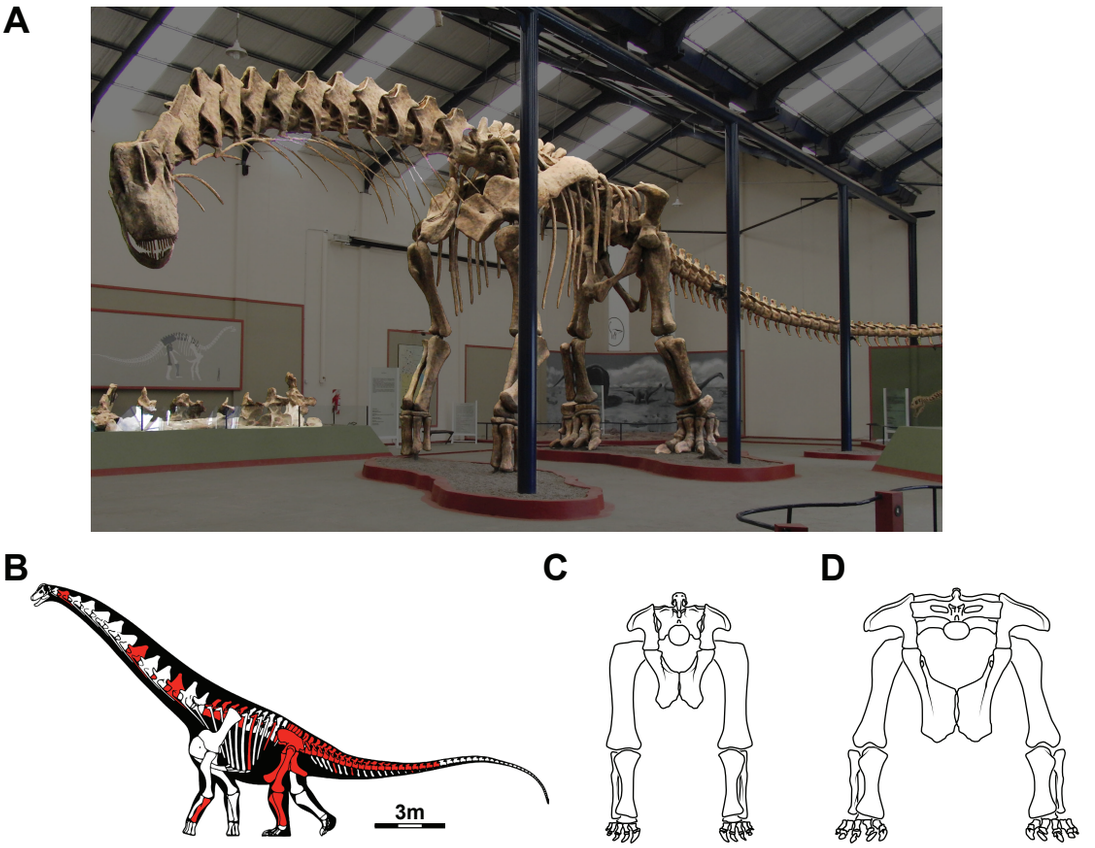

Fig.I.1. Basic body plan of the titanosaur sauropods. (A) *Argentinosaurus huinculensis* reconstruction in the Museo Carmen Funes (Plaza Huincul, Neuquén, Argentina). (B) *Lohuecotitan pandafilandi* skeleton composition. (C) Sauropod pelvic girdle and hindlimbs with "narrow-gauge" stance. (D) Titanosaur pelvic girdle and hindlimbs with "wide-gauge" stance. Modified from Wilson & Carrano (1999).

This diverse group of sauropods included some of the biggest known species (e.g. Argentinosaurus huinculensis, see Fig.I.1.A). Despite the massive size of some of their representatives, they could present a variety of morphologies in the limb skeleton. They probably achieved the largest body sizes thanks to several key features, some of them acquired in its appendicular skeleton. The limbs of the titanosaurs were arched instead of columnar, with the zeugopodium placed farther from the main proximodistal axis of the body compared to other non-titanosaur sauropods (see Fig.I.1.C). This type of limb posture is known as wide-gauge and it is so characteristic that the derived type of quadrupedal locomotion produces a type of foot tracks easily associated to titanosaurian track-makers, which is not common among other ichnological records (Wilson & Carrano, 1999). This posture is also associated with a combination of morphological features observable on the appendicular skeleton that allow to identify the fossil bones to this group of sauropods (see below).

All sauropod taxa studied in the current PhD project as well as present in the Late Cretaceous of Ibero-Armorican domain, pertain to the most inclusive group of Titanosauria.

I.2. THE PHYLOGENETIC DEFINITION OF TITANOSAURIA

First mention to Titanosauria was coined with the definition of Argentinosaurus (Bonaparte & Coria, 1993). While there was a diagnosis of the species, it lacked a formal phylogenetical definition of the new sauropod group. It has been loosely equivalent to the more general clade Titanosauridae defined by Lydekker (1885). The Titanosauridae is a derived group of sauropods predominant in the Late Cretaceous, initially defined for grouping all known "Titanosaurus" genera (Lydekker, 1877, 1893). They are characterized by deep hollows on the vertebrae, forming irregular shaped pleurocoels. Vertebral spines are directed backward, with transverse processes directed more dorsally than lateral. Caudal vertebrae are strongly procoelous, with prominent posterior convexity and neural arch on front half of the centrum, sometimes invading more than a half of the previous vertebra anteroposterior length (McIntosh, 1990a). Both pectoral and pelvic girdles are robust, and the preacetabular process of the ilium is swept outward from the main sagittal axis of the body and become more horizontal (McIntosh, 1990a; Salgado, Coria, & Calvo, 1997). The appendicular skeleton forms a characteristic arched stance instead of the more columnar stance as seen in other sauropod groups (e.g. McIntosh, 1990a; Salgado *et al.*, 1997; Carrano, 1998; Wilson & Carrano, 1999). First taxa included in this group were the Late Cretaceous "Titanosaurus" spp. from India, Madagascar and South America (Lydekker, 1893). In 1997, Leonardo Salgado, Rodolfo A. Coria and Jorge Calvo made the first comprehensive phylogenetic definition of "titanosaurid" sauropods, including both Titanosauridae and Titanosauria (Salgado *et al.*, 1997). The phylogenetic node based definition of Titanosauria is as follows in Salgado *et al.* (Salgado *et al.*, 1997):

> *"The clade including the most recent common ancestor of Andesaurus delgadoi and Titanosauridae and all of its descendants"*

And for Titanosauridae follows:

> *"The name Titanosauridae refers to the clade including most recent common ancestor of Epachthosaurus scuttoi, Malawisaurus dixey, Argentinosaurus huinculensis, Trigonosaurus pricei. (Titanosauria indet. DGM "Series B": Campos et al., 2005), Opisthocoelicauda skarzynskii, Aeolosaurus spp., Alamosaurus sanjuanensis and Saltasaurinae and all of its descendants"*

The Titanosauridae clade node based definition might not be dependant on any of original "*Titanosaurus*" species, being that recent studies have deemed invalid most of the species in that genus (Wilson & Upchurch, 2003). The stem-based definition of the clade Titanosauria is more suitable for this group of derived sauropods. Titanosauridae has been proposed for abandonment as well as other rank-taxa clade terms based on the "Titanosaurus" genus. Coincidently, Salgado *et al.* (1997) indicate that the phylogenetic definition of Titanosauria is rather similar to definition of Titanosauridae in Powell (1986). From now on, we will use Titanosauria instead of Titanosauridae even if some of the oldest references mention the later.

With this consideration, the diagnostic features of Titanosauria as per Salgado *et al.* (Salgado *et al.*, 1997) are as follows:

- Character 20: Eye-shaped pleurocoels in trunk vertebrae.
- Character 21: Posterior trunk vertebrae with ventrally widened, slightly forked infradiapophyseal laminae.
- Character 22: Presence of centro-parapophyseal lamina in posterior trunk vertebrae.
- Character 21 and 22 from Salgado *et al.* (1997) already introduced in the diagnosis of Titanosauria by Bonaparte and Coria (Bonaparte & Coria, 1993).
- Character 23: Procoelous anterior caudals contrary to amphyplatyan or slightly platycoelous in other Sauropoda outside Titanosauria.
- Character 24: Pubis longer than ischium, measured from the puboischial symphysis.

And a phylogenetic definition simplifying the proposal of Bonaparte and Coria (Bonaparte & Coria, 1993), after revision of Salgado *et al.* (1997):

> *Titanosauria: Andesaurus delgadoi (Calvo & Bonaparte, 1991), Saltasaurus loricatus (Powell, 1980) their most recent common ancestor and all descendant.*

Titanosauria as a group was also defined based on several early discoveries. Early phylogenetic hypothesis included several outdated characteristics e.g. the presence of a sixth sacral vertebra, the lack of hyposphene-hypantrum in dorsal vertebrae (Bonaparte and Coria 1993, Salgado *et al.* 1997). However, more recent titanosaur discoveries permit to observe that these features are variable among Sauropoda and therefore not synapomorphies of Titanosauria (Sanz *et al.*, 1999; González Riga, 2003; Apesteguía, 2005a; Curry Rogers, 2005; Salgado, Apesteguía, & Heredia, 2005; Wilson, 2011).

Early cladistic analyses (Salgado *et al.*, 1997; Wilson & Sereno, 1998; Upchurch, 1998; Sanz *et al.*, 1999; Curry Rogers & Forster, 2001; Wilson, 2002; González Riga, 2003; Upchurch *et al.*, 2004) resolved disputed phylogenetic hypotheses over the position of this group within Sauropoda (Gilmore, 1946; Romer, 1966; Steel, 1970; McIntosh, 1990b; Bonaparte & Coria, 1993). Titanosauria is a derived group of Titanosauriformes sauropods (see fig.I.2). These phylogenetic hypotheses have been stable over the decades and after dozens of new titanosaur discoveries. However, the relationships within Titanosauria are still uncertain.

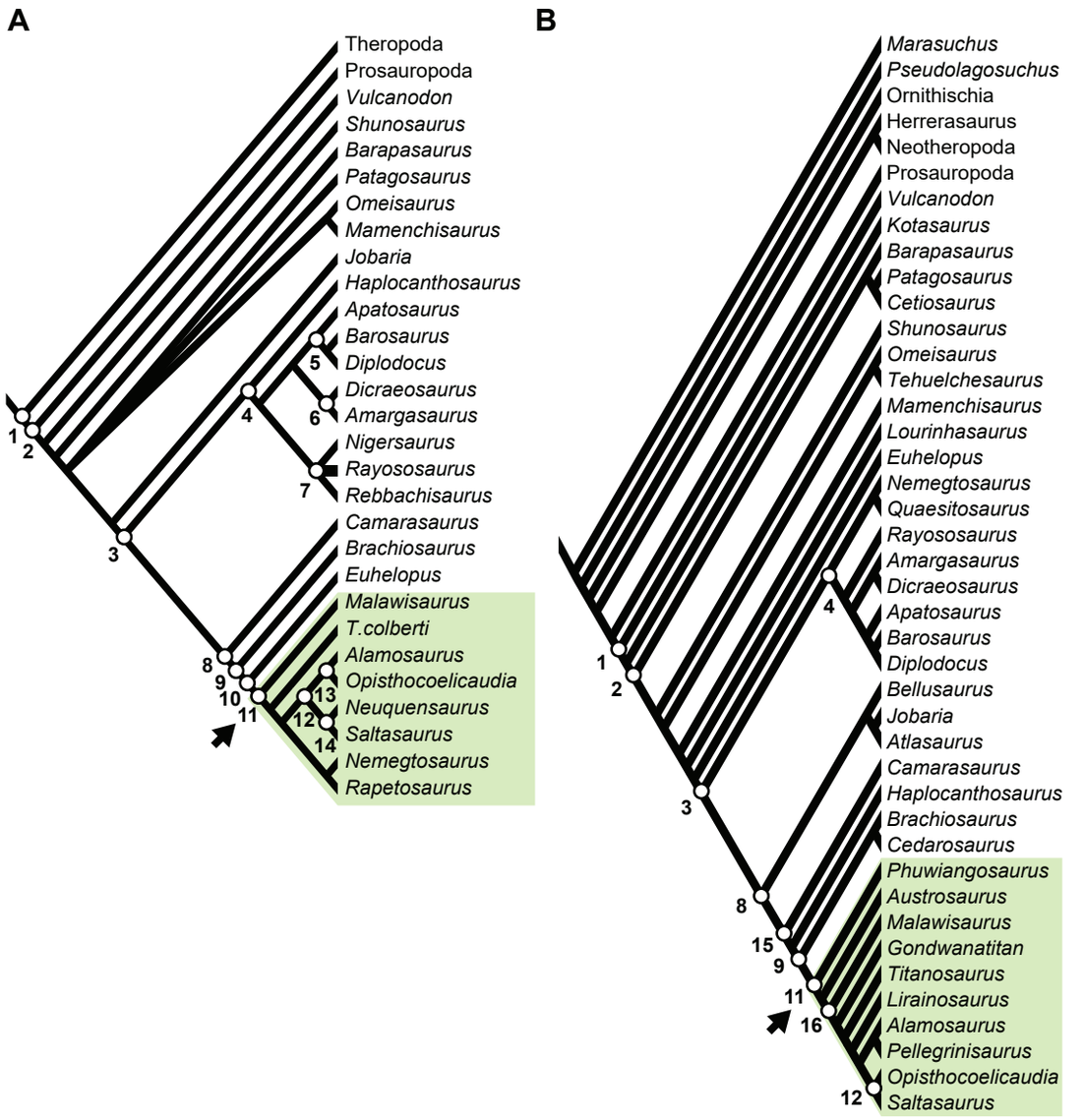

Fig.I.2. General phylogeny of Sauropoda. (A) Hypothesis of Wilson (2002). (B) Hypothesis of Upchurch *et al.* (2004)

The current PhD study is limited to the appendicular skeleton of titanosaurian sauropods which is also characteristic beside it is not diagnostic per se (as commented before). Several anatomical changes occur In derived Titanosauriformes, related with the acquisition of the characteristic "wide-gauge" (Wilson & Carrano, 1999; Carrano, 2000; Upchurch *et al.*, 2004; D'Emic, 2012; García *et al.*, 2015; Bates *et al.*, 2016; Ullmann, Bonnan, & Lacovara, 2017).

Sauropod trackways can be divided in "narrow-gauge" and "wide-gauge", the latter commonly found in the Cretaceous (Lockley *et al.*, 1994; Lockley & Hunt, 1995; Wilson & Carrano, 1999). This track type has been attributed to a major postural change in the evolution of Titanosauriformes

and more basal Titanosauria forms (Sereno *et al.*, 1999; Carrano, 2005; D'Emic, 2012; Ullmann *et al.*, 2017). During this transition, manual phalanges are periodically lost until they are completely absent in Saltasauridae (Borsuk-Bialynicka, 1977; Salgado *et al.*, 1997; Upchurch, 1998; Wilson & Carrano, 1999; Apesteguía, 2005b). Metatarsal bones lose part of the anterior projection of the distal end and together present a more moon-shaped contour than forming a beam-like in the distal part of the forelimb, with metacarpal I and V less opposed in the posterior part of the limb (Bonnan, 2003; Apesteguía, 2005b). The olecranon process is slightly reduced in more derived sauropod taxa as part of this postural change (Bonnan, 2003). The humerus increase its length proportional to the femur in Titanosauria (Bonnan, 2007; Ullmann *et al.*, 2017) and its more elongated and lateromedially narrow with a more quadrangular proximal part in anterior or posterior face than in more basal Neosauropoda (Ullmann *et al.*, 2017; see also Otero, 2018) as well as more medially oriented humeral heads (Ullmann *et al.*, 2017).

Most notable changes occur in the pelvic girdle and hindlimb (Wilson & Carrano, 1999), except for the pes morphology which is rather conservative in Neosauropoda (Bonnan, 2005) and recently found differences might be more related with different morphofunctional specializations (González Riga *et al.*, 2016). The angle between the the main sacral axis and the pubic peduncle increase in derived Titanosauriformes (Borsuk-Bialynicka, 1977; Salgado *et al.*, 1997), and the highest point of the iliac blade is displaced more anteriorly in lateral face (Salgado *et al.*, 1997). Also more derived forms include a more flattened iliac blade expandind outward from the main sacral axis as well as an absence of the ischiatic peduncle in the posterior part in Saltasauridae (Salgado *et al.*, 1997; Powell, 2003; Royo-Torres, 2009; D'Emic & Wilson, 2011). The titanosaurian pubis is longer than the ischium (Salgado *et al.*, 1997; Upchurch, 1998; Wilson, 2002), with absence of ambiens process (Salgado *et al.*, 1997; Royo-Torres, 2009). Part of the arched morphology of the limbs in the "wide-gauge" stance is thank to the arching of the hindlimb (Carrano, 1998; Wilson & Carrano, 1999; Bonnan, 2007; Otero & Vizcaíno, 2008; Ullmann *et al.*, 2017).

The femoral head is displaced, with a dorsally directed head and distal condyles that are perpendicular to medially beveled (Wilson & Carrano, 1999; Ullmann *et al.*, 2017). The fourth trochanter is positioned on the posteromedial region rather than in the posterior face of the femur shaft as in more basal Sauropoda (Ullmann *et al.*, 2017).

The tibia of titanosaurs presents a major development of distal anterior ascending process (aap: Wilson & Upchurch, 2003) to accommodate the new stance. Some authors have cited that there is also a development on the lateromedial width of the distal end (Salgado *et al.*, 1997; Sanz *et al.*, 1999), but other sauropods present similar development and might not be exclusive of Titanosauria (see Royo-Torres, 2009). Similarly, the distal condyle of the tibia of some titanosaurs presents a rotation along the shaft axis but this character has not been described in most non-Titanosauria taxa in order to compare it (Sanz *et al.*, 1999; Royo-Torres, 2009).

The fibula presents a characteristic triangular shaped distal end with the apex pointing slightly anteriorly (Royo-Torres, 2009; Upchurch, Mannion, & Taylor, 2015; González Riga *et al.*, 2018).

Thus, titanosaurian sauropod isolated appendicular elements can be identified with certain combination of those characters related with this novel stance acquisition.

Majority of recent published studies agree that European titanosaurs can be included in Lithostrotia (Upchurch *et al.*, 2004), a clade which node-based taxon definition is:

The most recent common ancestor of Malawisaurus dixeyi and Saltasaurus loricatus and all of its descendants.

The diagnostic features include strongly procoelous caudal centra and presence of strong procoelly in distal caudals. Partial association of caudal vertebrae from most of the European titanosaur taxa (including Chera morph 2, Lo Hueco morph 2, "Massecap titanosaur") present those characters. Referral of other European Late Cretaceous titanosaur morphotypes, which lacks record of axial skeleton, is uncertain (see below). This clade is similar to the proposal of Eutitanosauria from Sanz *et al.* (1999; see also in Calvo *et al.*, 2007; Filippi, García, & Garrido, 2011; Carballido *et al.*, 2017).

Among the uncertainties in Titanosauria, the phylogenetic position of the basal lithostrotian titanosaur taxa, the ingroup relationships between the gondwanan Lognkosauria, and the derived clades of Saltasauridae and Aeolosaurini is still discussed, including the relationships with the key lithostrotitan titanosaur Malawisaurus dixeyi. This might affect our understanding on the evolutionary relationships of European titanosaur taxa (like *Lirainosaurus astibiae* or *Ampelosaurus atacis*), although the most part of the phylogenetic hypotheses include the Ibero-Armorican titanosaurs among basal Lithostrotia, less derived than Aeolosaurini or Saltasauridae sauropods (Sanz *et al.*, 1999; Calvo & González Riga, 2003; González Riga, 2003; Curry Rogers, 2005). On the other hand, other analyses recover Lirainosaurus as more derived than Aeolosaurini and as sister taxon of Saltasauridae (Curry Rogers, 2005; Calvo *et al.*, 2007; Filippi *et al.*, 2011).

I.3. FOSSIL RECORD OF CRETACEOUS SAUROPODS OF THE IBERO-ARMORICAN DOMAIN

During the Late Cretaceous, almost all fragments of current European plate have already collided (Scotese, 1991; Dias & Ribeiro, 1995) save from Apulian fragments (Alonso *et al.*, 1994). The west domain was conformed by current Iberian Peninsula and France, without the uplifting of Pyrenees, which were instead an open basin facing West to the Atlantic Ocean (Alonso & Mas, 1982; Souquet, 1988; Alonso *et al.*, 1994; Rosenbaum, Lister, & Duboz, 2002). All along the Campanian contraction phase of pre-alpine orogeny along the Adria-Apulian front, there was a proliferation of south-west European basins (Kley & Voigt, 2008). Also, sea level raised in the course of the Late Cretaceous great transgression (Hancock & Kauffman, 1979; Alonso *et al.*, 1994; Dunhill *et al.*, 2016). As a result, the Campanian-Maastrichtian European archipelago appeared (Hancock & Kauffman, 1979; Tyson & Funnell, 1987; Ziegler, 1987; Scotese, 1991; Alonso *et al.*, 1994; Hay *et al.*, 1999; Golonka, 2004; Kley & Voigt, 2008).

From this complex of islands during Late Cretaceous, current PhD project will be centered on the titanosaur remains found in Lo Hueco fossil site (Fuentes Cuenca), located in the Campanian-Maastrichtian Ibero-Armorican domain. The Ibero-Armorican domain was one mega-island during the Late Cretaceous (Scotese, 1991; Le Loeuff, 1991b; Alonso *et al.*, 1994; Hay *et al.*, 1999; Philip *et al.*, 2000; Vera, 2004). However, regional changes in tectonic motions and sea level during Campanian and Maastrichtian induced landmasses fragmentation and re-connection between the different sub-basins of the Ibero-Armorican domain (Hancock & Kauffman, 1979; Ziegler, 1987; Alonso *et al.*, 1994; Kley & Voigt, 2008; Csiki *et al.*, 2015). It is discussed this fragmentation in several close islands is associated with the faunal turnover in the Maastrichtian near K-Pg extinction event (Buffetaut &

Le Loeuff, 1991; Le Loeuff, Buffetaut, & Martin, 1994b; Le Loeuff & Laurent, 2000; Riera *et al.*, 2009; Le Loeuff, 2012; Csiki *et al.*, 2015; Canudo *et al.*, 2016; Vila, Sellés, & Brusatte, 2016; Fondevilla *et al.*, 2019).

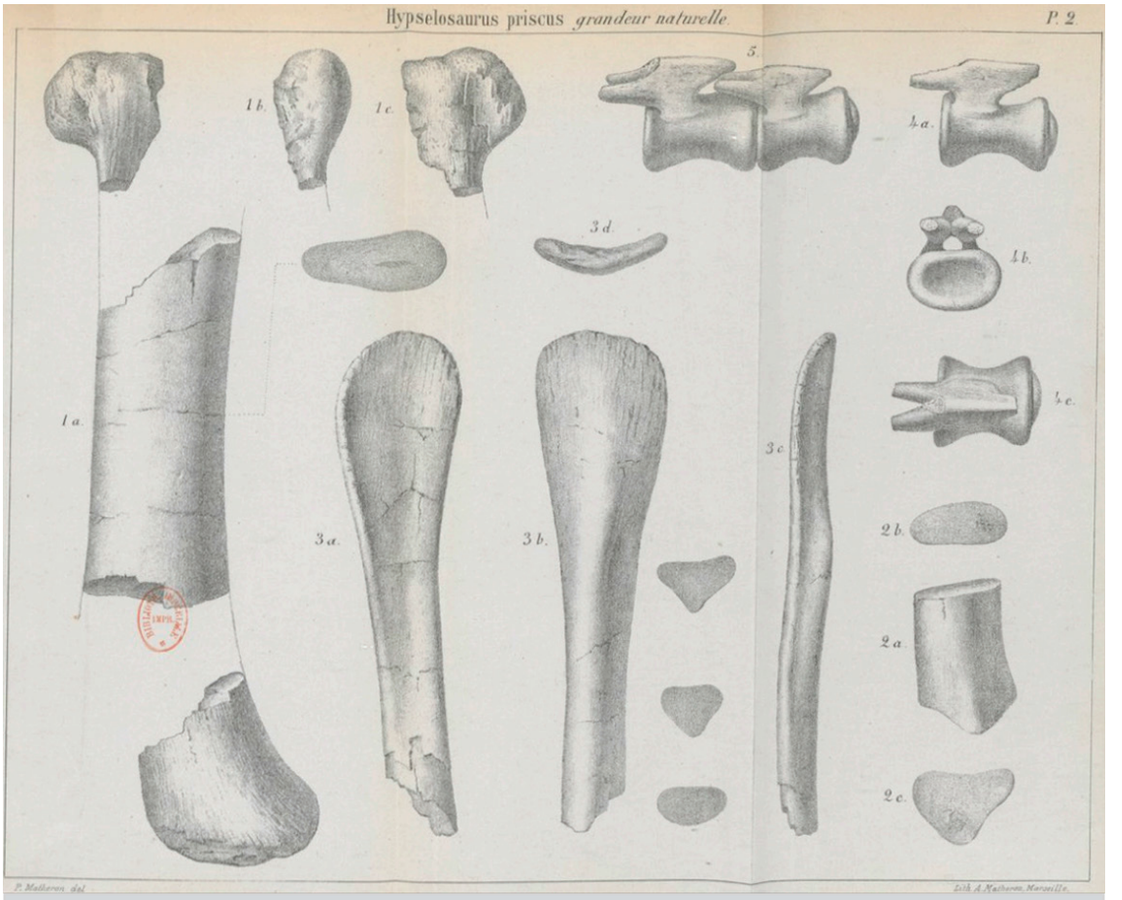

Fig.I.3. *Hypselosaurus priscus* remains, Matheron (1869).

I.3.1. HISTORICAL PALEONTOLOGY AND STRATIGRAPHIC BACKGROUND

First discoveries of putative sauropod remains from the Ibero-Armorican domain (Southern France – Spain) date from middle XIX century but not described until definition of "*Hypselosaurus priscus*" Matheron 1869 (Fig.I.3). Several fragments of a hindlimb and two fragmentary caudal vertebrae were found in Maastrichtian sediments of the Provence area, France (Matheron, 1846, 1869). There is also evidence of a possible sauropod remain from the Cenomanian of Mondragon, Vaucluse (Déperet, 1894) resembling "*Aepisaurus*" (but disputed by Boule, 1894). Unfortunately, those remains have been disappeared (Buffetaut, Cuny, & Le Loeuff, 1991). Although the rich vertebrate localities of the Late Cretaceous deposits of the Pyrenees and Tremp area of Lleida were early studied by some authors at the end of ninetieth century and the first half of twentieth century respectively (Gaudry, 1890; Lapparent & Aguirre, 1956a), it was not until mid-twentieth century when first systematic excavations and study of sauropod remains began. On the one hand, isolated and fragmentary sauropod material was recovered

and described from Fox-Amphoux, Provence, France (Lapparent, 1947). On the other hand, several remains from Tremp Basin, Catalonia, Spain (Lapparent & Aguirre, 1956b) and Soria, Spain (Lapparent *et al.*, 1957) were identified as "*Titanosaur* cf. *indicus*" and "*Hypselosaurus* sp.".

Since second half of twentieth century, new Late Cretaceous localities have been found and systematic excavations have been carry out (e.g. Broin *et al.*, 1980; Le Loeuff, 1991a; Sanz *et al.*, 1999; Canudo, 2001; Pereda Suberbiola *et al.*, 2015; Martín Jimenez *et al.*, 2017). Up to date, five sauropod taxa have been described in the Ibero-Armorican domain. We will divide the historical discoveries from this point into the French record and Spanish record. For a brief summary see Fig.I.4. and Table.I.1 and Table.I.2.

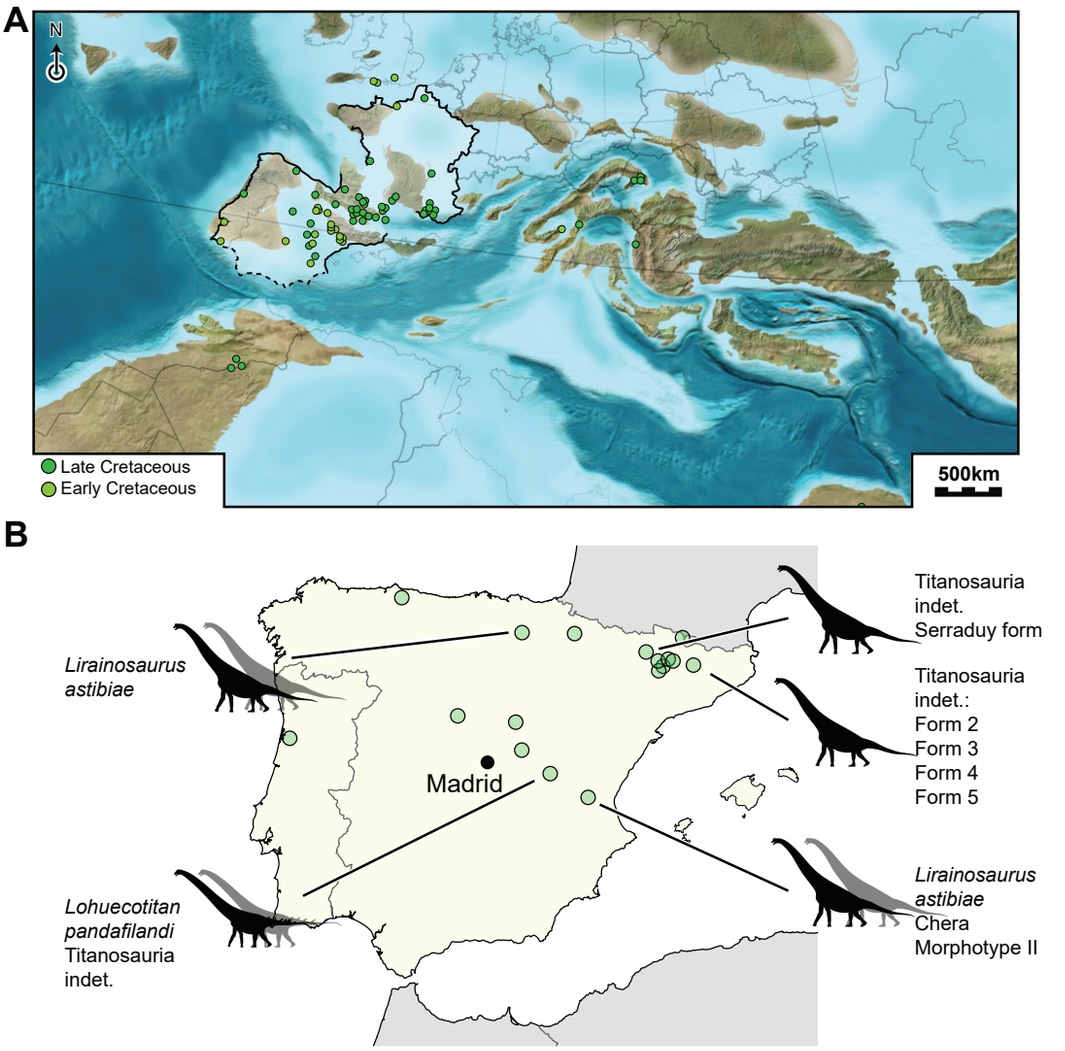

Fig.I.4. General map of the Ibero-Armorican domain during the Campanian-Maastrichtian. (A) Paleogeographical reconstruction with all the fossil sites of the European and North African fossil sites of the Cretaceous. (B) Described titanosaur forms of Spain.

Country	Locality	Fossil record	Morphotype	Age
France	Chateau de la Revelette	bones	Titanosauria indet.	late Campanian
	Jas Neuf Nord	bones	Titanosauria indet.	late Campanian
	La Boucharde	bones	Titanosauria indet.	late Campanian
	Pourcieux-Highway	bones	Titanosauria indet.	late Campanian
	Pourrières-Les Eysarettes	bones	Titanosauria indet.	late Campanian
	Tercis-les-Bains	bones	Titanosauria indet.	late Campanian
	Velaux-La Bastide Neuve	bones	*Atsinganosaurus velauciensis*	late Campanian
	Basségat	bones	Titanosauria indet.	late Campanian-early Maastrichtian
	Champ-Garimond	bones	Titanosauria indet.	late Campanian-early Maastrichtian
	Fox-Amphoux-Métisson	bones	Titanosauria indet.	late Campanian-early Maastrichtian
	La Cairanne	bones + teeth	Titanosauria indet.	late Campanian-early Maastrichtian
	Massecaps (Cruzy)	bones	Titanosauria indet.	late Campanian-early Maastrichtian
	Montouliers	bones	Titanosauria indet.	late Campanian-early Maastrichtian
	MontPlô-Nord	bones	Titanosauria indet.	late Campanian-early Maastrichtian
	Quarante	bones	Titanosauria indet.	late Campanian-early Maastrichtian
	Rousset-Highway 3	bones	Titanosauria indet.	late Campanian-early Maastrichtian
	Sainte-Foy	bones	Titanosauria indet.	late Campanian-early Maastrichtian
	St Estève Janson	bones	Titanosauria indet.	late Campanian-early Maastrichtian
	Bellevue	bones	*Ampelosaurus atacis* +Form1	early Maastrichtian
	Campagne-les-Bains	bones	Titanosauria indet.	early Maastrichtian
	Gabre	bones	Titanosauria indet.	early Maastrichtian
	Le Gourg de l'Encantado	bones	Titanosauria indet.	early Maastrichtian
	Le Mas d'Azil	bones	Titanosauria indet.	early Maastrichtian
	Rennes-le-Château	bones	Titanosauria indet.	early Maastrichtian

Table.I.1. List of titanosaurian fossil sites and record of the Ibero-Armorican domain.

I. 3.1.1. HISTORICAL RECORD IN FRANCE

Until mid-twentieth century, only several indeterminate remains from Fox-Amphoux and "*Hypselosaurus priscus*" Matheron 1846, were known in France.

The initial steps on systematic excavation and study of fossil material of different dinosaur taxa, and particularly Sauropoda, start almost at same time in France and Spain deposits. The French record is deemed one of the most abundant and important in order to understand the Late Cretaceous faunas of Europe due to the existence of dozens of fossil localities in the South of France (Buffetaut *et al.*, 1991). Most of the discovered fossil sites come from the northern part of Pyrenees in Midi-Pyrenees and Languedoc-Rousillon, and from the Provence region in the South-East.

The paleontologist Albert-Félix de Lapparent conducted the first excavation in the Late Cretaceous of Fox-Amphoux in 1947 and reviewed the material studied by Matheron and housed in Paris. In the monograph, he attributed the main titanosaur remains to "*Titanosaurus indicus*" (Lydekker, 1888), "*Hypselosaurus priscus*" (Matheron, 1846), and remarked the relative abundance of the last one in Bassin d'Aix and some presences in Nerthe and Languedoc. It is important to know that today, both taxa are considered nomina dubia (Le Loeuff, 1993, 2005; Wilson & Upchurch, 2003).

De Lapparent committed its entire life to the dinosaur paleontology and he made important discoveries in Late Cretaceous sediments of Spain (see below). However, it was after his death in 1975, when other fossil sites were discovered in France.

Although most of these fossil localities are from Campanian-Maatrichtian age, it is remarkable that a caudal vertebra attributed to titanosaurian sauropod was found in the Cenomanian of Le Mans, Sarthe (Buffetaut, 1989a), being one of the oldest remains of Titanosauria from the French record.

At the same time, four caudal vertebrae were discovered in the Upper Campanian of Ribérac region (Platel, 1989). Suddenly, titanosaur discoveries and record richness increased in a brief time span of a decade. All the prospected localities at this time also present chronostratigraphic correlation (Buffetaut *et al.*, 1991), especially when including the recent South Pyrenees discoveries in Spain (Buffetaut & Le Loeuff, 1991; Pereda Suberbiola, 2009; Canudo *et al.*, 2016; Fondevilla *et al.*, 2019). Several fragmentary remains that could be attributable to Titanosauria were recovered in the rediscovered Maastrichtian site of Mas d'Azil, Ariége (Villatte, Taquet, & Bilotte, 1986; Le Loeuff, 1991a) as part of the fossil vertebrate assemblage.

There are several cranial and postcranial remains of titanosaur sauropods found in the Maastrichtian of Fox-Amphoux-Métisson, Var (Broin *et al.*, 1980; Le Loeuff, 1989; Buffetaut *et al.*, 1991; Díez Díaz *et al.*, 2012a), the same locality where Lapparent excavated in 1947. Among other prospected localities in Var department, a titanosaur braincase is recovered in the Maastrichtian levels of the synclinal (Le Loeuff, 1989), which further expand the knowledge on titanosaur skull as cranial remains are scarce in this sauropods. Lastly in this decade, an haemal arch attributable to Titanosauria recovered in Pourcieux, Var (Le Loeuff, 1993).

At the beginning of the 90s, several sites from the Lower Maastrichtian of Corbiére, l'Aude, were found shortly (Le Loeuff, 1993). This area was mentioned in early nineteenth century but it was not rediscovered until last part of twentieth century (Clottes & Raynaud, 1983; Buffetaut *et al.*, 1989; Le Loeuff, 1991b). In several sites near Bellevue, l'Aude, it has been recovered dozens of vertebrate

fossil remains with abundant material assigned to titanosaurs. Within this association of partial skeletons, it was described the first Ibero-Armorican titanosaur considered as valid nowadays. The mid-sized species *Ampelosaurus atacis* Le Loeuff 1995 was described based on a series of four dorsal vertebrae. However, several partial skeletons are known (Le Loeuff, 1995, 2005; Buffetaut & Le Loeuff, 1997; Knoll *et al.*, 2013), including cranial and dermal material. There is also material that could be referred to probable juvenile individuals (Le Loeuff, 2005; Klein *et al.*, 2012). During the next part of the decade, the extraction of material from several sites of Bellevue locality will be continued.

Other localities from the Pyrenees area and Hérault Department were prospected, providing abundant material of this group. Most of this fragmentary remains coming from the Maastrichtian of Montpellier, Saint-Chinian or La Boissière (Le Loeuff, 1993). In the last part of the decade, several cranial, postcranial and dermal remains partly articulated were found in the Campanian-Maastrichtian of Massecap locality, Cruzy (Buffetaut *et al.*, 1999). For now, only Ampelosaurus sp. have been identified on this fossil site (Buffetaut *et al.*, 1999). Probably a new titanosaur morphotype is present, insight as the "Massecap titanosaur" from Hérault locality (Klein *et al.*, 2012; Díez Díaz, Tortosa, & Le Loeuff, 2013). It is also during early 90s that several remains were discovered from the Upper Campanian of La Bastide Neuve, Velaux, Aix-en-Provence (Garcia *et al.*, 2010). However, this site was not excavated until much later. By the early 90s, given the amount of titanosaur material recovered, the description of the first valid titanosaur taxa and the importance of some of the discoveries (e.g. presence of sauropod braincases, juvenile specimens, eggs, etc.) some authors consider the South of France a key region for the understanding of Late Cretaceous dinosaur faunas (Buffetaut *et al.*, 1991). The succession of dinosaur remains and the differences in titanosaur sample between the Campanian and Maastrichtian allowed the proposal of the first hypothesis of faunal turnover at the Ibero-Armorican Late Cretaceous (Buffetaut & Le Loeuff, 1991; Le Loeuff, 1991b; Le Loeuff *et al.*, 1994b)

At the end of the 90s, several fossil sites were discovered from Maastrichtian deposits in the area of Petites-Pyrénées of Arège and Haute-Garonne (Laurent, Cavin, & Bilotte, 1999), where several fragmentary and isolated material attributable to titanosaurs were recovered (Laurent *et al.*, 2001; Laurent, 2002).

In 2009 and 2012, the Upper Campanian fossil site of La Bastide Neuve, Velaux was re-excavated and several remains assigned to titanosaurs were recovered in partial articulation. A dwarf titanosaur taxa was described, *Atsinganosaurus velauciensis* (Garcia *et al.*, 2010; Díez Díaz *et al.*, 2018a), but probably a second titanosaur morphotype is present in the site (Díez Díaz *et al.*, 2018b). Also the locality of Métison in the area nearby, yielded several titanosaur cranial remains, including a partial braincase, rom three putative individuals of a new undescribed morphotype (Díez Díaz *et al.*, 2012a)

I. 3.1.2. HISTORICAL RECORD IN SPAIN AND PORTUGAL

The first discoveries in Spain occurred in South Pyrenees, from the Late Cretaceous of Tremp Basin, Catalonia, by José Royo y Gómez in the 1920s (Marín & Bataller, 1929). But there was no other mention to dinosaur material in this area until mid-part of twentieth century. Javier de Mendizábal y Cortázar collected several remains of vertebrates from the Cretaceous of Suterranya during a geological survey in 1940 (Sanz *et al.*, 1987). The first systematic excavations

Country	Locality	Fossil record	Morphotype	Age
France	La Nerthe	bones	Titanosauria indet.	early Maastrichtian
	Le Gourg de l'Encantado	bones	Titanosauria indet.	early Maastrichtian
	Le Mas d'Azil	bones	Titanosauria indet.	early Maastrichtian
	Rennes-le-Château	bones	Titanosauria indet.	early Maastrichtian
	Ausseing	bones	titanosauria indet.	late Maastrichtian
	Cassagnau	teeth	Titanosauria indet.	late Maastrichtian
	Vitrolles-La Plaine	bones	Titanosauria indet.	late Maastrichtian
Portugal	Taveiro	bones	Titanosauria indet.	late Campanian-early Maastrichtian
Spain	Apellániz	bones	titanosauria indet.	late Campanian-early Maastrichtian
	Armuña	bones	Titanosauria indet.	late Campanian-early Maastrichtian
	Chera	Bones + eggs	Lirainosaurus astibiae + Chera Morphotype II	late Campanian-early Maastrichtian
	El Encinar	bones	titanosauria indet.	late Campanian-early Maastrichtian
	La Castellana	bones	*Lirainosaurus astibiae*	late Campanian-early Maastrichtian
	Laño	bones	*Lirainosaurus astibiae*	late Campanian-early Maastrichtian
	Lo Hueco	bones	*Lohuecotitan pandafilandi* + Titanosauria indet.	late Campanian-early Maastrichtian
	Sacedón	Bones + eggs	cf. *Lirainosaurus* sp. + Titanosauria indet.	late Campanian-early Maastrichtian
	Cirugeda	bones	Titanosauria indet.	early Maastrichtian
	Santa Llúcia	bones	Titanosauria indet.	early Maastrichtian
	Cubilla	bones	Titanosauria indet.	early Maastrichtian
	Figuerola	bones	Titanosauria indet.	early Maastrichtian
	Fontllonga	bones	titanosauria	early Maastrichtian
	Castelltallat	bones	Titanosauria indet.	late Maastrichtian
	Els Nerets	bones	Titanosauria indet.	late Maastrichtian
	L'Estanyó	bones	Titanosauria indet.	late Maastrichtian
	Lo Bas-1	bones	Titanosauria indet.	late Maastrichtian
	Orcau-1 to 3	bones	Titanosauria indet.	late Maastrichtian
	Peguera-1	bones	Titanosauria indet.	late Maastrichtian
	Presa de Sant Antoni	bones	Titanosauria indet.	late Maastrichtian
	Serraduy	bones	Titanosauria indet.	late Maastrichtian
	Suterranya-Mina de lignit	bones	Titanosauria indet.	late Maastrichtian

Table.I.2. List of titanosaurian fossil sites and record of the Ibero-Armorican domain.

in the Late Cretaceous of Tremp Basin were conducted by Walter Georg Kühne in 1954 and later continued by Kühne, Emiliano Aguirre and Albert-Félix de Lapparent (Lapparent & Aguirre, 1956b). Several fragmentary remains assigned to titanosaur were reported from the later campaigns and prospection of Aguirre and de Lapparent in the area of Suterranya, specifically in Locality-5 (Orcau-1 sensu Ardèvol, Casanovas, & Santafé, 1995; Vila *et al.*, 2016)

The systematic excavations in this area continued with the works of María Lourdes Casanovas, who discovered titanosaur remains from the Late Cretaceous of Els Nerets and Fontllonga, in Tremp Basin, Lleida (Casanovas-Cladellas, 1992a). Dozens of localities were found on Tremp and Della Basins, recovering fragmentary material attributable to titanosaurs (Casanovas & Santafé, 1993; Ardèvol *et al.*, 1995; Casanovas-Cladellas *et al.*, 1995). It is remarkable the discovery of fragmentary appendicular elements, among which stands out the probable proximal part of a humerus from the Maastrichtian of L'Estanyó (Masriera & Ullastre, 1988).

At this time, the first putative titanosaurian teeth remains from Portugal are found in the re-excavation of Viso and the prospections on Aveiro and Taveiro, Maastrichtian levels near Arazede, in Portugal .(Antunes & Sigogneau-Russell, 1992, 1996; Antunes & Mateus, 2003). The Iberian titanosaur record comes mostly from Tremp Basin and these Portuguese localities by mid 80s.

The first reports of titanosaurian sauropod material outside Tremp Basin in Spain were reported from the Late Cretaceous of Armuña, Segovia, and Quintanilla del Coco, Burgos (Sanz & Buscalioni, 1987; Sanz *et al.*, 1992) which was the first record of putative armoured titanosaurs in the Ibero-Armorican domain (see also Le Loeuff *et al.*, 1994a). In addition, one isolated caudal vertebra from the Maastrichtian of Cubilla, Soria (Pereda Suberbiola & Ruiz-Omeñaca, 2001), and appendicular elements from the Campano-Maastrichtian of Apellaniz, Alava (Xabier Pereda, 1999).

However, the major discovery from the later 80s and first half of the 90s came from the Campanian levels of Laño fossil site, Treviño, Burgos (Astibia *et al.*, 1990) which have yielded abundant material from several vertebrate groups coming from continental and marine levels since the first campaigns in 1988. Among the material discovered in this site, several titanosaur remains in partial articulation were found. This allowed to define the first titanosaur species of the Iberian Peninsula: the dwarf sauropod *Lirainosaurus astibiae* (Sanz *et al.*, 1999), with several individuals (Pereda Suberbiola *et al.*, 1999; Sanz *et al.*, 1999) and the presence of one juvenile specimen (Díez Díaz, Pereda Suberbiola, & Sanz, 2012b; Díez Díaz, 2013).

At the end of the 90s several of the fragmentary remains allowed to question the presence of only two main titanosaur forms in the Ibero-Armorican Late Cretacoeus. The abundant titanosaur discoveries from the Pyrenees area insight the possibility of more undescribed exclusive forms within this group, like the femur from Serraduy, Huesca (Canudo, 2001). Also at the end of this decade several excavations were conducted on Campanian-Maastrichtian of Chera locality, Valencia (Company *et al.*, 1998; Company, Ruiz-Omeñaca, & Pereda Suberbiola, 1999), though the abundant titanosaurian remains will not be described until much further in the first decade of early XXI century.

The first discovery in the mid early XXI were several fragmentary remains from the Maastrichtian of Cirugeda, Teruel (Canudo, Infante, & Murelaga, 2005).

It is at the second half of the decade when remains of this group are found during the TAV railway constructions in the area of Fuentes, Cuenca in 2006-2007, several Campanian-Maastrichtian

levels were excavated and Lo Hueco fossil site was discovered (Ortega *et al.*, 2008; fig.I.6). The abundance of vertebrate fossil remains, especially titanosaurs, is comparable to the diverse and abundant remains found in the French bonebeds discovered in the Corbière (l'Aude) area (Ortega *et al.*, 2015). Based on the material found in Lo Hueco, the second species of titanosaur of the Late Cretaceous of Iberian Peninsula was described: the mid-sized sauropod *Lohuecotitan pandafilandi* (Díez Díaz *et al.*, 2016; see fig.I.1.C). This species preserves one of the most complete holotypes of the Ibero-Armorican titanosaurian record up to this date. In addition, several other individuals partially articulated have been found, with probable presence of juvenile specimens (Díez Díaz, Ortega, & Sanz, 2014; Páramo, Ortega, & Sanz, 2015a; Páramo *et al.*, 2018). Nowadays, the diversity of titanosaurian faunas present in Lo Hueco is discussed (Knoll *et al.*, 2013, 2015; Díez Díaz *et al.*, 2014; Ortega *et al.*, 2015; Páramo *et al.*, 2017; Vidal *et al.*, 2017; Mocho *et al.*, 2018), but at least another exclusive form could be distinguished in this fossil site (Ortega *et al.*, 2015; Vila *et al.*, 2016).

At the same time, the first presence of an Iberian titanosaur taxa in a second locality was described with the discovery of several titanosaurian remains attributed to Lirainosaurus in Chera locality, Valencia (Company, Suberbiola, & Ruiz-Omeñaca, 2009). However, nowadays some of this variability previously found is regarded as a probable existence of a second Chera titanosaurian morphotype (Díez Díaz, Pereda Suberbiola, & Company, 2015). On the other hand, the analysis of the fragmentary remains from Late Maastrichtian of Tremp and Della Basin could be referable to four probable different titanosaurian morphotypes (Vila *et al.*, 2012).

The implications of these diverse titanosaurian discoveries from Lo Hueco, Chera and south Pyrenees were included for first time in the analysis of the "Faunal turnover" of the Ibero-Armorican domain in the Maastrichtian (Canudo *et al.*, 2016; Vila *et al.*, 2016). This event is already known in other dinosaur groups of the Ibero-Armorican domain, but also in dinosaur tracksites, eggshell and nest record). During the last part of first decade of XXI century, a caudal vertebra centrum was discovered in the Campanian-Maastrichtian of Poyos, near Sacedón, Guadalajara (Ortega & Pérez-García, 2009). It was previously referred to cf. *Lirainosaurus astibiae*, the known Iberian titanosaur taxa at that time. But more recent campaigns from 2016 to this date in several levels of this locality, highlights the probable presence of other Iberian titanosaurian morpho. It has been recovered several partly articulated sauropod skeletons as well as an abundant and exceptionally preserved titanosaur nesting area among other vertebrate groups (Perez-Garcia, Gasco, & Ortega, 2017).

I. 3.2. EVOLUTIONARY HISTORY OF EUROPEAN TITANOSAURS

Some cladistic analyses have included European titanosaur taxa among their input data. So often, the inclusion of these taxa was limited to *L. astibiae* (Sanz *et al.*, 1999; Calvo & González Riga, 2003; González Riga, 2003; Upchurch *et al.*, 2004; Bonaparte, González Riga, & Apesteguía, 2006; Hocknull *et al.*, 2009; Gallina & Apesteguía, 2011; Filippi *et al.*, 2011; Gorscak *et al.*, 2014; Salgado, Gallina, & Paulina Carabajal, 2015; Gorscak & O'Connor, 2016; Carballido *et al.*, 2017). Among the analyses that includes *Magyarosaurus* spp., Paludititan nalaztensis, *Atsinganosaurus velauciensis*, *Lohuecotitan pandafilandi*, *Lirainosaurus astibiae* and/or *Ampelosaurus atacis*, the latter two were regarded as closer forms (Curry Rogers, 2005) or sometimes within a common group (Curry Rogers, 2005; Díez Díaz *et al.*, 2018a). While, the Haţeg Basin titanosaurs (*Magyarosaurus* spp., P. nalaztensis) are not so close related to western European titanosaur forms (Csiki *et al.*, 2010; Díez Díaz *et al.*, 2018b). The group *A. atacis* + *L. astibiae* would be

Lithostrotian titanosaur closer to Saltasauridae than to Malawisaurus dixeyi (Díez Díaz *et al.*, 2018a). On the other hand, the phylogenetic position of *Lohuecotitan pandafilandi* is unclear among Lithostrotitan titanosaurs. The species was initially regarded as a more basal Lithostrotitan taxa closely related to *Malawisaurus* (Díez Díaz *et al.*, 2016), but inclusion of Lognkosauria + European titanosaurian taxa in the data input results in a more derived position than typical lognkosaurian titanosaurs, closely related to the north african *Mansourasaurus shahinae* and less derived than *Lirainosaurus astibiae* (Sallam *et al.*, 2018; fig.I.9.D). Both M. shahinae and *L. astibiae* are regarded as a derived non-Saltasauridae Lithostrotia in this analysis, and slightly more derived than *Lohuecotitan pandafilandi*. The group *Ampelosaurus atacis* + Paludititan nalatzensis is also recovered as slightly more basal titanosaurs than *L. pandafilandi* (Sallam *et al.*, 2018).

However, in one analysis including all South European titanosaurian forms and the Early Cretaceous titanosaurs Normaniasaurus genceyi from Le Havre (Díez Díaz *et al.*, 2018a) the results divide the European titanosaurian taxa in two groups away from each other. The group *Lohuecotitan pandafilandi* + *Paludititan nalatzensis* are recovered as basal Lithostrotia, closely related to *Malawisaurus dixeyi* and the non-Lithostrotita Titanosauria *Normanniasaurus genceyi* (Díez Díaz *et al.*, 2018a; see fig.I.9.C). While *Lirainosaurus astibiae* + *Ampelosaurus atacis* + *Atsinganosaurus velauciensis* are recovered in the same group, and regarded as Lirainosaurinae among derived Lithostrotia and close related to Saltasauridae (Díez Díaz *et al.*, 2018a). But more detailed studies of titanosaur taxa are needed, including a reassessment of *Magyarosaurus* spp. (noted in Díez Díaz *et al.*, 2018a).

These recent phylogenetic hypotheses could represent also possible paleobiogeographical hypotheses for the European titanosaur faunas, different from previous studies (e.g. Mannion & Upchurch, 2011; Le Loeuff, 2012; Sallam *et al.*, 2018). As a first consideration, it exists the possibility of a South European-African connection and faunal exchange during Cenomanian age (Sallam *et al.*, 2018). Part of the evolution of the European island archipelago included the rotation and incorporation of the Iberian plate (and in minor effect until Paleogene, the Alboran plate) toward the main European craton (Alonso *et al.*, 1987; Scotese, 1991; Gómez, Vergés, & Riaza, 2002; Golonka, 2004; Golonka *et al.*, 2006; Kley & Voigt, 2008).

During Cenomanian-Santonian-Early Campanian, main separation from northern emerged part of African plate occurred in the southern part of Iberian peninsula (Tyson & Funnell, 1987; Alonso *et al.*, 1994; Hay *et al.*, 1999; Martín-Chivelet *et al.*, 2002; Golonka, 2004). Some authors have disregarded possible faunal connections during this interval and consider the European Late Cretaceous faunas as endemic (Upchurch, Hunn, & Norman, 2002; Pereda Suberbiola, 2009; Weishampel *et al.*, 2010; Brusatte *et al.*, 2013; Pérez-García, Gasulla, & Ortega, 2014). These faunas came from the European bioprovince and then evolved in each Campanian-Maastrichtian landmass like the Ibero-Armorican island or the Haţeg Basin island, suggesting a long time presence of endemic (high endemism sensu Le Loeuff, 2012) faunas in the Late Cretaceous of European island archipelago (see also Le Loeuff, 1991b; Upchurch *et al.*, 2002; Martin & Delfino, 2010; Weishampel *et al.*, 2010; Buscalioni *et al.*, 2011; Csiki *et al.*, 2015). However, an Early to Late Cretaceous connection between Africa and the European island archipelago could have been possible. While small sized vertebrate faunas are mostly endemic (see Evans, Raia, & Barbera, 2004; Rage, 2013; Csiki *et al.*, 2015), it is known now that several macrovertebrate groups were endemic but others came from radiations of other bioprovinces. Among the European endemic faunas there were the crocodylomorphs, represented by two major groups: Allodaposuchidae (Buscalioni *et al.*, 2011; Narváez *et al.*, 2016) and Hylaeochampsidae

(Martin & Delfino, 2010). However, the Testudines present a different evolutionary history between the two major group registered in the European Cretaceous faunas. The members of Pleurodira proceeded from Gondwanan groups that penetrated in the European region after the Cenomanian with representatives as Algorachelus peregrinus (Pérez-García, 2017). While, Bothremydidae were only present in Laurasia, and later as endemic groups during the Cretaceous of Europe and North America (Joyce, 2007; Pereda Suberbiola, 2009; Pérez-García, 2017).

The ornithischian dinosaur groups present in Ibero-Armorican domain represented a mixture of pre-Maastrichtian endemic faunas of the European post-Cenomanian realms (Butler *et al.*, 2009; Haluza *et al.*, 2012; Ősi *et al.*, 2012; Csiki *et al.*, 2015; Godefroit *et al.*, 2017; Madzia, Boyd, & Mazuch, 2018) though there is a possible exception within rhabdodontid dinosaurs if phylogenetic hypothesis including Australian taxa *Muttaburrasaurus* as a Rhabdodontomorpha (McDonald, 2012; Madzia *et al.*, 2018). The most derived hadrosaurids, present in the Maastrichtian, were the only group with probable Eurasian distribution and almost no local representatives during the Campanian (Prieto-Márquez *et al.*, 2013). This group enters the Ibero-Armorican domain as part of the proposed Campano-Maastrichtian dinosaur faunal turnover (~72 m.y.; see Vila *et al.*, 2016; Fondevilla *et al.*, 2019).

On the other hand, most of the Theropoda groups represented in the European island archipelago were widespread and had a Gondwanan origin (Buffetaut, 1988, 1989b; Pereda Suberbiola, 2009; Ősi & Buffetaut, 2011; Carrano, 2012; Csiki *et al.*, 2015). Based on the description of Balaur bondoc, Dromaeosauridae theropods are the only group discussed as representative of endemic European faunas or somewhat Laurasian origin within this clade (Brusatte *et al.*, 2013). This complex scenario can be explained with an Asian realm connection (Weishampel & Jianu, 2011; Brusatte *et al.*, 2013) as well as an Adriatic Tethys or Apulian Tethys connection between North Africa and European realms in the Late Cretaceous around Cenomanian age (Dalla Vecchia, 2002, 2005; Canudo *et al.*, 2009; Martin & Delfino, 2010; Prieto-Márquez *et al.*, 2013). The more accepted hypothesis is that it was a probable migration of several of these dinosaur groups from other bioprovinces of north of Gondwana or Laurasia (see Buffetaut, 1988, 1989b; Le Loeuff, 1991b; Canudo *et al.*, 2009; Martin & Delfino, 2010; Weishampel *et al.*, 2010; Weishampel & Jianu, 2011; Ezcurra & Agnolín, 2012; Sallam *et al.*, 2018)

Recent phylogenetic hypothesis for European titanosaur taxa could insight two different titanosaurian groups, with a previous Campanian-Maastrichtian fauna composed by Paludititan nalatzensis + *Lohuecotitan pandafilandi*, and a second group including Lirainosauridae titanosaurs (Díez Díaz *et al.*, 2018a). Other possibility is that one of these groups is representative of North African titanosaur faunal migration occurred in pre-Cenomanian. This North African migration of titanosaur faunas is based on the phylogenetic hypothesis of Sallam *et al.* (2018), which results show the affinities of *Lohuecotitan pandafilandi* and the Egyptian titanosaur Mansourasaurus shahinae. This paleobiogeographical hypothesis might be backed by the presence of several similar titanosaur teeth between European and African Late Cretaceous remains (Holwerda *et al.*, 2018). Titanosaurs could be represented by an endemic Laurasia faunas and a second group of North African migration like in turtles, lizards, atoposaurid crocodyliformes and theropod dinosaurs (e.g. Pereda Suberbiola *et al.*, 2015; see before).

A second implication of the disparity between current European Titanosauria phylogenetic hypotheses is related with the Late Cretaceous Ibero-Armorican faunal turnover (Le Loeuff *et al.*, 1994b; Laurent, Bilotte, & Le Loeuff, 2002; Prieto-Márquez, 2010; Canudo *et al.*, 2016;

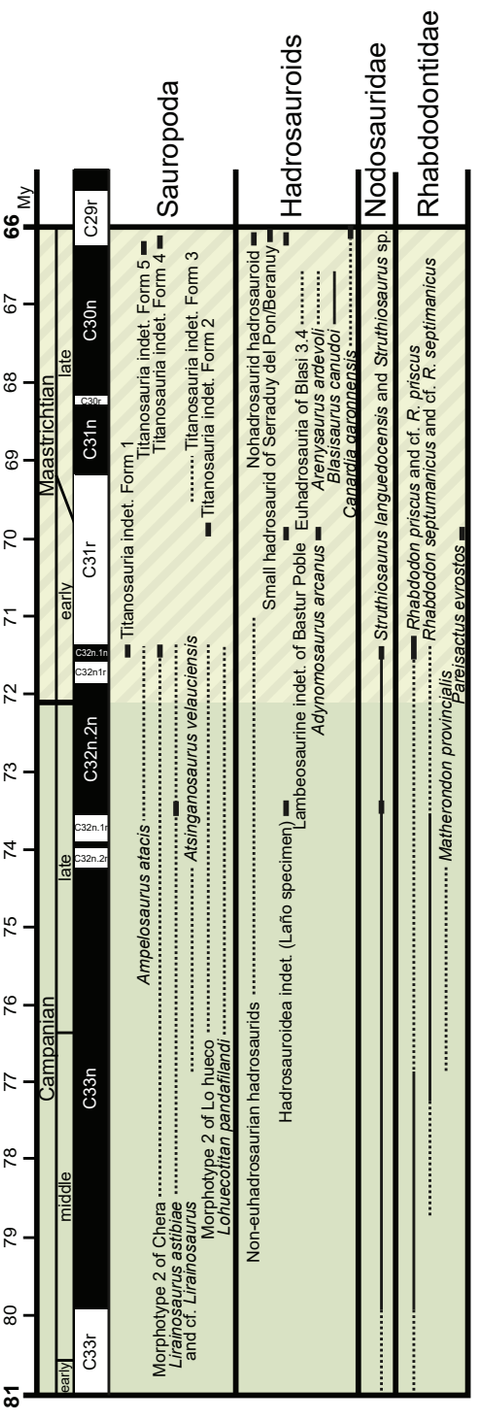

Fig.I.5. Late Cretaceous herbivorous faunal turnover in the Ibero-Armorican domain. Modified after Fondevilla *et al.* (2018)

Vila *et al.*, 2016; Prieto-Márquez *et al.*, 2018; Fondevilla *et al.*, 2019), which has been described in most dinosaur and non-dinosaur vertebrate faunas from the Maastrichtian of this domain (Vila *et al.*, 2012, 2016; Canudo *et al.*, 2016; Fondevilla *et al.*, 2019; see hadrosaurids before). Initial works highlighted a possible hiatus in titanosaurian record during Late Cretaceous that coincides with the entrance of derived hadrosauroid Ornithopoda in the Ibero-Armorican domain (Casanovas-Cladellas, 1992b; Le Loeuff *et al.*, 1994b; Casanovas *et al.*, 1999; Laurent, 2002). This process was regarded as a turn-over from a titanosaur dominated to an hadrosaurian dominated herbivorous macrovertebrate communities at the early Maastrichtian (Le Loeuff *et al.*, 1994b).

But attending to the new findings, it now knows that titanosaurian sauropods were present up to the Late Maastrichtian (Vila *et al.*, 2012). Moreover, the combination of skeletal remains, ichnological and dinosaur egg parataxa suggest a complex scenario with several dinosaur groups disappearing while other were replaced by different in-group clades (see Laurent, 2002; Le Loeuff, 2012; Canudo *et al.*, 2016; Vila *et al.*, 2016). Two different ootaxa associations are recovered between the Early and Late Maastrichtian, as well as several ichnological remains from Late Maastrichtian (Vila *et al.*, 2016).

Titanosaur taxa described in the Ibero-Armorican domain are mostly Campanian to Early Maastrichtian (see Pereda Suberbiola, 2009; Canudo *et al.*, 2016; Vila *et al.*, 2016), thought there are several undescribed titanosaurian morphotypes identified on isolated appendicular elements from the Maastrichtian of South of France and Pyrenees that are probably not related with known titanosaur taxa from Early Maastrichtian (Vila *et al.*, 2012 see also Table I.1. and Table I.2., Fig.I.3 and Fig.I.4). It has been explained as a change in the dominant titanosaurian forms at this age (~72 m.y.; Vila *et al.*, 2016), but phylogenetic relationships are unknown due to the fact that

these morphotypes are based on isolated appendicular elements. Similarly in other dinosaur groups, rhabdodontid and nodosaurid Ornithopoda dissapeared in the Early Maastrichtian and were substituted by Hadrosauridae taxa (Arenysaurus ardevoli Pereda Suberbiola *et al.*, 2009; Blasisaurus canudoi Cruzado-Caballero, Pereda-Suberbiola, & Ruiz-Omeñaca, 2010; Adynomosaurus arcanum Prieto-Márquez *et al.*, 2018) and undescribed morphotypes identified in Late Maastrichtian (see Vila *et al.*, 2016). Theropod dinosaurs are mostly known from teeth and fragmentary material (Torices *et al.*, 2015; Canudo *et al.*, 2016). Some changes in the composition of the different groups in the communities have been detected (Vila *et al.*, 2016), but the presence of several groups among Dromaeosauridae as well as the presence of Arcovenator scotae and cf. Arcovenator during all Maastrichtian suggest that theropod faunas did not been greatly affected during the Late Maastrichtian turn-over (Vila *et al.*, 2016; Fondevilla *et al.*, 2019).

In addition, recent studies of the chronostratigraphic and synthesis over all the possible fossil sites indicate that the turn-over was not as abrupt as previously have been observed during the transition between Early and Late Maastrichtian (Fondevilla *et al.*, 2019). One of the most recent titanosaur phylogenetic hypothesis (Díez Díaz *et al.*, 2018a) includes the possibilities that at least one of this groups are involved in the Maastrichtian turn-over, be it starting earlier in a Campanian-Maastrichtian or Early Maastrichtian, or the substitution of one of the earlier European clades (*Lohuecotitan* + Paludititan) for a more derived group of Lirainosauridae.

There is an abundant presence of undescribed morphotypes, including different sauropod remains found in Lo Hueco (Ortega *et al.*, 2015) with at least two distinct morphotypes (Knoll *et al.*, 2013, 2015; Díez Díaz *et al.*, 2014; Páramo *et al.*, 2015a), but probably up to four different taxa (Mocho *et al.*, 2016; Vidal *et al.*, 2017), the second morphotype at Chera (Company *et al.*, 2009; Díez Díaz *et al.*, 2015), the undescribed Late Maastrichtian titanosaur morphotypes (Vila *et al.*, 2012), a probable new titanosaur from South of France (Díez Díaz *et al.*, 2013) and the recent discovery of titanosaurian remains in Poyos, an Late Cretaceous locality near Sacedón, Guadalajara, Spain (Perez-Garcia *et al.*, 2017).

Assessment of possible morphological affinities between these undescribed morphotypes would help us to understand the titanosaurian Late Cretaceous turn-over in the Ibero-Armorican domain.

	Relative abundance (%)			
	Total	From total vertebrates	From total dinosaurs	
Vertebrates	79.04%	~100%		
Dinosaurs	20.96%	26.52%		
Dinosaurs + indet.	49.94%	63.19%	~100%	
Sauropoda	17.43%	22.05%	34.90%	
Ornithischia	0.63%	0.79%	1.26%	
Theropoda	2.90%	3.67%	5.81%	
Dinosauria indet.	28.98%	36.70%	58.03%	
Sauropoda + Dinosauria indet.				**~93%**

Table.I.3. Percentage of macrovertebrate fossil remains recovered from the Lo Hueco site. *indet.* - indeterminate remains probable from titanosaur sauropods.

I.4. LO HUECO FOSSIL SITE

The fossil site of Lo Hueco was discovered in Campanian-Maastrichtian levels in the locality of Fuentes, Cuenca (Castilla-La Mancha, Central Spain) during the works on the Spanish high-speed railway Madrid-Levante (TAV-AVE) in 2007. Lo Hueco is considered a Konzentrat-Lagerstätte yielding thousands of fossil remains, especially vertebrates (Ortega *et al.*, 2008, 2015). Among them, one of the most abundant groups represented in the sample is Dinosauria, especially those attributable to Titanosauria (Sauropoda). See summary of the abundance of fossil remains sampled in table I.3.

This fossil locality was discovered in South-Western branch of Iberian ranges on the Arcas-Fuentes Syncline, in levels known in the literature as the "Garumn" facies (Ortega 2008, Barroso-Barcenilla 2009). The garumnian facies are a series of clay and marls generally of reddish colours and relative to several shallow marine to continental interdigiting transgression levels from early Campanian to middle Eocene age found in most of the Late Cretaceous of Ibero-Armorican domain (Ramírez del Pozo, Portero, & Olivé, 1975; Vilas *et al.*, 1982; García-Gil, 1995; Vera, 2004). In a more detailed geological study, the site of Lo Hueco is located in six lithosomes of the upper part of the Margas, Arcillas y Yesos de Villalba de la Sierra Formation, of upper Campanian-lower Maastrichtian age (Ortega *et al.*, 2008; Barroso-Barcenilla *et al.*, 2009). The fossil remains have been discovered in four of the six stratigraphic lithosomes, coming mainly from level G1 and G2 interpreted as part of a flooded muddy plain (Barroso-Barcenilla *et al.*, 2009; Barroso-barcenilla, Cambra-moo, & Segura, 2010; Cambra-Moo *et al.*, 2012; see also fig.I.6). Main lithology is a marly mudstone with high proportion of clay minerals (>85%, see Ortega *et al.*, 2015). There is also a moderate proportion of gypsum (<15%) present in all lithosomes (Barroso-Barcenilla *et al.*, 2009; Ortega *et al.*, 2015).

I.4.1. TAPHONOMY OF LO HUECO

Much of fossil remains found in this site were found in partial articulation or isolated, with light and moderate scattering in "G1" and "G2" levels respectively (Barroso-barcenilla *et al.*, 2010; Cambra-Moo *et al.*, 2012; Ortega *et al.*, 2015). Most of the partially articulated sauropod skeletons come from "G1" level, proposed as the flooded muddy plain surrounding canals like the ones produced in level "C" (Barroso-barcenilla *et al.*, 2010). They are subject of low dispersion, but several parts of the skeletons have been lost (see specimen HUE-EC-1 of the holotype material of *Lohuecotitan pandafilandi*: (Díez Díaz *et al.*, 2016). Also several of the individuals were found intermingled with isolated specimens or other partially articulated individuals (common in bonebed sites). This make difficult to refer bone elements to a single specimen.

The study of bone preservation indicates that fossil remains were buried fast with low post-mortem subaerial exposal (Cambra-Moo *et al.*, 2012). The fossil bone material usually presents fractures and microfractures. Internal structure is well preserved in most cases, but in histological sampling it can be seen that many of the structures present microfractures caused by demineralization (Cambra-Moo *et al.*, 2012; see fig.I.7). Clay minerals penetrate in bone fractures and features related to sauropod bone pneumatization (Marcos-Fernández *et al.*, 2018). Many secondary osteons of the histological framework are filled with gypsum crystals affecting the stability of the specimens (Cambra-Moo *et al.*, 2012; see fig.I.7). However, sometimes growth of gypsum crystals is related with heavy mineral replacement. There are several specimens (e.g., the pubes HUE-3086 and the femur HUE-3108 of the holotype specimen of *Lohuecotitan pandafilandi*; see fig.I.7) where the gypsum crystals are decimeter long and extrude from the

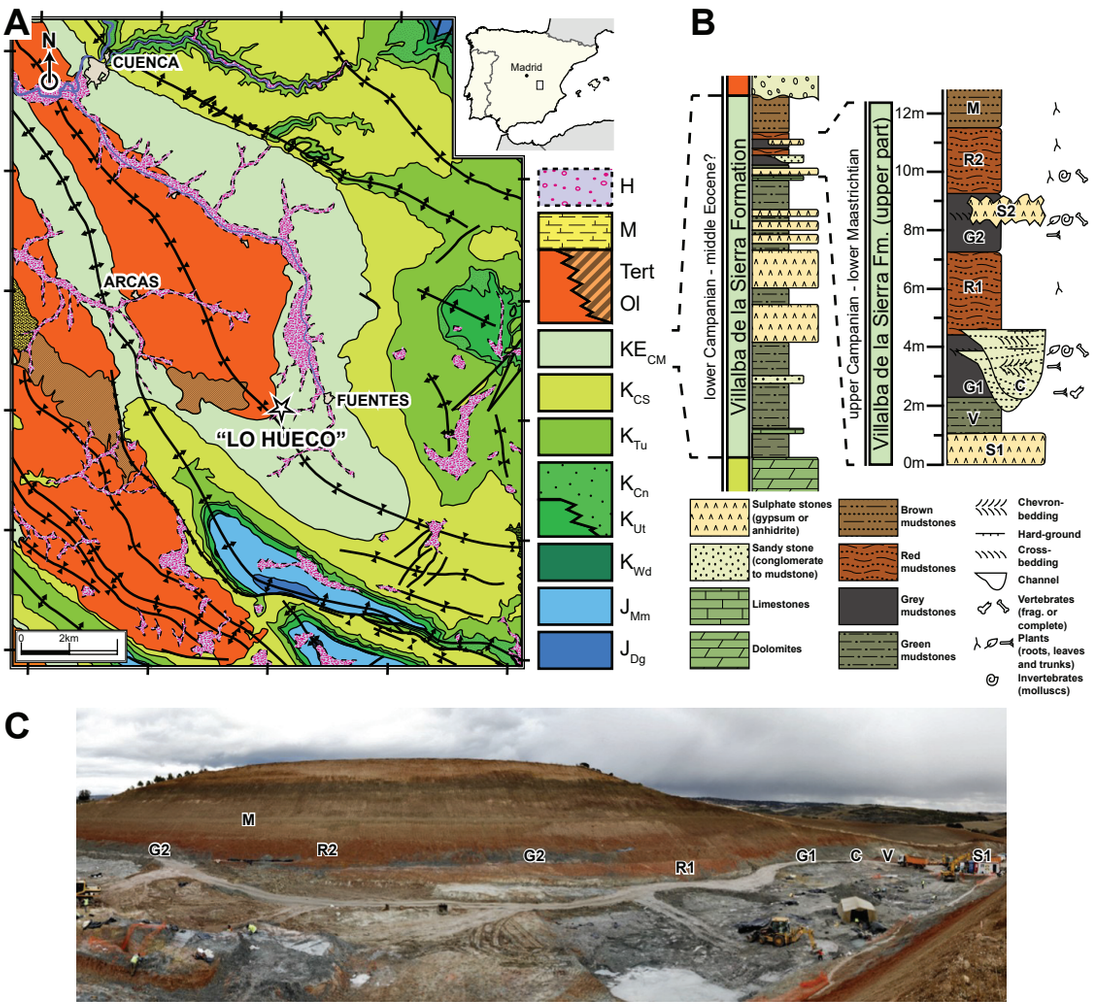

Fig.V.1. Lo Hueco fossil site location and stratigraphy. (A) Geological map of Cuenca (Spain). (B) General stratigraphic column of the Villalba de la Sierra Formation and the Lo Hueco fossil site. (C) Photography of the Lo Hueco site during the 2007 campaign. Labels indicates the levels of the stratigraphic column.

bone surface (fig.I.7). There is also a common second replacement of bone periosteum by iron minerals creating a ferruginous crust over fossil bone surface (Cambra-Moo *et al.*, 2012; Marcos-Fernández *et al.*, 2014, 2018; Ortega *et al.*, 2015). As it is a mineral replacement of the most external bone layer, it is not possible to eliminate and it can obscure some anatomical features (see Fig.I.7).

All the fossil remains are affected by all of these processes: e.g. long bones present common breakage of proximal and distal ends (Páramo *et al.*, 2017) and some of the elements might present also fractures perpendicular to the axis of the shaft, although generally they are simple planes that are easily recoverable during preparation phase (Páramo *et al.*, 2017; see also Chapter III). Sometimes, there are longitudinal fractures in some long bones that produce collapses of bone surfaces in conjunction with the internal microscopic focal destruction at histological level

and gypsum crystal replacement of the bone hydroxyapatite (see Cambra-Moo *et al.*, 2012). This process, together with the action of postburial compression, crushes some long bones, but generally it is not problematic for morphological feature recognition. The long bone shaft are only collapsed in the inner part while the more lateral or medial face preserve their width (Páramo *et al.*, 2016, 2017). Finally, the position of anatomical structures (e.g., deltopectoral crest of the humerus, fourth trochanter of the femur, lateral trochanter of the fibula) does not suffer significant displacement from the expected position in each long bone. Nonetheless, it is necessary that taphonomical deformation in long bones, including by bone crushing, be considered in any morphological studies.

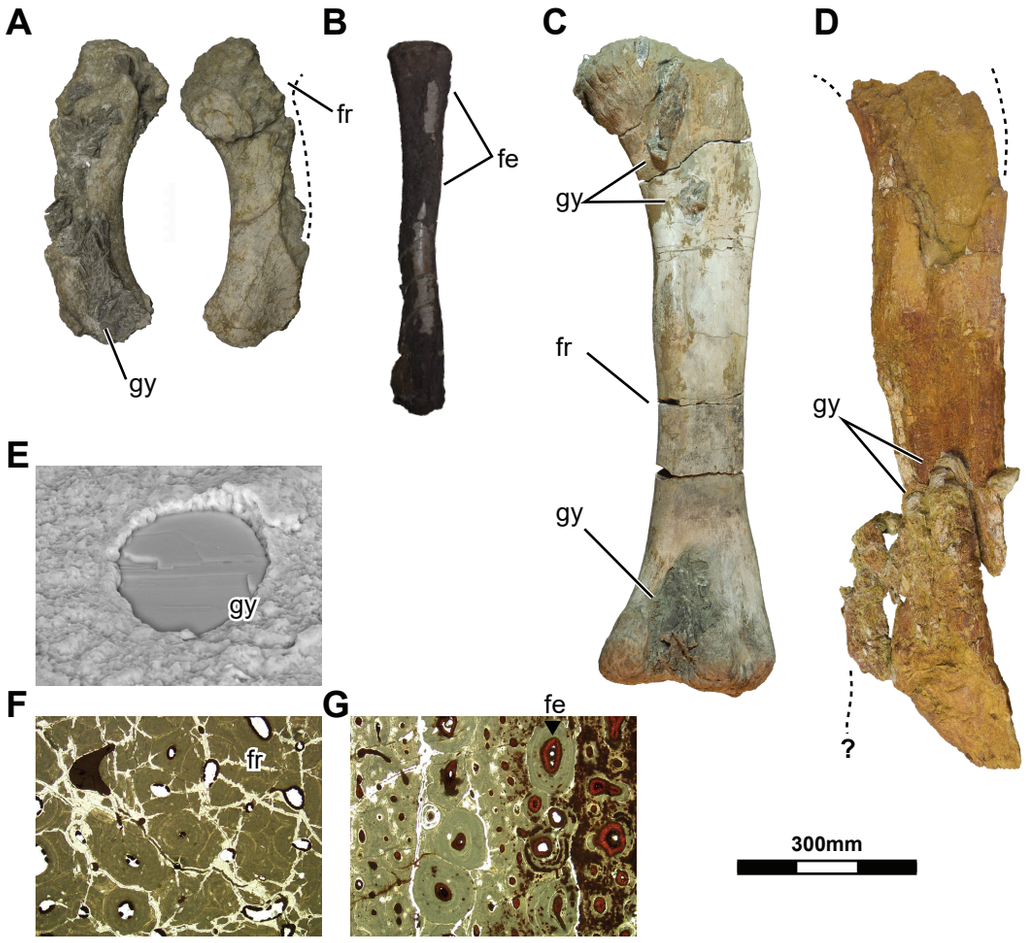

Fig.I.7. Taphonomy of the titanosaur remains from Lo Hueco. (A) Pubis HUE-3086. (B) Fibula HUE-1377 covered in iron oxide crust. (C) *Lohuecotitan pandafilandi* holotype EC-1; femur HUE-3108.(D) Femur HUE-1756. (E) Gypsum growth in a haversian canal, EC-1. (F) Paleohistology sample: Internal fracture of the histological structure, EC-1. (G) Paleohistology sample: Infilling of the haversian canals with iron oxide, remplacement of the bone periosteum EC-2.

I.4.2 .TITANOSAUR SAMPLE FROM LO HUECO

As previously mentioned, hundreds of specimens referable to titanosaurian sauropods have been found within the sample of macrovertebrates from Lo Hueco site (Ortega *et al.* 2015; see Table.I.3). Among this sample, there are at least sixteen individuals partially articulated skeletons. However, several other specimens have been found in partial articulation (e.g., specimen HUE-1612, a tibia and fibula and specimen HUE-1158, a distal forelimb). Some of the partially articulated skeletons preserve part of the appendicular skeleton, and many of the isolated specimens correspond to long bones.

This sample of appendicular specimens from Lo Hueco, allows to observe a wide range of variation similar to other bonebeds from the Ibero-Armorican domain (see Vila *et al.*, 2012). The taxonomic assessment of the sauropod macrofauna assemblage in Lo Hueco is difficult due to this variability. To this date, only a putative lithostrotian titanosaur taxa has been described in this site: *Lohuecotitan pandafilandi* Díez-Díaz, Mocho, Páramo, Escaso, Marcos-Fernández, Sanz and Ortega (2016).

Previous studies on cranial skeleton from the titanosaurs from Lo Hueco have highlighted two probable titanosaurs in this site. The analysis of titanosaur teeth show two main morphotypes (Díez-Díaz *et al.*, 2014). The morphotype-A are robust teeth with D-shaped section, a marked central ridge and compressed in mesial to labialy. This morphotype also presents fine "meteor shower" microwear pattern and has been related to a high soft stem eater (Díez-Díaz *et al.*, 2014). The morphotype-B corresponds to more cylindrical teeth, more slender, with the anteroposterior width almost the same as the mesial-labial width, slightly more expanded in the later. This morphotype presents similar microwear pattern like the morphotype A, but with wider (~0.7mm) scratches, suggesting the intake of lightly more harder elements within similar high soft stem diet (contra e.g. diplodocoids, see teeth in Whitlock, 2011). Based on these differences, it has been proposed that it could be related with niche-partitioning between the two studied teeth morphotypes (Díez Díaz *et al.*, 2014).

The study of two distinct braincases highlights again the presence of two different titanosaur morphotypes in Lo Hueco. The analysis of the virtual cranial cavity endocast and the inner ear of specimen HUE-8741 shows one morphotype closer to Ampelosaurus sp. (Knoll *et al.*, 2013). The brain lobe proportions, the vestibular system of the labyrinth and the morphology of the semicircular canals suggest a less head movement and generally a less agile sauropod (Knoll *et al.*, 2013). Virtual cranial cavity endocast of the Ampelosaurus sp braincase morphotype is more related with *A. atacis* and Camarasaurus lentus brain (Knoll *et al.*, 2013). The other cranial specimenHUE-1667 indicates a second morphotype with short and deep skull morphology closer to *Jainosaurus septentrionalis* (Knoll *et al.*, 2015). This second morphotype presents an expanded labyrinth, especially the semicircular canals. The proportions and morphology closer to Spinophorosaurus nigerensis, Rapetosaurus krausei and Giraffatitan brancai, suggesting a more agile morphotype (Knoll *et al.*, 2015).

Contrary to the cranial remains, the postcranial skeleton yielded a more abundant sample. The analysis of postcranial remains shows high morphological variability among the studied sample. The taxonomic assessment is complex and different cluster distribution have been observed in each region of the skeleton (Mocho *et al.*, 2016, 2018; Páramo *et al.*, 2016; Vidal *et al.*, 2017). There

	Specimens	Relative abundance (%)	
		From total Sauropoda	From total Sauropoda + Dinosauria indet.
Girdles	257	14.45%	5.43%
Forelimb	351	**19.74%**	**7.41%**
Hindlimb	365	**20.53%**	**7.71%**
Metapoda	169	9.51%	3.57%
Indeterminate bones	99	5.57%	2.09%

Table.I.4. Relative abundance of the different appendicular elements in the sample of titanosaurs from Lo Hueco.

are at least two main morphotypes identified in the appendicular skeleton of the titanosaurs from Lo Hueco (Ortega *et al.*, 2015; Páramo *et al.*, 2016). However, the study of the dorsal axial skeleton distinguishes three main groups of titanosaurs in the site (Mocho *et al.*, 2016). Also recent studies in the caudal axial skeleton highlight four probable titanosaur morphotypes (Vidal *et al.*, 2017; Mocho *et al.*, 2018).

The preliminary study of titanosaur femora from Lo Hueco shows two main groups. One group is closer to the morphology of the femur of *Jainosaurus septentrionalis*, while the other is closer to *Ampelosaurus atacis* or *Mendozasaurus neguyelap* (see Páramo *et al.*, 2016). The sample of titanosaur postcranial remains also shows important size differences (Páramo *et al.* 2014). No juvenile specimens were detected in the study of titanosaur teeth (Díez Díaz *et al.*, 2014), but there are reports on small vertebrae of juvenile sauropods in the fossil site (Díez-Díaz & Ortega, 2013). In addition, the sample of appendicular elements is more numerous and there are several specimens that could pertain to juvenile individuals (Páramo *et al.*, 2014). They exhibit some morphological differences with other bigger specimens.

I.4.3. INTRASPECIFIC VARIABILITY OR INTERESPECIFIC DISPARITY?

The analysis and assessment of this mophological variation is necessary for understanding the titanosaur taxonomy and interespecific relationships in Lo Hueco. The presence of small individuals can be attributed to juvenile individuals (Páramo *et al.*, 2014; see also fig.I.8), but there are other dwarf titanosaur taxa like *Magyarosaurus* spp. and *Paludititan nalatzensis* from the Hateg Basin (see Nopsca, 1915; Csiki & Benton, 2010) or the small to medium sized titanosaur *Lirainosaurus astibiae* (Sanz *et al.*, 1999; Company *et al.*, 2009; Company, 2011; Díez Díaz *et al.*, 2015). Size differences cannot be regarded accurately to different ontogenetic stages, as it may be size differences between specimens of similar age (see Ikejiri, 2004). Whether those differences are producing during the ontogenetic development of long bones in the sample of titanosaurs from Lo Hueco, or presence of putative dwarf titanosaur taxa must be addressed.

The presence of probable juvenile individuals as well as the wide sample of long bones is an opportunity to apply statistical framework on the study of titanosaur appendicular skeleton variability.

I.5. INTRASPECIFIC VARIABILITY OF THE APPENDICULAR SKELETON IN TITANOSAURIA

I.5.1. STATE OF THE KNOWLEDGE ON THE INTRASPECIFIC VARIABILITY OF SAUROPODA

The presence of morphological differences have been noted for long time in sauropod dinosaurs (e.g. Mook, 1918). However, it has been a lack of understanding of intraspecific variation in sauropod skeleton with detailed assessment of (i) character variation during ontogenetic development (ii) characters related with sexual dimorphism, (iii) individual variation within the population. This is partly caused by the lack of sauropod bone beds or new sauropod taxa with multiple individuals referred until the last part of XX century (e.g. *Phuwiangosaurus sirindhornae*, see Martin, 1994a; Martin, Buffetaut, & Suteethorn, 1994; *Ampelosaurus atacis*, see Le Loeuff, 1995). In general, studies on dinosaur intraspecific variation have come later in sauropods than in other dinosaur groups: e.g., within Theropoda (Molnar, 1990), in taxa as *Allosaurus fragilis* (Madsen, James H., 1976; Smith, 1998), *Coelophysis bauri* (see Colbert, 1990), *Deinonychus antirrhopus* (see Ostrom, 1969) and *Tyrannosaurus rex* (see Carpenter, 1990; Carr, 1999) among others; Ornithischia as in *Chasmosaurus* spp. (see Lehman, 1990), *Iguanodon bernissartensis* (see Norman, 1980) and *Maiasaura peeblesorum* (see Horner, 1982, 1983; Varricchio & Horner, 1993), among others. On the contrary, most of knowledge in Sauropodomorpha comes from *Plateosaurus engelhardi* (see Weishampel & Chapman, 1990; Wellhnöfer, 1993; Galton, 2000), and the Upper Jurassic sauropod faunas from Morrison Formation: *Camarasaurus* spp., *Diplodocus* spp. and *Apatosaurus* spp. (Carpenter & McIntosh, 1994; McIntosh *et al.*, 1996b,a; Wilhite, 1999, 2003; Bonnan, 2004; Ikejiri, 2004). This kind of sample is problematic due to the difficulty to distinguish species (McIntosh, 1990b; McIntosh *et al.*, 1996a; Wilson & Upchurch, 2003; Bonnan, 2003; Ikejiri, 2004). The taxonomical assessment of several classic taxa (e.g., *Titanosaurus* spp.) demonstrates that some of the morphological feature variation might not be diagnostic (Powell, 2003; Wilson & Upchurch, 2003). Some authors have proposed instead the use of phylogenetic taxonomy (Sereno, 2007).

Phylogenetic taxonomy is useful for taxon determination based on phylogenetic grouping of specimens and character disparity instead of isolated morphological features (Tschopp, Mateus, & Benson, 2015), or worse, relative proportions (McIntosh, 1990b,a; contra McIntosh *et al.*, 1996a; Wilson & Upchurch, 2003). The understanding of intraspecific variability, including individual variation and ontogeny, and quantifying the impact on morphological characters use in data matrices is important for this task as noted in other non-quantitative studies (e.g. Weishampel & Horner, 1994).

Most of the studies on sauropod appendicular skeleton intraspecific variation are related with ontogeny. The appendicular skeleton presents an isometric growth (Wilhite, 1999, 2003, 2005; Bonnan, 2004; Ikejiri, 2004; Tidwell & Wilhite, 2005; Curry Rogers *et al.*, 2016), and few morphological features are different between juvenile and adult specimens. Some juvenile specimens present feeble accessory trochanters in the femora i.e. *Phuwiangosaurus sirindhornae* and *Giraffatitan brancai* (Martin *et al.*, 1994). Other elements present small differences in deflection or torsion of structures, i.e., fibular deflection to anteromedial in Camarasaurus spp. (Ikejiri, 2004). The main differences between juvenile and adult specimens however, are restricted to proportions of the shaft and the proximal and distal ends (Martin, 1994b; Wilhite, 1999; Ikejiri, 2004; Tidwell & Wilhite, 2005; Díez Díaz *et al.*, 2015). While these proportion differences are noticeable, statistical

analysis on the relationships of shape and long bone size are isometric (Wilhite, 1999; Bonnan, 2004, 2007; Tidwell & Wilhite, 2005; Curry Rogers *et al.*, 2016). Early juvenile sauropods present appendicular elements with overall similar morphology to the adult specimens (Carpenter & McIntosh, 1994; Martin, 1994b; Martin *et al.*, 1994; Martin, Suteethorn, & Buffetaut, 1999; McIntosh *et al.*, 1996a,b; Wilhite, 1999; Bonnan, 2004; Tidwell & Wilhite, 2005; Curry Rogers *et al.*, 2016).

Preliminary studies on the titanosaurs of Lo Hueco show similar results with probable juvenile specimens with similar morphology to the adult specimens (see fig. I.7, see also Páramo *et al.*, 2014; Páramo, Ortega, & Sanz, 2015b). It is however, an unusual morphological feature differences between smaller appendicular specimens and the bigger specimens of each bone type of the sample from Lo Hueco (see Páramo *et al.*, 2018; see also Chapter V and VI). Whether those character-scoring differences in the morphological data sets occur by differences in the stages during ontogenetic development must be assessed.

Fig.I.8. Morphological variability in the titanosaur appendicular elements from Lo Hueco. Including probable juveniles (A) Humerus HUE-1434. (B) Ulna HUE-1139. (C) Radius HUE-1140. (D) Femur HUE-1319. (E) Femur HUE-3108. (F) Tibia HUE-3082. (G) Humerus HUE-XXYY. (H) Ulna HUE-2865. (I) Radius HUE-1166. (J) Femur HUE-10007. (K) Femur HUE-2636. (L) Tibia HUE-4632.

I.5.2. PHYLOGENETIC IMPLICATIONS OF THE INTRASPECIFIC VARIABILITY IN THE TITANOSAUR APPENDICULAR SKELETON

The importance of understanding the intraspecific variation in the appendicular skeleton is not only related to the taxonomic assessment of isolated specimens. The intraspecific variability can affect the morphological features used as osteological characters in studies on sauropod systematics. The differences in scorings among specimen of the same species can potentially alter the phylogenetic tree topology. The most common effect reported is the topological differences related to intraspecific variability related to ontogenetic changes (e.g. Chapman & Brett-Surman, 1990; Raath, 1990; Weishampel & Horner, 1994; Chapman *et al.*, 1997; Ikejiri, 2004; Griffin, 2018).

Current hypothesis on sauropod growth and precocity on the acquisition of adult morphology in the appendicular skeleton (Tidwell & Wilhite, 2005; Curry Rogers *et al.*, 2016) should result in few morphological differences in character scoring between specimens at different ontogenetic stages. However, even small amounts of character variation can result in different character scorings among distinct specimens of the same species (see features in Carpenter & McIntosh, 1994; character scorings in Carballido & Sander, 2014).

There are other types of intraspecific variation (e.g. probable sexual dimorphism and individual variation), that could affect the character score. As commented above, some European titanosaurs present differences in the appendicular skeleton e.g. *Magyarosaurus dacus*, M. hungaricus and M. transilvanicus (see Huene, 1932). This variability cannot be fully regarded as proper taxonomical differences in the light of current knowledge on sauropod interspecific variation in the appendicular skeleton (Wilson & Upchurch, 2003). Moreover, recent studies among the sample of specimens of *Ampelosaurus atacis* (see Le Loeuff, 1995, 2005) revealed that some specimens can be regarded as a second morphotype, closer to cf. *Lirainosaurus astibiae* (Vila *et al.*, 2012). These osteological features explored by Vila *et al.* (2012), can be potential new character definitions, though it is necessary assess whether they show taxonomic differences or intraspecific variation.

Most of the morphological characters considered on sauropods systematics are defined mainly in the axial skeleton and the girdles since first character data matrices (see Bonaparte, 1986; McIntosh, 1990a) and studies on sauropod morphology with systematic relevance (see McIntosh, 1990b). First phylogenetic studies using cladistics only considered the humerus-femur ratio relationships (Russell & Zheng, 1993; Calvo & Salgado, 1995). Posteriorly, several of the early studies on sauropod phylogenetics recognized the lateromedial expansion of the pelvic girdle in derived Titanosauriformes, the relationship with the expansion of the lateral bulge, deflection to medial of the femoral head as well as the anteroposterior compression of the femoral shaft and the lateromedial expansion of the tibia among Titanosauria (Salgado *et al.*, 1997). However, all of these observations were translated to only two morphological character definitions (2 of 38 characters, ~5.3% of the dataset), related with the femur of all the proposed dataset used for the analysis (Salgado *et al.*, 1997). While the knowledge of "titanosaurid" sauropod expands, number of appendicular characters increases, especially related with the humerus and tibia, given the discovery of *Lirainosaurus astibiae* and the first definition of the anteroposterior rotation of the distal end in the tibia of this species (Sanz *et al.*, 1999: 4 of 43 characters, ~9.3% of the dataset).

Most of the modern studies on sauropod systematics are based on two major works on sauropod systematics: Upchurch (1995) and Wilson & Sereno (1998). These works from the mid-

late 90's represent a formal morphological character definition and the associated character data matrices.

The first expanded sauropod data matrix presents 174 osteological characters (Upchurch, 1995) but was extended shortly after up to 205 osteological characters for 26 sauropod genera (Upchurch, 1998). This hypothesis presents for first time a detailed definition of morphological characters in each bone element of the appendicular skeleton, including a total of 34 characters (~16.6% of the dataset). Also, it includes several coding in order to record variable characters within a genera as well as pseudo-quantitative definitions (Upchurch, 1998).

The other main dataset introduced at that time included 109 osteological characters for ten sauropod terminal taxa and two outgroups, where the terminal taxa were a mix of sauropod genera plus the summarizing taxonomic unit for Diplodocoidea, Brachiosauridae and Titanosauria (Wilson & Sereno, 1998). This hypothesis included a detailed description of 40 characters for all the elements of the appendicular skeleton (~36.70% of the dataset).

As well as in the previous work of Upchurch (1998), the author included definitions based on qualification of quantitative characters, though Wilson and Sereno (1998) did not included polymorphic character scoring in the dataset. These works constitutes the set-up of modern sauropod cladistics and where updated in their most stable and widely used forms in the early 2000's.

The hypothesis and dataset carried out by Paul Upchurch, Paul M. Barrett and Peter Dodson included 309 osteological characters for 41 genera (introducing the Operative Taxonomic Unit, scorings summarizing all the interspecific and intraspecific variation within the genera) and six outgroups (Upchurch *et al.*, 2004). There are a comprehensive total of 36 character definitions on the appendicular skeleton (~11.33% of the dataset; see fig.I.7.A). These characters include polymorphic scorings of several OTUs. They also present several characters that include pseudo-quantification like humeral-femoral length (character 216) or the midshaft robustness of the radius (character 225).

The hypothesis and dataset of Jeffrey A. Wilson (2002) present 234 osteological characters for 23 OTUs and six outgroups. There is a comprehensive description of 28 appendicular characters (~11.97% of total dataset; see fig.I.7.B). These characters include this time several polymorphic scorings among the OTUs and several characters with pseudo-quantification like the eccentricity of the femur shaft (character 198) and the distal transverse breadth ratio of the tibia (character 205).

At this time, several other works especially focused on titanosaur sauropods start to appear in the literature (e.g. Curry Rogers & Forster, 2001; González Riga, 2003) with expanded character descriptions based on early titanosaur phylogenetic hypotheses (see Salgado *et al.*, 1997; Sanz *et al.*, 1999). From the first decade of the 2000's our current known on sauropod systematics have greatly expanded. Most of the works early based on these phylogenetic hypotheses have expanded from these early datasets using most of these proposed definitions.

Appendicular skeleton continues to represent a proportionally small amount of the morphological characters in the datasets used for sauropod systematics. They range from ~10% up to ~15% (Carballido *et al.*, 2017; González Riga *et al.*, 2018; Sallam *et al.*, 2018; Díez Díaz *et al.*, 2018a; see fig.I.7.C and D). As commented above, several quantitative characters scorings can be affected in the same species with individuals sampled at different ontogenetic stages (see Ikejiri,

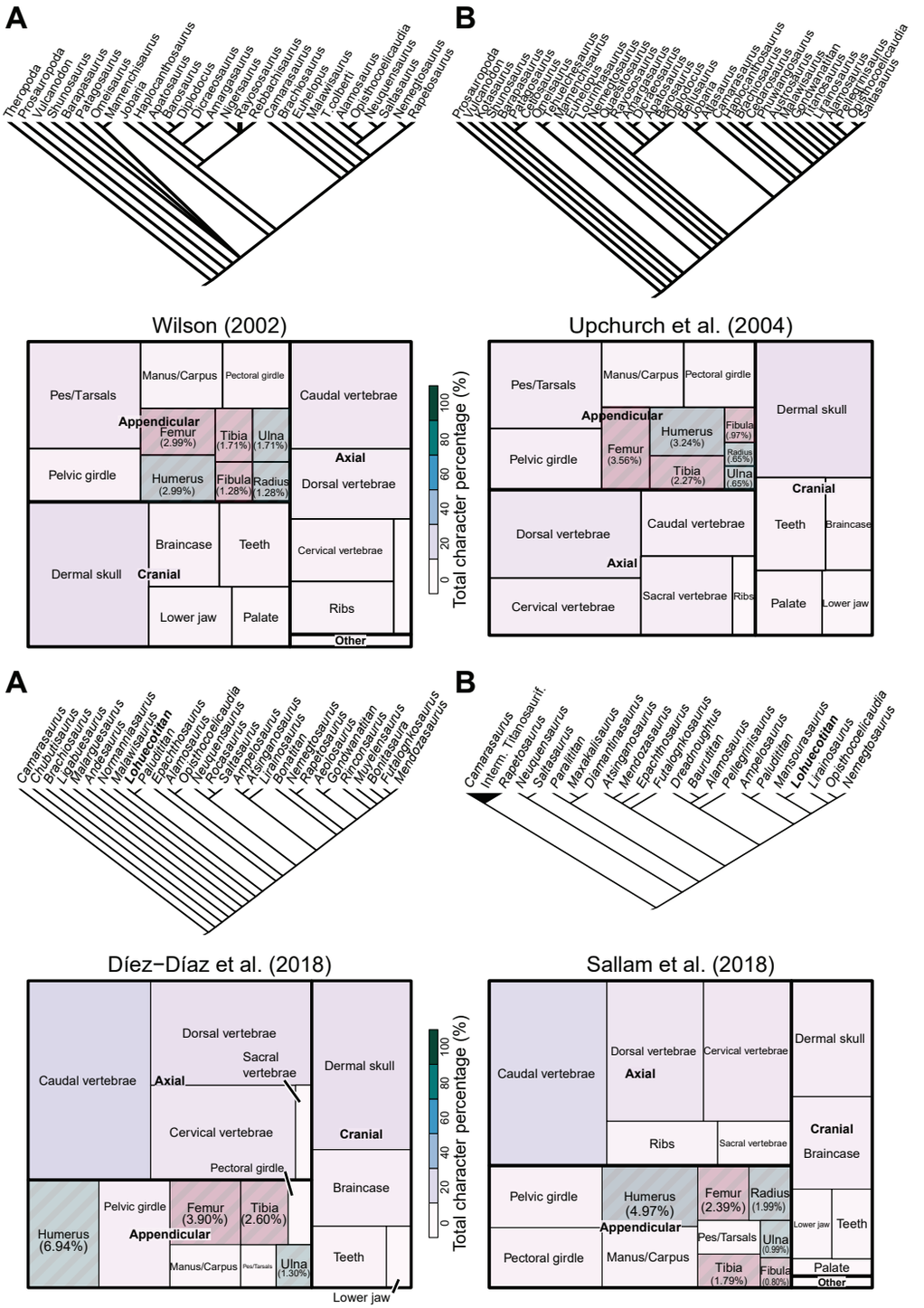

Fig.I.9. Osteological character distributions between different character data matrices. (A) Wilson (2002). (B) Upchurch et al. (2004) compared with recent (C) Díez Díaz *et al.* (2018) and (D) Sallam *et al.* (2018)

2004; Díez Díaz *et al.*, 2015). Also, some of the current morphological character datasets include autapomorphic or exclusive feature combinations in their coding (see Gorscak *et al.*, 2017; Sallam *et al.*, 2018). This is expected to be more sensitive to intraspecific variation than characters defined to cover a wide range of interespecific differences and less variable higher rank groups of the phylogeny.

Some attemtps into including morphometrics characters have been made in the past (Mannion *et al.*, 2013). The quantification of the intraspecific variation and quantitative methods for exploring interespecific differences can help to calibrate and evaluate the potential impact of the variability in these features.

Also, although several morphological features have been considered in sauropod systematics in the past while not incorporated in majority of phylogenetic analyses for now (McIntosh, 1990b; see osteological character definitions in Royo-Torres, 2009; see morphological features discussed in Vila *et al.*, 2012).

Probably, the inclusion of a comprehensive study on the variation of these morphological features can help to evaluate their potential for sauropod systematics and the taxonomic assessment of Ibero-Armorican titanosaurs.

1.6. STRUCTURE OF THE PHD THESIS

The current manuscript will includes a complete methodology chapter with comprehensive description of all the method employed. Then, there are three main chapters, presented in scientific article format, related with the main research of this thesis. All of them includes a brief introduction to the subject, an introduction to the fossil site (the Fig. 1.6. is used in all these commentaries) as well as a brief description of the methodology used for that particular analyses.

The Chapter IV is dedicated to the morphotype description and the analyses deployed for the specimen allocation. The identification of the probable appendicular morphotypes in the Lo Hueco sample will be carried out in the hindlimb elements. The femur is one of the most abundant appendicular elements found in Lo Hueco as well as in the sample of titanosaur fossil remains from the Cretaceous of the Ibero-Armorican domain, as commented before. The Chapter IV.I includes an approach based on previous studies in the morphological variability and probable diversity of Ibero-Armorican titanosaur morphotypes based on the isolated femoral remains (Vila *et al.* ,2012). The other analyses will be carried out in the complete hindlimb based in the well established association for several individuals from Lo Hueco, that preserve partially articulated skeletons, as well as the number of other isolated elements recovered.

After the analysis of the morphological variation referable to putative taxonomical differences, the Chapter V includes the analyses of the intraspecific variability in the complete appendicular skeleton. With the assessment of the morphotype distribution and the intraspecific variability in each morphotype, the Chapter VI presents the analyses of the intraspecific variability related with ontogenetic development.

The curernt PhD thesis present all the citation and bibliography following the format of The Zoological Journal of the Linnean Society.

I.7. BIBLIOGRAPHY

Alonso Á, Floquet M, Mas R, Meléndez A. 1987. Origine et Évolution du Détroit Ibérique au Crétacé Supérieur. In: Salomon J, ed. Transgressions et Régressions au Crétacé. *Mémories Géologiques de L'Université de Dijon*, 1–3.

Alonso Á, Mas R. 1982. Correlación y Evolución Paleogeográfica del Cretácico al Norte y al Sur del Sistema Central. *Cuadernos de Geología Ibérica* 8: 145–166.

Alonso Á, Mas R, Floquet M, Meléndez A. 1994. Late Cretaceous Carbonate Platforms: Origin and Evolution, Iberian Range, Spain. *AAPG Memoir* 56: 298–313.

Antunes MT, Mateus O. 2003. Dinosaurs of Portugal. *Comptes Rendus Palevol* 2: 77–95.

Antunes MT, Sigogneau-Russell D. 1992. La faune de petits dinosaures du Crétacé terminal portugais. *Comunicações dos Serviços Geológicos de Portugal* 78: 49–62.

Antunes MT, Sigogneau-Russell D. 1996. Le Crétacé terminal portugais et son apport au problème de l'extinction des dinosaures. *Bulletin du Museum National d'Histoire Naturelle Section C Sciences de la Terre Paleontologie Geologie Mineralogie* 18: 595–606.

Apesteguía S. 2005a. Evolution of the Hyposphene-hypantrum Complex within Sauropoda. In: Tidwell V, Carpenter K, eds. *ThunderLizards The Sauropodomorph Dinosaurs*. Indiana University Press, 248–267.

Apesteguía S. 2005b. Evolution of the Titanosaur Metacarpus. In: Tidwell V, Carpenter K, eds. *Thunder-Lizards: The Sauropodomorph Dinosaurs*. Bloomington and Indianopolis: Indiana University Press, 321–345.

Ardèvol L, Casanovas ML, Santafé JV. 1995. Restos de dinosaurios del Maastrichtiense de la Conca de Tremp, Lleida, cuenca de antepaís pirenaica meridional. *XI Jornadas de Paleontología*.25–27.

Astibia H, Buffetaut É, Buscalioni ÁD, Cappetta H, Corral JC, Estes R, Garcia-Garmilla F, Jaeger JJ, Jimenez-Fuentes E, Le Loeuff J, Mazin JM, Orue-Etxebarria X, Pereda Suberbiola X, Powell JE, Rage JC, Rodriguez-Lazaro J, Sanz JL, Tong H. 1990. The fossil vertebrates from Lano (Basque Country, Spain); new evidence on the composition and affinities of the Late Cretaceous continental faunas of Europe. *Terra Nova* 2: 460–466.

Barroso-Barcenilla F, Cambra-Moo O, Escaso F, Ortega F, Pascual A, Pérez-García A, Rodríguez-Lázaro J, Sanz JL, Segura M, Torices A. 2009. New and exceptional discovery in the Upper Cretaceous of the Iberian Peninsula: the palaeontological site of "Lo Hueco", Cuenca, Spain. *Cretaceous Research* 30: 1268–1278.

Barroso-barcenilla F, Cambra-moo O, Segura M. 2010. Estudio preliminar sobre Geología y Tafonomía del yacimiento paleontológico de " Lo Hueco " (Cretácico Superior , Cuenca , España). *Boletín de la Real Sociedad de Historia Natural.* 104: 57–70.

Bates KT, Mannion PD, Falkingham PL, Brusatte SL, Hutchinson JR, Otero A, Sellers WI, Sullivan C, Stevens KA, Allen V. 2016. Temporal and phylogenetic evolution of the sauropod dinosaur body plan. *Royal Society Open Science* 3: 150636.

Bonaparte JF. 1986. Les dinosaures (Carnosaures, Allosauridés, Sauropodes, Cétiosauridés) du Jurassique Moyen de Cerro Cóndor (Chubut, Argentina). *Annales de Paléontologie (Vertébrés-Invertebrés)* 72: 247–289.

Bonaparte JF, Coria RA. 1993. Un nuevo y gigantesco sauropodo titanosaurio de la Formacion

Rio Limay (Albiano-Cenomaniano) de la provincia del Neuquen, Argentina. *Ameghiniana* 30: 271–282.

Bonaparte JF, González Riga BJ, Apesteguía S. 2006. *Ligabuesaurus leanzai* gen. et sp. nov. (Dinosauria, Sauropoda), a new titanosaur from the Lohan Cura Formation (Aptian, Lower Cretaceous) of Neuquén, Patagonia, Argentina. *Cretaceous Research* 27: 364–376.

Bonnan MF. 2003. The evolution of manus shape in sauropod dinosaurs: implications for functional morphology, forelimb orientation, and phylogeny. *Journal of Vertebrate Paleontology* 23: 595–613.

Bonnan MF. 2004. Morphometric analysis of humerus and femur shape in Morrison sauropods: implications for functional morphology and paleobiology. *Paleobiology* 30: 444–470.

Bonnan MF. 2005. Pes Anatomy in sauropod Dinosaurs: Implications for Functional Morphology, Evolution and Phylogeny. In: Tidwell V, Carpenter K, eds. *Thunder-Lizards: The Sauropodomorph Dinosaurs*. Bloomington and Indianopolis: Indiana University Press, 346–380.

Bonnan MF. 2007. Linear and geometric morphometric analysis of long bone scaling patterns in Jurassic neosauropod dinosaurs: their functional and paleobiological implications. *Anatomical Record* 290: 1089–111.

Borsuk-Bialynicka M. 1977. A New Camarasaurid Sauropod *Opisthocoelicaudia skarzynskii* gen. n., sp. n. from the Upper Cretaceous of Mongolia. *Paleontologia Polonica* 37: 5–64.

Boule M. 1894. Réponse à C. Depéret sur un os de Dinosaurien (*Oepysaurus*) du Cénomanicn de Mondragon (Vaucluse). *Bulletin de la Société Géologique de France*, 3e série 22.

Broin F de L de, Buffetaut É, Cappetta H, Kerourio P, Koeniguer J, Russell DA, Secretan S, Sigogneau-Russell D, Taquet P, Wenz S. 1980. Nouvelles découvertes de vertébrés maestrichtiens dans le gisement de Fox-Amphoux (Var). *8ème Réunion Anuelle des Sciences de la Terre*.83.

Brusatte SL, Vremir M, Csiki Z, Turner AH, Watanabe A, Erickson GM, Norell MA. 2013. The Osteology of Balaur bondoc, an Island-Dwelling Dromaeosaurid (Dinosauria: Theropoda) from the Late Cretaceous of Romania. *Bulletin of the American Museum of Natural History* 374: 1–100.

Buffetaut É. 1988. Un dinosaure Téropode d'afnités gondwaniennes dans le Crétacé supérieur Provance. *Comptes Rendus de l'Academie des Sciences de Paris* II 306: 153–158.

Buffetaut É. 1989a. Une vertèbrc de dinosaure titanosauridé dans le Cénomanien du Mans et ses implications paléobiogéographiques. *Comptes Rendus de l'Academie des Sciences de Paris* 309: 437–443.

Buffetaut É. 1989b. Archosaurian reptiles with Gondwanan affinities in the Upper Cretaceous of Europe. *Terra Nova* 1: 69–74.

Buffetaut É, Clottes P, Cuny G, Ducrocq S, Le Loeuff J, Martin M, Powell JE, Raynaud C, Tong H. 1989. Les gisements de dinosaures maastrichtiens de la haute vallée de l'Aude (France). *Comptes Rendus de l'Academie des Sciences de Paris* 309: 1723–1727.

Buffetaut É, Cuny G, Le Loeuff J. 1991. French dinosaurs: the best record in Europe? *Modern Geology* 16: 17–42.

Buffetaut É, Le Loeuff J. 1991. Late Cretaceous dinosaur faunas of Europe: Some correlation problems. *Cretaceous Research* 12: 159–176.

Buffetaut É, Le Loeuff J. 1997. Late Cretaceous dinosaurs from the foothills of the Pyrenees. *Geology Today* 13: 60–68.

Buffetaut É, Le Loeuff J, Tong H, Duffaud S, Cavin L, Garcia G, Ward DJ. 1999. Un noveau gisement de vertébrés du Crétacé supérieur à Cruzy (Hérault, Sud de la France). *Comptes Rendus de l'Académie des Sciences - Series IIA - Earth and Planetary Science* 328: 203–208.

Buscalioni ÁD, Piras P, Vullo R, Signore M, Barbera C. 2011. Early eusuchia crocodylomorpha from the vertebrate-rich Plattenkalk of Pietraroia (Lower Albian, southern Apennines, Italy). *Zoological Journal of the Linnean Society* 163: S199–S227.

Butler RJ, Barrett PM, Kenrick P, Penn MG. 2009. Diversity patterns amongst herbivorous dinosaurs and plants during the Cretaceous: implications for hypotheses of dinosaur/angiosperm co-evolution. *Journal of evolutionary biology* 22: 446–59.

Calvo JO, Bonaparte JF. 1991. *Andesaurus delgadoi* gen. et sp. nov. (Saurischia-Sauropoda), Dinosaurio Titanosauridae de la Formación Rio Limáy (Albiano-Cenomaniano), Nequen, Argentina. *Ameghiniana* 28: 303–310.

Calvo JO, González Riga BJ. 2003. *Rinconsaurus caudamirus* gen. et sp. nov., a new titanosaurid (Dinosauria, Sauropoda) from the Late Cretaceous of Patagonia, Argentina. *Revista Geológica de Chile* 30: 233–353.

Calvo JO, Porfiri JD, González Riga BJ, Kellner AWA. 2007. A new Cretaceous terrestrial ecosystem from Gondwana with the description of a new sauropod dinosaur. *Anais da Academia Brasileira de Ciências* 79: 529–41.

Calvo JO, Salgado JL. 1995. *Rebbachisaurus tesonei* sp. nov. a new Sauropoda from the Albian-Cenomanian of Argentina; new evidence on the origin of the Diplodocidae. *GAIA* 33: 13–33.

Cambra-Moo O, Barroso-barcenilla F, Berreteaga A, Carenas B, Elvira A, Escaso F, Domingo L, Peyrot D, Sanz JL, Segura M, Ortega F, Sopelana A. 2012. Preliminary taphonomic approach to "'Lo Hueco'" palaeontological site. *Geobios* 45: 157–166.

Campos D de A, Kellner AWA, Bertini RJ, Santucci RM. 2005. On a titanosaurid (Dinosauria, Sauropoda) vertebral column from the Bauru Group, Late Cretaceous of Brazil. *Arquivos do Museo Nacional, Rio de Janeiro* 63: 565–893.

Canudo JI. 2001. Descripción de un fragmento proximal de fémur de Titanosauridae (Dinosauria, Sauropoda) del Maastrichtiense superior de Serraduy (Huesca). In: Meléndez G, Herrera Z, Delvene G, Azanza B, eds. *XVII Jornadas de Paleontología. Los fósiles y la Paleogeografía*. Albarracín, Zaragoza: Sociedad Española de Paleontología y Área y Museo de Paleontología de la Universidad de Zaragoza, 255–262.

Canudo JI, Barco JL, Pereda Suberbiola X, Ruiz-Omeñaca JI, Salgado JL, Torcida Fernández-Baldor F, Gasulla JM. 2009. What Iberian dinosaurs reveal about the bridges said to exist between Gondwana and Laurasia in the Early Cretaceous. *Bulletin de la Societe Geologique de France* 180: 5–11.

Canudo JI, Infante P, Murelaga X. 2005. Primer registro de vertebrados continentales (Dinosauria y Quelonii) en el Maastrichtiense de Teruel (Cirugeda, Aliaga). *¡Fundamental!* 06: 57–61.

Canudo JI, Oms O, Vila B, Galobart À, Fondevilla V, Puértolas E, Sellés AG, Cruzado-Caballero P, Dinarès-Turell J, Vicens E, Castanera D, Company J, Burrel L, Estrada R, Marmi J, Blanco A. 2016. The upper Maastrichtian dinosaur fossil record from the southern Pyrenees and its contribution to the topic of the Cretaceous-Palaeogene mass extinction event. *Cretaceous Research* 57: 540–551.

Carballido JL, Pol D, Otero A, Cerda IA, Salgado JL, Garrido AC, Ramezani J, Cúneo NR, Krause JM. 2017. A new giant titanosaur sheds light on body mass evolution among sauropod

dinosaurs. *Proceedings of the Royal Society B: Biological Sciences* 284: 20171219.

Carballido JL, Sander PM. 2014. Postcranial axial skeleton of *Europasaurus holgeri* (Dinosauria, Sauropoda) from the Upper Jurassic of Germany: implications for sauropod ontogeny and phylogenetic relationships of basal Macronaria. *Journal of Systematic Palaeontology* 12: 335–387.

Carpenter K. 1990. Variation in *Tyrannosaurus rex*. In: Carpenter K, Currie PJ, eds. *Dinosaurs Systematics: Approaches and Perspectives*. Cambridge University Press, 141–145.

Carpenter K, McIntosh JS. 1994. Upper Jurassic sauropod babies from the Morrison Formation. In: Carpenter K, Hirsch KF, Horner JR, eds. *Dinosaur Eggs and Babies*. Cambridge: Cambridge University Press, 265–278.

Carr TD. 1999. Craniofacial ontogeny in Tyrannosauridae (Dinosauria, Coelurosauria). *Journal of Vertebrate Paleontology* 19: 497–520.

Carrano MT. 1998. Locomotion in non-avian dinosaurs: Integrating data from hindlimb kinematics, in vivo strains, and bone morphology. *Paleobiology* 24: 450–469.

Carrano MT. 2000. Homoplasy and the evolution of dinosaur locomotion. *Paleobiology* 26: 489–512.

Carrano MT. 2005. The Evolution of Sauropod Locomotion. In: Curry Rogers KA, Wilson JA, eds. *The Sauropods: Evolution and Paleobiology.* University of California Press, 229–250.

Carrano MT. 2012. Dinosaurian faunas of the later Mesozoic. In: Brett-Surman MK, Holtz TR, Farlow JO, eds. *The Complete Dinosaur*. Bloomington: Indiana University Press, 1003–1026.

Casanovas-Cladellas ML. 1992a. Novedades en el registro fósil de dinosaurios del Levante español. *Zubia* 10: 139–151.

Casanovas-Cladellas ML. 1992b. Novedades en el Registro Fósil de Dinosaurios del Levante Español. *Zubia* 10: 139–151.

Casanovas-Cladellas ML, Santafé-Llopis JV, Sanz JL, Powell JE. 1995. Nuevos restos de dinosaurios (Titanosauria y Ornithopoda) de El Cretácico Superior de la Cuencas de Tremp y Della (Lleida, España). *Estudios Geológicos*: 277–283.

Casanovas ML, Pereda Suberbiola X, Santafé JV, Weishampel DB. 1999. A primitive euhadrosaurian dinosaur from the uppermost Cretaceous of the Ager syncline (Southern Pyrenees, Catalonia). *Geologie en Mijnbouw* 78: 345–356.

Casanovas ML, Santafé JV. 1993. Presencia de Titanosáuridos (Dinosauria) en el Cretácico superior de Fontlionga (Lleida, España). *America* 80.

Cerda IA, Paulina Carabajal A, Salgado JL, Coria RA, Reguero M a., Tambussi CP, Moly JJ. 2012. The first record of a sauropod dinosaur from Antarctica. *Die Naturwissenschaften* 99: 83–87.

Chapman RE, Brett-Surman MK. 1990. Morphometric observations on hadrosaurid ornithopods. In: Carpenter K, Currie PJ, eds. *Dinosaur Systematics: Approaches and Perspectives*. Cambridge University Press, 163–178.

Chapman SC, Weishampel DB, Hunt G, Rasskin-Gutman D. 1997. Sexual Dimorphism in Dinosaurs. *Dinofest International Proceedings*.83–93.

Clottes P, Raynaud C. 1983. Le gisement à dinosauriens de Campagne-sur-Aude–Esperaza. Observations préliminaires. Premiers résultats. *Bulletin de la Société d'Études Scientifiques de l'Aude* 83: 5–14.

Colbert EH. 1990. Variation in *Coelophysis bauri*. In: Carpenter K, Currie PJ, eds. *Dinosaur Systematics: Approaches and Perspectives*. Cambridge University Press, 81–90.

Company J. 2011. Bone histology of the titanosaur *Lirainosaurus astibiae* (Dinosauria: Sauropoda) from the Latest Cretaceous of Spain. *Die Naturwissenschaften* 98: 67–78.

Company J, Galobart Lorente À, Gaete R, Galobart À, Gaete R. 1998. First data on the hadrosaurid dinosaurs (Ornithischia, Dinosauria) from the Upper Cretaceous of Valencia, Spain. *Oryctos* 1: 121–126.

Company J, Ruiz-Omeñaca JI, Pereda Suberbiola X. 1999. A long-necked pterosaur (Pterodactyloidea, Azhdarchidae) from the Upper Cretaceous of Valencia, Spain. *Geologie en Mijnbouw* 78: 319–333.

Company J, Suberbiola XP, Ruiz-Omeñaca JI. 2009. Nuevos restos fósiles del dinosaurio Lirainosaurus. *Ameghiniana* 46: 391–405.

Cruzado-Caballero P, Pereda-Suberbiola X, Ruiz-Omeñaca JI. 2010. *Blasisaurus canudoi* gen. et sp. nov., a new lambeosaurine dinosaur (Hadrosauridae) from the Latest Cretaceous of Arén (Huesca, Spain). *Canadian Journal of Earth Sciences* 47: 1507–1517.

Csiki Z, Benton MJ. 2010. An island of dwarfs — Reconstructing the Late Cretaceous Haţeg palaeoecosystem. *Palaeogeography, Palaeoclimatology, Palaeoecology* 293: 265–270.

Csiki Z, Buffetaut É, Ősi A, Pereda Suberbiola X, Brusatte SL. 2015. Island life in the Cretaceous - faunal composition, biogeography, evolution, and extinction of land-living vertebrates on the Late Cretaceous European archipelago. *ZooKeys*: 1–161.

Csiki Z, Codrea VA, Jipa-Murzea C, Godefroit P. 2010. A partial titanosaur (Sauropoda, Dinosauria) skeleton from the Maastrichtian of Na'lat-Vad, Hateg Basin, Romania. *Neues Jahrbuch fur Geologie und Palaontologie - Abhandlungen* 258: 297–324.

Curry Rogers K. 2005. Titanosauria: A phylogenetic overview. In: Curry Rogers K, Wilson JA, eds. *The Sauropods: Evolution and Paleobiology.* Berkeley: University of California Press, 50–103.

Curry Rogers K, Forster CA. 2001. The last of the dinosaur titans: a new sauropod from Madagascar. *Nature* 412: 530–4.

Curry Rogers K, Whitney M, D'Emic MD, Bagley B. 2016. Precocity in a tiny titanosaur from the Cretaceous of Madagascar. *Science* 352: 450–453.

D'Emic MD. 2012. The early evolution of titanosauriform sauropod dinosaurs. *Zoological Journal of the Linnean Society* 166: 624–671.

D'Emic MD, Wilson JA. 2011. New remains attributable to the holotype of the sauropod dinosaur *Neuquensaurus australis*, with implications for saltasaurine systematics - *Acta Palaeontologica Polonica*. *Acta Palaeontologica Polonica* 56: 61–73.

Dalla Vecchia FM. 2002. Cretaceous dinosaurs in the Adriatic–Dinaric Carbonate Platform (Italy and Croatia): paleoenvironmental implications and paleogeographical hypotheses. *Memorie della Società Geologica Italiana* 57: 89–100.

Dalla Vecchia FM. 2005. Between Gondwana and Laurasia: Cretaceous sauropods in an Intracoceanic Carbonate Platform. In: Carpenter K, Tidwell V, eds. *Thunder-Lizards: The Sauropodomorph Dinosaurs*. Bloomington and Indianopolis: Indiana University Press, 395–429.

Déperet C. 1894. Sur la découverte d'un os dc Dinosaurien du genre *Oepysaurus* dans le Cénomanien saumâtre de Mondragon (Vaucluse). *Compte Rendu Sommaire des séances de la Société Géologique de France* 22.

Dias R, Ribeiro A. 1995. The Ibero-Armorican Arc: A collision effect against an irregular continent? *Tectonophysics* 246: 113–128.

Díez Díaz V. 2013. Revisión del Dinosaurio Saurópodo *Lirainosaurus astibiae* del cretácico Superior de la Península Ibérica: Comparación con otros titanosaurios del suroeste de Europa. Hipótesis filogenética y paleobiogeográfica. Unpublished thesis, Universidad del País Vasco/ Euskal Herriko Unibersitatea.

Díez Díaz V, Garcia G, Knoll F, Pereda Suberbiola X, Valentin X. 2012a. New cranial remains of titanosaurian sauropod dinosaurs from the Late Cretaceous of Fox-Amphoux-Métisson (Var, SE France). *Proceedings of the Geologists' Association* 123: 626–637.

Díez Díaz V, Garcia G, Pereda-Suberbiola X, Stein KHW, Jentgen-Ceschino B, Godefroit P, Valentin X. 2018a. The titanosaurian dinosaur *Atsinganosaurus velauciensis* (Sauropoda) from the Upper Cretaceous of southern France: New material, phylogenetic affinities, and palaeobiogeographical implications. *Cretaceous Research* 91: 429–456.

Díez Díaz V, Garcia G, Pereda Suberbiola X, Jentgen-Ceschino B, Stein KHW, Godefroit P, Valentin X. 2018b. A new titanosaurian sauropod from the Late Cretaceous of Velaux-La Bastide Neuve (southern France). *XVI Annual Meeting of the European Association of Vertebrate Paleontologists*. Caparica, Lisbon, 60.

Díez Díaz V, Mocho P, Páramo A, Escaso F, Marcos-Fernández F, Sanz JL, Ortega F. 2016. A new titanosaur (Dinosauria, Sauropoda) from the Upper Cretaceous of Lo Hueco (Cuenca, Spain). *Cretaceous Research* 68: 49–60.

Díez Díaz V, Ortega F. 2013. Dorsal vertebrae of a juvenile titanosaur from the Late Cretaceous of "Lo Hueco" (Cuenca, Spain). *XI Annual Meeting of the European Association of Vertebrate Paleontologists*. 35A.

Díez Díaz V, Ortega F, Sanz JL. 2014. Titanosaurian teeth from the Upper Cretaceous of "Lo Hueco" (Cuenca, Spain). *Cretaceous Research* 51: 285–291.

Díez Díaz V, Pereda Suberbiola X, Company J. 2015. Updating titanosaurian diversity (Sauropoda) from the Late Cretaceous of Spain: The fossil site of Laño and Chera. *Spanish Journal of Palaeontology* 30: 293–306.

Díez Díaz V, Pereda Suberbiola X, Sanz JL. 2012b. Juvenile and adult teeth of the titanosaurian dinosaur *Lirainosaurus* (Sauropoda) from the Late Cretaceous of Iberia. *Geobios* 45: 265–274.

Díez Díaz V, Tortosa T, Le Loeuff J. 2013. Sauropod diversity in the Late Cretaceous of southwestern Europe: The lessons of odontology. *Annales de Paléontologie* 99: 119–129.

Dunhill AM, Bestwick J, Narey H, Sciberras J. 2016. Dinosaur biogeographical structure and Mesozoic continental fragmentation: a network-based approach. *Journal of Biogeography* 43: 1691–1704.

Evans SE, Raia P, Barbera C. 2004. New lizards and rhyncocephalians from the Lower Cretaceous of southern Italy. *Acta Paleontologica Polonica* 49: 393–408.

Ezcurra MD, Agnolín FL. 2012. A new global palaeobiogeographical model for the late mesozoic and early tertiary. *Systematic Biology* 61: 553–566.

Filippi LS, García RA, Garrido AC. 2011. A New Titanosaur Sauropod Dinosaur from the Upper Cretaceous of North Patagonia, Argentina. *Acta Palaeontologica Polonica* 56: 505–520.

Fondevilla V, Riera V, Vila B, Sellés AG, Dinarès-Turell J, Vicens E, Gaete R, Oms O, Galobart À. 2019. Chronostratigraphic synthesis of the latest Cretaceous dinosaur turnover in south-western Europe. *Earth-Science Reviews* 191: 168–189.

Gallina PA, Apesteguía S. 2011. Cranial anatomy and phylogenetic position of the titanosaurian sauropod Bonitasaura salgadoi. *Acta Palaeontologica Polonica* 56: 45–60.

Galton PM. 2000. The prosauropod dinosaur *Plateosaurus* MEYER, 1837 (Saurischia : Sauropodomorpha). I. The syntypes of P. engelhardti MEYER, 1837 (Upper Triassic, Germany), with notes on other European prosauropods with 'distally straight' femora. *Neues Jahrbuch Fur Geologie Und Palaontologie-Abhandlungen* 216: 233–275.

García-Gil S. 1995. Evolución sedimentaria en la zona de enlace Cordillera Ibérica-Sistema Central, margen occidental de la cuenca del Tethys durante el Triásico Medio. *Cuadernos de Geología Ibérica* 19: 99–128.

Garcia G, Amico S, Fournier F, Thouand E, Valentin X. 2010. A new Titanosaur genus (Dinosauria, Sauropoda) from the Late Cretaceous of southern France and its paleobiogeographic implications. *Bulletin de la Société Géologique de France* 181: 269–277.

García RA, Salgado L, Fernández MS, Cerda IA, Carabajal AP, Otero A, Coria RA, Fiorelli LE, Salgado JL, Fernández MS, Cerda IA, Carabajal AP, Otero A, Coria RA, Fiorelli LE. 2015. Paleobiology of Titanosaurs: Reproduction, Development, Histology, Pneumaticity, Locomotion and Neuroanatomy from the South American Fossil Record. *Ameghiniana* 52: 29–68.

Gaudry JA. 1890. *Les Enchainements du monde animal dans les termes géologiques: Fossiles secondaires*. Paris, France.

Gilmore CW. 1946. Reptilian fauna of the North Horn Formation of central Utah. United States *Geological Survey Professional Paper* 201–C: 29–53.

Godefroit P, Garcia G, Gomez B, Stein KHW, Cincotta A, Lefèvre U, Valentin X. 2017. Extreme tooth enlargement in a new Late Cretaceous rhabdodontid dinosaur from Southern France. *Scientific Reports* 7: 1–9.

Golonka J. 2004. Plate tectonic evolution of the southern margin of Eurasia in the Mesozoic and Cenozoic. *Tectonophysics* 381: 235–273.

Golonka J, Gahagan L, Krobicki M, Marko F, Oszczypko N, Ślączka A. 2006. Plate-tectonic Evolution and Paleogeography of the Circum-Carpathian Region. The Carpathians and Their Foreland: Geology and Hydrocarbon Researces: *AAPG Memoir 84*. Tulsa, Oklahoma, U.S.A.: The American Association of Petroleum Geologists, 11–46.

Gómez M, Vergés J, Riaza C. 2002. Inversion tectonics of the northern margin of the Basque Cantabrian Basin. *Bulletin de la Société Géologique de France* 173: 449–459.

González Riga BJ. 2003. A New Titanosaur (Dinosauria, Sauropoda) from the Upper Cretaceous of Mendoza Province, Argentina. *Ameghiniana* 40: 155–172.

González Riga BJ, Lamanna MC, Ortiz David LD, Calvo JO, Coria JP. 2016. A gigantic new dinosaur from Argentina and the evolution of the sauropod hind foot. *Scientific Reports* 6: 1–15.

González Riga BJ, Mannion PD, Poropat SF, Ortiz David LD, Coria JP. 2018. Osteology of the Late Cretaceous Argentinean sauropod dinosaur *Mendozasaurus neguyelap*: implications for basal titanosaur relationships. *Zoological Journal of the Linnean Society*: 1–46.

Gorscak E, O'Connor PM. 2016. Time-calibrated models support congruency between Cretaceous continental rifting and titanosaurian evolutionary history. *Biology Letters* 12: 20151047.

Gorscak E, O'Connor PM, Roberts EM, Stevens NJ. 2017. The second titanosaurian (Dinosauria: Sauropoda) from the middle Cretaceous Galula Formation, southwestern Tanzania, with remarks on African titanosaurian diversity. *Journal of Vertebrate Paleontology* 37: e1343250.

Gorscak E, O'Connor PM, Stevens NJ, Roberts EM. 2014. The basal titanosaurian *Rukwatitan bisepultus* (Dinosauria, Sauropoda) from the middle Cretaceous Galula Formation, Rukwa Rift Basin, southwestern Tanzania. *Journal of Vertebrate Paleontology* 34: 1133–1154.

Griffin CT. 2018. Developmental patterns and variation among early theropods. *Journal of Anatomy* 232: 604–640.

Haluza A, Canale JI, Otero A, Pérez LM, Scanferla CA, Scanferla A, Otero A, Pérez LM, Scanferla CA, Taylor P, Haluza A, Canale JI, Scanferla A, Otero A, Municipal M, Bachmann E, Chocón V EI, Pérez LM, Scanferla CA. 2012. Changes in vertebral laminae across the cervicodorsal transition of a well-preserved rebbachisaurid (Dinosauria, Sauropoda) from the Cenomanian of Patagonia, Argentina. *Journal of Vertebrate Paleontology* 32: 219–224.

Hancock JM, Kauffman EG. 1979. The great transgressions of the Late Cretaceous. *Journal of the Geological Society* 136: 175–186.

Hay WW, DeConto RM, Wold CN, Wilson KM, Voigt S, Schulz M, Wold AR, Dullo WC, Ronov AB, Balukhovsky AN, Söding E. 1999. Alternative global Cretaceous paleogeography. *Special Paper 332: Evolution of the Cretaceous Ocean-Climate System*. Geological Society of America, 1–47.

Hocknull SA, White MA, Tischler TR, Cook AG, Calleja ND, Sloan T, Elliott DA. 2009. New Mid-Cretaceous (latest Albian) dinosaurs from Winton, Queensland, Australia. *PloS ONE* 4: e6190.

Holwerda FM, Díez Díaz V, Blanco A, Montie R, Reumer JWF. 2018. Late Cretaceous sauropod tooth morphotypes may provide supporting evidence for faunal connections between North Africa and Southern Europe. *PeerJ* 6: e5925.

Horner JR. 1982. Evidence of a colonial nesting and 'site fidelity' among ornithischian dinosaurs. Nature 297: 675–676.

Horner JR. 1983. Cranial osteology and morphology of the type specimen of Maiasaura peeblesorum (Ornithischia: Hadrosauridae), with discussion of its phylogenetic position. *Journal of Vertebrate Paleontology* 3: 29–38.

Huene FF von. 1932. Die fossile Reptil-Ordnung Saurischia, ihre Entwicklung und Geschichte. *Monographien zur Geologie und Paläontologie* I: 564.

Ikejiri T. 2004. Anatomy of *Camarasaurus lentus* (Dinosauria: Sauropoda) from the Morrison Formation (Late Jurassic), Thermopolis, central Wyoming, with Determination and Interpretation of Ontogenetic, Sexual Dimorphic and Individual Variation in the Genus. Unpublished thesis, State University.

Joyce WG. 2007. Phylogenetic relationships of Mesozoic turtles. *Bulletin of the Peabody Museum* 48: 3–102.

Klein N, Sander PM, Stein KHW, Le Loeuff J, Carballido JL, Buffetaut É. 2012. Modified Laminar Bone in *Ampelosaurus atacis* and Other Titanosaurs (Sauropoda): Implications for Life History and Physiology (AA Farke, Ed.). *PloS ONE* 7: e36907.

Kley J, Voigt T. 2008. Late Cretaceous intraplate thrusting in central Europe: Effect of Africa-Iberia-Europe convergence, not Alpine collision. *Geology* 36: 839–842.

Knoll F, Ridgely RC, Ortega F, Sanz JL, Witmer LM. 2013. Neurocranial Osteology and Neuroanatomy of a Late Cretaceous Titanosaurian Sauropod from Spain (*Ampelosaurus* sp.). *PloS ONE* 8: e54991.

Knoll F, Witmer LM, Ridgely RC, Ortega F, Sanz JL. 2015. A new titanosaurian braincase from the cretaceous 'Lo Hueco' locality in Spain sheds light on neuroanatomical evolution within

titanosauria. *PloS ONE* 10: 1–24.

Lapparent AF de. 1947. Les dinosauriens du Crétacé supérieur du Midi de la France. *Mémories de la Société Géologique de France* 56: 1–54.

Lapparent AF de, Aguirre E. 1956a. Présence de Dinosauriens dans le Crétacé supérieur du bassin de Tremp (province de Lérida, Espagne). *Comptes Rendus Sommaire de la Société Géologique de France* 14: 261–262.

Lapparent AF de, Aguirre E. 1956b. Algunos yacimientos de Dinosaurios del Cretácico Superior de la Cuenca de Tremp. *Estudios Geológicos* 31–32: 377–382.

Lapparent AF de, Aguirre E, Quintero I, Trigueros E. 1957. Descubrimiento de huesos de dinosaurios en el Cretácico terminal de Cubillas (provincia de Soria). *Notas y Comunicaciones del Instituto Geológico y Minero de España* 45: 61–63.

Laurent Y. 2002. *Les faunes de vertébrés continentaux du Maastrichtien supérieur d'Europe : systématique et biodiversité*. Unpublished thesis, Université Paul Sabatier.

Laurent Y, Bilotte M, Le Loeuff J. 2002. Late Maastrichtian continental vertebrates from southwestern France: Correlation with marine fauna. *Palaeogeography, Palaeoclimatology, Palaeoecology* 187: 121–135.

Laurent Y, Cavin L, Bilotte M. 1999. Découverte d'un gisement à vertébrés dans le Maastrichtien supérieur des Petites-Pyrénées. *Comptes Rendus de l'Académie des Sciences - Series IIA - Earth and Planetary Science* 328: 781–787.

Laurent Y, Le Loeuff J, Bilotte M, Buffetaut É, Odin GS. 2001. Chapter D10 Campanian-Maastrichtian continental-marine connection at the Aquitaine-Pyrenees-Provence area (S France). *The Campanian-Maastrichtian stage boundary — Characterisation at Tercis les Bains (France) and correlation with Europe and other Continents*.657–674.

Lehman TM. 1990. The ceratopsian subfamily Chasmosaurinae: sexual dimorphism and systematics. In: Carpenter K, Currie PJ, eds. *Dinosaur Systematics: Approaches and Perspectives*. Cambridge University Press, 211–230.

Lockley MG, Hunt AP. 1995. *Dinosaur Tracks*. New York, USA: Columbia University Press.

Lockley MG, Meyer CA, Hunt AP, Lucas SG. 1994. The distribution of sauropods tracks and trackmakers. *Gaia* 10: 233–248.

Le Loeuff J. 1989. Un arrière-crâne de dinosaure titanosauridé (Saurischia, Sauropoda) dans le Crétacé supérieur du Var (Provence, France). *Comptes Rendus de l'Académie des Sciences*. Série II 309: 851–857.

Le Loeuff J. 1991a. Les vertébrés maastrichtiens du Mas d'Azil (Ariége, France): etude de la collection Pouech. *Revue de Paléobiologie* 10: 61–67.

Le Loeuff J. 1991b. The Campano-Maastrichtian vertebrate faunas from southern Europe and their relationships with other faunas in the world; palaeobiogeographical implications. *Cretaceous Research* 12: 93–114.

Le Loeuff J. 1993. European titanosaurids. *Revue de Paléobiologie*, Volume Spéciale 7: 105–117.

Le Loeuff J. 1995. *Ampelosaurus atacis* (nov, gen., nov. sp.), un nouveau Titanosauridae (Dinosauria, Sauropoda) du Crétacé supérieur de la Haute Vallée de l'Aude (France). *Comptes Rendus de l'Académie des Sciences à Paris*, Série IIa 321: 693–699.

Le Loeuff J. 2005. Osteology of *Ampelosaurus atacis* (Titanosauria) from Southern France. In:

Tidwell V, Carpenter K, eds. *Thunder-Lizards: The Sauropodomorph Dinosaurs*. Bloomington: Indiana University Press, 115–137.

Le Loeuff J. 2012. Paleobiogeography and biodiversity of Late Maastrichtian dinosaurs: how many dinosaur species went extinct at the Cretaceous-Tertiary boundary? *Bulletin de la Societe Geologique de France* 183: 547–559.

Le Loeuff J, Buffetaut É, Cavin L, Martin M, Martin V, Tong H. 1994a. An armoured titanosaurid sauropod from the Late Cretaceous of Southern France and occurence of osteoderms in the Titanosauridae. *Gaia* 10: 155–159.

Le Loeuff J, Buffetaut É, Martin M. 1994b. The last stages of dinosaur faunal history in Europe: a succession of Maastrichtian dinosaur assemblages from the Corbières (southern France). *Geological Magazine* 131: 625.

Le Loeuff J, Laurent Y. 2000. Biodiversity of Late Maastrichtian Dinosaurs. *3rd Catastrophic events and mass extinctions Conference* 1386: 3126.

Lydekker R. 1877. Notices of a new and other Vertebrata from Indian Tertiary and Secondary Rocks. *Geological Survey of India* 10: 30–43.

Lydekker R. 1885. Indian Pre-Tertiary Vertebrata. The Reptilia and Amphibia of the Maleri and Denwa Groups. *Palaeontologia Indica* (ser.4) 1: 1–35.

Lydekker R. 1888. *Catalogue of fossil Reptilia and Amphibia in the British Museum. Part 1. Containing the Orders Ornithosauria, Crocodilia, Dinosauria, Squamata, Rhynchocephalia, and Proterosauria*. British Museum of Natural History.

Lydekker R. 1893. The Dinosaurs of Patagonia. *Anales del Museo de la Plata* 2: 1–14.

Madsen, James H. J. 1976. *Allosaurus fragilis*: A revised osteology. *Utah Geological and Mineral Survey Bulletin* 109: 1–163.

Madzia D, Boyd CA, Mazuch M. 2018. A basal ornithopod dinosaur from the Cenomanian of the Czech Republic. *Journal of Systematic Palaeontology* 16: 967–979.

Mannion PD, Schwarz D, Upchurch P, Wings O. 2019. Taxonomic affinities and biogeographic implications of the putative titanosaurs (Dinosauria: Sauropoda) from the Late Jurassic Tendaguru Formation of Tanzania. *Journal of Vertebrate Paleontology* XX: 1–126.

Mannion PD, Upchurch P. 2011. A re-evaluation of the 'mid-Cretaceous sauropod hiatus' and the impact of uneven sampling of the fossil record on patterns of regional dinosaur extinction. *Palaeogeography, Palaeoclimatology, Palaeoecology* 299: 529–540.

Mannion PD, Upchurch P, Barnes RN, Mateus O. 2013. Osteology of the Late Jurassic Portuguese sauropod dinosaur *Lusotitan atalaiensis* (Macronaria) and the evolutionary history of basal titanosauriforms. *Zoological Journal of the Linnean Society* 168: 98–206.

Marcos-Fernández F, Bartolomé S, López S, Martínez I, Navarro E, Onrubia M, Páramo A, Vidal D, Yagüe A, Ortega F. 2018. La conservación-restauración de la cintura pélvica de un dinosaurio Titanosaurio del yacimiento de Lo Hueco (Fuentes, Cuenca). *XXXIV Jornadas de Paleontología y IV Congreso Ibérico de Paleontología*. Vila Real, 181–187.

Marcos-Fernández F, Mocho P, Elvira A, Páramo A, Escaso F, Ortega F. 2014. The sauropod that stopped the train. *74th Annual Meeting of the Society of Vertebrate Paleontology*. Berlin, Germany, 177–178.

Marín A, Bataller JR. 1929. Nuevos datos sobre el Cretácico Superior de la cuenca de Tremp (Lérida). *Asociación Española Para el Programa de las Ciencias* Congreso d: 25–28.

Martín-Chivelet M, Berasategui X, Rosales I, Vilas L, Vera JA, Caus E, Gräfe KU, Mas R, Puig C, Segura M, Robles S, Floquet M, Quesada S, Ruiz-Ortiz PA, Fregenal-Martinez M, Salas R, Arias C, García A, Martín-Algarra A, Meléndez MA, Chacón B, Molina JM, Sanz JL, Castro JMB de, García-Hernández M, Carenas B, García-Hidalgo JF, Gil J, Ortega F. 2002. Cretaceous. In: Gibbons JW, Moreno T, eds. *The Geology of Spain*. The Geological Society of London, 255–292.

Martin V. 1994. Baby Sauropod from the Sao Khua Fm (Lower Cretaceous) in Northeastern Thailand. *Gaia* 10: 147–153.

Martin V, Buffetaut É, Suteethorn V. 1994. A New Genus of Sauropod Dinosaur from the Sao-Khua Formation (Late Jurassic or Early Cretaceous) of Northeastern Thailand. *Comptes Rendus de l'Academie des Sciences* Serie II 319: 1085–1092.

Martin JE, Delfino M. 2010. Recent advances on the comprehension of the biogeography of Cretaeous European eusuchians. *Palaeogeography, Palaeoclimatology, Palaeoecology* 293: 406–418.

Martín Jimenez M, Sanchez-Chillon B, Escaso F, Mocho P, Narvaez I, Ortega F, Perez-Garcia A. 2017. Systematic study of the historical material of Upper Cretaceous reptiles from the Tremp Basin (Catalonia, Spain) housed at the Museo Nacional de Ciencias Naturales (Madrid). *Journal of Iberian Geology* 43: 217–233.

Martin V, Suteethorn V, Buffetaut É. 1999. Description of the type and referred material of *Phuwiangosaurus sirindhorna*e Martin, Buffetaut and Suteethorn, 1994, A sauropod from the Lower Cretaceous of Thailand. *Oryctos* 2: 39–91.

Masriera A, Ullastre J. 1988. Nuevos datos sobre las capas maestrichtienses con *Septorella*: su presencia al norte del Montsec (Pirineo catalán). *Acta Geológica Hispánica* 23: 71–77.

Matheron P. 1846. Sur les terrains traversés par le souterrain de la Nerthe, près Marseille. *Bulletin de la Société Géologique de France* 4: 261–269.

Matheron P. 1869. Note sur les reptiles fossiles des dépôts fluvio-lacustres crétacés du bassin à lignite de Fuveau. *Memoires de L'Academie Impériale des Sciences, BellesLettres et Arts de Marseilles* 26: 781–795.

Mazzetta G V., Christiansen P, Fariña R a. 2004. Giants and Bizarres: Body Size of Some Southern South American Cretaceous Dinosaurs. *Historical Biology* 16: 71–83.

McDonald AT. 2012. Phylogeny of basal iguanodonts (Dinosauria: Ornithischia): an update. *PloS ONE* 7: e36745.

McIntosh JS. 1990a. Sauropoda. In: Weishampel DB, Dodson P, Osmólska H, eds. *The Dinosauria*. University of California Press, 345–401.

McIntosh JS. 1990b. Species determination in sauropod dinosaurs with tentative suggestions for their classification. In: Carpenter K, Currie PJ, eds. *Dinosaur Systematics*. Cambridge: Cambridge University Press, 53–70.

McIntosh JS, Miles CA, Cloward KC, Parker JR. 1996a. A new nearly complete skeleton of *Camarasaurus*. *Bulletin of Gunma Museum of Natural History* 1: 1–87.

McIntosh JS, Miller WE, Stadtman KL, Gillette DD. 1996b. The Osteology of *Camarasaurus lewisi* (Jensen, 1988). BYU Geology Studies 41: 73–115.

Mocho P, Escaso F, Marcos-Fernández F, Páramo A, Vidal D, Ortega F. 2018. The morphological variability on titanosaur caudal series from Lo Hueco: taxonomic diversity, intra-specific variability or both? *XVI Annual Meeting of European Association of Vertebrate Paleontologists*. 126.

Mocho P, Páramo A, Díez Díaz V, Escaso F, Marcos-Fernández F, Sanz JL, Ortega F. 2016. Looking

through the axial skeleton of the Lo Hueco titanosaurs. In: Torcida Fernández-Baldor F, Canudo JI, Huerta P, Pereda X, eds. *VII International Symposium about Dinosaurs Palaeontology and their Environment*.99–100.

Molnar RE. 1990. Variation in theory and in theropods. In: Carpenter K, Currie PJ, eds. *Dinosaurs Systematics: Approaches and Perspectives*. Cambridge University Press, 71–79.

Mook CC. 1918. The habitat of the sauropod dinosaurs. *Journal of Geology* 26: 459–470.

Narváez I, Brochu CA, Escaso F, Pérez-García A, Ortega F. 2016. New Spanish Late Cretaceous eusuchian reveals the synchronic and sympatric presence of two allodaposuchids. *Cretaceous Research* 65: 112–125.

Nopsca BF. 1915. Die dinosaurier der Siebenbürgischen landesteile Ungarns. *Ungarischen Geologischen Reichsanstalt* 23: 1–24.

Norman DB. 1980. On the ornithischian dinosaur Iguanodon bernissartensis from the Lower Cretaceous of Bernissart (Belgium). *Memoires de l'Institut Royal des Sciences Naturelles de Belgique* 178: 1–103.

Ortega F, Bardet N, Barroso-Barcenilla F, Callapez PMPM, Cambra-moo O, Daviero- Gómez V, Díez Díaz V, Domingo L, Elvira A, Escaso F, García-Oliva M, Gómez B, Houssaye A, Knoll F, Marcos-Fernández F, Martín M, Mocho P, Narváez I, Pérez-García A, Peyrot D, Segura M, Serrano H, Torices A, Vidal D, Sanz JL. 2015. The biota of the Upper Cretaceous site of "Lo Hueco" (Cuenca, Spain). *Journal of Iberian Geology* 41: 83–99.

Ortega F, Pérez-García A. 2009. cf. *Lirainosaurus* sp. (Dinosauria: Titanosauria) en el Cretácico Superior de Sacedón (Guadalajara). *Geogaceta*: 87–90.

Ortega F, Sanz JL, Barroso-barcenilla F, Fernández FM. 2008. El yacimiento de macrovertebrados fósiles del Cretácico Superior de "Lo Hueco" Fuentes, Cuenca). *Palaeontologia Nova* 8:119–131.

Ősi A, Buffetaut É. 2011. Additional non-avian theropod and bird remains from the early Late Cretaceous (Santonian) of Hungary and a review of the European abelisauroid record. *Annales de Paléontologie* 97: 35–49.

Ősi A, Prondvai E, Butler RJ, Weishampel DB. 2012. Phylogeny, Histology and Inferred Body Size Evolution in a New Rhabdodontid Dinosaur from the Late Cretaceous of Hungary (AR Evans, Ed.). *PloS ONE* 7: e44318.

Ostrom JH. 1969. Osteology of Deinonychus antirrhopus, an unusual theropod from the Lower Cretaceous of Montana. *Peabody Museum of Natural History Bulletin*: 1–165.

Otero A. 2018. Forelimb musculature and osteological correlates in Sauropodomorpha (Dinosauria, Saurischia). *PloS ONE* 13: e0198988.

Otero A, Vizcaíno SF. 2008. Musculatura y función del miembro posterior de *Neuquensaurus australis* (Sauropoda: Titanosauria). *Ameghiniana* 45: 333–348.

Páramo A, Mocho P, Marcos-Fernández F, Ortega F, Sanz JL. 2017. 3D Geometric Morphometrics on the Hind Limb of the Titanosaurs from Lo Hueco: Dwarf taxa or Small Individuals? *15th Annual Meeting of the European Association of Vertebrate Paleontologists*.

Páramo A, Mocho P, Ortega F, Sanz JL. 2018. Intraspecific variability in and its effects on systematic assessment of the titanosaurs from Lo Hueco (Late Cretaceous. Cuenca, Spain). *XVI Annual Meeting of European Association of Vertebrate Paleontologists*.147.

Páramo A, Ortega F, Escaso F, Narváez I, Sanz JL. 2014. Ejemplares juveniles de titanosaurio (Sauropoda) del yacimiento de Lo Hueco (Fuentes, Cuenca). In: Royo-Torres, R.; Verdú, F.J.;

Alcalá, L. (coord.). *XXX Jornadas de Paleontología de la Sociedad Española de Paleontología. ¡Fundamental!* 24: 149–151.

Páramo A, Ortega F, Mocho P, Sanz JL. 2016. Femoral variability in two titanosaur taxa from Lo Hueco (Cuenca, Spain): Insights for iberoarmorican titanosaur diversity assessment. In: Torcida F, Jose IC, Huerta P, Pereda-Suberbiola X, eds. *VII International Symposium about Dinosaurs Palaeontology and their Environment*. Salas de los Infantes, Burgos: Colectivo Arqueológico y Paleontológico de Salas, 107–108.

Páramo A, Ortega F, Sanz JL. 2015a. Preliminar assessment of the morphological variability of appendicular bones of titanosaurs (Dinosauria, Sauropoda) from Lo Hueco (Fuentes, Cuenca). *XXXI Jornadas de la Sociedad Española de Paleontología*.

Páramo A, Ortega F, Sanz JL. 2015b. Two types of appendicular bones of titanosaurs (Dinosauria, Sauropoda) from Lo Hueco (Fuentes, Cuenca). In: Dyke GJ, Marshall J, Naish D, Young MT, Wujeck JL, Martin-Silverstone L, Pond S, Roberts A, Hansford J, Taylor C, Blackwell G, Riddington K, eds. *63rd Symposium for Vertebrate Paleontology and Comparative anatomy & 24th Symposium of Palaeontological Preparation and Conservation with the Geological Curator's Group*. 100.

Pereda Suberbiola X. 2009. Biogeographical affinities of Late Cretaceous continental tetrapods of Europe: A review. *Bulletin de la Societe Geologique de France* 180: 57–71.

Pereda Suberbiola X, Canudo JI, Cruzado-Caballero P, Barco JL, López-Martínez N, Oms O, Ruiz-Omeñaca JI. 2009. The last hadrosaurid dinosaurs of Europe: A new lambeosaurine from the Uppermost Cretaceous of Aren (Huesca, Spain). *Comptes Rendus Palevol* 8: 559–572.

Pereda Suberbiola X, Corral JC, Astibia H, Badiola A, Bardet N, Berreteaga A, Buffetaut É, Buscalioni ÁD, Cappetta H, Cavin L, Díez Díaz V, Gheerbrant E, Murelaga X, Ortega F, Pérez-García A, Poyato-Ariza F, Rage JC, Sanz JL, Torices A. 2015. Late cretaceous continental and marine vertebrate assemblages from the Laño quarry (Basque-Cantabrian Region, Iberian Peninsula): an update. *Journal of Iberian Geology* 41.

Pereda Suberbiola X, Murelaga X, Baceta JI, Corral JC, Badiola A, Astibia H. 1999. Nuevos restos fósiles de vertebrados continentales en el Cretácico Superior de Álava (Región Vasco-Cantábrica): sistemática y posición estratigráfica. *Geogaceta* 26: 79–82.

Pereda Suberbiola X, Ruiz-Omeñaca JI. 2001. Un dinosaurio saurópodo (Titanosauria) del Cretácico superior de Cubilla, Soria (España). *Geogaceta* 30: 175–178.

Pérez-García A. 2017. A new turtle taxon (Podocnemidoidea, Bothremydidae) reveals the oldest known dispersal event of the crown Pleurodira from Gondwana to Laurasia. *Journal of Systematic Palaeontology* 15: 709–731.

Perez-Garcia A, Gasco F, Ortega F. 2017. A Singular Uppermost Cretaceous Dinosaur Nesting Area in the Villalba de la Sierra Formation (Guadalajara, Central Spain). *77th Annual Meeting of the Society of Vertebrate Paleontology*: 176.

Pérez-García A, Gasulla JM, Ortega F. 2014. *Eodortoka morellana* gen. et sp. nov., the first pan-pleurodiran turtle (Dortokidae) defined in the Lower Cretaceous of Europe. *Cretaceous Research* 48: 130–138.

Philip J, Floquet M, Platel JP, Bergerat F, Sandulescu M, Baraboshkin E, Amon E, Poisson A, Guiraud R, Vaslet D, Le Nindre Y, Ziegler M, Bouaziz S, Guezou J. 2000. Late Maastrichtian (69.5-65 Ma). In: Dercpurt J, Gaetani M, Vrielynck B, Barrier E, Biju-Duval B, Brunet MF, Cadet JP, Crasquin S, Sandulescu M, eds. *Atlas Peri-Tethys, Palaeogeographic maps. Explanatory notes*. Paris, 145–152.

Platel JP. 1989. Le Crétacé supérieur de la plate-forme septentrionale du Bassin d'Aquitaine. Stratigraphie et évolution géodynamique. *Documents du B.R.G.M.* 164: 1–572.

Powell JE. 1980. Sobre la presencia de una armadura dérmica en algunos dinosaurios titanosáuridos. *Acta Geologica Lilloana* 15: 41–47.

Powell JE. 1986. Revisión de los Titanosáuridos de América del Sur. Unpublished thesis, Universidad Nacional de Tucumán.

Powell JE. 2003. Revision of South American titanosaurid dinosaurs: Palaeobiological, palaeobiogeographical and phylogenetic aspects (TH Rich, K Dimmack, and JR Macdonald, Eds.). *Records of the Queen Victoria Museum* 111: 1–179.

Prieto-Márquez A. 2010. Global phylogeny of Hadrosauridae (Dinosauria: Ornithopoda) using parsimony and Bayesian methods. *Zoological Journal of the Linnean Society* 159: 435–502.

Prieto-Márquez A, Dalla Vecchia FM, Gaete R, Galobart À, Vila B, Oms O, Galobart À, Bates KT, Egerton VM, Manning PL. 2013. Diversity, Relationships, and Biogeography of the Lambeosaurine Dinosaurs from the European Archipelago, with Description of the New Aralosaurin Canardia garonnensis. *PloS ONE* 8: e69835.

Prieto-Márquez A, Fondevilla V, Sellés AG, Wagner JR, Galobart À. 2018. *Adynomosaurus arcanus*, a new lambeosaurine dinosaur from the Late Cretaceous Ibero-Armorican Island of the European Archipelago. *Cretaceous Research* 96.

Raath MA. 1990. Morphological variation in small theropods and its meaning in systematics: evidence from *Syntarsus rhodensis*. In: Carpenter K, Currie PJ, eds. *Dinosaurs Systematics: Approaches and Perspectives*. Cambridge University Press, 91–108.

Rage JC. 2013. Mesozoic and Cenozoic squamates of Europe. Palaeobiodiversity and Palaeoenvironments 93: 517–534.

Ramírez del Pozo J, Portero JM, Olivé A. 1975. *Fuentes*, 635 (24-25). Mapa Geológico de España 1:50.000 Segunda Serie.

Riera V, Oms O, Gaete R, Galobart À. 2009. The end-Cretaceous dinosaur succession in Europe: The Tremp Basin record (Spain). *Palaeogeography, Palaeoclimatology, Palaeoecology* 283: 160–171.

Romer AS. 1966. *Vertebrate Paleontology*. Chicago: University of Chicago Press.

Rosenbaum G, Lister GS, Duboz C. 2002. Relative motions of Africa, Iberia and Europe during Alpine orogeny. *Tectonophysics* 359: 117–129.

Royo-Torres R. 2009. *El saurópodo de Peñarroya de Tastavins*. Teruel: Instituo de Estudios Turolenses y Fundación Conjunto Paleontológico de Teruel-Dinópolis.

Russell DA, Zheng Z. 1993. A large mamenchisaurid from the Junggar Basin, Xinjiang, People's Republic of China. *Canadian Journal of Earth Sciences* 30: 2082–2095.

Salgado JL, Apesteguía S, Heredia S. 2005. A New Specimen of *Neuquensaurus australis*, a Late Cretaceous Saltasaurine titanosaur from North Patagonia. *Journal of Vertebrate Paleontology* 25: 623–634.

Salgado JL, Coria RA, Calvo JO. 1997. Evolution of the titanosaurid sauropods I: Phylogenetic analysis based on the postcranial evidence. *Ameghiniana* 34: 3–32.

Salgado JL, Gallina PA, Paulina Carabajal A. 2015. Redescription of *Bonatitan reigi* (Sauropoda: Titanosauria), from the Campanian–Maastrichtian of the Río Negro Province (Argentina). *Historical Biology* 27: 525–548.

Sallam HM, Gorscak E, O'Connor PM, El-Dawoudi IA, El-Sayed S, Saber S, Kora MA, Sertich JJW, Seiffert ER, Lamanna MC. 2018. New Egyptian sauropod reveals Late Cretaceous dinosaur dispersal between Europe and Africa. *Nature Ecology & Evolution* 2: 445–451.

Sanz JL, Buscalioni ÁD. 1987. New evidence of armoured dinosaurs in the Upper Cretaceous of Spain. In: Currie PJ, Koster EH, eds. 4th Symposium on Mesozoic Terrestrial Ecosystems. *Occasional Papers of the Tyrrel Museum of Paleontology* 3, 199–204.

Sanz JL, Buscalioni ÁD, Casanovas ML, Santafé JV. 1987. Dinosaurios del Cretácico Inferior de Galve (Teruel, España). *Estudios Geológicos* extr.: 45–64.

Sanz JL, Buscalioni ÁD, Pérez-Moreno BP, Moratalla JJ, Jiménez García S. 1992. Los dinosaurios de Castilla y León. *Vertebrados fósiles de Castilla y León.* Salamanca: Museo Provincial de Salamanca, 47–57.

Sanz JL, Powell JE, Le Loeuff J, Martínez RN, Pereda Suberbiola X. 1999. Sauropod remains from the Upper Cretaceous of Laño (north central Spain). Titanosaur phylogenetic relationships. *Estudios del Museo de Ciencias Naturales de Alava* 14: 235–255.

Scotese CR. 1991. Jurassic and cretaceous plate tectonic reconstructions. *Palaeogeography, Palaeoclimatology, Palaeoecology* 87: 493–501.

Sereno PC. 2007. Basal sauropodomorpha: Historical and recent phylogenetic hypotheses, with comments on *Ammosaurus major* (MARSH, 1889). *Special Papers in Palaeontology* 77: 261–289.

Sereno PC, Beck AL, Dutheil DB, Larsson HCE, Lyon GH, Moussa B, Sadleir RW, Sidor CA, Varricchio DJ, Wilson GP, Wilson JA. 1999. Cretaceous Sauropods from the Sahara and the Uneven Rate of Skeletal Evolution Among Dinosaurs. *Science* 286: 1342–1347.

Smith DK. 1998. A morphometric analysis of *Allosaurus*. *Journal of Vertebrate Paleontology* 18: 126–142.

Souquet P. 1988. Evolución del margen noribérico en los pirineos durante el Mesozoico. *Revista de la Sociedad Geológica de España* 1: 349–356.

Steel R. 1970. *Handbuch der Paläherpetology, Saurischia*. Jena: Gustav Fischer Verlag.

Tidwell V, Wilhite RD. 2005. Ontogenetic variation and isometric growth in the forelimb of the Early Cretaceous sauropod *Venenosaurus*. In: Carpenter K, Tidwell V, eds. *Thunder-Lizards: The Sauropodomorph Dinosaurs*. Indiana University Press, 187–196.

Torices A, Currie PJ, Canudo JI, Pereda Suberbiola X. 2015. Theropod dinosaurs from the Upper Cretaceous of the South Pyrenees Basin of Spain. *Acta Palaeontologica Polonica* 60: 611–626.

Tschopp E, Mateus O, Benson RBJ. 2015. A specimen-level phylogenetic analysis and taxonomic revision of Diplodocidae (Dinosauria, Sauropoda). *PeerJ* 3: e857.

Tyson R V., Funnell BM. 1987. European cretaceous shorelines, stage by stage. *Palaeogeography, Palaeoclimatology, Palaeoecology* 59: 69–91.

Ullmann PV., Bonnan MF, Lacovara KJ. 2017. Characterizing the Evolution of Wide-Gauge Features in Stylopodial Limb Elements of Titanosauriform Sauropods via Geometric Morphometrics. *The Anatomical Record* 300: 1618–1635.

Upchurch P. 1995. The evolutionary history of sauropod dinosaurs. *Philosophical Transactions of the Royal Society B: Biological Sciences* 349: 365–390.

Upchurch P. 1998. The phylogenetic relationships of sauropod dinosaurs. *Zoological Journal of the Linnean Society* 124: 43–103.

Upchurch P, Barrett PM, Dodson P. 2004. Sauropoda. In: Weishampel DB, Dodson P, Osmólska H, eds. *The Dinosauria*. Berkeley: University of California Press, 259–322.

Upchurch P, Hunn CA, Norman DB. 2002. An analysis of dinosaurian biogeography: evidence for the existence of vicariance and dispersal patterns caused by geological events. *Proceedings of the Royal Society B* 269: 613–621.

Upchurch P, Mannion PD, Taylor MP. 2015. The Anatomy and Phylogenetic Relationships of "*Pelorosaurus*" *becklesii* (Neosauropoda, Macronaria) from the Early Cretaceous of England. *PloS ONE* 10: e0125819.

Varricchio DJ, Horner JR. 1993. Hadrosaurid and lambeosaurid bone beds from the Upper Cretaceous Two Medicine Formation of Montana: taphonomic and biologic implications. Canadian *Journal of Earth Sciences* 30: 997–1006.

Vera JA. 2004. *Geología de España*. Salamanca, Spain: Sociedad Geológica de España-Instituto Geológico y Minero de España.

Vidal D, Sanz JL, Mocho P, Páramo A, Escaso F, Marcos-Fernández F, Ortega F. 2017. The titanosaur tails from Lo Hueco (Cuenca, Spain): Four different ways to shake? In: Farke AA, Mackenzie SA, Miller Camp J, eds. *77th Annual Meeting of the Society of Vertebrate Paleontology*. Calgary, 208.

Vila B, Galobart À, Canudo JI, Le Loeuff J, Dinarès-Turell J, Riera V, Oms O, Tortosa T, Gaete R. 2012. The diversity of sauropod dinosaurs and their first taxonomic succession from the latest Cretaceous of southwestern Europe: Clues to demise and extinction. *Palaeogeography, Palaeoclimatology, Palaeoecology* 350–352: 19–38.

Vila B, Sellés AG, Brusatte SL. 2016. Diversity and faunal changes in the latest Cretaceous dinosaur communities of southwestern Europe. *Cretaceous Research* 57: 552–564.

Vilas L, Mas R, García A, Alonso A, Meléndez N, Rincón R. 1982. Ibérica Suroccidental. In: García A, ed. *El Cretácico de España*. Universidad Complutense de Madrid, 457–508.

Villatte J, Taquet P, Bilotte M. 1986. Noveaux restes de Dinosauriens dans le Crétacé terminal de l'anticlinal de Dreuilhe. Etat des connaissances dans le domaine sous-pyrénéen. Les Dinosaures de la Chine à la France. Toulouse: Muséum d'Histoire Naturelle de Toulouse, 89–111.

Weishampel DB, Chapman RE. 1990. Morphometric study of *Plateosaurus* from Trossingen (Barden - Württembeerg, Federal Republic of Germany). In: Carpenter K, Currie PJ, eds. *Dinosaur Systematics: Approaches and Perspectives*. Cambridge University Press, 43–52.

Weishampel DB, Csiki Z, Benton MJ, Grigorescu D, Codrea VA, Csiki Z, Benton MJ, Grigorescu D, Codrea VA. 2010. Palaeobiogeographic relationships of the Haţeg biota — Between isolation and innovation. *Palaeogeography, Palaeoclimatology, Palaeoecology* 293: 419–437.

Weishampel DB, Horner JR. 1994. Life history syndromes, heterochrony and the evolution of Dinosauria. In: Carpenter, K., Hirsch, K.F., Horner, J.R. (eds.) *Dinosaur Eggs and Babies*. 229–243.

Weishampel DB, Jianu CM. 2011. *Transylvanian dinosaurs*. Baltimore: John Hopkins University Press.

Wellhnöfer P. 1993. Prosauropod dinosaurs from the Feuerletten (Middle Norian) of Ellingen near Weissenbur in Bavaria. *Revue de Paléobiologie*, Volume Spéciale 7: 263–271.

Wilhite RD. 1999. Ontogenetic variation in the appendicular skeleton of the genus *Camarasaurus*. Unpublished thesis, Brigham Young University.

Wilhite RD. 2003. Biomechanical Reconstruction of the Appendicular Skeleton in Three North American Jurassic Sauropods. Unpublished thesis, Louisiana State University.

Wilhite RD. 2005. Variation in the Appendicular Skeleton of North American Sauropod Dinosaurs: Taxonomic Implications. In: Tidwell V, Carpenter K, eds. *Thunder-Lizards: The Sauropodomorph Dinosaurs*. Indiana University Press, 268–301.

Wilson JA. 2002. Sauropod dinosaur phylogeny: critique and cladistic analysis. *Zoological Journal of the Linnean Society* 136: 215–275.

Wilson JA. 2011. Anatomical Terminology for the Sacrum of Sauropod Dinosaurs. *Contributions from the Museum of Paleontology*, University of Michigan 32: 59–69.

Wilson JA, Carrano MT. 1999. Titanosaurs and the Origin of 'wide-gauge' trackways: A Biomechanical and Systematic Perspective on Sauropod Locomotion. *Paleobiology* 25: 252–267.

Wilson JA, Sereno PC. 1998. Early Evolution and High-level Phylogeny of Sauropod Dinosaurs. *Journal of Vertebrate Paleontology* 18: 1–68.

Wilson JA, Upchurch P. 2003. A revision of Titanosaurus Lydekker (Dinosauria - Sauropoda), the first dinosaur genus with a 'Gondwanan' distribution. *Journal of Systematic Palaeontology* 1: 125–160.

Xabier Pereda. 1999. Las Faunas Finicretácicas de Dinosaurios Ibéricos. *Zubía* 17: 259–279.

Ziegler PA. 1987. Late Cretaceous and Cenozoic intra-plate compressional deformations in the Alpine foreland-a geodynamic model. *Tectonophysics* 137: 389–420.

CHAPTER II:

Research hypotheses and objectives of the current PhD thesis project

II.1 RESEARCH HYPOTHESES

Main Research Hypothesis.

H0 – The variability observed in the sample of sauropod appendicular remains from Lo Hueco fossil site (Late Cretaceous. Fuentes, Cuenca) can be explained by the presence of at least two forms, so far exclusive from the fossil site. One gracile species closer to *Jainosaurus septentrionalis,* and one robust species closer to *Ampelosaurus atacis*.

Research Hypothesis no.2.

H0 – There is an observable variation in size among the appendicular remains forming the sample of Lo Hueco fossil site. Several elements overlap in morphology and size with small taxa from the Ibero-Armorican domain such as *Lirainosaurus astibiae*, and so they may be referred to a closely related dwarf titanosaur.

Research Hypothesis no.3.

H0 – There are two main sauropod morphs from Lo Hueco, all the more robust appendicular elements of each bone type are referable to one of these morphswhile all the slender specimens of each bone type correspond to the more gracile titanosaur taxon.

Research Hypothesis no.4.

H0 –There is no significant relationship between ontogenetical stage, and features observable in the specimens, as long bone growth is isometric. The possible juvenile individuals are similar to the adult individuals of the same morph.

Research Hypothesis no.5.

H0 - Size is a bad predictor for the possible ontogenetical stage. Previous studies based on histological sampling, cortical area of long bone and estimated mass of sauropod dinosaurs observe high disparity in sizes (up to 1 tn of body mass) among adult forms of similar age.

Research Hypothesis no.6.

H0 – The Sauropoda body plan is conservative and there is a loss of plasticity along the evolution of its skeleton. Discrete features usually employed in cladistics data matrices present little to no intraspecific variation. Observable shape differences do not alter severely character codifications among the sample of the same taxa.

Research Hypothesis no.7.

H0 - Among the taxa sampled in Lo Hueco, most of the morphologic changes occur in early developmental stages.

Research Hypothesis no.8.

H0 - Based on other known sauropod megafaunas, like the one of the Morrison Formation, high sauropod diversity can be explained by subtle resource partitioning. The robust morphotype and gracile morphotype of Lo Hueco can be attributed to different morphofunctional specialisation within a niche-partitioning scenario.

Research Hypothesis no.9.

H0 - There are no significant differences between the appendicular skeleton growth models of both titanosaur morphs at Lo Hueco.

II.2 RESEARCH OBJECTIVES

Objective no.1.

Describe the variability among appendicular non-autopodial bones of the titanosaur sauropods sampled from Lo Hueco (Cuenca, Spain)

Objective no.2.

Evaluate the most probable number of groups of titanosaur appendicular elements in the sample of Lo Hueco.

Objective no.3.

Assess the association of isolated appendicular element and articulated individuals according to morphospace exploration. Characterize the variation of the Lo Hueco morphs.

Objective no.4.

Digitize a representative sample of different types of appendicular elements in order to use the geometric morphometric tool-kit. We will conduct several tests in order to confirm the probable taxonomical assessment.

Objective no.5.

Identify the appendicular elements pertaining to *Lohuecotitan pandafilandi*. Assess the taxonomical status of unassigned morphs among the sample of Lo Hueco testing the presence of other iberoarmorican titanosaur taxa (*Ampelosaurus atacis*, *Lirainosaurus astibiae*,*Atsinganosaurus velauciensis*).

Objective no.6.

Assess the taxonomical status of the smaller individuals among the sample of Lo Hueco testing the presence of dwarf titanosaur.

Objective no.7.

Elaborate a classification method to assess taxonomical status of isolated appendicular remains from Lo Hueco.

Objective no.8.

Test the correlation between morphofunctional or ecomorphological traits and shape variables. We will test the hypothesis of resource niche-partitioning in the sauropod megafauna. Compare the distribution of these morphological traits in the fauna of Lo Hueco with other sauropod taxa.

Objective no.9.

Identify the ontogenetical sequences present in the sample of titanosaurs appendicular elements from Lo Hueco.

Objective no.10.

Explore the variance referable to ontogenetical changes.

Objective no.11.

Identify morphological characters to establish the ontogenetical stage within ontogenetical sequences identified in the sample of titanosaurs appendicular elements of Lo Hueco. Test variability among the ontogenetical changes and assess which of the morphological characters mark developmental stages for the taxa of Lo Hueco.

Objective no.12.

Build data matrices based on main discrete characters used in cladistics analyses of Titanosauria. Explore the intraspecific variation of the characters in data matrices Identify the variability in character scoring. Identify the intraspecific disparity referable to ontogenetical changes. Test the staging acquisition of morphological features.

Objective no.13.

Calculate morphological disparity between the two main titanosaur morphs from Lo Hueco at different ontogenetial stages. Test the similarity of both morphs from Lo Hueco at early ontogenetical stages.

Objective no.14.

Calculate appendicular size disparity within each taxa of titanosaur from Lo Hueco at different ontogenetical stages. Test correlation between the size and the ontogenetical stages. Assess size variability at different ontogenetical stages for the different morphs of Lo Hueco.

Objective no.15.

Assess the differences between the appendicular skeleton growth models for the titanosaur morphs from Lo Hueco.

CHAPTER III:

Materials and Methods

III.1 MATERIALS

III.1. 1. LO HUECO TITANOSAUR SAMPLE

In this PhD project, appendicular elements of the material associated to several individual in partial articulation from Lo Hueco fossil site are analyzed. In addition, a random sample of the isolated appendicular elements of titanosaur sauropods from Lo Hueco fossil site were also included in this study..

Specimen	Type	Side	Assoc.	Strat.	Digitized	Accuracy (mm)
HUE-1316	Femur	Right	iso	GI	Kinect	3.000
HUE-1357	Femur	Left	iso	GI	Kinect	3.000
HUE-1440	Femur	Left	iso	GI	Kinect	3.000
HUE-1508	Femur	Left	iso	GI	Kinect	3.000
HUE-1521	Femur	Left	iso	GI	Kinect	3.000
HUE-1590	Femur	Right	iso	GI	Kinect	3.000
HUE-2903	Femur	Right	iso	GI	Kinect	3.000
HUE-3237	Femur	Right	iso	GI	Kinect	3.000
HUE-3583	Femur	Left	iso	GII	Kinect	3.000
HUE-1060	Humerus	Right	iso	GI	Kinect	3.000
HUE-1143	Humerus	Left	iso	GI	Kinect	3.000
HUE-1356	Humerus	Left	iso	GI	Kinect	3.000
HUE-1434	Humerus	Left	iso	GI	Kinect	3.000
HUE-1499	Humerus	Right	iso	GI	Kinect	3.000
HUE-3196	Humerus	Left	iso	GI	Kinect	3.000
HUE-3228	Humerus	Right	iso	GI	Kinect	3.000
HUE-3829	Humerus	Left	iso	GI	Kinect	3.000
HUE-4208	Humerus	Right	iso	GI	Kinect	3.000
HUE-4343	Humerus	Right	iso	GI	Kinect	3.000
HUE-4522	Humerus	Right	iso	GII	Kinect	3.000
HUE-1149	Tibia	Left	iso	GI	Kinect	3.000

Table.III.1. Lo Hueco specimen digitized in 3D for the current thesis project. Sampled via Kinect™ v.1. RGB-D camera for Windows®. *Assoc.* - associated material; *Strat.* - stratigraphic level. *iso* - isolated specimen.

Specimen	Type	Side	Assoc.	Strat.	Digitized	Accuracy (mm)
HUE-594	Femur	Right	iso	GI	Photoscan	0.508
HUE-902	Femur	Right	iso	GI	Photoscan	0.333
HUE-930	Femur	Right	EC11	GI	Photoscan	0.217
HUE-1183	Femur	Left	EC13	GI	Photoscan	0.045
HUE-1187	Femur	Left	iso	GI	Photoscan	8.882
HUE-1319	Femur	Right	iso	GI	Photoscan	0.662
HUE-1366	Femur	Right	EC05	GI	Photoscan	0.699
HUE-2338	Femur	Left	iso	GI	Photoscan	0.107
HUE-2420	Femur	Right	EC06	GI	Photoscan	0.835
HUE-2636	Femur	Right	iso	GI	Photoscan	0.188
HUE-3108	Femur	Right	EC01	GI	Photoscan	0.596
HUE-8801	Femur	Left	iso	NA	Photoscan	0.165
HUE-10007	Femur	Right	iso	NA	Photoscan	0.003
HUE-1068	Fibula	Right	iso	GI	Photoscan	0.160
HUE-1082	Fibula	Right	iso	GI	Photoscan	0.060
HUE-1146	Fibula	Left	iso	GI	Photoscan	8.557
HUE-1175	Fibula	Right	iso	GI	Photoscan	4.703
HUE-1335	Fibula	Left	iso	GI	Photoscan	0.178
HUE-1377	Fibula	Right	iso	GI	Photoscan	2.900
HUE-1476	Fibula	Right	iso	GI	Photoscan	0.057
HUE-1507	Fibula	Left	iso	GI	Photoscan	9.356
HUE-1513	Fibula	Left	iso	GI	Photoscan	0.385
HUE-1520	Fibula	Right	iso	GI	Photoscan	2.884
HUE-1570	Fibula	Right	iso	GI	Photoscan	0.049
HUE-1612b	Fibula	Left	HUE-1612	GI	Photoscan	0.014
HUE-2426	Fibula	Right	EC06	GI	Photoscan	0.035
HUE-2669	Fibula	Right	iso	GI	Photoscan	0.156
HUE-2804	Fibula	Right	iso	GI	Photoscan	0.081
HUE-2806	Fibula	Left	iso	GI	Photoscan	0.135
HUE-2904	Fibula	Left	iso	GI	Photoscan	5.176
HUE-2977	Fibula	Right	iso	GI	Photoscan	0.335
HUE-3000	Fibula	Left	iso	GI	Photoscan	0.715
HUE-3075	Fibula	Left	EC01	GI	Photoscan	0.014
HUE-3087	Fibula	Right	EC01	GI	Photoscan	0.474
HUE-4359	Fibula	Right	iso	GI	Photoscan	0.438
HUE-4416	Fibula	Right	iso	GII	Photoscan	4.822
HUE-5232	Fibula	Left	iso	GII	Photoscan	0.049
HUE-7802	Fibula	Right	iso	GI	Photoscan	0.280

Table.III.2. Lo Hueco specimen digitized in 3D for the current thesis project. Sampled via stereophotogrammetry. *Assoc.* - associated material; *Strat.* - stratigraphic level; *iso* - isolated.

Specimen	Type	Side	Assoc.	Strat.	Digitized	Accuracy (mm)
HUE-817	Humerus	Left	EC11	GI	Photoscan	0.339
HUE-940	Humerus	Left	iso	GI	Photoscan	0.436
HUE-1463	Humerus	Right	iso	GI	Photoscan	3.928
HUE-1502	Humerus	Right	iso	GI	Photoscan	2.775
HUE-1549	Humerus	Right	iso	GI	Photoscan	0.010
HUE-1549	Humerus	Left	iso	GI	Photoscan	0.001
HUE-1647	Humerus	Left	EC13	GI	Photoscan	0.104
HUE-2356	Humerus	Right	EC03	GI	Photoscan	0.158
HUE-2727	Humerus	Right	iso	GI	Photoscan	1.002
HUE-2772	Humerus	Left	iso	GI	Photoscan	0.372
HUE-2801	Humerus	Left	EC03	GI	Photoscan	0.035
HUE-3057	Humerus	Left	iso	GI	Photoscan	0.474
HUE-3662	Humerus	Left	iso	GII	Photoscan	0.041
HUE-4828	Humerus	Left	iso	NA	Photoscan	0.010
HUE-XXYY	Humerus	Left	EC02	GI	Photoscan	4.833
HUE-1140	Radius	Left	HUE-1139	GI	Photoscan	0.178
HUE-1166	Radius	Left	iso	GI	Photoscan	0.079
HUE-1340	Radius	Right	iso	GI	Photoscan	1.010
HUE-2711	Radius	Left	EC03	GI	Photoscan	0.012
HUE-1063	Tibia	Right	iso	GI	Photoscan	0.279
HUE-1165	Tibia	Left	iso	GI	Photoscan	0.311
HUE-1317	Tibia	Right	iso	GI	Photoscan	0.242
HUE-1410	Tibia	Right	iso	GI	Photoscan	0.305
HUE-1500	Tibia	Right	iso	GI	Photoscan	2.818
HUE-1573	Tibia	Left	iso	GI	Photoscan	0.018
HUE-1612	Tibia	Left	HUE-1612	GI	Photoscan	0.082
HUE-2117	Tibia	Right	iso	GI	Photoscan	0.133
HUE-2355	Tibia	Left	iso	GI	Photoscan	0.276
HUE-2425	Tibia	Right	EC6	GI	Photoscan	0.035
HUE-2799	Tibia	Right	iso	GI	Photoscan	0.171
HUE-3082	Tibia	Right	EC1	GI	Photoscan	0.880
HUE-4055	Tibia	Right	iso	GI	Photoscan	0.415
HUE-4344	Tibia	Left	iso	GI	Photoscan	0.057
HUE-4404	Tibia	Left	iso	GII	Photoscan	0.246
HUE-4632	Tibia	Right	iso	GII	Photoscan	0.146
HUE-964	Ulna	Left	EC05	GI	Photoscan	0.048
HUE-1103	Ulna	Right	iso	GI	Photoscan	0.107
HUE-1137	Ulna	Left	iso	GI	Photoscan	0.477
HUE-1139	Ulna	Left	HUE-1140	GI	Photoscan	0.107

Table.III.2.-continues

Specimen	Type	Side	Assoc.	Strat.	Digitized	Accuracy (mm)
HUE-1158	Ulna	Left	iso	GI	Photoscan	0.085
HUE-1338	Ulna	Right	iso	GI	Photoscan	0.488
HUE-2865	Ulna	Right	iso	GI	Photoscan	0.444
HUE-3044	Ulna	Left	EC01	GI	Photoscan	0.023
HUE-3462	Ulna	Left	iso	GI	Photoscan	0.074
HUE-4357	Ulna	Right	iso	GI	Photoscan	0.220

Table.III.2.-continues

III.1.2. MATERIAL ACCESSED AND INSTITUTIONAL ABBREVIATIONS

Taxa cited and accessed in this PhD project:

Aeolosaurus spp. (Salgado & Coria, 1993; Salgado, Coria, & Calvo, 1997a; García & Salgado, 2013), *Agustinia ligabuei* – Bonaparte 1999, *Ampelosaurus atacis* – Le Loeuff 1995; *Antarctosaurus giganteus* - Huene 1927, *Antarctosaurus wichmannianus* – Huene 1927, *Argentinosaurus huinculensis* – Bonaparte & Coria 1993, *Argyrosaurus superbus* – Lydekker 1893, *Bonatitan reigi* – Martinelli & Forasiepi 2004, *Bonitasaura salgadoi* – Apesteguía 2004, *Choconsaurus baileywillisi* – Simón, Salgado & Calvo, 2018, *Chubutisaurus insignis* – del Corro 1978, *Duriatitan humerocristatus* – Barret, Benson & Upchurch 2010, *Elaltitan lilloi* – Mannion & Otero 2012, *Haestasaurus becklesi* – Mantell 1852, *Jainosaurus cf. septentrionalis* (Wilson, Barrett, & Carrano, 2011), *Ligabuesaurus leanzai* – Bonaparte, González Riga & Apesteguía 2006, *Lirainosaurus astibiae* – Sanz, Powell, Le Loeuff, Martínez & Pereda-Suberbiola 1999, cf. *Lirainosaurus astibiae* (Company, Suberbiola, & Ruiz-Omeñaca, 2009; Díez Díaz, Pereda Suberbiola, & Company, 2015); *Malarguesaurus florenciae* – González Riga, Previtera & Pirrone 2009, *Magyarosaurus dacus* – Nopsca 1915, *Magyarosaurus "hungaricus"* – Nopsca 1915, *Magyarosaurus "transsylvanicus"* – Nopsca 1915, *Magyarosaurus* spp. (see Nopsca, 1915), *Mendozasaurus neguyelap* – González Riga 2003, *Muyelensaurus pecheni* – Calvo, González Riga, Porfiri 2007, *Narambuenatitan palomoi* – Filippi, García & Garrido 2011, *Neuquensaurus australis* – Lydekker 1893, *"Neuquensaurus robustus"* – Lydekker 1983, cf. *Neuquensaurus* - (Powell, 2003; Otero, 2010a,b), *Notocolossus gonzalezparejasi* – González Riga, Lamanna, Ortiz David, Calvo & Coria 2016, *Overosaurus paradasorum* – Coria, Filippi, Chiappe, García & Arcucci 2013, *Petrobrasaurus puestohern&ezi* – Filippi, Canudo, Salgado, Garrido, García, Cerda & Otero 2011, *Pitekunsaurus macayai* – Filippi & Garrido 2008, *Rinconsaurus caudamirus* – Calvo & González Riga 2003, *Rocasaurus muniozi* – Salgado & Azpilicueta 2000, *Saltasaurus loricatus* – Bonaparte & Powell 1980. AMNH – American Museum of Natural History, New York, USA; BYU – Brigham Young University, Museum of Paleontology, Provo, USA; CM – Carnegie Museum of Natural History, Pittsburg, USA; DMNS – Denver Museum of Nature & Sciences, Denver, USA; DNM – Dinosaur National Monument, Jensen, USA; FMNH – Field Museum of Natural History, Chicago, USA; GMNH – Gunma Museum of Natural History, Gunma, Japan; IANIGLA – Instituto Argentino de Nivología, Glaciología y Ciencias Ambientales, Mendoza, Argentina; NHMUK – Natural History Museum, London, United Kingdom; MACN – Museo Argentino de Ciencias Naturales "Bernardino Rivadavia", Buenos Aires, Argentina; MAU/MRS – Museo Argentino Urquina, Rincón de los Sauces, Neuquén, Argentina; MB.R – Museum für Naturkunde, Berlin, Germany; MCF

– Museo Carmen Funes, Plaza Huincul, Neuquén, Argentina; MCNA – Museo de las Ciencias Naturales de Álava/Arabako Natur Zientzien Museoa, Vitoria-Gasteitz, Spain; MLP – Museo de La Plata, La Plata, Buenos Aires, Argentina; MNHN - Muséum national d'Histoire Naturelle, Paris, France; MMCh-PV – Museo Municipal Ernesto Bachmann, Villa el Chocón, Neuquén, Argentina; MSC – Museo de Cinco Saltos, Río Negro, Argentina; MGUV – Museo de Geolgía de la Universidad de Valencia, Burjasot, Spain; MPCA – Museo Provincial Carlos Ameghino, Cipoletti, Río Negro, Argentina; MUPA- Museo de Paleontología de Castilla-La Mancha, Cuenca, Spain; OMNH – Sam Noble Ocklahoma Museum of Natural History, Norman, USA; SMa – Sauriermuseum Aathal, Aathal, Switzerl&; PVL – Instituto Migue Lillo, Tucumán, Argentina; UW – University of Wyoming Geological Museum, Laramie, USA; YPM – Yale Peabody Museum, Yale, USA.

III.1.3. ANATOMICAL NOMENCLATURE AND ABBREVIATIONS

Humerus:

aep – anterior entepycondyle/entepycondylar process; af – anconeal fossa; alp – antero-lateral process; amp – antero-medial process; dpc – deltopectoral crest; dpcar – deltopectoral accessory ridge; hh – humeral head; pat – posterior accessory trochanter rac – radial condyle; ulc – ulnar condyle.

Ulna:

adp – anterior distal process; alp – antero-lateral process; amdf – anterior middle distal fossa (articulation with the radius); amp – antero-medial process; olc – olecranon; op – olecranon process; rds – radial distal scar; raf – radial fossa (proximal radial articulation).

Radius

antf – anterior fossa; mp – medial process; pldc – posterolateral distal condyle; pmdc – posteromedial distal condyle; rmi – ridge for muscle insertion (mm. biceps + brachialis).

Femur:

4th – fourth trochanter; at – accessory trochanter; epi – lateral epicondyle; gt – greater trochanter; if – intercondylar fossa; lb – lateral bulge; lic – linea intermuscularis cranialis; fc – fibular condyle; fh – femoral head; tc – tibial condyle; ts – trochanteric shelf.

Tibia:

aap – anterior ascending process of distal condyles; cc – cnemial crest; pc – posterior condyle.

Fibula:

ap – anterior process; alp – anterolateral crest (proximal); lt – lateral trochanter; ts – tibial articulation scar.

Common abbreviations:

at – accessory trochanter; ri – ridge; s – sulcus; tr - trochanter

III.2 METHODS

III.2.1. 3D DIGITIZING TECHNIQUES

The sampled specimens were analyzed through 3D geometric morphometrics tool kit. In order to carry out this set of techniques, a 3D mesh representation of the sampled specimens is appropriate following a custom made 3D digitizing workflow (Fig.III.3). Nowadays an important variety of digitizing methods are available. Based on shared features, these methods can be differentiated into two major groups: Transmissive digitizing methods and Reflective digitize methods (Zollikofer & Ponce de León, 2006; Sutton, Rahman, & Garwood, 2014; Lachat *et al.*, 2015; Lautenschlager, 2016; Davies *et al.*, 2017). Transmissive digitizing methods capture information of the entire specimens, both the external shape as internal structures (Sutton, 2008; Sutton *et al.*, 2014). This set of techniques are generally related with Computed Tomography scanning (CT-scan) and, nowadays, are considered as a widespread methodology for study some internal structures on fossil material and in dinosaur remains in particular (see various examples in Rogers, 1998; Balanoff, Bever, & Ikejiri, 2010; Porter, Sedlmayr, & Witmer, 2016). In addition to CT-scanning techniques a plethora of other radiation methods varying the definition, resolution or sample sizes requirements, etc. are now applied (Schwarz *et al.*, 2005; Curtin *et al.*, 2012; Staedler, Masson, & Schönenberger, 2013; Gignac *et al.*, 2016; Lautenschlager, 2016; Davies *et al.*, 2017). In all these cases, a high energy radiation is emitted over the sampled specimen. The bombarded particles reflect and refract in several layers of the specimen and so they are measured (Sutton *et al.*, 2014). From the raw measurements of these particles, it is possible to reconstruct the density of the material that were bombarded with the high energy radiation from the slice. Then the slice stack is computed to produce a 3D digital model of the specimen with high accuracy given a known measurement error based on the specification of the scanner.

The other main group of digitizing techniques are those methods that rely on reflective 3D measurement; therefore, it can be only obtained data for the surface. There is also a difference between optical methods like use of computer-aided reconstruction from photographic material, structured light imaging, manual 3D space coordinate registration, RGB measurements or non-optical laser-beam scatter registration or 3D coordinate detection. Those are several techniques usually employed in 3D digitization of fossil and heritage material (Pieraccini, Guidi, & Atzeni, 2001; Sutton *et al.*, 2001, 2014; Pavlidis *et al.*, 2007; Cunningham *et al.*, 2014; Lautenschlager, 2016; Davies *et al.*, 2017). All of them coincides in the way the information is captured from the digitized specimen. Usually the input is a set of measurements over the sampled surface, either a photography (color pixels that can be compared or measured over), a direct point-cloud detection over the surface, line pattern reticules, a laser light-distance or a RGB value variation measurements over the scene. In these cases, an image or measurement of a radiation that does not penetrate the sampled specimen contrary to CT-scan techniques is obtained (Sutton *et al.*, 2014; Davies *et al.*, 2017). Therefore, surface digitizing techniques cannot be employed to study internal anatomy, but in several cases their surface resolution and accuracy can be comparable to CT-scanning (Challis & Kerwin, 1992; Baltsavias, 1999; Hennessy *et al.*, 2005; Cunningham *et al.*, 2014; Mallison & Wings, 2014; Fahlke & Autenrieth, 2016).

Here the external surface morphology from a sample of different appendicular specimens of titanosaur sauropods is studied. For these studies, photogrammetry and structured light set of techniques were carried out. These techniques have a moderate cost in comparison with

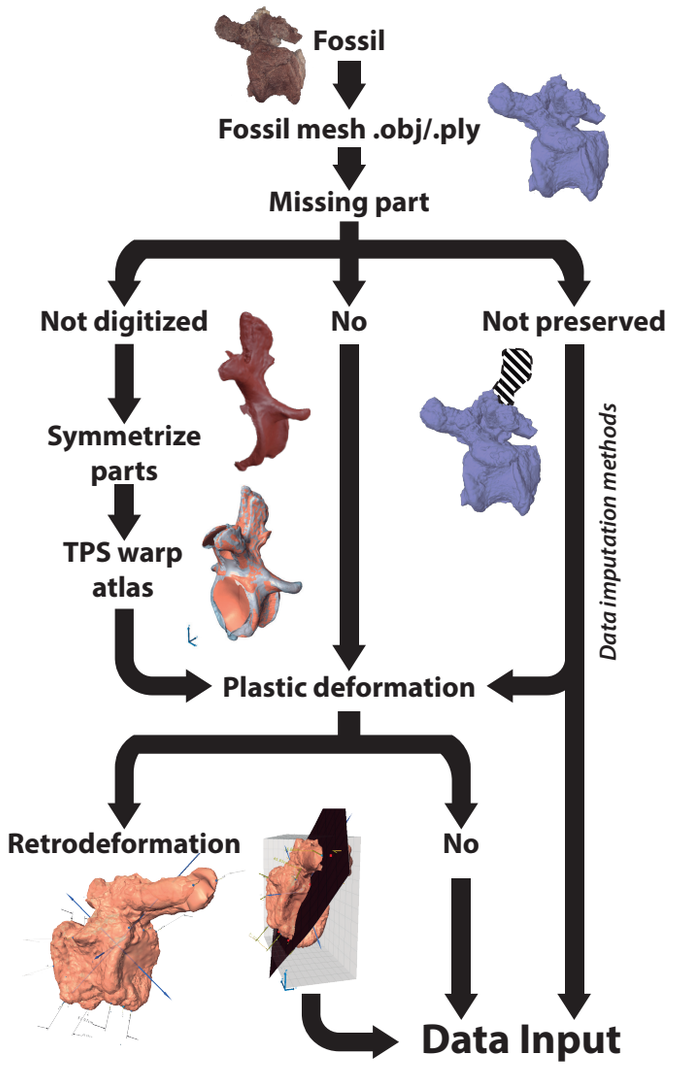

Fig.III.3. The 3D digitizing workflow proposed for the current PhD thesis project. Generalised protocol for all anatomical elements, note lack of symmetry in titanosaur long bones.

CT-scanning methods or LIDAR and other laser-beam surface registration techniques (Mallison, 2010, 2011; Falkingham, 2012, 2013; Davies *et al.*, 2017). They are also better suited for digitizing of large specimens like sauropod appendicular bones (Wilhite, 2003a; Mallison, 2011; Lautenschlager, 2017). Large elements are often difficult to digitize through CT-scan methods as usual medical or micro-CT-scan size requirements are far from the sauropod limb bone scales (see some scale ranges in Cunningham *et al.*, 2014). Some of the sampled specimens and the usual sauropod size are only in the range of industrial CT-scans. One of the advantages of these techniques is that are easy to apply and carried out when visiting paleontological collections, which allow to increase the sample easily. Some LIDAR (see Baltsavias, 1999; Bates *et al.*, 2009) or Microscribe™ digitizers (Marcus, Hingst-Zaher, & Zaher, 2000; Wilhite, 2003b) are porTable too, but the costs are far from the requirements for photogrammetry or RGB and structured light methods (Falkingham, 2012,

2013; Mallison & Wings, 2014). With the availability of a digital camera and a RGB-D camera, it is possible to compute a virtual 3D volumetric representation of the specimens of the study with the following workflow (Fig.III.2). For this work all digitizing and processing was made in an ASUS ROG g750 with Intel® Core™ i7-4700HQ CPU 2.40 GHz and a graphic card NVIDIA® GeForce GTX 870M with 3 Gb dedicated memory and 16 Gb DDR3 RAM allocated.

III.2.1.1. STRUCTURED LIGHT

Structure light method uses an active optical input to calculate the depth of field and reconstruct a 3D point cloud (Rocchini *et al.*, 2001; Zollikofer & Ponce de León, 2006; McPherron, Gernat, & Hublin, 2009; Sutton *et al.*, 2014; Pöhlmann *et al.*, 2016). Traditional methods depend on a projection of known image patterns that are captured by a sensor and then computer-aided reconstruction calculates the point cloud based on comparison from several of the warped patterns and the triangulation among them (Pieraccini *et al.*, 2001; Rocchini *et al.*, 2001; Pavlidis *et al.*, 2007; McPherron *et al.*, 2009; Sutton *et al.*, 2014). Other methods use the shape from shading, capturing depth information from shades over a 3D real object (Pavlidis *et al.*, 2007). But present-day methods can perform a real-time capture of depth through a combination of structured light traditional methods, video tracking and multi-layered shape from shading. In 2010 Microsoft® launched Microsfot Kinect™ v.1. followed by ASUS® Xtion Pro RGB-D motion tracking cameras (Falkingham, 2013) opened a new field of user-aided motion capture devices (Guidi, Gonizzi, & Micoli, 2016). They were intended mainly as video game and application motion tracking devices that can recognized the movement through RGB-D technology (see Fig.III.4). This technology stands for Red-Blue-Green-Depth, which is a mixture of structured light methods as commented before. This technology can recognize volume through filtering shadow and patterns of RGB color shading and grading in the camera infrared sensor (Guidi *et al.*, 2016).

This method can provide an easy and affordable digitize rig with high accuracy (Lachat *et al.*, 2015; Guidi *et al.*, 2016; Pöhlmann *et al.*, 2016; Marchal & Lygren, 2017). However, some problems must be taken into account with this method: the low resolution captured, especially

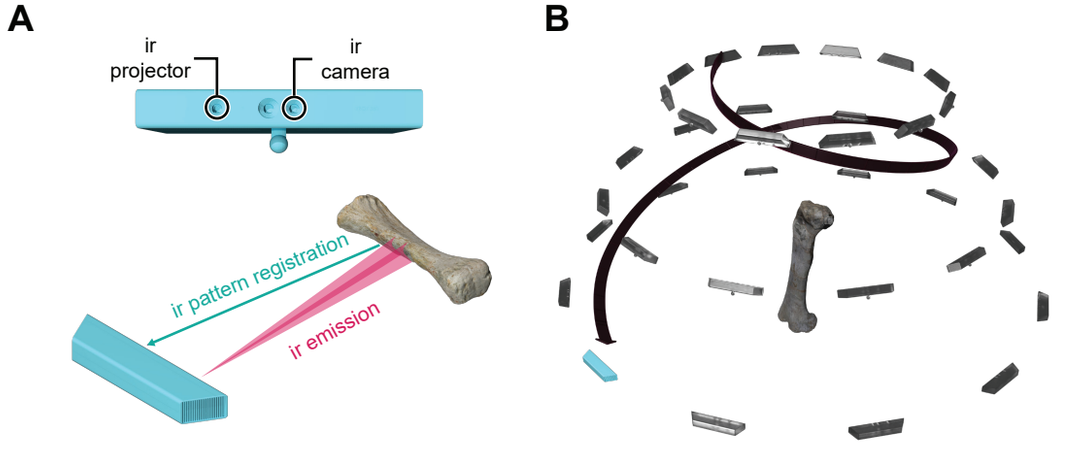

Fig.III.4. Structured light scanning method. (A) Principles of a infrared camera scan. (B) Scan path of the IR-camera for digitizing the complete specimen.

of the surface texture thanks to a 640x480 VGA camera in-built (Falkingham, 2013; White *et al.*, 2013; Guidi *et al.*, 2016; Das *et al.*, 2017) and the noise in this first generation sensor device (Falkingham, 2013; Das *et al.*, 2017). Because sauropod long bone lack complex structures (Upchurch, Barrett, & Dodson, 2004) here we used this method on several appendicular bones.

A Kinect™ v.1. RGB-D camera for Windows® as main device with Windows Kinect SDK™ v1.8. was used for 3D digitizing (Fig.III.4 and 5). The used software was ReconstructMe™ non-commercial console version (see Falkingham, 2013). To obtain the minimum structure width than can be captured with reliability the device was calibrated with several small objects (see Das *et al.*, 2017). Titanosaur long bones do not have any structure that fall under the 5mm width threshold of the capturing device. However, this method was intended for capturing sauropod girdle elements (which are not included in this PhD thesis project) or fragmentary structures over Lo Hueco titanosaur long bones.

Several long bones from Lo Hueco do not preserve proximal and distal ends, so Kinect™ could have difficulties to digitize. In order to assess the reliability of the method on those problematic areas these a priori analyses were carried out. Also, the models were calibrated based on a 2D scale and a 3D scale with a known measurement object (a rubric cube with preset measurements) that were digitized in each model.

The captured point clouds were aligned (anterior-posterior face digitize session of each element, see Fig.III.5) and reconstruction processed in MeshLab 64bit v2016.12 (Cignoni *et al.*, 2008). Mesh reconstruction was constructed following Falkignham (2013) and Lachat *et al.* (2015) but see similar processes over available 3D point clouds (Falkingham, 2013; Das *et al.*, 2017). This method produces 3D mesh objects in ".ply" format that were correctly scaled and post-processed. The complete sample taken with this method can be seen in Table III.1.

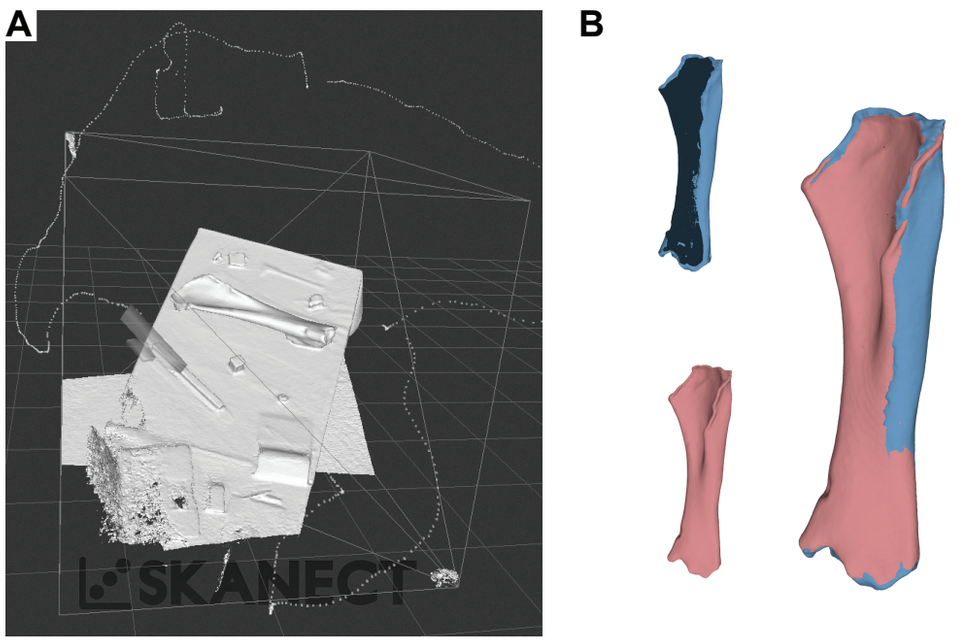

Fig.III.5. Structured light scanning interface. (A) Scan pattern of the anterior face of the humerus HUE-1356. (B) Aligment of the anterior and posterior face scans.

III.2.1.2. PHOTOGRAMMETRY

For 3D volume reconstruction of the sampled photogrammetry methods were performed. Photogrammetry or stereophotogrammetry is an active optical digitize method (Rocchini *et al.*, 2001; Lachat *et al.*, 2015) based on the reconstruction of 3D point clouds through photographic image sequences (Baltsavias, 1999; Falkingham, 2012; Mallison & Wings, 2014; Davies *et al.*, 2017). Here Short-Range Stereophotogrammetry were used (Matthews, 2008; Mallison & Wings, 2014), with an inset of photographs from the sampled specimens and without laser-scanning input contrary to common procedures in aerial stereophotogrammetry.

Photogrammetry is based on data acquisition as photographic material of the desired 3D object or scene. The software search for comparable pixels in the data input fed into the pipeline and tries to triangulate the pixel position in 3D space (Mallison & Wings, 2014). With this initial sparse cloud of points in 3D space, it is possible to compute several processes to increase the 3D model detail or generate a 3D mesh object as a basic volume reconstruction of the digitized specimen (Mallison, 2011; Falkingham, 2012). Despite photogrammetry depends on the data input (i.e. number of photographs and image quality) the object 3D resolution and detail are much greater than in structured-light RGB-D Kinect™ method.

In order to control data input, a quality control over the photographs taken was set up. For this work it was followed the methodology proposed by Mallison & Wings (2014). For smaller specimens (~600 mm or less), and when it was possible, it was used a turntable with a softbox to control light input (Fig.III.6). For mounted skeletons or bones, material with difficult access (e.g. not completely prepared or stored in security supports) or with size exceeding the Table dimensions, overlapping photographs around the specimens were employed. Every photograph was taken at ~30 ° (Fig.III.6) in every direction. The specimens were digitized using both Canon EOS 1100D and Canon Eos 80D. The lenses used for this study were Canon 18-55 mm f3.5-5.6, Canon 50 mm f1.8 and Sigma 17-50 mm f2.8. Both cameras are crop-sensor type which name indicates that the frame is cropped approximately 1.6 lens width, the areas where most lens distortion occur especially at wider angles or extremes of ranged focal length lenses like Canon 18-55 mm f3.5-5.6.

Nowadays available software can deal with image distortion and standard patterns of correction. However, the probable distortion in our data input could be reduced. When it was possible a 35 mm as main focal length for photographs taken with the wide-range lenses was used. 35 mm is the focal length that minimize distortion in Canon 18-55 mm f3.5-5.6 and Sigma 17-50 mm f2.8 (see also Třebický *et al.*, 2016). Canon 50 mm f1.8 (and most of 50 mm lenses) have already near 0 points of distortion in the frame area. Distortion and color aberration were corrected with Adobe® Camera RAW™ with standards correction profiles designed for our set of lenses.

Point cloud calculation and mesh reconstruction was carried out in Agisoft® Photoscan™ v1.41 (Fig.III.7). Sparse cloud reconstruction to "high" and processed dense cloud for all the specimens prior mesh reconstruction was set. It was obtained two distinct meshes, one high poly and high resolution, 500k triangle-polygon meshes, and one at lower resolution about 150k poly mesh. The 150k poly mesh was used as our main working virtual sample for the landmark definitions and all the calculations of the current thesis project. They were exported for post-processing in ".ply" and ".obj" 3D object with the available ".mtl" text metadata associated and photorealistic texture in ".jpeg" format.

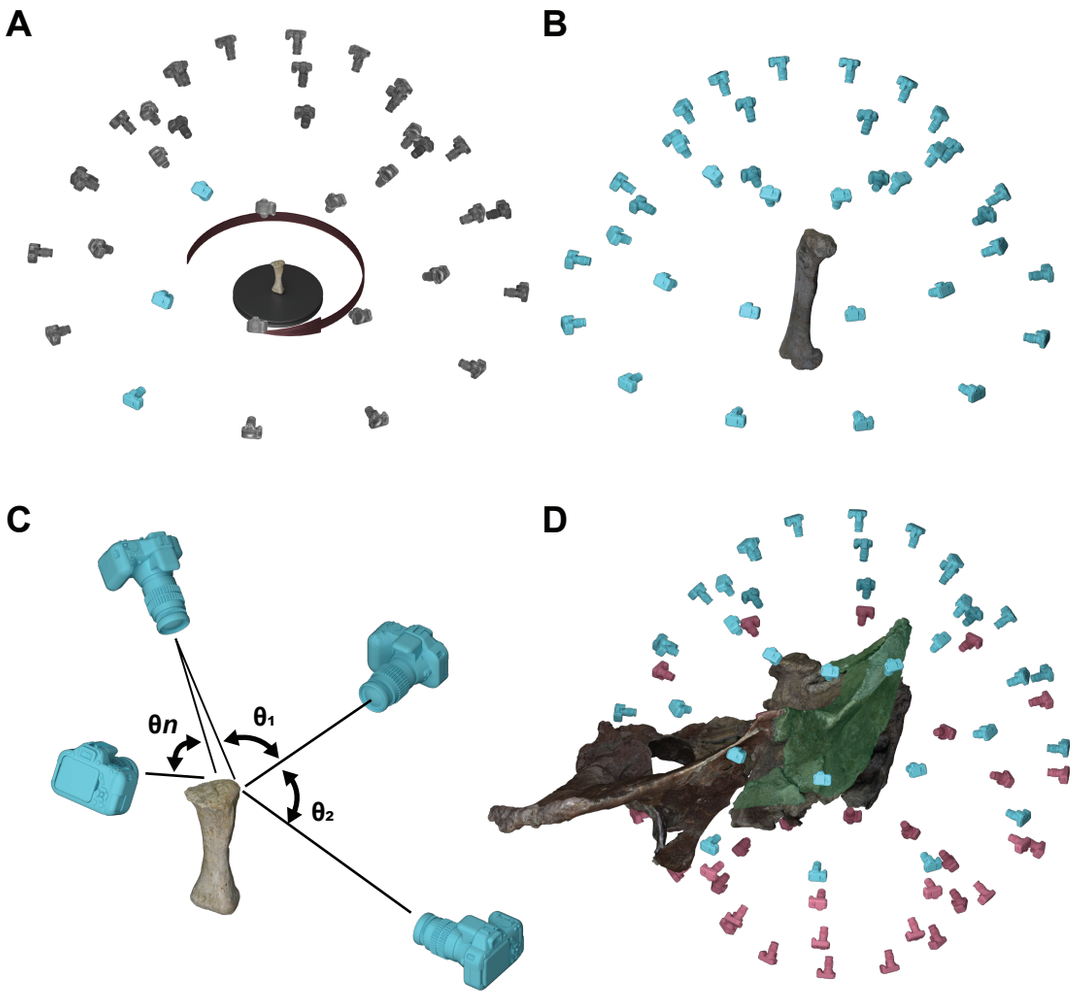

Fig.III.6. Stereophotogrammetry scanning method. (A) Scheme of sample photographs final position whith a rotating turning table and small specimen (HUE-2983). (B) Scheme of sample photographs needed in a immobile specimen (e.g. HUE-3108). (C) Principle of triangulation between several photographs (D) Final position of all the photographs for the ilium of specimen HUE-2957, after automatic aligment by the software.

III.2.1.3. MESH POST-PROCESSING

Meshes produced with this volumetric estimation methods can have artifacts, either during aligning and merging of the two sides of the scan within the structured light RGB-D camera digitizing pipeline or after mesh reconstruction in photogrammetry method. These artifacts are usually extruded vertex, zero area or zero length edges, small holes or non-manifold vertex among others.

All meshes were imported in MeshLab and Blender v2.79 3D modelling software (Blender Online Community, 2018). Zero area vertices and cleared original holes or ones resulting in problematic vertex were erased. Also, non-manifold vertices were corrected.

In the structured light method and for some problematic meshes a complete re-mesh with catmull-clark subdivision and 150k polygons limit on the final mesh was conducted. (Fig.III.8)

Several specimens were too fragmentary to digitize in original anatomical position via manual mounting and use of fossil external supports. Other specimens are almost complete but present a combination of complex fractures and a not easy preparation. Conservation criteria prevent complete extraction of a fossil if manipulation may be dangerous for the structural integrity of the specimen, like the two fragments of the tibia and fibula HUE-2425 and HUE-2426. One of the advantages of specimen virtual models is the capabilities or reconstruction of fragmentary, fractured or distorted structures. An entire field is committed to retrodeformation or virtual recovering of missing areas (Motani, Amenta, & Wiley, 2005; Arbour & Currie, 2012; Tschopp & Dzemski, 2013; Sutton *et al.*, 2014; Tallman *et al.*, 2014; Kwok, Yeung, & Wang, 2014; Taylor, 2015; Dumoncel *et al.*, 2016; Lautenschlager, 2016; Vidal & Díez Díaz, 2017; Schlager *et al.*, 2018; Molnar *et al.*, 2018), either absence of digitizing (fossil embedded in sediment) or sometimes these structures are completely loss by taphonomical processes (absent after fossilization).

In most specimens manual deformation of the 3D models with sculpture tools or distortion modifiers was avoided. As it was analyzing the bone morphology, and fossil material present an inherent taphonomical deformation, it cannot be manipulated virtual specimens in ways that increase the input error. Considering this problematic, we opted to not recover majority of crushed structures in 3D modelling software. Only manual restoration of the position of several structures like condyles and bulges, or manually close fragmentary areas in condyles or the shaft where the morphology respond to a curved surface instead of a straight sequence of NURBs (Fig.III.8) wfollowingformed. When it was possible gypsum crystals extruding from the original specimens were erased. For missing areas was opted for Statistical Shape modelling and data estimation through multiple imputation methods and resort on landmark based geometric morphometric techniques (Gunz *et al.*, 2009; Molnar, Pierce, & Hutchinson, 2012; Brown, Arbour, & Jackson, 2012a; Clavel, Merceron, & Escarguel, 2014; Lautenschlager, 2017; Schlager *et al.*, 2018). Data estimation methods will be covered later in this chapter.

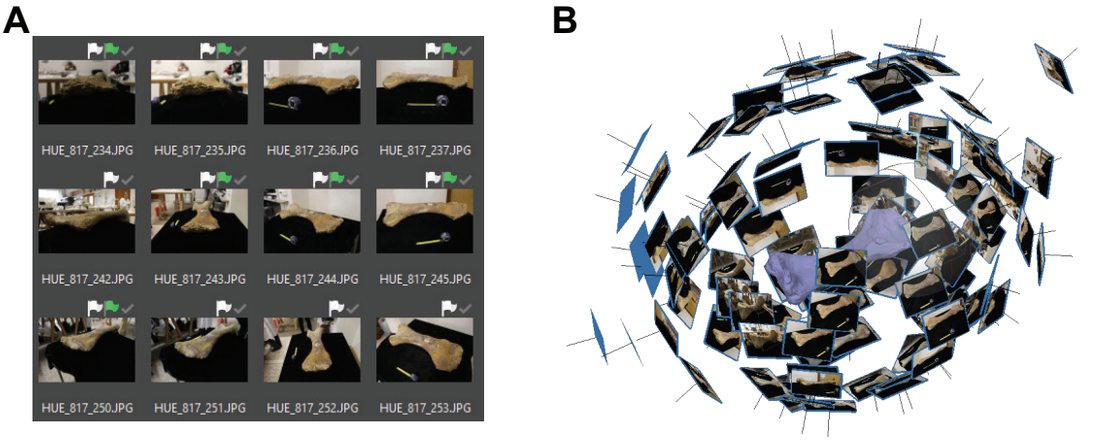

Fig.III.7. Current photogrammetry interface, humerus HUE-817. (A) Selection of some of the sampled photographs. (B) Estimation of the position of all the photographs, reconstruction of the surface mesh.

Only a minor set up of sampled specimens were partly recovered with sculpting methods in Blender. Those specimens that present a simple shearing or fracture and, that are present in two or more fragments were manually joined. In the case of long bones preserved in several fragments with complex contact, but shaft morphology make easy attach, those fragments, as in the left fibula HUE-1146 (Fig.III.8), were joined digitally. Other specimens present post-burial fractures and distortions and these specimens were conventionally digitized. Then in Blender, the displaced or bended fragments were cut and rejoined them in a straight shaft e.g. the proximal end of HUE-1146 or the distal part of HUE-2420 (see Fig.III.8). Shearing was only recovered in easy planes like the tibia shaft of HUE-2595 (Fig.III.8). Contrary, fractures and uncertain areas

Fig.III.8. Mesh post-processing. (A) Erasing of simple gypsum crystals extruding from the surface (e.g. HUE-3075). (B) Identification of simple fractures and (C) filling the gap via NURB curves (e.g. HUE-1146). (D) Cutting the mesh along simple fracture planes and (D) rejoining them (e.g. HUE-2595). (F) Mesh retopologize to fix non-manifold vertex and other surface errors.

that are absent e.g. the proximal end of the left femur HUE-2338 (see Landmark estimation methods below) were considered unrecoverable without heavy mesh manipulation on 3D modelling software. Instead it is considered for landmark estimation and virtual reconstruction via the Statistical Shape Modelling workflow and geometric morphometrics tool kit (see below).

III.2.2. STATISTICAL BACKGROUND

During this PhD thesis project, several morphological relationships and hypotheses based on morphological features were tested through a statistical framework. One of the major advantages of Lo Hueco fossil site is the sample potential to assess several of the common sauropod taxonomic problems from a statistical perspective. Linear morphometrics based on anatomical measurements and virtual paleontology permits us to visualize and employ a data-mining approach to detect morphological variance in other ways than conventional studies based on comparative anatomy. Strengthens of these methods depend on the abilities of decompose, discretize and structure the sample variance in several layers or components (Hatcher, 1994; Stegmann & Gomez, 2002; Baur & Leuenberger, 2011; Botton-Divet *et al.*, 2015; Bookstein, 2015). With data-mining approach

and several morphometric techniques it is possible to add or subtract effects that add confusion such as size (Mosimann, 1970, 2014; Isaac, 2005; Claude, 2008; Hammer & Harper, 2008; Berner, 2011). And as introduced before, size is a major problem for assessing taxonomical differences among isolated elements from Late Cretaceous iberoarmorican sauropods (Garcia *et al.*, 2010; Vila *et al.*, 2012; Díez Díaz *et al.*, 2015, 2018) as well as among the sample of Lo Hueco titanosaurs (Páramo *et al.*, 2014, 2017; Vidal *et al.*, 2017; Mocho *et al.*, 2018a). With a set of measurements for linear morphometrics or landmark coordinates also it is possible to display several discriminant algorithms (Claude, 2008; Hewson, 2009; Mitteroecker & Bookstein, 2011) in order to assess different clustering hypothesis project within the morphological variability present among the appendicular specimens of Lo Hueco titanosaurs. Also, it can be tested correlation and covariation hypothesis project between morphological features summarized in form of linear measurements or landmark coordinates and several ecomorphological variables (Claude, 2008; Kaliontzopoulou, Carretero, & Llorente, 2010; Cantalapiedra *et al.*, 2017). Several of these methods have been already deployed within the study of sauropod long bone morphology (Wilhite, 2005; Bonnan & Senter, 2007; Franz *et al.*, 2009; Schwarz & Böhm, 2012; Ullmann, Bonnan, & Lacovara, 2017).

A wide set of methods for i) quantify morphological traits and explore sample variance, ii) assess morphological differences and iii) test different paleobiological hypothesis project based on traditional comparative anatomy are here applied. Finally, to assess several morphological traits and evolutionary patterns and to test correlation between the morphological variables and several ecomorphological traits are the main aims of the PhD project.

In addition, to help us calibrate the probable ontogenetic series, preliminary identified based on morphological features, quantification methods were used (see also Páramo *et al.*, 2014). All analyses were computed in R statistical software v3.5.1 (The R Core Team, 2016) with R-studio gui (RStudio Team, 2015). All statistical analyses were conducted with six cores in parallel processing with package "snow" and "snowfall" (Knaus, 2015). The seed was set to 500. A list of R packages used in this thesis project can be accessed in each of the chapters. In addition, a comprehensive list of all available packages used in current thesis project can be accessed in Supplementary Material S.3 before the R-code and the list of custom functions developed during this research.

III.2.2.1. LINEAR MORPHOMETRICS AND LINEAR MODELS

Despite linear measurements were common early in sauropods studies (Owen, 1861; Marsh, 1878; Cope, 1887; Lull, 1919) it is not until the late XX century that these sets of measurement were applied to test biological hypothesis project (Coombs, 1978; Anderson, Hall-Martin, & Russell, 1985; Janis & Carrano, 1992; Carrano, 1998, 2001) focused on bone scaling patterns and biomechanical constraints of dinosaur skeleton. Nowadays is a common set-up for hypothesis project testing in paleobiology. A set of traditional statistical techniques for linear modelling in order to assess correlation of several morphological and morphofunctional variables and to test the proposed ecomorphological hypothesis project were used.

Linear measurements use as morphometric variables in present study can be developed in Chapter IV and Chapter V and cthe orresponding Supplementary Materials. it was also used the specimen length for several comparisons with ontogenetic stages and sequences in Chapter 6.

For now, a comprehensive data set of all appendicular elements sampled in this study can be

found in Supplementary Material. However only femora among the appendicular bones sample were analyzed (see Chapter IV) with the complete data set. The robustness of the specimens was analyzed within Chapter V. Data acquired for these linear morphometric variables was acquired with a digital caliper (E ~1 mm) on the sample from Lo Hueco or accessed material during current thesis project. For other specimens included in the analysis and no studied by firsthand, available open data sets for bibliography were employed. Unfortunately, not all the measurements are available in current bibliography of sauropod dinosaurs, and when it was possible linear measurements were achieved by published or available photographic material. For these measurements, the software ImageJ v.2.0.0-rc/1.51j8 were used (Schindelin *et al.*, 2015; Rueden *et al.*, 2017).

Linear models are used for testing correlation (i.e. some degree of linear variation) among the variables (Hammer & Harper, 2008). The mentioned morphometric variables can be related among them or to other set of discrete or continuous variables through an equation of type:

$$Y_i = mX_i + b + \varepsilon_i$$

(eq. III.1)

There is an abundant and detailed literature about the principles of linear regression, linear models and the advances toward general linear modelling (Sokal & Rohlf, 1987; Flury, 1997; Hastie, Tibshirani, & Friedman, 2000, 2009; Claude, 2008; Hammer & Harper, 2008; Hewson, 2009; Zelditch, Swiderski, & Sheets, 2012a). It is not going to discuss basic elements of statistical foundations but the selected methods applicable for the current thesis project will be commented.

It is possible to introduce the differences between model I linear regression and model II used in Chapter 4.1. Common use of linear regression appeals Least Squares (Dean, 2000; Hammer & Harper, 2008). The main objective is to determine the *m* and *b* parameters of the eq.III.1 and to assess the statistical signification and its effect (also if they are biologically relevant, see Zelditch *et al.*, 2012a: p.191). In order to estimate the best parameters m and b in least squares approach it was derived the estimator by an error function that can be expressed as:

$$\sum_{i=1}^{N} \varepsilon_i^2 = \sum_{i=1}^{N} (y_i - mx_i - b)^2$$

(eq.III.2)

Where x_i equals the $X_i - \langle X \rangle$ from eq.III.1 and is a difference between the observed variable and mean sample, and y_i equals $Y_i - \langle Y \rangle$ which is the difference between the observed value and expected value $\langle Y \rangle$. This is a sum of residuals (Zelditch *et al.*, 2012a) and minimization of the sum of squared residuals that it can be lead to estimate *m*, the slope in eq.III.1. With this set-up it can be extended the bivariate distribution to a multivariate problem following:

$$\{Y_1, Y_2, Y_3, \ldots Y_p\} = \{m_1, m_2, m_3, \ldots m_p\} X + \{b_1, b_2, b_3, \ldots b_p\} + \{\varepsilon_1, \varepsilon_2, \varepsilon_3, \ldots \varepsilon_p\}$$

(eq.III.3)

In addition, some of the requisites of linearity and general least squares methods such as the normality and homogeneity of variance to multivariate space can be extended with the General Linear Models (GLM). The GLM is a generalization over linear regression model that can fit a wide variety of different models with heterogeneous variances and nonlinearity errors (Chambers & Hastie, 1992). Instead of a variable transformation to fit the Gaussian errors (normality of errors), GLM compute two set of functions: (1) a link functions that describe how the mean depends on the linear predictors expressed by equations such as eq.III.1 (see Chambers & Hastie, 1992) and (2) a variable function that captures the variance of *Y* that depends on $var(Y) = \phi V(\mu)$. Where ϕ is a constant and μ a variance function selected by the corresponding distribution (Gaussian, Gamma, Poisson, etc.) (Chambers & Hastie, 1992; Zeileis, Kleiber, & Jackman, 2007; Zelditch *et al.*, 2012a). Here the analysis was focused around an extension of the bivariate/multivariate linear model of eq.III.1 applied for discrete data (Chambers & Hastie, 1992; Zelditch *et al.*, 2012a). It can be expressed that equation in a response to, for example, two binary categorical variable such as:

$$Y_i = A_i + B_i + A_i \times B_i + \beta(A, B, B \times A)X_i + \varepsilon_i$$

(eq.III.4)

Where *Y* is the dependent variable (or a multivariate set) for ith specimen (Zelditch *et al.*, 2012a, p. 196) such as shape variables. *A* and *B* are categorical variables or "factor" (as formally presented and as object class in R environment). *A*×*B* denotes the interaction between both factors. And the slope in this case is β which is a function of the factors and their interaction. In multivariate problems this vector will be a set of several coefficients for each variable/factor. In this work this kind of model for testing the interaction between a cladistic factor (taxa) and an morphofunctional variable was used in Chapter V.

Another consideration for the current thesis project is the assumption under the Least Square model or Model I regression. As mentioned before, linear regression parameters to check the relationships among variables (eq.III.1 and 3) is made through a derivation of the error function (eq.III.2) in order to assess the best model parameters.

However, several problems require minimizing the residuals of both dependent and explanatory variables. This is called Model II regression (see Sokal & Rohlf, 1987; Hammer & Harper, 2008) and comprise several approximations which usually appeal fitting both sets of variables into a regression line. It was considered Reduced or Standard Major Axis (RMA) as a method for such calculations in current thesis project. RMA fits the line to data by a triangulation method, minimizing the area of the triangles between the data point and the fitting line (Warton, Wright, & Falster, 2006; Friedman, Bohonak, & Levine, 2013), which considering eq.III.1 is slightly modified and the estimation of the slope translates in:

$$\hat{m} = sign\left(\sum_{i=1}^{n} x_i y_i * \sqrt{\frac{\sum_{i=1}^{n} y_i^2}{\sum_{i=1}^{n} x_i^2}}\right)$$

(eq.III.5)

This is an usual regression method in morphometrics (Bonnan, 2004; Hammer & Harper, 2008; Kilbourne & Makovicky, 2010; Harper, 2014) and given the assumptions over the error of both the variable set we used it in Chapter IV.

III.2.2.2. DISCRIMINANT ANALYSIS

Several discrimination techniques were used during the current thesis project in order to assess the morphotype distribution in Lo Hueco and iberoarmorican sauropod limb bone samples. These techniques are derived from the current methodological framework of machine learning and usually used for discrimination among factors of a set of data (Hastie *et al.*, 2009; Kassambara, 2017). Here it is briefly introduced unsupervised exploratory techniques first, as they set the foundation of one of the main methods used in the current thesis project.

Principal Component Analysis (PCA) is a method of unsupervised data exploration widely employed for multivariate visualization of variance distribution summarized in so called "principal components" (PC; Hatcher, 1994; Hammer & Harper, 2008; Abdi & Williams, 2010). Each component is an orthogonal linear combination of original variables (Campbell & Atchley, 1981; Hatcher, 1994; Hammer & Harper, 2008; Abdi & Williams, 2010) using an eigen-function to extract each axis. Therefore, a data matrix of $N \times p$ variables X can be reduced via singular value decomposition as:

$$X = UDV^T$$

(eq.III.6)

Where V is the singular vector, a $p \times p$ orthogonal matrix, and UD the principal components of the data matrix X. PC are calculated maximizing the variance of original observations and present some symmetry with the methodology of RMA commented before (Hastie *et al.*, 2009).

Based on this method there are two statistics useful for data classification: i) Between-Groups Principal Component Analysis (bg-PCA) which is not a strict discrimination method but the variance decomposition method can be helpful (Boulesteix, 2005; Mitteroecker & Bookstein, 2011) and ii) Discriminant Function Analysis (DFA) also known as Canonical Variate Analysis (CVA) or Linear Discriminant Analysis (LDA) following traditional Fisher's discriminant function (Darlington, Weinberg, & Walberg, 1973; Campbell & Atchley, 1981; Claude, 2008; Hammer & Harper, 2008; Mitteroecker & Bookstein, 2011).

The bg-PCA extracts the orthogonal axes with the particularity of maximizing the variance between a factor F which can be a taxonomical discrete category (*Apatosaurus, Ampelosaurus*, *Lohuecotitan*, etc.) in the set of morphological variables. The eigenvector will be calculated as:

$$V\left(aT_x \mid F\right)$$

(eq.III.7)

This method is not considered strictly a discrimination method and can be understand as a semi-unsupervised method to summarize variance of the sample within a set of categorical variables. On the contrary, LDA is an active machine learning method used for discrimination analyses. It uses a scaling function based on Mahalanobis distances (Darlington *et al.*, 1973; Claude, 2008). The LDA finds linear combinations of variables that describe intergroup variance (Claude, 2008; Fig.III.9). These eigenvectors over the group variance-covariance matrix are scaled by within-group variance-covariance contra bg-PCA. Nevertheless, that particular property permits to use it as a discriminant method, as take the Mahalanobis distance d_m among groups that take into account within-group variance. The distance for each

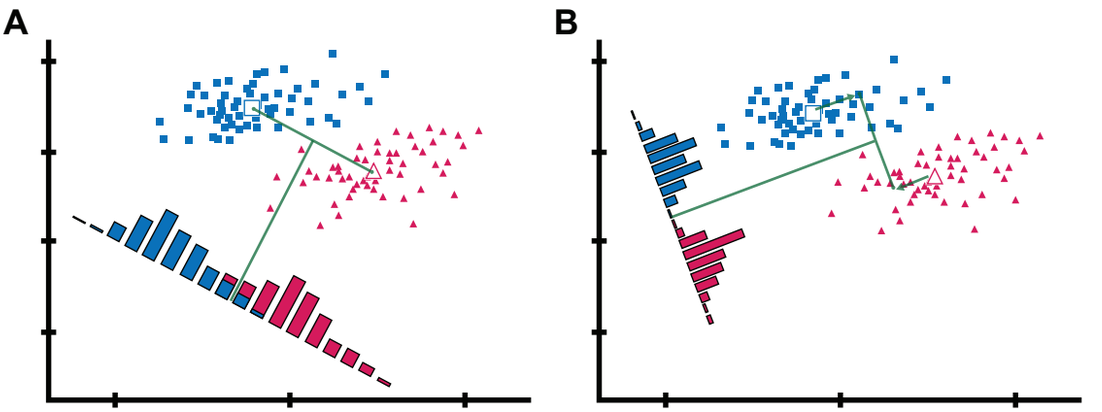

Fig.III.9. Linear Discriminant Analysis. (A) Axis of major variance as per PCA. (B) Algorithm reassessing the axis based on Mahalanobis distances in order to separate the groups.

point is not only its distance from the centroid of each group Fi, but also a function of the variance of the scatter of points (Claude, 2008). The equation of this distance is therefore:

$$d_m\left(X_i\right) = \sqrt{\left(X_i - \bar{X}\right)' V_w^{-1} \left(X_i - \bar{X}\right)}$$

(eq.III.8)

This equation corresponds to a generalization of Mahalanobis distance between a group mean and the observation (Claude, 2008, p. 115). This discrimination method has been applied also in linear and geometric morphometrics of sauropod and theropod dinosaurs (Smith, Vann, & Dodson, 2005; Bonnan, 2007; Bonnan *et al.*, 2010, 2013; Schwarz & Böhm, 2012; Serrano-Martínez *et al.*, 2015; Gerke & Wings, 2016; Malafaia *et al.*, 2017; Ullmann *et al.*, 2017). However, it is prone to problematics by sampling bias, normality of the data and unevenness among the groups, as larger groups can affect the classification methods.

Partitioning algorithms also suffer from feature space overlap, which in this case is the morphological similarities among sauropod appendicular bones as sauropods present a conservative bauplan (McIntosh, 1990a; Wilson, 2002; Bonnan, 2004; Upchurch *et al.*, 2004; Ullmann *et al.,* 2017). This can lead misclassification among different close morphospaces (see demonstration in Fig.III.10), especially in groups with few representatives toward the one with bigger N specimens. This is a common problem in Titanosauria (Upchurch *et al.*, 2004; D'Emic, Wilson, & Thompson, 2010; D'Emic, 2012; Mocho *et al.*, 2018b)

Several methods for dealing with the problem are present in modern machine learning, such as the inclusion of kernel functions to calculate the between-group variance decomposition (see Hastie *et al.*, 2009; Clemmensen *et al.*, 2011; Gopi & Palanisamy, 2014; Wu, Wipf, & Yun, 2015; Morgan, 2018).

In current thesis project an alternative classificatory algorithm for comparison was selected. The classification was carried out also by support vector machine (SVM; Boser, Guyon, & Vapnik, 1992; Cortes & Vapnik, 1995; Vapnik, 1995). The SVM does not require Gaussian data distribution and it is independent of the featured space dimensionality. Factor *Fi* is separated

by a hyperplane, maximizing the margin among the factors (Vapnik, 1995) instead of a between-group and within-group variance decomposition defining the classificatory hyperplane as in LDA. The method uses quadratic programming that provides only global minima. So local minima (mentioned problematics with uneven groups and overlapping feature space in LDA) are avoided. The SVM works normally through a kernel function that can be tooled for defining such hyperplane (Cortes & Vapnik, 1995; Vapnik, 1995). The kernel functions of the SVM work significantly different from the kernel functions of the LDA. As the algorithm is focused on the frontier rather than the group distributions, the quadratic programming optimization uses data points near the hyperplane to measure the margin, named the "*support vectors*". This method differs from LDA which calculates the centroid of each class and the scatter distribution of the population (Vapnik, 1995; Karatzoglou, Meyer, & Hornik, 2006; Brereton & Lloyd, 2010). The number of support vectors tend to be minimized and when the classes are not linearly separable, the SVM tries to find hyperplanes maximizing the margin whereas minimizing the quantity in proportion to misclassification error by a cost (see Fig.III.9 and 12 for comparison between LDA and SVM). The Cost constant commented above is set up in this preliminary step and works like a "*trade of*" when defining the hyperplane (Cortes & Vapnik, 1995). The SVM were developed as two class classification methods but have been adapted to multiclass classification like LDA or other machine learning methods such as logistic regression (Vapnik, 1995; Hastie *et al.*, 2009). All of them where in origin two-groups discrimination methods (Macqueen, 1967). Multiclass discriminant methods in SVM, logistic regression, lasso, etc. depend on several strategies and "One Against One" approach was selected. This method generates the hyperplane separating for all the possible pairs (Knerr, Personnaz, & Dreyfus, 1990; Pal, 2008) and then applies a "voting strategy" with the class label obtained. Each specimen receives the class label that occur the most after passing for all the classifiers. Multiclass SVM are conducted with the package "e1071" (Meyer *et al.*, 2017) which already includes in the code the "One Against One Approach" voting

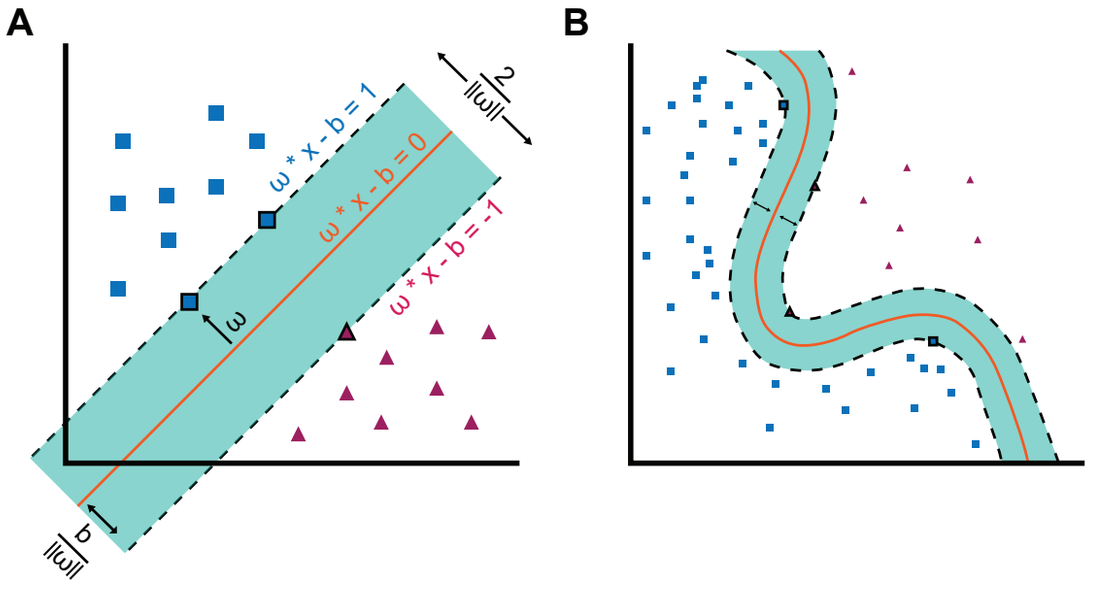

Fig.III.12. Support Vector Machine. (A) Algorithm searching for the support vector for assessment of the decission surface. (B) Kernel SVM defining a curved hyper-plane.

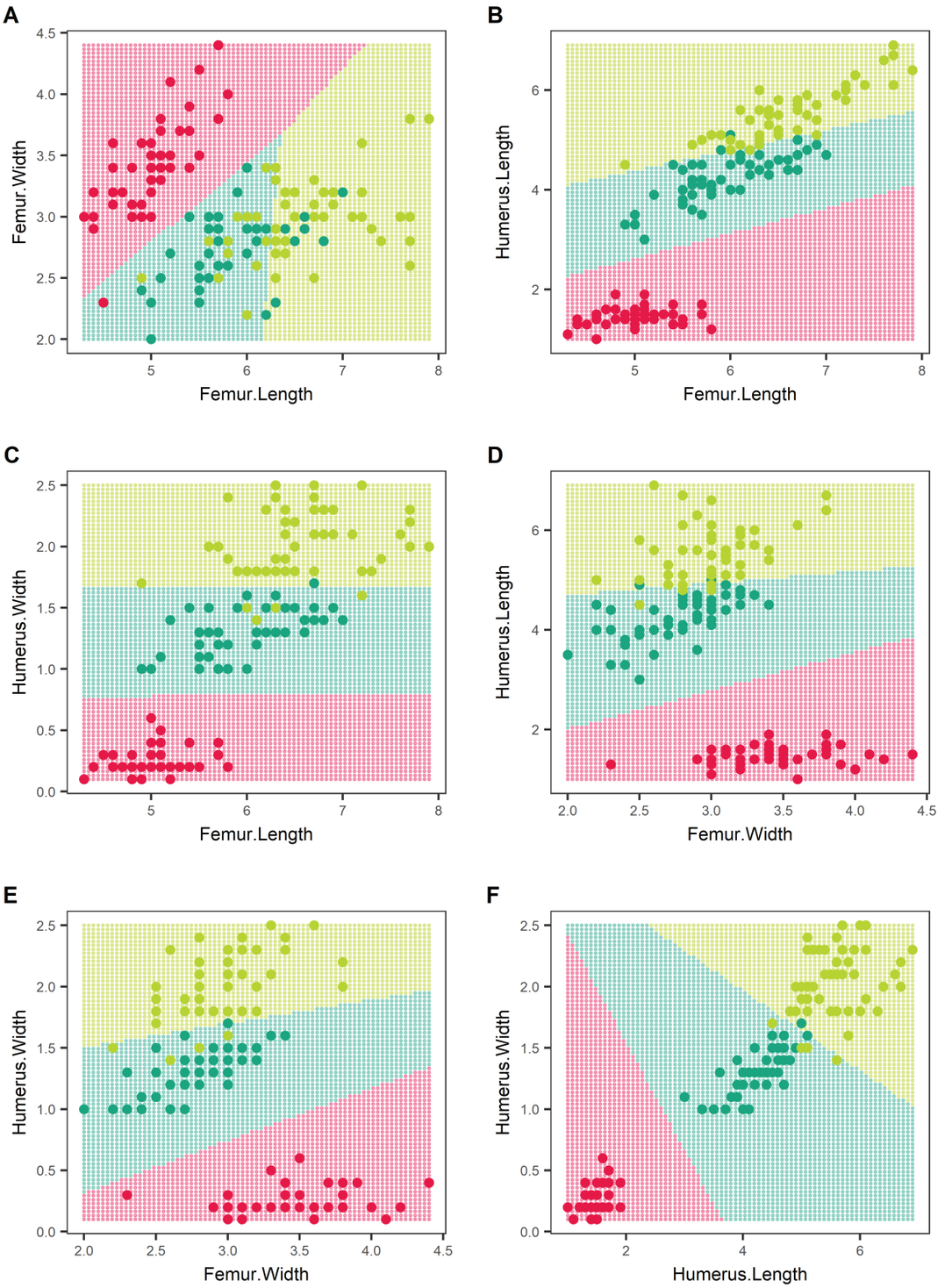

Fig.III.10. Linear Discriminant Analysis example over dummy data.

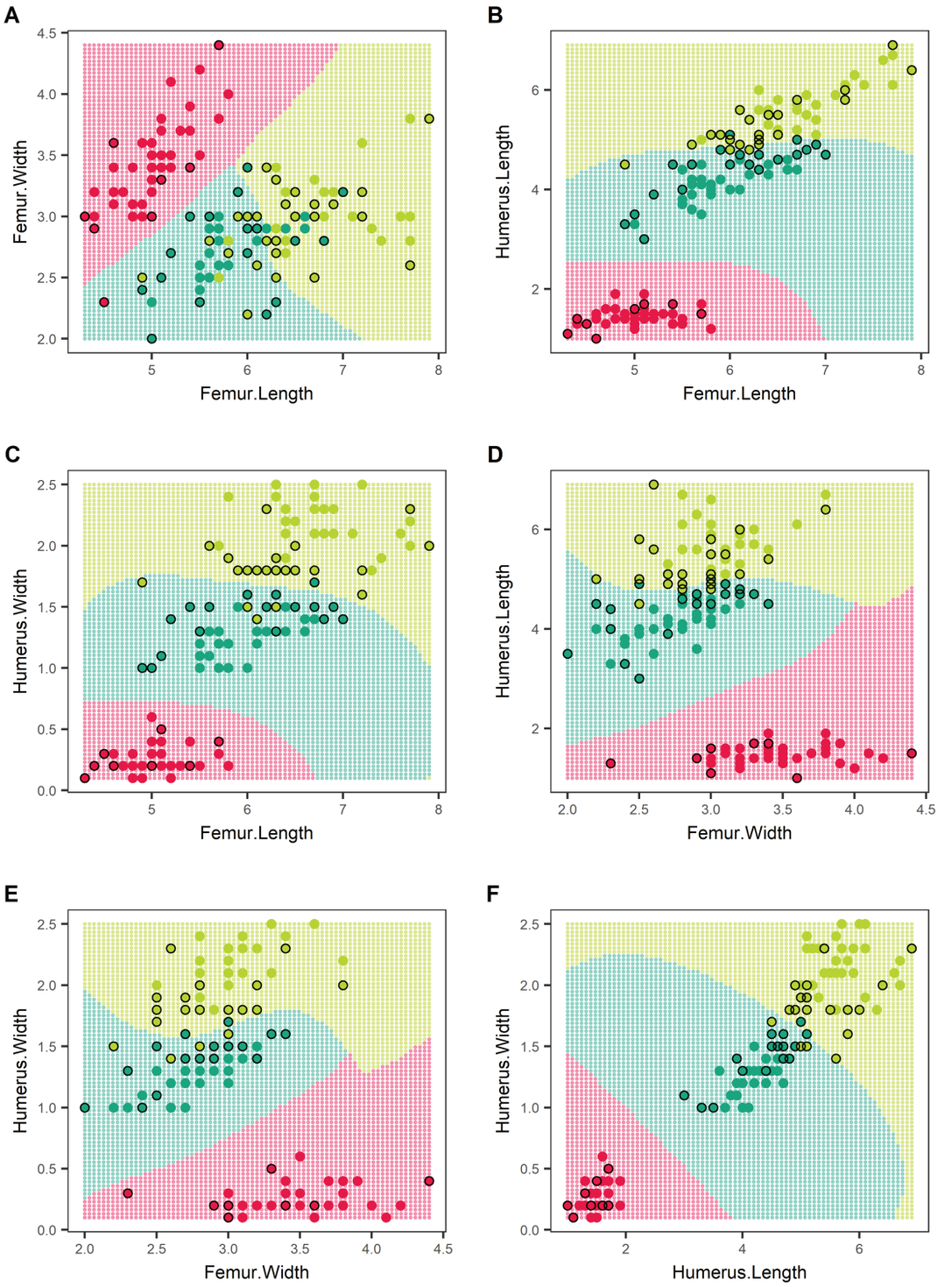

Fig.III.11. Support Vector Machine decission surfaces over dummy data. Black line around the specimen indicates that it is a *support vector.*

strategy (Hsu & Lin, 2002; Pal, 2008) and therefore can produce multiple decision surfaces between the different groups (Fig.III.11). In order to avoid overfitting, a conservative Cost value in a tuning of our model with a pre-processing session was selected. Several grading values between a minimal cost of 1 and 500 and a radial kernel with ɣ ranging from .0001 to .1 was developed. Further comments can be seen in Chapter IV when this technique was deployed.

III.2.2.3. CLUSTER ANALYSIS

Cluster analysis is an exploratory machine learning method (Rokach & Maimon, 2007a; see review in Hastie *et al.*, 2009). This type of analysis compromises several algorithm types for variable grouping or clustering. All of the methods depend on calculation of a similarity-dissimilarity distance across the sample and a linking function that groups them based on such distances. Contrary to discriminant methods, clustering methods are useful when the grouping factor or the grouping structure of the sample are unclear or unknown, respectively. Problematics like this are found in the sample from Lo Hueco (see Chapter, I), where no clear taxonomic pattern is assessed in the sample of appendicular elements of titanosaurs and attempts to preliminary classification are difficult. These methods can be used then for allocation, contra DFA, SVM and similar machine learning algorithms. Cluster analysis have been commonly used for assessing morphological similarities (Hammer & Harper, 2008; Longrich & Field, 2012; Serrano-Martínez *et al.*, 2016) or phenotypic traits within species or across similar species (de Queiroz & Good, 1997; Merilä, Kruuk, & Sheldon, 2001; Neustupa & Škaloud, 2007; Mitteroecker, 2009). This type of analysis is used here with similar purpose in an exploratory fashion and with algorithm variation for hypothesis project testing.

First, it is necessary to distinguish between distance calculations given the differences in data input types. Data input can be both discrete characters or numeric data (e.g. morphometric measurements or landmark coordinates) and therefore the method to calculate the similarities among the sampled specimens is different. An euclidean metric has no meaning with categorical data input (Gower, 1971). For numerical variables the standard distance method employed can be the euclidean distance between the standardized (equal weight if none prior weight is given, see Rokach & Maimon, 2007a) variable sets (Fig.III.13).

For calculate the euclidean distance and assess the similarity/dissimilarity of the data matrix, it is computed a variation of the Minkowski metric (Rokach & Maimon, 2007a; Jiawei Han, Micheline Kamber, 2011):

$$d\left(x_i, x_j\right) = \left(\left|x_{i1} - x_{j1}\right|^g + \left|x_{i2} - x_{j2}\right|^g + \cdots + \left|x_{ip} - x_{jp}\right|^g\right)^{\frac{1}{g}}$$

(eq. III.9)

This metric is useful for calculation of several other distances simply by an alteration of the *g* attribute. Euclidean distances are obtained when *g*=2 (Rokach & Maimon, 2007a) and the resultant distance matrix can be seen as example of Fig.III.11.

This measurement is a generalization of the equation of a triangle between both specimens or variables analyzed and has no significant meaning for discrete (factor) characters. In those cases, it is appealed to other types of index. Gower's similarity/dissimilarity index (Gower, 1971) is one of the most common and readily available metrics, but there are additional methods

(Sokal, 1961, 1963; Real & Vargas, 1996; de Queiroz & Good, 1997; Zhang & Srihari, 2003; Rokach & Maimon, 2007b). Gower dissimilarity among categorical variables is calculated based on comparisons on averaged coincidences among the character scores of two specimens:

$$d\left(x_i, x_j\right) = \frac{\sum_{k=1}^{\upsilon} S_{ijk}}{\sum_{k=1}^{\upsilon} \delta_{ijk}}$$

(eq.III.10)

Where the sumatory of the denominator is the total number of character that can be compared, δ_{ijk} is the possibility of establishing a comparison of the character *k* between specimen *i* and *j*, and S_{ijk} is the similarity between both scorings. As in previous example, a similarity data matrix for discrete data works like in Fig.III.14.

With these distance metrics established, it can be estimated the clustering relationships among the specimens of the sample using different sets of algorithms. It is possible to investigate

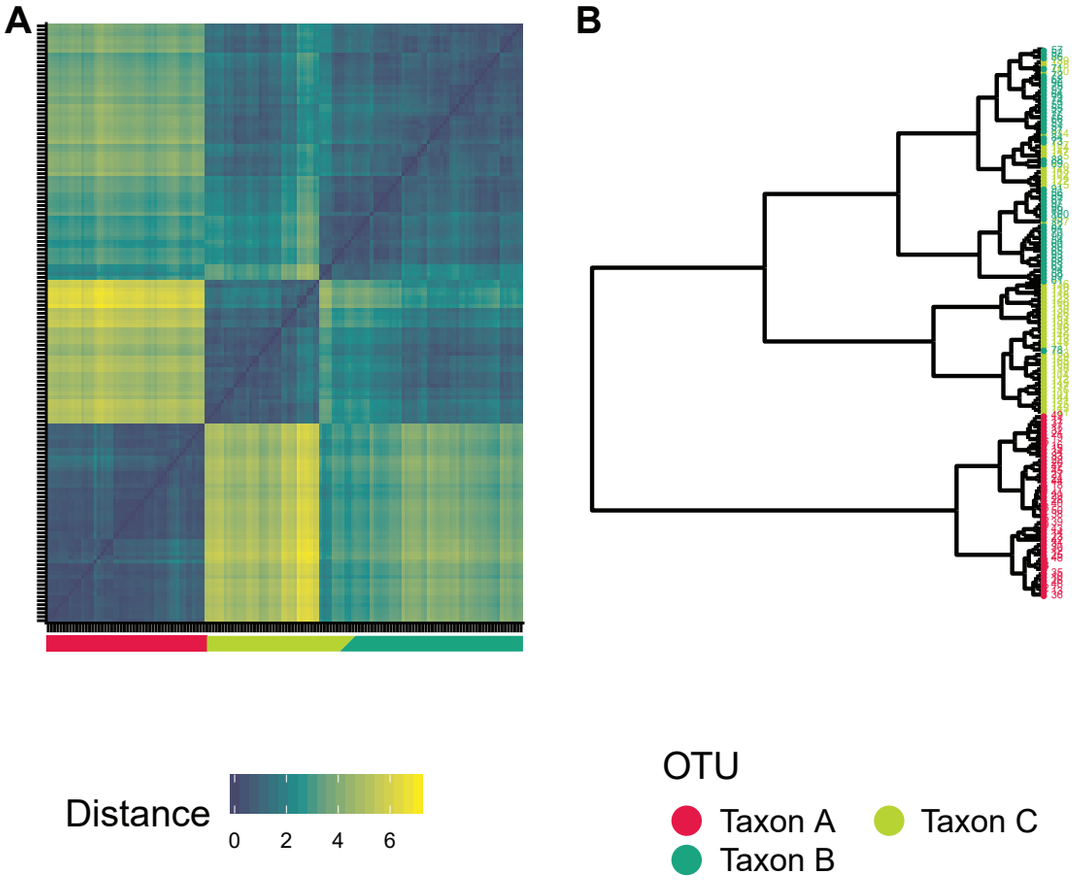

Fig.III.13. Hierarchical clustering over continous data. (A) Distance matrix. (B) Specimen dendrogram.

the clustering of the numeric data based on the euclidean distances among others. In the case of landmark coordinates, it is here uses procrustes distances, but it is a particularization of the euclidean distances for landmark coordinates translated, rotated and scaled via a Generalized Procrustes Analysis into tangential or Kendall tangent space (Claude, 2008). For processing this distances, it is similar to determine the euclidean distances over a set of GPA transformed coordinates (see below, see also Fig.III.15) assuming that there is low variation between Procrustes and Euclidean distances (Kendall, 1984; Rohlf, 1998, 1999).

Specimen	FL	FW	HL	HW
Spc 1	5.10	3.50	1.40	0.20
Spc 2	4.90	3.00	1.30	0.20
Spc 3	6.00	2.90	4.50	1.50
Spc 4	6.90	3.20	5.70	3.20
...				

Table.III.3. Numerical data example. FL = femur length; FW = femur width; HL = humerus length; HW = humerus width.

Specimen	Char.1	Char.2	Char.3	Char.4
Spc 1	0	1	1	1
Spc 2	1	0	0	2
Spc 3	0	1	0	1
Spc 4	0	0	1	1
...				

Table.III.4. Categorical data example. Char = character.

After calculation of a dissimilarity metric between the specimens and/or variables, it can be evaluated how they are grouping. It can be assessed hierarchical grouping via agglomerative or divisive algorithms, so the results obtained here shows the different groups and subgroups, often represented in a dendrogram. Additionally, it can be use partitional clustering to determine an a priori number of hypothesize groups in our sample and see how they reassess the specimen within this preset of each run of the algorithm.

III.2.2.3.2. PARTITIONAL CLUSTERING

The aim is to classify an *N* sample of specimens into *K* groups; therefore, it can also be tested via a partitioning of our data into several groups given an a priori hypothesis project. Instead of an hierarchical grouping having no idea on the number of groups that will be interpreted over the resulting dendrogram, it is possible to define k-means in which allocate the sample (Hartigan & Wong, 1979; Bow, 1984; Selim & Ismail, 1984; Rokach & Maimon, 2007a; Claude, 2008; Hammer & Harper, 2008). Having categorical data, it can be used a particularization of these methods as is the case of the k-modes algorithm (Huang, 1998; He, 2004) or computation derived from Lloyd's algorithm (Lloyd, 1982). This secondary method is only cited here to show that there are capabilities of perform these analysis on discrete characters also, but they were not used in the current study and may be applied elsewhere (see Páramo *et al.*, 2018). The number of groups is defined as k and functions as a mixture model in which each specimen mixture membership is calculated based on the mean, covariance and sampling probabilities of each cluster (Symons, 1981). From the different mixture models, k-means is a particularization in which covariance is assumed as spherical and all the different k clusters have similar sampling probability. The algorithm assigns each specimen *s to* a cluster c randomly and it calculates the cluster centroids. Then the algorithm reassess each classification of the sj specimens to the closer centroid until the centroid error function cannot be decreased further (Rokach & Maimon, 2007a). The allocation iterative process is based on assessing whether point *I* (a specimen) remains to cluster *L1* or *L2*, comparing *R1* to *R2* whereas the minimizing *R2* criteria (Hartigan & Wong, 1979), where *R2* corresponds to the equation:

$$R1 = \frac{\left[NC\left(L1\right) * d\left(I, L1\right)^2\right]}{\left[NC\left(L1\right) - 1\right]} \qquad R2 = \frac{\left[NC\left(L2\right) * d\left(I, L2\right)^2\right]}{\left[NC\left(L2\right) - 1\right]}$$

(eq. III.11)

N is the number of dimensions and *C* is a *k*N* array relative to each cluster center. It is a comparison of the distance of the point I to the center (centroid) of each cluster, if *R2* is less than *R1*, *L1* grouping is not updated, and otherwise the algorithm will assess the new grouping and update all the parameters. An example using the linear morphometrics data (see Fig.III.11, see Table.III.3) can be accessed in Fig.III.16.

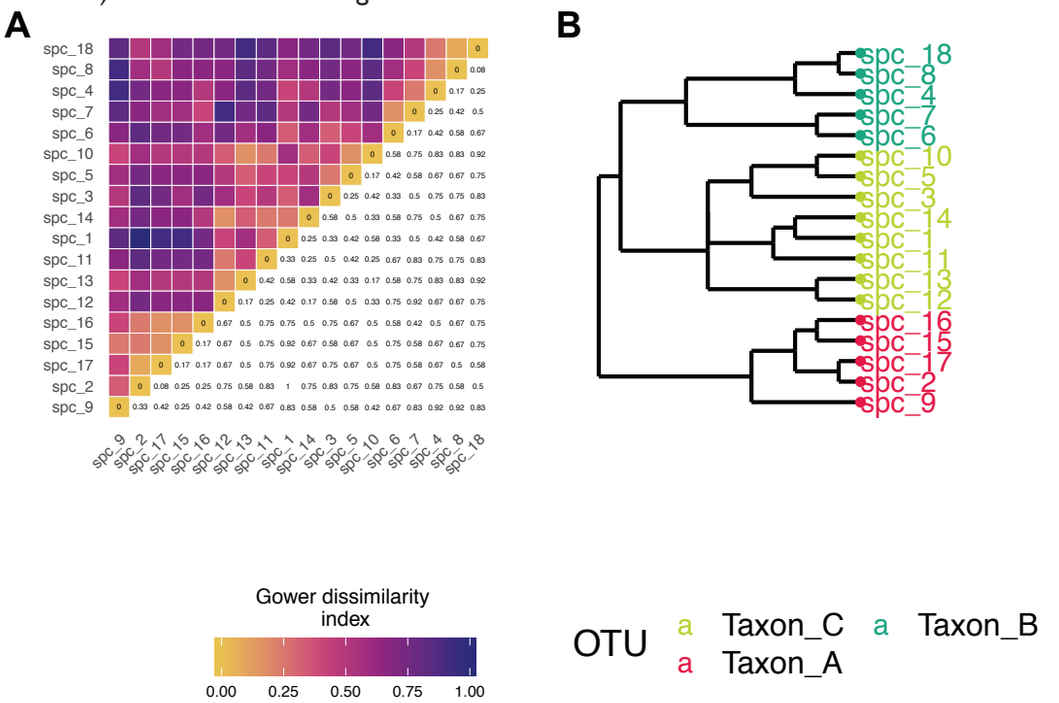

Fig.III.14. Hierarchical clustering over categorical data. (A) Gower distance matrix. (B) Specimen dendrogram.

It is also possible to explore different cluster patterns based on several criterion derived of the *R2* minimization process. It can be assessed the optimal number of cluster with several methods like the "*elbow rule*" or calculation of the Bayesian Information Criteria (Kass & Wasserman, 1995; Volinsky & Raftery, 1998; Scott Shaobing Chen & Gopalakrishnan, 2018). The "elbow rule" represents a calculation of the total between-groups variance sum of squares and dividing by the total sum of squares of the entire sample for each hypothesis project of K groups. Then, it can be assumed that the optimal number of groups are obtained when this ratio forms an "elbow" in the plot. In other words, in the case that the between-group variance cannot be further improved significantly whereas the number of groups are increasing (Rousseeuw, 1987; Kaufman & Rousseeuw, 1990). In addition, it is possible to test which number of clusters are the optimal reducing the within group variance while maximizing the between group variance. BIC works similarly, it is calculated the likelihood of the model for a given sample of points n minus the

maximized values of the likelihood function for the model *M* that it is being establish. Therefore, the equation is:

$$BIC\,(M) = lnL\,(X, M) - \frac{1}{2} * M \times ln\,(n)$$

(eq.III.12)

Where #*M* represents the parameters of the model. *L(X,M)* is the maximized values of the likelihood function for the model *M* (Scott Shaobing Chen & Gopalakrishnan, 2018). However, it is important to note that a caveat of this technique it is based on the absence of strong requisites that are susceptible to non-isotropic cluster distributions, presence of outliers or noisy samples (Rokach & Maimon, 2007a).

These methods are often employed in conjunction with hierarchical clustering or other mixture models in a typical machine learning workflow. Use of partitional clustering permit to fix an optimal number of clusters in pre-processing step, especially on difficult or computation consuming workflows. This study is focused on taxonomical clustering hypothesis project testing. Here it is employed this allocation algorithms to assess probable morphological similarities present in the sample, and the resulting grouping structure. After clusters are produced, it is possible to assess whether those resulting groups resemble natural groups with taxonomical meaning, or present other paleobiological significance.

III.2.3. LANDMARK BASED GEOMETRIC MORPHOMETRICS

Landmark based morphometrics use 2D or 3D points for quantification of the morphology. They substitute traditional measurement morphometrics for the analysis of morphology by means of representation based on coordinates in 2D or 3D space of the analyzed features by means of those points and the relative position with each other (Bookstein, 1991; Rohlf, 1993). Moreover, the advantage of landmark based geometric morphometrics comes also from use of Generalized Procrustes Analysis over the set of coordinates variables. The set of coordinates summarizes in fewer dimensions the morphology of the sample (Bookstein, 1991) and we can extract the sample variation caused by size, rotation of each specimen, and size of each specimen (Kendall, 1977; Rohlf & Slice, 1990; Bookstein, 1991; Rohlf, 1999). Therefore, we can analyze the shape variation in absolute terms between the specimens of the sample.

III.2.3.1. LANDMARKS

Each landmark is a "discrete anatomical loci that can be recognized as the same point in all specimens of the sample" (Zelditch *et al.*, 2012a; Zelditch, Swiderski, & Sheets, 2012b). These are homologous points representative of structures such as bone contacts, muscle insertion, foramina, etc. (Bookstein, 1991). Another requirement linked to the principle of homology is recognized among the sample both the geometric and the biological homology. For this reason, landmarks are scarce, especially in areas of interest relative to soft tissue insertion. Zelditch *et al.* (2012a) used the example of a squirrel jaw, where no clear point can be representative of all the insertion of one of the jaw muscles. For these cases it is also necessary to use semilandmarks (see below). Landmarks along a curve cannot be by definition, homologous in all the sample, it is needed

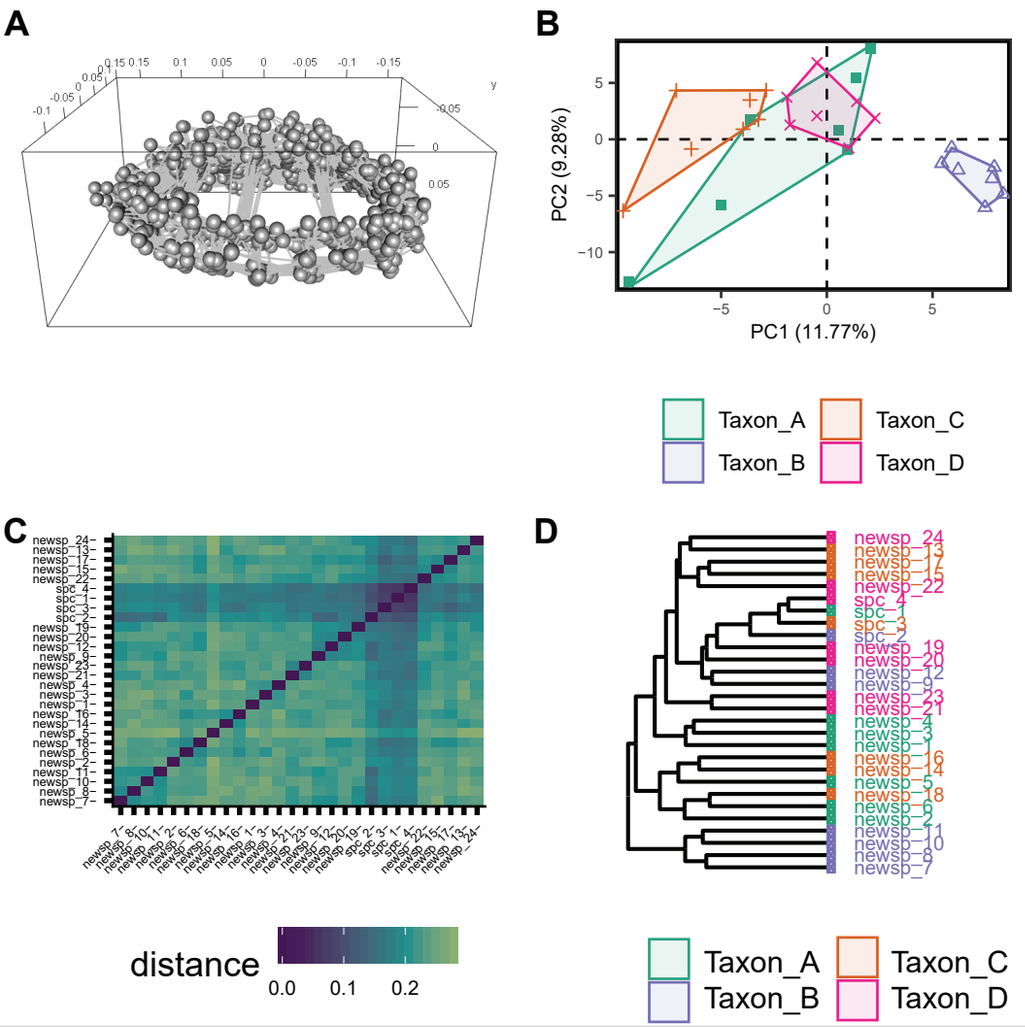

Fig.III.15. Hierarchical clustering over landmark data. (A) Generalized Procrustes Analyis over a sample of dummy turtle backplate data. (B) PCA morphospace exploration. (C) procrustes distance matrix. (D) hierarchical cluster over the procrustes distances matrix.

to appeal to particularities in form of semilandmarks (Bookstein, 1997; Gunz, Mitteroecker, & Bookstein, 2005; Sheets *et al.*, 2006; Mitteroecker & Gunz, 2009; Gunz & Mitteroecker, 2013).

Also, not all the landmarks present the requirements tightly, instead, sometimes repeatability or pure geometric homology is not fulfilled. For this reason Bookstein (1991) introduced a classification of landmarks in three categories that are followed in this PhD project: I) Type I landmarks which are the optimal and marked at the juxtaposition of two or more tissues. These tissues do not need to be of the same type. In this category it falls the contact among three bone sutures, foramina, muscle insertion in trochanters, etc. ii) Type II landmarks, which are problematic or barely considerable as landmarks at all, do not fulfill completely the requirements commented before. They are not surrounded by tissue and defined by far located structures, so some variation may apply when registered in all specimens from the sample. They have a geometrical definition. iii) Type III fall between both extremes previously commented, are locally

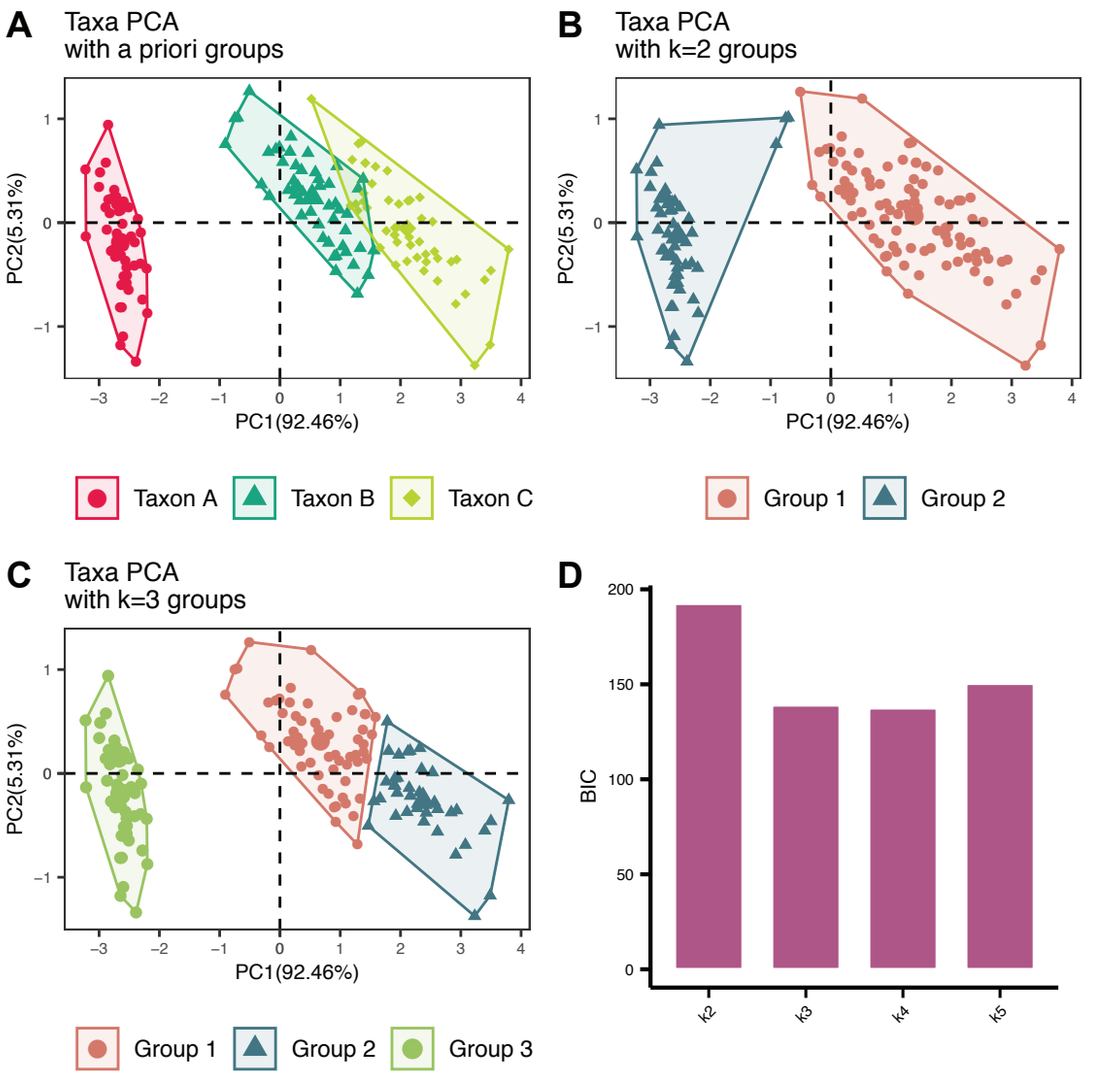

Fig.III.16. K-means clustering over dummy data. (A) PCA with the original morphospaces. (B) Group allocation with k=2 groups. (C) Group allocation with k=3 groups. (D) Bayesian Information Criterion for k=2 to k=5 groups tested.

defined (following Zelditch *et al.*, 2012a) but not so locally as in Type I. This type of landmarks is usually defined as the tip of a structure, or a maximum or minimum point of a curve, etc. An example of the procedure identifying morphological features to definition of the landmarks a sauropod long bone (e.g. the femur) is found in Fig.III.17. In addition, complete landmark dataset with each landmark type can be accessed in the corresponding chapter and supplementary material with the type and definition (see Chapter IV.2, Chapter V). Here it is avoided Type III landmark definition as they are deficient or ambiguous (Bookstein, 1997; Gunz *et al.*, 2005; Perez, Bernal, & Gonzalez, 2006). However, it is certainly that some structures of the sauropod long bones do not leave marks of tissue location after fossilization process. Places like the distal end of

the lateral bulge of the femur or the lateral trochanter of the fibula do not have an unambiguous landmark. Other similar structures present some local minima as the case of the distal end of the deltopectoral crest in the humerus or the distal end of cnemial crest in the tibia. Those places are ideally covered by a Type II landmark, as they are curvature changes often associated with muscular group insertions.

III.2.3.2. SLIDING SEMILANDMARKS

Several structures of interest are not described only by a landmark or may be an area of muscle insertion or curved structure, in which the whole area is the subject of analysis. As commented before with the Bookstein's typology of landmarks, it is not possible to define enough coverage of landmarks along the curve as they do not fulfill the requirement of homology. Instead, they are a geometric constructed and arbitrarily placed along a curve, however they are not true landmarks but semilandmarks (Bookstein, 1997; Gunz *et al.*, 2005; Perez *et al.*, 2006; Zelditch *et al.*, 2012a; Gunz & Mitteroecker, 2013).

To compare the semilandmarks, several protocols have been generated in order to produce some kind of geometric homology among specimens of the sample. Each curve must have the same regular number of sliding semilandmarks in every specimen. Then it can be proceeded to the sliding along the curve or surface so they are evenly spaced and the effect of initial arbitrary placing is removed (Gunz & Mitteroecker, 2013). It is important to note that equidistant spaced points along the curve continues to be an arbitrary assumption and should be considered thereof (Bookstein, 1997; Gunz *et al.*, 2005). The sliding process is iterative and use several relaxation algorithms to produce an evenly spaced curve in 2D or 3D (Marcus, Bello, & García-Valdecasas, 1993; Bookstein, 1997; Gunz *et al.*, 2005; Perez *et al.*, 2006; Sheets *et al.*, 2006; Gunz & Mitteroecker,

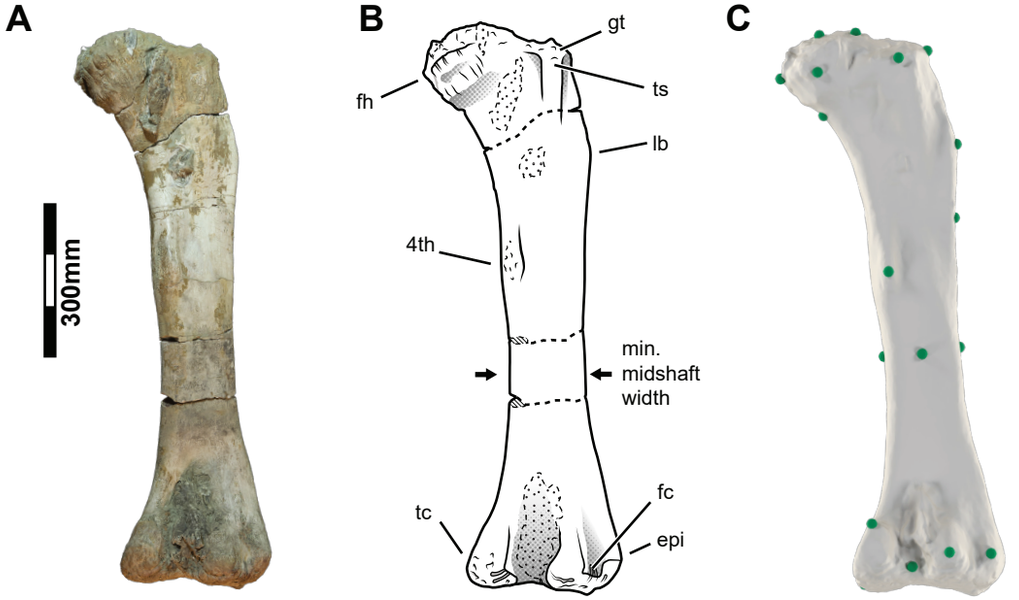

Fig.III.17. Landmark definition workflow. (A) Original specimen (e.g. HUE-3108). (B) Identification of osteological features. (C) Landmark definition with type I and type II over the ostological characters.

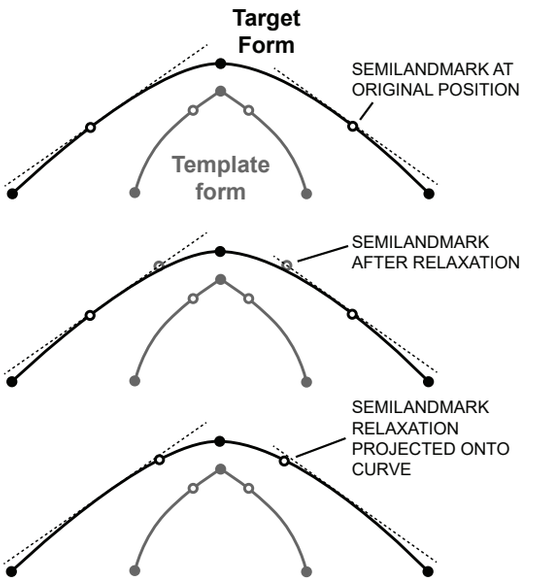

Fig.III.18. Semilandmark sliding method. Modified from Gunz (2005)

2013). The minimum Bending Energy method combined with Thin-Plate Spline is here used (Bookstein, 1996, 1997; Green, 1996; Gunz *et al.*, 2005; Perez *et al.*, 2006). The minimization of Bending Energy seeks "the smoothest possible deformation of one curve [the reference specimen] into the other, using a generally accepted mathematical definition of smoothness" (Perez *et al.*, 2006). In each iteration the TPS will relax the semilandmarks toward the curve or over a surface until minima is achieved (Fig.III.18). Or until the gaining after each iteration is not perceptible, it can be set up the number of iterations of the algorithm (Gunz, 2005; Perez *et al.*, 2006; Bastir *et al.*, 2013; Gunz & Mitteroecker, 2013; García-Martínez, Recheis, & Bastir, 2016; Schlager *et al.*, 2018). Curve semilandmarks were digitized with IDAV Landmark™ editor v3.0.7 (Wiley *et al.*, 2005: www.idav.ucdavis.edu/research/EvoMorph). For surface semilandmark an automation procedure was developed, instead of recording a surface in an external software. Here it is used a derivation of the method from Souter *et al.* (2010; see also Botton-Divet *et al.*, 2015).

For semilandmark placement a simplified mesh (see Souter *et al.*, 2010) for each appendicular bone analyzed in the current PhD project was modelled. Within this atlas the landmark and semilandmark for sliding relaxation via TPS were placed (following Gunz *et al.*, 2005; Perez *et al.*, 2006). In addition, from this atlas a regular mesh (much like the postprocessing pipeline) with the number of vertices equaling the number of surface semilandmarks desired for the analysis was calculated. The surface semilandmarks are extracted from the mesh vertex in R via the package "mesheR" (Schlager, 2016). And with these semilandmarks over the atlas mesh, then relaxed to each specimen (see Fig.III.19) following the usual procedure (Gunz *et al.*, 2005; Gunz & Mitteroecker, 2013). Not to confound with pseudolandmark automated placement (Gonzalez *et al.*, 2016; Vitek *et al.*, 2017). The semilandmarks points come from a regularly

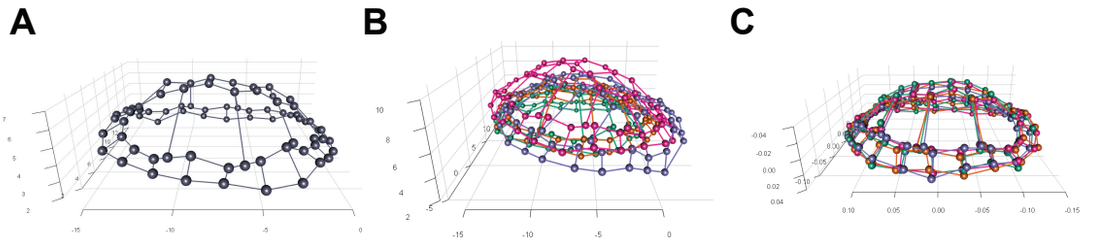

Fig.III.20. Landmark Generalized Procrustes Analysis. (A) Initial landmark definition of the dummy turtle backplate. (B) Example of different species backplate landamrks. (C) Rotation and scaling of all the specimens via GPA.

spaced initial mesh and then projected from this atlas. In fact this method has parallels with the method included and deployed within other commercial software like DHAL Viewbox 4™ (www.dhal.com) or the methodology for eigensurface sampling grids (Sievwright & MacLeod, 2012). Sliding semilandmarks were computed through R package "Morpho" (Schlager, 2017) with no limit on the number of iterations until convergence is reached with threshold of 0.00001.

III.2.3.3. GENERALIZED PROCRUSTES ANALYSIS

Was commented before the advantages of GM method in the study of shape making a definition similar to the one provided by Kendall (1977). Shape is the geometric information left after scaling, rotation and translation of sampled specimens. Initial landmarks and semilandmarks are in what it is called pre-shape space (Dryden & Mardia, 1998; Dean, 2000; Zelditch *et al.*, 2012a). In pre-shape space the coordinates of the different points that defines each specimen morphology are present, but it cannot be directly compared them as they do not share similar position in 2D/3D space (achievable through the translation and rotation of the specimens). Neither they have similar size, it can be extracted this variation from the coordinates and depending on what it is studying, incorporate later to our analysis. When those transformation are applied the sample into Kendall's shape space is moved (Zelditch *et al.*, 2012a). Though it is uses in reality an Euclidean approximation to Kendall's shape space (Kendall, 1984; Rohlf, 1998; Claude, 2008; Zelditch *et al.*, 2012a). There are several methods for this transformation, like the Baseline registration proposed by Bookstein (Bookstein, 1991, 2017; Rohlf, 2000; Claude, 2008) or the reference shape method. Here it is used the Generalized Procrustes Analysis (GPA), which permit this transformation via Procrustes Superimposition (Rohlf & Slice, 1990; Bookstein, 1997; Rohlf, 1999; Claude, 2008; Zelditch *et al.*, 2012a). The Procrustes Distances (which in this analysis is equivalent to Euclidean distances) are reduced by rotation and translation of each specimen to a sample average. In order to extract the size it is used the Centroid Size, the squared root of all the landmark distances to the centroid of a configuration for each specimen (Kendall, 1984; Rohlf & Slice, 1990; Goodall, 1991; Dryden & Mardia, 1998; Rohlf, 2003; Rohlf & Bookstein, 2003; Zelditch *et al.*, 2012a). These transform every configuration into the euclidean space proxy of shape space (but beware Slice, 2001). GPA was conducted within R with aid of package "Morpho" after the sliding of semilandmarks. Differences between registered landmarks and configurations after GPA can be seen in Fig.III.20.

As was commented before, with this method it can be analyzed shape (following Kendall, 1977), but extracting the centroid size, it can be used it for analyze the form (Gonzalez, Bernal, & Perez, 2009; Mitteroecker & Gunz, 2009; Mitteroecker & Bookstein, 2011). Using centroid size or other approximation of the specimen size can be valuable for test growth hypothesis project like allometrical relationship during development (see Bookstein, 1991; Klingenberg, 1996; Hood, 2000) or phylogenetic scaling patterns (Mitteroecker & Bookstein, 2011; Bonnan *et al.*, 2013; Chamero *et al.*, 2014). Use of size variables derived from geometric morphometrics was briefly included in Chapter VI.

III.2.4. MULTIVARIATE ESTIMATION METHODS

Fossil material is often incomplete or fragmentary (Wilson & Upchurch, 2003; Upchurch *et al.*, 2004; Molnar *et al.*, 2012; Arbour & Brown, 2014; Lautenschlager, 2016) and not all measurements

or landmarks required for study can be obtained. But not only the absence of a structure caused by fracture can affect data input. Strong postburial distortion may affect landmark placement or precise measurement of limb features (Motani, Amenta, & Wiley, 2008; Arbour & Currie, 2012; Molnar *et al.*, 2012; Tschopp & Dzemski, 2013; Tallman *et al.*, 2014; Vidal & Díez Díaz, 2017; Schlager *et al.*, 2018). It is necessary to consider also the size of sauropod remains, difficulties of fossil handling that can hide information. Additionally, embeded fossils in the original matrix, fossil supports for stabilizing material, or for exhibition can difficult the studies (Mallison, 2010; Molnar *et al.*, 2012; Mocho, Royo-Torres, & Ortega, 2014; Lautenschlager, 2017). The fossil site of Lo Hueco have yielded an abundant and diverse sample of Titanosauria sauropod remains, especially appendicular elements, but many of them present taphonomical distortion and/or fractures. The preservation of the fossil material is affected by gypsum growth, iron crusts that substitutes the periosteum and surficial layer of bone (Cambra-Moo *et al.*, 2012). Specimens of study are sometimes fragmentary, affected by loss of information in some areas, especially in the articular facets including long bone proximal and distal ends.

For those reasons, dataset construction in fossil material must evaluate these issues, either reducing variables/landmarks, input specimens (with a requirement of completion), or by estimation methods. Data estimation is a field on its own, with several sub-branches covering all methods used in current PhD project among others (see Schafer & Olsen, 1998; Schafer, 1999; Allison, 2000; van Buuren, 2007; Hammer & Harper, 2008; Dray & Josse, 2015). Modern day imputation methods do not only seek obtaining a precise estimated value for the missing data. Data estimation methods also need to retain an approximate structure of the original data

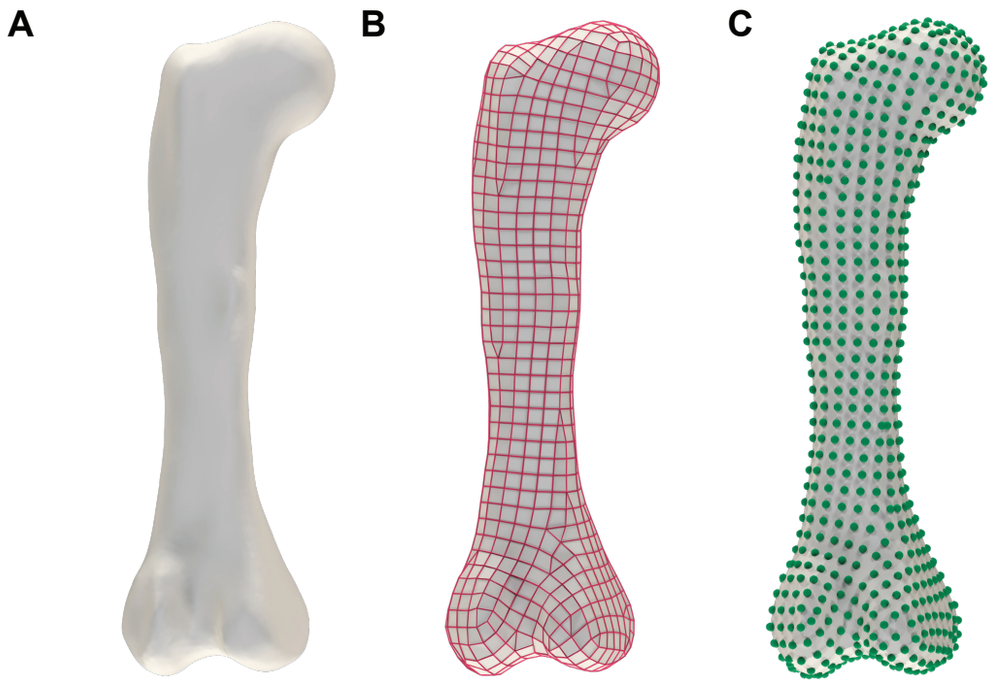

Fig.III.19. Surface semilandmark projection method. (A) Template mesh. (B) Retopologize to a quadratic regular mesh. (C) Conversion of the mesh vertices to surface landmarks.

properties such as its variance-covariance relationships (Schafer, 1999; Allison, 2000; Schafer & Graham, 2002; Oba *et al.*, 2003; Strauss & Atanassov, 2006; Abayomi, Gelman, & Levy, 2008; van Buuren, 2012; Brown *et al.*, 2012a; Arbour & Brown, 2014; Clavel *et al.*, 2014; Dray & Josse, 2015). Data imputation can be useful in order to prevent anatomical loss, ecological or in this case, morphometric information (Schafer, 1999; Royston, 2004; Brown *et al.*, 2012b; Clavel *et al.*, 2014; Bak & Hansen, 2016). Imputation methods are common after all, and some statistical software treats data input with them as default, like the average by column mean for missing values in PAST (Hammer, Harper, & Ryan, 2001). Here it is used a multiple imputation (MI) method instead of column average applied in PAST. Multivariate imputation (or estimation) methods used in this project are separated in multivariate morphometric imputation methods and landmark imputation methods. Multivariate morphometric estimation are based on the package "mice" v.2.0. (van Buuren & Groothuis-Oudshoorn, 2011). Here it is used the Bayesian linear regression (Minka, 1999; van Buuren & Groothuis-Oudshoorn, 2011) with a set of 50 different imputations and 1000 replications of each imputation. This method minimize the Procrustes sum of squared errors (PSSE, see Fig.III.21) and retain a fine and accurate estimation even when missing values exceed 25-30% of the values of total database (Clavel *et al.*, 2014; Bak & Hansen, 2016).

Common landmark estimation methods require an abundant sample ranging from dozens to hundred specimens (see the original works in Schæfer *et al.*, 2004; Gunz, 2005; Gunz *et al.*, 2005; Gunz & Mitteroecker, 2013). And while data imputation is a decades-long field, few literature consider the estimation of semilandmarks despite the proposed use of the original algorithm for thin plate spline to slide and also estimate semilandmark position (Gunz *et al.*, 2009; Gunz & Mitteroecker, 2013). TPS algorithm, as commented before, is an interpolation algorithm and therefore, it ca be used for estimation of missing landmarks (Gunz *et al.*, 2005, 2009; Schlager, 2013; Gunz & Mitteroecker, 2013; Schlager *et al.*, 2018). Or it is even possible to slide the semilandmarks

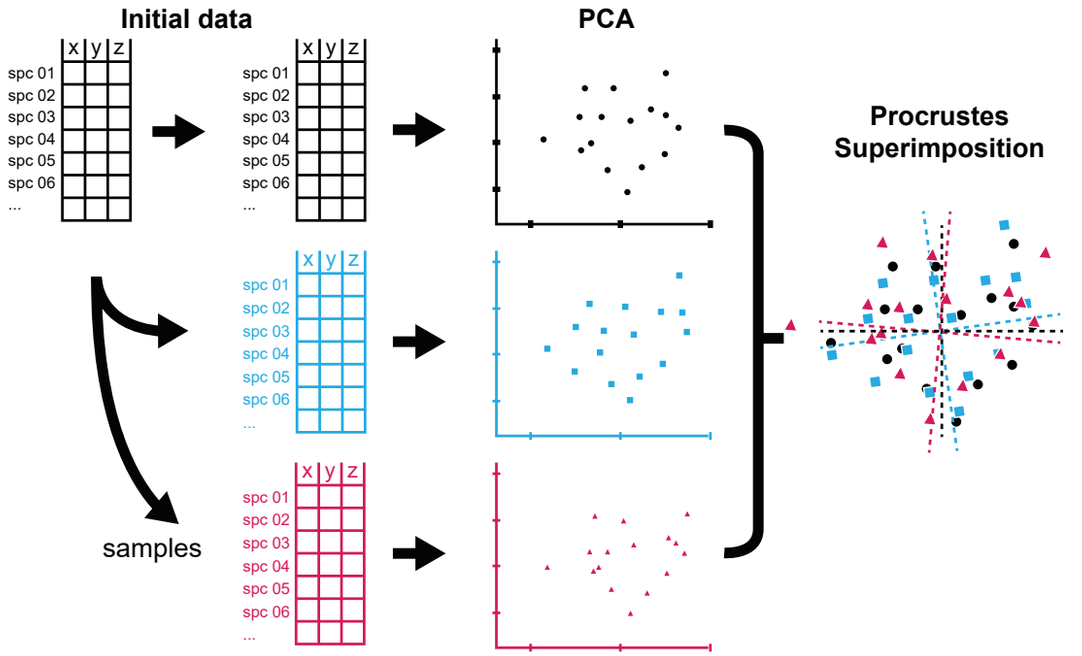

Fig.III.21. Procrustes Sum of Squared Errors calculation.

without the use of a surface where they may slide, using the proper bending energy minimization during the sliding to reorganize the curves or surface semilandmarks (Schlager, 2017). TPS can be useful for geometric estimation of morphology, the lack of available complete specimens in this study can hinder the results. Other reconstruction methods are available through digital modelling based on the actual specimens (Stevens & Parrish, 2005; Hutchinson *et al.*, 2011; Molnar *et al.*, 2012; Stevens, 2013; Lautenschlager, 2017). But in this thesis project it is analyzed the morphological changes and especially the variation in a population whether it is unknown the interspecific or intraspecific variation (including individual variation), so manual distortion of the specimens is not a suiTable input. The estimation methods cannot depend on a manual digital sculpture of the elements, as it would increase error and morphological biases. It is also important to note that the morphological variation analyzed is referred to biologically analogous landmarks (Bookstein, 1997; Molnar *et al.*, 2012). It is here appealed statistical warping of the mesh and estimation of the structure to recover those fragmentary or lost features much like in Multivariate morphometrics estimation methods. Statistical Shape modelling (Davies *et al.*, 2001; Stegmann & Gomez, 2002; Mei *et al.*, 2008; Souter *et al.*, 2010) combined with multiple imputation methods is here appealed (Gunz, 2005; Molnar *et al.*, 2012; Brown *et al.*, 2012a; Arbour & Brown, 2014; Schlager *et al.*, 2018). Nevertheless, direct geometrical distortion of the mesh even by TPS based on the actual landmarks can produce distortions that are not biologically relaTable. The transformation of a mean shape mesh into incomplete specimens is dubious for a geometric morphometrics study (Gunz *et al.*, 2009).

A combination of methods for landmark estimation and propose a virtual reconstruction pipeline is selected (Fig.III.22). The use of techniques proved in recent reconstruction studies permit us to estimate the coordinates safely but also generate meshes that can be used for use of semilandmarks along curves and surfaces. In the different studies of the current PhD project, it is developed: i) a reconstruction using TPS in absence of meshes demonstrates that while some problems and deviation in low presence of low sample, it is sure for landmarks and curve semilandmarks; ii) a reconstructed mesh generation after imputation and previous to TPS, where semilandmarks can slide, is introduced as a mid-step to final landmark estimation-sliding pre-process before generalized procrustes analysis.

The missing data from the landmark database was estimated with multiple imputation methods as with multivariate morphometrics. It is herein used two different algorithms to estimate the missing coordinates and curves, the commonly used Thin Plate Spline (TPS) following Gunz *et al.* (2009) and Bayesian principal component analysis (BPCA) of the most complete specimens to impute the partial aligned missing elements (Oba *et al.*, 2003; Arbour & Brown, 2014). This phase produces a complete set of landmarks and semilandmarks with adequate estimations of the landmark positions (see Chapter IV and Chapter V for more details).

The atlas was then iteratively processed via partial-GPA to each specimen and then warped. The mesh warping procedure was using the original landmarks and curves of the atlas and relaxing them to the landmarks and semilandmarks (also the estimated ones) for the corresponding specimen via TPS of all the mesh (Bookstein *et al.*, 2003; see multiple previous uses of this methodology like in Tschopp & Dzemski, 2013; Schlager *et al.*, 2018). It was produced also meshes for the original, complete specimens, so all the sample have this setup as an initial step, and it can be minimized the error between complete and imputated specimens. After the ,computation it is found that the original morphology is completely preserved and therefore the methodology is ready for use as standardization procedure for all the sample.

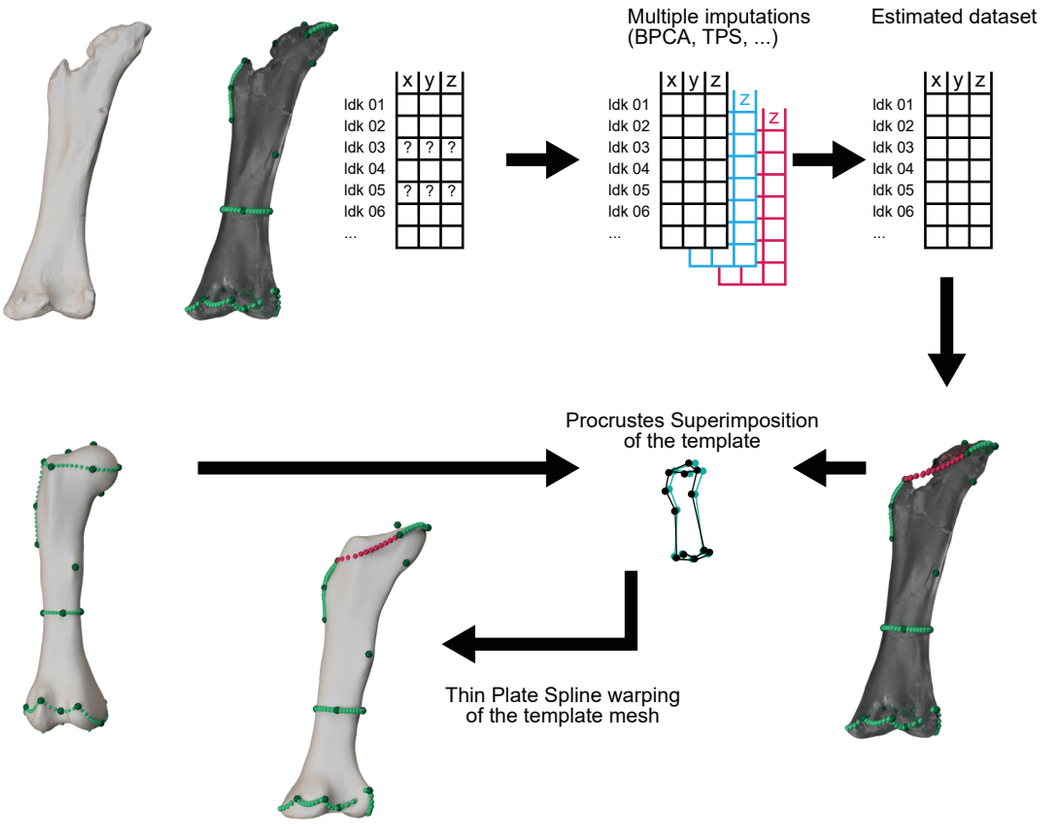

Fig.III.22. Landmark estimation pipeline. e.g. femur HUE-2338 with a fragmentary proximal end which cannot be virtually restored manually.

Some semilandmarks can produce overhanging vertices or several mesh problems like with stereophotogrammetry mesh reconstruction (see before, this Chapter) resultant during TPS-warping phase. It is treated them like those reconstruction errors and corrected using NURBs (see Molnar *et al.*, 2012) over those areas or mesh holes produced by the warp of the atlas. Instead of manually sculpting the area, this specimen reconstruction pipeline results in a rather accurate reconstruction that can help as proxy of incomplete elements. NURBs are only applied over mesh errors, holes or outlier vertices that may extrude over the surface ad should be erased. The missing data were imputed with package "mice" v3.3.0 (van Buuren & Groothuis-Oudshoorn, 2011), the package "LOST" (Arbour & Brown, 2014) and package "Morpho" (Schlager, 2017).

III.2.5. DISCRETE CHARACTERS

It has been mentioned before the use of categorical or discrete data. This kind of data is not numerical and in paleontology usually refer to ecomorphological variables as well as morphological features. These features correspond to the morphological characters previously mentioned in the sauropod anatomy epigraph that are usually employed in the morphological phylogenetic data matrices. It was also defined a series of morphological discrete characters based on features that change with ontogenetical development of the sauropod appendicular skeleton (see Chapter VI).

These characters are nominal, referring to a category (Chapter V) like "*wide gauge*" or the value "*narrow gauge*", or are usually referred to different character states in the phylogenetic and ontogenetic data matrices. Those states refer to several character changes or differences found within the sample and they are codified as "0", "1" or more states if necessary. Commonly, the different states can be related to the "absence" or "presence" of a feature (e.g. the lateral bulge of the posterior face of the femur, an accessory trochanter on the posterior face of the humerus, etc.) or to the development of distinct elements during ontogeny (e.g. a basal state "0" linked to smooth surface over the tibial proximal end in early ontogenetic stages and a state "1" referable to the development of a rugosity and other derived features in later ontogenetic stages). These ontogenetic characters are mainly related to muscular attachments and development of articulations and the sauropod cartilaginous articular caps (Schwarz, Wings, & Meyer, 2007; Holliday *et al.*, 2010).

Usually these morphological characters of sauropod dinosaurs have been used to determine the phylogenetic relationships within the different clades (McIntosh, 1990b; Upchurch, 1995; Salgado, Coria, & Calvo, 1997b; Wilson & Sereno, 1998; Sanz *et al.*, 1999; Wilson, 2002; González Riga, 2003; Upchurch *et al.*, 2004). However, the aim of the current thesis project is to know the similarities among the different morphotypes found in the sample of Lo Hueco titanosaurs. It is used traditional clustering techniques instead of *Cladistics* to evaluate cluster distribution within each of the appendicular bone studied (as commented in Cluster Analysis, this Chapter) and to compare with other types of analysis as the Ontogenetic Sequence Analysis. For the treatment of phenotypic character several data matrices were constructed, one for each appendicular bone. For this purpose, a suite of new characters were defined and used for this data matrices (see Table Chapter VI). Additionally, for the new data matrix several of the Sauropoda morphological discrete characters commonly employed will be added. Characters derived from sauropod phylogenetic data matrices are also summarized in Chapter VI. As an approximation to phenotype relationships and similarities, this data matrices are treated as commented in the clustering section (this chapter).

The ontogenetic characters defined during this thesis project will be treated following Brochu (1996) and Colbert & Rowe (2008). After character definition each specimen was coded. Sometimes, the specimens studied are incomplete or fragmentary and might be problematic. Furthermore, they may represent redundant operational units, with similar character scoring. here it is used as operational unit the semaphoront (Hennig, 1966; de Queiroz, 1985; Rieppel, 2003; Sharma, Clouse, & Wheeler, 2017), which is a summarizing "OTU" made with the most complete sequence of characters that defines a concrete character scoring. Taken as example, with the specimens of the data matrix in Table.III.5, the specimen A, B and C will be regarded too similar; but as B is incomplete, B and D are also similar. Then we code these initial specimens in the semaphoronts of Table.III.6. Note that specimen F is maintained as semaphoront C because it represents an unique operational unit on its own beside the missing data (see Griffin & Nesbitt, 2016a). Semaphoronts are used for analytical purpose. The more mature stage is generally represented by the semaphoronts with the higher number of state changes needed to pass from an all "0" score to its codification. One caveat of this technique applied to fossil titanosaur data is that it would results in many semaphoronts underscored at early ontogenetical stages. For example, with the character score sequence "0?201?" the correspondent stage is four, similar to specimen which score "011011". But note that character three has a derived scoring in state "2" which would be much more mature than suggested. Another problem with fossil data is that it would increase noisy information with

Specimen	Ontogenetic Character					
	Char. 1	Char. 2	Char. 3	Char. 4	Char. 5	Char. 6
Specimen A	0	1	2	0	1	1
Specimen B	0	?	2	0	1	?
Specimen C	1	1	2	1	2	1
Specimen D	0	1	2	0	1	1
Specimen E	0	2	2	0	1	1
Specimen F	0	1	0	1	0	0
Specimen G	0	0	?	0	?	1
Specimen H	0	0	0	?	0	1

Table.III.5. Ontogenetic character example. Char = character. Note affinities with each semaphoront definition (see color).

Semaphoront	Ontogenetic Character					
	Char. 1	Char. 2	Char. 3	Char. 4	Char. 5	Char. 6
Semaph. A	0	1	2	0	1	1
Semaph. B	1	1	2	1	2	1
Semaph. C	0	1	0	1	0	1
Semaph. D	0	2	2	0	1	1
Semaph. E	0	1	0	0	0	1
Semaph. 0	0	0	0	0	0	0

Table.III.6. Semaphoront definitions. Char = character.

too many incomplete specimens. In order to not increase redundant information with incomplete specimens, it is used Safe Taxonomic Reduction. Only specimens with relevant character combinations that are not found in other specimens/semaphoronts are included in this study.

Here it is preferred to estimate a probable ontogenetic stage of the available titanosaur long bone sample, normally determined with methods like paleohistological sampling (de Ricqlès, 2001; Sander *et al.*, 2004; Erickson, 2005; Sander & Klein, 2005; Klein & Sander, 2008; Organ, Brusatte, & Stein, 2009; Stein, 2010; Curtin *et al.*, 2012; Klein, Christian, & Sander, 2012). However, several difficulties are found that difficult an extensive use of this set of destructive techniques (see also Chapter I). In a normal workflow, specimen age estimation would be carried out by analysis of paleohistological data. Several Histological Ontogenetical Stages (Klein & Sander, 2008) have been defined and act as standarized chart of comparison for a given set of characteristics of the sauropod long bone histological structure. For a series of common features of all Sauropodomorpha (Stein, 2010), or within group characters, it can be determined a HOS relaTable to different age stages of the individual life history. Some paleohistological samples have been studied parallel to the present thesis project (Gascó *et al.*, 2018) and their results help us understand the ontogenetic development of the titanosaurs of Lo Hueco. However, even in the best scenario, sampling all the specimens of study is not achievable. In addition, individual determination is also impossible, as many of the specimens of study are found isolated within the level G1 and G2 of the Lo Hueco bonebed as commented before.

Here it is used the method of Brochu (1996) to estimate probable, relative ontogenetic stage (as well as the OSA). This method depend on irreversible treatment of ontogenetical characters, assuming each state ("lump") is acquired in ordered fashion after the previous state, and all the ontogenetical changes cannot be reversed to previous least mature conditions (Brochu, 1996). With this assumption it was search the Most Parsimonious Trees (MPTs) considering each ontogenetic character sequence = semaphoront as an OTU instead of a species (Wilson, 2002; Upchurch *et al.*, 2004) or individual (like in Tschopp, Mateus, & Benson, 2015). The MPT search conducted over the semaphoront data matrices follows normal procedures (see Brochu, 1996; Griffin & Nesbitt, 2016b) and was carried out using TNT v1.1 (Goloboff, Farris, & Nixon, 2008). Parameters and detailed description of this method can be found in Chapter VI.

With the resulting MPTs, the OSA estimation workflow (see below) was used and a consensus tree for determining each "lump" stage was estimated. To determine the consensus tree in each appendicular bone a 50% majority rule was used. With this consensus tree, it can be estimated a relative ontogenetic stage based on the position of each semaphoront as in Fig.III.23. Because some degree of uncertainty is present, some specimens may be relaTable to more than one semaphoront in the case of missing data. It is possible to determine the least mature stage whether it is considered the least mature semaphoront having similar features. In the case of the most mature stage this can be referred based on the most mature semaphoront. With this method it is possible to determine the error margin of the relative developmental stage of appearance of the ontogenetic characters.

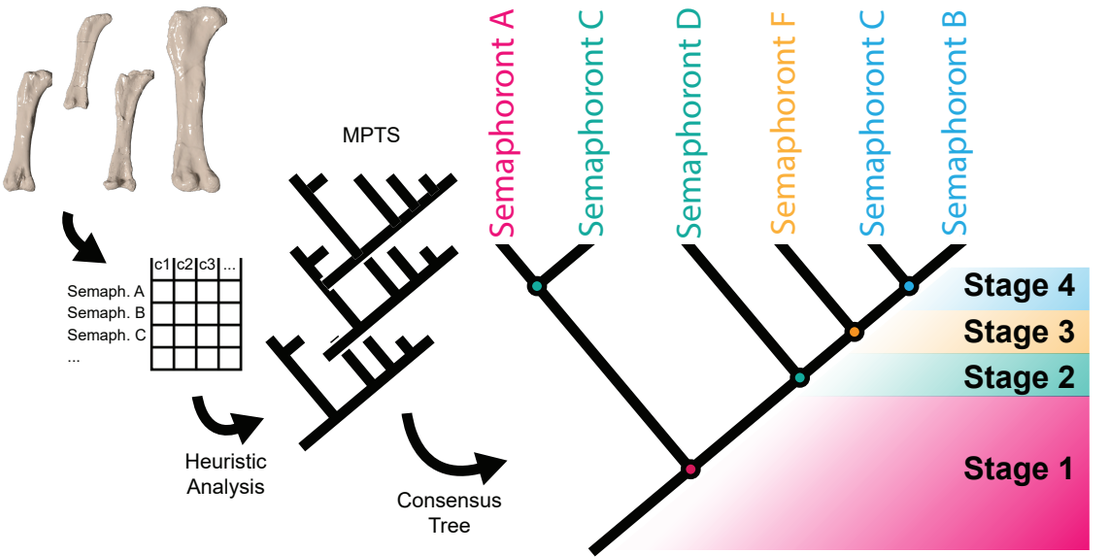

Fig.III.23. Ontogenetic stage estimation (following Brochu, 1996). MPTs - Most parsimonious trees.

III.2.6. ONTOGENETICAL SEQUENCE ANALYSIS

Ontogenetic Sequence Analysis is a method for analyze the developmental sequences of morphological character acquisition that is also sensitive to possible intraspecific variation on the ontogenetic development (Colbert & Rowe, 2008). This method is employed to plot and evaluated the developmental stage in which each morphological feature related with bone ossification is acquired (Colbert & Rowe, 2008; Griffin & Nesbitt, 2016b). This method also permit to plot different developmental paths in case of intraspecific variation acting on the maturity age in which a bone shows different ossification states (Colbert & Rowe, 2008). The way these paths are estimated also permit to infer probable semaphoronts unregistered in the original specimen sample at different ontogenetic stages.

The OSA is based on a derivation of the methodology used in cladistic estimation of developmental stages (Brochu, 1996). Here it is referred the method proposed by Brochu (1996) as Ontogenetic *Cladistics* Sequence Analysis (OCSA) in order to differentiate from OSA method in the present work. While OCSA use a consensus tree of the MPTs result from the search over the ontogenetic characters treated as ordered and irreversible, in the OSA it was conducted

a second search (Colbert & Rowe, 2008). This second search is made reversing the character scores and using the most mature specimen as an outgroup for the search. With this treatment, it can be observed the different connections (in form of branches of the MPTs) with the individual or semaphoront representing the most mature state. Instead of attribute a developmental stage based on the nodes of the tree, it is ordered the different maturation stage in a way of acquiring more morphological complexity or development more ossified and fused bones: a) Within an epistemological way, it refers to the roots behind semaphoront definition and use to observe different developmental stages (Hennig, 1966; de Queiroz, 1985; Cantino *et al.*, 1999; Rieppel, 2003; Sharma *et al.*, 2017); b) it is required to know all the possible steps into different combinations of character development but not a summarizing stage (Colbert & Rowe, 2008; Griffin, 2018). It is ordered the different relative maturity stages with the maturity score, which is the consecutive sum of all possible changes (i.e. steps) that must be acquired from an all "0" semaphoront of the most juvenile form up to the most mature combination of character scores. From each MPTs it will be traced a connection among the semaphoront based on the branches of the tree. When several individuals/semaphoronts are found in a new cluster or subtree, this method implies an intermediate unregistered step needed to explain that particular change from the previous semaphoront to the ones immediately connected by the subtree branch (see Fig.III.24). By this procedure it can be explained how it could be acquired all the observed combinations of character present in the semaphoronts of the sample. With the second reversed search, it can be estimated all probable connections with the most mature semaphoront or semaphoronts registered in the sample. Therefore, it can be obtained all probable connection unregistered in the first, normal tree search or biased by absence of enough sample. Thus, it can be lost some of the combinations of character ossification/acquisition with more derived developmental stages (Colbert & Rowe, 2008; de Jong *et al.*, 2009; Olori, 2013; Griffin & Nesbitt, 2016b; Griffin, 2018).

This method includes a dimensionless score useful as a support value that represents the frequency of representation of a particular semaphoront in the sample. This value is called the weight and it represents a proportion of information backing that particular combination. The semaphoront weight is determined after summing the complete individuals that represent that particular combination of ontogenetical characters (Fig.III.24 - Semaphoront ontogenetic stage). It is here included a change derived from Griffin & Nesbitt (2016b) as this method was developed for extant organism that have no problematic with incomplete individuals (Griffin & Nesbitt, 2016a; Griffin, 2018). It is summed a proportion of characters that has a similar score instead of numbers of individuals composing that particular semaphoront. In the previous example, if the semaphoront "012011" is represented by two individuals, then its weight is two. Griffin & Nesbitt (2016b) resolve the problematic determining that those cases the specimens with missing data summed 0.5 to the weight of the semaphoront. To better represent the weight of information backing each semaphoront a fraction representing the total missing information was added. So, if we composed the semaphoront "012011" with the second incomplete individual "0?201?" of the previous example, the total weight will be one plus four sixth of total possible character scores for a total of 1.67.

In this method, all the MPTs are used instead of the consensus tree, as we are transforming all the possible unions among the terminal specimens (therefore the node information) into connections. For tracing all the possible paths of connection with the most mature semaphoronts recovered in the studied sample, it is necessary to reverse the analysis. In order to do so, all the character scores (0 being the most developed state → 1/2/3... being the least) are reversed and repeat the MPT search with the most mature semaphoront defined in the sample. Then the

MPTs of the reverse analysis it is used to trace all the possible paths and character acquisitions connecting with the more mature specimens at the root (Colbert & Rowe, 2008). Fossil data normally suites high proportion of missing data but probably some interesting features among the represented characters. In such cases it is applied the modification of the original method proposed by Griffin (Griffin, 2018). None of the analysis performed here diverge so much and several of the standard sequences represent intermediate semaphoronts that need to be manually connected with the least mature or more mature semaphoront. In our cases, the degree of estimation of those polymorphic sequences match the low frequency weights. In some MPTs several semaphoronts are recovered in subtrees or small clusters. In that cases OSA method permit to infer a semaphoront that is not represented in the studied sample and unite the previous semaphoront with the members of that subtree. The weight of those inferred nodes is zero for the calculation of the modal sequence. Summing the semaphoront weights permit us to trace the most frequent sequence of maturation in that particular appendicular bone and taxa.

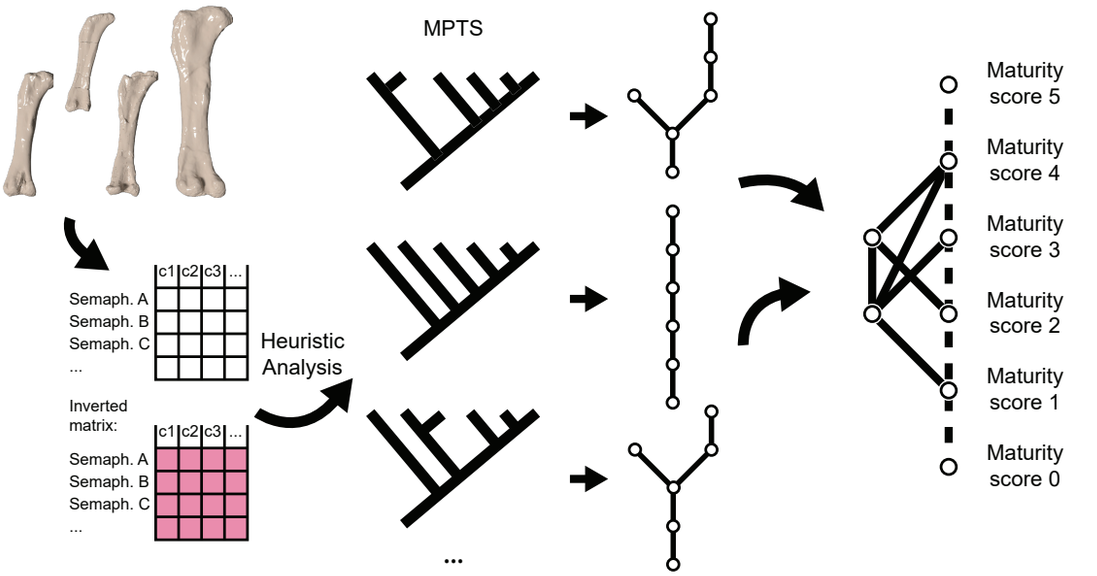

Fig.III.23. Ontogenetic Sequence Analysis (following Colbert & Rowe, 2008; after Griffin & Nesbitt, 2016). MPTs - Most parsimonious trees.

III.3. BIBLIOGRAPHY

Abayomi K, Gelman A, Levy M. 2008. Diagnostics for multivariate imputations. *Journal of the Royal Statistical Society. Series C: Applied Statistics*. 57: 273-291

Abdi H, Williams LJ. 2010. Principal component analysis. *Wiley Interdisciplinary Reviews: Computational Statistics* 2: 433–459.

Allison PD. 2000. Multiple imputation for missing data: A cautionary tale. *Sociological Methods and Research*. 28: 301-309.

Anderson JF, Hall-Martin A, Russell DA. 1985. Long-bone circumference and weight in mammals, birds and dinosaurs. *Journal of Zoology* 207: 53–61.

Apesteguía S. 2004. *Bonitasaura salgadoi* gen. et sp. nov.: A beaked sauropod from the Late Cretaceous of Patagonia. *Naturwissenschaften* 91: 493–497.

Arbour JH, Brown CM. 2014. Incomplete specimens in geometric morphometric analyses. *Methods in Ecology and Evolution* 5: 16–26.

Arbour VM, Currie PJ. 2012. Analyzing taphonomic deformation of ankylosaur skulls using retrodeformation and finite element analysis. *PLoS ONE* 7: 1–13.

Bak N, Hansen LK. 2016. Data Driven Estimation of Imputation Error—A Strategy for Imputation with a Reject Option. *PLoS ONE* 11: e0164464.

Balanoff AM, Bever GS, Ikejiri T. 2010. The Braincase of *Apatosaurus* (Dinosauria : Sauropoda) Based on Computed Tomography of a New Specimen with Comments on Variation and Evolution in Sauropod Neuroanatomy. *American Museum Novitates*: 1–29.

Baltsavias EP. 1999. A comparison between photogrammetry and laser scanning. *ISPRS Journal of Photogrammetry and Remote Sensing* 54: 83–94.

Barrett PM, Benson RBJ, Upchurch P. 2010. Dinosaurs of Dorset: Part II, the sauropod dinosaurs (Saurischia, Sauropoda) with additional comments on the theropods. *Proceedings of the Dorset Natural History and Archaeological Society* 131: 113–126.

Bastir M, García Martínez D, Recheis W, Barash A, Coquerelle M, Rios L, Peña-Melián Á, García Río F, O'Higgins PM. 2013. Differential Growth and Development of the Upper and Lower Human Thorax. *PLoS ONE* 8: 1–13.

Bates KT, Manning PL, Hodgetts D, Sellers WI. 2009. Estimating Mass Properties of Dinosaurs Using Laser Imaging and 3D Computer Modelling. *PLoS ONE* 4: e4532.

Baur H, Leuenberger C. 2011. Analysis of ratios in multivariate morphometry. *Systematic Biology* 60: 813–825.

Berner D. 2011. Size correction in biology: How reliable are approaches based on (common) principal component analysis? *Oecologia* 166: 961–971.

Blender Online Community. 2018. Blender - a 3D modelling and rendering package.

Bonaparte JF, González Riga BJ, Apesteguía S. 2006. *Ligabuesaurus leanzai* gen. et sp. nov. (Dinosauria, Sauropoda), a new titanosaur from the Lohan Cura Formation (Aptian, Lower Cretaceous) of Neuquén, Patagonia, Argentina. *Cretaceous Research* 27: 364–376.

Bonaparte JF, Powell JE. 1980. A continental assemblage of tetrapods from the Upper Cretaceous bed of El Brete, northwestern Argentina (Sauropoda-Coelurosauria-Carnosauria-Aves). *Memoires de la Société Géologique de la France* Nouvelle Série 139: 19–28.

Bonnan MF. 2004. Morphometric analysis of humerus and femur shape in Morrison sauropods: implications for functional morphology and paleobiology. *Paleobiology* 30: 444–470.

Bonnan MF. 2007. Linear and geometric morphometric analysis of long bone scaling patterns in Jurassic neosauropod dinosaurs: their functional and paleobiological implications. *Anatomical Record* 290: 1089–111.

Bonnan MF, Sandrik JL, Nishiwaki T, Wilhite RD, Elsey RM, Vittore C. 2010. Calcified cartilage shape in archosaur long bones reflects overlying joint shape in stress-bearing elements: Implications for nonavian dinosaur locomotion. *The Anatomical Record: Advances in Integrative Anatomy and Evolutionary Biology* 293: 2044–2055.

Bonnan MF, Senter P. 2007. Were the basal sauropodomorph dinosaurs *Plateosaurus* and *Massopondylus* habitual quadrupeds? *Special Papers in Palaeontology* 77: 139–155.

Bonnan MF, Wilhite RD, Masters SL, Yates AM, Gardner CK, Aguiar A. 2013. What Lies Beneath: Sub-Articular Long Bone Shape Scaling in Eutherian Mammals and Saurischian Dinosaurs Suggests Different Locomotor Adaptations for Gigantism. *PLoS ONE* 8: e75216.

Bookstein FL. 1991. *Morphometric tools for landmark data: geometry and biology*.

Bookstein FL. 1996. Applying landmark methods to biological outline data. In: Mardia K V., Gill CA, Dryden IL, eds. *Image Fusion and Shape Variability*. Leeds: University of Leeds Press, 79–87.

Bookstein FL. 1997. Landmark methods for forms without landmarks: morphometrics of group differences in outline shape. *Medical image analysis. IEEE*, 225–243.

Bookstein FL. 2015. The Relation Between Geometric Morphometrics and Functional Morphology, as Explored by Procrustes Interpretation of Individual Shape Measures Pertinent to Function. *The Anatomical Record* 298: 314–327.

Bookstein FL. 2017. A Newly Noticed Formula Enforces Fundamental Limits on Geometric Morphometric Analyses. *Evolutionary Biology*.

Bookstein FL, Gunz P, Mitteroecker P, Prossinger H, Schæfer K, Seidler H. 2003. Cranial integration in *Homo*: singular warps analysis of the midsagittal plane in ontogeny and evolution. *Journal of Human Evolution* 44: 167–187.

Boser BE, Guyon IM, Vapnik VN. 1992. A training algorithm for optimal margin classifiers. *Proceedings of the Fifth Annual Workshop on Computational Learning Theory - COLT '92*. 144–152.

Botton-Divet L, Houssaye A, Herrel A, Fabre AC, Cornette R. 2015. Tools for quantitative form description; an evaluation of different software packages for semi-landmark analysis. *PeerJ* 3: e1417.

Boulesteix AL. 2005. A note on between-group PCA. *International Journal of Pure and Applied Mathematics* 19: 359–366.

Bow ST. 1984. *Pattern recognition*. New York: Marcel Dekker.

Brereton RG, Lloyd GR. 2010. Support Vector Machines for classification and regression. *The Analyst* 135: 230–267.

Brochu CA. 1996. Closure of neurocentral sutures during crocodilian ontogeny: Implications for maturity assessment in fossil archosaurs. *Journal of Vertebrate Paleontology* 16: 49–62.

Brown CM, Arbour JH, Jackson DA. 2012a. Testing of the Effect of Missing Data Estimation and Distribution in Morphometric Multivariate Data Analyses. *Systematic Biology* 61: 941–954.

Brown CM, Evans DC, Campione NE, O'Brien LJ, Eberth DA. 2012b. Evidence for taphonomic size

bias in the Dinosaur Park Formation (Campanian, Alberta), a model Mesozoic terrestrial alluvial-paralic system. *Palaeogeography, Palaeoclimatology, Palaeoecology.* 372:108-122

van Buuren S. 2007. Multiple imputation of discrete and continuous data by fully conditional specification. *Statistical Methods in Medical Research* 16: 219–242.

van Buuren S. 2018. Flexible imputation of missing data. Chapman & Hall. 326pp.

van Buuren S, Groothuis-Oudshoorn K. 2011. mice : Multivariate Imputation by Chained Equations in R. *Journal of Statistical* Software 45.

Calvo JO, González Riga BJ. 2003. *Rinconsaurus caudamirus* gen. et sp. nov., a new titanosaurid (Dinosauria, Sauropoda) from the Late Cretaceous of Patagonia, Argentina. *Revista Geológica de Chile* 30: 233–353.

Calvo JO, González Riga BJ, Porfiri JD. 2007. A New Titanosaur Sauropod from the Late Cretaceous of Neuquén, Patagonia, Argentina. *Arquivos do Museu Nacional, Rio de Janiero* 65: 485–504.

Cambra-Moo O, Barroso-barcenilla F, Berreteaga A, Carenas B, Elvira A, Escaso F, Domingo L, Peyrot D, Sanz JL, Segura M, Ortega F, Sopelana A. 2012. Preliminary taphonomic approach to "Lo Hueco" palaeontological site. *Geobios* 45: 157–166.

Campbell NA, Atchley WR. 1981. The Geometry of Canonical Variate Analysis. *Systematic Biology* 30: 268–280.

Cantalapiedra JL, Prado JL, Hernández Fernández M, Alberdi MT. 2017. Decoupled ecomorphological evolution and diversification in Neogene-Quaternary horses. *Science* 355: 627–630.

Cantino DP, Bryant HN, Queiroz K De, Donoghue MJ, Eriksson T, Hillis DM, Lee MSY, Olmstead R. 1999. Species Names in Phylogenetic Nomenclature. *Systematic Biology* 48: 790–807.

Carrano MT. 1998. Locomotion in non-avian dinosaurs: Integrating data from hindlimb kinematics, in vivo strains, and bone morphology. *Paleobiology* 24: 450–469.

Carrano MT. 2001. Implications of limb bone scaling, curvature and eccentricity in mammals and non-avian dinosaurs. *Journal of Zoology* 254: 41–55.

Challis JH, Kerwin DG. 1992. Accuracy assessment and control point configuration when using the DLT for photogrammetry. *Journal of Biomechanics* 25: 1053–1058.

Chambers JM, Hastie T. 1992. *Statistical Models in S*. London: Chapman & Hall.

Chamero B, Buscalioni ÁD, Marugán-Lobón J, Sarris I. 2014. 3D geometry and quantitative variation of the cervico-thoracic region in crocodylia. *Anatomical Record* 297: 1278–1291.

Cignoni P, Callieri M, Corsini M, Dellepiane M, Ganovelli F, Ranzuglia G. 2008. MeshLab: an Open-Source Mesh Processing Tool. In: Scarrano V, Chiara R de, Erra U, eds. *Eurographics Italian Chapter Conference*. The Eurographic Association, .

Coria RA, Filippi LS, Chiappe LM, García RA, Arcucci AB. 2013. *Overosaurus paradasorum* gen. et sp. nov., a new sauropod dinosaur (Titanosauria: Lithostrotia) from the Late Cretaceous of Neuquén, Patagonia, Argentina. Zootaxa 3683: 357.

Claude J. 2008. *Morphometrics with R*. New York, NY: Springer New York.

Clavel J, Merceron G, Escarguel G. 2014. Missing Data Estimation in Morphometrics: How Much is Too Much? *Systematic Biology* 63: 203–218.

Clemmensen L, Witten D, Hastie T, Ersbøll B. 2011. Sparse Discriminant Analysis. *Technometrics* 53: 406–413.

Colbert MW, Rowe TB. 2008. Ontogenetic Sequence Analysis: using parsimony to characterize

developmental sequences and sequence polymorphism. *Journal of experimental zoology. Part B, Molecular and developmental evolution* 310: 398–416.

Company J, Suberbiola XP, Ruiz-Omeñaca JI. 2009. Nuevos restos fósiles del dinosaurio *Lirainosaurus*. *Ameghiniana* 46: 391–405.

Coombs WPJ. 1978. Theoretical Aspects of Cursorial Adaptations in Dinosaurs. *The Quarterly Review of Biology* 53: 393–418.

Cope ED. 1887. A Contribution to the History of the Vertebrata of the Trias of North America. *Proceedings of the American PhiloAmerican Philosophical Society* 24: 209–228.

Cortes C, Vapnik VN. 1995. Support-Vector Networks. *Machine Learning* 20: 273–297.

Cunningham JA, Rahman IA, Lautenschlager S, Rayfield EJ, Donoghue PCJ. 2014. A virtual world of paleontology. *Trends in Ecology and Evolution* 29: 347–357.

Curtin AJ, Macdowell AA, Schaible EG, Roth VL. 2012. Noninvasive histological comparison of bone growth patterns among fossil and extant neonatal elephantids using synchrotron radiation X-ray microtomography. *Journal of Vertebrate Paleontology* 32: 939–955.

D'Emic MD. 2012. The early evolution of titanosauriform sauropod dinosaurs. *Zoological Journal of the Linnean Society* 166: 624–671.

D'Emic MD, Wilson JA, Thompson R. 2010. The end of the sauropod dinosaur hiatus in North America. *Palaeogeography, Palaeoclimatology, Palaeoecology* 297: 486–490.

Darlington RB, Weinberg SL, Walberg HJ. 1973. Canonical Variate Analysis and Related Techniques. *Review of Educational Research* 43: 433.

Das AJ, Murmann DC, Cohrn K, Raskar R. 2017. A method for rapid 3D scanning and replication of large paleontological specimens. *PLoS ONE* 12: 1–13.

Davies RH, Cootes TF, Twining CJ, Taylor CJ. 2001. An Information Theoretic Approach to Statistical Shape Modelling. *Procedings of the British Machine Vision Conference* 2001: 2.1-2.10.

Davies TG, Rahman IA, Lautenschlager S, Cunningham JA, Asher RJ, Barrett PM, Bates KT, Bengtson S, Benson RBJ, Boyer DM, Braga J, Bright JA, Claessens LPAM, Cox PG, Dong XP, Evans AR, Falkingham PL, Friedman M, Garwood RJ, Goswami A, Hutchinson JR, Jeffery NS, Johanson Z, Lebrun R, Martínez-Pérez C, Marugán-Lobón J, O'Higgins PM, Metscher B, Orliac M, Rowe TB, Rücklin M, Sánchez-Villagra MR, Shubin NH, Smith SY, Starck JM, Stringer C, Summers AP, Sutton MD, Walsh SA, Weisbecker V, Witmer LM, Wroe S, Yin Z, Rayfield EJ, Donoghue PCJ. 2017. Open data and digital morphology. *Proceedings of the Royal Society B: Biological Sciences* 284: 20170194.

Dean D. 2000. Statistical Shape Analysis. *Journal of Human Evolution* 38: 455–457.

del Corro G. 1975. Un nuevo saurópodo del Cretácico Superior. *Chubutisaurus insignis* gen. et sp. nov. (Saurischia-Chubutisauridae nov.) del Cretácico Superior (Chubutiano), Chubut, Argentina. *Actas I Congreso Argentino de Paleontologia y Bioestratigrafia*.229–240.

Díez Díaz V, Garcia G, Pereda-Suberbiola X, Stein KHW, Jentgen-Ceschino B, Godefroit P, Valentin X. 2018. The titanosaurian dinosaur *Atsinganosaurus velauciensis* (Sauropoda) from the Upper Cretaceous of southern France: New material, phylogenetic affinities, and palaeobiogeographical implications. *Cretaceous Research* 91: 429–456.

Díez Díaz V, Pereda Suberbiola X, Company J. 2015. Updating titanosaurian diversity (Sauropoda) from the Late Cretaceous of Spain: The fossil site of Laño and Chera. *Spanish Journal of Palaeontology* 30: 293–306.

Dray S, Josse J. 2015. Principal component analysis with missing values: a comparative survey of methods. *Plant Ecology* 216: 657–667.

Dryden IL, Mardia K V. 1998. *Statistical Shape Analysis*.

Dumoncel J, Subsol G, Durrleman S, Jessel JP, Beaudet A, Braga J. 2016. How to Build an Average Model When Samples are Variably Incomplete? Application to Fossil Data. 2016 *IEEE Conference on Computer Vision and Pattern Recognition Workshops (CVPRW)*. IEEE, 541–548.

Erickson GM. 2005. Assessing dinosaur growth patterns: a microscopic revolution. *Trends in Ecology & Evolution* 20: 677–84.

Fahlke JM, Autenrieth M. 2016. Photogrammetry Vs. Micro-Ct Scanning for 3D Surface Generation of a Typical Vertebrate Fossil -a Case Study. *Journal of Paleontological Techniques* 14: 1–18.

Falkingham PL. 2012. Acquisition of high resolution three-dimensional models using free, open-source, photogrammetric software. *Paleontologia Electronica* 15: 1–15.

Falkingham PL. 2013. Low cost 3D scanning using off-the-shelf video gaming peripherals. *Journal of Paleontological Techniques*. 11: 1–9.

Filippi LS, Garrido AC. 2008. *Pitekunsaurus macayai* gen. et sp. nov., nuevo titanosaurio (Saurischia, Sauropoda) del Cretácico Superior de la Cuenca Neuquina, Argentina. *Ameghiniana* 45: 575–590.

Filippi LS, García RA, Garrido AC. 2011. A New Titanosaur Sauropod Dinosaur from the Upper Cretaceous of North Patagonia, Argentina. *Acta Palaeontologica Polonica* 56: 505–520.

Flury B. 1997. A First *Course in Multivariate Statistics*. New York, NY: Springer.

Franz R, Hummel J, Kienzle E, Kolle P, Gunga HC, Clauss M. 2009. Allometry of visceral organs in living amniotes and its implications for sauropod dinosaurs. *Proceedings of the Royal Society B: Biological Sciences* 276: 1731–1736.

Friedman J, Bohonak AJ, Levine RA. 2013. When are two pieces better than one: Fitting and testing OLS and RMA regressions. *Environmetrics* 24: 306–316.

García-Martínez D, Recheis W, Bastir M. 2016. Ontogeny of 3D rib curvature and its importance for the understanding of human thorax development. *American Journal of Physical Anthropology* 159: 423–431.

Garcia G, Amico S, Fournier F, Thouand E, Valentin X. 2010. A new Titanosaur genus (Dinosauria, Sauropoda) from the Late Cretaceous of southern France and its paleobiogeographic implications. *Bulletin de la Société Géologique de France* 181: 269–277.

García RA, Salgado JL. 2013. The titanosaur sauropods from the late Campanian–early Maastrichtian Allen Formation of Salitral Moreno, Río Negro, Argentina. *Acta Palaeontologica Polonica* 58: 269–284.

Gascó F, Vidal D, Páramo A, Mocho P, Ortega F. 2018. New insights into the palaeohistology of the titanosaur sauropods from the Upper Cretaceous of Lo Hueco (Cuenca, Spain). *XVI Annual Meeting of European Association of Vertebrate Paleontologists*. 76.

Gerke O, Wings O. 2016. Multivariate and cladistic analyses of isolated teeth reveal sympatry of theropod dinosaurs in the Late Jurassic of Northern Germany. *PLoS ONE* 11: 1–52.

Gignac PM, Kley NJ, Clarke JA, Colbert MW, Morhardt AC, Cerio D, Cost IN, Cox PG, Daza JD, Early CM, Echols MS, Henkelman RM, Herdina AN, Holliday CM, Li Z, Mahlow K, Merchant S, Müller J, Orsbon CP, Paluh DJ, Thies ML, Tsai HP, Witmer LM. 2016. Diffusible iodine-

based contrast-enhanced computed tomography (diceCT): An emerging tool for rapid, high-resolution, 3-D imaging of metazoan soft tissues. *Journal of Anatomy* 228: 889–909.

Goloboff PA, Farris JS, Nixon K. 2008. TNT: Tree analysis using New Technology, vers. 1.1 (Will Henning Edition). Program and documentation. Available at: http://www.zmuc.dk/public/phylogeny/tnt.

Gonzalez PN, Barbeito-Andrés J, D'Addona LA, Bernal V, Perez SI. 2016. Technical note: Performance of semi and fully automated approaches for registration of 3D surface coordinates in geometric morphometric studies. *American Journal of Physical Anthropology* 160: 169–178.

Gonzalez PN, Bernal V, Perez SI. 2009. Geometric morphometric approach to sex estimation of human pelvis. *Forensic Science International* 189: 68–74.

González Riga BJ. 2003. A New Titanosaur (Dinosauria, Sauropoda) from the Upper Cretaceous of Mendoza Province, Argentina. *Ameghiniana* 40: 155–172.

González Riga BJ, Previtera E, Pirrone C a. 2009. *Malarguesaurus florenciae* gen. et sp. nov., a new titanosauriform (Dinosauria, Sauropoda) from the Upper Cretaceous of Mendoza, Argentina. *Cretaceous Research* 30: 135–148.

Goodall C. 1991. Procrustes Methods in the Statistical Analysis of Shape. *Journal of the Royal Statistical Society. Series B (Methodological)* 53: 285–339.

Gopi ES, Palanisamy P. 2014. Maximizing Gaussianity using kurtosis measurement in the kernel space for kernel linear discriminant analysis. *Neurocomputing* 144: 329–337.

Gower JC. 1971 A General Coefficient of Similarity and Some of Its Properties. *Biometrics* 27: 857–874.

Green WDK. 1996. The thin-plate spline and images with curving features. In: Mardia KV., Gill CA, Dryden IL, eds. *Image Fusion and Shape Variability*. Leeds: University of Leeds Press, 79–87.

Griffin CT. 2018. Developmental patterns and variation among early theropods. *Journal of Anatomy* 232: 604–640.

Griffin CT, Nesbitt SJ. 2016a. Anomalously high variation in postnatal development is ancestral for dinosaurs but lost in birds. *Proceedings of the National Academy of Sciences* 113: 14757–14762.

Griffin CT, Nesbitt SJ. 2016b. The femoral ontogeny and long bone histology of the Middle Triassic (?late Anisian) dinosauriform *Asilisaurus kongwe* and implications for the growth of early dinosaurs. *Journal of Vertebrate Paleontology* 36.

Guidi G, Gonizzi S, Micoli L. 2016. 3D capturing performances of low-cost range sensors for mass-market applications. *International Archives of the Photogrammetry, Remote Sensing and Spatial Information Sciences - ISPRS Archives* 41: 33–40.

Gunz P. 2005. Statistical and geometric morphometric reconstruction of hominid crania. Reconstructing autralopithecine ontogeny. Unpublished thesis project, University of Vienna.

Gunz P, Mitteroecker P. 2013. Semilandmarks: a method for quantifying curves and surfaces. *Hystrix, the Italian Journal of Mammalogy* 24: 103–109.

Gunz P, Mitteroecker P, Bookstein FL. 2005. Semilandmarks in three dimensions. In: Slice DE, ed. *Modern Morphometrics in Physical Anthropology*. Kluwer Academic Publ., 73–98.

Gunz P, Mitteroecker P, Neubauer S, Weber GW, Bookstein FL. 2009. Principles for the virtual reconstruction of hominin crania. *Journal of Human Evolution* 57: 48–62.

Hammer Ø, Harper DAT. 2008. *Paleontological Data Analysis*. Wiley-Blackwell Publishing.

Hammer Ø, Harper DAT, Ryan PD. 2001. PAST: Paleontological Statistics Software Package for Education and Data Analysis. *Paleontologia Electronica* 4: 9pp.

Harper W V. 2014. Reduced Major Axis Regression: Teaching Alternatives to Least Squares. In: Makar K, Sousa B de, Gould R, eds. *Sustainability in statistics education. Proceedings of the Ninth International Conference on Teaching Statistics*.

Hartigan JA, Wong MA. 1979. Algorithm AS 136: A K-Means Clustering Algorithm. *Applied Statistics* 28: 100.

Hastie T, Tibshirani R, Friedman J. 2000. *The Elements of Statistical Learning: Data Mining, Inference, and Prediction*. Springer.

Hastie T, Tibshirani R, Friedman J. 2009. The Elements of Statistical Learning. *Bayesian Forecasting and Dynamic Models* 1: 1–694.

Hatcher L. 1994. Principal Component Analysis. *A Step-By-Step Approach to Using the SAS System for Factor Analysis and Structural Equation Modeling*: 1–56.

He Z. 2004. Approximation Algorithms for K-Modes Clustering. *Igarss* 2014: 1–5.

Hennessy RJ, Mclearie S, Kinsella A, Waddington JL. 2005. Facial surface analysis by 3D laser scanning and geometric morphometrics in relation to sexual dimorphism in cerebral – craniofacial morphogenesis and cognitive function. *J. Anat.* 207: 283–295.

Hennig W. 1966. *Phylogenetic Systematics*. Urbana, Illinois, USA: University of Illinois Press.

Hewson PJ. 2009. *Multivariate Statistics with R*: 189pp

Holliday CM, Ridgely RC, Sedlmayr JC, Witmer LM. 2010. Cartilaginous Epiphyses in Extant Archosaurs and Their Implications for Reconstructing Limb Function in Dinosaurs. *PLoS ONE* 5: e13120.

Hood CS. 2000. Geometric morphometric approaches to the study of sexual size dimorphism in mammals. *Hystrix* 11: 11–90.

Hsu CW, Lin CJ. 2002. A comparison of methods for multiclass support vector machines. *IEEE Transactions on Neural Networks* 13: 415–425.

Huang Z. 1998. Extensions to the k-Means Algorithm for Clustering Large Data Sets with Categorical Values. *Data Mining and Knowledge Discovery* 2: 283–304.

Huene FF von. 1927. Sichtung der Grundlagen der jetzigen Kenntnis der Sauropoden. *Eclogae Geologicae Helvetiae* 20: 444–470.

Hutchinson JR, Bates KT, Molnar JL, Allen V, Makovicky PJM. 2011. A computational analysis of limb and body dimensions in *Tyrannosaurus rex* with implications for locomotion, ontogeny, and growth. *PLoS ONE* 6: e26037.

Isaac JL. 2005. Potential causes and life-history consequences of sexual size dimorphism in mammals. *Mammal Review* 35: 101–115.

Janis CM, Carrano MT. 1992. Scaling of reproductive turnover in archosaurs and mammals: why are large terrestrial mammals so rare? *Annales Zoologici Fennici* 28: 201–216.

Jiawei Han, Micheline Kamber JP. 2011. *Data Mining – Concepts & Techniques*.

de Jong IML, Colbert MW, Witte F, Richardson MK. 2009. Polymorphism in developmental timing: Intraspecific heterochrony in a Lake Victoria cichlid. *Evolution and Development* 11: 625–635.

Kaliontzopoulou A, Carretero MA, Llorente GA. 2010. Intraspecific ecomorphological variation: Linear and geometric morphometrics reveal habitat-related patterns within *Podarcis bocagei* wall lizards. Journal of *Evolutionary Biology* 23: 1234–1244.

Karatzoglou A, Meyer D, Hornik K. 2006. Support Vector Algorithm in R. *Journal of Statistical Software* 15: 1–28.

Kass RE, Wasserman L. 1995. A reference Bayesian test for nested hypotheses and its relationship to the schwarz criterion. *Journal of the American Statistical Association* 90: 928–934.

Kassambara A. 2017. *Practical Guide to Cluster Analysis in R: Unsupervised Machine Learning*: Volume 1 (Multivariate Analysis).

Kaufman L, Rousseeuw PJ. 1990. *Finding Groups in Data*. Hoboken, NJ, USA, USA: John Wiley & Sons, Inc.

Kendall DG. 1977. The diffusion of shape. *Advances in Applied Probability* 9: 428–430.

Kendall DG. 1984. Shape Manifolds, Procrustean Metrics, and Complex Projective Spaces. *Bulletin of the London Mathematical Society* 16: 81–121.

Kilbourne BM, Makovicky PJM. 2010. Limb bone allometry during postnatal ontogeny in non-avian dinosaurs. *Journal of Anatomy* 217: 135–52.

Klein N, Christian A, Sander PM. 2012. Histology shows that elongated neck ribs in sauropod dinosaurs are ossified tendons. *Biology Letters*. 8: 1032-1035.

Klein N, Sander PM. 2008. Ontogenetic stages in the long bone histology of sauropod dinosaurs. *Paleobiology* 34: 247–263.

Klingenberg CP. 1996. Multivariate allometry. *Advances in Morphometrics* 284: 23–49.

Knaus J. 2015. snowfall: Easier cluster computing (based on snow).. R package version 1.84-6.1. https://CRAN.R-project.org/package=snowfall.

Knerr S, Personnaz L, Dreyfus G. 1990. Single-layer learning revisited: a stepwise procedure for building and training a neural network. *Neurocomputing*. Berlin: Springer, 41–50.

Kwok TH, Yeung KY, Wang CCL. 2014. Volumetric template fitting for human body reconstruction from incomplete data. *Journal of Manufacturing Systems* 33: 678–689.

Lachat E, Macher H, Landes T, Grussenmeyer P. 2015. Assessment and calibration of a RGB-D camera (Kinect v2 Sensor) towards a potential use for close-range 3D modeling. *Remote Sensing* 7: 13070–13097.

Lautenschlager S. 2016. Reconstructing the past: methods and techniques for the digital restoration of fossils. *Royal Society Open Science* 3: 160342.

Lautenschlager S. 2017. From bone to pixel—fossil restoration and reconstruction with digital techniques. *Geology Today* 33: 155–159.

Li C, Wang B. 2014. *Fisher Linear Discriminant Analysis*.

Lloyd SP. 1982. Least Squares Quantization in PCM. *IEEE Transactions on Information Theory* 28: 129–137.

Longrich NR, Field DJ. 2012. *Torosaurus* is not *Triceratops*: ontogeny in chasmosaurine ceratopsids as a case study in dinosaur taxonomy. *PLoS ONE* 7: e32623.

Lull RS. 1919. The sauropod dinosaur *Barosaurus* Marsh: redescription of the type specimens in the Peabody Museum, Yale University. *Memoirs of the Connecticut Academy of Arts and Sciences* 6: 1–42.

Malafaia E, Escaso F, Mocho P, Serrano-Martínez A, Torices A, Cachão M, Ortega F. 2017. Analysis of diversity, stratigraphic and geographical distribution of isolated theropod teeth from the Upper Jurassic of the Lusitanian Basin, Portugal. *Journal of Iberian Geology* 43: 257–291.

Mallison H. 2010. The Digital Plateosaurus I: Body Mass, Mass Distribution and Posture Assesed Using CAD and CAE on a Digitally Mounted Complete Skeleton. *Palaeontologia Electronica* 13: 1–26.

Mallison H. 2011. Digitizing Methods for Paleontology: Applications, Benefits and Limitations. In: Elewa A, ed. *Computational Paleontology*. Berling: Springer, 7–43.

Mallison H, Wings O. 2014. Photogrammetry in Paleontology - A Practical Guide. *Journal of Paleontological Techniques* 12: 1–13.

Mannion PD, Otero A. 2012. A reappraisal of the Late Cretaceous Argentinean sauropod dinosaur *Argyrosaurus superbus*, with a description of a new titanosaur genus. *Journal of Vertebrate Paleontology* 32: 614–638.

Marchal G, Lygren T. 2017. The Microsoft Kinect : validation of a robust and low-cost 3D scanner for biological science. Technical report.

Marcus LF, Bello E, García-Valdecasas A. 1993. *Contributions to morphometrics*.

Marcus E, Hingst-Zaher E, Zaher H. 2000. Application of landmark morphometrics to skulls representing the orders of living mammals. *Hystrix* 11: 27–47.

Martinelli AG, Forasiepi AM. 2004. Late Cretaceous vertebrates from bajo de Santa Rosa (Allen Formation), Río Negro province, Argentina, with the description of a new sauropod dinosaur (Titanosauridae). *Revista del Museo Argentino de Ciencias Naturales* 6: 257–305.

Marsh OC. 1878. Notice of New Dinosaurian Reptiles. *American Journal of Science* XV: 241–244.

Matthews NA. 2008. *Aerial and Close-Range Photogrammetric Technology: Providing Resource Documentation, Interpretation, and Preservation.* Technical Note 428. Denver, Colorado: U.S. Department of the Interior, Bureau of Land Management, National Operations Center.

McIntosh JS. 1990a. Sauropoda. In: Weishampel DB, Dodson P, Osmólska H, eds. *The Dinosauria*. University of California Press, 345–401.

McIntosh JS. 1990b. Species determination in sauropod dinosaurs with tentative suggestions for their classification. In: Carpenter K, Currie PJ, eds. *Dinosaur Systematics*. Cambridge: Cambridge University Press, 53–70.

McPherron SP, Gernat T, Hublin J jacques. 2009. Structured light scanning for high-resolution documentation of in situ archaeological finds. *Journal of Archaeological Science* 36: 19–24.

Mei L, Figl M, Darzi A, Rueckert D, Edwards P. 2008. Sample sufficiency and PCA dimension for statistical shape models. *Lecture Notes in Computer Science (including subseries Lecture Notes in Artificial Intelligence and Lecture Notes in Bioinformatics) 5305 LNCS*: 492–503.

Merilä J, Kruuk LEB, Sheldon BC. 2001. Cryptic evolution in a wild bird population. *Nature* 412: 76–79.

Meyer D, Dimitriadou E, Hornik K, Weingessel A, Leisch F. 2017. e1071: Misc Functions of the Department of Statistics, Probability. R package version 1.6-8. https://CRAN.R-project.org/package=e1071.

Michener CD, Sokal RR. 1957. A Quantitative Approach to a Problem in Classification. *Evolution* 11: 130.

Milligan GW. 1980. An examination of the effect of six types of error perturbation on fifteen clustering algorithms. *Psychometrika* 45: 325–342.

Milligan GW, Sokol LM. 1980. A Two-Stage Clustering Algorithm with Robust Recovery Characteristics. *Educational and Psychological Measurement* 40: 755–759.

Minka T. 1999. Bayesian linear regression. *Machine Learning* 631: 1–12.

Mitteroecker P. 2009. The developmental basis of variational modularity: Insights from quantitative genetics, morphometrics, and developmental biology. *Evolutionary Biology* 36: 377–385.

Mitteroecker P, Bookstein FL. 2011. Linear Discrimination, Ordination, and the Visualization of Selection Gradients in Modern Morphometrics. *Evolutionary Biology* 38: 100–114.

Mitteroecker P, Gunz P. 2009. Advances in Geometric Morphometrics. *Evolutionary Biology* 36: 235–247.

Mocho P, Escaso F, Marcos-Fernández F, Páramo A, Vidal D, Ortega F. 2018a. The morphological variability on titanosaur caudal series from Lo Hueco: taxonomic diversity, intra-specific variability or both? *XVI Annual Meeting of European Association of Vertebrate Paleontologists*. 126.

Mocho P, Pérez-García A, Martín-Jiménez M, Ortega F. 2018b. New remains from the Spanish Cenomanian shade light on the Gondwanan origin of European Early Cretaceous titanosaurs. *Cretaceous Research* 95: 164–190.

Mocho P, Royo-Torres R, Ortega F. 2014. Phylogenetic reassessment of *Lourinhasaurus alenquerensis*, a basal Macronaria (Sauropoda) from the Upper Jurassic of Portugal. *Zoological Journal of the Linnean Society* 170: 875–916.

Molnar JL, Diogo R, Hutchinson JR, Pierce SE. 2018. Evolution of Hindlimb Muscle Anatomy Across the Tetrapod Water-to-Land Transition, Including Comparisons With Forelimb Anatomy. *The Anatomical Record*: 1–43.

Molnar JL, Pierce SE, Hutchinson JR. 2012. Idealized landmark-based geometric reconstructions of poorly preserved fossil material: a case study of an early tetrapod vertebra. *Palaeontologia Electronica* 15: 1–18.

Morgan P. 2018. *Machine Learning Is Changing the Rules*.

Mosimann JE. 1970. Size allometry: Size and shape variables with characterizations of the lognormal and generalized gamma distributions. *Journal of the American Statistical Association* 65: 930–945.

Mosimann JE. 2014. Size and Shape Analysis. Wiley StatsRef: *Statistics Reference Online*. Chichester, UK: John Wiley & Sons, Ltd, .

Motani R, Amenta N, Wiley DF. 2005. Possibilities and Limitations of Three Dimensional Retrodeformation of a Trilobite and Plesiosaur Vertebrae. *PaleoBios* 25.

Motani R, Amenta N, Wiley DF. 2008. Possibilities and limitations of three dimensional retrodeformation of a trilobite and plesiosaur vertebrae. *PaleoBios* 25: 88.

Neustupa J, Škaloud P. 2007. Geometric morphometrics and qualitative patterns in the morphological variation of five species of *Micrasterias* (Zygnemophyceae, Viridiplantae). *Preslia* 79: 401–417.

Nopsca BF. 1915. Die dinosaurier der Siebenbürgischen landesteile Ungarns. *Ungarischen Geologischen Reichsanstalt* 23: 1–24.

Oba S, Sato M aki, Takemasa I, Monden M, Matsubara K ichi, Ishii S. 2003. A Bayesian missing value estimation method for gene expression profile data. *Bioinformatics* (Oxford, England) 19: 2088–2096.

Olori JC. 2013. Ontogenetic sequence reconstruction and sequence polymorphism in extinct taxa: an example using early tetrapods (Tetrapoda: Lepospondyli). *Paleobiology* 39: 400–428.

Organ CL, Brusatte SL, Stein KHW. 2009. Sauropod dinosaurs evolved moderately sized genomes unrelated to body size. *Proceedings. Biological sciences / The Royal Society* 276: 4303–8.

Otero A. 2010a. Comments on the taxonomic status of *Neuquensaurus robustus* (Huene) (Sauropoda, Titanosauria). X Congreso Argentino de Paleontología y Bioestratigrafía -VII Congreso Latinoamericano de Paleontología.A.

Otero A. 2010b. The appendicular skeleton of *Neuquensaurus*, a Late Cretaceous saltasaurine sauropod from Patagonia, Argentina. *Acta Palaeontologica Polonica* 55: 399–426.

Owen R. 1861. *A Monograph of the Fossil Reptilia of the Liassic Formations*. London: Palaeontographical Society.

Pal M. 2008. *Multiclass Approaches for Support Vector Machine Based Land Cover Classification*.

Páramo A, Mocho P, Marcos-Fernández F, Ortega F, Sanz JL. 2017. 3D Geometric Morphometrics on the Hind Limb of the Titanosaurs from Lo Hueco: Dwarf taxa or Small Individuals? *15th Annual Meeting of the European Association of Vertebrate Paleontologists*.

Páramo A, Mocho P, Ortega F, Sanz JL. 2018. Intraspecific variability in and its effects on systematic assessment of the titanosaurs from Lo Hueco (Late Cretaceous. Cuenca, Spain). *XVI Annual Meeting of European Association of Vertebrate Paleontologists*. 147.

Páramo A, Ortega F, Escaso F, Narváez I, Sanz JL. 2014. Ejemplares juveniles de titanosaurio (Sauropoda) del yacimiento de Lo Hueco (Fuentes, Cuenca). In: Royo-Torres, R.; Verdú, F.J.; Alcalá, L. (coord.). *XXX Jornadas de Paleontología de la Sociedad Española de Paleontología. ¡Fundamental!* 24: 149–151.

Pavlidis G, Koutsoudis A, Arnaoutoglou F, Tsioukas V, Chamzas C. 2007. Methods for 3D digitization of Cultural Heritage. *Journal of Cultural Heritage* 8: 93–98.

Perez SI, Bernal V, Gonzalez PN. 2006. Differences between sliding semi-landmark methods in geometric morphometrics, with an application to human craniofacial and dental variation. *Journal of Anatomy* 208: 769–784.

Pieraccini M, Guidi G, Atzeni C. 2001. 3D digitizing of cultural heritage. *Journal of Cultural Heritage* 2: 63–70.

Pöhlmann STL, Harkness EF, Taylor CJ, Astley SM. 2016. Evaluation of Kinect 3D Sensor for Healthcare Imaging. *Journal of Medical and Biological Engineering* 36: 857–870.

Porter WR, Sedlmayr JC, Witmer LM. 2016. Vascular patterns in the heads of crocodilians: blood vessels and sites of thermal exchange. *Journal of Anatomy* 229: 800–824.

Powell JE. 2003. Revision of South American titanosaurid dinosaurs: Palaeobiological, palaeobiogeographical and phylogenetic aspects (TH Rich, K Dimmack, and JR Macdonald, Eds.). *Records of the Queen Victoria Museum* 111: 1–179.

de Queiroz K. 1985. The Ontogenetic Method for Determining Character Polarity and its Relevance to Phylogenetic Systematics. *Systematic Zoology* 34: 280.

de Queiroz K, Good DA. 1997. Phenetic Clustering in Biology: A Critique. *The Quarterly Review of Biology* 72: 3.

Real R, Vargas JM. 1996. The Probabilistic Basis of Jaccard's Index of Similarity. *Systematic Biology* 45: 380.

de Ricqlès AJ. 2001. Vertebrate palaeohistology: Past and future. *Comptes Rendus Palevol* 10: 509–515.

Rieppel O. 2003. Semaphoronts, cladograms and the roots of total evidence. Biological *Journal of the Linnean Society* 80: 167–186.

Rocchini C, Cignoni P, Montani C, Pingi P, Scopigno R. 2001. A low cost 3D scanner based on structured light. *Eurographics Symposium on Geometry Processing* 20: 1–10.

Rogers SW. 1998. Exploring Dinosaur Neuropaleobiology : Viewpoint Computed Tomography Scanning and Analysis of an Allosaurus fragilis Endocast. *Neuron* 21: 673–679.

Rohlf FJ. 1993. Relative warp analysis and an example of its application to mosquito wings. *Contributions to morphometrics*. 8:129-132.

Rohlf FJ. 1998. On Applications of Geometric Morphometrics to Studies of Ontogeny and Phylogeny. *Systematic Biology* 47: 147–158.

Rohlf FJ. 1999. Shape statistics: Procrustes superimpositions and tangent spaces. *Journal of Classification* 16: 197–223.

Rohlf FJ. 2000. Statistical power comparisons among alternative morphometric methods. American *Journal of Physical Anthropology*. 111: 463-478.

Rohlf FJ. 2003. Bias and error in estimates of mean shape in geometric morphometrics. *Journal of Human Evolution* 44: 665–683.

Rohlf FJ, Bookstein FL. 2003. Computing the uniform component of shape variation. *Systematic Biology*.

Rohlf FJ, Slice D. 1990. Extensions of the Procrustes Method for the Optimal Superimposition of Landmarks. *Systematic Zoology*. 39: 40-59.

Rokach L, Maimon O. 2007. Clustering methods. In: Rokach L, Maimon O, eds. Series in Machine Perception and Artificial Intelligence. *Data Mining with Decision Trees*. World Scientific, 321–352. Rousseeuw PJ. 1987. Silhouettes: A graphical aid to the interpretation and validation of cluster analysis. Journal of Computational and Applied Mathematics 20: 53–65.

Royston P. 2004. Multiple imputation of missing values. *The Stata Journal*. 4:227-241.

RStudio Team. 2015. RStudio: Integrated Development for R. RStudio, Inc., Boston, MA URL http://www.rstudio.com/.

Rueden CT, Schindelin J, Hiner MC, DeZonia BE, Walter AE, Eliceiri KW. 2017. ImageJ2: ImageJ for the next generation of scientific image data.

Salgado JL, Coria RA. 1993. El género *Aelosaurus* (Sauropoda, Titanosauridae) en la Formación Allen (Campaniano-Maastrichtiano) de la Provincia de Río Negro, Argentina. *Ameghiniana* 30: 119–128.

Salgado JL, Coria RA, Calvo JO. 1997a. Presencia del género *Aeolosaurus* (Sauropoda, Titanosauridae) en la Formación Los Alamitos, Cretácico Superior de la Provincia de Río Negro, Argentina. *Geociencias* 2: 44–49.

Salgado JL, Azpilicueta C. 2000. Un nuevo saltasaurino (Sauropoda, Titanosauridae) de la provincia de Río Negro (Formación Allen, Cretácico Superior), Patagonia, Argentina. *Ameghiniana* 37: 259–264.

Salgado JL, Coria RA, Calvo JO. 1997b. Evolution of the titanosaurid sauropods I: Phylogenetic analysis based on the postcranial evidence. *Ameghiniana* 34: 3–32.

Sander PM, Klein N. 2005. Developmental Plasticity in the Life History of a Prosauropod Dinosaur. *Science* 310: 1800–1802.

Sander PM, Klein N, Buffetaut É, Cuny G, Suteethorn V, Le Loeuff J. 2004. Adaptive radiation in sauropod dinosaurs: bone histology indicates rapid evolution of giant body size through acceleration. *Organisms Diversity & Evolution* 4: 165–173.

Sanz JL, Powell JE, Le Loeuff J, Martínez RN, Pereda Suberbiola X. 1999. Sauropod remains from the Upper Cretaceous of Laño (north central Spain). Titanosaur phylogenetic relationships. *Estudios del Museo de Ciencias Naturales de Alava* 14: 235–255.

Schæfer K, Mitteroecker P, Gunz P, Bernhard M, Bookstein FL. 2004. Craniofacial sexual dimorphism patterns and allometry among extant hominids. *Annals of anatomy = Anatomischer Anzeiger* 186: 471–8.

Schafer JL. 1999. Multiple imputation: A primer. *Statistical Methods in Medical Research* 8: 3–15.

Schafer JL, Graham JW. 2002. Missing data: Our view of the state of the art. *Psychological Methods*. 7: 147-177.

Schafer JL, Olsen MK. 1998. Multiple imputation for multivariate missing-data problems: A data analyst's perspective. *Multivariate Behavioral Research*. 33: 545-571.

Schindelin J, Rueden CT, Hiner MC, Eliceiri KW. 2015. The ImageJ ecosystem: An open platform for biomedical image analysis. *Molecular Reproduction and Development* 82: 518–529.

Schlager S. 2013. Soft-tissue reconstruction of the human nose: Population differences and sexual dimorphism. Unpublished thesis project, Albert-Ludwigs Universität Freiburg.

Schlager S. 2016. mesheR: Meshing Operations on Triangular Meshes. R package version 0.4.160301.

Schlager S. 2017. Morpho and Rvcg – Shape Analysis in R. In: Zheng G, Li S, Szekely G, eds. *Statistical Shape and Deformation Analysis*. Elsevier, 217–256.

Schlager S, Profico A, Vincenzo F Di, Manzi G. 2018. Retrodeformation of fossil specimens based on 3D bilateral semi-landmarks: Implementation in the R package "Morpho". *PLoS ONE* 13.

Schwarz D, Böhm N. 2012. A morphometric approach to the specific separation of the humeri and femora of *Dicraeosaurus* from the Late Jurassic of Tendaguru, Tanzania. *Acta Palaeontologica Polonica* 59: 81–98.

Schwarz D, Vontobel P, Lehmann EH, Meyer CA, Bongartz G. 2005. Neutron tomography of internal structures of vertebrate remains: a comparison with X-ray computed tomography. *Palaeontologia Electronica* 8: 1–11.

Schwarz D, Wings O, Meyer CA. 2007. Super sizing the giants: first cartilage preservation at a sauropod dinosaur limb joint. *Journal of the Geological Society* 164: 61–65.

Scott Shaobing Chen, Gopalakrishnan PS. 2018. Clustering via the Bayesian information criterion with applications in speech recognition. Proceedings of the 1998 *IEEE International Conference on Acoustics, Speech and Signal Processing, ICASSP '98* (Cat. No.98CH36181). IEEE, 645–648.

Selim SZ, Ismail MA. 1984. K-Means-Type Algorithms: A Generalized Convergence Theorem and Characterization of Local Optimality. *IEEE Transactions on Pattern Analysis and Machine Intelligence* 6: 81–87.

Serrano-Martínez A, Ortega F, Sciscio L, Tent-Manclús JE, Fierro Bandera I, Knoll F. 2015. New theropod remains from the Tiourarén Formation (?Middle Jurassic, Niger) and their bearing on the dental evolution in basal tetanurans. *Proceedings of the Geologists' Association* 126: 107–118.

Serrano-Martínez A, Vidal D, Sciscio L, Ortega F, Knoll F. 2016. Isolated theropod teeth from the Middle Jurassic of Niger and the early dental evolution of Spinosauridae. *Acta Palaeontologica Polonica* 61: 403–415.

Sharma PP, Clouse RM, Wheeler WC. 2017. Hennig's semaphoront concept and the use of ontogenetic stages in phylogenetic reconstruction. *Cladistics* 33: 93–108.

Sheets HD, Covino KM, Panasiewicz JM, Morris SR. 2006. Comparison of geometric morphometric outline methods in the discrimination of age-related differences in feather shape. *Frontiers in Zoology* 3: 15.

Sievwright H, MacLeod N. 2012. Eigensurface analysis, ecology, and modelling of morphological adaptation in the falconiform humerus (Falconiformes: Aves). *Zoological Journal of the Linnean Society* 165: 390–419.

Simón E, Salgado JL, Calvo JO. 2018. A New Titanosaur Sauropod from the Upper Cretaceous of Patagonia, Neuquén Province, Argentina. *Ameghiniana* 55: 1–29.

Slice DE. 2001. Landmark Coordinates Aligned by Procrustes Analysis Do Not Lie in Kendall's Shape Space. *Systematic Biology* 50: 141–149.

Smith JB, Vann DR, Dodson P. 2005. Dental morphology and variation in theropod dinosaurs: Implications for the taxonomic identification of isolated teeth. *The Anatomical Record Part A: Discoveries in Molecular, Cellular, and Evolutionary Biology* 285A: 699–736.

Sokal RR. 1961. Distance as a Measure of Taxonomic Similarity. *Systematic Zoology* 10: 70.

Sokal RR. 1963. The Principles and Practice of Numerical Taxonomy. *Taxon* 12: 190.

Sokal RR, Michener CD. 1958. A statistical method for evaluating systematic relationships. *University of Kansas Science Bulletin* 38: 1409–1438.

Sokal RR, Rohlf FJ. 1987. *Introduction to bioestatistics*. W. H. Freeman and Company.

Souter T, Cornette R, Pedraza J, Hutchinson JR, Baylac M. 2010. Two applications of 3D semi-landmark morphometrics implying different template designs: the theropod pelvis and the shrew skull. *Comptes Rendus Palevol* 9: 411–422.

Staedler YM, Masson D, Schönenberger J. 2013. Plant Tissues in 3D via X-Ray Tomography: Simple Contrasting Methods Allow High Resolution Imaging. *PLoS ONE* 8.

Stegmann MB, Gomez DD. 2002. A brief introduction to statistical shape analysis. *Informatics and Mathematical Modelling*: 1–15.

Stein KHW. 2010. Long bone histology of basalmost and derived Sauropodomorpha : the convergence of fibrolamellar bone and the evolution of giantism and nanism. Unpublished thesis project, Universität Bonn.

Stevens KA. 2013. The Articulation of Sauropod Necks: Methodology and Mythology. *PLoS ONE* 8: e78572.

Stevens KA, Parrish JM. 2005. Digital Reconstructions of Sauropod Dinosaurs and Implications for Feeding. *The Sauropods: Evolution and Paleobiology*. University of California Press, 178–200.

Strauss RE, Atanassov MN. 2006. Determining best complete subsets of specimens and characters for multivariate morphometric studies in the presence of large amounts of missing data. *Biological Journal of the Linnean Society* 88: 309–328.

Sutton MD. 2008. Tomographic techniques for the study of exceptionally preserved fossils. *Proceedings of the Royal Society B: Biological Sciences* 275: 1587–1593.

Sutton MD, Briggs DEG, Siveter DJ, Siveter DJ. 2001. Methodologies for the Visualization and Reconstruction of Three-Dimensional Fossils from the Silurian Herefordshire Lagerstätte. *Palaeontologia Electronica* 4: 1–17.

Sutton MD, Rahman I, Garwood R. 2014. *Techniques for Virtual Palaeontology*. John Wiley & Sons.

Symons MJ. 1981. Clustering Criteria and Multivariate Normal Mixtures. *Biometrics* 37: 35–43.

Tallman M, Amenta N, Delson E, Frost SR, Ghosh D, Klukkert ZS, Morrow A, Sawyer GJ. 2014. Evaluation of a New Method of Fossil Retrodeformation by Algorithmic Symmetrization: Crania of Papionins (Primates, Cercopithecidae) as a Test Case. *PLoS ONE* 9: e100833.

Taylor MP. 2015. Almost all known sauropod necks are incomplete and distorted. *PeerJ* Not Peer R: e1418v1.

The R Core Team. 2016. A language and environment for statistical computing. R Foundation for

Statistical Computing, Vienna, Austria. URL https://www.R-project.org/.

Třebický V, Fialová J, Kleisner K, Havlíček J. 2016. Focal length affects depicted shape and perception of facial images. *PLoS ONE* 11: 1–14.

Tschopp E, Dzemski G. 2013. Retrodeformation as a test for the validity of phylogenetic characters: an example from diplodocid sauropod vertebrae. *Paleontologia Electronica* 16: 1–23.

Tschopp E, Mateus O, Benson RBJ. 2015. A specimen-level phylogenetic analysis and taxonomic revision of Diplodocidae (Dinosauria, Sauropoda). *PeerJ* 3: e857.

Ullmann PV., Bonnan MF, Lacovara KJ. 2017. Characterizing the Evolution of Wide-Gauge Features in Stylopodial Limb Elements of Titanosauriform Sauropods via Geometric Morphometrics. *The Anatomical Record* 300: 1618–1635.

Upchurch P. 1995. The evolutionary history of sauropod dinosaurs. *Philosophical Transactions of the Royal Society B: Biological Sciences* 349: 365–390.

Upchurch P, Barrett PM, Dodson P. 2004. Sauropoda. In: Weishampel DB, Dodson P, Osmólska H, eds. *The Dinosauria*. Berkeley: University of California Press, 259–322.

Vapnik VN. 1995. *The Nature of Statistical Learning Theory*. New York, NY: Springer.

Vidal D, Díez Díaz V. 2017. Reconstructing hypothetical sauropod tails by means of 3D digitization: *Lirainosaurus* astibiae as case study. *Journal of Iberian Geology* 43: 293–305.

Vidal D, Sanz JL, Mocho P, Páramo A, Escaso F, Marcos-Fernández F, Ortega F. 2017. The titanosaur tails from Lo Hueco (Cuenca, Spain): Four different ways to shake? In: Farke AA, Mackenzie SA, Miller Camp J, eds. *77th Annual Meeting of the Society of Vertebrate Paleontology*. Calgary, 208.

Vila B, Galobart À, Canudo JI, Le Loeuff J, Dinarès-Turell J, Riera V, Oms O, Tortosa T, Gaete R. 2012. The diversity of sauropod dinosaurs and their first taxonomic succession from the latest Cretaceous of southwestern Europe: Clues to demise and extinction. *Palaeogeography, Palaeoclimatology, Palaeoecology* 350–352: 19–38.

Vitek NS, Manz CL, Gao T, Bloch JI, Strait SG, Boyer DM. 2017. Semi-supervised determination of pseudocryptic morphotypes using observer-free characterizations of anatomical alignment and shape. *Ecology and Evolution* 7: 5041–5055.

Volinsky CT, Raftery AE. 1998. Bayesian Information Criterion for Censored Survival. *Biometrics* 56: 256–262.

Ward Jr. JH. 1963. Hierarchical Grouping to Optimize an Objective Function. *Journal of the American Statistical Association* 58: 236–244.

Warton DI, Wright IJ, Falster DS. 2006. Bivariate line-fitting methods for allometry. *Biological Reviews* 81: 259–291.

White MA, Falkingham PL, Cook AG, Hocknull SA, Elliott DA. 2013. Morphological comparisons of metacarpal I for Australovenator wintonensis and Rapator ornitholestoides: implications for their taxonomic relationships. *Alcheringa* 37: 435–441.

Wiley DF, Amenta N, Alcantara DA, Ghosh D, Kil YJ, Delson E, Harcourt-Smith W, Rohlf FJ, John K St., Hamann B, St John K, Hamann B, John K St., Hamann B. 2005. *Evolutionary Morphing. Proceedings of IEEE Visualization 2005*. Minneapolis, 1–8.

Wilhite RD. 2003a. Biomechanical Reconstruction of the Appendicular Skeleton in Three North American Jurassic Sauropods. Unpublished thesis project, Louisiana State University.

Wilhite RD. 2003b. Digitizing Large Fossil Skeletal Elements for Three-Dimensional Applications. *Palaeontologia Electronica* 5: 10pp.

Wilhite RD. 2005. Variation in the Appendicular Skeleton of North American Sauropod Dinosaurs: Taxonomic Implications. In: Tidwell V, Carpenter K, eds. *Thunder-Lizards: The Sauropodomorph Dinosaurs*. Indiana University Press, 268–301.

Wilson JA. 2002. Sauropod dinosaur phylogeny: critique and cladistic analysis. *Zoological Journal of the Linnean Society* 136: 215–275.

Wilson JA, Barrett PM, Carrano MT. 2011. An associated partial skeleton of *Jainosaurus* cf. *septentrionalis* (Dinosauria: Sauropoda) from the Late Cretaceous of Chhota Simla, Central India. *Palaeontology* 54: 981–998.

Wilson JA, Sereno PC. 1998. Early Evolution and High-level Phylogeny of Sauropod Dinosaurs. *Journal of Vertebrate Paleontology* 18: 1–68.

Wilson JA, Upchurch P. 2003. A revision of *Titanosaurus* Lydekker (Dinosauria - Sauropoda), the first dinosaur genus with a 'Gondwanan' distribution. *Journal of Systematic Palaeontology* 1: 125–160.

Wu Y, Wipf D, Yun JM. 2015. Understanding and Evaluating Sparse Linear Discriminant Analysis. *Artificial Intelligence and Statistics* 2015 38: 1070–1078.

Zeileis A, Kleiber C, Jackman S. 2007. Regression models for count data in R. Research Report Series / Department of Statistics and Mathematics 53.

Zelditch ML, Swiderski DL, Sheets HD. 2012a. *Geometric Morphometrics for Biologists*. Elsevier.

Zelditch ML, Swiderski DL, Sheets HD. 2012b. Obtaining Landmarks and Semilandmarks. *Geometric Morphometrics for Biologists: A Primer*. Academic Press, 1–31.

Zhang B, Srihari SN. 2003. Binary Vector Dissimilarity Measures for Handwriting Identification. In: Kanungo T, Barney Smith EH, Hu J, Kantor PB, eds. *Proceedings of SPIE - The International Society for Optical Engineering*. 28–38.

Zollikofer CPE, Ponce de León MS. 2006. *Virtual Reconstruction: A Primer in Computer-Assisted Paleontology and Biomedicine*. Wiley and Sons.

CHAPTER IV.I:

Multivariate analysis of the femoral variability of the titanosaur sauropods from Lo Hueco (Cuenca, Spain): Insights in the Late Cretaceous Ibero-Armorican sauropod diversity

IV.I. ABSTRACT

The Ibero-Armorican domain presents a wide sample of sauropod isolated elements in several fossils sites of Campanian-Maastrichtian age. The sauropod femur lacks many distinctive features for taxonomical assessment. This problematic is relevant for analysis of the Late Cretaceous titanosaur faunal turn-over, as part of the Campanian titanosaur faunas are replaced by several indeterminate titanosaurian forms and hadrosaurids. The Campanian-Maastrichtian Konzentrat-Lagerstätte of Lo Hueco (Spain) have yielded a large amount of isolated titanosaur appendicular elements. There is also a visible variability among these elements. In this study we employed a set of unsupervised clustering and discrimination techniques with the sample of femora from Lo Hueco site. The base for this study is a recent proposal of several measurements (morphometrics variables) used for taxonomic assessment of the Ibero-Armorican Maastrichtian indeterminate titanosaurian forms as it was based on isolated femora. This study includes other neosauropods taxa as reference for the statistical framework with use of advanced machine learning techniques. There is also a description of the possible variability in the femora of the titanosaurs of Lo Hueco.

The results shows two probable major groups of femora in the sample from Lo Hueco. One form, Morphotype I, is closer to the exclusive form *Lohuecotitan pandafilandi*, while the other, Morphotype II, could be a potentially second exclusive form from Lo Hueco. While it is possible that other titanosaur taxa are present in the sample, no other major group was detected and any of the sampled specimens from Lo Hueco resemble other titanosaur forms described in the Campanian-Maastrichtian of the Ibero-Armorican domain.

The analysis of the neosauropods sample shows the major evolutionary trends of Titanosauriformes, including the acquisition of the wide-gauge stance. The results show some differences among the morphospaces of titanosauriformes for the first time, though there is still overlapping between the different genera. The use of advanced machine learnings techniques others than Discriminant Function Analysis shows improvements in classification with the overlapping of morphospaces. Despite data imputation and morphological similarities, Support Vector Machines shows accurate results and can be employed for taxonomical assessment of sauropod isolated appendicular elements.

IV.I.1 INTRODUCTION

Titanosaurs were a diverse and widespread group of sauropods that reached all emerged land masses and its record spans from the early Cretaceous (Barremian) up to the Cretaceous-Paleogene boundary (e.g. Upchurch, Barrett, & Dodson, 2004; Cerda *et al.*, 2012; Gorscak & O'Connor, 2016). This group achieved an important peak of diversity, especially well-recorded on South America and Europe, right before the Cretaceous-Paleogene extinction event (Vila *et al.*, 2012; Le Loeuff, 2012; Díez Díaz, Tortosa, & Le Loeuff, 2013b; Vieira *et al.*, 2014). The members of this group acquired a characteristic and a rather conservative bauplan despite its many adaptations to different locomotion types on a multi-tonned body (e.g., Carrano, 1998; Wilson & Carrano, 1999; Upchurch *et al.*, 2004; González-Riga *et al.*, 2016). The study of the sauropod appendicular bones is an important source of information for the comprehension of their paleobiology and systematics. The morphology of the hindlimb in titanosaurian sauropods develops several adaptations to the locomotion known as "wide-gauge" (Salgado, Coria, & Calvo, 1997a; Wilson & Carrano, 1999; Wilson, 2002; Upchurch *et al.*, 2004a; Carballido *et al.*, 2011b; D'Emic, 2012), as well as other specializations within derived titanosaurian clades (Wilson & Carrano, 1999; Powell, 2003; González Riga *et al.*, 2016; Ullmann, Bonnan, & Lacovara, 2017). Despite several unique features within Titanosauria, recent studies in the morphology of the titanosaur femur suggest that it is not enough informative for taxonomic determination at genus or species level (see Powell, 2003; Wilson & Upchurch, 2003; Vila *et al.*, 2012).

In the past, some titanosaurian species have been differentiated due its variation on the appendicular bones based mostly on proportion changes within the sample. A detailed revision of these specimens have rendered those species invalid as they lack unique features which cannot separate them from other taxa of the same genera e.g. *Nequensaurus australis* and the lack of features to differentiate "*Neuquensaurus robustus*", *Antarctosaurus wichmanniannus* and the dubious *Antarctosaurus? giganteus* (Powell 2003). The presence of "intermediate" forms of titanosaurs between gondwanan groups and the ones described in the European record have been described in the past e.g. "*Iuticosaurus valdensis*" (= "*Titanosaurus valdensis*", Huene, 1929) and a second morphotype ("*Titanosaurus* sp. B") from the material described by Lydekker (Lydekker, 1888; Naish & Martill, 2001; Wilson & Upchurch, 2003). There is also some material reassessed from "*Titanosaurus indicus*" and a second morphotype separated from the referred material of *Hypsaelosaurus* (Lapparent, 1947; Wilson & Upchurch, 2003). It is important to note here the case of "*Titanosaurus*" genus. Wilson & Upchurch,(2003) concluded that some material could be attributed to new forms such as *Isisaurus colberti* or already known taxa (e.g. *Magyarosaurus* spp. as per Huene, 1932, and *Neuquensaurus* spp. as per Powell, 2003). While the remaining unattributed material after that revision of "*Titanosaurus* spp." are now regarded as invalid unkown taxa (see Lydekker, 1893; Gilmore, 1922; Huene, 1929; Janensch, 1929, with more recent opinions from Le Loeuff, 1993; Powell, 2003; Wilson & Upchurch, 2003). One of the aspects that this revision emphasizes is the lack of taxonomic value of some of the metric or observations of the different proportions. The robustness of the elements as well as ratios between some of the measurements (e.g. the eccentricity of the shaft) are regarded as non-characteristic within Titanosauria, while others are regarded as non-informative at species level. Today we know that some of the past comparisons made with these early measurements may be more widespread than in a single taxa or genus, including features heterogeneously distributed within Sauropoda (Wilson & Upchurch, 2003; see also continous character comments in Mannion *et al.*, 2013). In general, the relative

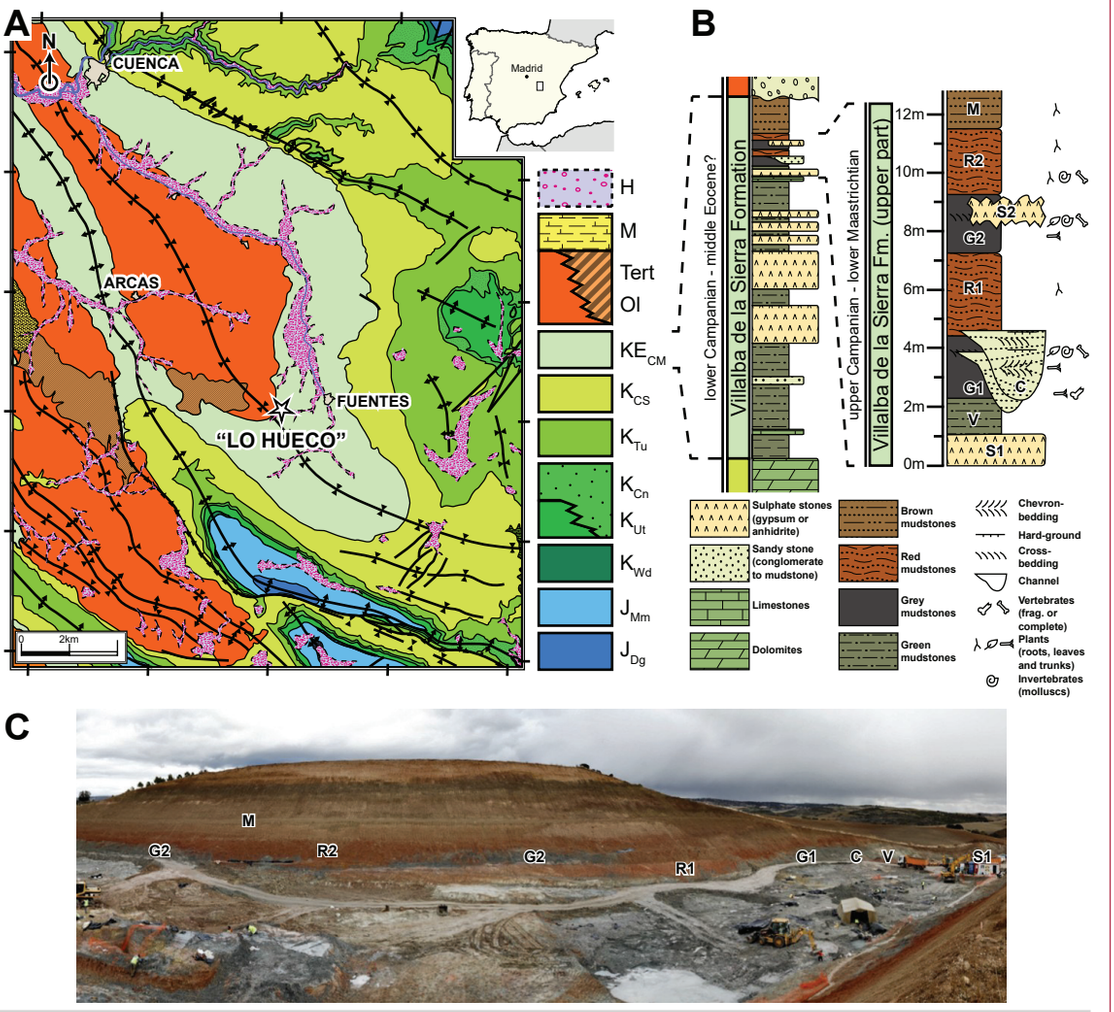

Fig.IV.I.1. Lo Hueco fossil site location and stratigraphy. (A) Geological map of Cuenca (Spain). (B) General stratigraphic column of the Villalba de la Sierra Formation and the Lo Hueco fossil site. (C) Photography of the Lo Hueco site during the 2007 campaign. Labels indicates the levels of the stratigraphic column.

gracility or robustness in qualitative sense, are not useful for taxonomic definition while useful to some extent in the respective description.

Some ratios are coded into categorical characters used in the majority of modern day systematic studies of sauropod dinosaurs (Wilson, 2002; see Upchurch *et al.*, 2004a; Whitlock, 2011; Carballido *et al.*, 2011b; D'Emic, 2012; Mannion *et al.*, 2013; Mocho, Royo-Torres, & Ortega, 2014; Tschopp, Mateus, & Benson, 2015; Gorscak *et al.*, 2017; González Riga *et al.*, 2018). The information given by appendicular element metrics can be important but its relevance on the assessment at different taxonomical levels is not clear.

The record of the titanosaur sauropods in the Maastrichtian-Campanian (Late Cretaceous)

of the Ibero-Armorican domain is relatively abundant and diverse, including many axial and appendicular specimens (coming from partial skeleton as well as isolated specimens). Four titanosaurian taxa have been described: the French *Ampelosaurus atacis* (Bellevue site; Le Loeuff, 1995, 2005a) and *Atsinganosaurus velauciensis* (Velaux-La Bastide Neuve site; Garcia *et al.*, 2010), and the Spanish forms *Lirainosaurus astibaie* (Laño site; Sanz *et al.*, 1999) and *Lohuecotitan pandafilandi* (Lo Hueco site; Díez Díaz *et al.*, 2016). Nevertheless, numerous isolated elements were also collected in this territory (Lapparent, 1947; Casanovas-Cladellas, 1992; Le Loeuff, 1993, 1998; Casanovas-Cladellas *et al.*, 1995; Sanz *et al.*, 1999; Canudo, 2001; López-Martínez, 2001; Ortega & Pérez-García, 2009; Company, Suberbiola, & Ruiz-Omeñaca, 2009; Tortosa *et al.*, 2012; Vila *et al.*, 2012; Csiki *et al.*, 2015; Ortega *et al.*, 2015; Pereda Suberbiola *et al.*, 2015; Perez-Garcia, Gasco, & Ortega, 2017; Martín Jimenez *et al.*, 2017; Pérez-García *et al.*, 2018; Díez Díaz *et al.*, 2018b). Many of these bones come from the pectoral girdle, pelvic girdle, forelimb and hindlimb region of the skeleton. In most of the cases, its taxonomic relationships are difficult to establish due the lack of diagnostic features at a generic and species level (Casanovas-Cladellas *et al.*, 1995; Canudo *et al.*, 2009; Vila *et al.*, 2012; Martín Jimenez *et al.*, 2017; Mocho *et al.*, 2017; Pérez-García *et al.*, 2018). The detailed analyses of some of these bones have been used to propose the presence of undescribed titanosaur taxa different from those described, and consequently, a possible higher diversity than reported only by the described taxa (Tortosa *et al.*, 2012; Vila *et al.*, 2012).

In 2007 during the construction of the high-speed train railway Madrid-Levante near the locality of Fuentes (Cuenca, Spain), the Lo Hueco fossil site was discovered (Fig.IV.I.1). The partial excavation of a hill exposed a large portion of fossiliferous levels that yielded an abundant quantity of vertebrate fossil remains (Ortega *et al.,* 2015). Almost one half of the fossil collected can be attributed to titanosaurs. Despite almost 20 partially articulated titanosaur skeletons were recovered, several other remains correspond to isolated bones. Previous attempts to study the diversity of some of these isolated bones point out the presence of at least two main morphotypes based on teeth (Díez Díaz, Ortega, & Sanz, 2014), skull remains (Knoll *et al.*, 2013b,a) and appendicular bones according to preliminary studies (Páramo *et al.*, 2014; Páramo, Ortega, & Sanz, 2015; Páramo *et al.*, 2016; Díez Díaz *et al.*, 2016; this project). Recent preliminary studies of caudal and pelvic material insight of up to four possible different morphotypes (Mocho *et al.*, 2016b, 2018; Vidal *et al.*, 2017). Majority of these studies tend to differentiate the two main morphotypes in a robust form and a gracile form, both of them probably unique from Lo Hueco fossil site (Díez-Díaz *et al* 2016, Vidal *et al* 2016). One of these morphotypes should be attributed to the recently described titanosaur species from Lo Hueco, *Lohuecotitan pandafilandi* (Díez-Díaz *et al.*, 2016). The taxonomic assessment of the fossil record of Lo Hueco is still under study.

In addition, the systematics of the European titanosaur is still in debate (e.g. Díez Díaz *et al.*, 2016, 2018a; Sallam *et al.*, 2018). The discovery of this fossil site is an important opportunity to understand the intra- and interspecific variability of the European titanosaurs and the proposed high diversity of forms in the Late Cretaceous. The study of intraspecific shape variation in the titanosaur skeleton permit us to recognize the differences in morphological features relatable to presence of new undescribed taxa or else referable to already known taxa. This will be key on the establishment of a more robust systematic context for the European titanosaurs, and valuable to understand the evolutionary history of this group, as well as, the European faunal composition during the Late Cretaceous. Previous assessment of isolated titanosaur appendicular specimens in the Ibero-Armorican domain highlights a high diversity of titanosaur forms with paleobiogeographical and paleoecological implications during the Late Cretaceous

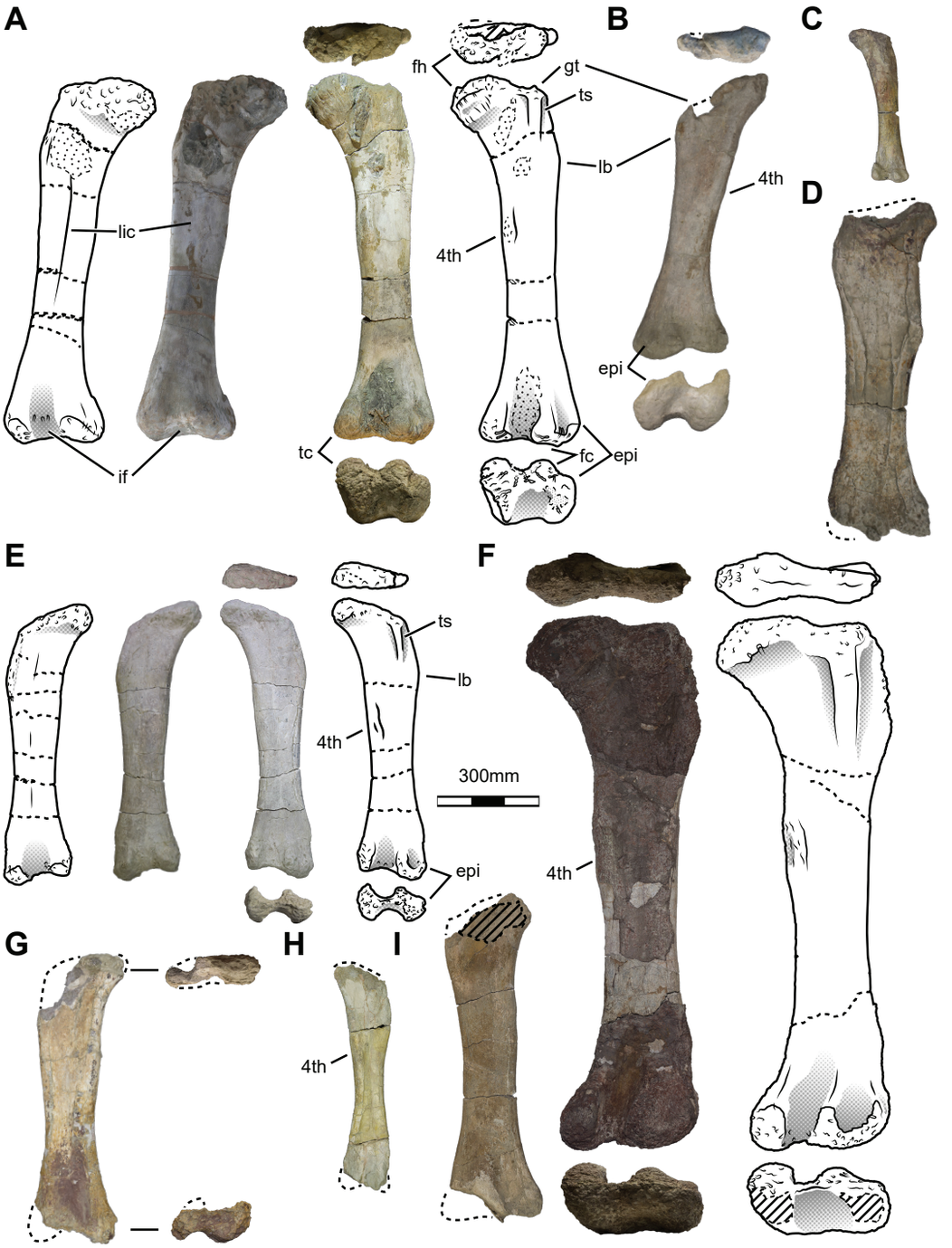

Fig.IV.1.2. Femoral sample of Lo Hueco titanosaurs. (A) HUE-3108 in anterior, dorsal, posterior and ventral face. (B) HUE-2338 in posterior face. (C) HUE-2636 posterior face. (D) HUE-1187 posterior face. (E) HUE-1319 in anterior, dorsal, posterior and ventral face. (F) HUE-594 in proximal, posterior and distal face. (G) HUE-3583 posterior face. (H) HUE-10007 posterior face. (I) HUE-1508 posterior face.

faunal turnover (Vila *et al.*, 2012; Vila, Sellés, & Brusatte, 2016; Le Loeuff, 2012; Csiki *et al.*, 2015; Pereda Suberbiola *et al.*, 2015). The assessment of titanosaur morphological diversity can also help to understand the Cretaceous-Paleogene extinction event and the impact on a rather diverse European titanosaur biota (see López-Martínez, 2001; Vila *et al.*, 2012; Le Loeuff, 2012).

The first studies on sauropod bones provided measurements on interesting features that helps describe these elements, especially for appendicular bones, like the total length of the elements, the expansion of the femoral or humeral head. Other measurements help us visualize and give an idea of the position of crests or trochanters (e.g. the position of the fourth trochanter respective to the proximal end). While other refer to ratios such as robustness of the elements or relationships between length of the different elements of the forelimb and hindlimb. Most of these measurements were supportive in descriptive comparisons between the early sauropod discoveries (Lydekker, 1893; Riggs, 1901, 1903; Broom, 1904; Huene, 1915, 1929; Huene & Matley, 1923; Janensch, 1929; Marsh, 1986), generally scarce and limited in information at the time (Wilson & Upchurch, 2003). But some of these relationships between measurements were noted as relevant not only in a descriptive way, but also as features shared by different groups in the sauropod phylogeny (McIntosh, 1990a,b; Salgado *et al.*, 1997a; Sanz *et al.*, 1999). These measurements ended coded in some of the characters from the data matrices readily employed in sauropod cladistics as commented before. However, few studies have incorporated these measurements into a morphometrics framework. These scarce studies are generally devoted to the analysis of the scaling patterns and the biomechanical specialization in Sauropoda (Coombs, 1978; Carrano, 1998, 2001; Wilhite, 1999, 2003; Wilson & Carrano, 1999; Bonnan, 2004, 2007; Tidwell & Wilhite, 2005; Ullmann *et al.*, 2017), but also the incorporation of some measurements into quantitative characters in systematics (Mannion *et al.*, 2013).

In addition, some recent studies proposed the inclusion of new measurements, exploring new morphological features in the femur and the incorporation of standardized indexes to make easily readable comparison between species such as the Robustness Index (Wilson & Upchurch, 2003; Company *et al.*, 2009) and the Eccentricity Index (Royo-Torres, 2009). This new set of morphometric and morphological variables was used to discuss the presence of several undescribed Maastrichtian titanosaur forms based in the description of isolated femora in the Ibero-Armorican domain (Vila *et al.*, 2012). These forms are also different to earlier, Campanian titanosaur faunas (Vila *et al.*, 2012, 2016). Moreover, several specimens previously referred to *Ampelosaurus atacis* were reassessed as cf. *Lirainosaurus* and other, undescribed Titanosauria indet. forms (Vila *et al.*, 2012). As well as an increase on measured information (i.e. variables to account) in each bone type (Royo-Torres, 2009; Vila *et al.*, 2012). Those studies report valuable databases and possible variable sets to compare bone types within a statistical framework.

Though discrete morphological characters of the femur are not enough to assess in titanosaurs a precise taxonomical approach at genus and species level on isolated specimens, it may not be impossible to establish a classification method. Several, different methodologies have been applied in other dinosaur groups and other anatomical elements in order to estimates and evaluate possible taxonomic diversity. For example, the study through multivariate statistic of isolated theropod teeth have been expanded in recent years, both using several classical measurements for theropod teeth (see Buscalioni *et al.*, 1997). While other studies expand on this idea adding more measurements to the available datasets (e.g. Smith, Vann, & Dodson, 2005; Hendrickx, Mateus, & Araújo, 2014; Gerke & Wings, 2016). Multivariate statistics are used with these datasets

in order to generate a classification framework of the isolated theropod teeth collected (Smith *et al.*, 2005; Larson & Currie, 2013; Hendrickx *et al.*, 2014; Gerke & Wings, 2016; Serrano-Martínez *et al.*, 2016; Malafaia *et al.*, 2017). This methodology can be applied to assess the taxonomic position of isolated and incomplete remains otherwise they could not be guessed at the same level. However, some authors argue that this methodology should be supportive or at least with elements discovered with some degree of association with other skeletal remains, which permit to stablish and analyze morphological characters, to support these results (Williamson & Brusatte, 2014). No similar study have been conducted among sauropod isolated bones.

Preliminary approach to the morphological variability of Lo Hueco appendicular specimens share similar methodologies with those proposed by Vila *et al.* (2012). We compared several measurments like eccentricity of the specimens and robustness of the bone through Robustness Index as well as other features. We found two main morphotypes among humerus and femur (Páramo *et al.*, 2014, 2015). These morphotypes are congruent with previous hypothesis based on the skull and teeth morphology (Knoll *et al.*, 2013b,a; Díez Díaz *et al.*, 2014; Ortega *et al.*, 2015). However, in order to test the presence of three different morphotypes (Mocho *et al.*, 2016b) or four distinct morphotypes in Lo Hueco (Vidal *et al.*, 2017; Mocho *et al.*, 2018) we set a clustering and multivariate statistical framework. These statistical analyses follows the metholodology proposed by Smith *et al.* (2005) for theropod teeth, as we want to: i) explore the number of morphotypes present in a sample of titanosaur femora from Lo Hueco. ii) elaborate a multivariate classificatory that help assess the clustering of isolated femora of Lo Hueco and applicable to other fossil sites. iii) test whether some of this morphometric characters in the femora are significant at different phylogenetical levels up to species level. In order to assess the precision of the method and the morphotype distribution in the fossil site of Lo Hueco, we developed also an unsupervised clustering workflow. The unsupervised clustering methods do not require an a priori morphotype hypothesis, therefore they can be used to discuss morphological similarities among the studied specimens (see clustering techniques in Hammer & Harper, 2008).

In this study, a sample of 21 femora recovered from Lo Hueco site (Cuenca, Spain) are analysed though a statistical framework. Here we study the femur, as it is one of the most abundant isolated bones found in the Ibero-Armorican domain (Le Loeuff, 2005a; Company *et al.*, 2009; Vila *et al.*, 2012; Díez Díaz, Suberbiola, & Sanz, 2013a; Díez Díaz, Pereda Suberbiola, & Company, 2015; Díez Díaz *et al.*, 2018a; Ortega *et al.*, 2015). This analysis will help to test the proposed hypotheses about the diversity of the titanosaur fauna of Lo Hueco, which was considered to comprise two main morphotypes (or eventually more). In order to confirm this hypothesis, the results of the statistical workflow must render two distinct group sets with the a priori description provided. The results also add valuable information for the study of other multi-specimen fossil sites of the Late Cretaceous of the Iberarmorican domain, such as Belleveu, Laño and Chera (Le Loeuff, 2005a; Company *et al.*, 2009; Díez Díaz *et al.*, 2015; Pereda Suberbiola *et al.*, 2015).

The current state of knowledge about the morphological variability on sauropod skeletons comes mostly from Neosauropod non-titanosaur faunas (Wilhite, 1999, 2003; Bonnan, 2004, 2007; Ikejiri, 2004, 2008; Carpenter & Tidwell, 2005; McIntosh, 2005; Tidwell & Wilhite, 2005; Remes, 2006, 2009; Schwarz & Böhm, 2012; Tschopp *et al.*, 2015), while much fewer studies are focused in titanosaurian appendicular shape variation (Company *et al.*, 2009; Curry Rogers, 2009; Otero, 2010a; Mannion & Otero, 2012; Vila *et al.*, 2012; Díez Díaz *et al.*, 2015; Curry Rogers *et al.*, 2016). Also, previous works have highlighted the possible presence of small appendicular elements that

may be referable to putative juvenile individuals (Páramo *et al.*, 2014). This hypothesis is based on the size among other characteristics. While size alone is not an indicative of the ontogenetical stage (e.g. Brochu, 1996; Sander *et al.*, 2006; Carballido & Sander, 2014; see also Chapter VI), the methodology of the statistical workflow needs to address its potential difference in the sample of the same morphotype. Also, there is a great variability in the size of the titanosaurs e.g. giants forms as *Antarctosaurus* spp. (Huene, 1929; see also Powell, 2003), *Argyrosaurus* spp. (see Mannion & Otero, 2012) and *Patagonatitan mayorum* (Carballido *et al.*, 2017), dwarf taxa as *Europasaurus holgeri* (Carballido & Sander, 2014) and *Magyarosaurus* spp. (Nopsca, 1915; Le Loeuff, 2005b). There is also a small to medium-sized taxa in the Ibero-Armorican domain, *Lirainosaurus astibaie* (Sanz *et al.*, 1999; Company *et al.*, 2009). The statistical framework needs to reflect this variability and allow us to assess these small elements (e.g. HUE-2636) cluster with more exclusive morphotypes from Lo Hueco or they resemble a completely different group, probably more similar to other small European titanosaurs like *L. astibaie* and *Magyarosaurus* spp. It is expected that after extracting the size variance from the sample, the smallest specimens from Lo Hueco are allocated to large, probable adult specimens, from our exclusive titanosaur forms.

Specimen	Side	Genus	Assoc.	Length	Pr. Length	Robustness	Eccentricity
HUE-1521	Left	Morphotype I	isolated	910	901	0.21	2.64
HUE-2338	Left	Morphotype I	isolated	860	860	0.22	2.09
HUE-2420	Right	Morphotype I	HUE-EC6	1151	1151	0.22	1.96
HUE-2636	Right	Morphotype I	isolated	455	455	0.21	1.29
HUE-2903	Right	Morphotype I	isolated	955	955	0.2	2.78
HUE-3108	Right	*L. pandafilandi*	HUE-EC1	1010	1010	0.23	2.5
HUE-8801	Left	Morphotype I	isolated	600	570	0.18	1.82
						0.21	**2.09**
HUE-594	Right	Morphotype II	isolated	1550	1550	0.21	1.83
HUE-1316	Right	Morphotype II	isolated	1000	965	0.26	2.86
HUE-1319	Right	Morphotype II	isolated	840	840	0.21	2.55
HUE-1357	Left	Morphotype II	isolated	860	840	0.23	2.08
HUE-1590	Right	Morphotype II	isolated	850	814	0.2	5
HUE-3583	Left	Morphotype II	isolated	900	840	0.23	2.31
HUE-10007	Right	Morphotype II	isolated	740	703	NA	3
						0.22	**2.67**
HUE-902		T. indet	isolated	1100	959	NA	2.97
HUE-930	Right	T. indet	HUE-EC11	1050	960	NA	3.1
HUE-1183	Left	T. indet	HUE-EC13	870	840	0.19	3.02
HUE-1187	Left	T. indet	isolated	965	965	0.25	3.33
HUE-1440		T. indet	isolated	1460	1430	NA	1.51
HUE-1508	Left	T. indet	isolated	870	857	0.24	3.62
HUE-3237	Right	T. indet	isolated	815	820	0.23	2.59

Table.IV.I.1. Sample of femora for current study. *Assoc.* - associated specimen. *Strat.* - stratigraphic level provenance. *T.indet.* - Titanosauria indet. *Pr. Length* - Preserved Length. Robustness Index as per Wilson & Upchurch, 2003. Eccentricity Index as per Wilson & Carrano, 1999..

Institutional abbreviations:

NHMUK – Natural History Museum, London, United Kingdom; MCNA – Museo de las Ciencias Naturales de Álava/Arabako Natur Zientzien Museoa, Vitoria-Gasteitz, Spain; MGUV – Museo de Geolgía de la Universidad de Valencia, Burjasot, Spain; MUPA- Museo de Paleontología de Castilla-La Mancha; PVL – Instituto Migue Lillo, Tucumán, Argentina.

Anatomical abbreviations:

4th – fourth trochanter; at – accessory trochanter; epi – lateral epicondyle; gt – greater trochanter; if – intercondylar fossa; lb – lateral bulge; lic – linea intermuscularis cranialis; fc – fibular condyle; fh – femoral head; tc – tibial condyle; ts – trochanteric shelf; s – sulcus.

Other abbreviations:

EXPDB – Database with the expanded set of variables proposed in this study; ORGDB – Database with the original set of variables from Vila *et al.* (2012); RDB – Database with the partial and complete Robustness Index as per Wilson & Upchurch (2003).

IV.I.2 MATERIAL AND METHODS

IV.I.2.1. DATASETS

A random sample of 21 femora (Table.IV.I.1, Fig.IV.I.2) from Lo Hueco fossil site was described and compared with other Neosauropoda and especially titanosaurian sauropod taxa (see complete list Supplementary Material IV.I.A), in particular those from Iberian Peninsula and other Late Cretaceous taxa. In these comparative analyses, a priori femoral morphotypes were established with descriptions based on some specimens (see Anatomical Description, below) while other specimens not referred to any of these previous described morphotypes were included to process in the statistic workflow. In our analysis, we used a modified version of the measurement matrix of Vila *et al.* (2012). The original dataset was previously used for support comparisons between several femoral morphotypes of the Late Cretaceous Ibero-Armorican domain. That matrix is expanded and modified in the present study (see Supplementary Material IV.I.B to D) by adding some new variables as well as increasing the sample with the femora from Lo Hueco as well as several other Neosauropoda. For referring to each database they will be called:

(i) Database with the original proposed variable set (ORGDB): derived from the variables proposed on the dataset of Vila *et al.* (2012) and based on Royo-Torres (2009) with the sample from Lo Hueco and other Neosauropoda taxa. See Supplementary Material IV.I.B.

(ii) Database with the expanded variable dataset (EXPDB): a database built from the measurement variables proposed by Bonnan (2004), Royo-Torres (2009), Vila *et al.* (2012) and some new ones introduced in this study (Fig.IV.I.3), measured for the sample from Lo Hueco and other Neosauropoda taxa. See Supplementary Material IV.I.C.

(iii) A database only from the partial robustness relationships and Robustness Index (RDB): with the ratios between the proximal, midshaft and distal width divided by the proximodistal length. Here it is also included the Eccentricity, which is a ratio between the anteroposterior width and lateromedial width of the midshaft. Measured in the sample from Lo Hueco and several other Neosauropoda taxa. See Supplementary Material IV.I.D.

The measurement of the Lo Hueco sample as well as other titanosaurian specimens (see Supplementary Material IV.I.A: accessed material) was conducted with a digital calliper (E ~1mm). Measurements are indicated in the Table.IV.I.2 and Fig.IV.I.3, and they are taken between the corresponding landmarks that delimits each of the proposed measurements with the same criteria as Type I and Type II landmarks used in geometric morphometrics (Bookstein, 1991). These landmarks are main features which bound the classical measurements used in this and previous studies (see Carrano, 1998, 2001; Bonnan, 2004; Royo-Torres, 2009).

Other neosauropod specimens were incorporated in the present data matrices using the available bibliography. If a specimen lack some of our measurements in the available information, we took measurements from the figuration whether it was possible. Figuration measurements were processed with the software ImageJ v2.0.0-rc-43/1.51j8 (Schindelin *et al.*, 2015; Rueden *et al.*, 2017). Also this software was used to measure angles in all the specimens, both the ones sampled in this study and the ones from bibliographical sources. A total of 195 femora were measured

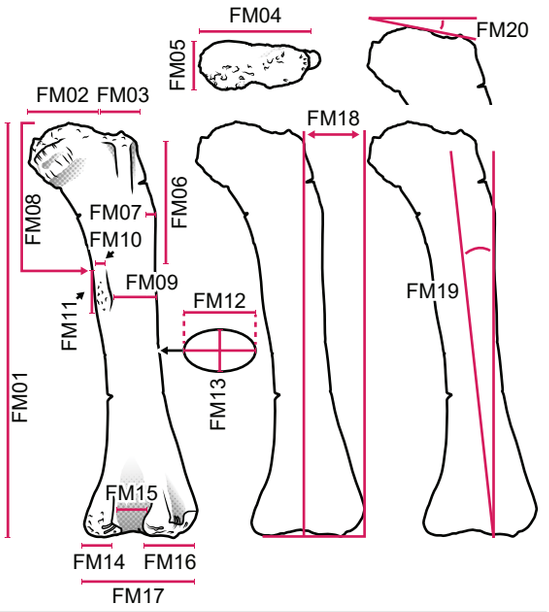

Fig.IV.1.3. Measurements used in this study.

by a combination of these methods. The sample range from some Upper Jurassic basal neosauropods and Brachiosauridae, to Late Cretaceous titanosaurian taxa representative from Lithostrotia, including member of the groups Aeolosaurini and Saltasauridae.

We tested all the statistical analyses for the three sets of variables with the complete databases, as well as in two subsets: (i) one subset of only Ibero-Armorican domain titanosaur taxa and (ii) other subset with only our sample from Lo Hueco fossil site. The EXPDB with all sauropod taxa accomplish a 51.97% completeness of the sample, while the ORGDB accomplish a 56.36% completeness. Reducing the number of variables from our database to the original set of variables from Vila *et al.* (2012) improve the completeness in less than ~5%. The RDB with all sauropod taxa accomplish 87.30% of completeness.

IV.1.2.2. STATISTICAL ANALYSES

Apart from the traditional description of the appendicular elements, measurement matrix was used to assess the statistical differences between the proposed morphotypes described in this study. All statistical analyses were conducted in R v3.6.1. statistical software (The R Core Team, 2016) with the R-Studio v1.0.136 interface (RStudio Team, 2015) and all analyses running in parallel processing with six Intel® i7-4700HQ 2.40 GHz cores via the package "snowfall" (Knaus, 2015) and the seed set to 500.

Some packages are not referred in the main text as they are employed for graphical display or mundane methods of data-matrix manipulation applied in the procedure without further comment here. A comprehensive list of the local libraries used is provided (see Supplementary Material III).

Preparation of the databases require handling the effects of missing values, as reported before, and the size differences between the specimens. Missing data imputation methods are commonly used by some statistical software such as the average by column values in PAST v3.26 (Hammer, Harper, & Ryan, 2001). The scope of imputation methods is not only to obtain a precise estimated value for the missing data but also to retain an approximate structure of the original data such as its variance-covariance relationships. This is useful in order to not lose anatomical or eoclogical information (Schafer, 1999; Royston, 2004; Brown *et al.*, 2012; Clavel, Merceron, & Escarguel, 2014; Bak & Hansen, 2016). Here we use a multiple imputation (MI) method instead of column average applied in other softwares (e.g. PAST) and estimation is based on the package "mice" v.2.0. (van Buuren & Groothuis-Oudshoorn, 2011). We used the Bayesian linear regression (Minka, 1999;

van Buuren & Groothuis-Oudshoorn, 2011) with a set of 50 different imputations and 1000 replications of each imputation. This method minimize the Procrustes sum of squared errors (PSSE) and retain a good and accurate estimation even when missing values exceed 25-30% of the data base (Clavel *et al.*, 2014; Bak & Hansen, 2016). Accuracy of this method and computing time is reported in Supplementary Material IV.I.F.

	Variable	EXPDB	ORGDB	RDB
FM01	Proximodistal length	x	x	
FM02	Greater trochanter lateromedial width	x	x	
FM03	Femoral head lateromedial width	x	x	
FM04	Proximal end width	x	x	
FM05	Femoral head anteroposteiror width	x		
FM06	Lateral bulge proximodistal length	x	x	
FM07	Lateral bulge lateromedial width	x	x	
FM08	Proximal end to 4th trochanter height	x	x	
FM09	Distance of 4th trochanter to lateral face	x	x	
FM10	4th trochanter lateromedial width	x		
FM11	4th trochanter proximodistal length	x	x	
FM12	Minimum midshaft lateromedial width	x	x	
FM13	Minimum midshaft anteroposterior width	x	x	
FM14	Tibial condyle lateromedial width	x	x	
FM15	Posterior intercondylar fossa width	x		
FM16	Fibular condyle lateromedial width	x	x	
FM17	Distal end lateromedial width	x	x	
FM18	Femoral shaft bevelling to medial	x		
FM19	Angle between the condylar plane and shaft axis	x		
FM20	Angle between femoral head and greater trochanter	x		
PROX_ROB	Proximal partial robustness index			x
MID_ROB	Minimum midshaft partial robustness index			x
DIST_ROB	Distal partial robustness index			x
ECC	Eccentricity Index			x

Table.IV.I.2. Measurements definitions and relationships with each dataset.

The variables are also standardized prior any statistical analysis. A log-transformation is made. controlling for some 0-value variables (cases with no biological sense, like the lateral bulge development in non-titanosaurian sauropods):

$$Log_{10}\left(Variable + 1\right)$$

For all the analyses, some conventions were assumed for the taxonomical assessment. Some of the taxa analysed have only one specimen per taxa, e.g. *Diamantinasaurus matildae* AODF-603 (Hocknull *et al.*, 2009; Poropat *et al.*, 2015) and *Andesaurus delgadoi* MUCPv-132 (Calvo & Bonaparte, 1991; Mannion & Calvo, 2011). While other of the taxonomical units used at "species" level (= morphotype) report similar problematics e.g. the *Aeolosaurus* sp. left femur MPCA-Pv-27177 (Salgado & Coria, 1993) or the right femur FMNH-13018 from a titanosauria indet. referred as cf. *Argyrosaurus* sp. (Powell, 2003; Mannion & Otero, 2012). We adopted a classification with OTUs at genus level. Those specimens assessed as confer of species that have two or more individuals, maintain that designation as a unique OTU, i.e. the right and left femur MLP-26-316 referred to cf. *Antarctosaurus giganteus* (Huene, 1929; Powell, 2003) which becomes the cf. *Antarctosaurus* category. However, those isolated specimens (i.e. FMNH-13018 discussed before) or the morphotypes described in the Tremp basin and South of France (Canudo, 2001; Vila *et al.*, 2012) are labeled as Titanosauria indet. which is used as a mélange that incorporates several undescribed species or undiagnostic material. In other studies, this last label could be counter-productive. However, we are assessing morphotype differences with use of classificatory methods, therefore having such a mélange group can be used for the classificatory algorithms to have the option of a class labeling that do not resemble to other, already described taxa. The Titanosauria indet. also present several specimens from Lo Hueco that have not been assessed in the a priori description of the morphotypes. These specimens instead are placed directly in the testing group, a sample of specimens to assess the validity of the algorithm. In the case of the supervised classification algorithms deployed for this study cannot guess new, undescribed classes, as they are discrimination method (working with a known set of classes as input). So if for example we have a new undescribed taxa in our sample from Lo Hueco, and it is different to the exclusive form *Lohuecotitan pandafilandi* (Díez Díaz *et al.*, 2016) or other, already known species of Ibero-Armorican domain, it is expected that: (a) classification algorithms will report those specimens as similar to previously described taxa completely different from the other Ibero-Armorican taxa; (b) or instead, labelling those specimens as Titanosauria indet. and we could discuss further is they may be attributable to one of the undescribed forms previously reported in the Late Cretaceous of the Ibero-Armorican domain (Vila *et al.*, 2012; Díez Díaz *et al.*, 2015).

A Shapiro-Wilks and Levene test of the homogeneity of variance as part of the pre-processing shows that multivariate normality is not reached in all the analysed databases and is slightly increased after the imputed data. While the multiple imputation methods preserve better the original inherent structure of the data and retain the biological information (Clavel *et al.*, 2014; Bak & Hansen, 2016), also tend to superimpose the effect of uneven sample sizes of the database. Other imputation methods can account better for this effect, however non-multiple imputation techniques increase too much error with high missing data (>25%) such as in our case. Multiple Imputation was better tool for estimation of the missing values nonetheless, and such high proportion of missing data has been taken into account when designing the experimental classification framework and in the discussion. The three databases are explored after data imputation with unsupervised classification methods like clustering methods and visualized with Principal Component Analysis (PCA). The PCA were obtained by "factoMineR" package

(Lê, Josse, & Husson, 2008) with escalation of the variables setting on and limiting the possible PCs retained to 10. The different unsupervised cluster methods for the complete sample will be available in Supplementary Material IV.1.H and I. We will show the morphospaces observed for the complete sample of sauropods in the EXPDB and ORGDB, and a comparison between Ibero-Armorican domain titanosaur only and Lo Hueco sample alone. Here we will also present the unsupervised clustering for the Ibero-Armorican titanosaur and for the sample of Lo Hueco within each database. PCA will be available for visualization of the classification algorithms (see below). A complete set of several PCA and clusters over all the databases and for complete Neosauropoda, Ibero-Armorican domain titanosaurs and sample of Lo Hueco alone.

After data imputation and before size standardization of the sample, we built the Robustness database (RDB). Robustness in a non standardized way after Wilson & Upchurch (2003) have been used to differentiate specimen or even sauropod taxa since the first sauropod discoveries. However this method has been regarded as undiagnostic without the combination with other characters (Osborn & Mook, 1921; Huene, 1929; Gilmore, 1936a; Powell, 2003; Naish & Martill, 2007; Otero, 2010b; Mannion & Otero, 2012). Here we use a database based on the use of Robustness Index according to Wilson & Upchurch (2003) to assess its usefulness at our OTU level. The Robustness Index is useful at more inclusive clade levels outside of the common phylogenetical definition of genus (see data matrices used in Sauropoda phylogenies in: Wilson, 2002; Upchurch *et al.*, 2004; Carballido *et al.*, 2011a, 2017; D'Emic, 2012; Gorscak *et al.*, 2014; Tschopp *et al.*, 2015; Salgado, Gallina, & Paulina Carabajal, 2015; González Riga *et al.*, 2018). We test the Proximal, Midshaft and Distal partial-Robustness indices to check if they report significant differences between the OTUs. We also included the Robust Index and the shaft Eccentricity. The Eccentricity Index is another interesting character included in this database as is a characteristic feature acquired in Titanosauria (Salgado *et al.*, 1997a; Wilson & Carrano, 1999; Carrano, 2005; Curry Rogers, 2005). We also found main differences in robustness and eccentricity within the sample of Lo Hueco femora (see Description). The Eccentricity of the long bone as per Wilson & Carrano (1999) is the minimum lateromedial width of the shaft divided by the minimum anteroposterior width of the shaft and was also used for comparison by Vila *et al.* (2012).

Previous works on fragmentary specimens have used a proxy of the Robustness Index via the midshaft partial robustness index (Company *et al.*, 2009; Vila *et al.*, 2012). For this purpose, we can assume that the robustness partial index on the midshaft is a good proxy for the Robustness Index if they show correlation and covariation as proposed. If they do not show a significant correlation or covariation (as the Robustness Index is the mean value of the proximal, midshaft and distal partial robustness indices) it means that the loss of the proximal and distal widths cannot be approximated only by midshaft robustness calculation. We tested the correlation-covariation between the Robustness Index and the partial robustness index of the midshaft with Kendal tau rank correlation (Claude, 2008) and see the correlation between both variables via reduced major axis (RMA) regression with the package "smatr" (Warton *et al.*, 2012).

IV.1.2.3. EFFECT OF SIZE

Size differences were found within the sample of Lo Hueco, and also among all the sampled specimens of Neosauropoda, sometimes from an order of magnitude. Also there is an added complexity whether some of those specimens come from possible juvenile individuals, especially among the sample from Lo Hueco. The ontogenetic development is beyond the scopes of this

work and will be covered elsewhere. However, the relationships between the size and shape may be a confounding component of the variance (see Marko & Jackson, 2001). Some methods to address or extract the size component of the variance have been explored, like transforming all the morphometric variables into ratios (e.g. dividing by the specimen length) but this method may increase unnecessarily the covariation (Claude, 2008). Others studies used the regression varimax-rotated orthogonal (see SAS Institute, 1999) in order to obtain the residual of non-ratio based variables (see Smith *et al.*, 2005). However, this methodology is not desirable to be applied on our database due the high amount of missing data. Another attempt usually resort to the use of the scaling properties on principal component analysis (PCA) and its orthogonal axis PC1 normally assumed to represent the size variance in analysis of measured distances (Claude, 2008; Hammer & Harper, 2008). However, we also use PCA to visualize all the variable values of the performed analyses, and we are using similar techniques such as Discriminant Function Analysis (DFA). The PCA scaling method can create an unnecessary convolution on the posterior visualization and analysis by DFA methods and make difficult to read the meaning of the components. We followed the traditional implementation of Mosiman extraction of the size effect (Mosimann, 1970) instead. This method is somewhat comparable to the one of Smith *et al.* (2005) for extracting the size effect but without the problematics dealing with missing data.

IV.I.2.4. LO HUECO SAMPLE DIFFERENCES AND UNSUPERVISED CLUSTERING

We tested if there is a significant difference between the two described morphotypes from Lo Hueco for all the databases after conducting the PCA for dimensionality reduction. PCs are not normally distributed (as commented before), so a Kruskal-Wallis test is desirable over other tests (Sokal & Rohlf, 1987). Kruskal-Wallis test ranks the data and therefore it is not affected by violation of the normality of distribution or equality of variances. We can test differences between both morphotypes described in Lo Hueco (Table.IV.I.3) and for all the OTUs (Supplementary Material IV.I.G). Kruskal-Wallis non parametric test was conducted with "coin" package (Hothorn *et al.*, 2006, 2008). A Mann-Whitney U test (Choi & Marden, 1997) was also conducted for comparison of the taxa differences, pairwise by OTUs (results on the sample of Lo Hueco alone: Table.IV.I.3; Complete databases: Supplementary G). These tests however only test group differences with each variable independently and we want to assess the classification power within multivariate datasets.

For specimen allocation, the K-means solution was deployed as it is an algorithm for classification without an a priori hypothesis of clustering but instead, a hypothesis of number of clusters available in the sample (Bow, 1984; Selim & Ismail, 1984; Rokach & Maimon, 2007). K-means algorithm assigns each specimen to different centroids at random and then tunes the classification iteratively. In each iterations, the reclassification is based on a decreasing of the within group variance with the new centroid until it cannot be further improved (Rokach & Maimon, 2007). The K-means solution clustering will be only applied in the sample from Lo Hueco, as this method is unreliable in its standard form for high quantity of groups with uneven distribution (see Rokach & Maimon, 2007). A two group k-mean analysis is complemented with a test of the optimal k-groups that could explain the variation in the sample. To test the optimal number of clusters and the derived classification we can repeat this analysis several times inputting an increasing number of hypothesized clusters. Then we calculate the total between-groups variance sum of squares and plot for all the k-means analyses applying the "elbow rule". The optimal

number of clusters available in our sample is the one that plotted produces an "elbow", or in other words, it cannot further improve or the gain is minimal on the between-groups variance (Rousseeuw, 1987; Tibshirani, Walther, & Hastie., 2001; Morissette & Chartier, 2013). We use the implementation in the package "factoextra" package (Kassambara & Mundt, 2017) in R.

IV.1.2.5. STATISTICAL CLASSIFICATION WORKFLOW

The statistical workflow proposed by Smith *et al.* (2005) was used with all the databases of this study, however, some modifications applied are derived from the statistical differences of our data and the anatomical perspective. As the sauropod body plan is so conservative and similar between groups, we reproduced a secondary statistical workflow using a different algorithm from the original study proposed for theropod teeth (Smith *et al.*, 2005). The workflow proposed by Smith *et al.* (2005) was based around Linear Discriminant Analysis, or Discriminant Function Analysis (DFA) that will be conducted with the "MASS" package (Venables & Ripley, 2002). The DFA assess the differences between groups in each database, using MANOVA to determine significant difference functions between a set of OTUs and can be used to classify each data to the group with which is more similar. However, this functions maximize the variation between the groups and are somewhat analogous to PCA (Schulte-Hostedde, Millar, & Gibbs, 2004; Hammer & Harper, 2008; Hewson, 2009) but the MANOVA function is sensible to group unevenness (i.e. number of sampled specimens per sauropod taxa) and group centroid size (i.e. overlapping between morphospaces).

In this study we chose as alternative classificatory algorithm the support vector machine (SVM; Boser, Guyon, & Vapnik, 1992; Cortes & Vapnik, 1995; Vapnik, 1995). The SVM does not require normal distribution and it is independent of the dimensionality of featured space. The main idea behind this method is to separate classes by a hyperplane, maximizing the margin between the classes (Vapnik, 1995). The method uses quadratic programming, which only provides a global minima and thus, it is not prone to misclassify due to local minima. The SVM works through a kernel function that can be tooled for defining such hyperplane (Vapnik, 1995). The kernel functions of the SVM work significantly different from the kernel functions implemented in the DFA. Furthermore, the flaws of uneven sampling can be tooled in a tuning pre-processing with a "training" dataset in order to establish a proper cost of misclassification for the SVM. The quadratic programming optimization uses data points near the hyperplane to measure the margin, the "support vectors", instead the centroid of each class like other discriminant analyses (Vapnik, 1995; Brereton & Lloyd, 2010). The number of support vectors tend to be minimized and when the classes are not linearly separable, the SVM tries to find hyperplanes maximizing the margin while minimizing the quantity in proportion to misclassification error by a cost. The Cost constant commented above is set up in this preliminary step and works like a "trade of" when defining the hyperplane (Cortes & Vapnik, 1995). The SVM were developed as two class classification methods but have been adapted to multiclass classification like other discriminant methods like DFA or logistic regression, which in origin where two-groups classificatory also (Macqueen, 1967). Multiclass SVM were conducted with the package "e1071" (Meyer *et al.*, 2017), which already includes in the code the "One Against One Approach" (see Hsu & Lin, 2002; Pal, 2008). This method generate SMVs for all the possible pairs (Knerr, Personnaz, & Dreyfus, 1990; Pal, 2008) and then apply a "voting strategy" with the class label obtained. Each specimen receive the class label that occur the most after passing for all the classifiers. In order to set the training data, the initial databases were sampled dividing in a subset of 66% random selected specimens in the training data and the rest for the testing data in which

measure the accuracy of the SVM. The kernel function used is a radial basis function, and the parameters used were selected during the tuning process with a conservative strategy, electing a lesser cost while suboptimal if the accuracy reported is nearly similar and the dispersion retained low in order to not overfit the kernel function and the classifier over the training data.

The DFA produces a set of functions and a new classification used to visualize the overall percentage of accuracy and can be used for cross validation. While SVM report the weight of each variable used in the definition of the hyperplane. Discriminant functions and output parameters of the SVM are reported in Table.IV.I.7. The package "caret" (Kuhn *et al.*, 2017) is used for elaboration of confusion matrices and also reporting accuracy rates. Results of both classificators will be discussed and assessed with the unsupervised methods.

IV.I.3 ANATOMICAL DESCRIPTION

IV.I.3.1. MORPHOTYPE I

Material:

HUE-3108 (type femur of *Lohuecotitan pandafilandi*), HUE-902, HUE-1183, HUE-1440, HUE-1508, HUE-1521, HUE-2338, HUE-2420, HUE-2636, HUE-2903, HUE-3587 and HUE-8801.

Description:

The specimen HUE-3108 is an almost complete right femur that lacks part of the anterior edge of the distal surface of the greater trochanter. HUE-2420 is almost complete right femora, being one of the biggest appendicular elements found in Lo Hueco.HUE-2420 is fractured in the distal end, with an oblique crack over the fibular condyle. HUE-2636 and HUE-8801 are two small right and left femora, respectively, rather complete except from part of the proximalmost surface of the femoral head and the greater trochanter in HUE-8801. HUE-1521 is a left femur that preserve the shaft, part of the femoral head except the proximalmost portion, the lateral bulge and the proximal part of the posterior surface of the tibial condyle. In HUE-1521, the trochanteric shelf can be followed in its distal part but lacks all the proximal and the greater trochanter. This femur also have some collapsing of the anterior face extending medially to the lateral bulge. HUE-2338 is an almost complete left femur despite some loss of the proximal end especially over the greater trochanter and the lateral face of the femoral head. HUE-2903 is a long and well preserved right femur that only lacks the proximalmost part of the femoral head and the greater trochanter. HUE-1183 is a left femur that lacks part of the fibular condyle, the greater trochanter and the proximal part of the lateral bulge. Both HUE-1366 and HUE-1183 experiment crushing and anteroposterior deformation with little extend. HUE-1508 has lost the fibular condyle and great part of proximal end, preserving only the proximalmost part of the proximal end and half the lateral bulge. It also present some crushing in the anterior part under the greater trochanter (not preserved in this specimen). Finally, HUE-1440 is a large left femur that lacks the distal condyles, part of its head and great portion of the lateral bulge due to a massive growth of gypsum crystals.

This morphotype has a rather slender shaft with low eccentricity ranging from 128 to 200% (eccentricity as the Eccentricity Index * 100, so it can be reported as percentage) by titanosaurian

standards (see Table.IV.I.1). The shaft section is subcircular to a low eccentricity ellipse. This kind of low eccentric shafts resemble the condition present in *Jainosaurus* cf. *septentrionalis* (Wilson *et al.*, 2009; Wilson, Barrett, & Carrano, 2011; pers. obs. APB 2016), *Euhelopus zdanskyi* (Wilson & Upchurch, 2009), *Opisthocoelicaudia skarzynskii* (Borsuk-Bialynicka, 1977), *Tastavinsaurus sanzi* (Canudo, Royo-Torres, & Cuenca-Bescós, 2008; Royo-Torres, Alcalá, & Cobos, 2012) and some femora referred to *Magyarosaurus* spp. (Huene, 1932 pers. obs. APB 2016). The femora referred to the Morphotype I differ from more anteroposteriorly compressed femora, which characterizes the other European titanosaurs from similar age (Le Loeuff, 2005a; Company *et al.*, 2009; Vila *et al.*, 2012; Díez Díaz *et al.*, 2013a, 2015, 2018a). The femora are columnar with a straight shaft lightly medially defelcted with a marked beveling of the distal condyles. The head is globous with little anteroposterior compression and a bit dorsally directed, differing from dorsomedial projected head of other femora belonging to the Morphoptype II of Lo Hueco (see below) and the European titanosaurs *Ampelosaurus atacis* (Le Loeuff, 2005a), *Lirainosaurus astibaie* (Díez Díaz *et al.*, 2013a, APB pers. observ.; absent in some femora referred in Company *et al.*, 2009; Díez Díaz *et al.*, 2015). They also differ from the morphotypes identified in Vila *et al.* (2012). It presents a step-like outline of the proximal end like *Rocasaurus muniozi* (Salgado & Azpilicueta, 2000) or *Saltasaurus loricatus* (Powell, 2003) with a sulcus between the femoral head and the greater trochanter. HUE-2338 presents a continuous proximal end between what is left of the greater trochanter and proximal lateral bulge, and the femoral head. The femoral head of HUE-2338 is also projected upward. In HUE-2338, the proximal part of the greater trochanter is lost so it cannot be described in detail; however, the lateral sector of the femoral head only shows a little anteroposterior constriction and this suggest that the step-like morphology is not as pronounced in this specimen as in other femora referred to the Morphotype I. In HUE-2636, there is difference between the height of the femoral head and the greater trochanter but the step-like outline is not well developed. Except for HUE-2338 (which is fragmentary), this morphotype present the somewhat stepped morphology between a bulbous femoral head, an anteroposteriorly expanded greater trochanter.

This morphotype presents a lateromedially wide trochanteric shelf in posterior view that extends parallel to almost all the length of the lateral bulge. The lateral bulge is well developed, and anteroposteriorly expanded. There is a low stepped transition between the greater trochanter and the lateral bulge. This character will be commented in the Discussion. HUE-8801 presents a low developed trochanteric shelf. Specimen HUE-8801 and HUE-2636 present a low development of the trochanteric shelf in posterior face. Both specimens may be relatable to juvenile specimens. So it cannot be regarded as truly loss of the trochanteric shelf development but instead an early stage of development of this ridge in posterior face.

The fourth trochanter is present in the posterior face of the femoral shaft, near its medial edge, sometimes extending directly from the medial border like in HUE-2338 or HUE-8801. In general the fourth trochanter is projected posterior to posteromedial in all the specimens. The dorsal tip of the fourth trochanter coincides with the distal end of the lateral bulge. The trochanteric shelf can reach a distalmost position than the distal end of the lateral bulge, such as in HUE-1183, HUE-3108, HUE-2636.

The shaft has an asymmetrical cross-section as in many other sauropods like *Jainosaurus* cf. *septentrionalis* specimen NHM-R931, *Antarctosaurus giganteus* (Powell, 2003), *Bonatitan reigi* (Salgado *et al.*, 2015; pers. obs. APB 2016) or *Lirainosaurus astibaie*, being anteroposteriorly wider near the medial border than near the lateral one. However, there are other titanosaurs which do not present this asymmetry or is lightly developed like *Saltasaurus loricatus* (Powell,

2003), *Neuquensaurus australis* and "*N. robustus*" (Powell, 2003; Otero, 2010a) or the majority of *Magyarosaurus* spp. (Nopsca, 1915; pers. obs. APB 2016). This asymmetry is weak and the cross-section retain its sub-elliptical outline. However, this cross-section is less eccentric than other derived titanosaurs, similar to the cross-section present in several non-titanosaurian sauropods (Wilson & Carrano, 1999; Carrano, 2001; Wilson & Upchurch, 2003; Bonnan, 2004; Royo-Torres, 2009; Carballido *et al.*, 2011a; Mocho *et al.*, 2014). The eccentricity can vary along the sample referred to the Morphotype I, some with a more rounded morphology such as HUE-1521, but others with a marked such as HUE-2903 (276%). The distribution of the overall robustness and eccentricity based on the corresponding indices can be observed in Table.IV.I.1. Majority of elements do not present such high values of eccentricity (albeit being the normal values among Titanosauria). Average eccentricity maintain at ~200 %. However, the eccentricity on HUE-2903 may be caused partially by some degree of crushing exerted on the bones.

In anterior face, the femora present a linea intermuscularis cranialis that extends in the mid axis of the shaft from the greater trochanter sulcus with the femoral head down to the separation of the intercondylar fossa, as it can be seen in HUE-3108 or HUE-1508. However, not all the specimens present this linea such as in HUE-2420, HUE-2636 and HUE-8801.It is interesting to note that HUE-2636 or HUE-8801 present a slightly convex area where the linea intermuscularis cranialis is present in other specimens. It may be a character that vary with the ontogeny also, if HUE-1636 and HUE-8801 are more juvenile specimens of Morphotype I. The histological analysis of these specimens will be important to test this hypothesis and assess the less development trochanteric shelf and linea intermuscularis craniales in HUE-2636 and HUE-8801.

The distal condyles are characterized by a medial deflection, more pronounced in the fibular condyle in some of the specimens. This morphotype have large, anteroposteriorly wide distal condyles. The condyles present a light expansion of the articulation into the anterior face. The posterior expansion of the condyles is more significant, denoting a possible high angle of flexion of the tibia and fibula and contrasting with the morphology of the Morphotype II, which has much more development of the posterior face. The lateromedial expansion is not as marked like in other titanosaurs of the Ibero-Armorican domain e.g. *Ampelosaurus atacis* (Le Loeuff, 2005a) and *Lirainosaurus astibaie* (Díez Díaz *et al.*, 2013a). These taxa loss also the anterior projection of the distal condyles and develop more the posterior face of the distal end.

Only few specimens preserve a complete distal end being difficult to compare the morphology of this sector in all femora referred to Morphotype I. Many of the specimens, even in the fragmentary ones (e.g. HUE-1521), preserve part of the tibial condyle, especially the posterior dorsal top of the articulation. They present the upward projection of the posterior face of the condyle. In posterior view, the distal end shows a medial rotation of the distal condyles. This characteristic cannot be observed in HUE-1183 or HUE-1508 due the preservation (the condyles are not completely preserved). The lateral epicondyle is wide, posterolaterally oriented, and bulbous in lateral view. The mid-intercondylar fossa is deep and extendss smoothly between the anterior and posterior view in almost all the specimens. Other sauropods develops a step or small concavity in distal face which separate the anterior face of the distal condyles and the posterior face in distal like *Ampelosaurus atacis* (Le Loeuff, 2005a; Vila *et al.*, 2012). Only HUE-2420 present a stepped margin in the transition to posterior view of the fossa that resemble to Morphotype II femora.

IV.I.3.2. MORPHOTYPE II

Material:

HUE-594, HUE-930, HUE-1187, HUE-1316, HUE-1319, HUE-1357, HUE-1590, HUE-3237, HUE-10007.

Description:

The specimen HUE-594 is one of the largest femora recovered in Lo Hueco fossil site. This femur presents some minor crushing in the anterior part of the proximal end, under the greater trochanter. The specimens HUE-930, HUE-1316 and HUE-1357 are rather incomplete right femora that have lost both the proximal and distal ends. HUE-930 exhibits a gypsum growth out of the shaft by cracks in the posterior side. Its trochanteric shelf is obliterated by the gypsum but the lateral bulge is completely preserved. The lateral bulge has some deflection to anterior face in HUE-1316 while the trochanteric shelf is mostly preserved but cracked under the greater trochanter (not preserved). The trochanteric shelf is not a proper ridge like in morphotype I, is weakly developed but present. The distal condyles are lost but the initial part of their lateromedial expansion is seems to suggest a wide and robust distal condyles, which coincides with the shaft and preserved proximal end. HUE-1187 has a complete preserved shaft but lacks the greater trochanter, part of the anterior face of the femoral head, and most of the distal end (except for the posterior face of the tibial condyle and part of the intercondylar fossa). The shaft has a minimal collapsing but the anteroposterior width loss in the midpoint of the femoral length is minimal. HUE-1319 is a complete, well preserved right femur. HUE-10007 has a complete shaft and a partially preserved femoral head. HUE-10007 has lost also part of the anteroposterior width and the tip of the greater trochanter. It presents a slight anterior torsion of the lateral bulge, and an anteroposteriorly compressed shaft.

The femora referred to the Morphotype II are robust, with a wider shaft relatively to the length of the femur with a lateromedially expanded femoral head and distal condyles. This morphotype resemble other European forms such as *Ampelosaurus atacis* (Le Loeuff, 2005a; Vila *et al.*, 2012), *Lirainosaurus astibaie*, and the femora described by Vila *et al.* (2012). There is also a remarkable eccentricity of the shaft, much greater than in Morphotype I ranging from 307 to 354%. The robustness overall ranges from 0.24 to 0.3, which slightly overlaps with the robustness index values present in the Morphotype I (i.e. RI: 0.19-26, see Table.IV.I.1). However the sample of specimens referred to Morphotype II tend to be more robust as well as having more eccentric shaft then the average morphology of Morphotype I.

The femoral head is not well preserved among the sampled specimens. Few of the femora preserve a complete femoral head but in general this region form a square angle respective to the main axis of the shaft like HUE-594. Some specimens like HUE-1319 present a femoral head upwardly directed. without step-like morphology between the greater trochanter and femoral head as in *Lirainosaurus astibaie*. But other specimens like HUE-594 develops this stepped outline between the femoral head and the greater trochanter, which has a "platform" morphology. This "platform" morphology of the greater trochanter is also caused by a projected edge in anterior face, connecting the interarea between femoral head and greater trochanter, and extending sometimes to the proximalmost of the lateral bulge. The upward head without

stepped morphology between the femoral head and the greater trochanter is observed in both morphotypes (seen in HUE-2338)

In the Morphotype II, the proximal end is markedly anteroposteriorly compressed than in the Morphotype I. The shaft present the typical titanosaurian medial and slightly anteriorly deflection of the femoral head,It is not as marked as in Morphotype I as the distal condyles are not as bevelled. This medial deflection is much less pronounced than in Morphotype I femora (e.g. in HUE-594, HUE-1357 or HUE-3237). The trochanteric shelf is present and it is shallow and extends parallel to almost the same proximodistal height as the lateral bulge. Contrary to the Morphotype I, the trochanteric shelf extends parallel to all the length of the lateral bulge (e.g. HUE-1319, HUE-1357 or HUE-10007), being longer than the ones of the Morphotype II. The lateral bulge is not as wide anteroposteriorly as in Morphotype I. It is also short and limited to proximal fourth of the femur. The lateral bulge is anteriorly deflected at its mid-length, but presents a light posterior deflection of its proximal tip (e.g. HUE-1319). This result in a very light sigmoidal shaft, observed in lateral view.

The minimum lateromedial width is positioned distally to the mid length of the femur. The apparent proximodistal position in which the shaft is more constricted change slightly depending on the view (anterior or posterior) because a light rotation of the shaft. This character is described for the femora analysed by Vila *et al.* (2012) and *Lirainosaurus astibaie* (Díez Díaz *et al.*, 2013a). The fourth trochanter is completely located in the posterior face, near the medial edge of the femoral shaft, not extending to the medial face of the femur like in the Morphotype I. The trochanter is long and pronounced in posterior face. The light linea intermuscularis cranialis can be identified in some of the specimens like HUE-594, HUE-1319, HUE-1187, while is absent in HUE-10007.

The distal expansion of the femur is placed more distally and expands more abruptly than the gentle distal expansion of the distal end in Morphotype I. The distal condyles are projected posteriorly but presenting a low anterior projection, less developed than in the Morphotype I. The distal end tends to be lateromedially wider, more robust and more compressed anteroposteriorly than the Morphotype I. Sometimes, the tibial condyle is slighlt medially beveled, much less than in Morphotype I. The tibial condyle has a light medial concavity (e.g. HUE-1187 and HUE-1319). The fibular condyle is expanded lateromedially and the epicondyle ranges from a lateroposterior projection to a fully lateral projection as occur in HUE-1319. The intercondylar fossa is wide and lightly more expanded in anterior view. The transition from the anterior to the posterior face presents a stepped concavity such as in *A. atacis*. This anterior concavity is separated from the posterior fossa by the presence of a transversely elongated ridge, which connects the fibular and tibial condyles.

IV.II.3.3. FRAGMENTARY MATERIAL WITH DIFFICULT ASSESSMENT

Some fragmentary femora have been difficult to assess into one of the described morphotypes. Here we describe this difficulties in the assessment. Lo Hueco conforms a diverse and abundant sample but many appendicular elements have lost some features that are important to provide a accurate description. Some specimen are herein described as they may be relevant due their association with partially complete and associated/articulated titanosaurian sets found in Lo Hueco. Some of the described elements have lost the proximal and distal ends and do not present enough features to clearly assess their affinities.

HUE-902 is one of those specimens as it is found in the proximity of the individual HUE-EC-3, as well as the femur HUE-930. The lateral bulge is long and its absence of marked anterior deflection may suggest affinities with Morphotype I. However, the overall robustness of HUE-902 resembles the robustness shown by Morphotype II femora. The eccentricity is also high (327%). This may be partially caused by the crushing of the anterior face of the shaft. Also the fourth trochanter is posteriorly positioned near the midshaft like in Morphotype II.

HUE-1183 is another example of morphological mosaic of features from the two morphotypes and the absence of the proximal and distal ends avoid a more accurate assessment. HUE-1183 is a long and gracile femur with a proximodistally long lateral bulge. The proximal end of the lateral bulge (and possible the greater trochanter, which is not preserved) has a slightly posterior deflection. The lateral bulge is anteroposteriorly narrow and the middle part is not anteriorly flexed. A long trochanteric shelf project parallel and up to the end of the lateral bulge . The shaft is quite eccentric, almost 300% and lacks marks of collapsing besides presenting cracks and gypsum growing in the mid part, at the proximal third of the femoral length. The fourth trochanter is posteromedially positioned, extending to the medial face of the shaft. It is weakly developed. A linea intermuscularis cranialis is developed in anterior face. The minimum lateromedial width of the mid-shaft is located distally under the midpoint of the proximodistal length of the femur. The distal end has been lost, preserving near the medial face the proximal part of tibial condyle. A low lateromedial expansion for the distal condyles can be interpreted, The tibial condyle is not aligned with the femoral head in anterior or posterior view.

Some femora like HUE-1508 or HUE-1440 are also classified as unknown for analytical purpose. Some features like the eccentricity of the shaft or the development of the tibial condyle as well as a marked linea intermuscularis cranialis allow us to infer that they probably belong to Morphotype I. Due the poor preservation of these specimens, this assessment will be tested following statistical techniques. Similar situation occurs with HUE-3237, which is preliminary referred to the Morphotype II based on the eccentric shaft. Therefore we included these femora in the statistical analysis as part of the unknown Lo Hueco sample.

IV.I.4 RESULTS

IV.I.4.1. UNSUPERVISED ANALYSES AND MORPHOSPACE DEFINITION

The PCA over the complete datasets resulted in twenty (our setting maximum) PCs for the EXPDB, fifteen for the ORGDB and only four PCs for the RDB. We analysed which PCs are meaningful (explain enough variance over a threshold compared with its successor). We used Bookstein method (Bookstein, 2014, p. 324) included in package "Morpho" (Schlager, 2017) which use a test that resemble the Anderson's X^2 (Bonnan, 2007) based on a comparison of the respective eigenvalues with a Chi-squared type test (see also Anderson, 2003; Zelditch, Swiderski, & Sheets, 2012). With this test, we found that only six PCs are worth commenting in EXPDB, four in ORGDB and three on RDB. When considering the Ibero-Armorican domain sample alone, meaningful PCs decreased to only the first in the EXPDB and ORGDB, while RDB maintain three first PCs as meaningful. No meaningful PCs are found for the sample of Lo Hueco alone and this is addressed in the discussion.

In the EXPDB the first PC explains 68.96% of variance while the second and third PCs explain only a modest 8% aand 5.95% respectively. The six first PCs considered meaningful according to the test explain a cumulative variance of 92.5%. In ORGDB the first PC explain 27.05 % of total variance and the second ~16.52% of variance. The four first PCs are found meaningful and explain s a cumulative ~66.33% of total variance. It is necessary to observe up to the sixth PC to explain 80.93% of cumulative variance. The RDB on the other hand presents a first PC that explain 55.88% of variance and the second PC 26.75%. Both of them help explain a cumulative 82.64% of total variance, that increase to ~92.5% with the third PC which was considered meaningful. We can observe an even contribution of almost all the variables to the first component of the analysis in EXPDB (see Supplementary Material E). The variables that conrtibutes the most to this PC are the proximodistal length, proximal end width, femoral head lateromedial width, proximodistal development of the lateral bulge, height of the fourth trochanter respective to proximal end, minimum lateromedial width of the midshaft and the distal end expansion width are the variablesHowever, if we observe the way they are contributing to the first component, we can observe main differences in the medial displacement of the femur. If we see the biplot with the distribution of femoral morphospaces by clade (Fig.IV.I.4) we can observe main differences between the morphospaces occupation of Diplodocidae + more basal Macronaria and Titanosauriformes along PC1. On the other hand, the second PC results are more influenced by the anteroposterior width of the femoral head, the lateromedial width of the lateral bulge and the angle between the planes of the condyles and the main axis of the shaft (or medial bevelling of the shaf). The PC2 contrast with PC1 in less separation between Titanosauriformes and non-Titanosauriformes sauropods. However, the titanosauriforms morphospaces tend to be tighter than more basal neosauropods (Fig.IV.I.4). At genus level (see Supplementary E) we can observe light differences between Upper Jurassic non-Titanosauriformes sauropods of the Morrison and Tendaguru formations on the positive values of PC1. We can distinguish *Diplodocus* spp. and *Giraffatitan brancai* morphospaces at slightly more positive values of PC2. Overlapping with those taxa, *Camarasaurus* spp. and *Apatosaurus* spp. are projected toward more negative values of PC2. While *Dicraeosaurus* spp. are present near the point 0 values of PC2, at an intermediate morphospaces. More derived macronarian sauropods are projected toward 0 or negative values of PC1 (e.g. *Europasaurus holgeri* or *Haplocanthosaurus* spp.) but not overlapping with most of the Titanosauriformes morphospaces at more negative values in PC1. Another observable trend is the swift between more slender and elongated femora of diplodocines and non-derived Titanosauriformes, projected at more positive values of PC1 (e.g. *Diplodocus* spp. and *Giraffatitan brancai*) and across all values of PC2. In the other hand, slender forms of titanosauriformes (e.g. Lo Hueco Morphotype I, *Bonatitan reigi*, *Phuwiangosaurus sirindhornae*) are projected at more negative values of PC1 and PC2. While more robust forms of titanosaur sauropods are subdivided in two different of morphospaces. Robust yet eccentric type of femora (e.g. *Ampelosaurus atacis*, *Magyarosaurus* spp., the cf. *Lirainosaurus*, Lo Hueco Morphotype II and *Antarctosaurus* spp.) are projected at more positive values of PC2. While other robust forms with less eccentric shaft and anteroposteriorly expanded proximal and distal end are projected at point 0 values of PC2 and towards more negative values of PC2. The exception of this subdivision is *Lirainosaurus astibaie* that is projected at more negative values with a slightly more robust and eccentric femur. Probably it is projected at more negative values based on the anteroposteriorly narrow proximal end (but not as narrow as in *A. atacis*) and the proximodistally long lateral bulge which represent roughly >45% of the variance in the PC2 and is shared with other taxa in the same values (see Supplementary Material IV.I.E variable eigenvalues).

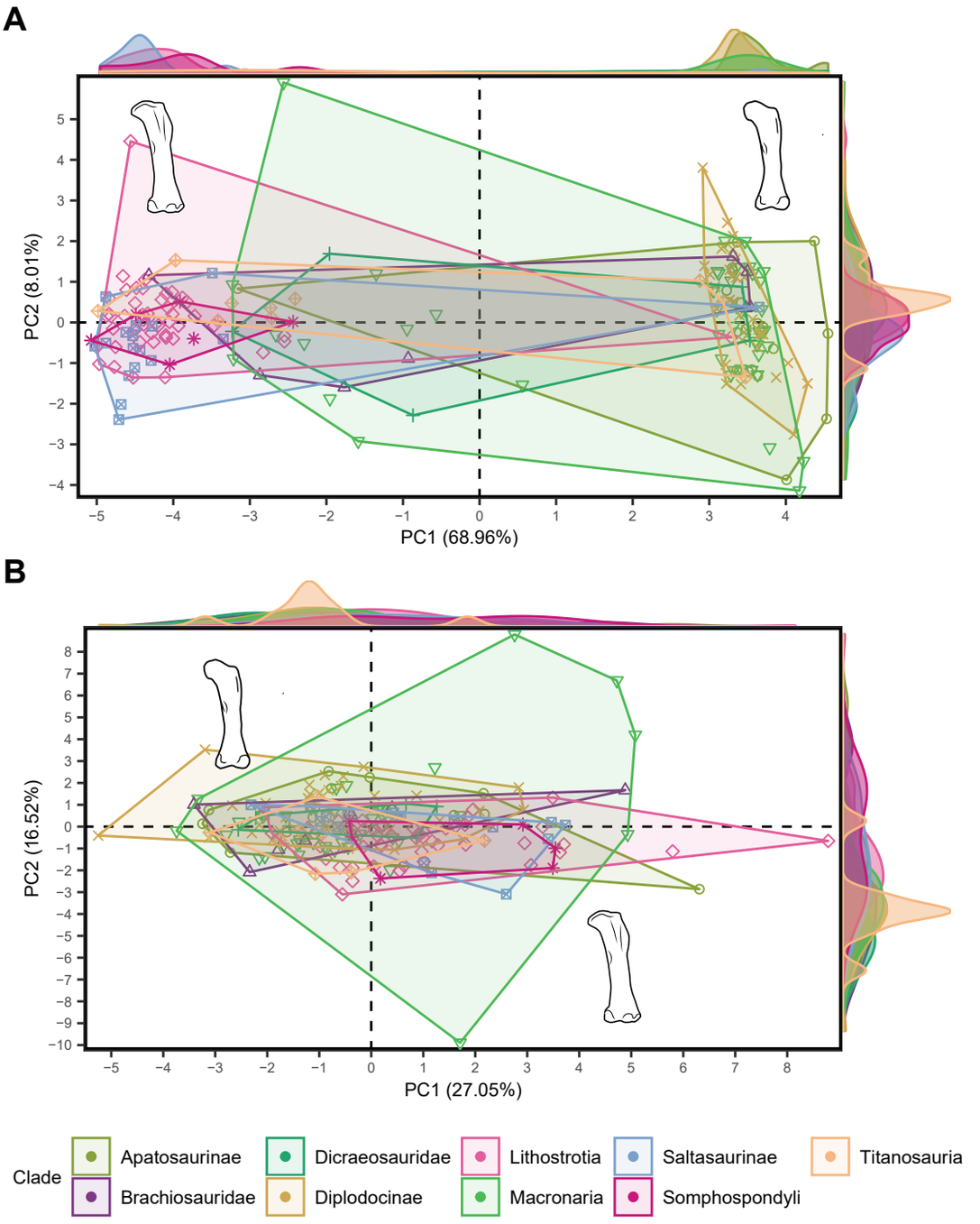

Fig.IV.1.4. Results of the shape PCA. Main morphospace occupation by the more inclusive clades. (A) PC1-PC2 of the analysis of EXPDB. (B) PC1-PC2 of the analysis of ORGDB.

The ORGDB on the other hand produces more overlapping between morphospaces in each PC (Fig.IV.I.4, see also Supplementary Material IV.I.E.). The first PC of this dataset represent less variance than the first PC on the EXPDB (27.08% contra 68.96% PC1 in EXPDB). Contrary to the EXPDB, not all the variables contributes almost equally to the first PC on ORGDB. The PC1 of ORGDB is composed mainly by variance of proximodistal length of the femur, the lateromedial width of the distal end and the minimum lateromedial width of the midshaft. Also, there are other variables help explain slightly less variance: the lateromedial width of the fourth trochanter, the proximodistal length of the lateral bulge, the lateromedial width of the proximal end and the position of the fourth trochanter respective to lateral face. Titanosauriformes sauropods tend to occupy more positive extreme of this PC, but differences with non-titanosauriformes are minimal. Macronaria femora also have one of the widest morphospaces overlapping all the other sauropod clades types of femora. PC2 in this dataset represent the variation in the minimum anteroposterior and lateromedial width of midshaft, the lateromedial width of the fourth trochanter and its position relative to lateral face and proximal end. Non-titanosauriform neosauropods tend to be projected on negative values while the Titanosauriformes morphospaces represent more positive values. However, separation is again minimal and Macronaria type femora englobes a morphospace that overlaps with other femur types. When observing the ORGDB morphospaces plot at genus level (Supplementary Material IV.I.E), similar trend to the observed in EXPDB between more robust and gracile types of femur is present within Titanosauriformes. However, the morphospaces overlap all near point 0 to positive values of PC1. Differences between genera are not so easy to establish and this dataset is less helpful assessing trends toward morphospaces occupation at genus level. Lastly, the RDB shows complete overlap of almost all morphospaces in PC1 and PC2. The first PC comprises the variance on all the variables, while PC2 corresponds mainly to variance in the Eccentricity Index. Some comparisons can be established in those PCs between several clade morphospaces occupation like differences between Diplodocinae + Dicraeosauridae against Apatosaurinae + Macronaria, or in the same way Lithostrotia against more derived Saltasaurinae. Between clade morphospaces occupation can be assessed easier than with ORGDB, however we loss information about transition between non-Titanosauriformes Neosauropoda and Titanosauriformes seen in the other two datasets. When inspecting the morphospaces at genus level (see Supplementary Material IV.I.E) the problematics of morphospaces overlapping worse. Differences can be assessed when comparing determinate taxa between them like the different morphospaces occupation of *Diplodocus* spp. at more negative values of PC1 and positive values of PC2 while *Camarasaurus* spp. and *Apatosaurus* spp. project at more positive values of PC1 and negative values of PC2. But the overlapping of most of the morphospaces impedes assess any trend among Neosauropoda at genus level.

Within the Ibero-Armorican titanosaurs sample the EXPDB first PC decrease to 54.03 % of variance explained and it is necessary nine PCs to explain ~93.5% of cumulative variance similar to the meaningful components of the complete dataset. The second PC of the EXPDB analysis in the sample of Ibero-Armorican titanosaurs returns a 8.97% and the third PC a total of 7.57% of variance explained. The results of the analysis in the ORGDB for the Ibero-Armorican sauropods present a first PC that explain 26.09% and it would be necessary the five first PCs to explain ~70.5% cumulative variance. The differences are minor respective to the ones found in the analysis of EXPDB between all neosauropods and between the Ibero-Armorican titanosaurs sample alone. On the other hand, the RDB explains slightly more variance in the first PC with 56.80% in the analysis of Ibero-Armorican titanosaurs. Within EXPDB there are few differences

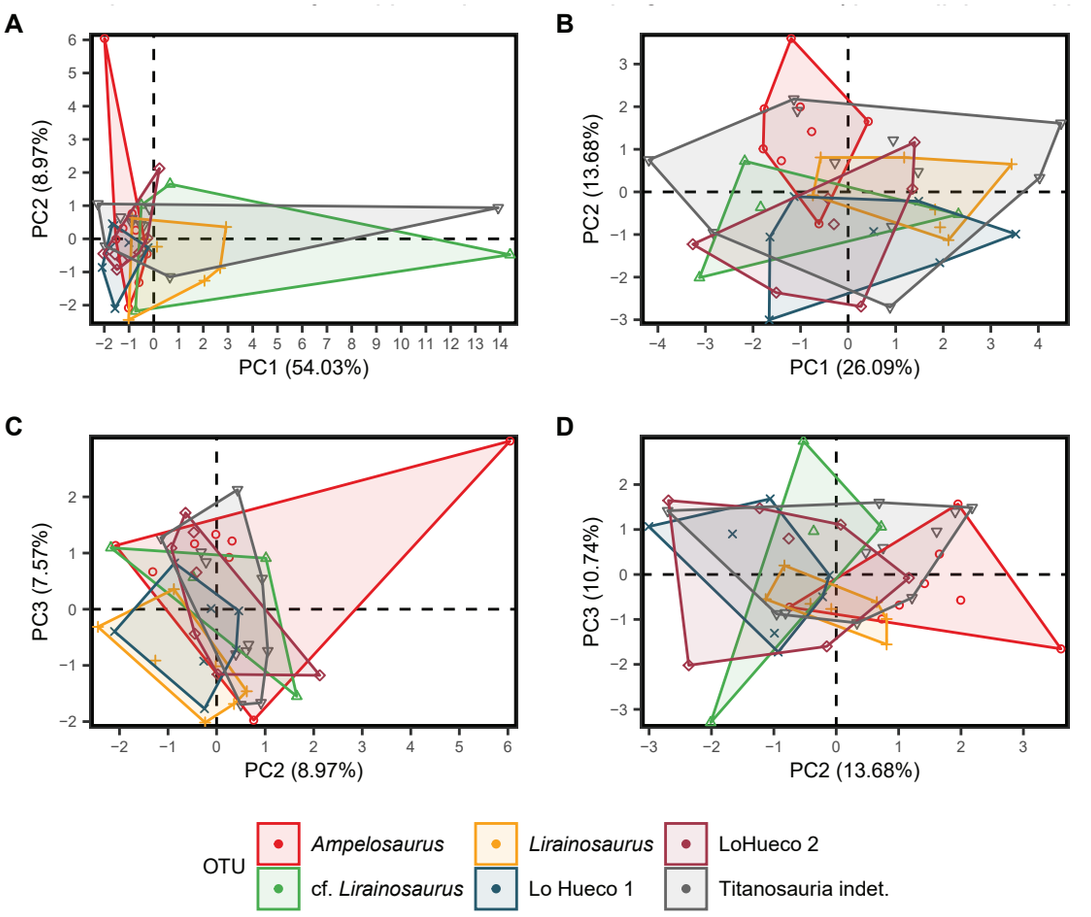

Fig.IV.I.5. Shape PCA results of the analysis of the Ibero-Armorican sample. (A) PC1-PC2 and (C) PC2-PC3 of the analysis of EXPDB. (B) PC1-PC2 and (D) PC2-PC3of the analysis of ORGDB. LoHueco 1 - Morphotype I. LoHueco 2 - Morphotype II.

the variance explained in this PC. The PC2 shows main variance in femoral head anteroposterior width and the lateromedial development of the lateral bulge. When inspecting the biplot we can observe an apparent overlapping of almost all the morphospaces in the first three PCs (Fig.IV.I.5). We can difference between *Lirainosaurus astibiae* + cf. *Lirainosaurus* toward the point 0 of PC1 and negative values of PC2. The Morphotype II of Lo Hueco is displayed at negative values of PC1 and near point 0 of PC2, while Morphotype I of Lo Hueco occupy negative values of PC1 and near point 0 to more negative values of PC2. *Ampelosaurus atacis* will be found in a wide morphospaces near point 0 values of PC1 and expanding along PC2, in a morphospace similar to Morphotype II from Lo Hueco. ORGDB dataset analysis for the Ibero-Armorican titanosaurs contrast with the analysis of the complete Neosauropoda in the importance of several variables. The PC1 shows that proximal end expansion is not as relevant and there is less variance in the distal end expansion. On the other hand, there is more variance in the minimum lateromedial midshaft width and the lateromedial width of the fourth trochanter. In the second PC the variance of the height of the fourth trochanter relative to proximal end contributes greatly (~34%) to the variance of this component. The distance of the fourth trochanter to lateral face is also relevant

with more variance in the Ibero-Armorican sample. Other variables relative to the development of the fourth trochanter or the anteroposterior expansion of midshaft are not as relevant, while there is an important portion of variance in the lateromedial width of the femoral head and the femur proximodistal length. The biplot on ORGDB PCA exhibits a more difficult to assess morphospaces distribution. The PC1 produces more overlap between all the morphospaces. Morphotype I and *Lirainosaurus astibaie* lean to positive values in PC1 and show some differences between them in negative values of PC2. While cf. *Lirainosaurus* and Morphotype II occupy negative values of PC1 and negative values of PC2, exerting some differences between both of them in the PC2. The only taxon that shows great differences in morphospaces occupation between the Ibero-Armorican titanosaurs, is *Ampelosaurus atacis,* projected in negative values of PC1 near point 0, with tight distribution in this axis, and also projected in positive values of PC2 (Fig.IV.I.5). The analysis of the Ibero-Armorican titanosaurs in the RDB shows similar trends with even greater overlap of morphospaces in each PC. First PC shows a trend between less robust and less eccentric femora of cf. *Lirainosaurus* + Morphotype I from Lo Hueco at more negative values. At near point 0 values of PC1 we found the more robust femora of *Lirainosaurus astibie* and some of the morphotypes defined in the south Pyrenees (Canudo, 2001; Vila *et al.*, 2012) as well as some specimens of Morphotype II from Lo Hueco and *Ampelosaurus atacis*. At more positive values we found the morphospaces of *A. atacis* and several of the specimens described by Vila *et al.* (2012). PC2 is not that useful to visualize morphospaces differences between the Ibero-Armorican titanosaurs as *A. atacis* variability overlap all other taxa from more negative up to more positive values. When decomposing the eigenvalues of PC1 we found that the proximal partial robustness index contributes less to the overall variance *contra* the analysis on all Neosauropoda. In the analysis of Ibero-Armorican titanosaurs, the eccentricity contributes more in the first PC, with almost same percentage as proximal robustness. The PC2 on the contrary represents slightly less variance in the Eccentricity Index than in the analysis of complete Neosauropoda sample (Ibero-Armorican sample ~47%; complete Neosauropoda ~75%). Moreover the contribution of the proximal robustness increases from ~12% in the complete Neosauropoda sample, to ~37% of variance in PC2 of the Ibero-Armorican sample.

The analysis of the sample of titanosaur femora of Lo Hueco on each dataset shows less separation in between the morphospaces than in the previous analyses with other neosauropods taxa. In absence of other sauropod taxa, PC1 of EXPDB represents much less of cumulative variance of the sample. It shows mostly the variance in distance of the fourth trochanter respective to the lateral face, the variation in the minimum lateromedial width of the midshaft, the distal lateromedial expansion and the lateromedial width of the fibular condyle. Main variance contribution on PC2 comes from the anteroposterior and lateromedial width of the femoral head, lateromedial expansion of proximal end, height of the fourth trochanter respective to proximal end, lateromedial width of tibial condyle and the femoral shaft bevelling to medial (but not the angle between the plane of the distal condyles and main axis of the shaft). Several of those features are variable in both morphotypes and so the morphospaces present a great overlap in PC1-PC2 plot while PC3 presents some differences with Morphotype I morphospaces at more negative values and the Morphotype II morphospaces projected at more positive values (Fig.IV.I.6). ORGDB present a similar pattern variance contribution between the PC1 and the PC1 of EXPDB. Both analyses share similar variables with somewhat similar percentage of contribution when decomposing the eigenvalue of PC1. Differences are observable in PC2 and PC3, which do not show great differences between morphospaces of Morphotype I and II.

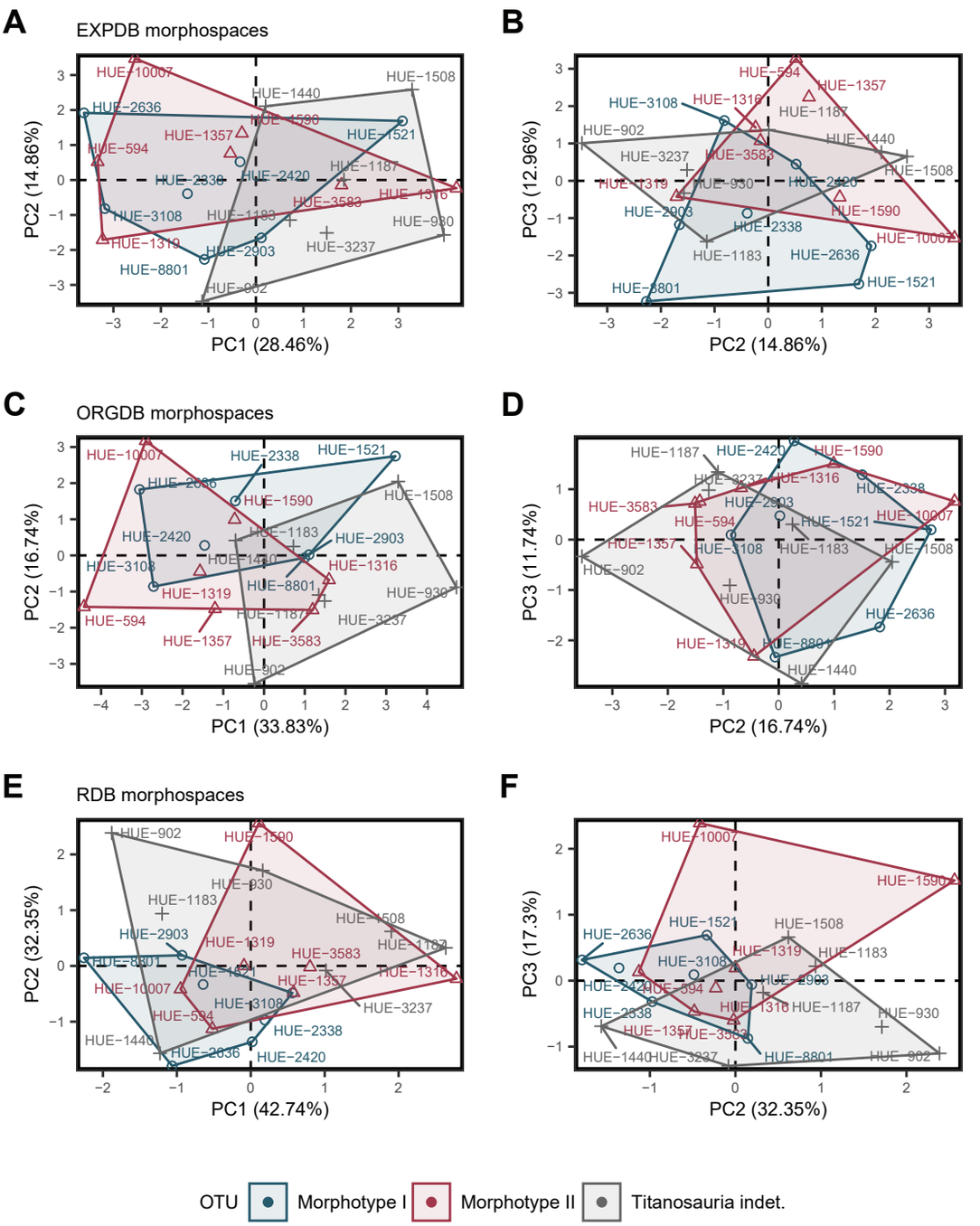

Fig.IV.I.5. Shape PCA results of the analysis of the Lo Hueco sample. (A) PC1-PC2 and (B) PC2-PC3 analysis of the EXPDB. (C) PC1-PC2 and (D) PC2-PC3 analysis of ORGDB. (E) and (F) analysis of RDB.

While the EXPDB PC2 and 3 shows the variance on the femoral medial bevelling of the shaft as one of the main contributors, this variable is absent in ORGDB, and therefore does not capture differences in this feature. Finally, RDB shows differences between both morphotypes morphospaces occupation. Morphotype I is projected in more negative values of PC1 and PC2, however, several of the possible specimens that could be assessed as Morphotype I are projected onto PC2 more negative values. Morphotype II occupy more positive values in PC1 and PC2, with only HUE-594 and HUE-10007 projected onto negative values of PC1 and PC2. PC3 shows less separation between both morphotype morphospaces, unless we consider some of the dubious specimens referred to Morphotype I. As before, if we include HUE-902, HUE-1440 between others, Morphotype I would occupy more negative values of PC2 and a range between near point 0 values to negative values in PC3. On the contrary, Morphotype II would project a morphospaces between positive values of PC3 and PC2 up to positive near point 0 values of PC2 and PC3.

There are significant differences between groups found both in Kruskal-Wallis and Mann-Whitney's U test over the PCs in all the database for the complete sample and for the analysis of the EXPDB and ORGDB with the Ibero-Armorican titanosaurs sample only (see complete set in supplementary G, for the Ibero-Armorican titanosaur sample see Table.IV.I.3, 4 and 5). The Kruskal-Wallis test presents slightly better results in the ORGDB database derived from Vila *et al.* (2012) with the complete set of genera and within the Ibero-Armorican titanosaur sample, as there are more PCs that show significant differences between the taxa (Table.IV.I.3 and 4). While the RDB shows only the PC1 over the EXPDB with significant differences between the taxa (Table.IV.I.6), no significant PCs show the differences in the analysis of the Ibero-Armorican titanosaur sample nor in the Lo Hueco sample. The Mann Whitney U test of EXPDB database for all Neosauropoda pairwise differences returned significant differences among most of taxa in PC1, PC8 and PC9. When comparing only the Ibero-Armorican titanosaurs, differences are found in PC9, as not many of the titanosaur taxa present significant differences in all the PCs as shown by the pair-wise Mann-Whitney U tests. We will highlight taxa that do not present pair-wise significant differences in few or any of the PCs. Among *L. astibaie* and cf. *Lirainosaurus* there are significant differences in only one PC (PC10). Morphotype I from Lo Hueco can be assessed different from the indeterminate titanosaurian morphotypes from Ibero-Armorican domain in

	Complete sample		Ibero-Armorican sample		Lo Hueco sample	
	χ^2	p-value	χ^2	p-value	χ^2	p-value
PC1	135.686	**<0.001***	13.337	0.120	0.037	0.902
PC2	29.560	0.798	5.628	1.000	0.494	0.535
PC3	22.568	1.000	10.810	0.330	3.433	0.073
PC4	34.350	0.209	8.077	0.912	0.102	0.805
PC5	15.018	1.000	3.816	1.000	0.200	0.710
PC6	23.679	1.000	12.716	0.156	0.004	1.000
PC7	23.994	1.000	4.259	1.000	0.494	0.535
PC8	40.521	**0.038***	5.014	1.000	0.102	0.805
PC9	36.914	0.095	15.773	**0.048***	5.588	**0.017***
PC10	29.578	0.798	4.204	1.000	0.331	0.620

Table.IV.I.3. Kruskal Wallis and Mann-Whitney U's test in EXPDB.

two PC (PC1 and PC9); and also with *L. astibaie* in PC1 and PC10. There are no significant differences between Morphotype I and II, as well as Morphotype II from Lo Hueco and *L. astibiae* (and cf. *L astibiae*), and between Morphotype II and the Titanosauria indet. This however might be partially caused by the presence of several specimens that could be referable to both morphotypes among the indeterminate titanosaurian femora. After all, the Titanosauria indet. comprises both the putative undescribed Ibero-Armorican forms and the unassessed specimens from Lo Hueco. The analysis of the ORGDB presents significant differences among taxa for PC1, PC2 and PC6 when comparing the complete Neosauropoda sample. However, among Ibero-Armorican titanosaurs only PC2 and PC6 show significant differences among sampled taxa.

When highlighting the differences in pairwise comparison among Ibero-Armorican titanosaurs, we can observe that most of the significant differences are found in PC6. While *A. atacis* presents significant differences with Morphotype I and II from Lo Hueco in one PC each (PC2 and 5 respectively), *L. astibaie* presents significant differences in one PC with Morphotype I from Lo Hueco (PC4) and with the specimens referred as Titanosauria indet (PC2, 6 and 8). The Morphotype I and II from Lo Hueco appear as significantly different in PC6 as well as Morphotype II form the indeterminate specimens from the titanosaurs of the Ibero-Armorican domain. The taxon that presents the least significant differences was cf. *Lirainosaurus*. Significant differences with Morphotype II from Lo Hueco or the Titanosauria indet. specimens were observed in one PC each (PC2). No significant differences were detected between cf. *Lirainosaurus* and *L. astibaie* or the Morphotype I from Lo Hueco in the Mann-Whitney U test over the Ibero-Armorican titanosaur sample in ORGDB.

The RDB shows significant differences between the complete Neosauropoda sample just in PC1. Despite this, from all the four PCs (Table IV.I.5) present significant differences in the pairwise Mann-Whitney U test with few exceptions, e.g. comparison of *A. atacis* with majority of sampled taxa. However when analysing the Ibero-Armorican sample alone, no significant differences are detected on Kruskal-Wallist test for all the PCs as well as the fewest significant differences between the genera in the pairwise comparisons. We only found significant differences between *Ampelosaurus atacis* and *Lirainosaurus astibaie* + Morphotype I from Lo Hueco on PC1.

	Complete sample		Ibero-Armorican sample		Lo Hueco sample	
	χ^2	p-value	χ^2	p-value	χ^2	p-value
PC1	54.915	**<0.001***	9.098	0.630	0.655	0.710
PC2	69.038	**<0.001***	17.082	**0.024***	0.142	0.165
PC3	27.761	1.000	4.969	1.000	0.565	0.620
PC4	23.576	1.000	7.547	1.000	0.338	0.383
PC5	31.421	0.494	6.553	1.000	0.655	0.710
PC6	50.491	**<0.001***	22.166	**<0.001***	0.338	0.383
PC7	20.311	1.000	3.211	1.000	0.655	0.710
PC8	31.991	0.418	3.636	1.000	0.013	**0.011***
PC9	27.072	1.000	5.819	**1.000**	0.655	0.710
PC10	26.621	1.000	5.599	1.000	0.949	1.000

Table.IV.I.4. Kruskal Wallis and Mann-Whitney U's test in ORGDB.

	Complete sample		Ibero-Armorican sample		Lo Hueco sample	
	χ^2	p-value	χ^2	p-value	χ^2	p-value
PC1	95.119	**<0.001***	10.430	0.384	2.159	0.142
PC2	30.961	0.551	4.318	1.000	0.918	0.338
PC3	50.146	**<0.001***	6.390	1.000	0.037	0.848
PC10	30.749	0.589	2.797	1.000	2.551	0.110

Table.IV.I.5. Kruskal Wallis and Mann-Whitney U's test in RDB.

IV.I.4.2. CLUSTERING ANALYSES AND K-MEAN SOLUTIONS

We conducted the cluster analyses over the original variables in all the datasets. However, here we will only comment the results of the analyses for the sample of Ibero-Armorican domain titanosaurs and the sample from Lo Hueco alone. Complete cluster analyses of all Neosauropoda present low resolution both at genus level, as many of the specimens do not fall in same cluster. They can be found in Supplementary Materials IV.I.H nonetheless.

In the analysis of EXPDB we can distinguish two major clusters that groups most of the specimens of cf. *Lirainosaurus*, *Ampelosaurus atacis* and some of the specimens referred mainly to Morphotype I from Lo Hueco as well as several of the indeterminate morphotypes previously described in the Ibero-Armorican domain (Vila *et al.*, 2012). In this cluster (Fig.IV.7.A; superior cluster) several of the specimens of *A. atacis* form one minor cluster (Fig.IV.7.A; inferior cluster) as well as some of the elements of Morphotype I from Lo Hueco. Other specimens from the referred taxa are scattered between the clusters. On the second cluster we recoverd most of the elements of *Lirainosaurus astibaie*, Morphotype I from Lo Hueco and most of the specimens referred to Morphotype II from Lo Hueco. From those taxa, *L. astibaie* and Morphotype I from Lo Hueco represent two closer clusters.There is a third cluster with several of the referred specimens of Morphotype II from Lo Hueco near a small cluster composed by specimens of *L. astibaie* from Laño, Chera and a cf. *Lirainosaurus*. However, several of the specimens clearly referable to Morphotype II from Lo Hueco are recoered spread among all the other clusters. The resolution of the clusters is low in order to correctly assess clusters relevant for taxonomical allocation.

The analysis of the ORGDB on the other hand presents better definition of a cluster composed by *A. atacis*. Other cluster presents many of the specimens of Morphotype II from Lo Hueco, and other of the major groups presents the specimens of *Lirainosaurus astibaie* (Fig.IV.I.7.B.). However, several of the specimens referred to Morphotype II from Lo Hueco, which are clearly different from Morphotype I (e.g. HUE-594 and HUE-1319), are recovered mixed within other clusters. Morphotype I is also found mixed among several clusters, mainly with *L. astibaie*. One of the referred specimens, HUE-3108, the femur from the holotype of *Lohuecotitan pandafilandi*, is arranged within the same cluster as HUE-594, HUE-1319 and the Titanosauria indet. Form 1 and Form 4 previously described in the Ibero-Armorican domain (Vila *et al.*, 2012). All this specimens present morphological differences with the holotype material of *L. pandafilandi*. Although there is an a priori slightly better resolution of the clusters of the sampled taxa, those clusters hardly reflect taxonomical similarities again.

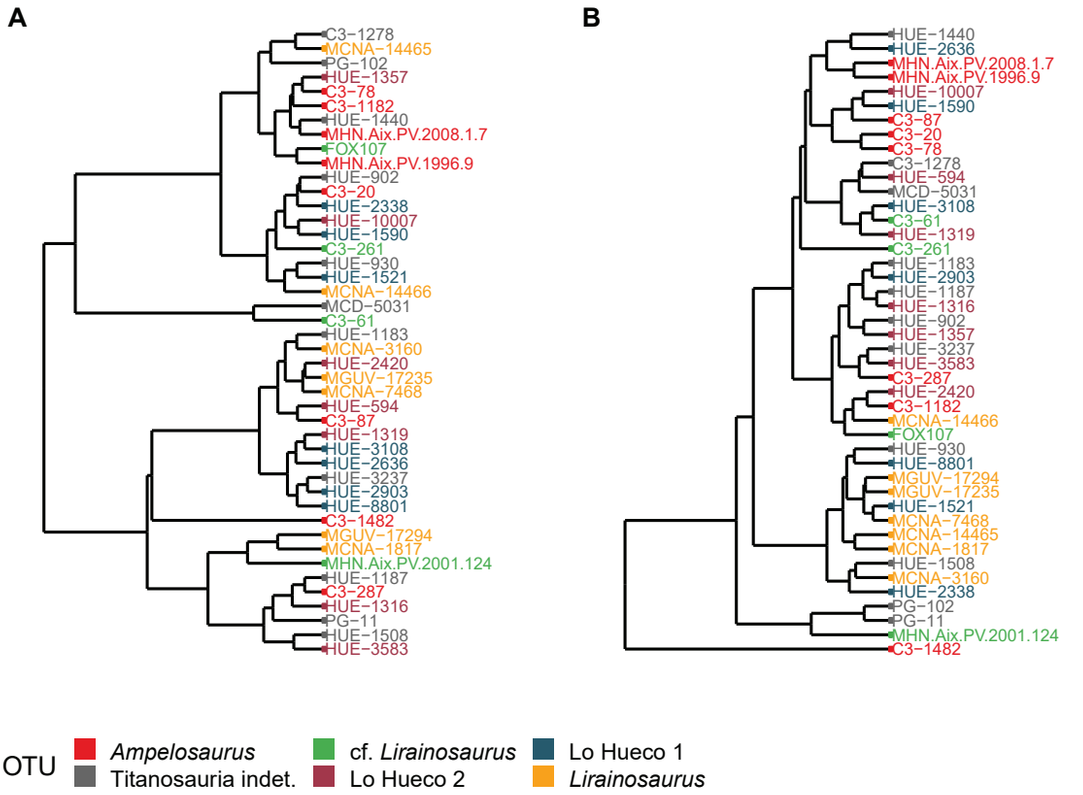

Fig.IV.I.7. Cluster analysis with the sample of Ibero-Armorican titanosaurs. (A) Cluster analysis in EXPDB. (B) Cluster analysis in ORGDB. Lo Hueco 1 - Morphotype I. Lo Hueco 2 - Morphotype II.

The clustering pattern was also assessed via k-means for the Ibero-Armorican titanosaur sample and Lo Hueco femora sample alone. We inspected the optimal number of clusters with reduction on the Bayesian Information Criterion and comparing the results with the titanosaur taxa already defined in the Ibero-Armorican domain. We conducted these comparisons in order to assess whether the clusters obtained show any paleobiological significance relevant for taxonomical classification of the sampled specimens. Current known species in the Ibero-Armorican domain with described femora are *Ampelosaurus atacis, Lirainosaurus astibaie*, *Lohuecotitan pandafilandi,* and it is probable that Morphotype II from Lo Hueco (based on the current work). The EXPDB analysis shows an optimal distribution of five clusters, with three, four, six and seven clusters hypotheses (in that order) with similar BIC (Fig.IV.I.9). EXPDB partitioning in four clusters reflect Lo Hueco Morphotype I cluster, includes Morphotype II from Lo Hueco into the *A. atacis* cluster and somewhat recognizes *L. astibaie* (although some of the specimens are reported in the similar morphospaces as Lo Hueco Morphotype I (Fig.IV.I.9). From the specimens of the Ibero-Armorican morphotypes previously recognized as well as cf. *Lirainosaurus*, only two form are present in distinct cluster, and might be separated by its position in PC1. However, the differences in PC1 within these specimens may overestimated as a by-product of the imputation methods. When increasing the number of clusters, *A. atacis* and Morphotype II from Lo Hueco are assigned to several clusters with the most robust elements of *L. astibaie* and the Ibero-Armorican undescribed morphotypes.

Within the sample of Lo Hueco, we observe that optimal number of clusters are three or four, followed by five different clusters. However, none of the distributions follows any of the differences observed in the described material (Fig.IV.I.10). The four groups hypothesis is the one that shows the most congruence with the described morphological differences but includes in the same clusters specimens that show differences referable to at least distinct taxonomical unit, like HUE-1319 and HUE-594 within the same cluster of HUE-3108 and HUE-2636 or the fragmentary specimen HUE-1440 within the same cluster of HUE-10007.

The analysis in ORGDB shows five clusters as the most optimal solution followed by four three and six clusters respectively. However, none of them presents similarities between the clusters and the already known species of the Ibero-Armorican domain. The six clusters solution resembles largely the morphospace distribution between the described taxa (Fig.IV.I.11). But in close inspections some morphospaces do not resemble natural groups, like cluster six which group part of the specimens from the unknown Ibero-Armorican titanosaurs, sample from Lo Hueco (of both described morphotypes) and specimens referred as cf. *Lirainosaurus*. With the sample of Lo Hueco alone we observe the more optimal solution in three or maybe two groups, followed by four and five probable clusters as the optimal result. We detected that for two clusters, all the specimens with difficult assessment are reported as a distinct group while the other cluster are the specimens which has been assessed already as Morphotype I or II by the description of the material. Additionally three cluster solution report two main clusters mixing several specimens referred to each morphotype and a third group formed by HUE-1521, HUE.-1508 and HUE-930 which are some of the specimens related with Morphotype I and occupying more positive values of PC1.

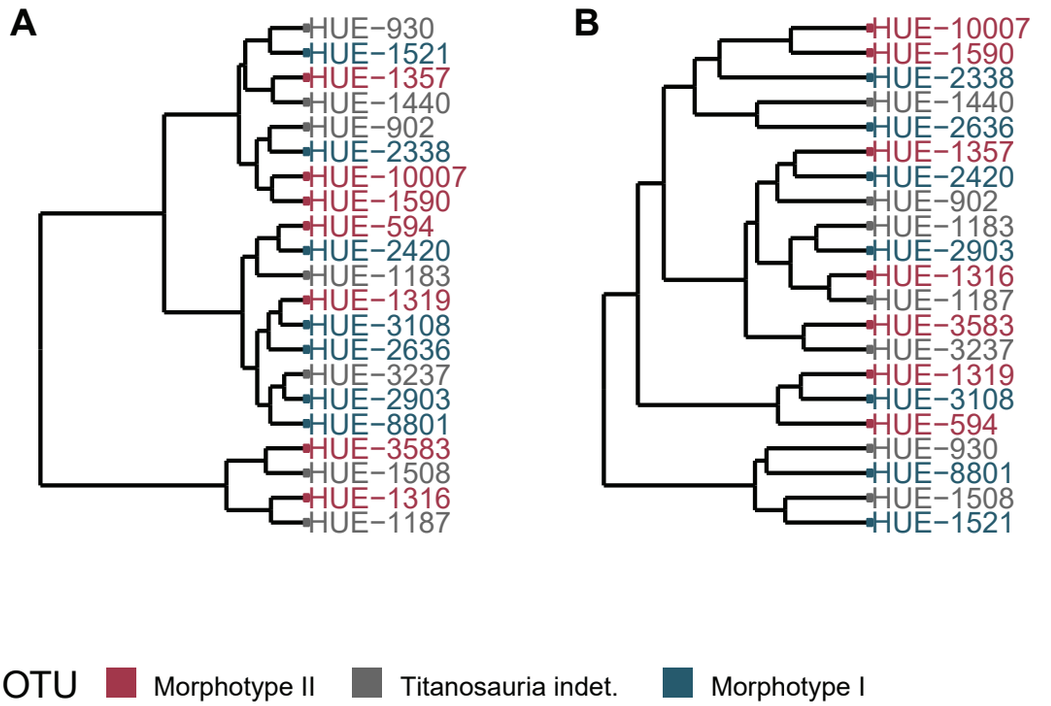

Fig.IV.I.8. Cluster analysis with the sample of Lo Hueco femora. (A) Cluster analysis in EXPDB. (B) Cluster analysis in ORGDB.

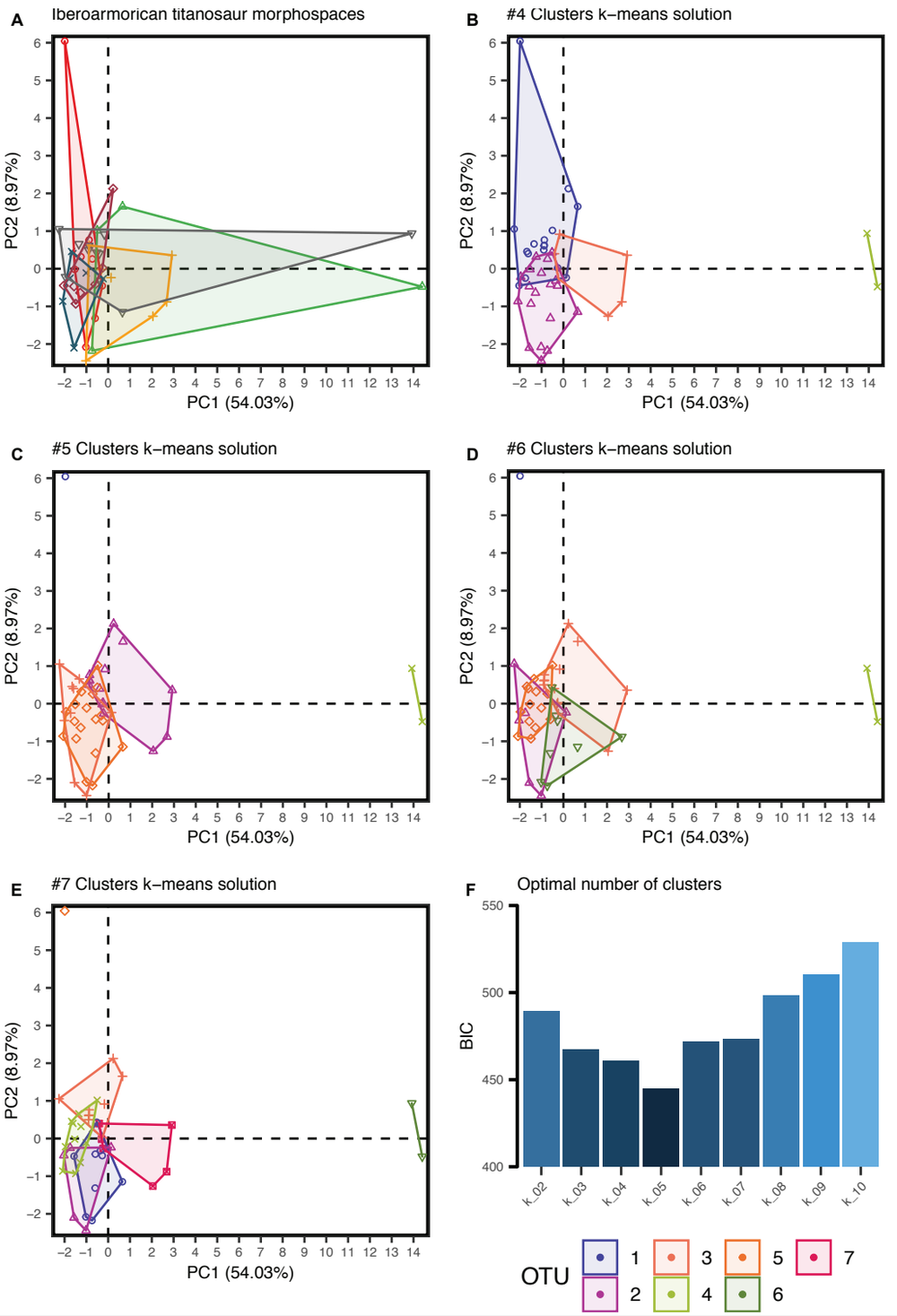

Fig.IV.I.9. Results of the k-means analysis in EXPDB within the Ibero-Armorican sample. (A) Original morphospaces in PC1-PC2. (B) Classification for k= 4 groups. (C) k= 5 groups. (D) k = 6 groups. (E) k = 7 groups. (F) BIC after partition of the morphospace into k groups.

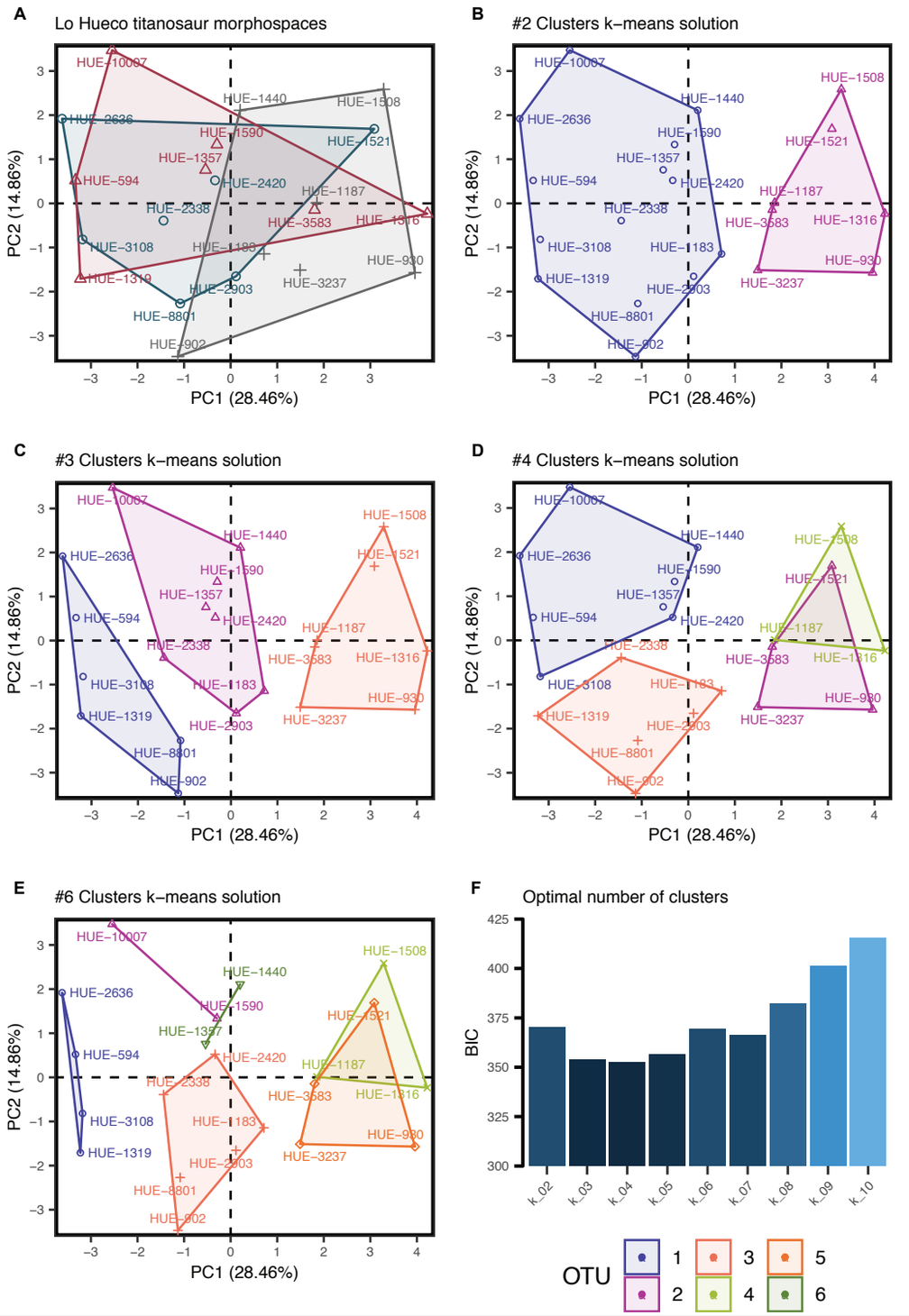

Fig.IV.I.10. Results of the k-means analysis in EXPDB within the Lo Hueco sample. (A) Original morphospaces in PC1-PC2. (B) Classification for k= 5 groups. (C) k= 3 groups. (D) k = 4 groups. (E) k = 6 groups. (F) BIC after partition of the morphospace into k groups.

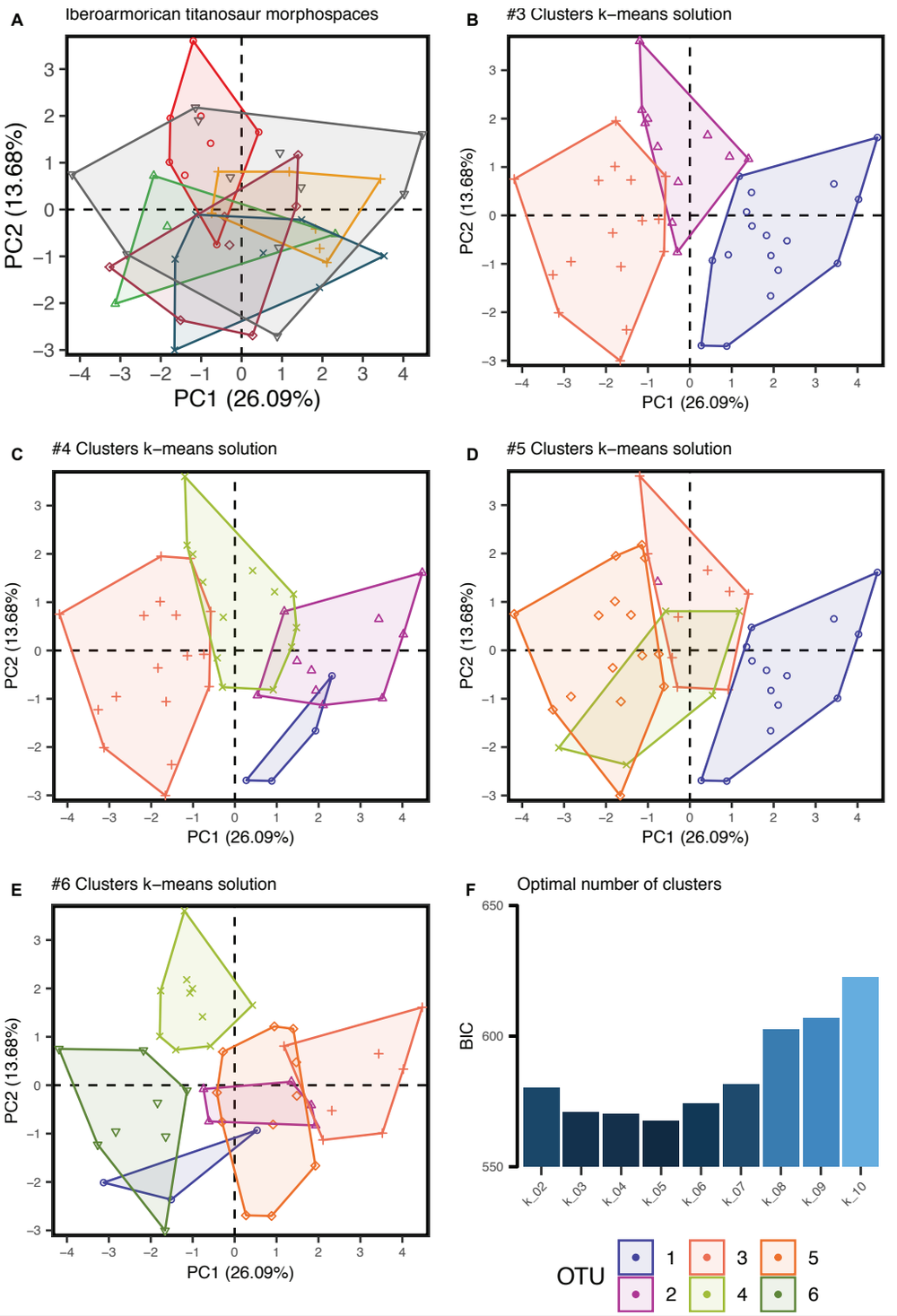

Fig.IV.I.11. Results of the k-means analysis in ORGDB within the Ibero-Armorican sample. (A) Original morphospaces in PC1-PC2. (B) Classification for k= 4 groups. (C) k= 5 groups. (D) k = 6 groups. (E) k = 7 groups. (F) BIC after partition of the morphospace into k groups.

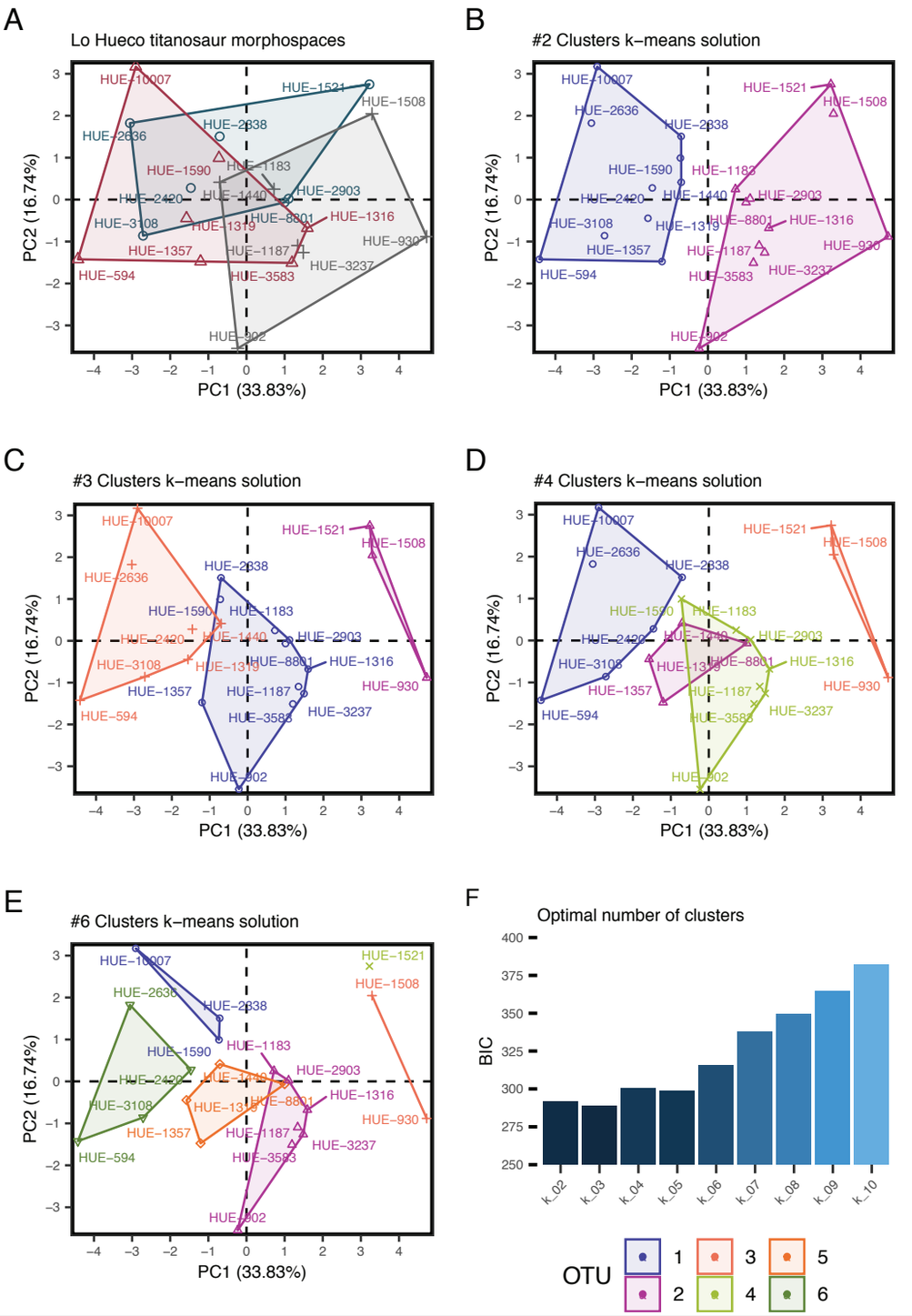

Fig.IV.1.12. Results of the k-means analysis in ORGDB within the Lo Hueco sample. (A) Original morphospaces in PC1-PC2. (B) Classification for k= 2 groups. (C) k= 3 groups. (D) k = 4 groups. (E) k = 6 groups. (F) BIC after partition of the morphospace into k groups.

Finally, the analysis of RDB found three, four and two respective clusters (in that order) as the optimal clusters solutions. However, none of the clustering solution report a pattern referable to the known Ibero-Armorican titanosaurs, and it is highly unlikely that these results resemble any biological cluster with taxonomic value (see supplementary). Analysis based on robustness indices alone shows the worst results in majority of unsupervised exploratory analyses.

IV.I.4.3. SUPERVISED CLASSIFICATION METHODS

The discriminant function analyses as per Smith *et al.* (2005) return classification accuracy overall. Table.IV.I.7 shows accuracy of each classification method used onto the three datasets. Discriminant function analysis can be affected by the uneven distribution of the classes (sauropod genus and morphotypes in this case) of the input data. Best performance is achieved with the analysis of EXPDB dataset (mean accuracy 37.04%, see Table.IV.I.7), and also the classification is significant (the symmetries between DFA and MANOVA permit us to obtain p-value like when calculating Wilk's Lambda). Moreover, EXPDB is the only datasets that exhibit significant differentiation between the input OTUs ($p= 0.003$). A detailed report of the classification accuracy via cross validation of the testing sample can be accessed in Supplementary Material IV.I.J. The majority of misclassified specimens come from species that share similar morphospaces, like the low sensitivity of *Apatosaurus* spp. which is classified in majority of specimens of testing group as *Camarasaurus* spp. Some specimens of Morphotype II from Lo Hueco (both classified or between undetermined Titanosauria indet. specimens) classified as *Ampelosaurus* sp. or *Neuquensaurus* sp.

When comparing this results with ORGDB and RDB, none of the latter have an accuracy greater than 50%. It is worth noting that RDB classify better with DFA algorithm and results are slightly more accurate by 2% approximate (both the lower and higher accuracy rates reported). Each discriminant function (DF/LD) can be plotted similarly to PCs. Here we show first and second DFs on EXPDB and ORGDB (Fig.IV.I.13), but a comprehensive visualization of first to third DFs in each dataset can be shown in Supplementary Material IV.I.J.

On the other hand, the SVM presents much better results in accuracy than the DFA. EXPDB dataset reports the best accuracies with a mean of 42.59% rate (see Table.IV.I.7). ORGDB and RDB have a mean accuracy of 35.19% and 33.33% respectively, but their higher accuracy is near 50% in both cases. All the results present significant differentiation between the OTUs (EXPDB p-value >0.05, ORGDB and RDB p-value >0.05). A comprehensive result of the cross-validation and a detailed report of the accuracy can be found on Supplementary Material IV.I.K. It is worth noting that in this case, ORGDB presents slightly better results compared with RDB. Also, all the analyses improve specially in the lower accuracy, generally as much as 5% more precise in all the datasets than the lower accuracy reported in DFA analyses, while the higher accuracy rate is only an slightly better by 2% per dataset compared to DFA. Another difference reported between SVM and DFA is in the sensitivity and estimated probabilities. Sensitivity of the SVM is greater in some of the OTUs, while less classes are accurately classified. When assessing the probabilities, we can observe that primary and secondary probabilities are much more even between them. The DFA usually report a 1st class probability whereasother probable classes shows residual probabilities. SVM voting strategy present much more similar probabilities between all the classes, but the morphospaces separation is better nonetheless. This leads to few OTUs correctly classified but the ones that are correctly

Dataset	Classificator	Accuracy					Cohen's Kappa
		Mean	Lower	Upper	Null	p-value	
EXPDB	LDA	37.04 %	24.29 %	51.26 %	20.37 %	**0.003***	0.292
	SVM	42.59 %	29.23 %	56.79 %	20.37 %	**<0.001***	0.336
ORGDB	LDA	27.78 %	16.46 %	41.64 %	20.37 %	0.120	0.178
	SVM	35.19 %	22.68 %	49.38 %	20.37 %	**0.008***	0.206
RDB	LDA	29.63 %	17.98 %	43.61 %	20.37 %	0.069	0.152
	SVM	33.33 %	21.09 %	47.47 %	20.37 %	**0.018***	0.179

Table.IV.I.7. Report of the DFA and SVM classificators.

classified present high sensitivity and recall. The morphospaces are correctly separated from other forms even in cases of high overlapping between the OTUs (e.g. Neuquensaurus spp.).

The accuracy of the method can also be observed by Cohen's Kappa (Cohen, 1960; Bakeman *et al.*, 1997; Bruckner & Yoder, 2006) which is a measurement of agreement of classification given the possibility of allocation at random. All the Cohen Kappa's values of SVM are greater than in DFA (Table.IV.I.7). For further comparison, we highlighted the classified specimens of the testing group over the results of PC1 and PC2 plot of EXPDB (Fig.IV.I.14) and ORGDB (Fig.IV.I.15). We can observe that SVM classifies better (accurately estimated the OUT) in the limits of morphospaces and also where several morphospaces are overlapped. On the other hand, DFA accurate classifications are concentrated near group means but worse in the morphospace frontiers, especially when several OTUs present similar morphospaces.

IV.I.5 DISCUSSION

IV.I.5.1. CHARACTER OVERVIEW AND SYSTEMATICS ASSESSMENT

The femora described here can be referred to Titanosauriformes based on the presence of a trochanteric shelf in the proximal third of the posterior face. The trochanteric shelf is a parallel ridge medially located to the developed lateral bulge. In the studied specimens the trochanteric shelf and the lateral bulge have the same length that extends to the position of the fourth trochanter (the trochanteric shelf is slightly shorter than the lateral bulge in HUE-1366). The trochanteric shelf has been considered autapomorphic of saltasaurine titanosaurs (Otero, 2010a) but it is known also in other more basal titanosauriformes: e.g. *Giraffatitan brancai* (Janensch, 1961), *Lirainosaurus astibaie,* a new titanosauriform from Sant Antoni de la Vespa (Mocho *et al.*, 2016a), *Tastavinsaurus sanzi* (Royo-Torres, 2009) and *Huaebisaurus allocotus* (D'Emic *et al.*, 2013). There is also a marked medial deflection of the femoral head in the majority of specimens, when comparing the angle between the base of the distal condyles and the proximal end. This deflection have been reported in more derived titanosauriforms and is part of the features of wide-gauge acquisition of titanosaur sauropods (Wilson & Carrano, 1999; Ullmann *et al.*, 2017). Also the presence of a straight and somewhat eccentric midshaft is common among sauropods (Wilson & Sereno, 1998; Wilson, 2002; Upchurch *et al.*, 2004a). However, an eccentric midshaft approximately two times wider lateromedially than anteroposteriorly is relatable to more derived forms (Wilson, 2002; Upchurch *et al.*, 2004a). It was considered a synapomorphy of Saltasauridae (Wilson, 2002) but is probably a common feature in Titanosauriformes (Carballido *et al.*, 2011b; Mannion *et al.*, 2013).

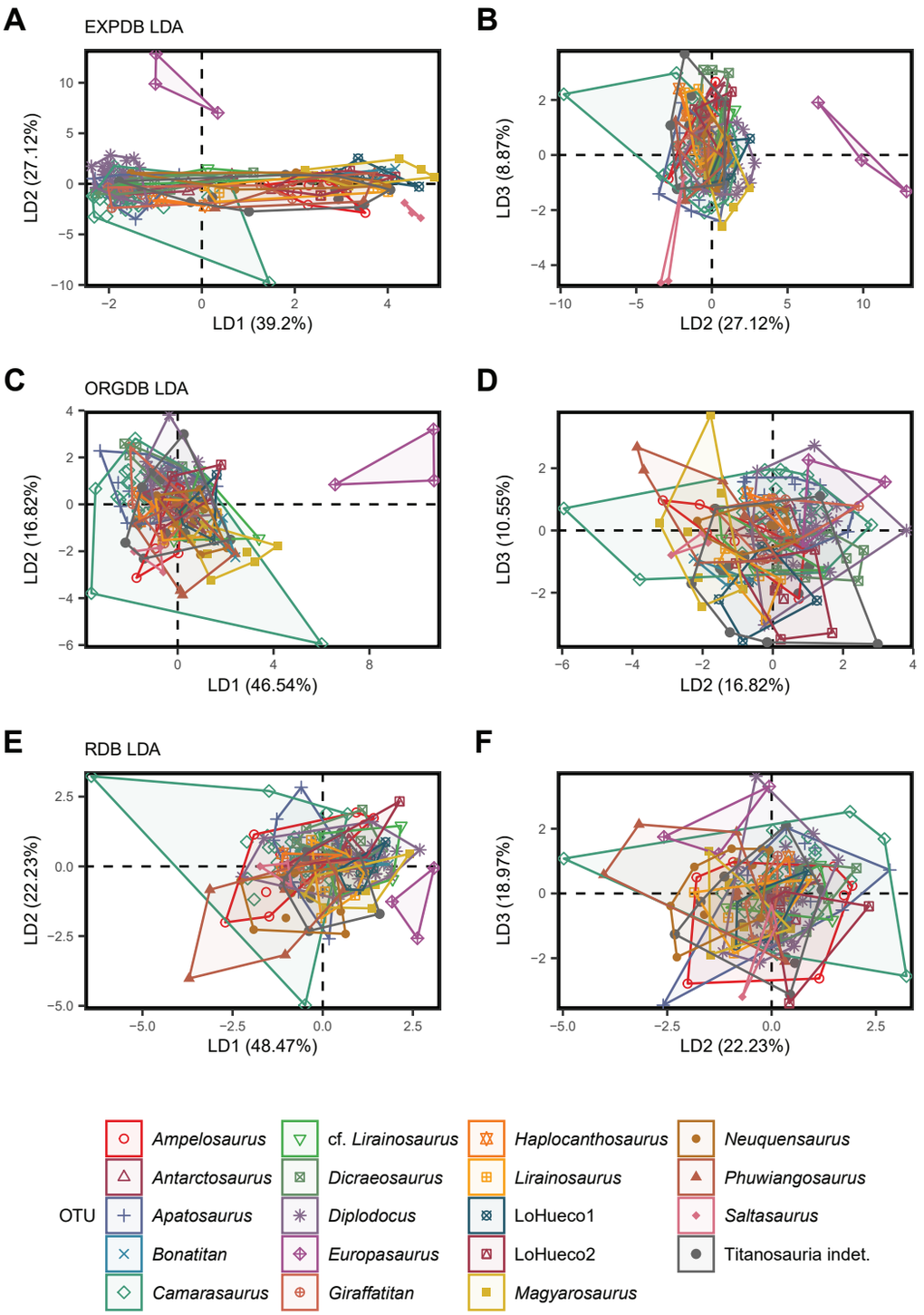

Fig.IV.1.13. Results of the DFA/LDA. (A) LD1-LD2 and (B) LD2-LD3 of the analysis of the EXPDB. (C) LD1-LD2 and (D) LD2-LD3 of the analysis of the ORGDB. (E) LD1-LD2 and (F) LD2-LD3 of the analysis of the RDB.

The more slender femora of *Lohuecotitan pandafilandi* and Morphotype I present a stepped femoral head respectively to the greater trochanter, but no constriction as in other titanosaur sauropods (Salgado *et al.*, 1997a). The Morphotype II does not present any constriction and rarely present a step between the femoral head and the greater trochanter is absent. Hwever, This characteristic is variable among sauropods, and instead of a constriction between the femoral head and greater trochanter, we can observe a reduction in the anteroposterior width of the proximal end at lateromedial position of the greater trochanter. This feature is shared with other titanosaurs like *Mendozasaurus neguyelap* or *Elaltitan lilloi*, and contrary to the wide femoral head and greater trochanter of more basal Neosauropoda like *Camarasaurus* spp. (Osborn & Mook, 1921; McIntosh *et al.*, 1996a,b; Woodruff & Foster, 2017). All the femora of Lo Hueco present a less developed fourth trochanter in comparison to non-titanosauriform sauropods like *Camarasaurus* spp. (Osborn & Mook, 1921; Gilmore, 1925; McIntosh *et al.*, 1996b), *Diplodocus* spp. (Hatcher, 1901; Holland, 1906; Tschopp *et al.*, 2015), *Haplocanthosaurus priscus* (Hatcher, 1903) and *Spinophorosaurus nigerensis* (Remes *et al.*, 2009). The fourth trochanter is more similar to the ones present in titanosauriforms e.g. *Giraffatitan brancai* (Janensch, 1961) and *Jainosaurus* cf. *septentrionalis* (left femur NHM-R5903). The reduction of the fourth trochanter to a low ridge (generally not visible in anterior view) is shared within titanosauriformes supporting its assessment as at least a titanosauriform type of femora (Wilson & Sereno, 1998; Sanz *et al.*, 1999; Gallina & Apesteguía, 2005; Whitlock, 2011; D'Emic, 2012). Some caveats apply, as *Lohuecotitan pandafilandi* + Morphotype I present a fourth trochanter slightly placed in the edge of medial and posterior faces. Generally, they are not visible in anterior view except for some specimens (e.g. HUE-2903) that present a light bump visible in the anteromedial view. However, some other non titanosauriformes may have fourth trochanter not visible in anterior face like *Brontosaurus excelsus* (Whitlock, 2011; Mannion *et al.*, 2013; Tschopp *et al.*, 2015). Some femora of Morphotype II present a straighter shaft compared with the marked deflection to proximomedial present in most of titanosaurs. The derived Macronaria in general presents a gentle angle between the axis of the shaft and a perpendicular axis with the plane of the distal condyles, as seen in *Tastavinsaurus sanzi* (Royo-Torres, 2009), *Aragosaurus ischiaticus* (Sanz *et al.*, 1987) or *Brachiosaurus altithorax* (Riggs, 1903; Paul, 1988; Taylor, 2009). More derived titanosauriformes share a proximomedial deflection of the shaft of 10° or more. This deflection to medial of the femoral head and bevelling of the distal end is related with a displacement upward of the tibial condyle (Salgado *et al.*, 1997a; Wilson & Sereno, 1998; Wilson & Carrano, 1999; Wilson, 2002; Carrano, 2005; Royo-Torres, 2009; D'Emic, 2012; Mannion *et al.*, 2013; Gorscak *et al.*, 2017; Ullmann *et al.*, 2017). The Morphotype II present less development of the medial deflection contrary to Morphotype I, but there is some deflection nonetheless (contra non-titanosauriform sauropods). Values range in intermediate values between those of more basal titanosaurifomres or derived non-titanosauriform macronarians (e.g. *B. altithorax*, *A. ischiaticus* or *T. sanzi*) and more derived titanosaurian forms e.g. *Opisthocoelicaudia skarzyinski* (Borsuk-Bialynicka, 1977), *Neuquensaurus australis* or *Saltasaurus loricatus* (Powell, 2003). In fact, they are comparable to other robust titanosaur femora like the ones from *Ampelosaurus atacis* which present straighter shaft than other titanosaurs (Le Loeuff, 2005a; Vila *et al.*, 2012).

Another character already used for recognition of isolated elements in the Ibero-Armorican domain has been the presence or absence of a linea intermuscularis cranialis in the anterior part of the femur (Vila *et al.*, 2012). This structure was identified by Powell (Powell, 2003) and separates the insertions of the M. femorotibialis externus and internus (Otero & Vizcaíno, 2008; Otero, 2010a). It has been regarded as a saltasaurine synapomorphy in recent

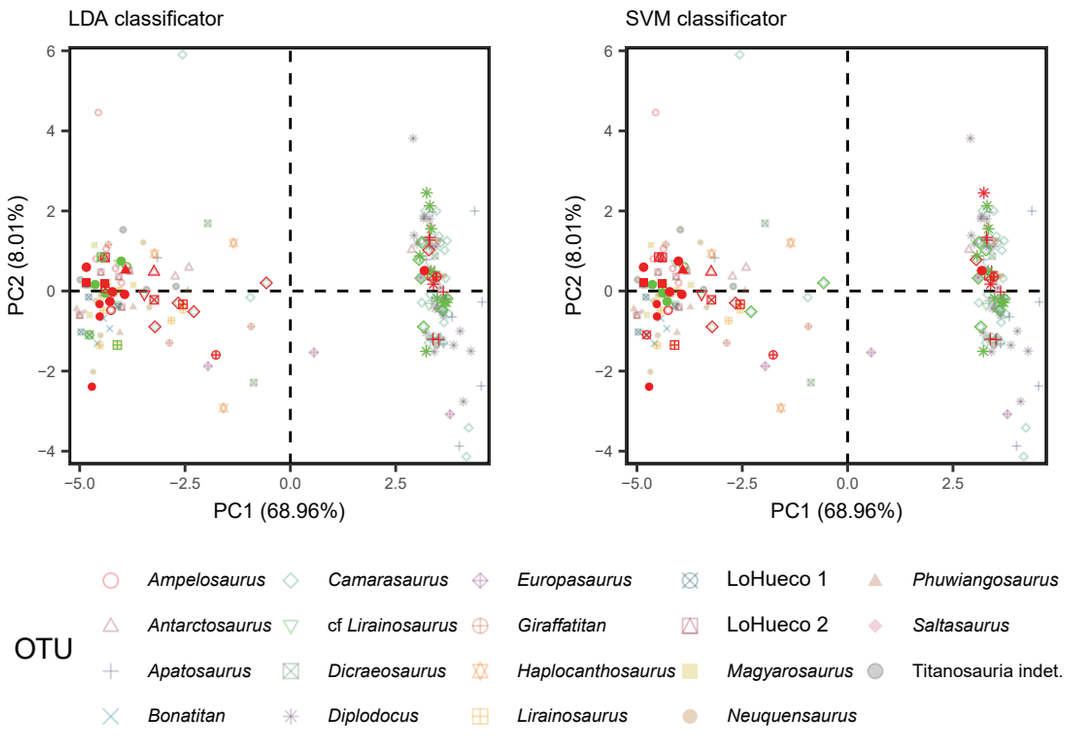

Fig.IV.I.14. Comparison between the DFA/LDA and the SVM results in the EXPDB. LoHueco 1 - Morphotype I. Lo Hueco 2 - morphotype II. In red the missclassifications of the testing sample. In green the accurate classfications of the testing sample.

systematic studies (D'Emic, 2012; Mannion *et al.*, 2013). In the studied sample it can be observed the presence of this ridge and its variability. Some elements attributed to Morphotype I (e.g. HUE-2420 and HUE-3108, the Lohuecotitan type femur) and Morphotype II (HUE-1319, HUE-1187 and to some extent in HUE-594) present this structure. Other femoral forms from the Ibero-Armorican Late Cretaceous also share the present of linea intermuscularis cranialis (Vila *et al.*, 2012). This character may be characteristic of a more inclusive group of derived titanosaurs than Saltasauridae contrary to D'Emic (2012) based on current phylogenetic hypothesis for *Lohuecotitan pandafilandi* (Sallam *et al.*, 2018; Díez Díaz *et al.*, 2018a).

When comparing the two main morphotypes described with the holotype material of *Lohuecotitan pandafilandi* as well as other titanosaurian sauropods, the Morphotype I share with *L. pandafilandi* several features. The distal condyles present some medial bevelling, especially the tibial condyle with the highest torsion to medial. However, this medial torsion of the tibial condyle is not as marked as in *L. astibaie*. The the lateromedial width of the tibial condyle is almost equal to the fibular condyle width (including the lateral epicondyle) in all of the elements attributable to this type, like in HUE-3108, the holotype of *L. pandafilandi*, and contrary to Morphotype II. This character is also shared with *Lirainosaurus astibaie*. The lateromedially narrow (with lateromedially subequal condyles) and anteroposteriorly wide distal end is also similar to other titanosauriforms e.g. *Jainosaurus* cf. *septentrionalis* (Wilson *et al.*, 2011), *Euhelopus zdanskyi* (Wilson & Upchurch, 2009), *Narambuenatitan palomoi* (Filippi, García, & Garrido, 2011), *Gobititan*

shenzhouensis (You, Tang, & Luo, 2003) and "*Titanosaurus*" *falloti* (Hoffet, 1942; Wilson & Upchurch, 2003; D'Emic *et al.*, 2013). Though it is not exclusive of titanosauriforms and it is also similar to some diplodocoids like in *Apatosaurus ajax* (Upchurch *et al.*, 2004b). The Morphotype II presents anteroposteriorly compressed condyles, only posteriorly projected and perpendicular to the shaft with no medial bevelling. The shaft is slightly more robust than in Morphotype I and much more eccentric (Mean Eccentricity Index ~2.7 compared to ~2.1 of Morphotype I, see Table. IV.I.1). These characteristics are shared with *Ampelosaurus atacis* (Le Loeuff, 2005a; Vila *et al.*, 2012), *Petrobrasaurus puestohernandenzi* (Filippi *et al.*, 2013) or *Antarctosaurus wichmannianus* (Powell, 2003).

Other character that differs between both morphotypes is the present of a smooth transition between the greater trochanter to the lateral bulge in Morphotype I. It lacks the pronounced step from the lateral bulge to the greater trochanter as in other sauropods e.g. *Alamosaurus sanjuanensis* (Gilmore, 1946), *Bonatitan reigi* (Salgado *et al.*, 2015), *Aeolosaurus* sp. specimen MPCA-Pv-27177 (Salgado, Coria, & Calvo, 1997b; García & Salgado, 2011), *Magyarosaurus* spp. (Nopsca, 1915), *Opisthocoelicaudia skarzynskii* (Borsuk-Bialynicka, 1977), and the Titanosauria indet. TMM-46052-1 (Wick & Lehman, 2014). On the contrary, the transition between the greater trochanter and the lateral bulge is more glentle like in *Rapetosaurus krausei* (Curry Rogers, 2009; Curry Rogers *et al.*, 2016), *Aragosaurus ischiaticus* (Sanz *et al.*, 1987), *Elaltitan lilloi* (Mannion & Otero, 2012), *Lohuecotitan pandafilandi* and the specimen of Titanosauria indet. UTEP-P-25 (Wick & Lehman, 2014).

Meanwhile, the Morphotype II presents a more usual stepped morphology between the greater trochanter and the lateral bulge (e.g. HUE-594) that is less marked than in *Bonatitan reigi* (e.g. left femur MACN-PV-RN-821) or *Aeolosaurus* sp. (e.g. MPCA-27177). However, it is much more marked than in *Lohuecotitan pandafilandi* and comparable to the greater trochanter-lateral bulge transition in *Alamosaurus sanjuanensis* (Lehman & Coulson, 2002). Or the stepped morphology posterior to the greater trochanter similar to less derived Neosauropoda without lateral bulge like *Camarasaurus* spp. (Osborn & Mook, 1921; Gilmore, 1925; McIntosh *et al.*, 1996a; Ikejiri, 2004).

When compared with other European titanosaur taxa, some differences are observed in the anteroposterior compression of the femoral head of *Ampelosaurus atacis* (see Vila *et al.*, 2012) contrary to the more expanded femoral head of *Lohuecotitan pandafilandi* and *Lirainosaurus astibaie* (e.g. MCNA-7468). The Morphotype II presents the anteroposterior compression of the femoral head similar to *A. atacis*. The majority of specimens referred to Morphotype I present at least the medial part of the femoral head and it is possible to observe that it is anteroposteriorly expanded like in *Lohuecotitan pandafilandi* or at least as expanded as in *Lirainosaurus astibaie*. When comparing the proximal end of Morphotype I to *L. astibaie*, some differences can be observed. While *Lirainosaurus* femoral head is more expanded anteroposteriorly than in *Ampelosaurus* femora, they are not as anteroposteriorly wide as Morphotype I and *Lohuecotitan pandafilandi*. The only other European sauropod with this anteroposterior expansion of the femoral head is *Magyarosaurus* spp. like in specimens NHM-R3856, NHM-R3859 or even fragmentary femur NHM-R4898. (pers. obs. APB 2016). Another feature of Morphotype I shared with other European titanosaur taxa is the anteroposterior expanded condyles like in *L. pandafilandi*, *Magyarosaurus* spp. and *Lirainosaurus astibaie*. The Morphotype II does not present anteroposteriorly expanded condyles and resembles the anteroposteriorly compressed and lateromedially expanded condyles which characterizes *Ampelosaurus atacis* (see the distal end in distal view in Vila *et al.*, 2012). Other important feature to distinguish the femora morphotypes from Lo Hueco is the morphology of

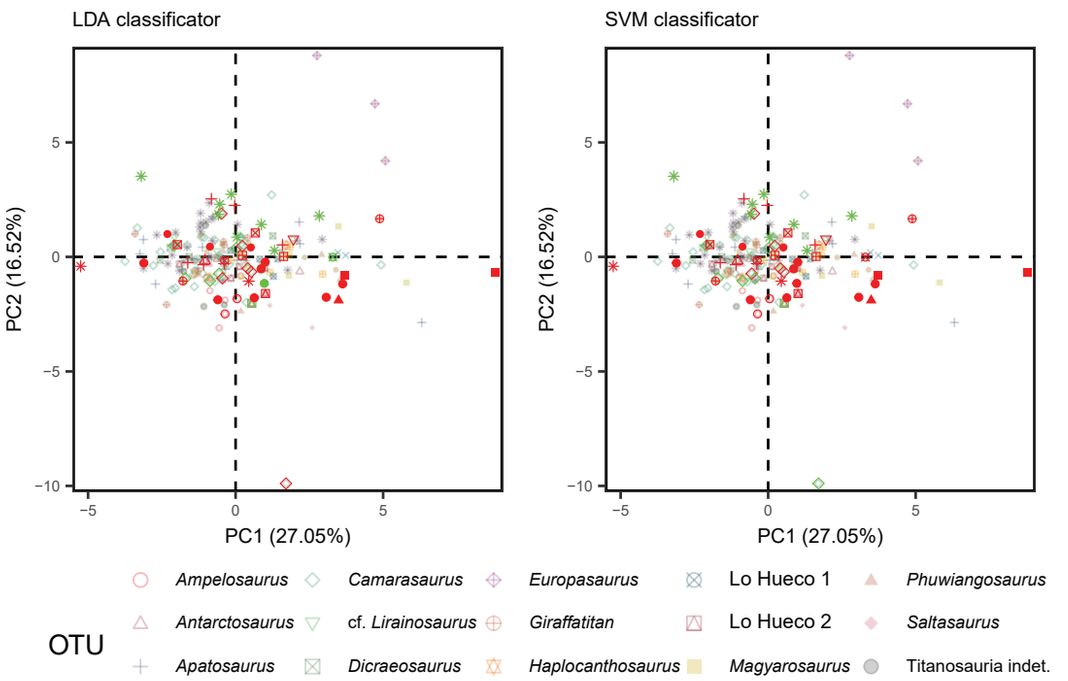

Fig.IV.I.14. Comparison between the DFA/LDA and the SVM results in the ORGDB. LoHueco 1 - Morphotype I. Lo Hueco 2 - morphotype II. In red the missclassifications of the testing sample. In green the accurate classfications of the testing sample.

the distal condyles. In Morphotype II, the overall the distal condyles morphology resemble that of *Ampelosaurus atacis* (Le Loeuff, 2005a; Vila *et al.*, 2012). The distal end is compressed anteroposteriorly, more similar to *Ampelosaurus atacis* than to cf. *Lirainosaurus astibaie*, and to the Form 1, 2 and 3 of Vila *et al.* (2012). Both distal condyles extend parallel and have low medial torsion. The medial edge of the tibial condyle is not as posetriorly projected as in *A. atacis*.

Main morphological differences overserved across all the analyses that includes the sample from Lo Hueco suggests the presence of two distinct morphotypes. However, we tested the presence of three and four distinct groups among the sample from Lo Hueco (after Vidal *et al.*, 2017; Mocho *et al.*, 2018). The presence of some variable features suggests that it could be possibe that more than two appendicular morphotpyes are present in this site. The presence/absence of some structures and the combination with other discrete and continuous related characters already present in the appendicular elements opens the possibility of having more than two morphotypes similarly to the morphological variation observed in the axial skeleton. These characters includes the relative position of the fourth trochanter in posterior face, the eccentricity of the shaft, the robustness of the proximal or distal ends, the midshaft, or the overall bone in sensu lato, as well as the rotation of tibial and fibular condyle. For example, some of the features discussed by Vila *et al.* (2012) as the presence of an accessory trochanter of the fourth trochanter (e.g. HUE-2338) or not (e.g. HUE-3108), is variable among specimens referred to the same morphotype (Morphotype I). Several of these features are also variable in other Ibero-Armorican titanosaurs (e.g. the presence of the linea intermuscularis cranialis and the Eccentricity Index among specimens from the same taxa).

The possibility of several small specimens that are attributed to the Morphotype I pertain to small taxa is also discussed here. The smallest specimens (e.g. HUE-2636, HUE-8801) present similar morphology with Morphotype I, i.e. anteroposteriorly wide and lateromedially narrow proximal and distal end, subcircular shaft section and medial di of the proximal end. The shaft of these specimens is slightly less eccentric than the shaft of *Lirainosaurus astibaie* (Eccentricity Index ~2.1-2.7) nor cf. *Lirainosaurus astibaie* (Eccentricity Index ~2-2.3 Vila *et al.*, 2012). However, there are some exceptions e.g. MCNA-7468 referred to *L. astibiae* (Eccentricity index ~1.7; pers. obs. APB 2016) and specimen MHN.AIX-PV-2001.124 reffered to cf. *L. astibiae* (Eccentricity Index ~1.7; Vila *et al.* 2012). The proximal end is more bulbous and anteroposteriorly expanded than *L. astibaie* (and cf. *L. asitbiae*). The position of the fourth trochanter vary but it is posteromedially located in Morphotype I and *Lirainosaurus astibaie* (e.g. MCNA-3160). The distal end is anteroposteriorly wide as in Morphotype I, with some medial bevelling in the tibial condyle but not as pronounced as in *L. astibaie* (and cf. *L. astibaie*). It is possible that these small femora from Lo Hueco pertain to the Morphotype I as they present different features in the proximal and distal end compared to *L. astibaie* (and cf. *L. astibaie*). Whether they are putative juvenile or present some intraspecific variability should be covered elsewhere (see Chapter V, Chapter VI). Further commentary on the development of this organisms is beyond the scope of this work.

The Form 1 and 2 from Vila *et al.* (2012) also have low eccentric shaft as seen in the Morphotype I of Lo Hueco. Comparing these forms with Morphotype I some differences can be identified: (i) a robust fourth trochanter, not so expanded proximodistally and located on the medioposterior edge of the femoral shaft in Morphotype I contra Form 1 and 2 in which the fourth trochanter is medially located and seen in anterior view; and (ii) absence of a developed trochanteric shelf in Form 1 and 2. The loss of proximal and distal parts of both specimens of Form1 and 2 (Vila *et al.*, 2012) render difficult to assess if they share the characteristic anteroposteriorly wide morphology of the distal part of the Morphotype I from Lo Hueco. The feature combination does support the differences between all the specimens referred to Morphotype I and Form 1 and 2 from the Maastrichtian of the Ibero-Armorican domain. Moreover, there are no specimen from Lo Hueco that resemble neither forms.

The second morphotype is more robust, with an eccentric midshaft, distal condyles more separated by a greater intercondylar fossa than in Morphotype 1. The distal condyles are not so medially bevelled and less anteriorly projected. On the other hand they are well posteriorly projected. They resemble the femur from *Ampelosaurus atacis* (Le Loeuff 2005) and the Form 4 from the Maastrichtian of the Ibero-Armorican domain (Vila *et al.*, 2012). However, in the Morphotype II the intercondylar fossa is less transversely expanded than in *A. atacis,* without the intercondylar proximodistal sulcus present in the middle of the fossa that is characteristic from *A. atacis* (Le Loeuff, 2005, see details in Vila *et al.*, 2012). Also some degree of ventral projection of the tibial condyle is present in many of the specimens from the Morphotype II while in *A. atacis*, the distal part is straight in its basal plane. This is also an important character that differentiates Morphotype I and Morphotype II. Some of these characters are obscured in some of the specimens of the studied sample and it is difficult to assess whether they belong to the Morphotype II, *A. atacis* or other Ibero-Armorican form with an eccentric diaphysis and medially displaced fourth trochanter. At least the combination of characters permit to rule outthe possibility of having *Lirainosaurus astibaie* (or cf. *Lirianosaurus*) among this femoral sample of specimens from Lo Hueco.

IV.I.5.2. MORPHOMETRICS OF THE IBERO-ARMORICAN TITANOSAURS

When selecting the appropriate set of morphometric variables for the data matrices, several important features were determined as not suitable based on the available sample. For example some features commented in the anatomical comparison such as the medial deflection of the tibial condyle, the projection on anterior view of the femoral head and minimal shaft torsion among others are difficult to include in the data matrix as it was not possible to access in all the studied specimens in this study. They are also variables not registered in previous studies, and sometimes the available photographic material with an appropriate view for digital measurement is scarce. This is especially relevant as some of the taxa with more missing information in those variables are taxa with comprehensive anatomical descriptions already published e.g. *Camarasaurus* spp., *Giraffatitan brancai*, *Diplodocus* spp., *Apatosaurus* spp. or *Phuwiangosaurus sirindhornae* (Mook, 1903; Osborn & Mook, 1921; Gilmore, 1936b; Janensch, 1961; Martin, Buffetaut, & Suteethorn, 1994; Suteethorn *et al.*, 2010). An early attempt in the construction of the present data matrices with the incorporation of those variables could lead to imputation rates over 75% of these measurements, which is not desirable for the present analyses.

The PCA (Fig.IV.I.4 and Supplementary Material IV.I.E) and cluster analysis (Supplementary Material IV.I.H) of the EXPDB permit to visualize and differentiate two major sauropod groups within Neosauropoda. One of the groups is composed by Diplodocoidea (Apatosaurinae + Dicraeosauridae + Diplodocinae), as well as some Brachiosauridae and Non-Titanosauriformes Macronaria, This group represent more positive values in PC1 and occupies a wide range of values from negative to positive values of PC2. There is a mix of Non-Titanosauriformes Macronaria and Somphospondyli in several intermediate clusters between the two major groups reported. The Non-Titanosauriformes macronarian femora are found in the negative values of PC1 and PC2 or among the cluster of mainly Somphospondyli sauropods might be due exaggerated values by the estimation method. Some of these specimens are partially incomplete either by fragmentary state or because not all measurements were available in the literature (neither image to digitally measure). Moreover, one of these cases is CM-11338, one of the most complete specimens of *Camarasaurus lentus* (see Gilmore, 1925). Specimen CM-11338 is a juvenile individual of *C. lentus* with a slightly eccentric femora and anteroposteriorly compressed proximal and distal condyles in comparison with other individuals of the same species (Ikejiri, Tidwell, & Trexler, 2005) as well as a gentle medial displacement of the femoral head without the medial bevelling proper of wide-gauge stance. The measurements related to these features present some missing data and after estimation, it present a combination of values more similar to Somphospondyli sauropods than could be expected. This by-product of the estimation method might have caused also that some titanosaur femora are projected on the other way e.g. MCD-5031 of the Ibero-Armorican domain Titanosauria indet. Form 4 (Vila *et al.*, 2012) or MLP-Ly Titanosaur indet. femora from General Roca (Powell, 2003), located more towards macronarian sauropods in the PCA and far from other Titanosauria in the cluster analysis. Despite these specimens overlapping within non-somphospondylian morphospace, we can distinguish between a cluster of columnar hindlimb sauropods without wide-gauge posture and the more derived somphospondyles with wide-gauge stance. Our results show similar trends to the published results of 2D landmark geometric morphometrics analyses on all the inclusive clades of Sauropoda (Bonnan *et al.*, 2013; Ullmann *et al.*, 2017). In this study there is not enough sample among basal titanosaurs in order

to assess significant differences between Non-Titanosauriformes Macronaria and more basal forms of Titanosauria thought. We relay on the comparison between Somphospondyli and Non-Titanosauriformes Macronaria. Among more derived neosauropods groups in negative values of PC1 of EPXDB, and the more derived cluster (Suplementary Material IV.I.H) we can observe the overlapping between Somphospondyli Titanosauriformes morphospaces similar to previous studies on Titanosauriformes femoral morphology (Canudo & Cuenca-Bescós, 2004). While these major group differences are easy to observe in morphospace occupation, differences at generic level are not so evident. Morphospace overlapping between Neosauropoda genera is persistent among all the clades. We can observe a common cluster for Lohuecotitan pandafilandi + Morphotype I from Lo Hueco, *Saltasaurus loricatus*, *Neuquensaurus* spp., *Antarctosaurus wichmannianus* and at least two morphotypes of *Magyarosaurus* (from the sample in Nopsca, 1915). Other taxa sampled in this work are located mixed in each cluster with specimen from completely different sauropod clades (see supplementary H). Almost no differences can be seen among titanosauriforms nor among titanosaurs (see Supplementary Material IV.I.E. and H.). Similar to other studies, there are enough differences between the morphospaces of the different genera in Morrison formation neosauropods (Bonnan, 2004) or Tendaguru Formation sauropods (Schwarz & Böhm, 2012) but among more derived taxa, many of the morphospaces overlap and it is difficult to assess diferences (Wilhite, 2005; Bonnan, 2007; Ullmann *et al.*, 2017). This study also includes the measurement data of Bonan (2004, 2007) into our analyses. Nevertheless, when including more neosauropods groyps we cannot distinguish either between groups that have been previously reported as significantly different like *Apatosaurus* spp., *Diplodocus* spp. and *Camarasaurus* spp. (Bonnan, 2004; Wilhite, 2005). When the sample is reduced only to Ibero-Armorican domain titanosaur taxa we detected less dispersion between the more robust, eccentric and columnar femora as in *Ampelosaurus atacis* + Morphotype II from Lo Hueco + Ibero-Armorican Titanosauria indet. Form 3 (Vila *et al.*, 2012) and more slender but not as eccentric forms as in *Lirainosaurus astibaie* + cf. *Lirainosaurus astibaie* + Titanosauria indet. Form 1 and 2. However, only *Lohuecotitan pandafilandi* + Morphotype I from Lo Hueco produce a common cluster. *A. atacis* is recovered in several groups, connected with both Ibero-Armorican morphotypes as commented before. *Lirainosaurus astibaie* is located closer to *L. pandafilandi* + Morphotype I from Lo Hueco. but intermingled with specimens of *A. atacis* + Morphotype II from Lo Hueco. As the PCA shows (Fig.IV.I.5) the majority of Ibero-Armorican titanosaurs present overlap between the femoral morphospaces. One of the most different morphospaces in PC1 and PC2 negative values is *L. pandafilandi* + Morphotype I from Lo Hueco, several of the specimen present similarities with Morphotype II of Lo Hueco + *A. atacis* and it is reflected in the cluster analysis, represented by the sister subcluster that group *A. atacis* + Morphotype II from Lo Hueco + Ibero-Armorican Titanosauria indet. Form 3. This is congruent with the k-means first and second most optimal results, dividing the Ibero-Armorican titanosaur femoral morphospaces in four or five clusters. The group of *L. pandafilandi* + Morphotype I from Lo Hueco (including the specimens we incorporated as Titanosauria indet.) are recovered within the same cluster. A difference between both solutions is the separation of one of the specimens of Morphotype I defining the extreme of its morphospace in more negative values of PC2, as it is found closer to the *A. atacis* + Morphotype II from Lo Hueco cluster. The *L. pandafilandi* + Morphotype I from Lo Hueco cluster includes several specimens referred to *Lirainosaurus astibaie,* which is divided between the *Ampelosaurus* + Morphotype II cluster. Also result in a third cluster composed mainly by *Lirainosaurus* + cf. *Lirainosaurus* and some specimens from *A.atacis* + Morphotype II from Lo Hueco (including some specimens which we regarded as Titanosauria indet. for the

analyses, referred to this morphotype). The results on the morphometric analysis are consistent with comparative anatomy. The PC2 reflect variance in lateromedial width of the lateral bulge, anteroposterior width of femoral head, and the angle of the shaft respective to the plane of distal condyles, features in which we can appreciate differences between *Lohuecotitan pandafilandi* + Morphotype I from Lo Hueco + *Lirainosaurus astibae* + cf. *Lirainosaurus* and *Ampelosaurus atacis* + Morphotype II from Lo Hueco + Ibero-Armorican Titanosauria indet. Form 1 and 3. At least between the specimens referred to Morphotype I from Lo Hueco it seems that no more than one group is currently present in our sample. Among specimens referred to Morphotype II from Lo Hueco, it is more complicated as they do not produce a main cluster, but instead, several cluster normally with specimens referred to *A. atacis*.

With the sample from Lo Hueco alone, it is hard to assess morphological differences with clustering techniques (see Fig.IV.I.8). Without a comparative context with other Ibero-Armorican titanosaurian taxa, specimens seems to be mixed, still with a subcluster composed by *Lohuecotitan* + several Morphotype I specimens. The reason behind this problematic can be observed in the PCA (Fig.IV.I.6 and 10), as both morphotypes (and the specimens included as Titanosauria indet.) present great overlapping between the morphospaces in many PCs. None of the k-mean solutions represent those two groups or an alternative taxonomically relevant (Fig.IV.I.10). For example, every k-means solution cluster together specimens with greatly different features like the eccentricity or position of fourth trochanter (e.g. HUE-1357, HUE-1440, HUE-10007; see also Fig.IV.I.2).

With the suggested variables of Vila *et al.* (2012) in the ORGDB group differences are more difficult to assess. With this dataset, group differences at clade level are not so evident, as between more inclusive clades their morphospaces overlap and no differences between non-Titanosauriformes Macronaria + Diplodocoidea and Titanosauriformes are detected like in EXPDB analyses. Analysis over ORGDB at genus level is also not conclusive and it has least resolution than EXPDB. Few clusters relatable to actual OTUs are recovered. *Neuquensaurus*, *Saltasaurus*, *Europasaurus*, *Dicraeosaurus* and several subclusters referable to *Camarasaurus* spp. with the type or referred individuals grouped together (see Supplementary Material IV.I.H). Majority of taxa specimens are recovered intermingled, as in the PCA (Supplementary Material IV.I.E), without a clear distinction between major clades either. When the analysis of ORGDB is reduced to the Ibero-Armorican titanosaur taxa, some differences can be observed, but much worse than in the analysis of EXPDB. The k-means clustering again offer little resolution as no partitioning alternative have taxonomical significance. Coincidently, the cluster analysis results in a common cluster for several specimens of Morphotype I and II from Lo Hueco, mixed with *Ampelosaurus atacis*. There is another subcluster with the main groups of specimens from Morphotype II from Lo Hueco and other subcluster Morphotype I + *Lirainosaurus astibae*, as well as closely related the Titanosauria indet. Form 3 (Fig.IV.I.7). Some differences can be observed in the PCA along PC2 (Fig.IV.I.5 and 11). This PC summarizes the variance of the minimum width of the midshaft, both anteroposteriorly and lateromedially, and the position of the fourth trochanter. Several differences can be found between *A. atacis* and Morphotype II in this regard, but most significantly against *Lirainosaurus astibae* + *Lohuecotitan pandafilandi* + Morphotype I from lo Hueco. However, the lack on information of the anteroposterior development of the proximal or distal ends in this dataset, do not permit us to establish significant differences between *L. astibae* and *L. pandafilandi* + Morphotype I from Lo Hueco. If the cluster analysis is reduced to the specimens from Lo Hueco alone, it is much more difficult to assess morphotype differences contrary to the

analysis over EXPDB. The PCA over ORGDB for the Lo Hueco sample alone present a great overlapping between both morphotypes and difficulties to assess the morphotype allocation for the specimens that we included as Titanosauria indet. for analytical purpose. This might be caused also by the lack of information on the anteroposterior development of the proximal end, or information on the medial displacement of the shaft, main characters to distinguish at least the two morphotypes previously identified.

The k-means solution recovers the two and three cluster hypothesis as the most optimal partitions. The suggestion of k=2 partitions correspond mostly to the two a priori groups we assessed between the specimens included as indeterminate for the analyses. While the three cluster hypothesis assess several specimens from Morphotype I to the second cluster where majority of Morphotype II femora are allocated. Third cluster at more positive values of PC1 correspond to three femora (HUE-930, HUE-1508 and HUE-1521) with lateromedially short lateral bulge, the fourth trochanter displaced to the medial edge of the posterior face, slightly visible as a bump from anterior face. They also present what seems to be expanded distal condyles (as it cannot be fully seen because they are fragmentary), and they have some separation of the tibial condyle respective to the axis of the shaft. However, we doubt this correspond to a natural group, as this fragmentary distal end present similarity to the tibial condyle slightly deflected medially seen in Morphotype I (e.g. HUE-2338, HUE-3108).

Lastly the analysis of RDB show worst results overall (see Supplementary Material E, H, I). The analysis recovered distinct clusters at clade level that can be referred to inclusive groups like non-Lithostrotia Titanosauria, non-Titanosauriformes Neosauropoda (three major subclusters, one only composed by macronarian sauropods, two subclusters grouping Diplodocoidea + non-Titanosaurfirmes Macronaria including Brachiosauridae). However, at genus level there is no clear pattern and it is difficult to find a cluster defining a putative OTU, with the exception only for *Neuquensaurus* spp. When we analysed only the Ibero-Armorican domain titanosaurs, differences are less evident than in EXPDB or ORGDB, and no partitioning within k-means solution found a natural group. Coincidently, the Kruskal-Wallis and Mann-Whitney's U tests found significant differences in the analysis of all Neosauropoda in RDB at least along the PC1. Differences in robustness index and Eccentricity between different taxa can be assessed within cross clade comparisons of morphological extremes, and it is congruent with observations and its use in classic and modern osteological character data matrices (Upchurch, 1998; Wilson, 2002; Upchurch *et al.*, 2004a; Royo-Torres & Upchurch, 2012; D'Emic, 2012; Mannion *et al.*, 2013; Mocho *et al.*, 2014; Tschopp *et al.*, 2015; Carballido *et al.*, 2017; González Riga *et al.*, 2018; Sallam *et al.*, 2018). However, not enough differences in the relative robustness or eccentricity are found among many of the analysed neosauropods taxa, neither among the Ibero-Armorican titanosaurian sample. Another interesting result is in the analysis of only the sample from Lo Hueco fossil site. As seen in the cluster analysis and k-means partitioning, RDB is hardly useful to distinguish natural groups, as all partitioning hypothesis have little taxonomical meaning. However, it can be observed at least two different morphospaces in PCA, and thus it may be less useful for specimen allocation than all previous datasets, but better for morphospace visualization than the ORGDB.

In addition, if we compare the results on the Kruskal-Wallis and Mann-Whitney's U tests across all the datasets, we can find the ORGDB present the slightly better results than the EXPDB in order to differentiate between morphotypes and OTUs in majority of the PCs. The EXPDB show less significant differences but some of the PCs permit us to assess OTUs differences between

majorities of the analysed taxa and the morphospaces are easier to visualize. The RDB reported significant differences among PC1 and PC3 (Table.IV.I.5), but when inspecting the Mann-Whitney U's test (Supplementary material IV.I.G) the significant differences are only visible when comparing basal Neosauropoda outside Titanosauriformes, or between non-Titanosauriformes and derived Titanosauria OTUs, while several intermediate genera or taxa inside each of these inclusive clades, cannot be distinguished. The RDB have special difficulties between titanosaurian sauropods, as majority of them present overlapping between the morphospaces also congruent with previous observation on the (small) differences in robustness between titanosaur taxa (Wilson & Upchurch, 2003; Ullmann *et al.*, 2017). The usefulness of this dataset is therefore limited when comparing the sample of Ibero-Armorican titanosaurs. Robustness and eccentricity differences alone are much less accentuated among majority of taxa, which follows the problematic underlying previous attempts at classification of different undescribed titanosaurian forms of the Ibero-Armorican domain (Company *et al.*, 2009; Vila *et al.*, 2012; Díez Díaz *et al.*, 2015; Páramo *et al.*, 2015).

We found significant differences in all analysis, especially in the dataset proposed for this study (EXPDB). However, direct application of partitioning and unsupervised clustering methods showed few correspondence with the known OTUs. Many of the known Neosauropoda used in current study present overlap between morphospaces, caused partially because the femur morphology is similar among genera from close clades. Major differences are found between the non-Somphospondyli Neosauropoda and Somphospondyli taxa. THE EXPDB is useful for easily visualize this relationships, but in general all datasets show significant differences in comparisons between OTUs from both major Neosauropoda groups (among other comparisons) as shown by the Mann Whitney's U test results. The wide-gauge acquisition in derived Titanosauriformes or probably at the base of Titanosauria is involved in a series of major morphological feature acquisition responsible of the limb morphological reconfiguration. This morphological changes are shown in the morphospaces of the current analyses for all the dataset analyses. This results are congruent with phylogenetic analyses (Salgado *et al.*, 1997a; Wilson, 2002; D'Emic, 2012; Carballido *et al.*, 2017), ichnological and biomechanical evidence (Wilson & Carrano, 1999; Otero, 2010a; Vila *et al.*, 2013; Fronimos & Wilson, 2016) as well as previous results in 2D geometric morphometrics studies (Ullmann *et al.*, 2017). However, outside this major morphological reconfiguration of the hindlimb, all Neosauropoda present overlapping morphospace occupation between sister genera (e.g. *Diplodocus* spp., *Magyarosaurus* spp., *Camarasaurus* spp.). This is also valid for close clades like Saltasauridae + European titanosauria which is not helpful to resolve the current phylogenetic problematics, whether some of these groups are saltarsaurid sauropods or closer groups (Sallam *et al.*, 2018; Díez Díaz *et al.*, 2018a). Sometimes even distant clades of Neosauropoda reports morphological similarities, see non-Titanosauria Somphospondyli with Lithostrotia, and non-Titanosauria Somphospondyli with Saltasaurinae in all datasets. On the other hand, while EXPDB present this problems, slightly bigger differences can be observed between those clades. In addition, at genus level there is a better separation in the analysis of EXPDB between ingroups inside non-Titanosauria Somphospondyli and Lithostrotia contra the analysis of ORGDB. The variable selection is also important to distinguish between the resulting morphospaces, and so we observe improvement when we include information on the anteroposterior width of different femoral features. Another characteristic that is helpful to distinguish between genera is the angle of the shaft and the plane of the distal condyles, as seen in PC2 of EXPDB PCA (Supplementary Material IV.I.E). This feature may seem to be redundant with the medial displacement of the femur, however, it reflects also the degree of bevelling of the

distal condyles (Royo-Torres, 2009: page 319). Furthermore we included this variable as it has been useful to erect formal opinion in taxonomical assessment among asian titanosauriformes, which present problematics of morphological similitudes and isolated elements like in the case of "*Titanosaurus*" *falloti*. The femur previously assessed as "*Titanosaurus*" *falloti* (Allain *et al.*, 1999; Wilson & Upchurch, 2003) was also suggested as probable *Huabeisaurus allocotus* (Pang & Cheng, 2000) but D'Emic *et al.* (2013) points out some differences in the absence of the unique combination of femoral characters in this taxa. The femur from *H. allocotus* presents distinct bevelling to medial on the anterior face of the distal condyles (D'Emic *et al.*, 2013) compared to "*T.*" *falloti* femur. This feature can be also used to distinguish among the sample from Ibero-Armorican titanosaurs e.g. *Ampelosaurus atacis* – no bevelling, Morphotype II – small to no bevelling, Morphotype I – some medial bevelling, *Lirainosaurus astibaie* – strong medial bevelling. The anteroposterior width of the distal end is also relevant, however, not all the sampled specimens present this information neither good photographed material to measure it, hence it was excluded from the data matrices (see selection of morphometric variables, above). Our datasets rely heavily on imputation of data, hence increasing the covariation, as few published measurements or photographic material on those characters is available (see the Caveats), so it is important to consider that EXPDB, the dataset that show better separation between the morphospaces, could offer greater between group variance if the complete specimens are included without imputation.

IV.II.5.3. CLASSIFICATION ANALYSES WITH THE SAMPLE OF LO HUECO

The development of statistical classification-discrimination pipeline based on machine learning methods produce rather accurate results in the assessment of isolated sauropod femora despite the high percentage of missing information. As DFA and SVM are discrimination methods, even if the most probable groups recovered are not taxonomically possible (e.g. a diplodocine in a sample from the Maastrichtian), differences between the result groups are useful for assessment of faunal diversity on the sample (e.g. the specimen is allocated as probable *Diplodocus* spp. as it shares its slender and subcircular shaft, a unique morphology among titanosaurs). As established before, one major problematic among the Ibero-Armorican domain titanosaurs, but not exclusive within this group of sauropods, is the morphological similarities and lack of unique morphological feature combinations in the femur. Understanding the variation of some of the described characters is also necessary in order to develop a discrimination tool kit. However discussion over a data matrix of discrete morphological characters is beyond the scopes of this work. However, the analysis of EXPDB permits to distinguish the different Ibero-Armorican titanosaurs with relative accuracy and observe two major types of femora in Lo Hueco. The ORGDB analyses recover a slightly less accurate classification of the Ibero-Armorican titanosaur forms but two main groups are found: i) a group of similar Lo Hueco Morphotype I + *Lirainosaurus astibaie* + *Bonatitan reigi* in the LDA, or a *Diplodocus*-like group in the SVM; ii) another group of *Ampelosaurus atacis* + Lo Hueco Morphotype II + *Phuwiangosaurus sirindhornae* in the LDA, or a *Camarasaurus*-like group in the SVM. The RDB in the other hand is much more inconclusive as all neosauropods taxa present great overlapping of their morphospaces (see Supplementary Material IV.I.I).

Initial reports based on the DFA show low accuracy values not greater than 51.26% (Table. IV.I.7), while mean accuracy is 37.04%. The EXPDB analysis shows the best results, while ORGDB mean accuracy decay to 27.78% and RDB surprisingly presents a mean accuracy slightly better at

29.63%. All the datasets present lower accuracy rates when DFA is deployed. One cause might be the DFA, requirement of independent samples with multivariate normality, both between the specimens and variables (Claude, 2008; Hammer & Harper, 2008; Hastie, Tibshirani, & Friedman, 2009). Therefore the discrimant analysis is sensible to the increase in multivariate heterocedasticity of the imputed databases caused by the estimation of missing data itself. It is important to note that the Robustness dataset (RDB) shows better results than ORGDB, which is congruent with the increase in heterocedasticy causes for low accuracy, as RDB present less missing data. The lack of imputation in RDB could explain why it offers better results while the morphospaces present much more overlapping and there are less PCs with significant discrimination between the analysed taxa (and there was no cluster biologically meaningful, see Fig.IV.I.7 and 8, see also Supplementary Material IV.I.H). The DFA is also affected by general morphospace distribution, as it calculates the classes based on the distance from the OTU morphospace centroid. All the datasets shows various degrees of morphospace overlapping, from the EXPDB with slightly better separation, to RDB as the worse. In addition, when we take into account the Cohen's Kappa we see this mentioned tendency in the classificators, as RDB shows slightly more accurate results than ORGDB but worse Kappa (see Table IV.I.7). Therefore, there are fewer differences from a result at random than an accurate classification in the RDB than in the ORGDB DFA results.

On the other hand, the SVM results in better rates of accuracy with moderate Kappa values (see Table.IV.I.7), which indicates better agreement than the DFA between an accurate classification and a result at random. This method clearly outperform DFA analysis because is less sensitive to non-Gaussian distribution of the data and is not so biased by uneven distribution of classes (both in number of sampled specimens and overlapping morphospaces). Also, the SVM classifier was tuned by a kernel function which trace a complex non-linear hyperplane (in this case an elliptic hyperplane) which may work better to separate the high overlap between derived sauropod morphospaces in the EXPDB and the similarities between all the morphospaces in ORGDB and RDB. All the SVM results improve ~5% or more the accuracy in comparison to the DFA results and present higher kappa values (Table IV.I.7).

The probability of each classification in the testing sample was also calculated in order to discuss the assessment following other similar studies e.g. Smith *et al.* (2005), Hendrickx *et al.* (2014), Serrano-Martínez *et al.* (2016), Gerke and Wings (2016), and Malafaia *et al.* (2017). After exploring how the classifier assign probabilities to each of the studied specimen, it is possible to verify how each of the method's principles perform better in those specimens that are far from the centroid of each morphospace. The DFA analysis results in mean high first probabilities but low accuracy rate in all the tests. Most probable groups suggested in cases where the specimen was misclassified, present low probability (around 50%) and class determined is one of the taxa which morphospace overlap. Like the *Giraffatitan* femur MFN-Bg21 determined as *Haplocanthosaurus* with first probability of 55% (see Supplementary Material IV.I.J). There are also cases such as HUE-2420 or HUE-3237 which present a lightly eccentric shaft, bulbous femoral head and toward the robust values of robust index of Morphotype I, determined by the algorithm as *Neuquensaurus*. There are some misclassification between phylogenetically distant clades, which is especially relevant between Titanosauria and non-Titanosauria type of femur (after wide-gauge acquisition). The ORGDB on the contrary presents lower accuracy among many non-Titanosaurifromes, misclassified with Titanosauria taxa. While RDB present better accuracy than ORGDB, the suggested classes present lower probabilities, with first class rarely passing more than 50% probability rate. RDB might be underperforming while accuracy rate is lightly

better, as there is no all the probabilities are mixed between the femora of Late Cretaceous of Europe and those from the Upper Jurassic of North America and probabilities are extremely low, scoring euqally probable to other similar taxa.

The SVM presents some improvement in the discrimination over DFA with lower first and second probability percentages (Supplementary Material IV.I.L). Apart from the slightly better accuracy, we can observe improvement in the discrimination of specimens that were in the frontier between morphospaces (see Fig.IV.I.14, comparison with morphospaces in Fig.IV.I.4). However one problematic reading results of the cross validation in the SVM is the way the one-against-all voting strategy works. First and second probabilities are less useful than in DFA, as they are extremely low. The algorithm does not allocate the specimens in base of the higher probability across the entire sample but instead by comparison between many similar probabilities for every class, determining the one that is more different in the voting system (Liu & Zheng, 2005).

The DFA also performs worse in some taxa with overlapping morphospaces and unbalanced toward the class with the biggest number of specimens overall. For example the femora referred to *Giraffatitan* or *Dicraeosaurus* score generally as *Camarasaurus*. In addition, some specimens of *Camarasaurus* that are in the limit of the morphospace toward other morphospaces that overlap like *Phuwiangosaurus*, *Apatosaurus*, etc (see Fig.IV.I.14, Supplementary Material IV.I.L). This trend is more marked in ORGDB and RDB, as titanosaurian sauropods also overlap with the more basal neosauropods groups. The SVM on the other hand present no clear pattern of misclassification, the hyperplane traced does not fail toward morphospace limits on overlapping areas. Neither the hyperplane fails toward groups with bigger sample e.g. the majority of Ibero-Armorican titanosaur misclassifications on EXPDB for the SVM are referred to *Ampelosaurus*, *Neuquensaurus*, or in some cases *Magyarosaurus* and Morphoype I from Lo Hueco, which are not the most populated groups in that particular area of the morphospace (see *Saltasaurus* and *Phuwiangosaurus*). On ORGDB for example, almost all the misclassifications are referred to *Camarasaurus* and *Diplodocus*, besides *Diplodocus* is not much more populated than e.g. *Apatosaurus*. The missclassification might be determined by the actual complete overlapping between morphospaces in multivariate space rather than sample numbers, which is a benefit in the SVM when analysing the uneven sauropod fossil record. While the SVM performs better on frontiers, in situations like ORGDB and RDB where all sauropods occupy similar morphospace barely different between them, all misclassification are due to assign the data to *Camarasaurus*, *Diplodocus* or *Apatosaurus* not based on the *N* of their sample, but instead because they have the biggest (and more variable) morphospaces in most of the PCs. Thus, in SVM, the class boundary does not set a big role defining the shape of the boundary in the featured space (Hastie *et al.*, 2009). This might support the previous observations that the classes do not have an easy separation using a linear hyperplane such as in traditional DFA, so the SVM results in overall better accuracy rates as high as ~55%. This better performance in titanosaurian sauropods is related to the degree they share much part of the feature space and the differences in the algorithm of classificators. The SVM classify them by the margin and their specimens most distant from the group centroid (grand mean) of the feature space, not by the centroid itself and covariation of the classes (Vapnik, 1995; Hammer & Harper, 2008; Hastie *et al.*, 2009). Contrary to the DFA, while the most probable classes retain a high probability over the second one, the SVM return in class probabilities closer between the most probable and the second higher probability. This also can be caused by the distribution of the complex feature space of each taxa and the a priori decisions made during this study. Kernel function is an improvement in cases of complex overlaps of the classes in the featured space, and in our case, morphospaces

and the SVM benefits from this potential feature of the method. This is not exclusive to SVM as it is applicable to almost all other machine learning algorithms including DFA (see a review in Hastie *et al.*, 2009). When setting up the kernel functions, a radial kernel seems to be the best for the sample of Neosauropoda. However, overlaps in feature space may produce an increase in support vectors which it is not a desirable objective. Also, as some studies on simulation data suggest, high costs with low gamma values of the radial kernel increases the error rate (Hastie *et al.*, 2009). The cost might was maintained low in order to avoid overfitting and the tuning process suggest low gamma values for the classifier function (see Supplementary Material IV.I.K).

All these problematics united on the significant overlapping between genera morphospaces render the traditional DFA worse than the alternative SVM with kernel function. However, an increase in the completeness provided by the input data sampling derived from non-titanosaurian neosauropods is necessary. Many of these taxa lack measurements nor photographic material in where to obtain more morphometric data. It is expected that all results on EXPDB and ORGDB (for both DFA and SVM) improve with less data estimated thanks to a direct measuring over the specimen in future research. Another problem experienced by DFA algorithms is the uneven distribution of fossil taxa samples. The DFA tends to produce equally weighted partitions in multivariate space (Claude, 2008). This is unavoidable nonetheless, as several taxa are represented only by one or two specimens, while OTUs like *Camarasaurus*, *Diplodocus*, *Apatosaurus*, *Phuwiangosaurus*, *Neuquensaurus* or the morphotypes from this study might have from half a dozen up to several dozens of specimens.

In the end, all the results of the SMV are improvements in accuracy and stability (marked by kappa values) compared with the DFA because the featured space is explored in a more efficient way with the SVM.

IV.II.5.4. CAVEATS OF THIS STUDY

Morphometric methods are surpassed by 2D and 3D geometric morphometrics in almost every way for visualizing and capture morphological changes over the studied specimens (Bookstein, 1991; Rohlf, 2000; Claude, 2008; Zelditch *et al.*, 2012). Geometric morphometrics tool kit surpass traditional morphometrics in the power of mapping and representation of shape variation (Claude, 2008; Zelditch *et al.*, 2012; Klingenberg, 2013) but also in the advances of modern shape analysis (Claude, 2008). Considering that each landmark can capture much more information than a linear measurement as they can capture the same information as several measurments that are made between those landmarks with fewer variables (Bookstein, 1991; Zelditch *et al.*, 2012). Therefore, a complex set of measurements can be summarize with a set of few landmarks (see extreme examples of Strauss & Bookstein, 1982; Bookstein *et al.*, 1985; summarized in Zelditch *et al.*, 2012).

However, this is the first Multivariate analysis performed in order to assess the variability of the titanosaur appendicular elements from Lo Hueco site and the Ibero-Armorican domain. New analyses on other appendicular bones, as well as, in axial elements are being performed and will complete the analysis of the morphological variability of Lo Hueco titanosaurs. In order to build a statistical framework as a first approach and for the sake of constructing a classifier, linear morphometrics were selected instead of their 2D and 3D counterpart. 2D geometric

morphometrics (GM) have proven to be valuable tool for distinction of non-titanosauriform neosauropod appendicular elements between closer taxa in multispecimen bone-beds (Wilhite, 2003, 2005; Bonnan, 2004, 2007; Schwarz & Böhm, 2012). 2D GM are also useful for the assessing of intraspecific variability and statistical processing of shape variables in other dinosaur taxa (Barden & Maidment, 2011; Maiorino *et al.*, 2013, 2015) and for the study of major trends in dinosaur evolution and comparison among sauropod dinosaurs and other clades (Bonnan *et al.*, 2013; Van Buren *et al.*, 2014; Ullmann *et al.*, 2017). It is a successful set of techniques already applied to dinosaur taxa, however, 2D GM have difficulties for analysing the morphological similarities among titanosaur taxa (e.g. Bonnan, 2007) probably based on the three dimensional variation of some osteological features. As commented before, some main differences arise in the anteroposterior morphology of the several features of the femora and we wanted to capture them in the current study. Many of the analysed specimens also lack published figuration available and would be excluded from our sample, as 2D geometric morphometrics relay on landmark placement, while at least some measurements are already available. For these causes, the employment of 2D GM has been disregarded for this study as they would have greatly limited the set of techniques applicable.

The 3D GM can be used for analysing those features that present some variation between titanosaur taxa (e.g. the tibial condyle distal bevelling, projection of fourth trochanter, anteroposterior width of femoral head). However, there are no current public libraries of 3D scans for many of the sauropod sampled for this study. Many techniques can be applied to transform the landmark in multiple 2D planes into a set of 3D coordinates (Chiari *et al.*, 2008; Claude, 2008), and there are new methodologies to estimate 3D morphology from 2D photography (see Zhou *et al.*, 2015). The available photographic material especially for historical specimens is scarce, and several views of the bone are not available on the published material.. For this reason, the measurement database continues to be a more optimal approach especially for deployment of machine learning techniques.

The lack of openly available measurements and photographic material (which can be digitally measured) have a great impact in the data input, as large portions of the data matrices needed to be estimated. The lack of available photographs means lack of possibility digitize the measurements via software in case of not having access to all the studied specimens from different institutions across the world and with different degrees of preservation that could hardly justify such comprehensive task. Another consideration is the fragmentary state of the appendicular elements, especially relevant for European titanosaur specimens. Vila *et al.* (2012) analysed a sample of fragmentary isolated femora tentatively attributed to cf. Lirainosaurus and unknown titanosaur taxa. The paratype material attributed to *Lirainosaurus* lacks some portions of the condyles (specimen MCNA-3160, MCNA-1817, FOX-105 pers. obs. P.Mocho 2015). Similarly, some referred specimens of *Magyarosaurus* (NHM-R3859-2, NHM-R4882 pers. obs. APB 2016) lack portions of the shaft and miss parts of their condyles. The imputation of information is unavoidable even when all the sampled specimens could be accessed. Data imputation is not an unknown field of study nowadays, and several methods could be applied to this situations (Schafer, 1999; Arbour & Brown, 2014). However both problematics commented here and the patterns underlying the missing data may be resulting in a much worse classifier than the expected with measurement morphometrics. We think that part of the lower accuracies reported are caused by the high amount of data imputation. Available data could improve much more the results, especially with the SVM, though data imputation is still needed by the fragmentary nature of many fossil materials. Reduction of variables in order to decrease missing data is not desirable. The EXPDB showed better results in all the analysis that outperform ORGDB and RDB, which has

less variables and therefore less missing data. Overall, the ORGDB is also useful in quantitative analysis but lacks information of the third dimension to account for the anteroposterior position of several osteological features. We think that with increasing sampled specimens, including those that could not be directly measured in this study, the number of variables accounting for these morphological features could be also increased. Some features like the anteroposterior bevelling (angle) of the distal condyles, projection of the fourth trochanter among others that were excluded from this study could add valuable information in future works.

Also switching to geometric morphometric methods can be helpful, as they need less dimensions to explain much more morphological information. However, building a data base for 2D or 3D GM with the N number of specimens covered in the current study could require much more effort.

IV.1.6 CONCLUSIONS

The detailed description provided here recognizes two different morphotypes in the sample of titanosaurian femora of Lo Hueco fossil site (Campanian-Maastrichtian, Spain). The Morphotype I is characterized by more gracile femora with low eccentric shafts. The femoral head is more rounded, expanded anteroposteriorly. The lateral bulge is well developed, forming a light curvature in the proximal third of the shaft. A robust trochanteric shelf extends parallel to the bulge, and it is wide lateromedially. It has a fourth trochanter positioned in posterior face, somewhat medially but not extending to the medial margin of the shaft. Distally, it has slender condyles and anteriorly projected (tibial condyle is also projected medially). These characters are congruent with the description of *Lohuecotitan pandafilandi* holotype.

We found that the most probable partitioning of the sample from Lo Hueco might be two distinct morphotypes, one form closer to *Lohuecotitan pandafilandi,* the other, Morphotype II, a more robust and eccentric type closer in morphology to *A. atacis*. The sample from Lo Hueco also includes several specimens of smaller individuals in order to assess the relationship with European dwarf taxa like *Magyarosaurus* or *Lirainosaurus*. These specimens are closer to Morphotype I, and HUE-10007 to Morphotype II from Lo Hueco than to other known small-sized titanosaurian forms of the European record like *Lirainosaurus*, cf. *Lirainosaurus* and *Magyarosaurus*. Neither HUE-10007 or the other small specimens of Morphotype I are closer to the juvenile specimens of *Ampelosaurus atacis*, so they are probably small individuals of Lo Hueco Morphotype I and II respectively. This might support the presence of juvenile specimens in Lo Hueco referred to Morphotype I but further analyses are necessary

The other main morphotype is more robust, with an eccentric shaft, and anteroposteriorly compressed proximal and distal ends, but not as compressed as in *Ampelosaurus atacis* referred material. Some characters also differentiates the femora of the Morphotype II from *A. atacis*: (i) distal condyles are not as anteroposteriorly compressed as in *A. atacis*; and (ii) absence of the vertical sulcus in the intercondylar fossa in posterior face of distal condyles. We also found significant differences between Morphotype II and *A. atacis* at least in ORGDB. Morphospace occupation is difficult to differentiate due to overlapping, but the partitioning results do not clearly refer all the specimens from both OTUs to the same cluster. The performed analyses tend to support that they might pertain to a second and unnamed titanosaur taxa from Lo Hueco site, at least there are differences with majority of Titanosauria

indet. forms described in Ibero-Armorican domain. However, further analyses are needed to correctly assess if they are a closer form to *A. atacis* or a new, exclusive form from Lo Hueco.

Proposed phenotypic discrete data matrix such as Vila *et al.* (2012) based on Royo-Torres (2009) variables can help dealing with identification of isolated material. Its original database render some accurate results with significant differences. However, this study shows that it would lack some three dimension information regarding features with anteroposterior variation in the sauropod femur. Increase in morphometrics variables is desirable. This study also demonstrates that some measurements like the Robustness Index, the position of the fourth trochanter in posterior face, the position of the femur head respective to the greater trochanter, the distal condyle orientation, or the tibial-fibular lateromedial width of distal condyles used in systematic study are variable between elements of the same species. These features alone should not be used to distinguish between different morphotypes or sauropod taxa, as it is better to relay in the combination of several features and support from other discrete characters. Some of them experiment more intraspecific variation than other, like the Robustness Index, and the robustness of the element should be used qualitatively and only as tentative support. Our results are congruent with previous studies like Wilson and Upchurch (2003). The analysis of the database with only robustness and eccentricity information showed the worst results overall.

Inclusion of measurements and quantification of some patterns may help to assess possible taxonomical identification. The ORGDB is a good starting dataset to those morphometric analyses. Our proposed dataset, named here as EXPDB, improves the results of discrimination methods and showed better morphospace differences. Moreover, the EXPDB showed similar results with other 2D GM previous studies as we can identify the transition toward Titanosauria and the acquisition of wide-gauge. However, the EXPDB analysis showed some improvements when including measurements in 3D as we found major morphological within Titanosauria.

The classificators provided here have a moderate accuracy, which is partially related with a scarce bibliographical sample that should be completed in future works. Another part of the problematics arises from a complex and similarities in the morphology between titanosauriform femora. The featured space (or morphospace here) overlaps between genera so a separation of the morphotypes is complicated. However, we found that the SVM outperforms in this case the DFA. Both algorithms are easy to implement nonetheless, the DFA may only be surpassed by the scarcity of the sample. The increase in multivariate heterogeneity of the sample by imputation methods could also affect the DFA results. Further analysis might be necessary when data completion is increased.

Morphological differences between titanosaur taxa, or between non-Titanosauriformes taxa is generally hard to assess. While significant differences are found in statistical analysis (e.g. Mann-Whitney's U) is hard to visualize those differences. Especially in ORGDB, as this dataset does not consider some variables regarding anteroposterior development of proximal and distal end, or the medial deflection of the shaft. The SVM perform much better under those conditions in the areas which two or more morphospaces limit and overlap with each other. While the DFA is prone to misclassify in favour of the bigger *N* sample in those areas.

For assess this problems further analyses of the titanosaur skeleton intraspecific variability should be conducted. While the classification methods based on morphometric data are desirable and useful for taxonomical assessment of isolated specimens, unsupervised morphospace exploration is probably better approached with geometric morphometrics techniques.

IV.I.7 BIBLIOGRAPHY

Allain R, Taquet P, Battail B, Dejax J, Richir P, Véran M, Limon-Duparcmeur F, Vacant R, Mateus O, Sayarath P, Khenthavong B, Phouyavong S. 1999. Un nouveau genre de dinosaure sauropode de la formation des Grès supérieurs (Aptien-Albien) du Laos. *Comptes Rendus de l'Académie des Sciences* - Series IIA - Earth and Planetary Science 329: 609–616.

Anderson TW. 2003. *An introduction to multivariate statistical analysis*. Wiley.

Arbour JH, Brown CM. 2014. Incomplete specimens in geometric morphometric analyses. *Methods in Ecology and Evolution* 5: 16–26.

Bak N, Hansen LK. 2016. Data Driven Estimation of Imputation Error—A Strategy for Imputation with a Reject Option. *PLoS ONE* 11: e0164464.

Bakeman R, McArthur D, Quera V, Robinson BF. 1997. Detecting sequential patterns and determining their reliability with fallible observers. *Psychological Methods* 2: 357–370.

Barden HE, Maidment SCR. 2011. Evidence for sexual dimorphism in the stegosaurian dinosaur *Kentrosaurus aethiopicus* from the Upper Jurassic of Tanzania. *Journal of Vertebrate Paleontology* 31: 641–651.

Bonnan MF. 2004. Morphometric analysis of humerus and femur shape in Morrison sauropods: implications for functional morphology and paleobiology. *Paleobiology* 30: 444–470.

Bonnan MF. 2007. Linear and geometric morphometric analysis of long bone scaling patterns in Jurassic neosauropod dinosaurs: their functional and paleobiological implications. *Anatomical Record* 290: 1089–111.

Bonnan MF, Wilhite RD, Masters SL, Yates AM, Gardner CK, Aguiar A. 2013. What Lies Beneath: Sub-Articular Long Bone Shape Scaling in Eutherian Mammals and Saurischian Dinosaurs Suggests Different Locomotor Adaptations for Gigantism. *PLoS ONE* 8: e75216.

Bookstein FL. 1991. *Morphometric tools for landmark data: geometry and biology*.

Bookstein FL. 2014. *Measuring and Reasoning: Numerical Inference in the Sciences*. Cambridge University Press.

Bookstein FL, Chernoff B, Elder RL, Humphries JJM, Smith GR, Strauss RF. 1985. *Morphometrics in evolutionary biology: the geometry of size and shape change, with examples from fishes*. Academy of Natural Sciences of Philadelphia.

Borsuk-Bialynicka M. 1977. A New Camarasaurid Sauropod *Opisthocoelicaudia skarzynskii* gen. n., sp. n. from the Upper Cretaceous of Mongolia. *Paleontologia Polonica* 37: 5–64.

Boser BE, Guyon IM, Vapnik VN. 1992. A training algorithm for optimal margin classifiers. *Proceedings of the Fifth Annual Workshop on Computational Learning Theory - COLT '92*. 144–152.

Bow ST. 1984. *Pattern recognition*. New York: Marcel Dekker.

Brereton RG, Lloyd GR. 2010. Support Vector Machines for classification and regression. *The Analyst* 135: 230–267.

Brochu CA. 1996. Closure of neurocentral sutures during crocodilian ontogeny: Implications for maturity assessment in fossil archosaurs. *Journal of Vertebrate Paleontology* 16: 49–62.

Broom R. 1904. On the occurrence of an Opisthocoelian Dinosaur (*Algoasaurus bauri*) in the Cretaceous Beds of South Africa. *Geological Magazine Decade* 5: 445–447.

Brown CM, Evans DC, Campione NE, O'Brien LJ, Eberth DA. 2012. Evidence for taphonomic size

bias in the Dinosaur Park Formation (Campanian, Alberta), a model Mesozoic terrestrial alluvial-paralic system. *Palaeogeography, Palaeoclimatology, Palaeoecology* 372: 108-122.

Bruckner CT, Yoder P. 2006. Interpreting Kappa in Observational Research: Baserate Matters. *American Journal on Mental Retardation* 111: 433.

Van Buren NC, Curtin AJ, Narasimhan E, Harvey DB, Meier JD. 2014. Caregiver-Reported Outcomes and Indirect Costs of Pediatric Tonsillectomy. *Otolaryngology – Head and Neck Surgery* 151: 100.

Buscalioni ÁD, Gasparini ZB, Pérez-Moreno BP, Sanz JL. 1997. Argentinean theropods: first morphological analysis on isolated teeth. *Proceedings from the First European Workshop on Vertebrate Palaeontology*. Geological Museum, Copenhagen University, 1–4.

van Buuren S, Groothuis-Oudshoorn K. 2011. mice : Multivariate Imputation by Chained Equations in R. *Journal of Statistical Software* 45.

Calvo JO, Bonaparte JF. 1991. *Andesaurus delgadoi* gen. et sp. nov. (Saurischia-Sauropoda), Dinosaurio Titanosauridae de la Formación Rio Limáy (Albiano-Cenomaniano), Nequen, Argentina. *Ameghiniana* 28: 303–310.

Canudo JI. 2001. Descripción de un fragmento proximal de fémur de Titanosauridae (Dinosauria, Sauropoda) del Maastrichtiense superior de Serraduy (Huesca). In: Meléndez G, Herrera Z, Delvene G, Azanza B, eds. *XVII Jornadas de Paleontología. Los fósiles y la Paleogeografía.* Albarracín, Zaragoza: Sociedad Española de Paleontología y Área y Museo de Paleontología de la Universidad de Zaragoza, 255–262.

Canudo JI, Barco JL, Pereda Suberbiola X, Ruiz-Omeñaca JI, Salgado JL, Torcida Fernández-Baldor F, Gasulla JM. 2009. What Iberian dinosaurs reveal about the bridge said to exist between Gondwana and Laurasia in the Early Cretaceous. *Bulletin de la Societe Geologique de France* 180: 5–11.

Canudo JI, Cuenca-Bescós G. 2004. Morphometric approach to Titanosauriformes (Sauropoda, Dinosauria) femora: Implications to the paleobiogeographic analysis. *Morphometrics.* Springer Berlin Heidelberg, 143–156.

Canudo JI, Royo-Torres R, Cuenca-Bescós G. 2008. A new sauropod: *Tastavinsaurus sanzi* gen. et sp. nov. from the Early Cretaceous (Aptian) of Spain. *Journal of Vertebrate Paleontology* 28: 712–731.

Carballido JL, Pol D, Cerda IA, Salgado JL. 2011a. The Osteology of *Chubutisaurus insignis* Del Corro, 1975 (Dinosauria: Neosauropoda) from the 'Middle' Cretaceous of Central Patagonia, Argentina. *Journal of Vertebrate Paleontology* 31: 93–110.

Carballido JL, Pol D, Otero A, Cerda IA, Salgado JL, Garrido AC, Ramezani J, Cúneo NR, Krause JM. 2017. A new giant titanosaur sheds light on body mass evolution among sauropod dinosaurs. *Proceedings of the Royal Society B: Biological Sciences* 284: 20171219.

Carballido JL, Rauhut OWM, Pol D, Salgado JL. 2011b. Osteology and phylogenetic relationships of *Tehuelchesaurus benitezii* (Dinosauria, Sauropoda) from the Upper Jurassic of Patagonia. *Zoological Journal of the Linnean Society* 163: 605–662.

Carballido JL, Sander PM. 2014. Postcranial axial skeleton of *Europasaurus holgeri* (Dinosauria, Sauropoda) from the Upper Jurassic of Germany: implications for sauropod ontogeny and phylogenetic relationships of basal Macronaria. *Journal of Systematic Palaeontology* 12: 335–387.

Carpenter K, Tidwell V. 2005. Reassessment of the Early Cretaceous Sauropod *Astrodon johnstoni* Leidy 1865 (Titanosauriformes). In: Tidwell V, Carpenter K, eds. *Thunder-Lizards: The Sauropodomorph Dinosaurs*. Bloomington and Indianopolis: Indiana University Press, 38–77.

Carrano MT. 1998. Locomotion in non-avian dinosaurs: Integrating data from hindlimb kinematics, in vivo strains, and bone morphology. *Paleobiology* 24: 450–469.

Carrano MT. 2001. Implications of limb bone scaling, curvature and eccentricity in mammals and non-avian dinosaurs. *Journal of Zoology* 254: 41–55.

Carrano MT. 2005. The Evolution of Sauropod Locomotion. In: Curry Rogers KA, Wilson JA, eds. *The Sauropods: Evolution and Paleobiology.* University of California Press, 229–250.

Casanovas-Cladellas ML. 1992. Novedades en el Registro Fósil de Dinosaurios del Levante Español. *Zubia* 10: 139–151.

Casanovas-Cladellas ML, Santafé-Llopis JV, Sanz JL, Powell JE. 1995. Nuevos restos de dinosaurios (Titanosauria y Ornithopoda) de El Cretácico Superior de la Cuencas de Tremp y Della (Lleida, España). *Estudios Geológicos*: 277–283.

Cerda IA, Paulina Carabajal A, Salgado JL, Coria RA, Reguero M a., Tambussi CP, Moly JJ. 2012. The first record of a sauropod dinosaur from Antarctica. *Die Naturwissenschaften* 99: 83–87.

Chiari Y, Wang B, Rushmeier H, Caccone A. 2008. Using digital images to reconstruct three-dimensional biological forms: A new tool for morphological studies. *Biological Journal of the Linnean Society* 95: 425–436.

Choi K, Marden J. 1997. An Approach to Multivariate Rank Tests in Multivariate Analysis of Variance. *Journal of the American Statistical Association* 92: 1581–1590.

Claude J. 2008. *Morphometrics with R.* New York, NY: Springer New York.

Clavel J, Merceron G, Escarguel G. 2014. Missing Data Estimation in Morphometrics: How Much is Too Much? *Systematic Biology* 63: 203–218.

Cohen J. 1960. A Coefficient of Agreement for Nominal Scales. *Educational and Psychological Measurement* 20: 37–46.

Company J, Suberbiola XP, Ruiz-Omeñaca JI. 2009. Nuevos restos fósiles del dinosaurio *Lirainosaurus*. *Ameghiniana* 46: 391–405.

Coombs WPJ. 1978. Theoretical Aspects of Cursorial Adaptations in Dinosaurs. *The Quarterly Review of Biology* 53: 393–418.

Cortes C, Vapnik VN. 1995. Support-Vector Networks. *Machine Learning* 20: 273–297.

Csiki Z, Buffetaut É, Ősi A, Pereda Suberbiola X, Brusatte SL. 2015. Island life in the Cretaceous - faunal composition, biogeography, evolution, and extinction of land-living vertebrates on the Late Cretaceous European archipelago. *ZooKeys*: 1–161.

Curry Rogers K. 2005. Titanosauria: A phylogenetic overview. In: Curry Rogers K, Wilson JA, eds. *The Sauropods: Evolution and Paleobiology*. Berkeley: University of California Press, 50–103.

Curry Rogers K. 2009. The postcranial osteology of *Rapetosaurus krausei* (Sauropoda: Titanosauria) from the Late Cretaceous of Madagascar. *Journal of Vertebrate Paleontology* 29: 1046–1086.

Curry Rogers K, Whitney M, D'Emic MD, Bagley B. 2016. Precocity in a tiny titanosaur from the Cretaceous of Madagascar. *Science* 352: 450–453.

D'Emic MD. 2012. The early evolution of titanosauriform sauropod dinosaurs. *Zoological Journal of the Linnean Society* 166: 624–671.

D'Emic MD, Mannion PD, Upchurch P, Benson RBJ, Pang Q, Zhengwu C. 2013. Osteology of *Huabeisaurus allocotus* (Sauropoda: Titanosauriformes) from the Upper Cretaceous of China. *PLoS ONE* 8: e69375.

Díez Díaz V, Garcia G, Pereda-Suberbiola X, Stein KHW, Jentgen-Ceschino B, Godefroit P, Valentin X. 2018a. The titanosaurian dinosaur *Atsinganosaurus velauciensis* (Sauropoda) from the Upper Cretaceous of southern France: New material, phylogenetic affinities, and palaeobiogeographical implications. *Cretaceous Research* 91: 429–456.

Díez Díaz V, Garcia G, Pereda Suberbiola X, Jentgen-Ceschino B, Stein KHW, Godefroit P, Valentin X. 2018b. A new titanosaurian sauropod from the Late Cretaceous of Velaux-La Bastide Neuve (southern France). *XVI Annual Meeting of the European Association of Vertebrate Paleontologists*. Caparica, Lisbon, 60.

Díez Díaz V, Mocho P, Páramo A, Escaso F, Marcos-Fernández F, Sanz JL, Ortega F. 2016. A new titanosaur (Dinosauria, Sauropoda) from the Upper Cretaceous of Lo Hueco (Cuenca, Spain). *Cretaceous Research* 68: 49–60.

Díez Díaz V, Ortega F, Sanz JL. 2014. Titanosaurian teeth from the Upper Cretaceous of "Lo Hueco" (Cuenca, Spain). *Cretaceous Research* 51: 285–291.

Díez Díaz V, Pereda Suberbiola X, Company J. 2015. Updating titanosaurian diversity (Sauropoda) from the Late Cretaceous of Spain: The fossil site of Laño and Chera. *Spanish Journal of Palaeontology* 30: 293–306.

Díez Díaz V, Suberbiola XP, Sanz JL. 2013a. Appendicular skeleton and dermal armour of the Late Cretaceous titanosaur *Lirainosaurus astibae* (Dinosauria: Sauropoda) from Spain. *Palaeontologia Electronica* 16: 18 p.

Díez Díaz V, Tortosa T, Le Loeuff J. 2013b. Sauropod diversity in the Late Cretaceous of southwestern Europe: The lessons of odontology. *Annales de Paléontologie* 99: 119–129.

Filippi LS, García RA, Garrido AC. 2011. A New Titanosaur Sauropod Dinosaur from the Upper Cretaceous of North Patagonia, Argentina. *Acta Palaeontologica Polonica* 56: 505–520.

Filippi LS, Martinelli AG, Garrido AC, S. Filippi L, Martinelli AG, C. Garrido A. 2013. Registro de un dinosaurio aeolosaurini (Sauropoda, Titanosauria) en el cretácico superior (Formación plottier) del norte de la Provincia de Neuquén, Argentina, y comentarios sobre los Aeolosaurini sudamericanos. *Revista Brasileira de Paleontologia* 16: 147–156.

Fronimos JA, Wilson JA. 2016. Concavo-Convex Intercentral Joints Stabilize the Vertebral Column in Sauropod Dinosaurs and Crocodylians. *Ameghiniana* 54: 151–176.

Gallina PA, Apesteguía S. 2005. *Cathartesaura anaerobica* gen. et sp. nov., a new rebbachisaurid (Dinosauria, Sauropoda) from the Huincul Formation (Upper Cretaceous), Río Negro, Argentina. *Revista del Museo Argentino de Ciencias Naturales* 7: 153–166.

Garcia G, Amico S, Fournier F, Thouand E, Valentin X. 2010. A new Titanosaur genus (Dinosauria, Sauropoda) from the Late Cretaceous of southern France and its paleobiogeographic implications. *Bulletin de la Société Géologique de France* 181: 269–277.

García RA, Salgado JL. 2011. The titanosaur sauropods from the Allen Formation (late Campanian-early Maastrichtian) of Salitral Moreno (Patagonia, Río Negro, Argentina). *Acta Palaeontologica Polonica* 58: 269-284.

Gerke O, Wings O. 2016. Multivariate and cladistic analyses of isolated teeth reveal sympatry of theropod dinosaurs in the Late Jurassic of Northern Germany. *PLoS ONE* 11: 1–52.

Gilmore CW. 1922. Discovery of a sauropod dinosaur from the Ojo Alamo formation of New Mexico. *Smithsonian Miscellaneous Collections* 81: 1–9.

Gilmore CW. 1925. A nearly complete articulated skeleton of *Camarasaurus*, a saurischian dinosaur from the Dinosaur National Monument. *Memoirs of the Carnegie Museum* 10: 347–384.

Gilmore CW. 1936a. The osteology of *Apatosaurus* with special reference to specimens in the Carnegie Museum. *Memoirs of the Carnegie Museum* 11: 175–300.

Gilmore CW. 1936b. Osteology of *Apatosaurus* with special comments on the specimens of the Carnegie Museum.

Gilmore CW. 1946. Reptilian fauna of the North Horn Formation of central Utah. United States *Geological Survey Professional Paper* 201–C: 29–53.

González Riga BJ, Lamanna MC, Ortiz David LD, Calvo JO, Coria JP. 2016. A gigantic new dinosaur from Argentina and the evolution of the sauropod hind foot. *Scientific Reports* 6: 19165.

González Riga BJ, Mannion PD, Poropat SF, Ortiz David LD, Coria JP. 2018. Osteology of the Late Cretaceous Argentinean sauropod dinosaur *Mendozasaurus neguyelap*: implications for basal titanosaur relationships. *Zoological Journal of the Linnean Society*: 1–46.

Gorscak E, O'Connor PM. 2016. Time-calibrated models support congruency between Cretaceous continental rifting and titanosaurian evolutionary history. *Biology Letters* 12: 20151047.

Gorscak E, O'Connor PM, Roberts EM, Stevens NJ. 2017. The second titanosaurian (Dinosauria: Sauropoda) from the middle Cretaceous Galula Formation, southwestern Tanzania, with remarks on African titanosaurian diversity. *Journal of Vertebrate Paleontology* 37.

Gorscak E, O'Connor PM, Stevens NJ, Roberts EM. 2014. The basal titanosaurian *Rukwatitan bisepultus* (Dinosauria, Sauropoda) from the middle Cretaceous Galula Formation, Rukwa Rift Basin, southwestern Tanzania. *Journal of Vertebrate Paleontology* 34: 1133–1154.

Hammer Ø, Harper DAT. 2008. *Paleontological Data Analysis*. Wiley-Blackwell Publishing.

Hammer Ø, Harper DAT, Ryan PD. 2001. PAST: Paleontological Statistics Software Package for Education and Data Analysis. *Paleontologia Electronica* 4: 9pp.

Hastie T, Tibshirani R, Friedman J. 2009. The Elements of Statistical Learning. B*ayesian Forecasting and Dynamic Models* 1: 1–694.

Hatcher JB. 1901. *Diplodocus* Marsh*: its osteology, taxonomy, and probate habits, with a restoration of the skeleton*. Pittsburgh: Published under authority of the Board of Trustees of the Carnegie Museum.

Hatcher JB. 1903. Osteology of *Haplocanthosaurus*, with description of a new species, and remarks on the probable habits of the Sauropoda and the age and origin of the *Atlantosaurus* Beds. *Memoirs of the Carnegie Museum* 2: 1–72.

Hendrickx C, Mateus O, Araújo R. 2014. The dentition of Megalosauridae (Theropoda: Dinosauria). *Acta Palaeontologica Polonica* 56: 463–475.

Hewson PJ. 2009. *Multivariate Statistics with R.* 189pp.

Hocknull SA, White MA, Tischler TR, Cook AG, Calleja ND, Sloan T, Elliott DA. 2009. New Mid-Cretaceous (latest Albian) dinosaurs from Winton, Queensland, Australia. *PloS ONE* 4: e6190.

Hoffet JH. 1942. Description de quelques ossements de Titanosauriens du Sénonien du Bas-Laos. *Comptes Rendus des Séances du Conseil des Recherches Scientifiques de l'Indochine*: 1–8.

Holland WJ. 1906. The osteology of *Diplodocus* Marsh: with special reference to the restoration of the skeleton of *Diplodocus* carnegie Hatcher, presented by Mr. Andrew Carnegie to the British museum, May 12, 1905. *Memoirs of the Carnegie Museum* 2: 1–68.

Hothorn T, Hornik K, van de Wiel MA, Zeileis A. 2006. A Lego System for Conditional Inference. *The American Statistician* 60: 257–263.

Hothorn T, Hornik K, van de Wiel MA, Zeileis A. 2008. Implementing a Class of Permutation Tests: The coin Package. *Journal of Statistical Software*: 1–23.

Hsu CW, Lin CJ. 2002. A comparison of methods for multiclass support vector machines. IEEE *Transactions on Neural Networks* 13: 415–425.

Huene FF von. 1915. On Reptiles of the New Mexican Trias in the Cope Collection. *Bulletin of the American Museum of Natural History* 34: 485–508.

Huene FF von. 1929. Los Saurisquios y Ornitisquios del Cretáceo Argentino. *Anales del Museo de la Plata* III: 263.

Huene FF von. 1932. Die fossile Reptil-Ordnung Saurischia, ihre Entwicklung und Geschichte. *Monographien zur Geologie und Paläontologie* I: 564.

Huene FF von, Matley. 1923. The Cretaceous Saurischia and Ornithischia of the central provinces of India. *Memoirs of the Geological Survey of India* 21: 1–74.

Ikejiri T. 2004. *Anatomy of Camarasaurus lentus (Dinosauria: Sauropoda) from the Morrison Formation (Late Jurassic), Thermopolis, central Wyoming, with Determination and Interpretation of Ontogenetic, Sexual Dimorphic and Individual Variation in the Genus*. Unpublished thesis, State University.

Ikejiri T. 2008. Slender and robust morphs of *Camarasaurus* (Dinosauria, Sauropoda) from the Morrison Formation (Late Jurassic) of the Rocky Mountain Region and Its Implications for possible sexual dimorphism. In: Farley GH, Choate JR, eds. *Unlocking the Unknown: Papers honoring Dr. Richard J. Zakrzewski. Fort Hays Special Studies number* 2. Hays, Kansas: Fort Hays State University, 31–44.

Ikejiri T, Tidwell V, Trexler D. 2005. New adult specimens of *Camarasaurus lentus* highlight ontogenetic variation within the species. In: Carpenter K, Tidwell V, eds. *Thunder-Lizards: The Sauropodomorph Dinosaurs*. Bloomington: Indiana University Press, 157–179.

Janensch W. 1929. Material und Formengehalt der Sauropoden in der Ausbeute der Tendaguru-*Expedition. Palaeontographica* 1: 1–34.

Janensch W. 1961. Die Gliedmaszen und Gliedmaszengürtel der Sauropoden der Tendaguru-Schichten. *Palaeontographica* 3: 177–235.

Kassambara A, Mundt F. 2017. Factoextra: extract and visualize the results of multivariate data analyses. R package version 1: 1–76.

Klingenberg CP. 2013. Cranial integration and modularity: Insights into evolution and development from morphometric data. *Hystrix* 24: 43–58.

Knaus J. 2015. snowfall: Easier cluster computing (based on snow). R package version 1.84-6.1. https://CRAN.R-project.org/package=snowfall.

Knerr S, Personnaz L, Dreyfus G. 1990. Single-layer learning revisited: a stepwise procedure for building and training a neural network. *Neurocomputing*. Berlin: Springer, 41–50.

Knoll F, Ridgely RC, Ortega F, Sanz JL, Witmer LM. 2013a. Neurocranial Osteology and Neuroanatomy of a Late Cretaceous Titanosaurian Sauropod from Spain (*Ampelosaurus*

sp.) *PLoS ONE* 8: e54991.

Knoll F, Witmer LM, Ridgely RC, Ortega F, Sanz JL. 2013b. A new titanosaur sauropod neurocranium from the Late Cretaceous of Spain. *73rd Annual Meeting of the Society of Vertebrate Paleontology*. Los Angeles, CA, 122.

Kuhn M, Contributions from ., Wing J, Weston S, Williams A, Keefer C, Engelhardt A, Cooper T, Mayer Z, Kenkel B, The R Core Team, Benesty M, Lescarbeau R, Ziem A, Scrucca L, Tang Y, Candan C, Hunt. T. 2017. caret: Classification and Regression Training. R package version 6.0-76. https://CRAN.R-project.org/package=caret.

Lapparent AF de. 1947. Les dinosauriens du Crétacé supérieur du Midi de la France. *Mémories de la Société Géologique de France* 56: 1–54.

Larson DW, Currie PJ. 2013. Multivariate analyses of small theropod dinosaur teeth and implications for paleoecological turnover through time. *PloS ONE* 8: e54329.

Lehman TM, Coulson AB. 2002. A Juvenile Specimen of the Sauropod Dinosaur *Alamosaurus sanjuanensis* from the Upper Cretaceous of Big Bend National Park, Texas. *Journal of Paleontology* 76: 156–172.

Liu Y, Zheng YF. 2005. One-against-all multi-class SVM classification using reliability measures. *Proceedings of the International Joint Conference on Neural Networks. IEEE*, 849–854.

Le Loeuff J. 1993. European titanosaurids. *Revue de Paléobiologie, Volume Spéciale* 7: 105–117.

Le Loeuff J. 1995. *Ampelosaurus atacis* (nov, gen., nov. sp.), un nouveau Titanosauridae (Dinosauria, Sauropoda) du Crétacé supérieur de la Haute Vallée de l'Aude (France). *Comptes Rendus de l'Académie des Sciences à Paris*, Série IIa 321: 693–699.

Le Loeuff J. 1998. Les dinosaures du Crétacé supérieur de l'Île Ibéro-Armoricaine. In: Carvalho AMG de, Andrade AM, Santos VF dos, Cascalho J, Taborda R, eds. *I Encontro Internacional sobre Paleobiologia dos Dinossáurios*. Museu Nacional de História Natural, Lisboa, 49–64.

Le Loeuff J. 2005a. Osteology of *Ampelosaurus atacis* (Titanosauria) from Southern France. In: Tidwell V, Carpenter K, eds. *Thunder-Lizards: The Sauropodomorph Dinosaurs*. Bloomington: Indiana University Press, 115–137.

Le Loeuff J. 2005b. Romanian late cretaceous dinosaurs: Big dwarfs or small giants? *Historical Biology* 17: 15–17.

Le Loeuff J. 2012. Paleobiogeography and biodiversity of Late Maastrichtian dinosaurs: how many dinosaur species went extinct at the Cretaceous-Tertiary boundary? *Bulletin de la Societe Geologique de France* 183: 547–559.

López-Martínez N. 2001. New dinosaur sites correlated with Upper Maastrichtian pelagic deposits in the Spanish Pyrenees: implications for the dinosaur extinction pattern in Europe. *Cretaceous Research* 22: 41–61.

Lydekker R. 1888. *Catalogue of fossil Reptilia and Amphibia in the British Museum. Part 1. Containing the Orders Ornithosauria, Crocodilia, Dinosauria, Squamata, Rhynchocephalia, and Proterosauria*. British Museum of Natural History.

Lydekker R. 1893. *Contributions to a knowledge of the fossil vertebrates of Argentinia*. La Plata: [s.n.].

Macqueen J. 1967. Some methods for classification and analysis of multivariate observations. *Proceedings of the Fifth Berkeley Symposium on Mathematical Statistics and Probability* 1: 281–297.

Maiorino L, Farke A a, Kotsakis T, Piras P. 2013. Is *Torosaurus Triceratops*? Geometric morphometric evidence of late maastrichtian ceratopsid dinosaurs. *PloS ONE* 8: e81608.

Maiorino L, Farke A a., Kotsakis T, Piras P. 2015. Males Resemble Females: Re-Evaluating Sexual Dimorphism in *Protoceratops andrewsi* (Neoceratopsia, Protoceratopsidae). *PLOS ONE* 10: e0126464.

Malafaia E, Escaso F, Mocho P, Serrano-Martínez A, Torices A, Cachão M, Ortega F. 2017. Analysis of diversity, stratigraphic and geographical distribution of isolated theropod teeth from the Upper Jurassic of the Lusitanian Basin, Portugal. *Journal of Iberian Geology* 43: 257–291.

Mannion PD, Calvo JO. 2011. Anatomy of the basal titanosaur (Dinosauria, Sauropoda) *Andesaurus delgadoi* from the mid-Cretaceous (Albian-early Cenomanian) Río Limay Formation, Neuquén Province, Argentina: implications for titanosaur systematics. *Zoological Journal of the Linnean Society* 163: 155–181.

Mannion PD, Otero A. 2012. A reappraisal of the Late Cretaceous Argentinean sauropod dinosaur *Argyrosaurus superbus*, with a description of a new titanosaur genus. *Journal of Vertebrate Paleontology* 32: 614–638.

Mannion PD, Upchurch P, Barnes RN, Mateus O. 2013. Osteology of the Late Jurassic Portuguese sauropod dinosaur *Lusotitan atalaiensis* (Macronaria) and the evolutionary history of basal titanosauriforms. *Zoological Journal of the Linnean Society* 168: 98–206.

Marko PB, Jackson JBC. 2001. Patterns of morphological diversity among and within arcid bivalve species pairs separated by the Isthmus of Panama. *Journal of Paleontology* 75: 590–606.

Marsh OC. 1986. *The Dinosaurs of North America*.

Martin V, Buffetaut É, Suteethorn V. 1994. A New Genus of Sauropod Dinosaur from the Sao-Khua Formation (Late Jurassic or Early Cretaceous) of Northeastern Thailand. *Comptes Rendus de l'Academie des Sciences Serie* II 319: 1085–1092.

Martín Jimenez M, Sanchez-Chillon B, Escaso F, Mocho P, Narvaez I, Ortega F, Perez-Garcia A. 2017. Systematic study of the historical material of Upper Cretaceous reptiles from the Tremp Basin (Catalonia, Spain) housed at the Museo Nacional de Ciencias Naturales (Madrid). *Journal of Iberian Geology* 43: 217–233.

McIntosh JS. 1990a. Species determination in sauropod dinosaurs with tentative suggestions for their classification. In: Carpenter K, Currie PJ, eds. *Dinosaur Systematics*. Cambridge: Cambridge University Press, 53–70.

McIntosh JS. 1990b. Sauropoda. In: Weishampel DB, Dodson P, Osmólska H, eds. *The Dinosauria*. University of California Press, 345–401.

McIntosh JS. 2005. The Genus *Barosaurus* Marsh (Sauropoda, Diplodocoidea). In: Tidwel V, Carpenter K, eds. *Thunder-Lizards: The Sauropodomorph Dinosaurs*. Indiana University Press, 512.

McIntosh JS, Miles CA, Cloward KC, Parker JR. 1996a. A new nearly complete skeleton of *Camarasaurus*. *Bulletin of Gunma Museum of Natural History* 1: 1–87.

McIntosh JS, Miller WE, Stadtman KL, Gillette DD. 1996b. The Osteology of *Camarasaurus lewisi* (Jensen, 1988). *BYU Geology Studies* 41: 73–115.

Meyer D, Dimitriadou E, Hornik K, Weingessel A, Leisch F. 2017. e1071: Misc Functions of the Department of Statistics, Probability. R package version 1.6-8. https://CRAN.R-project.org/package=e1071.

Minka T. 1999. Bayesian linear regression. *Machine Learning* 631: 1–12.

Mocho P, Escaso F, Gasulla JM, Galobart À, Poza B, Santos-Cubedo A, Sanz JL, Ortega F. 2016a. A new titanosauriform sauropod from the Arcillas de Morella Formation (Early Cretaeous). *VII International Symposium about Dinosaurs Palaeontology and their Environment*.97–98.

Mocho P, Escaso F, Marcos-Fernández F, Páramo A, Vidal D, Ortega F. 2018. The morphological variability on titanosaur caudal series from Lo Hueco: taxonomic diversity, intra-specific variability or both? *XVI Annual Meeting of European Association of Vertebrate Paleontologists*.126.

Mocho P, Páramo A, Díez Díaz V, Escaso F, Marcos-Fernández F, Sanz JL, Ortega F. 2016b. Looking through the axial skeleton of the Lo Hueco titanosaurs. In: Torcida Fernández-Baldor F, Canudo JI, Huerta P, Pereda X, eds. *VII International Symposium about Dinosaurs Palaeontology and their Environment*.99–100.

Mocho P, Pérez-García A, Gasulla JM, Ortega F. 2017. High sauropod diversity in the upper Barremian Arcillas de Morella Formation (Maestrat Basin, Spain) revealed by a systematic review of historical material. *Journal of Iberian Geology* 43: 111–128.

Mocho P, Royo-Torres R, Ortega F. 2014. Phylogenetic reassessment of *Lourinhasaurus alenquerensis*, a basal Macronaria (Sauropoda) from the Upper Jurassic of Portugal. *Zoological Journal of the Linnean Society* 170: 875–916.

Mook CC. 1903. The Fore and Hindlimb of *Diplodocus*. *Bulletin American Museum of Natural History* 37: 815–820.

Morissette L, Chartier S. 2013. The k-means clustering technique: General considerations and implementation in Mathematica. *Tutorials in Quantitative Methods for Psychology* 9: 15–24.

Mosimann JE. 1970. Size allometry: Size and shape variables with characterizations of the lognormal and generalized gamma distributions. *Journal of the American Statistical Association* 65: 930–945.

Naish D, Martill DM. 2001. Saurischian dinosaurs 1: Sauropods. In: Martill DM, Naish D, eds. *Dinosaurs of the Isle of Wight*. London: Palaeontological Association, 185–241.

Naish D, Martill DM. 2007. Dinosaurs of Great Britain and the Role of the Geological Society of London in Their Discovery: Basal Dinosauria and Saurischia. *Journal of the Geological Society* 164: 493–510.

Nopsca BF. 1915. Die dinosaurier der Siebenbürgischen landesteile Ungarns. *Ungarischen Geologischen Reichsanstalt* 23: 1–24.

Ortega F, Bardet N, Barroso-Barcenilla F, Callapez PMPM, Cambra-moo O, Daviero- Gómez V, Díez Díaz V, Domingo L, Elvira A, Escaso F, García-Oliva M, Gómez B, Houssaye A, Knoll F, Marcos-Fernández F, Martín M, Mocho P, Narváez I, Pérez-García A, Peyrot D, Segura M, Serrano H, Torices A, Vidal D, Sanz JL. 2015. The biota of the Upper Cretaceous site of "Lo Hueco" (Cuenca, Spain). *Journal of Iberian Geology* 41: 83–99.

Ortega F, Pérez-García A. 2009. cf. *Lirainosaurus* sp. (Dinosauria: Titanosauria) en el Cretácico Superior de Sacedón (Guadalajara). *Geogaceta*: 87–90.

Osborn HF, Mook CC. 1921. *Camarasaurus, Amphicoelias*, and other sauropods of Cope. *Memoirs of the American Museum of Natural History* 3: 247–387.

Otero A. 2010a. The appendicular skeleton of *Neuquensaurus*, a Late Cretaceous saltasaurine sauropod from Patagonia, Argentina. *Acta Palaeontologica Polonica* 55: 399–426.

Otero A. 2010b. Comments on the taxonomic status of *Neuquensaurus robustus* (Huene)

(Sauropoda, Titanosauria). *X Congreso Argentino de Paleontología y Bioestratigrafía -VII Congreso Latinoamericano de Paleontología*. A.

Otero A, Vizcaíno SF. 2008. Musculatura y función del miembro posterior de *Neuquensaurus australis* (Sauropoda: Titanosauria). Ameghiniana 45: 333–348.

Pal M. 2008. Multiclass Approaches for Support Vector Machine Based Land Cover Classification. ArXiv: 0802.2411

Pang Q, Cheng Z. 2000. A new family of sauropod dinosaur from the Upper Cretaceous of Tianzhen, Shanxi Province, China. *Acta Geologica Sinica* 74: 1–9.

Páramo A, Ortega F, Escaso F, Narváez I, Sanz JL. 2014. Ejemplares juveniles de titanosaurio (Sauropoda) del yacimiento de Lo Hueco (Fuentes, Cuenca). In: Royo-Torres, R.; Verdú, F.J.; Alcalá, L. (coord.). *XXX Jornadas de Paleontología de la Sociedad Española de Paleontología. ¡Fundamental!* 24: 149–151.

Páramo A, Ortega F, Mocho P, Sanz JL. 2016. Femoral variability in two titanosaur taxa from Lo Hueco (Cuenca, Spain): Insights for iberoarmorican titanosaur diversity assessment. In: Torcida F, Jose IC, Huerta P, Pereda-Suberbiola X, eds. *VII International Symposium about Dinosaurs Palaeontology and their Environment. Salas de los Infantes*, Burgos: Colectivo Arqueológico y Paleontológico de Salas, 107–108.

Páramo A, Ortega F, Sanz JL. 2015. Preliminar assessment of the morphological variability of appendicular bones of titanosaurs (Dinosauria, Sauropoda) from Lo Hueco (Fuentes, Cuenca). *XXXI Jornadas de la Sociedad Española de Paleontología*.

Paul GS. 1988. The *Brachiosaurus* giants of the Morrison and Tendaguru with a description of a new supergenus, Giraffatitan, and comparison of the world's largest dinosaurs. *Hunteria* 2: 1–14.

Pereda Suberbiola X, Corral JC, Astibia H, Badiola A, Bardet N, Berreteaga A, Buffetaut É, Buscalioni ÁD, Cappetta H, Cavin L, Díez Díaz V, Gheerbrant E, Murelaga X, Ortega F, Pérez-García A, Poyato-Ariza F, Rage JC, Sanz JL, Torices A. 2015. Late cretaceous continental and marine vertebrate assemblages from the Laño quarry (Basque-Cantabrian Region, Iberian Peninsula): an update. *Journal of Iberian Geology* 41.

Pérez-García A, Bardet N, Martín-Jiménez M, Mocho P, Narváez I, Torices A, Ortega F. 2018. Los reptiles del yacimiento Cenomaniense de Algora (Guadalajara, España): nuevos datos y síntesis faunística. *IV Congresso Ibérico de Paleontologia e XXXIV Jornadas de Paleontologia*. Coimbra, A.

Perez-Garcia A, Gasco F, Ortega F. 2017. A Singular Uppermost Cretaceous Dinosaur Nesting Area in the Villalba de la Sierra Formation (Guadalajara, Central Spain). *77th Annual Meeting of the Society of Vertebrate Paleontology*: 176.

Poropat SF, Upchurch P, Mannion PD, Hocknull SA, Kear BP, Sloan T, Sinapius GHK, Elliott DA. 2015. Revision of the sauropod dinosaur *Diamantinasaurus matildae* Hocknull *et al.*, 2009 from the mid-Cretaceous of Australia: Implications for Gondwanan titanosauriform dispersal. *Gondwana Research* 27: 995–1033.

Powell JE. 2003. Revision of South American titanosaurid dinosaurs: Palaeobiological, palaeobiogeographical and phylogenetic aspects. *Records of the Queen Victoria Museum* 111: 1–179.

Remes K. 2006. Revision of the Tendaguru Sauropod dinosaur *Tornieria africana* (Fraas) and its

relevance for sauropod paleobiogeography. *Journal of Vertebrate Paleontology* 26: 651–669.

Remes K. 2009. Taxonomy of Late Jurassic diplodocid sauropods from Tendaguru (Tanzania). *Fossil Record* 12: 23–46.

Remes K, Ortega F, Fierro I, Joger U, Kosma R, Marín Ferrer JM, Ide OA, Maga A. 2009. A New Basal Sauropod Dinosaur from the Middle Jurassic of Niger and the Early Evolution of Sauropoda. *PLoS ONE* 4: e6924.

Riggs ES. 1901. The Largest Known Dinosaur. *Science* 13: 549–550.

Riggs ES. 1903. Brachiosaurus altithorax, the largest known dinosaur. *American Journal of Science* s4-15: 299–306.

Rohlf FJ. 2000. Statistical power comparisons among alternative morphometric methods. *American Journal of Physical Anthropology* 111: 463-478.

Rokach L, Maimon O. 2007. Clustering methods. In: Rokach L, Maimon O, eds. *Series in Machine Perception and Artificial Intelligence. Data Mining with Decision Trees*. World Scientific, 321–352.

Rousseeuw PJ. 1987. Silhouettes: A graphical aid to the interpretation and validation of cluster analysis. *Journal of Computational and Applied Mathematics* 20: 53–65.

Royo-Torres R. 2009. *El saurópodo de Peñarroya de Tastavins. Teruel*: Instituo de Estudios Turolenses y Fundación Conjunto Paleontológico de Teruel-Dinópolis.

Royo-Torres R, Alcalá L, Cobos A. 2012. A new specimen of the Cretaceous sauropod *Tastavinsaurus sanzi* from El Castellar (Teruel, Spain), and a phylogenetic analysis of the Laurasiformes. *Cretaceous Research* 34: 61–83.

Royo-Torres R, Upchurch P. 2012. The cranial anatomy of the sauropod *Turiasaurus riodevensis* and implications for its phylogenetic relationships. *Journal of Systematic Palaeontology* 10: 1–31.

Royston P. 2004. *Multiple imputation of missing values*. The Stata Journal.

RStudio Team. 2015. RStudio: Integrated Development for R. RStudio, Inc., Boston, MA URL http://www.rstudio.com/.

Rueden CT, Schindelin J, Hiner MC, DeZonia BE, Walter AE, Eliceiri KW. 2017. ImageJ2: ImageJ for the next generation of scientific image data.

Salgado JL, Azpilicueta C. 2000. Un nuevo saltasaurino (Sauropoda, Titanosauridae) de la provincia de Río Negro (Formación Allen, Cretácico Superior), Patagonia, Argentina. *Ameghiniana* 37: 259–264.

Salgado JL, Coria RA. 1993. El genero *Aeolosaurus* (Sauropoda, Titanosauridae) en la Formacion Allen (Campaniano-Maastrichtiano) de la Provincia de Rio Negro, Argentina. *Ameghiniana* 30: 119–128.

Salgado JL, Coria RA, Calvo JO. 1997a. Evolution of the titanosaurid sauropods I: Phylogenetic analysis based on the postcranial evidence. *Ameghiniana* 34: 3–32.

Salgado JL, Coria RA, Calvo JO. 1997b. Presencia del género *Aeolosaurus* (Sauropoda, Titanosauridae) en la Formación Los Alamitos, Cretácico Superior de la Provincia de Río Negro, Argentina. *Geociencias* 2: 44–49.

Salgado JL, Gallina PA, Paulina Carabajal A. 2015. Redescription of *Bonatitan reigi* (Sauropoda: Titanosauria), from the Campanian–Maastrichtian of the Río Negro Province (Argentina). *Historical Biology* 27: 525–548.

Sallam HM, Gorscak E, O'Connor PM, El-Dawoudi IA, El-Sayed S, Saber S, Kora MA, Sertich JJW,

Seiffert ER, Lamanna MC. 2018. New Egyptian sauropod reveals Late Cretaceous dinosaur dispersal between Europe and Africa. *Nature Ecology & Evolution* 2: 445–451.

Sander PM, Mateus O, Laven T, Knötschke N. 2006. Bone histology indicates insular dwarfism in a new Late Jurassic sauropod dinosaur. *Nature* 441: 739–41.

Sanz JL, Buscalioni ÁD, Casanovas ML, Santafé JV. 1987. Dinosaurios del Cretácico Inferior de Galve (Teruel, España). *Estudios Geológicos* extr.: 45–64.

Sanz JL, Powell JE, Le Loeuff J, Martínez RN, Pereda Suberbiola X. 1999. Sauropod remains from the Upper Cretaceous of Laño (north central Spain). Titanosaur phylogenetic relationships. *Estudios del Museo de Ciencias Naturales de Alava* 14: 235–255.

SAS Institute. 1999. SAS/GRAPH Software: Reference, Version 8.

Schafer JL. 1999. Multiple imputation: A primer. *Statistical Methods in Medical Research* 8: 3–15.

Schindelin J, Rueden CT, Hiner MC, Eliceiri KW. 2015. The ImageJ ecosystem: An open platform for biomedical image analysis. *Molecular Reproduction and Development* 82: 518–529.

Schlager S. 2017. Morpho and Rvcg – Shape Analysis in R. In: Zheng G, Li S, Szekely G, eds. *Statistical Shape and Deformation Analysis*. Elsevier, 217–256.

Schulte-Hostedde AI, Millar JS, Gibbs HL. 2004. Sexual selection and mating patterns in a mammal with female-biased sexual size dimorphism. *Behavioral Ecology* 15: 351–356.

Schwarz D, Böhm N. 2012. A morphometric approach to the specific separation of the humeri and femora of *Dicraeosaurus* from the Late Jurassic of Tendaguru, Tanzania. *Acta Palaeontologica Polonica* 59: 81–98.

Selim SZ, Ismail MA. 1984. K-Means-Type Algorithms: A Generalized Convergence Theorem and Characterization of Local Optimality. *IEEE Transactions on Pattern Analysis and Machine Intelligence* 6: 81–87.

Serrano-Martínez A, Vidal D, Sciscio L, Ortega F, Knoll F. 2016. Isolated theropod teeth from the Middle Jurassic of Niger and the early dental evolution of Spinosauridae. *Acta Palaeontologica Polonica* 61: 403–415.

Smith JB, Vann DR, Dodson P. 2005. Dental morphology and variation in theropod dinosaurs: Implications for the taxonomic identification of isolated teeth. *The Anatomical Record* 285A: 699–736.

Sokal RR, Rohlf FJ. 1987. *Introduction to bioestatistics*. W. H. Freeman and Company.

Strauss RE, Bookstein FL. 1982. The Truss: Body Form Reconstructions in Morphometrics. *Systematic Biology* 31: 113–135.

Suteethorn S, Le Loeuff J, Buffetaut É, Suteethorn V. 2010. Description of topotypes of *Phuwiangosaurus sirindhornae*, a sauropod from the Sao Khua Formation (Early Cretaceous) of Thailand, and their phylogenetic implications. *Neues Jahrbuch für Geologie und Paläontologie Abhandlungen* 256: 109–121.

Taylor MP. 2009. A Re-evaluation of *Brachisaurus altitorax* Riggs 1903 (Dinosauria, Sauropoda), and its generic separation from *Giraffatitan brancai* (Janesch 1914). *Journal of Vertebrate Paleontology* 29: 787–806.

The R Core Team. 2016. A language and environment for statistical computing. R Foundation for Statistical Computing, Vienna, Austria. URL https://www.R-project.org/.

Tibshirani R, Walther G, Hastie. T. 2001. Estimating the number of clusters in a dataset via the gap

statistic. *Journal of the Royal Statistical Society: Series B* (Statistical Methodology) 63: 411–423.

Tidwell V, Wilhite RD. 2005. Ontogenetic variation and isometric growth in the forelimb of the Early Cretaceous sauropod *Venenosaurus*. In: Carpenter K, Tidwell V, eds. *Thunder-Lizards: The Sauropodomorph Dinosaurs*. Indiana University Press, 187–196.

Tortosa T, Dutour Y, Cheylan G, Buffetaut É. 2012. New discovery of titanosaurs (Dinosauria, Sauropoda) from Provence (SE France): Implications on local paleobiodiversity. *¡Fundamental!*: 259–262.

Tschopp E, Mateus O, Benson RBJ. 2015. A specimen-level phylogenetic analysis and taxonomic revision of Diplodocidae (Dinosauria, Sauropoda). *PeerJ* 3: e857.

Ullmann P.V., Bonnan MF, Lacovara KJ. 2017. Characterizing the Evolution of Wide-Gauge Features in Stylopodial Limb Elements of Titanosauriform Sauropods via Geometric Morphometrics. *The Anatomical Record* 300: 1618–1635.

Upchurch P. 1998. The phylogenetic relationships of sauropod dinosaurs. *Zoological Journal of the Linnean Society* 124: 43–103.

Upchurch P, Barrett PM, Dodson P. 2004a. Sauropoda. In: Weishampel DB, Dodson P, Osmólska H, eds. *The Dinosauria*. Berkeley: University of California Press, 259–322.

Upchurch P, Tomida Y, Barrett PM, Yukimitsu T, Barrett PM. 2004b. A New Specimen of *Apatosaurus ajax* (Sauropoda: Diplodocidae) from the Morrison Formation (Upper Jurassic) of Wyoming, USA. Tokyo, Japan: *National Science Museum Monographs* 26: 156pp.

Vapnik VN. 1995. *The Nature of Statistical Learning Theory*. New York, NY: Springer.

Venables WN, Ripley BD. 2002. *Modern Applied Statistics with S*. Springer.

Vidal D, Sanz JL, Mocho P, Páramo A, Escaso F, Marcos-Fernández F, Ortega F. 2017. The titanosaur tails from Lo Hueco (Cuenca, Spain): Four different ways to shake? In: Farke AA, Mackenzie SA, Miller Camp J, eds. *77th Annual Meeting of the Society of Vertebrate Paleontology. Calgary*, 208.

Vieira WLS, Vieira KS, Nóbrega RP, Montenegro PFGP, Pereira Filho GA, Santana GG, Alves RRN, Almeida WO, Vasconcellos A. 2014. Species Richness and Evidence of Random Patterns in Assemblages of South American Titanosauria during the Late Cretaceous (Campanian–Maastrichtian). *PLoS ONE* 9: e108307.

Vila B, Galobart À, Canudo JI, Le Loeuff J, Dinarès-Turell J, Riera V, Oms O, Tortosa T, Gaete R. 2012. The diversity of sauropod dinosaurs and their first taxonomic succession from the latest Cretaceous of southwestern Europe: Clues to demise and extinction. *Palaeogeography, Palaeoclimatology, Palaeoecology* 350–352: 19–38.

Vila B, Oms O, Galobart À, Bates KT, Egerton VM, Manning PL. 2013. Dynamic Similarity in Titanosaur Sauropods: Ichnological Evidence from the Fumanya Dinosaur Tracksite (Southern Pyrenees). *PLoS ONE* 8: e57408.

Vila B, Sellés AG, Brusatte SL. 2016. Diversity and faunal changes in the latest Cretaceous dinosaur communities of southwestern Europe. *Cretaceous Research* 57: 552–564.

Warton DI, Duursma RA, Falster DS, Taskinen S. 2012. smatr 3- an R package for estimation and inference about allometric lines. *Methods in Ecology and Evolution* 3: 257–259.

Whitlock JA. 2011. A phylogenetic analysis of Diplodocoidea (Saurischia: Sauropoda). Zoological *Journal of the Linnean Society* 161: 872–915.

Wick SL, Lehman TM. 2014. A complete titanosaur femur from West Texas with comments regarding hindlimb posture. *Cretaceous Research* 49: 39–44.

Wilhite RD. 1999. *Ontogenetic variation in the appendicular skeleton of the genus Camarasaurus*. Unpublished thesis, Brigham Young University.

Wilhite RD. 2003. *Biomechanical Reconstruction of the Appendicular Skeleton in Three North American Jurassic Sauropods*. Unpublished thesis, Louisiana State University.

Wilhite RD. 2005. Variation in the Appendicular Skeleton of North American Sauropod Dinosaurs: Taxonomic Implications. In: Tidwell V, Carpenter K, eds. *Thunder-Lizards: The Sauropodomorph Dinosaurs*. Indiana University Press, 268–301.

Williamson TE, Brusatte SL. 2014. Small Theropod Teeth from the Late Cretaceous of the San Juan Basin, Northwestern New Mexico and Their Implications for Understanding Latest Cretaceous Dinosaur Evolution. *PLoS ONE* 9: e93190.

Wilson JA. 2002. Sauropod dinosaur phylogeny: critique and cladistic analysis. *Zoological Journal of the Linnean Society* 136: 215–275.

Wilson JA, Barrett PM, Carrano MT. 2011. An associated partial skeleton of *Jainosaurus* cf. *septentrionalis* (Dinosauria: Sauropoda) from the Late Cretaceous of Chhota Simla, Central India. *Palaeontology* 54: 981–998.

Wilson JA, Carrano MT. 1999. Titanosaurs and the Origin of 'wide-gauge' trackways: A Biomechanical and Systematic Perspective on Sauropod Locomotion. *Paleobiology* 25: 252–267.

Wilson JA, D'Emic MD, Curry Rogers K, Mohabey DM, Sen S. 2009. Reassessment of Sauropod Dinosaur *Jainosaurus* (= '*Antarctosaurus*') *septentrionalis* from the Upper Cretaceous of India. *Contributions from the Museum of Paleontology University of Michigan* 32: 17–40.

Wilson JA, Sereno PC. 1998. Early Evolution and High-level Phylogeny of Sauropod Dinosaurs. *Journal of Vertebrate Paleontology* 18: 1–68.

Wilson JA, Upchurch P. 2003. A revision of *Titanosaurus* Lydekker (Dinosauria - Sauropoda), the first dinosaur genus with a 'Gondwanan' distribution. *Journal of Systematic Palaeontology* 1: 125–160.

Wilson JA, Upchurch P. 2009. Redescription and reassessment of the phylogenetic affinities of *Euhelopus zdanskyi* (Dinosauria: Sauropoda) from the Early Cretaceous of China. *Journal of Systematic Palaeontology* 7: 199–239.

Woodruff DC, Foster JR. 2017. The first specimen of *Camarasaurus* (Dinosauria: Sauropoda) from Montana: The northernmost occurrence of the genus. *PLoS ONE* 12: e0177423.

You H, Tang F, Luo Z. 2003. A New Basal Titanosaur (Dinosauria: Sauropoda) from the Early Cretaceous of China. *Acta Geologica Sinica* 77: 424–429.

Zelditch ML, Swiderski DL, Sheets HD. 2012. *Geometric Morphometrics for Biologists*. Elsevier.

Zhou X, Leonardos S, Hu X, Daniilidis K. 2015. 3D shape estimation from 2D landmarks: A convex relaxation approach. *Proceedings of the IEEE Computer Society Conference on Computer Vision and Pattern Recognition* 07-12-June: 4447–4455.

CHAPTER IV.II:

3D Geometric morphometrics of the hindlimb in the titanosaur sauropods from Lo Hueco (Cuenca, Spain)

IV.II. ABSTRACT

The Campanian-Maastrichtian Konzentrat-Lagerstätte of Lo Hueco (Spain) have yielded tens of appendicular specimen referable to titanosaurs. There is a high variability in the morphology among this abundant sample. The taxonomical assessment is difficult, as many of the fossil remains present various degrees of preservation and also many of the appendicular elements are isolated. Among the hindlimb elements there are several specimens in partial association. This gives the opportunity to analyse the morphological variability and establish a taxonomical assessment of the hindlimb elements of the titanosaurs of Lo Hueco. The partial association of several of these specimens allow us to test several morphotype hypothesis proposed in previous studies of the cranial and axial skeleton of these titanosaurs.

The geometric morphometrics tool kit is a suitable methodology to explore the morphological variability of these anatomical elements. In this study several femora, tibiae and fibulae of Lo Hueco are digitized. The resultant mesh representations are used for definition of 3D landmarks analysed through geometric morphometric methods. The use of clustering techniques and statistical workflow over the shape variables allow us to test and discuss several a priori morphotype hypotheses. The presence of two main morphotypes is the most probable distribution among the sample of titanosaur hindlimb elements of Lo Hueco.

IV.II.1 INTRODUCTION

Previous works on limb scaling and quantitative morphology in sauropod dinosaurs have been carried out using 2D geometric morphometrics landmark dataset (Bonnan, 2004, 2007; Wilhite, 2005; Schwarz & Böhm, 2012; Ullmann, Bonnan, & Lacovara, 2017). The advantage of 2D landmark geometric morphometrics over traditional morphometrics is the capability of summarize more morphological changes in fewer dimensions (Bookstein, 1991; Rohlf, 1993; Zelditch, Swiderski, & Sheets, 2012a). The use of fewer dimensions means less statistical difficulties relative to sample availability, especially useful in paleontology (Hammer & Harper, 2008; Zelditch *et al.*, 2012a; Brown, Arbour, & Jackson, 2012; Polly & Motz, 2016). The obvious problematics of 2D landmark geometric morphometrics is the lack of information on features that changes in the third dimension of the analysed specimen. There is a trade-off between 2D and 3D geometric morphometrics, as the advantages of 2D data input is the availability photographic while few 3D scans are already available for wide range of sauropod (or other fossil groups) collections (e.g., Cunningham *et al.*, 2014; Davies *et al.*, 2017; Lautenschlager, 2017).

The Campanian-Maastrichtian Konzentrat-Lagerstätte of Lo Hueco (Spain; Fig.IV.II.1) have yielded tens of specimens referable to titanosaur sauropods in partial articulation. At least sixteen titanosaur individuals in partial articulation and tens of isolated bones have been recovered (Ortega *et al.*, 2015). Preliminary studies on cranial and appendicular skeleton of the titanosaurs from Lo Hueco reveals the presence of at least two distinct morphotypes of titanosaurs (Knoll *et al.*, 2013, 2015; Díez Díaz, Ortega, & Sanz, 2014). The study of one of those individuals has abled us to define an exclusive form of European titanosaur, *Lohuecotitan pandafilandi* (Díez Díaz *et al.*, 2016). The wide sample of specimens and high degree of morphological variability in the skeleton of the titanosaurs allow us to analyse the sauropod intraspecific variability and the use of 3D geometric morphometrics methods (Páramo, Ortega, & Sanz, 2015a; see Fig.IV.II.2, this study). The study of appendicular skeleton reveals two possible main morphotypes in the sample of titanosaurs from Lo Hueco (Páramo *et al.*, 2016) and the study of the axial skeleton reported the probable presence of three or four distinct morphotypes (Mocho *et al.*, 2016, 2018; Vidal *et al.*, 2017). The assessment of morphological features with taxonomic relevance have been proved problematics with the current sample of vertebral specimens and the high morphological variation between the characters (Mocho *et al.*, 2018). Use of discrete morphological characters on the appendicular skeleton of the titanosaurs of Lo Hueco is also difficult as titanosaur appendicular bones lack enough autapomorphies or combination of features that permit us a precise taxonomical assessment (e.g., Wilson & Upchurch, 2003; Wilson, Barrett, & Carrano, 2011; Díez Díaz, Pereda Suberbiola, & Company, 2015). And also the material is fragmentary and few specimens present partial articulation, which add a difficulty to differentiate between interspecific and intraspecific morphological variation in discrete characters (see again Mocho *et al.*, 2018).

The analysis of Campanian-Maastrichtian titanosaur material of the Ibero-Armorican domain has yielded a sauropod faunal assemblage with several described species: *Ampelosaurus atacis* (Le Loeuff, 1995), *Atsinganosaurus velauciensis* (Garcia *et al.*, 2010), *Lirainosaurus astibiae* (Sanz *et al.*, 1999), the mentioned taxa *Lohuecotitan pandafilandi* (Díez Díaz *et al.*, 2016); and several undescribed titanosaur morphotypes that are proposed as probable different species based on morphological dissimilarities in the appendicular skeleton (i.e., Vila, Sellés, & Brusatte, 2016). This sauropod assemblage is also related with a faunal turnover affecting most of the herbivorous dinosaurs of the Ibero-Armorican domain (e.g., Vila *et al.*, 2016; Fondevilla *et al.*,

2019). Assessment of morphological features variable within the titanosaur hindlimb skeleton can be helpful for understanding the sauropod taxonomy during this Late Cretaceous event.

There are some possible appendicular morphotypes in Lo Hueco sample with differences related with the three dimensional position and shape of the morphological features in the distinct elements types. With the use of the geometric morphometrics toolkit we will address different grouping hypotheses in order to test the presence of two or more titanosaur morphs in Lo Hueco sample. To provide a statistical discriminant framework will be helpful for taxonomical assessment in complex bonebed associations.

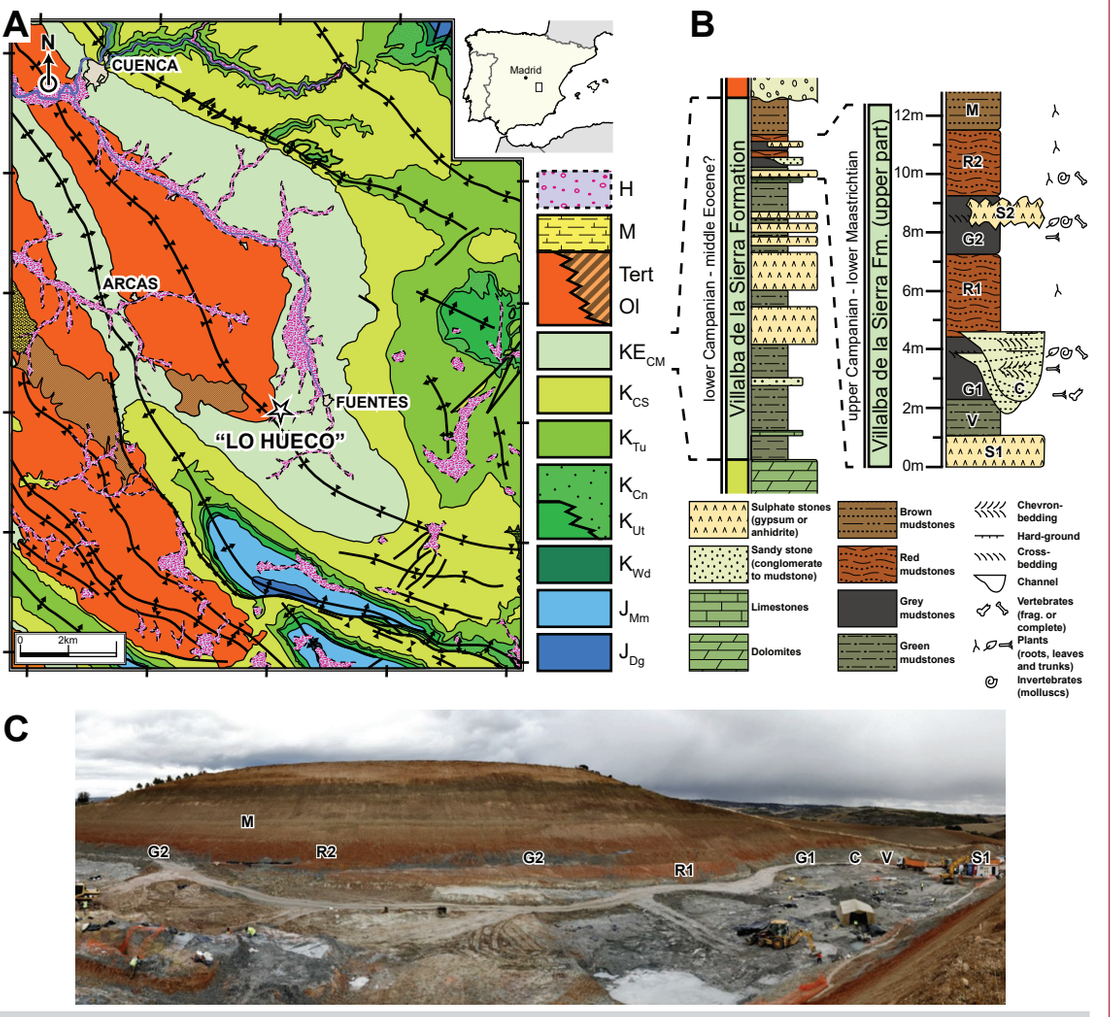

Fig.IV.II.1. Lo Hueco fossil site location and stratigraphy. (A) Geological map of Cuenca (Spain). (B) General stratigraphic column of the Villalba de la Sierra Formation and the Lo Hueco fossil site. (C) Photography of the Lo Hueco site during the 2007 campaign. Labels indicates the levels of the stratigraphic column.

Anatomical abbreviations:

4th – fourth trochanter; aap – anterior ascending process of distal condyles; ac – anerolateral crest (distal); alp – anterolateral crest (proximal); ap – anterior process; at – accessory trochanter; cc – cnemial crest; dac – distal anterior concavity; epi – lateral epicondyle; gt – greater trochanter; if – intercondylar fossa; lb – lateral bulge; lic – linea intermuscularis cranialis; lt – lateral trochanter; fc – fibular condyle; fh – femoral head; fia – fibular articulation; pc – posterior condyle; pvp – posterior ventral process; ri – ridge; s – sulcus; tc – tibial condyle; ts – trochanteric shelf; tbs – tibial articulation scar; tr - trochanter

Institutional abbreviations:

CPP – Centro de Pesquisas Paleontológicas Lewellyn Price, Peirópolis, Brasil. CRILAR – Centro Regional de Investigaciones Científicas y Transferencia Tecnológica de La Rioja, Anillaco, Argentina. DINO – Dinosaur National Monument, Utah, USA. FMNH – Field Museum of Natural History, Chicago, USA. IANIGLA – Instituto Argentino de Nivología, Glaciología y Ciencias Ambientales, Colección de Paleovertebrados, Mendoza, Argentina. MACN – Museo Argentino de Ciencias Naturales "Bernardino Rivadavia", Buenos Aires, Argentina. MAU/MRS – Museo Municipal Argentino Urquiza, Rincón de los Sauces, Argentina. MB.R – Collection of Fossil reptiles in the Museum für Naturkunde, Berlin, Germany. MCD – Museu de la Conce Dellà, Lleida, Spain. MCF – Museo "Carmen Funes", Neuquén, Argentina. MCS – Museo Municipal de Cinco Saltos, Cinco Saltos, Argentina. MDE – Musée des Dinosaures, Espéraza, France. MHN – Museum d'Histoire Naturelle, Aix-en-Provence, France. MNHN – Museum National d'Histoire Naturelle, Paris, France. MMS-CVN – Musée Moulin Seigneurial/Velaux-La Bastide Neuve, Bouches-du-Rhône, France. NHM – Natural History Museum, London, UK. MCNA – Museo de Ciencias Naturales de Álava / Arabako Natur Zientzien Museoa, Vitoria-Gasteiz, Spain. MLP – Museo de La Plata, La Plata, Argentina. MPCA – Museo Provincial "Carlos Ameghino", Cipolletti, Argentina. MPD – Institute of Paleontology and Geology, Ulaan Baatar, Mongolia. MUCPv – Museo de la Universidad Nacional del Comahue, Paleontología de Vertebrados, Neuquén. MUPA – Museo de Paleontología de Castilla-La Mancha, Cuenca, Spain. MUVHN – Museu de la Universitat de València d'Història Natural, Valencia, Spain. PVL – Colección de Vertebrados Fósiles – Fundación Miguel Lillo, Tucumán, Argentina. UNPSJB-PV – Universidad Nacional de la Patagonia "San Juan Bosco" – Paleovertebrados, Comodoro Rivadavia, Argentina.

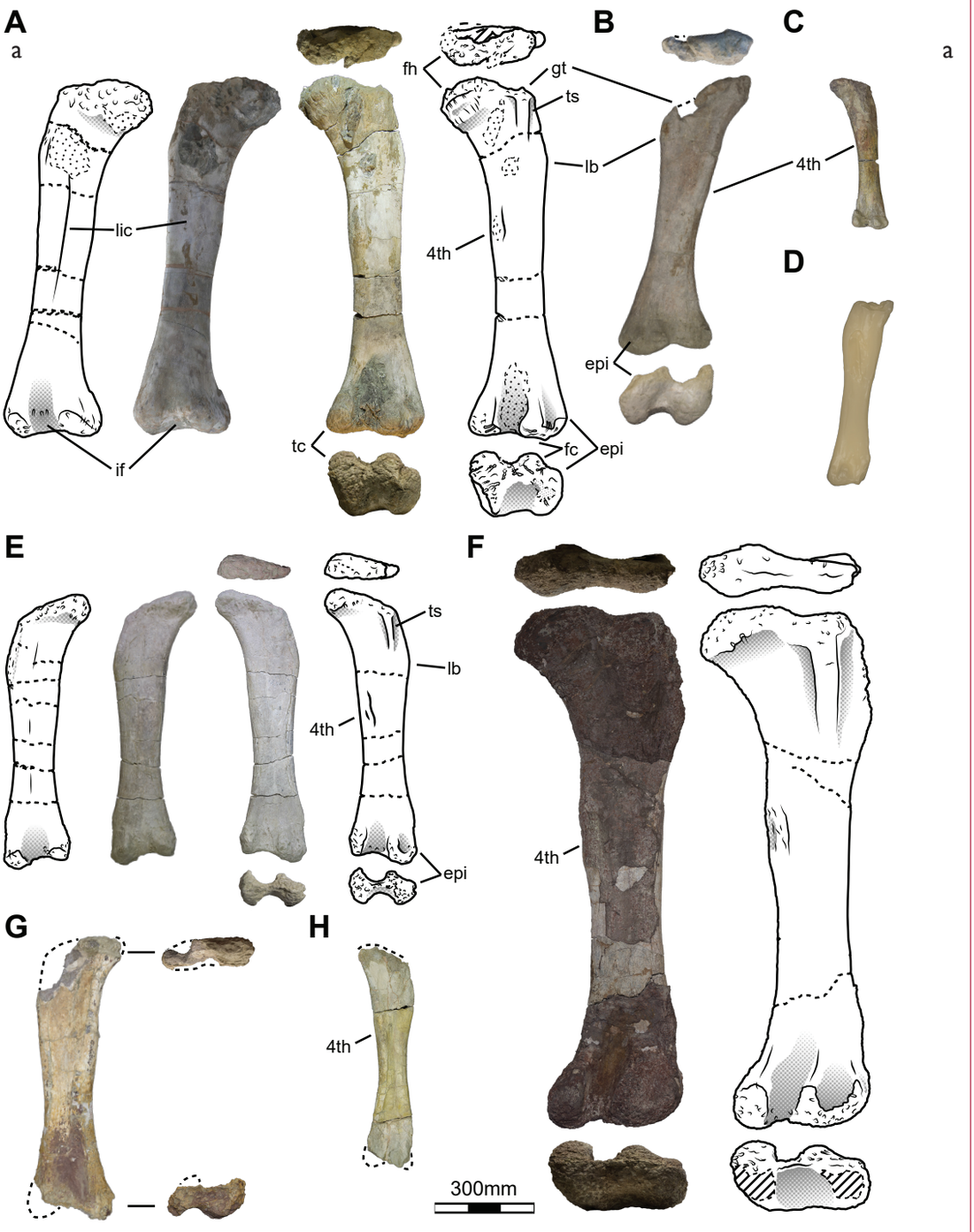

Fig.IV.II.2. Femoral sample of Lo Hueco titanosaurs. (A) HUE-3108 in anterior, dorsal, posterior and ventral face. (B) HUE-2338 in posterior face. (C) HUE-2636 posterior face. (D) HUE-8801 mesh posterior face. (E) HUE-1319 in anterior, dorsal, posterior and ventral face. (F) HUE-594 in proximal, posterior and distal face. (G) HUE-3583 posterior face. (H) HUE-10007 posterior face.

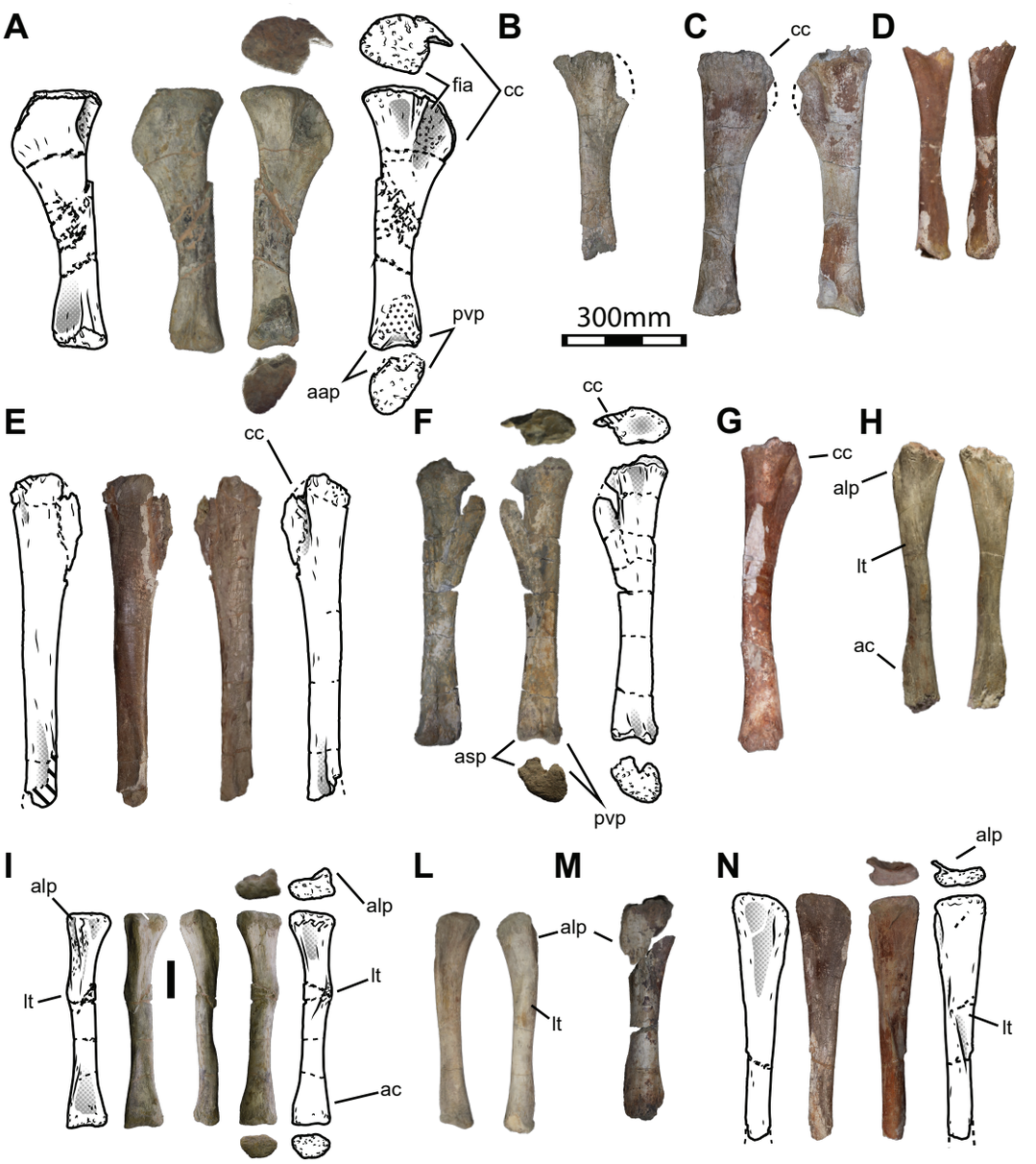

Fig.IV.II.3. Tibiae and fibulae sample of Lo Hueco titanosaurs. Tibiae: (A) HUE-3082. in medial, proximal, lateral and distal face. (B) HUE-4632 in lateral face. (C) HUE-1573 in medial and lateral face. (D) HUE-1612 in medial and lateral face. (E) HUE-1149 in medial, proximal, lateral and distal face. (F) HUE-2117 in lateral face. Fibulae: (G) HUE-3087 in medial, anterior, proximal, lateral and distal face. (H) HUE-1570 in medial and lateral face. (I) HUE-1335 in medial and lateral face. (K) HUE-1612 in medial, proximal and lateral face. (L) HUE-2806 in medial and lateral face. (M) HUE-1146 in lateral face.

IV.II.2 MATERIAL AND METHODS

Previous morphological and morphometric studies on the titanosaurs from Lo Hueco addressed the need of incorporate features like the anteroposterior development or relative torsion of several structures of the elements (Páramo, Ortega, & Sanz, 2015b; Páramo *et al.*, 2016). Also, current research on traditional morphometrics of these titanosaurs appendicular elements highlights advantages of including variables capturing the morphological variation along the anteroposterior development of the long bones (Chapter IV.I). Some authors have proposed that 2D is a bad proxy for 3D structures in studies of intraspecific variation (Hedrick *et al.*, 2019). This problematic is partially addressed with inclusions of features that captures information on the third dimension like the use of midshaft cortical area (Bonnan, 2007). However, this solution is not enough to capture some of the variation found in the titanosaur appendicular elements from Lo Hueco. Some of this variation is related to the anterolateral torsion of some features of the appendicular elements, e.g. the lateral bulge of the femur or the cnemial crest of the tibia. While these features might be included with a combination of measurements on the lateromedial and anteroposterior width, the relative position of each part of the structure is not easily summarized in 2D, and these features may not be properly reflected in 2D analyses.

For these reasons and considering the available sample of appendicular specimens from Lo Hueco (more than a ten of specimens in this study; see Fig.IV.II.2 and 3), 3D geometric morphometrics represent an adequate tool to assess the intraspecific variation in the hindlimb morphotypes of titanosaurs.

The base of current study is the set of femoral landmarks proposed by Bonnan (2004) which are defined in a 2D space and cover major anatomical structures of the femur. We expanded his proposal with more structures in 3D, capturing the morphology of the anterior face of the femur, as well as the anteroposterior and lateromedial morphology of proximal and distal ends. We set the landmarks in main key morphological features that will be considered as type I (and some type II) landmarks following the basic principles in the definition of landmarks (Bookstein, 1991; see also Zelditch *et al.*, 2012a; Zelditch, Swiderski, & Sheets, 2012b). Also, for purpose of visualization of morphological changes along curved features, like the morphology of cnemial crest, proximal and distal end of the femur, tibia and fibula, etc., curve and surface semilandmarks methods are herein used (see in Gunz, Mitteroecker, & Bookstein, 2005; Gunz & Mitteroecker, 2013; Botton-Divet *et al.*, 2015).

Sliding semilandmarks is a powerful tool for analysing the variation in morphology along curves (Bookstein, 1996a, 1997; Gunz *et al.*, 2005; Sheets *et al.*, 2006; Gunz & Mitteroecker, 2013). It has been already employed in many studies of 3D geometric morphometrics in non-avian dinosaurs (Bonnan *et al.*, 2013; Ullmann *et al.*, 2017) and it is widely used on the study of shape in birds (e.g., Bright *et al.*, 2016; Navalón *et al.*, 2018; Felice, Randau, & Goswami, 2018). Sliding semilandmarks may be used for study curved structures like, among others, the femoral head, the relative position between this structure and the greater trochanter, the lateral bulge, the lateromedial contour of the distal condyles, the cnemial crest in the tibia, or the lateral trochanter of the fibula (see Table. IV.II.4, IV.II.5 and IV.II.6). In this study a suite of landmarks, sliding semilandmarks and surfaces related to main anatomy of the femur, tibia and fibula are proposed.

Specimen	Type	Side	Assoc.	Strat.	Morphotype	Taxa	R.I.	Ecc. (%)
HUE-1183	Femur	Left	HUE-EC13	GI	Morphotype I	T.i.	0.18	297.34
HUE-1366	Femur	Right	HUE-EC5	GI	Morphotype I	T.i.	0.21	203.31
HUE-1508	Femur	Left	iso	GI	Morphotype I	T.i.	0.23	354.40
HUE-1521	Femur	Left	iso	GI	Morphotype I	T.i.	0.20	259.19
HUE-2338	Femur	Left	iso	GI	Morphotype I	T.i.	0.21	208.62
HUE-2420	Femur	Right	HUE-EC6	GI	Morphotype I	T.i.	0.21	194.13
HUE-2636	Femur	Right	iso	GI	Morphotype I	T.i.	0.20	128.89
HUE-2903	Femur	Right	iso	GI	Morphotype I	T.i.	0.19	276.75
HUE-3108	Femur	Right	HUE-EC1	GI	Morphotype I	*L. pandafilandi*	0.22	250.00
HUE-8801	Femur	Left	iso	NA	Morphotype I	T.i.	0.17	180.70
					Morphotype I	**Average**	**0.20**	**226.94**
HUE-594	Femur	Right	iso	GI	Morphotype II	T.i.	0.20	182.61
HUE-930	Femur	Right	HUE-EC11	GI	Morphotype II	T.i.	NA	307.05
HUE-1187	Femur	Left	iso	GI	Morphotype II	T.i.	0.25	327.89
HUE-1316	Femur	Right	iso	GI	Morphotype II	T.i.	0.25	283.90
HUE-1319	Femur	Right	iso	GI	Morphotype II	T.i.	0.21	255.10
HUE-1357	Femur	Left	iso	GI	Morphotype II	T.i.	0.22	207.58
HUE-1590	Femur	Right	iso	GI	Morphotype II	T.i.	0.20	486.56
HUE-3237	Femur	Right	iso	GI	Morphotype II	T.i.	0.22	254.46
HUE-3583	Femur	Left	iso	GII	Morphotype II	T.i.	0.22	230.77
HUE-10007	Femur	Right	iso	NA	Morphotype II	T.i.	NA	300.00
					Morphotype II	**Average**	**0.22**	**273.82**

Table.IV.II.1. Sample of femora for current study. *Assoc.* - assocaited specimen. *Strat.* - stratigraphic level provenance. *iso.* - isolated. *T.i.* - Titanosauria indet. *R.I.* - Robustness Index (Wilson & Upchurch, 2003). *Ecc.* - Eccencitricty Index (Wilson & Carrano, 1999).

While forelimb specimens have been found mainly isolated in Lo Hueco fossil site, we have several hindlimb partially articulated (Páramo, Ortega, & Sanz, 2018). We restricted the analysis to a sample of femora, tibiae and fibulae of the titanosaurs from Lo Hueco. At least two types of femora, tibiae and fibulae have been recognized in preliminary analyses of morphological features (Páramo *et al.*, 2016), and the presence of two main morphs is the hypothesis tested in this study.

The material referred to each morphotype and analysed in present study can be accessed in Table.IV.II.1, IV.II.2 and IV.II.3.

Specimen	Type	Side	Assoc.	Strat.	Morphotype	Taxa	R.I.	Ecc. (%)
HUE-1165	Tibia	Left	iso	GI	Morphotype I	T.i.	0.18	70.00
HUE-1410	Tibia	Right	iso	GI	Morphotype I	T.i.	-	62.50
HUE-1573	Tibia	Left	iso	GI	Morphotype I	T.i.	0.15	149.18
HUE-2425	Tibia	Right	HUE-EC6	GI	Morphotype I	T.i.	0.13	177.05
HUE-2669	Tibia	Left	iso	GI	Morphotype I	T.i.	NA	52.08
HUE-2799	Tibia	Right	HUE-EC3	GI	Morphotype I	T.i.	-	173.47
HUE-3082	Tibia	Right	HUE-EC1	GI	Morphotype I	*L. pandafilandi*	0.15	155.00
HUE-4344	Tibia	Left	iso	GII	Morphotype I	T.i.	0.18	162.96
HUE-4404	Tibia	Left	iso	GII	Morphotype I	T.i.	0.16	58.42
HUE-4632	Tibia	Right	iso	GII	Morphotype I	T.i.	NA	75.32
					Morphotype I	**Average**	**0.16**	**101.50**
HUE-1149	Tibia	Left	iso	GI	Morphotype II	T.i.	0.12	148.00
HUE-1317	Tibia	Right	iso	GI	Morphotype II	T.i.	-	65.93
HUE-1500	Tibia	Right	iso	GI	Morphotype II	T.i.	0.12	175.71
HUE-1612a	Tibia	Left	HUE-1612	GI	Morphotype II	T.i.	0.10	115.87
HUE-2117	Tibia	Right	iso	GI	Morphotype II	T.i.	0.13	75.95
HUE-4055	Tibia	Right	iso	GI	Morphotype II	T.i.	0.11	53.25
					Morphotype II	**Average**	**0.13**	**89.24**

Table.IV.II.2. Sample of tibiae for current study. *Assoc.* - assocaited specimen. *Strat.* - stratigraphic level provenance. *iso.* - isolated. *T.i.* - Titanosauria indet. *R.I.* - Robustness Index (Wilson & Upchurch, 2003). *Ecc.* - Eccencitricty Index (Wilson & Carrano, 1999).

IV.II.2.1. GEOMETRIC MORPHOMETRICS

We explored the morphological variability of the titanosaurian hindlimb bones from Lo Hueco using a geometric morphometrics toolkit (GM: Bookstein, 1991; Zelditch *et al.*, 2012a). This set of methods allows to explore and quantify shape in absence of size variation. Landmark types follows Bookstein (1991, 1997), landmark proposal for the femur is based on Bonnan (2004) and Wilhite (2005), and it has been defined several news landmarks on the femur, tibia and fibula. These landmarks are based on main anatomical features like scars for principal muscle attachments: e.g., the femoral fourth trochanter or the anteriormost point of the cnemial crest of the tibia, (Otero & Vizcaíno, 2008; Gallina, 2011) among others. Anatomical features in sauropod long bones related with proximal distal or curved structures are described by a combination of surface curvature and rugosity on the epiphyses (Britt & Naylor, 1994; Carpenter & McIntosh, 1994; Schwarz, Wings, & Meyer, 2007; Holliday *et al.*, 2010). However, sometimes these structures does not present a clear anatomical correlate (see examples in Remes, 2007; Otero & Vizcaíno, 2008; Gallina, 2011; Otero, 2018). The lack of rugosity at the edge of the epiphyses may be related with ontogenetical development or taphonomical preservation and it should be discussed elsewhere. Related to landmark definition, this lack of osteological feature leaves the position on several of these structures as dubious (e.g. the anterior projection of the distal tibial and fibula condyles of HUE-2636). Therefore, those landmarks are considered as Type-II. Other structures like the bottom end of lateral bulge of the femur has no clear border with lateral margin of the shaft. They should be considered Type-III, as they are geometrically homologous, though, with difficult anatomical correlation assessment.

Specimen	Type	Side	Assoc.	Strat.	Morphotype	Taxa	R.I.	Ecc. (%)
HUE-1068	Fibula	Right	iso	GI	Morphotype I	T.i.	0.19	120.00
HUE-1175	Fibula	Right	iso	GI	Morphotype I	T.i.	0.15	186.21
HUE-1335	Fibula	Left	iso	GI	Morphotype I	T.i.	0.20	120.00
HUE-1377	Fibula	Right	iso	GI	Morphotype I	T.i.	0.17	136.84
HUE-1476	Fibula	Left	iso	GI	Morphotype I	T.i.	0.20	125.81
HUE-1513	Fibula	Left	iso	GI	Morphotype I	T.i.	-	108.82
HUE-1520	Fibula	Right	iso	GI	Morphotype I	T.i.	0.15	113.33
HUE-1570	Fibula	Right	iso	GI	Morphotype I	T.i.	0.17	183.87
HUE-2426	Fibula	Right	HUE-EC6	GI	Morphotype I	T.i.	0.17	122.92
HUE-3000	Fibula	Left	iso	GI	Morphotype I	T.i.	0.16	114.55
HUE-3075	Fibula	Left	HUE-EC1	GI	Morphotype I	*L. pandafilandi*	0.18	87.27
HUE-3087	Fibula	Right	HUE-EC1	GI	Morphotype I	*L. pandafilandi*	0.20	83.33
HUE-4359	Fibula	Left	iso	GII	Morphotype I	T.i.	0.11	94.23
HUE-7802	Fibula	Right	iso	NA	Morphotype I	T.i.	-	110.53
					Morphotype I	**Average**	**0.17**	**111.77**
HUE-1082	Fibula	Right	iso	GI	Morphotype II	T.i.	0.17	132.50
HUE-1146	Fibula	Left	iso	GI	Morphotype II	T.i.	0.18	126.67
HUE-1507	Fibula	Left	iso	GI	Morphotype II	T.i.	-	113.79
HUE-1612b	Fibula	Left	HUE-1612	GI	Morphotype II	T.i.	-	142.50
HUE-2669	Fibula	Right	iso	GI	Morphotype II	T.i.	0.11	122.58
HUE-2804	Fibula	Right	iso	GI	Morphotype II	T.i.	-	135.85
HUE-2806	Fibula	Left	iso	GI	Morphotype II	T.i.	0.17	111.67
HUE-2977	Fibula	Right	HUE-EC4	GI	Morphotype II	T.i.	0.23	167.31
HUE-4416	Fibula	Right	iso	GII	Morphotype II	T.i.	0.19	168.42
HUE-5232	Fibula	Left	iso	GII	Morphotype II	T.i.	0.15	165.22
					Morphotype II	**Average**	**0.17**	**137.16**

Table.IV.II.3. Sample of fibulae for current study. *Assoc.* - associated specimen. *Strat.* - stratigraphic level provenance. *iso.* - isolated. *T.i.* - Titanosauria indet. *R.I.* - Robustness Index (Wilson & Upchurch, 2003). *Ecc.* - Eccencitricty Index (Wilson & Carrano, 1999).

For landmark placement, a 3D model for each specimen were acquired mainly by photogrammetry methods (following Falkingham, 2012; Mallison & Wings, 2014; Falkingham *et al.*, 2018). Photographs were taken with a Canon 1100D camera and Canon 18-55mm f3.5-5.6 IS-II lens at 35mm focal length which has a distortion of almost 0 points. Several other elements were digitized using a Canon 50mm f1.8 which distortion is null by default. Reduction of lens deformation pattern has been addressed as they can affect the results (observed in 2D GM studies: Mullin & Taylor, 2002; Třebický *et al.*, 2016; Collins & Gazley, 2017). Undistorted photographs were also processed from RAW data using the standard algorithm and calibration setup (e.g. Challis & Kerwin, 1992; Stein, 1997) customize for each objective as provided in Photoshop Camera Raw v10.4. The photogrammetry reconstruction precision is important and the model accuracy (Error measurement in mm) obtained from the software is provided in the Supplementary Material.IV.II.A. Several elements from an early sampling were reconstructed using a Microsoft® KinectTM for Xbox360TM RGB-D camera (following methodology of Falkingham, 2013; Das *et al.*, 2017). Reconstruction precision is also provided

(Supplementary Material.IV.II.A). All elements were decimated to meshes of 150.000 polygons each, post processed in Autodesk® Meshmixer™ v3.4.35 and Blender® v2.79 3D modelling software (Blender Online Community, 2018). 3D digitized models were exported as .obj files.

The landmark input was made using the methodology proposed by Souter *et al.* (2010) and a simplified sculpt of a femur, tibia and fibula are used as Template meshes for landmark placement, sliding and representation of results. The landmarks and semilandmarks were collected using the IDAV LandmarkTM editor v3.0.7 (Wiley *et al.*, 2005: www.idav.ucdavis.edu/research/EvoMorph). Curve and surface semilandmarks were defined by landmarks as boundaries following Gunz (2005), except for the lateral trochanter of the fibula, which has no clear boundary in posterodistal end and is treated as an open curve.

The fragmentary nature of many of the fossil elements recovered in Lo Hueco (see Cambra-Moo *et al.*, 2012; Ortega *et al.*, 2015) difficults the placement of all the landmarks in every specimen. Usually the ends of the long bone are partially or completely lost by fracturing. In addition, the gypsum crystal growth may produce loss of bone (Cambra-Moo *et al.*, 2012). Also, the gypsum crystal extruding on the surface of the bone can obstruct semilandmark placement and the sliding process. We are studying morphological changes, so it is not possible to introduce further error in the sample by manual digital restoration via 3D sculpting tools for those fragmentary zones, distorted areas or gypsum growths like in other studies (e.g., Molnar, Pierce, & Hutchinson, 2012; Lautenschlager, 2013, 2017; Cunningham *et al.*, 2014; Vidal & Díez Díaz, 2017). Consequently, several pre-processing options were taken before analysis:

- In order to produce a correct sliding surface several gypsum crystal were erased digitally for the specimens where the surface could be reconstructed easily without producing significant deformation. In cases where gypsum removal was in particularly complex areas, the hole was left in the mesh instead, and reconstructed with the same tool used to analyse morphological extremes and semilandmark curves; the Thin Plate Spine (TPS: Bookstein, 1989; see below).

- The fragmentary specimens where several fragments cannot be digitized in connection and in anatomical position, they were joined with 3D modelling software. This include reuniting fragments with simple fractures (e.g. distal end of the femur HUE-2420).

Further virtual restoration was carried out within a Statistical Shape Modelling framework (see Gunz *et al.*, 2009; Souter *et al.*, 2010; Molnar *et al.*, 2012; Lautenschlager, 2016a; Wang, Munsell, & Richardson, 2017; Schlager *et al.*, 2018). It is not uncommon in geometric morphometrics to use the reconstruction of lost elements prior landmark placement (i.e., Strauss & Bookstein, 1982; Gunz *et al.*, 2005, 2009; Motani, Amenta, & Wiley, 2008; Molnar *et al.*, 2012; Foth & Rauhut, 2013; Arbour & Brown, 2014; Lautenschlager, 2016a). However, in this study it was preferred not to use any method that might incorporate artefacts due to manual manipulation in modelling software. The reconstruction of incomplete specimens is made by multivariate imputation methods (Schafer, 1997; Arbour & Brown, 2014) and the use of TPS (Bookstein, 1996b; Little & Mardia, 1996; Gunz *et al.*, 2005). This method has been used in the reconstruction of the elements of the hind limb of HUE-EC6: the fibular condyle of the femur (HUE-2420), the areas covered by sediment of the lateral face of the tibia (HUE-2425) and the medial face of the fibula (HUE-2426). The tibia and fibula of HUE- EC6 are complete but divided in two fragments embedded in sediment. The sediment was removed from the model, the fragments joined and the simple holes

filled with NURBs curves following Molnar *et al.* (2012). The use of NURBs curves was limited in the areas lacking digitized information in order to avoid speculative manual virtual restorations. Instead, the landmarks and semilandmarks were estimated with multiple imputation methods and surfaces reconstructed with TPS warping of the Template mesh to this new set of coordinates.

The defined landmarks and semilandmarks where imported and analysed in R v3.4.4 statistical software (The R Core Team, 2016) with RStudio gui (RStudio Team, 2015). Data import, Procrustes superimposition and sliding of semilandmarks were carried with the "Morpho" package (Schlager, 2017) and also using some functions of the package "geomorph" (Adams & Otárola-Castillo, 2013; Adams *et al.*, 2017). The complete set of landmarks can be accessed in Fig.IV.II.4

Some authors suggest reducing the landmark set in order to palliate as much as possible incomplete information (see Hammer & Harper, 2008; Gunz *et al.*, 2009; Zelditch *et al.*, 2012a; Brown *et al.*, 2012). We tested possible advantages of this approach using two separate landmark sets for each bone type. One set is downsampled to landmarks with at least 75% complete data (Table. IV.II.5, 6 and 7). The other set is the entire landmark set and the missing data are estimated with use of TPS (Gunz *et al.*, 2005, 2009) as commented before. The incompleteness of the long bones also difficult the projection of the semilandmark from the Template configuration and sliding over the actual mesh of the specimen like in the workflow of Souter *et al.* (2010) derived from Gunz *et al.* (2005). We slided the semilandmarks via TPS minimizing the Bending Energy (see Green, 1996; Bookstein, 1997) with no specimen mesh using the sliding function in "Morpho" (Schlager, 2017).

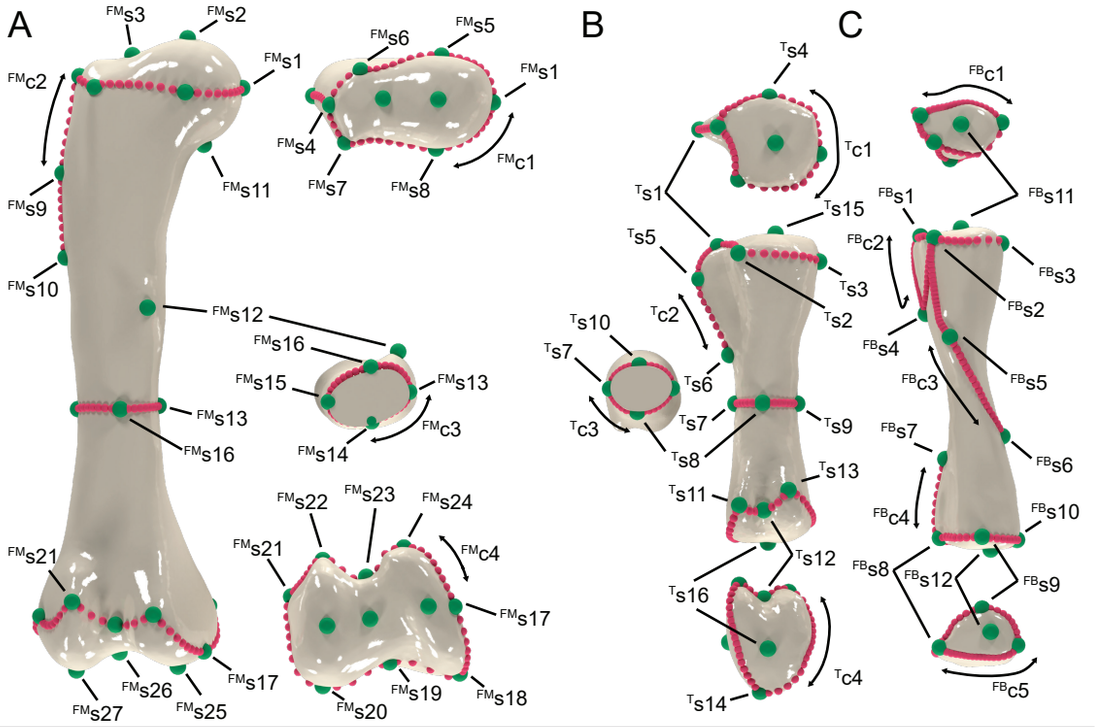

Fig.IV.4. Landmark definitions in the current sample. (A) Selection of some of the sampled photographs. (B) Estimation of the position of all the photographs, reconstruction of the surface mesh.

		Definition	Missing %
Ladnmarks	s1	Medial point Femoral Head	26.32%
	s2	Roof of Femoral Head	36.84%
	s3	Lateral border of Femoral Head	57.89%
	s4	Proximolateral border of the Greater Trochanter	15.79%
	s5	Anterior Femoral Head	31.58%
	s6	Anterior Greater Trochanter	52.63%
	s7	Greater Trochanter top Trochanteric Shelf	57.89%
	s8	Posterior Femoral Head	36.84%
	s9	Lateral bulge	0.00%
	s10	Distal end lateral bulge	0.00%
	s11	Deflection femoral head	0.00%
	s12	Fourth trochanter	0.00%
	s13	Minimum midshaft width medial	0.00%
	s14	Minimium midshaft width anterior	0.00%
	s15	Minimum midshaft width lateral	0.00%
	s16	Minimum midshaft width posterior	0.00%
	s17	Tibial condyle medial margin	31.58%
	s18	Tibial condyle anteroproximal	47.37%
	s19	Anterior intercondylar fossa	31.58%
	s20	Fibular condyle anteroproximal	52.63%
	s21	Lateral epicondyle	42.11%
	s22	Fibular condyle posteroproximal	36.84%
	s23	Posterior intercondylar fossa	15.79%
	s24	Tibial condyle posteroproximal	0.00%
	s25	Distalmost bottom of tibial condyle	42.11%
	s26	Intercondylar fossa	36.84%
	s27	Distalmost bottom of fibular condyle	52.63%
Curves	c1	Proximal end outline	63.16%
	c2	Lateral bulge	15.79%
	c3	Midshaft outline	0.00%
	c4	Distal articular condyles outline	57.89%

Table.IV.II.4. Femur landmark definitions.

The taphonomical deformation is another source of morphological variation between the sampled specimens. In order to assess biologically significant morphological variation, the effects of deformation induced by taphonomy should be controlled. Taphonomical deformation is not an exclusive problem from the Lo Hueco site but a common preservation problem in paleontological analyses (e.g. Tschopp & Dzemski, 2013; Taylor, 2015). Taphonomical processes produce unequal changes in shape among elements into a sample. While some tools for retrodeformation have been proposed, they relay on bilateral symmetry (e.g., Motani, Amenta, & Wiley, 2005; Wiley *et al.*, 2005; Tschopp & Dzemski, 2013; Tallman *et al.*, 2014; Lautenschlager, 2017). Sauropod long bones lack bilateral symmetry and deformation imposed as well as bone breaking along the shaft (see

		Definition	Missing %
Landmarks	s1	Top of cnemial crest	6.67%
	s2	Top of medial crest of the articular fossa	40.00%
	s3	Posterior tibial head	20.00%
	s4	Medial of tibial head	26.67%
	s5	Cnemial crest	6.67%
	s6	Distal end of cnemial crest	0.00%
	s7	Anterior midshaft	0.00%
	s8	Lateral midshaft	0.00%
	s9	Posterior midshaft	0.00%
	s10	Medial midshaft	0.00%
	s11	Anterior ascending process of distal	46.67%
	s12	Intercondylar sulcus	40.00%
	s13	Posterior ventral process of distal	40.00%
	s14	Distal condyle medial process	53.33%
	s15	Top proximal end	26.67%
	s16	Bottom distal end	33.33%
Curves	c1	Tibial proximal end outline	46.67%
	c2	Cnemial crest	46.67%
	c3	Midshaft outline	0.00%
	c4	Tibial distal end outline	73.33%

Table.IV.II.5. Tibia landmark definitions.

		Definition	Missing %
Landmarks	s1	Top anterior crest	13.64%
	s2	Top border anterior crest sulcus	4.55%
	s3	Posterior proximal end	27.27%
	s4	Bottom border anterior crest	0.00%
	s5	Lateral trochanter	0.00%
	s6	Bottom of the tibial scar	0.00%
	s7	Top of the anterolateral crest	0.00%
	s8	Anterior distal ending	36.36%
	s9	Lateral distal ending	36.36%
	s10	Posterior distal ending	45.45%
	s11	Top proximal end	36.36%
	s12	Bottom distal end	36.36%
Curves	c1	Proximal end outline	36.36%
	c2	Anterior fossa	18.18%
	c3	Lateral trochanter ridge	4.55%
	c4	Anterolateral crest	36.36%
	c5	Distal end outline	50.00%

Table.IV.II.6. Fibula landmark definitions.

Cambra-Moo *et al.*, 2012) is too complex for current GM retrodeformation efforts. Using bilateral symmetry of the body for recovering elemets is not possible as much of our sample comes from isolated specimens. Also there are sauropods that present high individual variation (see Poropat *et al.*, 2014). We addressed the effects of taphonomical deformation on the morphology of each specimen with the introduction of the concept of taphomorphospace (Hedrick & Dodson, 2013). This assumption allows us to explore the shape space considering that morphological variation is a combination of biological differences and taphonomy. The possible effects of this deformation will be also briefly addressed and discussed with the results of GM analyses, as well as their implications for the study of the hindlimb morphology of the titanosaurs of Lo Hueco (see Discussion).

The Principal Component Analyses are made with "FactoMineR" package (Lê, Josse, & Husson, 2008). Number of PCs retained are set to a maximum of 50 that describes 75% of sample variance. We also assessed the number of meaningful PCs obtained with the method proposed by Bookstein (2014: pp.324) implemented in the "Morpho" package (Schlager, 2017). This method is similar to those of the Anderson's Chi implemented by Bonnan (2007).

IV.II.2.2. MORPHOLOGICAL CLUSTER ANALYSIS

Our current clustering hypothesis proposes two main morphotypes based on cranial and preliminary analysis of appendicular material. Other grouping hypotheses tested are the presence of three (three possible morphotypes based on description of dorsal vertebrae) and four groups (based on description of caudal vertebrae). We explored grouping of the sampled specimen using cluster analysis and euclidean distances between GPA aligned landmark configuration. We assumed that there is a low variation between Procrustes and Euclidean distances (Kendall, 1984; Rohlf, 1998, 1999).

In order to test the presence of more than two distinct morphological groups for each element from the sample Lo Hueco titanosaurs, a k-means clustering analysis is applied to shape

	Femur		Tibia		Fibula	
	Complete dataset	Reduced dataset	Complete dataset	Reduced dataset	Complete dataset	Reduced dataset
Landmarks	s1, s2, s3, s4, s5, s6, s7, s8, s9, s10, s11, s12, s13, s15, s16, s17, s19, 20, s21, s22, s23, s24, s25, s26, s27	s1, s2, s4, s5, s8, s9, s10, s11, s12, s13, s14, s15, s16, s17, s18, s19, s21, s22, s23, s24, s25, s26	s1, s2, s3, s4, s5, s6, s7, s8, s9, s10, s11, s12, s13, s14, s15, s16	s1, s2, s3, s4, s5, s6, s7, s8, s9, s10	s1, s2, s3, s4, s5, s6, s7, s8, s9, s10, s11, s12	s1, s2, s3, s4, s5, s6, s7, s8, s9, s10, s11, s12
Curves	c1, c2, c3, c4	c2, c3	c1, c2, c3, c4	c1, c2, c3	c1, c2, c3, c4, c5	c1, c2, c3, c4, c5

Table.IV.II.7. Complete dataset and alternative reduced dataset list of landmarks.

variables. K-means is a type of unsupervised analysis that partition a sample of specimens into a predefined number of groups (Hastie, Tibshirani, & Friedman, 2000; Hammer & Harper, 2008). The k-means algorithm defines *k* partitions to which they assign iteratively the n specimens of the sample (Hubert & Levin, 1975; Hartigan & Wong, 1979; Hammer & Harper, 2008; Morissette & Chartier, 2013). The iteration continues reassessing the specimens to the closest centroid until a stable centroid position is achieved reducing the within-cluster variation sum of squares (Hubert & Levin, 1975; Hartigan & Wong, 1979; Hammer & Harper, 2008). We followed the "elbow criterion" to estimate the optimal number of groups achieved (Claude, 2008). This criterion is based on testing the improvement on within-group variance against the total variance with its iteration, that is suggested as a stability measurement (Pollard & van der Laan, 2002; Lange *et al.*, 2004; Claude, 2008; Charrad *et al.*, 2014; Kassambara, 2017). For testing the grouping hypothesis, this stability measurement was calculated for a solution with two possible groups (morphotypes) up to ten different groups, and for the set of Monte Carlo samples to 1000. This is achieved with a function implemented in the "factoextra" package (Kassambara & Mundt, 2017) which is also based in the "NbClust" package (Charrad *et al.*, 2014). We will discuss the taxonomical meaning of the suggested partitions.

IV.II.3. DESCRIPTION

IV.II.3.1. MORPHOTYPE I

Femora:

The femora are slender (Mean Robustness Index= .20 see Table.IV.II.5) with bulbous and rounded head. The diaphysis has a round cross-section, with low eccentricity (Table.IV.II.5). The femoral head is slightly dorsal to the greater trochanter with a step between them. Some elements present also a femoral head directed upward (e.g., HUE-2338). The lateral bulge develops one third of the proximodistal length of the femur. The proximal end of the lateral bulge presents a slight anterior deflection. In some elements such as HUE-2420, HUE-3108 and HUE-8801, this anterior deflection results in an anterior shallow concavity just below the greater trochanter. In the posterior surface there is a long and robust trochanteric shelf parallel to the lateral bulge. The fourth trochanter is present at one third of the femoral length level with the distal end of the lateral bulge. In some specimens, there is an accessory trochanter at the mid-line of the shaft, medially to the fourth trochanter (e.g., HUE-2338). The fourth trochanter is posteriorly prominent and proximodistally elongated even in the smaller elements. In some specimens the fourth trochanter is posteriorly located near the medial edge of the shaft (e.g., HUE-2338, HUE-3108). However, in most specimens, it is located in the posteromedial edge and projected perpendicular from the femoral shaft. Sometimes the fourth trochanter is visible in anterior view as it is the case for specimens HUE-2420, HUE-2903, HUE-3108 and HUE-8801 (see Fig.IV.II.2).

There is a marked linea intermuscularis cranialis (sensu Otero & Vizcaíno, 2008; Otero, 2010; see also in D'Emic, 2012) in the anterior face in most specimens. Some femora present a connection between tibial and fibular condyles to this ridge. The distal condyles are almost as anteroposteriorly expanded as lateromedially wide contrary to the more usual anteroposteriorly compressed titanosaurian distal condyles. The femoral distal condyles are thereof bulbous and

rounded, with a tibial condyle greater in anteroposterior than the fibular condyle and medially bevelled. The distal end presents a well-developed epicondyle in the lateral part of the fibular condyle. The distal articulation reaches almost the same height in anterior than in posterior face. The area between the condyles is rounded and continuous. Most of the specimens do not present any structure in the intercondylar fossa (differing from the Morphotype II, see below). However, some elements such as HUE-2903 present a weak and gently ventral ridge between the anterior and posterior intercondylar fossa in the anterodistal view (sensu Mannion *et al.*, 2019) and the distal popliteal surface in posterior face.

Tibiae:

The tibia is a robust element with an expanded head both anteroposteriorly and lateromedially. The proximal end has a subquadrangular articular outline. The proximal fibular articulation is greatly expanded in lateral face, and shows a robust ridge that extends parallel to the fossa of the cnemial crest (e.g., HUE-3082 and HUE-1573). However, in some elements (e.g. HUE-4344), the projection of the fibular articulation is abrupt in the tibial head without a marked ridge below. The cnemial crest is rounded, projected anterolaterally and it forms a deep fossa between the shaft and the crest. The cnemial crest reaches one third of the proximodistal length of the tibia. Some specimens (e.g., HUE-2425, HUE-2669 and HUE-4344), present a cnemial crest with a more rounded triangular morphology in lateral or medial face. The muscle scar of mid-distal cnemial crest is marked with a visible rugosity, forming a lateromedially wide ridge. The diaphysis is circular in cross-section, slightly anterospoteriorly wider. The distal condyles are prominent, lateromedially expanded with the anterior ascending process anterolateraly projected. The ascending process of the distal end is laterally more prominent and directed slightly upward. Some specimens present distal end directed to posterolateral instead (e.g., HUE-1573).

Fibulae:

The fibula is almost straight in lateromedial with few elements deflecting anteriorly with a gentle curvature of the shaft, but without developing a great sigmoid (e.g. HUE-1476 and HUE-3075). In the specimens where the fibula and tibia are associated, the fibula is slightly shorter than the tibia. The proximal end of the fibula has a rectangular outline. It is wider anteroposteriorly than lateromedially. Also in proximal view, the anterior flange forms a quadrangular border surrounding a small surface between the anterior edge of the lateral trochanter and the medial border of the anerolateral crest. The anerolateral crest is deflected medially and dorsally contributes to form the medial part of the quadrangular margin of the fibular head. The anerolateral crest is developed up to one third of the shaft proximodistal length, as the same level with the lateral trochanter. It is anteroposteriorly narrow but forms a marked step in medial, forming an L shape in proximal view (see also Díez Díaz *et al.*, 2016). Some elements (e.g., HUE-1520, HUE-1513 or HUE-1377; see Fig.IV.II.3) show an anteroposteriorly wide anterolateral crest. Some fibulae present a marked tibial insertion ridge in medial face, from a slightly convex area (e.g. HUE-3000) to a fully developed fibular knob (*sensu* Salgado & De Souza Carvalho, 2008) seen in the posterior part of the medial edge of the proximal end (e.g. HUE-3087) or in the medial face when the proximal end is not preserved (e.g. HUE-1476). The tibial ridge extends from mid- to distal point of the anterolateral crest proximodistal length to the posterior part of proximal edge.

The lateral trochanter is displaced anteriorly in most of the specimens referred to this

morphotype. The lateral trochanter shows a significant variation between elements. Most of the specimens present an anteriorly displaced trochanter with a single crest or an oval-shaped muscular attachment. In several specimens (e.g. HUE-1513, HUE-1377) the lateral trochanter comprises a main crest at midline of the trochanter, and a secondary one anteriorly located resulting in a bifurcated muscular attachment. In some fibulae (e.g. HUE-3082), the lateral trochanter are slightly more anteriorly directed than the other and present a single crest slightly anteriorly displaced.

IV.II.3.1. MORPHOTYPE I

Femora:

The femora are robust elements and have anteroposteriorly compressed shafts (see Table .IV.II.5). The femoral head is compressed anteroposteriorly. The area between the greater trochanter and femoral head extends smoothly without marked step (e.g. HUE-1319). However, some specimens present this step (e.g. HUE-594) though not as marked as in other sauropods and the femoral head is only slightly above the proximal height of the greater trochanter. The lateral bulge is short spanning about one fourth of the proximodistal length of the femur. It flexes to anterior in its lateralmost part, surrounding laterally a shallow concavity in the anterior face of the proximal end under the greater trochanter. The lateral bulge is narrow anteroposteriorly, except for its middle part, which present a marked muscular insertion, slightly wider than the rest of the bulge. Parallel and medially to the lateral bulge there is a straight trochanteric shelf. The trochanteric shelf is shallow (e.g. HUE-1316) compared to other titanosaur sauropods.

The shaft is greatly compressed anteroposteriorly (mean Eccentricity ~273%, see Table.IV.II.1). Usually the minimum lateromedial width is two times bigger than the minimum anteroposterior width for all the femora referred to this morphotype (e.g. HUE-594 and HUE-1319). Some degree of crushing is shown in many of the specimens, however, the anteroposterior width of the shaft is not greatly affected in the studied specimens (e.g. HUE-1187 and HUE-3583). The fourth trochanter is proximally placed respective to the midshaft, at the level of the lateral bulge distal end. The trochanter is placed in the postero-medial border and posteriorly projected. The fourth trochanter is not visible from anterior face for most of the specimens. The specimen HUE-1187 presents a fourth trochanter medially displaced but it only form a convex area visible from anterior face. The fourth trochanter is not visible itself (as it projects in the posterior face).

The distal end is anteroposteriorly compressed in the femora that preserve enough of distal end. The tibial condyle is a little wider anteroposteriorly than the fibular one. Both condyles are parallel and projected posteriorly perpendicular to the lateromedial plane. Some specimens like HUE-1366, HUE-1357 and HUE-10007 exhibit a shallow medial deflection of the condyles. All the elements present a step between the posterior intercondylar fossa and the anterior face of the distal end. There is also a strong posterolateral projection of the fibular epicondyle.

Tibiae:

The tibia is a rather slender element in contrast to the femur. The shaft is elongated and cylindrical in section with little anteroposterior development of both proximal and distal ends. The proximal end is almost quadrangular in proximal view with a similar development of the anteroposterior and posterolateral width. The anteroposterior width is also much similar to the lateromedial width across

all the head; it is not the common triangle-shaped tibial head. The posterior edge is posterolaterally expanded resulting in its lateral projection. It sometimes presents a second ridge parallel to the anterior proximal articulation with the fibula. In addition, in the specimens that preserve the complete proximal end it can be seen a shallow oval-shaped concavity in the middle of proximal face.

The cnemial crest is proximodistally long but narrow anteroposteriorly. Some elements (e.g. HUE-1149 and HUE-2117, see Fig.IV.3) present a wide muscle attachment in midpoint of cnemial crest, suggesting a strong development of the M. ambiens/femorotibialis. Sometimes the cnemial crest does not present a robust insertion in midpoint but instead present a triangle-shaped morphology (seen in lateral face) e.g. HUE-4055. The midshaft has low eccentricity being sometimes wider lateromedially than anteroposteriorly. The cross section of the tibia is slightly compressed lateromedially and tend to be slightly oval-shaped.

The distal end is almost as expanded anteroposteriorly than lateromedially. The anterior ascending process is deflected upwards like in most sauropods. The processes of the distal condyle are directed laterally and lateroposteriorly instead of projected anteriorly like in most sauropods (Sanz *et al.*, 1999). Some tibiae (e.g. HUE-1149 and HUE-1500) present a shallow concave surface on the anterior face of the anterior ascending process.

Fibula:

The fibula is anteroposteriorly wide, with a rather eccentric shaft lateromedially compressed (mean Eccentricity ~137%). The fibular proximal end is compressed lateromedially with the anterior process slightly bevelled medially forming a gently angle. This process is wide anteroposteriorly and proximodistally long up to one third of the shaft. Some elements like HUE-1082 and HUE-4416 also present a raised posterior part of the proximal end. Some elements present a little step between the lateral part of the shaft in the transition between the proximal end of the lateral trochanter and the aanterolateral crest like in HUE-1612 and HUE-2806 (see Fig.IV.II.3). The anterolateral crest is anteriorly directed instead medially as in the Morphotype I, which results in a continuous lateral face for the fibular proximal end, resembling a slightly compressed D-shaped head in cross-section.

In the medial surface, there is no tibial scar nor concavity in any of the elements. The lateral trochanter is well developed, anteroposteriorly wide and present a single crest projected in the middle of the lateral trochanter. Some specimens like HUE-1146 presents a bifurcated lateral trochanter, in form of two parallel crests. The shaft is straight in anterior view, with little medial flexion except for the distal end, especially in some elements like HUE-1570. However, some fibulae have a little anteroposterior displacement of the proximal and distal ends. There is much more contribution to the anterior projection of proximal end by the expansion of the anterolateral crest than to actual displacement or development of a curved shaft (e.g. HUE-1082 and HUE-1612). The described deflection of the distal and proximal ends never results in a well-defined sigmoid outline of the fibular shaft which characterizes the fibulae of some somphospondylans (Powell, 1992; Salgado & De Souza Carvalho, 2008; Royo-Torres, 2009).

The distal end is incomplete for the most part of the studied specimens, being preserved in HUE-1082, HUE-4416 and HUE-1570. The distal end is lateromedially compressed with a quadrangular morphology in distal view. Sometimes, the distal end is bevelled anteriorly especially in those specimen with sigmoidal shaft as HUE-1082.

	Femur				Tibia				Fibula			
	Complete		Reduced		Complete		Reduced		Complete		Reduced	
Shape PC	Chi-sq	p-value	Chi-sq	p-value	Chi-sq	p-value	Chi-sq	p-value	Chi-sq	p-value	Chi-sq	p-value
PC1	9.627	**0.002***	0.167	0.683	6.615	**0.01***	8.640	**0.003***	8.039	**0.005***	5.078	**0.024***
PC2	1.707	0.191	0.667	0.414	0.735	0.391	0.060	0.806	4.452	**0.035***	6.074	**0.014***
PC3	0.007	0.935	0.060	0.806	0.540	0.462	0.015	0.903	0.109	0.742	0.179	0.673
PC4	0.540	0.462	0.027	0.870	1.500	0.221	0.240	0.624	0.070	0.792	0.005	0.944
PC5	0.807	0.369	0.327	0.568	1.215	0.270	0.240	0.624	0.735	0.391	1.607	0.205
PC6	0.027	0.870	8.167	0.004	-	-	-	-	0.070	0.792	0.124	0.725
PC7	4.507	**0.034***	-	-	-	-	-	-	0.004	0.947	-	-

Table.IV.II.8. Kruskal-Wallis results on the PCA shape variables.

IV.II.4. RESULTS

The analyses over the complete set of landmarks and curve semilandmarks shows better results on Kruskal-Wallis for differentiation between the morphotypes in at least one PC (see Table.IV.II.8). Reduced dataset shows worse results in the analysis over the femora, with no significant differences between morphotypes in any PC. On the analysis over complete dataset we found significant differences between proposed morphotypes in PC1 and PC7 (see Table.IV.II.8). The analysis of the fibula present slightly worse results for the reduced dataset but significant differences in PC1 and PC2 for both analysis. The tibia reduced dataset is the only one that presents improvement when removing too much missing data. With the tibia reduced dataset (which includes only the proximal end), slightly better results are returned when assessing the significant differences in PC1 (see Table.IV.II.8). The complete sets, despite needing more landmark estimation, are more informative than the reduced dataset with the most complete sample but fewer landmarks and semilandmarks. A comparison between meaningful PCs in the complete set and the reduced sets for each element type is presented in Table.IV.II.9. We will focus our description and discussion of the morphospaces based on the three main PCs. Those PCs describe ~50% of variance in all bone types whether complete or reduced datasets. All the PCs recovered in the PCA of each bone type and dataset can be accessed in Supplementary Material.IV.II.B.

IV.II.4.1. FEMUR SHAPE TAPHOMORPHOSPACES

For the first principal component (PC1: 20.57% variance), the analysis of the complete set shows the difference between more robust elements (plotted with negative scores) and the slightly less robust elements (plotted at more positive scores). More negative values of PC1 are characterized by having femoral heads and distal condyles lateromedially expanded together with more eccentric shafts that are compressed anteroposteriorly, especially in the distal condyles (see Fig.IV.II.5.a). A more rounded femoral head and distal condyles characterize the more positive values of PC1. Positive scores also reflect femora with less eccentric shafts and more anteroposteriorly expanded distal condyles, showing a slight medial bevelling (see Fig.IV.II.5.b).

Femora analysis		Df	SS	MS	Rsq	F	Z	pval
Morphotype I vs Morphotype II		1	0.011	0.011	0.136	2.683	2.463	0.004*
	Residuals	17	0.068	0.004	0.864			
	Total	18	0.079					
k2 groups		1	0.016	0.016	0.207	4.429	3.593	0.001*
	Residuals	17	0.063	0.004	0.793			
	Total	18	0.079					
k3 groups		1	0.015	0.015	0.191	4.015	3.457	0.001*
	Residuals	17	0.064	0.004	0.809			
	Total	18	0.079					
k4 groups		1	0.013	0.013	0.164	3.345	3.015	0.001*
	Residuals	17	0.066	0.004	0.836			
	Total	18	0.079					
k5 groups		1	0.009	0.009	0.116	2.227	1.993	0.022*
	Residuals	17	0.070	0.004	0.884			
	Total	18	0.0793					

Table.IV.II.9. PERMANOVA results on the GPA aligned coordinates of the femora.

When compared with the subsampled dataset PC1 (25.01%), they show similar results in most areas. However, the lack of landmarks sampling like the complete contour of the femoral head and the fibular condyle, as well as those curves (curve #1 and #4 not sampled in reduced dataset, see Table.IV.II.7) difficult assessing clear differences between the two taphomorphospaces as reported variance represent more discrete differences in the sampled landmarks. The subsample dataset only captures the position and deepness of the intercondylar fossae, where there are major differences in the morphology of the femoral distal condyles. The position of the posterior dorsal margin of the tibial condyle is registered and it is different between the PC1 negative and positive values. However, its relative position respective to the fibular condyle and the morphology of the distal condyles in general cannot be shown with the reduced configuration (Fig.IV.II.5).

In addition, PC1 reflects differences between the height where the distal tip of the lateral bulge ends and the position of the midshaft least lateromedial width in the complete database, with more positive values representing a lateral bulge placed more proximally. The midshaft lateromedial minimum width outline is placed more distally on positive values of PC1. Negative values represent femora with lateral bulge slightly placed more distally and midshaft minimum width outline more proximally. The midshaft minimum width outline in more positive values represents more eccentric shafts, slightly more expanded. More negative values represent less eccentric, more anteroposteriorly expanded midshaft minimum width outlines. Also, more negative values present a bump on the anterior face in the midshaft minimum width, similar to the presence of linea intermuscularis cranialis. The reduced database reflects a more distal position for the lateral bulge and the fourth trochanter and a downward placement of the femoral head respective to the greater trochanter, and contrary to the complete dataset, in the negative values of PC1. Apart from the exaggerated differences between the position of the lateral bulge extension and distal tibial posterior condyle, taphomorphospaces reflect the same variance. The differences are less evident between the taphomorphospaces.

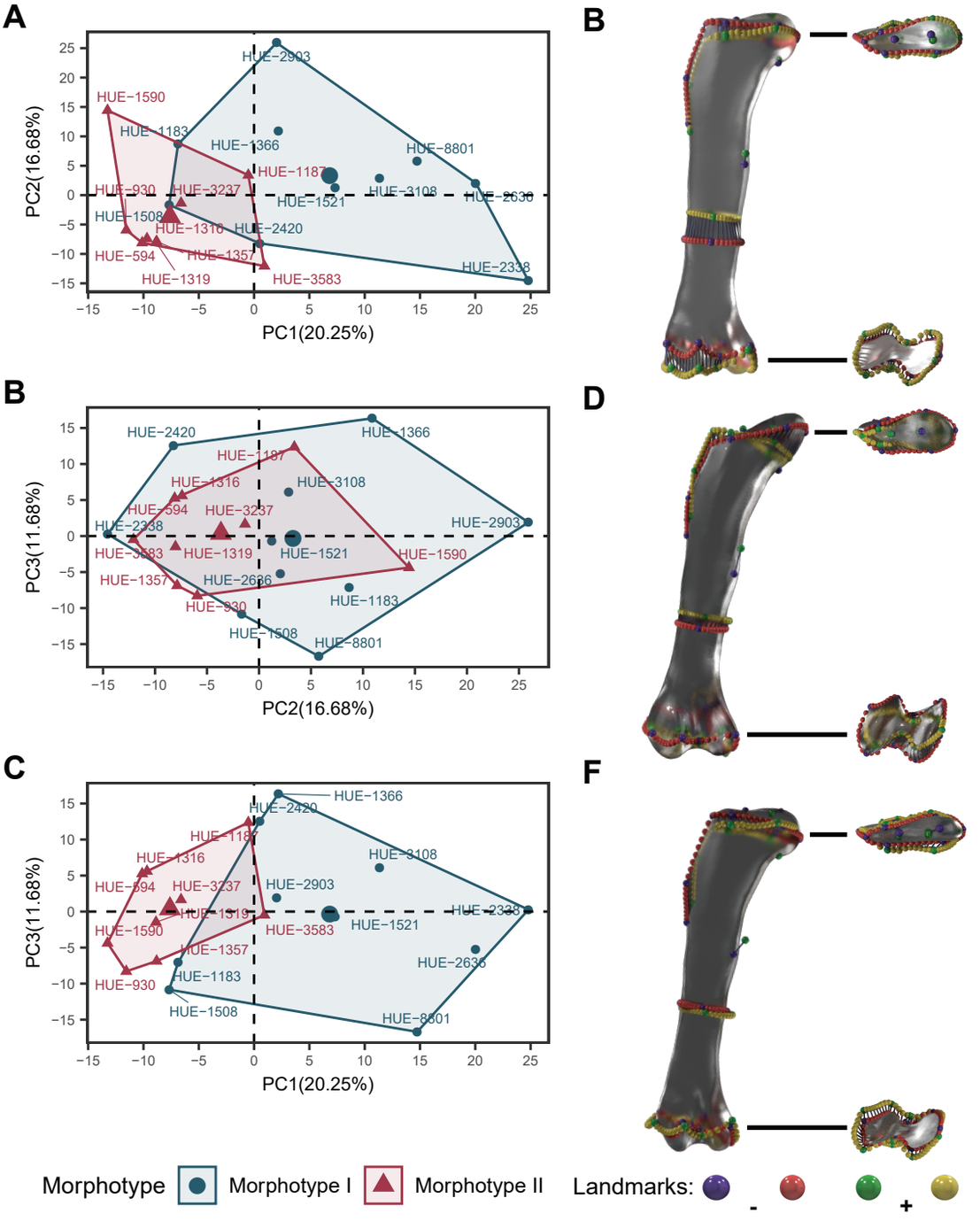

Fig.IV.II.5. Femur shape PCA results with highlighted taphomorphospaces. (A) PC1-PC2. (B) PC2-PC3. (C) PC1-PC3. (D) Landmark configuration at the extremes of PC1 axis. (C) at the extrmes of PC2 axis. (F) at the extremes of PC3 axis.

It is in the second principal component (PC2: 16.79% of variance) where differences between taphomorphospaces are more remarkable. In more negative values there is a more downward position of the femoral head. In addition, PC2 reflects a more anteroposterior developed femoral head relative to the lateromedial width of the greater trochanter. Here it is important to highlight that medium values represent elements with a developed step between the femoral head and the greater trochanter. The more negative values represent femora characterized by straight and eccentric shafts, an extreme compression of the distal condyles and a more lateral position of the epicondyle. This differs to the relative position of the epicondyle respective to the distal condyles in posterior face and the anteroposterior expansion of the distal condyles reflected by positive values. More positive values represent a more upward position of the femoral head and more expanded distal condyles as well as a more posterior position of the lateral epicondyle. Both morphotypes are as differentiated in this component as both shows some degree of variation in the position of the femoral head especially, in specimens referred to Morphotype I (e.g., HUE-2338). These specimens have a femoral head directed dorsally similar to the elements assigned to the Morphotype II. The reduced dataset PC2 (16.68% variance) shows similar results to the complete dataset PC2 but with inverted values (see Supplementary Material.IV.II.C). Negative values show femora with more straight proximal end, with the femoral head placed at same height to the lateral bulge to slightly lower position. The fourth trochanter is more proximally placed and the distal end has the fibular end more distally placed. Positive values are represented by femora with more upward projection of the femoral head, more distally placed fourth trochanter and fibular condyle and intercondylar fossa in anterior face more proximally placed. However, lack of landmarks especially on the greater trochanter area and the anterior face of distal end makes difficult to assess if there is some bevelling of the shaft contrary to the complete dataset. Comparing the PC1-PC2 plot of the complete sample (Fig.IV.II.5.a) with the plot of the subsampled dataset (Supplementary Material.IV.II.C) we can observe that both taphomorphospaces overlap in both PCs for the subsampled analysis, contrary to the analysis on complete dataset.

The third principal component (PC3: 11.55%) reflects the variation in the lateromedial development and the torsion of the fibular condyle and a weak rotation of the complete distal condyles (Fig. IV.II.5). Positive values show femora with less lateromedially expanded femoral head and shorter lateral bulge. Both the proximodistal development of the lateral bulge and the femoral head position also reflect some residual variation relative to the previous principal components (as variation is seen in PC1 and PC2). Positive values also represent more anterosposteriorly wide femoral head, more proximal fourth trochanter and more anteroposteriorly expanded midshaft minimum width outline and distal end. Negative values represent proximal end more expanded lateromedially, with the femoral head more proximodistally expanded but not deflected proximally. The lateral bulge in more negative values is a bit longer, with fourth trochanter more posterodistally placed. The midshaft is more eccentric and the distal condyles are more anteroposteriorly compressed.

The variation along PC3 concentrates in the position of the femoral head respective to greater trochanter, proximodistal length of the lateral bulge and the anteroposterior development of distal condyles (i.e., fibular and tibial condyles). The more negative values represent femora with a lower femoral head respective to the greater trochanter, weakly compressed anteroposteriorly. The lateral bulge is a bit longer and with the midpoint of the bulge more placed distally. There are subtle differences in the overall more proximal position of minimum midshaft contour. The midshaft is also more eccentric in those values whereas there are no differences in the lateromedial minimum width of the midshaft. The distal condyles are anteroposteriorly

compressed, with little medial deflection in distal face. The fibular condyle is also in an upward position respective to the tibial condyle. Some specimens are representative of negative values (e.g. HUE-1366 and HUE-2903), which present fragmentary proximal and distal ends and both are lateromedially compressed but rather slender elements. On the contrary, values that are more positive shows elements having lightly more anteroposteriorly wide femoral head and greater trochanter. The femoral head is placed at same height to the greater trochanter. The lateral bulge is slightly shorter but the proximal part is deflected in the anterior face. The fourth trochanter is placed proximally and medially. The midshaft is less eccentric and the minimum width placed slightly more distal. The distal condyles are more expanded anteroposteriorly. They are medially deflected, bulkier and more bulbous fibular and tibial condyles. The reduced dataset PC3 (11.61% variance) shows similar results to the complete dataset for the proximal end of the femur. While we lose some information about the proximal contour, differences in femoral head position and the anterior deflection of the lateral bulge in more positive values are captured. However, fewer differences in fourth trochanter placement and the relative position of the femoral head are reported along this PC. The midshaft results are similar, but the distal condyles are less informative and it is harder to distinguish the medial deflection in more positive values. Instead, it seems an exaggerated difference in the angle of deflection, having fewer differences in the tibial condyle landmarks while much more in the medial or fibular landmarks. The lack of landmark sampling in the distal end does not permit us to show the major differences on this area between both morphotypes. Moreover, with the Procrustes superimposition based on the landmark of the more proximal part of the shaft, this dataset exaggerates the anteroposterior rotation of the distal end. The reduced dataset does not show the expansion of the anterior landmarks of the distal end along the PC3 seen in the complete dataset.

IV.II.4.2. TIBIA SHAPE TAPHOMORPHOSPACES

First principal component of the complete analysis (PC1: 30.1% variance) reflects a trend from more robust (both with lateromedially and anteroposteriorly expanded proximal and distal ends) on the more positive values to more gracile elements (and shafts with more constant width) represented toward more negative values (Fig.IV.II.6). It is also important to note that more positive values shows the most anteroposteriorly expanded cnemial crest against negative values featured by anteroposteriorly shorter cnemial crests with more triangular shape. There is also a weak flexion of the cnemial crest to lateral in more positive values while more negative values remain anteroposteriorly straight. In more positive values the proximal end is more expanded anteroposteriorly and lateromedially, especially in the fibular articulation, and the posterior part forms a subtriangular-oval-shaped. More negative values reflect a slightly circular, narrower proximal end. Negative values reflect similar oval-shaped but much more narrow both in anteroposterior and lateromedial.

Lastly, positive values reflects a more expanded distal end with the condyle facing perpendicular to slightly anterior in lateral face. Negative values present a narrower distal end in anteroposterior and lateromedial, with the condyle articulation facing slightly to lateroposterior.

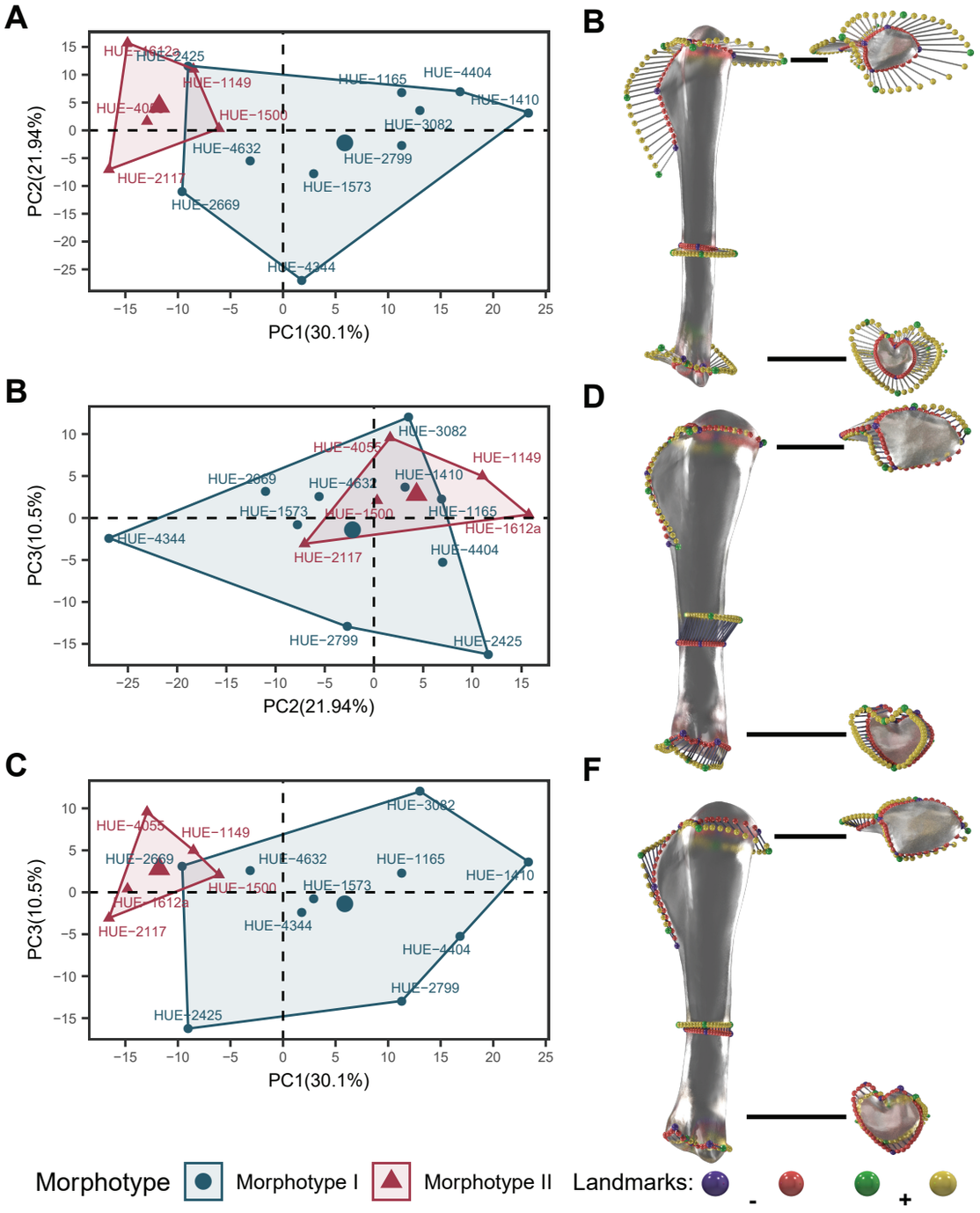

Fig.IV.II.6. Tibia shape PCA results with highlighted taphomorphospaces. (A) PC1-PC2. (B) PC2-PC3. (C) PC1-PC3. (D) Landmark configuration at the extremes of PC1 axis. (C) at the extrmes of PC2 axis. (F) at the extremes of PC3 axis.

The reduced dataset PC1 (36.15% variance) shows similar results but with an inverted PC compared to the complete dataset. Negative values present a more distally placed cnemial crest midpoint whereas positive values shows tibiae with more proximally placed triangular-shaped midpoint of cnemial crest (see Supplementary Material.IV.II.5.B). Differences can be observed on the position of the anterior ascending process of the distal end between positive values (more expanded and upward position) and negative values (more medially and posteriorly placed, rotation of the condyle to lateroposterior). However, the lack of the distal end landmarks compared to the complete dataset does not allow us to see possible displacement of the anterior part of distal end nor its rotation.

The second principal component of the complete dataset analysis (PC2: 21.94% variance) shows the main differences between tibiae with lateromedially compressed proximal ends (in positive values) up to the more anterior-anterolaterally expanded tibial heads with more upward placed anterior proximal part of the cnemial crest (in negative values). The elements on positive values present a minimum midshaft width distally placed. While the negative values show a more proximal positioned minimum midshaft width, more proximal to the cnemial crest distal end. Thre are minor differences in the contour of the distal end in this PC, as only a weak increase in anteroposterior width in more positive values. There are differences in the position of the distal end along this axis. Positive values represent a distal displacement of the condyle, with a more upward placed of the anterior ascending process and a distal flexion of the entire contour and posterior half in medial and lateral face. On the contrary, values that are more negative represent distal ending that maintain similar height of the anterior and posterior parts of the condyle.

Main differences between the complete dataset and the reduced dataset arise in results for PC2. The reduced dataset PC2 (15.76% variance) only comprises proximal landmarks and curves so the anteroposterior expansion of the distal condyles and the rotation of the fibular articulation in the distal end is not captured. For this reason, there is less differences between both taphomorphospaces in the reduced dataset than in the analysis of the complete dataset.

Tibiae analysis		Df	SS	MS	Rsq	F	Z	pval
Morphotype I vs Morphotype II		1	0.027	0.027	0.234	3.971	2.700	0.005*
	Residuals	13	0.090	0.007	0.766			
	Total	14	0.117					
k2 groups		1	0.035	0.035	0.298	5.516	3.432	0.001*
	Residuals	13	0.082	0.006	0.702			
	Total	14	0.117					
k3 groups		1	0.021	0.021	0.176	2.775	2.178	0.019*
	Residuals	13	0.096	0.007	0.824			
	Total	14	0.117					
k4 groups		1	0.028	0.028	0.237	4.034	2.897	0.003*
	Residuals	13	0.089	0.007	0.763			
	Total	14	0.117					
k5 groups		1	0.005	0.005	0.040	0.546	-0.952	0.824
	Residuals	13	0.112	0.009	0.960			
	Total	14	0.117					

Table.IV.II.10. PERMANOVA results on the GPA aligned coordinates of the tibiae.

The third principal component (PC3: 10.5% variance) shows similar trends to the PC2 but reflecting more the divergence between the anteriorly and posteriorly rotated distal condyles. In this regard, analysing the reduced dataset, the PC3 (9.76% variance) only shows minor differences between the lateromedially compressed proximal head as shown in negative values, and the more expanded in positive values. The differences between taphomorphospaces are less evident in this PC.

IV.II.4.3. FIBULA SHAPE TAPHOMORPHOSPACES

The analysis of the complete dataset present a first principal component (PC1: 19.82% variance) which positive values are characterized by fibulae with a deflected proximal end so the anterior part is directed downward; and a medially deflected anterolateral crest (in lateral view this crest shows a shorter anteroposterior width due to this flexion, see Fig.IV.II.7). The proximal end is expanded lateromedially equal to the anteroposterior width. The negative values are characterized by a lateromedially compressed proximal end with the anterior facing upward, and the posterior part more distally placed. The anterolateral crest faces anterior to anteromedial and it is more expanded than in positive values. The positive values show a lateral trochanter projected anteriorly and slightly proximally. On the contrary, negative values shows a lateral crest less anteriorly placed and longer distally. The positive values show fibulae with shorter lateral trochanter while positive values show fibulae with longer lateral trochanter that reach the posterior edge of the fibula. The positive values are defined by a medial flexion of the anterior crest. They also show a flexion downward of the anterior part of the distal end. Negative values show fibulae with an expanded anerior crest, with a distal end slightly bevelled to proximal in anterior (while the posterior part is more distally placed).

The first PC of the analysis of the reduced dataset (PC1: 21.23% variance, see Supplementary Material.IV.II.C) shows weak differences between negative and positive values. The more positive values show proximal ends slightly more distally placed with an anerolateral crest shorter proximodistally and medially deflected. The negative values show a proximal end more upwardly directed, with a proximodistally longer anerolateral crest. The lateral crest is more distally placed in positive values. The distal part of the lateral bulge is placed more posteriorly in the positive values as well. The distal end differ with more distally placed medial midpoint landmark in positive values.

On the analyses of the complete dataset, the second principal component (PC2: 16.81% variance) reproduces the variation between a slight medially flexed proximal end in more positive values and the lateral deflection of the proximal end in negative values. It also reflects a similar pattern in the distal end. In the more positive values, the distal end deflectes to more posteromedial position while in negative values, the fibulae have more anterolaterally enlarged distal ends. There is a large overlapping toward central values of PC2, with few differences between both morphotypes near the 0 value. An exception to this is the specimen HUE-2804 which is projected in the most negative values of PC2. Morphotype I is placed in slightly more positive values while the Morphotype II is projected toward more negative values. The differences are minor in this axis.

The analysis of the reduced dataset (PC2: 17.86% variance) shows very similar results as majority of change seen in PC2 of the analysis on the complete dataset. Both set of landmarks captures enough of the overall morphology, with the reduced dataset lacking some landmarks

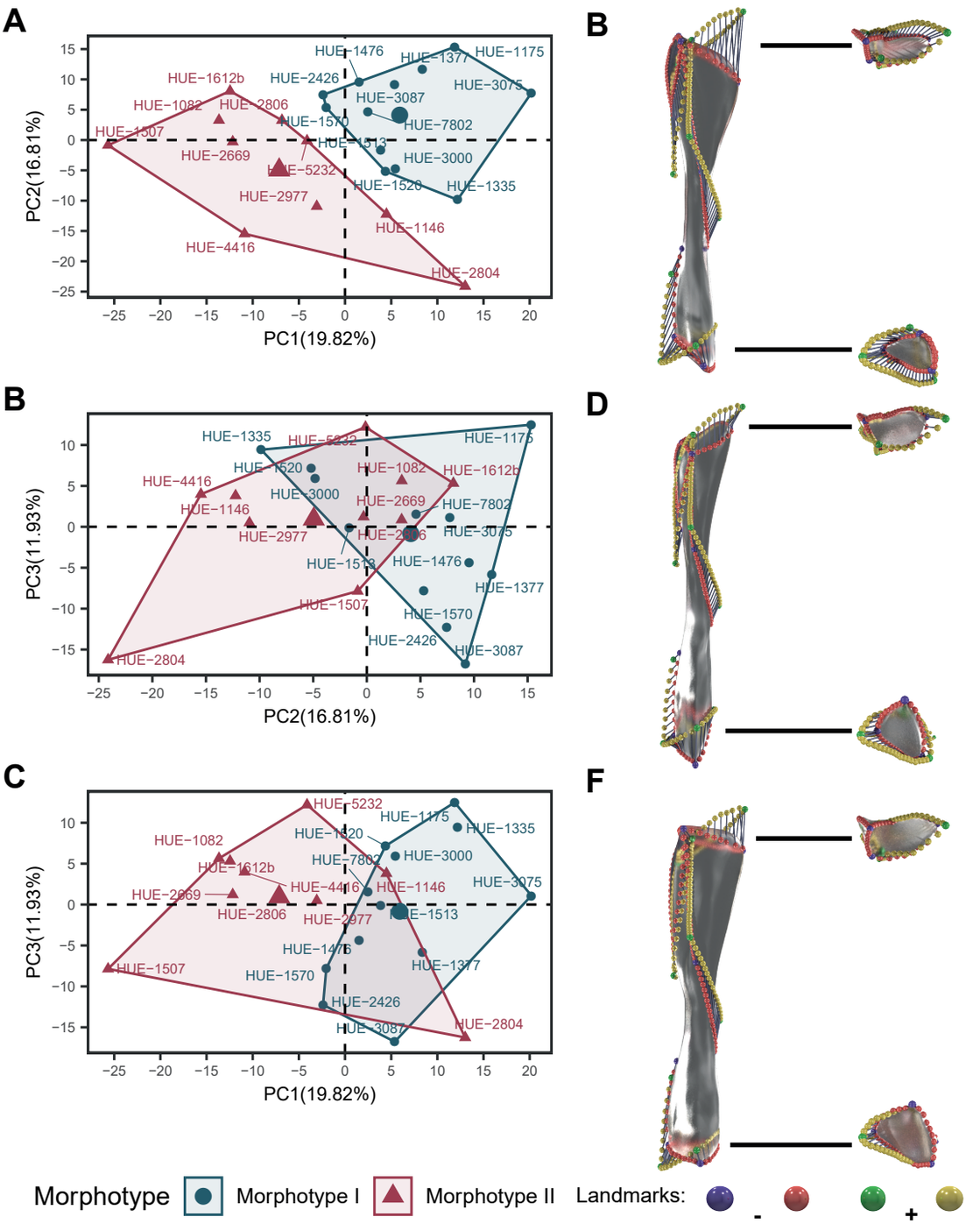

Fig.IV.II.7. Fibula shape PCA results with highlighted taphomorphospaces. (A) PC1-PC2. (B) PC2-PC3. (C) PC1-PC3. (D) Landmark configuration at the extremes of PC1 axis. (C) at the extrmes of PC2 axis. (F) at the extremes of PC3 axis.

on the medial face and the proximal and distal curves. This causes less marked differences in the proximal part of the lateral trochanter and it is harder to see the variation in the anterolateral crest, as there is no landmark and curve in the medial face of the proximal end for reference.

The third principal component of the PCA over complete dataset (PC3: 11.93%) shows minor differences in the anerolateral crest, in the articulation of the tibia and in the anterolateral crest of the distal end. The positive values recovered longer anterolateral crests in the distal end. The distal end is also flexed ventrally with a more upward medial face. The negative values recovered shorter anterolateral crests and more upward anterior part of the distal end, with a lower, more anteriorly placed medial face of the condyle. No major differences between the two morphotypes are reported. The analysis of the reduced dataset (PC3: 13.09%) shows minor differences in the anerolateral crest with more variation in the lateral trochanter position and the distal landmark recorded at the end of the lateral crest. Negative values show fibulae with longer and straighter lateral trochanter, and the anterior crest is more proximal placed. Positive values show fibulae with lateral trochanter shorter, more flexed with the proximal half more anteriorly placed. The distal end of the lateral trochanter is placed slightly more posterior. The lateral crest in distal is more anterior and distally placed. However, lack of landmark information compared to complete dataset do not allow to see deflection of the anterolateral crest and the anerolateral crest in distal respective to the medial face.

IV.II.4.4. GROUP DIFFERENCES

A priori group differences reported in the description of the elements are tested. After Principal Components Analysis on the Procrustes coordinates, a Kruskal-Wallis test is performed over the principal components, and the results can be seen in Table.IV.II.8. A priori grouping shows statistical

Tibiae analysis		Df	SS	MS	Rsq	F	Z	pval
Morphotype I vs Morphotype II		1	0.027	0.027	0.234	3.971	2.700	0.005*
	Residuals	13	0.090	0.007	0.766			
	Total	14	0.117					
k2 groups		1	0.035	0.035	0.298	5.516	3.432	0.001*
	Residuals	13	0.082	0.006	0.702			
	Total	14	0.117					
k3 groups		1	0.021	0.021	0.176	2.775	2.178	0.019*
	Residuals	13	0.096	0.007	0.824			
	Total	14	0.117					
k4 groups		1	0.028	0.028	0.237	4.034	2.897	0.003*
	Residuals	13	0.089	0.007	0.763			
	Total	14	0.117					
k5 groups		1	0.005	0.005	0.040	0.546	-0.952	0.824
	Residuals	13	0.112	0.009	0.960			
	Total	14	0.117					

Table.IV.II.11. PERMANOVA results on the GPA aligned coordinates of the fibulae.

significant differences in the test of the complete dataset for all the element types in at least one PC. The femur, tibia and fibula show significant differences in the PC1 (Femur: X^2=9.627, p=.002, Tibia: X^2=6.615, p=.01, Fibula: X^2=8.039, p=.003). There are also significant differences in the femur PC7 (X^2=4.507, p=.034) and the fibula PC2 (X^2=4.452, p=.035). The reduced dataset was also tested and it has been found no significant differences between femora morphotypes. The tibiae present differences between the proposed morphotypes in the PC1 (X^2=8.640, p=.003). The fibulae show differences in the same PCs (PC1: X^2=5.078, p=.024, PC2: X^2=6.074, p=.014).

The cluster analysis over Procrustes distances can be observed in Fig.IV.II.8. The cluster of the femur complete dataset (Fig.IV.II.8.a) shows two distinct clusters resemble Morphotype I and Morphotype II respectively, with only specimen HUE-1508 (attributed to Morphotype I) in the cluster of Morphotype II specimens. Two other clusters are observed with mixed specimens from the two morphotypes. The cluster analysis of the femur reduced dataset recovered two distinct clusters resembling the two described morphotypes except for specimens HUE-1319 and HUE-1508 (see Fig.IV.II.8.b). Two other clusters are found with mixed specimens from the described morphotypes. The analysis of the complete and the reduced tibia datasets returned two distinct clusters for each analysis (Fig.IV.II.8.c and d). The only exceptions are specimen HUE-1500 defined in this work as Morphotype II and recovered in the cluster of Morphotype I;and the specimen HUE-2425, described as Morphotype I and observable in the other major cluster. The differences found between both analyses are in the number of internal clusters recognized in the main group of specimens from Morphotype I. Two different clusters can be seen among specimens of Morphotype I in analysis of complete dataset (Fig.IV.II.8.c), while there are three to four distinct clusters among Morphotype I in the analysis of the reduced dataset (Fig.IV.II.8.d). The analysis for the complete fibula dataset recovered two groups of specimens from Morphotype II intermingled with different clusters of specimens from Morphotype I, suggesting few differences between them (see Fig. IV.II.8.e). The specimens HUE-1507 and HUE-2804 from Morphotype II are much more different from the other specimens of the sample. The analysis of the reduced dataset results in a cluster of specimens from Morphotype II at the base of the tree, much more similar to HUE-1507 and HUE-2804 (Fig.IV.II.8.f). Three distinct clusters formed by specimens of Morphotype I are found also in this analysis, with several specimens (HUE-1146, HUE-2977, HUE-4416 and HUE-5232) mixed.

The K-means solutions are implemented over the PC eigenvalues for each individual. Comparative plots of the first and second PCs with the grouping alternative hypothesis are reported as well as the optimal number of clusters. For the complete set of landmarks and curves, femur and fibula report an optimal number of two groups. Both reflect similar clustering of the specimens as in the morphotypes defined during the description. Differences between the alternative grouping hypotheses will be discussed later.

Most of the analyses recovered two clusters as one of the optimal grouping hypothesis. These groups shows similarities with the a priori description of Morphotype I and Morphotype II. Femora and tibiae show as most optimal grouping hypothesis the presence of three clusters with slightly better average silhouette widths (see Fig.IV.II.9.f, 10.f. and11.f). As the average silhouette width between two and three groups is so similar, both grouping hypothesis are regarded as the most optimal. The taxonomical significance for this different grouping hypothesis is assessed (see Discussion). It is necessary to note that k-means clustering tend to produce groups with no overlapping. Despite the two-groups hypothesis coincides in most of the a priori group description, several specimens are re-classified based on this principle of the

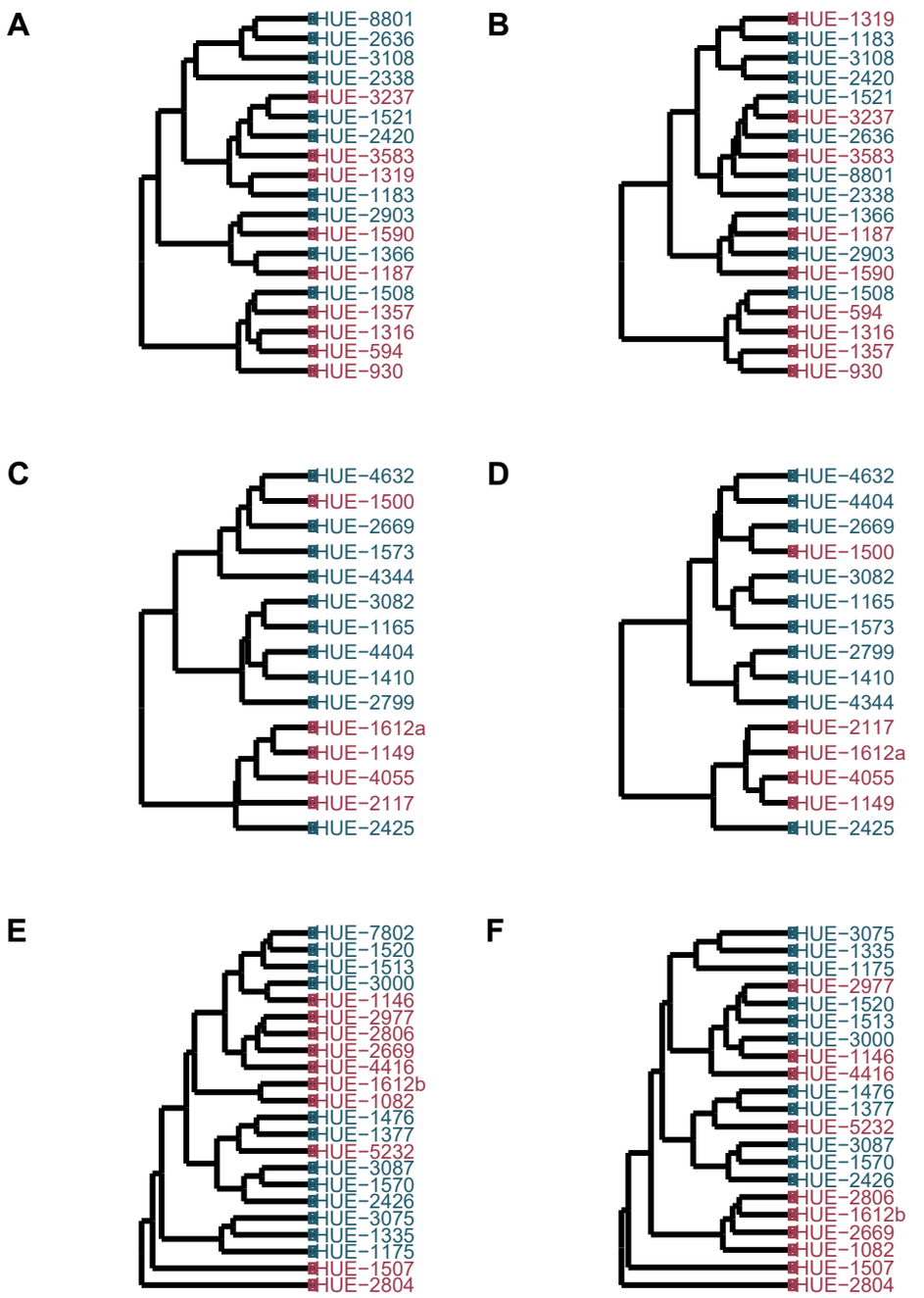

Fig.IV.II.8. Cluster analysis of the GPA aligned coordinates. (A) Femur, complete dataset. (B) Femur, reduced dataset of landmarks. (C) Tibia, complete dataset. (D) Tibia, reduced dataset. (E) Fibula, complete dataset. (F) Fibula, complete dataset.

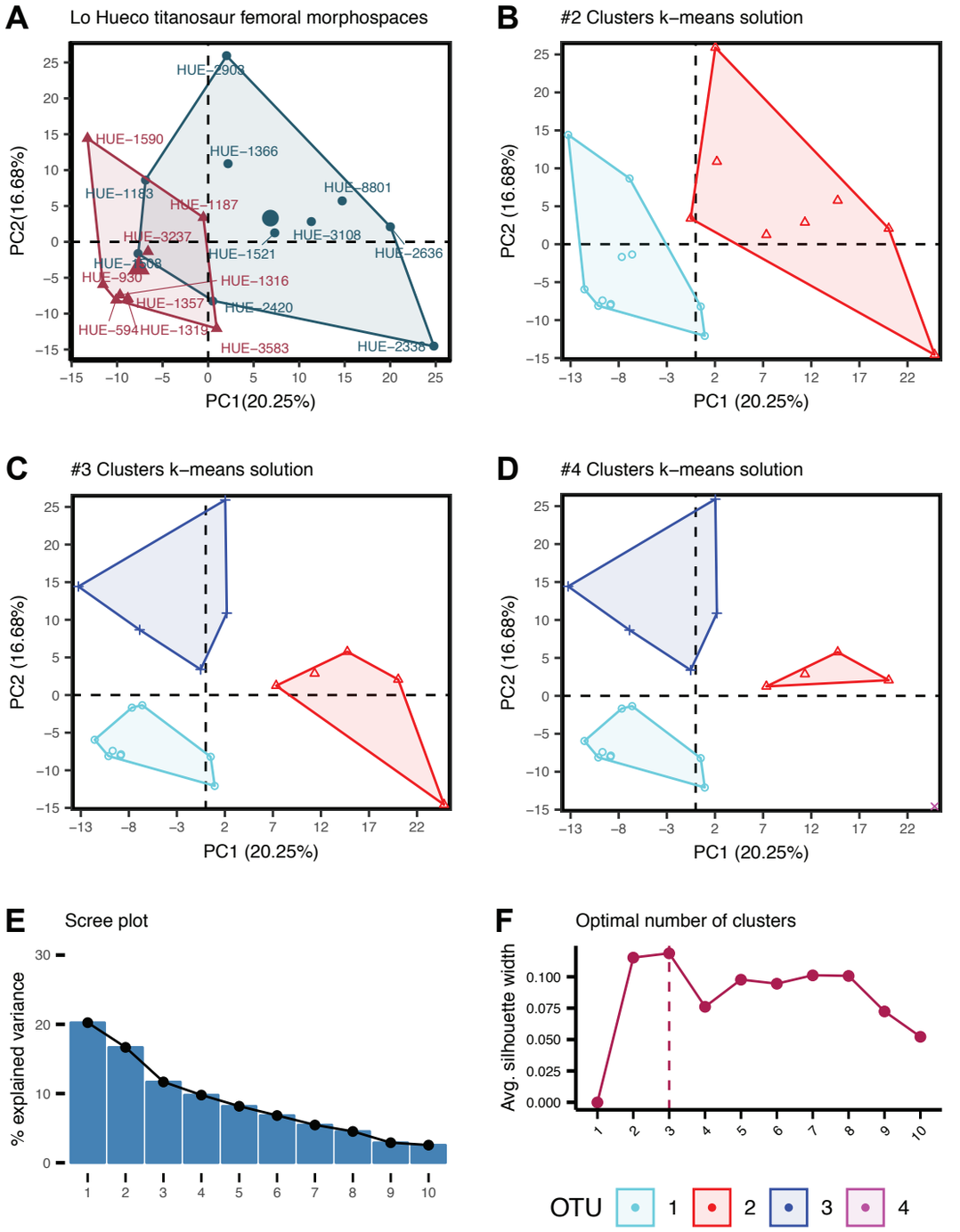

Fig.IV.II.9. Femora group assessment via k-means algorithm. (A) Shape PCA PC1-PC2 with a priori morphotypes. (B) Classification for k= 2 groups. (C) k= 3 groups. (D) k = 4 groups (E) Variance explained by each PC. (F) Average silhouette width after partition of the morphospace into k groups.

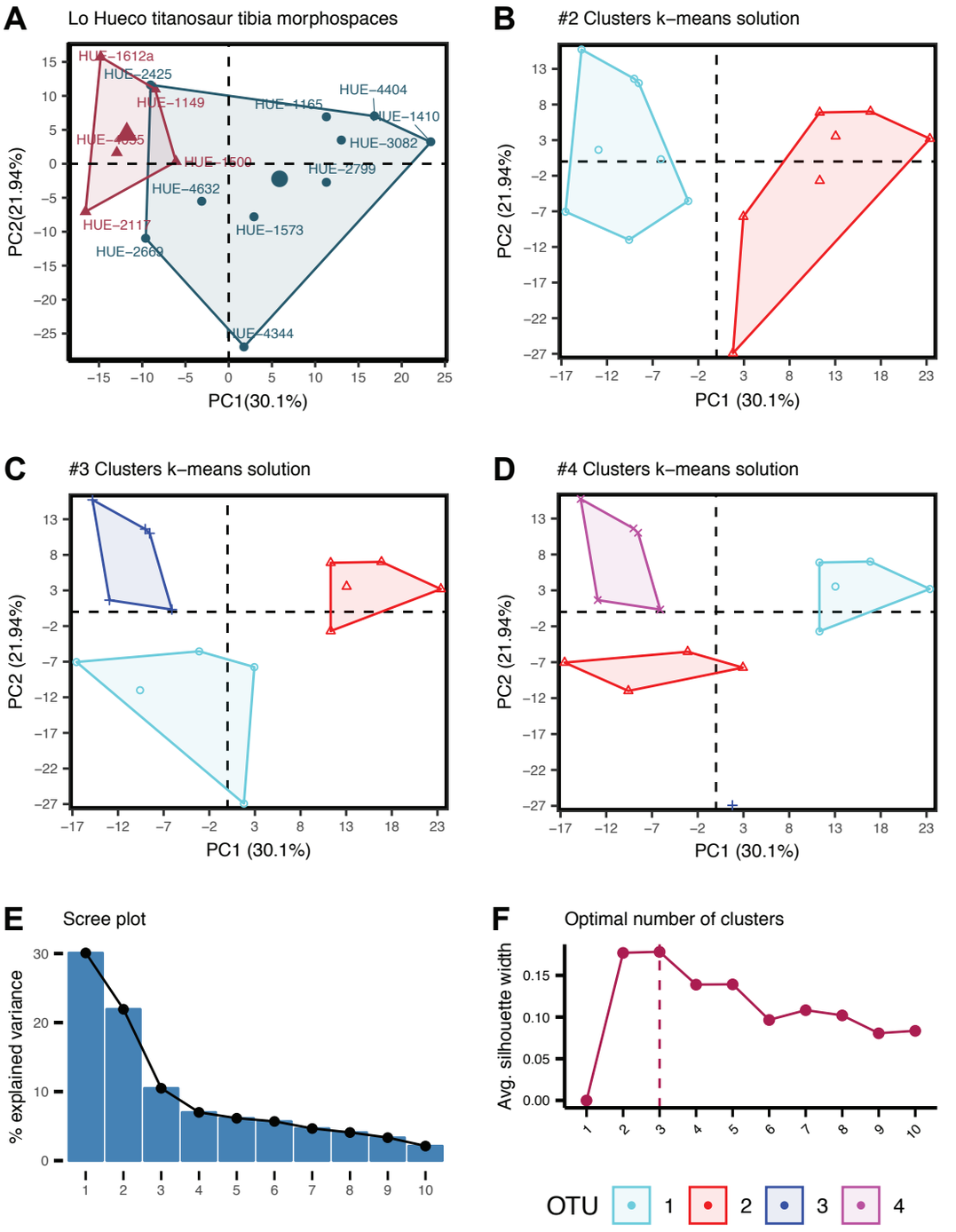

Fig.IV.II.10. Tibiae group assessment via k-means algorithm. (A) Shape PCA PC1-PC2 with a priori morphotypes. (B) Classification for k= 2 groups. (C) k= 3 groups. (D) k = 4 groups (E) Variance explained by each PC. (F) Average silhouette width after partition of the morphospace into k groups.

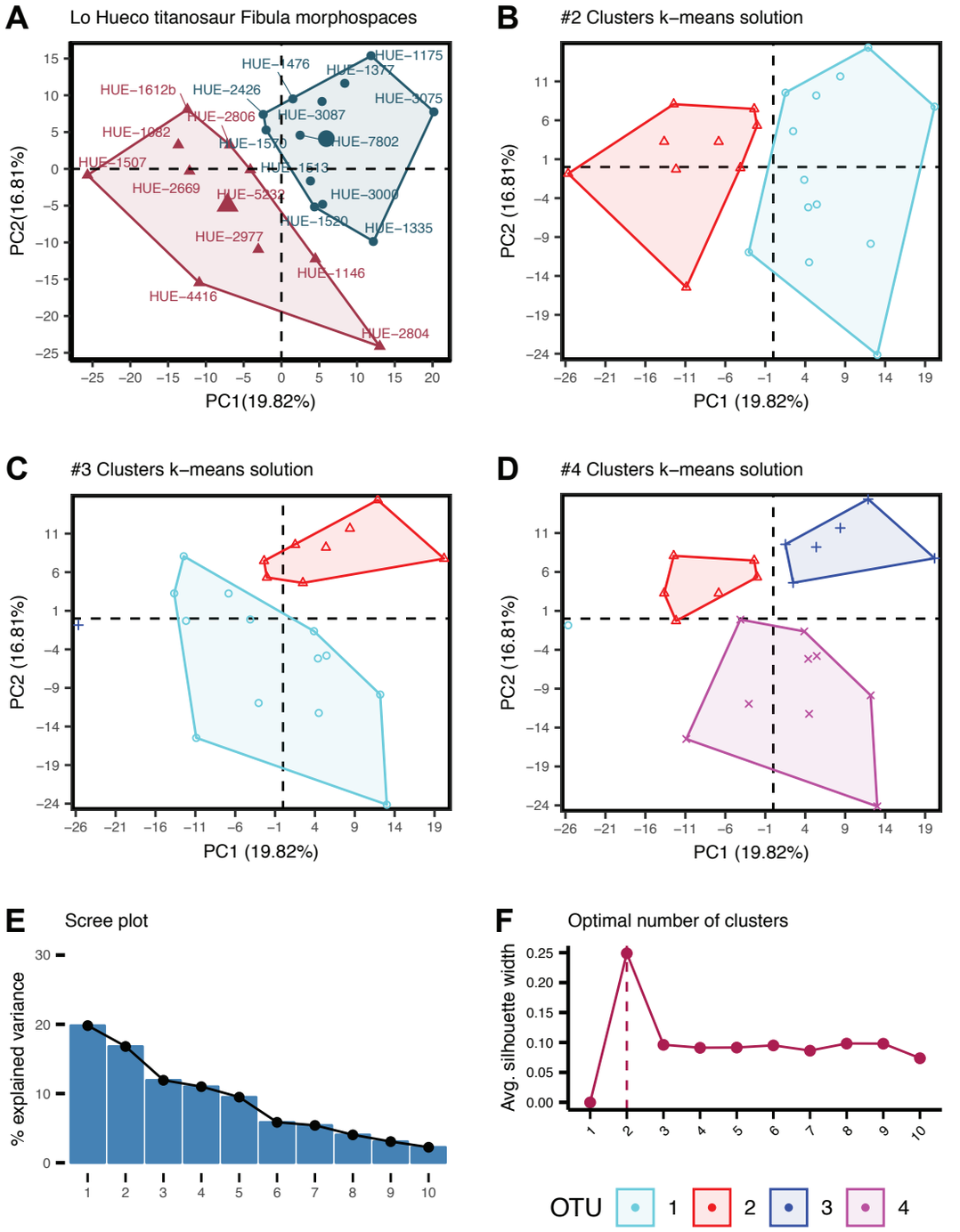

Fig.IV.II.11. Fibulae group assessment via k-means algorithm. (A) Shape PCA PC1-PC2 with a priori morphotypes. (B) Classification for k= 2 groups. (C) k= 3 groups. (D) k = 4 groups (E) Variance explained by each PC. (F) Average silhouette width after partition of the morphospace into k groups.

algorithm. The four groups hypothesis is not supported in any of the k-means clustering of the morphometric variables. The tibia is the only element that present a closer silhouette width for four and five probable groups. However the inspection of the results (Fig.IV.II.10.d) shows that the four group is represented by specimen HUE-4344 alone. The three groups hypothesis and four group hypothesis subdivide also Morphotype II specimens HUE-1573, HUE-2669 and HUE-4632 as well as specimen HUE-2117 of Morphotype II into a new group. This group defines a taphomorphospace in negative values of PC1 and PC2 (Fig.IV.II.10.c and d). All these elements resemble the tibia of *Lohuecotitan pandafilandi*, (specimen HUE-3082), with some variation in the overhanging of the articulation of the fibula (specimen HUE-4344) or the rotation to lateroposterior of the distal end (specimen HUE-1573). The specimen HUE-2117 is the only one exhibiting more differences with the tibia of *L. pandafilandi*, showing a slender and elongated shaft, least lateromedially expanded distal end and the engrossed mid-part of the cnemial crest.

Another result recovered in all the analysis is the presence of specimen HUE-EC-6 as part of Morphotype II on the alternative grouping hypothesis. The analyses of the femur (Fig. IV.II.9), the tibia (Fig.IV.II.10) and the fibula (Fig.IV.II.11) classify the elements of the hindlimb from individual HUE-EC-6 in the same group as most of the elements from Morphotype II. The probable assessment of HUE-EC-6 as Morphotype II is discussed further below.

The k-mean clustering for the subset datasets recovered 2 groups as the most optimal clustering solution for all the element types. Group distribution however is difficult to assess as taxonomical significant for the femur and the fibula, clustering together strongly different specimens. The analysis can be accessed in Supplementary Material.IV.II.C. Another observation on the results is the consideration of the specimens referred to the hindlimb of individual HUE-EC-6 as part of a group with most of the Morphotype II specimens. However, the analysis of the fibulae also recovered the right fibula of *L. pandafilandi*, individual HUE-EC-1 (HUE-3087) as Morphotype II with the fibula of HUE-EC-6 (HUE-2426). The left fibula of HUE-EC-1 (HUE-3075) however is classified in the other cluster with most of specimens from the Morphotype I.

Problems for morphospace separation in the reduced dataset can be related to the lack of information on some areas as highlighted in the results of the principal components (see Femur, Tibia and Fibula shape taphomorphospaces before). The great overlap in the femora and fibulae produces difficulties to assess group differences because k-means separates the tightest group possible without overlap. Lack of information in the femoral head or distal end of the femur as well as proximal and distal end of the fibula difficult the clustering, as those areas are the most variables between both morphotypes.

IV.II.5. DISCUSSION

IV.II.5.1. MORPHOTYPE I ASSESSMENT

According to the description of the elements at least two main groups of specimens can be recognized in all the bone element types studied. The hindlimb of Morphotype I is characterized by more gracile but less eccentric femur, with a rather robust distal elements. This robustness of the distal elements is due to the presence of relatively short tibia and fibula with both anteroposteriorly and lateromedially expanded proximal and distal ends. This morphotype has

an arched hindlimb in anterior view with medial deflection of the femoral head and a medial and dorsal bevelling of the distal condyles. The tibial anterior ascending process is elevated relative to the fibular condyle resulting in the medial deflection of the distal end common in several titanosaurian sauropods (Salgado, Coria, & Calvo, 1997; Wilson & Sereno, 1998; Sanz *et al.*, 1999; Wilson & Carrano, 1999; D'Emic, 2012). The femur presents a prominent lateral bulge, condition considered as synapomorphy of Titanosauriformes and some other stem forms (e.g. Salgado *et al.*, 1997; Wilson, 2002; Upchurch, Barrett, & Dodson, 2004; Carballido *et al.*, 2011; Royo-Torres, Alcalá, & Cobos, 2012; D'Emic, 2012; D'Emic *et al.*, 2013; Mannion, Allain, & Moine, 2017). All these femora are different to other known European species such as *Lirainosaurus astibiae* (e.g. MCNA-3160, MCNA-7468 and MUVHN-17235), *Ampelosaurus atacis* (e.g. MDE C3-87 and MDE C3-1182, Le Loeuff, 2005; Vila *et al.*, 2012) or *Atsinganosaurus velauciensis* (specimen MMS/VBN-09.126, Díez Díaz *et al.*, 2018) with rather robust femora, especially in lateromedial expanded distal ends and with an eccentric shaft. Femora referred to *A. atacis* show some degree of variation in the position of the fourth trochanter and the proximodistal height of the lateral bulge (e.g. MDE C3-87, MDE C3-287, MDE C3-1182). The relative robustness of the midshaft is variable as seen in the right femur MDE C3-1182 which bears a more slender midshaft, but the proximal and distal ends present similar robustness (e.g. Vila *et al.*, 2012) greater than in most of the specimen of Morphotype I and *L. pandafilandi*. The fourth trochanter of *A. atacis* is placed distally in posterior face, almost in the midshaft, with a short lateral bulge ending more proximal. Morphotype I present some variation but the lateral bulge is long and extends up to the same proximodistal height as the fourth trochanter (e.g. HUE-1366). However, there are some specimen of *A. atacis* with the lateral bulge ending almost at the same height as the fourth trochanter (e.g. MDE C3-87, MDE C3-287, Le Loeuff, 2005; Vila *et al.*, 2012). The fourth trochanter is not visible in anterior face in all the femora referred to *A. atacis*, contrary to Morphotype I specimens which present a fourth trochanter migrated to medial on the posterior face and some of them visible in anterior face (e.g. HUE-2903, HUE-3108). All the femora of *A. atacis* also present similar robustness of the proximal end and especially robustness of the distal end despite the variation observed in the midshaft (e.g. Vila *et al.*, 2012: Table 1; see also Supplementary Material.IV.D, this study). The femoral head is not preserved in all the femora of *A. atacis* but none shows the anteroposterior expansion and the bulbous morphology on proximal end (e.g. MDE C3-203) contrary to the specimens of Morphotype I and *Lohuecotitan pandafilandi* (HUE-3108). In the specimens that preserve the distal end from Morphotype I and *A. atacis* there are differences in anteroposterior compression of the distal condyles between both sauropod forms. The distal end of the femora of *A. atacis* are compressed anteroposteriorly, without noticeable medial deflection of any of the condyles. There is a lateral epicondyle posteriorly directed as in *Epachthosaurus sciuttoi* (UNPSJB-PV-920, Martínez *et al.*, 2004) and the Morphotype II of Lo Hueco. On the contrary, the Morphotype I has an epicondyle facing more lateroposteriorly. Morphotype I presents a medial deflexion of the tibial and fibular condyle. Instead, the distal end of Morphotype I is similar to the anteroposterior expanded distal end of *Jainosaurus* cf. *septentrionalis* (specimen NHM-R.5903), *Huaebisaurus allocotus* (e.g. HBV-20001, D'Emic *et al.*, 2013) and also visible in more primitive Titanosauriformes as in *Giraffatitan brancai* (Janensch, 1961)

Some specimens of Morphotype I present a marked linea cranialis intermuscularis in anterior face, which is not present in *Ampelosaurus atacis* (e.g. Vila *et al.*, 2012), *Lirainosaurus astibiae* (Díez Díaz, Suberbiola, & Sanz, 2013; but see specimen MCNA-14471), cf. *Lirainosaurus* (Vila *et al.*, 2012) and the Titanosauria indet. Form 2, Form

3 and Form 4 described in the Ibero-Armorican Late Cretaceous (Vila *et al.*, 2012).

The indeterminate titanosaur Form 1 (MDE C3-1278) described by Vila *et al.* (2012) presents a linea intermuscularis cranialis in anterior face and a medial deflection of the fourth trochanter. It also presents a less eccentric shaft. However, none of the sampled specimen referred to Morphotype 1 from Lo Hueco have the fourth trochanter posteromedially placed and directed to medial as in titanosaur Form 1 (see Fig.4, Vila *et al.*, 2012).

Some small specimens sampled in Lo Hueco were previously attributed to this morphotype (see Páramo *et al.*, 2014) but another hypothesis highlights probable affinities with small or putative dwarf taxa from the Late Cretaceous of Europe. None of these elements (e.g. HUE-8801 and HUE-2636) resemble the femora of *Lirainosaurus astibiae* (small sized taxa, see Company, 2011) nor *Magyarosaurus* spp. Moreover, these small specimens, as well as, the other specimens attributed to Morphotype 1, are recovered both in the description of the specimens and in all the analysis as being closer, to the femur of the holotype of *Lohuecotitan pandafilandi* (HUE-3108). The small femora from Lo Hueco present some of the least eccentric shafts with almost circular midshaft section as in Morphotype 1 specimen HUE-1440 and also resembling *Jainosaurus* cf. *septentrionalis* specimen NHM-R.5903. They differ greatly from the anteroposterior compressed and eccentric midshaft of *L. astibiae*. There are also differences with the femora of *Magyarosarus* spp. (e.g. NHM-R3934, NHM-R4882), much more slender but with less bulbous femoral proximal end (but see NHM-R3859). Also, *Magyarosaurus* spp. present a step morphology between the trochanteric shelf and the lateral bulge (e.g. proximal cross-section on the distal lateral bulge of NHM-R3934, specimen NHM-R3856), not present in any of the specimens of Morphotype 1.

The tibia is lateromedially expanded, with a somewhat developed anerolateral crest process of the fibular articulation that extends parallel to the cnemial crest. The proximal end is rounded and lateromedially expanded, and different to the lateromedial compressed tibia of *Lirainosaurus astibiae* (specimen MCNA-13860), *Atsinganosaurus velauciensis* (e.g. MMS/VBN.09.132, Díez Díaz *et al.*, 2018) and one of the specimens referred to *Magyarosaurus* sp. (e.g. NHM-R.3812). The tibial proximal and distal ends resemble the tibia of *Jainosaurus* cf. *septentrionalis* (e.g. NHM-R.5903), *Antactosaurus wichmannianus* (e.g. MACN-6804 no.22), *Bonatitan reigi* (e.g. MACN-PV-RN-821 no.5) and *Bonitasaura salgadoi* (e.g. MPCA-468, see also distal of MPCA-467) or *Neuquensaurus* spp. (e.g. MCS-5/25, MCS-6). There is a marked fibular articular facet in the lateral face of proximal third, forming one of the vertex of the triangle-shaped tibial proximal end (eg. HUE-3082, HUE-4344; see Fig.IV.II.3). Sometimes there is a slight concavity on lateral face between this marked fibular articulation and posterior face of the shaft (e.g. HUE-4632). Most of the specimens from Morphotype 1 do not present this concavity differing from other sauropods as in *A. atacis* (e.g. MDE C3-138), *Atsinganosaurus velauciensis* (e.g. MMS/VBN.02.132, Díez Díaz *et al.*, 2018) and *Mendozasaurus neguyelap* (e.g. IANIGLA-73-2). Also note that some of the specimens of *A. atacis* presents a concavity between two convex lines in the proximal end in lateral face (e.g. MDE C3-138) but do not present a true ridge like in specimens of Morphotype 1 (e.g. HUE-3082, HUE-1573). The cnemial crest is weakly medially curved but narrow without a marked thickening of the medial muscle attachment, contrary to the short and recurved cnemial crest of *Magyarosaurus* spp. (e.g. NHM-R.3853). There is also a difference with other robust tibia which present a thickening of the cnemial crest in medial and possibly distal as *A. atacis* (e.g. MDE C3-173, MDE C3-1303), *J.* cf. *septentrionalis* (NHM-R.5903), *Aeolosaurus* sp. (e.g. MPCA-27100-8) or *Neuquensaurus* spp. (e.g. MCS-6).

The distal ascending process and the posteroventral process are directed anteriorly as in most sauropods. There are some variation in the torsion of the distal end and some of the specimens show a slightly medial-posterior directed distal end (e.g. HUE-1500, HUE-1165). This has been considered characteristic of *Lirainosaurus astibiae* (Sanz *et al.*, 1999; Díez Díaz *et al.*, 2013). But it is also shared with other sauropods as *Antarctosaurus wichmannianus* (e.g. MACN-6804-22), *Mendozasaurus neguyelap* (e.g. IANIGLA-74-1), *Diamantinasaurus matildae* (e.g. AODF-603, Poropat *et al.*, 2015) and *Neuquensaurus* spp. (e.g. MLP-CS-1264). In fact, some sauropods show slightly variation in the torsion of distal end as *Mendozasaurus neguyelap* (e.g. IANIGLA-73-2, but might present some taphonomical deformation) or *Neuquensaurus* spp. (e.g. MLP-CS-1054, MLP-CS-1123).

The tibia of Morphotype I is therefore different from other Ibero-Armorican titanosaurs, with much more expanded anteroposteriorly and lateromedially proximal and distal ends. All of the sample specimens present a more anterior expansion of the cnemial crest in comparison to *Magyarosaurus* spp. The most similar tibiae are from the referred material of *Ampelosaurus atacis*, which present some variation in its elements. The more robust type of tibia attributed to this taxa presents a lateromedially expanded proximal and distal ends. However, the cnemial crest is shorter than in the specimens from Lo Hueco, and the midshaft is also more eccentric in *A. atacis* (e.g. MDE-C3-144, MDE-C3-138 Le Loeuff, 2005).

The fibulae of the Morphotype I is sigmoid but not at the degree of other titanosaurs such as *Lirainosaurus astibiae* (e.g. MCNA-9410, but see MCNA-7472), *Rapetosaurus krausei* (e.g. FMNH-PR-2209, Curry Rogers, 2009), *Alamosaurus sanjuanensis* (e.g. TMM-43621-1 Lehman & Coulson, 2002), *Ampelosaurus atacis* (e.g. MDE-C3-48, MDE-C3-137 Le Loeuff, 2005), and *Tastavinsaurus sanzi* (e.g. MPZ99/9 Canudo, Royo-Torres, & Cuenca-Bescós, 2008; Royo-Torres, 2009). They retain the derived condition of a sigmoid fibula but with a more weakly developed curvature as in *Phuwiangosaurus sirindhornae* (e.g. P.W.1-18, Martin, Suteethorn, & Buffetaut, 1999), *Epachtosaurus sciuttoi* (e.g. UNPSJB-PV-920, Martínez *et al.*, 2004), *Aelosaurus* sp. (e.g. MPCA-27100-8) and *Saltasaurus loricatus* (e.g. PVL-4017-85). They show differences with the fibula of *L. astibiae* and *Atsinganosaurus velauciensis*, which are compressed lateromedially and lack the pronounced medial deflection of the anerolateral crest. The lateromedial compression is much more pronounced in proximal and distal ends of *L. astibiae* (e.g. MCNA-9410) and *A. velauciensis* (e.g. MMS/VBN.09.132, Díez Díaz *et al.*, 2018) in contrast with all the specimen referred to Morphotype I, including the smallest individuals (e.g. HUE-1175, HUE-7802). The fibulae of Morphotype I present small differences with *Magyarosaurus* spp. The lateral trochanter is placed in the middle of the shaft in *Magyarosaurus* spp. (e.g. NHM-R3853) contrary to the more anteriorly placed in Morphotype I (e.g. HUE-3087, HUE-1476). Both of them share the anerolateral crest medially displaced, e.g. *Magyarosaurus* spp. as seen in specimen NHM-R.3853; and Morphotype I in specimen HUE-1570. However, the fibulae of *Magyarosaurus* spp. present a bifurcated lateral trochanter, and a distal anterolateral crest greatly medially diverted with an accessory ridge extending parallel in lateral face (e.g. NHM-R.3853 and see also NHM-R.3850). Despite not all the specimens of Morphotype I present a bifurcated lateral trochanter (e.g. HUE-1513) and none share the presence of this accessory distal ridge in lateral face. Morphotype I fibulae also differ from *Ampelosaurus atacis*, which present a slightly sigmoidal fibula with anteriorly placed lateral trochanter and a low eccentric transverse section of the shaft (e.g. MDE-C3-1468). None of the referred fibulae of *A. atacis* present the anerolateral crest medially deflected, nor the anterior surface observed in the Morphotype I from Lo Hueco (e.g. HUE-3087).

The presence of a fibular knob in the posterior part of the proximal end in medial face (e.g. HUE-1476, HUE-3087) is also present in *Uberabatitan riberoi* (e.g. CPP-1107-UrHo, Salgado & De Souza Carvalho, 2008) and *Argentinosaurus huinculensis* (specimen MCF-PVH-1). This feature is not present in any of the fibulae from other Ibero-Armorican titanosaurs.

IV.II.5.2. MORPHOTYPE II ASSESSMENT

The second morphotype represents a more robust and straight hind limb. The limb are more columnar, with less lateral torsion from sagittal plane. The femora are robust, with little medial deflection of the femoral head and the distal condyles. They resemble the femora of *Ampelosaurus atacis* (e.g. MDE-C3-87, MDE-C3-1182, Le Loeuff, 2005). The shaft is also more eccentric than in Morphotype I. The proximal and distal ends are expanded lateromedially, while the anteroposterior expansion is more subtle. The femoral head is less bulbous, more compressed anteroposteriorly and slightly bevelled proximally based on the curvature of the shafts under the femoral head (e.g. HUE-3237). Specimens tend to have an upward femoral head; however few specimens attributed to this morphotype present a complete femoral head (e.g. HUE-1316, HUE-1319 and HUE-3237). They are similar to some of the specimens of *A. atacis*, which show a proximally bevelled femoral head based on the morphology of the area under femoral head (e.g. MDE-C3-513, MDE-C3-1182). Some of the specimens from Morphotype II show a proximal ridge connecting the anterior part of the femoral head and the greater trochanter (e.g. HUE-594, HUE-1319) not seen in *A. atacis* (e.g. MDE-C3-87). Both sauropods share eccentric shafts, a short lateral bulge in the proximal one fourth of the proximodistal length. The fourth trochanter in both taxa is almost in the middle of proximodistal length and medially placed, facing to posterior and not visible from anterior face (e.g. HUE-594). However, in Morphotype II it is not visible from anterior face in any of the specimens (see Gallina & Apesteguía, 2005; Mannion *et al.*, 2013), contra Morphotype I (e.g. HUE-2338, HUE-3108) and other titanosaurs such as *A. atacis* (e.g. MDE-C3-87, Le Loeuff, 2005), *Saltasaurus loricatus* (e.g. PVL-4017-83) and *Opisthocoelicaudia skarzyinskii* (e.g. MPC-D100/404, Borsuk-Bialynicka, 1977), Ibero-Armorican Titanosauria indet. Form 1 and Form 2 (Vila *et al.*, 2012).

The distal condyles are anteroposteriorly compressed and parallel between them, mostly posteriorly projected. However, in Morphotype II they extends slightly into lateral face (e.g. HUE-1316) whereas in *A. atacis* are comprised only to posterior face and slightly posteriorly bevelled in lateral or medial face (e.g. MDE-C3-87, Vila *et al.*, 2012). The distal end of the Morphotype II femora is more similar to *Antarctosaurus giganteus* (e.g. MLP-26-316), *Petrobrasaurus puestohernandezi* (e.g. MAU-Pv-PH-449/8) and Lithostrotia indet. CRILAR-Pv-509c (Hechenleitner *et al.*, 2018) with an eccentric shaft, slightly anteroposteriorly compressed proximal and distal ends but with the weak expansion of the distal end to anterior face. The lateral epicondyle is also placed toward posterior in Morphotype II (e.g. HUE-594, HUE-1319). This type of anteroposteriorly compressed distal end with lateral epicondyle facing posteriorly is also reported in more basal Titanosauriformes as in *Brachiosaurus altithorax* (specimen FMNH P25107, Riggs, 1903) and *Phuwiangosaurus sirindhornae* (e.g. P.W.1-17, Martin *et al.*, 1999). *A. atacis* shows that lateral epicondyle is shallow and directed posterolaterally (e.g. MDE-C3-87, Vila *et al.*, 2012). These features contrast with eccentric shaft, more gracile proximal and distal ends as well as expanded in anteroposterior of the femora in *Aeolosaurus* sp. (e.g. MPCA-27100), *Andesaurus delgadoi* (e.g. MUCPv-132, Mannion & Calvo, 2011), *Magyarosaurus* spp. (e.g. NHM-R.3934) and Morphotype I (e.g. HUE-1508, HUE-2338, HUE-3108).

Several specimens of Morphotype II femora are small and slightly more gracile (e.g. HUE-10007, estimated Robustness Index ≈ 0.18) and may pertain to other known small to medium sized titanosaur taxa with eccentric femoral shaft as *Atsinganosaurus velauciensis* and *Lirainosaurus astibiae*. The femora from Morphotype II do not share the medial bevelling of the distal end of the femora, especially of the tibial condyle of cf. *Lirainosaurus astibiae* (e.g. MNHN-FOX-107, MDE-C3-261, Vila *et al.*, 2012) and *L. astibiae* (e.g. MCNA-7468). The specimens referred to cf. *Lirainosaurus astibiae* are gracile (i.e. RI: 0.116-0.166, see Vila *et al.*, 2012) fall bellow the most gracile of the specimens of Morphotype II (i.e. RI: 0.2-0.25, see Table.IV.II.1). *L. astibiae* Robustness Indices (i.e. RI: 0.2-0.21, Díez Díaz *et al.*, 2013) overlap with the most gracile elements of Morphotype II; but the morphology of the distal end, and the low eccentricity (i.e. EI: 197-265%, see Díez Díaz *et al.*, 2013) are different from any specimens of Morphotype II. The Ibero-Armorican Titanosauria indet. Form 4 (specimen MCD-5031, Vila *et al.*, 2012) has eccentric femora but the fourth trochanter is displaced to the middle of the lateromedial width, and the lateral bulge is longer to those of any specimen of Morphotype II. Some of the specimens of Morphotype II present a weakly developed linea intermuscularis cranialis but not as pronounced as in the Ibero-Armorican Titanosauria indet. Form 1 (specimen MDE-C3-1278, Vila *et al.*, 2012). On the other hand, the titanosaur Form 1, Form 2 and Form 3 are much more gracile in comparisons to Morphotype II (Vila *et al.*, 2012: table 2).

The tibia-fibula of Morphotype II are much more slender and elongated (e.g. HUE-1612) than in Morphotype I (e.g. tibia HUE-3082, fibula HUE-3087) or more robust titanosaurs as *Magyarosaurus* spp. (e.g. NHM-R.3859), *Aeolosaurus* sp. (e.g. MPCA-27100), *Jainosaurus* cf. *septentrionalis* NHM-R.5903), and most of the specimens referred to *Ampelosaurus atacis* (e.g. MDE-C3-138, Le Loeuff, 2005). The tibia is gracile with a proximal end as wide anteroposteriorly than lateromedially. Some of them present some lateromedial compression. The cnemial crest is proximodistally shorter and more pointed with a triangular shape. The morphology of the proximal end and the cnemial crest is different to those of other slender tibiae as in *Atsinganosaurus velauciensis* (e.g. MMS/VBN.02.90, Díez Díaz *et al.*, 2018), *Lirainosaurus astibiae* (specimen MCNA-13860), *Rapetosaurus krausei* (e.g. FMNH-PR-2209 Curry Rogers, 2009), *Mendozasaurus neguyelap* (e.g. IANIGLA-74-2), *Petrobrasaurus puestohernandezi* (e.g. MAU-PV-449-9) and *Muyelensaurus pecheni* (e.g. MAU-PV-162). In general the presence of a robust muscular attachment in the middle of the cnemial crest is related to more robust tibiae e.g. *Saltasaurus loricatus* (e.g. PVL-4017-87), *Neuquensaurus australis* (e.g. MCS-5/25) and *"Magyarosaurus hungaricus"* (e.g. NHM-R.3853). The tibiae of Morphotype II resemble the gracile tibiae with narrow proximal end of *Huabeisaurus allocotus* (specimen HBV-20001, D'Emic *et al.*, 2013), the Titanosauria indet. Morphotype-2 from Chera, specimen MUVHN-17843 (Díez Díaz *et al.*, 2015), some specimens referred to *Ampelosaurus atacis* (e.g. MDE-C3-48, MDE-C3-1303 MDE-C3-1489) and cf. *Argyrosaurus* sp. (e.g. FMNH-P13020, Powell, 2003). However, in Morphotype II there is a marked muscular attachment that produce a concavo-convex area proximodistally elongated (e.g. HUE-1612, HUE-4055) whereas this attachment in the specimens referred to *A. atacis* presents a recess or ridge in the posteromedial proximal end (e.g. MDE-C3-970, MDE-C3-1303). The tibial proximal end in this second type of tibiae referred to *A. atacis* also presents an expanded fibular articulation (e.g. MDE-C3-1303, Le Loeuff, 2005). Contrary to this morphology, Morphotype II presents a laterally projected fibular articulation but without further expansion on the anterior part of proximal end in lateral face. None of the specimens of *A. atacis* develop the accessory ridge or convexity parallel to the fibular articulation as in Morphotype II (e.g. HUE-1612). The latter is more similar to those of the lectotype of

Laplatasaurus araukanicus (specimen MLP-CS-1128; see lateral face) and of some Titanosauriformes as the associated material of *Abydosaurus mcintoshi* (e.g. DINO-10913; pers. obs. P.M. 2018).

The distal end is weakly expanded lateromedially and anteroposteriorly, almost as wide anteroposteriorly as the shaft, and with the anterior ascending process and posterior ventral process facing posteriorly (e.g. HUE-1612, HUE-1149). Posterior projection of the anterior ascending process and posterior ventral process have been reported in *L. astibiae* (specimen MCNA-13860) and is also present in *Ampelosaurus atacis* (e.g. MDE-C3-1303, Le Loeuff, 2005), *Antarctosaurus wichmannianus* (e.g. MACN-6804 no.22), *Muyelensaurus pecheni* (e.g. MAU-PV-161), the Titanosauria indet. Morphotype-2 from Chera (e.g. MUVNH-17843, Díez Díaz *et al.*, 2015) and in some somphospondylii such as *Chubutisaurus insignis* (MACN-182-22-41), among others. The gracile morphology of the distal end with a remarkable lateromedial compression and a lateromedial width almost equal to anteroposterior width is also known in other titanosaurs as *A.atacis* (e.g. MDE-C3-1303, Le Loeuff, 2005), *Ligabuesaurus leanzai* (specimen MCF-PHV-233-18), *Mendozasaurus neguyelap* (e.g. IANIGLA-73-3) and Titanosauria indet. Morphotype-2 from Chera (e.g. MUVNH-17843, Díez Díaz *et al.*, 2015). However, this feature combination is only present in the tibia of Morphotype II and the Titanosauria indet. Morphotype-2 from Chera.

The fibula is mediolaterally compressed and the anerolateral crest expands to anterior in lateral or medial face and the contour is D-shaped in proximal face, similar to *Alamosaurus sanjuanensis* (e.g. TMM-43621-1, Lehman & Coulson, 2002), *Epachthosaurus sciuttoi* (e.g. UNPSJB-PV 920, Martínez *et al.*, 2004; Ibiricu, Martínez, & Casal, 2018), *Mendozasaurus neguyelap* (specimen IANIGLA-74-3), *Aelosaurus* sp. (e.g. MPCA-27100/9) and *Lirainosaurus astibiae* (e.g. MCNA-14471. Morphotype II fibulae are much more compressed than the fibulae of *Aeolosaurus* spp. (e.g. MPCA-27100/7) and the shaft of *A. sanjuanensis*. The lateromedial compression of morphotype II also differs to other slightly more robust and lateromedially expanded fibulae as those of *Rapetosaurus krausei* (e.g. FMNH PR 2209, Curry Rogers, 2009), Morphotype I (e.g. HUE-3087, HUE-1476), *Magyarosaurus* spp. (e.g. NHM-R3850) and *Aeolosaurus* sp. (e.g. MPCA-27100/7). There is an accessory shallow ridge parallel to the anterolateral crest in some specimens (e.g. HUE-1612) but it is not as marked as the feature accessory crest of *Lohuecotitan pandafilandi* (e.g. HUE-3087). Instead, this accessory ridge in the anterior face of proximal end is more similar to the shallow ridge seen in some specimens of *L. astibiae* (e.g. MCNA-14471). However, not all the specimens referred to Morphotype II present this ridge (e.g. HUE-1082) and this character weakly developed in *L. astibiae* is also variable (e.g. MCNA-9410). The lateral trochanter is placed in the middle of the anteroposterior width of the shaft, differing from the more anteriorly placed trochanter of Morphotype I (e.g. HUE-1476, HUE-3087) and some specimens referred to *Ampelosaurus atacis* (e.g MDE C3-137, Le Loeuff, 2005). The lateral trochanter is also placed in Morphotype II in the proximal third of the proximodistal height of the shaft as in *M. neguyelap* (specimen IANIGLA-74-3), differing from the more distally placed lateral trochanter of *L. astibiae* (e.g. MCNA-7472, MCNA-9410). In addition, the lateral trochanter is narrow and crest-like differing from the more massive and oval-shaped lateral trochanter seen in Morphotype I (e.g. HUE-1175, HUE-3087), *Laplatasaurus araukanicus* (e.g. MLP-CS-1127), *Magyarosaurus* spp. (e.g. NHM-R.3850) and *Neuquensaurus australis* (e.g. MCS-5/26). While most of the specimens develop the anteroproximal fossa in the anterior to lateral part of the anterolateral crest and the proximal part of the lateral trochanter, none present the anteroproximal margin (sensu Gallina & Otero, 2015) as in other titanosaurs with a gracile fibula as *M. neguyelap* (specimen IANIGLA-74-3).

The distal end is only preserved in some of the fibulae but it has a triangle-shaped distal outline as common in titanosaurian as *Alamosaurus sanjuanensis* (e.g.TMM-43621-1, Lehman & Coulson, 2002), *Laplatasaurus araukanicus* (e.g. MLP-CS-1127), *Bonatitan reigi* (specimen MACN-PV-RN-821/4), *Bonitasaura salgadoi* (e.g. MPCA-460) and *Lohuecotitan pandafilandi* (e.g. HUE-3082) among others. The only variation observed is the relative position between the height of anterior and posterior part of the distal end. This is related to the development of the anteroposterior sigmoid shaft in lateral face and the consequent anterior projection of the fibular proximal end. More sigmoid specimens present proximal deflection of the anterior part of the distal end (e.g. HUE-1082).

There are few differences between both morphotypes from Lo Hueco. The Morphotype II presents a shorter and more distally developed anerolateral crest (e.g. HUE-1082) while in the Morphotype I is proximodistally longer and more slightly medially deflected (e.g. HUE-3087).

IV.II.5.3. MORPHOMETRICS ANALYSES

The analysis of femoral shape variation through PCA shows significant differences between two proposed morphotypes in PC1 and PC6 for the complete dataset (Kruskal-Wallis report Table .V.2.8, Procrustes PERMANOVA Table.IV.II.9). Main variation along PC1 shows differences in the anteroposterior compression of the proximal and distal ends, eccentricity of the shaft and presence of a probable linea intermuscularis cranialis among more positive values (Fig.IV.II.5, 10 and 12). The variation along PC6 differences the femora with slightly compressed distal ends in anteroposterior, more posterior expansion of the tibial condyle, and more robust and anteroposteriorly compressed shaft in negative value against positive values along PC6 that represent specimens with more subcircular shaft, more anteroposteriorly wide distal end, and lateromedially narrow midshaft and distal end. The taphomorphospace of Morphotype II is placed in the negative values whereas taphomorphospace of Morphotype I is present in values that are more positive.

The variance described by PC1 and PC6 is congruent with main morphological differences found between sauropod taxa (see before). The taphomorphospaces of both morphotypes overlap toward negative values, and the morphotype assessment of several of the specimens may be discussed based on k-means clustering alternatives. Among the Morphotype I specimens recovered in more negative values, the femur of HUE-EC-06 and HUE-EC-13 as well as specimen HUE-1508 do not present a proximally deflected femoral head. Specimen HUE-1508 (R.I. = .23, see Table.IV.II.1) is slightly more robust than other specimens referred to Morphotype I (e.g. HUE-3108, R.I. = .22). HUE-EC-06 and HUE-EC-13 present femora with similar robustness to other specimens of Morphotype I, but slightly more eccentric shaft and lighter anteroposterior compression of proximal and distal ends. These specimens also present a linea intermuscularis cranialis, a more bulbous femoral head in HUE-EC-06 (specimen HUE-2420), fourth trochanter displaced to medial edge and with distal end slightly medially bevelled (specimen HUE-2420). These features are referable to the Morphotype I and also recovered by the landmarks that are present in more positive values of PC1 that correspond to the taphomorphospace of Morphotype I. The two specimens referred to Morphotype II that are recovered near the point 0 and positive values (i.e. HUE-1187, HUE-3583), which present slightly eccentric shafts, without medial displacement of the femoral head, anteroposteriorly expanded distal end and medially placed fourth trochanter. Specimen HUE-3583 presents a shaft with a light convexity, probably related

with the linear intermuscularis cranialis in anterior face. The displacement of fourth trochanter to medial, the anteroposteriorly expanded distal end and the presence of a linear intermuscularis cranialis increase toward more positive values (Fig.IV.II.10 and 12). However, the analysis might be affected by missing data and the estimation method, as the specimens HUE-1183, HUE-1187 and HUE-3583 lack part of the proximal and distal ends and the shaft of specimen HUE-1183 and HUE-3583 are slightly crushed proximodistally.

The analysis of k-mean clustering of the PC shape variables suggests two to three clusters as the most optimal grouping hypotheses. The two groups hypothesis includes the specimens HUE-1508 and the femora of HUE-EC-06 and HUE-EC-13 into the space of Morphotype II, while HUE-1187 is placed on the cluster of Morphotype I.

The three groups hypothesis subdivides the described taphomorphospace in two groups in point 0 and negative values of PC1 and Morphotype I (with part of the described specimens) in positive values (Fig.IV.II.9). The Morphotype II is recovered with some of its characteristic specimens (e.g. HUE-594, HUE-1316, see Description) in negative values of PC1 and PC2. The third cluster include the femora of HUE-EC-05, HUE-EC-13, and the specimens HUE-1187, HUE-1590 and HUE-2903. This third cluster could represent femora with slightly compressed proximal and distal ends, not as much as in most of the specimens described in Morphotype II (e.g. HUE-1316). The lateral bulge is shorter than in *L. pandafilandi* (specimen HUE-3108), but not reduced to the proximal one fourth of the proximodistal length (e.g. HUE-1366). The fourth trochanter is placed proximally (e.g. HUE-2903). While the distal end is proximodistally compressed, PC2 positive values represent some degree of medial deflection of the tibial condyle (e.g. HUE-1366). However, some of the specimens included in this cluster does not share all these traits as k-means separates based on dispersion from the centroid of Morphotype II taphomorphospace and found them too far from its mean shape. HUE-1183 is a slender specimen from Morphotype II, but have an anteroposteriorly compressed shaft. There is a *weakly* developed linea intermuscularis cranialis in anterior face of HUE-1183, similar to the one present in HUE-594 and contrary to greatly developed linea intermuscularis cranialis within a convex anterior face of the shaft seen in Morphotype I. Proximal and distal ends are fragmentary and these landmarks are estimated. Other specimens similar to HUE-1183 like HUE-1357 are recovered in the cluster of Morphotype II. The specimen HUE-1187 on the contrary is much more robust, clearly compressed anteroposteriorly, with the *weakly* developed linea intermuscularis cranialis as those of the specimens of Morphotype II (e.g. HUE-594 and HUE-1316). These specimens are completely different to other elements recovered in this cluster (e.g. HUE-1366, HUE-2903) except for the light medial deflection of the tibial condyle and distal end (which is present in specimen HUE-1187, in positive values of PC2).

We consider here that the presence of a third morphotype is unlikely, as some of the specimens referred to this cluster can be considered more similar to Morphotype II (e.g. HUE-1187) and the lack of some specimens that resemble the commented features of this cluster (e.g. HUE-1357, HUE-3237) are placed in Morphotype II cluster. This third cluster is also not corroborated by the cluster analysis of procrustes distances (Fig.IV.II.8) where several specimens are found close to Morphotype II main cluster and other are grouped in Morphotype I or intermingled with specimens from Morphotype I and Morphotype II (e.g. HUE-1183 femur of HUE-EC-13).

The PERMANOVA over procrustes configurations (Table.IV.II.9) result in significant differences among the defined morphotypes and all the alternative grouping hypotheses (see Group

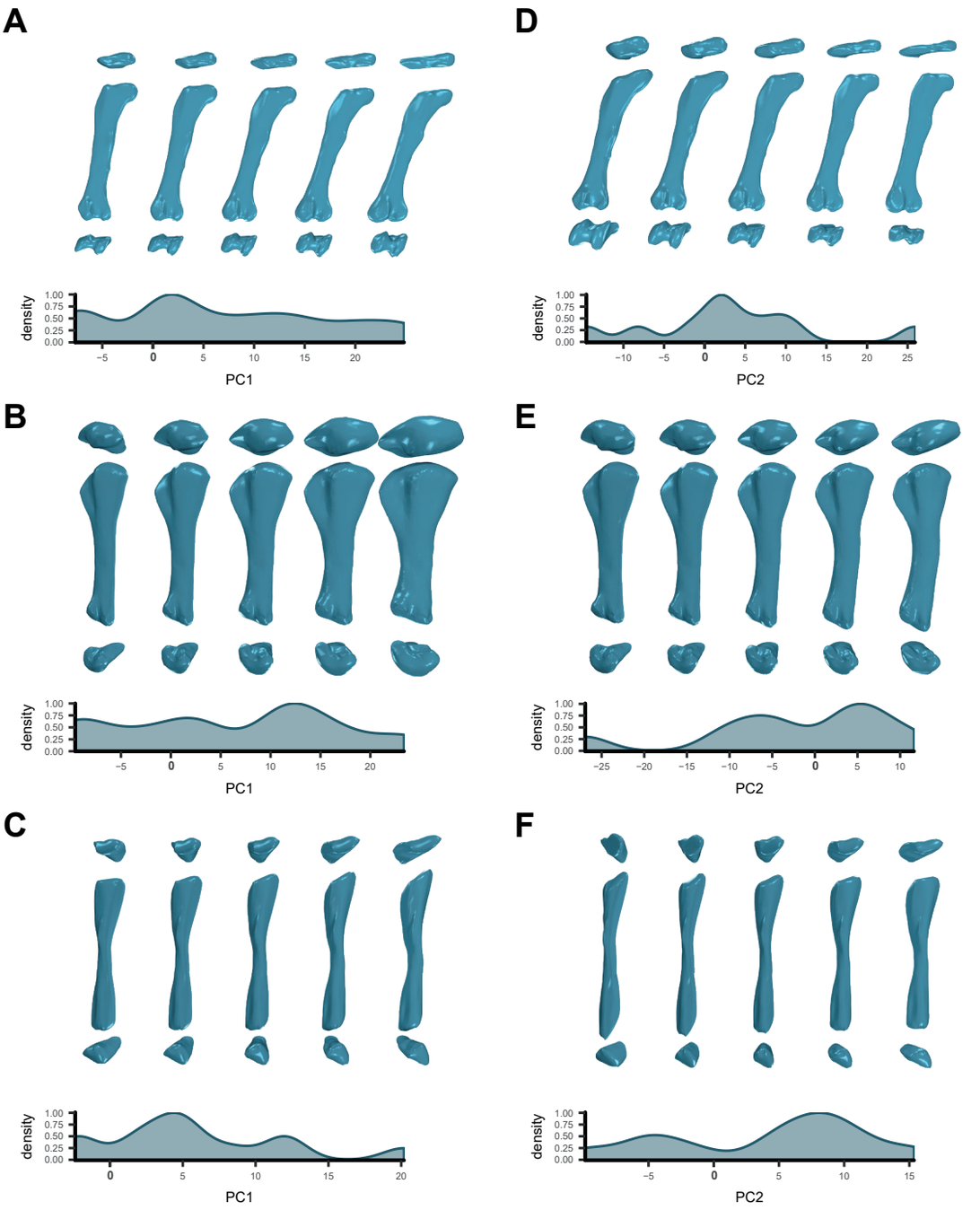

Fig.IV.II.12. Morphological variation in Morphotype I in each shape PCA. *Femora:* (A) Along PC1 axis. (B) Along PC2 axis. Tibiae: (C) Along PC1 axis. (D) Along PC2 axis. Fibulae: (E) along PC1 axis. (F) Along PC2 axis.

differences). The k = 2 groups distribution present slightly better results than k= 3 grouping hypothesis (Fk=2 = 4.429 against Fk=3 = 4.015). The account of total variance explained range from 13.6% considering two femora morphotypes, to 20.7% considering the two clusters suggested by k-means clustering over shape PCA variables. The intraspecific variability found in the sample is 79.3-86.4% of the total variance found in the procrustes configurations. We can consider instead the variance explained by the shape PCA in the PCs that present significant differences among morphotypes: 27.09% of total variance (PC1: 20.25%, PC6: 6.84%). The variance not relatable to morphotype differences is 72.91% of the total, slightly less than in the direct analysis of the procrustes coordinates. The variation not attributable to morphotype or taxonomic differences affects to the relative position of the femoral head, with medial displacement respective to the greater trochanter and the proximal part of the lateral bulge (see Fig.IV.II.5). There is some variation within each morphotype in the midshaft eccentricity (e.g. HUE-1366 and HUE-2338 in Morphotype I, specimen HUE-594 and HUE-3583 in Morphotype II), and also the relative proximodistal position of the fourth trochanter respective to the midshaft (e.g. HUE-1366 and HUE-3108 in Morphotype I; see similar results within morphotypes in Vila *et al.*, 2012). There is also variation in the relative anteroposterior development between the tibial condyle and fibular condyle in posterior face: i.e. a tibial condyle much more posteriorly expanded, far from the fibular condyle specimen HUE-2338 in more negative values of PC2, identical condyles posteriorly expanded in specimen HUE-1366 in more positive values of PC2. There is also a slight variation in the anterior face of the outline of the midshaft, with some concavity in the middle of the lateromedial width (e.g. positive values of PC2, negative values of PC3). This is because there are some specimens with marked convexity and a linea intermuscularis cranialis in the Morphotype I (e.g. HUE-1366, HUE-3108) whereas there are specimens that do not have these features (e.g. HUE-2338, negative values of PC2). There are some specimens of Morphotype II that present a linea intermuscularis cranialis with some convexity of the midshaft (e.g. HUE-1590) while most of them do not present this marked convexity (e.g. HUE-1357) even among those femora that present a linea intermuscularis cranialis in Morphotype II (e.g. HUE-594).

The analysis of the PCA shape variables on the tibia presents significant differences between the morphotypes in PC1. This PC represents the variation between slender specimens with anteroposteriorly and lateromedially narrow proximal end, more anteroposterior short cnemial crest with subtriangular morphology, and gracile midshaft and distal end in more negative values, represented by Morphotype II taphomorphospace (e.g. HUE-1612; see Fig.IV.II.8 and 13). Less negative values near point 0 to positive values shows specimens referable to Morphotype I taphomorphospace, presenting progressively more anteroposterior expansion of tibial head, much greater than the midshaft,; and with the cnemial crest anteroposteriorly expanded. The midshaft is slightly lateromedially narrower and the distal end is robust, lateromedially wider than anteroposteriorly (e.g. HUE-2799, HUE-3082).

The result of the PC1 is congruent with anatomical differences between the tibiae in comparison with other sauropod taxa (see Discussion before). It is also noticeable in the negative values of PC1, with slender and elongated tibia, with a tibial head and distal end as anteroposteriorly wide as lateromedially. It represents a unique combination of features of the tibiae of Morphotype II (only found in other titanosaurs such as *Ampelosaurus atacis*, Le Loeuff, 2005; Titanosauria indet. Morphotype-2 from Chera, Díez Díaz *et al.*, 2015).

The k-means clustering over the procrustes PCA shape variables resulted in two and three

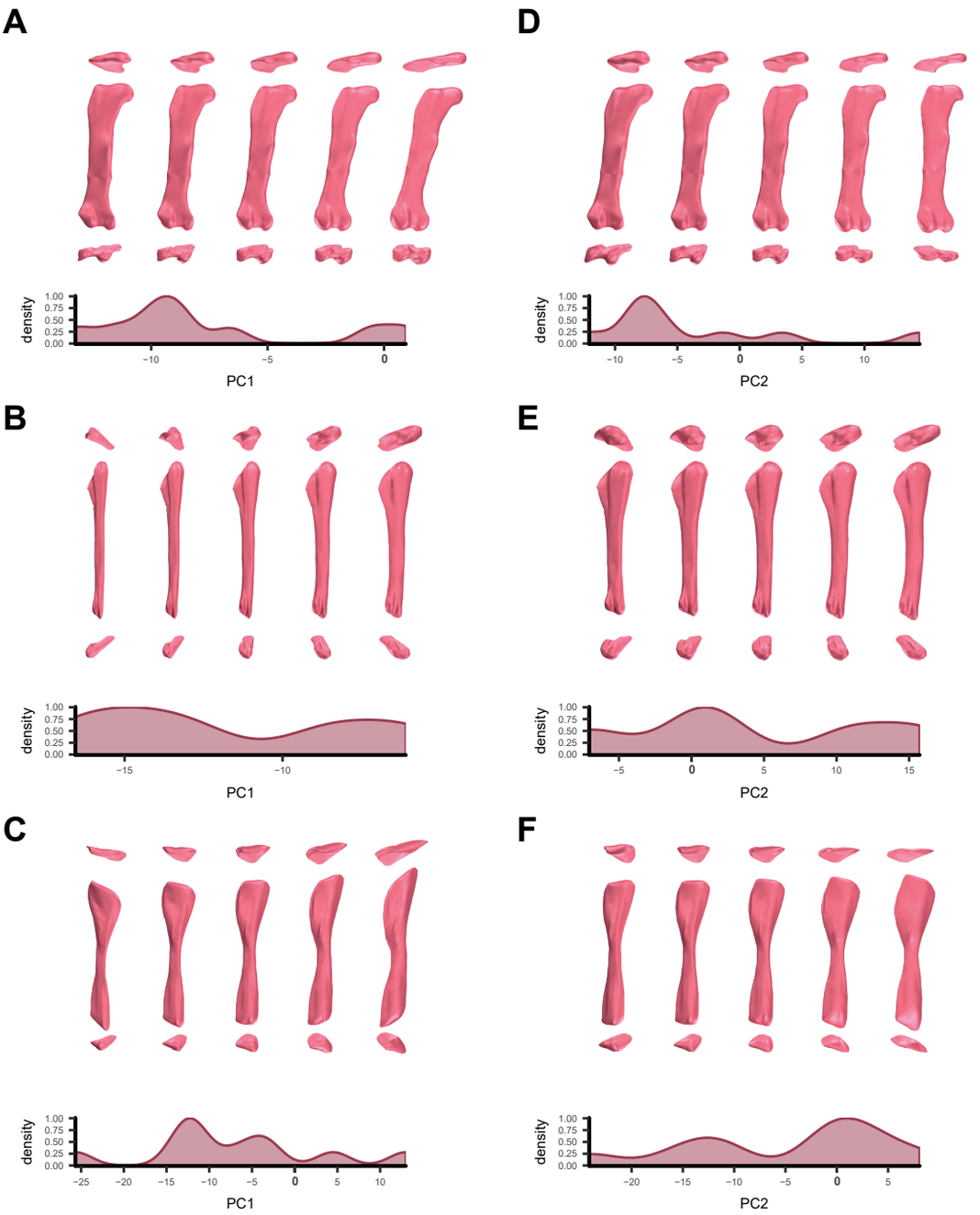

Fig.IV.II.13. Morphological variation in Morphotype II in each shape PCA. *Femora:* (A) Along PC1 axis. (B) Along PC2 axis. Tibiae: (C) Along PC1 axis. (D) Along PC2 axis. Fibulae: (E) along PC1 axis. (F) Along PC2 axis.

different groups as the most optimal solution among the sampled specimens (Fig.IV.II.10). The hypothesis with two probable groups resembles the initial morphotype description with small differences. There are three specimens at point 0 values of PC1 and PC2 that are suggested as Morphotype II instead of pertaining to Morphotype I (Fig.IV.II.10). This hypothesis found a cluster in positive values without the overlapping at 0 point values that is the remaining Morphotype I as described before. The specimen HUE-2669 present a slightly lateromedial compressed shaft, a cnemial crest anteriorly expanded with a developed and slightly distal muscular attachment in the middle of cnemial crest. It lacks the proximal most part and part of the distal end, which is laterally to slightly posterolaterally bevelled. The specimen HUE-2669 is similar to HUE-4632. The cnemial crest is fragmentary in the proximal end, but is longer than those of Morphotype II. The tibia of HUE-EC-06 is elongated, slender and with marked fibular articulation but restricted to the lateral of the tibial proximal end. It seems that there is no ridge of the fibular articulation parallel to the cnemial crest, somewhat visible in lateroposterior proximal part of the shaft. However, the presence of a ridge of the fibular articulation extending parallel to the cnemial crest cannot be disregarded due to the presence of sediment obscuring this area. Only the tibia HUE-EC-06 (specimen HUE-2425) resembles in some features to other specimens referred to Morphotype II. The specimens HUE-2669 and HUE-4632 present a longer cnemial crest and the proximal and distal ends, while fragmentary, are not as anteroposteriorly narrow as other specimens of Morphotype II (e.g. HUE-1612). However for the analysed landmarks, the proximal and distal ends are very narrow, barely expanded respective to the shaft section and it is probably exaggerated by the landmark estimation method in these specimens. The three clusters alternative hypothesis presents two groups similar to Morphotype I and Morphotype II as described here, except for a new cluster along negative values of PC2, reassessing some specimens of Morphotype I. Morphotype I loss the specimens HUE-1573, HUE-2669, HUE-4344, HUE-4632 and separates from centre values of PC1 and PC2 (Fig.IV.II.10).

Two groups are present in negative values of PC1 and separated along values of PC2 (Fig. IV.II.10). The specimens from the "blue" cluster are in negative values of PC1 and positive values of PC2 and are the described Morphotype II except for specimen HUE-2117 which is regarded into the third cluster. The specimens in PC2 positive values present expanded posterior part of the posterior proximal end, with more oval-shaped instead of triangle-shaped proximal end, and an accessory fibular trochanter. The distal end is also laterally or posteriorly rotated in positive values of PC2. The cluster near 0 point and negative values of PC1 and negative values of PC2 (Fig.IV.II.10.c: cluster #1 or "cyan") group specimens with narrower posterior part of proximal end, a longer cnemial crest and slightly more anteroposterior expanded distal ends. However, the third group in negative values of PC2 does not represent a coherent morphology that can be referred to only one morphotype. The specimens HUE-1612, HUE-2117 and HUE-4055 from Morphotype II present morphological similarities and combination of features despite the reassessment of HUE-2117 into the third cluster. Among the few differences in these specimens, there is a greater posterior development of the proximal end in specimen HUE-2117, the relative length of cnemial crest and the lateral displacement of the distal end. However, differences are minor and other specimens also present displacement of the distal end in both morphotypes. Also, specimen HUE-2117 lacks the posterior part of proximal end, and this expansion in the landmarks can be exaggerated by the estimation method (see similarities between HUE-1149 and HUE-2117 despite it distance along PC2). Other sauropod taxa also present variable morphology in these features of the tibiae (e.g. *Ampelosaurus atacis*, see Le Loeuff, 2005; *Bonatitan reigi*, see

Salgado, Gallina, & Paulina Carabajal, 2015). It is noticeable in the tibiae of *Bonatitan reigi* right tibia MACN-PV RN 821 presents more expanded posterior part of proximal end than in the left tibia MACN-PV RN 821, which has triangular-shaped outline in proximal. The proximal end is also different to the posterior part of the proximal end of tibia MACN-PV RN 1061 (the anterior part has been lost). Also the distal end of the left tibia MACN-PV RN 821 faces lateral while the anterior ascending process and posterolateral process of the left tibia MACN-PV RN 1061 face to posterior. This variation are similar to the variation seen in specimens from Morphotype I and Morphotype II along PC2 that conditions the k = 3 clusters hypothesis in this case.

The cluster analysis of the procrustes distances between the specimens shows two major clusters coinciding with the morphotypes described in the sample (Fig.IV.II.8.c). Another possibility is interpreting the major cluster of specimens from Morphotype I as two subclusters (Fig.IV.II.8.c). However, in doing so, none of these alternatives distributions resemble the clusters suggested the k-means algorithm. Also when analysed the procrustes configurations via PERMANOVA, only the initial grouping hypothesis and from k = 2 up to k = 4 clusters hypotheses are significant ($p < .05$). The hypothesis of k = 3 clusters explain less variance of the sample (Finitial = 3.971, Fk=2 = 5.516, Fk=3 = 2.775, see Table.IV.II.9). The most optimal distribution in the available sample is the presence of two morphotypes among the tibiae, whether we consider the initial description or the alternative offered by the algorithm. The hypothesis of three clusters in the sample cannot be regarded to three different tibiae morphotypes, and therefore it is rejected. The test also shows that the variance explained by group differences ranges from 21% to 35%. It is similar to the femora, which majority of the sample variance is referable to within morphotype variation (79-65%). If we consider the variance explained from PCA shape variables, 30.1% variance of the sample summarize morphological differences between the morphotypes (PC1 present significant differences between groups), while 69.9% of the total variance can be related to intra-morphotype variability.

The analysis of fibula PCA shape variables shows significant differences between the proposed morphotypes for PC1 and PC2 (Table.IV.II.8). The variation along PC1 summarized variation between slightly lateromedially wider fibulae with more anteriorly placed lateral trochanter and anterolateral crest medially deflected in positive values and lateromedially narrower and much more gracile specimens in more negative values (see Fig.IV.II.7.a and 12). The PC2 show similar results (Fig.IV.II.7.b and 12), with the more robust and anteriorly leaning sigmoid shaft in positive values, and more gracile with posterior leaning sigmoid in negative values. The taphomorphospace occupied by Morphotype I is in the positive values of PC1 and PC2 while Morphotype II present specimens in negative values of PC1 and PC2. Along these two PCs there are also differences in deflection and length of the anterolateral crest. Positive values of PC1 and PC2 present longer anterolateral crest, more directed toward medial, while negative values present shorter but more anteriorly expanded anterolateral crest. There is also a difference between more anteriorly placed lateral trochanter in positive values of PC1 and more laterodistally and smooth curve of the lateral trochanter in negative values of PC1. These morphological differences have also been found between specimens of different sauropod taxa (see before) and are congruent with taxonomical differences.

The k-mean analysis over the PCA shape variables resulted in two groups as the most optimal hypothesis. The two groups resultant are similar to the described morphotypes except for allocation of two specimens from Morphotype I regarded as Morphotype II (HUE-1570, HUE-EC-06) and three specimen of Morphotype II to Morphotype I (specimens HUE-1146, HUE-2804, HUE-2977; see Fig.IV.II.11). The k-mean algorithm seems to differentiate the two groups

based mostly on PC1 differences, as both morphotypes do not overlap in the initial description but in the k-means solution the two groups are separated in PC1 values (see Fig.IV.II.11.b).

The specimen HUE-1570 and the fibula of HUE-EC-06 (specimen HUE-2426) have a quadrangular outline of the proximal end. They also have medial deflection of the anterolateral trochanter and the lateral trochanter is anteriorly projected. The sediment hides the proximal part of the anterior face and the medial face of the fibula of HUE-EC-06, but overall morphology of the anterolateral crest can be seen in the proximal and in the medial face of the shaft. All morphological features indicates that, at least HUE-1570 can be referred to Morphotype I with confidence. The specimen HUE-1146 is slightly wider lateromedially but the lateral trochanter is placed in medial part of the shaft and the anterolateral crest is not medially deflected. The specimen HUE-2977 presents slightly lateromedially compressed shaft as HUE-1146 but the lateral trochanter is placed more anteriorly thought it is not oval-shaped as in most specimens of Morphotype I (e.g. HUE-3087) and present some weakly bifurcated crest instead. The specimen HUE-2804 is fragmentary and from the cited features it can only be seen some anterior displacement of the lateral trochanter but not as marked as in other specimens of Morphotype I (e.g. 1570, HUE-3087).

The specimens HUE-1570 and probably HUE-1146 and HUE-2807 could be referred to Morphotype I. Specimen HUE-2977 resembles most of the specimens of Morphotype II and the cluster analysis of the procrustes configurations shows morphological similarities with one unique cluster of Morphotype II specimens. The specimen HUE-2426 presents few differences with other specimens which bear most of the defining features of morphotype I (e.g. the fibulae HUE-3087, HUE-3075 from individual HUE-EC-01). However, the absence of information on the anterolateral crest make impossible to disregard the affinities of this specimen to Morphotype II. The PERMANOVA over the procrustes configurations shows significant results for all grouping hypotheses, but k = 3 groups hypothesis is found as the most suboptimal of all the results of the algorithm, without barely improving the morphotype distribution as commented before. The variance explained by group differences range between 9.3% and 16.8% of variance on the shape configuration. If we consider instead the PCA shape variables, the two PCs that present significant differences between the two morphotypes explain 36.63% variance (PC1: 19.82%, PC2: 16.81%, Supplementary Material.IV.II.B). This result in 63.37% of variance attributable to intra-morphotype differences.

All the analyses found two main groups among the sample as the most optimal distribution, coinciding mostly with the initial morphotype definition. The k-means alternative clusters suggests different clustering for all the specimens of the individual HUE-EC-06. This hindlimb resemble in some features the combination of characters described in HUE-EC-01. The femur of HUE-EC-06 is more gracile and slightly less eccentric than the femur of *Lohuecotitan pandafilandi* (RI of EC-06: .21, ECC of EC-06: 194.13%, RI of EC-01: .22, ECC of EC-01: 250%). However, the tibia and fibula are much more gracile (see Table.IV.II.2 and 3), and several of the features analysed via comparison in hand and landmark geometric morphometrics are not visible by the sediment. This is especially noticeable in key features such as the projection of the proximal anterolateral crest of the fibula or the presence of a ridge in the fibular proximal articulation of the tibia. All the landmarks associated with main morphological features have been estimated instead.

Some specimens resemble small-sized titanosaur *Lirainosaurus astibiae* (see Discussion before), but our analyses did not find them as morphologically different from the described morphotypes or their alternative hypotheses. It would be possible to detect the presence of small sized

titanosaur taxa if the smallest specimens of the sample were clustered together. Our results do not cluster the smallest specimens in one cluster, so this hypothesys is unlikely. We also assessed several of the smallest specimens to Morphotype I (e.g. the femora HUE-2636, HUE-8801) and possible related with probable juvenile specimens of this titanosaur form. However, it is necessary to include a comparison with the specimens referred to *L. astibiae* in order to disregard this hypothesis. Some variability is observable in Morphotype II and could be associated with taxonomic differences whether it is a form closer to *L. astibiae* or other indeterminate titanosaur. Several of the alternative hypotheses recovered by the k-mean algorithm separates the Morphotype II taphomorphospace. However, Morphotype I is recovered in all the analysis with little differences from its initial definition and the allocation of the specimens referred to this group.

IV.II.5.4. MORPHOTYPE I AND *LOHUECOTITAN PANDAFILANDI*

Most of the specimens referred to Morphotype I present many of the morphological features of the hindlimb of *Lohuecotitan pandafilandi* (specimen HUE-EC-01). Morphotype I presents similar hindlimb morphology, with slightly more slender femora with subcircular shaft section and anteroposteriorly expanded distal condyles, robust tibiae with lateromedially expanded proximal and distal ends and robust fibulae with the characteristic deflection of the anterolateral crest, presence in some specimens of the accessory crest in proximal end and anteriorly placed lateral trochanter. Morphological differences related to small changes in the height of the fourth trochanter, bevelling of the lateral epicondyle, eccentricity of the shaft of the femur, as well as the proximodistal development of the fibular articulation of the tibia or small changes on the proximodistal development of the anterolateral crest in the fibula can be related to intraspecific variation. All the analyses show that these differences cannot be related with probable taxonomic differences, neither in our initial hypothesis or in the alternatives found by the k-means algorithm. Comparisons with other sauropod taxa are congruent with shape configuration analyses and with observation of some feature variation, as the presence of a bifurcation of the lateral trochanter of the fibula, a more crest-like trochanter, or an oval-shaped trochanter. In fact, *L. pandafilandi* shows some individual variation in those features, as it presents a slightly lateromedial compression of the fibula, a more crest-like lateral trochanter (fibula HUE-3075), more robust and less eccentric section in the shaft and more anteriorly placed fibular lateral trochanter with a robust, oval-shaped muscular attachment (specimen HUE-3087).

IV.II.5.5. CAVEATS OF THIS STUDY

Two main caveats of this study must be discussed. One is the landmark and semilandmark estimation techniques and their implications on posterior analyses. Some authors suggest that the specimens with missing values may be directly excluded from the analysis (see Little, 1988; Gornbein, Lazaro, & Little, 1992; Wiens, 2003). Missing data are common in paleontological data and techniques to reconstruct the morphology or data estimation is unavoidable in some studies (Little, 1988; Wiens, 2003; Hammer & Harper, 2008; Neeser, Ackermann, & Gain, 2009; Gunz *et al.*, 2009; Zelditch *et al.*, 2012a; Brown *et al.*, 2012; Arbour & Brown, 2014; Clavel, Merceron, & Escarguel, 2014; Lautenschlager, 2016b). However, both the estimation method and the reduction of variables

and/or specimens with missing information can lead to distinct and possibly biased results. Unfortunately, the exclusion of specimens with missing information reduces significantly the size of the available sample (Gauthier, Landry, & Lapointe, 2003) which can have an important impact on the results of studies on paleontological samples (Proschan *et al.*, 2001; Gauthier *et al.*, 2003; Strauss & Atanassov, 2006; Nakagawa & Freckleton, 2008; Arbour & Brown, 2014; Clavel *et al.*, 2014).

Therefore, the choice between the dataset reduction and the estimation of morphometric data come with a trade-offs of each choice. We addressed missing data with a consensus methodological choice between reduction of sampled landmarks and the use of estimation methods for landmarks and semilandmarks. Also for this regard, we slided the semilandmarks with the use of minimum bending energy and an approximation based on the landmark point cloud in absence of the complete specimen mesh when the original specimen is fractured and have lost some features. This method is based on the same algorithm of Gunz *et al.* (2009) of TPS that can be used both for sliding of curve and surface semilandmark, and for estimation of landmark coordinates based on the correlation among nearest landmarks.

Use of these correlation or covariation methods to estimate landmarks has been developed and refined over last decades (Oba *et al.*, 2003; Strauss, Atanassov, & Alves de Oliveira, 2003; Brown *et al.*, 2012; Dray & Josse, 2015). However some studies suggest that the extensive use of these imputation methods may exaggerate covariation effects, underestimate variances and potentially lead to errors of type I (Little, 1988; Gornbein *et al.*, 1992; Strauss *et al.*, 2003). Also, they are ultimately dependent on the availability of sampling of complete specimens and sample number for a good power of the estimation method and reliability. The lack of sample and/or the missing data on the available data may reduces their reliability (Strauss *et al.*, 2003; Brown *et al.*, 2012; Clavel *et al.*, 2014). Despite the sample of Lo Hueco represents an unusual sample among sauropod taxa (see Introduction) the number of available specimens is still a problem that is also found in the present sample.

Results for some specimens suggest that the estimation method and the effect of taphonomical deformation may be exaggerating some morphological patterns and the altering the position of the specimen in the taphomorphospace. As discussed before, one example of this effect can be related to the PC2 variation in proximal and distal ends of the fibulae. There is some variation in the deflection of the fibular ends in each of the morphotypes described in this work (e.g. HUE-1476, HUE-1570 and HUE-3087). However, this variation is not as accused as the analysis of the landmarks suggest. The proximal and distal ends of the fibulae are fragmentary in many specimens, and the lack of complete fibulae may be producing that many landmark configuration present an exaggeration on the dorsal or ventral deflection of one of those ends (e.g. HUE-1335 incomplete specimens with the landmark configuration estimated for the proximal end).

For this reason we have decided to discuss the results of the clustering methods with the anatomy of other known taxa and opted for more conservative solutions when possible. The other option was to reduce the dataset in order to estimate less missing data as other studies suggest to proceed (e.g. Hammer & Harper, 2008).

Results from the analyses complete landmark datasets are much more informative than the results from the reduced sets of landmarks. Except in the analysis of the tibiae, all the reduced datasets show worse results, with few differences between the taphomorphospaces. The fibulae and femora reduced landmark datasets results in non-significant differences

between morphotypes in any PCA shape variable. This may be caused by the lack of information in areas that are related with morphological differences between sauropod taxa as seen in the comparative anatomy. It is preferred the inclusion of more landmarks besides needing estimation of more landmarks, than down sample the structure of key morphological features. However, further testing of the accuracy and probably with a selective procedural algorithm of the best (less missing values) dataset (e.g. Strauss & Atanassov, 2006) might be required in future studies to palliate the effect of taphonomy as commented before.

Other caveat in present study is the use of k-means algorithm for classification.These algorithms are dependent on the sample as they require to assess iteratively the predefined number of groups with the lowest similarities between them (see Hastie *et al.*, 2000). This means that very similar titanosaurs with morphospace overlapping could not be classified correctly with this method (see original algorithm by Hastie *et al.*, 2000; see also differences in algoirthm in Morissette & Chartier, 2013). The effect of common taphonomical deformation may also produce artefacts like the one commented before, reducing the between group variance among the sampled sauropod groups. The k-means uses the calculation of group centroid to assess the sum of squares / Euclidean distances between the specimen and the mean of the group (Macqueen, 1967; Hastie *et al.*, 2000). Thus, the group centroid is biased by size of the sample and larger groups, which produce morphospace overlapping and larger centroids, may obscure small and unevenly distributed groups. This method does not translate the multivariate sample to a tangential space which maximizes the differences like a discriminant analysis do (Claude, 2008; see Hammer & Harper, 2008) but can be used with "*unlabelled*" data for exploring grouping of specimens in the sample. This theoretical problem is addressed using the k-means results backed by other qualitative observations with the comparative anatomy, a suggested use according to other authors (e.g. Bookstein, 2015).

In future studies this effect may be tested and probable solutions could be use of other machine learning methods, including refining the k-mean algorithm with the use of a Learning Vector and/or a Gaussian function (see Morissette & Chartier, 2013). However, for this study, the Fisher's algorithm implemented in R was used and the results have been discussed in the light of the k-mean algorithm theory.

IV.II.6. CONCLUSIONS

For the present sample of hindlimb elements from Lo Hueco referred to Lithostrotita, it has been identified two main morphotypes. Without taking into account the size variation and possible allometrical effects, there are two main groups of femora, tibiae and fibulae. These groups present differences attributable to possible taxonomical differences as they are beyond the intraspecific variation observable in other Ibero-Armorican forms like *Ampelosaurus atacis* or *Lirainosaurus astibiae*, and also in other titanosaurian forms with multiple specimens of hindlimb elements. These results are congruent with previous works on the cranial material of Lo Hueco. The presence of some articulated or partially associated titanosaurian sets (e.g., HUE-EC1 - holotype of *Lohuecotitan pandanfilandi*) that can be attributed a unique individual indicates that the femoral, tibial and fibular Morphotype I can be referred to the same taxon. Similarly, we also can conclude that the tibial and fibular Morphotype II belongs to the same taxonomic unit (they are found in partial articulation: e.g. HUE-1612). The femoral Morphotype

II was not found in association with the fibular and tibial Morphotype II. However, the most parsimonious hypothesis would allow to refer these elements to same form. It is possible that individual HUE-EC-06 may pertain to Morphotype II instead of Morphotype I; however, assessment with description of material of other parts of the skeleton may be necessary.

The analysis of shape variations within groups, permit us to assess some patterns affecting the proportion and position of some of the principal morphological structures of each element. Some of these characters are found in the specimen description and summarized in geometric morphometric analysis. For example the relative position of the fourth trochanter and the presence of a linea intermuscularis cranialis in the anterior surface of the femur is observed in both analysis. The linea intermuscularis cranialis is generally absent in the femora of Morphotype II and the fourth trochanter is positioned more posteriorly than posteromedially. On the contrary the Morphotype I presents a marked linea intermuscularis cranialis, recorded by the landmarks on the midshaft and a fourth trochanter medially directed and visible in anterior view. However, both morphotypes present elements with the opposite conditions. Some specimens from Morphotype I do not present this structure (e.g. HUE-8801) but might be related with ontogenetic development. The Morphotype II also has some elements (e.g. HUE-594) that develops the linea intermuscularis cranialis. The significant variation as quantified in this region among the morphotypes coincides with observation of morphological differences between sauropod taxa in comparative anatomy. The quantification of morphological differences, referable to possible taxonomic differences, allowed us to calculate the residual variance. The intraspecific variability is high in the sample of Lo Hueco titanosaur and all the analysis show that more than 70% of the shape variance are not related with interspecific variation in all of the bone elements, at least in current analysis between both morphotypes.

The discussion of morphological features shows variation within each sample attributable to intraspecific differences, such as (i) the presence or absence of accessory trochanter of the femoral fourth trochanter; (ii) the position of the enlargement of the insertion of the tibial cnemial crest, (iii) and bifurcation of the lateral trochanter of the fibula. All these variances are associated to muscular attachment, subject to ontogenetical and individual variation within taxa.

A third group is discussed for some elements of the femora and the tibiae from Lo Hueco and could be related to the presence of a possible less common titanosaur form in the sample. However more sample and comparison with other Ibero-Armorican taxa such as *Lirainosaurus astibiae* is required. However, these tests are beyond the scopes of the present work.

The use of geometric morphometric tool kit allowed us to quantify shape variance and help taxonomic assessment of the titanosaurs from Lo Hueco. Thanks to this set of techniques we have observed that majority of shape variability in the hindlimb elements is among each morphotype. Differences between the two main titanosaur morphotypes from Lo Huecco only account for one fourth of the total shape variation in each element of the hindlimb.

IV.II.7. BIBLIOGRAPHY

Adams DC, Collyer ML, Kaliontzopoulou A, Sherratt E. 2017. Geomorph: Software for geometric morphometric analyses. R package version 3.0.5. https://cran.r-project.org/package=geomorph.

Adams DC, Otárola-Castillo E. 2013. geomorph: an r package for the collection and analysis of geometric morphometric shape data. *Methods in Ecology and Evolution* 4: 393–399.

Arbour JH, Brown CM. 2014. Incomplete specimens in geometric morphometric analyses (S Nakagawa, Ed.). *Methods in Ecology and Evolution* 5: 16–26.

Blender Online Community. 2018. Blender - a 3D modelling and rendering package.

Bonnan MF. 2004. Morphometric analysis of humerus and femur shape in Morrison sauropods: implications for functional morphology and paleobiology. *Paleobiology* 30: 444–470.

Bonnan MF. 2007. Linear and geometric morphometric analysis of long bone scaling patterns in Jurassic neosauropod dinosaurs: their functional and paleobiological implications. *Anatomical Record* 290: 1089–111.

Bonnan MF, Wilhite RD, Masters SL, Yates AM, Gardner CK, Aguiar A. 2013. What Lies Beneath: Sub-Articular Long Bone Shape Scaling in Eutherian Mammals and Saurischian Dinosaurs Suggests Different Locomotor Adaptations for Gigantism. *PLoS ONE* 8: e75216.

Bookstein FL. 1989. Principal Warps: Thin-Plates Splines and the decompostion of deformations. *IEEE Transactions on Pattern Analysis and Machine Intelligence* 11: 567–585.

Bookstein FL. 1991. *Morphometric tools for landmark data: geometry and biology.*

Bookstein FL. 1996a. Applying landmark methods to biological outline data. In: Mardia K V.,, In: Gill CA,, In: Dryden IL, eds. *Image Fusion and Shape Variability.* Leeds: University of Leeds Press, 79–87.

Bookstein FL. 1996b. Landmark methods for forms without landmarks: localizing group differences in outline shape. *Proceedings of the Workshop on Mathematical Methods in Biomedical Image Analysis. IEEE*, 279–289.

Bookstein FL. 1997. Landmark methods for forms without landmarks: morphometrics of group differences in outline shape. *Medical image analysis. IEEE*, 225–243.

Bookstein FL. 2014. *Measuring and Reasoning: Numerical Inference in the Sciences.* Cambridge University Press.

Bookstein FL. 2015. No quantification without qualification, and vice versa. *Biological Theory* 10: 212–227.

Borsuk-Bialynicka M. 1977. A New Camarasaurid Sauropod *Opisthocoelicaudia skarzynskii* gen. n., sp. n. from the Upper Cretaceous of Mongolia. *Paleontologia Polonica* 37: 5–64.

Botton-Divet L, Houssaye A, Herrel A, Fabre AC, Cornette R. 2015. Tools for quantitative form description; an evaluation of different software packages for semi-landmark analysis. *PeerJ* 3: e1417.

Bright JA, Marugán-Lobón J, Cobb SN, Rayfield EJ. 2016. The shapes of bird beaks are highly controlled by nondietary factors. *Proceedings of the National Academy of Sciences* 113: 5352–5357.

Britt BB, Naylor BG. 1994. An embryonic *Camarasaurus* (Dinosauria, Sauropoda) from the Upper Jurassic Morrison Formation (Dry Mesa Quarry, Colorado). In: Carpenter K, Hirsch KF,

Horner JR, eds. *Dinosaur Eggs and Babies*. Cambridge: Cambridge University Press, 256–264.

Brown CM, Arbour JH, Jackson DA. 2012. Testing of the Effect of Missing Data Estimation and Distribution in Morphometric Multivariate Data Analyses. *Systematic Biology* 61: 941–954.

Cambra-Moo O, Barroso-barcenilla F, Berreteaga A, Carenas B, Elvira A, Escaso F, Domingo L, Peyrot D, Sanz JL, Segura M, Ortega F, Sopelana A. 2012. Preliminary taphonomic approach to "'Lo Hueco'" palaeontological site. *Geobios* 45: 157–166.

Canudo JI, Royo-Torres R, Cuenca-Bescós G. 2008. A new sauropod: *Tastavinsaurus sanzi* gen. et sp. nov. from the Early Cretaceous (Aptian) of Spain. *Journal of Vertebrate Paleontology* 28: 712–731.

Carballido JL, Pol D, Cerda IA, Salgado JL. 2011. The Osteology of *Chubutisaurus insignis* Del Corro, 1975 (Dinosauria: Neosauropoda) from the 'Middle' Cretaceous of Central Patagonia, Argentina. *Journal of Vertebrate Paleontology* 31: 93–110.

Carpenter K, McIntosh JS. 1994. Upper Jurassic sauropod babies from the Morrison Formation. In: Carpenter K, Hirsch KF, Horner JR, eds. *Dinosaur Eggs and Babies*. Cambridge: Cambridge University Press, 265–278.

Challis JH, Kerwin DG. 1992. Accuracy assessment and control point configuration when using the DLT for photogrammetry. *Journal of Biomechanics* 25: 1053–1058.

Charrad M, Ghazzali N, Boiteau V, Niknafs A. 2014. NbClust : An R Package for Determining the Relevant Number of Clusters in a Dataset. *Journal of Statistical Software* 61.

Claude J. 2008. *Morphometrics with R.* New York, NY: Springer New York.

Clavel J, Merceron G, Escarguel G. 2014. Missing Data Estimation in Morphometrics: How Much is Too Much? *Systematic Biology* 63: 203–218.

Collins KS, Gazley MF. 2017. Does my posterior look big in this? the effect of photographic distortion on morphometric analyses. *Paleobiology* 43: 508–520.

Company J. 2011. Bone histology of the titanosaur *Lirainosaurus astibiae* (Dinosauria: Sauropoda) from the Latest Cretaceous of Spain. *Naturwissenschaften* 98: 67–78.

Cunningham JA, Rahman IA, Lautenschlager S, Rayfield EJ, Donoghue PCJ. 2014. A virtual world of paleontology. *Trends in Ecology and Evolution* 29: 347–357.

Curry Rogers K. 2009. The postcranial osteology of *Rapetosaurus krausei* (Sauropoda: Titanosauria) from the Late Cretaceous of Madagascar. *Journal of Vertebrate Paleontology* 29: 1046–1086.

D'Emic MD. 2012. The early evolution of titanosauriform sauropod dinosaurs. *Zoological Journal of the Linnean Society* 166: 624–671.

D'Emic MD, Mannion PD, Upchurch P, Benson RBJ, Pang Q, Zhengwu C. 2013. Osteology of *Huabeisaurus allocotus* (Sauropoda: Titanosauriformes) from the Upper Cretaceous of China. *PLoS ONE* 8: e69375.

Das AJ, Murmann DC, Cohrn K, Raskar R. 2017. A method for rapid 3D scanning and replication of large paleontological specimens. *PLoS ONE* 12: 1–13.

Davies TG, Rahman IA, Lautenschlager S, Cunningham JA, Asher RJ, Barrett PM, Bates KT, Bengtson S, Benson RBJ, Boyer DM, Braga J, Bright JA, Claessens LPAM, Cox PG, Dong XP, Evans AR, Falkingham PL, Friedman M, Garwood RJ, Goswami A, Hutchinson JR, Jeffery NS, Johanson Z, Lebrun R, Martínez-Pérez C, Marugán-Lobón J, O'Higgins PM, Metscher B, Orliac M, Rowe TB, Rücklin M, Sánchez-Villagra MR, Shubin NH, Smith SY, Starck JM, Stringer C,

Summers AP, Sutton MD, Walsh SA, Weisbecker V, Witmer LM, Wroe S, Yin Z, Rayfield EJ, Donoghue PCJ. 2017. Open data and digital morphology. *Proceedings of the Royal Society B: Biological Sciences* 284: 20170194.

Díez Díaz V, Garcia G, Pereda-Suberbiola X, Stein KHW, Jentgen-Ceschino B, Godefroit P, Valentin X. 2018. The titanosaurian dinosaur *Atsinganosaurus velauciensis* (Sauropoda) from the Upper Cretaceous of southern France: New material, phylogenetic affinities, and palaeobiogeographical implications. *Cretaceous Research* 91: 429–456.

Díez Díaz V, Mocho P, Páramo A, Escaso F, Marcos-Fernández F, Sanz JL, Ortega F. 2016. A new titanosaur (Dinosauria, Sauropoda) from the Upper Cretaceous of Lo Hueco (Cuenca, Spain). *Cretaceous Research* 68: 49–60.

Díez Díaz V, Ortega F, Sanz JL. 2014. Titanosaurian teeth from the Upper Cretaceous of "Lo Hueco" (Cuenca, Spain). *Cretaceous Research* 51: 285–291.

Díez Díaz V, Pereda Suberbiola X, Company J. 2015. Updating titanosaurian diversity (Sauropoda) from the Late Cretaceous of Spain: The fossil site of Laño and Chera. *Spanish Journal of Palaeontology* 30: 293–306.

Díez Díaz V, Suberbiola XP, Sanz JL. 2013. Appendicular skeleton and dermal armour of the Late Cretaceous titanosaur *Lirainosaurus astibiae* (Dinosauria: Sauropoda) from Spain. *Palaeontologia Electronica* 16: 18 p.

Dray S, Josse J. 2015. Principal component analysis with missing values: a comparative survey of methods. *Plant Ecology* 216: 657–667.

Falkingham PL. 2012. Acquisition of high resolution three-dimensional models using free, open-source, photogrammetric software. *Paleontologia Electronica* 15: 1–15.

Falkingham PL. 2013. Low cost 3D scanning using off-the-shelf video gaming peripherals. *Journal of Paleontological Techniques*: 1–9.

Falkingham PL, Bates KT, Avanzini M, Bennett M, Bordy EM, Breithaupt BH, Castanera D, Citton P, Díaz-Martínez I, Farlow JO, Fiorillo AR, Gatesy SM, Getty P, Hatala KG, Hornung JJ, Hyatt JA, Klein H, Lallensack JN, Martin AJ, Marty D, Matthews NA, Meyer CA, Milàn J, Minter NJ, Razzolini NL, Romilio A, Salisbury SW, Sciscio L, Tanaka I, Wiseman ALA, Xing LD, Belvedere M. 2018. A standard protocol for documenting modern and fossil ichnological data. *Palaeontology* 61: 469–480.

Felice RN, Randau M, Goswami A. 2018. A fly in a tube: Macroevolutionary expectations for integrated phenotypes. *Evolution* 72: 2580-2594.

Fondevilla V, Riera V, Vila B, Sellés AG, Dinarès-Turell J, Vicens E, Gaete R, Oms O, Galobart À. 2019. Chronostratigraphic synthesis of the latest cretaceous dinosaur turnover in South-Western Europe. *Earth-Science Reviews* 191: 168-189.

Foth C, Rauhut OWM. 2013. The good, the bad, and the ugly: the influence of skull reconstructions and intraspecific variability in studies of cranial morphometrics in theropods and Basal saurischians. *PloS ONE* 8: e72007.

Gallina PA. 2011. *Estudio Anatómico, Sistemático Y Paleobiológico De Bonitasaura salgadoi (Dinosauria, Sauropoda): Su Importancia En El Contexto De La Evolución De Los Titanosaurios Del Cretácico Superior De La Argentina*. PhD Theis, 340pp.

Gallina PA, Apesteguía S. 2005. *Cathartesaura anaerobica* gen. et sp. nov., a new rebbachisaurid (Dinosauria, Sauropoda) from the Huincul Formation (Upper Cretaceous), Río Negro,

Argentina. *Revista del Museo Argentino de Ciencias Naturales* 7: 153–166.

Gallina PA, Otero A. 2015. Reassessment of *Laplatasaurus araukanicus* (Sauropoda: Titanosauria) from the Upper Cretaceous of patagonia, Argentina. *Ameghiniana* 52: 487–501.

Garcia G, Amico S, Fournier F, Thouand E, Valentin X. 2010. A new Titanosaur genus (Dinosauria, Sauropoda) from the Late Cretaceous of southern France and its paleobiogeographic implications. *Bulletin de la Société Géologique de France* 181: 269–277.

Gauthier O, Landry PA, Lapointe FJ. 2003. Missing data in craniometrics: A simulation study. *Acta Theriologica* 48: 25–34.

Gornbein JA, Lazaro CG, Little RJA. 1992. Incomplete data in repeated measures analysis. Statistical *Methods in Medical Research* 1: 275–295.

Green WDK. 1996. The thin-plate spline and images with curving features. In: Mardia K V., Gill CA, Dryden IL, eds. *Image Fusion and Shape Variability*. Leeds: University of Leeds Press, 79–87.

Gunz P. 2005. *Statistical and geometric morphometric reconstruction of hominid crania. Reconstructing autralopithecine ontogeny.* Unpublished thesis, University of Vienna.

Gunz P, Mitteroecker P. 2013. Semilandmarks: a method for quantifying curves and surfaces. *Hystrix, the Italian Journal of Mammalogy* 24: 103–109.

Gunz P, Mitteroecker P, Bookstein FL. 2005. Semilandmarks in three dimensions. In: Slice DE, ed. *Modern Morphometrics in Physical Anthropology*. KLUWER ACADEMIC PUBL, 73–98.

Gunz P, Mitteroecker P, Neubauer S, Weber GW, Bookstein FL. 2009. Principles for the virtual reconstruction of hominin crania. *Journal of Human Evolution* 57: 48–62.

Hammer Ø, Harper DAT. 2008. *Paleontological Data Analysis*. Wiley-Blackwell Publishing.

Hartigan JA, Wong MA. 1979. Algorithm AS 136: A K-Means Clustering Algorithm. *Applied Statistics* 28: 100.

Hastie T, Tibshirani R, Friedman J. 2000. *The Elements of Statistical Learning: Data Mining, Inference, and Prediction*. Springer

Hechenleitner EM, Fiorelli LE, Martinelli AG, Grellet-Tinner G. 2018. Titanosaur dinosaurs from the Upper Cretaceous of La Rioja province, NW Argentina. *Cretaceous Research* 85: 42–59.

Hedrick BP, Dodson P. 2013. Lujiatun Psittacosaurids: Understanding Individual and Taphonomic Variation Using 3D Geometric Morphometrics. *PLoS ONE* 8: e69265.

Hedrick BP, Natanson LJ, Brennan PLR, Antalek-Schrag P, Conith AJ. 2019. Variability and asymmetry in the shape of the spiny dogfish vagina revealed by 2D and 3D geometric morphometrics. *Journal of Zoology*: 1–12.

Holliday CM, Ridgely RC, Sedlmayr JC, Witmer LM. 2010. Cartilaginous Epiphyses in Extant Archosaurs and Their Implications for Reconstructing Limb Function in Dinosaurs. *PLoS ONE* 5: e13120.

Hubert LJ, Levin JR. 1975. A General Statistical Framework for Assessing Categorical Clustering in Free Recall. *Psychological Bulletin*: 12–27.

Ibiricu LM, Martínez RD, Casal GA. 2018. The pelvic and hindlimb myology of the basal titanosaur *Epachthosaurus sciuttoi* (Sauropoda: Titanosauria). *Historical Biology* 00: 1–16.

Janensch W. 1961. Die Gliedmaszen und Gliedmaszengürtel der Sauropoden der Tendaguru-Schichten. *Palaeontographica* 3: 177–235.

Kassambara A. 2017. *Practical Guide to Cluster Analysis in R: Unsupervised Machine Learning:* Volume 1 (Multivariate Analysis).

Kassambara A, Mundt F. 2017. Factoextra: extract and visualize the results of multivariate data analyses. R package version 1: 1–76.

Kendall DG. 1984. Shape Manifolds, Procrustean Metrics, and Complex Projective Spaces. *Bulletin of the London Mathematical Society* 16: 81–121.

Knoll F, Ridgely RC, Ortega F, Sanz JL, Witmer LM. 2013. Neurocranial Osteology and Neuroanatomy of a Late Cretaceous Titanosaurian Sauropod from Spain (*Ampelosaurus* sp.). *PLoS ONE* 8: e54991.

Knoll F, Witmer LM, Ridgely RC, Ortega F, Sanz JL. 2015. A new titanosaurian braincase from the cretaceous 'Lo Hueco' locality in Spain sheds light on neuroanatomical evolution within titanosauria. *PLoS ONE* 10: 1–24.

Lange T, Roth V, Braun ML, Buhmann JM. 2004. Stability-Based Validation of Clustering Solutions. *Neural Computation* 16: 1299–1323.

Lautenschlager S. 2013. Cranial myology and bite force performance of *Erlikosaurus andrewsi*: A novel approach for digital muscle reconstructions. *Journal of Anatomy* 222: 260–272.

Lautenschlager S. 2016. Reconstructing the past: methods and techniques for the digital restoration of fossils. *Royal Society Open Science* 3: 160342.

Lautenschlager S. 2017. From bone to pixel—fossil restoration and reconstruction with digital techniques. *Geology Today* 33: 155–159.

Lê S, Josse J, Husson F. 2008. FactoMineR : An R Package for Multivariate Analysis. *Journal of Statistical Software* 25.

Lehman TM, Coulson AB. 2002. A Juvenile Specimen of the Sauropod Dinosaur *Alamosaurus sanjuanensis* from the Upper Cretaceous of Big Bend National Park, Texas. *Journal of Paleontology* 76: 156–172.

Little RJA. 1988. A test of missing completely at random for multivariate data with missing values. *Journal of the American Statistical Association* 83: 1198–1202.

Little J, Mardia K. 1996. *Edgels and Tangent Planes in Image Warping. Advances in Morphometrics*. Boston, MA: Springer US, 263–270.

Le Loeuff J. 1995. *Ampelosaurus atacis* (nov, gen., nov. sp.), un nouveau Titanosauridae (Dinosauria, Sauropoda) du Crétacé supérieur de la Haute Vallée de l'Aude (France). *Comptes Rendus de l'Académie des Sciences à Paris*, Série IIa 321: 693–699.

Le Loeuff J. 2005. Osteology of *Ampelosaurus atacis* (Titanosauria) from Southern France. In: Tidwell V, Carpenter K, eds. *Thunder-Lizards: The Sauropodomorph Dinosaurs*. Bloomington: Indiana University Press, 115–137.

Macqueen J. 1967. Some methods for classification and analysis of multivariate observations. *Proceedings of the Fifth Berkeley Symposium on Mathematical Statistics and Probability* 1: 281–297.

Mallison H, Wings O. 2014. Photogrammetry in Paleontology - A Practical Guide. Journal of *Paleontological Techniques* 12: 1–13.

Mannion PD, Allain R, Moine O. 2017. The earliest known titanosauriform sauropod dinosaur and the evolution of Brachiosauridae. *PeerJ* 5: e3217.

Mannion PD, Calvo JO. 2011. Anatomy of the basal titanosaur (Dinosauria, Sauropoda) *Andesaurus delgadoi* from the mid-Cretaceous (Albian-early Cenomanian) Río Limay Formation, Neuquén Province, Argentina: implications for titanosaur systematics. *Zoological Journal of the Linnean Society*. 163: 155-181

Mannion PD, Schwarz D, Upchurch P, Wings O. 2019. Taxonomic affinities and biogeographic implications of the putative titanosaurs (Dinosauria: Sauropoda) from the Late Jurassic Tendaguru Formation of Tanzania. *Journal of Vertebrate Paleontology* XX: 1–126.

Mannion PD, Upchurch P, Barnes RN, Mateus O. 2013. Osteology of the Late Jurassic Portuguese sauropod dinosaur *Lusotitan atalaiensis* (Macronaria) and the evolutionary history of basal titanosauriforms. *Zoological Journal of the Linnean Society* 168: 98–206.

Martin V, Suteethorn V, Buffetaut É. 1999. Description of the type and referred material of *Phuwiangosaurus sirindhornae* Martin, Buffetaut and Suteethorn, 1994, A sauropod from the Lower Cretaceous of Thailand. *Oryctos* 2: 39–91.

Martínez RD, Giménez O, Rodríguez J, Luna M, Lamanna MC. 2004. An articulated specimen of the basal titanosaurian (Dinosauria: Sauropoda) *Epachthosaurus sciuttoi* from the early Late Cretaceous Bajo Barreal Formation of Chubut Province, Argentina. *Journal of Vertebrate Paleontology* 24: 107–120.

Mocho P, Escaso F, Marcos-Fernández F, Páramo A, Vidal D, Ortega F. 2018. The morphological variability on titanosaur caudal series from Lo Hueco: taxonomic diversity, intra-specific variability or both? *XVI Annual Meeting of European Association of Vertebrate Paleontologists*. 126.

Mocho P, Páramo A, Díez Díaz V, Escaso F, Marcos-Fernández F, Sanz JL, Ortega F. 2016. Looking through the axial skeleton of the Lo Hueco titanosaurs. In: Torcida Fernández-Baldor F, Canudo JI, Huerta P, Pereda X, eds. *VII International Symposium about Dinosaurs Palaeontology and their Environment*. 99–100.

Molnar JL, Pierce SE, Hutchinson JR. 2012. Idealized landmark-based geometric reconstructions of poorly preserved fossil material: a case study of an early tetrapod vertebra. *Palaeontologia Electronica* 15: 1–18.

Morissette L, Chartier S. 2013. The k-means clustering technique: General considerations and implementation in Mathematica. *Tutorials in Quantitative Methods for Psychology* 9: 15–24.

Motani R, Amenta N, Wiley DF. 2005. Possibilities and Limitations of Three Dimensional Retrodeformation of a Trilobite and Plesiosaur Vertebrae. *PaleoBios* 25.

Mullin SK, Taylor PJ. 2002. The effects of parallax on geometric morphometric data. *Computers in Biology and Medicine* 32: 455–464.

Nakagawa S, Freckleton RP. 2008. Missing inaction: the dangers of ignoring missing data. *Trends in Ecology and Evolution* 23: 592–596.

Navalón G, Bright JA, Marugán-Lobón J, Rayfield EJ. 2018. The evolutionary relationship between beak shape, mechanical advantage, and feeding ecology in modern birds. *Evolution*: evo.13655.

Neeser R, Ackermann RR, Gain J. 2009. Comparing the accuracy and precision of three techniques used for estimating missing landmarks when reconstructing fossil hominin crania. American *Journal of Physical Anthropology* 140: 1–18.

Oba S, Sato M aki, Takemasa I, Monden M, Matsubara K ichi, Ishii S. 2003. A Bayesian missing value estimation method for gene expression profile data. *Bioinformatics* 19: 2088–2096.

Ortega F, Bardet N, Barroso-Barcenilla F, Callapez PM, Cambra-Moo O, Daviero- Gómez V, Díez Díaz V, Domingo L, Elvira A, Escaso F, García-Oliva M, Gómez B, Houssaye A, Knoll F, Marcos-Fernández F, Martín M, Mocho P, Narváez I, Pérez-García A, Peyrot D, Segura M, Serrano H, Torices A, Vidal D, Sanz JL. 2015. The biota of the Upper Cretaceous site of "Lo Hueco" (Cuenca, Spain). *Journal of Iberian Geology* 41: 83–99.

Otero A. 2010. The appendicular skeleton of *Neuquensaurus*, a Late Cretaceous saltasaurine sauropod from Patagonia, Argentina. *Acta Palaeontologica Polonica* 55: 399–426.

Otero A. 2018. Forelimb musculature and osteological correlates in Sauropodomorpha (Dinosauria, Saurischia). *PLoS ONE* 13: e0198988.

Otero A, Vizcaíno SF. 2008. Musculatura y función del miembro posterior de *Neuquensaurus australis* (Sauropoda: Titanosauria). *Ameghiniana* 45: 333–348.

Páramo A, Ortega F, Escaso F, Narváez I, Sanz JL. 2014. Ejemplares juveniles de titanosaurio (Sauropoda) del yacimiento de Lo Hueco (Fuentes, Cuenca). In: Royo-Torres, R.; Verdú, F.J.; Alcalá, L. (coord.). *XXX Jornadas de Paleontología de la Sociedad Española de Paleontología. ¡Fundamental!* 24: 149–151.

Páramo A, Ortega F, Mocho P, Sanz JL. 2016. Femoral variability in two titanosaur taxa from Lo Hueco (Cuenca, Spain): Insights for iberoarmorican titanosaur diversity assessment. In: Torcida F, Jose IC, Huerta P, Pereda-Suberbiola X, eds. *VII International Symposium about Dinosaurs Palaeontology and their Environment.* Salas de los Infantes, Burgos: Colectivo Arqueológico y Paleontológico de Salas, 107–108.

Páramo A, Ortega F, Sanz JL. 2015a. Preliminar assessment of the morphological variability of appendicular bones of titanosaurs (Dinosauria, Sauropoda) from Lo Hueco (Fuentes, Cuenca). *XXXI Jornadas de la Sociedad Española de Paleontología*.

Páramo A, Ortega F, Sanz JL. 2015b. Two types of appendicular bones of titanosaurs (Dinosauria, Sauropoda) from Lo Hueco (Fuentes, Cuenca). In: Dyke GJ,, Marshall J, Naish D, Young MT, Wujeck JL, Martin-Silverstone L, Pond S, Roberts A, Hansford J, Taylor C, Blackwell G, Riddington K, eds. *63rd Symposium for Vertebrate Paleontology and Comparative anatomy & 24th Symposium of Palaeontological Preparation and Conservation with the Geological Curator's Group*. 100.

Páramo A, Ortega F, Sanz JL. 2018. Modularity in the titanosaurian appendicular skeleton: insights from Lo Hueco fossil site. *XVI Annual Meeting of European Association of Vertebrate Paleontologists*. 146.

Pollard KS, van der Laan MJ. 2002. A Method to Identify Significant Clusters in Gene Expression Data A Method to Identify Significant Clusters in Gene Expression Data. Proceedings, SCI (*World Multiconference on Systemics, Cybernetics and Informatics*) 2: 318–325.

Polly PD, Motz GJ. 2016. Patterns and Processes in Morphospace: Geometric Morphometrics of Three-Dimensional Objects. *The Paleontological Society Papers* 22: 71–99.

Poropat SF, Mannion PD, Upchurch P, Hocknull S a., Kear BP, Elliott D a. 2014. Reassessment of the non-titanosaurian somphospondylan *Wintonotitan wattsi* (Dinosauria: Sauropoda: Titanosauriformes) from the mid-Cretaceous Winton Formation, Queensland, Australia (R Benson, Ed.). *Papers in Palaeontology*: 1: 59-106.

Poropat SF, Upchurch P, Mannion PD, Hocknull SA, Kear BP, Sloan T, Sinapius GHK, Elliott DA. 2015. Revision of the sauropod dinosaur *Diamantinasaurus matildae* Hocknull *et al.* 2009 from the mid-Cretaceous of Australia: Implications for Gondwanan titanosauriform dispersal. *Gondwana Research* 27: 995–1033.

Powell JE. 1992. Osteología de *Saltasaurus loricatus* (Sauropoda-Titanosauridae) del Cretácico Superior del noroeste argentino. In: Sanz JL, Buscalioni AD, eds. *Los Dinosaurios y Su Entorno Biotico Actas del Segundo Curso de Paleontologia in Cuenca.* Cuenca, España: Instituto 'Juan Valdes', 166–229.

Powell JE. 2003. Revision of South American titanosaurid dinosaurs: Palaeobiological, palaeobiogeographical and phylogenetic aspects (TH Rich, K Dimmack, and JR Macdonald, Eds.). *Records of the Queen Victoria Museum* 111: 1–179.

Proschan MA, McMahon RP, Shih JH, Hunsberger SA, Geller NL, Knatterud G, Wittes J. 2001. Sensitivity analysis using an imputation method for missing binary data in clinical trials. *Journal of Statistical Planning and Inference* 96: 155–165.

Remes K. 2007. *Evolution of the Pectoral girdle and Forelimb in Sauropodomorpha (Dinosauria, Saurischia): Osteology, Myology and Fuction*. Unpublished thesis, Ludwig-Maximilians-Universität München.

Riggs ES. 1903. *Brachiosaurus altithorax*, the largest known dinosaur. *American Journal of Science* s4-15: 299–306.

Rohlf FJ. 1993. Relative warp analysis and an example of its application to mosquito wings. *Contributions to morphometrics*.

Rohlf FJ. 1998. On Applications of Geometric Morphometrics to Studies of Ontogeny and Phylogeny. *Systematic Biology* 47: 147–158.

Rohlf FJ. 1999. Shape statistics: Procrustes superimpositions and tangent spaces. *Journal of Classification* 16: 197–223.

Royo-Torres R. 2009. *El saurópodo de Peñarroya de Tastavins*. Teruel: Instituo de Estudios Turolenses y Fundación Conjunto Paleontológico de Teruel-Dinópolis.

Royo-Torres R, Alcalá L, Cobos A. 2012. A new specimen of the Cretaceous sauropod *Tastavinsaurus sanzi* from El Castellar (Teruel, Spain), and a phylogenetic analysis of the Laurasiformes. *Cretaceous Research* 34: 61–83.

RStudio Team. 2015. RStudio: Integrated Development for R. RStudio, Inc., Boston, MA URL http://www.rstudio.com/.

Salgado JL, Coria RA, Calvo JO. 1997. Evolution of the titanosaurid sauropods I: Phylogenetic analysis based on the postcranial evidence. *Ameghiniana* 34: 3–32.

Salgado JL, Gallina PA, Paulina Carabajal A. 2015. Redescription of *Bonatitan reigi* (Sauropoda: Titanosauria), from the Campanian–Maastrichtian of the Río Negro Province (Argentina). *Historical Biology* 27: 525–548.

Salgado JL, De Souza Carvalho I. 2008. *Uberabatitan ribeiroi*, a new titanosaur from the Marília Formation (Bauru Group, Upper Cretaceous), Minas Gerais, Brazil. *Palaeontology* 51: 881–901.

Sanz JL, Powell JE, Le Loeuff J, Martínez RN, Pereda Suberbiola X. 1999. Sauropod remains from the Upper Cretaceous of Laño (north central Spain). Titanosaur phylogenetic relationships. *Estudios del Museo de Ciencias Naturales de Alava* 14: 235–255.

Schafer JL. 1997. Analysis of Incomplete Multivariate Data.

Schlager S. 2017. Morpho and Rvcg – Shape Analysis in R. In: Zheng G, Li S, Szekely G, eds. *Statistical Shape and Deformation Analysis*. Elsevier, 217–256.

Schlager S, Profico A, Vincenzo F Di, Manzi G. 2018. Retrodeformation of fossil specimens based on 3D bilateral semi-landmarks: Implementation in the R package "Morpho". *PLoS ONE* 13.

Schwarz D, Böhm N. 2012. A morphometric approach to the specific separation of the humeri and femora of *Dicraeosaurus* from the Late Jurassic of Tendaguru, Tanzania. *Acta Palaeontologica Polonica* 59: 81–98.

Schwarz D, Wings O, Meyer CA. 2007. Super sizing the giants: first cartilage preservation at a sauropod dinosaur limb joint. *Journal of the Geological Society* 164: 61–65.

Sheets HD, Covino KM, Panasiewicz JM, Morris SR. 2006. Comparison of geometric morphometric outline methods in the discrimination of age-related differences in feather shape. *Frontiers in Zoology* 3: 15.

Souter T, Cornette R, Pedraza J, Hutchinson JR, Baylac M. 2010. Two applications of 3D semi-landmark morphometrics implying different template designs: the theropod pelvis and the shrew skull. *Comptes Rendus Palevol* 9: 411–422.

Stein GP. 1997. Lens distortion calibration using point correspondences. *Proceedings of IEEE Computer Society Conference on Computer Vision and Pattern Recognition*: 602–608.

Strauss RE, Atanassov MN. 2006. Determining best complete subsets of specimens and characters for multivariate morphometric studies in the presence of large amounts of missing data. *Biological Journal of the Linnean Society* 88: 309–328.

Strauss RE, Atanassov MN, Alves de Oliveira J. 2003. Evaluation of the principal- component and expectation- maximization methods for estimating missing data in morphometric studies. *Journal of Vertebrate Paleontology* 23: 284–296.

Strauss RE, Bookstein FL. 1982. The Truss: Body Form Reconstructions in Morphometrics. *Systematic Biology* 31: 113–135.

Tallman M, Amenta N, Delson E, Frost SR, Ghosh D, Klukkert ZS, Morrow A, Sawyer GJ. 2014. Evaluation of a New Method of Fossil Retrodeformation by Algorithmic Symmetrization: Crania of Papionins (Primates, Cercopithecidae) as a Test Case. *PLoS ONE* 9: e100833.

Taylor MP. 2015. Almost all known sauropod necks are incomplete and distorted. *PeerJ* Not Peer R.

The R Core Team. 2016. A language and environment for statistical computing. R Foundation for Statistical Computing, Vienna, Austria. URL https://www.R-project.org/.

Třebický V, Fialová J, Kleisner K, Havlíček J. 2016. Focal length affects depicted shape and perception of facial images. *PLoS ONE* 11: 1–14.

Tschopp E, Dzemski G. 2013. Retrodeformation as a test for the validity of phylogenetic characters: an example from diplodocid sauropod vertebrae. *Paleontologia Electronica* 16: 1–23.

Ullmann PV., Bonnan MF, Lacovara KJ. 2017. Characterizing the Evolution of Wide-Gauge Features in Stylopodial Limb Elements of Titanosauriform Sauropods via Geometric Morphometrics. *The Anatomical Record* 300: 1618–1635.

Upchurch P, Barrett PM, Dodson P. 2004. Sauropoda. In: Weishampel DB, Dodson P, Osmólska H, eds. *The Dinosauria*. Berkeley: University of California Press, 259–322.

Vidal D, Díez Díaz V. 2017. Reconstructing hypothetical sauropod tails by means of 3D digitization: *Lirainosaurus astibiae* as case study. *Journal of Iberian Geology* 43: 293–305.

Vidal D, Sanz JL, Mocho P, Páramo A, Escaso F, Marcos-Fernández F, Ortega F. 2017. The titanosaur tails from Lo Hueco (Cuenca, Spain): Four different ways to shake? In: Farke AA, Mackenzie SA, Miller Camp J, eds. *77th Annual Meeting of the Society of Vertebrate Paleontology.* Calgary, 208.

Vila B, Galobart À, Canudo JI, Le Loeuff J, Dinarès-Turell J, Riera V, Oms O, Tortosa T, Gaete R. 2012. The diversity of sauropod dinosaurs and their first taxonomic succession from the latest Cretaceous of southwestern Europe: Clues to demise and extinction. *Palaeogeography,*

Palaeoclimatology, Palaeoecology 350–352: 19–38.

Vila B, Sellés AG, Brusatte SL. 2016. Diversity and faunal changes in the latest Cretaceous dinosaur communities of southwestern Europe. *Cretaceous Research* 57: 552–564.

Wang S, Munsell B, Richardson T. 2017. Correspondence Establishment in Statistical Shape Modeling: Optimization and Evaluation. *Statistical Shape and Deformation Analysis*: 67–87.

Wiens JJ. 2003. Missing data, incomplete taxa, and phylogenetic accuracy. *Systematic Biology* 52: 528–538.

Wiley DF, Amenta N, Alcantara DA, Ghosh D, Kil YJ, Delson E, Harcourt-Smith W, Rohlf FJ, John K St., Hamann B, St John K, Hamann B, John K St., Hamann B. 2005. Evolutionary Morphing. *Proceedings of IEEE Visualization 2005*. Minneapolis, 1–8.

Wilhite RD. 2005. Variation in the Appendicular Skeleton of North American Sauropod Dinosaurs: Taxonomic Implications. In: Tidwell V, Carpenter K, eds. *Thunder-Lizards: The Sauropodomorph Dinosaurs*. Indiana University Press, 268–301.

Wilson JA. 2002. Sauropod dinosaur phylogeny: critique and cladistic analysis. *Zoological Journal of the Linnean Society* 136: 215–275.

Wilson JA, Barrett PM, Carrano MT. 2011. An associated partial skeleton of *Jainosaurus* cf. *septentrionalis* (Dinosauria: Sauropoda) from the Late Cretaceous of Chhota Simla, Central India. *Palaeontology* 54: 981–998.

Wilson JA, Carrano MT. 1999. Titanosaurs and the Origin of 'wide-gauge' trackways: A Biomechanical and Systematic Perspective on Sauropod Locomotion. *Paleobiology* 25: 252–267.

Wilson JA, Sereno PC. 1998. Early Evolution and High-level Phylogeny of Sauropod Dinosaurs. *Journal of Vertebrate Paleontology* 18: 1–68.

Wilson JA, Upchurch P. 2003. A revision of *Titanosaurus* Lydekker (Dinosauria - Sauropoda), the first dinosaur genus with a 'Gondwanan' distribution. *Journal of Systematic Palaeontology* 1: 125–160.

Zelditch ML, Swiderski DL, Sheets HD. 2012a. *Geometric Morphometrics for Biologists*. Elsevier.

Zelditch ML, Swiderski DL, Sheets HD. 2012b. *Obtaining Landmarks and Semilandmarks. Geometric Morphometrics for Biologists: A Primer*. Academic Press, 1–31.

CHAPTER V:

Geometric Morphometric Analysis of the Intraspecific Variability in the Appendicular Skeleton of the Titanosaur Sauropods from Lo Hueco (Cuenca, Spain): Functional Implications

V. ABSTRACT

The fossil site of Lo Hueco have yielded several titanosaur individuals partially articulated as well as several hundreds of isolated specimens. The collection of appendicular elements of titanosaurs from Lo Hueco presents a high variance of forms as well as size between the elements. Assessment of the taxonomic differences as well as intraspecific shape variation is important to determine the number and composition of the titanosaur sample present in this fossil site. The 3D digitizing of the elements and extensive use of landmark based geometric morphometric methods are selected as a helpful tool to quantify the variance of a sample from each appendicular element. Other advantage of this method is that it permits extracting the confounding effect of the size component of the form and compare the specimens from Lo Hueco with modern machine learning techniques.

With these landmark and semilandmark information several statistical analyses were used to assess several grouping hypothesis based on previous studies that range from the possible scenario of two available morphotypes up to four different titanosaur forms. Two main morphotypes have been reported as the more parsimonious hypothesis. Also the geometric morphometric tool kit permit us to refer the material attributed across all the bone types analyzed as labelled as Morphotype I to the exclusive titanosaur taxon found in the fossil site, *Lohuecotitan pandafilandi*. The Morphotype II might corresponds to another exclusive form not previously described in the Ibero-Processorican domain during the Late Cretaceous. There are also some specimens referred to cf. *Lirainosaurus astibiae*.

The differences between the morphotypes can be attributed to a morphofunctional specialization with Morphotype I occupying a more traditional low browsing titanosaurian role while Morphotype II present a characteristic gracile morphology of the forelimb that might be associated with high browser feeding niche exploitation. A dataset of linear measurements of several Neosauropoda taxa including the titanosaurian specimens from Lo Hueco was also analyzed. The hypothesis of morphofunctional specialization is proved and several trends in the architecture of the limbs are found and related to the high browsing capabilities of the feeding envelope. *Lohuecotitan pandafilandi* should have been a lower browsing sauropod while the sauropod of the Morphotype II acquired capabilities to feeding on a higher envelope based statistical proxy models presented in this study..

V.1 INTRODUCTION

In 2007 during the construction of the Spanish high-speed (AVE) railway connection Madrid-Valencia, the fossil site of Lo Hueco was found in the nearby of Fuentes (Cuenca; Fig.V.1). The dismantling of the hill needed for such type of railways revealed thousands of vertebrate fossils in Campanian-Maastrichtian strata (Ortega *et al.*, 2015). The most abundant fossil material are dinosaur remains, to which at least 87% can be attributed to titanosaur sauropods. Several individuals are in connection but most of the material are isolated and without a clear association between specimens.

Previous studies have found two possible different taxa based on the cranial material (Knoll *et al.*, 2013, 2015; Díez Díaz, Ortega, & Sanz, 2014b) and a partial sample of appendicular material (Páramo *et al.*, 2016, 2017; see also Chapter IV). However preliminary studies on the axial and pelvic skeleton of the titanosaurs of Lo Hueco suggested that more morphotypes can be described (Mocho *et al.*, 2016; Vidal *et al.*, 2017). Also one exclusive titanosaur sauropod was established from the site, *Lohuecotitan pandafilandi* (Díez Díaz *et al.*, 2016). These studies noted for a high morphological variation within the sample of Lo Hueco titanosaurs. Differences between those morphotypes described in different areas of the skeleton cannot be confidently assessed as taxonomic differences or intraspecific variability. In addition, it is important to highlight that there are important differences in size between many elements in the sample suggesting the presence of juvenile titanosaurian individuals or a dwarf taxon. In the Ibero-Processorican domain, the presence of small taxa has been referred with *Lirainosaurus astibiae* (Sanz *et al.*, 1999; see also Company, Suberbiola, & Ruiz-Omeñaca, 2009) as well as other known European titanosaur taxa , *Magyarosaurus* spp. (Nopsca, 1915; Csiki, 1999; Stein *et al.*, 2010) and *Paludititan nalatzensis* (Csiki *et al.*, 2010).

The presence of more than one titanosaur form in the same fossil site is not unheard of in the sauropod fossil record (Salgado & Coria, 1993; Vila *et al.*, 2012; Díez Díaz, Pereda Suberbiola, & Company, 2015; Canudo *et al.*, 2016). There are also known bone beds with representatives of multiple sauropod taxa. These sauropod communities shows morphological differences that may suggest different feeding niche exploitation (Stevens & Parrish, 2005a; Mallon & Anderson, 2013; Tschopp & Mateus, 2017). For example, in the fossil sites of Tendaguru Formation there are gracile form and upper-canopy feeders, such as *Giraffatitan brancai*, and low browsers and more robust forms, such as *Dicraeosaurus sattleri* and *D. hansemanni* (Janensch, 1929a, 1961; Christiansen, 2000; Gunga *et al.*, 2002; Taylor, 2009a; Schwarz & Böhm, 2012). Similar scenario is reported in the Morrison Formation with the more robust forms (e.g., apatosaurines and *Camarasaurus* spp.) cohabiting with the specialized and more gracile forms (e.g., the diplodocines *Diplodocus* spp. and *Barosaurus* spp.; and the brachiosaurid *Brachiosaurus altithorax*; Osborn, 1898; Hatcher, 1901; Riggs, 1903; Lull, 1919; Osborn & Mook, 1921; Gilmore, 1925, 1936; McIntosh *et al.*, 1996; McIntosh, 2005).

In this study we will test: I) the presence of at least two morphotypes in the sample of titanosaur appendicular elemetns from Lo Hueco; II) compare the sample of Lo Hueco to the other small titanosaur taxon of the Ibero-Processorican domain, *Lirainosaurus astibiae*, as some of the smallest specimens from Lo Hueco can be referred to the morphs already described in this site; III) the main morphological variance in the sample is intraspecific variability; IV) the morphological differences between the titanosaur morphs described in the sample can be related to differences in feeding niche occupation as suggested in previous studies of the cranial skeleton in the sample of Lo Hueco.

In order to analyze the morphological variation and assess the titanosaur morphs present

in the sample, it is necessary to address the size differences among each bone type. In this study we propose the use of geometric morphometrics (GMM) to analyze the morphological variability in a sample of titanosaur appendicular elements from Lo Hueco site. The GMM tool kit is a reliable method to explore morphological differences without the confounding effects of size and isolating the component of shape (see Bookstein, 1991; Hammer & Harper, 2008; Zelditch, Swiderski, & Sheets, 2012). This methodology also permits quantify the shape variables and use exploratory and classification techniques (Zelditch *et al.*, 2012).

Preliminary studies indicates that one of the described appendicular morphotypes of Lo Hueco, the Morphotype I, presents less robust proximal hindlimb elements (Páramo *et al.*, 2016, 2017; see Chapter IV) but short and slightly robust forelimb elements (Páramo, Ortega, & Sanz, 2015; this chapter). The relationships between the forelimb and hindlimb retain also the typical wide-gauge titanosaurian plan (see Wilson & Carrano, 1999; Carrano, 2005). While the Morphotype II has a more robust hindlimb than in the Morphotype I (Páramo *et al.*, 2015, 2016) but an exceptionally slender and elongated forelimb (Páramo *et al.*, 2015). Traditionally the high browser sauropods have been identified with brachiosaurids: *Brachiosaurus altithorax* and *Giraffatitan brancai* have been reconstructed several times with different biomechanical hypothesis (Bakker, 1987; Paul, 1988; Gunga *et al.*, 1995, 1999, 2002; Christian, Heinrich, & Golder, 1999; Christian, 2002; Stevens & Parrish, 2005a; Dzemski & Christian, 2007; Taylor, Wedel, & Naish, 2009; Taylor, 2009b). Despite differences on the reconstructions of the posture of the neck and head, all the hypotheses coincidesuggests a high browser feeding specialization thanks to particularly neck morphology, pectoral girdle modification, and rotation of the sacrum angle respective to the axial plane. But more important to our study, its long and slender forelimb which supersede the length of the hindlimb, a specialized condition within Sauropoda. Thanks to the forelimb and rotation of the girdle, the neck could reach more height than other sauropods whether it face upward or arch gently. This dorsiflexion of the neck and upward posture permit to reach greater heights without need to develop specialized mechanisms, such as occasional bipedalism (Mallison, 2011; Paul, 2017).

Other sauropod taxa with a high browser feeding envelope tend to have a proportionally greater anterior half of the body (Bates *et al.*, 2016). Instead of a longer forelimb than hindlimb they tend to acquire higher browsing capabilities through other combination of characters as the development of longer necks with more dorsiflexion capabilities (McIntosh, 2005; Christian, 2010). Some of these sauropod taxa maintain the normal sauropod humerus-femur length relationship (see character #214 and #215 in Upchurch, Barrett, & Dodson, 2004; see also Supplementary Material.V.A). However, there are some sauropods with great development of the anterior half of the body, long neck and low browsing feeding capabilities such as the case of the genus *Mamenchisaurus* (Christian *et al.*, 2013). Therefore, a greater development of anterior part of the body can be related with other ingroup specializations and not only with the development of a dorsoventrally higher feeding envelope capabilities.

In order to assess the hypothesis of two main morphotypes present in Lo Hueco we will use GMM tool kit to analyze the shape variation within the sample. We will also compare the shape of each bone type with other small size titanosaur from the Ibero-Processorican domain: *Lirainosaurus astibiae* (Laño site, Spain). In order to test if our results are compatible with two different ecomorphological specialization and a possible feeding niche partitioning, a proxy model will be developed to analyze several morphological traits of the forelimb and hindlimb with feeding specialization comparing with published biomechanical results from other sauropods.

The sample of Lo Hueco is an opportunity to test the hypothesis of ecomorphological specialization. The morphological variation between the Lo Hueco appendicular specimens can be related with results obtained of paleoneuroanatomical analyses and dietary habits as well as compare with other known sauropod bonebeds.

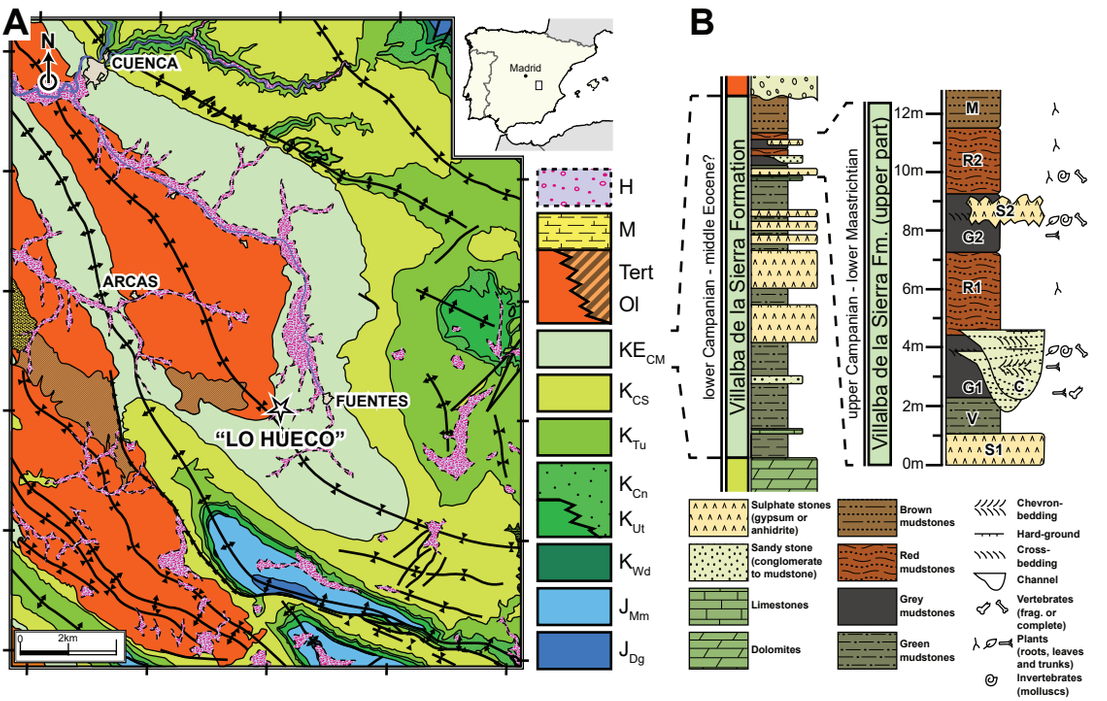

Fig.V.1. Lo Hueco fossil site location and stratigraphy. (A) Geological map of Cuenca (Spain). (B) General stratigraphic column of the Villalba de la Sierra Formation and the Lo Hueco fossil site. (C) Photography of the Lo Hueco site during the 2007 campaign. Labels indicates the levels of the stratigraphic column.

Methodology abbreviations:

bpca – Bayesian Principal Component Analysis; GMM – Geometric Morphometrics; GLM – Generalized Linear Model; GPA – Generalized Procrustes Analysis; km – K-means cluster; LDA – Linear Discriminant Analysis; PC – Principal component; PCA - Principal Component Analysis; tps – Thin Plate Spline.

Anatomical abbreviations:

Humerus:

aep – anterior entepycondyle/entepycondylar process; af – anconeal fossa; alp – antero-lateral process; amp – antero-medial process; dpc – deltopectoral crest; dpcar – deltopectoral accessory ridge; hh – humeral head; pat – posterior accessory trochanter rac – radial condyle; ulc – ulnar condyle.

Ulna:

adp – anterior distal process; alp – antero-lateral process; amdf – anterior middle distal fossa (articulation with the radius); amp – antero-medial process; olc – olecranon; op – olecranon process; rds – radial distal scar; raf – radial fossa (proximal radial articulation).

Radius

antf – anterior fossa; mp – medial process; pldc – posterolateral distal condyle; pmdc – posteromedial distal condyle; rmi – ridge for muscle insertion (mm. biceps + brachialis).

Femur:

4th – fourth trochanter; at – accessory trochanter; epi – lateral epicondyle; gt – greater trochanter; if – intercondylar fossa; lb – lateral bulge; lic – linea intermuscularis cranialis; fc – fibular condyle; fh – femoral head; tc – tibial condyle; ts – trochanteric shelf.

Tibia:

aap – anterior ascending process of distal condyles; cc – cnemial crest; pc – posterior condyle.

Fibula:

ap – anterior process; alp – anterolateral crest (proximal); lt – lateral trochanter;

ts – tibial articulation scar.

Common abbreviations:

at – accessory trochanter; ri – ridge; s – sulcus; tr - trochanter

Institutional abbreviations:

MUPA – Museo de Paleontología de Castilla La Mancha, Cuenca, Spain; MCNA – Museo de Ciencias Naturales de Álava / Arabako Natur Zientzien Museoa, Vitoria-Gasteiz, Spain.

The complete report of the institutional abbreviations of the sampled specimens in the statistical analysis can be accessed in Chapter III.I.

V.2 MATERIAL AND METHODS

The comparison between several of Lo Hueco specimens and other taxa of the Ibero-Processorican domain up to specimen level is important to discern the variation attributable to different taxonomic units to the intraspecific variation. Several morphological differences are detected in the contour of the elements such as the humerus proximal morphology (Páramo *et al.*, 2015). Previous studies have found taxonomic differences in the analysis of the outline of appendicular specimens (e.g. Ruscillo, 2000; see also ontogenetic changes in the appendicular skeleton of the sauropod *Rapetosaurus krausei* Curry Rogers *et al.*, 2016) and with the analysis via 2D geometric morphometrics specifically in Sauropod dinosaurs (Bonnan, 2004, 2007; Canudo & Cuenca-Bescós, 2004; Wilhite, 2005; Schwarz & Böhm, 2012). However, 2D shape variables obtanied through GMM tool kit may be not enough for assess differences among derived Titanosauria. The adaptation to gigantism in Titanosauriformes is related with a conservative morphology and fixation of several features of the appendicular skeleton. Therefore its morphology is more related with the acquistion of wide-gauge posture and the dynamic stability on the appendicular skeleton (Ullmann, Bonnan, & Lacovara, 2017) rather than present significative differences among the operative taxonomical units (Ullmann & Lacovara, 2016; Ullmann *et al.*, 2017). Also, previous studies on Late Cretaceous Ibero-Processorican titanosaur femora present differences on morphological features that also involves the third dimmension, the anteroposterior development of the specimen (see Vila *et al.*, 2012) not captured in previous 2D GMM studies on sauropod appendicular skeleton (e.g. Wilhite, 2005; Bonnan, 2007; Schwarz & Böhm, 2012).

For this reason, the comparative analyses between the morphotypes of Lo Hueco and *Lirainosaurus astibiae* as well as quantification of shape variables will be obtained from 3D landmarks and semilandmarks over 3D model representation of each sampled specimen. Specimen digitizing was carried out with a photogrammetry array (see Mallison, 2011). We use a Canon EOS 1100D and Canon EOS 80D with Canon EFS 18-55mm f3.5-5.6, Canon 50mm f1.8 and Sigma 17-50mm f2.8 for the pictures needed in the photogrammetry process. Photographs were made when possible in 35mm focal distance, as it is the closer to no lens distortion in both wide-range lenses. 50mm lenses produce near 0 distortion by default. It is also important to note that both cameras are APS-C sensor type so the edge of the lenses where the distortion occurs is greatly cropped for about a factor of x1.6. Also the photograph RAWs were processed with Camera RAW™ standard correction algorithm for each lens type. Photogrammetry was processed in Agisoft Photoscan™ v1.4. Some of the elements were digitized in an early stage of this research via IR device with an XboX 360 Kinect™ sensor (see Falkingham, 2013). This device produce low resolution digital models accurate up to the millimeter. Accuracy of the model reconstructions is provided in Supplementary Material.V.B. All the 3D models used for the analyses herein performed are meshes of 150.000 polygons representative of the original specimen.

In order to construct an ecomorphological proxy linear model, several measurements related with the length and robustness of each bone element. Measurement database for the morphometric multivariate statistics were sampled with two different methods. Measurements for the sample of Lo Hueco specimens and other taxa accessed during this study were taken with measurement tape and a caliper. Other specimens included for comparison were accessed from the available bibliography and measurements were taken with ImageJ v2.0.0 (Rueden *et al.*, 2017). Measurements used in this study as well as citation of the material from bibliography are available in Supplementary Material.V.C.

V.2.1. 3D LANDMARK BASED GEOMETRIC MORPHOMETRICS

The definition of each landmark and semilandmark is based on major anatomical structures of sauropod limb elements. They are placed over a sculpted theoretical template of each bone following Souter *et al.* (2010; see also Botton-Divet *et al.*, 2015). The landmarks are based mostly on type I and II biologically homologous points among the sample (Bookstein, 1997). Semilandmark curves are delimited by landmarks at their extremes and sometimes at midpoints of complex curves. However, sauropod dinosaur appendicular elements might lack points of clear intersection or ending in some structures (e.g. limits of the articulation of the femoral head, distal end of the lateral trochanter of the fibula). On other hand, structures like the lateral bulge of the femur, the cnemial crest of the tibia and the deltopectoral crest of the humerus have clear definite endings (see Romer, 1956; McIntosh, 1990; Otero, 2018). This can lead to delimit several of those structures by type II or even type III landmarks. However, the type III landmarks are not as consistent and the homology can be problematic and have been avoided when possible. Definition of each landmark and semilandmark curve as well as landmark type and number of semilandmarks along each curve can be found in Table.V.1. Landmarks and curve semilandmarks were collected with the software IDAV Landmark™ editor v3.0.7 (Wiley *et al.*, 2005: www.idav.ucdavis.edu/research/EvoMorph).

One of the main problems of the sauropod record is the fragmentary state of many of the specimens (see Upchurch *et al.*, 2004; Tschopp, Mateus, & Benson, 2015). This is more accentuated in the record of titanosaur sauropods. A significant number of titanosarian taxa are erected using incomplete specimens, being the caudal vertebrae and limb bones the most common elements represented on these associations (e.g. Upchurch *et al.*, 2004; Tschopp & Dzemski, 2013). Lo Hueco fossil site have yielded a diverse and abundant sample of titanosaurian bones, which show high degree of variability. Unfortunately, the preservation of part of this material is highly affected, including gypsum growth and the presence of iron crusts in the bone surface, as these crusts substitute the periosteum of bone (Cambra-Moo *et al.*, 2012; Marcos-Fernández *et al.*, 2014, 2019). Several elements are only partially preserved, and some parts have been totally lost, especially the articular faces, such as the proximal and distal ends of long bones.

It is necessary some considerations for the assessment of intraspecific variability in Lo Hueco sample but also in the sauropod record. Usually in this kind of scenarios one way to deal with specimen incompleteness is to develop a reduced database of measurements or landmarks (Zelditch *et al.*, 2012; Brown, Arbour, & Jackson, 2012). However, some studies have found that reduced database both via variable trimming and/or downsampling can lead to analytical bias (Brown *et al.*, 2012; Arbour & Brown, 2014; Clavel, Merceron, & Escarguel, 2014).

Landmark estimation method as well as general multivariate dataset imputation methods have been developed for decades (e.g. Schafer, 1999; Gauthier, Landry, & Lapointe, 2003; Gunz *et al.*, 2009; Arbour & Currie, 2012). The usage of more common landmark estimation methods requires an abundant sample ranging from dozens to hundred specimens (see the original works of Schæfer *et al.*, 2004; Gunz, 2005; Gunz, Mitteroecker, & Bookstein, 2005; Gunz & Mitteroecker, 2013). The very same tool used for sliding of the semilandmarks and adjust the coordinates to the curve of the anatomical feature can be used to estimate missing landmarks (Gunz *et al.*, 2009; Molnar, Pierce, & Hutchinson, 2012; Schlager, 2013). While thin plate spline can be useful for geometric estimation of morphology, the lack of available complete specimens in this study can

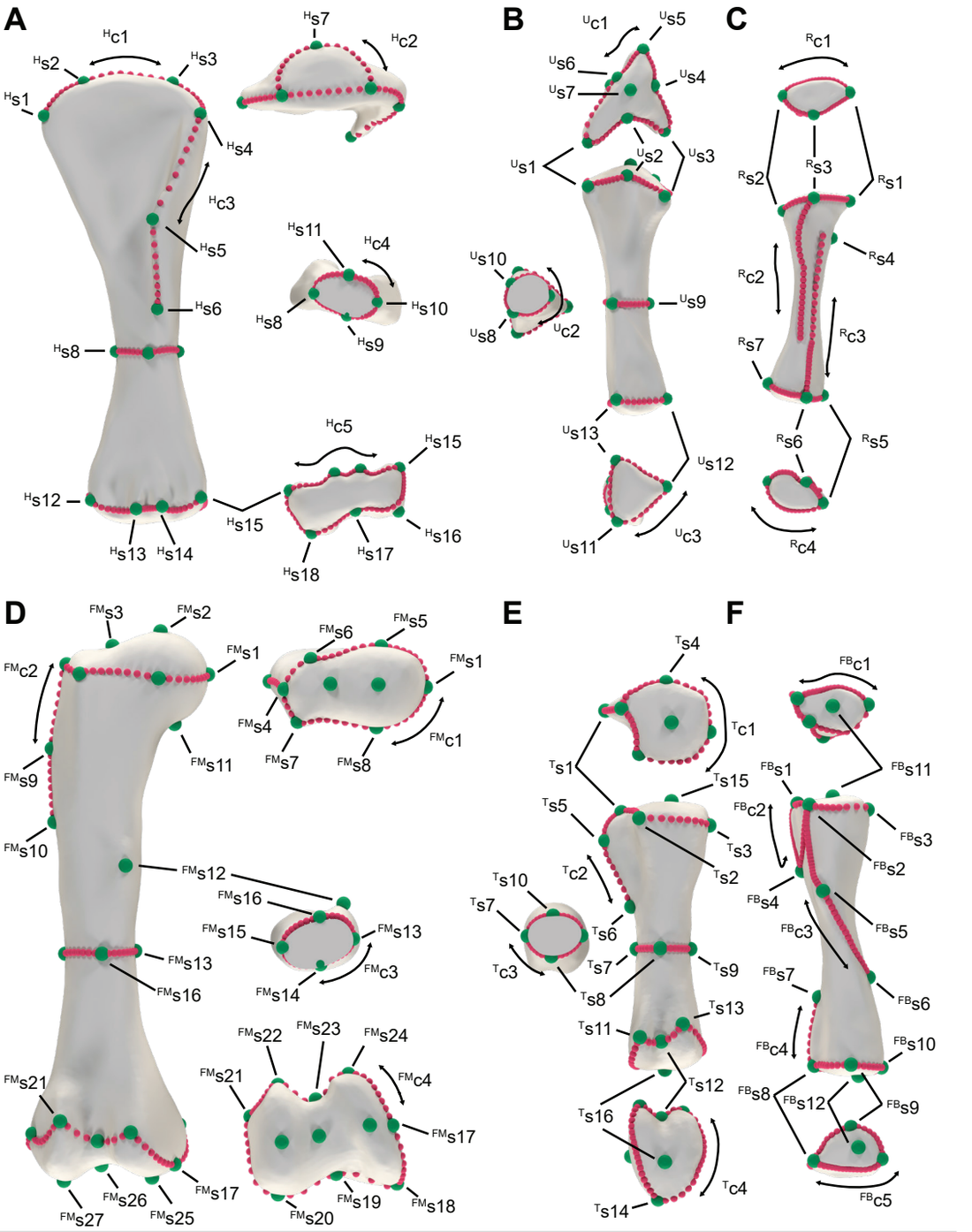

Fig.V.2. Landmark definitions used in the current study. (A) Humerus in anterior, proximal, midshaft cross-section and distal view. (B) Ulna in proximal, anterior, midshaft cross-section and distal view. (C) Radius in proximal, posterior and distal view. (D) Femur in posterior, proximal, midshaft cross-section and distal view. (E) Tibia in proximal, lateral, midshaft cross-section and distal view. (F) Fibula in proximal, lateral and distal view.

			Semilandmarks		
	N	Landmarks	N	Curves	Missing
Humerus	18	s1-s18			20.78%
			30	c1	60.71%
			20	c2	64.29%
			20	c3	42.86%
			40	c4	3.57%
			70	c5	50.00%
			783	surface	
Ulna	13	s1-s13			26.92%
			60	c1	50.00%
			30	c2	0.00%
			30	c3	43.33%
			810	surface	
Radius	7	s1-s7			2.78%
			28	c1	0.00%
			28	c2	0.00%
			46	c3	0.00%
			41	c4	25.00%
			687	surface	
Femur	24	s1-s24			25.33%
			50	c1	68.00%
			20	c2	20.00%
			40	c3	0.00%
			60	c4	60.00%
			898	surface	
Tibia	14	s1-s14			22.93%
			40	c1	47.37%
			20	c2	52.63%
			40	c3	0.00%
			50	c4	73.68%
			655	surface	
Fibula	10	s1-s10			16.30%
			40	c1	37.04%
			40	c2	25.93%
			44	c3	3.70%
			10	c4	37.04%
			40	c5	48.15%
			719	surface	

Table.V.1. Landmark and semilandmark used in the current study. The definition of each landmark and semilandmark dataset can be accessed in Supplementary Material V.E.

obscure the results. Other reconstruction methods are available through digital modelling based on the actual specimens (Stevens & Parrish, 2005b; Hutchinson *et al.*, 2011; Hutchinson, 2012; Molnar *et al.*, 2012; Stevens, 2013; Lautenschlager, 2017). Taking into account the morphological changes and especially the variation in a population whether it is interspecific or intraspecific variation (including individual variation), manual distortion of the specimens is not acceptable. The estimation methods cannot rely on a manual digital sculpture of the elements, as it would increase error and morphological biases. The method implemented in this study is a combination of landmark estimation method and virtual reconstruction techniques. The use of techniques that were tested in recent reconstruction studies permit us to reliably estimate the coordinates but also generate meshes that can be applied for the usage of semilandmarks along curves and surfaces. A previous study using TPS in absence of meshes demonstrate that while there is some deviation in presence of low sample, it is reliable for estimation of the missing surface of the specimens (Páramo, 2018).

The missing data from the landmark database was estimated with multiple imputation methods. Multiple imputations preserve better the original structure of the data with low dispersion from the original variation-covariation from the data (Schafer, 1997; Schafer & Olsen, 1998; van Buuren, 2007; Brown *et al.*, 2012; Clavel *et al.*, 2014). This implies that they retain the biological information accurately (Clavel *et al.*, 2014; Bak & Hansen, 2016).

Several methods have been discussed in the literature (Schafer, 1999, 2003; Oba *et al.*, 2003; van Buuren, 2008; Abayomi, Gelman, & Levy, 2008; Mitra, 2011; Clavel *et al.*, 2014; Dray & Josse, 2015). Here we use two different algorithms to estimate the missing coordinates and curves; the commonly used Thin Plate Spline (TPS) following Gunz *et al.* (2009) and Bayesian principal component analysis (BPCA) of the most complete specimens to impute the partial aligned missing elements (Oba *et al.*, 2003; Arbour & Brown, 2014). This stage of the data pre-process produces a complete set of landmarks and semilandmarks with acceptable estimations of the landmark positions (see Supplementary Material.V.C for accuracy calculation). There are two separate landmark dataset, one dataset of landmarks after estimation via BPCA- algorithm and another after estimation via TPS- algorithm.

In order to slide the semilandmarks, we generate a consensus mesh based on a projection of the template mesh to the landmark and semilandmark configuration (or estimated configuration if there was any missing landmarks initially) after the previous stage. The template is aligned and warped via TPS-algorithm both for the TPS-landmark dataset and BPCA-landmark dataset (following Gunz *et al.*, 2009; Tschopp & Mateus, 2012; Gunz & Mitteroecker, 2013). The TPS-algorithm used over an actual 3D polygon mesh acts in a similar way as sculpting with NURB curves (Molnar *et al.*, 2012) with the exception that it is automated and not manually placed, avoiding the commented problematics on manual reconstruction of missing structures.

The meshes produced with this method do not differ greatly from original scans of the specimens (see Supplementary Material.V.C). With this method, the original morphology is preserved accurately, specimens with missing parts are virtually reconstructed and all the specimens share the same baseline bias, so it may not further distort the analysis of the incomplete specimens. We imputed the missing data with package "mice" v3.3.0 (van Buuren & Groothuis-Oudshoorn, 2011), the package "LOST" (Arbour & Brown, 2014).

With an available surface for all the specimens including those initially incomplete, projection of surface semilandmarks and sliding of the curves and surfaces can be done. For the definition of surface semilandmarks the original template mesh was retopologized in a quadrangular poly mesh with a reduced number of vertex equal to the desired number of surface semilandmarks. This method is used to produce meshes of regular spaced polygons with similar area. We can use this tool to produce an equidistant and regular point cloud used as surface semilandmarks prior to sliding. This process was made in Instant Mesher v1.0 (Jakob *et al.*, 2015: http://igl.ethz.ch/projects/instant-meshes/). The retopologized meshes were imported in R and the vertex converted into 3D coordinates over the atlas using the package "mesheR" (Schlager, 2016). The coordinates were projected into each specimen following standard procedures proposed by Souter *et al.* (2010). For the projection of the surface semilandmark configurations, we used the warped meshes for each specimen instead of the original meshes, as some of them are incomplete specimen in origin. The number of surface semilandmarks used can be found also in Table.V.1 and the projection over atlas in Fig.V.2. This method resembles what other software can do within an interface, e.g. in semilandmark relaxation methods from the atlas surface to each specimen in DHAL Viewbox 4™ and IDAV Landmark™. Also, surface semilandmark automatic or semiautomatic methods are already in use as in the creation of eigensurface sampling grids and projection (Sievwright & MacLeod, 2012).

V.2.2. GENERALIZED PROCRUSTES ANALYSIS AND DISCRIMINANT ANALYSIS

The landmark and semilandmarks are slided following Gunz *et al.* (2005) recommendations. We used 10 iterations of recursive sliding, based on Bending energy minimization (Bookstein, 1996; Gunz *et al.*, 2005; Perez, Bernal, & Gonzalez, 2006) with the default threshold provided in the "Morpho" package sliding function (Schlager, 2017). The results are then aligned via Procrustes Generalized Analysis (Gower, 1975) to ensure they are centered, size effect removed and translated to an standardized position in which can be analyzed.

There is a practical problem with the post-burial deformation and taphonomical warping of the specimens when we try to analyze fossil shape variables. Fossil material is often affected by the inherit deformation of the embedding strata in which they are preserved (Motani, Amenta, & Wiley, 2005; Arbour & Currie, 2012; Tschopp & Dzemski, 2013; Hedrick & Dodson, 2013). The different processes post-mortem to which the fossil material is exposed can produce diverse outcomes in the preservation of the material even in the same fossil site (e.g. Lo Hueco site in Díez Díaz *et al.*, 2016; Marcos-Fernández *et al.*, 2018). Taphonomical and post-mortem warping assessment is beyond the scope of this work. However, one way to deal with this problem is to adapt the Geometric Morphometrics (GMM) method to an analysis of both shapes as a combination of the biological and taphonomical processes. Both processes are united here as an analysis of the taphomorphospaces following Hedrick & Dodson (2013). We consider that the results in each Principal Component Analysis (PCA) summarize variance in morphology by taphonomical warping and the biological processes. We then proceed to discuss the reported variation trends within the sample taking into account the effect of possible taphonomical deformation in our results.

Morphological variation can be observed with PCA over the procrustes coordinates after centering and scaling all the specimens in each bone type dataset. PCA is a multivariate tool

often used in dimensional reduction. It transforms correlated variables into orthogonal axis that maximize the variance of original observations (Campbell & Atchley, 1981; Sainani, 2014). The results are a new space in which each Principal Component (PC) is uncorrelated to the other axes and each PC express the maximum variance in all the variables or landmarks in GMM.

PCA were carried out for each type of element over the procrustes coordinates with the package "pcaMethods" (Stacklies *et al.*, 2007) with a maximum of 50 components saved in each analysis. A list of PCs recovered with the variance and cumulative variance explained, as well as, the eigenvectors is available in the Supplementary Material.V.D.

In this study we discuss the possible assessment of the described morphotypes in previous Chapters and their differences from other Late Cretaceous taxa of the Ibero-Processorican domain. Calculation of shape variance attributable to intraspecific variance in appendicular elements is also analyzed after testing for morphotype differences. In order to test the proposed morphotype description we compared this a priori grouping assumption via pair-wise Kruskall Wallis tests between the morphotypes and between each morphotype and Ibero-Processorican titanosaur *Lirainosaurus astibiae*.

Among the ordination methods useful for testing grouping hypotheses it is normally employed the Linear Discrimination Analysis. However, the available sample does not meet the requisites for a traditional Linear Discriminant Analysis as the number of variables exceed the number of specimens as well as presenting an uneven group distribution among the different sampled species e.g. *Lirainosaurus astibiae* (see Claude, 2008; Zelditch *et al.*, 2012; see explaination in Supplementary Material.V.E.).

Clustering patterns based on the data without an a priori assumption can be made with the k-means algorithm (Bow, 1984; Selim & Ismail, 1984; Rokach & Maimon, 2007). The k-means function differs from other unsupervised exploratory techniques on the absence of an a priori assumption of grouping. Instead of exploring the most probable distribution from an initial grouping hypothesis; the k-means uses an a priori hypothesis of number of clusters instead. The algorithm assign randomly each specimen *s* to a cluster *c* and calculates the cluster centroids. Then the algorithm reassesses each classification of the *sj* specimens to the closer centroid until the centroid error function cannot be decreased further (Rokach & Maimon, 2007). Optimal number of cluster can be assessed by the "elbow rule". This "rule" implies the calculation of the total between-groups variance sum of squares is calculated and divided by the total sum of squares of all the sample, the optimal number of groups is when this ratio form an "elbow" if plotted.

In other words, it is considered optimal when between group variance/total variance ratio cannot be improved significantly increasing the number of groups (Rousseeuw, 1987). As several iterations of the algorithm can be run with different number of clusters to search, it is a desirable method to assess clustering distribution without several different a priori group hypotheses. So we can observe in our results if the presence of two, three or more morphotypes explain better the variance of our sample and which specimens are referred to each cluster for the n iterations. However this technique, while do not have strong requisites, is susceptible to non-isotropic cluster distributions, presence of outliers and noisy samples (Rokach & Maimon, 2007). So here it is also discussed the biological significance of the final grouping distribution reported by the algorithm

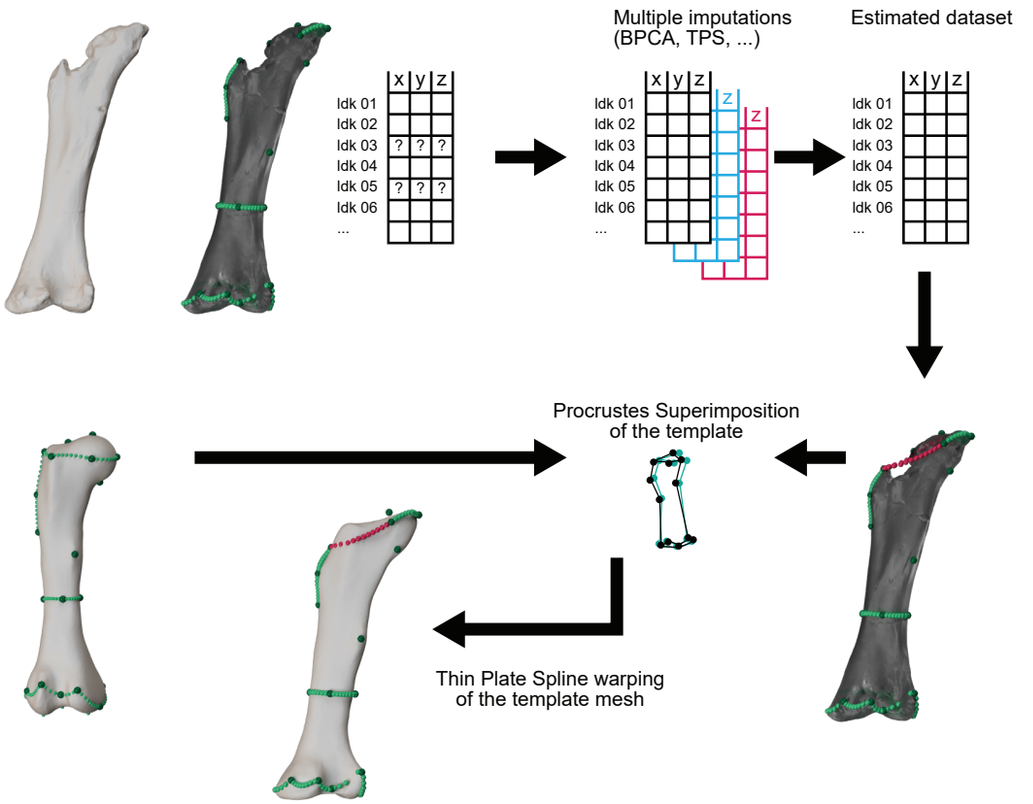

Fig.V.3. Virtual restoration workflow. From estimation of missing landmarks to generation of the new specimen mesh through warping of the template mesh to the estimated landamrk configuration

to check if it is representative of the morphotype distribution of the sample. Or else, the algorithm only reports differences between morphologies without biological significance (i.e. dividing in different clusters specimens which are clearly assessed for the same morphotype).

V.2.3. MORPHOFUNCTIONAL LINEAR MODELLING

To test the ecomorphological specialization hypothesis, we have used a database of several standard measurements in sauropod paleontology. These measurements of the appendicular elements are listed in Table.V.2 and are related with robustness of each specimen. The robustness of a specimen can be summarized and quantified by the robustness index (Wilson & Upchurch, 2003). This is the ratio of the mean relationship between measurements of the width on the proximal, middle and distal part of each element type, to the length of the specimen.

For testing the relationships of the bone robustness in each element of the forelimb and hindlimb with a morphofunctional specialization, the comparative species were sampled based on several studies of the feeding envelope and body bauplan within the clade Neosauropoda (Tütken, 2011; Stevens, 2013; Bates *et al.*, 2016; Ullmann *et al.*, 2017). However, the range of species in which we know the neck posture with certainty is low, especially among titanosaur sauropods.

For many species the neck posture is unknown but can be estimated by extrapolation. For this reasons we have included several other species, which biomechanics and neck posture (see Barrett & Upchurch, 1994; Christian, Dzemski, & Moeller, 2009; Christian *et al.*, 2013; Christian & Dzemski, 2011; Stevens, 2013) are not assessed but we know the volume distribution within the sauropod body plan evolution for many more species (Bates *et al.*, 2016). There are studies on sauropod body mass and vertebral morphology related with feeding envelope and maximum dorsiflexion range (Paul, 2017). There are also studies of dental microwear (Fiorillo, 1998; Whitlock, 2011) and isotopic composition relatable to different types of plant consumption (Tütken, 2011) that insight differences in vegetation consumption relatable to different feeding niche exploitation in height. These species have been included, feeding envelope specialization assessed based on greater development of anterior portion of the body or data on their probable feeding. Forelimb and hindlimb element measurements were taken from bibliography or *in situ* observation with all the caveats commented before for the sample of Lo Hueco. The complete list of taxa (Table.V.2) summarizes the available *N* of each specimen type, the feeding envelope and gauge (a posture acquired within Titanosauria) as biomechanical specializations, as well as, the method assessment of the feeding envelope and related neck and limb posture.

Some considerations on the sampled taxa for the linear models in this study regard some taxonomic reassessment over recent years (Remes, 2006, 2009; Taylor, 2009b; Tschopp *et al.*, 2015). Some species were also considered invalid (Remes, 2007b, 2009; Tschopp *et al.*, 2015). *Barosaurus* spp. have been included both the North American record and the Tendaguru material attributed to "*Barosaurus africanus*" (Fraas, 1908; Janensch, 1929b, 1961). In the case of the Tendaguru material, all species previously attributed to "*B. africanus*" have been considered to be relatable to the feeding envelope hypothesis attributed to *Barosaurus* following *Barosaurus lentus* - Marsh 1890 reviewed by McIntosh (2005) and based on the body plan estimations of Bates *et al.* (2016). Also all the corresponding taxon names have been updated to its more recent taxonomical determination, as some of the material was regarded as *Tornieria africana* (see Remes, 2006), while other material have not been precisely reassessed yet. For this study, the material of the third sauropod form genus cited in the Tendaguru bed is regard as "*Barosaurus africanus*" (see Remes, 2009). The inclusion of extremely giant lognkosaurian forms as high browser is based on extrapolation from body mass distribution and vertebral morphology (see Paul, 2017).

Not all the specimens are complete, in some (few) cases by lacking published measurements and photographical material where digital measurement could be established. The complete set of variables derived from the estimation method have been log 10 transformed to ensure normality of distribution as some element types suffer from platykurtic and slightly asymmetrical distributions. Size is another problem when we are taking account of such different sauropod groups. In one hand, some of the sampled specimens are from juvenile individuals of *Rapetosaurus krausei* (Curry Rogers, 2009; Curry Rogers *et al.*, 2016), *Camarasaurus* spp. (Carpenter & McIntosh, 1994; Foster, 2005; Ikejiri, Tidwell, & Trexler, 2005) and *Apatosaurus* sp. (Foster, 2005). Also some taxa have extreme size differences such as the small to medium sized taxa *Lirainosaurus astibiae* (Sanz *et al.*, 1999; Company *et al.*, 2009) and *Patagotitan mayorum* (Carballido *et al.*, 2017). Extracting size effect over linear measurements can be done by multiple methods. The most extended method is dividing the lateromedial width (or any other measurement) by the length (Wilson & Upchurch, 2003; Bonnan, 2004; Ikejiri, 2004; Bonnan, Farlow, & Masters, 2008; Stubbs & Benton, 2016).

Table.V.2. Sauropod taxa included in the ecomorphological proxy model. *N* - sample. *Rob.* - Robustness Index following Wilson and Upchurch (2003). Complete bibliography of the dataset in Supplementary Material V.A.

		Humerus		Ulna		Radius		Femur		Tibia		Fibula			
Genus	Taxa / Morphotype	N	Rob.	N	Rob.	N	Rob.	N	Rob.	N	Rob.	N	Rob.	Feeding Envelope	Gauge
Amphicoelias	*Amphicoelias altus*	-	-	-	-	-	-	1	0.20	-	-	-	-	Low Browser	Narrow
Apatosaurus	*Apatosaurus ajax*	1	0.31	1	0.36	1	0.29	1	0.26	1	0.28	1	0.17	Low Browser	Narrow
	Apatosaurus louisae	4	0.36	1	0.19	1	0.25	4	0.24	1	0.33	1	0.19	Low Browser	Narrow
	Apatosaurus sp.	17	0.36	15	0.27	10	0.24	25	0.27	14	0.27	13	0.19	Low Browser	Narrow
Barosaurus	*Barosaurus lentus*	1	0.25	-	-	1	0.12	1	0.23	1	0.21	-	-	High Browser	Narrow
	Barosaurus sp.	2	0.25	1	0.16	1	0.19	-	-	-	-	1	0.15	High Browser	Narrow
	"Barosaurus africanus"	7	0.29	3	0.20	1	0.16	9	0.22	4	0.24	5	0.15	High Browser	Narrow
Brachiosaurus	*Brachiosaurus altithorax*	2	0.21	2	0.24	-	-	1	0.25	1	0.25	-	-	High Browser	Narrow
Brontosaurus	*Brontosaurus excelsus*	2	0.35	1	0.27	1	0.26	2	0.28	3	0.29	2	0.20	Low Browser	Narrow
	Brontosaurus parvus	2	0.33	1	0.25	-	-	1	0.24	-	-	1	0.19	Low Browser	Narrow
	Brontosaurus sp.	-	-	1	0.26	-	-	-	-	-	-	-	-	Low Browser	Narrow
Camarasaurus	*Camarasaurus cfsupremus*	1	0.28	1	0.32	1	0.20	-	-	-	-	-	-	Low Browser	Narrow
	Camarasaurus grandis	9	0.26	5	0.24	6	0.21	5	0.26	5	0.27	6	0.16	Low Browser	Narrow
	Camarasaurus lentus	15	0.31	6	0.25	8	0.24	14	0.27	5	0.30	7	0.18	Low Browser	Narrow
	Camarasaurus lewisi	1	0.26	1	0.21	1	0.20	-	-	-	-	1	0.17	Low Browser	Narrow
	Camarasaurus sp.	38	0.30	17	0.24	15	0.21	40	0.26	16	0.27	15	0.16	Low Browser	Narrow
	...														

Table.V.2. -continues.

Genus	Taxa	Humerus N	Humerus Rob.	Ulna N	Ulna Rob.	Radius N	Radius Rob.	Femur N	Femur Rob.	Tibia N	Tibia Rob.	Fibula N	Fibula Rob.	Feeding Envelope	Gauge
	Camarasaurus supremus	2	0.32	1	0.24			2	0.29	3	0.29	2	0.16	Low Browser	Narrow
Cedarosaurus	*Cedarosaurus weiskopfae*	-	-	-	-	1	0.15	-	-	-	-	-	-	High Browser	Narrow
Dicraoesaurus	*Dicraeosaurus hansemanni*	1	0.33	1	0.22	-	-	4	0.24	2	0.28	1	0.20	Low Browser	Narrow
	Dicraeosaurus sattleri	4	0.28	1	0.23	1	0.20	3	0.21	1	0.24	1	0.16	Low Browser	Narrow
	Diplodocus carnegii	-	-	-	-	-	-	-	-	1	0.21	1	0.15	Low Browser	Narrow
Diplodocus	*Diplodocus hallorum*	2	0.30	-	-	1	0.20	1	0.20	-	-	1	0.16	Low Browser	Narrow
	Diplodocus longus	-	-	-	-	-	-	3	0.22	-	-	-	-	Low Browser	Narrow
	Diplodocus sp.	18	0.28	15	0.22	27	0.19	40	0.22	23	0.22	26	0.15	Low Browser	Narrow
Dreadnoughtus	*Dreadnoughtus schrani*	1	0.33	1	0.29	1	0.22	2	0.35	2	0.30	1	0.21	High Browser	Wide
Galeamopus	*Galeamopus hayi*	2	0.32	1	0.19	2	0.20	1	0.23	1	0.25	1	0.17	Low Browser	Narrow
Giraffatitan	*Giraffatitan brancai*	8	0.23	1	0.22	1	0.19	9	0.24	3	0.30	5	0.19	High Browser	Narrow
Lirainosaurus	*Lirainosaurus astibiae*	5	0.31	1	0.22	-	-	5	0.23	1	0.21	4	0.15	Low Browser	Wide
Lo Hueco Morphotype I	*LoHueco 1*	5	0.32	6	0.27	3	0.18	11	0.21	10	0.16	10	0.16	Low Browser	Wide
Lo Hueco Morphotype II	*LoHueco 2*	17	0.27	4	0.16	1	0.18	11	0.22	7	0.13	14	0.15	High Browser	Wide
Mendozasaurus	*Mendozasaurus neguyelap*	2	0.25	1	0.24	1	0.20	-	-	4	0.20	1	0.16	High Browser	Wide
	…														

Genus	Taxa	Humerus		Ulna		Radius		Femur		Tibia		Fibula		Feeding Envelope	Gauge
		N	obustnes	N	obustnes	N	obustnes	N	obustnes	N	obustnes	N	obustnes		
Neuquensaurus	*Neuquensaurus australis*	9	0.33	4	0.24	2	0.23	9	0.26	4	0.26	3	0.19	Low Browser	Wide
	"Neuquensaurus robustus"	1	0.31	4	0.30	3	0.29	4	0.28	2	0.31	1	0.27	Low Browser	Wide
	cf. Neuquensaurus	-	-	-	-	1	0.20	-	-	-	-	-	-	Low Browser	Wide
Patagotitan	*Patagotitan mayorum*	1	0.28	1	0.33	1	0.28	3	0.24	-	-	-	-	High Browser	Wide
Rapetosaurus	*Rapetosaurus krausei*	3	0.25	1	0.30	1	0.20	2	0.24	2	0.23	3	0.16	High Browser	Wide
Saltasaurus	*Saltasaurus loricatus*	10	0.36	5	0.29	5	0.33	3	0.26	4	0.28	2	0.20	Low Browser	Wide
Tornieria	*Tornieria africana*	2	0.32	-	-	-	-	-	-	1	0.27	1	0.19	High Browser	Narrow

Table.V.2. -continues.

However the creation of ratio based variables can increase the amount of covariation of the data. We decided to employ a scaling function instead of ratios for the linear models(the partial robustness and actual Robustness Index following Wilson & Upchurch, 2003). Other methods include PCA over the original variables in order to rotate and scale in multidimensional space and it is assumed that PC1 correspond to size or size-shape variation, therefore working on the other PC or residual eigenvalues it is the same as working with shape variables. But as our problem does not suffer from high dimensionality, we chose the Mosimann size extraction method instead (Mosimann, 1970). Mosimann equations permit to extract the effect of centroid size in multivariate space and return a transformation of the original variables to shape variables (Mosimann, 1970; Claude, 2008). The multivariate linear models included the categorical variables of the feeding envelope and gauge type, as well as an interaction of both factors given the equation:

log Length ~ *log* Proximal/Midshaft/Distal width + Feeding Envelope * Gauge

This allowed to test the relationships between the partial robustness (width/length of the bone) with the inferred feeding envelope and the limb posture as some of the species of this study pertain to derived Titanosauriformes and this feature is related with major changes on appendicular skeleton (see Wilson & Carrano, 1999). This interaction may translate in e.g. significant relationships among the robustness of some elements of the forelimb and the feeding envelope but only among non wide-gauge sauropods.The interaction of the factors were also tested with Akaike Informaiton Criterion (AIC) in order to see if the model improved including both factors or the interaction between them.

The null hypothesis is no effect by the morphofunctional variables, the linear model only report a significant effect of the width with the length of the element.

V.3 DESCRIPTIVE ANATOMY

V.3.1. MORPHOTYPE I

Humeri:

The humeri are short in comparison to the femora (Table.V.2). They are somewhat robust (see Table.V.3) with an expanded proximal end, two times the midshaft width at least. The proximal end is slightly concave with the humeral head medially flexed (see HUE-817, Fig.V.4). The lateral margin of the proximal expansion presents sometimes a rugosity and an engrossment in anteroposterior but without losing the slightly curved morphology. The transition to the deltopectoral crest is not abrupt, the curvature of the proximal expansion transform in a gently concavity of the lateral margin of the humerus. Some specimens present a straight lateral margin such as HUE-2727, HUE-3054 and HUE-XXYY, but with a weak curvature still. In addition, those elements that present an apparent, straighter lateral margin also have lost the proximal part of the lateral margin and deltopectoral crest. Therefore, it may only be an artefact of preservation. The medial margin presents an abrupt transition from the curved proximal expansion and the shaft. The proximal expansion is convex and continuous with the proximalmost top of the curvature at the humeral head. The deltopectoral crest forms a step-like structure with the Mm. supracoracoideus insertion, which is located distally to one third of the humeral proximodistal length. The crest also has little projection to the interior part of the proximal expansion. The lateral margin presents a marked trochanter in the posterolateral part of the deltopectoral crest. Sometimes this trochanter is slightly upward relative to the M. coracobrachialis insertion. The posterior presents an accessory trochanter near the midline under the lateral fossa (slightly lateral to the level of the humeral head in proximal view).

The ulnar and radial condyles are marked with a subtle distal concavity between them. The medial anterodistal condyle is positioned between the middle part of the distal end and its lateral side. The ulnar and radial component (medial and lateral anterodistal process *sensu* Upchurch, Mannion, & Taylor, 2015) are not separated as in other titanosaurs. The posterior face of the distal end has a triangular and proximodistally elongated anconeal fossa, which extends from the minimum lateromedial width of the shaft to the distal end. The distal condyles form two diverging ridges surrounding the anconeal fossa. The ulnar condyle is more anteroposteriorly expanded. There is a well developed anterior ectepicondylar process slightly medially rotated. Some variation occurs between the proximodistally-expanded distal condyle (e.g. HUE-817, HUE-3057, Fig.V.4) and some elements that present a more anteroposteriorly compressed distal end (e.g. HUE-XXYY) but all retain similar morphology and an anterior ectepicondylar process. Moreover, this differences in the compression do not produce any difference in the rotation of the ulnar and radial condyles, specially the medial face of the ulnar condyle (different to the overall morphology of Morphotype II, see below).

Ulna:

The ulna has some degree of variation in the overall robustness (Table.V.4). It is a rather short element compared to the radius (see Table.V.3 and 4). All the elements in which the proximal end is present have a marked convexity of the olecranon with slightly concave anteromedial process proximal surface. The anteromedial process is slightly curved to

anterior (see Fig.V.4). The anteromedial process is the more robust and up to twice as wide as the posterior process in lateromedial, and slightly wider than the anterior process (e.g. HUE-1137 and HUE-1139). Some differences are found in the proximal and minimum midshaft transverse width. Some elements (e.g. HUE-964 and HUE-3067) present a narrow anteromedial process with the same width as the anterior process. While the proximal part is fragmentary, these specimens do not seems to reach the wide morphology seen in more robust specimens (e.g. HUE-1137). Both HUE-1139 and HUE-654 however present the same expansion in the anteromedial process slightly curved surrounding the articulation of the radius.

Distally, the ulna presents a marked oblique linea in the articulation for the radius from the middle of the proximodistal length to the anteromedial part of the distal end. The midshaft is narrower than the proximal and distal expansions, but it is still robust in some specimens (e.g. HUE-964, HUE-3057). The distal end presents a marked anteromedial to posterior expansion. Especially with the development of a prominent anterior distal process. The distal end is subcircular to slightly triangular with the expansion of this anterior flange.

Specimen	Type	Side	Assoc.	Strat.	Morphotype	Length	R.I.	Ecc. (%)
HUE-817	Humerus	Left	EC11	GI	Morphotype I	631	0.29	202.41
HUE-2356	Humerus	Right	EC03	GI	Morphotype I	588	0.31	246.94
HUE-2727	Humerus	Right	iso	GI	Morphotype I	NA	NA	211.74
HUE-2772	Humerus	Left	iso	GI	Morphotype I	NA	NA	182.70
HUE-3057	Humerus	Left	iso		Morphotype I	NA	NA	172.61
HUE-3228	Humerus	Right	iso	GI	Morphotype I	1010	0.24	180.13
HUE-XXYY	Humerus	Left	EC02	GI	Morphotype I	NA	NA	318.52
					Morphotype I	**Average**	**0.28**	**211.85**
HUE-940	Humerus	Left	iso	GI	Morphotype II	705	NA	230.95
HUE-1060	Humerus	Right	iso	GI	Morphotype II	880	0.20	203.77
HUE-1143	Humerus	Left	iso	GI	Morphotype II	780	NA	248.85
HUE-1356	Humerus	Left	iso	GI	Morphotype II	NA	NA	217.91
HUE-1463	Humerus	Right	iso	GI	Morphotype II	640	0.25	209.66
HUE-1549	Humerus	Right	iso	GI	Morphotype II	1110	0.25	221.43
HUE-1434	Humerus	Left	iso	GI	Morphotype II	840	0.22	238.75
HUE-1499	Humerus	Right	iso	GI	Morphotype II	749	0.28	228.25
HUE-1502	Humerus	Right	iso	GI	Morphotype II	530	NA	234.04
HUE-1530	Humerus	Left	iso	GI	Morphotype II	NA	NA	183.51
HUE-1647	Humerus	Left	EC13	GI	Morphotype II	712	0.25	239.22
HUE-3196	Humerus	Left	iso	GI	Morphotype II	750	0.25	185.78
HUE-3662	Humerus	Left	iso	GII	Morphotype II	512	NA	NA
HUE-3829	Humerus	Left	iso	GI	Morphotype II	NA	NA	197.45
HUE-4208	Humerus	Right	iso	GI	Morphotype II	860	NA	266.04
HUE-4343	Humerus	Right	iso	GI	Morphotype II	690	0.19	180.06
HUE-4522	Humerus	Right	iso	GII	Morphotype II	NA	NA	255.31
HUE-4828	Humerus	Left	iso	NA	Morphotype II	460	0.24	187.18
					Morphotype II	**Average**	**0.23**	**217.77**

Table.V.3. Sample of humeri specimens from Lo Hueco. *iso.* - isolated. *R.I.* - Robustness Index following Wilson & Upchurch (2003). *Ecc.* - Eccentricity Index following Royo-Torres (2009).

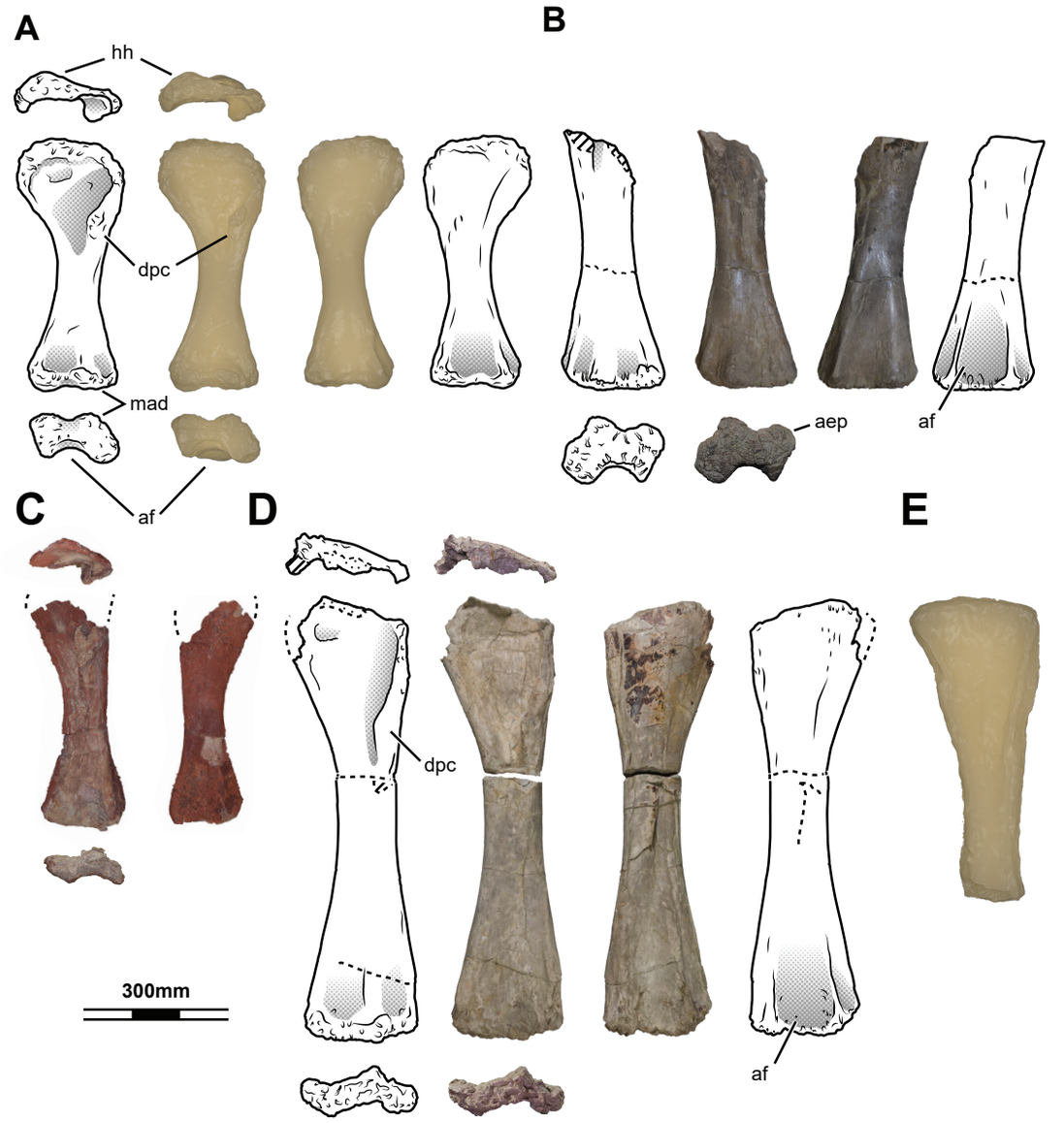

Fig.V.4. Sample of humeri specimens from Lo Hueco. (A) HUE-817 mesh in proximal, anterior, distal and posterior face. (B) HUE-2727 in anterior, distal and posterior face. (C) HUE-XXYY in proximal, anterior, distal and posterior face. (D) HUE-1434 in proximal, anterior, distal and posterior face. (E) HUE-940 in anterior face.

Radius:

The radius is straight with a marked anterolateral projection of the proximal end and posteromedial projection of the distal end. Two marked ridges extend along the posterior face of the shaft, straight to each other. One comes from the proximal end and forms an elongated interosseous ridge. This extends to almost all the shaft down to the distal end as can be seen in specimen HUE-1140. As the sample is the smallest of all the bone types, major differences in size can be observed between the available radii analyzed in this study.

The distal end present a marked concavity between the posterior medial distal condyle and posterior lateral distal condyle (pmdc and pldc following Upchurch *et al.*, 2015)..

Femora:

The hindlimb is gracile in general, especially the femur, and it spreads outside the body sagittal plane much more than the forelimb. The femur of this morphotype is relatively more slender than the distal part of the hindlimb (tibia and fibula; see Fig. V.7, V.8, see also Table. V.6, V.7 and V.8), and present a great medial deflection. The femur presents a bulbous femoral head, transversely expanded. The femoral head is sometimes proximally deflected (e.g. HUE-2338) or slightly upward forming a step between the femoral head and the greater trochanter (e.g. HUE-3108, HUE-2636 and HUE-1366). The greater trochanter presents a laterally abrupt end at the start of the lateral bulge. The lateral bulge is slightly anteriorly flexed in its proximal to middle part. Parallel to the lateral bulge it extends an elongated trochanteric shelf down to the distal end of the lateral bulge. The lateral bulge is robust and expands almost to one third of the proximodistal length.

The fourth trochanter is located distally in the posteromedial edge of the shaft or event in the medial side of the shaft. It starts usually at the same proximodistal length where the lateral bulge ends. The fourth trochanter is deep and marked, sometimes proximodistally elongated, but weakly posteriorly projected. Some elements (e.g. HUE-3108 and HUE-2903) present a robust fourth trochanter. However, other elements (e.g. HUE-1366, HUE-2636 and HUE-8801) does not present it and instead resembles a shallow convexity in posteromedial face. However, latter specimens may be a result of differences related with the ontogenetical stage of development (see Chapter VI).

The shaft is slightly eccentric as in most titanosauriformes elliptical in section (Table. V.6). In the anterior face of the femoral shaft, there is the linea intermuscularis cranialis (Otero, 2010; D'Emic, 2012). The distal condyles are weakly expanded lateromedially. Both condyles present a deep development in anteroposterior. In cases such as HUE-3108, they are more anteroposteriorly wide than lateromedially. The tibial condyle is more posteriorly projected and developed than the fibular one. The tibial condyle is medially flexed. The intercondylar fossa is wide and extends smoothly between anterior and posterior. The distal condyles extends slightly to the anterior face of the distal end. The lateral epicondyle of the fibular condyle is projected posterolaterally with more emphasis on the posterior projection.

Tibiae:

The tibia has a wide, triangular shaped head. The lateromedial width is almost the anteroposterior width of the tibial proximal end. There is a marked fibular trochanter laterally projecting in the proximal end. The cnemial crest is rounded, lateromedially wide and proximodistally long, being developed up to one third of the proximodistal length of the tibia. Some elements present a long posterior ridge of the trochanter mentioned before that extends almost as long as the cnemial crest, parallel to the cnemial crest fibular fossa, similar to the "second cnemial crest" of *Janenschia* (Bonaparte, W.-D. Heinrich, & Wild, 2000; e.g. HUE-1573, HUE-3082,). However, other elements present a shorter ridge and the transition from the shaft to the fibular projection or trochanter in the fibular articulation is more abrupt like in HUE-1573 and HUE-1063. Some elements that are referred to this morphotype (e.g., HUE-1063) lacks part of the proximal end. In these bones, the shaft along the cnemial crest is preserved and does not show a remarkable ridge down the position where the fibular articulation protrusion might have been located, much more similar to HUE-4632.

The tibial shaft is slightly eccentric (Table.V.7) but retains the subcircular to subtriangular morphology with only a slight lateromedial compression of the midshaft (see Fig.V.7). Distally, the anterior ascending process is projected slightly upward respective to the posterior ventral process as in most sauropods. This condyle is more lateromedially long than the posterior ventral process. Both condyles extend completely perpendicular to the anteroposterior width of the shaft or slightly anteriorly bevelled. The distal end is triangular, with a wide lateromedial expansion and the anterior ascending process curved upward. The distal end tends to be convex rather than straight in most specimen (e.g. HUE-1063, HUE-EC3 or HUE-3082).

Fibulae:

The fibula is straight with a slight sigmoid development and a proximal anteriorly bevelling. The proximal end is subectangular in proximal view with a marked anterior trochanter extendning long and medially flexed. This medial deflection is also accompanied with a long anterior sulcus parallel to the anterior trochanter and characteristic in *Lohuecotitan pandafilandi* (HUE-3087) and also present in other fibulae specimens referred to Morphotype I (e.g. HUE-1377 and HUE-1476; see Fig.V.7). The lateral trochanter or M. iliofibularis insertion expanding slightly forward. This trochanter is also robust and oval-shaped in general, projecting from the shaft and rugose in almost all the specimens.

Specimen	Type	Side	Assoc.	Strat.	Morphotype	Length	R.I.
HUE-964	Ulna	Left	EC05	GI	Morphotype I	666	0.19
HUE-1103	Ulna	Right	iso	GI	Morphotype I	NA	NA
HUE-1137	Ulna	Left	iso	GI	Morphotype I	810	0.19
HUE-1139	Ulna	Left	HUE-1140	GI	Morphotype I	614	0.27
HUE-3044	Ulna	Left	EC01		Morphotype I	550	0.26
HUE-2865	Ulna	Right	iso	GI	Morphotype I	493	0.20
					Morphotype I	**Average**	**0.22**
HUE-1158	Ulna	Left	iso	GI	Morphotype II	626	0.15
HUE-1338	Ulna	Right	iso	GI	Morphotype II	676	0.16
HUE-3462	Ulna	Left	iso	GI	Morphotype II	550	0.14
HUE-4357	Ulna	Right	iso	GI	Morphotype II	620	0.14
					Morphotype II	**Average**	**0.15**

Table.V.4. Sample of ulnae specimens from Lo Hueco. *iso.* - isolated. *R.I.* - Robustness Index following Wilson & Upchurch (2003).

Specimen	Type	Side	Assoc.	Strat.	Morphotype	Length	R.I.
HUE-1140	Radius	Left	EC05	GI	Morphotype I	772	0.24
HUE-1340	Radius	Right	iso	GI	Morphotype I	608	0.19
HUE-2711	Radius	Left	iso	GI	Morphotype I	312	0.23
					Morphotype I	**Average**	**0.22**
HUE-1166	Radius	Left	iso	GI	Morphotype II	279	0.21
					Morphotype II	**Average**	**0.21**

Table.V.5. Sample of radii specimens from Lo Hueco. *iso.* - isolated. *R.I.* - Robustness Index following Wilson & Upchurch (2003).

In medial face, the tibial insertion area is an equilateral triangle surrounded anteriorly by the medial expansion of the anterior trochanter and posteriorly by a light flange in the proximal part (e.g.,HUE-3087 and HUE-1377).

The distal anterolateral crest corresponds to almost one quarter of the proximodistal length. This crest is well developed and projected slightly to medial instead of projecting exclusively to anterior.The distal end presents sometimes a flange between the medial and lateral part of the shaft and the ventral face. This end is triangular shaped or slightly rounded, as wide lateromedial than anteroposterior., sometimes slightly bevelled, especially in the posterior as occurs in HUE-1335.

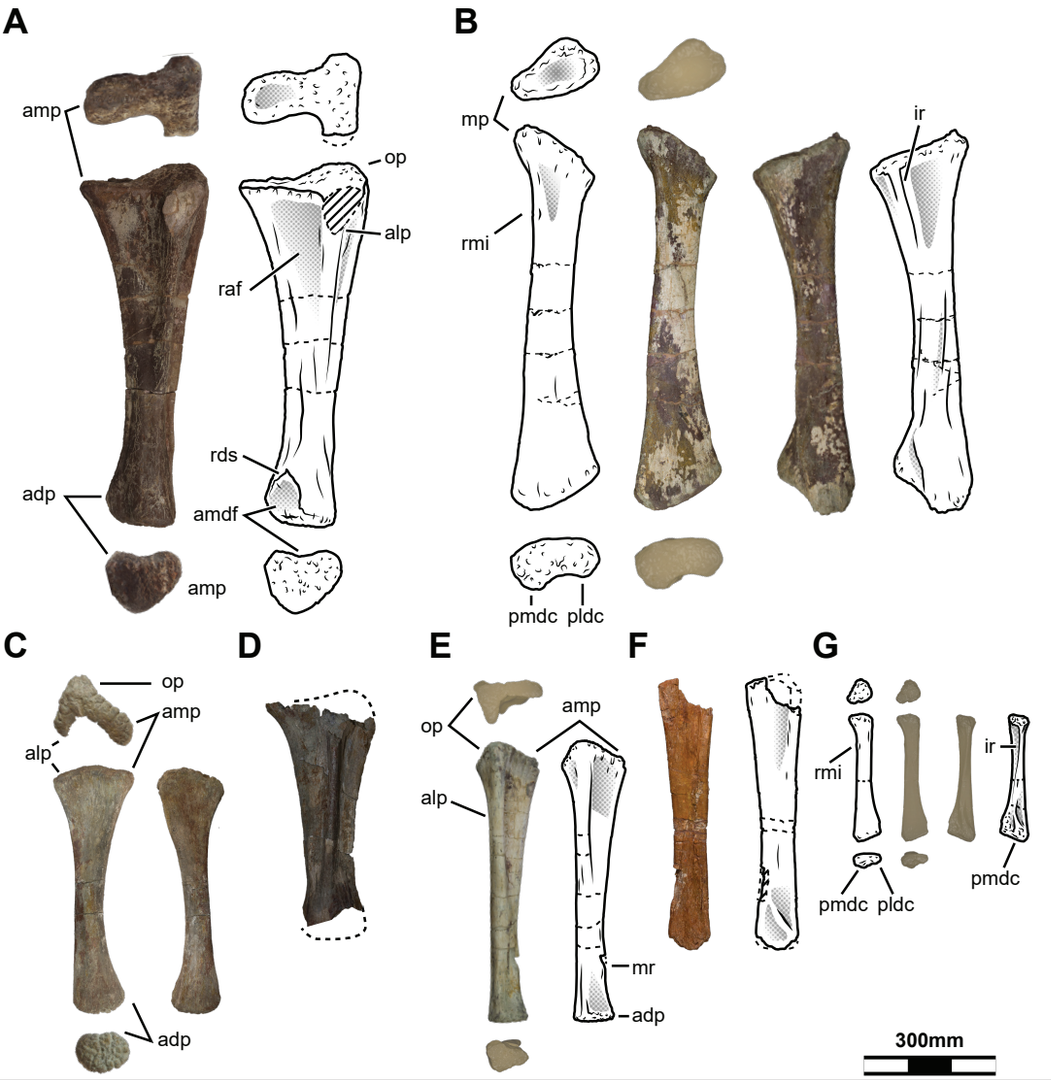

Fig.V.5. Sample of ulnae and radii specimens from Lo Hueco. (A) Ulna HUE-1139 in proximal, anteromedial and distal view. (B) Radius HUE-1140 in proximal (mesh), anterior, distal (mesh) and posterior view. (C) Ulna HUE-2865 in proximal, anterior, distal and posterior view. (D) Ulna HUE-3044 in anteromedial view. (E) Ulna HUE-1158 in proximal, anterolateral and distal view. (F) Ulna HUE-4357 in anterolateral view. (G) Radius HUE-1166 mesh in proximal, anterior, distal and posterior view.

V.3.2. MORPHOTYPE II

Humeri:

The humerus is a straight element with the proximal end is expanded and quadrangular in anterior view, with a squared proximolateral edge (e.g. HUE-940, HUE-1463, HUE-1499; Fig.V.4). Some specimens are slightly fractured in the lateral part of the proximal end, but the quadrangular morphology can still be observed (e.g. HUE-1434, HUE-1502). Some elements present a slightly curved lateral margin, but the curvature is extremely reduced as in HUE-1060 and is almost straight. The medial margin is slightly curved, forming a small step with the humeral head in anterior face (e.g. HUE-1463, HUE-1647). The medial margin has a triangular morphology and the proximal part is slightly more distal than the proximal part of the lateral margin (e.g. HUE-940, HUE-1434, HUE-1463). The humeral head position varies, from a slightly medially placed humeral head as in most sauropods (e.g. HUE-940) to mid part of the proximal end in posterior face (e.g., HUE-1060 , HUE-1463). There is an associated posterior straight to slightly medially deflected ridge, which extends distally from the humeral head (e.g., HUE-940). The deltopectoral crest is projected anteriorly, sometimes with some anterolateral deflection of the entire anterior face, as occurs in the specimens HUE-1143, HUE-1356, HUE-1499 and HUE-3196. However, most of time this deflection is not as pronounced like the deltopectoral crest in HUE-1060, HUE-1463 or HUE-4343, which are anteriorly projected with only slightly deflection of the lateral margin. The M. coracobrachialis insertion of the deltopectoral crest extends into humeral shaft to midpoint of its lateromedial width and it is not limited to the lateral part of the expansion. The proximodistal development of the deltopectoral crest is variable, with some elements that present the insertion of Mm. supracoracoideus and M. pectoralis more proximal to the midpoint of the deltopectoral crest proximodistal length (e.g., HUE-4343). However, in the majority of the preserved humeri present a deep deltopectoral crest, with the main muscular insertion positioned more distally from the humeral head and near the minimum midshaft width (e.g. HUE940, HUE-1434, HUE-3196). The deltopectoral crest is also slender and is slightly recurved outward from the shaft, with a flat anterolateral edge. The deltopectoral crest presents an accessory posterior trochanter in latera edge to posterior face, at the middle of its proximodistal length. This is possibly the typical insertion of the M. teres major and dorsalis scapulae *sensu* Wilhite (2003) and equivalent to the "posterior rounded ridge" from *Haestasaurus becklesii* (Upchurch *et al.*, 2015). Some elements, such as HUE-1060, HUE-3196, HUE-3228 and HUE-4208, present an accessory trochanter near the middle ridge of the posterior face of the shaft. This second accessory trochanter is much less developed than the accessory trochanter of the deltopectoral crest and slightly more distally placed and related with the insertion of the M. latissimus dorsi. (Otero, 2018). Other specimens have a weak convexity instead (e.g., HUE-1356).

The midshaft is slender and much more anteroposteriorly than lateromedially compressed (Table.V.3). The lateral face of the humerus is slightly concave to straight. Many of the specimens present a proximodistal narrow ridge extending two thirds of proximodistal length to the distal end, surrounding the anterolateral fossa (e.g.HUE-1060 and HUE-1434). The distal expansion is subequal or slightly transversely shorter than the proximal expansion as occur in HUE-1060 (thought the majority of elements have lost the dorsalmost part of the proximal end and a portion of the distal condyles, being impossible to assess the ratio between the transverse width of the proximal end and distal end). In the elements that the distal expansion is preserved, the distal condyles form a flat surface, with little to no concavity in the

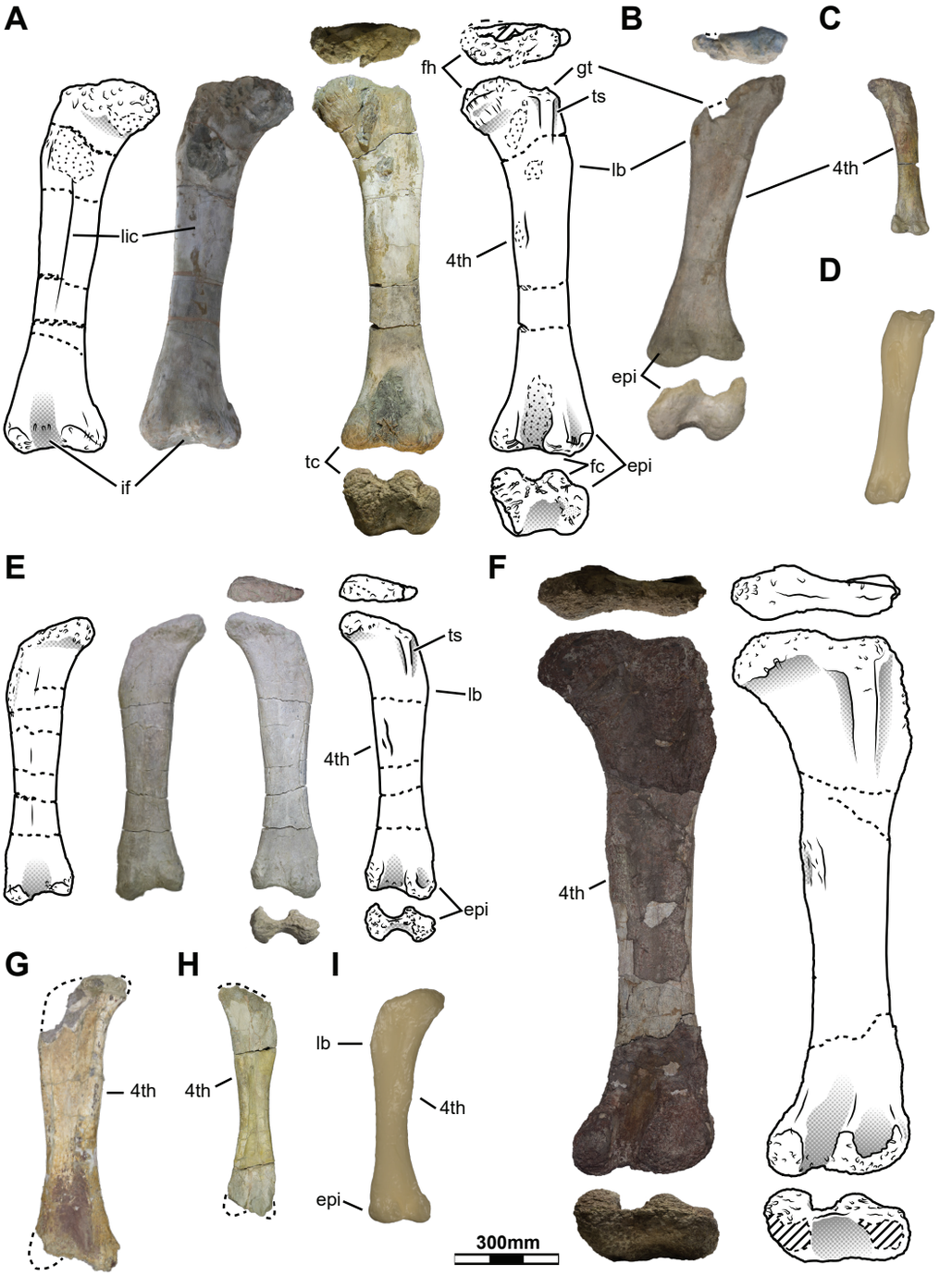

Fig.V.6. Sample of femora specimens used in this study. (A) HUE-3108 in anterior, dorsal, posterior and ventral face. (B) HUE-2338 in posterior face. (C) HUE-2636 posterior face. (D) HUE-8801 mesh posterior face. (E) HUE-1319 in anterior, dorsal, posterior and ventral face. (F) HUE-594 in proximal, posterior and distal face. (G) HUE-3583 posterior face. (H) HUE-10007 posterior face. (I) *Lirainosaurus astibiae* MCNA-7468 mesh posterior face.

intercondylar area. The distal end is greatly anteroposteriorly compressed, but with radial and ulnar condyles presents a marked anterior projection. The medial ulnar and radial condyle are the area with most anteroposterior expansion of the distal condyle, and they are not bifurcated as in most titanosaurian sauropods. The lateral face of the distal end forms an acute flange and present a lightly concave surface down to the distalmost part of the lateral face of the distal end. There is a lightly developed ectepicondylar process in the medial margin of the distal end in anterior face. Posteriorly, two parallel and acute ridges extend from the ulnar and radial condyles surrounding the anconeal fossa. There is also a concave surface in the medial face of the radial condyle. The condyles are also medially bevelled (e.g. HUE-1434, HUE-1463).

Specimen	Type	Side	Assoc.	Strat.	Morphotype	Length	R.I.	Ecc. (%)
HUE-902	Femur	Right	iso	GI	Morphotype I	1100	NA	295.80
HUE-930	Femur	Right	EC11	GI	Morphotype I	1050	NA	307.05
HUE-1366	Femur	Right	EC05	GI	Morphotype I	1019	0.21	203.31
HUE-1440	Femur	Left	iso	GI	Morphotype I	1460	NA	150.85
HUE-1521	Femur	Left	iso	GI	Morphotype I	910	0.20	259.19
HUE-1590	Femur	Right	iso	GI	Morphotype I	850	0.20	333.54
HUE-2338	Femur	Left	iso	GI	Morphotype I	860	0.21	208.62
HUE-2636	Femur	Right	iso	GI	Morphotype I	455	0.20	128.89
HUE-2903	Femur	Right	iso	GI	Morphotype I	955	0.19	276.75
HUE-3108	Femur	Right	EC01	GI	Morphotype I	1010	0.22	250.00
HUE-3583	Femur	Left	iso	GII	Morphotype I	900	0.22	230.77
HUE-8801	Femur	Left	iso	NA	Morphotype I	600	0.17	180.70
					Morphotype I	**Average**	**0.20**	**226.96**
HUE-594	Femur	Right	iso	GI	Morphotype II	1550	0.20	182.61
HUE-1183	Femur	Left	EC13	GI	Morphotype II	870	0.18	297.34
HUE-1187	Femur	Left	iso	GI	Morphotype II	965	0.25	327.84
HUE-1316	Femur	Right	iso	GI	Morphotype II	1000	0.25	283.90
HUE-1319	Femur	Right	iso	GI	Morphotype II	840	0.21	255.10
HUE-1357	Femur	Left	iso	GI	Morphotype II	860	0.22	207.57
HUE-1508	Femur	Left	iso	GI	Morphotype II	870	0.23	354.40
HUE-1756	Femur	Right	iso	GI	Morphotype II	1320	NA	325.40
HUE-2420	Femur	Right	EC06	GI	Morphotype II	1151	0.21	194.13
HUE-3237	Femur	Right	iso	GI	Morphotype II	815	0.22	254.46
HUE-10007	Femur	Right	iso	NA	Morphotype II	740	NA	300.00
					Morphotype II	**Average**	**0.22**	**265.25**

Table.V.6. Sample of femora specimens from Lo Hueco. *iso.* - isolated. *R.I.* - Robustness Index following Wilson & Upchurch (2003). *Ecc.* - Eccentricity Index following Royo-Torres (2009).

Fig.V.7. [right] Tibiae and fibulae sample used in this study. Tibiae: (A) HUE-3082 in medial, proximal, lateral and distal face. (B) HUE-4632 in lateral face. (C) HUE-1573 in medial and lateral face. (D) HUE-2117 in lateral face. (E) HUE-1612 in medial and lateral face. (F) HUE-1149 in medial, proximal, lateral and distal face. (G) *Lirainosaurus astibiae* MCNA-13860 in medial, proximal, lateral and distal face. Fibulae: (H) HUE-3087 in medial, anterior, proximal, lateral and distal face. (I) HUE-1570 in medial and lateral face. (J) HUE-1335 in medial and lateral face. (K) HUE-1612 in medial, proximal and lateral face. (L) HUE-2806 in medial and lateral face. (M) HUE-1146 in lateral face. (N) *L. astibiae* MCNA-9410 in proximal, lateral, distal and medial face.

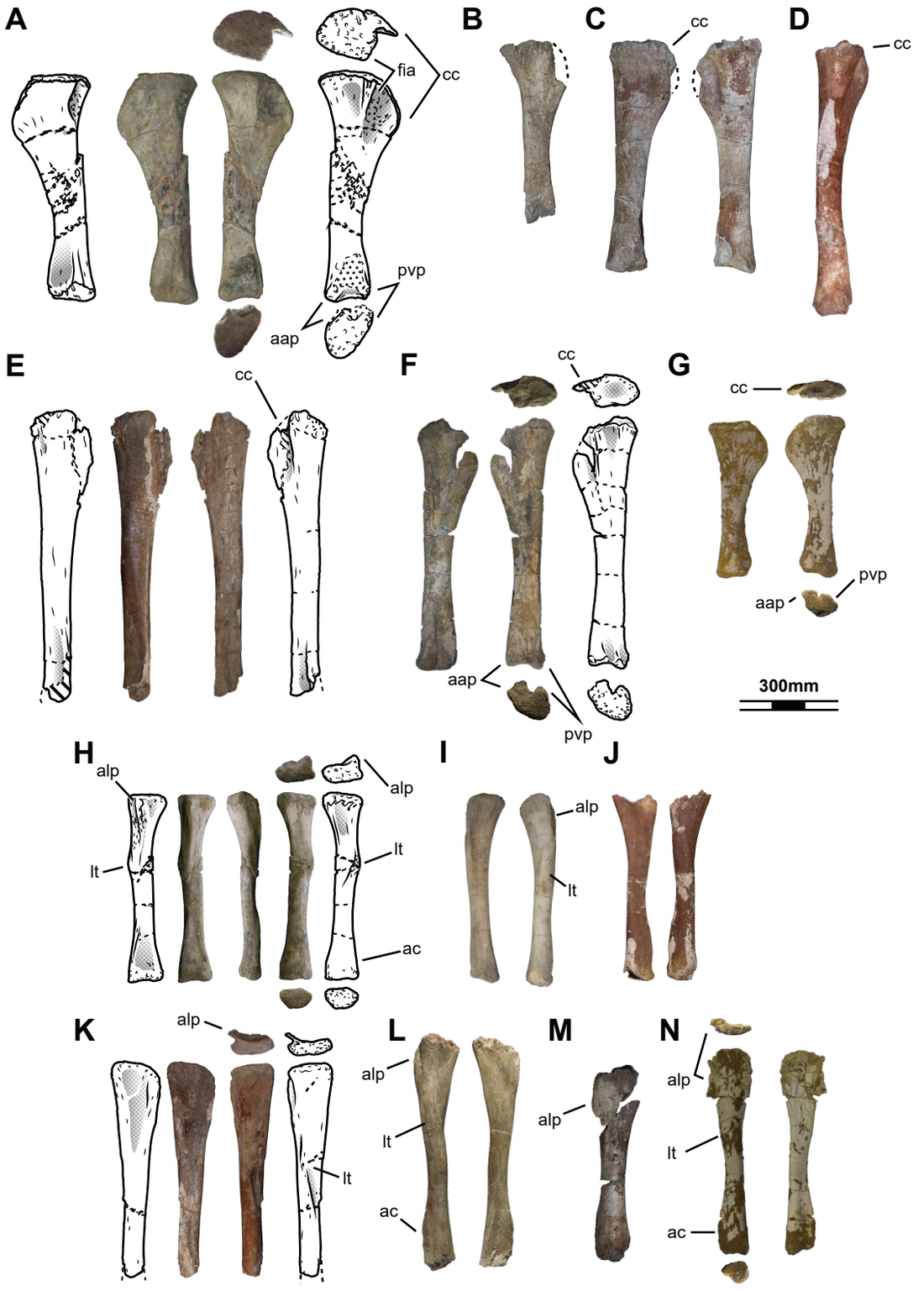
A
fia
cc
pvp
aap
B
C
cc
D
cc
E
cc
F
cc
aap
pvp
G
cc
pvp
aap
300mm
H
alp
alp
lt
lt
ac
I
alp
lt
J
K
alp
lt
L
alp
lt
ac
M
alp
N
alp
lt
ac

Ulnae:

The ulna is a slender and elongated element (Table.V.). The proximal expansion is small in comparison to the total elongation of the element (Fig.V.5). There is a dorsally expanded olecranon, but only lightly from the proximal surface with a gentle convexity. The posterior process of the ulna lean downward from the olecranon produncing a robust posterior ridge while the other process of the ulna are rather slender elements. The anterior process is almost straight and short (see HUE-1158 and HUE-1338), lateromedially longer than the medial process nonetheless as shown in HUE-1158. There is a longitudinal ridge straight and extends from the proximal end in the middle of the radial anterior fossa up to the radial articulation. In some elements like HUE-1338 and HUE-4357, this ridge is well-defined, while in other elements as HUE-3462, it has much rudimentary shape. In the elements HUE-1158 and HUE-4357, the radial longitudinal ridge is not present. The presence of this ridge and its development is related with the insertion of the M. interosseous (Borsuk-Bialynicka, 1977). The shaft is slender and proximodistally straight in anterior and lateral views (Table.V.4). Proximal and distal end are particularly expanded relatively to the midshaft unlike the ulnae referred to the Morphotype I.

Distally the anteromedial edge of the posterior expansion is marked by a stepped morphology. There is an initial bump at one fourth of the proximodistal length. Then it follows a slight concavity and finally the expansion of the distal condyles. The distal end expansion is small and much less developed than the proximal expansion (e.g., HUE-1158 and HUE-1338). There is a concavity in the anterior face of the distal end, visible in distal view. The distal end is also anteroposteriorly compressed and D-shaped in outline, instead the typical triangular shape morphology as the anterior distal fossa is not visible in distal view by a stepped straight edge distal on the radial articulation.

Radii:

The small radius HUE-1166 is interpreted as belonging to the Morphotype II, but it is not found in association any other element from this morphotype. This interpretation is based on the distinct morphology when compared to the previous described Morphotype I and to the fact that only two appendicular morphotypes have been so far identified in Lo Hueco, one of them referred with confidence to the previous Morphotype I.

In addition, this radius might be belongs to a possible juvenile individual based on its small size (Fig.V.5) in comparison with the available ulnae sampled for this morphotype (Table.V.5). The shaft is straight and has a small flange in the proximomedial edge. The distal end is slightly leaning upward in the lateral side. The shaft does not have a proper oblique ridge in the anterior face but it has a small incline between the proximal and the distal end. In the posterior face there is a well-developed interosseous ridge, forming an extruding trochanter in the proximal end and extending straight down to distal end. At midshaft, the interosseous ridge expands parallel to another marked ridge, which comes from the posteromedial edge of the distal end.

Femora:

The femora are robust and eccentric (Table.V.6), with an anteroposteriorly compressed shafts. In anterior view, some elements present a continuous proximal edge (e.g. HUE-1319, Fig.V.6) without a step between the femoral head and greater trochanter and the femoral head bevelling to proximal. While other elements such as HUE-594 and HUE-2420 have small step between the

femoral head and the greater trochanter in proximal but without a proximal deflection of the femoral head. The lateral bulge is short in most elements comprising one fourth of the femoral proximodistal length. The lateral bulge is anteroposteriorly narrow and has a light anterior flexion at midpoint of its proximodistal length. Parallel to the lateral bulge there is a shallow and straight trochanteric shelf. The lateromedial width of the shaft is usually two times the anteroposterior width of the shaft (see Eccentricity Index; Table. V.6). Some elements present a higher robustness index related to the marked expansion of the proximal and distal ends (e.g., HUE-1316 and HUE-1187).

However, some femora may present a low robustness (e.g. HUE-594, HUE-1183, see Table. V.6) but the differences are small in comparison with all the sample and most of the other features on the proximal and distal ends as well as the lateral bulge. The eccentricity might be exaggerated by taphonomy in some elements that are affected by longitudinal cracks (e.g. HUE-10007). But generally, this specimen present a great anteroposterior compression of the shaft and it is not caused by taphonomical deformation (see Table. V.6). The fourth trochanter is proximally placed respectively to the midshaft, at the same height that the lateral bulge ends. The fourth trochanter is posteriorly located near the medial edge and exclusively posteriorly projected. The muscle insertion does not extends the medial face of the femoral shaft and it is not visible in anterior view, except from some elements that reach the posterior part of medial face (e.g. HUE-1187, HUE-1508, HUE-2420).

Distal condyles are slightly anteroposteriorly compressed. The condyles are posteriorly projected with small extension of the anterior face. The tibial condyle is more developed anteroposteriorly than the fibular condyle. Some elements present a small bevelling of the tibial condyle to medial (e.g., HUE-1357 and HUE-10007). However, majority of the elements the distal surface of the

Specimen	Type	Side	Assoc.	Strat.	Morphotype	Length	R.I.	Ecc. (%)
HUE-1063	Tibia	Right	iso	GI	Morphotype I	727	NA	147.14
HUE-1165	Tibia	Left	iso	GI	Morphotype I	364	0.18	70.00
HUE-1410	Tibia	Right	iso	GI	Morphotype I	NA	NA	62.50
HUE-1573	Tibia	Left	iso	GI	Morphotype I	685	0.15	149.18
HUE-2355	Tibia	Left	iso	GI	Morphotype I	690	NA	52.08
HUE-2799	Tibia	Right	iso	GI	Morphotype I	482	NA	173.47
HUE-3082	Tibia	Right	EC01	GI	Morphotype I	670	0.15	155.00
HUE-4344	Tibia	Left	iso	GI	Morphotype I	539	0.18	162.96
HUE-4404	Tibia	Left	iso	GII	Morphotype I	590	0.16	58.42
HUE-4632	Tibia	Right	iso	GII	Morphotype I	526	NA	75.32
					Morphotype I	**Average**	**0.16**	**99.64**
HUE-1149	Tibia	Left	iso	GI	Morphotype II	692	0.12	148.00
HUE-1317	Tibia	Right	iso	GI	Morphotype II	550	NA	65.93
HUE-1500	Tibia	Right	iso	GI	Morphotype II	813	0.12	175.71
HUE-1612a	Tibia	Left	HUE-1612	GI	Morphotype II	825	0.10	115.87
HUE-2117	Tibia	Right	iso	GI	Morphotype II	769	0.13	75.95
HUE-2425	Tibia	Right	EC06	GI	Morphotype II	746	0.13	177.05
HUE-4055	Tibia	Right	iso	GI	Morphotype II	735	0.11	53.25
					Morphotype II	**Average**	**0.12**	**105.16**

Table. V.7. Sample of tibiae specimens from Lo Hueco. *iso.* - isolated. *R.I.* - Robustness Index following Wilson & Upchurch (2003). *Ecc.* - Eccentricity Index following Royo-Torres (2009).

condyles is perpendicular to the axis of the shaft. The lateral epicondyle is slightly laterally projected and mostly located in the posterior face of the distal end. All the elements that preserve the distal condyles present a step between the anterior and posterior part of the distal end in the intercondylar fossa.

Tibiae:

In contrast with the proximal part of the hindlimb, the tibia and fibula are much more slender elements in comparison. The tibia present an elongated, sometimes straight shaft (Table.V.7, see Fig.V.7). The tibial proximal end is quadrangular with similar development of the anteroposterior and lateromedial widths. The anterior part of the tibial head does not present a true lateral ridge and the articulation of the fibula have been reduced to a prominent trochanter only in the proximalmost part. This ridge does not reach distally the height of the cnemial crest muscular insertion (contra to Morphotype I; see Fig.V.7). This lateral trochanter forms an projecting flange contributing to the quadrangular morphology of the tibial head and it is not a true "secondary cnemial crest" (Bonaparte, 1999). Some elements like HUE-4055 present a secondary accessory flange in the posterior part of the proximal end, with a total of two flanges in the lateral face of the tibial head (and only limited to the proximal, without extending distally on the shaft). The cnemial crest is proximodistally long and anteroposteriorly narrow. The crest is robust, with a slightly sigmoid muscular insertion in the anterior face and an associated concavity in the posterolateral edge of the cnemial crest. Besides this excavation, the resultant fibular fossa between the cnemial crest and the rest of the shaft is rather shallow. Normally deep fossae are delimited by the lateral ridge but as in this morphotype the ridge is reduced to a proximal trochanter and there is only a small step dividing the cnemial lateral fossa from the shaft.

The midshaft has low eccentricity (Table.V.7), but it is still slightly lateromedially compressed. The distal end is almost as expanded lateromedially than anteroposteriorly. The anterior ascending process (aspa; see Wilson & Sereno, 1998) is deflected upwards while the posterior ventral process (pvp; see Wilson & Sereno, 1998) is straight facing lateromedial. The condyles are perpendicular to the lateromedial width of the shaft, but in some elements as HUE-1149 they are lateroposteriorly projected. Some elements (e.g. HUE-1149 and HUE-1500) present a concavity in the anterior face of the anterior ascending process.

Fibulae:

The fibula have anteroposterior expanded (slightly robust, mean Robustnes Index ~0.17 but many specimens present Robust Index over 0.20; Table.V.8) proximal and distal ends. Also, most of the specimens present an eccentric shaft (Eccentricty Index ~134%, Table.V.8) that is compressed lateromedially. The fibular anterior trochanter is slightly medially bevelled forming a gentle and subtle angle. In proximal view, this end forms a lightly compressed D-shape. The anterior trochanter is anteroposteriorly expanded and proximodistally elongated (sometimes up to one third of the fibular proximodistal length). The shaft is straight with a marked lateral trochanter. Some elements present a small ridge in proximolateral, surrounding the fossa between the lateral and the anterior trochanter (e.g. HUE-1612; see Fig.V.6). It forms a shallow flange with an anterior sulcus like in HUE-1612 and HUE-2806. The anterior trochanter is mainly anteriorly directed and extends continuously to the lateral face of the shaft (no sulcus associated as occurs in the Morphotype I; Fig.V.6). There is no remarkable tibial scar nor a defined area of articulation

with the tibia in the medial face of the proximal end. Some elements like HUE-1146 present a bifurcated lateral trochanter with a double crest in the insertion (see Fig.V.6). The lateral trochanter is well developed both proximodistally and anteroposteriorly. Thought the muscle insertion is sometimes a ridge (e.g. HUE-1082, HUE-1612) with a marked lateraly projection and placed in the middle of the anteroposterior width of the shaft.

The shaft is mostly straight in anterior view with little medial flexion except for the distal end, as occurs in HUE-1570. There is a small deflection of the proximal part of the fibula to anterior in lateral face in some elements (e.g. HUE-1612, HUE-2669). However, this deflection is small and the shaft does not present a truly sigmoid shaft as in other somphospondylians (Powell, 1992; Salgado & De Souza Carvalho, 2008)

The distal end is fragmentary in most of the elements, being preserved in HUE-1082, HUE-4416 and HUE-1570. The distal end is lateromedially compressed and has rectangular distal face.

Specimen	Type	Side	Assoc.	Strat.	Morphotype	Length	R.I.	Ecc. (%)
HUE-1335	Fibula	Left	iso	GI	Morphotype I	507	0.20	120.00
HUE-1377	Fibula	Right	iso	GI	Morphotype I	534	0.17	136.84
HUE-1476	Fibula	Right	iso	GI	Morphotype I	702	0.20	125.81
HUE-1513	Fibula	Left	iso	GI	Morphotype I	640	NA	108.82
HUE-1570	Fibula	Right	iso	GI	Morphotype I	572	0.17	183.87
HUE-2804	Fibula	Right	iso	GI	Morphotype I	480	NA	135.85
HUE-2904	Fibula	Left	iso	GI	Morphotype I	490	NA	131.37
HUE-3075	Fibula	Left	iso	GI	Morphotype I	525	0.18	87.27
HUE-3087	Fibula	Right	EC01	GI	Morphotype I	638	0.20	83.33
HUE-4359	Fibula	Right	iso	GI	Morphotype I	569	0.11	94.23
HUE-7802	Fibula	Right	iso	GI	Morphotype I	445	NA	110.53
					Morphotype I	**Average**	**0.17**	**116.93**
HUE-1068	Fibula	Right	iso	GI	Morphotype II	500	0.19	120.00
HUE-1082	Fibula	Right	iso	GI	Morphotype II	707	0.17	132.50
HUE-1146	Fibula	Left	iso	GI	Morphotype II	720	0.18	126.67
HUE-1175	Fibula	Right	iso	GI	Morphotype II	430	0.15	186.21
HUE-1507	Fibula	Left	iso	GI	Morphotype II	570	NA	113.79
HUE-1520	Fibula	Right	iso	GI	Morphotype II	440	0.15	113.33
HUE-1612b	Fibula	Left	HUE-1612	GI	Morphotype II	810	NA	142.50
HUE-2426	Fibula	Right	EC06	GI	Morphotype II	724	0.17	122.92
HUE-2669	Fibula	Right	iso	GI	Morphotype II	905	0.11	122.58
HUE-2806	Fibula	Left	iso	GI	Morphotype II	709	0.17	111.67
HUE-2977	Fibula	Right	iso	GI	Morphotype II	532	0.23	167.31
HUE-3000	Fibula	Left	iso	GI	Morphotype II	550	0.16	114.55
HUE-4416	Fibula	Right	iso	GII	Morphotype II	564	0.19	168.42
HUE-5232	Fibula	Left	iso	GII	Morphotype II	676	0.15	165.22
					Morphotype II	**Average**	**0.17**	**134.26**

Table.V.8. Sample of fibulae specimens from Lo Hueco. *iso*. - isolated. *R.I.* - Robustness Index following Wilson & Upchurch (2003). *Ecc.* - Eccentricity Index following Royo-Torres (2009).

V.4 RESULTS

V.4.1. 3D GEOMETRIC MORPHOMETRICS RESULTS

While as much as 10 PCs are stored as shape variables in each analysis, only three of them are meaningful following the method introduced by Bookstein (2014). Therefore, only up to the third PC in each PCA over procrustes coordinates of each type of bone will be shown. The most variable elements are located in the distal hindlimb. The tibia and fibula present more than ~80% of variance not relatable to significant differences between the different titanosaur morphotypes (as per PCA and Kruskal-Wallis test and Mann-Whitney's U test, see below; see also Supplementary Material.V.D).

Humerus taphomorphospace

The humeri present a variation between elements with a more transversely expanded proximal end, and with the humeral head slightly medially flexed at more negative values of the first principal component (PC1). This component explains 22.36% of all the variance. It also shows a more rounded proximal expansion as well as a more anteriorly projected humeral head. On the contrary, more positive values in the PC1 present a humerus with more quadrangular proximal end, a less lateromedially wide and more anteroposteriorly compressed humeral head. The humeral head is closer to the sagittal plane of the element. The deltopectoral crest is longer, projected anteriorly and the M. supracoracoideus insertion (see Diogo & Abdala, 2010) is at one third of the proximodistal length in more negative values. While more positive values represent a anterosteriorly and proximodistally shorter deltopectoral crest, with a proximal step-like morphology and extending to the interior part of the anterior expansion.

Few differences are identified in the midshaft region with both morphotypes sharing similar anteroposterior and lateromedial widths and therefore the morphology of the oval midshaft section. Values that are more negative present a more distal location for the midshaft minimum width relatively to the anterior expansion and the deltopectoral crest. On the contrary, the values on the positive extreme present a slight deflection of the distal end of the humeral crest to the mid part of the shaft and the midshaft minimum width is more proximally located and near the distal part of the deltopectoral crest.

Distal end presents a concavity between the ulnar and radial condyle of the in ventral face in the negative extreme of the first PC in more negative values. Positive values represent a transversely flat distal end. The anterior and lateral face of the ulnar condyle distal end form a marked angle also in the positive values of PC1. The anconeal fossa is surrounded by two narrow and well developed ridges projecting from the condyles. However PC1 positive extreme is represented by a less posteriorly projected and less acute ridges delimiting the anconeal fossa. The medial part of the distal end is also more angular in negative values of PC1 while values that are more positive represent a curved radial condyle slightly medially deflected.

The second principal component (PC2) represents 16.66% of the variance. It presents differences in the anteroposterior development of the humerus. The proximal end is less anteroposteriorly wide, and the humeral head is lateromedially reduced in the negative values of PC2. The proximal expansion is less medially developed in negative values. The deltopectora

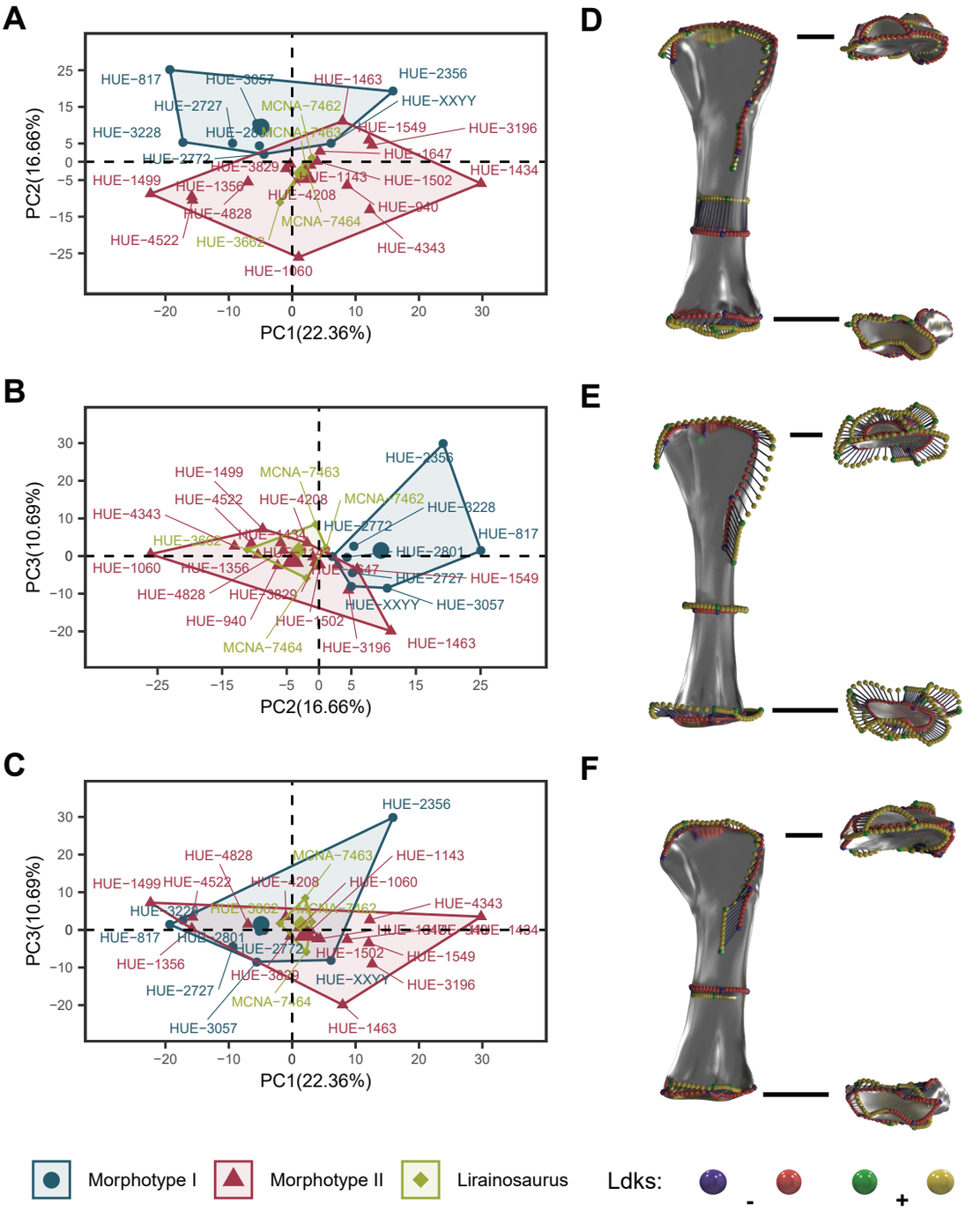

Fig.V.8. Humerus shape PCA results with highlighted taphomorphospaces. (A) PC1-PC2. (B) PC2-PC3. (C) PC1-PC3. (D) Landmark configuration at the extremes of PC1 axis. (C) at the extremes of PC2 axis. (F) at the extremes of PC3 axis.

crest presents a more abrupt step-like morphology in the proximal part of the lateral edge. The positive values present a more expanded humeral head, both anteroposteriorly and especially lateromedially. In the positive values of the PC2, the medial part of the anterior expansion is proximodistal deeper, and the deltopectoral crest does not present an abrupt step in proximal or a quadrangular lateral as in negative values. The deltopectoral crest is slightly anteriorly projected and expanded lateromedially in positive values. The M. supracoracoideus insertion is slightly distally placed in positive values of PC2.

The midshaft is elliptical in both extremes of the PC2 but the negative values present humeral minimum midshaft width with slightly more eccentric condition as well as smaller section than in positive values.

The distal end is a more anteroposteriorly compressed and less lateromedially expanded when compared to the total length of the humerus in negative values. The anterior face is straight and less developed medial condyle. The lateral ectepicondyle is also more laterally expanded in negative values. The lateral face is more rounded anteroposteriorly in distal view in the lateral face after the ectepicondyle. The radial condyle is more medially bevelled. Meanwhile the positive values of PC2 comprise a more expanded distal end, especially the radial condyle. This condyle is rounder and more anteromedially developed, with less medial or lateral bevelling. The anconeal fossa is slightly deeper with a more posterior projected ridge on the radial condyle. The anterior face also presents a more developed medial condyle. The lateral edge of the humeral distal end is acute with less developed lateral ectepycondyle but with more pronounced fossa between the medial condyle and the lateral edge of the distal end in anterior face.

Lastly, the third principal component (PC3) represents only a 10.69% of the variance. In total this three components (PC1, PC2 and PC3) represent 49.7% of the total variance of the sample, with little gaining including the next principal components. As the next 5 principal components help explaining only an additional 28.79% of the variance to a significant minimum of >75% (78.507%). The PC3 captures the medial deflection of the humeral head in more negative values as well as the less expanded deltopectoral crest into the mid part of the anterior expansion. Meanwhile, more positive values show a humeral head placed in the middle of the lateromedial width of the proximal expansion. The medial edge of the proximal expansion is more quadrangualar. The positive values of PC3 also show an expansion of the deltopectoral crest into the interior part of the proximal expansion but with no anterior projection. Negative values of PC3 are represented by a more curved medial proximal expansion, a wide humeral head inclined to medial. The proximal of the deltopectoral crest producing a quadrangular edge of the proximal expansion in lateral and present a step between proximal and the deltopectoral crest. The M. supracoracoideus insertion of the deltopectoral crest is also slightly deflected to anterolateral in negative values of PC3.

More negative values of PC3 show a more lateromedially expanded minimum width of the midshaft as well as a posterior face of radial condyle which is more upward and projected. The negative extreme of the PC3 also reflects the presence of an anteroposteriorly compressed of distal end. Meanwhile positive extreme values reflect a slender midshaft, with similar eccentricity but much smaller diameter and an anteroposteriorly developed distal end with expanded ulnar condyle. The distal end also preserves a weak torsion respectively to the proximal end.

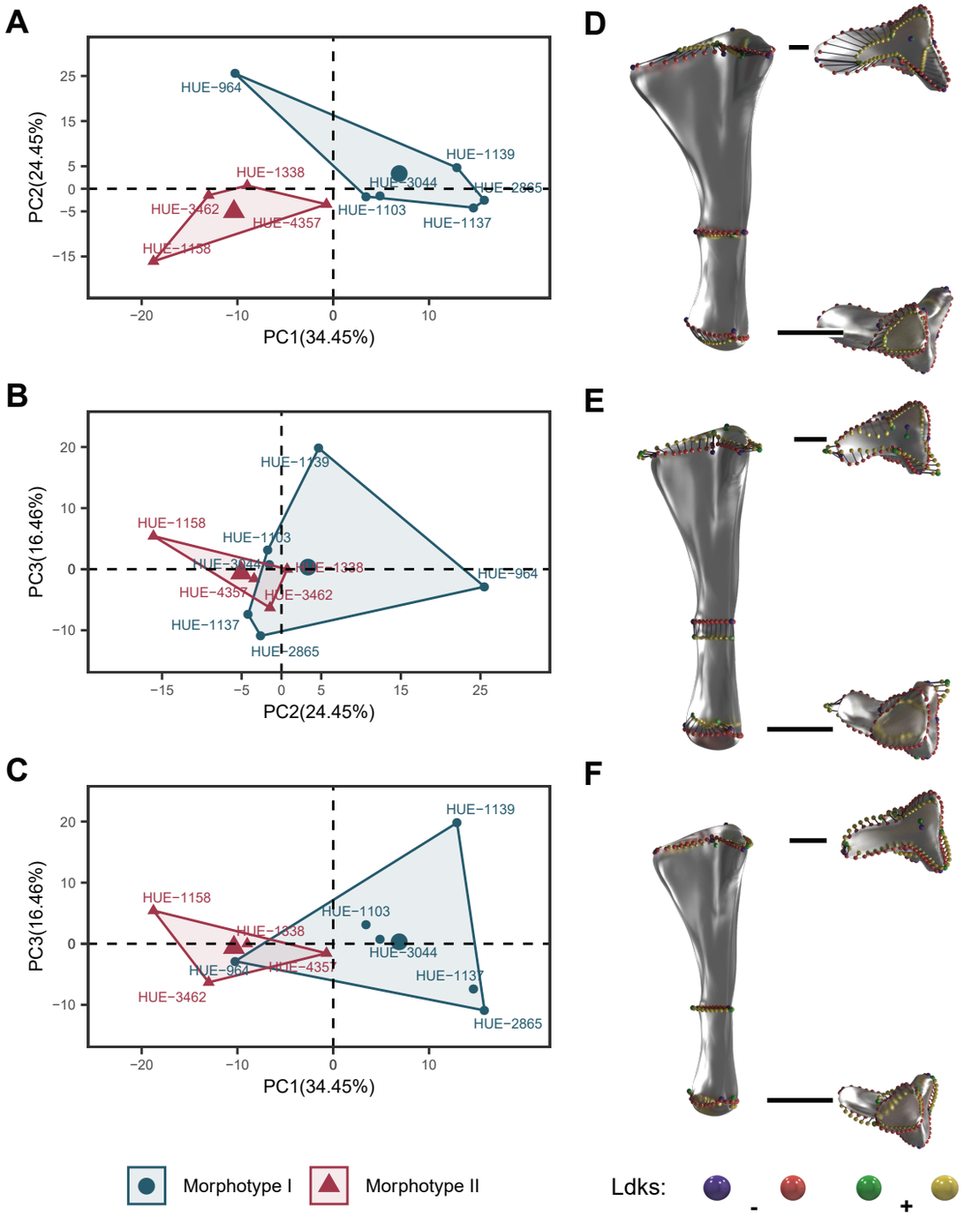

Fig.V.9. Ulna shape PCA results with highlighted taphomorphospaces. (A) PC1-PC2. (B) PC2-PC3. (C) PC1-PC3. (D) Landmark configuration at the extremes of PC1 axis. (C) at the extremes of PC2 axis. (F) at the extremes of PC3 axis.

Ulna taphomorphospace

Ulnar PC1 represents a total of 34.45% of the variance. PC1 negative values comprises the more robust elements with expanded anterior and lateral processes. This extreme of the PC also records ulnae with a lateromedially wider and anteriorly expanded anterior process. The olecranon is slightly posteriorly placed. Meanwhile the positive PC1 values represent a more slender and less expanded ulnar proximal end, with closest anterior and lateral processes, forming a more rectangular to acute angle in comparison to the negative values characterized by angles higher than 90°.

The minimum midshaft width is more robust in more negative values, with a slightly concave lateroposterior face contrary to the more slender triangle-shaped midshaft with almost no concavity between the latera and posterior processes at midshaft on more positive values.

Distal end differences are minor. More negative values represent a more expanded ulnar distal condyle toward the posterior flange, which curves upward. On the contrary, more positive values represent a flat and straight distal condyle with a triangle to D-shaped outline.

The PC2 represents 24.45% of the sample variance. It shows main differences between an expanded anterior process in more negative values, also characterized by a wide posterior process and a downward deflection of the lateral process. Meanwhile more positive values describe elements with narrow anterior and lateral process and a shallower olecranon. The anterior processes in the negative extreme also presents a small lateral flexion.

Most of the midshaft differeces along this PC occur in the anterior face. The positive values present a small concavity in anterior part and anteroposteriorly narrower midshaft. Also, more negative values the minimum midshaft width is placed more proximally, while in the negative values it is placed distally.

Positive values represent an expanded distal end with the radial articulation facing forward and straight, forming a D-shape in distal. While negative values represent slightly smaller distal end, with the posterior part slightly medially bevelled and a weak concavity in anterior face.

Finally, PC3 only shows 16.46% of the total variance, reaching with the PC1 and PC2 74.74% of variance. The differences in this axis are extremely subtle. In more negative values, the ulnae are characterized by an expanded posterior process, an anteroposteriorly narrow midshaft as well as an anterior expansion of the distal end. Meanwhile, the positive values represent elements with a narrower posterior part of the olecranon, a more anteroposteriorly expanded midshaft as well as narrower distal condyle with an upward development of the posterior part.

Radius taphomorphospace

This element presents a small sample and only three principal components were recoverd. PC1 only explains 47.24% of the variance of the sample. Negative values of PC1 represent a radius with a transversely expanded proximal end. There is also a marked and straight interosseous ridge in the lateral posterior face extending downward. The Mm. biceps brachii and brachialis scar (see Borsuk-Bialynicka, 1977; Otero, 2018) is placed more proximally in medial face of more negative values. The proximal wend is anteroposteriorly

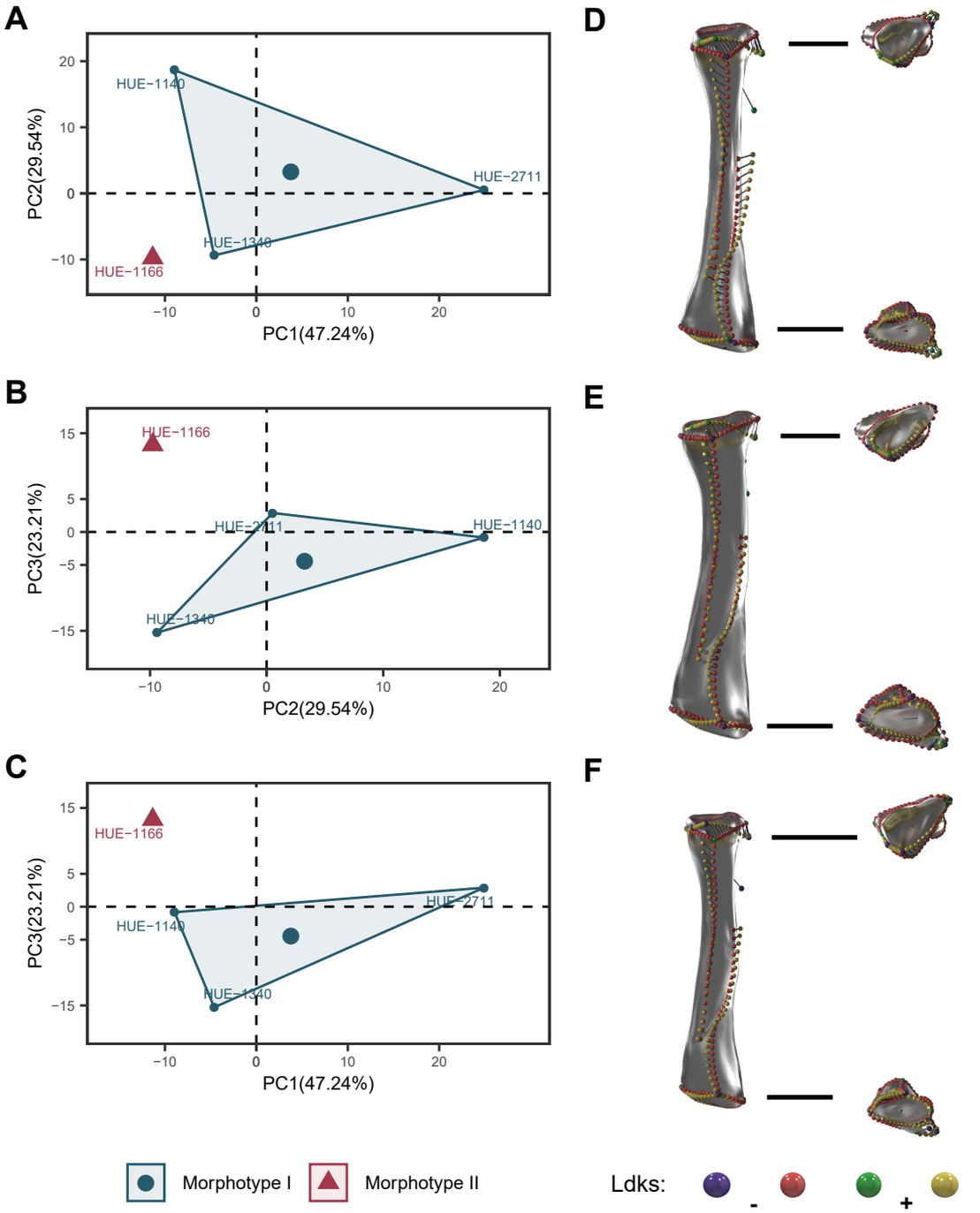

Fig.V.10. Radius shape PCA results with highlighted taphomorphospaces. (A) PC1-PC2. (B) PC2-PC3. (C) PC1-PC3. (D) Landmark configuration at the extremes of PC1 axis. (C) at the extremes of PC2 axis. (F) at the extremes of PC3 axis.

compressed in positive values, with a distal deflection of the lateral edge of the proximal end. The Mm. biceps brachii and brachialis insertion is more distal. The interosseous ridge is straight but the distal parallel ridge is slightly sigmoid in negative values, with the proximal part medially bevelled.

The distal end is anteromedially to posterolaterally expanded in more positive values, with a marked concavity between the pmdc and the pldc. More negative values present anteroposteriorly compressed distal end without a marked concavity between pmdc and pldc. The pldc is also more developed in negative values as the lateral interosseous ridge forms a sigmoid ridge distally.

The PC2 reports 33% of the variance and shows smaller deviations in the morphology of the proximal end as well as the muscle attachment represented by the lateral flange. Negative values report a proximal flexion of the proximal end as well as a more dorsal position for the Mm. biceps brachii and bracialis insertion. They also are representative of a more expanded distal end in the pmdc. Positive values show a more straight proximal end, a more distal muscular insertion in medial face and a more developed and posteriorly projected distal ridge over the pmdc.

The PC3 sums all the rest of variance up to 100% and represents mostly the variance in the proximodistal flexion of the proximal end. The more negative values represent a marked proximal deflection of the radial proximal end in medial view while more positive values retain a straight proximal end.

Femur taphomorphospace

The three first principal components alone define only a total of 45.93% of the total morphological variance recorded in the Lo Hueco femora. It is necessary to observe up to the sixth principal component to explain 76.37% of the total variance.

The PC1 represents 19.80% of the variance and the main differences are related with the anteroposterior compression and position of midshaft elements. The negative values define elements that are featured by more compressed shafts and ends. The femoral head inclines upward without much difference in the position of the plane of the proximal end. The fourth trochanter is placed distally, a little below the end of the lateral bulge and near the midshaft. The midshaft is anteroposteriorly compressed with a small concavity in the midline of posterior face.

While more positive values represent a femur with more anteroposteriorly expanded and globous femoral head, which is straight in anterior or posterior view. The fourth trochanter and the midshaft has a more proximal position. The midshaft is also less eccentric with a weak concavity in the middle of the posterior face, probably related with the development of the linea intermuscularis cranialis.

More negative values show an anteroposteriorly compressed distal end. The surface of condyles is perpendicular to the axis of the shaft, and it is slightly more development in the posterior face than in anterior face despite the compression. The fibular condyle is laterally expanded and rounded, therefore the lateral epicondyle is exclusively posteriorly projected. The positive extreme, on the contrary, shows a more anteroposteriorly expanded distal condyles with a deeper intercondylar fossa. The condyles are also medially bevelled especially the tibial condyle The lateral face of the fibular condyle is rounded and not particularly lateromedially expanded.

The positive extreme of this component shows a posterolaterally projected epicondyle.

The PC2 explains 13.78% of total variance. The PC2, on the contrary, does not reflect great changes in the overall anteroposterior compression of the shaft and the respective ends. Instead more negative values represent femora with more lateromedially expanded proximal end. Also these values comprise the presence of a longer lateral bulge. The proximal and mid part of the lateral bulge is slightly inclined to anterior face and the fourth trochanter is more laterally and distally placed. More positive values in the other hand represent a less expanded proximal end in lateromedial. The lateral bulge is proximodistally shorter and does not present bevelling. The fourth trochanter is more proximal located and slightly more posteriorly projected. More positive values present also the bump in anterior face of the minimum midshaft width while negative values present a smooth outline.

In the distal end. more positive values of this PC correspond to a tibial condyle top positioned upward, and similarly identified for the fibular condyle. Negative values present less development in the posterior excursion of both condyles.

The PC3 explains 11.08% and shows great differences in the morphology of the proximal end and in the expansion of distal end, but without the bevelling of the proximal or distal end similar to PC1. More negative values represent a femur with a straight femoral head, an abrupt transition from the greater trochanter to the lateral bulge, and an anteroposteriorly compressed midshaft and distal condyles. The distal condyles are greatly anteroposteriorly compressed but present a more lateromedially expanded tibial condyle than in more positive values. On the other hand, positive values in the PC3 are characterized by femora with a bulbous, dorsally projected and more anteroposteriorly expanded head. The midshaft is less eccentric, more rounded with an convexity at midline of the anterior face. On more positive values, the distal condyles are more anteroposteriorly expanded. Furthermore, the medial face of the tibial condyle is straight and the lateral face of the distal end is more rounded. The intercondylar fossa and the posterior fossa between the epicondyle and the fibular condyle are also deeper in this extreme.

Tibia taphomorphospace

The PC1, PC2 and PC3 sum a total cumulative variance explained of 54.05%, being necessary to consider the next three components to explain more than 75% (76.37%) of the morphological variance of the sample.

The PC1 represents 23.51% of the total variance and shows great differences in the mediolateral expansion of the proximal end. The negative values are represented by a compressed end both anteroposteriorly and mediolaterally. The result is a square shaped or somewhat rounded tibial head. The cnemial crest is less expanded in anteroposterior and part of the curvature is placed dorsally with a smooth distal end. On the contrary, more positive values present a more expanded tibial proximal end, with the typical triangle-shaped head. The lateral fibular ridge is expanded and well developed in the lateral face. The posterior face of the proximal end expands greatly in more positive values forming the typical triangular outline in proximal. While more negative values show a small and semicircular proximal end. The cnemial crest is curved with the midpoint being the area of maximal curvature in both extremes, The positive values shows a semicircular cnemial crest in lateral face while more negative values present a triangular cnemial crest with gentle

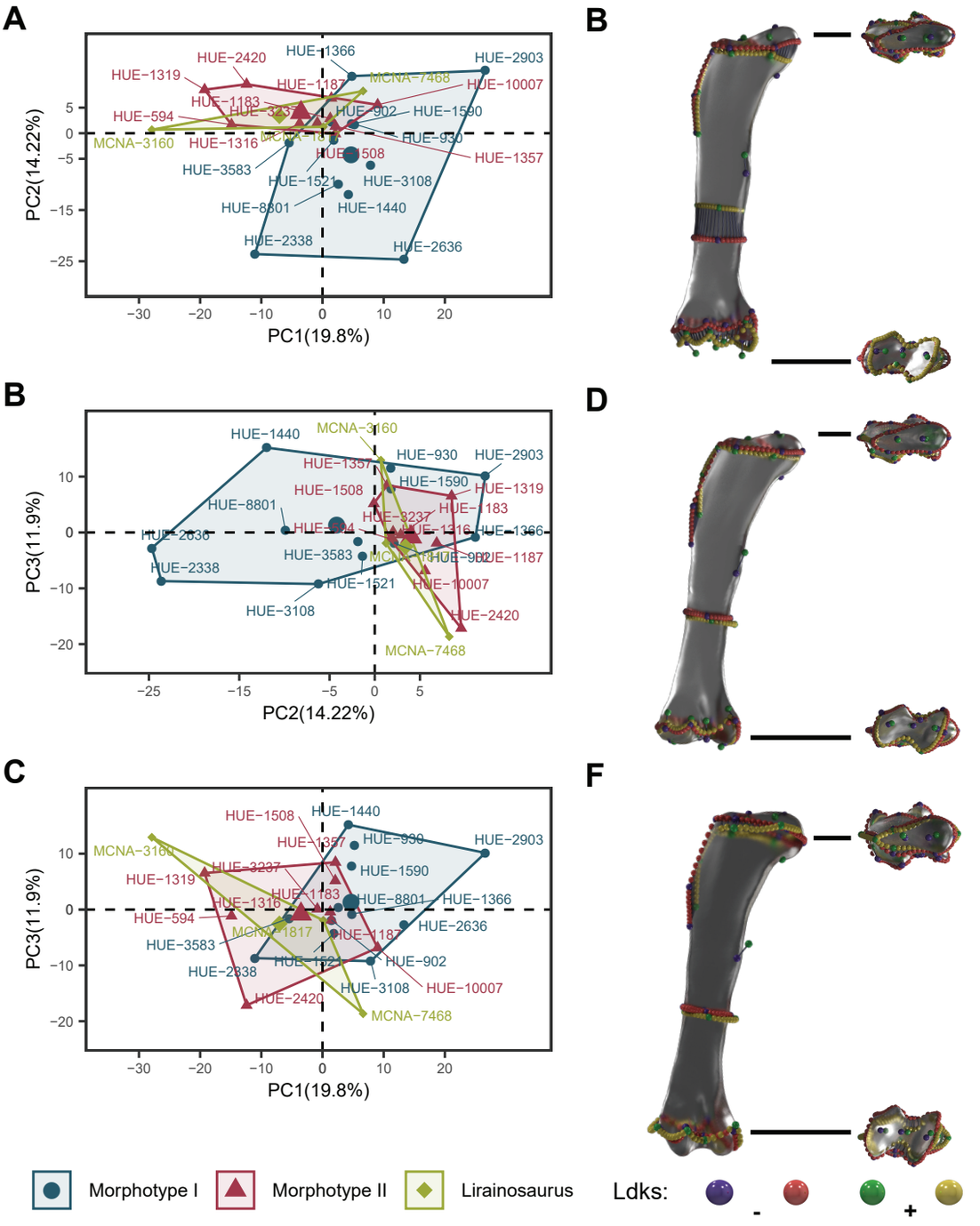

Fig.V.11. Femur shape PCA results with highlighted taphomorphospaces. (A) PC1-PC2. (B) PC2-PC3. (C) PC1-PC3. (D) Landmark configuration at the extremes of PC1 axis. (C) at the extremes of PC2 axis. (F) at the extremes of PC3 axis.

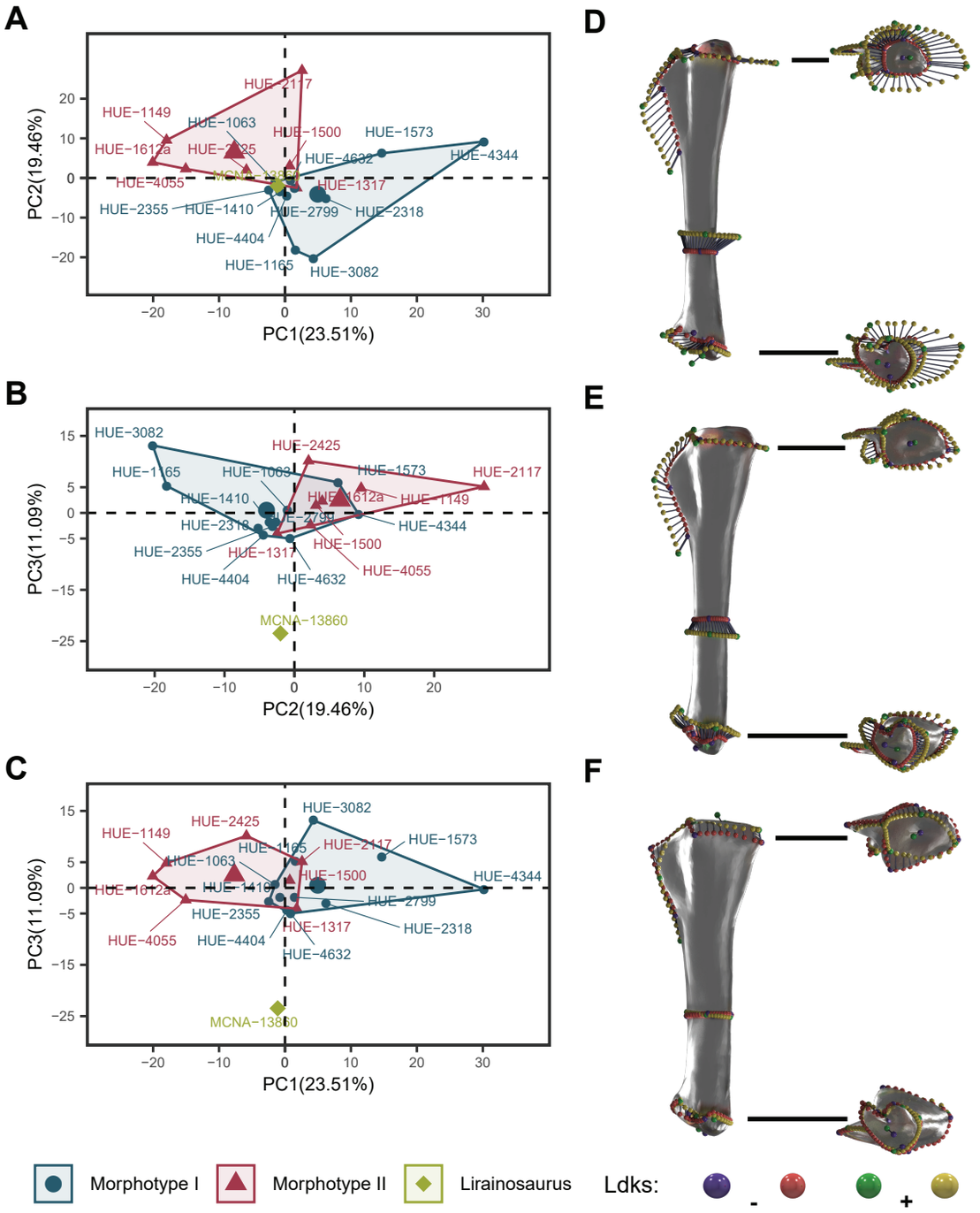

Fig.V.12. Tibia shape PCA results with highlighted taphomorphospaces. (A) PC1-PC2. (B) PC2-PC3. (C) PC1-PC3. (D) Landmark configuration at the extremes of PC1 axis. (C) at the extremes of PC2 axis. (F) at the extremes of PC3 axis.

curvature in the distal portion of the crest. In addition, the cnemial crest is proximodistally longer in positive values.

The position of the midshaft, in more negative values, is slightly distally located. The midshaft in this extreme is also more constricted in all directions and shows a small concavity at the midline of its lateral face. More positive values show a more proximal midshaft height. The midshaft is also more robust than in negative values.

The distal end shows a perpendicular to posteriorly projected aap and pvp in more negative values, with a more posteriorly bevelled aap and pvp. While positive values represent a more anteriorly bevelled distal end.

The PC2 explains 19.46% of the variance. It represents differences in the morphology of cnemial crest and the distal end. The positive values of PC2 represents specimens with greater and more abrupt lateral ridge of the fibular articulation in proximal view, more anteriorly expanded cnemial crest, and more anteroposteriorly expanded and eccentric midshaft and distal end. The negative values show gentler curved proximal end in lateral view with less expansion of the posterior part and less abrupt fibular articulation ridge. The cnemial crest and the distal end are less anteroposteriorly expanded. The midshaft is more anteroposteriorly constricted and positioned dorsally in the negative values, but less eccentric than in positive values. Also the distal end is deeper, with a longer shaft, placed more distally than in positive values, with an aap less flexed upward.

The PC3 corresponds to 11.09% of the variance. Minor differences between extremes can be found here, and the changes are more subtle. The major trend in this PC is the variation in the development of the lateral proximal ridge of the articulation of the fibula and in the morphology of the cnemial crest. The negative extreme represents the lateral expansion of this ridge generating a more triangular shaped proximal end. The cnemial crest is more proximally placed being triangular-shaped in lateral view and the insertion of the group Mm. ambiens, femorotibialis and iliotibialis (see Borsuk-Bialynicka, 1977) is pointing slightly upward. There is also some degree of posterior bevelling of the distal sector of the cnemial crest. Positive values represent a less developed lateral ridge in the proximal end and a round shaped cnemial crest, as well as, a straight proximal end in lateral view.

Fibula taphomorphospace

The fibula is the single element which the three first principal components explains a variance of 43.49% only, the lowest cumulative variance for the three first PCs on all the bone elements analyzed. It is necessary to consider eighth first principal components to explain more than 75% (77.61%) of the variance. The PC1 explains an 18.06% of the variation. The negative extreme shows a more proximodistally expanded anterior trochanter and a more sinuous lateral trochanter. This trochanter is slightly inclined forward in this component, and also more curved distally up to the posterior face of the shaft. On the other hand, more positive values represent a shorter anterior trochanter of the fibula. The lateral trochanter is longer, less forwardly, and its curvature ends in the lateral face of the shaft.

The PC2 represent 13.19% of the variance and helps visualize differences in the development of the fibular proximal end and the lateral trochanter. Negative values represent a D-shaped

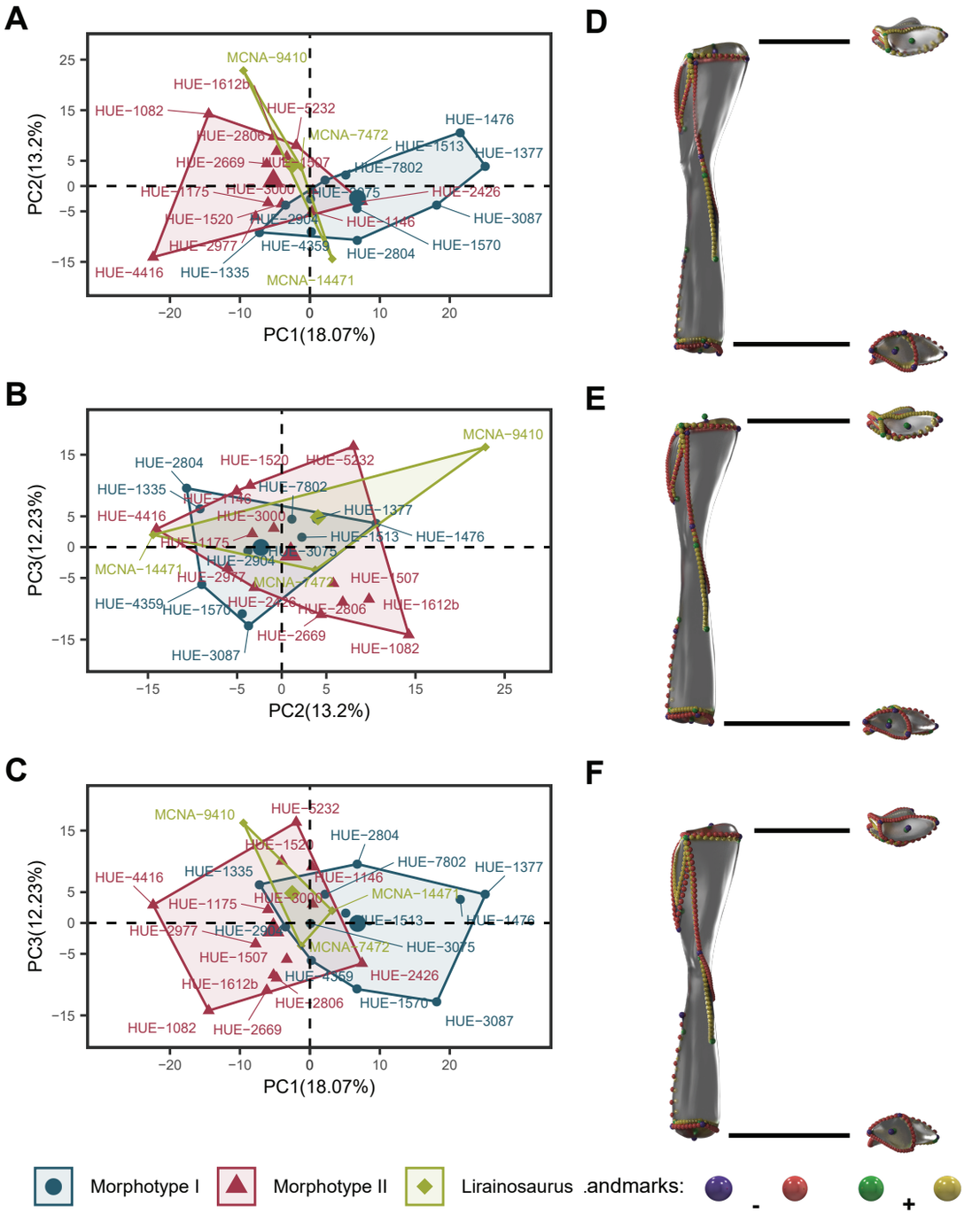

Fig.V.13. Fibula shape PCA results with highlighted taphomorphospaces. (A) PC1-PC2. (B) PC2-PC3. (C) PC1-PC3. (D) Landmark configuration at the extremes of PC1 axis. (C) at the extremes of PC2 axis. (F) at the extremes of PC3 axis.

proximal end. The anterior trochanter does not bevel medially but instead is anteriorly expanded with light medial bevelling. There is no sulcus between the anterior trochanter and the rest of lateral face of the shaft and proximal end, and there is a smooth transition from the anterior trochanter to the lateral trochanter in proximal view. The lateral trochanter is shorter proximodistally. Meanwhile more positive values represent a fibula with medially bevelled anterior trochanter and the development of a step or sulcus between the anterior trochanter and the lateral face of the shaft. This step is also related with the presence of the lateral trochanter more anteriorly and proximally located. Also more positive values represent a distally longer lateral trochanter.

Minor differences are reported in distal end, with more negative values presenting a distal end slightly bevelling to posterior while positive values are represented by more straight distal end.

The PC3 sums only 12.23% of the variance. Significant changes in this component are only observed in the proximodistal development of the crests and trochanters. Minor differences are recorded between the length of the anterior trochanter and anterolateral crest of the distal end. The negative values represents longer anterior trochanter and anterolateral crest of the distal end. The anterolateral crest of distal end is proximally longer and has a small anterior expansion. The lateral trochanter is proximodistally shorter. Positive values represent proximodistally shorter anterior trochanter and also proximodistally shorter anterolateral crest. The lateral trochanter is proximodistally longer.

V.5.2. ASSESSMENTS OVER TAPHOMORPHOSPACES

Morphological trends observable in the taphomorphospaces are congruent with the observed differences between the morphotypes as discussed before. The comparison with *Lirainosaurus astibiae* material as well as inclusion of several specimens has allowed to assess previous allocations on some specimens (see Chapter IV)

The use of k-means algorithm in each bone type with an increase number of clusters allowed to test the optimal number of clusters in the sample of Lo Hueco site + *L. astibiae*. Another previous study have tried to apply this method with good results assessing the differences only in the hindlimb (based in the better known association of the material among hindlimb elements from Lo Hueco). However, when increasing the sample with some conflicting specimens and *Lirainosaurus astibiae*, the results show significant overlaps in many of the analyzed bone types, as previously commented, differing from the initial descriptions and therefore recovering distinct clustering patterns. Some resemblances still apply to the previous assessment, and this method helps us to explore the hypothesis of more than two main clusters. Despite the reassessment of some elements, there are still two main morphotypes in the sample of Lo Hueco.

The comparison between the a priori definition and the few specimens reassessed in this Chapter can be accessed in Supplementary Material.V.H.

Generally, the two taphomorphospaces that usually overlaps are the *Lirainosaurus astibiae* taphomorphospace and the Morphotype II from Lo Hueco. Both forms have been assessed as different morphotypes but they share more similitudes than Morphotype I with the Morphotype II and the Morphotype I with *L. astibiae*. In addition, some specimens have been allocated to *L. astibiae* or closely related form after this study. None of these specimens have reassessed from

previous hypotheses (commented before), and all the specimens referred to *L. astibiae* or closely related form in this study are analyzed here for the first time.

The humeral morphotypes overlap slightly over PC1 and PC2 as well as in PC2 and PC3 (Fig.V.8) based on the similar compression of the distal condyle of the specimens of HUE-XXYY, HUE-1463 and HUE-2772. These three specimens are regarded as different morphotypes. Contrary, PC1 produces a considerable overlap, as the main areas of variance are centered on the midshaft expansion and its relative position along the shaft, and in the position of the deltopectoral crest. As discussed before, this structure has a great degree of variation especially between elements of the Morphotype II.

The PC1 shows no significant differences between the morphotypes, however, there is a variation in the morphology of the proximal end, the deltopectoral crest and the overall position of the midshaft in each morphotype, which is the variation that summarizes this PC. The Morphotype II taphomorphospace ranges from specimen HUE-1499 (rounded head, less lateromedially compressed shaft, anteriorly expanded deltopectoral crest) at more negative values. On the other extreme it is specimen HUE-1434, with extreme compression of the shaft compared to its elongation at all heights, less expanded deltopectoral crest and the minimum midshaft width more proximally placed in the positive extreme. Also, positive values shows a slightly more recurved medial edge of the proximal end in anterior face contra the more squared proximal end of negative values.

		Kruskal-Wallis test		Mann-Whitney U-test		
		Chi squared	p-value	Morphotype I - Morphotype II	Morphotype I - *Lirainosaurus*	Morphotype II - *Lirainosaurus*
Humerus	PC1	2.401	0.301	0.192	0.214	0.617
	PC2	11.280	**0.004***	**0.001***	**0.004***	0.963
	PC3	0.852	0.653	0.742	0.461	0.494
	PC4	3.410	0.182	0.264	0.933	0.080
	PC5	1.679	0.432	0.417	0.683	0.290
	PC6	0.574	0.751	0.653	0.570	0.682
	PC7	0.018	0.991	0.928	0.808	1.000
	PC8	6.748	**0.034***	0.106	**0.016***	0.122
	PC9	2.882	0.237	0.653	0.570	0.064
	PC10	3.633	0.163	0.106	0.933	0.211
Ulna	PC1	4.545	**0.033***	**0.038***		
	PC2	0.409	0.522	0.610		
	PC3	0.045	0.831	0.914		
	PC4	0.182	0.670	0.762		
	PC5	0.409	0.522	0.610		
	PC6	0.045	0.831	0.914		
	PC7	0.045	0.831	0.914		
	PC8	1.136	0.286	0.352		
	PC9	0.182	0.670	0.762		
Radius	PC1	1.800	0.180	0.500		
	PC2	0.200	0.655	1.000		
	PC3	1.800	0.180	0.500		

Table.V.9. Kruskal Wallis and Mann-Whitney U's test for the forelimb shape PCA.

However, the PC1 can also be affected by the extreme position of HUE-1356, HUE-1499 and HUE-4522 (Fig.V.8) and by estimation of the morphology of the proximal end. Its position can be exaggerated based on the preservation status of the elements that have been under high landmark estimation. HUE-4522 is clearly referable to Morphotype II; however, it lacks the proximal and distal ends, which present some of the feature variation in PC1. HUE-1499 lost a great part of the proximalmost part of the humeral head; thought, it show a marked quadrangular lateral edge characteristic of the Morphotype II (the medial part is not preserved). HUE-1434 presents the landmark of the medial edge of the proximal end but not the medial edge of the humeral head. The proximal end is slightly rotated in HUE-1434 and this could be related with a weak distal displacement of the humeral head. The humeral head is also strongly medially deflected, rather than gently curved as in Morphotype I. Similarly, variation in Morphotype I may be exaggerated between much more negative values (e.g. HUE-817) and more positive specimens HUE-2356 and HUE-XXYY. In both specimens the minimal diameter of the midshaft is distally placed, and they lack most of the deltopectoral crest. The estimation of this structure might be relatable to its overlapping with specimens from Morphotype II that present the gentle curvature of the proximal end (more positive values of PC1). The PC2 separates better the taphomorphospace of the Morphotype I, within more positive values. *Lirainosaurus astibiae* and Morphotype II taphomorphospaces are projected toward more negative values, with slender shafts, anteroposteriorly compressed proximal and distal ends, quadrangular proximal end, more medially placed deltopectoral crest and straight distal end in anterior face. There are some overlapping between both morphotypes (e.g. HUE-1463 of Morphotype II toward positive values), which presents a slight anteroposterior compression of the proximal and distal ends compared with other specimens of Morphotype II (e.g. HUE-1434). There is also some weak similarities between this specimen and *L. astibiae*, but, as we discussed before, the feature combination is different among both taxa. There are also differences in the angle of the shaft and the morphology of the proximal end with HUE-3662, the only specimen from Lo Hueco referred to *L. astibiae* or as a closely related form, which is projected in more negative values of PC2 with a more anteroposteriorly compressed and slender shaft than other specimens from *L. astibiae*.

Humeri classification by k-means suggests that the best clustering is between two groups. K-means suggests that the Morphotype I does not include specimens like HUE-XXYY and HUE-2356 but instead includes the specimens HUE-1356, HUE-1499 and HUE-4522 (see Supplementary Material.V.G.1). Nevertheless, this sub cluster probably presents an exaggerated separation from other specimens due taphonomical warping and the estimation of the missing structures. All these specimens resemble the ones of the Morphotype II in all the osteological features.

The specimen HUE-XXYY presents anteroposteriorly compressed distal condyles, and the preserved lateral edge of the shaft is straight. It has also a deltopectoral crest inclined slightly to the midline. Some of the mentioned features are found in the Morphotype II. However, the distal condyles are placed more laterally like in the Morphotype I. HUE-XXYY also presents a concavity between both condyles in the distal face, characteristic of the Morphotype I. In the posterior face, the medial ridge that projects from the humeral head is medially deflected as in other humeri of the Morphotype I. Only some specimens of Morphotype II presents the humeral head more medially displaced (e.g. HUE-940, HUE-1463), but only HUE-1463 is placed near the point 0 or positive values as HUE-XXYY.

The specimen HUE-2356 is considered as other separated Morphotype. Its morphology resembles HUE-817 but there are two key features that are probably causing this separation, and, consequently similar with HUE-XXYY. As discussed before, HUE-2356 presents a medial expansion of the muscular attachment in the deltopectoral crest. However, this area might be slightly variable in different taxa, as other specimens of Morphotype II (see Fig.V.8; this study) and *Ampelosaurus atacis* (e.g. C3-1297, C3-1506; pers. obs. APB 2019) present differences in the muscular attachment. The other major change in PC1 and PC3 is the position of the humeral head, where HUE-2356 diverges the most from other specimens within the Morphotype I taphomorphospace. However, the lack of humeral head and the estimation over this region might exaggerates the divergence of this element similarly to HUE-XXYY.

The ulnae present two clusters as the most optimal solution, and three clusters as another possible hypothesis based on the silhouette width distribution (Supplementary Material.V.G.2). These clusters resemble the taphomorphospaces of the described morphotypes despite the separation of HUE-964 from its original proposed morphotype (Morphotype I) to the Morphotype II based on the narrowing of the process and ulnar head. As commented before, despite these morphological differences, the specimen HUE-964 is considered more similar to the Morphotype I (similar features e.g. HUE-3044). However, the lack of preservation of the distal end and lack of the posterior protuberance of the distal end might affect this classification, as well as, the presence or absence of a trochanter medial to the radial articulation, which is an exclusive feature of the Morphotype II. On the other hand, this condyle is not as anteroposteriorly compressed as in other specimens from Morphotype II. Also, the anteromedial and lateroposterior process are markedly expanded resulting in a slightly negative PC1 (Fig.V.9). On the contrary, most of the taphomorphospace of Morphotype II is located on negative values and its characterized by shorter proximal anteromedial and lateroposterior process, as well as, a compressed distal end (Fig.V.9). The k-mean analysis suggests to relocate HUE-4357 in the Morphotype I. This ulna shares with morphotype I the open angle between anterolateral and posteromedial process. However, this is variable character in the Morphotype II and HUE-4357 corresponds to one of the extremes of the Morphotype II taphomorphospace. All the other features are common in the Morphotype II and none of the diagnostic features of the Morphotype I are found in HUE-4357 despite the angle between the processes.

The radii present some variation along PC1. Morphotype I presents some differences in the anteroposterior compression of the proximal end and also in the medial expansion part of the proximal end in proximodistal. The only specimen of the Morphotype II is placed in more negative values, with an anteroposterior compression of proximal end and more sigmoid morphology of the distal interosseous ridge. The analysis of k-means of the radii reported two and four probable clusters (Supplementary Material.V.G.3). The only difference in the k-means analysis with the distribution of the specimens is considering HUE-1166 as part of the Morphotype I and HUE-2711 as part of the Morphotype II in the two cluster hypothesis. Also, both the a priori hypothesis and the k=2 hypothesis results cannot be ruled out due the presence of such small sample. Based on a unique specimen referred to Morphotype II, it is not possible to differentiate whether consider the current morphotypes or the alternative hypothesis proposed by the algorithm.

The femora present an overlapping among taphomorphospaces based on the difficulties to assess the differences between the compressed femoral shafts of *Lirainosaurus astibiae* and Morphotype II (Fig.V.11). This great overlap can be caused by the relative position of the femoral

		Kruskal-Wallis test		Mann-Whitney U-test		
		Chi squared	p-value	Morphotype I - Morphotype II	Morphotype I - *Lirainosaurus*	Morphotype II - *Lirainosaurus*
Femur	PC1	4.990	0.082	**0.025***	0.365	0.937
	PC2	4.025	0.134	0.059	0.448	0.469
	PC3	0.262	0.877	0.923	0.734	0.692
	PC4	4.904	0.086	0.418	0.180	**0.014***
	PC5	0.825	0.662	0.381	0.945	0.811
	PC6	3.431	0.180	0.456	0.448	0.028
	PC7	3.601	0.165	0.582	0.136	0.077
	PC8	2.777	0.249	0.539	0.233	0.112
	PC9	0.200	0.905	0.722	0.840	0.937
	PC10	4.415	0.110	0.974	0.136	0.014
Tibia	PC1	3.927	0.140	0.069	0.500	1.000
	PC2	6.076	**0.048***	**0.015***	0.833	0.500
	PC3	3.366	0.186	0.425	0.167	0.250
	PC4	0.325	0.850	0.860	0.667	1.000
	PC5	2.507	0.286	0.536	0.333	0.250
	PC6	1.201	0.549	1.000	0.333	0.750
	PC7	0.144	0.930	1.000	1.000	0.750
	PC8	2.139	0.343	1.000	0.333	0.250
	PC9	0.419	0.811	0.596	0.833	1.000
	PC10	2.195	0.334	0.479	0.333	0.500
Fibula	PC1	7.833	**0.02***	**0.006***	0.170	0.611
	PC2	1.404	0.496	0.252	0.659	1.000
	PC3	0.704	0.703	0.649	0.659	0.521
	PC4	0.356	0.837	0.608	0.885	0.800
	PC5	4.626	0.099	0.569	0.060	0.057
	PC6	2.069	0.355	0.733	0.291	0.189
	PC7	3.049	0.218	0.186	0.170	0.611
	PC8	0.494	0.781	0.531	0.769	0.900
	PC9	4.593	0.101	0.106	0.126	0.296
	PC10	0.236	0.889	0.649	1.000	0.900

Table.V.10. Kruskal Wallis and Mann-Whitney U's test for the hindlimb shape PCA.

(e.g. HUE-594) as is shown in PC1. The shaft is also an important component of variation in the PC1, which is affected by the taphonomical compression and bone breaking. This might affect the position of some specimens in PC1. The high anteroposterior compression of the shaft is present in the Morphotype II and *L. astibiae*, however, in the latter this is exaggerated by post-burial warping (e.g. MCNA-3160; pers. obs. APB 2014). In addition, some elements of the Morphotype I that overlap with the taphomorphospace of *L. astibiae* and the Morphotype II (e.g. HUE-3583)

shows some shaft breakage and compression. Originally, the midshaft should have been less eccentric, suggesting that this taphomorphospace has a more reduced PC1 expansion. Despite the problems probably related with taphonomical processes, the PC1 and PC2 expose some differences in the fourth trochanter and in the distal position of the epicondyle. These differences are not so obvious considering the breakage and preservation of the Lo Hueco material.

We can also recognize a greater variation in the position of the femoral head and the overall projecting the head to medial in Morphotype I (Fig.V.17). Contrary, the Morphotype II is more constant, with low degree of variation (Fig.V.19) despite having specimens with or without medial deflection. The Morphotype I is the most variable with the widest taphomorphospace both in PC1 and PC2 (Fig.V.11). Several elements presenting a proximal deflection of the femoral head, while reducing the midshaft and bevelling the condyles (e.g. HUE-2338) in negative values of PC1 and PC2. Other specimens present a slight proximal deflection of the femoral head and similarly anteroposteriorly expanded distal end (e.g. HUE-2636) in more negative values of PC1. On the other extreme of the PC1 and PC2 biplot (Fig.V.11), the femoral morphology is marked by a low medial bevelling of the distal condyles, a low femoral upward deflection and a more pronounced anterior torsion of the lateral bulge as in HUE-1366 and HUE-2903. Also, the specimen HUE-2903 presents a higher degree of anterior deflection of the lateral bulge but probably due to the crushing of the anterior face of the shaft proximal end.

The femora k-means analysis suggests the presence of two main clusters as the unique most optimal hypothesis, followed by hypothesis considering three and four clusters. The two clusters are found resembling the previous description. It is the Morphotype II, the cluster with most changes proposed by the algorithm. Most of the elements that are located within the overlap area between the two taphomorphospace are suggested as part of the Morphotype I in all the PCs, including the specimens of *Lirainosaurus astibiae*. As commented before, several of the specimens located in this region of the taphomorphospace have been affected by taphonomical processes so the femoral head and/or the distal condyles are not preserved; and the shaft can have some degree of collapse. This is the case of the specimen HUE-902, which presents a morphology similar to HUE-1316. However, HUE-1316 have an anteroposteriorly compressed shaft, a short lateral bulge, and a lateromedially compressed tibial distal end (not anteriorly expanded). On other the hand, HUE-902 has a longer lateral bulge and the fourth trochanter is positioned slightly more distally (not beyond the distal tip of the lateral bulge end as occurs in HUE-1316 and in the Morphotype II). The shaft of HUE-902 seems to have undergone anteroposterior cracking and crushing so the medial face is similar to the Morphotype I and the other elements recovered near HUE-EC-03 (HUE-930).

The three clusters hypothesis splits Morphotype I in two different groups with no natural significance, as some of the specimens separated from the original Morphotype I are clearly similar to *Lohuecotitan* femur (e.g. HUE-2338, HUE-2636, HUE-8801; Supplementary Material.V.G.4.C.: blue cluster). The cluster that includes the specimen HUE-3108 (Supplementary Material.V.G.4.C: yellow cluster) also includes some specimens from Morphotype II (e.g. HUE-1187, HUE-10007) and some specimens referred to *Lirainosaurus astibiae* (e.g. MCNA-1817, MCNA-7468). The third group (Supplementary Material.V.G.4.C: cyan cluster) includes the remaining specimens of Morphotype II and some of the specimens of Morphotype I (e.g. HUE-1508, HUE-3583) and *L. astibiae* (e.g. MCNA-3160). None of these clusters resemble a biological significant group. Similarly, the four groups cluster hypothesis subdivides further the yellow cluster of the previous

Specimens	Morphotype	K-means clustering k=2	k=3	k=4
HUE-817	Morphotype I	2	2	3
HUE-2356	Morphotype I	2	1	2
HUE-2727	Morphotype I	2	1	4
HUE-2772	Morphotype I	2	1	4
HUE-2801	Morphotype I	2	1	4
HUE-3057	Morphotype I	2	1	1
HUE-3228	Morphotype I	1	2	3
HUE-XXYY	Morphotype I	2	1	1
HUE-940	Morphotype II	2	1	1
HUE-1060	Morphotype II	1	3	4
HUE-1143	Morphotype II	2	1	1
HUE-1356	Morphotype II	1	3	4
HUE-1434	Morphotype II	2	1	1
HUE-1463	Morphotype II	2	1	1
HUE-1499	Morphotype II	1	3	4
HUE-1502	Morphotype II	2	1	1
HUE-1549	Morphotype II	2	1	1
HUE-1647	Morphotype II	2	1	1
HUE-3196	Morphotype II	2	1	1
HUE-3829	Morphotype II	2	1	1
HUE-4208	Morphotype II	2	1	4
HUE-4343	Morphotype II	2	1	1
HUE-4522	Morphotype II	1	3	4
HUE-4828	Morphotype II	1	3	4
HUE-3662	*Lirainosaurus*	1	3	4
MCNA-7462	*Lirainosaurus*	2	1	1
MCNA-7463	*Lirainosaurus*	2	1	1
MCNA-7464	*Lirainosaurus*	2	1	1

Table.V.11. Results of k-means clustering over the Humeri GPA coordinates.

Specimens	Morphotype	K-means clustering k=2	k=3	k=4
HUE-964	Morphotype I	1	3	4
HUE-1103	Morphotype I	2	2	4
HUE-1137	Morphotype I	2	2	3
HUE-1139	Morphotype I	2	2	2
HUE-2865	Morphotype I	2	2	3
HUE-3044	Morphotype I	2	2	4
HUE-1158	Morphotype II	1	1	1
HUE-1338	Morphotype II	1	1	4
HUE-3462	Morphotype II	1	1	4
HUE-4357	Morphotype II	2	2	4

Table.V.12. Results of k-means clustering over the Ulnae GPA coordinates.

hypothesis. One of these cluster includes the most slender specimens of Morphotype I (i.e. HUE.1366, HUE-2903; Supplementary Material.V.G.4.D.: olive cluster), and the specimens HUE-10007 and MCNA-7468. The second cluster comprises most of the specimens near the point 0 of PC1 and PC2. Again, these grouping hypothesis have little biological significance as the morphological features are too different (see Morphotype Differences and discussion about those specimens). However, several specimens can be reassessed based on the different grouping hypothesis and they resemblance according to the taphomorphospaces. Some specimens of the Morphotype I are recovered as Morphotype II in all the results of k-means clustering (e.g. HUE-1183, HUE-1508, HUE-2420). They present an anteroposteriorly compressed shaft, posteriorly placed fourth trochanter without projecting in the medial face, and they lack a marked linea cranialis intermuscularis (sometimes absent as in HUE-2420). They are probably more related with the femora of the Morphotype II. Similarly, several specimens of the Morphotype II are reassessed as Morphotype I in all hypotheses (e.g. 930, HUE-1590, HUE-3583). Most of them present an anteroposteriorly compressed shaft, but this might be exaggerated by taphonomical compression and fracture (e.g. HUE-3583). The fourth trochanter is posteromedially placed projecting into the medial face (e.g. HUE-930, HUE-1590). Some of them does not have a marked lic, which might be obscured by crushing (e.g. HUE-930), other femora have a well-developed lic (e.g. HUE-3583). They probably belong to the Morphotype I, according to the previous taphomorphospace reassessment (e.g. HUE-930, HUE-1590) or closer sharing all the morphological features (e.g. HUE-3583).

The tibial taphomorphospaces present a weak overlapping near the point zero of PC1 and PC2 (Fig.V.12). Contrary to other elements, the tibiae of *Lirainosaurus astibiae* (specimen MCNA-13960) resemble the tibiae of Morphotype I overlapping its taphomorphospace (Fig.V.12).

Analyzing via k-means, no significant results were recovered and the most optimal solution yields seven clusters (Supplementary Material.V.G.5.F), followed by six different clusters, which are not biologically meaningful. However, two and three clusters hypotheses present almost the same silhouette width and can be commented here instead. After the k=3 (k is number of clusters), each new iteration of the algorithm subdivides Morphotype I and Morphotype II taphomorphospaces in smaller clusters until the complete atomization of these taphomorphospaces.

The combination of so many specimens with low preservation of key structures, such as the distal condyles, is possibly causing this unforseen behavior to the algorithm. None of the explored suboptimal clusters bears biological significance.

In the analysis of the tibiae, the two clusters hypothesis yields several specimens initially referred to the Morphotype I as part of tMorphotype II (e.g. HUE1063, HUE-1410, HUE-2318, HUE-2355, HUE-2425, HUE-2799; Supplementary Material.V.G.5.B: yellow cluster) as well as the tibia referred to *Lirainosaurus astibiae* (MCNA-13960). However, as seen before, none of these specimens resemble the extremely elongated tibiae of Morphotype II.

The k=3 groups hypothesis propose a main group similar to the one main group discussed before (Supplementary Material.V.G.5.C: cyan cluster) and two small groups. One of these groups corresponds to the remaining elements of the Morphotype I including the tibia of *Lohuecotitan pandafilandi* (i.e. HUE-3082; Supplementary Material.V.G.5.C: blue cluster) after the separation of original Morphotype I taphomorphospace. The other groups comprises the specimens HUE-1573, HUE-2117, HUE-4344 (Supplementary Material.V.G.5.C: yellow cluster). The specimen HUE-2117 however, does not resemble any of the other specimens in this cluster with an extremely slender shaft and more lateromedially expanded and yielding a subcircular outline (see Morphotype Differences). Any of the proposed groups have biological meaning. On the other hand, specimen HUE-2425 (initially Morphotype I) overlaps with the taphomorphospace of the Morphotype II and it is reassessed in all the results of the k-means algorithm.

The fibula taphomorphospaces present a strong overlapping near point 0 values and negative values of PC1 and positive values of PC2 (Fig.V.13). Supplementary Material.V.G.6.A). The fibulae show more subtle differences between the analyzed taxa (Fig.V.13;Table.V.10). This is also reflected among the percentage of variance explained with each principal component. Each of them explain few of the total variance contrary to other elements (Table.V.10). Almost all the variance is concentrated in the zones that describe the sigmoid profile of the shaft, the anteroposteriorly development of the lateral trochanter, and the expansion of the anterior trochanter.

However, the morphology of the lateral trochanter does not change greatly despite the presence of two main different positions described in this study (see Morphotype Differences). The way that the anterior trochanter rotates to medial while the lateral trochanter is forwardly projected, is similar. The landmarks, this feature combination translates in few differences when includes the bevelling of the anterior trochanter, the position of the lateral trochanter and the deflection of the shaft that forms the sigmoid morphology of the shaft (Fig.V.13). Instead of a PC1 with strong changes between positive and negative values, we have few variance explained by each PC. These low-variance explaining PCs summarize different combinations of the rotation and position of these structures despite the lack of the complex morphological features seen in others elements as the humerus and femur.

Specimens	Morphotype	K-means clustering k=2	k=3	k=4
HUE-902	Morphotype I	1	1	1
HUE-930	Morphotype I	1	3	1
HUE-1366	Morphotype I	1	1	4
HUE-1440	Morphotype I	2	2	3
HUE-1521	Morphotype I	1	1	1
HUE-1590	Morphotype I	1	3	1
HUE-2338	Morphotype I	2	2	3
HUE-2636	Morphotype I	2	2	3
HUE-2903	Morphotype I	1	1	4
HUE-3108	Morphotype I	2	1	3
HUE-3583	Morphotype I	1	3	1
HUE-8801	Morphotype I	2	2	3
HUE-594	Morphotype II	1	3	2
HUE-1183	Morphotype II	1	1	1
HUE-1187	Morphotype II	1	1	1
HUE-1316	Morphotype II	1	3	1
HUE-1319	Morphotype II	1	3	2
HUE-1357	Morphotype II	1	3	1
HUE-1508	Morphotype II	1	3	1
HUE-2420	Morphotype II	1	1	2
HUE-3237	Morphotype II	1	3	1
HUE-10007	Morphotype II	1	1	4
MCNA-1817	*Lirainosaurus*	1	1	1
MCNA-3160	*Lirainosaurus*	1	3	2
MCNA-7468	*Lirainosaurus*	1	1	4

Specimens	Morphotype	K-means clustering k=2	k=3	k=4
HUE-1063	Morphotype I	1	3	1
HUE-1165	Morphotype I	2	2	4
HUE-1410	Morphotype I	1	3	1
HUE-1573	Morphotype I	2	1	2
HUE-2318	Morphotype I	1	3	1
HUE-2355	Morphotype I	1	3	1
HUE-2799	Morphotype I	1	3	1
HUE-3082	Morphotype I	2	2	4
HUE-4344	Morphotype I	2	1	2
HUE-4404	Morphotype I	1	3	1
HUE-4632	Morphotype I	1	3	1
HUE-1149	Morphotype II	1	3	3
HUE-1317	Morphotype II	1	3	1
HUE-1500	Morphotype II	1	3	1
HUE-1612a	Morphotype II	1	3	3
HUE-2117	Morphotype II	1	1	2
HUE-2425	Morphotype II	1	3	3
HUE-4055	Morphotype II	1	3	3
MCNA-13860	*Lirainosaurus*	1	3	1

Table.V.14. Results of k-means clustering over the Tibiae GPA coordinates.

Table.V.13.[left] Results of k-means clustering over the Femora GPA coordinates.

In more positive values, the shaft is straighter but (e.g. HUE-3082) with proximodistally and anteroposteriorly shorter anterior trochanter fully medially deflected, and more distally and anteriorly placed lateral trochanter. The Morphotype II overlaps in the positive values near point 0 of PC1, with a slightly sigmoidal shaft, proximodistally short and slightly medially deflected anterior trochanter, as well as, more distally placed lateral trochanter (e.g. HUE-1146). In more negative values, they present the typical straight shaft with more anteroposterior expansion of the proximal and distal end (e.g. HUE-1082, HUE-2669). As commented before, the PC1 summarizes few morphological features differences, however, this small range of variation summarizes greater qualitative differences when inspecting the osteological features. In this case, the landmark configuration shows small differences in structrures like the lateral trochanter, with similarities along PC1 on the curvature between the two different morphotypes. However, these small differences in the landmark configuration represent a more typical anterior trochanter seen in Morphortype II and the characteristic morphology of the anterior trochanter in *Lohuecotitan pandafilandi* (specimen HUE-3087). In the same way, the anterior trochanter morphology is also very similar between the described morphotypes. The major differences in the morphology of the anterior trochanter among those specimens (Morphotype I and *L. pandafilandi*) are the presence of a complete medial deflection and the anterior sulcus. However, the medial deflection of the anterior trochanter might be affected by reconstruction of this area in several specimens (e.g. HUE-2669) while the sulcus area is not covered by standard landmarks and semilandmarks (see Fig.V.2). We can infer the displacement of this structure not by the warping

Specimens	Morphotype	K-means clustering k=2	k=3	k=4
HUE-1335	Morphotype I	2	2	4
HUE-1377	Morphotype I	1	2	1
HUE-1476	Morphotype I	1	2	1
HUE-1513	Morphotype I	1	3	4
HUE-1570	Morphotype I	1	3	1
HUE-2804	Morphotype I	2	2	1
HUE-2904	Morphotype I	2	3	4
HUE-3075	Morphotype I	2	3	4
HUE-3087	Morphotype I	1	3	1
HUE-4359	Morphotype I	2	3	4
HUE-7802	Morphotype I	2	2	4
HUE-1082	Morphotype II	1	1	4
HUE-1146	Morphotype II	2	2	4
HUE-1175	Morphotype II	2	3	4
HUE-1507	Morphotype II	1	3	4
HUE-1520	Morphotype II	2	2	4
HUE-1612b	Morphotype II	1	1	4
HUE-2426	Morphotype II	1	3	3
HUE-2669	Morphotype II	1	3	4
HUE-2806	Morphotype II	1	3	4
HUE-2977	Morphotype II	2	3	4
HUE-3000	Morphotype II	2	3	4
HUE-4416	Morphotype II	2	1	2
HUE-5232	Morphotype II	2	2	3
MCNA-7472	*Lirainosaurus*	1	3	4
MCNA-9410	*Lirainosaurus*	2	1	4
MCNA-14471	*Lirainosaurus*	2	2	1

Table.V.15. Results of k-means clustering over the Fibulae GPA coordinates

vectors reported in those similar structures. Instead, we can use the lack of displacement in these areas that records a great change in their morphology. The anterior trochanter changes less than the sulcus and the proximal part of the lateral trochanter. The anteroposteriorly shorter anterior trochanter with slightly medially deflected landmarks respective to the fibular proximal end might be related with this characteristic medial deflection described in the Morphotype I and *L. pandafilandi*. The proximodistally short lateral trochanter with shorter distance between the landmark in the attachment of the M. iliofibularis (see Otero & Vizcaíno, 2008) may indicate a more anteriorly placed lateral trochanter in the shaft, which is characteristic of the Morphotype I and *L. pandafilandi*. However, this anterior projection is less intuitive than in other element types analyzed herein. This area is difficult to sample based on the lack of features with Type I landmarks and the preservation across the studied specimens.

The main differences between the taphomorphospaces are therefore subtle changes related with these morphological features in the proximal end and the lateral trochanter. This might difficult the assessment of several specimens, such as HUE-2426. In previous studies (see Chapter IV.2), HUE-2426 was projected toward the taphomorphospace of Morphotype II based on the overall straight shaft and the position of the lateral trochanter respectively to the anterior face. However, the shaft is extremely warped and fractured, and an extensive effort to reconstruct this specimen was peformed. The anterior trochanter is projected to medial at least in the proximal part (where it is not obscured by sediment in the specimen) presenting the anterior sulcus, as in *L. pandafilandi*. The lateral trochanter is reduced to a light muscular attachment instead of the robust and oval-shaped morphology in other specimens of the Morphotype I (e.g. HUE-1476, HUE-2804, HUE-3087). The presence of a sulcus is also identified in the specimen HUE-1612 from the Morphotype II. Considered as an autapomorphy of *L. pandafilandi* (see Díez Díaz *et al.*, 2016), this feature is shared with other titanosaurs, such as *Jainosaurus* cf. *septentrionalis* (e.g. NHM-R5903, pers. obs. APB 2016) and *Laplatasaurus araukanicus* (e.g. MLP-CS-1127; pers. obs. APB 2016). In the specimen HUE-1612 referred to the Morphotype II, this sulcus is not marked distally *contra L. pandafilandi* (e.g. HUE-3087), *J.* cf. *septentrionalis* and *L. araukanicus*. In the specimen HUE-2425, the distal part of the anterior trochanter is covered by sediment in the original specimen, being impossible to test the presence of this feature.

The GMM also help us to assess some problems related with the variability of *Lirainosaurus astibiae*. As commented before, part of the overlap might results from a wide and spread taphomorphospace that can be a result of preservation status of the specimens. The PC1 (Fig.V.13) shows a low variation in the position of the lateral trochanter (located at midline of the shaft), and the anterolateral crest of the distal end. The PC3 summarizes the light variation in the development of the distal part of the lateral trochanter, as in some specimens of *L. astibiae* such as MCNA-9410, which generally present a straight profile. On the other hand, the PC2 presents a huge taphomorphospace expansion mainly related with the fragmentary state of the anterior trochanter. All elements of *L. astibiae* present some degree of loss in the proximal end and in the anterior trochanter. Thus, the PC2 reflects the variation between extremely expanded and anteriorly projected anterior trochanter of MCNA-14471 to an apparently reduced one in MCNA-9410. However, this is probable related with taphonomical deformation rather than to intraspecific variation.

The k-means analysis over shape variables returns a two clusters hypothesis as the most optimal number of clusters, followed by five, two and three clusters, respectively (Supplementary Material.V.G.6.F). As in the analysis of the tibiae, more than three groups do not seem feasible and biologically relevant. The k=2 groups hypothesis reassesses the specimens HUE-1082, HUE-1507, HUE-2806 and HUE-2669 within same group of Morphotype I specimens and *Lohuecotitan pandafilandi* (Supplementary Material.V.G.6.B: yellow cluster). The specimen MCNA-7472 of *Lirainosaurus astibiae* is also reassessed in this cluster. The specimen HUE-2806 presents a medial deflection of the anterior trochanter and a subcircular section of the shaft similar to the Morphotype I, while the shaft is straighter than in Morphotype I specimens. Oher specimens do not present the characteristic medial deflection of the anterior trochanter, nor the anteriorly placed lateral trochanter (e.g. HUE-2669).

The other proposed cluster (Supplementary Material.V.G.6.B) includes most of Morphotype II specimens with the addition of the specimens HUE-1335, HUE-1570, HUE-2904, HUE-3000, HUE-3075, HUE-4359, HUE-7802. The analyses also recovered the specimens of *Lirainosaurus astibiae* (e.g. MCNA-9410, MCNA-14471) within this cluster. This group seems to have no biological significance. Several specimens present all the features discussed in *Lohuecotitan pandafilandi* fibula (e.g. HUE-1335, HUE-1570; see Morphotype Differences). Moreover, the reassessment of the specimens of *L. astibiae* represents that the intraspecific variation for this group will cover all the variance observable in PC2 (Fig.V.13) including fibulae with lateromedially narrow and straight shaft towards a more sigmoid shaft, and a wide diversity of deflection from medial to anteriorly projected anterior trochanter.

The k=3 clusters hypothesis results in a peculiar distribution of the taphomorphospaces near the point 0 values of PC1 and PC2 (Supplementary Material.V.G.6.C). This hypothesis reassesses most of the specimens in two different clusters with high overlapping in this area of the PC biplot (Supplementary Material.V.G.6.C: cyan and blue cluster). Again, the distribution of the specimens produces unnatural groups with few biological significance, as many of the specimens regarded as part of the third cluster (Supplementary Material.V.G.6.C: cyan cluster) were discussed as clearly referable to Morphotype II with no morphological features from *Lohuecotitan pandafilandi* and Morphotype I. However, several specimens are reassessed to the same morphotype in all the alternative hypotheses, instead of their preliminary classification (see Chapter IV.2; see Supplementary Material.V.H). One specimen of Morphotype II (HUE-2804) is regarded as member of the same group as the fibula of *L. pandafilandi* (HUE-3087) in all the alternative hypotheses

resultant from the k-means algorithm. This specimen presents a slight sigmoid morphology of the shaft and some medial deflection of the anterior trochanter. The proximal end is not well preserved though, and therefore it cannot be seen if this fibula shares the characteristic morphology of *L. pandafilandi*. The estimation method produces this morphology for HUE-2804. This reassessement can be also supported by the analysis and the available features. Similarly, several specimens of Morphotype I (e.g HUE-1175, HUE-1520, HUE-3000) when compared with the inclusion of *Lirainosaurus astibiae*, are alternatively reassessed as part of the Morphotype II, and are projected near the centroid of its taphomorphospace (Fig.V.13). These specimens present some lateromedial compression, little to no medial deflection of the anterior trochanter (but beware, they are not well preserved), and a weak and wide concavity in the medial face of the shaft (e.g. HUE-1520) similar to other specimens of Morphotype II. They can be regarded as Morphotype II contrary to our previous description (Chapter IV, see also Chapter V Descriptive Anatomy).

Based on the taphomorphospace assessment as well as the closer inspection of the features, we can assess almost all the specimens to two morphotypes as previously hypothesized. Moreover, the Morphotype I specimens can be preliminary referred to *Lohuecotitan pandafilandi*, and so, the specimens referred to the individuals HUE-EC-02, HUE-EC-03, HUE-EC-05 and HUE-EC-11.

Some specimens have presented some minor discrepancies discussed in the previous chapters (Chapter IV), however in the light of several analyses and the available information, we cannot determine if the individuals HUE-EC-02 and HUE-EC-03 belong to *Lohuecotitan pandafilandi* or closely related form. More material from other regions of the skeleton must be considered. For now we regard the variance observable in this sample as part of the intraspecific shape variability of *L. pandafilandi*. In general terms, *Lohuecotitan* forelimb should be composed by a robust humerus, ulna and radius, with low degree of torsion and arched in the typical wide gauge titanosaurian body plan.

There is another morphotype which preliminary includes the individuals HUE-EC-06 and HUE-EC-13 that might be referred to a different and exclusive form of Lo Hueco. In previous studies (Chapter IV), we considered HUE-EC-06 as a possible variant of the Morphotype I. When *Lirainosaurus astibiae* specimens are included in the analyses, the hindlimb of the individual HUE-EC-06 is different from the cluster of the Morphotype I and could not be considered as closely related form to *Lohuecotitan pandafilandi*. HUE-2426 is the only fibula of the taphomorphospace of *Lohuecotitan pandafilandi* + Morphotype I that overlaps the taphomorphospace of Morphotype II. Several of the analyses assess it in the same cluster than Morphotype II specimens while other separates in a third new group (Supplementary Material.V.G.6). We cannot reliably assess in HUE-2436 the presence of several *L. pandafilandi* features due the sediment already obscuring several of them. It is slightly visible the presence of a medially deflected anterior trochanter, and a reduced and acute lateral crest placed in the midline of the shaft and somewhat inclined forward but not as much as in HUE-3087. However, the medial face is completely covered as well as part of the anterior edge.

The tibia HUE-2425 presents the characteristic triangular cnemial crest seen in other specimens of Morphotype II. The position is extremely warped by the fragmentary state of this specimen, however it can be seen that it is slender and compressed. The proximal end is expanded, but the projection of the lateral proximal edge and the articulation of the fibula resembles the enlarged ridge seen in HUE-4404 instead the secondary cnemial crest present in HUE-3082.

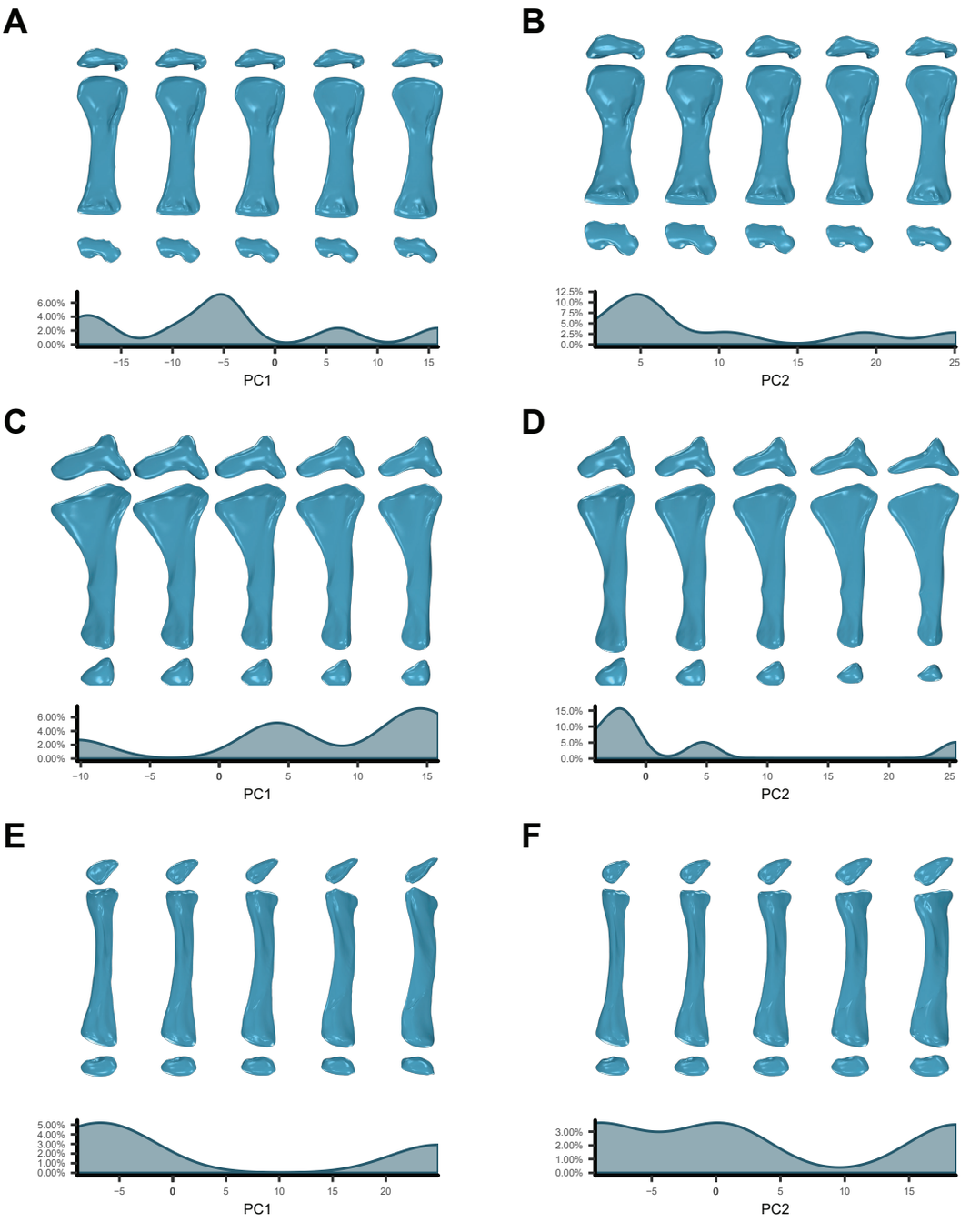

Fig.V.14. Morphological variation in the forelimb elements of Morphotype 1 for each shape PCA. *Humeri:* **(**A) Along PC1 axis. (B) Along PC2 axis. *Ulnae*: (C) Along PC1 axis. (D) Along PC2 axis. *Radii*: (E) along PC1 axis. (F) Along PC2 axis.

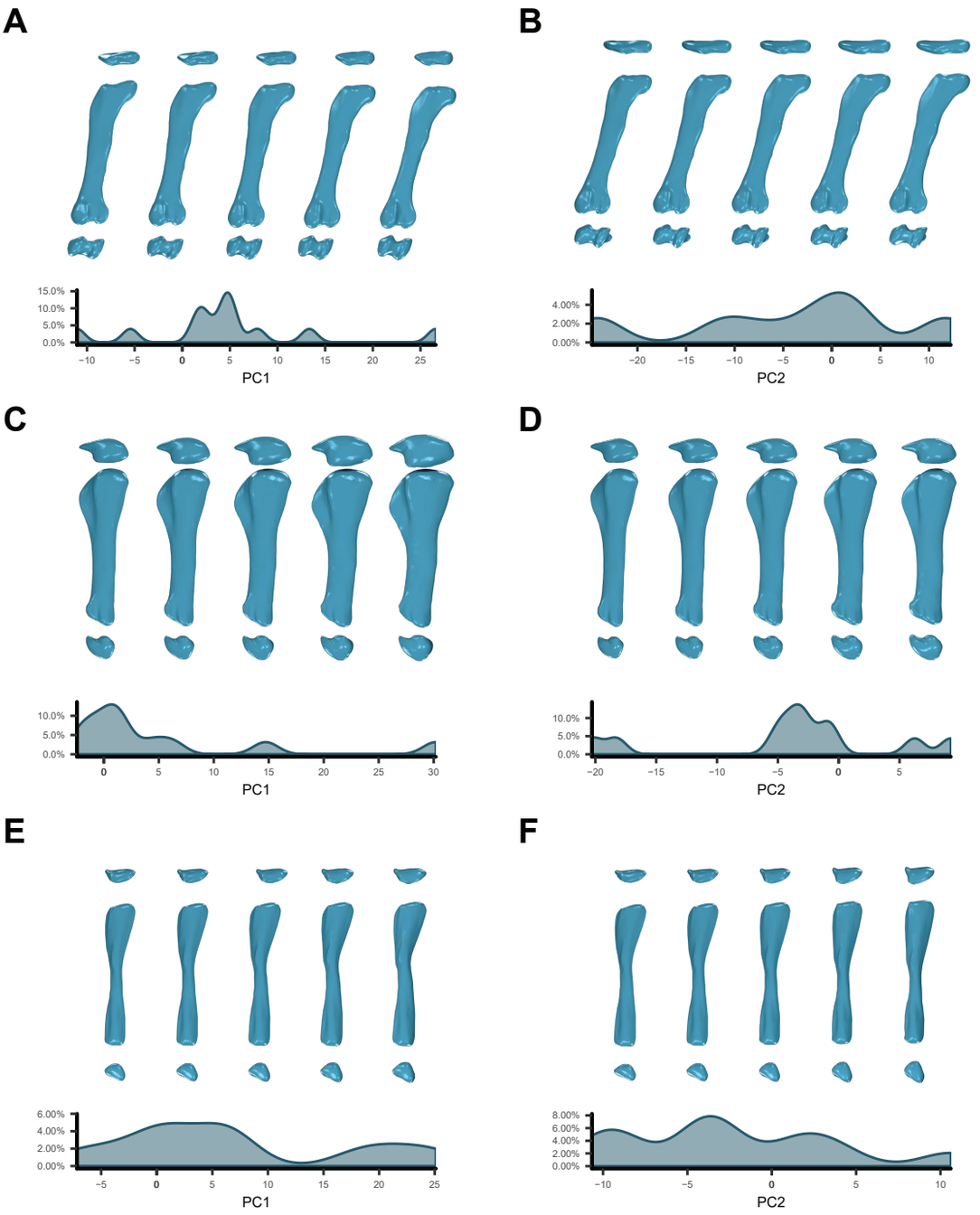

Fig.V.15. Morphological variation in the hindlimb elements of Morphotype I for each shape PCA. *Femora:* **(**A) Along PC1 axis. (B) Along PC2 axis. *Tibiae:* (C) Along PC1 axis. (D) Along PC2 axis. *Fibulae:* (E) along PC1 axis. (F) Along PC2 axis.

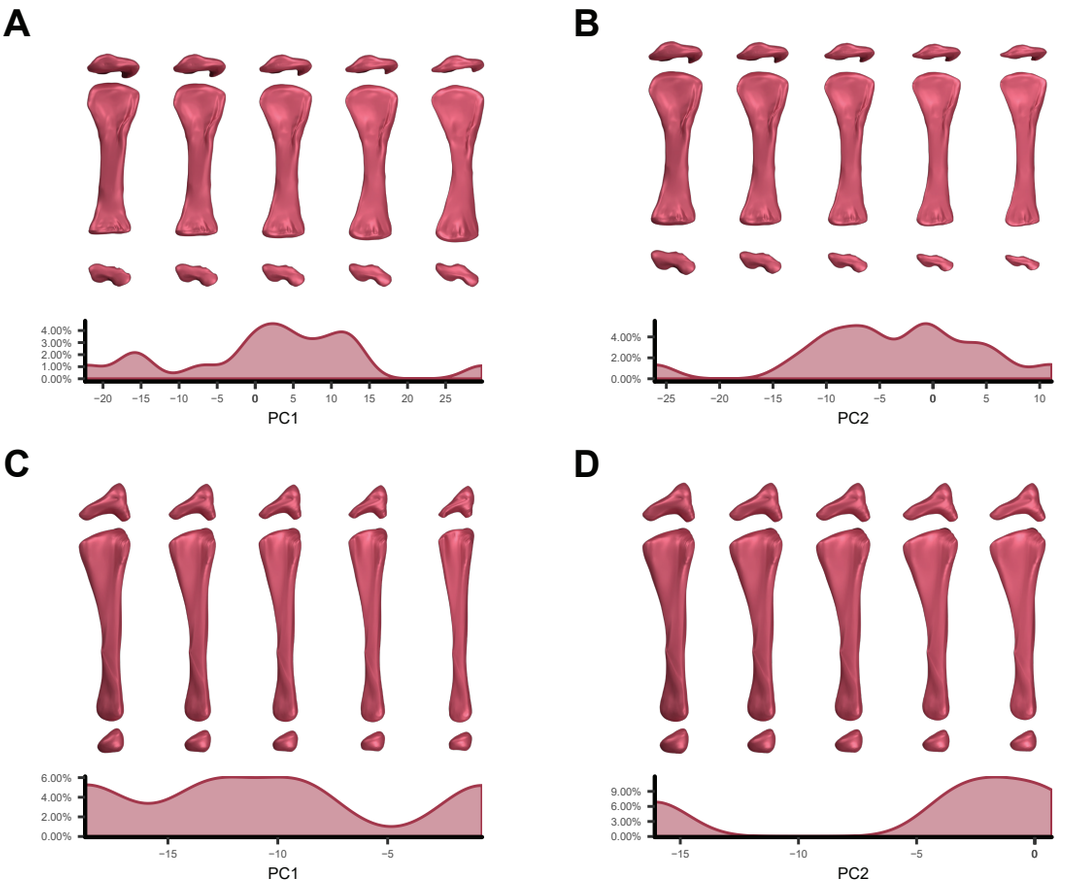

Fig.V.16. Morphological variation in the forelimb elements of Morphotype II for each shape PCA. *Humeri:* **(**A) Along PC1 axis. (B) Along PC2 axis. *Ulnae*: (C) Along PC1 axis. (D) Along PC2 axis. *Radii*: (E) along PC1 axis. (F) Along PC2 axis.

The femur HUE-2425 is completely projected in the taphomorphospace of the Morphotype II and closer to HUE-594. In this regard, HUE-EC-06 is a closely related form to HUE-EC-13 than to HUE-EC-1 and therefore different from *Lohuecotitan pandafilandi*. This might coincide with the analysis of the caudal axial skeleton associated to individual HUE-EC-06 (Vidal *et al.*, 2017; Mocho *et al.*, 2018a). The analysis of the other regions of the skeleton may shed light to the taxonomical assessment of this individual preliminary referred to Morphotype II.

Based on the present analysis, we have discarded the presence of more than one putative titanosaur form among the specimens referred to the Morphotype II. The relation between the humeri and femora can be established due their partial association in the field, as well as, the relationship between the elements on the hindlimb. The Morphotype II described in each bone element are interpreted as belonging to the same taxon (currently undescribed). The Morphotype II has a body plan that resembles brachiosaurid and lognkosaurian in the limb proportions, especially when considering forelimb elements. This gracile taxa present an elongated forelimb (see Table.V.19) with a mean forelimb to hindlimb ratio ~.77. The hindlimb

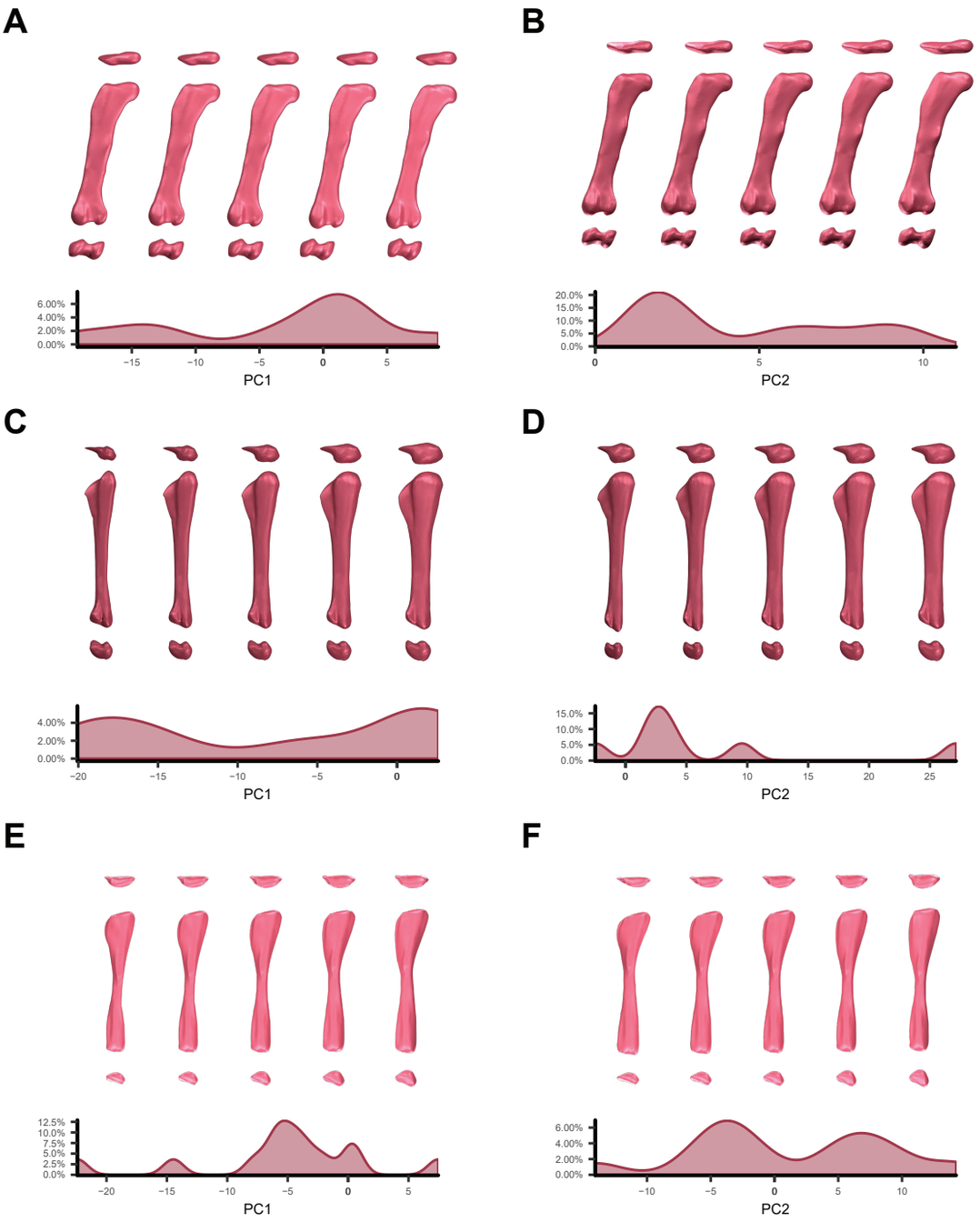

Fig.V.17. Morphological variation in the hindlimb elements of Morphotype II for each shape PCA. *Femora:* (A) Along PC1 axis. (B) Along PC2 axis. *Tibiae:* (C) Along PC1 axis. (D) Along PC2 axis. *Fibulae:* (E) along PC1 axis. (F) Along PC2 axis.

present a slightly more robust femora than Morphotype I, thought the hindlimb zeugopodium is much more elongated (Table.V.19) and slender (Table.V.3). There is common to see other gracile taxa with a with the femur and humerus equally robust as in *Mendozasaurus neguyelap* (González Riga *et al.*, 2018) or with more robust femora *Brachiosaurus altithorax* and *Giraffatitan brancai* (Gunga *et al.*, 1995; Christian *et al.*, 1999) and *Barosaurus* spp. (Robustness index of the femur= 0.21 compared to ~0.18-0.2 in the more robust *Camarasaurus grandis*, see McIntosh, 2005). This morphology and proportions are probably related with high browsing capabilities, as the forelimb is greatly elongated and related with the more upward position of the pectoral girdle (see Schwarz, Frey, & Meyer, 2007; Stevens, 2013). A manus with extremely elongated metacarpals was reported in the Lo Hueco fossil site (Díez Díaz *et al.*, 2014a), which might corresponds to this form with elongated forelimb.. Morphotype II seems to present a specialized forelimb yielding an elongated humerus and an extremely elongated ulnae. The hindlimb on the contrary is hypothesized to be more variable, suggesting the possibility that this titanosaurs with relative gracile forelimbs have a moderately robust hindlimbs. The Robustness Index is helpful to summarize this relationship (see Table.V.3 and 19). The robustness of the proximal elements of the hindlimb is closer among these gracile, high browsing feeders than to more stouter taxa. The distal elements of the hindlimb, however, present more significant differences that can be related to ecomorphological specialization. In order to test this hypothesis of morphological configuration we conducted the morphofunctional linear models between the measurements that conforms this index and several factors (see Morphofunctional differences, below).

V.5.3. INTRASPECIFIC VARIABILITY AND MORPHOLOGICAL CHARACTERS

We assessed the areas in each element that concentrates the greatest morphological variation via the analysis of high density surface semilandmarks and calculation of procrustes distances between the morphological extremes of each principal component of the shape variation (see Fig.V.18,V.19). The use of high density surface semilandmarks allowed us to track areas of maximum shape variation in the humerus (Fig.V.18.A and B). It can be observed that the deltopectoral crest presents higher procrustes distance differences concentrated in the deltopectoral crest (PC1-PC2 only, Fig.V.18.A and B). The area also covers the posterolateral trochanter of the deltopectoral crest and the area where some specimens present the accessory secondary trochanter in posterior face. These changes are more related with intraspecific variation and less with interspecific differences (see PCs of significant shape differences among morphotypes; Table.V.11).

Other areas observed are variable in both morphotypes is the minimum midshaft width. This area of the shaft can be more expanded in some specimens (e.g. more lateromedially expanded in HUE-1499, more lateromedially narrow in HUE-1463, HUE-1434; all of these specimens belongs to Morphotype II). The differences observed in the distal end and suggested as possible intraspecific variation are found among the areas with more variation in PC1 and especially in PC2 (Fig.V.18.A and B).

Considering several of the different morphological characters used in the study of sauropod systematics, the described intraspecific variation can have important impact on these analyses. In the proximal end, there is a slightly rugose process in the proximal part of the deltopectoral crest lateral edge (Upchurch, 1998). However, none of the Lo Hueco specimens present the well-developed process observed in some saltasaurids (e.g. *Neuquensaurus australis* MLP-Ly-25;

Saltsaurus loricatus PVL-4017-66; pers. obs. APB 2016). This area presents a convex development in several specimens of Lo Hueco (e.g. HUE-817, HUE-1463). The proximolateral edge of the humerus is one of the most variable areas in PC1, as well as, the entire deltopectoral crest (Fig.V.18.A). There are also some specimens that present a quadrangular shape of the proximal end (e.g. HUE-1463) and more rounded medial edge (e.g. HUE-1434) referred to the Morphotype II. While it is not as variable as the deltopectoral crest and the lateral edge in proximal, the medial edge of the proximal end is also one of the areas which present most of the shape variance in PC1, and especially in PC2 (see Fig.V.18.A and B). This can cause some score differences in the characters that summarize the overall morphology of the proximal end (Upchurch, 1998; González Riga, 2003; Gorscak *et al.*, 2017). The development of deltopectoral crest and its anterior to anteromedial projection also affects the scoring and it is the most variable character of the proximal end (Upchurch, 1998). While Morphotype I presents less variability in the deflection of the Mm. scapulohumerales insertion resulting in similar character scoring, the Morphotype II presents a higher variability within the sample (probably referable to intraspecific variability). Therefore, the Morphotype II in this case is the only one that can present different scoring and overlap with the characteristic morphology of Morphotype I.

The shaft presents some degree of torsion, but none of the observed differences between the morphotypes, nor the proposed intraspecific variation among specimens of Morphotype II can translate in significant differences in the scoring of the associated characters (see Tschopp *et al.*, 2015). On the contrary, we can observe significant differences in the morphology of the lateral margin related with the distal variability in the deltopectoral crest (Fig.V.18) that may affect the scoring of these characters, especially for the Morphotype II (see Curry Rogers, 2005). In addition, the variability observed in the midshaft robustness or anteroposterior compression can also be a source of variation in scoring of Morphotype humeri (Fig.V.18.B; see Carballido & Sander, 2014 after Wilson & Upchurch, 2003)

The analysis of the high density surface semilandmarks shows that the ulnar features with the most changes across PC1 are related with the morphology of the anteromedial and posterolateral processes. Light differences in the anteromedial part of the distal end can be recovered (Fig.V.18.C and D). The variation in the distal end includes the area where Morphotype II presents the small ridge, absent in all specimens of the Morphotype I. The PC2 also shows that the more variable areas are the anteromedial and posterolateral processes, as well as, the area between both processes. A slight variation can be observed in the anterior face of the midshaft where the ulnar ridge and the edges of the distal end are present. This second PC present a mix of differences between both morphotypes and the variability present in each morphotype, such as the development of the proximal processes, the anteroposterior expansion of the distal end, and the extension of the ulnar ridge in the midshaft.

Based on these findings, the angle of the anteromedial process and the posterolateral (see intraspecific variation in PC2, Fig.V.18.D) can cause different scorings among specimens of each morphotype (Tschopp *et al.*, 2015). Also, the distal end present some degree of variability both in PC1 and PC2, both within and among the morphotypes. This variability affects both in the scoring on the distal transverse expansion (see D'Emic, 2012; Mannion *et al.*, 2013; Tschopp *et al.*, 2015) and the robustness of the specimen (Curry Rogers, 2005) within the same morphotype.

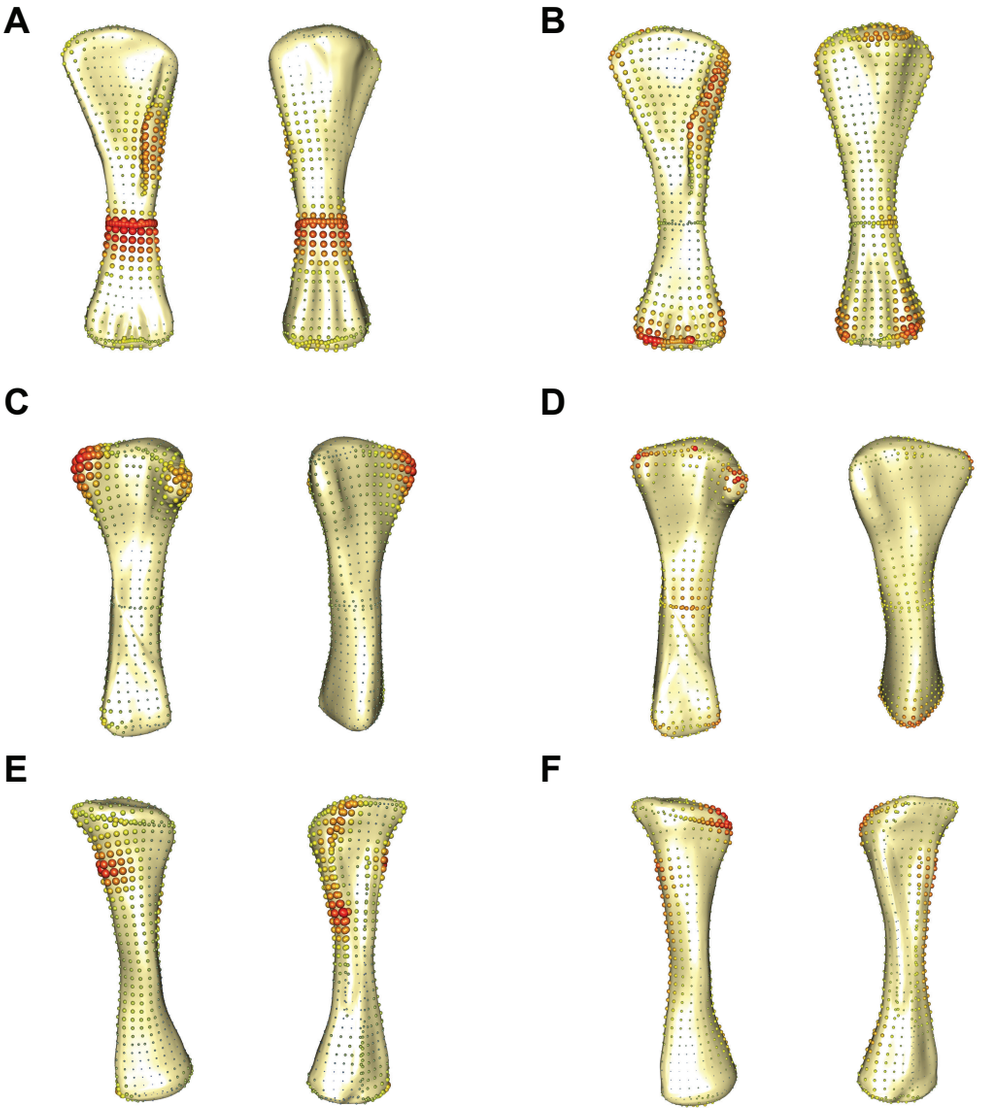

Fig.V.18. Morphological variation hot-spot in the high density surface semilandmarks shape PCA. *Humeri:* (A) Along PC1 axis. (B) Along PC2 axis. *Ulnae:* (C) Along PC1 axis. (D) Along PC2 axis. *Radii:* (E) along PC1 axis. (F) Along PC2 axis.

The variability in the high density surface semilandmarks of the radii shows that the areas with most of the variation in PC1 are the medial and posterolateral faces of proximal end, the area of the M. biceps brachii scar and the proximal part of the interosseous ridge (Fig.V.18.E). There is a weak variability in the medial part of the distal end, but lesser than in the other cited areas. In PC2 there is also variation, again, in the M. biceps brachii attachment area, as well as, in the posterolateral part of the proximal end and the lateral and medial edges of the shaft (Fig.V18.F).

With the available sample, we found little effect on character scoring among the traditional characters used in sauropod systematics. These characters are few in number compared with

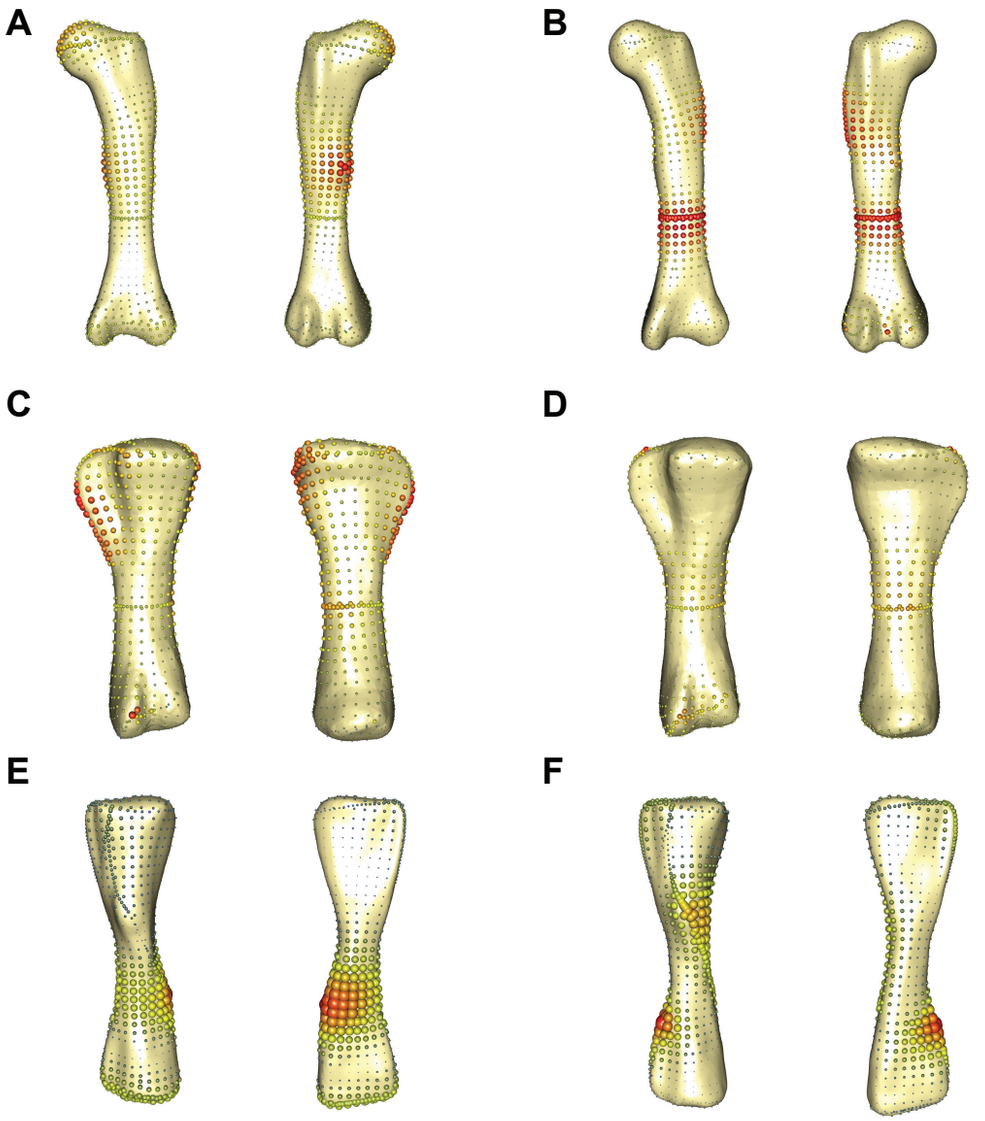

Fig.V.19. Morphological variation hot-spot in the high density surface semilandmarks shape PCA. *Femora:* **(**A) Along PC1 axis. (B) Along PC2 axis. *Tibiae:* (C) Along PC1 axis. (D) Along PC2 axis. *Fibulae:* (E) along PC1 axis. (F) Along PC2 axis.

other regions of the skeleton. The shape of the proximal end is one of the most variable areas in our sample (see Fig.V.18.E and D), but this is translated in no significant scoring differences among the specimens according to the character definitions (see Curry Rogers, 2005; Gorscak *et al.*, 2014).

The femora show major differences in the proximal and distal end as well as in the anteroposterior compression of the shaft and shape of the lateral bulge, which probably have taxonomical significance. These areas concentrate most of the variation in PC1 and PC2 (Fig.V.19) by the surface semilandmarks. In PC1 the variation is subtle than in the development of the distal part of the lateral bulge and the minimum midshaft width section, while most of the variation is

concentrates in the medial and proximal face of the femoral head, and in the fourth trochanter area. These changes have been discussed as main differences between both morphotypes: (i) morphology and relative position of the femoral head, (ii) development of the lateral bulge and the position, (iii) morphology of the medial face in the area of the fourth trochanter, and (iv) eccentricity of the midshaft. The PC2 also indicates that there is a slight variation in the position and eccentricity of the minimum midshaft width, in the distal development of the lateral bulge and in the distal end. The distal end bears most of this variation in the posterior face of the epicondyle and intercondylar fossa, while in the anterior face it is mostly concentrated in the proximal development of the distal condyles.

The variance on the position of the femoral head is related with differences between both morphotypes, but also variable within the same morphotype (e.g. HUE-2338, HUE-3108 in Morphotype I). This produces different scoring in the characters related with the dorsoventral position of this feature (Upchurch *et al.*, 2004). There is also some differences in the medial bevelling of the femoral head and the displacement of the shaft. These can affect the scoring depending on the character definition (see proposal in Royo-Torres, 2009; Gorscak *et al.*, 2017). In PC2 and PC3 (Fig.V.19.B; Supplementary Material.V.D.10.C) there is variation in the proximodistal development of the lateral bulge that is not entirely related with the morphotype differences. This intraspecific variability seen among several specimens (e.g. HUE-594, HUE-1319, HUE-2420) can affect the scoring on this character (see Salgado *et al.*, 1997a; Royo-Torres, 2009).

There is also a great difference in the overall robustness among the specimens of each morphotype, as well as the eccentricity of the shaft (Table.V.5) and the section of the minimum midshaft width (Fig.V.19.A and B). Several characters proposed in morphological datasets are focused in the codification of these features (see character #198 in Wilson, 2002; character #41, #42 and #43 in Mannion *et al.*, 2013) and their variability (see Vila *et al.*, 2012). While it is noticeable at first glance in all the sample (see Chapter I, Chapter IV; see also Páramo *et al.*, 2016), the variability in the scoring greatly depends on the way it is codified these morphological features. For example there are few differences in the scoring if we codify the anteroposterior midshaft section morphology as a discrete character (subcircular or elliptical; almost every specimen of both morphotypes are elliptical as in most Titanosauria, see Royo-Torres, 2009) than if we use it as a continuous or semi-quantitative character (ratio of anteroposerior width against lateromedial width, see Royo-Torres, 2009).

Finally, the distal end posterior projection of the tibial and fibular condyles present most of the variance in PC2 (Fig.V.19.B) and PC3 (Supplementary Material.V.D.10.C) indicating that there are not only variance between morphotypes but also some degree of intraspecific variability as discussed before (see Morphotype Differences). The relative orientation of the tibial condyle is much more variable in Morphotype II (e.g. HUE-594, HUE-2420). However, both morphotypes generally present distinct and congruent scorings for this character (Royo-Torres, 2009). The fibular-tibial condyle width ratio is also a character widely expanded in the literature of sauropod systematic (see definition in Wilson, 2002), which scoring can be also affected among specimens of Morphotype I (e.g. HUE-8801 with subequal condyles; HUE-3108 with wider fibular condyle).

The analysis of the high density surface semilandmarks on the tibiae shows in PC1 that most of the variability is centered in the morphology of the cnemial crest, especially in the distal part; the posterior part of the proximal end; the morphology of the posterior part of the midshaft; and

the positon of the aap (Fig.V.19.C). The PC2 shows that most of the variation is related to the proximal part of the cnemial crest, the midshaft, and the aspa. The PC1 variation coincides with the discussed interspecific variability, with the Morphotype I showing a more lateromedially expanded, a subtriangular proximal end with a developed fibular articulation and a secondary cnemial crest contra a less lateromedial expanded proximal end with more quadrangular posterior edge characteristic of the Morphotype II. Other major differences discussed herein are the relative position of the aap between both morphotypes and the extreme slenderness of the Morphotype II tibial shaft.

Most of the variability of the proximal end is is the cnemial crest and the area between the fibular articulation and the distal end of the cnemial crest fossa, which covers several morphological characters proposed in sauropod systematics. There is a proposal to include the morphology of the cnemial crest in lateral face (Royo-Torres, 2009) that could be affected by the variability in the distal part of the cnemial crest in Morphotype II (e.g. HUE-1317 subcircular, HUE-1500 subtriangular). The wider distal part of the cnemial crest in some specimens of the Morphotype II, probably associated with the muscular attachment (e.g. HUE-2117) could be discussed if is present a true fibular accessory trochanter on the cnemial crest (see Tschopp *et al.*, 2015). The variability on the development of the fibular articulation in proximal view in both morphotypes may also affects the scoring of the morphology of the proximal end (Wilson, 2002). There are some specimens with more anteroposteriorly elongated proximal end in both morphotypes (see variability in the posterior part of the proximal end, Fig.V.19.A; e.g. HUE-1149, HUE-1165). Most of the specimens present a more typical titanosaurian subcircular-subtriangular morphology (Wilson, 2002: character 203, state 1).

The proximodistal development of the fibular articulation is a clear morphological difference between both morphotypes (see Chapter IV, see also Morphological Differences, this chapter). However, both morphotypes present some differences in this area that can be relatable to ontogenetic differences, as smaller specimens present a less development (or shorter accessory cnemial crest in Morphotype I, e.g. HUE-2318). This character is therefore variable in both morphotypes, which can affect the scoring regardless with the presence of the secondary cnemial crest in one of the morphotypes of our sample (see character definition in Harris, 2007; Tschopp *et al.*, 2015; Mannion, Allain, & Moine, 2017).

The distal end presents some variability in each morphotype as shown in PC2 (Fig.V.19.D) with differences in the position of the aap among the same morphotype. This feature was one of the identified differences between both morphotypes of Lo Hueco. However, several specimens present a slightly different deflection in the aap in each morphotype (e.g. more perpendicular distal end to the axis of the shaft to more posteriorly deflected distal end among specimens of Morphotype II). This character was firstly proposed based on the description of *Lirainosaurus astibiae*, which have a more posteriorly deflected distal end (Sanz *et al.*, 1999; see also discussion about this character in Royo-Torres, 2009).

The analysis of the surface semilandmarks of the fibula shows that most of the variation concentrates in the distal end and the distal part of the lateral trochanter in PC1 (Fig.V.19.E). While it may be seen as counterintuitive at first, these features are related with the sigmoid development of shaft, which is one of the major differences between Morphotype I, *Lirainosaurus astibiae* and Morphotype II. On the PC2 most of the variation is related with the anterior trochanter in proximal view, the lateral trochanter, the shaft, and the anterolateral crest in distal

view. The variation in those areas is related with major differences between the morphotypes but also with the variability in the extension of the anterior trochanter and the extension of the area of the muscular attachment in the lateral trochanter, also related with the bifurcation or expansion of this trochanter (see morphotype differences and taphomorphospaces before).

The variability on the proximal part of the anterior trochanter (PC2: Fig.V.19.F.; PC3: Supplementary Material.V.D.10.I) and the anterior or slightly medially deflection in Morphotype II produces different scorings in this character (Royo-Torres, 2009; Wilson & Upchurch, 2009; D'Emic, 2012). The Morphotype I is also variable, but almost all the sampled specimens retain the medial deflection of the anterior trochanter forming a crux in proximal (D'Emic, 2012: character #111, state 1). The lateral trochanter also presents most of the variation in the proximal third of the fibula in PC2 (Fig.V.19.F). As it has been observed, several specimens of each morphotype present the development of a more oval-shaped lateral trochanter or a crest like trochanter, which can be bifurcated (e.g. HUE-1146, HUE-1513). While most of the specimens of Morphotype I present its characteristic oval-shaped lateral trochanter, this area can present some variation that might interfere in the character scoring as previously noted for datasets focused on titanosaurs (Curry Rogers, 2005). The variation found in this area can also affect the scoring on the morphology shaft cross-section at midpoint of the fibular total length (see Royo-Torres, 2009) with some specimens presenting a more circular section (e.g. HUE-1175) while others present a more lateromedially compressed outline with some concavity on medial face (e.g. HUE-1612). Also, the variation in the sigmoid of the shaft could also affect especially in Morphotype II, which presents a straighter shaft (see character 113, D'Emic, 2012 after Royo-Torres, 2009). The distal end also presents a high variability in each morphotype (distal end morphology, PC1: Fig.V.19.I, proximal part of the anterolateral crest, PC2: Fig.V.19.F.) but has no effect in the current established character related with the fibular distal end and the development of the anterolateral crest.

While this variability affects a small portion of the majority of appendicular characters defined on the analyzed elements (see a list of morphological characters of current use in sauropod systematics, Supplementary Material.V.I), our results show that they might affect the final character scorings in all the element types. Most of the current osteological characters used in sauropod systematics have a conservative definition not susceptible to the intraspecific variability reported in this study. However, the impact of the scoring differences between individuals of the same taxa in the small amount of characters sensible to intraspecific variability is unknown. Further work may be necessary in this issue, including scoring by individuals in order to better expose differences in the scoring and quantify the resultant differences, if any, in the tree topologies. Some areas with high variability identified in this study and the associated morphological character scoring differences may be relatable to ontogenetic changes. A more detailed study on the variability related with ontogenetic development should be addressed elsewhere (see Chapter VI).

V.5.4. MORPHOFUNCTIONAL DIFFERENCES

We tested the relationships between the variables length correlated with the proximal, medial and distal lateromedial widths, prior extracting the shape component (absent of the size noise component), and related with two factors. The acquisition of wide-gauge associated with derived titanosauriforms (Wilson & Carrano, 1999; Wilson, 2002; Upchurch *et al.*, 2004; D'Emic, 2012; García *et al.*, 2015; Bates *et al.*, 2016; Ullmann *et al.*, 2017) and the high browsing capabilities

derived of a specialized the body plan (Christian, 2002; Ullmann *et al.*, 2017).

We found a strong relationship (with high F effects and all significant effects) between the robustness development in the humerus and radius. The ulna presents a significant effect of the feeding envelope specialization and the acquisition of wide gauge locomotion type. When checking the statistical power of the effect in the ulna, we found that there is a greater effect of the acquisition of wide gauge.

In sauropods, the acquisition of high browsing capabilities is correlated with the elongation of the humerus or, in general, with presence of much more slender elements (Fig.V.20 and 22; Table.V.15 and 17). The intercept shows an inverse relation between the length and the width of the proximal end and the midshaft. The longer humeri usually present the narrower proximal ends and midshafts. While shorter humeri present wider proximal ends and midshaft. There is also a significant difference between sauropods with long, narrow humeri and high browsing feeding while the more robust humeri correspond to low browsing feeders. The distal end presents less variation but there are differences between low browsing feeders and high browsing feeders. The trend among high browsing sauropods is to increase the distal width (i.e. more robust distal) in association with the increase of the elongation (Fig.V.20). This is partially caused by a difference in the trend between non-wide gauge sauropods and titanosaur sauropods (Table.V.15). Titanosaurs present a divergent trend within sauropods. Titanosaurs present shorter, lateromedially robust distal end among low browsing sauropods and much more elongated and slightly more slender distal end in high browsing sauropods. On the contrary to the proximal end and midshaft lateromedial width, where titanosaurs present the same trend among other sauropod groups. This trend reported in the titanosaurs also produce a change in the slope of the distal end model among high browsing feeders only.

The ulna presents a significant relationship of the overall robustness and the feeding envelope as well as the type of gauge in the proximal and distal lateromedial width (Table.V.15). High feeding sauropods present much more slender elements, with narrower lateromedial width or more elongated ulnae with the same width than the low browsing feeder counterparts. However, there is also a marked effect of the wide gauge acquisition in the robustness of the element, as titanosaur sauropods present much more robust ulnae than non-titanosaurian sauropods (see Fig.V.20.B).

The radius presents significant effect of the browsing capabilities but in this case all the widths are positively correlated. There is an interaction between the type of gauge and the feeding specialization. Longer the elements are more lateromedially narrow with a slender shaft, especially among high browsing sauropods. This is partially caused by the extreme elongation among titanosaur sauropods with high browsing capabilities compared with non-titanosaur sauropods and low browsing feeder titanosaurs (Fig.V.20.C). However, the sample among high browser sauropods is extremely reduced and uneven, and therefore it may be affecting our linear models.

The hindlimb shows similar results but the effects on the tibiae are not clear, with no relationships between the elongation and the anteroposterior width. Hind limb elements do not present such a marked development towards the acquisition of high browsing specialization. When including the sample of Lo Hueco, we found significant effects, both in the specialization of the feeding envelope and the acquisition of wide gauge capabilities (see Table.V.17). However, if we exclude the sample from Lo Hueco, the only existing effect is the acquisition of wide gauge

Element	Effect	Proximal						Midshaft						Distal					
					without *Giraffatitan*						without *Giraffatitan*						without *Giraffatitan*		
		F-stat	*df*	*p-value*	*F-stat*	*df*	*p-value*	*F-stat*	*df*	*p-value*	*F-stat*	*df*	*p-value*	*F-stat*	*df*	*p-value*	*F-stat*	*df*	*p-value*
Humerus	Width	52.044	1	**0.000***	39.376	1	**0.000***	19.632	1	**0.000***	6.467	1	**0.012***	4.384	1	**0.038***	3.651	1	0.058
	Feeding Envelope	39.448	1	**0.000***	19.869	1	**0.000***	46.224	1	**0.000***	26.825	1	**0.000***	52.125	1	**0.000***	26.740	1	**0.000***
	Gauge	9.471	1	**0.002***	4.534	1	**0.035***	2.537	1	0.113	0.965	1	0.327	7.671	1	**0.006***	3.173	1	0.077
	Feeding Envelope X Gauge	0.233	1	0.630	3.960	1	**0.048***	1.041	1	0.309	6.267	1	**0.013***	0.525	1	0.470	5.664	1	**0.018***
Ulna	Width	12.892	1	**0.001***	14.209	1	**0.000***	22.995	1	**0.000***	22.651	1	**0.000***	43.032	1	**0.000***	42.971	1	**0.000***
	Feeding Envelope	17.485	1	**0.000***	15.158	1	**0.000***	15.450	1	**0.000***	16.466	1	**0.000***	11.896	1	**0.001***	10.726	1	**0.001***
	Gauge	10.380	1	**0.002***	11.368	1	**0.001***	3.458	1	0.066	4.598	1	**0.035***	15.226	1	**0.000***	16.789	1	**0.000***
	Feeding Envelope X Gauge	0.116	1	0.734	0.967	1	0.328	1.543	1	0.217	0.234	1	0.629	0.077	1	0.781	0.200	1	0.655
Radius	Width	0.344	1	0.559	0.269	1	0.605	4.999	1	**0.028***	4.920	1	**0.029***	12.377	1	**0.001***	10.476	1	**0.002***
	Feeding Envelope	13.303	1	**0.000***	11.512	1	**0.001***	13.617	1	**0.000***	11.784	1	**0.001***	10.730	1	**0.001***	12.374	1	**0.001***
	Gauge	0.250	1	0.619	0.218	1	0.642	0.010	1	0.921	0.020	1	0.887	0.049	1	0.826	0.045	1	0.832
	Feeding Envelope X Gauge	5.350	1	**0.023***	6.222	1	**0.014***	4.796	1	**0.031***	5.744	1	**0.019***	5.927	1	**0.017***	4.270	1	0.042*

Table.V.16. Results of the forelimb ecomorphological proxy GLM models.

on the proximal width ratio (see Table.V.18). The effect is not so marked (F=8.993) as expectable. The wide-gauge acquisition is correlated with a medial deflection of the proximal end. There is an increase in robustness of hindlimb elements among the members of Titanosauria when compared with non-titanosaurian neosauropods (see fig. 29).

On the other hand, the tibia reflects both the high browsing capabilities and the acquisition of wide gauge ($p<0.05$ all models; Fig.V.22 and Table.V.17). However if we exclude the sample of Lo Hueco, the effect in the acquisition of wide gauge is not significant ($p>0.05$ all models; Table.V.18, figs. V.23). Also, the effect of the feeding niche specialization is small and much less marked with the exclusion of the sample from Lo Hueco (F~11 with Lo Hueco specimens, F~4.4 without Lo Hueco specimens). There is a trend toward a more accentuated reduction of the shaft length among the high browser sauropods while the tibia get short, than in the non-high browsing feeder sauropods.

One interesting issue is the lack of relationship between the anteroposterior width and the length of the tibial shaft in our models. There is an important morphological change in the tibia lateromedial development of the proximal and distal end, especially toward the robust tibiae in titanosaurian sauropods (Wilson, 2002; D'Emic, 2012). Moreover, from the sauropods included in this study, there is a marked trend toward the reduction of the distal end observable in *Rapetosaurus krausei* (Curry Rogers, 2009b), *Mendozasaurus neguyelap* (González Riga, 2005b; González Riga *et al.*, 2018) and *Giraffattitan brancai* (Janensch, 1961) and other high browsing feeder or gracile sauropods included in this study. Nevertheless, the major reduction of the distal end width seems to be related with the lateromedial width of the tibial distal end rather to the anteroposterior width (which is a measurement not usually reported in the literature, nor registered in this PhD thesis.

Element	Effect	Proximal			Midshaft			Distal		
		F-stat	*df*	*p-value*	*F-stat*	*df*	*p-value*	*F-stat*	*df*	*p-value*
Humerus	Width	38.016	1	**0.000***	21.608	1	**0.000***	5.578	1	**0.019***
	Feeding Envelope	36.168	1	**0.000***	32.728	1	**0.000***	46.279	1	**0.000***
	Gauge	9.344	1	**0.003***	3.657	1	0.058	7.623	1	**0.006***
	Feeding Envelope X Gauge	0.393	1	0.532	1.015	1	0.315	1.111	1	0.293
Ulna	Width	5.428	1	**0.022***	17.406	1	**0.000***	46.647	1	**0.000***
	Feeding Envelope	6.513	1	**0.012***	4.265	1	**0.042***	2.032	1	0.158
	Gauge	31.327	1	**0.000***	16.665	1	**0.000***	46.195	1	**0.000***
	Feeding Envelope X Gauge	5.500	1	**0.021***	2.139	1	0.147	8.540	1	**0.004***
Radius	Width	0.975	1	0.326	7.856	1	**0.006***	19.128	1	**0.000***
	Feeding Envelope	23.237	1	**0.000***	22.708	1	**0.000***	19.377	1	**0.000***
	Gauge	4.295	1	**0.041***	2.019	1	0.159	1.619	1	0.207
	Feeding Envelope X Gauge	17.972	1	**0.000***	16.399	1	**0.000***	19.514	1	**0.000***

Table.V.17. Results of the forelimb ecomorphological proxy GLM models. Withouth the sample of Lo Hueco.

The effect and significance of the reduction on the lateromedial width instead of the anteroposterior width should be analyzed elsewhere.

Lastly the fibula reflects a small significant effect of the feeding specialization only after acquiring the wide gauge stance ($p<0.05$ interaction between factors, all models; Table.V.17 and V.18). The fibulae of titanosaurian sauropods tend to be more robust than the fibulae of non-titanosaurs and the effect of the wide gauge acquisition is also significant ($p<0.05$ all models). Moreover, it can be observed that in the proximal end the anteroposterior width relationship with the length is significant and its effect is more marked than in the distal end ($p<0.05$ both models; F ~16 anteroposterior width of proximal end, F ~5 anteroposterior width of distal end). There is also a more marked effect of the interaction between the specialization and the wide gauge than the wide gauge itself in the robustness of the proximal end (F ~8.5 interaction, F ~5.5 gauge type; Table.V.17). This effect may be caused by marked difference in the robustness of low browsing feeder titanosaurs against those with a higher feeding envelope capability, which are in general much more gracile despite the higher variation (much more dispersed with much shorter but gracile forms and some robust ones, see Fig.V.22.G and I).

There is a loss of the effect of wide gauge acquisition and the interaction with the feeding envelope specialization in the robustness of the proximal end when excluding the sample from Lo Hueco. Instead, there is only a small effect of the gauge type in the midshaft robustness (after exclusion of Lo Hueco: F ~6.4 midshaft width, $p=0.013$; Table.V.18). With the exclusion of the Lo Hueco sample, it can be seen that there is also a significant but small effect of the feeding specialization in the robustness of the element in midshaft and distal end (F ~ 6 in both models, $p<0.05$; Table.V.18). As seen with the tibiae, this may be cause after considering the anteroposterior width, usually reported in the literature. However, it may be interesting to test the effects on the lateromedial width. Among titanosaurs, some studies report extreme slender elements even among giant titanosaurs, such as *Argentinosaurus huinculensis* (e.g. MCF-PVH-1) and *Mendozasaurus neguyelap* (IANIGLA-74-3; see also González Riga *et al.*, 2019). They present straighter shaft with no sigmoid morphology as in other titanosaurs (D'Emic, 2012). *M. neguyelap*

also presents a considerable reduction of the proximal end with medial deflection of the anterior trochanter as well as a lateromedial narrower shaft (IANIGLA-74-3, pers. obs. APB 2016). In contrast, non-titanosaurian sauropods present a more direct relationship between a possible feeding niche specialization and the robustness of the elements, such as the lateromedially compressed and slender fibula of *Barosaurus lentus* (McIntosh, 2005; see also Lovelace, Hartman, & Wahl, 2007) and the robust fibula of *Apatosaurus louisae* (see Lovelace *et al.*, 2007).

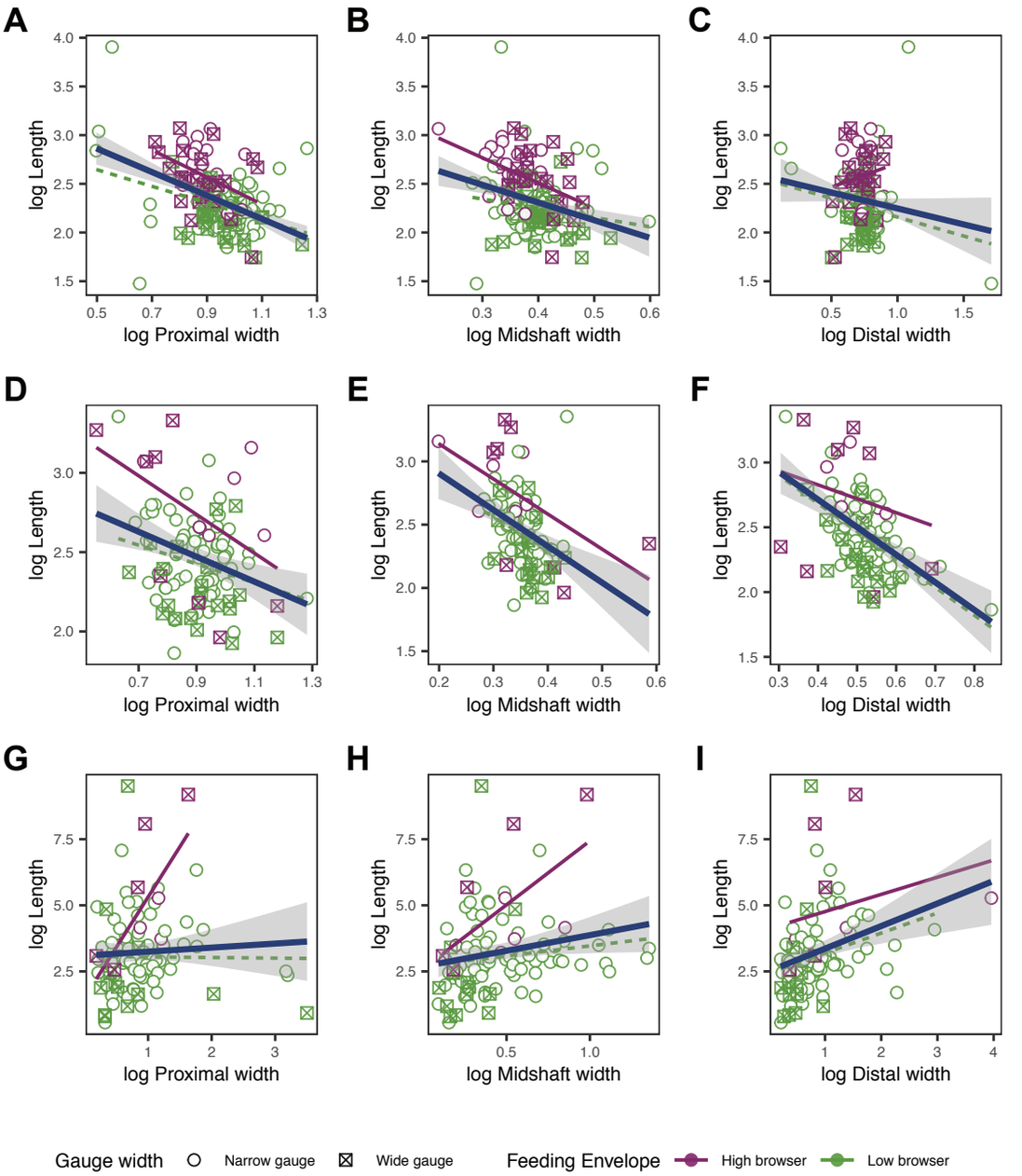

Fig.V.20. Results of the forelimb ecomorphological proxy GLM models..

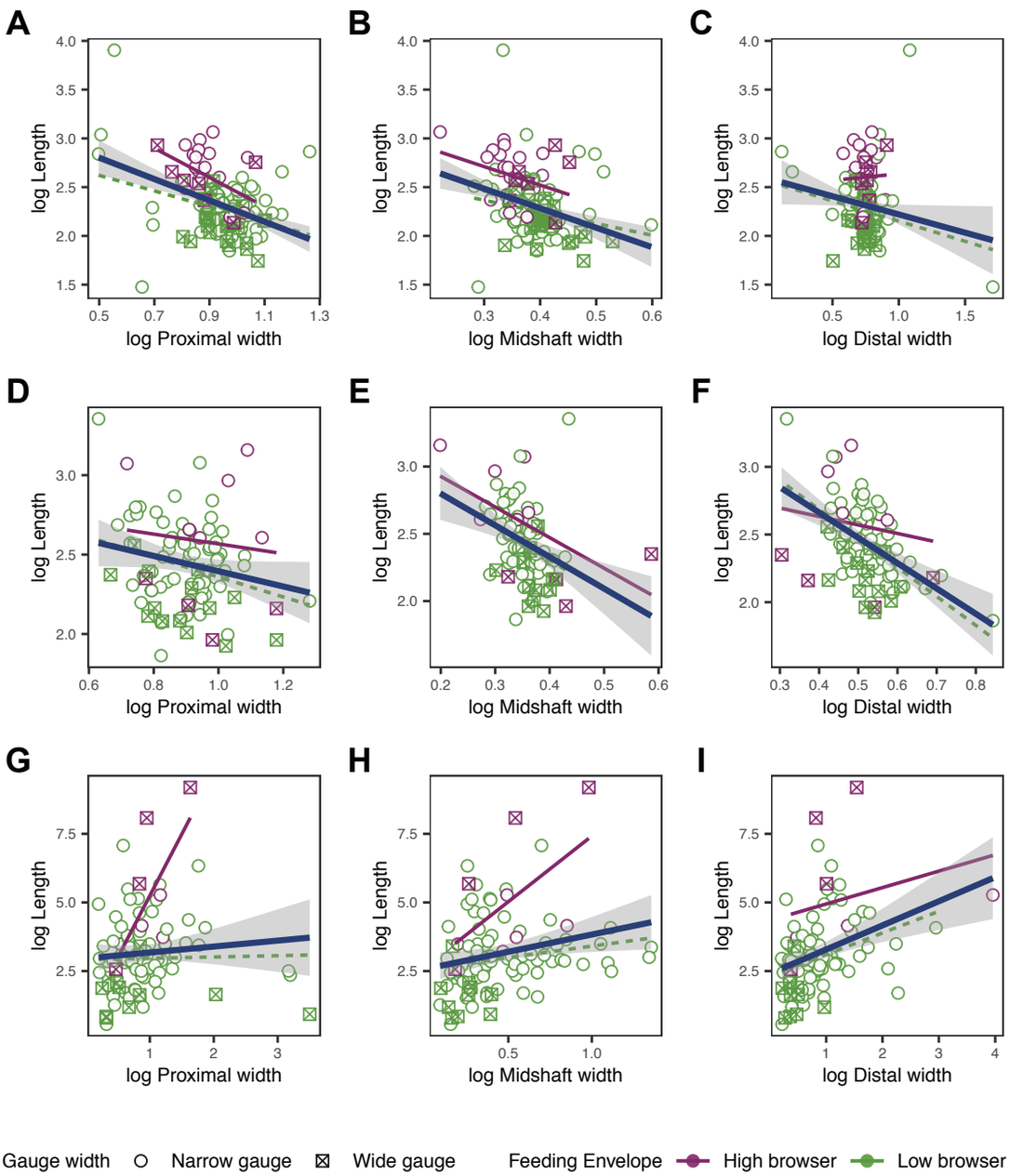

Fig.V.21. Results of the forelimb ecomorphological proxy GLM models. Withouth the sample from Lo Hueco.

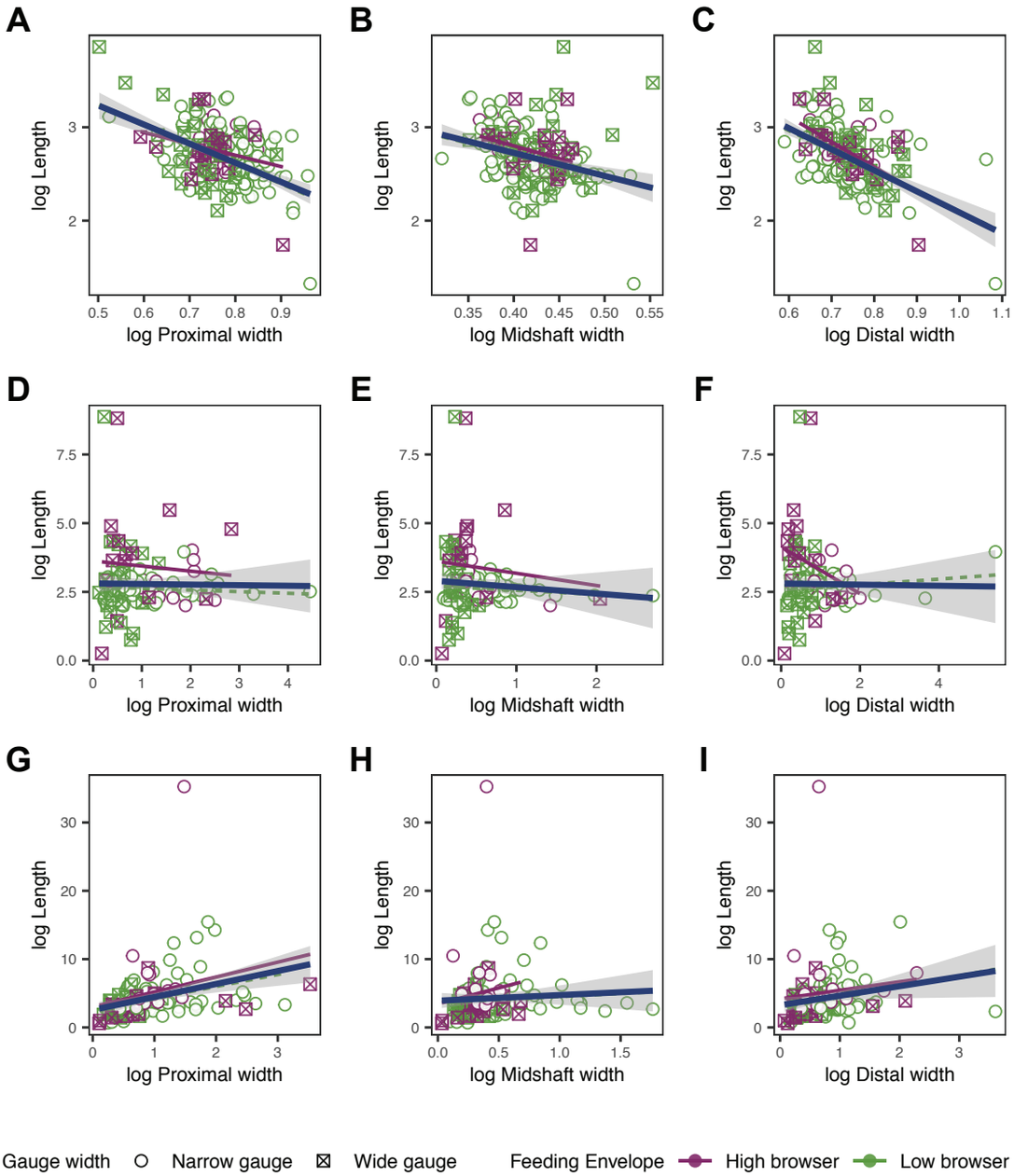

Fig.V.22. Results of the hindlimb ecomorphological proxy GLM models..

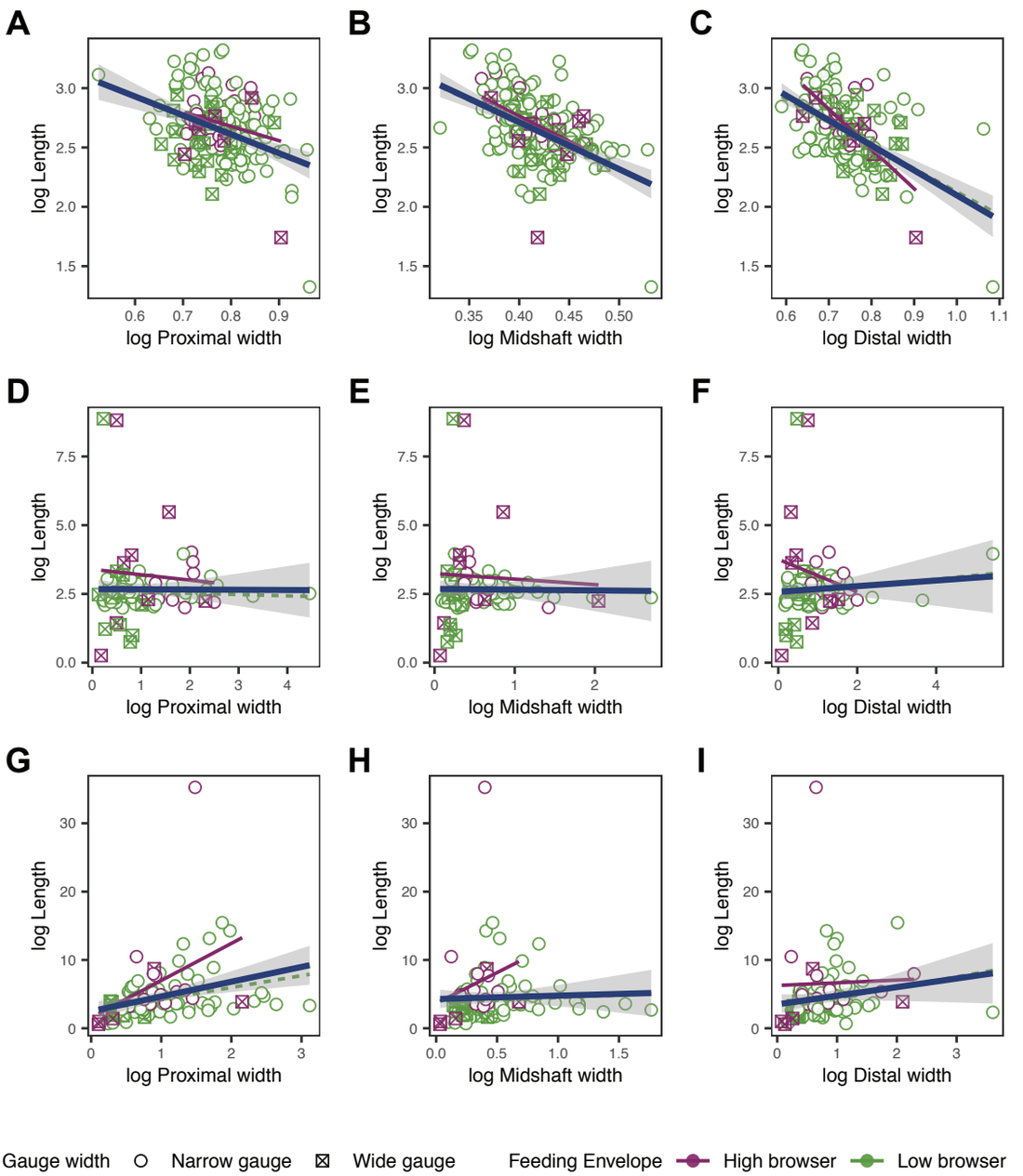

Fig.V.23. Results of the hindlimb ecomorphological proxy GLM models. Withouth the sample from Lo Hueco.

Table.V.18. Results of the hindlimb ecomorphological proxy GLM models.

Element	Effect	Proximal			Proximal without *Giraffatitan*			Midshaft			Midshaft without *Giraffatitan*			Distal			Distal without *Giraffatitan*		
		F-stat	*df*	*p-value*	*F-stat*	*df*	*p-value*	*F-stat*	*df*	*p-value*	*F-stat*	*df*	*p-value*	*F-stat*	*df*	*p-value*	*F-stat*	*df*	*p-value*
Femur	Width	62.716	1	**0.000***	65.362	1	**0.000***	20.855	1	**0.000***	19.538	1	**0.000***	77.661	1	**0.000***	76.796	1	**0.000***
	Feeding Envelope	1.481	1	0.225	2.510	1	0.115	3.204	1	0.075	3.970	1	**0.048***	3.429	1	0.065	4.766	1	**0.030***
	Gauge	0.460	1	0.498	1.313	1	0.253	5.977	1	**0.015***	4.921	1	**0.028***	9.318	1	**0.003***	7.848	1	**0.006***
	Feeding Envelope X Gauge	0.962	1	0.328	3.840	1	0.051	1.516	1	0.220	2.401	1	0.123	3.237	1	0.073	5.128	1	**0.025***
Tibia	Width	0.026	1	0.871	0.001	1	0.980	0.964	1	0.328	0.660	1	0.418	0.022	1	0.883	0.012	1	0.913
	Feeding Envelope	11.591	1	**0.001***	14.121	1	**0.000***	11.030	1	**0.001***	13.657	1	**0.000***	11.224	1	**0.001***	14.061	1	**0.000***
	Gauge	4.785	1	**0.031***	3.307	1	0.072	4.492	1	**0.036***	3.047	1	0.084	5.575	1	**0.020***	3.796	1	0.054
	Feeding Envelope X Gauge	1.777	1	0.185	0.665	1	0.416	1.846	1	0.177	0.678	1	0.412	1.943	1	0.166	0.727	1	0.396
Fibula	Width	15.805	1	**0.000***	23.375	1	**0.000***	0.598	1	0.441	2.241	1	0.137	4.812	1	**0.030***	13.502	1	**0.000***
	Feeding Envelope	1.792	1	0.183	0.836	1	0.362	2.294	1	0.132	0.356	1	0.552	2.335	1	0.129	0.270	1	0.604
	Gauge	5.516	1	**0.020***	1.825	1	0.179	9.300	1	**0.003***	4.711	1	**0.032***	6.640	1	**0.011***	1.747	1	0.189
	Feeding Envelope X Gauge	8.462	1	**0.004***	0.977	1	0.325	6.041	1	**0.015***	0.316	1	0.575	6.011	1	**0.016***	0.244	1	0.622

Table.V.20. Forelimb and Hindlimb measurments comparison between the analysed taxa.

OTU	Humerus Length	Ulna Length	Femur Length	Tibia Length	Forelimb Length	Hindlimb Length	Fo-Hi Ratio	H-U Ratio	F-T Ratio	Feeding niche
"Barosaurus africanus"	607.86	550	1128.89	817.5	1157.86	1946.39	0.59	1.11	1.38	High Browser
Barosaurus	927.67	791	1440	1050	1718.67	2490	0.69	1.17	1.37	High Browser
Brachiosaurus	1839	941	2019	947	2780	2966	0.94	1.95	2.13	High Browser
Dreadnoughtus	1600	1010	1600	1145	2610	2745	0.95	1.58	1.40	High Browser
Giraffatitan	1608.75	1300	1287.22	1046.67	2908.75	2333.89	1.25	1.24	1.23	High Browser
Mendozasaurus	1143	733	1530	835.75	1876	2365.75	0.79	1.56	1.83	High Browser
Morphotype II	713.97	618	998.27	732.86	1331.97	1731.13	0.77	1.16	1.36	High Browser
Patagotitan	1675	1050	2363.33	NA	2725	NA	NA	1.60	NA	High Browser
Rapetosaurus	280.33	372	424.5	313	652.33	737.5	0.88	0.75	1.36	High Browser
Tornieria	980	NA	NA	860	NA	NA	NA	NA	NA	High Browser
Amphicoelias	NA	NA	1750	NA	NA	NA	NA	NA	NA	Low Browser
Apatosaurus	767.73	612.35	1306.97	789.12	1380.08	2096.09	0.66	1.25	1.66	Low Browser
Brontosaurus	671	486	1169.67	985.67	1157	2155.33	0.54	1.38	1.19	Low Browser
Camarasaurus	841.77	648.9	1146.05	697.88	1490.67	1843.92	0.81	1.30	1.64	Low Browser
Dicraeosaurus	633	437.5	1128.57	686.67	1070.5	1815.24	0.59	1.45	1.64	Low Browser
Diplodocus	762.65	501.87	1189.51	778.54	1264.52	1968.05	0.64	1.52	1.53	Low Browser
Galeamopus	923	728	1448	935	1651	2383	0.69	1.27	1.55	Low Browser
Lirainosaurus	507.89	114	709.6	412	621.89	1121.6	0.55	4.46	1.72	Low Browser
Morphotype I	617.96	600.17	930.75	577.63	1218.13	1508.38	0.81	1.03	1.61	Low Browser
Neuquensaurus	520.8	308.5	724.15	451	829.3	1175.15	0.71	1.69	1.61	Low Browser
Saltasaurus	499.5	382.8	795	437.25	882.3	1232.25	0.72	1.30	1.82	Low Browser

Element	Effect	Proximal			Midshaft			Distal		
		F-stat	*df*	*p-value*	*F-stat*	*df*	*p-value*	*F-stat*	*df*	*p-value*
Femur	Width	31.282	1	**0.000***	59.610	1	**0.000***	69.729	1	**0.000***
	Feeding Envelope	1.775	1	0.184	1.384	1	0.241	1.869	1	0.173
	Gauge	8.993	1	**0.003***	1.784	1	0.183	0.049	1	0.824
	Feeding Envelope X Gauge	0.381	1	0.538	0.670	1	0.414	2.828	1	0.094
Tibia	Width	0.004	1	0.951	0.012	1	0.912	0.514	1	0.475
	Feeding Envelope	4.370	1	**0.039***	4.146	1	**0.044***	3.906	1	0.051
	Gauge	0.809	1	0.371	0.982	1	0.324	1.369	1	0.245
	Feeding Envelope X Gauge	0.965	1	0.328	1.002	1	0.319	1.096	1	0.298
Fibula	Width	12.476	1	**0.001***	0.164	1	0.686	2.789	1	0.098
	Feeding Envelope	6.441	1	**0.013***	6.426	1	**0.013***	5.777	1	**0.018***
	Gauge	1.769	1	0.186	4.331	1	**0.040***	3.560	1	0.062
	Feeding Envelope X Gauge	2.969	1	0.088	2.069	1	0.153	2.156	1	0.145

Table. V. 19. Results of the hindlimb ecomorphological proxy GLM models. Withouth the sample of Lo Hueco.

Given the results of our model and the interaction observed between the acquisition of the wide gauge, it also may be possible that more high feeder titanosaurs develop a more slender appendicular skeleton through there is a loss of the sigmoid morphology of the fibula (see *Rapetosaurus krausei*, Curry Rogers, 2009; Morphotype II, this study). Therefore, we estimate the relationships of the robustness with the feeding envelope based in the anteroposterior width of the element despite the fact that two taxa with different feeding niche may present similar robustness but changes in the sigmoid of the fibula (with an associated reconfiguration of the position of the zeugopodium). The relationships of the feeding niche on the fibulae can be tested through other methods: (i) the analysis through landmark based GMM of the possible sigmoid morphology of the shaft and the expression of the feeding niche specialization; and (ii) change to the lateromedial width of the shaft instead of the anterposterior width. However, these tests should be carried elsewhere.

To summarize, while sauropods specialize to high browsing capabilities, part of the shifting is concentrated on the anterior part of the body and is related with an increase in forelimb length, and in the acquisition of a more slender ratio among the robustness index of the elements. The forelimb is usually composed by more robust distal elements, as occurs in *Brachiosaurus* and *Giraffatitan*, but unlike some of the individuals of the Lo Hueco Morphotype II, and an indeterminate diplodocine of Tendaguru Formation (previously referred as "*Barosaurus africana*") and *Mendozasaurus neguyelap*.

This strong elongation of the forelimb with more slender elements is congruent with the current hypothesis of changes in the morphology and orientation of the pectoral girdle related with the neck position and increases in its vertical envelope (Christian & Dzemski, 2007; Schwarz *et al.*, 2007; Preuschoft & Klein, 2013; Stevens, 2013). Among low browser sauropods there is a thigh coupling of robust humerus-robust distal part in the forelimb. The differences are remarkable between this kind of forelimb and the gracile type of high browsing sauropods (including Morphotype I of Lo Hueco). On the other hand, the hindlimb presents an irregular pattern, where predominates the similarities between robust hindlimbs among high and low browsers.

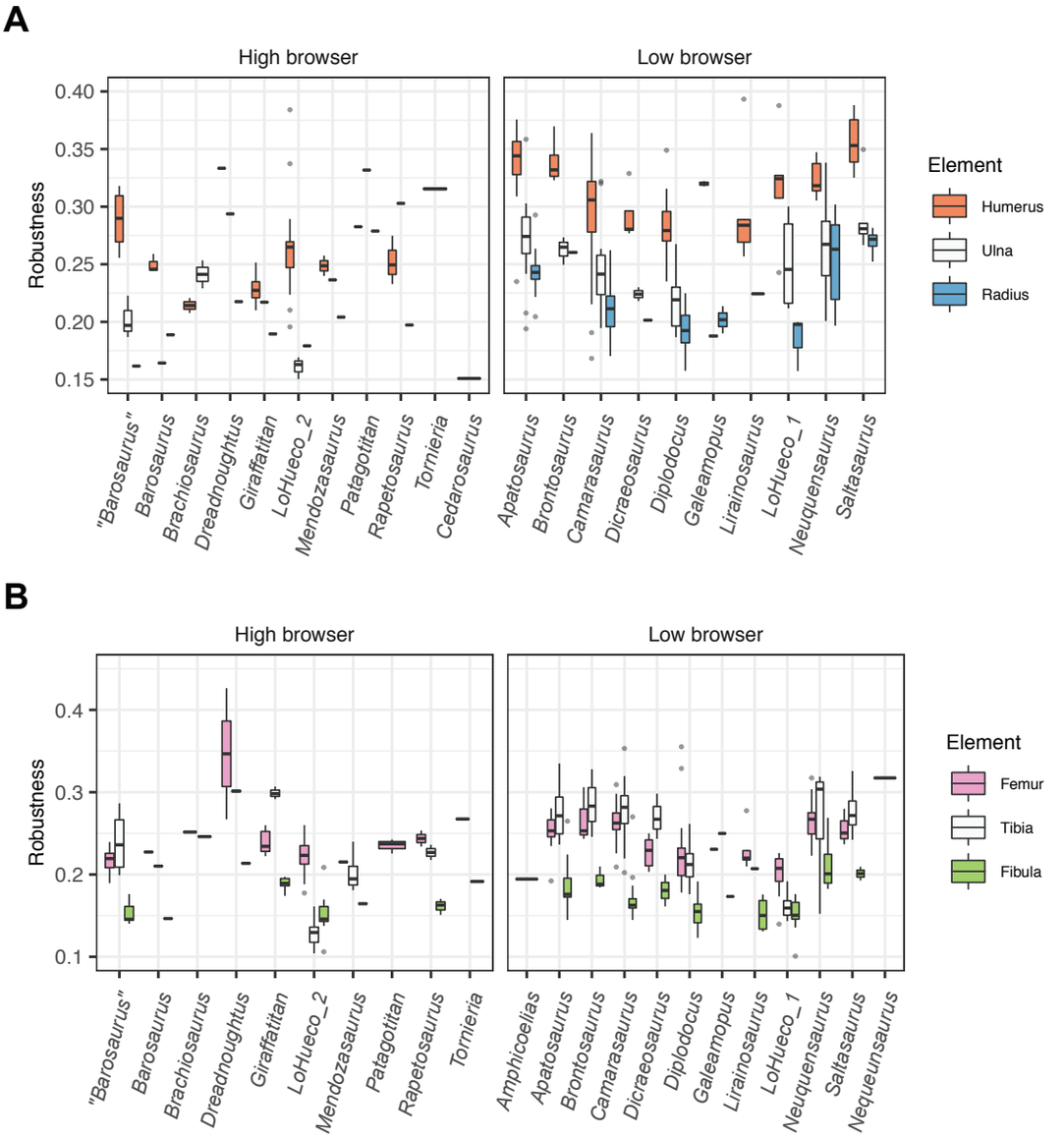

Fig.V.24. Comparison of the robustness indices among the two ecomorphological especializations explore in the analyses. LoHueco_1 - Morphotype I. LoHueco_2 - Morphotype II

Moreover, slender hindlimbs occur not only among high browsing feeding sauropod but within groups that develops specialized locomotion types outside wide-gauge, as seen in narrow gauge and low browsing feeders, such as *Diplodocus* and *Galeamopus* (see Wilhite, 2003; Tschopp & Mateus, 2017).

It is also remarkable that Morphotype II includes extremely slender tibiae and ulnae elements. The elongated zeugopodium has been also seen in other gracile taxa e.g. *Giraffatitan brancai* (Taylor, 2009b) which also present an elongated manus. This might be compatible with an extremely

gracile manus identified in Lo Hueco site (see Díez Díaz *et al.*, 2014a) despite it has not been associated to any morphotype and more work in this attribution is still necessary.

It is also important to note that this is a proxy model, and more studies on sauropod biomechanics especially in the neck vertical envelope are needed. We based our model in the available metadata, especially the Center of Masses. However, current study of the neck biomechanics insight that there are sauropods with long neck and anteriorly displaced Center of Masses that are actually low browsing feeders with low vertical envelope like *Mamenchisaurus youngi* (Christian *et al.*, 2013). Also, we based the attribution of several lognkosaurian taxa sampled in this study to high browsing feeders based on the (i) assumption of higher reach based in the gigantic size (ii) direct comparison on the vertebrae morphology and the cervico-dorsal spine positions following Stevens (2013) and (iii) the qualitative comparison between the estimated volumes of the neck, forelimb and hindlimb of *Patagotitan mayorum* (Carballido *et al.*, 2017) with other high browsing feeders after Bates *et al.* (2016). However, the axial skeleton and girdle specialization within this group may alter this preliminary assumption (Ullmann & Lacovara, 2016; Carballido *et al.*, 2017; González Riga *et al.*, 2019). Our results show an extremely robust forelimb in *Dreadnoughtus scharni* and *Patagotitan mayorum*, even compared to other sauropod of similar sizes or phylogenetically related. Further study in titanosaur neck biomechanics is also needed in the representatives of this group.

V.6 CONCLUSIONS

High shape variability have been found among the titanosaurian sauropods of Lo Hueco. Until now and with the given information, two main morphotypes have been detected. We used a series of comparisons to assess the interspecific and intraspecific morphological differences in a sample of forelimb and hindlimb elements from Lo Hueco.

The use of GMM methods help us quantify this morphological variation, test hypothesis of shape differences and also visualize those trends. Moreover, GMM and size extraction techniques over lineal variables allowed us to explore the shape variation with samples that range between specimens that differentiates greatly in size. We did not test the effect of size and possible ontogenetic effects on the shape variables as it was beyond the scope of this work. However, we assessed the presence of dwarf taxa and/or small non-fully grown individuals in the sample from Lo Hueco. None of the analysed small specimens of Lo Hueco belong to dwarf taxon, with the possible exception of HUE-3662. In general, no specimen was reassessed from previous description to other Ibero-Processorican titanosaur form. The humerus specimen HUE-3662, first described in this study, may be also the first presence of *Lirainosaurus astibiae* or a closely related form in the fossil site of Lo Hueco.

Moreover, we address that those morphotypes can be referred to different taxa. All the elements assessed as Morphotype I are referred herein to *Lohuecotitan pandafilandi*. The specimens assessed as Morphotype II, most likely, correspond to another and different exclusive titanosaurian sauropod present in Lo Hueco. This titanosaur might represent a new taxon from the Ibero-Processorican domain that still needs to be properly described.

These two taxa (not including the sole presence of a cf. *L. astibiae* humerus) present differences that also can be attributed to a more classical titanosaurian bauplan, including the case of

Lohuecotitan pandafilandi (Morphotype I), and the case of a highly specialized form (Morphotype II) that might be related to high browsing capabilities. This specialized form is characterized by the development of a gracile forelimb and hindlimb zeugopodium, and the limbs located straighter and near the sagittal plane.

We found that this trends are also present in other titanosaurian and non-titanosaurian neosauropods. There are several feature convergences in the body plan configuration acquired as part of the niche specialization for higher browsing capabilities in their feeding envelope.

V.7 BIBLIOGRAPHY

Abayomi K, Gelman A, Levy M. 2008. Diagnostics for multivariate imputations. *Journal of the Royal Statistical Society: Series C (Applied Statistics)* 57: 273–291.

Arbour JH, Brown CM. 2014. Incomplete specimens in geometric morphometric analyses. *Methods in Ecology and Evolution* 5: 16–26.

Arbour VM, Currie PJ. 2012. Analyzing taphonomic deformation of ankylosaur skulls using retrodeformation and finite element analysis. *PloS ONE* 7: 1–13.

Bak N, Hansen LK. 2016. Data Driven Estimation of Imputation Error—A Strategy for Imputation with a Reject Option. *PloS ONE* 11: e0164464.

Bakker RT. 1987. *The Dinosaur Heresies: a Revolutionary View of Dinosaurs*.

Barrett PM, Upchurch P. 1994. Feeding mechanism of *Diplodocus*. *Gaia*: 195–203.

Bates KT, Mannion PD, Falkingham PL, Brusatte SL, Hutchinson JR, Otero A, Sellers WI, Sullivan C, Stevens KA, Allen V. 2016. Temporal and phylogenetic evolution of the sauropod dinosaur body plan. *Royal Society Open Science* 3: 150636.

Benton MJ, Csiki Z, Grigorescu D, Redelstorff R, Sander PM, Stein KHW, Weishampel DB. 2010. Dinosaurs and the island rule: The dwarfed dinosaurs from Hațeg Island. *Palaeogeography, Palaeoclimatology, Palaeoecology* 293: 438–454.

Bonaparte JF. 1999. An processoured sauropod from the Aptian of Northern Patagonia, Argentina. In: Tomida Y, Rich TH, Vickers-Rich P, eds. Proceedings of the Second Gondwanan Dinosaur Symposyum. *Tokyo: National Science Museum Monographs*, 1–12.

Bonaparte JF, W.-D. Heinrich WD, Wild R. 2000. Review of Janenschia WILD, with the description of a new sauropod from the Tendaguru beds of Tanzania and a discussion on the systematic value of procoelous caudal vertebrae in the sauropoda. *Palaeontographica Abteilung A* 256: 25–76.

Bonnan MF. 2004. Morphometric analysis of humerus and femur shape in Morrison sauropods: implications for functional morphology and paleobiology. *Paleobiology* 30: 444–470.

Bonnan MF. 2007. Linear and geometric morphometric analysis of long bone scaling patterns in Jurassic neosauropod dinosaurs: their functional and paleobiological implications. *Anatomical Record* 290: 1089–111.

Bonnan MF, Farlow JO, Masters SL. 2008. Using linear and geometric morphometrics to detect intraspecific variability and sexual dimorphism in femoral shape in *Alligator mississippiensis* and its implications for sexing fossil archosaurs. *Journal of Vertebrate Paleontology* 28: 422–431.

Bookstein FL. 1991. *Morphometric tools for landmark data: geometry and biology.*

Bookstein FL. 1996. Landmark methods for forms without landmarks: localizing group differences in outline shape. *Proceedings of the Workshop on Mathematical Methods in Biomedical Image Analysis. IEEE*, 279–289.

Bookstein FL. 1997. Landmark methods for forms without landmarks: morphometrics of group differences in outline shape. *Medical image analysis. IEEE*, 225–243.

Bookstein FL. 2014. *Measuring and Reasoning: Numerical Inference in the Sciences*. Cambridge University Press.

Borsuk-Bialynicka M. 1977. A New Camarasaurid Sauropod *Opisthocoelicaudia skarzynskii* gen. n., sp. n. from the Upper Cretaceous of Mongolia. *Paleontologia Polonica* 37: 5–64.

Botton-Divet L, Houssaye A, Herrel A, Fabre AC, Cornette R. 2015. Tools for quantitative form description; an evaluation of different software packages for semi-landmark analysis. *PeerJ* 3: e1417.

Bow ST. 1984. *Pattern recognition*. New York: Marcel Dekker.

Brown CM, Arbour JH, Jackson DA. 2012. Testing of the Effect of Missing Data Estimation and Distribution in Morphometric Multivariate Data Analyses. *Systematic Biology* 61: 941–954.

van Buuren S. 2007. Multiple imputation of discrete and continuous data by fully conditional specification. *Statistical Methods in Medical Research* 16: 219–242.

van Buuren S. 2008. Improved accuracy when screening for human growth disorders by likelihood ratios. *Statistics in Medicine*.

van Buuren S, Groothuis-Oudshoorn K. 2011. mice : Multivariate Imputation by Chained Equations in R. *Journal of Statistical Software* 45.

Calvo JO, González Riga BJ, Porfiri JD. 2007. A New Titanosaur Sauropod from the Late Cretaceous of Neuquén, Patagonia, Argentina. *Arquivos do Museo Nacional, Rio de Janeiro* 65: 485–504.

Cambra-Moo O, Barroso-barcenilla F, Berreteaga A, Carenas B, Elvira A, Escaso F, Domingo L, Peyrot D, Sanz JL, Segura M, Ortega F, Sopelana A. 2012. Preliminary taphonomic approach to "'Lo Hueco'" palaeontological site. *Geobios* 45: 157–166.

Campbell NA, Atchley WR. 1981. The Geometry of Canonical Variate Analysis. *Systematic Biology* 30: 268–280.

Canudo JI, Cuenca-Bescós G. 2004. Morphometric approach to Titanosauriformes (Sauropoda, Dinosauria) femora: Implications to the paleobiogeographic analysis. *Morphometrics*. Springer Berlin Heidelberg, 143–156.

Canudo JI, Oms O, Vila B, Galobart À, Fondevilla V, Puértolas E, Sellés AG, Cruzado-Caballero P, Dinarès-Turell J, Vicens E, Castanera D, Company J, Burrel L, Estrada R, Mprocessi J, Blanco A. 2016. The upper Maastrichtian dinosaur fossil record from the southern Pyrenees and its contribution to the topic of the Cretaceous-Palaeogene mass extinction event. *Cretaceous Research* 57: 540–551.

Canudo JI, Royo-Torres R, Cuenca-Bescós G. 2008. A new sauropod: *Tastavinsaurus sanzi* gen. et sp. nov. from the Early Cretaceous (Aptian) of Spain. *Journal of Vertebrate Paleontology* 28: 712–731.

Carballido JL, Pol D, Otero A, Cerda IA, Salgado JL, Garrido AC, Ramezani J, Cúneo NR, Krause JM. 2017. A new giant titanosaur sheds light on body mass evolution among sauropod

dinosaurs. *Proceedings of the Royal Society B: Biological Sciences* 284: 20171219.

Carballido JL, Sander PM. 2014. Postcranial axial skeleton of *Europasaurus holgeri* (Dinosauria, Sauropoda) from the Upper Jurassic of Germany: implications for sauropod ontogeny and phylogenetic relationships of basal Macronaria. *Journal of Systematic Palaeontology* 12: 335–387.

Carpenter K, McIntosh JS. 1994. Upper Jurassic sauropod babies from the Morrison Formation. In: Carpenter K, Hirsch KF, Horner JR, eds. *Dinosaur Eggs and Babies*. Cambridge: Cambridge University Press, 265–278.

Carpenter K, Tidwell V. 2005. Reassessment of the Early Cretaceous Sauropod *Astrodon johnstoni* Leidy 1865 (Titanosauriformes). In: Tidwell V, Carpenter K, eds. *Thunder-Lizards: The Sauropodomorph Dinosaurs*. Bloomington and Indianopolis: Indiana University Press, 38–77.

Carrano MT. 2005. The Evolution of Sauropod Locomotion. In: Curry Rogers KA, Wilson JA, eds. *The Sauropods: Evolution and Paleobiology*. University of California Press, 229–250.

Christian A. 2002. Neck posture and overall body design in sauropods. *Fossil Record* 5: 269–279.

Christian A. 2010. Some sauropods raised their necks-evidence for high browsing in *Euhelopus zdanskyi*. *Biology Letters* 6: 823–5.

Christian A, Dzemski G. 2007. Reconsrtuction of the cervical skeleton posture of *Brachiosaurus brancai* Janensch 1914 by an analysis of the intervertebral stress along the neck and a comparison with the results of different approaches. *Fossil Record – Mitteilungen aus dem Museum für Naturkunde* 10: 37–48.

Christian A, Dzemski G. 2011. Neck Posture in Sauropods. *Biology of the Sauropod Dinosaurs: Understanding the life of giants*.251–262.

Christian A, Dzemski G, Moeller J. 2009. Posture and Mobility of the Neck and Variation in Feeding Strategy among Sauropod Dinosaurs. *Journal of Vertebrate Paleontology* 29: 78A.

Christian A, Heinrich WD, Golder W. 1999. Posture and Mechanics of the Forelimbs of *Brachiosaurus brancai* (Dinosauria: Sauropoda). *Fossil Record* 2: 63–73.

Christian A, Peng G, Sekiya T, Ye Y, Wulf MG, Steuer T. 2013. Biomechanical reconstructions and selective advantages of neck poses and feeding strategies of Sauropods with the example of *Mamenchisaurus youngi*. *PloS ONE* 8.

Christiansen P. 2000. Feeding mechanisms of the sauropod dinosaurs *Brachiosaurus, Camarasaurus, Diplodocus*, and *Dicraeosaurus*. *Historical Biology* 14: 137–152.

Claude J. 2008. *Morphometrics with R*. New York, NY: Springer New York.

Clavel J, Merceron G, Escarguel G. 2014. Missing Data Estimation in Morphometrics: How Much is Too Much? *Systematic Biology* 63: 203–218.

Company J, Suberbiola XP, Ruiz-Omeñaca JI. 2009. Nuevos restos fósiles del dinosaurio *Lirainosaurus*. *Ameghiniana* 46: 391–405.

Csiki Z. 1999. New evidence of processored titanosaurids in the Late Cretaceous - *Magyarosaurus dacus* from the Hateg Basin (Romania). Oryctos 2: 93–99.

Csiki Z, Codrea VA, Jipa-Murzea C, Godefroit P. 2010. A partial titanosaur (Sauropoda, Dinosauria) skeleton from the Maastrichtian of Na'lat-Vad, Hateg Basin, Romania. *Neues Jahrbuch fur Geologie und Palaontologie - Abhandlungen* 258: 297–324.

Curry Rogers K. 2005. Titanosauria: A phylogenetic overview. In: Curry Rogers K, Wilson JA, eds.

The Sauropods: Evolution and Paleobiology. Berkeley: University of California Press, 50–103.

Curry Rogers K. 2009. The postcranial osteology of *Rapetosaurus krausei* (Sauropoda: Titanosauria) from the Late Cretaceous of Madagascar. *Journal of Vertebrate Paleontology* 29: 1046–1086.

Curry Rogers K, Whitney M, D'Emic MD, Bagley B. 2016. Precocity in a tiny titanosaur from the Cretaceous of Madagascar. *Science* 352: 450–453.

D'Emic MD. 2012. The early evolution of titanosauriform sauropod dinosaurs. *Zoological Journal of the Linnean Society* 166: 624–671.

Díez Díaz V, Garcia G, Pereda-Suberbiola X, Stein KHW, Jentgen-Ceschino B, Godefroit P, Valentin X. 2018. The titanosaurian dinosaur *Atsinganosaurus velauciensis* (Sauropoda) from the Upper Cretaceous of southern France: New material, phylogenetic affinities, and palaeobiogeographical implications. *Cretaceous Research* 91: 429–456.

Díez Díaz V, Mocho P, Ortega F, Sanz JL. 2014a. A case of extreme manus elongation in sauropods from the Late Cretaeous of 'Lo Hueco' (Spain). In: Delfino M, Carnevale G, Pavia M, eds. *XII Annual Meeting of the European Association of Vertebrate Palaeontologists*. Torino, Italia, 52.

Díez Díaz V, Mocho P, Páramo A, Escaso F, Marcos-Fernández F, Sanz JL, Ortega F. 2016. A new titanosaur (Dinosauria, Sauropoda) from the Upper Cretaceous of Lo Hueco (Cuenca, Spain). *Cretaceous Research* 68: 49–60.

Díez Díaz V, Ortega F, Sanz JL. 2014b. Titanosaurian teeth from the Upper Cretaceous of "Lo Hueco" (Cuenca, Spain). *Cretaceous Research* 51: 285–291.

Díez Díaz V, Pereda Suberbiola X, Company J. 2015. Updating titanosaurian diversity (Sauropoda) from the Late Cretaceous of Spain: The fossil site of Laño and Chera. *Spanish Journal of Palaeontology* 30: 293–306.

Díez Díaz V, Suberbiola XP, Sanz JL. 2013. Appendicular skeleton and dermal processour of the Late Cretaceous titanosaur *Lirainosaurus astibiae* (Dinosauria: Sauropoda) from Spain. *Palaeontologia Electronica* 16: 18 p.

Diogo R, Abdala V. 2010. *Muscles of Vertebrates* (R Diogo and V Abdala, Eds.). Enfield, New Hampshire: Taylor & Francis.

Dray S, Josse J. 2015. Principal component analysis with missing values: a comparative survey of methods. *Plant Ecology* 216: 657–667.

Dzemski G, Christian A. 2007. Flexibility along the neck of the ostrich (*Struthio camelus*) and consequences for the reconstruction of dinosaurs with extreme neck length. *Journal of Morphology* 268: 701–14.

Falkingham PL. 2013. Low cost 3D scanning using off-the-shelf video gaming peripherals. *Journal of Paleontological Techniques*: 1–9.

Filippi LS, García RA, Garrido AC. 2011. A New Titanosaur Sauropod Dinosaur from the Upper Cretaceous of North Patagonia, Argentina. *Acta Palaeontologica Polonica* 56: 505–520.

Fiorillo AR. 1998. Dental micro wear patterns of the sauropod dinosaurs *Camarasaurus* and *Diplodocus*: Evidence for resource partitioning in the late Jurassic of North America. *Historical Biology* 13: 1–16.

Foster JR. 2005. New juvenile sauropod material from Western Colorado and the record of juvenile Sauropods from the Upper Jurassic Morrison Formation. In: Tidwell V, Carpenter K, eds. Life of the Past. *Thunder-Lizards: The Sauropodomorph Dinosaurs*. Bloomington and Indianopolis: Indiana University Press, 141–153.

Fraas E. 1908. Ostafrikanische Dinosaurier. *Palaeontographica* 55: 105–144.

Gallina PA. 2011. Estudio Anatómico, Sistemático Y Paleobiológico De *Bonitasaura salgadoi* (Dinosauria, Sauropoda): Su Importancia En El Contexto De La Evolución De Los Titanosaurios Del Cretácico Superior De La Argentina. : 340.

Gallina PA, Apesteguía S. 2015. Postcranial anatomy of *Bonitasaura salgadoi* (Sauropoda, Titanosauria) from the Late Cretaceous of Patagonia. *Journal of Vertebrate Paleontology* 35: e924957.

Gallina PA, Otero A. 2015. Reassessment of *Laplatasaurus araukanicus* (Sauropoda: Titanosauria) from the Upper Cretaceous of patagonia, Argentina. *Ameghiniana* 52: 487–501.

Garcia G, Amico S, Fournier F, Thouand E, Valentin X. 2010. A new Titanosaur genus (Dinosauria, Sauropoda) from the Late Cretaceous of southern France and its paleobiogeographic implications. *Bulletin de la Société Géologique de France* 181: 269–277.

García RA, Salgado JL. 2013. The titanosaur sauropods from the late Campanian–early Maastrichtian Allen Formation of Salitral Moreno, Río Negro, Argentina. *Acta Palaeontologica Polonica* 58: 269–284.

García RA, Salgado L, Fernández MS, Cerda IA, Carabajal AP, Otero A, Coria RA, Fiorelli LE, Salgado JL, Fernández MS, Cerda IA, Carabajal AP, Otero A, Coria RA, Fiorelli LE. 2015. Paleobiology of Titanosaurs: Reproduction, Development, Histology, Pneumaticity, Locomotion and Neuroanatomy from the South American Fossil Record. *Ameghiniana* 52: 29–68.

Gauthier O, Landry PA, Lapointe FJ. 2003. Missing data in craniometrics: A simulation study. *Acta Theriologica* 48: 25–34.

Gilmore CW. 1925. A nearly complete articulated skeleton of *Camarasaurus*, a saurischian dinosaur from the Dinosaur National Monument. *Memoirs of the Carnegie Museum* 10: 347–384.

Gilmore CW. 1932. On a newly mounted skeleton of *Diplodocus* in the United States National Museum. *Proceedings of the United States National Museum* 81: 1–21.

Gilmore CW. 1936. The osteology of *Apatosaurus* with special reference to specimens in the Carnegie Museum. *Memoirs of the Carnegie Museum* 11: 175–300.

González Riga BJ. 2003. A New Titanosaur (Dinosauria, Sauropoda) from the Upper Cretaceous of Mendoza Province, Argentina. *Ameghiniana* 40: 155–172.

González Riga BJ, Lamanna MC, Otero A, Ortiz David LD, Kellner AWA, Ibiricu LM. 2019. An overview of the appendicular skeletal anatomy of South American titanosaurian sauropods, with definition of a newly recognized clade. *Anais da Academia Brasileira de Ciências* 91: e20180374.

González Riga BJ, Mannion PD, Poropat SF, Ortiz David LD, Coria JP. 2018. Osteology of the Late Cretaceous Argentinean sauropod dinosaur *Mendozasaurus neguyelap*: implications for basal titanosaur relationships. *Zoological Journal of the Linnean Society*: 1–46.

González Riga BJ. 2005. Nuevos restos fósiles de *Mendozasaurus neguyelap* (Sauropoda, Titanosauria) del Cretácico Tardío de Mendoza, Argentina. *Ameghiniana* 42: 535–548.

Gorscak E, O'Connor PM, Roberts EM, Stevens NJ. 2017. The second titanosaurian (Dinosauria: Sauropoda) from the middle Cretaceous Galula Formation, southwestern Tanzania, with remarks on African titanosaurian diversity. *Journal of Vertebrate Paleontology* 37: e1343250

Gorscak E, O'Connor PM, Stevens NJ, Roberts EM. 2014. The basal titanosaurian *Rukwatitan bisepultus* (Dinosauria, Sauropoda) from the middle Cretaceous Galula Formation, Rukwa Rift Basin, southwestern Tanzania. *Journal of Vertebrate Paleontology* 34: 1133–1154.

Gower JC. 1975. Generalized Procrustes Analysis. *Psychometrika* 40: 33–51.

Gunga HC, Kirsch K, Baartz F, Röcker L, Heinrich WD, Lisowski W, Wiedemann A, Albertz J. 1995. New data on the dimensions of *Brachiosaurus brancai* and their physiological implications. *Naturwissenschaften* 82: 189–192.

Gunga HC, Kirsch K, Rittweger J, Clarke JA, Albertz J, Wiedemann A, Wher A, Heinrich WD, Schultze HP. 2002. Dimensions of *Brachiosaurus brancai*, *Dicraeosaurus hansemanni* and *Diplodocus carnegi* and their physiological implications for gravitational physiology. *Adaptation Biology and Medicine* 3: 156–169.

Gunga HC, Kirsch K, Rittweger J, Röcker L, Clarke A, Albertz J, Wiedemann A, Mokry S, Suthau T, Wehr A, Heinrich WD, Schultze HP. 1999. Body size and body volume distribution in two sauropods from the Upper Jurassic of Tendaguru (Tanzania). *Fossil Record* 2: 91–102.

Gunz P. 2005. Statistical and geometric morphometric reconstruction of hominid crania. Reconstructing autralopithecine ontogeny. Unpublished thesis, University of Vienna.

Gunz P, Mitteroecker P. 2013. Semilandmarks: a method for quantifying curves and surfaces. *Hystrix, the Italian Journal of Mammalogy* 24: 103–109.

Gunz P, Mitteroecker P, Bookstein FL. 2005. Semilandmarks in three dimensions. In: Slice DE, ed. *Modern Morphometrics in Physical Anthropology*. Kluwer Academy Publ., 73–98.

Gunz P, Mitteroecker P, Neubauer S, Weber GW, Bookstein FL. 2009. Principles for the virtual reconstruction of hominin crania. *Journal of Human Evolution* 57: 48–62.

Hammer Ø, Harper DAT. 2008. *Paleontological Data Analysis*. Wiley-Blackwell Publishing.

Harris JD. 2007. The appendicular skeleton of *Suuwassea emilieae* (Sauropoda: Flagellicaudata) from the Upper Jurassic Morrison Formation of Montana (USA). *Geobios* 40: 501–522.

Hatcher JB. 1901. *Diplodocus* Marsh: *its osteology, taxonomy, and probate habits, with a restoration of the skeleton*. Pittsburgh: Published under authority of the Board of Trustees of the Carnegie Museum.

Hedrick BP, Dodson P. 2013. Lujiatun Psittacosaurids: Understanding Individual and Taphonomic Variation Using 3D Geometric Morphometrics. *PloS ONE* 8: e69265.

Hocknull SA, White MA, Tischler TR, Cook AG, Calleja ND, Sloan T, Elliott DA. 2009. New Mid-Cretaceous (latest Albian) dinosaurs from Winton, Queensland, Australia. *PloS ONE* 4: e6190.

Huene FF von. 1932. Die fossile Reptil-Ordnung Saurischia, ihre Entwicklung und Geschichte. *Monographien zur Geologie und Paläontologie* I: 564.

Hulke JW. 1869. Note on a large Saurian Humerus from the Kimmeridge Clay of the Dorset Coast. Quarterly *Journal of the Geological Society* 25: 386–389.

Hutchinson JR. 2012. On the inference of function from structure using biomechanical modelling and simulation of extinct organisms. *Biology Letters* 8: 115–118.

Hutchinson JR, Bates KT, Molnar JL, Allen V, Makovicky PJM. 2011. A computational analysis of limb and body dimensions in *Tyrannosaurus rex* with implications for locomotion, ontogeny, and growth. *PloS ONE* 6: e26037.

Ikejiri T. 2004. Anatomy of *Camarasaurus lentus* (Dinosauria: Sauropoda) from the Morrison Formation (Late Jurassic), Thermopolis, central Wyoming, with Determination and Interpretation of Ontogenetic, Sexual Dimorphic and Individual Variation in the Genus. Unpublished thesis, State University.

Ikejiri T, Tidwell V, Trexler D. 2005. New adult specimens of *Camarasaurus lentus* highlight ontogenetic variation within the species. In: Carpenter K, Tidwell V, eds. *Thunder-Lizards: The Sauropodomorph Dinosaurs*. Bloomington: Indiana University Press, 157–179.

Jakob W, Tarini M, Panozzo D, Sorkine-Hornung O. 2015. Instant Field-Aligned Meshes. *ACM Transactions on Graphics (Proceedings of SIGGRAPH Asia 2015)*. 1–15.

Janensch W. 1929a. Die Wirbelsäule der Gattung *Dicraeosaurus*. *Palaeontographica* II: 37–133.

Janensch W. 1929b. Material und Formengehalt der Sauropoden in der Ausbeute der Tendaguru-Expedition. *Palaeontographica* 1: 1–34.

Janensch W. 1961. Die Gliedmaszen und Gliedmaszengürtel der Sauropoden der Tendaguru-Schichten. *Palaeontographica* 3: 177–235.

Knoll F, Ridgely RC, Ortega F, Sanz JL, Witmer LM. 2013. Neurocranial Osteology and Neuroanatomy of a Late Cretaceous Titanosaurian Sauropod from Spain (*Ampelosaurus* sp.) *PloS ONE* 8:e54991.

Knoll F, Witmer LM, Ridgely RC, Ortega F, Sanz JL. 2015. A new titanosaurian braincase from the cretaceous 'Lo Hueco' locality in Spain sheds light on neuroanatomical evolution within titanosauria. *PloS ONE* 10: 1–24.

Lautenschlager S. 2017. From bone to pixel—fossil restoration and reconstruction with digital techniques. *Geology Today* 33: 155–159.

Le Loeuff J. 2005a. Osteology of *Ampelosaurus atacis* (Titanosauria) from Southern France. In: Tidwell V, Carpenter K, eds. *Thunder-Lizards: The Sauropodomorph Dinosaurs*. Bloomington: Indiana University Press, 115–137.

Le Loeuff J. 2005b. Romanian late cretaceous dinosaurs: Big dwarfs or small giants? *Historical Biology* 17: 15–17.

Lovelace DM, Hartman SA, Wahl WR. 2007. Morphology of a specimen of *Supersaurus* (Dinosauria, Sauropoda) from the Morrison formation of Wyoming, and a Re-evaluation of Diplodocid phylogeny. *Arquivos do Museo Nacional, Rio de Janeiro* 65: 527–544.

Lull RS. 1919. The sauropod dinosaur *Barosaurus* Marsh: redescription of the type specimens in the Peabody Museum, Yale University. *Memoirs of the Connecticut Academy of Arts and Sciences* 6: 1–42.

Mallison H. 2011. Digitizing Methods for Paleontology: Applications, Benefits and Limitations. In: Elewa A, ed. *Computational Paleontology*. Berling: Springer, 7–43.

Mallon JC, Anderson JS. 2013. Skull Ecomorphology of Megaherbivorous Dinosaurs from the Dinosaur Park Formation (Upper Campanian) of Alberta, Canada. *PloS ONE* 8: e67182.

Mannion PD, Allain R, Moine O. 2017. The earliest known titanosauriform sauropod dinosaur and the evolution of Brachiosauridae. *PeerJ* 5: e3217.

Mannion PD, Otero A. 2012. A reappraisal of the Late Cretaceous Argentinean sauropod dinosaur *Argyrosaurus superbus*, with a description of a new titanosaur genus. *Journal of Vertebrate Paleontology* 32: 614–638.

Mannion PD, Upchurch P, Barnes RN, Mateus O. 2013. Osteology of the Late Jurassic Portuguese sauropod dinosaur *Lusotitan atalaiensis* (Macronaria) and the evolutionary history of basal titanosauriforms. *Zoological Journal of the Linnean Society* 168: 98–206.

Marcos-Fernández F, Bartolomé S, López S, Martínez I, Navarro E, Onrubia M, Páramo A, Vidal D, Yagüe A, Ortega F. 2018. La conservación-restauración de la cintura pélvica de un

dinosaurio Titanosaurio del yacimiento de Lo Hueco (Fuentes, Cuenca). *XXXIV Jornadas de Paleontología y IV Congreso Ibérico de Paleontología*. Vila Real, 181–187.

Marcos-Fernández F, Fernández Fernández E, Fernández Martínez J, Martínez Fernández I, Plaza Beltrán M, Ortega F. 2019. La limpieza química controlada en la restauración paleontológica: el uso de geles. *Zubia*.

Marcos-Fernández F, Mocho P, Elvira A, Páramo A, Escaso F, Ortega F. 2014. The sauropod that stopped the train. *74th Annual Meeting of the Society of Vertebrate Paleontology*. Berlin, Germany, 177–178.

Martínez RD, Giménez O, Rodríguez J, Luna M, Lamanna MC. 2004. An articulated specimen of the basal titanosaurian (Dinosauria: Sauropoda) *Epachthosaurus sciuttoi* from the early Late Cretaceous Bajo Barreal Formation of Chubut Province, Argentina. *Journal of Vertebrate Paleontology* 24: 107–120.

McIntosh JS. 1990. Sauropoda. In: Weishampel DB, Dodson P, Osmólska H, eds. *The Dinosauria*. University of California Press, 345–401.

McIntosh JS. 2005. The Genus *Barosaurus* Marsh (Sauropoda, Diplodocoidea). In: Tidwel V, Carpenter K, eds. *Thunder-Lizards: The Sauropodomorph Dinosaurs*. Indiana University Press, 512.

McIntosh JS, Miller WE, Stadtman KL, Gillette DD. 1996. The Osteology of *Camarasaurus lewisi* (Jensen, 1988). *BYU Geology Studies* 41: 73–115.

Mitra K. 2011. *Handling Outliers and Missing Data in Statistical Data Models*.

Mocho P, Escaso F, Marcos-Fernández F, Páramo A, Vidal D, Ortega F. 2018a. The morphological variability on titanosaur caudal series from Lo Hueco: taxonomic diversity, intra-specific variability or both? *XVI Annual Meeting of European Association of Vertebrate Paleontologists*. 126.

Mocho P, Pérez-García A, Martín-Jiménez M, Ortega F, Martín Jiménez M, Ortega F. 2018. New remains from the Spanish Cenomanian shade light on the Gondwanan origin of European Early Cretaceous titanosaurs. *Cretaceous Research* 95: 164–190.

Molnar JL, Pierce SE, Hutchinson JR. 2012. Idealized landmark-based geometric reconstructions of poorly preserved fossil material: a case study of an early tetrapod vertebra. *Palaeontologia Electronica* 15: 1–18.

Mook CC. 1903. The Fore and Hindlimb of *Diplodocus*. *Bulletin American Museum of Natural History* 37: 815–820.

Mosimann JE. 1970. Size allometry: Size and shape variables with characterizations of the lognormal and generalized gamma distributions. *Journal of the American Statistical Association* 65: 930–945.

Motani R, Amenta N, Wiley DF. 2005. Possibilities and Limitations of Three Dimensional Retrodeformation of a Trilobite and Plesiosaur Vertebrae. *PaleoBios* 25.

Nopsca BF. 1915. Die dinosaurier der Siebenbürgischen landesteile Ungarns. *Ungarischen Geologischen Reichsanstalt* 23: 1–24.

Oba S, Sato M aki, Takemasa I, Monden M, Matsubara K ichi, Ishii S. 2003. A Bayesian missing value estimation method for gene expression profile data. *Bioinformatics* (Oxford, England) 19: 2088–2096.

Osborn HF. 1898. Additional characters of the Great Herbivorous Dinosaur *Camarasaurus*. *Bulletin American Museum of Natural History* 10: 219–234.

Osborn HF, Mook CC. 1921. *Camarasaurus*, *Amphicoelias*, and other sauropods of Cope. *Memoirs of the American Museum of Natural History* 3: 247–387.

Otero A. 2010. The appendicular skeleton of *Neuquensaurus*, a Late Cretaceous saltasaurine sauropod from Patagonia, Argentina. *Acta Palaeontologica Polonica* 55: 399–426.

Otero A. 2018. Forelimb musculature and osteological correlates in Sauropodomorpha (Dinosauria, Saurischia). *PloS ONE* 13: e0198988.

Otero A, Vizcaíno SF. 2008. Musculatura y función del miembro posterior de *Neuquensaurus australis* (Sauropoda: Titanosauria). *Ameghiniana* 45: 333–348.

Páramo A. 2018. Ténicas de Restauración Virtual de Fósiles Basadas en Landmarks: Reconstruyendo los Titanosaurios de Lo Hueco. *XVI EJIP. Zarautz*, .

Páramo A, Mocho P, Marcos-Fernández F, Ortega F, Sanz JL. 2017. 3D Geometric Morphometrics on the Hind Limb of the Titanosaurs from Lo Hueco: Dwarf taxa or Small Individuals? *15th Annual Meeting of the European Association of Vertebrate Paleontologists*.

Páramo A, Ortega F, Mocho P, Sanz JL. 2016. Femoral variability in two titanosaur taxa from Lo Hueco (Cuenca, Spain): Insights for iberoprocessorican titanosaur diversity assessment. In: Torcida F, Jose IC, Huerta P, Pereda-Suberbiola X, eds. *VII International Symposium about Dinosaurs Palaeontology and their Environment.* Salas de los Infantes, Burgos: Colectivo Arqueológico y Paleontológico de Salas, 107–108.

Páramo A, Ortega F, Sanz JL. 2015. Two types of appendicular bones of titanosaurs (Dinosauria, Sauropoda) from Lo Hueco (Fuentes, Cuenca). In: Dyke GJ, Marshall J, Naish D, Young MT, Wujeck JL, Martin-Silverstone L, Pond S, Roberts A, Hansford J, Taylor C, Blackwell G, Riddington K, eds. *63rd Symposium for Vertebrate Paleontology and Comparative anatomy & 24th Symposium of Palaeontological Preparation and Conservation with the Geological Curator's Group*. 100.

Paul GS. 1988. The Brachiosaur Giants of the Morrison and Tendaguru with a description of a new subgenus, *Giraffatitan*, and a comparison of the world's largest dinosaurs. *Hunteria* 2: 1–14.

Paul GS. 2017. Restoring Maximum Vertical Browsing Reach in Sauropod Dinosaurs. *The Anatomical Record* 300: 1802–1825.

Perez SI, Bernal V, Gonzalez PN. 2006. Differences between sliding semi-landmark methods in geometric morphometrics, with an application to human craniofacial and dental variation. *Journal of Anatomy* 208: 769–784.

Poropat SF, Upchurch P, Mannion PD, Hocknull SA, Kear BP, Sloan T, Sinapius GHK, Elliott DA. 2015. Revision of the sauropod dinosaur *Diamantinasaurus matildae* Hocknull *et al.* 2009 from the mid-Cretaceous of Australia: Implications for Gondwanan titanosauriform dispersal. *Gondwana Research* 27: 995–1033.

Powell JE. 1990. *Epachthosaurus sciuttoi* (gen. et sp. nov.) un dinosaurio saurópodo del Cretácico de Patagonia (Provincia de Chubut, Argentina). *Actas del V Congreso Argentino de Paleontologia y Bioestratigrafia.* Tucumán, 123–128.

Powell JE. 1992. Osteología de *Saltasaurus loricatus* (Sauropoda-Titanosauridae) del Cretácico Superior del noroeste argentino. In: Sanz JL, Buscalioni AD, eds. *Los Dinosaurios y Su Entorno Biotico Actas del Segundo Curso de Paleontologia in Cuenca.* Cuenca, España: Instituto 'Juan Valdes', 166–229.

Powell JE. 2003. Revision of South American titanosaurid dinosaurs: Palaeobiological,

palaeobiogeographical and phylogenetic aspects. *Records of the Queen Victoria Museum* 111: 1–179.

Preuschoft H, Klein N. 2013. Torsion and Bending in the Neck and Tail of Sauropod Dinosaurs and the Function of Cervical Ribs: Insights from Functional Morphology and Biomechanics. *PloS ONE* 8: e78574.

Remes K. 2006. Revision of the Tendaguru Sauropod dinosaur *Tornieria africana* (Fraas) and its relevance for sauropod paleobiogeography. *Journal of Vertebrate Paleontology* 26: 651–669.

Remes K. 2007a. Evolution of the Pectoral girdle and Forelimb in Sauropodomorpha (Dinosauria, Saurischia): Osteology, Myology and Fuction. Unpublished thesis, Ludwig-Maximilians-Universität München.

Remes K. 2007b. A second Gondwanan diplodocid dinosaur from the Upper Jurassic Tendaguru Beds of Tanzania, East Africa. Palaeontology 50: 653–667.

Remes K. 2009. Taxonomy of Late Jurassic diplodocid sauropods from Tendaguru (Tanzania). Fossil Record 12: 23–46.

Riggs ES. 1903. *Brachiosaurus altithorax*, the largest known dinosaur. *American Journal of Science* s4-15: 299–306.

Rokach L, Maimon O. 2007. Clustering methods. In: Rokach L, Maimon O, eds. *Series in Machine Perception and Artificial Intelligence. Data Mining with Decision Trees*. World Scientific. 321–352.

Romer AS. 1956. *Osteology of the Reptiles*. Chicago: The University of Chicago Press.

Royo-Torres R. 2009. *El saurópodo de Peñarroya de Tastavins*. Teruel: Instituo de Estudios Turolenses y Fundación Conjunto Paleontológico de Teruel-Dinópolis.

Royo-Torres R, Alcalá L, Cobos A. 2012. A new specimen of the Cretaceous sauropod *Tastavinsaurus sanzi* from El Castellar (Teruel, Spain), and a phylogenetic analysis of the Laurasiformes. *Cretaceous Research* 34: 61–83.

Rueden CT, Schindelin J, Hiner MC, DeZonia BE, Walter AE, Arena ET, Eliceiri KW. 2017. ImageJ2: ImageJ for the next generation of scientific image data. *BMC Bioinformatics* 18: 529.

Ruscillo D. 2000. A Morphometric Exploration of Sexual Dimorphism in Mammalian Skeletons for Applicability in Archaeology. *Institute of Archaeology* 2: 704.

Sainani KL. 2014. Introduction to principal components analysis. *PM & R : the journal of injury, function, and rehabilitation* 6: 275–8.

Salgado JL, Apesteguía S, Heredia S. 2005. A New Specimen of *Neuquensaurus australis*, a Late Cretaceous Saltasaurine titanosaur from North Patagonia. *Journal of Vertebrate Paleontology* 25: 623–634.

Salgado JL, Azpilicueta C. 2000. Un nuevo saltasaurino (Sauropoda, Titanosauridae) de la provincia de Río Negro (Formación Allen, Cretácico Superior), Patagonia, Argentina. *Ameghiniana* 37: 259–264.

Salgado JL, Coria RA. 1993. El género *Aelosaurus* (Sauropoda, Titanosauridae) en la Formación Allen (Campaniano-Maastrichtiano) de la Provincia de Río Negro, Argentina. *Ameghiniana* 30: 119–128.

Salgado JL, Coria RA, Calvo JO. 1997a. Evolution of the titanosaurid sauropods I: Phylogenetic analysis based on the postcranial evidence. *Ameghiniana* 34: 3–32.

Salgado JL, Coria RA, Calvo JO. 1997b. Presencia del género *Aeolosaurus* (Sauropoda, Titanosauridae)

en la Formación Los Alamitos, Cretácico Superior de la Provincia de Río Negro, Argentina. *Geociencias* 2: 44–49.

Salgado JL, Gallina PA, Paulina Carabajal A. 2015. Redescription of *Bonatitan reigi* (Sauropoda: Titanosauria), from the Campanian–Maastrichtian of the Río Negro Province (Argentina). *Historical Biology* 27: 525–548.

Salgado JL, De Souza Carvalho I. 2008. *Uberabatitan ribeiroi*, a new titanosaur from the Marília Formation (Bauru Group, Upper Cretaceous), Minas Gerais, Brazil. *Palaeontology* 51: 881–901.

Sanz JL, Powell JE, Le Loeuff J, Martínez RN, Pereda Suberbiola X. 1999. Sauropod remains from the Upper Cretaceous of Laño (north central Spain). Titanosaur phylogenetic relationships. *Estudios del Museo de Ciencias Naturales de Alava* 14: 235–255.

Schæfer K, Mitteroecker P, Gunz P, Bernhard M, Bookstein FL. 2004. Craniofacial sexual dimorphism patterns and allometry among extant hominids. *Annals of anatomy = Anatomischer Anzeiger : official organ of the Anatomische Gesellschaft* 186: 471–8.

Schafer JL. 1997. *Analysis of Incomplete Multivariate Data*.

Schafer JL. 1999. Multiple imputation: A primer. *Statistical Methods in Medical Research* 8: 3–15.

Schafer JL. 2003. *Multiple imputation in multivariate problems when the imputation and analysis models differ*. Statistica Neerlandica.

Schafer JL, Olsen MK. 1998. Multiple imputation for multivariate missing-data problems: A data analyst's perspective. Multivariate Behavioral Research. 33: 545-571

Schlager S. 2013. Soft-tissue reconstruction of the human nose: Population differences and sexual dimorphism. Unpublished thesis, Albert-Ludwigs Universität Freiburg.

Schlager S. 2016. mesheR: Meshing Operations on Triangular Meshes. R package version 0.4.160301.

Schlager S. 2017. Morpho and Rvcg – Shape Analysis in R. In: Zheng G, Li S, Szekely G, eds. *Statistical Shape and Deformation Analysis*. Elsevier, 217–256.

Schwarz D, Böhm N. 2012. A morphometric approach to the specific separation of the humeri and femora of *Dicraeosaurus* from the Late Jurassic of Tendaguru, Tanzania. *Acta Palaeontologica Polonica* 59: 81–98.

Schwarz D, Frey E, Meyer CA. 2007. Novel reconstruction of the orientation of the pectoral girdle in sauropods. *The Anatomical Record* 290: 32–47.

Selim SZ, Ismail MA. 1984. K-Means-Type Algorithms: A Generalized Convergence Theorem and Characterization of Local Optimality. *IEEE Transactions on Pattern Analysis and Machine Intelligence* 6: 81–87.

Sievwright H, MacLeod N. 2012. Eigensurface analysis, ecology, and modelling of morphological adaptation in the falconiform humerus (Falconiformes: Aves). *Zoological Journal of the Linnean Society* 165: 390–419.

Souter T, Cornette R, Pedraza J, Hutchinson JR, Baylac M. 2010. Two applications of 3D semi-landmark morphometrics implying different template designs: the theropod pelvis and the shrew skull. *Comptes Rendus Palevol* 9: 411–422.

Stacklies W, Redestig H, Scholz M, Walther D, Selbig J. 2007. pcaMethods a bioconductor package providing PCA methods for incomplete data. *Bioinformatics* 23: 1164–1167.

Stein KHW, Csiki Z, Rogers KC, Weishampel DB, Redelstorff R, Carballido JL, Sander PM, Curry Rogers K, Weishampel DB. 2010. Small body size and extreme cortical bone remodeling

indicate phyletic dwarfism in *Magyarosaurus dacus* (Sauropoda: Titanosauria). *Proceedings of the National Academy of Sciences of the United States of America* 107: 9258–9263.

Stevens KA. 2013. The Articulation of Sauropod Necks: Methodology and Mythology. *PloS ONE* 8: e78572.

Stevens KA, Parrish JM. 2005a. Neck posture, dentition and feeding strategies in Jurassic sauropod dinosaurs. In: Tidwell V, Carpenter K, eds. *Thunder-Lizards: The Sauropodomorph Dinosaurs*. Bloomington: Indiana University Press, 212–232.

Stevens KA, Parrish JM. 2005b. Digital Reconstructions of Sauropod Dinosaurs and Implications for Feeding. In: Currii Rogers, K. and Wilson, J.A. (eds) *The Sauropods: Evolution and Paleobiology.* University of California Press, 178–200.

Stubbs TL, Benton MJ. 2016. Ecomorphological diversifications of Mesozoic marine reptiles: the roles of ecological opportunity and extinction. *Paleobiology* 42: 547–573.

Taylor MP. 2009a. Aspects of the history , anatomy, taxonomy and palaeobiology of sauropod dinosaurs.

Taylor MP. 2009b. A Re-evaluation of *Brachiosaurus altitorax* Riggs 1903 (Dinosauria, Sauropoda), and its generic separation from *Giraffatitan brancai* (Janesch 1914). *Journal of Vertebrate Paleontology* 29: 787–806.

Taylor MP, Wedel MJ, Naish D. 2009. Head and Neck Posture in Sauropod Dinosaurs Inferred from Extant Animals. *Acta Palaeontologica Polonica* 54: 213–220.

Tschopp E, Dzemski G. 2013. Retrodeformation as a test for the validity of phylogenetic characters: an example from diplodocid sauropod vertebrae. *Paleontologia Electronica* 16: 1–23.

Tschopp E, Mateus O. 2012. A sternal plate of a large-sized sauropod dinosaur from the Late Jurassic of Portugal. In: Royo-Torres R, Gascó F, Alcalá L, eds. *10th Annual Meeting of the European Association of Vertebrate Palaeontologists. ¡Fundamental!.* Teruel, 1–290.

Tschopp E, Mateus O. 2017. Osteology of *Galeamopus pabsti* sp. nov. (Sauropoda: Diplodocidae), with implications for neurocentral closure timing, and the cervico-dorsal transition in diplodocids. *PeerJ* 5: e3179.

Tschopp E, Mateus O, Benson RBJ. 2015. A specimen-level phylogenetic analysis and taxonomic revision of Diplodocidae (Dinosauria, Sauropoda). *PeerJ* 3: e857.

Tütken T. 2011. The diet of sauropod dinosaurs – Implications from carbon isotope analysis of teeth, bones, and plants. In: Klein N, Remes K, Gee CT, Sander PM, eds. *Biology of the Sauropod Dinosaurs: Understanding the life of giants*.57–82.

Ullmann PV., Bonnan MF, Lacovara KJ. 2017. Characterizing the Evolution of Wide-Gauge Features in Stylopodial Limb Elements of Titanosauriform Sauropods via Geometric Morphometrics. *The Anatomical Record* 300: 1618–1635.

Ullmann P V., Lacovara KJ. 2016. Appendicular osteology of *Dreadnoughtus schrani*, a giant titanosaurian (Sauropoda, Titanosauria) from the Upper Cretaceous of Patagonia, Argentina. *Journal of Vertebrate Paleontology* 36.

Upchurch P. 1998. The phylogenetic relationships of sauropod dinosaurs. *Zoological Journal of the Linnean Society* 124: 43–103.

Upchurch P, Barrett PM, Dodson P. 2004. Sauropoda. In: Weishampel DB, Dodson P, Osmólska H, eds. *The Dinosauria*. Berkeley: University of California Press, 259–322.

Upchurch P, Mannion PD, Taylor MP. 2015. The Anatomy and Phylogenetic Relationships of

"*Pelorosaurus*" *becklesii* (Neosauropoda, Macronaria) from the Early Cretaceous of England. *PloS ONE* 10: e0125819.

Vidal D, Sanz JL, Mocho P, Páramo A, Escaso F, Marcos-Fernández F, Ortega F. 2017. The titanosaur tails from Lo Hueco (Cuenca, Spain): Four different ways to shake? In: Farke AA, Mackenzie SA, Miller Camp J, eds. *77th Annual Meeting of the Society of Vertebrate Paleontology*. Calgary, 208.

Vila B, Galobart À, Canudo JI, Le Loeuff J, Dinarès-Turell J, Riera V, Oms O, Tortosa T, Gaete R. 2012. The diversity of sauropod dinosaurs and their first taxonomic succession from the latest Cretaceous of southwestern Europe: Clues to demise and extinction. *Palaeogeography, Palaeoclimatology, Palaeoecology* 350–352: 19–38.

Whitlock JA. 2011. Inferences of Diplodocoid (Sauropoda: Dinosauria) Feeding Behavior from Snout Shape and Microwear Analyses. *PloS ONE* 6: e18304.

Wiley DF, Amenta N, Alcantara DA, Ghosh D, Kil YJ, Delson E, Harcourt-Smith W, Rohlf FJ, John K St., Hamann B, St John K, Hamann B, John K St., Hamann B. 2005. Evolutionary Morphing. *Proceedings of IEEE Visualization 2005*. Minneapolis, 1–8.

Wilhite RD. 2003. Biomechanical Reconstruction of the Appendicular Skeleton in Three North American Jurassic Sauropods. Unpublished thesis, Louisiana State University.

Wilhite RD. 2005. Variation in the Appendicular Skeleton of North American Sauropod Dinosaurs: Taxonomic Implications. In: Tidwell V, Carpenter K, eds. *Thunder-Lizards: The Sauropodomorph Dinosaurs*. Indiana University Press, 268–301.

Wilson JA. 2002. Sauropod dinosaur phylogeny: critique and cladistic analysis. *Zoological Journal of the Linnean Society* 136: 215–275.

Wilson JA, Barrett PM, Carrano MT. 2011. An associated partial skeleton of *Jainosaurus* cf. *septentrionalis* (Dinosauria: Sauropoda) from the Late Cretaceous of Chhota Simla, Central India. Palaeontology 54: 981–998.

Wilson JA, Carrano MT. 1999. Titanosaurs and the Origin of 'wide-gauge' trackways: A Biomechanical and Systematic Perspective on Sauropod Locomotion. *Paleobiology* 25: 252–267.

Wilson JA, Sereno PC. 1998. Early Evolution and High-level Phylogeny of Sauropod Dinosaurs. *Journal of Vertebrate Paleontology* 18: 1–68.

Wilson JA, Upchurch P. 2003. A revision of *Titanosaurus* Lydekker (Dinosauria - Sauropoda), the first dinosaur genus with a 'Gondwanan' distribution. *Journal of Systematic Palaeontology* 1: 125–160.

Wilson JA, Upchurch P. 2009. Redescription and reassessment of the phylogenetic affinities of *Euhelopus zdanskyi* (Dinosauria: Sauropoda) from the Early Cretaceous of China. *Journal of Systematic Palaeontology* 7: 199–239.

Zelditch ML, Swiderski DL, Sheets HD. 2012. *Geometric Morphometrics for Biologists*. Elsevier.

CHAPTER VI:

Ontogenetic Sequences on the Appendicular Skeleton of the titanosaur of Lo Hueco (Cuenca, Spain)

VI. ABSTRACT

The knowledge of sauropod postnatal ontogeny has greatly expanded in recent years. On the other hand, the majority of this knowledge is based on paleohistological sampling and estimation of life history growth models. The study of morphological feature acquisition lacks in comparison with a noticeable increase in sauropod ontogenetic studies. Understanding trends of character changes during sauropod ontogeny is important for developing a comprehensive growth model for the titanosaur appendicular skeleton. The current growth hypothesis for Titanosauria suggests similarities between the long bone morphology of juveniles and adult individuals. We found a great intraspecific variability between titanosaur appendicular elements in several of the Late Cretaceous of South of France, Northeast and Central Spain fossil sites. This intraspecific variability is expressed in both morphological features and size differences. An abundant sample of titanosaur appendicular elements from Lo Hueco presents high morphological variation that can help us to understand this intraspecific variability. The finding of many appendicular elements at potentially different ontogenetic stages allow us to test several previous hypotheses. The possible presence of juvenile individuals is useful for testing feature acquisition during titanosaur postnatal ontogeny in the appendicular skeleton of two possible different titanosaur taxa, *Lohuecotitan pandafilandi* + Morphotype I and a second undescribed titanosaur form from Lo Hueco, which we refer as Morphotype II. In this study, we describe for the first time titanosaurian ontogenetic sequences in the Ibero-Armorican domain. This will help us to understand the acquisition of some morphological features along titanosaurian ontogeny, as well as improving our morphological character coding.

Herein, the detailed analysis of the titanosaurian long bone morphology including the observation of main muscular attachments allow defining a preliminary set of morphological ontogenetic characters. This set of ontogenetic characters was analysed with two published methods employed on the study of ontogenetic development in another taxa. The obtained ontogenetic sequences allow to assess the ontogenetical stages of the studied appendicular bones and the different paths of feature acquisition during sauropod growth. The polymorphism in the analysed ontogenetic sequences was also tested in the titanosaurian sauropods of Lo Hueco. Several of the osteological characters used in cladistic data matrices were also analysed in this study and present morphological variation relatable to ontogenetic development. Individuals of the same taxa in different ontogenetic stages may result in several different scorings. The detailed staging of these feature changes can help on the taxonomical assessment of appendicular elements and character scoring of appendicular skeleton for titanosaur phylogenetics.

V.1 INTRODUCTION

In recent years our knowledge of the ontogenetical changes based on histological studies of the sauropod long bones have greatly expanded (Sander *et al.*, 2011b; Sander, 2013). The understanding of bone growth rate and mass acquisition is now widespread among a sample of titanosaurian and non-titanosaurian sauropods (Cerda & Powell, 2009; Klein, Sander, & Suteethorn, 2009; González Riga, Previtera, & Pirrone, 2009; Stein *et al.*, 2010; Gallina, 2011; Sander *et al.*, 2011b; Company, 2011; Cerda & Chinsamy, 2012; Klein *et al.*, 2012b; García *et al.*, 2015; Curry Rogers *et al.*, 2016; Cerda *et al.*, 2017). The evolution of the development at histological level have improved significantly in the past decade, however the changes on the morphological shape in the appendicular skeleton during the postnatal ontogeny is still unknown.

Studies centered on sauropod ontogeny are relatively scarce. Varricchio (1997) proposed allometrical growth for sauropod neck. Some studies have been centered in the taxonomical implications of the ontogenetical changes, which are mainly focused in the variability present in the vertebral lamination of the axial skeleton (Carpenter & McIntosh, 1994; Martin, 1994a; Lehman & Coulson, 2002; Ikejiri *et al.*, 2005a; Ikejiri, Tidwell, & Trexler, 2005b; McIntosh, 2005; Schwarz *et al.*, 2007a; Allain & Aquesbi, 2008; Woodruff & Fowler, 2012; Carballido *et al.*, 2012; Carballido & Sander, 2014; Woodruff, 2015; Melstrom *et al.*, 2016; Tschopp & Mateus, 2017; Hanik, Lamanna, & Whitlock, 2017). On the other hand, limb morphology variation during ontogeny suggests for the presence of low disparity between juvenile and adult individuals and possible patterns of isometric growth (Carpenter & McIntosh, 1994; Martin, 1994a; Wilhite, 1999; Curry Rogers & Forster, 2001; Tidwell & Wilhite, 2005; Wilhite, 2005; Curry Rogers *et al.*, 2016).

In the case of the Ibero-Armorican titanosaurs, the preserved appendicular elements show significant morphological and size differences (Le Loeuff, 2005; Company, Suberbiola, & Ruiz-Omeñaca, 2009; Vila *et al.*, 2012; Vila, Sellés, & Brusatte, 2016; Canudo *et al.*, 2016). some of this morphological variability is attributed to distinct ontogenetic stages with the identification of juvenile, subadult and adult individuals (e.g. Le Loeuff, 2005; Díez Díaz, Pereda Suberbiola, & Company, 2015; Páramo *et al.*, 2017). In addition, several titanosaur nests have been discovered in the Upper Cretaceous of Ibero-Armorican domain (e.g. Sanz *et al.*, 1992; López-Martínez *et al.*, 2001; Vila, Jackson, & Galobart, 2010; Perez-Garcia, Gasco, & Ortega, 2017) and no embryo or early juvenile has been discovered yet.. Some studies have described the life-history of the Ibero-Armorican titanosaurs (e.g. Klein *et al.*, 2012b; Díez Díaz *et al.*, 2018) but a detailed analysis on the morphological variation during the ontogeny is so far unpublished.

More recently, the Campano-Maastrichtian konzentrat-lagerstätten of Lo Hueco (Cuenca, Spain) provided several partial articulated titanosaur specimens in addition to many isolated appendicular specimens (Ortega *et al.*, 2015). Within this large sample of appendicular elements, many of these bones exhibit both morphological and size variation (see Fig.VI.1). The analyses of the morphological interspecific and intraspecific shape variability conducted in the titanosaurian remains of Lo Huecto (see Chapter IV and V) suggest that most of the appendicular elements from the studied sample can be attributed to *Lohuecotitan pandafilandi* + Morphotype I, and tentatively, to a second exclusive titanosaur taxon. In addition, previous studies rejected the possibility of the smallest appendicular specimens of Lo Hueco pertain to a third, small to medium sized titanosaurian morph similar to other small to medium sized European Late Cretaceous titanosaurian taxa such as *Lirainosaurus astibiae* and *Magyarosaurus dacus*. (Chapter IV, Chapter

V) Most of the small specimens have been attributed to possible presence of juvenile titanosaur specimens in this fossil site (Díez Díaz & Ortega, 2013; Páramo *et al.*, 2017; see also Chapter V).

The large sample of titanosaurian appendicular bones of the konzentrat-lagerstätten of Lo Hueco represents an opportunity to describe ontogenetical series, only known for a few sauropod taxa (e.g. Martin, 1994a; Lehman & Coulson, 2002; Ikejiri *et al.*, 2005b; Klein *et al.*, 2009; Suteethorn *et al.*, 2010; Klein *et al.*, 2012b; Curry Rogers *et al.*, 2016). Two analytical methods have been used to estimate the relative maturity of a specimen based on the combination of morphological features that change between juvenile to adult individuals of the same taxa (Brochu, 1996; Colbert & Rowe, 2008; Griffin & Nesbitt, 2016b). Herein we propose the employment of analytics in order to identify ontogenetic sequences and assess morphological feature variation along the ontogeny in each titanosaur morph present in Lo Hueco. These sequences also help to determine the degree of polymorphism in osteological feature acquisition in the appendicular skeleton of Titanosauria during the postnatal development. Assessing the patterns of variation in the appendicular skeleton is important given that appendicular characters, while not as informative as axial skeleton, are usually included in data matrices employed in phylogenetic analyses and their proportion of the total characters is increasing (e.g. Wilson & Sereno, 1998; Wilson, 2002; Upchurch, Barrett, & Dodson, 2004; Curry Rogers, 2005). The osteological characters of the appendicular skeleton represent approximately from 10 to 15 % of the information of the data matrices used in the recent studies of titanosaur cladistics analyses (Carballido *et al.*, 2017; González Riga *et al.*, 2018; Sallam *et al.*, 2018; Díez Díaz *et al.*, 2018; see Fig. VI.2 and VI.3). Therefore, for the first time, in the present study we can quantify and test the impact of morphological changes during ontogeny in the scoring in character data matrices usually employed in phylogenetic analysis of Titanosauria.

Anatomical abbreviations:

Humerus:

aep – anterior entepycondyle/entepycondylar process; af – anconeal fossa; alp – antero-lateral process; amp – antero-medial process; dpc – deltopectoral crest; dpcar – deltopectoral accessory ridge; hh – humeral head; pat – posterior accessory trochanter rac – radial condyle; ulc – ulnar condyle.

Ulna:

adp – anterior distal process; alp – antero-lateral process; amdf – anterior middle distal fossa (articulation with the radius); amp – antero-medial process; olc – olecranon; op – olecranon process; rds – radial distal scar; raf – radial fossa (proximal radial articulation).

Radius:

antf – anterior fossa; mp – medial process; pldc – posterolateral distal condyle; pmdc – posteromedial distal condyle; rmi – ridge for muscle insertion (mm. biceps + brachialis).

Femur:

4th – fourth trochanter; at – accessory trochanter; epi – lateral epicondyle; gt – greater trochanter; if – intercondylar fossa; lb – lateral bulge; lic – linea intermuscularis cranialis; fc – fibular condyle; fh – femoral head; tc – tibial condyle; ts – trochanteric shelf.

Tibia:

aap – anterior ascending process of distal condyles; cc – cnemial crest; pc – posterior condyle.

Fibula:

ap – anterior process; alp – anterolateral crest (proximal); lt – lateral trochanter;

ts – tibial articulation scar.

Common abbreviations:

at – accessory trochanter; ri – ridge; s – sulcus; tr - trochanter

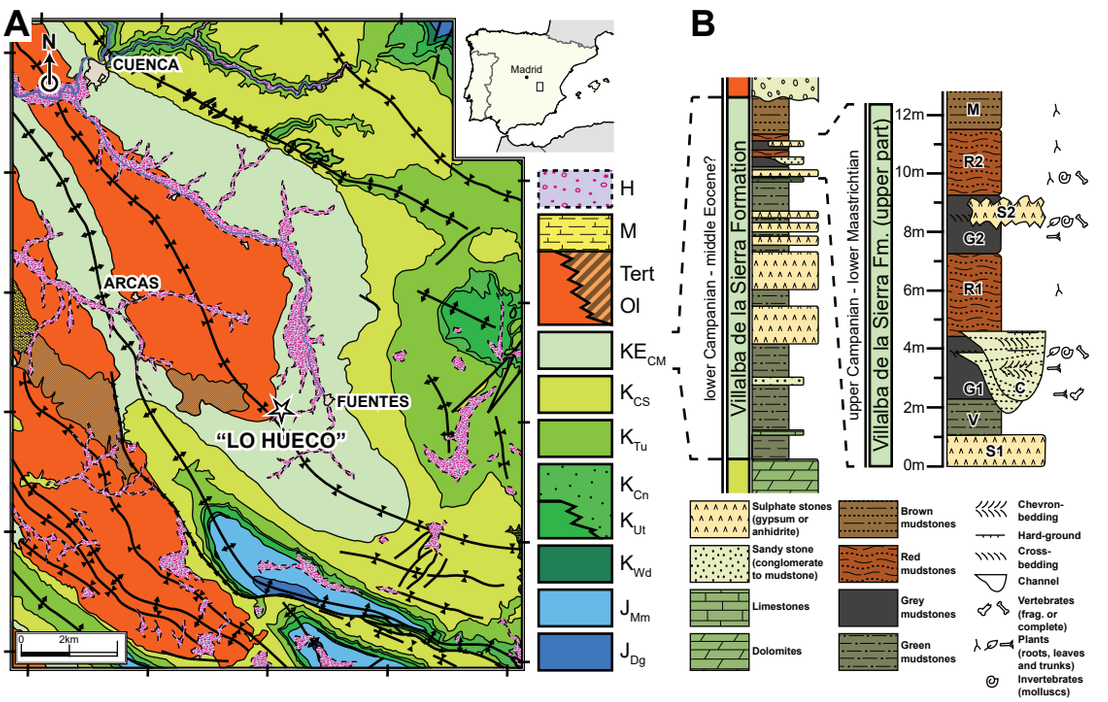

Fig.VI.1. Lo Hueco fossil site location and stratigraphy. (A) Geological map of Cuenca (Spain). (B) General stratigraphic column of the Villalba de la Sierra Formation and the Lo Hueco fossil site. (C) Photography of the Lo Hueco site during the 2007 campaign. Labels indicates the levels of the stratigraphic column.

Institutional abbreviations:

AMNH – American Museum of Natural History, New York, USA; BYU – Brigham Young University, Museum of Paleontology, Provo, USA; CM – Carnegie Museum of Natural History, Pittsburg, USA; FMNH – Field Museum of Natural History, Chicago, USA; IANIGLA – Instituto Argentino de Nivología, Glaciología y Ciencias Ambientales , Mendoza, Argentina; NHMUK – Natural History Museum, London, United Kingdom; MACN – Museo Argentino de Ciencias Naturales "Bernardino Rivadavia", Buenos Aires, Argentina; MCNA – Museo de las Ciencias Naturales de Álava/Arabako Natur Zientzien Museoa, Vitoria-Gasteitz, Spain; MLP – Museo de La Plata, La Plata, Buenos Aires, Argentina; MGUV – Museo de Geolgía de la Universidad de Valencia, Burjasot, Spain; MLP – Museo de La Plata, La Plata, Buenos Aires, Argentina; MPCA – Museo Provincial Carlos Ameghino, Cipoletti, Río Negro, Argentina; PVL – Instituto Miguel Lillo, Tucumán, Argentina; UW – University of Wyoming Geological Museum, Laramie, USA; YPM – Yale Peabody Museum, Yale, USA.

VI.1.1. CRITERIA FOR ONTOGENETIC CHARACTER DEFINITION

The large sample of titanosaurian appendicular elements from Lo Hueco represents two clusters with a high disparity in size (see Chapter IV.1 and IV.2). The identification of possible ontogenetical sequences can help to attribute the identified morphological feature changes to transformations during the postnatal growth. The morphological variation observed for each morphotype of Lo Hueco might be explained by the early acquisition of some morphological features during the postnatal growth. This was preliminary suggested by the study of several small specimens (Páramo *et al.*, 2014).

Understanding the morphological changes in the appendicular skeleton during the ontogeny will be important for the taxonomical assessment of other sauropod morphs from the Upper Cretaceous Ibero-Armorican domain. This domain is representative by several bonebeds which have yielded many titanosaur sauropod remains (see Vila *et al.*, 2016) including juvenile individuals. This sample is an opportunity to assess these ontogenetic changes in the skeleton of titanosaurs. However, only few studies mainly focused on the ontogeny of this titanosaur appendicular material have been presented (see brief commentaries in Le Loeuff, 2005; Company *et al.*, 2009; also see Company, 2011; Díez Díaz *et al.*, 2015). The available appendicular material presents remarkable size variation for each element type (see Le Loeuff, 2005; Company *et al.*, 2009; Company, 2011; Vila *et al.*, 2012; Díez Díaz, Suberbiola, & Sanz, 2013; Ortega *et al.*, 2015). These differences in size are also associated with important variability on morphological features that may be attributable to new undescribed taxa (Vila *et al.*, 2012) or to already known taxa (Company *et al.*, 2009; Vila *et al.*, 2012). Díez Díaz *et al.* (2015) suggest that several of these observed feature differences can be attributed to ontogenetical changes (e.g. Chera morph II humeri).

Nowadays we have limited understanding about the timing of postnatal acquisition of several of the morphological traits that characterize the titanosaurian appendicular skeleton and thereof the proportion of morphological variance that could be interpreted as ontogenetical changes. In general, we can assume fast and isometric growth for sauropods including titanosaurs (see Curtice & Wilhite, 1997; Wilhite, 1999, 2005; Bonnan, 2004, 2007). This implies that: (i) specimens attributed to juvenile individuals cannot be easily taxonomically misidentified because morphological features are acquired earlier in the ontogeny and, generally, early juveniles resemble adult individuals (Forster, 2005; Schwarz *et al.*, 2007a); and (ii) only a few morphological changes can occur between early

juveniles and adult individuals within the same species (see Curry Rogers *et al.*, 2016). Sauropods have lost developmental plasticity in comparison with the non-sauropod sauropodomorphs (Sander *et al.*, 2011a). Low developmental plasticity is plesiomorphic for archosaurs (including early dinosaurs), which probably related with their ectothermy, and secondary lost in sauropodomorphs (Sander & Klein, 2005). It is expected that we find few morphological changes during the development between early juvenile and adult individuals given Loss of developmental plasticity and the precocial growth strategy in titanosaur sauropods (Curry Rogers *et al.*, 2016). Additionally some histomorphological features seems to be acquired earlier in the ontogeny among more derived titanosaurs than in non-titanosaurian neosauropods, which suggests the presence of heterochrony (Company, 2011; Curry Rogers *et al.*, 2016). The occurrence of several individuals (including possible juveniles) in two different titanosaurian morphotypes from Lo Hueco allow us to test the presence of heterochrony in particularly for titanosaurian appendicular skeleton.

In addition to the presence of some degree of morphological variation during the ontogeny (Ekdale, 2010; Piechowski, Tałanda, & Dzik, 2014; Canale *et al.*, 2015; Foth, Hedrick, & Ezcurra, 2016), it can be observed that some taxa exhibits variation between the sequence of acquisition of morphological traits (Leigh & Terranova, 1998; Badyaev, 2002; Colbert & Rowe, 2008; Bever *et al.*, 2011; Griffin & Nesbitt, 2016b).

A good way to determine a sequence of bone maturation is via definition of several morphological features that can address different ontogenetical stage changes (Ikejiri, 2004). The recognition of these morphological features can be relatable to the Morphological Ontogenetical Stages (MOS) following Carballido & Sander (2014) which allow us to estimate the age of the individual. This is particularly useful in the absence of a paleohistological analysis. This is also important for the assessment of possible transformations of morphological features and their timing of acquisition during the ossification. The determination of the ontogenetic stages must be independent of the specimen size since different individuals with a similar age can present differences in body size (e.g., Ikejiri *et al.*, 2005b).

The framework to analyse ontogenetic changes is based on the determination of morphological features that usually changes along postnatal ontogeny in vertebrates, mainly in sauropod dinosaurs. These features are used to define a series of ontogenetic characters. The scoring of those characters for each individuals in a data matrix produce the semaphoronts (Hennig, 1966). In paleontology we only have isolated semaphoronts, a character combination representative of an individual in a developmental time of its life, instead of a complete ontogenetic sequence, i.e., the ontogenetic sequence is the complete sequence of semaphoronts of the individual (Hennig, 1966; Sharma, Clouse, & Wheeler, 2017). However, a proxy for the ontogenetic and some of the tokogenetic changes on that species can be estimated with the analysis of several semaphoronts (Brochu, 1996; Irmis, 2007b; Colbert & Rowe, 2008; Carballido & Sander, 2014; Griffin & Nesbitt, 2016a; Griffin *et al.*, 2019). The use of semaphoront data matrices can be analysed (Brochu, 1996; Colbert & Rowe, 2008) to estimate an order of acquisition and the possible variation within the sequence, resulting in the different Morphological Ontogenetic Stages (MOS) and the ordering the Ontogenetic Sequence.

The relative age of a sauropod individual is usually established based on the standardized Histological Ontogenetical Stages (Klein & Sander, 2008). These stages were initially established through the histological analysis of sauropod long bones (Padian, de Ricqlès, & Horner, 2001; Klein & Sander, 2008; Sander *et al.*, 2011b; Mitchell, Sander, & Stein, 2017) but can be determined

using other parts of the skeleton such as the ribs (Klein, Christian, & Sander, 2012a; Waskow & Sander, 2014; Waskow & Mateus, 2017). The HOS are usually employed to determine life history and growth curves (Klein & Sander, 2008; Sander *et al.*, 2011a,b). Some paleohistological analyses are starting to be performed in some titanosaurian elements from Lo Hueco titanosaurs (see Gascó *et al.*, 2018), and future analyses are necessary to calibrate our models.

The sample from Lo Hueco, as in other bonebeds, presents uncertainties due the presence of many isolated elements. The presence of more than one morph or taxon in sauropodomorph assemblages coming from bonebeds also difficult the paleohistological sampling effort and its interpretation, especially among isolated specimens (see Sander, 1992; Klein & Sander, 2007; Stein *et al.*, 2010). Some advances have been made in other bonebeds with taxa as *Phuwiangosaurus sirindhornae* (Klein *et al.*, 2009) *Lirainosaurus astibiae* (Company, 2011), *Magyarosaurus* spp. (Stein *et al.*, 2010) and *Ampelosaurus atacis* (Klein *et al.*, 2012b).

Methods that do not relay on paleohistological sampling usually assume an estimation via the size of the individual respective to a known putative adult specimen. But the overall size is a poor criteria given the size variation observable between individuals at different ontogenetical stages

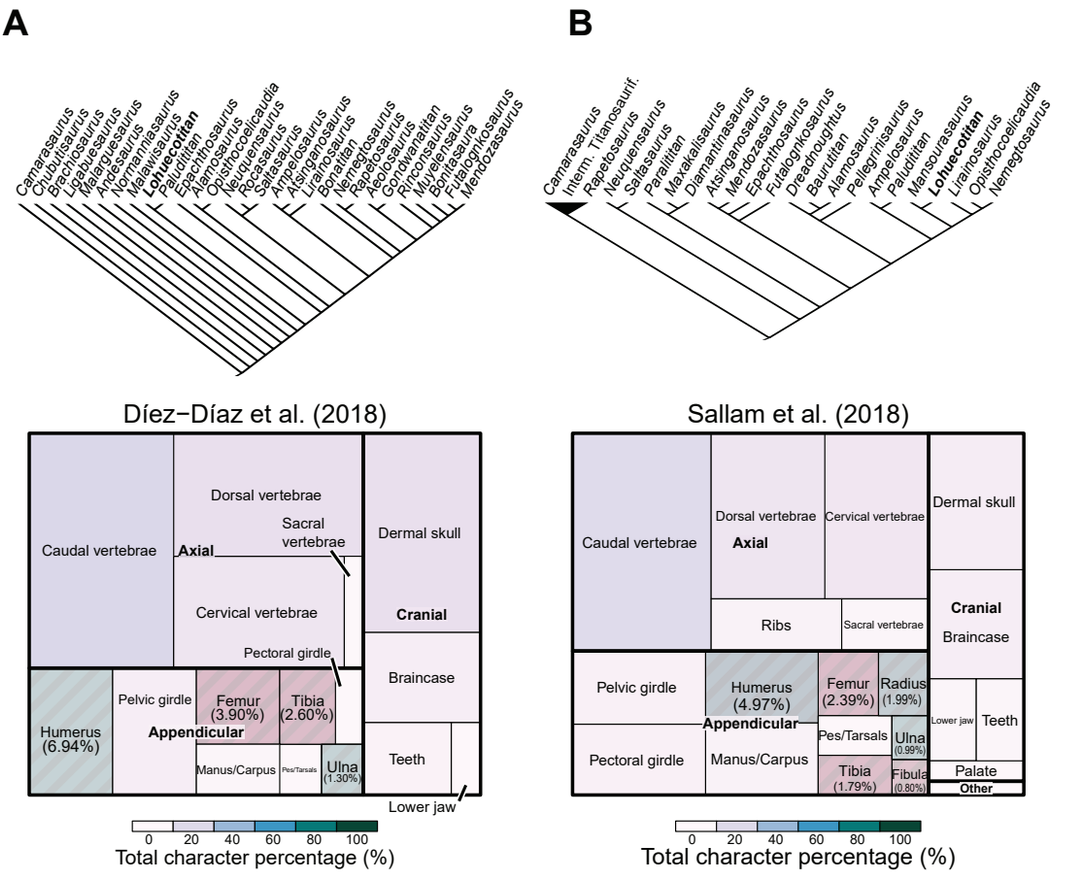

Fig.VI.3. Osteological character distribution. (A) Díez-Díaz *et al.* (2018) data matrix. (B) Sallam *et al.* (2017) data matrix.

(Brochu, 1996; Smith, 1998; Ikejiri, 2004; Taylor & Wedel, 2013). In Lo Hueco, we observe several size differences between titanosaurian specimens at apparent similar relative developmental stage in the same morphotype (see Fig.VI.1). The holotype individual of *Lohuecotitan pandafilandi* (HUE-EC1) is not the largest individual that can be referred to this taxon (see Table.VI.2) despite presenting an advanced mature and possibly senile adult stage (Gascó *et al.*, 2018). Several possible ontogenetical series of Lo Hueco are sequenced via the methodology employed by Brochu (1996) that it is named in this study as Ontogenetic Cladistic Sequence Analysis (OCSA). The Ontogenetic Sequence Analysis (OSA) was also employed in this study for estimation of ontogenetic sequences and polymorphism in the acquisition of MOS, following the methodology of Colbert & Rowe (2008). These methods are more reliable than the identification of isolated morphological features relatable to possible juvenile, subadult and adult specimens. Often these morphological features can appear at multiple ontogenetical stages and the range of appearance during growth might cause those features not as precise enough for this task (i.e., Garn & Rohmann, 1960; Ikejiri, 2004; Colbert & Rowe, 2008; Ekdale, 2010; Foth *et al.*, 2016). Moreover, several character appearances might interact with body mass and thereof its appearance timing is covariant between the age of the individual and its size (Garn & Rohmann, 1960). In absence of paleohistological analysis, these statistical methods and the use of multiple ontogenetical features (i.e., complete semaphoronts) can be used for estimate and analyse potential ontogenetic sequences.

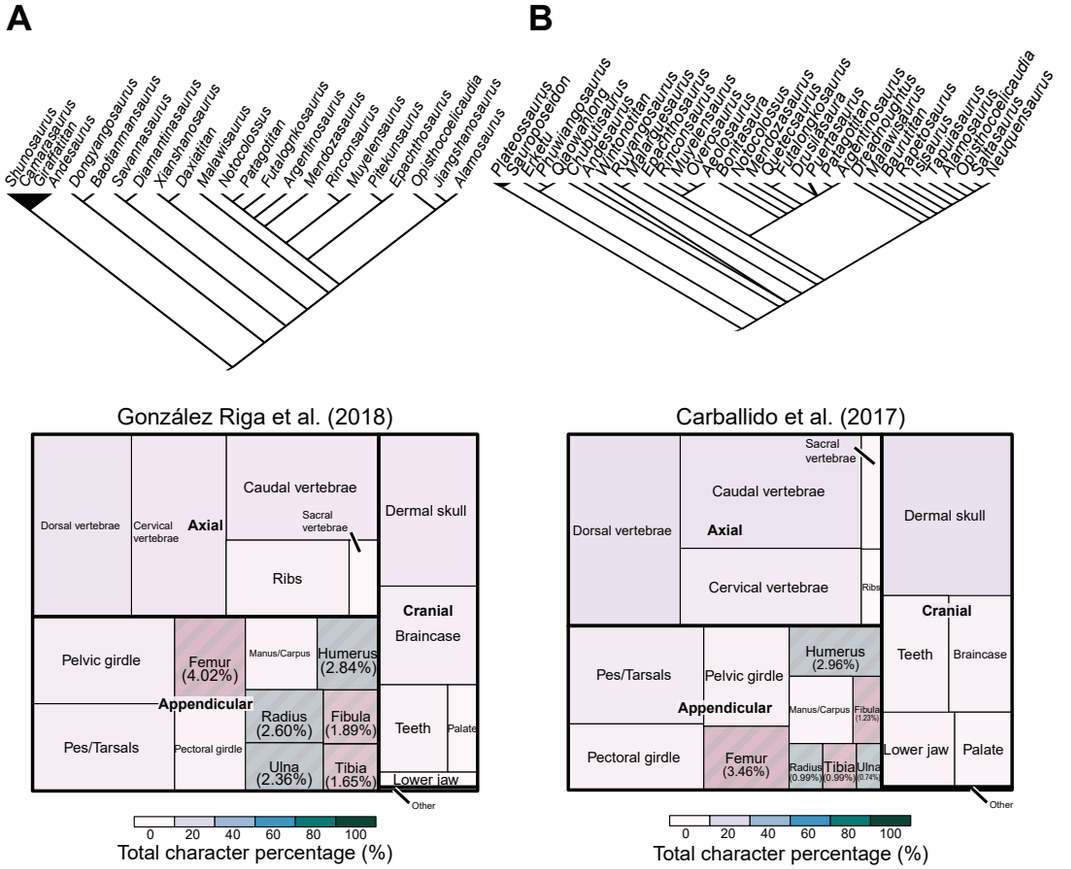

Fig.VI.3. Osteological character distribution. (A) González Riga *et al.* (2018) data matrix. (B) Carballido *et al.* (2017) data matrix.

VI.2. METHODOLOGY

VI.2.1. DEFINITION OF ONTOGENETIC CHARACTERS

The first step in the ontogenetic sequence estimation framework is the definition of the ontogenetic characters. These characters are morphological features that putatively varies during the ontogeny. These features allow defining the MOS therefore essential for the reconstruction of the ontogenetic sequence. Several ontogenetic characters proposed in studies *centered* on sauropod ontogeny, including data on long bone growth, are included in the present study (Ikejiri, 2004; Ikejiri *et al.*, 2005b; Carballido *et al.*, 2012). While other ontogenetic characters are derived from observations of morphological transformations during the growth (Martin, 1994a; Wilhite, 1999; Tidwell & Wilhite, 2005; Wilhite, 2005; Suteethorn *et al.*, 2010; Sander *et al.*, 2011b). We also propose new ontogenetic characters based on a comparative analysis of our sample and the findings of previous studies on morphological changes relatable to long bone growth (e.g., Bonnan, 2004; Ikejiri, 2004; Tumarkin-Deratzian, 2009; Carballido *et al.*, 2012; Griffin & Nesbitt, 2016a). For definition of these characters we observed features related with the pattern of chondrification and ossification of archosaurian long bones (e.g., McIntosh, 1990a; Brochu, 1996; Geist & Jones, 1996; Ikejiri, 2004; Hübner, 2011; Griffin & Nesbitt, 2016a; Hübner, 2018). Therefore, we can operate with overall rugosity of the long bone ends related with the sauropod long bone cartilaginous cap (Schwarz, Wings, & Meyer, 2007b; Holliday *et al.*, 2010). Other criteria includes the general development of structures like fossae, crests and trochanters and their relative texture that was associated with bone structure maturity (Carpenter & McIntosh, 1994; Geist & Jones, 1996; Ikejiri, 2004; Tumarkin-Deratzian, Vann, &

	Morphotype	Semaph.	Asoc.	Length (mm)
HUE-817	Morphotype I	S1	EC11	631
HUE-2356	Morphotype I	S2	EC03	588
HUE-2727	Morphotype I	S3	iso	501*
HUE-2772	Morphotype I	S4	iso	607*
HUE-3057	Morphotype I	S5	iso	526*
HUE-XXYY	Morphotype I	S5	EC02	451*
HUE-940	Morphotype II	S1, S5, S11	iso	705
HUE-1060	Morphotype II	S2, S8	iso	880
HUE-1143	Morphotype II	S1	iso	780
HUE-1356	Morphotype II	S3	iso	720*
HUE-1434	Morphotype II	S4	iso	840
HUE-1463	Morphotype II	S5	iso	640
HUE-1499	Morphotype II	S6, S10	iso	749
HUE-1502	Morphotype II	S5, S9	iso	530
HUE-1549	Morphotype II	S7	iso	1110
HUE-1647	Morphotype II	S8	EC13	712
HUE-3196	Morphotype II	S9	iso	750
HUE-3829	Morphotype II	S7	iso	660*
HUE-4208	Morphotype II	S10	iso	860
HUE-4343	Morphotype II	S11	iso	690
HUE-4828	Morphotype II	S1, S4, S10	iso	460
HUE-4522	Morphotype II	S5, S9	iso	420*

	Morphotype	Semaphoront	Asoc.	Length (mm)
HUE-1103	Morphotype I	S1, S2, S3, S4	iso	468*
HUE-1137	Morphotype I	S1	iso	614
HUE-1139	Morphotype I	S2	HUE-1140	817
HUE-2865	Morphotype I	S3	iso	493
HUE-3044	Morphotype I	S2	EC01	550
HUE-4399	Morphotype I	S4	iso	NA
HUE-964	Morphotype I	S1	iso	666
HUE-1158	Morphotype II	S1	iso	626
HUE-1338	Morphotype II	S2	iso	676
HUE-3462	Morphotype II	S3	iso	550
HUE-4357	Morphotype II	S4	iso	620

Table.V**I.2. Sample of ulnae for the current study.** Semaph. - Semaphoront where it is included (including similarities). *Assoc.* - Association. *iso* - isolated

Table.V**I.1. Sample of humeri for the current study.** Semaph. - Semaphoront where it is included (including similarities). *Assoc.* - Association. *iso* - isolated

	Morphotype	Semaphoront	Asoc.	Length (mm)
HUE-1140	Morphotype I	S1	HUE-1139	772
HUE-1340	Morphotype I	S2	iso	608
HUE-2711	Morphotype I	S3	EC03	312
HUE-1166	Morphotype II	S1	iso	279

Table.VI.3. **Sample of radii for the current study.** Semaph.- Semaphoront where it is included (including similarities). Assoc. - Association.

Dodson, 2006; Tumarkin-Deratzian, 2009; Hedrick, Tumarkin-Deratzian, & Dodson, 2012). The summary of the criteria used to establish the ontogenetic characters are available in Table.VI.1.

The definition of ontogenetic characters involving muscular attachments is based on the descriptions of forelimb and hindlimb muscle groups for non-avian dinosaurs such as Borsuk-Bialynicka (1977), Remes (2007), Otero & Vizcaíno (2008), Fechner (2009), Gallina (2011) and Otero (2018). Some muscular attachments have been interpreted differently by some authors. In these cases, the Extant Phylogenetical Bracketing (EPB: Witmer, 1995) is applied through the comparison with extant birds and crocodyles following Romer (1923, 1956), Diogo & Abadala (2007) and Diogo & Molnar (2014). The bone surface texture (see Tumarkin-Deratzian, 2009) and the rugosity are also used as a criteria for the definition of ontogenetic characters. These features are described through the direct observation of specimens and with the requirement of a hand lens. The rugosity over a muscle attachment can be hard to define. Different examples of rugosities for each character in different specimens can be accessed in Supplementary Data VI.A.

	Morphotype	Semaphoront	Asoc.	Length (mm)
HUE-902	Morphotype I	S1	iso	959*
HUE-930	Morphotype I	S2	EC11	960*
HUE-1366	Morphotype I	S3, S5	EC05	1019
HUE-1440	Morphotype I	S10	iso	1460
HUE-1521	Morphotype I	S4	iso	901*
HUE-1590	Morphotype I	S3, S5	iso	850
HUE-2338	Morphotype I	S6	iso	860
HUE-2636	Morphotype I	S7	iso	455
HUE-2903	Morphotype I	S8	iso	955
HUE-3108	Morphotype I	S9	EC01	1010
HUE-3583	Morphotype I	S10	iso	900*
HUE-8801	Morphotype I	S11	iso	600
HUE-594	Morphotype II	S1	iso	1550
HUE-1183	Morphotype II	S2	EC13	870
HUE-1187	Morphotype II	S3	iso	965
HUE-1316	Morphotype II	S4	iso	965*
HUE-1319	Morphotype II	S5	iso	840
HUE-1357	Morphotype II	S6	iso	840*
HUE-1508	Morphotype II	S3	iso	857*
HUE-2420	Morphotype II	S7	EC06	1151
HUE-3237	Morphotype II	S8	iso	814*
HUE-10007	Morphotype II	S9	iso	703*

Table.VI.4. **Sample of femora for the current study.** Semaph.- Semaphoront where it is included (including similarities). Assoc. - Association.

	Morphotype	Semaphoront	Asoc.	Length (mm)
HUE-1063	Morphotype I	S3, S6	iso	727
HUE-1165	Morphotype I	S1	iso	364
HUE-1410	Morphotype I	S2, S5	iso	415*
HUE-1573	Morphotype I	S3	iso	685
HUE-2318	Morphotype I	S2, S3, S5, S6, S9	EC3	484*
HUE-2355	Morphotype I	S2, S5	iso	667*
HUE-2799	Morphotype I	S2, S5	EC3	482
HUE-3082	Morphotype I	S6	EC1	670
HUE-4344	Morphotype I	S7	iso	539
HUE-4404	Morphotype I	S8	iso	575*
HUE-4632	Morphotype I	S9	iso	526
HUE-1149	Morphotype II	S1	iso	692
HUE-1317	Morphotype II	S2, S6, S7	iso	540*
HUE-1500	Morphotype II	S3	iso	813
HUE-1612	Morphotype II	S4	HUE-1612	825
HUE-2117	Morphotype II	S5	iso	769
HUE-2425	Morphotype II	S6	EC6	746
HUE-4055	Morphotype II	S7	iso	735

Table.VI.5. **Sample of tibiaee for the current study.** Semaph.- Semaphoront where it is included (including similarities). Assoc. - Association.

In this study, we codify a muscular attachment as absent when the bone surface is smooth and lack the projection of structures as crests, ridges and trochanters. This condition is considered the state 0. The development of a rugosity with mamellae or protuberances, and a crest or a trochanter is considered as state 1. Some multistate characters can be defined to describe a further development in some morphological structures, such as: (i) crests that develop a bifurcation (e.g. bifurcation of the medial distal condyle in the humerus Carpenter & McIntosh 1994), (ii) presence of longitudinal striation on the lateral margin of trochanters (e.g. development of the deltopectoral crest of the humerus; Fondevilla *et al.*, 2018), and (iii) depressions on the proximal and distal ends (development of the intercondylar fossa of the humerus Ikejiri, 2004).

These structures are related with maturation of tendinous caps over muscular attachments (e.g., Romer, 1956). Additionally, some studies suggested that the overall robustness of the specimen and the eccentricity can vary with the development (Martin, 1994a; Ikejiri *et al.*, 2005a; Díez Díaz *et al.*, 2015). The dependence of the characters derived from specimen's measurements are relevant in the test of possible allometrical relationships in the long bone growth of the titanosaurian sauropods (see Wilhite, 1999, 2005; Bonnan, 2004). We thought that a statistical workflow entirely committed to this question could be more appropriate to analyse these morphometric features. Therefore, morphometric variables and characters derived from measurements, such as the Robustness Index (RI) and Eccentricity (ECC) they were excluded in the definition of ontogenetical characters.

VI.2.2. ONTOGENETIC CHARACTER DATA MATRICES CONSTRUCTION

The ontogenetical data matrces are built in Mesquite v3.31 (Maddison & Maddison, 2011) with the proposed set of ontogenetic characters (see Ontogenetic Characters, below). Each row corresponds to one semaphoront, which acts as an Operative Taxonomic Unit (OTU) as in cladistic analysis. The semaphoronts result from the scoring of ontogenetic characters for a particular specimen. In fossil data however, many specimens lack an important portion of the character information. Semaphoronts with and redundant scorings and with a high proportion of missing data might increase the uncertainty on the estimation of ontogenetic sequences. This uncertainty is analogous to the one related with large portions of missing data and redundant OTUs, which comprise the morphological dataset used in cladistic analyse(Wilkinson, 1995, 2003; Wiens, 2003). In order to control this uncertainty, it is necessary to pextende uninformative specimens. First, we summarized specimens with identical scoring into one semaphoront (see Colbert & Rowe, 2008; Griffin & Nesbitt, 2016a). After this step, some semaphoronts can still have similar scorings, differing in only a few number of scorings or with the presence of a few missing data. These similar scorings might add no information for the sequence estimation. In order to clean the data matrices of uninformative and redundant semaphoronts we applied Safe Taxon Reduction following Wilkinson (1995) via "Claddis" package (Lloyd, 2016).

The OCSA and OSA, applied in this study, consider all the characters as additive, i.e. the morphological features acquired during ontogeny of an organism are stepwise. For example, one organism cannot develop a fully mature ossified cartilaginous cap without the previous mineralization of the cartilaginous shaft (Brochu, 1996; see also Fröbisch, 2008). The OCSA and OSA also assume that the changes of states are irreversible, i.e. the ossification patterns of

	Morphotype	Semaphoront	Asoc.	Length (mm)
HUE-1335	Morphotype I	S1	iso	507
HUE-1377	Morphotype I	S2	iso	534
HUE-1476	Morphotype I	S2	iso	702
HUE-1513	Morphotype I	S3	iso	640
HUE-1570	Morphotype I	S4	iso	572
HUE-2804	Morphotype I	S5	iso	469*
HUE-2904	Morphotype I	S6	EC3	470*
HUE-3075	Morphotype I	S7	iso	525
HUE-3087	Morphotype I	S8	EC1	638
HUE-7802	Morphotype I	S2, S7, S8	iso	399*
HUE-1082	Morphotype II	S1	iso	707
HUE-1146	Morphotype II	S1	iso	702*
HUE-1175	Morphotype II	S2	iso	430
HUE-1507	Morphotype II	S3	iso	428*
HUE-1520	Morphotype II	S4	iso	440
HUE-1612	Morphotype II	S5	HUE-1612	614*
HUE-2426	Morphotype II	S6	EC6	724
HUE-2669	Morphotype II	S7	iso	905
HUE-2806	Morphotype II	S8	iso	709
HUE-2977	Morphotype II	S9	EC4	532
HUE-3000	Morphotype II	S1	iso	525*
HUE-4416	Morphotype II	S10	iso	564
HUE-5232	Morphotype II	S11	iso	676

Table.V**I.2. Sample of ulnae for the current study.** Semaph.- Semaphoront where it is included (including similarities). Assoc. - Association.

epiphyses and muscular attachments cannot disappear. These assumptions related with the character changes are introduced using a step cost matrix coded in TNT. v.1.1 (see Goloboff, Farris, & Nixon, 2008a). The character cost of state reversion is codified as extremely high increase of steps (999). This cost matrix is applied in this study in order to treat the irreversible characters in a similar way as it was originally applied by OCSA (Brochu, 1996) and OSA (Colbert & Rowe, 2008) using the software PAUP (Swofford, 2002). With these ontogenetic characters we build a data matrix similar to osteological data matrices for phylogenetic analyses and here they are called ontogenetic matrices.

The sample of Lo Hueco do not preserve specimens at probable early development stages for all elements, i.e., a semaphoront scoring all "*0*". Therefore, in order to polarize the trees in both OCSA and OSA method, we created a virtual juvenile outgroup which it is "0" in all the character states. It is feasible to assume that sauropods in post-hatchling stage could have weakly ossified cartilaginous caps on their long bones and little to no development of several muscular attachments that will be described below (Curry Rogers *et al.*, 2016). Moreover, embryonary titanosaurs present no ossification of proximal and distal epiphyses with barely noticeable major structures like deltopectoral crest of the humerus (García *et al.*, 2010; pers. obs. APB 2016). . As they are included only for analytical purpose as outgroups, then they are removed from the ontogenetical consensus tree returned by OCSA and only included as root of the sequences at juvenile state in the OSA (Griffin, 2018).

Each ontogenetic data matrix is exported in TNT format with the step cost matrix of additive irreversible characters and the outgroup juvenile semaphoronts if needed. There is a total of five data matrices, one for each long bone of Morphotype I + *Lohuecotitan pandafilandi* forelimb and hindlimb excluding the radius which sample is too low (three possible distinct semaphoronts, only for Morphotype I). In addition, four data matrices, one for each long bone of Morphotype II fore and hindlimb. For Morphotype II there is no ulna ontogenetic data matrix as safe taxon reduction recovered only two valid semaphoronts and considered the other two available specimens as redundant information. From this point both methodologies differ in processing these ontogenetic data matrices. The Analytical methodology is commented below.

VI.2.3. PHYLOGENETIC DATA MATRICES

We are assessing possible intraspecific variation between morphological characters used in phylogenetic analysis of sauropod dinosaurs and the relationship with ontogenetic changes. In order to analyse possible clusters and the tempo of intraspecific changes, we built a data matrix of relevant morphological features already used in phylogenetic analysis and others that might be potentially useful. They are not necessarily characters used during the construction of the ontogenetic data matrices. Some of these characters relevant to sauropod systematics are related to muscular attachments that are also sensible to ontogenetic changes, so they may appear in both types of data matrices (e.g. presence of a prominent process in the lateral edge of the proxmal end following Upchurch, 1998; see also humerus ontogenetic character #10, see below; and the development of the posterolateral bulge in the deltopecoral crest following D'Emic, 2012; see also humerus ontogenetic character #6, see below).

Character definition is based on the criteria of first definition and any modification made in more recent studies. In this study, we have not covered in detail the individual association of several of the analysed specimens as most of the sample are isolated specimens. For this reason we do not analyse complete semaphoronts of the forelimb, hindlimb and all the appendicular skeleton as a whole. In the same way, we excluded characters based in ratios of fore- and hindlimb, and ratio characters that compare between bone types (e.g. the classical humerus-to-femur length ratio, and femur-tibia length, see McIntosh, 1990a; Wilson & Sereno, 1998; Wilson, 2002; Upchurch *et al.*, 2004) because they require an association between the different element specimens. Use of averaged values is not possible either as we present both the problematic of association and the degree of individual variance in size (see Chapter V) independently of the probable ontogenetic status of the specimen. A way to deal with this problem can be through scaling of numeric variables and operating in shape variables, like after a size-dependant principal component analysis to transform the original variables (Somers, 1986; Revell, 2009) or size extraction method following Mosimman (1970). However, an entire study with morphometric approach should cover this variation and these analytics are beyond the scope of the present work, thus the implications of ratio-based ontogenetical character will be covered elsewhere.

Assuming that titanosaur appendicular growth follows isometric relationships and fast, it is expected that individuals, even in early ontogenetic stages, will show the same combination of phylogenetical morphological traits as the adults of that same taxa. To test this hypothesis we will assess the similarities between specimens of the same morphotype and the ontogenetical stage appearance distribution. In order to test the similarities, we processed the phylogenetic character with cluster methods instead of cladistic methods. We want to test how teach specimen groups by similarities in the character combination via a distance metric, in this case a dissimilarity distances between categorical data. We do not want to know how the different morphotypes or groups relate in a phylogenetic context, only the resemblance among the more juveniles and the more adult individuals without an a priori assumption of character change i.e. see the basic assumptions of cladistic analysis following Hennig (1966). Hence, a clustering method based on averaged (UPGMA) aggregation is selected. Distance metrics in categorical characters were calculated via Gower distances (Gower, 1971). Euclidean distances are usually employed in clustering techniques of continuous (metric, numeric) data (Hammer & Harper, 2008). Euclidean distances have no meaning over categories like in our morphological data matrix, nonetheless. We chose a measurement of dissimilarities between the specimens

that accept missing values in the data input. Gower coefficient of dissimilarity is based on a comparison between the total character coincidences of two specimens and then the distance is calculated via the average score taken over all possible comparisons (Gower, 1971). For the comparison within a developmental context, we will plot the phylogenetic characters in the stages estimates by OCSA and OSA methods based on ontogenetical characters.

VI.2.4. ONTOGENETICAL STAGES ANALYSED VIA MAXIMUM PARSIMONY

The OCSA and OSA methods resemble each other in the character input and in the initial analytical step. Both use cladistic methods for assessment of the topology, producing a set of trees which hierarchical structure reflects the character acquisition and how the resultant groups relate to each other (see Hennig, 1966). In order to estimate this set of trees we use maximum parsimony methodology. The most parsimonious trees (MPTs) are calculated with the software TNT v1.1 (Goloboff *et al.*, 2008a). A heuristic search conducted with the least mature semaphoront (or the hypothetical juvenile semaphoront) as outgroup is conducted with 1000 replications of tree branch swapping over Wagner trees with tree bisection-reconnection algorithm and saving 100 trees per replication. The OCSA method is based in a cladistic treatment of those irreversible ontogenetical characters. For the OCSA we calculate a consensus tree via 50% majority rule, which is a common consensus estimation method, and that tree will be our basic estimation unit. The ontogenetic stage is inferred from the method of Brochu (1996), which is based on the node number described in tabular format. Each node is associated with a combination of character state changes that marks a new developmental stage. Tree polytomies are treated as similar, ontogenetical stages with indeterminate order between them, all semaphoronts occur in the same stage (as per the common node). If more than one cluster is present, similar counting strategy will be used (see Fig.VI.4). Each subtree node is then accounted, and it may be significant of different developmental routes differing from the node-developmental stage in which both subtrees diverge. The subtree nodes are not cumulative; semaphoronts with similar node count in different subtrees are at the same ontogenetic stage. Also, the total ontogenetic stages are determined by the longest branch (in subtree node count).

The developmental stage is then translated into a percentage of the total possible stages, indicating the grade of development estimated.

VI.2.4. ONTOGENETIC SEQUENCE ANALYSIS

While both methods use the parsimony search of MPTs, the OCSA *sensu* Brochu (1996) only calibrate the ontogenetical sequence based on the resulting consensus tree. The OSA in the other hand is used to search all the possible developmental paths and explore if there is some sort of sequence polymorphism and when it is produced (see Colbert & Rowe, 2008). The ontogenetical stage is set a priori summing the number of steps as character changes from the data matrix given the principle of stepped acquisition of the features and irreversible changes during the ontogeny (Colbert & Rowe, 2008). A semaphoronts with six characters and the codification as "*012011*" for example will result in a stage five, as the method consider the steps (character changes) as ontogenetic changes by maturation. The more mature stage is determined by the semaphoronts with the higher number of cumulative state changes

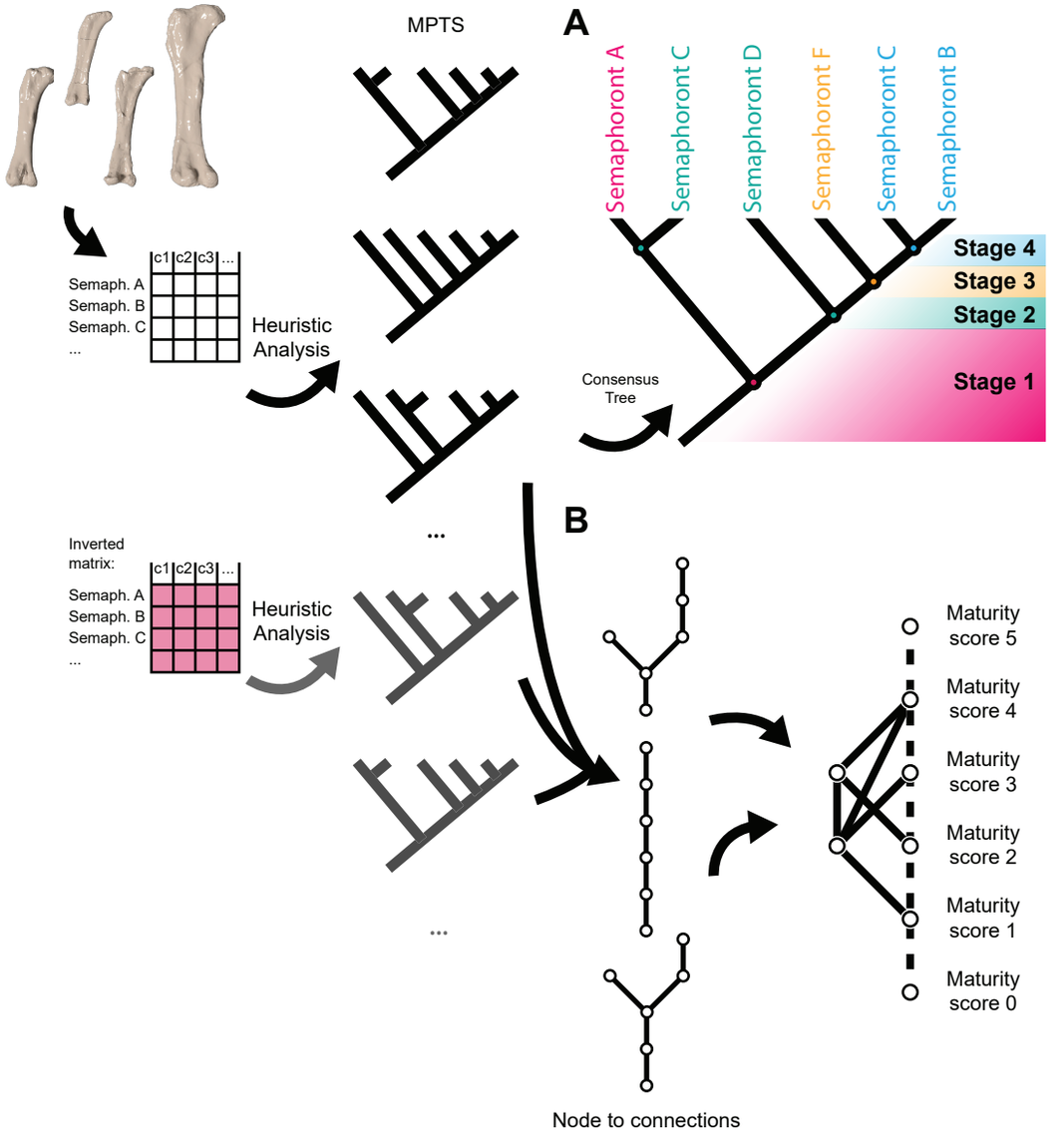

Fig. VI.4. Analysis of ontogenetic sequences using parsimony. (A) OCSA method following Brochu (1996), estimate Consensus Tree after MPTs heuristic search. Conversion of nodes to MOS. (B) MPTs heuristic search on the original dataset and inverted characters. Transformtion of all the MPTs topologies into connections between Semaphoronts and estimation of Modal Sequence.

needed to pass from an all "*0*" scoring (the hypothetical juvenile) to its current ontogenetic character scoring. This technique applied in fossil data would results in many semaphoronts underscored at early ontogenetical stages due to missing data. The same example with "*0?201?*" will score a stage four. For this matter, we used Safe Taxonomic Reduction (STR; see Wilkinson, 2003) before the tree search. This algorithm reports the specimens that are removable due to redundant or null information. Only those specimens that represent relevant semaphoronts with character combinations that are not found in other specimens/semaphoronts are included

in the tree search. The STR was carried in R with the "Claddis" v0.3 package (Lloyd, 2018). The similarities between specimens after STR, generally the most complete specimens, are reported in Table.VI.2., 3, 4, 5 and 6 This method include a dimensionless score that represents the frequency of representation of a particular semaphoront by specimens described in the sample. It can act as some sort of support as it is the weight of information backing that particular combination of characters. The semaphoront weight is determined summing the complete individuals that represent partially or completely that particular combination of ontogenetical characters (Colbert & Rowe, 2008). In the previous example if the semaphoront "*012011*" is represented by two individuals, then its weight will be of two. Some previous works on fossil material have addressed the relevance of specimens with missing data (Griffin & Nesbitt, 2016a; Griffin, 2018). In those cases, the specimens with missing data summed 0.5 to the weight of the semaphoront in order to account that the information is partial. We chose to sum a fraction representing the total missing information instead, as progressively more incomplete specimens backed much less the information of a particular semaphoront. So, if we compose the semaphoront "012011" with the second incomplete individual "0?201?" of our previous example, the total weight will be one plus four sixth of total possible character scores for a total of 1.67.

In this method, we operate with all the MPTs without the consensus tree, transforming all the possible nodes into connections between the semaphoronts. For tracing all the possible paths of connection with the most mature semaphoronts recovered in our sample, it is necessary to invert the analysis (see Colbert & Rowe, 2008). In order to do so, we will invert all the character scores ("*0*" being the most developed state → *1/2/3...* being the least developed) and repeat the MPT search with the most mature semaphoront defined in the sample as outgroup. Then the MPTs of the inverted analysis will be used to trace all the possible paths and character acquisitions connecting with the more mature specimens at the root (see Colbert & Rowe, 2008). Another effect of missing data in fossil taxa is the complete lack of preservation of intermediate ontogenetic stages or possible semaphoronts in determinate ontogenetic stage. These missing unique combinations of morphological features can be estimated to some degree following the method proposed by Griffin (2018). Some of the MPTs may present a subtree with several of the semaphoronts grouped together. This node can be translated into an unknown intermediate semaphoront that was not available in the sample at a stage between the subtree semaphoronts of the tree. We do not know the exact combination of characters of this semaphoront, but we can estimate the presence of another semaphoront in a determinate ontogenetic stage, so all the possible character change combinations are covered. These estimated semaphoronts have zero weight, as they do not add evidence on the ontogenetic trajectory as they are instead estimated from it. With all the paths traced, the total sum of semaphoront weights of each path can be summed up to calculate the modal sequence, the one with more evidence and probably more usual path of development of the osteological characters.

VI.3. ONTOGENETIC CHARACTERS

The characters described here are based on the criteria commented before (see Ontogenetic Character Definition). All the proposed characters are figured in the text, and additional photos and graphics can be found in Supplementary Material VI.A. The radii are excluded from these analyses due the lack of a representative sample. Only four radii have been recovered so far Lo Hueco. One specimen attributable to Morphotype II and three specimens referred to *Lohuecotitan pandafilandi*. There are major differences in size between the specimens of *L. pandafilandi*, and only minor morphological variability is observable. The range of this variability is comparable to the one found in other element types of the sample, suggesting that they might be referable to ontogenetic changes. Here we introduce several ontogenetic characters for the radius based on the present morphological variation; and this variability will be discussed (see Discussion).

VI.3.1. HUMERUS CHARACTERS

- H_{ont}1: Rugosity of the proximal and Hont2: rugosity of the distal end

The proximal and distal ends present some variation on the rugosity. The rugosity corresponds morphologically to a series of bumps and grooves, ranging from weak concavities and convexities to deep sulcus and mammillae. These rugosities are probably relatable to the presence of a cartilaginous cap common in the proximal and distal end of the dinosaur appendicular bones (e.g., Geist & Jones, 1996). Unfortunately, many sampled humeri of Lo Hueco have badly preserved the proximal and distal ends belonging to the Morphotype I (= *Lohuecotitan pandafilandi*, e.g. HUE-3044) and Morphotype II (e.g., HUE-1143). The humeri that preserve proximal and distal ends present minor differences in the rugosities (Fig. VI.5). The detailed description of the humeri from Lo Hueco and their comparison with other sauropod taxa allow defining three states of character. The state 0 can be attributed to the absence or a weakly development of rugose endings with a generally dimpled surface texture (e.g. HUE-4343, HUE-2727, see Fig. VI.5.A). In some specimens, the state 0 is related to a slightly grained bone texture (following Tumarkin-Deratzian *et al.*, 2006; see also Tumarkin-Deratzian, 2009) in the surface. The surface, however, does not develop proper grooves nor mammillae. The state 1 is represented by a strong rugosity and some longitudinal sulcus over the edges between the ends and the shaft (e.g. HUE-1463, see Fig. VI.6.B). The edges are engrossed (especially in proximal end, related with humerus ontogenetic character Hont10, see below). The transition between the proximal surface and the deltopectoral crest can be slightly rough. Finally, the state 2 is characterized by deeper grooves and longitudinal in proximal and distal ends. The texture of the bone is punctuated (following Tumarkin-Deratzian, 2009).

- H_{ont}3: Deltopectoral crest scar of the M. supracoracoideus

The scar at midpoint of the deltopectoral crest is the attachment of the M. supracoracoideus (Diogo & Abdala, 2010a). This structure is one of the main landmarks and more distinct morphological structures visible in the anterior face of sauropod humeri (e.g. McIntosh, 1990b; Upchurch *et al.*, 2004). Some authors interpret the attachment of the M. pectoralis in the inner side of the deltopectoral crest (Remes, 2007). The development of the M. supracoracoideus attachment is located at the midpoint to the distal part of the deltopectoral crest in all the Lo

Hueco specimens. The deltopectoral crest is sometimes fractured, especially in its upper part, but this insertion can be recognized easily in all the studied specimens. The state 0 is characterized by the presence of engrossment of this area without rugosity nor scars. The engrossment of the deltopectoral crest is restricted to its midpoint. The state 1 shows marked scars and rugosities. Some differences in the morphology of the M. supracoracoideus attachment and deltopectoral crest between both morphotypes can be described. In Morphotype I, the M. supracoracoideus becomes wider than Morphotype II, forming a round thick area in the distal part of a thick deltopectoral. In the Morphotype II this attachment is represented by a small, narrow and thick oval-shaped swelling, longer proximodistally than Morphotype II, placed on a narrow deltopectoral crest and extending to the lateral face of the crest (Fig. VI.5).

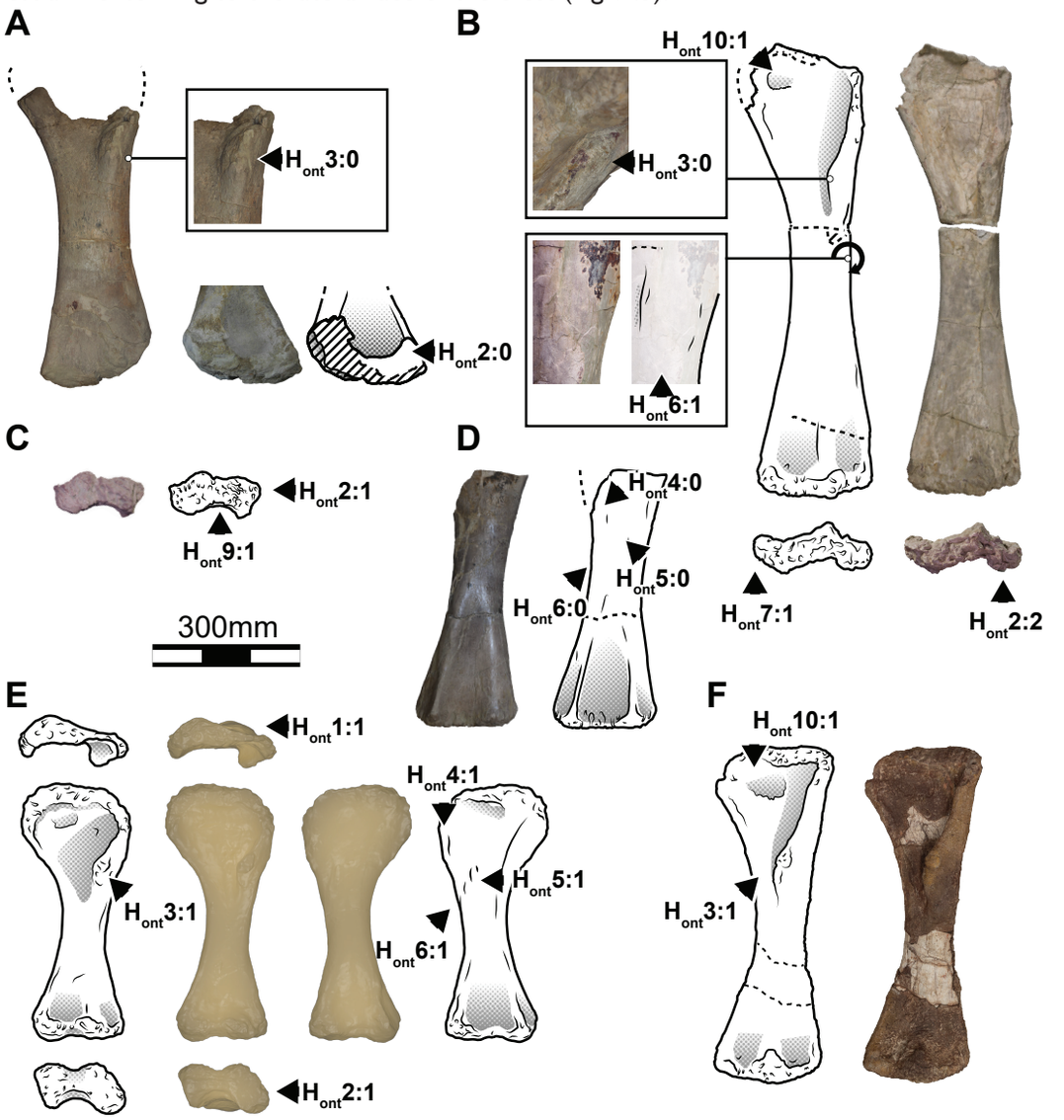

Fig. VI.5. Humeral ontogenetic characters. (A) HUE-2772 in anterior and posterior view. (B) HUE-1434 in anterior and distal view. (C) HUE-1060 in distal view. (D) HUE-2727 in posterior view. (E) HUE-817 in proximal, anterior, distal and posterior view. (F) HUE-1463 in anterior view.

- H_{ont}4: Development of the Mm. deltoideus scapularis + clavicularis ridge

In the posterior face of the humeral proximal end there is a bulge that usually extends behind the deltopectoral crest at the same level. This morphological structure has been observed and codified as a phylogenetic character in a few datasets (see character #80 in D'Emic, 2012). This bulge was attributed to the attachment of the M. deltoideus scapularis, and thefleshy insertion of M. deltoideus clavicularis by Remes (2007) and Otero (2018). This attachment is located in the lateral face of deltopectoral and it is discussed here. Both authors propose the fleshy insertion of the M. deltoideus scapularis in the posterior lateral face of the humerus. The hypothesis by Remes (2007) limits the extension to the posterolateral part of the humerus with no component in the deltopectoral crest. This hypothesis also suggests a more dorsal position and probably extending over the transition between the humeral proximal end and the deltopectoral crest. While the hypothesis of Otero (2018) includes a lateral component in the posterior part of the deltopectoral crest. In this work we consider this bulge as the most probable insertion for Mm deltoideus scapularis + clavicularis following both hypotheses, and by comparison with other muscle attachment from this region (see below). This bulge is located more ventrolateral to the attachment of the Mm. scapulohumerale group in the lateral part of the proximal end (e.g. Otero, 2018). It is possible to correlate the posterolateral bulge to the M. deltoideus scapularis crest as some titanosauriforms present a development of the transition of the proximal end and the deltopectoral crest (attachment of the Mm. scapulohumerale) and develop a ridge dividing the posterior face and the posterior part of deltopectoral crest following the hypothesis of Otero (2018): e.g. *Ligabuesaurus leanzai* (Bonaparte, González Riga, & Apesteguía, 2006) and *Neuquensaurus australis* (Otero, 2018; APB pers. observ. 2016). These taxa develop the posterolateral bulge from the proximal end to the height in which the deltopectoral crest ends in the posterolateral face of the humerus.

In some specimens of Lo Hueco site, this bulge is absent, with a smooth surface extendning from the lateral of the deltopectoral crest to posterior face of the humerus; or only slightly developed. This condition is considered the least mature state 0. The development of a bulge or a crest and a marked rugosity at the height of the deltopectoral crest in the posterolateral of the deltopectoral crest is considered the most mature state 1.

- H_{ont}5: Development of the Mm. latissimus dorsi and teres major crest located posteromedially and distally to the deltopectoral crest

Some sauropod taxa develop a secondary trochanter in the posterior face of the humerus and placed slightly more medially and distally to the bulge of the Mm. deltoideus scapularis + clavicularis ridge. This feature can be observed in both titanosaurian morphotypes of Lo Hueco site. This bulge is proposed by Otero (2018) as a type I inference of the attachment of the M. latissimus dorsi in sauropodomorph dinosaurs identifying the presence of this trochanter in *Rapetosaurus krausei* and *Neuquensaurus australis* among titanosaur taxa. Some differences have been observed and two states are defined: the absence or the presence of a smooth convexity considered as state 0 (e.g. HUE-2727 or the smooth convexity in HUE-2356; and the presence of a rugose bulge in the posterior face of the humeral diaphysis, defined as state 1 (e.g. HUE-1549).

- H_{ont}6: Presence of a Mm. triceps brachii caput humerali laterale and humeroradialis ridge

The M. tricep brachii caput humerali, which presence in sauropodomorph dinosaurs is inferred (see Diogo & Abdala, 2010b; Otero, 2018), starts in the separation between the M. deltoideus group and those that connect the anterior part of the scapulocoracoid proximal expansion. There is a pair of crossing ridges present under the deltopectoral crest in the posterior face of the humerus, as occur in *Neuquensaurus australis* (Otero, 2010; pers. obs. APB 2016), *Saltasaurus loricatus* (pers. observ. APB 2016), and *Elaltitan lilloi* (pers. obs. APB 2016) as well as both morphotypes from Lo Hueco. The more proximal of these ridges expands longitudinally to the lateral edge in posterior face of the deltopectoral crest, defining the edge between the lateral and posterior faces of the humerus. This ridge connects the M. deltoideus scapularis crest with the second ridge. The second ridge expands distally and slightly oblique from the posterior face to lateral edge of the shaft and can be associated to the insertion of the M. humeroradialis. This ridge contacts with the distal part of the deltopectoral crest and the M. triceps brachii caput humeralis laterale. The absence or the rudimentary development of the described pair of ridges is considered as state 0; and their full development as state 1 (see Fig. VI.6.B and D).

- H_{ont}7: Development of the lateral ectepicondyle

This structure is a ridge that serves as insertion of a complex group of muscles related to the distal lateral part of the humerus with connection of the rest of the forearm. The morphology observed for this ridge can be defined in two states. This ridge can be smooth and barely noticed (without a marked crest in the distal edge) and related with the shallower rugosity of the distal end. This state is considered as the least mature state (state 0). On the other hand, the most mature state (state 1) is somewhat related with the rugosities of the distal end, marked proximodistal sulcus in distal edge. Sometimes, there is a ridge expanding posteriorly and marking the lateral edge perpendicular to the distal end, with an associated concavity in anterolateral face (see the distal end of HUE-1434, HUE-817; Fig. VI.5.B and E).

- H_{ont}8: Step in posterodistal part of the anconeal fossa

The anconeal fossa is a concave area that extends in the posterior face of the distal end of the humerus and can extend to the region between the distal condyles in morphotypes or taxa that present a non-flat distal end of the humerus. In such cases it can reach the humeral distal end in anterior view (see character #163 in Wilson, 2002). Some specimens show a small step in the distal face associated with high rugosity of the distal condyles. This straight bar in distal view connects both radial and lateral ulnar condyle creating a step in the distal part of the anconeal fossa (Fig. VI.6.D). The absence of any step-in distal view is considered state 0 while the presence is considered as state 1.

- H_{ont}9: Posterior edge of the proximal end

Some of the specimens which present a developed rugosity in the proximal end, usually with associated mammillae or/and longitudinal grooves have a projected posterior edge. This edge is probably associated with the development of the proximal cartilaginous cap of the epiphysis in dinosaurs (Holliday *et al.*, 2010). And it is present in many sauropod humeri (see in McIntosh, 1990a; Wilson & Sereno, 1998; Upchurch *et al.*, 2004; Upchurch, Mannion, & Taylor, 2015; Otero, 2018; González Riga *et al.*, 2019). The proximal ending of the

attachment of the M. scapulohumerales can also be the M. suboracoideus cranial component (Remes, 2007) and maybe part of the M. deltoideus scapularis (see Remes, 2007 contra the extension as proposed by; Otero, 2018). The absence of this projected edge is considered as state 0 and the presence of a developed posterior edge in the proximal end is state 1.

- H_{ont}10: Development of striation in the M. coracobrachialis fossa located in the anterior face

This fossa is present in many sauropodomorph taxa (Galton & Upchurch, 2004; Upchurch *et al.*, 2004; Remes, 2007; Otero, 2018). The M. coracobrachialis expands all over the proximal part of the anterior expansion in the sauropod humeri and this fossa is its main area of attachment (Remes, 2007; see the anterior fossa in Otero, 2018). All specimens of the taxa represented in Lo Hueco has this anterior fossa suggesting that it might appear early in ontogeny. In some humeri, this fossa can preserve a well-developed striation. We considered the lack of this striation in the M. coracobrachialis fossa as state 0. It is probable that some early juvenile sauropod individuals also lacks

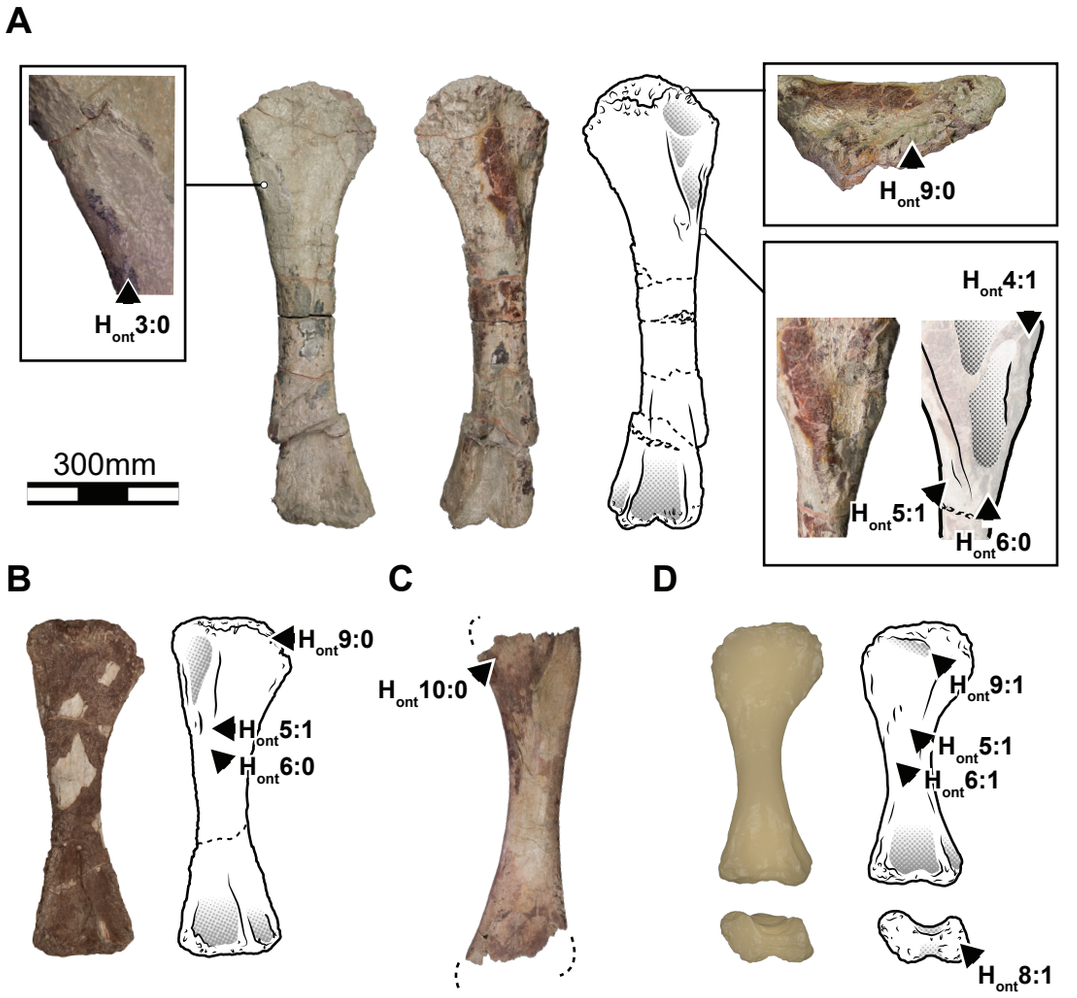

Fig.VI.6. Humeral ontogenetic characters. (A) HUE-1060 in anterior and posterior view. (B) HUE-1463 in posterior view. (C) HUE-3829 in anterior view. (D) HUE-817 in posterior view.

the M. coracobrachialis fossa as occur in the specimens OMNH-1277 and OMNH-1278 belonging to juvenile individuals referred to *Apatosaurus* sp., which only shows smooth anterior fossa in the proximal expansion (Carpenter & McIntosh, 1994). The mature state (state 1) is defined by the presence of longitudinal and marked striation in the distal border of this fossa (see Fig. VI.5, VI.6).

VI.3.2. ULNA CHARACTERS

- U_{ont}1: Rugosity on the proximal and U_{ont}2: Rugosity on the distal end of the ulna.

Similarly to the humerus and observed for all the bone types, the overall rugosity of the proximal/distal condyles is determined. Only HUE-3462 referred to Morphotype II lacks rugosity and the development of grooves and tubercles on the proximal end, which is representative of the state 0. The distal end of specimens HUE-4399 referred to Morphotype I and HUE-1158 and HUE-4357 referred to Morphotype II, have no rugosity in this area. The majority of the sampled specimens present a rugose proximal and distal ends considered as state 1., which is deeper while increasing the presence of sulcus in the proximal edge. Further development of the rugosity of this area include the appearance of longitudinal grooves on the edge of the proximal end, which defines the state 2. This can be observed in the HUE-2865, the holotype specimen of *Lohuecotitan pandafilandi* (HUE-3044), and HUE-1158 referred to Morphotype II. Sometimes this rugosity is also associated with the development of a proximal concavity over the anteromedial proximal process (e.g. HUE-1139).

- U_{ont}3: Ridge of the M. pronatus quadratus attachment.

There is a marked ridge or linea extendning longitudinally at the middle of the anterior face of the ulna. This linea is developed in the middle of the radial fossa in anterior face, slightly below the edge of the proximal end. The structure extend to the distal part of the radial fossa, and in some sauropods continues with the lateral flange of the radial articulation (e.g. HUE-3044) and some authors refer to it as the interosseous ridge without further comment (Poropat *et al.*, 2015; Upchurch *et al.*, 2015). It has been proposed as the correlate with the distal part of the attachment of the M. pronatus quadratus (Otero, 2018). This is ridge is absence in some of the specimens of Lo Hueco, especially among the ones referred to the Morphotype II. We consider the absence of this ridge as the state 0. The presence of a clearly visible ridge, whether it reaches to midshaft of the ulna or expands the radial articulation, is considered as state 1. Interestingly, HUE-1158 does not present this ridge. Nevertheless, it can be observed the development of pronounced proximal rugosity with longitudinal grooves.

- U_{ont}4: Distal component of the M. pronatus quadratus ridge with the M. abductor pollicis longus

There is a recurved ridge related to the attachment of the M. abductor pollicis longus (see Otero, 2018) located in the anteromedial surface of the distal end. We separate this character from the previous one based on some variation observed with the continuity of this ridge in the distal end. Some specimens referred to Morphotype I have the M. pronatus quadratus ridge or interosseous ridge (sensu Upchurch *et al.*, 2015) in the proximal part, at the height of the midshaft and expand down to the distal end. This ridge becomes less developed in the radial articulation, but it does not contact with the scar of the radial ligament. This condition might be related to ontogeny, as this weak development of the anterior part of radial

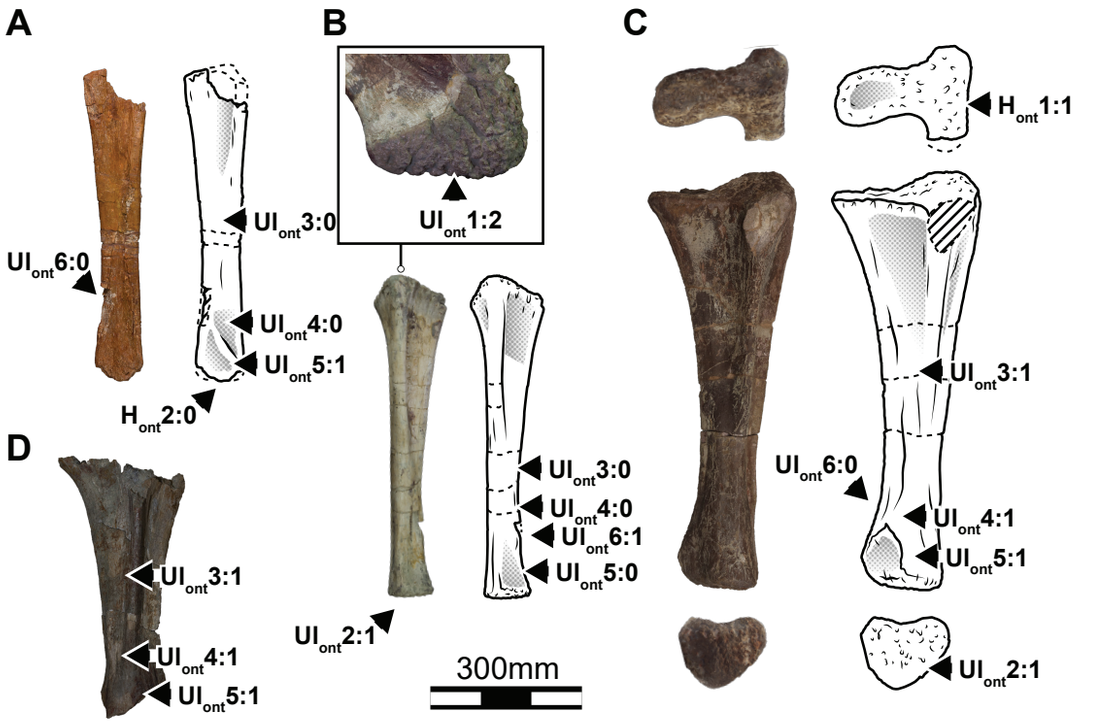

Fig.VI.7. Ulnar ontogenetic characters. (A) HUE-4357 in anterior view. (B) HUE-1158 in anterior view. (C) HUE-1139 in proximal, anterior and distal view. (D) HUE-3044 in anterior view.

articulation and the reduction to a weak bump following the interosseous ridge occurs in the smallest specimens of the studied sample. The presence of a weakly developed ridge in the distal anteromedial face, with smooth surface and the absence of the more anterior ramus of the ridge connecting the medial end of radial articulation with the interosseous ridge is considered as state 0. The presence of a recurved ridge extending from the interosseous ridge to the medial face of the distal end surrounding the radial articulation is the state 1. It is also important to denote that this character might be variable between distinct taxa. For example, the ulnae referred to the Morphotype II do not present a clear ridge on the edge of the M. abductor pollicis longus probable area of insertion. Similarly, other taxa show several differences in this ramus of the ridge and the position itself that does not alter, which might difficult the assessment of the attachment of M. abductor pollicis longus. The ulna of *Saltasaurus loricatus* (Powell, 2003; pers. obs. APB 2016) presents a developed scar toward the medial edge of the anterior face and the area of the attachment of M. abductor pollicis longus, which extends between two ridges formed by the distal attachment of the M. pronatus quadratus and the medial edge of the anteromedial process in distal.

- U_{ont}5: Radial ligament scar

In the anterior face of the ulnar distal end there is a common anterior projection in many sauropod taxa e.g. MPCA-PV-27174 referred to *Aeolosaurus* sp., IANIGLA-PVL-70-1 referred to *Mendozasaurus neguyelap* and PVL.4017-72 referred to *Satalsaurus loricatus*, and a triangle-shaped fossa next to it. This triangle-shaped area is associated with the development of radial ligament scar

and with the articulation of radial distal condyle. We can observe some differences in the degree of development of this area within the identified morphotypes of Lo Hueco. In type specimen and referred ulnae of *Lohuecotitan pandafilandi* + Morphotype I this area has a more common triangular fossa in the middle of distal anterior face of the ulna, The Morphotype II presents a triangular fossa more medially developed, delimited medially by a marked ridge delimiting the posteromedial part of the articulation . Laterally to this fossa there is sometimes a second ridge, connecting the M. pronatus quadratus medial ridge with the distal end. The ulna HUE-964 referred to *L. pandafilandi* does not present the marked ridges delimiting this distal triangular fossa. In the Morphotype II, the specimens HUE-3462 and HUE-4357 do not develop a clear separation of this fossa from the shaft surface in anterolateral, though this fossa can still be recognized. The absence or rudimentary triangular fossa in the anterior face of the distal end is considered the state 0 (the edges of the fossa are only poorly developed). The state 1, can be defined as the appearance of marked ridges at least in posteromedial, a rugose surface around the limits of the triangular fossa sometimes with a weakly rugose bone texture. These edges are remarkable and can be viewed even in poorly preserved distal ends as in the ulna HUE-3044 from *L. pandafilandi* holotype.

- U_{ont}6: Distal interosseous crest

The Morphotype II present a distal interosseous crest similar to that observed in other sauropods like *Vouivria damparіensis* (Mannion, Allain, & Moine, 2017) in spite of slightly shorter proximodistally. This ridge is associated with a curved distal part of the anteromedial edge, extendning from the anterior expansion of the distal end up to the interosseous ridge. Some specimens like HUE-3462 and HUE-4357 barely present this ridge. HUE-3462 has a small bump in this area. HUE-4357 is fragmentary and the area of where it should be present is poorly preserved. Nevertheless, this specimen lacks the noticeable concavity, dorsally and distally to the fractured area, as in other specimens with the developed crest. Lack of a marked crest or presence of a weak bump with smooth surface barely noticeable over the anterior projection of distal end is considered as state 0. While more or less developed crest with rugose surface, as it is easily observable in HUE-1158 and HUE-1338 is considered state 1.

VI.3.3. RADIUS CHARACTERS

- R_{ont}1: Rugosity of the proximal and R_{ont}2: Rugosity of the distal end of the radius.

These ends present a smooth surface in the specimen HUE-1166, which does not develop any rugose surface and tubercles and longitudinal grooves is considered as state 0. Meanwhile, the other specimens present markedly rugose ends with longitudinal small grooves all over the edge of the articulation. These specimens also have a significantly developed concavity in the surface of the proximal end. These features are considered as diagnostic of the state 1.

- R_{ont}3: Trochanter of the Mm. biceps brachii and humeroradialis

This small trochanter is recognizable in several sauropod taxa in the anteromedial face of the shaft right under the medial projection of the proximal end. This trochanter is associated with the attachment of the intersecting muscles that projects from the lateral distal end of the deltopectoral crest (Otero, 2018). Again, the specimen HUE-1166

presents a small concavity on this area instead of a proper trochanter or bulge and might be considered as state 0 relatable to least mature specimen. While the presence of this trochanter in the proximal part of the shaft, with a rugose surface is considered as state 1.

- R_{ont}4: Development of an interosseus ridge between Mm. pronatus teres and pronatus quadratus attachment in the posterior face of the radius

This ridge extends from a proximal interosseous ridge of the posterior face which articulates with the proximal radial fossa of the ulna. The specimen HUE-1340 have a weakly developed ridge, reduced to a smooth convexity in the proximal part, where the tendinous insertions with the ulna might have developed. The state 0 is characterized by a visible convexity but absence of a marked and acute ridge, and distal part of the ridge reaching the posterolateral edge of posterior face of the shaft. Both the largest specimens (HUE-1140), and the smallest specimen (HUE-1166) develop a marked and acute ridge, condition that is considered as state 1.

- R_{ont}5: Development of an interosseous ridge between the Mm. pronatus quadratus and supinator in the posterior face of the radius

The second major ridge extendning in the posterior face of the sauropod radius is placed at mid proximodistal length down to the posteromedial distal condyle. It is related with the development of the M. pronatus quadratus attachment and separates the area in which the M. supinator attachment in the anteromedial part of the radius under the M. humeroradialis trochanter (following Otero, 2018). This ridge is generally slightly developed in small specimens. The state 0, and least mature state, is characterized by the distal displacement of this ridge in the posterior face and a weak development, similarly to

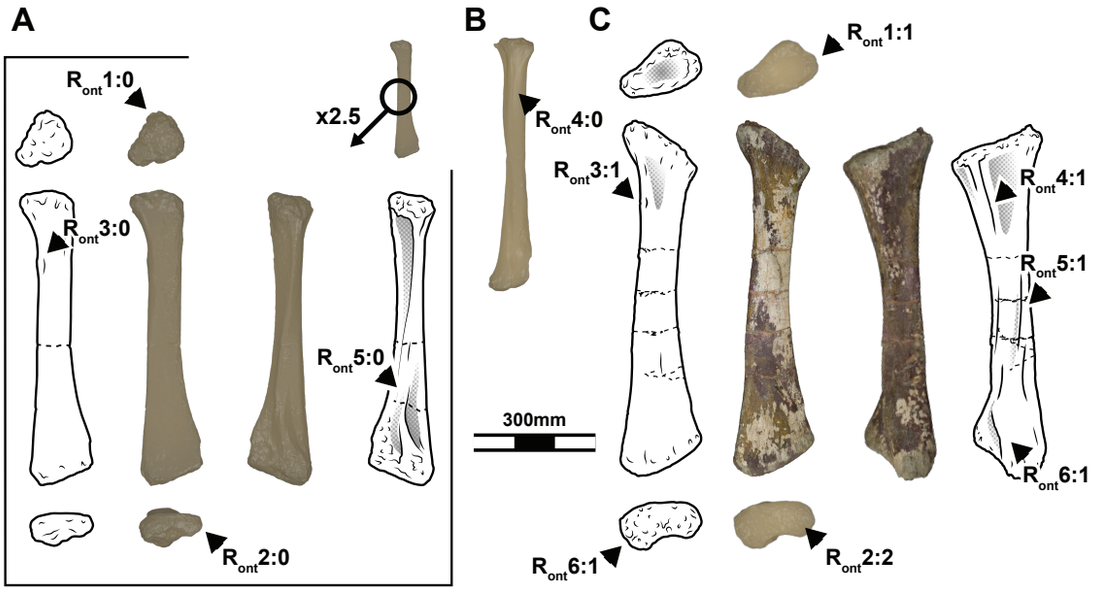

Fig.VI.8. Radial ontogenetic characters. (A) HUE-1166 mesh (x2.5 its scale) in proximal, anterior, distal and posterior view (B) HUE-1340 mesh in posterior view. (C) HUE-1140 in proximal, anterior, distal and posterior view.

the posterior proximal interosseous ridge. The ridge can also appear extendning up to proximal part of the shaft (e.g. HUE-1140, see Fig.VI.5), and is associated with the development of the posteromedial distal condyle (see below), which we consider as representative of state 1.

- R_{ont}6: Development of the posteromedial distal condyle articulation with the ulna in posterior face

The posteromedial distal condyle that articulates with the ulna presents also some differences between the smallest specimens of the sample, which present a less a developed crest, with a generally smooth bone surface and producing an acute curved ridge rather than the typical convexity seen in other sauropods (see Upchurch *et al.*, 2015). This morphology is considered as state 0. The specimen HUE-1140 presents a rugose and bulbous posteromedial distal condyle in posterior, with a wide convex surface and a marked and wide ridge ascending to proximal (see radial ontogenetic character #5). The presence of a robust distal crest dividing the insertion of the Mm. pronatus quadratus in distal and supinator and a bulbous posteromedial distal condyle is considered state 1.

VI.3.4. FEMUR CHARACTERS

- F_{ont}1: Rugosity of the proximal end and F_{ont}2: Rugosity on the distal end of the femur.

We observe several textural differences in the bone surface of the proximal and distal. There is also the presence of several specimens that might be related with early stages of development that show a smooth surface in proximal and distal ends, considered as state 0. The state 1 is the presence of a rugose area and a second derived most mature state 2 characterizes some specimens that develop longitudinal grooves along the edges of the proximal and distal end e.g. HUE-3108 from the type specimen of *Lohuecotitan pandafilandi*. The longitudinal grooves can be deep and some of them invade the intercondylar area in anterior and posterior faces of the distal end.

- F_{ont}3: Proximal edge of the greater trochanter and M. ilifemoralis attachment

The greater trochanter shows a stepped edge extendning from the femoral head up to the proximal part of the lateral bulge, probably related with the development of the proximal cartilaginous cap and the attachment of the M. iliofibularis on the lateral top of the greater trochanter connecting to said bulge. Some of the smaller specimens and those which have been discussed as probable putative juveniles (see Páramo *et al.*, 2014), lack this scar along the proximolateral edge of the greater trochanter(e-g- HUE-2636 and HUE-8801 referred to Morphotype I, HUE-10007 referred to Morphotype II). The absence is considered as state 0, as it may be related with less mature stages. The development of a small ridge for the muscular attachment or the presence of marked edge overhanging between the proximal of the greater trochanter and transition to the proximal of the latera bulge (e.g. HUE-594, see Fig.VI.9) isconsidered the state 1.

- F_{ont}4: Scar on the lateral bulge

The lateral bulge presents the attachment for Mm. pubioisquiofemoralis internus and externus especially visible in the first half of the proximodistal length. The most distal group of M. pubioischiofemoralis internus are developed in the proximal half of the lateral bulge (see Otero

& Vizcaíno, 2008; Gallina, 2011; Ullmann, Bonnan, & Lacovara, 2017). This attachment is hardly seen in smaller specimens, the lateral bulge has a smooth surface and characterizes the state 0. The presence of a a rugose lateral bulge with expansion of the anteroposterior width in the middle of the proximodistal length in lateral view is considered as the state 1.

- F_{ont}5: Scar of the M. ischiotronchantericus on the trochanteric shelf

The M. ischiotrochantericus attachment in sauropod dinosaurs attaches in the proximal part of the posterior face, in a ridge medial to the lateral edge of the shaft that is especially developed in titanosaurs as the trochanteric shelf. It has been proposed that this muscle attach to the trochanteric shelf for titanosaur sauropods based on observations in *Bonitasaura salgadoi* (Gallina, 2011). Some variation in the attachment of the M. ischiotrochantericus is present in the smaller specimens of the studied sample. The trochanteric shelf is lightly developed in smallest specimens, barely reduced to a longitudinal convexity parallel to the lateral bulge, more similar to the convexity present in non-titanosauriformes sauropods without a proper trochanteric shelf (e.g. *Camarasaurus* spp.; see in Ikejiri, 2004). We consider the less developed bump and light convexity under the greater trochanter as state 0 and probably related with least mature stages. It is important to consider taxonomic differences, as some specimens have shorter and less developed trochanteric shelf based between Morphotype II (shorter trochanteric shelf, e.g. HUE-594, HUE-1319) and Morphotype I (longer and robust trochanteric shelf, e.g. HUE-3108). The more mature state 1 is characterized by a well-developed trochanteric shelf, sometimes rugose or with a grooved texture in the surface of the bone (e.g. HUE-594, HUE-3108, see Fig.VI.6).

- F_{ont}6: Development of the fourth trochanter

The fourth trochanter is one of the major structures in the posterior face of sauropod femora (e.g. McIntosh, 1990a; Wilson & Sereno, 1998; Upchurch *et al.*, 2004). This trochanter is related with the attachment of the M. caudofemoralis longus as occur in several other dinosaurian clades (Hutchinson, 2002; Otero & Vizcaíno, 2008; Fechner, 2009; Gallina, 2011; Ibiricu, Lamanna, & Lacovara, 2014). This trochanter shows significant changes. The fourth trochanter can be a subtle protuberance on the posterior face and described as state 0, In the state 1, the fourth trochanter corresponds to a marked crest, posteriorly projected, with grooved bone surface and sometimes with longitudinal scars. Femora interpreted as belonging to more mature individuals present this state of the character.

- F_{ont}7: Development of the accessory trochanter of the M. caudofemoralis brevis

There is also a second trochanter in the posterior face of the femur near the midshaft of some specimens that can be related to the attachment of the M. caudofemoralis brevis as it extends laterally and parallel to caudofemoralis longus (Hutchinson, 2002; Otero & Vizcaíno, 2008; Gallina, 2011). The absence of the accessory trochanter is described as state 0 and probably related with least mature states (e.g. HUE-2636). On the other hand, the presence of this trochanter (state 1) is mainly observable in some specimens interpreted as belonging to mature individuals (e.g. HUE-2338, see Fig.VI.9). However, some specimens referred to possible mature individuals lacks this structure (e.g. HUE-3108).

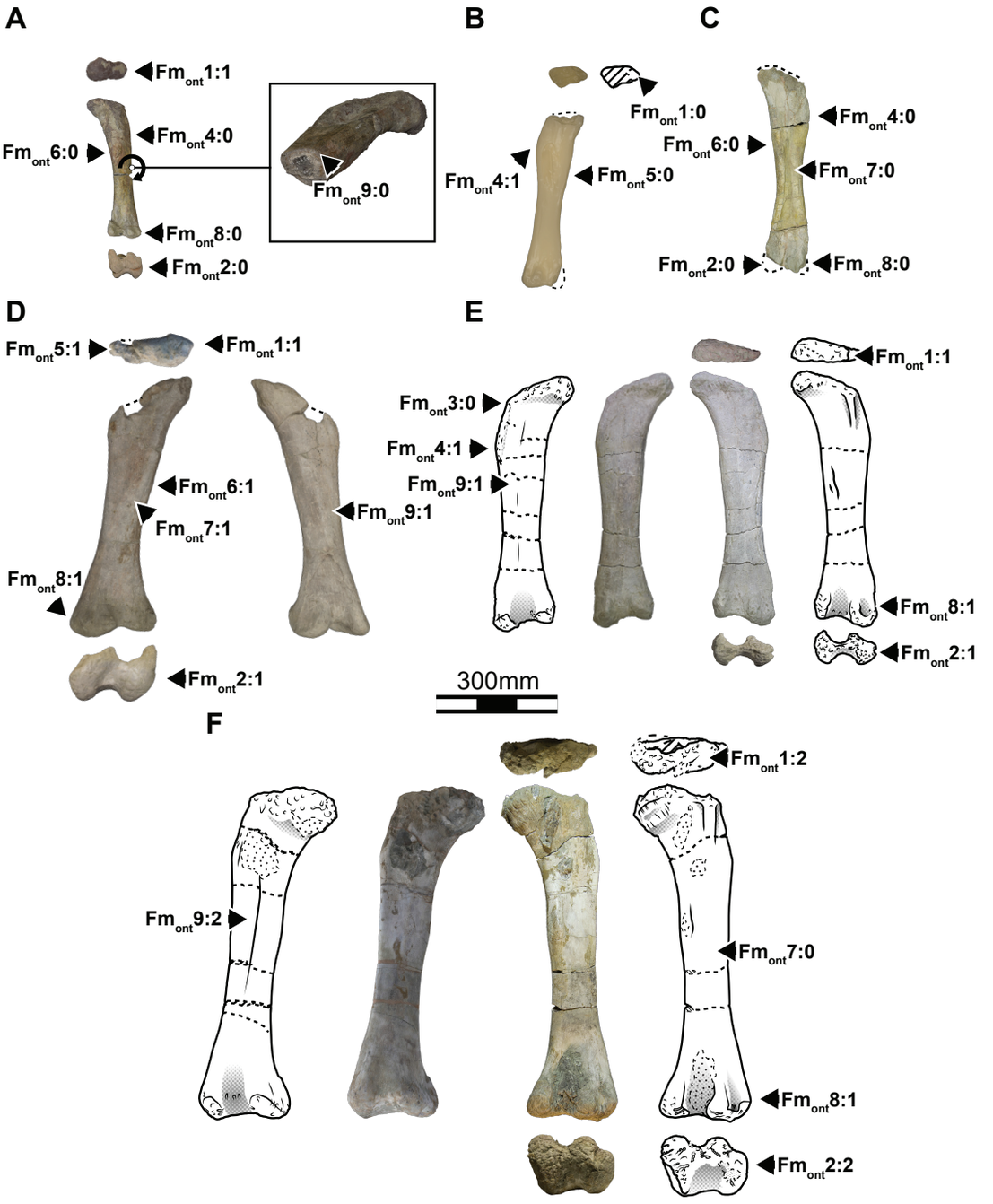

Fig.VI.10. Femoral ontogenetic characters. (A) HUE-2636 in anterior view. (B) HUE-8801 mesh in proximal and anterior view. (C) HUE-10007 in anterior view. (D) HUE-2338 in proximal, anterior, distal and posterior view. (E) HUE-1319 in anterior, proximal, posterior and distal view. (F) HUE-3108 in anterior, proximal, posterior and distal view.

- $F_{ont}8$: Development of the lateral epicondyle

The lateral part of the fibular condyle is related with the attachment of the Mm. gastrocnemius group (Otero & Vizcaíno, 2008; Gallina, 2011). The Mm. gastrocnemius group probably occupies the fossa resulting from the proximodistal ridges located over the fibula condyle and the lateral epicondyle. The epicondyle is always present in our sample, but it can be a smooth and lightly developed convexity projected to posterior or posterolateral like in HUE-2636 and considered state 0. Other specimens present a marked projection of the condyle with associated longitudinal grooves in the lateral edge and a deep fossa between the epicondyle and the condyle posterior projection and it is considered state 1 and probably related with more mature development. This morphology coincides with the presence of a more rugose distal end (see Font2).

- $F_{ont}9$: Development of the linea intermuscularis cranialis

The linea intermuscularis cranialis is present in both morphotypes of Lo Hueco. This linea located on the middle of the lateromedial width of the anterior face separates the Mm. femorotibialis group. This scar is absence of this ridge, or reduction to a light convexity difficult to observe in some specimens (e.g. HUE-2636, HUE-1357), which is considered as state 0. The presence of a weak linea that it is only developed in part of the proximodistal height is referred to the state 1 (e.g. HUE-1319, HUE-2338; see Fig. VI.9). Other specimens exhibit a marked ridge projecting over the middle of the anterior face of the femur (state 2: e.g. HUE-3108) and similar to the one described in other sauropods e.g. *Saltasaurus loricatus* (see Powell, 2003; D'Emic, 2012).

VI.3.5. TIBIA CHARACTERS

- $T_{ont}1$: Rugosity on the proximal and $T_{ont}2$: Rugosity on the distal end of the tibia.

The proximal and distal end of the tibia present an extended development of rugosities and coarse bone texture with increasing mammillae probably related with ontogenetic changes. As was referred in other elements (see above), these rugosities are related with the development of the cartilaginous cap which has a direct relationship with the ontogeny of the individual. In the current studied tibiae however, the entire sample present some degree of rugosity in the proximal and distal ends even in the smallest specimens. Other authors have identified specimens at probable early ontogenetic stages with smooth surface on the proximal and distal ends of the tibiae (Carpenter & McIntosh, 1994; Martin, 1994b; Curry Rogers *et al.*, 2016) so we consider this condition as state 0 following those observations and similarities in other types of elements also described in this study. The presence of a rugosity, mammillae and longitudinal sulcus around the edge of the proximal and distal end is considered as state 1.

- $T_{ont}3$: Scar of the Mm. iliotibialis + ambiens + Mm. femorotibiales on the proximal part of the cnemial crest

This complex muscular attachment is developed in the proximal half of the cnemial crest in proximal or proximolateral view (Borsuk-Bialynicka, 1977; Otero & Vizcaíno, 2008; Gallina, 2011). This attachment results in a small plateau or a slightly flat and rugose area on the proximal part of the crest in continuity with the surface of the proximal end. Some specimens lack the

rugosity and present a narrower proximal portion of the cnemial crest (e.g. HUE-4344). This is and considered as state 0. While more mature the state 1 is represented by specimens with a wide proximal half of the cnemial crest and an associated lateral small swelling (e.g., HUE-3082, type specimen of *Lohuecotitan pandafilandi*). This morphology is interpreted as referable to more mature stages in the ontogenetical development.

It is important to note that this small plateau is observable in many titanosaur sauropods but can present some taxonomic differences. Some taxa develop this area in proximal view e.g. *Laplatasaurus araukanicus* (MLP-CS-1128; pers. obs. APB 2016) or present a weakly engrossed edge e.g. *Mendozasaurus neguyelap* (IANIGLA-73-3, IANIGLA 74-1; pers. obs. APB 2016). Other taxa may present a plateau in the proximal half of the cnemial crest inclined slightly in the in the proximal toward medial face, at the proximal edge of the cnemial crest e.g. *Lirainosaurus astibiae* (MCNA-13860; pers. obs. APB 2014). All of these morphologies are related to the same muscular group attachment. The presence of a marked and probably rugose edge in the proximal half of the cnemial crest is considered the state 1.

- T_{ont}4: Scar of the Mm. femorotibialis + M. tibialis anterior in the middle to distal part of the cnemial crest

The distal half of the cnemial crest corresponds to the limit of the insertion of Mm. femorotibialis (the insertion of this muscle also occupies the proximal half of the cnemial crest) and also for the insertion the M. tibialis anterior responsible for the adduction of the metatarsals (connecting the external edge of the proximal end of the metatarsals, e.g. Gallina, 2011). The attachment of the M. tibialis anterior is slightly different in both morphotypes from Lo Hueco. In the Morphotype 1 + *Lohuecotitan pandafilandi* this attachment surface has some rugosities and the edge over the distal half of the cnemial crest lateral fossa as in other sauropods with lateromedially narrow cnemial crest e.g. *Bonitasaura salgadoi* (MPCA-468 Gallina, 2011; pers. obs. APB 2016) and *Lirainosaurus astibiae* (MCNA-13860, pers. obs. APB 2014). The Morphotype II presents a wide lateral trochanter from the midpoint to distal half of the cnemial crest. The presence of this trochanter can also be considered that the inference of this muscle attachment is level I like in *Neuquensaurus australis* (Otero & Vizcaíno, 2008; see distal cnemial crest on Otero, 2010; pers. obs. APB 2016) and *Bonatitan reigi* (MACN-PV-RN-1061; pers. obs. APB 2016). The presence of a small trochanter can be also variable in each morphotype, some specimens in Morphotype I present a small bump on the lateral face of middle cnemial crest (e.g. HUE-1573). The absence of rugosity or grooved surface texture on this area (e.g., HUE-1165), or lack of a marked trochanter the cnemial crest distal half reduced to a narrow lamina in lateromedial, is considered the state 0. While the appearance of striate or groove marks as well as the presence of a marked ridge or trochanter toward lateral face (e.g. HUE-2117) is considered the derived state 1.

- T_{ont}5: Ridge under the lateral articulation with the fibula

Some sauropod taxa presents a ridge under the lateral articulation with the fibula in proximal end, and shared in both taxa from Lo Hueco. This ridge is referrable to the proximal articulation with the fibula in lateral and delimits the posterior edge of the cnemial crest lateral fossa. This ridge is also related with the articulation of the anterior process of the fibula, and is especially developed in *Lohuecotitan pandafilandi*, which present a secondary cnemial crest (following Bonaparte, W.-D.

Heinrich, & Wild, 2000; see Chapter IV, Chapter V) in the tibia and an associated and characteristic medial deflection of the anterior trochanter of the fibula (Díez Díaz *et al.*, 2016; see Chapter IV and V). Some changes are observed in this ridge that is barely developed in some of the smallest specimens (e.g., HUE-1165), which is present a little stepped morphology between the cnemial crest lateral fossa and the shaft, with smooth bone surface and considered as state 0. The presence of a marked and acute step between the cnemial crest lateral fossa and the shaft, with small bump in lateral face (e.g., HUE-4344, HUE-1149) or the presence of a fully developed secondary cnemial crest in Morphotype I (e.g. HUE-3082, the type specimen of *L. pandafilandi*) are considered as state 1.

Note that we considered the possible taxonomical differences in the presence of a secondary cnemial crest, and the absence in many sauropod taxa. Therefore, we only considered the presence of a marked bump in the shaft or fully development of this feature in the same state (e.g. HUE-4344 and HUE-3082 among Morphotype I). Also, not all sauropods that present this secondary ridge, making difficult to assess a further state of the character, as it can be present as the secondary cnemial crest of *L. pandafilandi* (see Chapter IV and V), *Lusotitan atalaiensis* (Mannion *et al.*, 2013; Mocho, Royo-Torres, & Ortega, 2016) and

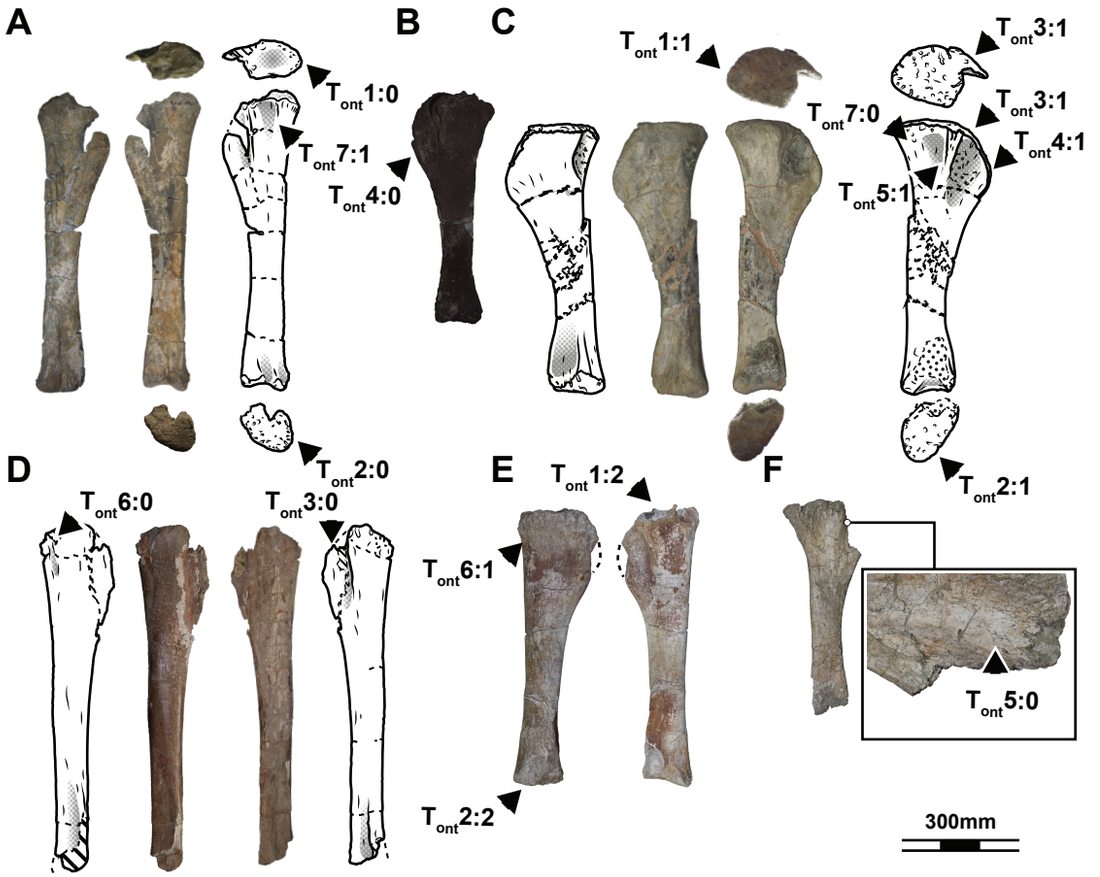

Fig. VI.11. Tibial ontogenetic characters. (A) HUE-1149 in medial, proximal, lateral and distal face. (B) HUE-1165 in lateral face. (C) HUE-3082 in medial, proximal, lateral and distal face. (D) HUE-1612 in medial and lateral face. (D) HUE-1573 in medial and lateral face. (F) HUE-4632 in lateral face.

Janenschia robusta (Bonaparte *et al.*, 2000; Mannion *et al.*, 2019) differ from the marked double ridge of *Diamantinasaurus matildae* (Poropat *et al.*, 2015 not considered a secondary cnemial crest). Based on these observations, we decided that our definition is based solely the fibular articulation of the fibula and related to possible ontogenetic differences on its development.

- T_{ont}6: Attachment of the posterior Mm. flexores and gastrocnemius of the tibia in posterior of the proximal medial face

There is a small concave rugose surface in the posterior proximal part of medial face of the tibia in both taxa from Lo Hueco. This small area have been proposed as the attachment of Mm. flexores (Otero & Vizcaíno, 2008) and part of the Mm. gastrocnemius (Borsuk-Bialynicka, 1977; Otero & Vizcaíno, 2008; contra Gallina, 2011). We observe that some specimens (e.g., HUE-1149) present a smooth concave surface barely recognisable and considered as state 0. Other specimens present a rugose surface or the presence of a small lamina or bump (e.g. HUE-1500), but there is an especially prominent ridge in the Morphotype II (e.g. HUE-2117) and both are referred as state 1

- T_{ont}7: Posterior proximal secondary crest and fossa on the lateral face

The Morphotype II does not present a secondary cnemial crest but instead present a proximal seconday crest and a small fossa between the fibular articulation and this secondary crest on the lateral face. The absence of this secondary crest (e.g. HUE-1612) in the posterior lateral face of the proximal end is considered state 0. This feature also presents some differences between the morphotypes as it is absent in *Lohuecotitan pandafilandi* + Morphotype I except for the probable presence in specimen HUE-1573. This specimen does not preserve the edge of the proximal end but present the lateral fossa posterior to the secondary cnemial crest and small bump that could be the distalmost part of this crest. The larger specimens present a fully developed crest in the lateral edge of the proximal end, and a short and acute ridge in lateral face, considered as state 1.

VI.3.6. FIBULA CHARACTERS

- Fb_{ont}1: Rugosity on proximal end and Fb_{ont}2: Rugosity on the distal end of the fibula

Similar to other appendicular elements herein described, the proximal and distal end might present some morphological variations in the rugosity and development of longitudinal sulcus in the edge of the proximal and distal edges. The fibula does not present development of mammillae in the rugosity of the proximal and distal end contrary to other elements. Similarly to the tibiae analysed in this study, few of them present a smooth surface that suggest earlier ontogenetic stages among the smallest specimens (slightly smooth proximal end in HUE-1520; contra the femora, e.g. HUE-2636, HUE-8801). A smooth surface of the proximal and distal end without marked sulcus in the edge is considered the state 0. The presence of a rugose proximal or distal end with longitudinal striation or sulcus in the edges (e.g. HUE-1570, HUE-3087, see Fig. VI.10) are considered the state 1.

- Fb_{ont}3: Rugosity on the anterior trochanter in the anterior to lateral face

The anterior trochanter develops in the lateral face anteriorly projected and slightly deflected in most sauropods, but some taxa present a medial deflection of this structure e.g. *Lohuecotitan pandafilandi* + Morphotype I, (this study). There is two different hypothesis on the attachment

of the M. iliofibulares, some authors propose the insertion in the anterior trochanter (Borsuk-Bialynicka, 1977; Wilson & Sereno, 1998) while other authors argue that this muscle attach more laterodistally in the lateral trochanter (Hutchinson, 2002; Otero & Vizcaíno, 2008) instead of the anterior crest (Borsuk-Bialynicka, 1977; Wilson & Sereno, 1998). We accept the latter hypothesis and consider that the development of the anterior trochanter is related with the articulation of the tibia. The differences on the texture of this surface among the sample of Lo Hueco can be related with the development of the tendinous connections of this articulation (see articulation in Bonaparte *et al.*, 2006; D'Emic & Wilson, 2011) and attachment of some muscles like M. ambiens (see subdivision in five different heads in the tibia + fibula in the bird line Hutchinson, 2002). The trochanter may present a smooth surface with almost no separation between the concave anterior surface of the trochanter and the shaft (e.g. HUE-5232 in proximal anterolateral view) and considered state 0. The development of a rugose surface and the presence of a small bump between the trochanter and the lateral of the shaft (e.g. HUE-1612) or the development of a stepped morphology and the anterior sulcus in Morphotype 1 + *L. pandafilandi* (e.g. HUE-1476, HUE-3087) are considered the state 1.

- Fb_{ont}4: Development of the M. iliofibularis attachment

The lateral trochanter of the fibula is related with the attachment of the M. iliofibularis which inserts to the postacetabular lobe of the ilium and the lateral trochanter (Hutchinson, 2002; Otero & Vizcaíno, 2008). It can be observed some variation between both morphotypes of Lo Hueco and among each morphotype that is not probably related only to ontogenetic development. An initial stage (state 0) is characterized by a shallow and single lateral trochanter with a smooth bone surface (e.g. HUE-1520, HUE-2804, see Fig. VI.10). The state 1 is marked by a developed lateral trochanter with rugose surface, anteroposteriorly wide and oval-shaped in *Lohuecotitan pandafilandi* + Morphotype 1 (e.g. HUE-3087; see Fig. VI.10) or an acute ridge projecting far from the surface of the shaft in lateral face (e.g. HUE-1612, HUE-2806; see Fig. VI.10). We also consider a state 2 referred to the development two bifurcated ridges and a grooved surface over the bone (with visible longitudinal striation) in the middle of the lateral trochanter of the fibula (e.g. HUE-1513, HUE-1570).

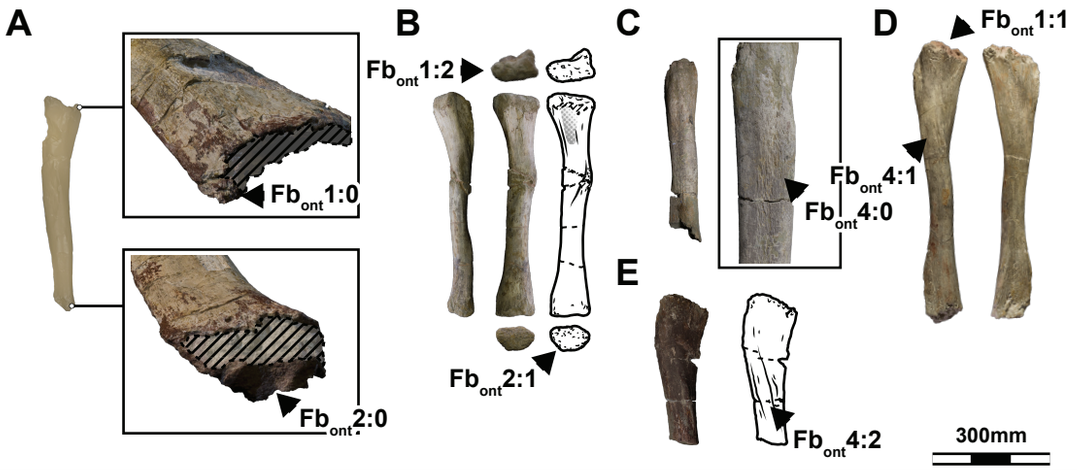

Fig. VI.11. Fibular ontogenetic characters. (A) HUE-5232 in lateral view. (B) HUE-3087 in anterior, proximal, lateral and distal view. (C) HUE-2904 in lateral view. (D) HUE-2806 in lateral and medial view. (E) HUE-1513 in lateral view.

- $Fb_{ont}5$: Development of the tibial scar

The tibial scar is commonly present in sauropod fibula in the posteroproximal part of the medial face. This structure is related with the articulation of the tibia similar to the anterior trochanter and is related with the development of articular cartilage and various tendinous insertions (Borsuk-Bialynicka, 1977; Bonaparte *et al.*, 2006). However, this structure is sometimes absent in Morphotype II, probably not related with ontogenetic development (e.g. HUE-1146). The absence of tibial scar in the posterior medial face is considered as state 0. In the specimens referred to *Lohuecotitan pandafilandi* + Morphotype I we found a weakly developed type, barely marked concavity on the surface of the tibial scar and considered state 0, relatable to least mature stage. The state 1 is defined by the development of triangular tibial scar on the medial face of the proximal end, with a the typical concavity between the posterior edge up to the anterior trochanter (e.g. HUE-3075). Some specimens develop a marked accessory ridge in the proximal end defining the posterior edge of the tibial scar and the concavity related to this structure (e.g. HUE-1570, HUE-2426 visible in proximal view despite the sediment) which is considered as state 2.

Note that Morphotype II has some variation in this scar as commented before. They show a much less developed tibial scar in general (see Chapter V) but there are specimens representatives of this feature in all the described states (e.g. HUE-1175, HUE-1612, HUE-2669).

- $Fb_{ont}6$: Development of the M. fibularis brevis insertion

The anterolateral crest of the distal end has been related to the attachment of the M. fibularis brevis (Gallina, 2011) among the distal extensor muscle group. This crest shows some taxonomic differences related on its orientation respective to the lateral or medial face of the shaft, but they do not differ greatly in relationship to the definition of the current ontogenetic character. Some specimens present a smooth surface in the lateral and medial face of the anterolateral crest in continuity with the surface of the shaft (e.g. HUE-1175) and is considered state 0. The anterolateral crest may present a weak concavity in lateral face and the development of a rugose crest in anterior face (e.g. HUE-2806, Fig.VI.10) or a much more wide edge in anterior view (e.g. HUE-1476, HUE-3087; Fig.VI.10) and both conditions are considered as state 1 and observable in larger specimens with feature combination probably related to more mature stages.

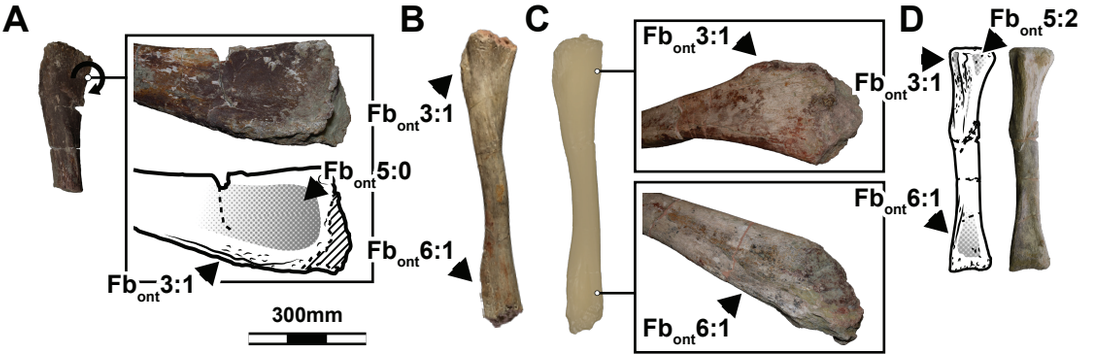

Fig.VI.12. Fibular ontogenetic characters. (A) HUE-1513 in lateral and medial view. (B) HUE-2806 in lateral view. (C) HUE-2669 mesh in medial view (details of the actual specimen). (D) HUE-3087 in medial view.

Possible Characters and Semaphoronts excluded

During the preliminary stage of this analysis, our observations in several ontogenetical series (Carpenter & McIntosh, 1994; Martin, 1994b; Lehman & Coulson, 2002; Ikejiri, 2004; Curry Rogers, 2009; Curry Rogers *et al.*, 2016) allow us to consider several other characters already described with possible variation during sauropod growth.. However, based on in the studied sample and their codification, some have been excluded due uncertainties and little or no variations across sampled specimens. Some of these characters have also been excluded based on a high proportion of missing information due preservation status of the sample from Lo Hueco, as including them can be problematic.

One of these problematic characters observed in more basal sauropods is the bifurcation and expansion of the anterior medial condyle in the humerus into the radial and ulnar ramus. Changes during ontogeny have been reports in this feature for several other sauropod taxa (e.g. Carpenter & McIntosh, 1994; Bonnan, 2004, 2007). However, bifurcation of the medial condyle is not present in all sauropods, only some present a markedly bifurcated anterior distal medial condyle *Haestasaurus becklesii* (Upchurch *et al.*, 2015), *Camarasaurus* grandis specimen YPM-1908 (Carpenter & McIntosh, 1994) and *Brontosaurus parvus* specimen UW-15556 (= '*Apatosaurus excelsus*', Gilmore, 1936). We report few changes in this character for the sequences given in each morphotype of Lo Hueco. The lack of preservation of this area difficult the correct assessment in the entire sample. Only minor differences can be reported in the better-preserved specimens but not resulting in noticeable changes in the character scoring.

Other taxa show post-hatchling increase in the bifurcation of medial condyle of the humerus, from no bifurcation as in the juvenile individual referred to *Apatosaurus* sp. (OMNH-1277), and *Brontosaurus excelsus* (= "*Apatosaurus* excelsus") and the left and right humerus of CM-566, Carpenter & McIntosh, 1994). While other more mature individuals present bifurcation of this condyle as in *Apatosaurus* sp. specimens OMNH-1275 and OMNH-1278 (Carpenter & McIntosh, 1994). A variation in the projection of the distal medial condyle is also discussed based on the juvenile material referred to *Astrodon johnsoni*, which does not present bifurcation (Carpenter & Tidwell, 2005). But A. johnsoni is only known from juvenile individuals and it may seem temptative to report differences in the ulnar and radial distal condyles compared to other Titanosauriformes as effect of ontogenetic development.

The lack of bifurcation in the medial condyle in the morphotypes of Lo Hueco seems to be related with the absence of this feature in most titanosaurs (see Upchurch *et al.*, 2015). There is no much variation in the development of this structure in each morphotype. Besides Morphotype I present a much more prominent medial condyle (see Chapter V) we found no significant differences that could be referred to ontogenetic development in neither of the morphotypes. This character was excluded from the performed analysis. improving the resolution of the recovered topology especially for Morphotype II, reducing the number of MPTs from 68 to 37 trees.

Other character considered initially was the tendinous attachment of M. triceps brachii which produces a rugose and crest-like edge in the olecranon process of some ulnae e.g. *Opisthocoelicaudia skarzynskii* (Borsuk-Bialynicka, 1977), *Saltasaurus loricatus* (e.g. PVL-4017-72; pers. obs. APB 2016), *Diamantinasaurus matildae* (Poropat *et al.*, 2015) and *Venenosaurus dicrocei* (Tidwell & Wilhite, 2005), among others (see also Remes, 2007; Otero, 2018). The morphology of

this insertion can be variable along post-natal ontogeny as discussed in other sauropods (Ikejiri, 2004; Tidwell & Wilhite, 2005). It has been recognized that juvenile specimens present a smooth surface in posterior face of the olecranon, and more adult individuals present a ridge or marked edge along the posteromedial fossa in proximal as part of the rugosity of the olecranon in proximal view (e.g. Tidwell & Wilhite, 2005). However, this variation is not observed in the sample from Lo Hueco. These stages are only recognized in some specimens referred to Morphotype I: (i) HUE-1103, which preserves a smooth surface; (ii) a proximal posteromedial edge in the of HUE-964 but it is fragmetary (iii) a fully developed edge with rugose texture and the deep proximodistal sulcus in HUE-1137 (= G1-C-187). A combination of poor preservation of this part of the ulnar proximal end across the sample of Lo Hueco might add unnecessary noise to the analyses. Besides the referred specimen above, this character is excluded from current study.

		Weights				
Morphotype	Semaphoront	Humerus	Ulna	Femur	Tibia	Fibula
Morphotype I	Semaphoront 1	1.00	2.00	0.63	1.00	0.83
	Semaphoront 2	0.55	1.17	0.75	2.43	2.67
	Semaphoront 3	0.73	1.17	1.75	1.00	0.83
	Semaphoront 4	0.36	0.33	0.75	2.00	1.00
	Semaphoront 5	1.36		1.75	1.29	0.67
	Semaphoront 6			0.88	1.00	0.50
	Semaphoront 7			1.00	0.43	1.67
	Semaphoront 8			1.00	1.43	1.67
	Semaphoront 9			2.00		
	Semaphoront 10			1.00		
	Semaphoront 11			0.88		
Morphotype II	Semaphoront 1	2.91		1.00	0.86	1.83
	Semaphoront 2	2.45		1.00	1.86	1.67
	Semaphoront 3	0.64		0.50	1.00	0.67
	Semaphoront 4	2.09		1.50	1.00	1.00
	Semaphoront 5	2.73		0.63	1.00	0.67
	Semaphoront 6	0.73	NA	0.88	1.14	0.83
	Semaphoront 7	1.00		1.00	1.14	1.00
	Semaphoront 8	0.55		0.88		0.83
	Semaphoront 9	2.09		0.88		0.83
	Semaphoront 10	0.82				1.00
	Semaphoront 11	1.00				1.00

Table.VI.7. **Semaphoronts defined in this study for each morphotype.** Weight = evidence weight calculation for each semaphoront following Griffin *et al.* (2016)

VI.4. RESULTS

VI.4.1. ONTOGENETIC MPTS AND CONSENSUS

A heuristic search of the ontogenetic data matrices was performed. If more than a single MPT (i.e. a single resolved tree with juvenile as root → adult), we estimated a 50% Majority Rule of the available trees. For the reverse (mature as root → juvenile) there was no need to establish a consensus as they are only used for tracing the OSA diagrams.

In the case of the appendicular elements referred to Morphotype I, the heuristic search yielded the following results. One MPT was recovered for humerus dataset in the normal search and two MPTs on the reversed one. For the ulna dataset, one MPT for the normal search and one MPT for the reversed search. 32 MPTs were recovered based on the normal search of the femur dataset and eight MPTs on the reversed one. The normal search on the tibia data matrix recovered ten MPTs and the reverse search yielded three MPTs. Finally, based on fibula dataset, the normal search and the reverse one resulted both in one MPT.

The analysis was also performed on the forelimb and hindlimb elements referred to the Morphotype II. Three MPTs after the normal search and 16 MPTs after the reversed search were found for the humerus dataset. The analyses performed on the ulna dataset resulted in one MPT after the normal search and one MPT after the reversed one. For the femur dataset, five MPTs were recovered on the normal search and one MPT in the reversed one; for the tibia dataset, nine MPTs after the normal search and two MPTs after the reversed one; and finally for the fibula dataset, three MPTs from the normal search and eight MPTs from the reversed one.

For estimating the OCSA stage sensu Brochu (1996) we conducted the consensus (Majority Rule 50%) also within TNT v1.1 (Goloboff, Farris, & Nixon, 2008b) for the recovered solutions with more than one MPT. The performed consensus tree over the ontogenetical sequences can be accessed in Supplementary Material VI.D. The ontogenetical stages obtained, as well as, the specimens representative of the earliest and latest ontogenetic stages can be accessed in table 3. All the MPTs resultant from the heuristic searches are available in Supplementary Material VI.G.

VI.4.2. OSA DIAGRAMS

The OSA reticulate diagrams are built based on the information obtained in the MPTs of the normal rooted and the reversed searches. The weight of the semaphoronts were calculated following Colbert & Rowe (Colbert & Rowe, 2008; after Griffin & Nesbitt, 2016b; see also Methodology). The modal sequence weight is calculated with the cumulative weights of the semaphoronts present in all the possible sequences. A summarized OSA reticulate diagram of each type of appendicular bone (humerus, ulna, radius, femur, tibia and fibula) were obtained for Morphotpye I + *Lohuecotitan pandafilandi* (see Fig.VI.13 and 14) and Morphotype II (Fig.VI.15 and 16). An expanded version indicating the semaphoront identity and the character changes in each path can be seen in Supplementary Material E. The Morphotype I + *L. pandafilandi* presents a polymorphism of five ontogenetical sequences of the humerus and present a modal ontogenetic sequence (Fig.VI.13.A) with 68.18% of the support weight. The ulnae are not polymorphic with only one ontogenetical sequence found (Fig.VI.13.B). The femora show a total of 37 possible ontogenetic sequences (Fig.VI.14.A) with the modal accounting for 64.65% of support weight. The tibiae present a polymorphism of 18 possible ontogenetical sequences (see Fig.VI.14.B) and the modal sequence account 77.03% of support weight. Finally, the fibulae have only three possible sequences (Fig.VI.14.C) and the modal sequence account for 73.85% of the support weight.

The Morphotype II on the other hand presents a polymorphism of 42 possible ontogenetic sequences on the humerus with the modal sequence (Fig.VI.14.A) accounting for 66.84% of the support weight. The ulnae present three possible sequences (Fig.VI.14.B) with a modal sequence represented by 100% of the support weight. The femora present a polymorphism of 56 ontogenetic sequences (Fig.VI.15.A) with a modal sequence accounting for 60.32% of the support weight.

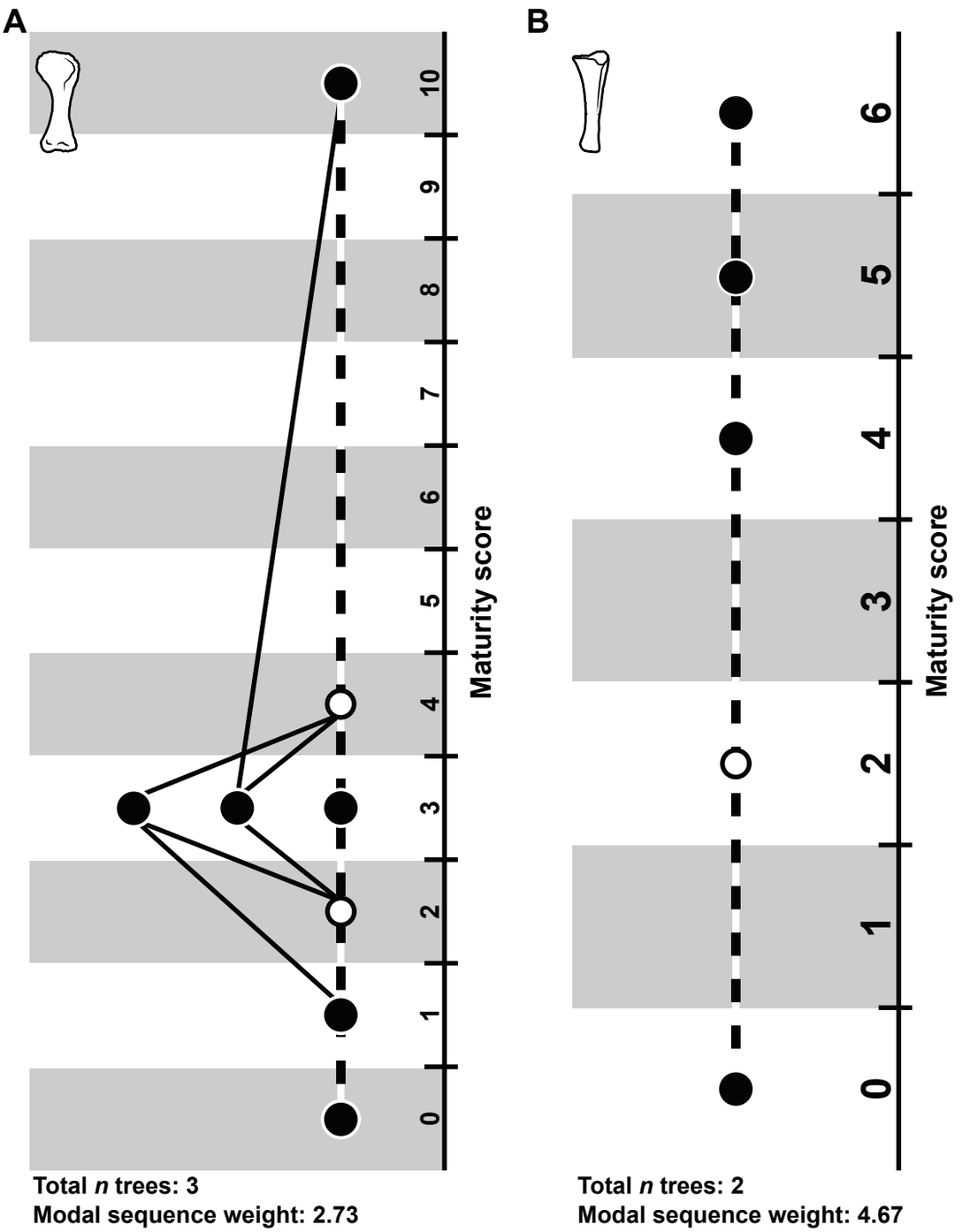

Fig.VI.13. Morphotype 1 forelimb elements ontogenetic sequence analysis results. (A) Humeri OSA. (B) Ulnae OSA.

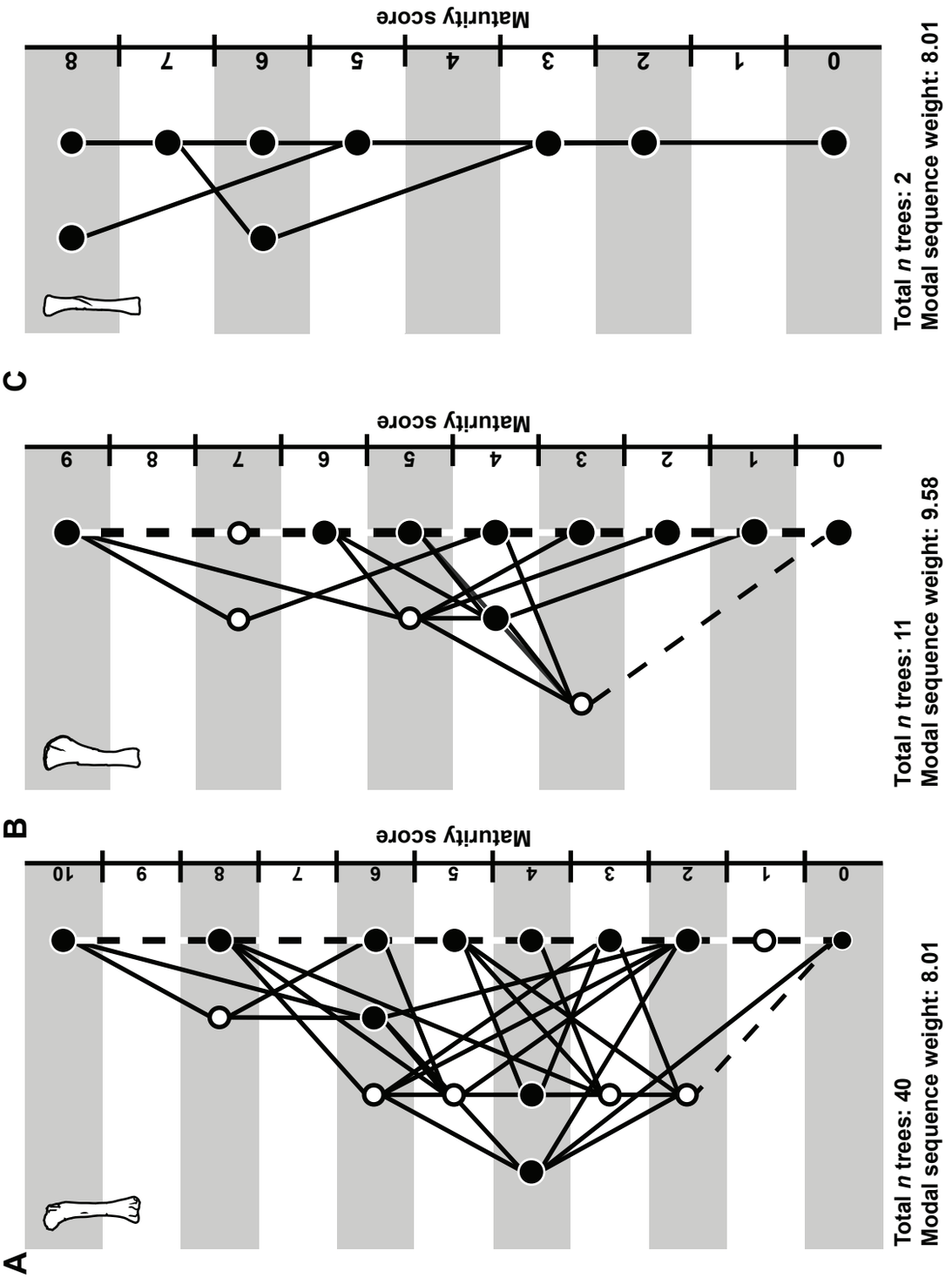

Fig.VI.14. Morphotype I hindlimb elements ontogenetic sequence analysis results. (A) Femora OSA. (B) Tibiae OSA. (C) Fibula OSA.

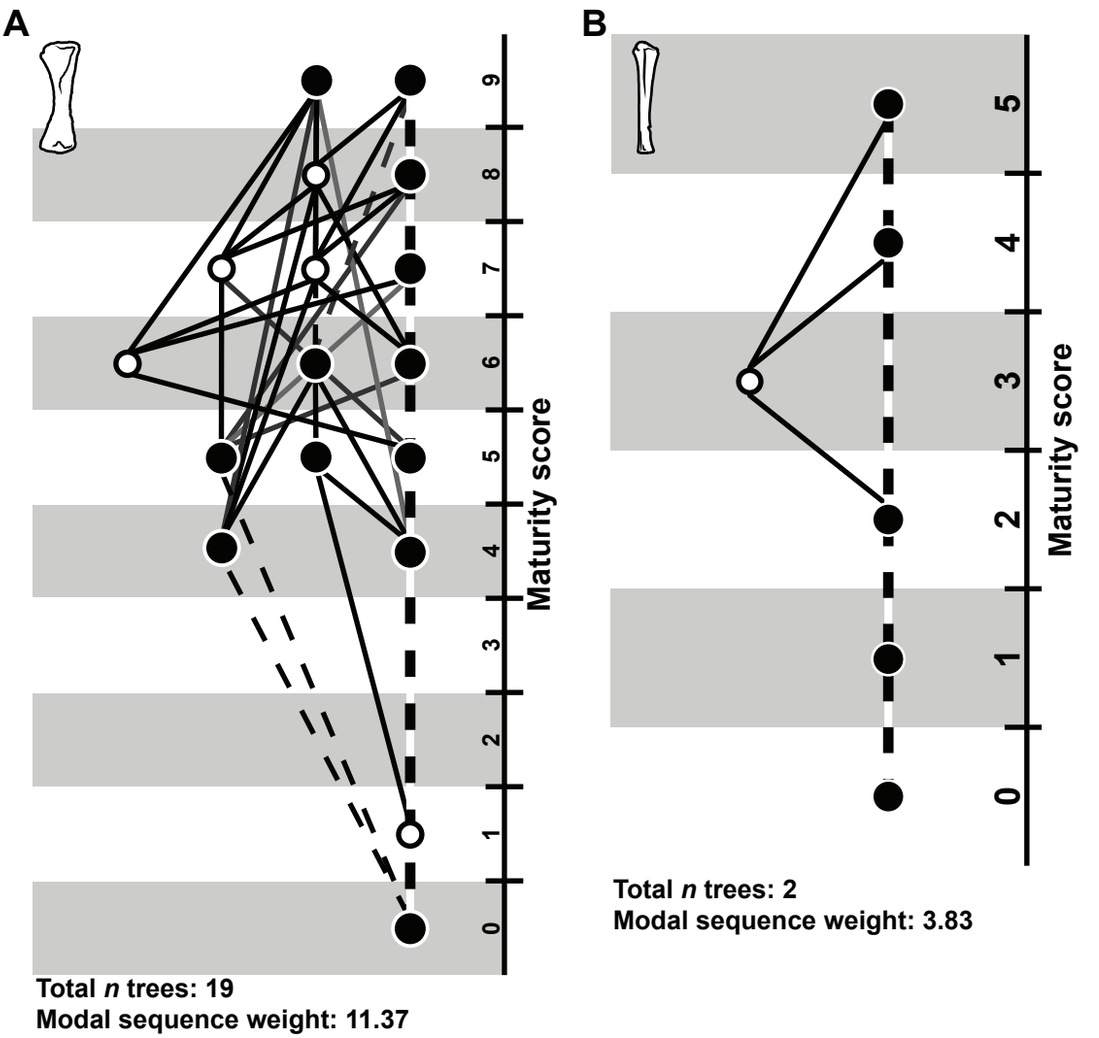

Fig.VI.15. Morphotype II forelimb elements ontogenetic sequence analysis results. (A) Humeri OSA. (B) Ulnae OSA.

While the tibiae present 53 possible ontogenetic sequences (Fig.VI.15.B) with the modal sequence accounting for the 89.29% of the support weight. The fibulae show a polymorphism of 45 possible sequences (Fig.VI.15.C) with the modal sequence accounting for 59.46% of the support weight.

VI.4.3. TITANOSAUR PHENOTYPE CLUSTERS FROM LO HUECO

We performed the cluster analysis over the phylogenetic character data matrices in order to see if there are intraspecific variability affecting those characters and assess possible ontogenetic patterning. Cluster analysis of Gower dissimilarity metric is presented with the MOS estimated by OCSA method and the length of the specimen. We coloured the clusters only for better visualization of closer sub-clusters and these colours are not based in any particular metric.

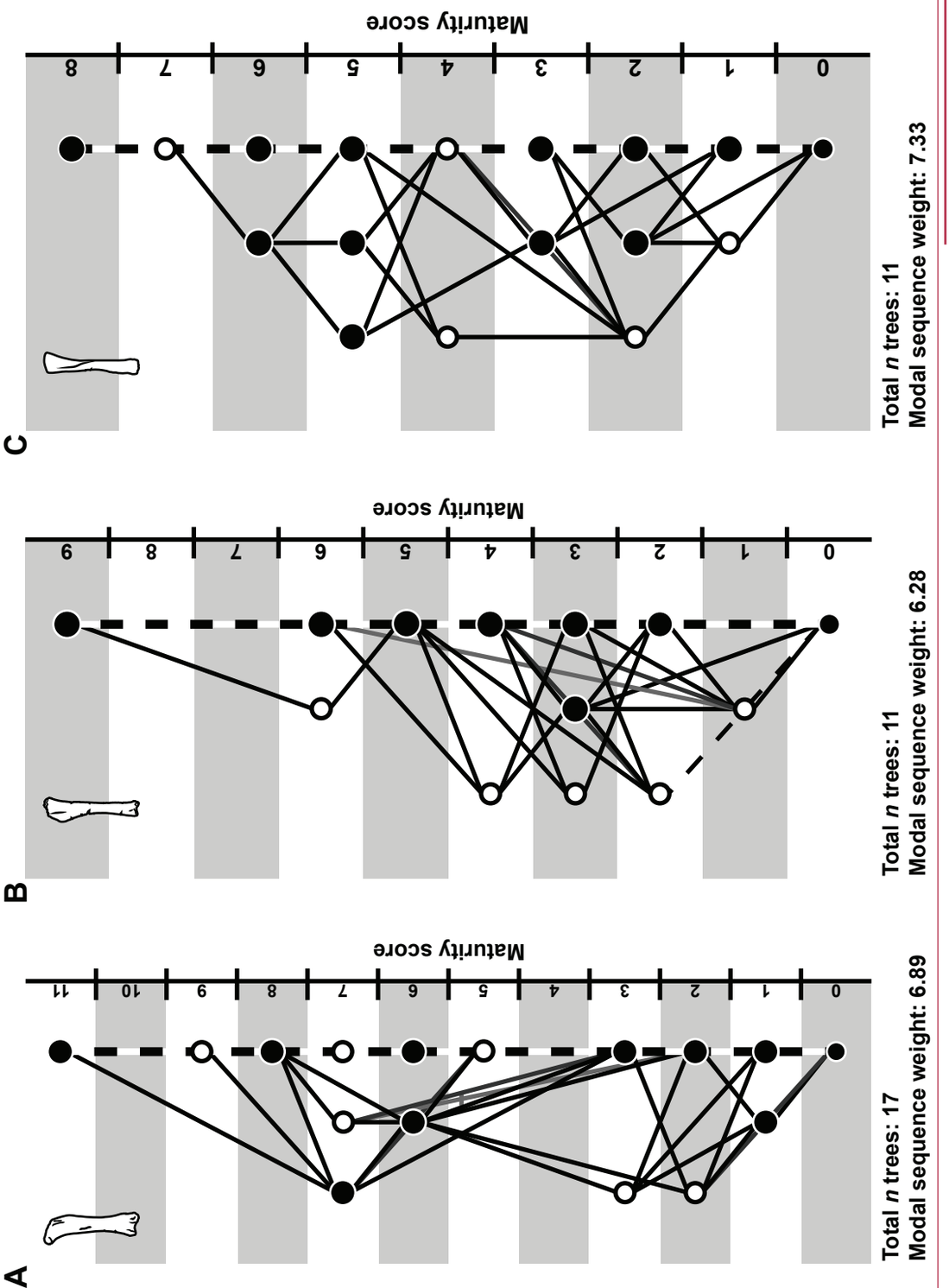

Fig. VI.16. Morphotype II hindlimb elements ontogenetic sequence analysis results. (A) Femora OSA. (B) Tibiae OSA. (C) Fibula OSA.

Morpho.	Element	Seq.	Modal seq. weight	Weight (%tot)
Morphotype I	Humerus	5	2.73	68.18%
	Ulna	1	4.67	100.00%
	Femur	37	8.00	64.65%
	Tibia	18	8.14	77.03%
	Fibula	3	8.00	73.85%
Morphotype II	Humerus	42	11.36	66.84%
	Ulna	2	3.83	100.00%
	Femur	56	4.75	60.32%
	Tibia	53	7.14	89.29%
	Fibula	45	7.33	59.46%

Table.VI.8. **Total sequences obtained in the OSA analyses.** Morpho. - Morphotype. Seq. - Sequence.

Forelimb and hindlimb clusters of Morphotype I + *Lohuecotitan pandafilandi* are present in Fig.VI.17, respectively. Forelimb and hindlimb clusters of Morphotype II are present in Fig.VI.18, respectively. The cluster analysis of the humeri, ulnae, femora, tibiae and fibular for both taxa are summarized in the Supplementary Material E.

Only a single radius actually referable to Morphotype II, and three specimen referred to Morphotype I. The small size of the sample does not allow an analysis for each taxa. The sample on radii is not enough to determine ontogenetic sequences. Herein, a combined cluster analysis for the radius of both taxa was performed. This cluster analysis without MOS determination can also be accessed at the Supplementary Material E.

VI.5. DISCUSSION

VI.5.1. ONTOGENETICAL STAGES

The obtained ontogenetical stages recovered some of the smallest specimens found in Lo Hueco as least mature (e.g., humeri HUE-XXYY, HUE-4828; ulna HUE-3462; femora HUE-2636, HUE-8801, tibiae HUE-1165 and HUE-1317). Those specimens show several features considered as probable indicators of juvenile status in previous preliminary studies (Páramo *et al.*, 2014, 2017). However, not all of the smallest specimens are estimated among the least mature stages, and some other specimens are found in early ontogenetic stages disregarding the size (e.g humeri HUE-2727, HUE-4343). When assessing the resulting clusters (Fig.VI.17 and VI.18) there is no clear pattern between the size of the specimen and the overall ontogenetical stage, especially among the intermediate sub-adult to adult stages. The hypothesized a priori informal ontogenetic determination was better support and congruent to current results (i.e. HUE-2636 femur from a possible juvenile individual, see Páramo *et al.*, 2014) based on a combination of morphological features previously described as variable during sauropod ontogeny in other ontogenetic series (e.g. Ikejiri, 2004; Curry Rogers *et al.*, 2016; see also Ontogenetic Characters). The different semaphoronts present an ontogenetical staging structure based on the tree topologies (see Supplementary Material C). If the ontogenetic characters has a random distribution, not following any means of sequential development, the recovered topologies would be characterized by a marked polytomy. Instead, we found several patterns and resulting imbalanced tree topologies similar to those observable in other ontogenetic sequencing studies applying the same methodology (Brochu, 1996; Carr, 2010).

After extracting the sequential information from the nodes of the consensus tree we estimated the number of MOS, the current stage represented by each semaphoront, and the MOS as a percentage of development dividing the stage by all the stages of the sequence (see Fig.VI.17, VI.18, VI.19 and VI.20; see Supplementary Data VI.D.2).

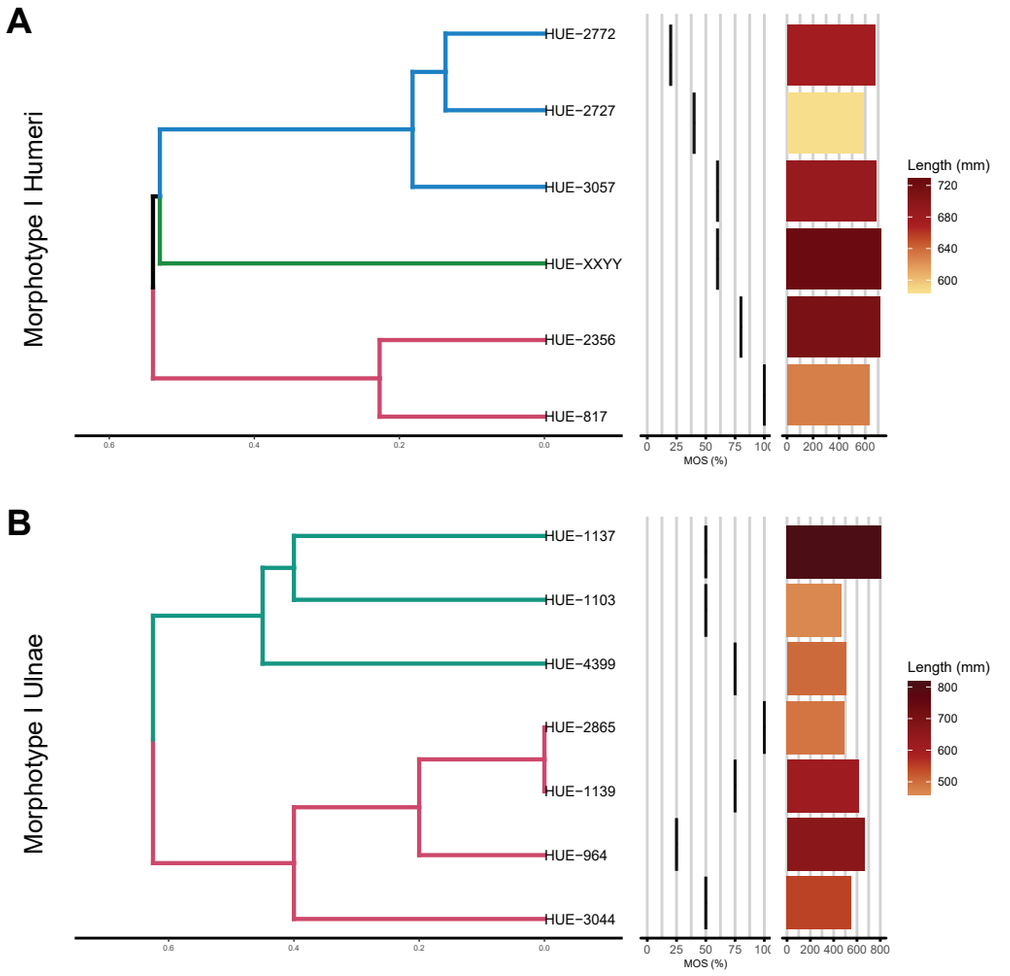

Fig. VI.17. Morphotype I forelimb elements cluster analysis results. Using the osteological (phylogenetic) characters. (A) Humeri cluster analysis. (B) Ulnae cluster analysis.

VI.5.2. ONTOGENETICAL SEQUENCE POLYMORPHISM

Ontogenetic sequence polymorphism is detected in majority of bone types for both morphotypes. We detect high intraspecific variability at various ontogenetical stages, affecting specially the ossification patterns in early stages of development except in humeri referred to the Morphotype II. We will discuss these sequences in strict order of fore- and hindlimb structure from the upper part of the limb to the lower part. Both morphotypes of Lo Hueco present high rates of intraspecific variability on earlier developmental stages in almost all the main bones of the hindlimb. Several of the different developmental paths are recovered within low maturity scores creating an asymptotic reticulate diagram towards the base. Only the fibulae of Morphotype I seem to present a low intraspecific variability effect on early stages of ontogenetical development.

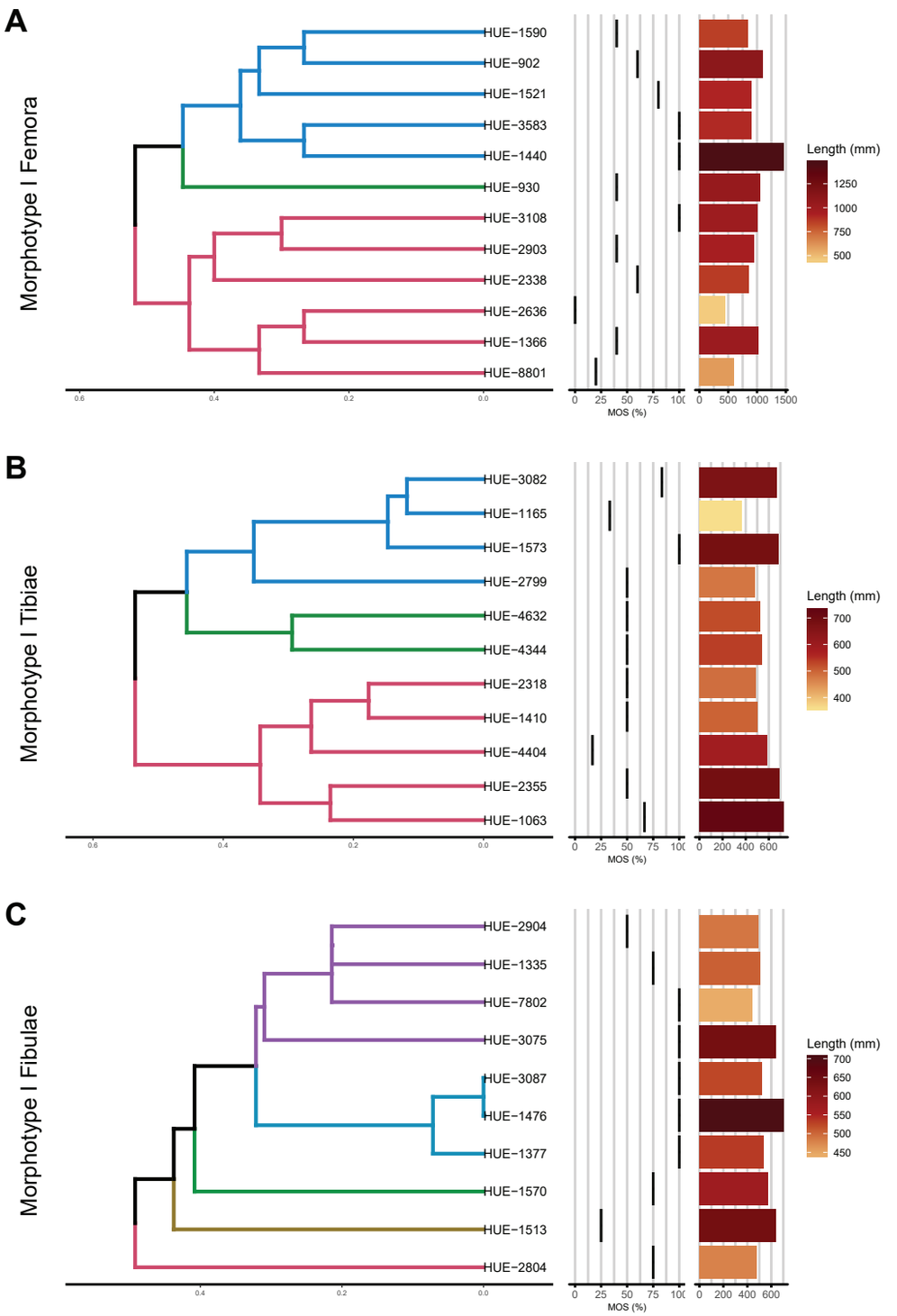

Fig. VI.18. Morphotype I hindlimb elements cluster analysis results. Using the osteological (phylogenetic) characters. (A) Femora cluster analysis. (B) Tibiae cluster analysis. (C) Fibulae cluster analysis.

The available sample for ulnae and radii is relatively low, being difficult to provide a strong evidence in the analysis for the forelimb zeugopodium. The radius have been excluded from the OSA because there is not enough sample for an heuristic search over ontogenetical characters.

Humeri:

The humeri are well sampled in Lo Hueco, with more specimens referred to the Morphotype II than to Morphotype I. However, both samples allow us to observe how the intraspecific variability affect at different stages in both morphotypes despite some bias that could affect to Morphotype II. The Morphotype I present a high variability at early stages of ontogenetic development with four different sequences between maturity score one and three out of 10 (Fig.VI.13). Some of the semaphoronts representative of early developmental stages are based in fragmentary specimens (i.e. HUE-2727, HUE-2772) as well as the specimen of the most mature semaphoront (i.e. HUE-3044). This may cause an underestimation of the ontogenetic stage in which the sequence polymorphism is found based on the maturity score calculation

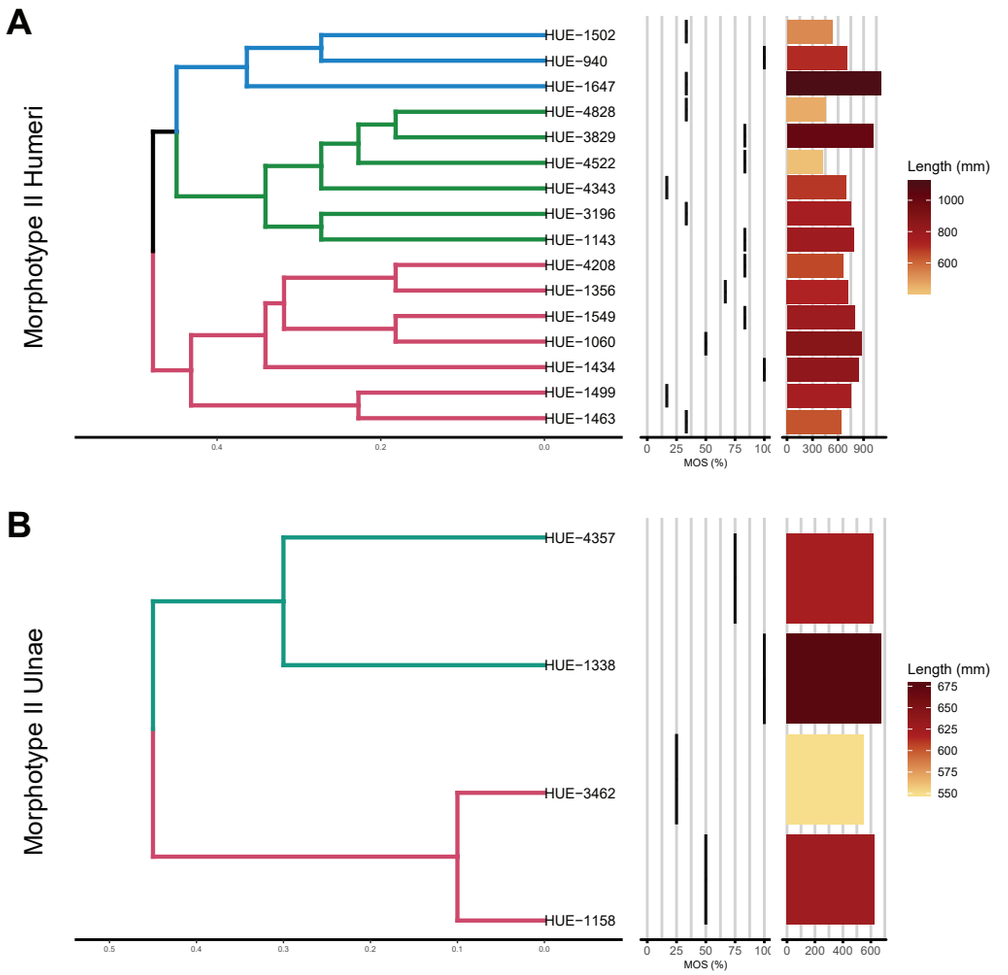

Fig.VI.19. Morphotype II forelimb elements cluster analysis results. Using the osteological (phylogenetic) characters. (A) Humeri cluster analysis. (B) Ulnae cluster analysis.

method. However, the fragmentary specimens representative of earlies juvenile semaphoront cannot be a misidentification of mature specimens as several of the morphological features present the least mature scoring. Therefore, the intraspecific variation can still produce sequence polymorphism but only at early stages of the ontogenetic development. Juvenile individuals present different ontogenetic paths of development at early stages in Morphotype I.

It is necessary to increase the sample further nonetheless, as we found several estimated nodes of the sequence (Fig.VI.13.A). These estimated nodes indicate that for the already sampled variation, it must be at least two more developmental stage in which the observed early polymorphic sequences coincide with the modal sequence at later ontogenetic stages (maturity score 2 and 4) to explain all possible semaphoront scoring combinations.

The humeri of Morphotype I includes two of the individuals which have a preliminary paleohistological analysis (Gascó *et al.*, 2018). The individual HUE-EC-02 (i.e. HUE-XXYY) is representative of a semaphoront found at early maturity score (see Fig.VI.13.A, 17 and 19) and exhibit histological features congruent with a juvenile individual. The holotype of *Lohuecotitan pandafilandi*, individual HUE-EC-01 (i.e. HUE-3044) is representative of the most mature semaphoront (see Fig.VI.13.A, 17 and 19) and its paleohistological analysis indicates the internal structure compatible to an adult to senile individual (Gascó *et al.*, 2018).

The humeri of the Morphotype II present also a high intraspecific variability in the ontogenetic paths between more adult specimens. There is an early diversification of ontogenetic sequences (Fig.VI.15.A), but majority of divergences observed occur among late maturity scores. Inferred nodes also appear at late stages and they are probably related with the two distinct late maturity scores registered. We have an underrepresentation of specimens in early developmental stages that may be reducing the appearance of polymorphism between juveniles. However, lack of inferred nodes at the base of the reticule indicates that there is a small number of different paths occurring in early postnatal developmental stages than in later stages. The estimation of several paths at early stages also indicates that ontogenetic sequence polymorphism occurs also among earlier developmental stages (contra the fibula of Morphotype II; Fig.VI.16).

The presence of more than one semaphoront at the most mature developmental stage (maturity score 9; Fig.VI.15.A) could be related to more than one titanosaur morph in the sample. However, previous studies of intraspecific variability disregarding the variation attributable to ontogenetic development, shows that there are no other major morphotype cluster among the sample of humeri from Lo Hueco (see Chapter V).

The lack of sample is not necessarily detrimental to our capabilities of infer high degrees of intraspecific variability at earlier and later stages. This method account for possible paths and unregistered semaphoronts in the current sample (Colbert & Rowe, 2008; Olori, 2013; Griffin & Nesbitt, 2016b; including in comparisons between different taxa Griffin, 2018), and they are expected to appear as branches grouping several semaphoronts in the input MPTs. Besides both morphotypes present sequence polymorphism at early stages as observed thanks to the path estimation, there are differences between the two morphotypes. It is more probable thatthe observed difference between the humeri of Morphotype I and between the humeri of the Morphotype II in the ontogenetic sequences are caused by different growth models than lack of information. Another difference is the presence of two distinct late stages in the

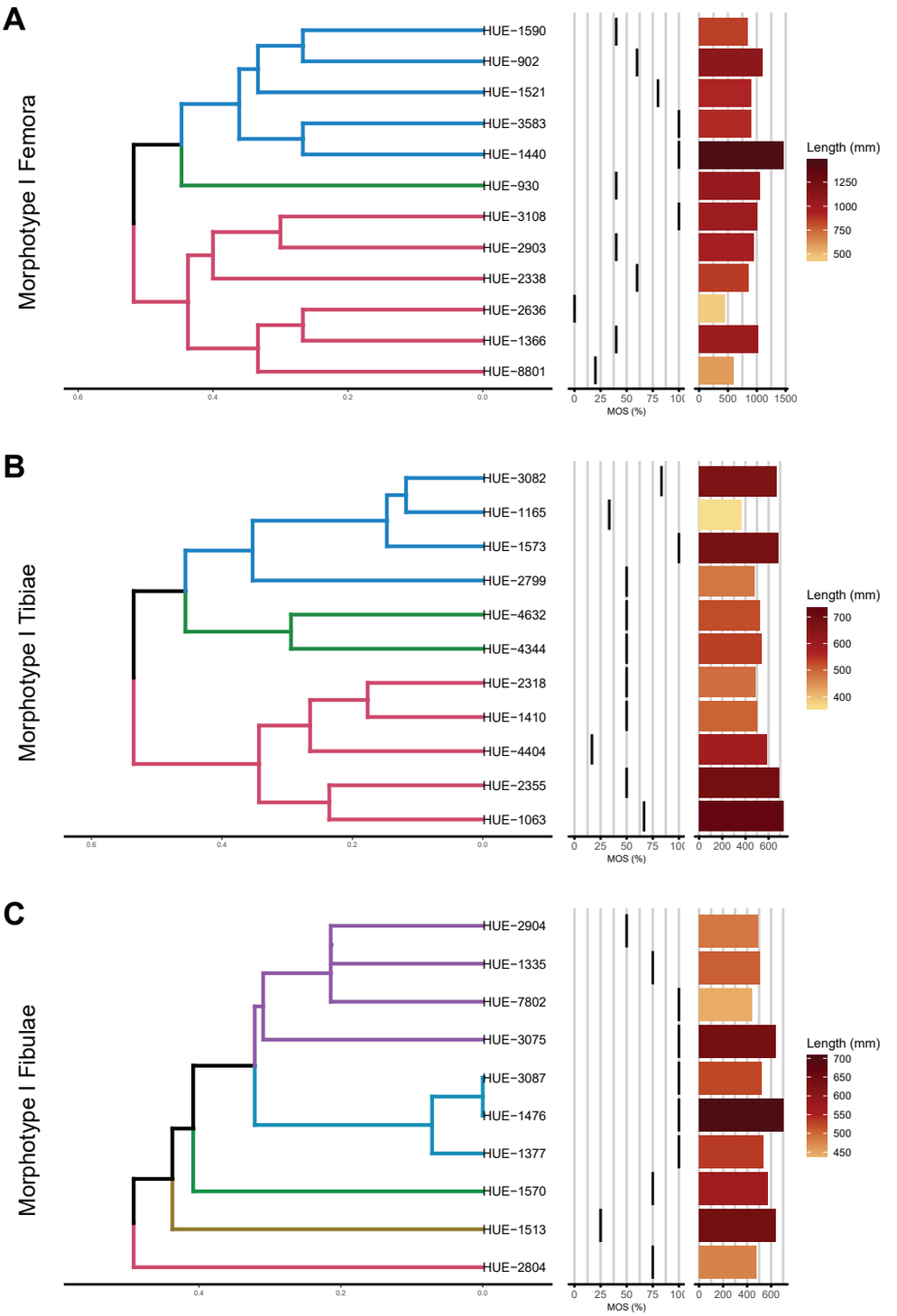

Fig. VI.20. Morphotype II hindlimb elements cluster analysis results. Using the osteological (phylogenetic) characters. (A) Femora cluster analysis. (B) Tibiae cluster analysis. (C) Fibulae cluster analysis.

humerus of Morphotype II. This can be caused by absence of record of more mature specimens in Morphotype II and therefore our sample only reach some previous, non-senile stages. Despite the maturity scores between both morphotypes are not directly homologous, the Morphotype II present one stage less tan Morphotype I, which is a possible senile specimen based also on the paleohistological analysis. Therefore, there are two probables most mature semaphoronts in Morphotype II as product of non-ontogenetical intraspecific variability, or the current sample lacks representatives of a more mature stage. The OSA method can estimate unregistered intermediate semaphoronts as commented before, but terminal stages is more difficult, as only the hypothetical juvenile can be given an all zero (= not developed) scoring with certainty. The contrary, an all developed scoring is not possible and actual comparisons between juveniles of one species and theoretical adults based on size alone and on comparisons with other taxa from the same clade have been is still debated (Longrich & Field, 2012; Woodruff & Fowler, 2012; Carballido & Sander, 2014).

Another insight on the lack of available sample of more mature specimens is the actual absence of derived character scorings for some key features. Some ontogenetical characters like the rugosity of the proximal end where the cartilaginous cap attaches reach state 1 in the most of the sample from Lo Hueco. However, other titanosaurian sauropods have a rugose humeral proximal surface with the development of the usual mamelons but also longitudinal grooves referred herein to state 2, such as *Mendozasaurus neguyelap* (IANIGLA-69-2, González Riga *et al.*, 2018; pers. obs. APB 2016), *Saltasaurus loricatus* (PVL-4017-65, Powell, 2003: but beware, the fractures in the medial side of humeral head should not be interpreted as longitudinal grooves; pers. obs. APB 2016) and "*Neuquensaurus robustus*" (Salgado, Apesteguía, & Heredia, 2005; Otero, 2010; pers. obs. APB 2016). However, as commented before, direct comparison between specimens of different ontogenetic stages in order to establish ontogenetic sequences can be misleading. Absence of more mature specimens among Morphotype II or differences in the growth model at more mature stages between Morphotype II and other known Gondwanan titanosaurs cannot be disregarded. Lastly, these two different semaphoront at mature stage could be representative of the presence of sexual dimorphs (see possible dimorphism patterns in Sauropoda in Ikejiri, 2008; Carballido & Sander, 2014; see dimorphism in appendicular skeleton of Theropoda discussion in Griffin, 2018), but as other hypothesis here considered cannot be ruled out.

Ulnae:

The ulna of both taxa does not present remarkable polymorphism, and almost no intraspecific variability over the ontogenetical sequences is found except for some differences between the latter stages in the ulnae of the Morphotype II (semaphoronts that includes e.g. HUE-1338, maturity stage 5). The small sample of ulnae from Morphotype II present a mature stage that is impossible to be related directly with the earlier stage semaphoront represented by specimen HUE-1158 (maturity stage 4). The character combination of this semaphoront of maturity score 4 includes some features with the least mature state. However, other features such as the proximal end presents rugose bone surface with longitudinal grooves, which is considered as state 2 (for the ontogenetical character #Uont1) and interpreted as representative of mature stages. The only possible path includes an intermediate, unregistered semaphoront, which is representative of a previous developmental stage between the semaphoront at maturity score 2 and the other more mature semaphoront.

Another implication of the presence of these marked rugosities in the proximal an distal end at small sizes and early ontogenetic stages (see also the tibiae and fibulae below) is an early development of the articulations in the zeugopodium. Some specimens representatives of semaphoronts in early stages (e.g. HUE-4357) present also a marked rugosity in the proximal end. Other specimens on the contrary, present rugose proximal and distal ends, even with developed grooves in the edge of the proximal end (state 2 in the ulnar ontogenetic character #2) but exhibit other character with least mature scores (e.g. HUE-G1-C-187 in Morphotype I). These observations suggests that the acquisition of a more rugose proximal and distal ends related to the development of the articulation cartilage can occur earlier in the development, and also being relatively more variable during the ontogeny than in humeri (and femora, see below). Also, the presence and development of the proximal end groove over the anteromedial process related with the presence of longitudinal grooves in the edge proximal and distal end should be revised after inclusion of more sauropod ontogenetic sequences. The concavity on the surface of the anteromedial process of the ulna have been identified and discussed as variable in the morphotypes of Lo Hueco (see Chapter V). A probable state 3 should considered in future studies as it is relatable to the appearance of a concavity in the proximal surface of the anterior process of the ulna. However, current sample in the fossil site of Lo Hueco do not permit to assess the relationship between these morphological features.

Femora:

The femur is the bone that recorded highest degree of polymorphism in both taxa regardless of sampling n and among all the bone types. Both taxa present high variation of ossification patterns especially at lower stages. Diversity in the developmental paths is present at the lower part of the sequences, so the OSA diagram tend to be asymmetrical. The Morphotype I present several inferred nodes in order to explain different ossification patterns at the early to middle ontogenetic stages, which already present high variability. Observed semaphoronts and inferred nodes represent a parallel path along majority of sampled ontogenetic stages. This could be indicative of some sort of dimorphism in Morphotype I, but further test are required to assess it accurately (see de Jong *et al.*, 2009; Griffin & Nesbitt, 2016b). Other possibility is the presence of two different groups related with different taxonomic units, this hypothesis, nonetheless, have been disregarded with the analysis of most optimal clusters (see Chapter IV, Chapter V). Most of the polymorphism occur among early developmental stages (maturity score 0 to 3; see Fig. VI.14). It is also important to note a common feature described before, the rugosity of the proximal and distal ends related with the ossification of the cartilaginous articular cap. These features can vary greatly the stage where they are developed, with semaphoronts representing the acquisition of first rugose surface at maturity score of 4 to 5 (see Fig.VI.14.A, see also supplementary material VI.E.5). In the other hand, development of the most derived state, a rugose surface with development of longitudinal grooves in the external edge of the proximal and distal ends, can be observed as early as semaphoronts with maturity score 5 (see Fig.VI.14.A, see also supplementary material VI.E.5).

Similarly to the size of the specimen (see Fig.V.18), the rugosity of the ends is not enough to identify the probable ontogenetic stage of the specimen. The combination of morphological features relatable to the ontogenetic development, as our set of ontogenetic characters (see similar sets of ontogenetic characters for theropod dinosaurs in Griffin, 2018) is the best approach.

The Morphotype II present also a high polymorphism in the ontogenetic sequences at early developmental stages (see Fig. VI.16.A). It also presents a structure of low polymorphism at middle ontogenetic stages (maturity scores 3 to 5; Fig. VI.16.A) and again a high polymorphism at middle to more mature stages (maturity score 5 to 8). It is probable that it is only a small artefact of a slightly smaller sample of specimen compared to Morphotype I, and instead, both morphotypes present similar trends. The estimated paths suggest that the decrease of polymorphism at maturity stage 4 is compensated by the high number of different paths registered at earlier stages and a higher number of character state changes in these ontogenetic sequences. Another possibility is that Morphotype II present a faster growth than Morphotype I, and so more characters changes are produced in less ontogenetic stages and at early development. Differences in growth speed is not unheard of in the European titanosaur faunas (e.g. Stein *et al.*, 2010). In order to test this hypothesis, further paleohistological sampling and analysis is needed in the specimens of Morphotype II.

Tibiae:

The tibiae of both morphotypes present similar growing models although Morphotype II presents higher polymorphism with a greater number of possible sequences at early stages (Fig. VI.16.B). Despite the similar number of MPTs resulted from the analysis, there is a in a higher number of different possible patterns recovered for the Morphotype II than for Morphotype I. There is more variation among the tibiae of Morphotype II, and a higher number of estimated semaphoronts which help explain all the possible combinations of feature acquisition.

Most of the specimens sampled for Morphotype I are representatives of the semaphoronts of the modal sequence. The high variability on more mature semaphoronts is explained by high polymorphism at early stages and a number of estimated semaphoronts (Fig. VI.14.B), especially at early to mid-ontogenetic stages (maturity score 3 to 5; Fig. VI.14.B). It is also possible that our sample is also slightly biased by poor preservation of the distal end of the tibia, especially in many specimens referred to Morphotype I. The codification has been conservative in this regard and a future increase of the sample of tibiae with better preserved distal end should improve the present analysis. It could be possible that decrease in missing values could increase the number of feature combinations therefore the number of sequences.

In the case of the tibiae of the Morphotype II, they are represented by a smaller sample with better preserved distal ends resulting in less missing information across the ontogenetic data matrix (average 87.12% of ontogenetic data completeness). There is a high variability in the development of the rugosity of the proximal and distal ends at early stages (maturity score 1 to 4) as well as the development of the proximal muscular scar on the cnemial crest (Tibial character #3, see ontogenetic characters; see fig V.16.B and VI.23).

Fibulae:

The fibula presents some diverging ontogenetic sequences between both taxa. The fibulae of Morphotype I show little polymorphism especially at lower maturity scores, highlighting few significant effects of intraspecific variability on the early ontogenetic stages. Different sequences at mature stages of development produce two different mature semaphoronts in the current sample. They present differences between the rugosity of proximal and distal end and the development of lateral and medial muscular attachments of the fibula. The specimen HUE-1570 represents one

of the most mature semaphoronts (see Supplementary Material B). This specimen has a marked tibial scar with development of an accessory posterior trochanter in medial face. As well as deep grooves in the lateral trochanter of the fibula. The specimen HUE-3087 represents the other mature semaphoront from the holotype material of *Lohuecotitan pandafilandi*. This specimen presents a marked proximal and distal end development with rugose bone surface and some grooves in the articulation edges. The lateral trochanter is robust and with a rugose surface but lacks the longitudinal grooves or scars that we considered as state 2 of the character and related to most mature stages. There is also variability in the tibial articulation and the presence of an accessory posterior ridge between more mature individuals. Those specimens that are probable subadults and show middle maturity scores 4 to 7, have a great development of the lateral and posterior proximomedial muscular attachment (see fibular ontogenetic character #4 and #5; see also variability in this area Chapter IV, Chapter V). Presence of two different clusters among the specimens of Morphotype I has been disregarded based on the geometric morphometrics analyses (see Chapter IV). In fact, specimen HUE-1570 exhibits a combination of morphological features similar to HUE-3087. On the other hand. some specimens as HUE-1513 referred to Morphotype I and HUE-2977 referred to the Morphotype II exhibit an advanced development of the M. iliofibularis attachment (fibular character #4, state 2) as well as a combination of least mature features, including the absence of the tibial articulation scar. It is probable that the differences mentioned in the tibial articulation are not entirely related to ontogenetic development and more related to other type of intraspecific variability (e.g. dimorphism and individual variability). Also, the Morphotype II present this feature less frequently (see Chapter IV). It is necessary to observe the development of a tibial articulation scar in other sauropod ontogenetic sequences to fully assess its importance during development.

The development of the lateral trochanter is also a remarkable feature. It is a common variable character among different polymorphic sequences (see Supplementary Material VI.E.5). It seems that the lateral trochanter rugosity is acquired at middle development stages (maturity scores 3-4 for both morphotypes). This also develops later than other characters related with the distal iliac muscle groups attaching in the hindlimb zeugopodium (tibial characters #3 and #4) which present a developed rugosity or scar at earlier maturity scores of the tibiae. However, we cannot establish if the external muscle groups that connects the pelvic girdle to the zeugopodium develop later in any of the Lo Hueco morphotypes until a comprehensive analysis of the paleohistology is carried out in order to establish homologies between the tibial and fibular ontogenetic stages. We found that development of bifurcated crest related with the attachment of M. iliofibularis and M. ischiotrochantericus can be variable regardless of ontogenetic stage for more mature state 2. This indicates that the change between the absence of clear attachment surface in the trochanter to the presence of a proper rugosity or trochanter of lateral crest of the fibula is informative for ontogenetic development stage determination. The appearance of a single or multiple crest is variable within taxa (see Chapter IV) and could be variable by other types of intraspecific variability (e.g. dimorphism and individual variation). Assessment of this feature in other sauropod taxa with ontogenetic sequences that exhibit a lateral trochanter bifurcation is important. In addition, this feature is variable among each morphotype from Lo Hueco, but it is more prominently present among Morphotype II specimens (see Chapter IV, Chapter V), so it could be more informative of taxonomic differences rather than ontogenetic development stages.

VI.5.3. MORPHOLOGICAL FEATURE ACQUISITION

We clustered the morphological features used in phylogenetic data matrices in order to see if there are more similarities between specimens at the same ontogenetic stage or there are no clear pattern, given that the appendicular skeleton in sauropod juvenile individuals resemble those of the adults (Bonnan, 2004; Tidwell & Wilhite, 2005; Wilhite, 2005; Curry Rogers *et al.*, 2016). We can assess the implications for these osteological characters based in the reported patterns of ontogenetic staging between the clusters in some of the bone types. The general trend between both morphotypes is that there are no clear major differences between juvenile specimens and adult forms for all the bone types (see Fig.VI.17, 18, 19 and 20).

In the Morphotype I, the small sample of humeral specimens is the only cluster that shows a pattern that reflects the ontogenetic sequence. The cluster branches reproduce the different ontogenetic stages, with the juvenile specimens closer between them than to the more mature specimens and vice versa (Fig.VI.17.A). However, there is no clear pattern in size, as it shows high intraspecific variability in size in the sample (see Fig.VI.17.A) and the size patterns do not resemble the ontogenetic stages. One of the more mature humerus specimens (e.g. iHUE-817) are smaller than the estimated length of more juvenile specimens of Morphotype I (e.g. HUE-2727,

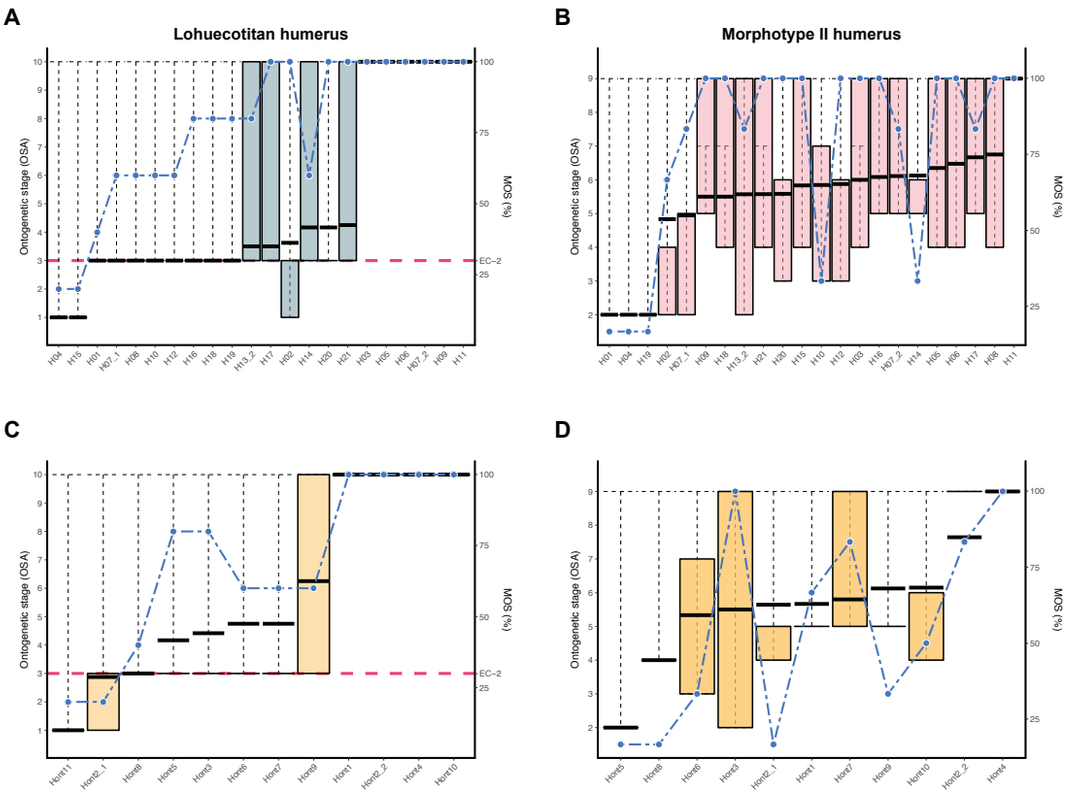

Fig.VI.21. Humeral ontogenetic character and osteological character developmental stages. (A) Morphotype I humeri osteological character relative development. (B) Morphotype II humeri osteological character relative development. (C) Morphotype I ontogenetic character development. (D) Morphotype II ontogenetic character development.

HUE-XXYY). Moreover, size differences not relatable to the ontogenetic stage are supported by the preliminary paleohistological analyses of HUE-EC-2 (i.e. HUE-XXYY) and HUE-EC-1 (i.e. HUE-3044).

The ulnae show no clear ontogenetic clustering pattern. Some disparity can be identified between a subcluster grouping the least mature and most mature specimens and another with intermediate specimens. A laddered pattern can be recognized in the ontogenetic stages among each subcluster (see Fig. VI.17. B). The small sample of ulnae from Lo Hueco does not allow a conclusion for this pattern, as there is no clear trend that reproduces the ontogenetic sequence. However, it could be related, as some small allometric effects have been preliminary reported in the relationships between size and shape in the ulnae of Morphotype I via 3D geometric morphometrics analysis (Páramo, Ortega, & Sanz, 2018; Páramo *et al.*, 2019). Another possibility of two different clusters could be the presence of dimorphs, but absence of sequence polymorphism seems to be against it, as the differences are minimal and do not produce different ontogenetic trajectories as in other taxa with dimorphism (de Jong *et al.*, 2009; Griffin & Nesbitt, 2016b). It is also noticeable the presence of the high intraspecific variability in the size for the sample specimens. There is a great size difference for specimens at similar ontogenetic stages (e.g. HUE-964, HUE-1103, HUE-4399; see Fig. VI.19.B) as well as specimens at early stages larger than specimens at later stages (e.g. HUE-2865, HUE-4399)

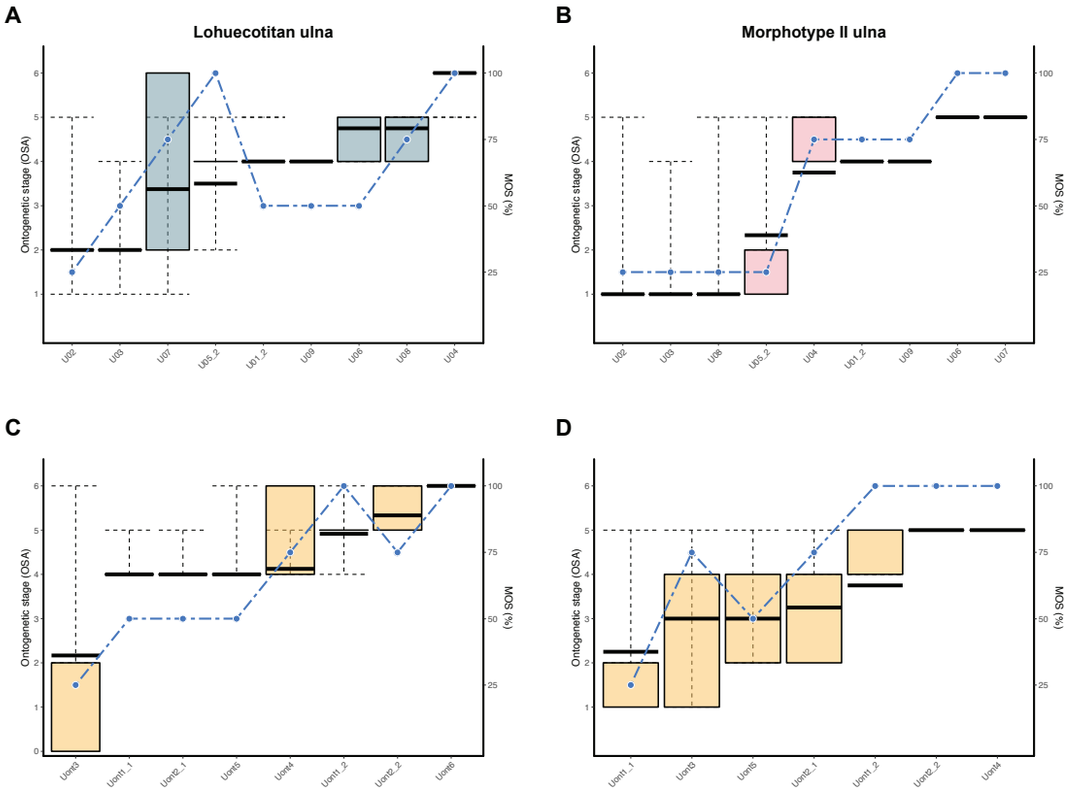

Fig. VI.22. Ulnar ontogenetic character and osteological character developmental stages. (A) Morphotype I ulnae osteological character relative development. (B) Morphotype II ulnae osteological character relative development. (C) Morphotype I ontogenetic character development. (D) Morphotype II ontogenetic character development.

In contrast, the hindlimb have little to no resemblance between the ontogenetic sequences with the resulting clusters. The femora of Morphotype I show some similarities between the smaller and early ontogenetic stage individuals, but we cannot conclude a clear relationship among specimens in the intermediate and most mature stages, as the different subclusters do not reproduce the ontogenetic sequence. Three possible main clusters can be identified (Fig. VI.18.A) but they do not reflect either two major trends of ontogenetic sequences commented before (see fig. 13, see Supplementary Material VI.E for the semaphoront labels and associated specimens; see Ontogenetical Sequences Polymorphism). Also, there lack of relationship between the clusters and the two major sequence trends could indicate that there are no clear dimorphs as most probable explanation of these two groups of sequences, as discussed before.

Tibiae show several similarities among specimens at equal MOS and similar sizes. The tibiae of Morphotype I also presents an important intraspecific variability in size at different several stages. The clusters present some laddered pattern between similar size and the morphology of the individuals, but only for one of the major subclusters. There is againbut there is some degree of overlapping between bone length and in different developmental stages. (e.g. HUE-4404, which is proposed to be referred to an early developmental stage but is much larger than HUE-1410, and HUE-2318; see Fig.VI.18.B). Some of the largest femora

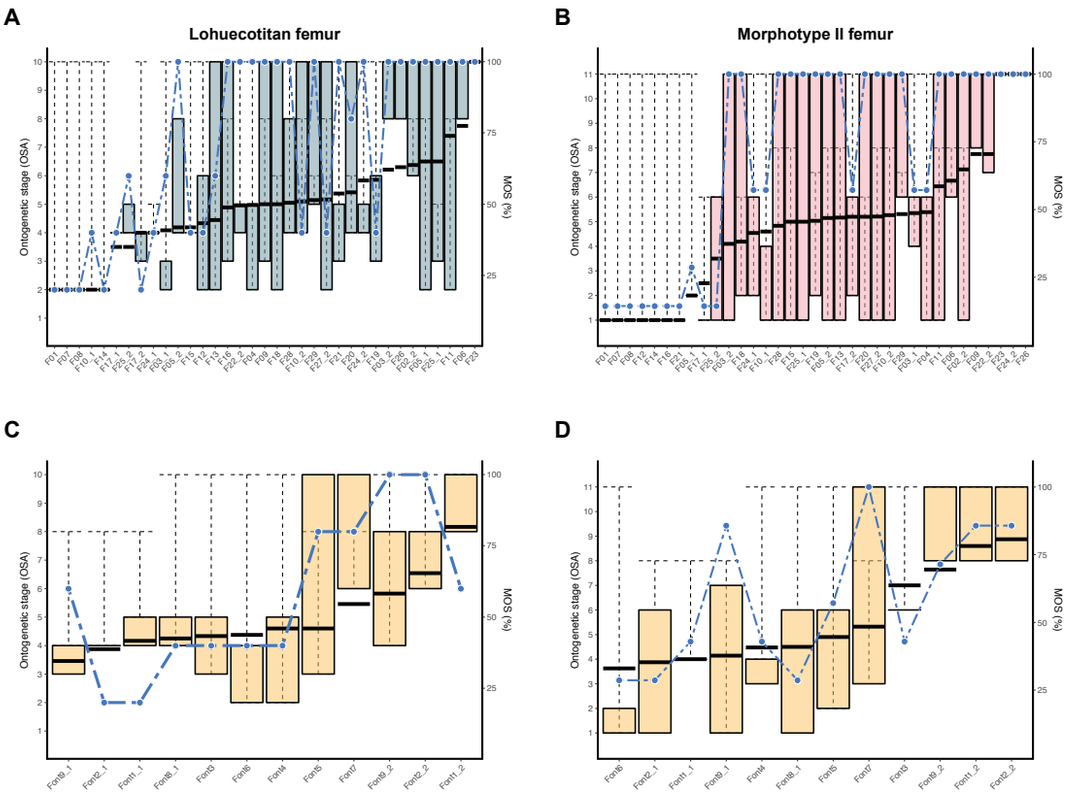

Fig.VI.23. Femoral ontogenetic character and osteological character developmental stages. (A) Morphotype I femora osteological character relative development. (B) Morphotype II femora osteological character relative development. (C) Morphotype I ontogenetic character development. (D) Morphotype II ontogenetic character development.

are associated with tibiae in mature stage of development (e.g. type specimen of *Lohueotitan pandafilandi*) but earlier stages are much more variable (e.g. HUE-2335, HUE-1063).

The fibulae do not present any remarkable pattern in the cluster composition. The intermingled structure shown by the different resulting clusters (Fig.VI.18.C) is the expected one in case of resemblance between juvenile individuals and adult forms. There is no remarkable pattern in the intraspecific variability on size of the fibula either. When compared the complete zeugopodium of Morphotype I however, it can be seen that there is also a high variability in size among the most mature specimens in the fibulae (e.g. HUE-3087 the type specimen of *L. pandafilandi*, HUE-7802) while the largest tibiae at least can be referred to more mature stages only (see Fig.VI.18.B and C). This could be related to the lack of sample of probable largest specimens among Morphotype I hypothetical population nonetheless, as we have already sampled other elements (e.g. femora HUE-1440) representative of adult individuals larger than *L. pandafilandi* holotype individual.

Morphotype II does not present a remarkable pattern in the humerus, except for a high intraspecific size variability between specimens at several different MOS (Fig.VI.19.A). Most of the specimens do not show any particular pattern in the size distribution or the ontogenetic stage of the individual. The different subclusters do not show any grouping that reflects the ontogenetic sequences obtained in the analyses (see fig VI.19.A, compare with Fig.VI.15). There are several humeral specimens that also present a high overlap despite the ontogenetic stage. Some of the smaller specimens are referable to a more mature development stage (e.g. HUE-4522). There are also several specimens with the longest elements at early ontogenetic stages (e.g. HUE-1499) and intermediate stages (e.g. HUE-1647). Some of these specimens are slightly fragmentary and the length have been estimated (see Chapter V). We estimate that preserved length is at least 75% of the complete proximodistal length. The preserved length is 421 mm contrasting with specimen HUE-1549 with a massive size of 1070 mm and HUE-3829 with an estimated total length of 1010 mm and similar developmental stage. The overlapping in size is therefore not caused by estimation and the fragmentary state of many specimens. It shows that the size intraspecific variability is high among the humeri of Morphotype II and it is not clearly related to the ontogenetic stage. There is also no pattern in de similarities of the specimens of Morphotype II, the juvenile individuals are similar to more mature specimen as they may be present intermingled in the same subcluster.

The small sample of ulnae referred to Morphotype II does not present any remarkable pattern. They are distributed in two groups and present some staggered pattern (see Fig.VI.19.B), but this analysis based only on four specimens and it is not possible to conclude any significant pattern. Given that there are only four specimens, further sampling is necessary to assess with more accuracy possible clustering structure.

The hindlimb presents a clear pattern of size and probable ontogenetical stage clustering of the characters in the femur (Fig.VI.20.A). The femoral smaller specimens are much more similar between them than to the larger ones, thought the ontogenetic stage is not clearly related. Several specimens among the juvenile and intermediate ontogenetic stages are the subculture with the smallest specimen (e.g. HUE-1319, HUE-3237, HUE-10007; see Fig.VI.20.A). There are some of the largest specimens are clearly the most mature of the analysed sample (e.g. HUE-594, HUE-2420). The gradation in sizes is therefore more marked than the clustering by MOS. It is possible that this small similarities between the morphological features, ontogenetic stages and

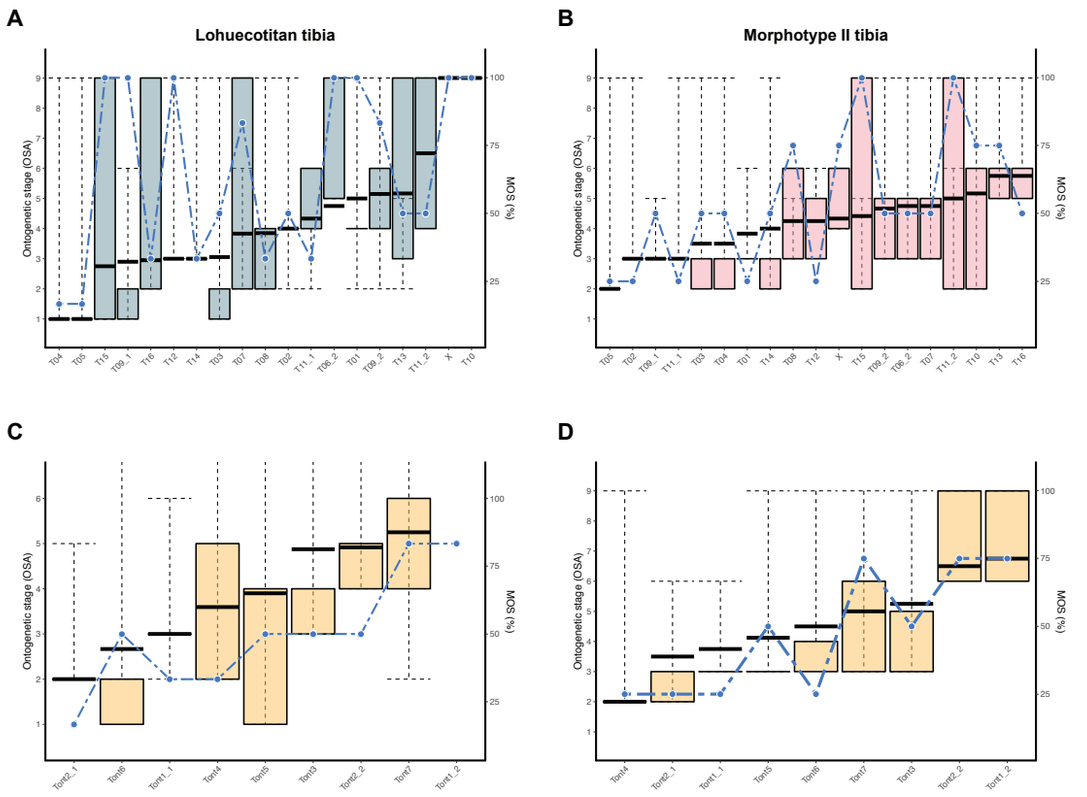

Fig.VI.24. Tibial ontogenetic character and osteological character developmental stages. (A) Morphotype I tibiae osteological character relative development. (B) Morphotype II tibiae osteological character relative development. (C) Morphotype I ontogenetic character development. (D) Morphotype II ontogenetic character development.

e.g. contra *Venenosaurus* Tidwell & Wilhite, 2005; ;see also the morphometric concept of allometry in Bonnan, 2007). Assessing the pattern between size and shape is necessary to clarify this relationships observable with morphological features. Preliminary analyses of the allometric relationships in Morphotype II do not indicate the presence of a significant allometric effect nonetheless (Páramo *et al.*, 2019). Another conclusion is that size could be somewhat related with the ontogenetic stage (contra the humerus of Morphotype II, as commented before), but it shows a wide overlapping especially among intermediate ontogenetic stages. It is unadvisable to use the size as sole estimation of the ontogenetic stage (see also Irmis, 2007a). Also, it is possible that the sample of specimens from Morphotype II do not reflect the earliest ontogenetic stages, as the representative of early stages are fragmentary, presenting the same problematic of the Morphotype I humeri sample. It is possible that the increase in sample of more complete early juveniles and intermediate ontogenetic stages increases this variability as most of the estimated semaphoronts and polymorphism found in Morphotype II occur at these stages (see Fig.VI.16).

The tibiae of Morphotype II present a weak pattern between the morphological features similarities, the ontogenetic stage and the size (Fig.VI.20.B). However, there are

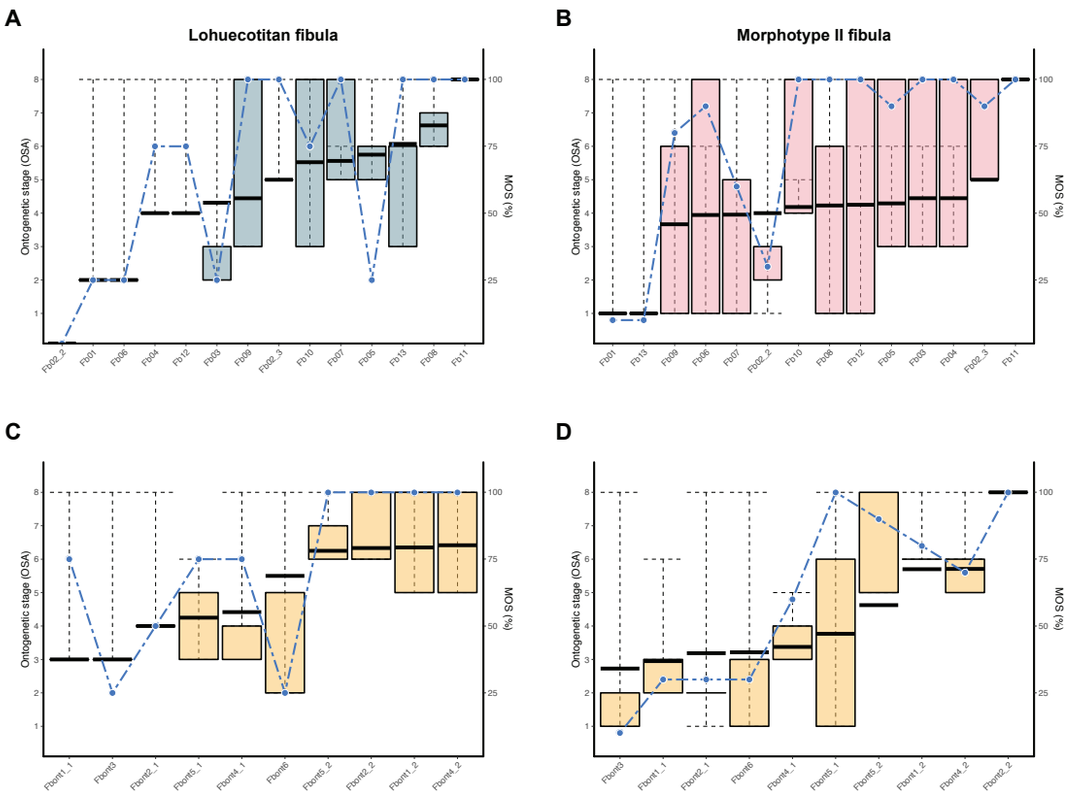

Fig.VI.25. Fibular ontogenetic character and osteological character developmental stages. (A) Morphotype I fibulae osteological character relative development. (B) Morphotype II fibulae osteological character relative development. (C) Morphotype I ontogenetic character development. (D) Morphotype II ontogenetic character development.

few specimens at early ontogenetic stages, and many of the sampled specimens are found at the same intermediate MOS. The sample of tibiae is small, but the pattern is very weak and it can be disregarded the presence of an allometric growth. The smallest specimens are not relatable to early ontogenetic stages (e.g. HUE-1317) and there is no clear differences between the juvenile and adult individuals as it is common in other titanosaurs.

The fibulae present a larger sample and do not show any remarkable patterns between the morphological features and the size and MOS. Clustering is caused by intraspecific not relatable to the ontogenetic development, neither when we take into account the ontogenetic sequence polymorphism (see Fig.VI.16). Also, similar to the tibiae, there is no remarkable pattern of size variability in the fibulae of Morphotype II. There are some specimens of fibula at lower MOS with larger size (e.g. HUE-2806) than more mature specimens (e.g. HUE-1507) suggesting that the size cannot be accurately related with the ontogenetic stage and it is unadvisable to use the size alone to estimate it.

VI.5.4. IMPLICATIONS FOR SAUROPOD SYSTEMATICS

Observing the intraspecific variability on the phylogenetic data matrix character and the maturity scores following the OSA method, and the MOS estimated by the OCSA method, we note for several scoring changes that are probably related with ontogenetic development. We can observe that several ontogenetic characters as well as some phylogenetic characters are acquired at some ontogenetic stage determined by the MOS and maturity score (see figs. VI.19, VI.20, VI.21, VI.22, VI.23).

We do not have sampled specimens at early ontogenetic stages for both morphotypes of humeri and several changes seems to appear in an earlier stage of developmental than those represented on the sample, as they appear among the more juvenile specimens. They are probably before the hatchling (see similar features early acquired during ontogeny in Carpenter & McIntosh, 1994; Martin, 1994a; Curry Rogers *et al.*, 2016) and are related with the morphology of the deltopectoral crest (e.g. humeral character #1 and #4; see character #219 and #220 in Upchurch *et al.*, 2004; see also the lateral margin of the humerus in Curry Rogers, 2005). However, the rugosity of the deltopectoral crest do not appear until later during the ontogeny as suggested by the first appearance (see Fig. VI.21). Those morphological characters that are preserved in almost all the specimen and appear at a determinate MOS can be attributable to ontogenetic changes in both morphotypes. They can be also related to several ontogenetic character changes at the same stage e.g. humeral ontogenetic characters #3, #5 and #6 determine maturity score 3 or intermediate ontogenetic stage (50% MOS). This combination allows us to identify ontogenetic characters that can mark important ontogenetic events and morphological characters used in systematic analysis data matrices that present some variation relatable to these stages. Direct comparison between the relative ontogenetic stages of each morphotypes is not possible, but some similarities can be established i.e. humeral ontogenetic character #6 and #8 are absent in post-hatchling juveniles prior our registered stages and are acquired at early stages in both morphotypes; though MOS estimation (contra the maturity score) indicates otherwise with humeral ontogenetic character #8, see Fig. VI.21.

The lateromedial projection of the deltopectoral crest can present differences scoring between juvenile and more mature specimens in both morphotypes as commented before. Other characters can also present more primitive scoring at early stages such as the difference in curvature in the distal end articulation (humeral character #7). However, this character can also present some variation after intermediate ontogenetic (possibly subadult) stages, as some of the posterior stages may or may not present similar scoring. There is also a variation in the presence of the posterolateral bulge to the deltopectoral crest at early ontogenetic stages (humeral character #19; character #80 in D'Emic, 2012), as it is absent in any specimen before the ontogenetic stage represented by the juvenile specimen HUE-EC-2 (see Morphotype I; Fig. VI.21.A). After these early ontogenetic stages, the bulge is present in all specimens (not variable, as in the distal end morphology commented before).

One of the new character analysed in this study and based on the morphological differences observed between both morphotypes (see Chapter V) is the presence of an accessory ridge under the deltopectoral crest in lateroposterior, related with the attachment of M. teres brachii (Humeral character #20; see Supplementary Material C). This character is absent among early

ontogenetic stages in both taxa, and can appear variably at intermediate ontogenetic stages in Morphotype II (see Fig.VI.21.B). Other taxa also present this ridge, and the observation in specimens that could be tentatively referred to sub-adult specimens (based mostly on size and some morphological features), this ridge is present though slightly less acute and well developed e.g. *Saltasaurus loricatus* (PVL-4017-70; pers. obs. APB 2016).

We consider that several characters like the development (e.g. Humeral ontogenetic character #1) and position of the humeral head (e.g. humeral character #16; see chararacter #270 in Curry Rogers, 2005) as well as the proximal expansion might be affected by lack of preservation on several of the specimens rather than ontogenetic development as commented before (see Ontogenetical Stages). For this reason, we cannot confidently assess the stage in which several morphological features related to the proximal end are acquired (e.g. the prominent process of the humerus proximal observed only in mature specimens in Morphotype I character #3; character #217 in Upchurch *et al.*, 2004).

The similarities in stage timing of some character differences of the ulnae allow us to compare these features despite the ontogenetic stages are relative (in each morphotype). Both morphotypes shows that the development of the rugosity in the proximal end (ulnar ontogenetic character #1) and the presence of a radial ligament scar (ulnar ontogenetic character #5) is related to more intermediate ontogenetic stages. On the contrary, the presence of a marked rugosity in the distal end is variable but present among earliest ontogenetic stages (at least in Morphotype II; see ulnar ontogenetic character #2, Fig.VI.22.C and D). It is also important to note that some specimens at early stages may not present the development of the M. pronatus quadratus ridge in the radial articular fossa in anterior face (ulnar ontogenetic character #3) but it is generally present among the earliest ontogenetic stages reported in our sample (see Fig.V.22.C and D).

Related to these ontogenetic characters, other morphological changes can affect the scoring in different data matrices of osteological morphological characters. We modified the development of the concavity in the proximal end of the ulna and convexity of the olecranon process (e.g. ulnar character #1; base in character 167 in Wilson, 2002; modified after Gorscak *et al.*, 2017). We observe a great development of the olecranon process that changes along ontogeny between juvenile and intermediate (= subadult) stages (new state 1 → state 2). We also observe at similar stage an increase in the distal transverse expansion (ulnar character #4; character #86 in D'Emic, 2012) and the covariant character, an increase in the ulnar length-to-proximal breadth ratio (ulnar character #9; based in character #168 in Wilson, 2002; modified in character #276 in Curry Rogers, 2005). The robustness of the elements have been proposed to change during the ontogeny and less derived states are expressed in juvenile forms as observed in other sauropod taxa (Ikejiri, 2004; Díez Díaz *et al.*, 2015). The sauropod growth in the appendicular skeleton is mostly isometric, so these proportion changes have been expected to produce light differences along the ontogeny (e.g. Bonnan, 2004; Ikejiri, 2004; Tidwell & Wilhite, 2005; e.g. titanosaur limb bone midshaft section changes during development Stein *et al.*, 2010). However, this analysis shows that the change can also be translated to different character scorings. Whether it shows insights of allometric relationships between size and shape in the ulna (preliminary reports Páramo *et al.*, 2019) should be tested elsewhere.

Lastly, the changes during the development can also affect the scoring on the distal end of the ulna articular surface (ulnar character #7), changing toward a more circular shaped in the more

mature stages. However, character scoring difference in late mature stages of Morphotype II is variable in Morphotype I, as some intermediate (= subadult) stages shows score differences (see Fig.VI.22.C). This feature has been also discussed as variable in the sample of Lo Hueco before (see Chapter V) and could be related to intraspecific variability not related with ontogenetic development. Further inclusion of more specimens as well as better preservation of the distal end could help to verify this morphological variability at different ontogenetic stages.

The radius have been excluded from most of the analyses as its sample is too small. It seems that the specimen HUE-1140 represent an adult individual while the specimens HUE-1340 and HUE-2711 are juveniles based on the morphological features. The major difference between the probable juvenile individuals and the specimen HUE-1140 are in the absence of a marked interosseous distal ridge in posterior face (radial ontogenetic character #5) and the development of a marked ridge in the distal trochanter of the ulnar articulation (radial ontogenetic character #6). There is also a marked development of the radial distal articulation rugosity (radial ontogenetic character #2) in specimen HUE-1140 that it is less developed in the juvenile individuals. Also, the Mm. triceps brachii and humeroradialis trochanter in the proximal of medial face (radial ontogenetic character #3) is less developed (= smooth surface, small bump) in the specimen HUE-1166. This specimen is referred to Morphotype II but it is also a probable early juvenile based in the morphological features (almost all are score 0, with weakly developed muscular attachment and no rugosity in the proximal and distal ends).

When inspecting the morphological features, the only intraspecific variability observable are among the juvenile specimens of Morphotype I, as Morphotype II do not present more than one specimen. But we cannot confidently assume that the morphological differences among the sample of Morphotype I can be related with a significant effect of ontogenetic development. The only character which variability could be somewhat related is the difference in the midshaft breath of the specimen HUE-2711 compared with the other ones of Morphotype I. This specimen is slightly more robust (radial character #2) than the other specimens, and it is also a juvenile specimen. Some other elements present light differences in the rusticity (Ikejiri, 2004) during ontogeny, so it is possible that this feature can also be affected. However, more sample is necessary, as our current sample do not allow us to conclude morphological changes during the ontogeny and comparisons with other taxa are difficult, as the growth of sauropod forelimb zeugopodium is almost unknown (see Ikejiri, 2004; Tidwell & Wilhite, 2005).

The femora of Lo Hueco present a larger sample than other elements and some and a more accurate representation of the different ontogenetic stages can be recognized (at least for Morphotype I; see also Fig.VI.14 and VI.16) like in the humeral sample. The absence of a clear development of the fourth trochanter (femoral ontogenetic character #6; see Fig.VI.23) and the scar over the middle of proximodistal length of lateral bulge (femoral ontogenetic character #4) are related to early ontogenetic stages. Other features indicative of early developmental stage are the rugosity of the proximal and distal ends (smooth surface; femoral ontogenetic character #1 and #2), the absence of a rugosity surrounding the lateral epicondyle (femoral ontogenetic character #8) and the development of the linea intermuscularis cranialis in anterior face (femoral ontogenetic character #9). However, among these characters the presence of a rugosity on the lateral epicondyle and the rugosity of the distal end in general can be variable among juvenile and intermediate (= subadult) stages at least in Morphotype II (see Fig.VI.23.D). The development of the linea intermuscularis cranialis is also variable between the juvenile and intermediate stages,

but also present differences between the morphotypes (see Chapter IV, chapter V). However, the presence of a fully developed linea intermuscularis cranialis is related only to the more mature stages, probably in the transition between subadult and adult stages (see Fig. VI.23.C and D). The most mature stages are also clearly marked in both morphotypes by the appearance of developed mammillae in the proximal and distal end, with longitudinal grooves in the edge (e.g. HUE-594, HUE-3108; see Fig. VI.23). This also indicates that other taxa could present this feature as indicative of adult stage rather than a morphological feature of taxonomic relevance e.g. the presence of the longitudinal grooves in the distal end intercondylar area of *Ampelosaurus atacis* (C3-87, not present in the juvenile specimen C3-1182 or other specimens Le Loeuff, 2005; pers. obs. APB 2019).

At early developmental stages it is observed a small change in the position of the fourth trochanter (characters #267 and #268 Upchurch *et al.*, 2004; see also character #166 in Royo-Torres, 2009) in Morphotype I. However, this minor difference may be intraspecific variability not related with ontogenetic development, as most of the specimen present a change between state 1 and state 2 of the same character in the same ontogenetic stage. This character have been also commented as variable among individuals of similar size (see Chapter IV, Chapter V). Therefore, the most probable change of state related to ontogenetic development is the state between state 1 and state 2. At early developmental stages there are differences in the anteroposterior expansion of the distal end articular surface (femoral character #24: state 0 to new state 1; character #202 in Wilson, 2002). In addition, there are potential changes in the proximal end displacement to medial (femoral character #3; character #154 in Royo-Torres, 2009; see also character #241 in Gorscak *et al.*, 2017) but only in Morphotype II. The Morphotype I also presented some intraspecific differences in the medial deflection of the proximal end and the position of the femoral head, however, these findings suggest that it is not relatable to ontogenetic development in this morphotype.

Other variable character at juvenile to early intermediate ontogenetic stages are the distal condyle orientation respective to the shaft (femoral character #19; based in character #168 and #169 in Royo-Torres, 2009), the lateromedial width ratio between the fibular and tibial condyles (femoral character #21) and a change between an added state in the dorsoventral development of the lateral bulge and the derived state 2 (femoral character #10; see Salgado, Coria, & Calvo, 1997; and character #162 in Royo-Torres, 2009). However, the time of the changes on the relative orientation of the distal end vary from morphotype I (intermediate ontogenetic stages) and Morphotype II (early ontogenetic stages). In addition, the Morphotype II do not present scoring differences relatable to ontogenetic development in the relationships of the fibular and tibial condyle width, neither in the development of the lateral bulge (see Fig. VI.23.B). A variable character in the intermediate developmental stages is the femoral head alignment with the condyles (femoral character #4), related with the position of the femoral head with medial of the shaft as seen before.

At later ontogenetic stages, probable in the subadult to adult individuals, several differences between character scorings can be observed. The displacement of the distal end previously commented experiment yet another score difference between intermediate stages and more mature stages (femoral character #3: new state 1 to state 2; character #154 in Royo-Torres, 2009; see also character #241 in Gorscak *et al.*, 2017) and the presence of an accessory trochanter to the fourth trochanter (following Vila *et al.*, 2012). It is also important to note that the later presence of this accessory trochanter only among mature specimens could be conditioning its relevance to identify morphotypes in several titanosaur morphotypes of the Ibero-Armorican

domain (Vila *et al.*, 2012; see Chapter IV). The variation on the position of the femoral head respective to the greater trochanter and the lateral half of the proximal end (femoral character #23; character #341 in Tschopp, Mateus, & Benson, 2015). There are also some scoring changes in the anteroposterior development of the distal end (femoral character #24: new state 1 to state 2; character #202 in Wilson, 2002). But in Morphotype I this change is produced at more intermediate stages rather than the most mature stages.

The variability at intermediate ontogenetic stages in the overall position of the femoral head (e.g. femoral character #2) and the relative position of the femoral head respective to the greater trochanter (femoral character #24) as well as the increasing rugosity of the proximal end (femoral ontogenetic character #1) are congruent with observation in other sauropod ontogenetic series. The femoral head have smoother bone surface as well as less development of the convexity of the femoral head as well as more anteroposteriorly compressed femoral head in specimens referred to least mature individuals, (Ikejiri, 2004; Ikejiri *et al.*, 2005b). The robustness of the femur present some differences between the juvenile and adult forms (Ikejiri, 2004) despite an isometric relationship between the size and the shape of the femur (Bonnan, 2004; Ikejiri, 2004). This variation is minimal. While we recovered also a light difference in the scoring of characters relative to the development of the minimum midshaft posterolateral width (femoral character #16) in Morphotype I, we cannot refer to the mentioned ontogenetic changes. This feature does not present variation in the morphotype II, and juvenile specimens present the same scoring as the adults (Fig.VI.23). The Morphotype I present some variability in the morphology of the shaft under the lateral bulge and the position of the midshaft minimum width may vary without relationship with changes on the overall robustness (see Chapter V). Also, few differences have been found between the minimum midshaft width of the Morphotype I (see Chapter IV.1) and none can be attributed to the specimens here estimated at juveniles (e.g. HUE-2636, HUE-8801). Therefore, based on these observations and the high variability in the timing of the scoring changes (see the range in Fig.VI.23.A) we can conclude that it is relatable to intraspecific variability with no significant effect of the ontogenetic development. Lastly, there is a variability on the twisting of the femoral head (femoral character #29) proposed here based on the subtle differences observed in other Ibero-Armorican titanosaur morphotypes (Vila *et al.*, 2012). The anterior twisting is only produced among the more mature specimens in each morphotype and therefore cannot be observed in juvenile individuals, which may have implications in order to use this feature to distinguish sauropod femoral morphotypes when they are isolated.

Among the proposed morphological characters, it is important to take into account the taxonomical differences on the trochanteric shelf when comparing ontogenetic changes among different sauropod groups (see Wilson & Carrano, 1999; D'Emic, 2012). We considered the femoral ontogenetic character #4 based on subtle differences on the bone surface the presence of a bone ridge connecting the greater trochanter to the lateral bulge. However, not all titanosaur sauropods present this structure (D'Emic, 2012), therefore the absence is independent to the ontogenetic stage. Other sauropod however, present a stout and step-like morphology between the trochanteric shelf and the lateral bulge e.g. *Aeolosaurus* sp. (Candeiro, 2010; pers. obs. APB 2016) and *Magyarosaurus* spp. (including the smaller, probable juvenile individuals Nopsca, 1915; pers. obs. APB 2016) and present this structure in most of the specimens regardless of the ontogenetic stage.

The tibiae present three easily recognized major ontogenetic events between the early

juvenile and more mature stages. Thought most of the specimen have a development of the proximal end rugosity and few present an early, smoother surface of the articulation. This character (tibial character #1) can be absent in some early ontogenetic stages (see Fig.VI.24) with the development of the distal end articulation surface (tibial ontogenetic character #2) and the absence of a muscular attachment in the middle to distal half of the cnemial crest (tibial ontogenetic character #4). Their development is probably in early juveniles, post-hatchling, as we recovered early differences in those characters for Morphotype I but all the early ontogenetic stages registered in the sample of Morphotype II present most of these features.

The intermediate ontogenetic stages present an overlapping between the scoring changes in several ontogenetic characters. A feature combination that potentially mark this event is the development of the proximal attachment in the cnemial crest (tibial ontogenetic character #3) with the lack of a marked ridge and fossa related with the M. gastrocnemius in the posterior medial face (tibial ontogenetic character #7). But it is necessary to take into account some taxonomical differences in the presence of this posterior proximal ridge, much more developed in Morphotype II, which also present at probably earlier developmental stages (see Fig.VI.24.D).

The more mature stages are identified by the presence of this ridge (tibial ontogenetic character #7) as well as fully developed and the marked rugosity with longitudinal grooves or sulcus in the edge of the proximal and distal end articulation (tibial ontogenetic character #1 and #2: state 2).

The osteological characters however present few different scorings related with the ontogenetic stages. At early stages the ratio between the anteroposterior and lateromedial width of the distal end (tibial character #12 based after Salgado *et al.*, 1997), the dorsal contour of the articular surface with the fibula (tibial character #8), the maximal lateromedial length of the distal end (tibial character #14; after Salgado *et al.*, 1997; see also character #277 in Upchurch *et al.*, 2004) and the complexity of the cnemial crest (tibial character #7; not confound with character #443 in Tschopp *et al.*, 2015). The maximal lateromedial length of the distal end is slightly different in Morphotype II up to intermediate ontogenetic stages. But this feature can be affected by the lack of preservation of the distal end especially in Morphotype II (see Chapter IV, Chapter V). As some of the specimens of Morphotype II present an acquisition of this feature at early ontogenetic stages (see Fig.VI.24.B) we prefer the more conservative assumption of early acquisition of the state 1 among the sample of Morphotype II similar to Morphotype I.

The torsion of the distal end (tibial character #11 based in Sanz *et al.*, 1999; and character #181 in Royo-Torres, 2009) and the morphology of the cnemial crest (character #6; based in character #177 in Royo-Torres, 2009) are acquired at intermediate ontogenetic stages. Thought both characters are variable in Morphotype II and can present the more developed scoring at early stages (see Fig.VI.23.B). While the only character that can be confidently assessed to present a intermediate to later developmental stages is the distal end contour (tibial character #13), which can be present slightly earlier in Morphotype I. Nevertheless, as with other characters elated to the distal end, it is possible that the lack of preservation in the sample of Morphotype II suggest a later development of this character than the actual, slightly earlier intermediate stage as in Morphotype I. It is important to note the possible taxonomic difference in the development of the posterior surface of the cnemial crest (tibial character #16, based in character #445 in Tschopp *et al.*, 2015). This character is acquired at late stages of development in Morphotype

II but at early stages in Morphotype I. As it is related with the development of the possible secondary cnemial crest of Morphotype I, probably this character is acquired earlier during the development of this morphotype. Therefore, it will be congruent with the variability of this feature and the early development in Morphotype I previously commented (related with the development of the fibular articulation, see tibial ontogenetic character #5).

The fibulae present a complex arrange of ontogenetic characters that could determine the overall ontogenetic stage of the individual (see Fig.VI.25). The early ontogenetic stages can be defined by the absence of a rugosity on proximal and distal end (fibular ontogenetic character #1 and #2), the absence of a clear ridge or rugosity in dividing the anterior trochanter from the shaft (fibular ontogenetic character #3). However, most of the specimens in the current sample present the development of the anterior trochanter and only one specimen (e.g. HUE-5232) lack a clear separation of this structure from the lateral face of the shaft. Lack of the ridge or rugosity would be indicative of post-hatchling juvenile individuals or some stage earlier than the juvenile specimens described in this study.

The more intermediate stages can be marked by the presence of the rugosity or marked ridge of the M. iliofibularis in the lateral trochanter (fibular ontogenetic character #4) and the tibial articulation scar (fibular ontogenetic character #5). At this time there is also the development of the anterolateral crest rugose surface on the edge and clearly differenced from the lateral face of the shaft (fibular ontogenetic character #6) as with the anterior trochanter in proximal. However, this character is variable from early to intermediate ontogenetic stages and the absence could not be easily associated with early juvenile or more developed individuals. In the other hand, its absence could be related with at least juvenile to subadult individuals.

In the other hand, four characters in the most derived state (Fig.VI.25) can identify the mature stage, probably related with adult forms. The presence of a fully developed tibial scar with a secondary ridge in the proximal posterior medial face (fibular ontogenetic character #5). There is also a marked and acute ridge, sometimes bifurcated, or the presence of a stout and rugose, oval shaped M. iliofibulares attachment in the lateral trochanter (fibular ontogenetic character #4) and the rugosity with mammillae in the proximal and distal end (fibular ontogenetic character #1 and #2). With all these features, the individual can be referred to a mature adult.

As well as other elements, several osteological characters seems to present some variation between different ontogenetic stages. The least mature individuals can present different scoring in the anterior trochanter development (fibular character #3; based on a combination of cahracter #189 and #190 in Royo-Torres, 2009) and the shape of the proximal end (fibular character #2; added several states to character #188 Royo-Torres, 2009). Up to intermediate ontogenetic stages, the presence of an anterolateral sulcus to the anterior trochanter can also present different scoring (fibular character #4; see also Royo-Torres, 2009: related also to fibular ontogenetic character #3). There is also a difference in character scoring in the complexity of the lateral trochanter (fibular character #10; based in character #192 in Royo-Torres, 2009; see also character #253 in Gorscak *et al.*, 2017) which is related with the fibular ontogenetic character #4, therefore can also present another different character scoring at more mature ontogenetic stages. There is also some variability in the stage in which the anteromedial directed crest can present a notch behind the cnemial crest of the tibia (fibular character #5; see character #447 in Tschopp *et al.*, 2015). This feature is probably developed at intermediate stages in Morphotype

I, much earlier than in Morphotype II, because the strong medial deflection of the anterior trochanter in this morphotype (e.g. HUE-3082).

The characters that present some differences at late stages are the morphology of the proximal end contour (fibular character #2; as there were some new stages added, see Supplementary Material C) and the transverse expansion of the distal end (fibular character #11; see Royo-Torres, 2009; see also character #448 in Tschopp *et al.*, 2015). We observed also the presence of a tranverse lamina in the medial face of the distal end related with medial concavity where the anterior ascending process of the tibia articulates. This distal transverse ridge or lamina in the medial distal edge can be present only among the late ontogenetic stages (fibular character #13).

Our observations coincides with some previous descriptions of ontogenetic changes in sauropod appendicular skeleton (Dong, 1990; Carpenter & McIntosh, 1994; Ikejiri, 2004; Tidwell & Wilhite, 2005; Schwarz *et al.*, 2007a). Also, some of these morphological changes on the appendicular skeleton have been identified in archosauria long bones(Barreto *et al.*, 1993; Carpenter & McIntosh, 1994; Geist & Jones, 1996; Ikejiri, 2004; Bybee, Lee, & Lamm, 2006; Tumarkin-Deratzian *et al.*, 2006; Fostowicz-Frelik & Sulej, 2009; Woodruff, 2015; Vieira *et al.*, 2016). The use of ontogenetic characters related mostly with muscular and tendinous attachments could help establish ontogenetic sequences and identify qualitative ontogenetic stages with better precision than with isolated ontogenetic characters or the use of the size of the specimen (see also Carballido & Sander, 2014).

We observed that several osteological characters can present a high variability between early juvenile and adult individuals, more than previously reported (e.g. Ikejiri *et al.*, 2005b; Tidwell & Wilhite, 2005). Despite this variability, the number of characters susceptible to significant effects of ontogenetic development are still low. Most of the character variability can be avoided by including only individuals that do not exhibit juvenile features (see discussion in Upchurch *et al.*, 2004; Carballido & Sander, 2014). However, some (few) characters present a variability in the character scores at late ontogenetic stages, which might be unavoidable. In addition, we identified several patterns of character variation during ontogeny that present differences between both morphotypes and could reflect taxonomical differences in the growth model. This ontogenetic variability can be taken into account in the codification and scoring of morphological datasets for phylogenetic analysis in order to avoid errors and misinterpretations by cautious practices on character scoring and taxa inclusion. Another possibility is to include ontogenetic characters that shows potential phylogenetic information. Though this should be tested, as for now we cannot assess if these differences in the tempo of character change between the morphotypes can represent major differences in the growth model with potential phylogenetic implications i.e. heterochrony (as suggested by Company, 2011). Another possibility is switching toward the scoring of specimens against the use of OTUs based on several individuals and assessing intraspecific variability (see discussion of intraspecific variability and taxnomic differences in Tschopp *et al.*, 2015).

Most of the character changes found in this study are among earlier ontogenetic stages, which is compatible also with the presence of ontogenetic sequence polymorphism at early stages of development (see Ontogenetic Sequence Analyses). The presence of different ossification patterns can produce more morphological variation among juveniles. In addition to this, the concentration of morphological variation at early stages and fast fixation of adult morphology (= scorings in this study) and similarities between juvenile and adult individuals (see cluster analysis

results) is congruent with current known fast and isometric growth of titanosaur sauropods. Most of the morphological changes are expected to happen among post-hatchling juveniles. Most of the sampled specimens here are probably from later stages, juvenile to sub-adult individuals in the earlier ontogenetic stages here reported. This has to be taken into consideration on what we know now about sauropod herd composition (e.g. Myers & Fiorillo, 2009; Castanera *et al.*, 2011). The structure recovered in the fossil site of Lo Hueco is compatible with the hypothesis introduced by those authors. Most of the sampled specimens are from juvenile to sub-adults forms with fewer early juvenile individuals. However, further sampling is required to test this hypothesis, as well as taphonomical analysis of the sample of Lo Hueco and compare other Ibero-Armorican sauropod ontogenetic sequences. A detailed study on the sauropod population composition in Lo Hueco should be covered elsewhere and is beyond the scopes of this work.

In order to test the presence of heterochronic development on the titanosaur appendicular skeleton, further sample is required. The inclusion of more than two Ibero-Armorican taxa is necessary to address the differences reported in the current study. It is also important to support analysis of more sauropod ontogenetic sequences with analyses of paleogistological samples. One caveat of the methods here deployed is the estimation of relative ontogenetic stages. In order to compare between different taxa, a homology must be established. The use of standard histological ontogenetic stages can help to determine common ontogenetic stages obtained by current methodologies. It is also important to further increase the analyses of Lo Hueco titanosaur with analyses of the complete limbs. For this reason, further sample of partially articulated individuals are needed.

VI.6. CAVEATS OF THIS STUDY

The ontogenetic stage estimation method presented here suffer from some limitations. First and more important consideration made in this study is the difficulty to establish a whole fore and hindlimb comparison or one that include the complete appendicular skeleton of *Lohuecotitan pandafilandi* + Morphotype I or the Morphotype II. The association between individuals in the konzentrat-lagerstätten site of Lo Hueco is difficult, as many of the specimens have been recovered isolated (Ortega *et al.*, 2015). This makes impossible to analyse each complete limb as one data matrix neither produce homology between the different estimated ontogenetic stages (e.g. Griffin *et al.*, 2019).

The OCSA and OSA are methodologies that only estimates a relative ontogenetic stage as we cannot assess the absolute time and age of an specific MOS (see Carballido & Sander, 2014). The tempo is relative to each taxon sampled and we cannot reliably assess whether the MOS three of the ulna of Morphotype I is acquired at the same maturity age as the MOS three of the ulna of Morphotype II. Histological sampling and calibration with the HOS of several specimens is necessary. This calibration will help us establishing those cross-taxa comparisons. As seen in this study however, there are some minor differences in growth patterns between the morphotypes despite the growth main mechanics seems to stay the same i.e. both morphotypes in general: typical titanosaur fast growth, morphological similarities between juvenile and adult specimens and early ontogenetic sequence polymorphism, see Results. This minor differences might support the heterochronic growth model proposed for the titanosaur appendicular skeleton (Company, 2011), but for now the sample compared might be too low. We prefer a conservative conclusion

of no proof of heterochronic growth among the sample from Lo Hueco. In future studies each OCSA and OSA stage estimation could be calibrated to the standard HOS, until then the interspecific comparison might be tentative. In addition, the application of this methodology in more taxa with a proper calibration to the more readily available HOS might help to test this hypothesis as two current morphotypes could not be enough to support the presence of heterochrony among the Late Cretaceous European titanosaur faunas. The report of ontogenetic character acquisition at different developmental stages, whether or not present ontogenetic sequence polymorphism, is a criteria for determining the growth mode. The presence of these ontogenetic changes in character scorings has been already used in other vertebrate groups (Geist & Jones, 1996; Sánchez-villagra, 2002; Prochel, Vogel, & Sánchez-Villagra, 2004; Weisbecker *et al.*, 2008; Mitgutsch *et al.*, 2011; Wilson & Sánchez-Villagra, 2011; Hautier *et al.*, 2013; Griffin & Nesbitt, 2016a; Griffin, 2018).

VI.7. CONCLUSIONS

We found several ontogenetic sequences on the long bones of the two titanosaur appendicular morphotypes from Lo Hueco. several characters were used to determine the presence of juvenile, subadult and adult specimens. Some morphological characters are variable during sauropod ontogenetic postnatal development as occur in other taxa, such as *Venenosaurus*, and *Camarasaurus* spp. We used those characters as well as the definition of new ones that has helped us to estimate the developmental stages in humeri, ulnae, radii, femora, tibiae and fibulae from Morphotype I + *Lohuecotitan pandafilandi* and a second titanosaur morphotype from Lo Hueco, which we believe that belongs to a distinct taxon. Based on this estimation we found ontogenetic sequence polymorphism caused by high intraspecific variability on ontogenetic development in the humeri, femora, tibiae of both morphotypes, and in the fibulae of Morphotype II. This polymorphism is concentrated at early stages of developmental except for Morphotype II humeri, which present higher sequence polymorphism at more mature developmental stages. This general trend also coincides with the precocity growth model proposed for titanosaur sauropods and observed in other sauropods as higher number of changes are expected among juvenile stages.

Our findings also point toward some minor differences in the growth models between the morphotypes, but for now our sample does not permit us to test the presence of heterochronic growth in European titanosaurs as suggested by other authors. An increase in the sample of both morphotypes from Lo Hueco (several specimens still need to be prepared) as well as in more Ibero-Armorican taxa will help to test this hypothesis.

This ontogenetic development effect on intraspecific variability and the possibility of several different growth dynamics among the titanosaurs of Lo Hueco are translated in several character scoring differences during ontogeny. We found that majority of morphological characters established for appendicular bones used in cladistics might be affected by ontogeny, i.e., the scoring might depend on the development stage of the scored individual. However, the performed analysis suggested that only a minor proportion of the morphological changes occur in later developmental stages and should impact the phylogenetic analyses if handled properly. There are also some insights that current character scoring differences and timing during the ontogeny could be related with allometric growth, but further analyses are necessary to prove it and should be published elsewhere.

The abundant sample of Lo Hueco aimed to test several developmental hypotheses and establish a detailed study on the morphological variation of the anatomy of fore- and hindlimb bones during ontogeny. Further studies and the calibration based on paleohistological sampling will be necessary to assess the complex patterns of feature acquisition during the postnatal ontogenetic development and establish comparison between other Ibero-Armorican titanosaurs..

VI.8. BIBLIOGRAPHY

Allain R, Aquesbi N. 2008. Anatomy and phylogenetic relationships of Tazoudasaurus naimi (Dinosauria, Sauropoda) from the late Early Jurassic of Morocco. *Geodiversitas* 30: 345–424.

Badyaev A V. 2002. Growing apart: an ontogenetic perspective on the evolution of sexual size dimorphism. *Trends in Ecology & Evolution* 17: 369–378.

Barreto C, Albrecht RM, Bjorling DE, Horner JR, Wilsman NJ. 1993. Evidence of the Growth Plate and the Growth of Long Bones in Juvenile Dinosaurs. *Science* 262: 2020–2023.

Bever GS, Brusatte SL, Balanoff AM, Norell MA. 2011. Variation, variability, and the origin of the avian endocranium: Insights from the anatomy of *Alioramus altai* (theropoda: Tyrannosauroidea). PLoS ONE 6.

Bonaparte JF, González Riga BJ, Apesteguía S. 2006. *Ligabuesaurus leanzai* gen. et sp. nov. (Dinosauria, Sauropoda), a new titanosaur from the Lohan Cura Formation (Aptian, Lower Cretaceous) of Neuquén, Patagonia, Argentina. *Cretaceous Research* 27: 364–376.

Bonaparte JF, W.-D. Heinrich WD, Wild R. 2000. Review of Janenschia WILD, with the description of a new sauropod from the Tendaguru beds of Tanzania and a discussion on the systematic value of procoelous caudal vertebrae in the sauropoda. *Palaeontographica Abteilung* A 256: 25–76.

Bonnan MF. 2004. Morphometric analysis of humerus and femur shape in Morrison sauropods: implications for functional morphology and paleobiology. *Paleobiology* 30: 444–470.

Bonnan MF. 2007. Linear and geometric morphometric analysis of long bone scaling patterns in Jurassic neosauropod dinosaurs: their functional and paleobiological implications. *Anatomical Record* 290: 1089–111.

Borsuk-Bialynicka M. 1977. A New Camarasaurid Sauropod *Opisthocoelicaudia skarzynskii* gen. n., sp. n. from the Upper Cretaceous of Mongolia. *Paleontologia Polonica* 37: 5–64.

Brochu CA. 1996. Closure of neurocentral sutures during crocodilian ontogeny: Implications for maturity assessment in fossil archosaurs. *Journal of Vertebrate Paleontology* 16: 49–62.

Bybee PJ, Lee AH, Lamm ETT. 2006. Sizing the Jurassic theropod dinosaur *Allosaurus*: Assessing growth strategy and evolution of ontogenetic scaling of limbs. *Journal of Morphology* 267: 347–359.

Canale JI, Novas FE, Salgado L, Coria RA. 2015. Cranial ontogenetic variation in *Mapusaurus roseae* (Dinosauria: Theropoda) and the probable role of heterochrony in carcharodontosaurid evolution. *Paläontologische Zeitschrift* 89: 983–993.

Candeiro CR a. 2010. Record of the genus *Aeolosaurus* (Sauropoda, Titanosauria) in the Late Cretaceous of South America: paleogeographic implications. *Estudios Geológicos* 66: 243–253.

Canudo JI, Oms O, Vila B, Galobart À, Fondevilla V, Puértolas E, Sellés AG, Cruzado-Caballero P,

Dinarès-Turell J, Vicens E, Castanera D, Company J, Burrel L, Estrada R, Marmi J, Blanco A. 2016. The upper Maastrichtian dinosaur fossil record from the southern Pyrenees and its contribution to the topic of the Cretaceous-Palaeogene mass extinction event. *Cretaceous Research* 57: 540–551.

Carballido JL, Marpmann JS, Schwarz D, Pabst B. 2012. New information on a juvenile sauropod specimen from the Morrison Formation and the reassessment of its systematic position. *Palaeontology* 55: 567–582.

Carballido JL, Pol D, Otero A, Cerda IA, Salgado JL, Garrido AC, Ramezani J, Cúneo NR, Krause JM. 2017. A new giant titanosaur sheds light on body mass evolution among sauropod dinosaurs. *Proceedings of the Royal Society B: Biological Sciences* 284: 20171219.

Carballido JL, Sander PM. 2014. Postcranial axial skeleton of *Europasaurus holgeri* (Dinosauria, Sauropoda) from the Upper Jurassic of Germany: implications for sauropod ontogeny and phylogenetic relationships of basal Macronaria. *Journal of Systematic Palaeontology* 12: 335–387.

Carpenter K, McIntosh JS. 1994. Upper Jurassic sauropod babies from the Morrison Formation. In: Carpenter K, Hirsch KF, Horner JR, eds. *Dinosaur Eggs and Babies*. Cambridge: Cambridge University Press, 265–278.

Carpenter K, Tidwell V. 2005. Reassessment of the Early Cretaceous Sauropod *Astrodon johnstoni* Leidy 1865 (Titanosauriformes). In: Tidwell V, Carpenter K, eds. *Thunder-Lizards: The Sauropodomorph Dinosaurs*. Bloomington and Indianopolis: Indiana University Press, 38–77.

Carr TD. 2010. A taxonomic assessment of the type series of *Albertosaurus sarcophagus* and the identity of Tyrannosauridae (Dinosauria, Coelurosauria) in the Albertosaurus bonebed from the Horseshoe Canyon Formation (Campanian–Maastrichtian, Late Cretaceous. *Canadian Journal of Earth Sciences* 47: 1213–1226.

Castanera D, Barco JL, Díaz-Martínez I, Gascón JH, Pérez-Lorente F, Canudo JI. 2011. New evidence of a herd of titanosauriform sauropods from the lower Berriasian of the Iberian range (Spain). *Palaeogeography, Palaeoclimatology, Palaeoecology* 310: 227–237.

Cerda IA, Chinsamy A. 2012. Biological implications of the bone microstructure of the Late Cretaceous Ornithopod Dinosaur *Gasparinisaura cincosaltensis*. *Journal of Vertebrate Paleontology* 32: 355–368.

Cerda IA, Chinsamy A, Pol D, Apaldetti C, Otero A, Powell JE, Martínez RN. 2017. Novel insight into the origin of the growth dynamics of sauropod dinosaurs. *PloS ONE* 12: e0179707.

Cerda IA, Powell JE. 2009. Microestructura ósea de los osteodermos de *Saltasaurus loricatus* Bonaparte y Powell, un titanosaurio del Cretácico Superior del norte argentino. *III Jornadas Argentinas de Paleontología de Vertebrados*. 19–20.

Colbert MW, Rowe TB. 2008. Ontogenetic Sequence Analysis: using parsimony to characterize developmental sequences and sequence polymorphism. *Journal of Experimental Zoology. Part B, Molecular and developmental evolution* 310: 398–416.

Company J. 2011. Bone histology of the titanosaur *Lirainosaurus astibiae* (Dinosauria: Sauropoda) from the Latest Cretaceous of Spain. *Die Naturwissenschaften* 98: 67–78.

Company J, Suberbiola XP, Ruiz-Omeñaca JI. 2009. Nuevos restos fósiles del dinosaurio *Lirainosaurus*. *Ameghiniana* 46: 391–405.

Curry Rogers K. 2005. Titanosauria: A phylogenetic overview. In: Curry Rogers K, Wilson JA, eds. *The Sauropods: Evolution and Paleobiology*. Berkeley: University of California Press, 50–103.

Curry Rogers K. 2009. The postcranial osteology of *Rapetosaurus krausei* (Sauropoda: Titanosauria) from the Late Cretaceous of Madagascar. *Journal of Vertebrate Paleontology* 29: 1046–1086.

Curry Rogers K, Forster CA. 2001. The last of the dinosaur titans: a new sauropod from Madagascar. *Nature* 412: 530–4.

Curry Rogers K, Whitney M, D'Emic MD, Bagley B. 2016. Precocity in a tiny titanosaur from the Cretaceous of Madagascar. *Science* 352: 450–453.

Curtice BD, Wilhite RD. 1997. A statistical analysis of sauropod limb elements. *Journal of Vertebrate Paleontology* 17: 41A.

D'Emic MD. 2012. The early evolution of titanosauriform sauropod dinosaurs. *Zoological Journal of the Linnean Society* 166: 624–671.

D'Emic MD, Wilson JA. 2011. New remains attributable to the holotype of the sauropod dinosaur *Neuquensaurus australis*, with implications for saltasaurine systematics. *Acta Palaeontologica Polonica* 56: 61–73.

Díez Díaz V, Garcia G, Pereda-Suberbiola X, Stein KHW, Jentgen-Ceschino B, Godefroit P, Valentin X. 2018. The titanosaurian dinosaur *Atsinganosaurus velauciensis* (Sauropoda) from the Upper Cretaceous of southern France: New material, phylogenetic affinities, and palaeobiogeographical implications. *Cretaceous Research* 91: 429–456.

Díez Díaz V, Mocho P, Páramo A, Escaso F, Marcos-Fernández F, Sanz JL, Ortega F. 2016. A new titanosaur (Dinosauria, Sauropoda) from the Upper Cretaceous of Lo Hueco (Cuenca, Spain). *Cretaceous Research* 68: 49–60.

Díez Díaz V, Ortega F. 2013. Dorsal vertebrae of a juvenile titanosaur from the Late Cretaceous of "Lo Hueco" (Cuenca, Spain). *XI Annual Meeting of the European Association of Vertebrate Paleontologists*. 35A.

Díez Díaz V, Pereda Suberbiola X, Company J. 2015. Updating titanosaurian diversity (Sauropoda) from the Late Cretaceous of Spain: The fossil site of Laño and Chera. *Spanish Journal of Palaeontology* 30: 293–306.

Díez Díaz V, Suberbiola XP, Sanz JL. 2013. Appendicular skeleton and dermal armour of the Late Cretaceous titanosaur *Lirainosaurus astibiae* (Dinosauria: Sauropoda) from Spain. *Palaeontologia Electronica* 16: 18 p.

Diogo R, Abdala V. 2007. Comparative anatomy, homologies and evolution of the pectoral muscles of bony fish and tetrapods: A new insight. *Journal of Morphology* 268: 504–517.

Diogo R, Abdala V. 2010a. *Muscles of Vertebrates* (R Diogo and V Abdala, Eds.). Enfield, New Hampshire: Taylor & Francis.

Diogo R, Abdala V. 2010b. *Muscles of vertebrates: comparative anatomy, evolution, homologies and development*. Taylor & Francis.

Diogo R, Molnar J. 2014. Comparative Anatomy, Evolution, and Homologies of Tetrapod Hindlimb Muscles, Comparison with Forelimb Muscles, and Deconstruction of the Forelimb-Hindlimb Serial Homology Hypothesis. *Anatomical Record* 297: 1047–1075.

Dong Z. 1990. Sauropoda from the Kelamaili region of the Junggar Basin, Xinjiang Autonomous Region. *Vertebrata Palasiatica* 28: 43–58.

Ekdale EG. 2010. Ontogenetic Variation in the Bony Labyrinth of *Monodelphis domestica* (Mammalia: Marsupialia) Following Ossification of the Inner Ear Cavities. *The Anatomical Record: Advances in Integrative Anatomy and Evolutionary Biology* 293: 1896–1912.

Fechner R. 2009. Morphofunctional Evolution of the Pelvic Girdle and Hindlimb of Dinosauromorpha on the Lineage to Sauropoda. Unpublished thesis, Ludwigs Maximilians Universität.

Fondevilla V, Dalla Vecchia FM, Gaete R, Galobart À, Moncunill-Solé B, Köhler M. 2018. Ontogeny and taxonomy of the hadrosaur (Dinosauria, Ornithopoda) remains from Basturs Poble bonebed (late early Maastrichtian, Tremp Syncline, Spain). *PLoS ONE* 13: e0206287.

Forster CA. 2005. New Juvenile Sauropod Material from Western Colorado, and the Record of Juvenile Sauropods from Up Juras Morrison Formation. Tidwell, V. & Carpenter, K. (eds). *Thunder-Lizards: The Sauropodomorph Dinosaurs*. Bloomington and Indianopolis: Indiana University Press, 141–153.

Fostowicz-Frelik Ł, Sulej T. 2009. Bone histology of *Silesaurus opolensis* Dzik, 2003 from the Late Triassic of Poland. *Lethaia* 43: 137–148.

Foth C, Hedrick BP, Ezcurra MD. 2016. Cranial ontogenetic variation in early saurischians and the role of heterochrony in the diversification of predatory dinosaurs. *PeerJ* 4: e1589.

Fröbisch NB. 2008. Ossification patterns in the tetrapod limb - Conservation and divergence from morphogenetic events. *Biological Reviews* 83: 571–600.

Gallina PA. 2011. Estudio Anatómico, Sistemático Y Paleobiológico De *Bonitasaura salgadoi* (Dinosauria, Sauropoda): Su Importancia En El Contexto De La Evolución De Los Titanosaurios Del Cretácico Superior De La Argentina. : 340.

Galton PM, Upchurch P. 2004. Prosauropoda. In: Weishampel DB, Dodson P, Osmolska H, eds. *The Dinosauria*. Berkeley: University of California Press, 232–258.

García RA, Salgado JL, Coria RAA, Chiappe LM. 2010. Osteología embrionaria de saurópodos titanosaurios de Neuquén (Argentina): aspectos ontogenéticos y evolutivos. *Ameghiniana* 47: 409–430.

García RA, Salgado L, Fernández MS, Cerda IA, Carabajal AP, Otero A, Coria RA, Fiorelli LE, Salgado JL, Fernández MS, Cerda IA, Carabajal AP, Otero A, Coria RA, Fiorelli LE. 2015. Paleobiology of Titanosaurs: Reproduction, Development, Histology, Pneumaticity, Locomotion and Neuroanatomy from the South American Fossil Record. *Ameghiniana* 52: 29–68.

Garn SM, Rohmann CG. 1960. Variability in the order of ossification of the bony centers of the hand and wrist. *American Journal of Physical Anthropology* 24: 101–116.

Gascó F, Vidal D, Páramo A, Mocho P, Ortega F. 2018. New insights into the palaeohistology of the titanosaur sauropods from the Upper Cretaceous of Lo Hueco (Cuenca, Spain). *XVI Annual Meeting of European Association of Vertebrate Paleontologists*. 76.

Geist NR, Jones TD. 1996. Juvenile skeletal structure and the reproductive habits of dinosaurs. *Science* 272: 712–714.

Gilmore CW. 1936. The osteology of *Apatosaurus* with special reference to specimens in the Carnegie Museum. *Memoirs of the Carnegie Museum* 11: 175–300.

Goloboff PA, Farris JS, Nixon K. 2008a. TNT: Tree analysis using New Technology, vers. 1.1 (Will Henning Edition). Program and documentation. Available at: http://www.zmuc.dk/public/phylogeny/tnt.

Goloboff PA, Farris JS, Nixon KC. 2008b. TNT, a free program for phylogenetic analysis. *Cladistics* 24: 774–786.

González Riga BJ, Lamanna MC, Otero A, Ortiz David LD, Kellner AWA, Ibiricu LM. 2019. An overview of the appendicular skeletal anatomy of South American titanosaurian sauropods,

with definition of a newly recognized clade. *Anais da Academia Brasileira de Ciências* 91: e20180374.

González Riga BJ, Mannion PD, Poropat SF, Ortiz David LD, Coria JP. 2018. Osteology of the Late Cretaceous Argentinean sauropod dinosaur *Mendozasaurus neguyelap*: implications for basal titanosaur relationships. *Zoological Journal of the Linnean Society*: 1–46.

González Riga BJ, Previtera E, Pirrone C a. 2009. *Malarguesaurus florenciae* gen. et sp. nov., a new titanosauriform (Dinosauria, Sauropoda) from the Upper Cretaceous of Mendoza, Argentina. *Cretaceous Research* 30: 135–148.

Gorscak E, O'Connor PM, Roberts EM, Stevens NJ. 2017. The second titanosaurian (Dinosauria: Sauropoda) from the middle Cretaceous Galula Formation, southwestern Tanzania, with remarks on African titanosaurian diversity. *Journal of Vertebrate Paleontology* 37.

Gower JC. 1971. A General Coefficient of Similarity and Some of Its Properties. Biometrics 27: 857–874.

Griffin CT. 2018. Developmental patterns and variation among early theropods. *Journal of Anatomy* 232: 604–640.

Griffin CT, Bano LS, Turner AH, Smith ND, Irmis RB, Nesbitt SJ. 2019. Integrating gross morphology and bone histology to assess skeletal maturity in early dinosauromorphs: new insights from *Dromomeron* (Archosauria: Dinosauromorpha). *PeerJ* 7: e6331.

Griffin CT, Nesbitt SJ. 2016a. Anomalously high variation in postnatal development is ancestral for dinosaurs but lost in birds. *Proceedings of the National Academy of Sciences* 113: 14757–14762.

Griffin CT, Nesbitt SJ. 2016b. The femoral ontogeny and long bone histology of the Middle Triassic (?late Anisian) dinosauriform *Asilisaurus kongwe* and implications for the growth of early dinosaurs. *Journal of Vertebrate Paleontology* 36.

Hammer Ø, Harper DAT. 2008. *Paleontological Data Analysis*. Wiley-Blackwell Publishing.

Hanik GM, Lamanna MC, Whitlock JA. 2017. A Juvenile Specimen of *Barosaurus* Marsh, 1890 (Sauropoda: Diplodocidae) from the Upper Jurassic Morrison Formation of Dinosaur National Monument, Utah, USA. *Annals of Carnegie Museum* 84: 253–263.

Hautier L, Bennett NC, Viljoen H, Howard L, Milinkovitch MC, Tzika AC, Goswami A, Asher RJ. 2013. Patterns Of Ossification In Southern Versus Northern Placental Mammals. *Evolution* 67: 1994–2010.

Hedrick BP, Tumarkin-Deratzian AR, Dodson P. 2012. Bone microstructure and relative age of the holotype specimen of the diplodocoid sauropod dinosaur *Suuwassea emilieae*. *Acta Palaeontologica Polonica* 59: 295–304.

Hennig W. 1966. *Phylogenetic Systematics*. Urbana, Illinois, USA: University of Illinois Press.

Holliday CM, Ridgely RC, Sedlmayr JC, Witmer LM. 2010. Cartilaginous Epiphyses in Extant Archosaurs and Their Implications for Reconstructing Limb Function in Dinosaurs. *PLoS ONE* 5: e13120.

Hübner TR. 2011. Ontogeny in *Dysalotosaurus lettowvorbecki*. Unpublished thesis, Ludwig-Maximilians-Universität.

Hübner TR. 2018. The postcranial ontogeny of *Dysalotosaurus lettowvorbecki* (Ornithischia: Iguanodontia) and implications for the evolution of ornithopod dinosaurs. *Palaeontographica Abteilung* A 310: 43–120.

Hutchinson JR. 2002. The evolution of hindlimb tendons and muscles on the line to crown-group birds. *Comparative biochemistry and physiology. Part A, Molecular & integrative physiology* 133: 1051–86.

Ibiricu LM, Lamanna MC, Lacovara KJ. 2014. The influence of caudofemoral musculature on the titanosaurian (Saurischia: Sauropoda) tail skeleton: morphological and phylogenetic implications. *Historical Biology* 26: 454–471.

Ikejiri T. 2004. Anatomy of *Camarasaurus* lentus (Dinosauria: Sauropoda) from the Morrison Formation (Late Jurassic), Thermopolis, central Wyoming, with Determination and Interpretation of Ontogenetic, Sexual Dimorphic and Individual Variation in the Genus. Unpublished thesis, State University.

Ikejiri T. 2008. Slender and robust morphs of *Camarasaurus* (Dinosauria, Sauropoda) from the Morrison Formation (Late Jurassic) of the Rocky Mountain Region and Its Implications for possible sexual dimorphism. In: Farley GH, Choate JR, eds. *Unlocking the Unknown: Papers honoring Dr. Richard J. Zakrzewski*. Fort Hays Special Studies number 2. Hays, Kansas: Fort Hays State University, 31–44.

Ikejiri T, Hays KS, Schwarz D, Breithaupt B. 2005a. A Nearly Complete Skeleton of a Baby Sauropod from the Lower Morrison Formation of the Howe Stephens Quarry, Wyoming: 'Little Steps' into Diplodocid ontogeny and taxonomy. *Journal of Vertebrate Paleontology* 25: 73.

Ikejiri T, Tidwell V, Trexler D. 2005b. New adult specimens of *Camarasaurus* lentus highlight ontogenetic variation within the species. In: Carpenter K, Tidwell V, eds. *Thunder-Lizards: The Sauropodomorph Dinosaurs*. Bloomington: Indiana University Press, 157–179.

Irmis RB. 2007. Axial skeleton ontogeny in the Parasuchia (Archosauria: Pseudosuchia) and its implications for ontogenetic determination in archosaurs. *Journal of Vertebrate Paleontology* 27: 350–361.

de Jong IML, Colbert MW, Witte F, Richardson MK. 2009. Polymorphism in developmental timing: Intraspecific heterochrony in a Lake Victoria cichlid. *Evolution and Development* 11: 625–635.

Klein N, Christian A, Sander PM. 2012a. Histology shows that elongated neck ribs in sauropod dinosaurs are ossified tendons. *Biology letters*. 8: 1032-1035.

Klein N, Sander PM. 2007. Bone histology and growth of the prosauropod dinosaur *Plateosaurus engelhardti* von Meyer, 1837 from the Norian bonebeds of Trossingen (Germany) and Frick (Switzerland) (PM Barrett and DJ Batten, Eds.). *Special Papers in Palaeontology* 7: 169–206.

Klein N, Sander PM. 2008. Ontogenetic stages in the long bone histology of sauropod dinosaurs. *Paleobiology* 34: 247–263.

Klein N, Sander PM, Stein KHW, Le Loeuff J, Carballido JL, Buffetaut É. 2012b. Modified Laminar Bone in *Ampelosaurus atacis* and Other Titanosaurs (Sauropoda): Implications for Life History and Physiology. *PLoS ONE* 7: e36907.

Klein N, Sander PM, Suteethorn V. 2009. Bone histology and its implications for the life history and growth of the Early Cretaceous titanosaur *Phuwiangosaurus sirindhornae*. *Geological Society, London, Special Publications* 315: 217–228.

Lehman TM, Coulson AB. 2002. A Juvenile Specimen of the Sauropod Dinosaur *Alamosaurus sanjuanensis* from the Upper Cretaceous of Big Bend National Park, Texas. *Journal of Paleontology* 76: 156–172.

Leigh SR, Terranova CJ. 1998. Comparative Perspectives on Bimaturism, Ontogeny, and Dimorphism

in Lemurid Primates. *International Journal of Primatology*.19: 723-750.

Lloyd GT. 2016. Estimating morphological diversity and tempo with discrete character-taxon matrices: implementation, challenges, progress, and future directions. *Biological Journal of the Linnean Society* 118: 131–151.

Lloyd GT. 2018. Journeys through discrete-character morphospace: synthesizing phylogeny, tempo, and disparity. *Palaeontology* 61: 637–645.

Le Loeuff J. 2005. Osteology of *Ampelosaurus atacis* (Titanosauria) from Southern France. In: Tidwell V, Carpenter K, eds. *Thunder-Lizards: The Sauropodomorph Dinosaurs*. Bloomington: Indiana University Press, 115–137.

Longrich NR, Field DJ. 2012. *Torosaurus* is not *Triceratops*: ontogeny in chasmosaurine ceratopsids as a case study in dinosaur taxonomy. *PloS ONE* 7: e32623.

López-Martıínez N, Canudo JI, Ardèvol L, Suberbiola XP, Orue-Etxebarria X, Cuenca-Bescós G, Ruiz-Omeñaca JI, Murelaga X, Feist M. 2001. New dinosaur sites correlated with Upper Maastrichtian pelagic deposits in the Spanish Pyrenees: implications for the dinosaur extinction pattern in Europe. *Cretaceous Research* 22: 41–61.

Maddison WP, Maddison DR. 2011. Mesquite: a modular system for evolutionary analysis.

Mannion PD, Allain R, Moine O. 2017. The earliest known titanosauriform sauropod dinosaur and the evolution of Brachiosauridae. *PeerJ* 5: e3217.

Mannion PD, Schwarz D, Upchurch P, Wings O. 2019. Taxonomic affinities and biogeographic implications of the putative titanosaurs (Dinosauria: Sauropoda) from the Late Jurassic Tendaguru Formation of Tanzania. *Journal of Vertebrate Paleontology* XX: 1–126.

Mannion PD, Upchurch P, Barnes RN, Mateus O. 2013. Osteology of the Late Jurassic Portuguese sauropod dinosaur *Lusotitan atalaiensis* (Macronaria) and the evolutionary history of basal titanosauriforms. *Zoological Journal of the Linnean Society* 168: 98–206.

Martin V. 1994a. Baby sauropods from the Sao Khua Formation (Lower Cretaceous) of northeastern Thailand. *Gaia* 10: 147–153.

McIntosh JS. 1990a. Sauropoda. In: Weishampel DB, Dodson P, Osmólska H, eds. *The Dinosauria*. University of California Press, 345–401.

McIntosh JS. 1990b. Species determination in sauropod dinosaurs with tentative suggestions for their classification. In: Carpenter K, Currie PJ, eds. *Dinosaur Systematics*. Cambridge: Cambridge University Press, 53–70.

McIntosh JS. 2005. The Genus *Barosaurus* Marsh (Sauropoda, Diplodocoidea). In: Tidwel V, Carpenter K, eds. *Thunder-Lizards: The Sauropodomorph Dinosaurs*. Indiana University Press, 512.

Melstrom KM, D'emic MD, Chure DJ, Wilson JA. 2016. A juvenile sauropod dinosaur from the Late Jurassic of Utah, U.S.A., presents further evidence of an avian style air-sac system. *Journal of Vertebrate Paleontology* 36: e1111898.

Mitchell J, Sander PM, Stein KHW. 2017. Can secondary osteons be used as ontogenetic indicators in sauropods? Extending the histological ontogenetic stages into senescence. *Paleobiology* 43: 321–342.

Mitgutsch C, Wimmer C, Sánchez-Villagra MR, Hahnloser R, Schneider RA. 2011. Timing of Ossification in Duck, Quail, and Zebra Finch: Intraspecific Variation, Heterochronies, and Life History Evolution. *Zoological Science* 28: 491–500.

Mocho P, Royo-Torres R, Ortega F. 2016. New data of the Portuguese brachiosaurid *Lusotitan atalaiensis* (Sobral Formation, Upper Jurassic). *Historical Biology* 29: 789–817.

Mosimann JE. 1970. Size allometry: Size and shape variables with characterizations of the lognormal and generalized gamma distributions. *Journal of the American Statistical Association* 65: 930–945.

Myers TS, Fiorillo AR. 2009. Evidence for gregarious behavior and age segregation in sauropod dinosaurs. *Palaeogeography, Palaeoclimatology, Palaeoecology* 274: 96–104.

Nopsca BF. 1915. Die dinosaurier der Siebenbürgischen landesteile Ungarns. *Ungarischen Geologischen Reichsanstalt* 23: 1–24.

Olori JC. 2013. Ontogenetic sequence reconstruction and sequence polymorphism in extinct taxa: an example using early tetrapods (Tetrapoda: Lepospondyli). *Paleobiology* 39: 400–428.

Ortega F, Bardet N, Barroso-Barcenilla F, Callapez PMPM, Cambra-moo O, Daviero- Gómez V, Díez Díaz V, Domingo L, Elvira A, Escaso F, García-Oliva M, Gómez B, Houssaye A, Knoll F, Marcos-Fernández F, Martín M, Mocho P, Narváez I, Pérez-García A, Peyrot D, Segura M, Serrano H, Torices A, Vidal D, Sanz JL. 2015. The biota of the Upper Cretaceous site of "Lo Hueco" (Cuenca, Spain). *Journal of Iberian Geology* 41: 83–99.

Otero A. 2010. The appendicular skeleton of *Neuquensaurus*, a Late Cretaceous saltasaurine sauropod from Patagonia, Argentina. *Acta Palaeontologica Polonica* 55: 399–426.

Otero A. 2018. Forelimb musculature and osteological correlates in Sauropodomorpha (Dinosauria, Saurischia). *PLoS ONE* 13: e0198988.

Otero A, Vizcaíno SF. 2008. Musculatura y función del miembro posterior de *Neuquensaurus australis* (Sauropoda: Titanosauria). *Ameghiniana* 45: 333–348.

Padian K, de Ricqlès AJ, Horner JR. 2001. Dinosaurian growth rates and bird origins. *Nature* 412: 405–8.

Páramo A, Mocho P, Escaso F, Sanz JL, Ortega F. 2019. Establishment of Ontogenetic Sequences for Ibero-Armorican Titanosaurs and their Implications for Phylogenetic Analysis. *International Congress of Vertebrate Morphology (ICVM) - Abstract Volume, Journal of Morphology.* Prague, S197.

Páramo A, Mocho P, Marcos-Fernández F, Ortega F, Sanz JL. 2017. 3D Geometric Morphometrics on the Hind Limb of the Titanosaurs from Lo Hueco: Dwarf taxa or Small Individuals? *15th Annual Meeting of the European Association of Vertebrate Paleontologists*.

Páramo A, Ortega F, Escaso F, Narváez I, Sanz JL. 2014. Ejemplares juveniles de titanosaurio (Sauropoda) del yacimiento de Lo Hueco (Fuentes, Cuenca). In: Royo-Torres, R.; Verdú, F.J.; Alcalá, L. (coord.). *XXX Jornadas de Paleontología de la Sociedad Española de Paleontología. ¡Fundamental!* 24: 149–151.

Páramo A, Ortega F, Sanz JL. 2018. Desarrollo ontogenético en el esqueleto apendicular de los Titanosaurios de Lo Hueco (Fuentes, Cuenca). In: Vaz N, Sá AA, eds. *XXXIV Jornadas de la Sociedad Española de Paleontología y V Encuentro Ibérico Anual. Yacimientos paleontológicos excepcionales en la península Ibérica*. Cuadernos del Museo Geominero. Vila Real, 195–201.

Perez-Garcia A, Gasco F, Ortega F. 2017. A Singular Uppermost Cretaceous Dinosaur Nesting Area in the Villalba de la Sierra Formation (Guadalajara, Central Spain). *77th Annual Meeting of the Society of Vertebrate Paleontology*: 176.

Piechowski R, Tałanda M, Dzik J. 2014. Skeletal variation and ontogeny of the Late Triassic

Dinosauriform Silesaurus opolensis. *Journal of Vertebrate Paleontology* 34: 1383–1393.

Poropat SF, Upchurch P, Mannion PD, Hocknull SA, Kear BP, Sloan T, Sinapius GHK, Elliott DA. 2015. Revision of the sauropod dinosaur Diamantinasaurus matildae Hocknull *et al.* 2009 from the mid-Cretaceous of Australia: Implications for Gondwanan titanosauriform dispersal. *Gondwana Research* 27: 995–1033.

Powell JE. 2003. Revision of South American titanosaurid dinosaurs: Palaeobiological, palaeobiogeographical and phylogenetic aspects. *Records of the Queen Victoria Museum* 111:1–179.

Prochel J, Vogel P, Sánchez-Villagra MR. 2004. Hand development and sequence of ossification in the forelimb of the European shrew *Crocidura russula* (Soricidae) and comparisons across therian mammals. *Journal of Anatomy* 205: 99–111.

Remes K. 2007. Evolution of the Pectoral girdle and Forelimb in Sauropodomorpha (Dinosauria, Saurischia): Osteology, Myology and Fuction. Unpublished thesis, Ludwig-Maximilians-Universität München.

Revell LJ. 2009. Size-correction and Principal Components for Interspecific Comparative studies. *Evolution* 63: 3258–3268.

Romer AS. 1923. Crocodilian pelvic muscles and their avian and reptilian homologues. *Bulletin of the American Museum of Natural History* 48: 533–552.

Romer AS. 1956. *Osteology of the Reptiles*. Chicago: The University of Chicago Press.

Royo-Torres R. 2009. *El saurópodo de Peñarroya de Tastavins*. Teruel: Instituo de Estudios Turolenses y Fundación Conjunto Paleontológico de Teruel-Dinópolis.

Salgado JL, Apesteguía S, Heredia S. 2005. A New Specimen of *Neuquensaurus australis*, a Late Cretaceous Saltasaurine titanosaur from North Patagonia. *Journal of Vertebrate Paleontology* 25: 623–634.

Salgado JL, Coria RA, Calvo JO. 1997. Evolution of the titanosaurid sauropods I: Phylogenetic analysis based on the postcranial evidence. *Ameghiniana* 34: 3–32.

Sallam HM, Gorscak E, O'Connor PM, El-Dawoudi IA, El-Sayed S, Saber S, Kora MA, Sertich JJW, Seiffert ER, Lamanna MC. 2018. New Egyptian sauropod reveals Late Cretaceous dinosaur dispersal between Europe and Africa. *Nature Ecology & Evolution* 2: 445–451.

Sánchez-villagra MR. 2002. Comparative patterns of postcranial ontogeny in therian mammals: An analysis of relative timing of ossification events. *Journal of Experimental Zoology* 294: 264–273.

Sander PM. 1992. The Norian Plateosaurus bonebeds of central Europe and their taphonomy. *Palaeogeography, Palaeoclimatology, Palaeoecology* 93: 255–299.

Sander PM. 2013. An Evolutionary Cascade Model for Sauropod Dinosaur Gigantism - Overview, Update and Tests. *PLoS ONE* 8: e78573.

Sander PM, Christian A, Clauss M, Fechner R, Gee CT, Griebeler EMM, Gunga HC, Hummel J, Mallison H, Perry SF, Preuschoft H, Rauhut OWM, Remes K, Tütken T, Wings O, Witzel U. 2011a. *Biology of the sauropod dinosaurs: the evolution of gigantism*. Biological reviews of the Cambridge Philosophical Society 86: 117–55.

Sander PM, Klein N. 2005. Developmental Plasticity in the Life History of a Prosauropod Dinosaur. *Science* 310: 1800–1802.

Sander PM, Klein N, Stein KHW, Wings O. 2011b. Sauropod Bone Histology and Its Implications

for Sauropod Biology. In: Klein N, Remes K, Gee CT, Sander PM, eds. *Biology of the Sauropod Dinosaurs: Understanding the Life of Giants*. Bloomington: Indiana University Press, 276–302.

Sanz JL, Buscalioni ÁD, Pérez-Moreno BP, Moratalla JJ, Jiménez García S. 1992. *Los dinosaurios de Castilla y León. Vertebrados fósiles de Castilla y León*. Salamanca: Museo Provincial de Salamanca, 47–57.

Sanz JL, Powell JE, Le Loeuff J, Martínez RN, Pereda Suberbiola X. 1999. Sauropod remains from the Upper Cretaceous of Laño (north central Spain). Titanosaur phylogenetic relationships. *Estudios del Museo de Ciencias Naturales de Alava* 14: 235–255.

Schwarz D, Ikejiri T, Breithaupt BH, Sander PM, Klein N. 2007a. A nearly complete skeleton of an early juvenile diplodocid (Dinosauria: Sauropoda) from the Lower Morrison Formation (Late Jurassic) of North central Wyoming and its implications for early ontogeny and pneumaticity in sauropods. *Historical Biology* 19: 225–253.

Schwarz D, Wings O, Meyer CA. 2007b. Super sizing the giants: first cartilage preservation at a sauropod dinosaur limb joint. *Journal of the Geological Society* 164: 61–65.

Sharma PP, Clouse RM, Wheeler WC. 2017. Hennig's semaphoront concept and the use of ontogenetic stages in phylogenetic reconstruction. *Cladistics* 33: 93–108.

Smith DK. 1998. A morphometric analysis of *Allosaurus*. *Journal of Vertebrate Paleontology* 18: 126–142.

Somers KM. 1986. Multivariate allometry and removal of size with principal components analysis. *Systematic Biology* 35: 359–368.

Stein KHW, Csiki Z, Rogers KC, Weishampel DB, Redelstorff R, Carballido JL, Sander PM, Curry Rogers K, Weishampel DB. 2010. Small body size and extreme cortical bone remodeling indicate phyletic dwarfism in *Magyarosaurus dacus* (Sauropoda: Titanosauria). *Proceedings of the National Academy of Sciences of the United States of America* 107: 9258–9263.

Suteethorn S, Le Loeuff J, Buffetaut É, Suteethorn V. 2010. Description of topotypes of *Phuwiangosaurus sirindhornae*, a sauropod from the Sao Khua Formation (Early Cretaceous) of Thailand, and their phylogenetic implications. *Neues Jahrbuch für Geologie und Paläontologie Abhandlungen* 256: 109–121.

Swofford DL. 2002. PAUP*: Phylogenetic Analysis Using Parsimony (and Other Methods).

Taylor MP, Wedel MJ. 2013. Why sauropods had long necks; and why giraffes have short necks. *PeerJ* 1: e36.

Tidwell V, Wilhite RD. 2005. Ontogenetic variation and isometric growth in the forelimb of the Early Cretaceous sauropod *Venenosaurus*. In: Carpenter K, Tidwell V, eds. *Thunder-Lizards: The Sauropodomorph Dinosaurs*. Indiana University Press, 187–196.

Tschopp E, Mateus O. 2017. Osteology of *Galeamopus pabsti* sp. nov. (Sauropoda: Diplodocidae), with implications for neurocentral closure timing, and the cervico-dorsal transition in diplodocids. *PeerJ* 5: e3179.

Tschopp E, Mateus O, Benson RBJ. 2015. A specimen-level phylogenetic analysis and taxonomic revision of Diplodocidae (Dinosauria, Sauropoda). *PeerJ* 3: e857.

Tumarkin-Deratzian AR. 2009. Evaluation of long bone surface textures as ontogenetic indicators in centrosaurine ceratopsids. *Anatomical Record* 292: 1485–500.

Tumarkin-Deratzian AR, Vann DR, Dodson P. 2006. Bone surface texture as an ontogenetic indicator in long bones of the Canada goose *Branta canadensis* (Anseriformes: Anatidae). *Zoological Journal of the Linnean Society* 148: 133–168.

Ullmann P.V., Bonnan MF, Lacovara KJ. 2017. Characterizing the Evolution of Wide-Gauge Features in Stylopodial Limb Elements of Titanosauriform Sauropods via Geometric Morphometrics. *The Anatomical Record* 300: 1618–1635.

Upchurch P. 1998. The phylogenetic relationships of sauropod dinosaurs. *Zoological Journal of the Linnean Society* 124: 43–103.

Upchurch P, Barrett PM, Dodson P. 2004. Sauropoda. In: Weishampel DB, Dodson P, Osmólska H, eds. *The Dinosauria*. Berkeley: University of California Press, 259–322.

Upchurch P, Mannion PD, Taylor MP. 2015. The Anatomy and Phylogenetic Relationships of "*Pelorosaurus*" *becklesii* (Neosauropoda, Macronaria) from the Early Cretaceous of England. *PLoS ONE* 10: e0125819.

Varricchio DJ. 1997. Growth and Embriology. In: Currie PJ, Padian K, eds. *Encyclopedia of dinosaurs*. San Diego: Academic Press, 282–288.

Vieira LG, Santos ALQ, Lima FC, Mendonça SHSTD, Menezes LT, Sebben A. 2016. Ontogeny of the Appendicular Skeleton in *Melanosuchus niger* (Crocodylia: Alligatoridae). *Zoological Science* 33: 372–383.

Vila B, Galobart À, Canudo JI, Le Loeuff J, Dinarès-Turell J, Riera V, Oms O, Tortosa T, Gaete R. 2012. The diversity of sauropod dinosaurs and their first taxonomic succession from the latest Cretaceous of southwestern Europe: Clues to demise and extinction. *Palaeogeography, Palaeoclimatology, Palaeoecology* 350–352: 19–38.

Vila B, Jackson F, Galobart À. 2010. First Data on Dinosaur Eggs and Clutches from Pinyes Locality (Upper Cretaceous, Southern Pyrenees). *Ameghiniana* 47: 79–87.

Vila B, Sellés AG, Brusatte SL. 2016. Diversity and faunal changes in the latest Cretaceous dinosaur communities of southwestern Europe. *Cretaceous Research* 57: 552–564.

Waskow K, Mateus O. 2017. Dorsal rib histology of dinosaurs and a crocodylomorph from western Portugal: Skeletochronological implications on age determination and life history traits. *Comptes Rendus Palevol* 16: 425–439.

Waskow K, Sander PM. 2014. Growth record and histological variation in the dorsal ribs of *Camarasaurus* sp. (Sauropoda). *Journal of Vertebrate Paleontology* 34: 852–869.

Weisbecker V, Goswami A, Wroe S, Sánchez-Villagra MR. 2008. Ossification heterochrony in the therian postcranial skeleton and the marsupial-placental dichotomy. *Evolution* 62: 2027–2041.

Wiens JJ. 2003. Missing data, incomplete taxa, and phylogenetic accuracy. *Systematic Biology* 52: 528–538.

Wilhite RD. 1999. Ontogenetic variation in the appendicular skeleton of the genus *Camarasaurus*. Unpublished thesis, Brigham Young University.

Wilhite RD. 2005. Variation in the Appendicular Skeleton of North American Sauropod Dinosaurs: Taxonomic Implications. In: Tidwell V, Carpenter K, eds. *Thunder-Lizards: The Sauropodomorph Dinosaurs*. Indiana University Press, 268–301.

Wilkinson M. 1995. Coping with Abundant Missing Entries in Phylogenetic Inference Using Parsimony. *Systematic Biology* 44: 501–514.

Wilkinson M. 2003. Missing entries and multiple trees: instability, relationships, and support in parsimony analysis. *Journal of Vertebrate Paleontology* 23: 311–323.

Wilson JA. 2002. Sauropod dinosaur phylogeny: critique and cladistic analysis. *Zoological Journal of*

the Linnean Society 136: 215–275.

Wilson JA, Carrano MT. 1999. Titanosaurs and the Origin of 'wide-gauge' trackways: A Biomechanical and Systematic Perspective on Sauropod Locomotion. *Paleobiology* 25: 252–267.

Wilson LAB, Sánchez-Villagra MR. 2011. Evolution and phylogenetic signal of growth trajectories: The case of chelid turtles. *Journal of Experimental Zoology Part B: Molecular and Developmental Evolution* 316 B: 50–60.

Wilson JA, Sereno PC. 1998. Early Evolution and High-level Phylogeny of Sauropod Dinosaurs. *Journal of Vertebrate Paleontology* 18: 1–68.

Witmer LM. 1995. The Extant Phylogenetic brakcet and the Importance of Reconstructing Soft Tissue in Fossils. In: Thomason J, ed. *Functional morphology in vertebrate paleontology*. Cambridge: Cambridge University Press, 19–33.

Woodruff DC. 2015. A new multi-faceted framework for deciphering diplodocid ontogeny. Unpublished thesis, Montana State University.

Woodruff DC, Fowler DW. 2012. Ontogenetic influence on neural spine bifurcation in diplodocoidea (Dinosauria: Sauropoda): A critical phylogenetic character. *Journal of Morphology* 273: 754–764.

CHAPTER V.II:

General Discussion

VII.1. DISCUSSION

The analysis of the titanosaur appendicular elements from Lo Hueco allowed the description of two main morphotypes among the sample of specimens in each bone type. These two morphotypes are congruent among all the bone elements and therefore they can be referred to putative titanosaur forms e.g. the Morphotype I of the humeri is the same as Morphotype I in the ulnae and femora, and so on. One of these morphotypes corresponds to the exclusive form *Lohuecotitan pandafilandi* previously described in Lo Hueco. This form presents some variation, especially in the morphology of the hindlimb. However, all the sampled specimens present a set of common features with *L. pandafilandi* (e.g. the linea cranialis intermuscularis in the anterior face of the femur, the secondary cnemial crest of the tibia, or the medially deflected anterior trochanter of the fibulae). All the specimen referred to this morphotype + *L. pandafilandi* share a feature combination of Lithostrotian sauropods thought they show similarities with less derived non-lithostrotian sauropods (as previously commented in Díez Díaz *et al.*, 2016) such as *Jainosaurus* cf. *septentrionalis* (Wilson, Barrett, & Carrano, 2011). Some analysis of the femoral morphology shows similarities with other femora with less eccentric shaft and more bulbous and anteroposteriorly expanded proximal and distal end (e.g. *Neuquensaurus*, see Chapter IV) congruent with previous anatomical comparisons with other sauropod taxa following Díez Díaz *et al.* (2016).

L. pandafilandi lacks most of the forelimb elements, with only one fragmentary ulna attributed to the holotype material (Díez Díaz *et al.*, 2016). The analysis of several specimens in partial association have allowed the referral of one of the humeral morphotypes and one of the radial morphotypes to Morphotype I + *L. pandafilandi*. The specimen HUE-EC-3 present a association of proximity in the field that has yielded a left and right humeri (HUE-2356, HUE-2801), a right radius (HUE-2711), two right tibae in proximity (HUE-2318, HUE-2799) and a left fibula (HUE-2904). This set is composed by more than one individual in the base of the duplicated specimens and the dispersion over the field map. The analyses that included all these elements allow referring them all to Morphotype I. This group of specimens is accepted as pertaining to a Morphotype I, thought the complex association difficult us to establish a relationship between the results of the different analyses based only on this individual. A comprehensive study on their association is beyond of the scopes of the current work. The specimen HUE-EC-5 preserves a left ulna (HUE-964) and a right femur (HUE-1366). Both elements are referred to Morphotype I. The femur present some differences compared to other specimens of Morphotype I (e.g. the anteroposterior compression of the shaft and the distal end) but these differences found in this specimen and other similar isolated femora (e.g. HUE-2903) are considered as intraspecific variability. The ulna (HUE-964) present similar features with the ulna of *L. pandafilandi* (HUE-3044). The specimen HUE-EC-11 preserves a left humerus (HUE-817) and a fragmentary right femur (HUE-930). This individual was initially assessed as a more robust morphotype based in its fragmentary humerus (HUE-930; see Chapter IV). Further comparison in this study have allowed its allocation as Morphotype I after comparison with other Ibero-Armorican titanosaurs and a comprehensive analysis of the variability in the femora through 3D geometric morphometrics Finally, the specimen HUE-EC-2 includes a small fragmentary humerus HUE-XXYY) and two other humeri from the proximity (HUE-2772, HUE-2727). The specimen HUE-EC-2 is currently under study and it has permited to determine that the later humeri are not part of the individual. Therefore, in this case, we can include them (HUE-2727 and HUE-2772) in the analyses as isolated. The specimen HUE-XXYY comes from a single individual in partial articulation. This specimen has been identified

as Morphotype I based in the 3D geometric morphometrics analyses. There is also a partially associated titanosaur zeugopodium (left ulna HUE-1139, left radius HUE-1140) referred to Morphotype I. These elements are also some of the biggest ulna and radius found in the fossil site.

The association of these individuals allowed us to establish the relationships among the results of the different analyses for the Morphotype I.

The Morphotype II present a slightly more robust femora, a more quadrangular and slender humeri and gracile zeugopodium in both limbs. The individual HUE-EC-13 preserves a left fragmentary humerus (HUE-1647) and a left femur (HUE-1183). These specimens are referred to Morphotype II based on 3D geometric morphometrics analysis. The specimen HUE-1183 was initially assessed to a more robust femoral morphotype (Chapter IV). However, comparison with other Ibero-Armorican titanosaurs and assessment of the morphospace with inclusion of several new specimens, allowed allocating this femur to Morphotype II, congruent with the results of the analysis including the humerus. Besides some similarities between HUE-EC-13 and HUE-EC-5 femora, the 3D-GM analysis shows that probably do not pertain to the same morphotype. The individual HUE-EC-6 preserves a right femur (HUE-2420), a right tibia (HUE-2426) and a right fibula (HUE-2426). The tibia and fibula are still partly obscured by sediment, as their preparation is difficult by the fragmentary state besides they preserve most of the shaft and proximal and distal ends. The 3D digitizing of the specimens and virtual restoration techniques allowed us to study their morphology through a virtual complete representation of both specimens. HUE-EC-6 was initially assessed as Morphotype I (Chapter VI) but presented several important differences (e.g. absence of a linea intermuscularis cranialis of the femur, step between anterior and posterior face in the distal end of the femur in distal view, absence of the secondary cnemial crest in the tibia, extremely elongated and narrow shaft of the tibia, etc.). The comparison with other Ibero-Armorican titanosaurs and 3D geometric morphometric analyses found some of these elements closer to the taphomorphospace of Morphotype II. They are probably referable to Morphotype II, which is congruent with differences found in other parts of the skeleton of this individual (e.g. differences between the caudal vertebrae of *L. pandafilandi* and HUE-EC-6, see Mocho *et al.*, 2018). There are also an associated tibia and fibula (HUE-1612) which are referred as Morphotype II and the 3D geometric morphometrics analysis show congruent results. The ulnae and radius of Morphotype II present no clear association with other elements analyzed in the current study. The gracile morphotype of ulna was referred to Morphotype II by exclusion of other alternative hypothesis as they do not present similarities with any of the ulnae associated to partially articulated individuals (and referred here to Morphotype I) and by the absence of a third group of ulnae in all the analyses, which could represent an alternative morphotype distribution. However, the only radius referred to Morphotype II is still discussed, as it is from a probable juvenile individual (see Chapter VI), but present morphological differences with the other sampled specimens (referred to Morphotype I) that are probably not intraspecific variation (see Chapter V, Chapter VI).

The Morphotype II presents differences with Morphotype I and with other Ibero-Armorican titanosaurs. Some initial similarities with other robust titanosaur form as *Ampelosaurus atacis* were tested. Morphotype II presents an elongated and gracile zeugopodium in both fore and hindlimbs that is different to the usual lithostrotian zeugopodium of *A. atacis* (e.g. short and lateromedially expanded ulna C3-1490, tibiae with both lateromedially and anteroposteriorly expanded proximal end as well as lateromedially wide distal end C3-138, C3-173). None of the alternative hypothesis explored in the 3D-GM analyses support the allocation of any specimen

of Lo Hueco to *A. atacis* or a closer form. It is important to note however that there are several specimens referred to *A. atacis* that present a morphology as variable as observed in Lo Hueco site (e.g. the slender and elongated tibia C3-1483) and some previous studies have identified at least two different morphotypes (*A. atacis* + cf. *Lirainosaurus*) among the femora of Bellevue titanosaurs (Vila *et al.*, 2012). Further study including these specimens is necessary.

The sample of Lo Hueco was also compared to the small lithostrotian titanosaur *Lirainosaurus* astibiae from the Ibero-Armorican domain. It is especially relevant as some small specimens were previously identified in the sample from Lo Hueco site (Páramo *et al.*, 2014). The anatomical comparison and 3D geometric morphometrics have allowed the comparison between the sampled specimens and none of the smallest specimen previously regarded as possible juvenile individuals were referred to *L. astibiae* or a closer form. Only one specimen of humerus (HUE-3662) from Lo Hueco could be referred to *Lirainosaurus* astibiae or a closer form. This specimen present most of the characteristic of *L. astibiae* in direct comparison of the specimen, and all the 3D geometric morphometrics analyses show a close relationship with the taphomorphospace of *L. astibiae*.

Another humerus specimen (HUE-3228) preliminary regarded here as Morphotype I present a completely odd morphology compared with other specimens from the sample of Lo Hueco. This humerus present an extremely twisted proximal end toward anterior, a slightly curved shaft with subcircular midshaft section and a reduced distal condyles as much anteroposteriorly expanded as lateromedially. This morphology is only found in few titanosaurs e.g. *Muyenlensaurus pecheni* (MAU-PV-70, MAU-PV-132).

It is possible that there is up to four different morphotypes in Lo Hueco. However, HUE-3662 and HUE-3228 are the only elements identified in the current study that may not pertain to the two main morphotypes, as they are extremely outnumbered in the Lo Hueco titanosaur faunas. Previous hypothesis on morphotype variability in the axial skeleton discuss up to four different possible morphotypes (Mocho *et al.*, 2016, 2018; Vidal *et al.*, 2017). However, the individuals analyzed in previous studies on the axial skeleton are found among the analyzed morphotypes (HUE-EC-1, HUE-EC-2, HUE-EC-3 and HUE-EC-11 referred Morphotype I; HUE-EC-6 and HUE-EC-13 referred Morphotype II). So these hypotheses are rejected and two different titanosaur forms probably explain the variability of most of the sample from Lo Hueco, with only isolated presence of other titanosaurs.

The overall morphology found in both morphotypes insight to different biomechanical specialization. Whether this relates with different feeding niche exploitation was unknown, as the current hypothesis insight two different types of niche occupation in the titanosaurs from Lo Hueco came from mainly isolated cranial material (Knoll *et al.*, 2013, 2015; Díez Díaz, Ortega, & Sanz, 2014). Also, many works on feeding niche exploitation relate are related with the neck posture and envelope in height, but few includes the overall posture and morphology of the rest of the sauropod body (Christian, 2002; Stevens, 2013; Paul, 2017; see also body volume distribution in Bates *et al.*2016). We used available information on neck posture and possible feeding niche exploitation for developing a simplified proxy model. This model is used to test possible correlation between main morphological trends of the appendicular skeleton with differences in feeding niche exploitation (i.e. low browsing feeders and high browsing feeders). Most of the information comes from non titanosaurian sauropods, so the deploy of glm-models with a secondary factor allowed to test the interaction of the acquisition of the "wide-gauge" limb configuration of titanosauriformes sauropods, which is a major body change between

non-titanosauriformes neosauropods and more derived titanosauriformes (Wilson & Carrano, 1999). The proxy models shows that there is a significant relationship between the robustness of the forelimb elements and a differential feeding niche exploitation among all the sampled neosauropods (Chapter V). Some elements (e.g the ulnae and tibiae) present also different trends among those titanosauriformes or more derived taxa after development of "wide-gauge" posture and non-titanosauriformes. While the radius present differences of the robustness related to different feeding niche capabilities only among titanosaur sauropods. Lastly, our proxy model found no relationships in the robustness of the femora and fibulae in relationship with the feeding envelope, but significant differences between non-titanosauriformes neosauropods and titanosauriformes after acquisition of the "wide-gauge" posture. Based on these results, it is possible that Morphotype I present a lower feeding envelope, related with its more usual titanosaur body plan. While the Morphotype II, which presents an extremely gracile forelimb with elongated zeugopodium, may be related with high browsing feeder capabilities. These results shall be tested within a full biomechanical analysis, including partial skeletons related with each morphotype.

The deployment of several imputation methods allowed us a precise allocation of the sampled specimens with 3D geometric morphometrics These techniques also permitted the study the intraspecific variability among the defined morphotypes. In the current work, the results show that estimation of morphometric variables and landmark variables is more desirable than variable reduction (Chapter IV). The use of less variables may reduce the missing information inherent in the study of fossil material. However, the analyses show that this may cost valuable information regarding the anteroposterior width and position of osteological structures in the use of linear morphometric data (Chapter IV.I). In the case of landmark based GM, the reduction on the number of landmarks may produce more overlapping between morphotypes with similar morphospace, lack of information on valuable osteological features and therefore loss of significant differences with taxonomic relevance (Chapter IV.II). Modern multivariate estimation methods can produce accurate results that resemble the initial structure (variation-covariation) of the sample (see Supplementary Material IV.I.F, IV.II.F, V.C). The actual accuracy reported in the current study is, for most of the specimens, lower than the 3D reconstruction accuracy (stereo-photogrammetry, Kinect™ IR-scanning). TPS warping is the most usual method employed for landmark estimation and it present a good accuracy (see Chapter IV.II, Chapter V), however, Bayesian PCA can produce improved landmark estimations at the cost of a light increase in variance-covariance of the sample and further overlap in the morphospaces (see Chapter V). The use of 3D-GM based virtual restoration techniques allows also the analysis of the complete 3D mesh representation of the specimens including those specimens that are fragmentary (Chapter V). It is possible to slide the semilandmarks using the own power of TPS algorithm (see Chapter IV.II), but this is not enough for deploying more advanced techniques such as high density surface semilandmarks. The complete specimen mesh can be obtained after landmark estimation via warping the initial landmark template mesh to the specimen of study, producing a complete and accurate representation of the specimen of study even if it was fragmentary. The analysis of the mesh warping indicates that most of the specimens do not present a warping of the new object mesh greater than the actual accuracy of the digitizing methods (see Supplementary Material V.C). The virtual restoration of fragmentary specimens allow the use of high density surface semilandmarks method to analyze the complete morphology despite the incomplete nature of many fossil specimens due to preservation.

It is necessary to maintain low levels of missing information thought, as our results show that increase in covariance among the variables may also impact the analyses and

difficult interpretation of the results (Chapter IV). It is especially relevant with the use of unsupervised clustering techniques, that are sensible to the morphological similarities already present among the Ibero-Armorican titanosaurs (Chapter IV, Chapter V).

The analysis of the intraspecific variability in each morphotype and L. asitibae shows that several osteological characters already in use in morphological data matrices used for sauropod systematics are susceptible to present different scoring among specimens of the same taxa. The use of 3D geometric morphometrics and especially high density surface semilandmarks allows to visualize and quantify the areas of the bone surface where there is more variance in the sample. Only a small amount of the total characters analyzed is susceptible of presenting differences in character scoring, however, all the bone elements present this pattern. The effect of intraspecific variability are generalized and a quantitative analysis of the impact of the character scoring differences in the same taxa over phylogenetic tree topologies should be covered elsewhere.

The analysis of the intraspecific variability in the sample from Lo Hueco also allow to discuss some morphological femoral characters previously applied in the differentiation of titanosaur indeterminate forms in the Late Cretaceous of Ibero-Armorican domain (Vila *et al.*, 2012). These osteological characters are not related with the ones used in studies of sauropod systematics but may be representative of morphological differences between sauropod taxa in the Ibero-Armorican domain. However, many of these characters are found as variable in the current study. The presence of a linea intermuscularis cranialis not only present among saltasaurid sauropods (Vila *et al.*, 2012; after proposal of D'Emic, 2012). This structure is present in other sauropod forms e.g. Titanosaur indet. Form 1 (Vila *et al.*, 2012), Morphotype I + *Lohuecotitan pandafilandi* (this study) and weakly developed in Morphotype II (this study). However, it may be variable among elements of the same sample (e.g. HUE-594 weak linea intermuscularis cranialis contra HUE-1319 in which is absent). The presence of an anterior trochanter to the fourth trochanter is also variable among specimens of the same taxa (e.g. HUE-2338: present, HUE-3108: absent; both referred to Morphotype I). The extension of structures like the lateral bulge or the trochanteric shelf (as well as the short and robust 'accesory pilaster' defined by Vila *et al.*, 2012) can also be variable among specimens of the same morphotype. The accessory posterior trochanter of the humerus seen in *Lirainosaurus* astibiae is also present in more sauropod forms (e.g. both morphotypes in this study). It is variable among specimens of the same morphotype (e.g. HUE-817: present, HUE-XXYY: absent; both referred to Morphotype I). These considerations shall apply when considering such characters to establish differences among isolated titanosaur forms.

There is also the potential effect of ontogenetic changes in the observable intraspecific variation, especially on some of these features commented before. Some of the lineas, trochanter and crests commented before are related with the development of the attachment of muscular groups (e.g. the linea intermuscularis cranialis of the femur, the presence of accessory trochanters to the femoral fourth trochanter, the posterolateral ridge under the deltopectoral crest in the humerus, etc.). Current developmental hypothesis for titanosaurs sauropods implies an early fixation of the appendicular morphology during the ontogeny (Curry Rogers *et al.*, 2016). However, while the main morphology can be found among the earliest juveniles of a titanosaur, the development of the articular caps and muscle attachment can produce morphological variation in the osteological features related to them (Ikejiri, 2004). Several ontogenetic sequences have been identified on both morphotypes from Lo Hueco for almost all the bone types (see Chapter VI). There are representatives of at least subadult stages in almost all the bone elements. The

analysis of the OCSA and OSA allowed to estimate the ontogenetic stage for the smallest specimens referred to both main morphotypes, including a selection of previously discussed probable juvenile specimens (see Páramo *et al.*, 2014). These specimens are representative of juvenile or at least subadult individuals. These methods permit to estimate a relative ontogenetic stage by each bone type. However, further analysis of paleohistological sampling is needed to assess precisely the ontogenetic stage according the standardized histological ontogenetic stage (following Stein, 2010). It is also necessary to establish a comparison between the stages obtained in each bone type as well as comparison between morphotypes (and other titanosaur taxa). The study of the paleohistological sampling is beyond the scopes of the current work. The morphological ontogenetic stage estimated in this study allowed to identify the presence of sequence polymorphism for the first time in sauropod dinosaurs. Most of the bone elements of Morphotype I + *Lohuecotitan pandafilandi* present several different possible ontogenetic sequences at early stages of development. The femora and tibiae are the most variable elements with several different paths of development of the morphological features e.g. the rugosity of the proximal and distal end, development of the femoral fourth trochanter, presence of a fully developed secondary cnemial crest, etc.; see Chapter VI). The fibulae present fewer sequence polymorphism and concentrated in the more mature developmental stages. While the ulnae have yielded a single ontogenetic sequence without variation in the character acquisition.

The Morphotype II in the other hand present high sequence polymorphism in the humeri, femora, tibiae and fibulae. The elements present most of the sequence variability at earlier ontogenetic stages, probably among juvenile specimens. Thought it is unclear for now if the specimens recovered at early stages in the sample of the femora and tibiae of Morphotype II are juvenile or subadult individuals. Regardless of a precise estimation, all the analyses indicates that most of the variability in the ontogenetic character acquisition is produced early on the ontogeny. The humeri may represent the only exception, with a high sequence polymorphism also at more mature ontogenetic stages. However, the method allowed to estimate a high diversity of path linking the earlier developmental stages with the more mature individuals which present a high variability on ontogenetic character traits. Only the ulna presenting a single, or probably two different ontogenetic sequences.

The analysis of the ontogenetic sequences also allow to map the morphological ontogenetic stage in which actual osteological characters used in data matrices for sauropod systematics may present variability in their scorings. The analysis of the results of the OCSA and OSA were used to estimate the stage in which a series of osteological characters may appear or present a change in the scoring. If the intraspecific variability observable is referable to ontogenetic changes, several character scores will be present only after a particular morphological ontogenetic stage. The results show that most of the character used in data matrices are affected by ontogenetic development changes. Thought majority of the osteological characters express similar scoring after early ontogenetic stages, which may limit the impact of ontogeny whenever we omit the sampling of early juvenile individuals. However, other characters present different scoring at later ontogenetic stages, and may be problematic, as excluding subadult individuals from the sampling may be difficult or unavoidable. More than half of the sampled specimens from Lo Hueco exhibit ontogenetic characters that indicates subadult or adults at different (mature) ontogenetic stages (see Chapter VI) and a small sample of specimens of juvenile individuals. The late development of osteological characters that present differences in scoring even among such mature specimens, translates in necessary polymorphic scoring for these characters, more sensible to ontogenetic development. Finally, the analyses yielded another, small amount of characters with

variable scoring along all the morphological ontogenetic stages. This indicates that those last characters present intraspecific variability but it is not related with ontogenetic development.

It was deployed a series of machine learning methods to help identify isolated femora in the Ibero-Armorican domain, which may be problematic otherwise as the femur does not present enough taxonomical information to establish a precise assessment. The use of Discriminant Function Analysis have been proposed for assessment of isolated theropod teeth by Smith *et al.* (2005) and it is an extended methodology. However, DFA is sensible to morphological similarities between sauropod femora and may result in difficulties to precisely assess an operative taxonomic unit. In this study, the Support Vector Machine with a radial kernel function was also deployed over several linear morphometric data matrices. The use of SVM, a classificatory method based on a decision surface not related with the group centroid (= grand mean) is better to allocate elements in cases where there is a great morphological variability and morphospace overlapping and an uneven sample between the taxa. The SVM present high accurate results despite the imputation of large parts of missing data in the data matrices used in the current thesis project (Chapter IV.I). The DFA is still a reliable method though it produces slightly worse results (Chapter IV.I). The data matrix of linear measurements proposed by Vila *et al.* (2012) after Royo-Torres (2009) represent a good base for deployment of machine learning and other clustering methods. However, it lacks information on the anteroposterior morphology of the femur and an improved data matrix is introduced in the current thesis project. This new data matrix allowed better morphospace visualization and assess significant differences between the different inclusive clades of neosauropoda analyzed (Chapter IV.I). Further completion of the morphometric variables of both data matrices is still needed.

VII.2. BIBLIOGRAPHY

Christian A. 2002. Neck posture and overall body design in sauropods. *Fossil Record* 5: 269–279.

Curry Rogers K, Whitney M, D'Emic MD, Bagley B. 2016. Precocity in a tiny titanosaur from the Cretaceous of Madagascar. *Science* 352: 450–453.

D'Emic MD. 2012. The early evolution of titanosauriform sauropod dinosaurs. *Zoological Journal of the Linnean Society* 166: 624–671.

Díez Díaz V, Mocho P, Páramo A, Escaso F, Marcos-Fernández F, Sanz JL, Ortega F. 2016. A new titanosaur (Dinosauria, Sauropoda) from the Upper Cretaceous of Lo Hueco (Cuenca, Spain). *Cretaceous Research* 68: 49–60.

Díez Díaz V, Ortega F, Sanz JL. 2014. Titanosaurian teeth from the Upper Cretaceous of "Lo Hueco" (Cuenca, Spain). *Cretaceous Research* 51: 285–291.

Ikejiri T. 2004. Anatomy of *Camarasaurus lentus* (Dinosauria: Sauropoda) from the Morrison Formation (Late Jurassic), Thermopolis, central Wyoming, with Determination and Interpretation of Ontogenetic, Sexual Dimorphic and Individual Variation in the Genus. Unpublished thesis, State University.

Knoll F, Witmer LM, Ridgely RC, Ortega F, Sanz JL. 2013. A new titanosaur sauropod neurocranium from the Late Cretaceous of Spain. *73rd Annual Meeting of the Society of Vertebrate Paleontology.* Los Angeles, CA, 122.

Knoll F, Witmer LM, Ridgely RC, Ortega F, Sanz JL. 2015. A new titanosaurian braincase from the cretaceous 'Lo Hueco' locality in Spain sheds light on neuroanatomical evolution within

titanosauria. *PLoS ONE* 10: 1–24.

Mocho P, Escaso F, Marcos-Fernández F, Páramo A, Vidal D, Ortega F. 2018. The morphological variability on titanosaur caudal series from Lo Hueco: taxonomic diversity, intra-specific variability or both? *XVI Annual Meeting of European Association of Vertebrate Paleontologists*. 126.

Mocho P, Páramo A, Díez Díaz V, Escaso F, Marcos-Fernández F, Sanz JL, Ortega F. 2016. Looking through the axial skeleton of the Lo Hueco titanosaurs. In: Torcida Fernández-Baldor F, Canudo JI, Huerta P, Pereda X, eds. *VII International Symposium about Dinosaurs Palaeontology and their Environment*. 99–100.

Páramo A, Ortega F, Escaso F, Narváez I, Sanz JL. 2014. Ejemplares juveniles de titanosaurio (Sauropoda) del yacimiento de Lo Hueco (Fuentes, Cuenca). In: Royo-Torres, R.; Verdú, F.J.; Alcalá, L. (coord.). *XXX Jornadas de Paleontología de la Sociedad Española de Paleontología. ¡Fundamental!* 24: 149–151.

Paul GS. 2017. Restoring Maximum Vertical Browsing Reach in Sauropod Dinosaurs. *Anatomical Record* 300: 1802–1825.

Royo-Torres R. 2009. *El saurópodo de Peñarroya de Tastavins*. Teruel: Instituo de Estudios Turolenses y Fundación Conjunto Paleontológico de Teruel-Dinópolis.

Smith JB, Vann DR, Dodson P. 2005. Dental morphology and variation in theropod dinosaurs: Implications for the taxonomic identification of isolated teeth. *The Anatomical Record Part A: Discoveries in Molecular, Cellular, and Evolutionary Biology* 285A: 699–736.

Stein KHW. 2010. Long bone histology of basalmost and derived Sauropodomorpha : the convergence of fibrolamellar bone and the evolution of giantism and nanism. Unpublished thesis, Universität Bonn.

Stevens KA. 2013. The Articulation of Sauropod Necks: Methodology and Mythology. *PLoS ONE* 8: e78572.

Vidal D, Sanz JL, Mocho P, Páramo A, Escaso F, Marcos-Fernández F, Ortega F. 2017. The titanosaur tails from Lo Hueco (Cuenca, Spain): Four different ways to shake? In: Farke AA, Mackenzie SA, Miller Camp J, eds. *77th Annual Meeting of the Society of Vertebrate Paleontology*. Calgary, 208.

Vila B, Galobart À, Canudo JI, Le Loeuff J, Dinarès-Turell J, Riera V, Oms O, Tortosa T, Gaete R. 2012. The diversity of sauropod dinosaurs and their first taxonomic succession from the latest Cretaceous of southwestern Europe: Clues to demise and extinction. *Palaeogeography, Palaeoclimatology, Palaeoecology* 350–352: 19–38.

Wilson JA, Barrett PM, Carrano MT. 2011. An associated partial skeleton of *Jainosaurus* cf. *septentrionalis* (Dinosauria: Sauropoda) from the Late Cretaceous of Chhota Simla, Central India. *Palaeontology* 54: 981–998.

Wilson JA, Carrano MT. 1999. Titanosaurs and the Origin of 'wide-gauge' trackways: A Biomechanical and Systematic Perspective on Sauropod Locomotion. *Paleobiology* 25: 252–267.

CHAPTER VIII:

Conclusions

Based on the results derived from the analyses of the titanosaur appendicular elements from the Campanian-Maastrichtian of Lo Hueco and attending the proposed hypotheses and objectives of the current PhD thesis, it can be concluded the following:

Conclusion no.1:

There are two main titanosaur appendicular morphotypes that help explain the morphological variance of the sample of the Lo Hueco fossil site. One form is a lithostrotian titanosaur that includes the appendicular skeleton of *Lohuecotitan pandafilandi*, an exclusive titanosaur from Lo Hueco. The second main morphotype can be attributed to a second undescribed lithostrotian titanosaur in Lo Hueco. Among the analysed sample, a single specimen, HUE-3662, is attributable to a form closely related to *Lirainosaurus astibiae*. Additionally, another single specimen, HUE-3228, can be related to a potential fourth undescribed titanosaur in Lo Hueco. However, none of them are associated with the partially articulated skeletons and are isolated. The previous hypothesis of three and four morphotypes that explain most of the morphological variance of the sample is therefore partly rejected. Despite the morphotype diversity is still of four titanosaur forms, the specimen distribution among the morphotypes is different [Main Research hypothesis is accepted; Research hypothesis no.2 is rejected – see also Conclusion no.2 below].

Conclusion no.2:

Most of the smallest specimens preserved in Lo Hueco are referable to the two main morphotypes. These specimens exhibit morphological features that clearly indicates they are juvenile individuals and not dwarf taxa. [Research hypothesis no. 2 is rejected]

Conclusion no.3:

The Morphotype I, including *Lohuecotitan pandafilandi*, share the same morphological features and present the same general morphology, with similarities to those of other primitive titanosaurian sauropods. Both of the limbs of this morphotype are slightly robust in general morphology. The Morphotype II is characterized by a gracile limb skeleton, with robust femora and gracile forelimb as well as the hindlimb zeugopodium, that is slightly more columnar than in Morphotype I. In addition, both morphotypes are clearly different from other known Ibero-Armorican titanosaurs. [Research hypothesis no. 3 is accepted].

Conclusion no.4:

Even at early ontogenetic stages, juvenile individuals from both morphotypes resemble the morphology of the adult individuals. There is no observable correlation between morphological clusters and ontogenetic stage except for the Morphotype I humeri. [Research hypothesis no.4 is accepted].

Conclusion no.5:

The size variability indicates that this sole parameter is not indicative of the developmental stage of the specimen. Moreover, some of the size variability is distributed among sub-adult to adult individuals. Exceptionally, some of the largest specimens are not the most mature individuals of the sample. [Research hypothesis no.5 is accepted].

Conclusion no.6:

The titanosaur body plan is conservative among lithostrotian sauropods during ontogenetic development. However, most of the ontogenetic sequences present some degree of polymorphism related with the presence of a greater developmental plasticity than previously observed. [Research hypothesis no.7 is partly rejected - see also Conclusion no.7 below]

Conclusion no.7:

Intraspecific variability related to ontogenetic development can modify the morphological character scoring for some specimens in the available character data matrices. Most of these changes are produced at early developmental stages, but differences in scoring can also appear at late developmental stages, producing character polymorphism in the scorings. [Research hypothesis no.6 is partly rejected; Research hypothesis no.7 is partially rejected as some changes affect the mature ontogenetic stages].

Conclusion no.8:

The morphological differences present between the two morphotypes can be confidently related to two distinct ecomorphological guilds and two different trophic strategies. The Morphotype I is clearly generalist forms characterized by a more lower feeding envelope, whereas Morphotype II presents morphological similarities with sauropods characterized by having higher feeding envelope capabilities [Research hypothesis no. 8 is accepted - see also Conclusion no.9 below].

Conclusion no.9:

There is a significant ecomorphological specialization relationship between the height of the feeding envelope and the robustness of the appendicular skeleton. For non-titanosaur neosauropods and titanosaurs this ecomorphological specialization relationship is especially related with the forelimb morphology [Research hypothesis no.8 is accepted].

Conclusion no.10:

For most of the bone types analysed, there are few differences between the ontogenetic sequences of the two main titanosaur morphotypes from Lo Hueco [Research hypothesis no.9 is rejected].

Basándonos en los resultados derivados de los análisis del esqueleto apendicular de los titanosaurios del yacimiento de Lo Hueco, y atendiendo a las hipótesis y objetivos propuestos en el presente manuscrito, se concluye lo siguiente:

Conclusión no.1:

En la colección procedente del yacimiento de Lo Hueco se han reconocido dos morfotipos apendiculares principales que nos permiten explicar la variabilidad morfológica de la muestra analizada. Una de estas formas corresponde a un titanosaurio Lithostrotia que incluiría a *Lohuecotitan pandafilandi*, un titanosaurio exclusivo del yacimiento de Lo Hueco. El segundo morfotipo principal corresponde a una forma aún no descrita de titanosaurio Lithostrotia. Dentro de la muestra analizada, se ha identificado un único ejemplar (HUE-3662) considerado como una forma cercana a *Lirainosaurus astibiae*, además de otro único ejemplar, HUE-3228, que puede estar relacionado con una cuarta forma de titanosaurio no descrita en Lo Hueco. Sin embargo, ninguno de estos dos ejemplares está asociado a los individuos encontrados en conexión, y han sido localizados de manera aislada dentro del yacimiento. La hipótesis previa que hace mención a la presencia de tres o cuatro morfotipos que permitiesen explicar la mayor parte de la variabilidad morfológica queda así parcialmente refutada. Si bien la diversidad detectada es semejante, la distribución de ejemplares entre los distintos morfotipos es diferente [Se confirma la hipótesis principal y se rechaza la hipótesis no.2 – ver también Conclusión no. 2 más abajo]

Conclusión no.2:

La mayoría de los ejemplares de pequeño tamaño preservados en Lo Hueco pueden incluirse dentro de los dos morfotipos principales encontrados. Estos ejemplares mantienen determinados caracteres morfológicos que indican su pertenencia a individuos juveniles y no a taxones enanos. [Se rechaza la hipótesis no.2]

Conclusión no.3:

El Morfotipo I, incluyendo *Lohuecotitan pandafilandi*, comparte los mismos caracteres osteológicos y presenta la misma morfología general que otros saurópodos titanosaurios más primitivos. Ambas extremidades, anterior y posterior, son ligeramente robustas en términos generales. El Morfotipo II se caracteriza por presentar un esqueleto apendicular relativamente gracil, con un fémur robusto, una extremidad anterior grácil y el zeugopodio de la extremidad posterior ligeramente más columnar que el del Morfotipo I. Ambos morfotipos muestran claras diferencias con otras formas de titanosaurios conocidas en el registro Ibero-Armoricano [Se confirma la hipótesis no.3]

Conclusión no.4:

Incluso en estadios tempranos del desarrollo, los individuos juveniles de ambos morfotipos se asemejan morfológicamente a los individuos adultos. No se aprecia correlación entre los clústers morfológicos y los estadios ontogenéticos excepto en el húmero del Morfotipo I [Se confirma la hipótesis no.4]

Conclusión no.5:

La variabilidad en tamaño encontrada indica que este parámetro no es útil por si mismo para estimar el estadio de desarrollo del ejemplar. Además, gran parte de la variabilidad en tamaño

también se distribuye en los estadios sub-adultos y adultos. Excepcionalmente, algunos de los ejemplares de mayor tamaño de la muestra no están entre los individuos más maduros. [Se confirman tanto la hipótesis no.5]

Conclusión no.6:

El plan corporal de los titanosaurios litostrotios es conservativo a lo largo de su desarrollo ontogenético. No obstante, en las secuencias ontogenéticas se produce un fenómeno de polimorfismo que implica una plasticidad morfológica mayor de la esperada [Se rechaza parcialmente la hipótesis no. 6 – ver también Conclusión no.7 más abajo]

Conclusión no.7:

La variabilidad intraespecífica relacionada con el desarrollo ontogenético modifica la codificación de algunos caracteres morfológicos en las matrices de caracteres disponibles. La mayoría de estos cambios se producen en estadios tempranos del desarrollo, aunque algunos ocurren en estadios tardíos, generando situaciones de polimorfismo en la codificación de algunos caracteres [Se rechaza parcialmente la hipótesis no.6; se rechaza parcialmente la hipótesis no.7, ya que algunos cambios afectan también a estadios ontogenéticos tardíos]

Conclusión no.8:

Las diferencias morfológicas encontradas entre los dos morfotipos apendiculares principales identificados en Lo Hueco permiten relacionarlos con dos distintos gremios ecomorfológicos y dos distintas estrategias tróficas. Morfotipo I es claramente una forma generalista caracterizada por una estrategia trófica de baja altura. El Morfotipo II presenta una morfología similar a la de otros saurópodos especializados en estrategias tróficas de altura elevada [Se confirma la hipótesis no.8 – ver también Conclusión no.9 más abajo]

Conclusión no.9:

Se observa una relación significativa entre la especialización ecomorfológica relacionada con una estrategia trófica de altura elevada y la robustez general de los elementos del esqueleto apendicular. Esta relación se observa tanto en neosaurópodos no titanosaurios, como en titanosaurios, principalmente en la morfología de la extremidad anterior [Se confirma la hipótesis no.8]

Conclusión no.10:

La mayoría de los elementos del esqueleto apendicular de los dos morfotipos principales reconocidos en Lo Hueco muestran pequeñas diferencias a lo largo de la secuencia ontogenética [Se rechaza la hipótesis no.9]

SUPPLEMENTARY MATERIALS

SUPP. MATERIAL IV.I:

3D Geometric morphometrics of the hindlimb in the titanosaur sauropods from Lo Hueco (Cuenca, Spain)

SUPPL.IV.I.D. RDB

SUPPL.IV.I.D. ROBUSTNESS COMPARISON AND LINEAR MODEL TEST

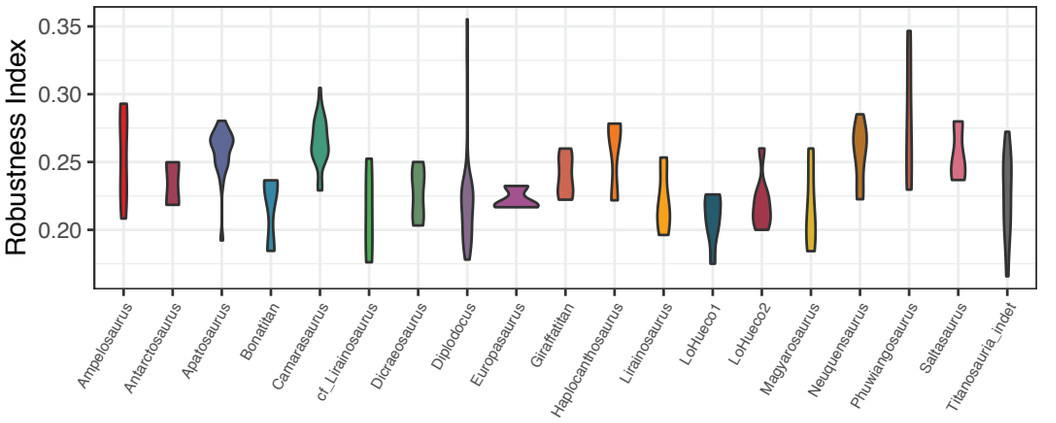

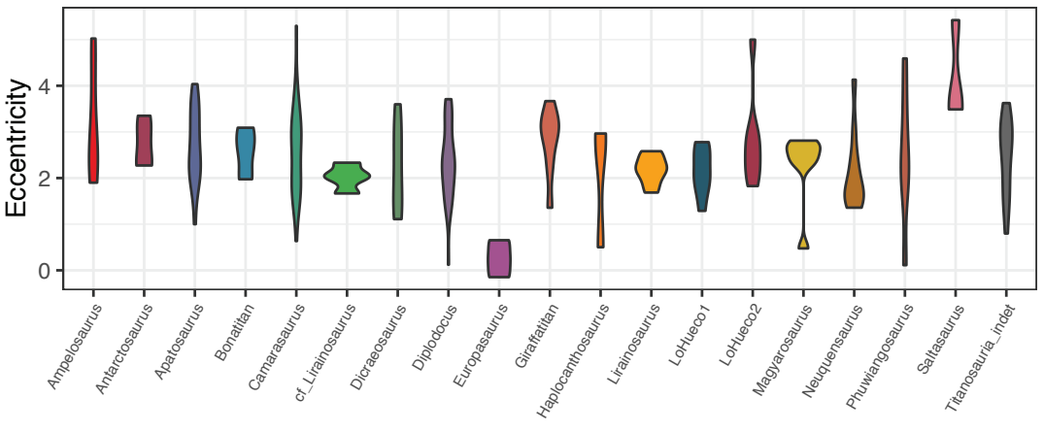

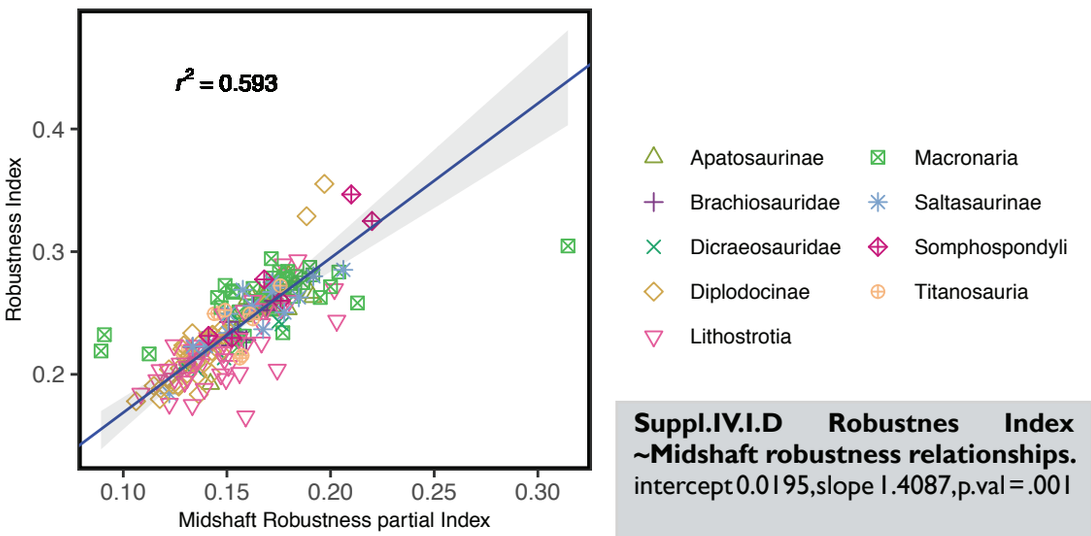

Suppl.IV.I.D Robustnes Index ~Midshaft robustness relationships. intercept 0.0195, slope 1.4087, p.val = .001

SUPPL.IV.I.E. PCA RESULTS

SUPPL.IV.I.E.1. COMPLETE PCA REPORTS

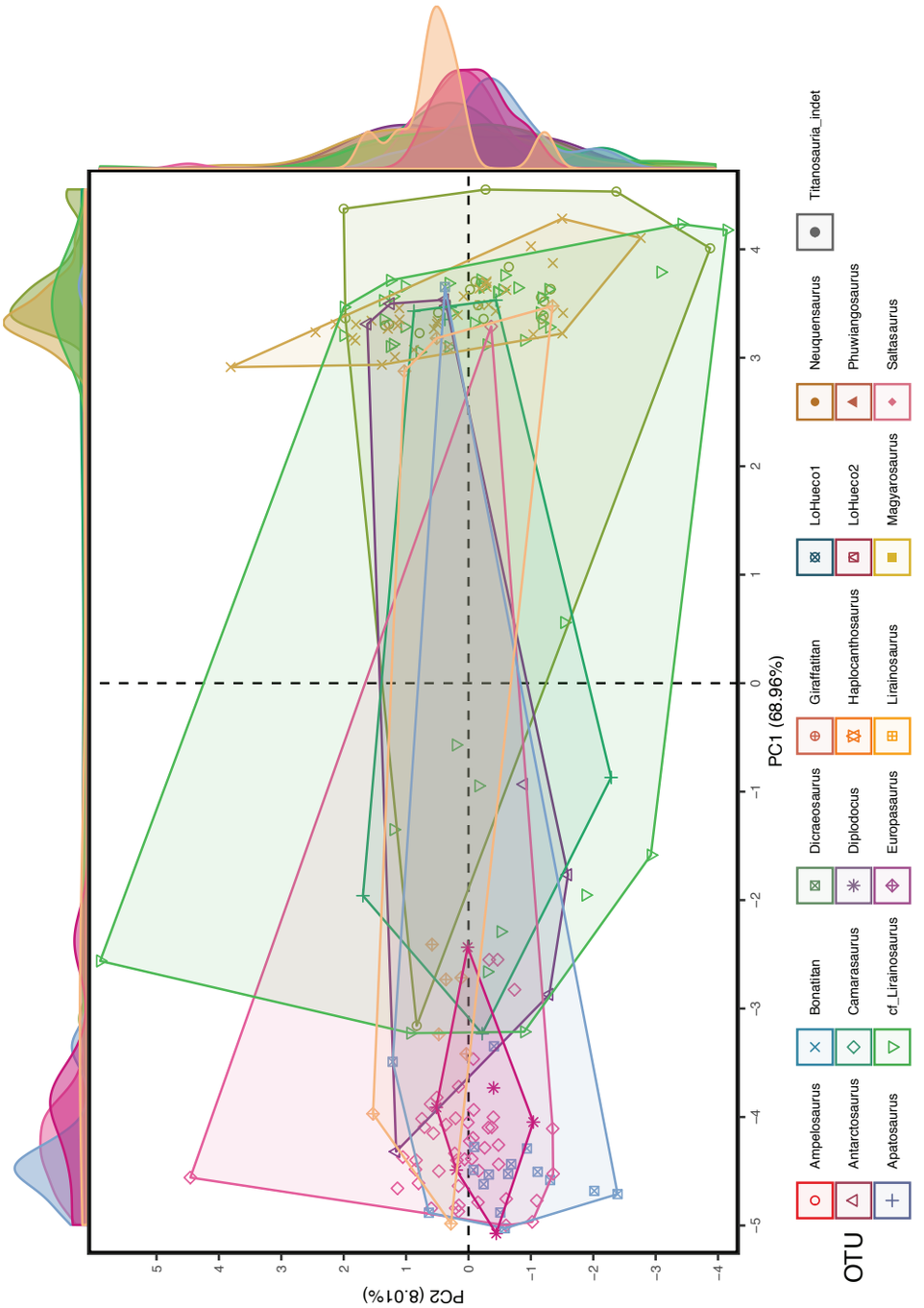

Suppl.IV.I.E.1. EXPDB PC1-PC2 with Clade morphospaces.

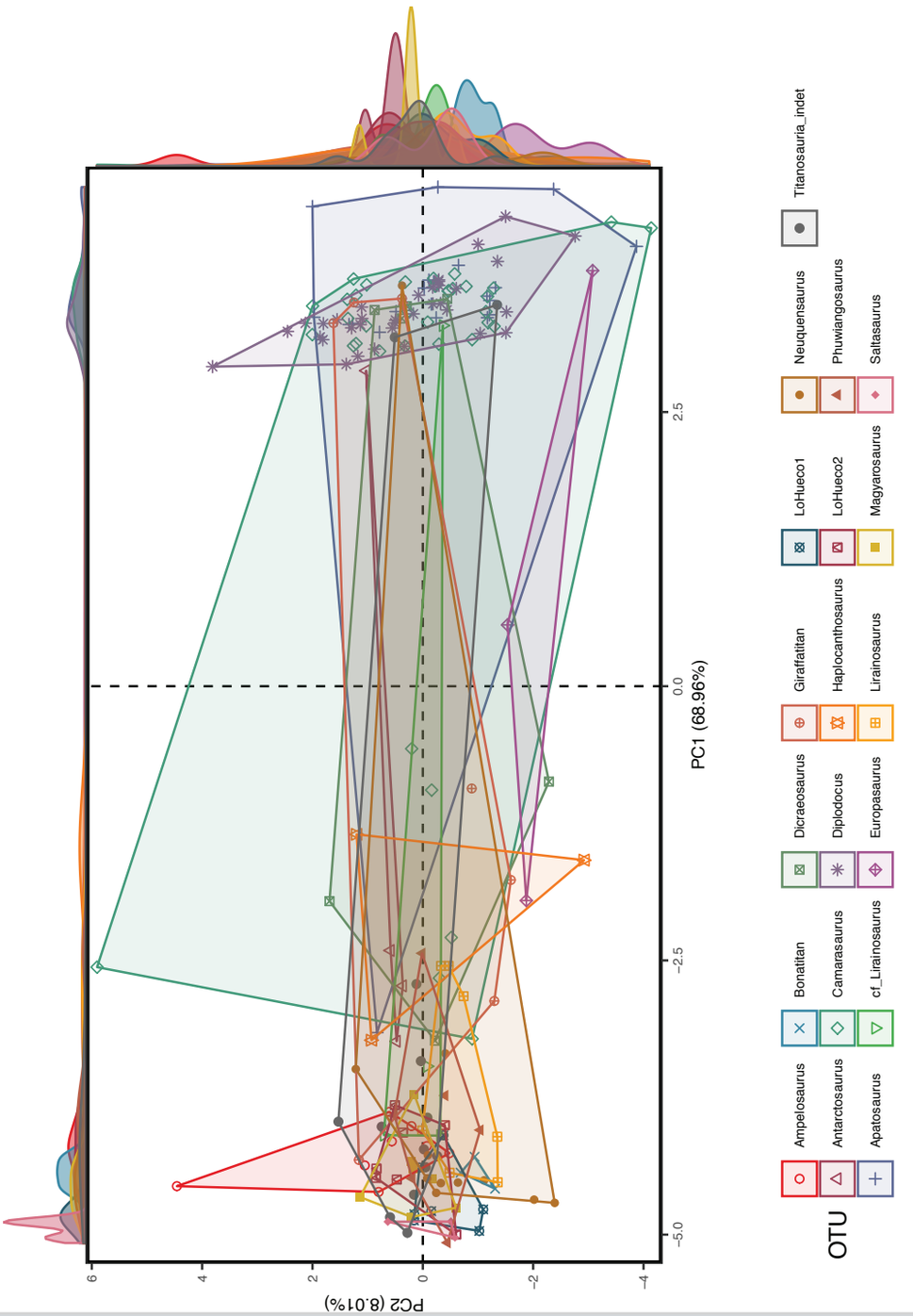

Suppl.IV.I.E.2. EXPDB PC1-PC2 with Genus morphospaces.

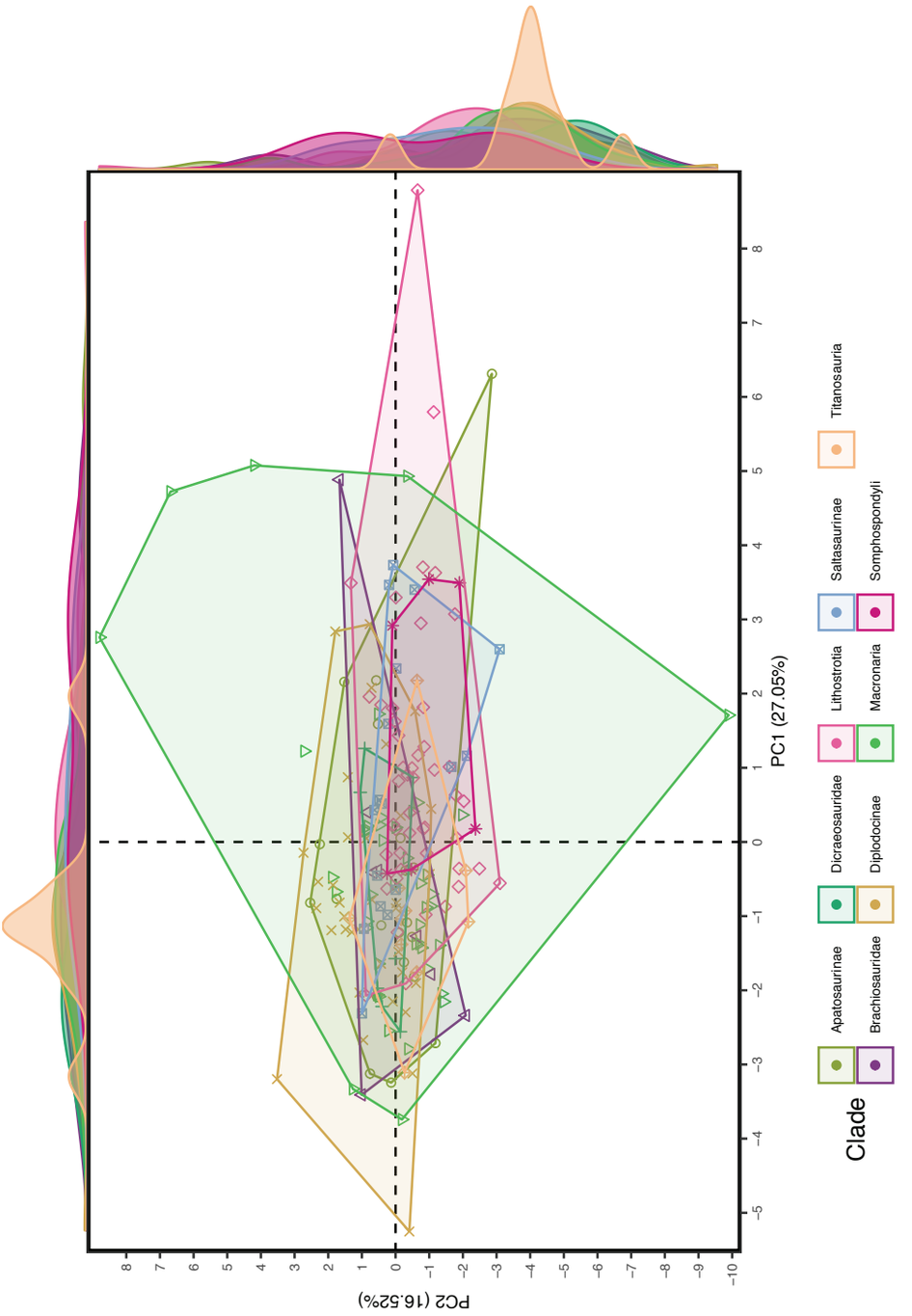

Suppl.IV.I.E.3. ORGDB PC1-PC2 with Clade morphospaces.

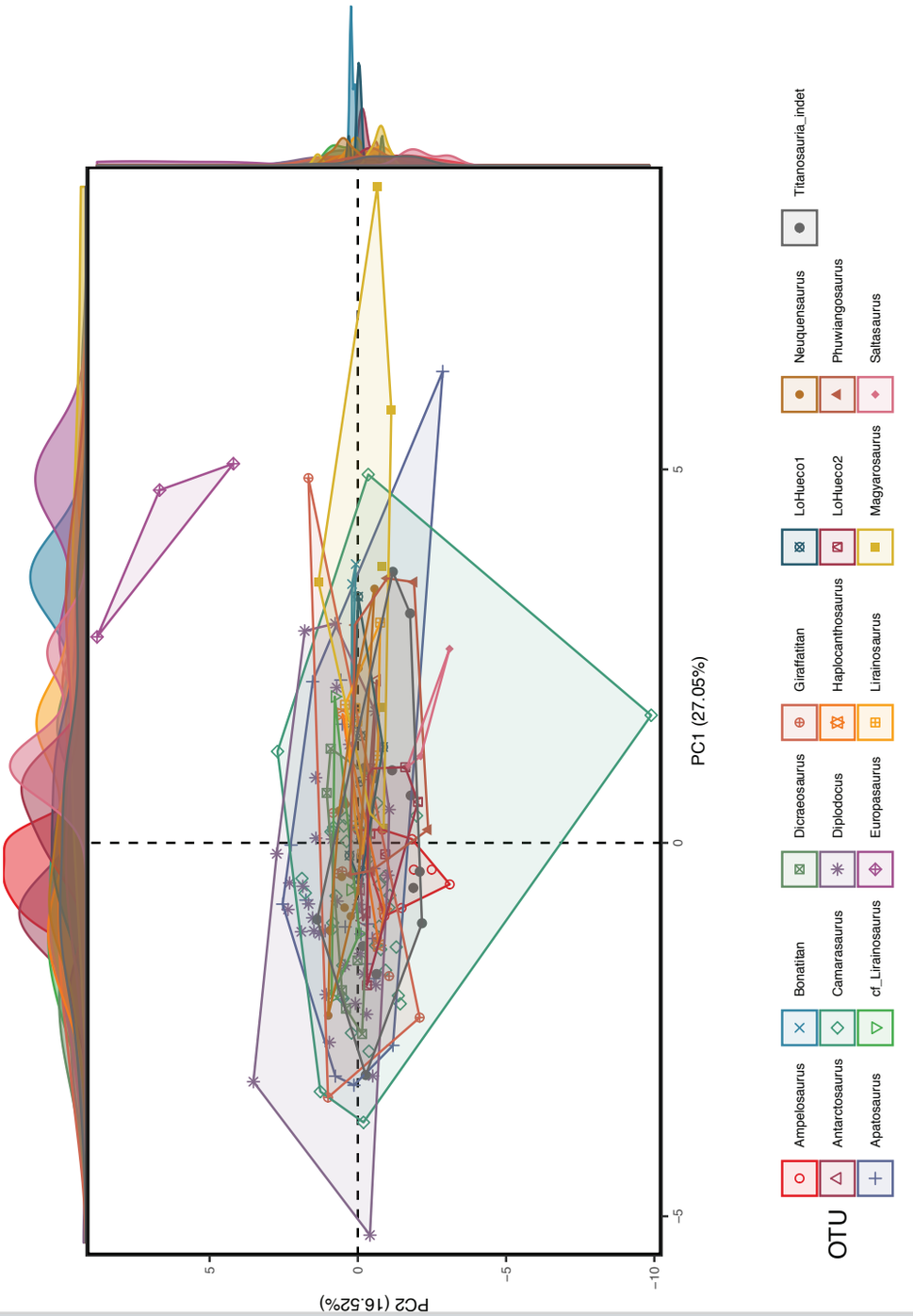

Suppl.IV.I.E.4. ORGDB PC1-PC2 with Genus morphospaces.

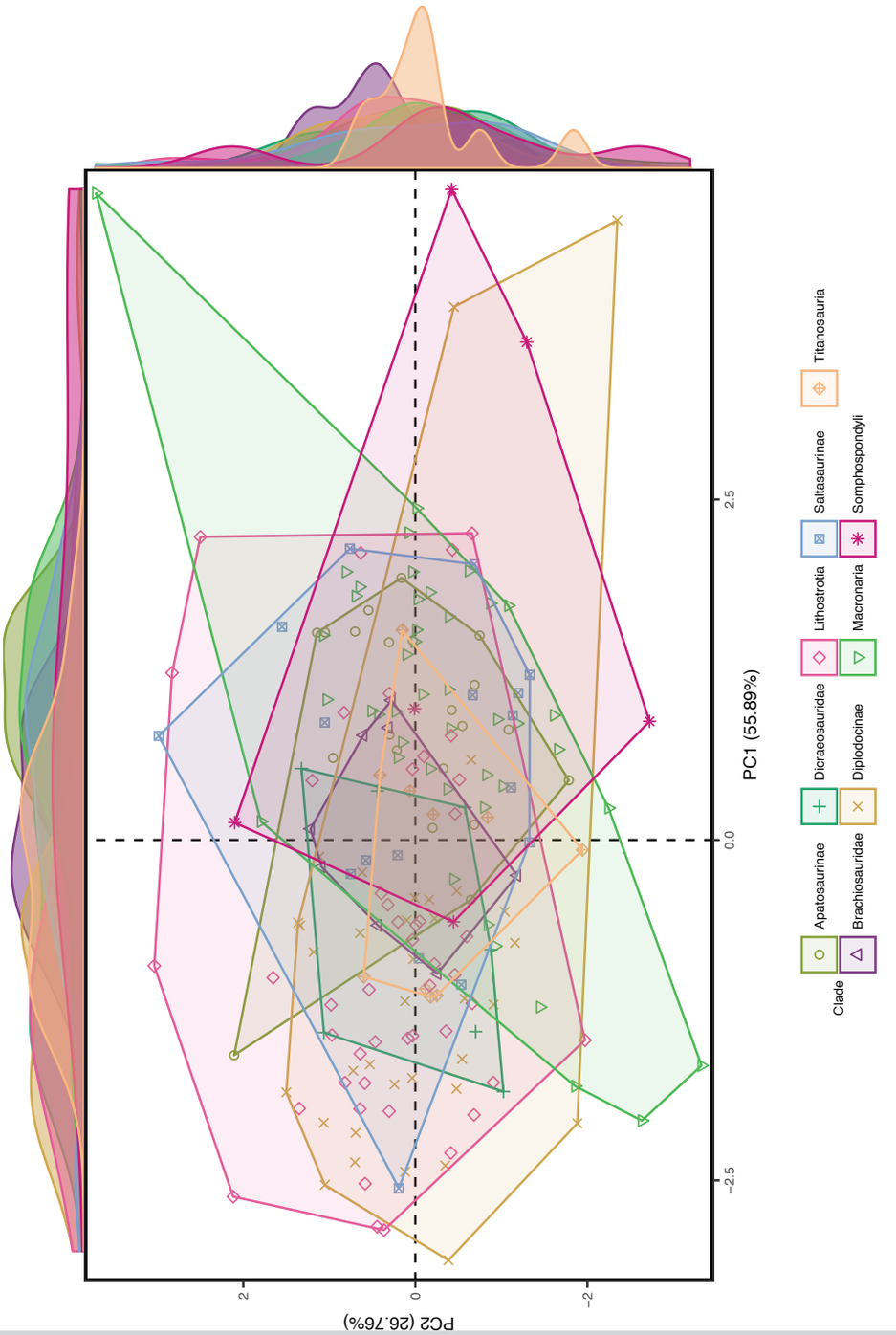

Suppl.IV.I.E.5. RDB PC1-PC2 with Clade morphospaces.

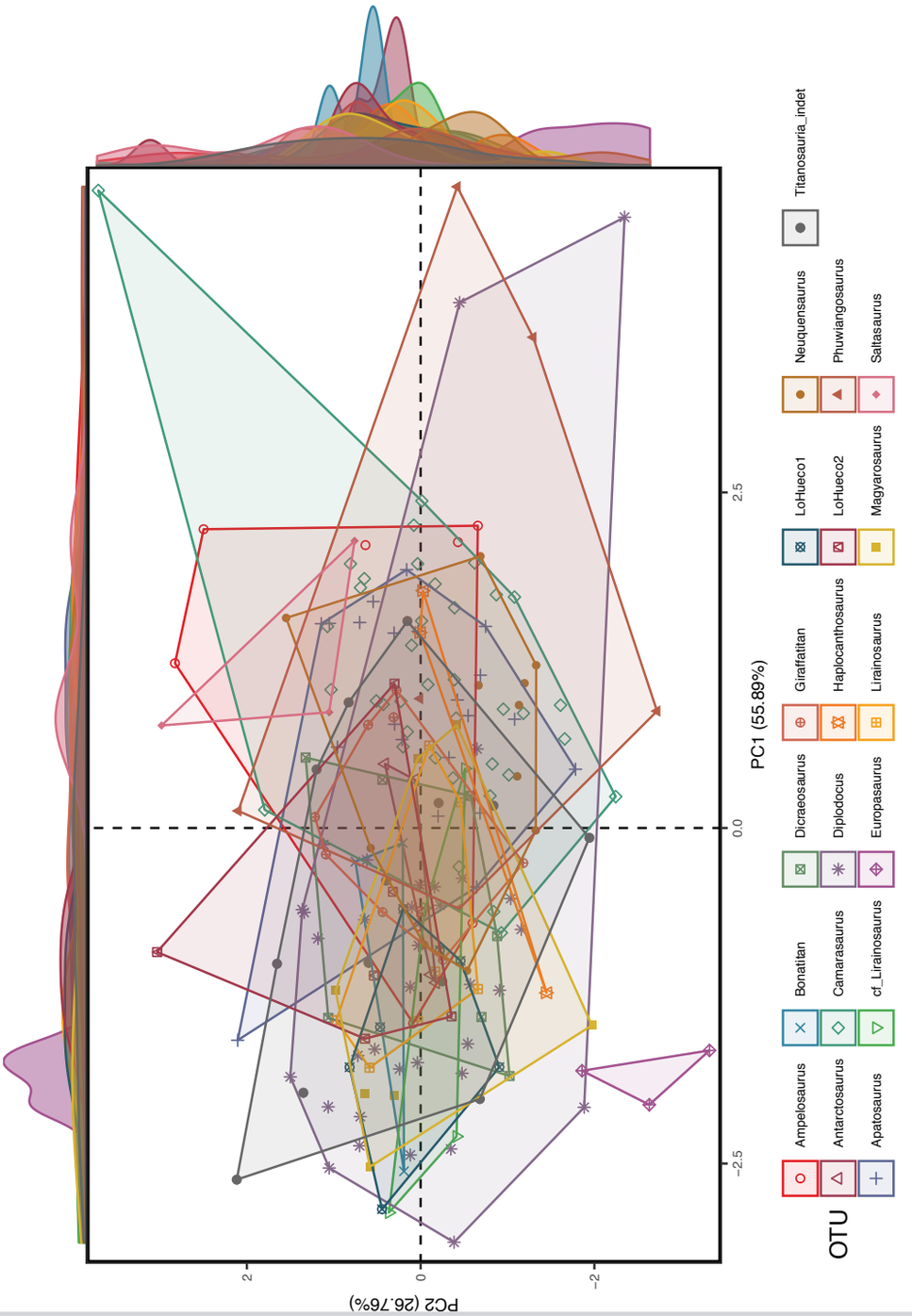

Suppl.IV.I.E.6. RDB PC1-PC2 with Genus morphospaces.

SUPPL.IV.I.E.2.VARIANCE EXPLAINED BY PCA

	EXPDB			ORGDB			RDB		
	Eigenval.	Variance (%)	Cum. Variance (%)	Eigenval.	Variance (%)	Cum. Variance (%)	Eigenval.	Variance (%)	Cum. Variance (%)
PC1	13.792	68.961	68.961	4.057	27.047	27.047	2.235	55.886	55.886
PC2	1.601	8.006	76.967	2.477	16.515	43.562	1.070	26.756	82.642
PC3	1.189	5.947	82.914	1.936	12.908	56.470	0.394	9.855	92.497
PC4	0.849	4.247	87.161	1.478	9.856	66.327	0.300	7.503	100.000
PC5	0.629	3.147	90.308	1.181	7.873	74.199			
PC6	0.442	2.212	92.520	1.010	6.732	80.932			
PC7	0.312	1.559	94.079	0.859	5.726	86.657			
PC8	0.266	1.332	95.411	0.647	4.312	90.969			
PC9	0.240	1.198	96.609	0.412	2.744	93.713			
PC10	0.155	0.774	97.383	0.331	2.204	95.917			
PC11	0.123	0.617	98.000	0.244	1.627	97.544			
PC12	0.119	0.594	98.594	0.168	1.117	98.661			
PC13	0.089	0.447	99.042	0.113	0.756	99.417			
PC14	0.073	0.365	99.406	0.066	0.439	99.856			
PC15	0.042	0.211	99.618	0.022	0.144	100.000			
PC16	0.036	0.178	99.796						
PC17	0.018	0.090	99.886						
PC18	0.012	0.061	99.947						
PC19	0.007	0.033	99.980						
PC20	0.004	0.020	100.000						

Suppl.IV.I.E.2.1. Eigenvalue descomposition of the Complete neosauropod sample PCAs.

	EXPDB			ORGDB			RDB		
	Eigenval.	Variance (%)	Cum. Variance (%)	Eigenval.	Variance (%)	Cum. Variance (%)	Eigenval.	Variance (%)	Cum. Variance (%)
PC1	10.806	54.031	54.031	3.914	26.094	26.094	2.272	56.803	56.803
PC2	1.794	8.971	63.003	2.052	13.677	39.771	1.063	26.578	83.381
PC3	1.514	7.570	70.573	1.611	10.737	50.508	0.425	10.635	94.016
PC4	1.244	6.220	76.792	1.577	10.513	61.021	0.239	5.984	100.000
PC5	1.048	5.238	82.030	1.425	9.498	70.519			
PC6	0.836	4.179	86.209	1.058	7.053	77.572			
PC7	0.565	2.823	89.032	0.888	5.922	83.495			
PC8	0.466	2.331	91.363	0.865	5.764	89.258			
PC9	0.429	2.143	93.506	0.570	3.801	93.059			
PC10	0.318	1.592	95.097	0.427	2.845	95.904			
PC11	0.264	1.322	96.420	0.222	1.477	97.381			
PC12	0.243	1.213	97.633	0.165	1.101	98.482			
PC13	0.155	0.775	98.408	0.140	0.936	99.418			
PC14	0.117	0.584	98.992	0.083	0.557	99.975			
PC15	0.077	0.385	99.376	0.004	0.025	100.000			
PC16	0.054	0.272	99.649						
PC17	0.031	0.154	99.803						
PC18	0.016	0.081	99.884						
PC19	0.014	0.068	99.952						
PC20	0.010	0.048	100.000						

Suppl.IV.I.E.2.2. Eigenvalue descomposition of the Ibero-Armorican titanosaur sample PCAs.

	EXPDB			ORGDB			RDB		
	Eigenval.	Variance (%)	Cum. Variance (%)	Eigenval.	Variance (%)	Cum. Variance (%)	Eigenval.	Variance (%)	Cum. Variance (%)
PC1	5.692	28.461	28.461	5.074	33.828	33.828	1.710	42.745	42.745
PC2	2.973	14.864	43.325	2.511	16.740	50.568	1.294	32.353	75.098
PC3	2.591	12.957	56.281	1.761	11.742	62.310	0.692	17.301	92.399
PC4	1.886	9.428	65.709	1.321	8.806	71.116	0.304	7.601	100.000
PC5	1.411	7.054	72.764	1.002	6.682	77.798			
PC6	1.145	5.724	78.487	0.909	6.063	83.861			
PC7	1.031	5.157	83.644	0.771	5.137	88.999			
PC8	1.004	5.020	88.664	0.667	4.447	93.446			
PC9	0.672	3.359	92.023	0.379	2.528	95.974			
PC10	0.532	2.662	94.686	0.234	1.558	97.532			
PC11	0.345	1.727	96.413	0.147	0.980	98.512			
PC12	0.279	1.395	97.808	0.118	0.788	99.300			
PC13	0.196	0.979	98.787	0.075	0.499	99.800			
PC14	0.088	0.441	99.228	0.030	0.197	99.997			
PC15	0.083	0.416	99.644	0.000	0.003	100.000			
PC16	0.039	0.193	99.837						
PC17	0.020	0.100	99.937						
PC18	0.010	0.051	99.988						
PC19	0.002	0.011	99.999						
PC20	0.000	0.001	100.000						

Suppl.IV.I.E.2.3. Eigenvalue descomposition of the Lo Hueco sample PCAs.

SUPPL.IV.I.H. CLUSTER ANALYSES

SUPPL.IV.I.H.1. CLUSTER ANALYSES WITH CLADE DISTRIBUTION

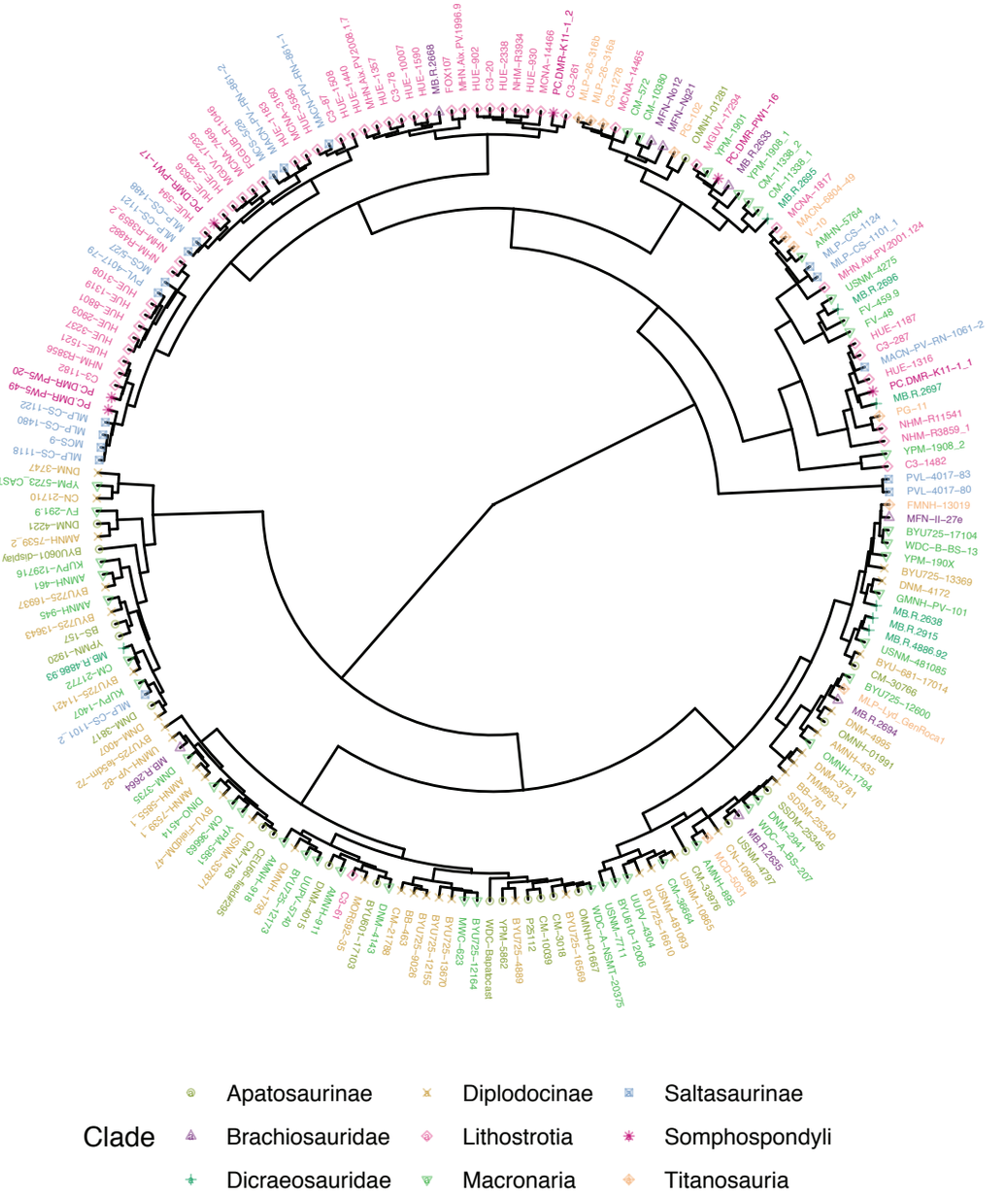

Suppl.IV.I.H.1. EXPDB cluster analysis with neosauropod sample. Coloured by clade.

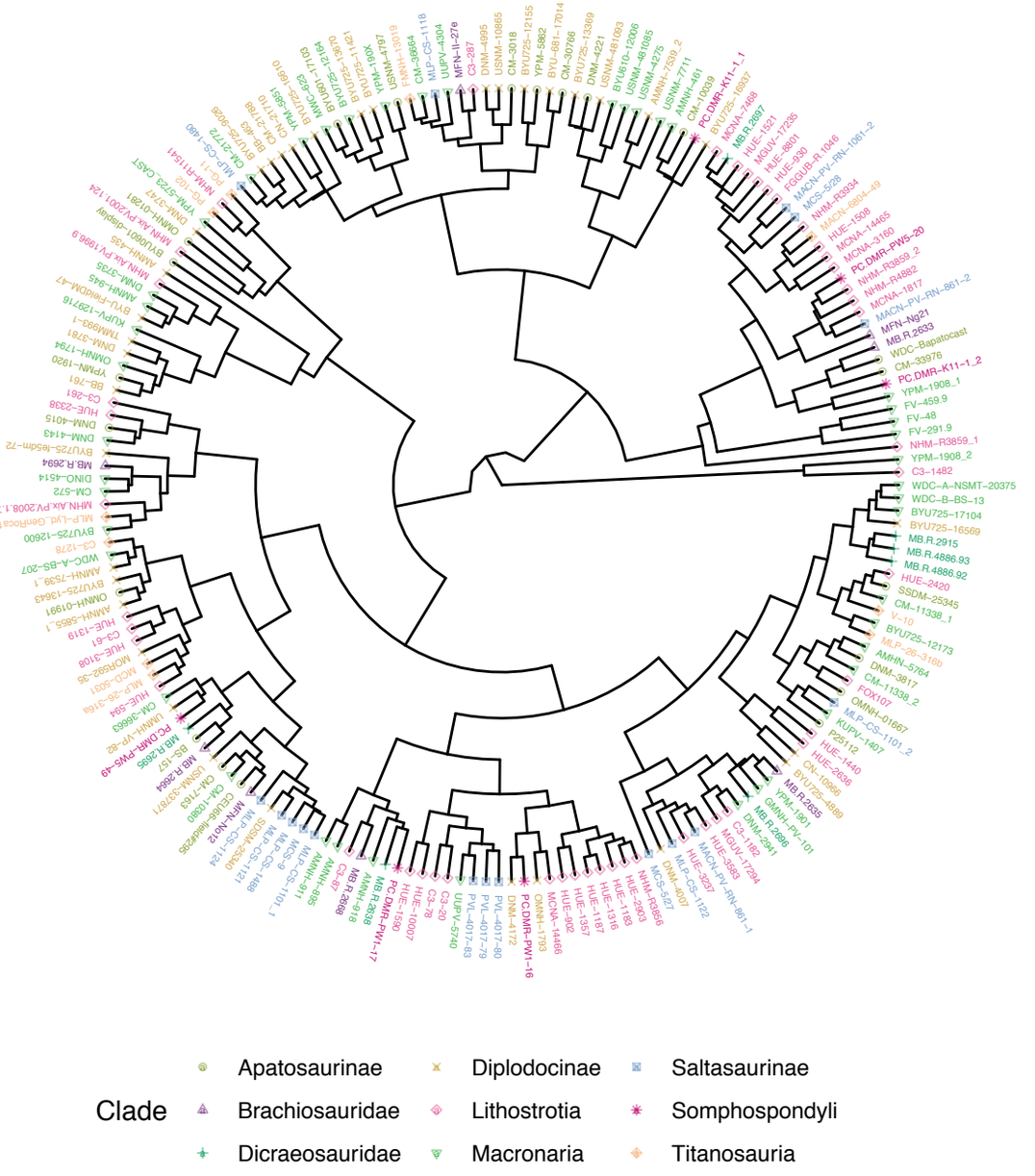

Suppl.IV.I.H.2. ORGDB cluster analysis with neosauropod sample. Coloured by clade.

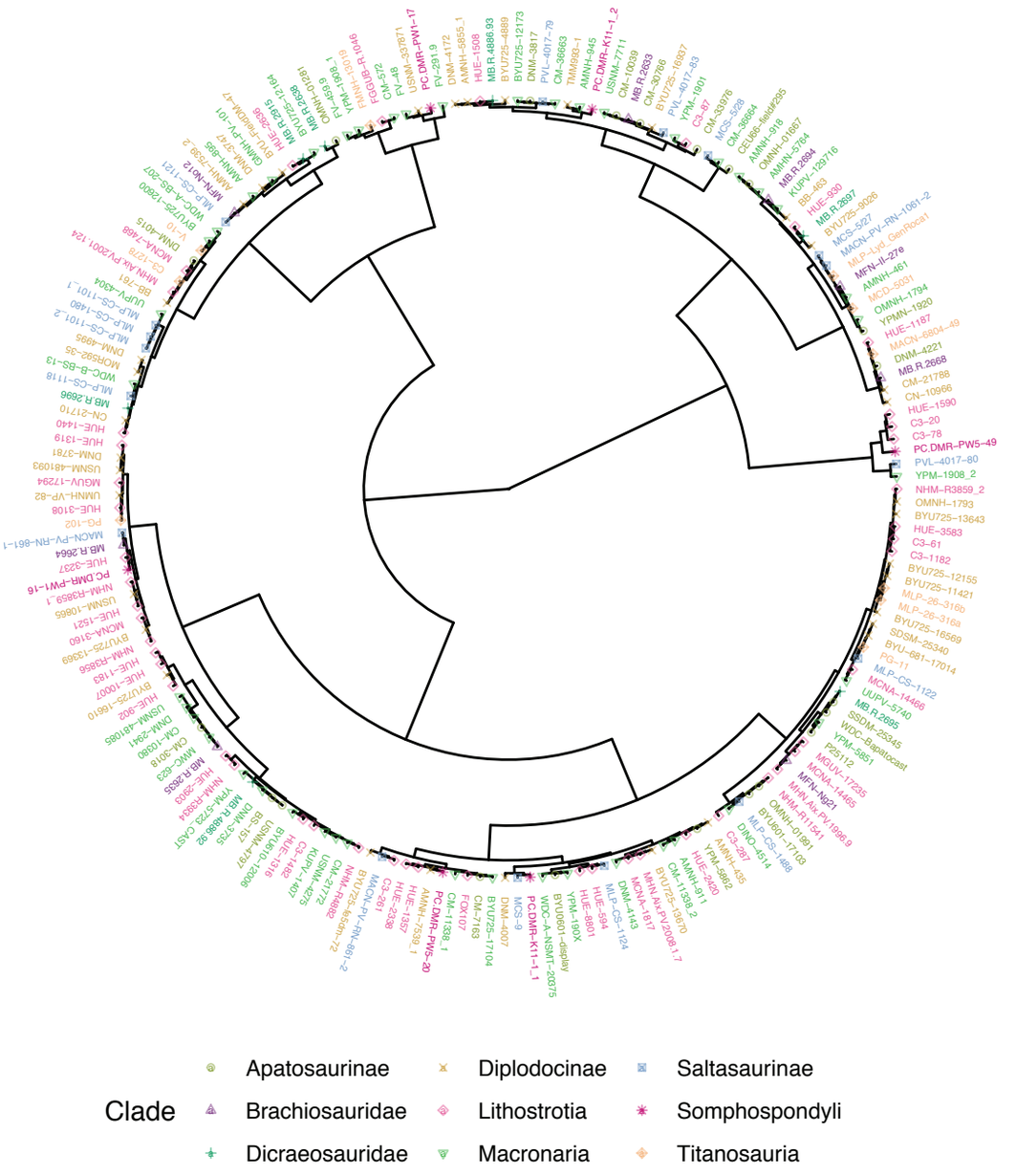

Suppl.IV.I.H.3. RDB cluster analysis with neosauropod sample. Coloured by clade.

SSUPPL.IV.I.H.2. CLUSTER ANALYSES WITH GENUS DISTRIBUTION

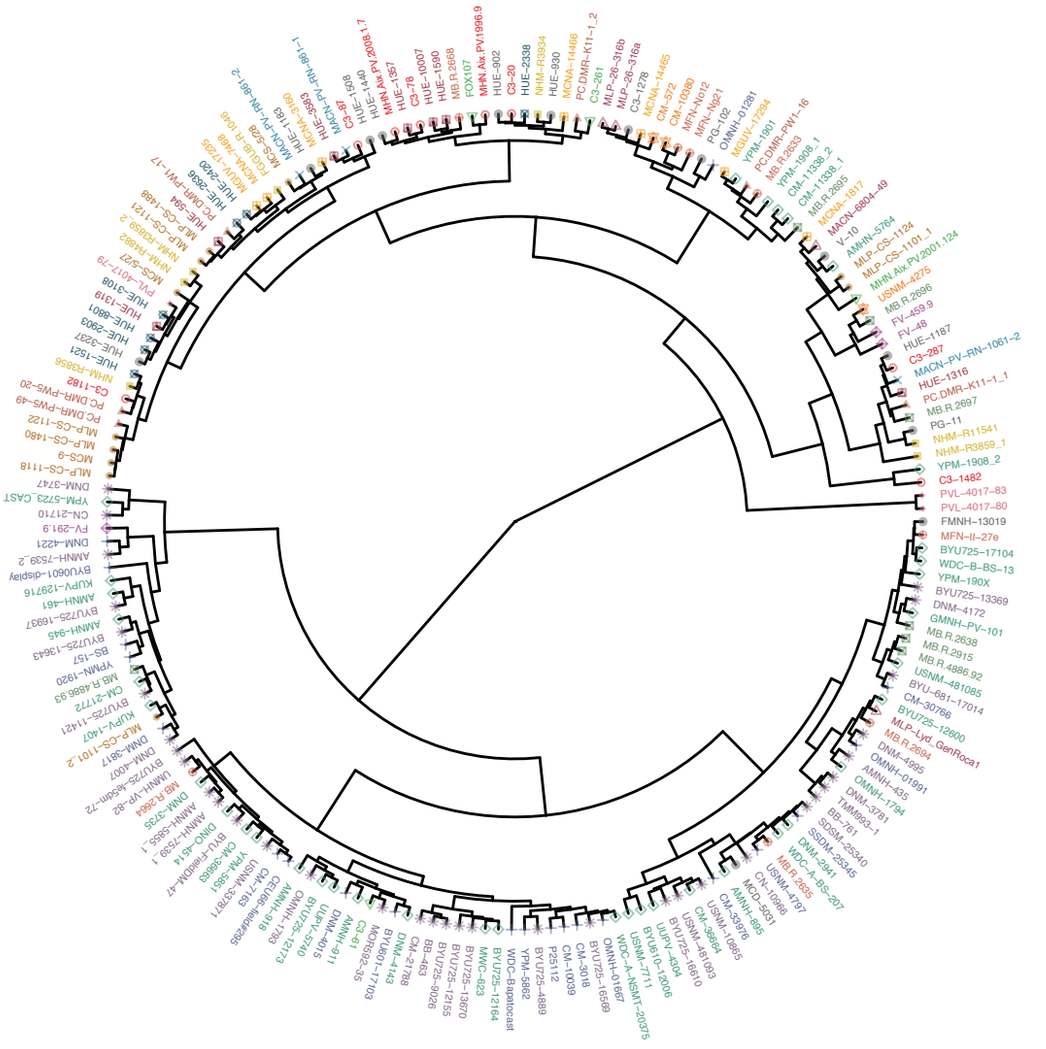

OTU

Ampelosaurus	cf_Lirainosaurus	Haplocanthosaurus	Neuquensaurus
Antarctosaurus	Dicraeosaurus	Lirainosaurus	Phuwiangosaurus
Apatosaurus	Diplodocus	LoHueco1	Saltasaurus
Bonatitan	Europasaurus	LoHueco2	Titanosauria_indet
Camarasaurus	Giraffatitan	Magyarosaurus	

Suppl.IV.I.H.4. EXPDB cluster analysis with neosauropod sample. Coloured by genus.

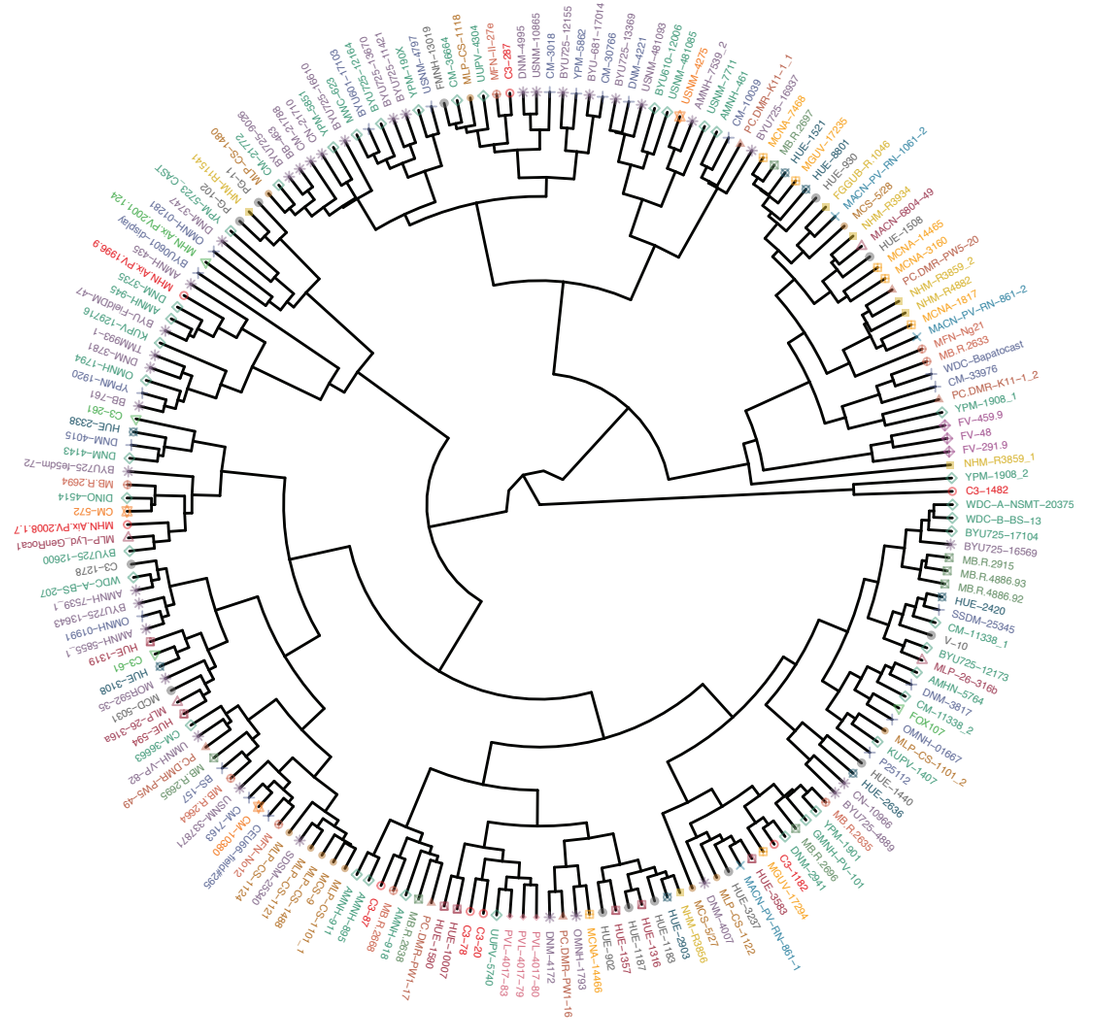

OTU

- Ampelosaurus
- Antarctosaurus
- Apatosaurus
- Bonatitan
- Camarasaurus
- cf_Lirainosaurus
- Dicraeosaurus
- Diplodocus
- Europasaurus
- Giraffatitan
- Haplocanthosaurus
- Lirainosaurus
- LoHueco1
- LoHueco2
- Magyarosaurus
- Neuquensaurus
- Phuwiangosaurus
- Saltasaurus
- Titanosauria_indet

Suppl.IV.I.H.5. ORGDB cluster analysis with neosauropod sample. Coloured by genus.

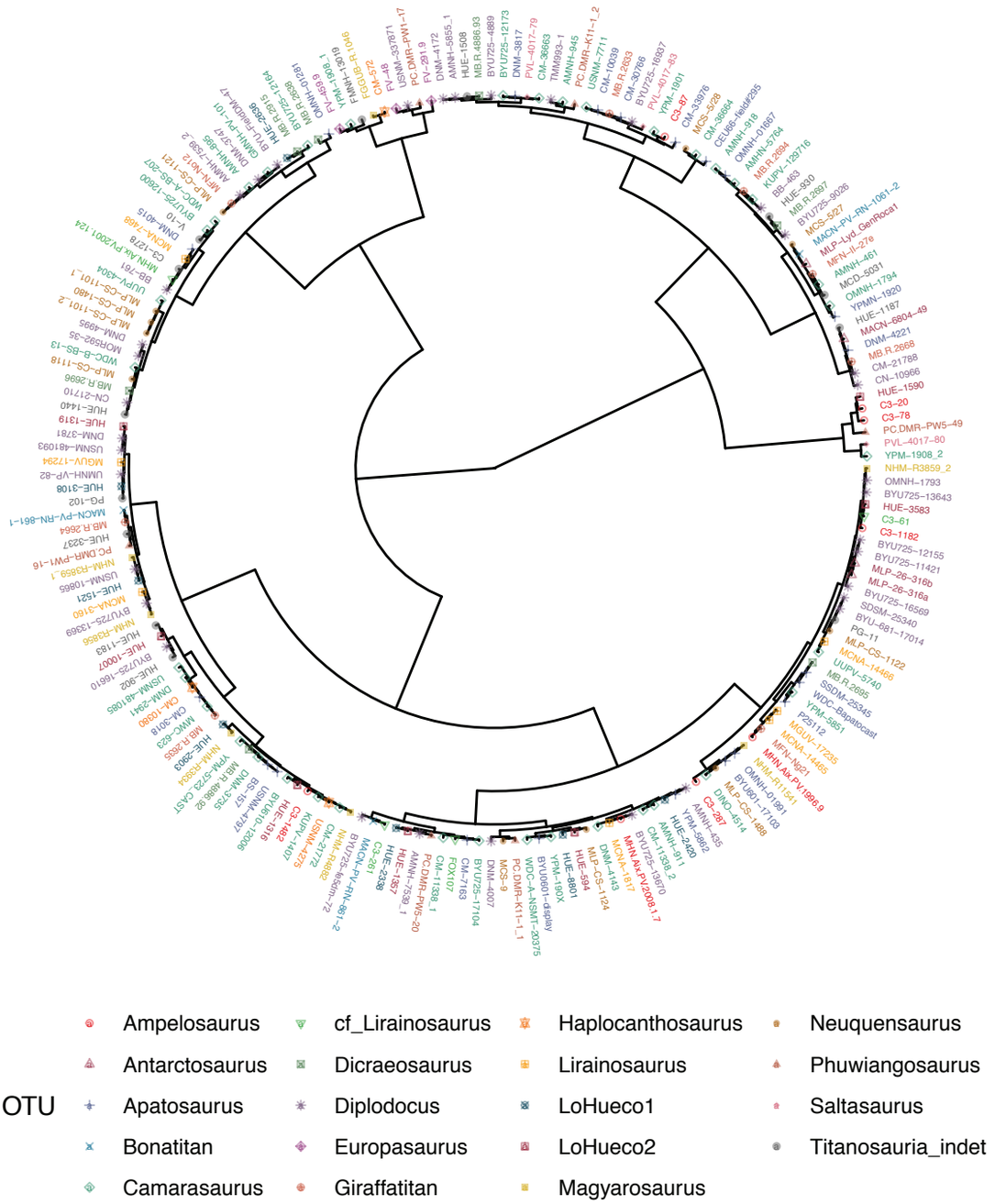

Suppl.IV.I.H.6. RDB cluster analysis with neosauropod sample. Coloured by genus.

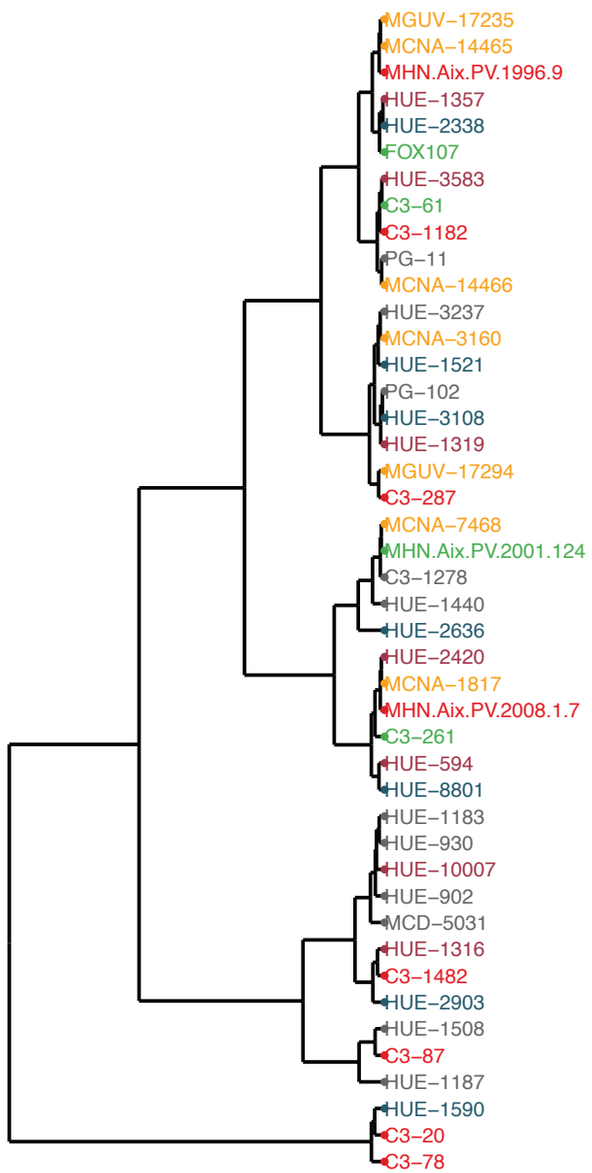

Suppl.IV.I.H.7. RDB cluster analysis with Ibero-Armorican sample. Coloured by genus.

SUPPL.IV.I.J. DISCRIMINANT FUNCTION ANALYSIS RESULTS

SUPPL.IV.I.J.1. PREDICTED ALLOCATION REPORT

Specimen	OTU	1st Prob	1st Class	2nd Prob	2nd Class
C3-287	Ampelosaurus	61.86	Phuwiangosaurus	27.3	Diplodocus
MHN.Aix.PV.2008.1.7	Ampelosaurus	48.88	Ampelosaurus	18.09	Magyarosaurus
MACN-6804-49	Antarctosaurus	74	Ampelosaurus	20.22	Diplodocus
CM-7163	Apatosaurus	67.65	Camarasaurus	25.34	Saltasaurus
BS-157	Apatosaurus	80.87	Camarasaurus	14.76	Magyarosaurus
CM-10039	Apatosaurus	64.27	Camarasaurus	24.59	Bonatitan
BYU601-17103	Apatosaurus	34.4	Giraffatitan	31.1	Magyarosaurus
YPM-5862	Apatosaurus	86.96	Camarasaurus	10.39	LoHueco2
OMNH-01991	Apatosaurus	41.01	Apatosaurus	33.33	Magyarosaurus
YPM-1908_1	Camarasaurus	90.76	Phuwiangosaurus	4.39	Diplodocus
YPM-1901	Camarasaurus	36.31	Haplocanthosaurus	35.9	Magyarosaurus
GMNH-PV-101	Camarasaurus	41.86	Camarasaurus	29.21	Magyarosaurus
CM-11338_2	Camarasaurus	68.47	Antarctosaurus	8.6	Magyarosaurus
WDC-B-BS-13	Camarasaurus	63.76	Camarasaurus	31.46	Magyarosaurus
DNM-2941	Camarasaurus	60.05	Camarasaurus	23.07	Magyarosaurus
CM-36663	Camarasaurus	76.68	Camarasaurus	16.76	Bonatitan
AMNH-945	Camarasaurus	55.07	Camarasaurus	28.73	LoHueco1
OMNH-1794	Camarasaurus	42.75	Camarasaurus	33.2	Bonatitan
AMHN-5764	Camarasaurus	48.61	Titanosauria_indet	39.01	Magyarosaurus
DNM-3735	Camarasaurus	35.08	Apatosaurus	32.27	Bonatitan
MHN.Aix.PV.2001.124	cf_Lirainosaurus	48.25	Titanosauria_indet	39.94	LoHueco1
MB.R.4886.92	Dicraeosaurus	39.48	Camarasaurus	31.39	Magyarosaurus
MB.R.2697	Dicraeosaurus	50.69	LoHueco2	32.73	Magyarosaurus
USNM-10865	Diplodocus	73.04	Diplodocus	20.5	Magyarosaurus
CM-21788	Diplodocus	94.55	Diplodocus	2.05	Bonatitan
BYU725-4889	Diplodocus	94.06	Diplodocus	4.79	LoHueco1
SDSM-25340	Diplodocus	54.03	Camarasaurus	24.83	Magyarosaurus
BYU725-13670	Diplodocus	94.65	Diplodocus	2.07	Magyarosaurus
BYU725-16569	Diplodocus	89.18	Diplodocus	7.69	Magyarosaurus
BYU725-13643	Diplodocus	63.88	Diplodocus	13.29	Magyarosaurus
BYU725-fe5dm-72	Diplodocus	91.09	Diplodocus	6.23	Magyarosaurus
MOR592-35	Diplodocus	94.95	Diplodocus	3.31	Magyarosaurus
UMNH-VP-82	Diplodocus	94.25	Diplodocus	2.18	Saltasaurus
MFN-II-27e	Giraffatitan	49.9	Camarasaurus	29.89	Bonatitan
MFN-Ng21	Giraffatitan	55	Haplocanthosaurus	33.84	Magyarosaurus
MCNA-14465	Lirainosaurus	56.08	Titanosauria_indet	22.51	Magyarosaurus
MGUV-17235	Lirainosaurus	39.85	Lirainosaurus	37.13	Saltasaurus
HUE-2636	LoHueco1	59.01	LoHueco1	38.91	Haplocanthosaurus
HUE-1590	LoHueco2	87.19	LoHueco2	6.47	Haplocanthosaurus
HUE-2420	LoHueco1	42.72	Neuquensaurus	26.72	Haplocanthosaurus
HUE-594	LoHueco2	70.53	Ampelosaurus	20.78	Apatosaurus
NHM-R3856	Magyarosaurus	40.04	LoHueco2	34.72	Haplocanthosaurus
NHM-R3859_2	Magyarosaurus	69.98	Magyarosaurus	17.53	Dicraeosaurus
MLP-CS-1480	Neuquensaurus	43.72	Phuwiangosaurus	28.78	Saltasaurus
MLP-CS-1122	Neuquensaurus	81.41	Neuquensaurus	5.93	Diplodocus
MCS-5/28	Neuquensaurus	59.53	Bonatitan	18.71	Diplodocus
PC.DMR-K11-1_2	Phuwiangosaurus	99.67	Phuwiangosaurus	0.16	Diplodocus
MCD-5031	Titanosauria_indet	42.62	Dicraeosaurus	25.01	Magyarosaurus
HUE-1440	Titanosauria_indet	98.11	LoHueco2	1.03	Magyarosaurus
HUE-902	Titanosauria_indet	86.22	LoHueco1	10.6	Antarctosaurus
HUE-1508	Titanosauria_indet	74.85	Ampelosaurus	12.13	Diplodocus
HUE-3237	Titanosauria_indet	78.51	Neuquensaurus	16.63	Dicraeosaurus
HUE-1183	Titanosauria_indet	63.47	LoHueco1	34.44	Saltasaurus
HUE-1187	Titanosauria_indet	48.26	LoHueco2	36.25	Diplodocus
HUE-930	Titanosauria_indet	41.24	Lirainosaurus	28.12	Diplodocus

Suppl.IV.I.J.1.1. DFA allocation results over the EXPDB testing group.

Specimen	OTU	1st Prob	1st Class	2nd Prob	2nd Class
C3-287	Ampelosaurus	37.96	Camarasaurus	9.98	cf_Lirainosaurus
MHN.Aix.PV.2008.1.7	Ampelosaurus	46.31	Saltasaurus	22.61	LoHueco2
MACN-6804-49	Antarctosaurus	29.72	Diplodocus	22.05	Bonatitan
CM-7163	Apatosaurus	41.53	Camarasaurus	24.51	Saltasaurus
BS-157	Apatosaurus	55.71	Diplodocus	18.38	Ampelosaurus
CM-10039	Apatosaurus	63.03	Camarasaurus	13.42	Saltasaurus
BYU601-17103	Apatosaurus	34.8	Camarasaurus	26.06	Saltasaurus
YPM-5862	Apatosaurus	42.22	Camarasaurus	23.26	LoHueco1
OMNH-01991	Apatosaurus	98.03	Diplodocus	1.09	Lirainosaurus
YPM-1908_1	Camarasaurus	99.08	Saltasaurus	0.92	Dicraeosaurus
YPM-1901	Camarasaurus	41.71	Camarasaurus	20.64	Saltasaurus
GMNH-PV-101	Camarasaurus	53.2	Dicraeosaurus	18.46	Magyarosaurus
CM-11338_2	Camarasaurus	24.17	Camarasaurus	23.73	Saltasaurus
WDC-B-BS-13	Camarasaurus	28.73	Diplodocus	28.64	Saltasaurus
DNM-2941	Camarasaurus	39.91	Neuquensaurus	19.13	Ampelosaurus
CM-36663	Camarasaurus	82.04	Diplodocus	8.07	Bonatitan
AMNH-945	Camarasaurus	52.86	Camarasaurus	23.77	LoHueco2
OMNH-1794	Camarasaurus	47.54	Haplocanthosaurus	24.65	Bonatitan
AMHN-5764	Camarasaurus	42.37	Camarasaurus	39.27	Saltasaurus
DNM-3735	Camarasaurus	21.45	Camarasaurus	21.44	Bonatitan
MHN.Aix.PV.2001.124	cf_Lirainosaurus	81.05	Ampelosaurus	15.16	Dicraeosaurus
MB.R.4886.92	Dicraeosaurus	35.78	Camarasaurus	18.84	cf_Lirainosaurus
MB.R.2697	Dicraeosaurus	38.5	Diplodocus	31.38	Bonatitan
USNM-10865	Diplodocus	84.83	Diplodocus	6.94	Bonatitan
CM-21788	Diplodocus	75.12	Diplodocus	13.09	Bonatitan
BYU725-4889	Diplodocus	70.36	Diplodocus	7.29	cf_Lirainosaurus
SDSM-25340	Diplodocus	87.08	Lirainosaurus	8.25	Haplocanthosaurus
BYU725-13670	Diplodocus	37.23	Diplodocus	30.74	Bonatitan
BYU725-16569	Diplodocus	93.08	Diplodocus	3.3	Bonatitan
BYU725-13643	Diplodocus	94.73	Diplodocus	1.76	Ampelosaurus
BYU725-fe5dm-72	Diplodocus	48.52	Diplodocus	15.6	Bonatitan
MOR592-35	Diplodocus	39.42	cf_Lirainosaurus	28.8	Magyarosaurus
UMNH-VP-82	Diplodocus	32.82	Diplodocus	15.72	Saltasaurus
MFN-II-27e	Giraffatitan	54.3	Camarasaurus	31.63	LoHueco1
MFN-Ng21	Giraffatitan	90.79	Lirainosaurus	6.73	LoHueco2
MCNA-14465	Lirainosaurus	32.08	Bonatitan	22.78	LoHueco2
MGUV-17235	Lirainosaurus	98.93	Bonatitan	0.51	Antarctosaurus
HUE-2636	LoHueco1	45.06	Diplodocus	32.92	Bonatitan
HUE-1590	LoHueco1	86.55	Lirainosaurus	9.57	Haplocanthosaurus
HUE-2420	LoHueco2	90.56	LoHueco2	4.86	Antarctosaurus
HUE-594	LoHueco2	33.66	Phuwiangosaurus	20.04	cf_Lirainosaurus
NHM-R3856	Magyarosaurus	65.63	Europasaurus	21.96	Dicraeosaurus
NHM-R3859_2	Magyarosaurus	46.91	Magyarosaurus	43.86	Apatosaurus
MLP-CS-1480	Neuquensaurus	32.85	Diplodocus	26.61	Bonatitan
MLP-CS-1122	Neuquensaurus	28.82	Neuquensaurus	21.59	Ampelosaurus
MCS-5/28	Neuquensaurus	34.77	Magyarosaurus	32.52	cf_Lirainosaurus
PC.DMR-K11-1_2	Phuwiangosaurus	64.37	Saltasaurus	13.04	LoHueco2
MCD-5031	Titanosauria_indet	26.59	Camarasaurus	20.12	Saltasaurus
HUE-1440	Titanosauria_indet	76.07	LoHueco2	17	cf_Lirainosaurus
HUE-902	Titanosauria_indet	69.1	LoHueco1	26.86	Saltasaurus
HUE-1508	Titanosauria_indet	80.57	Ampelosaurus	8.45	Neuquensaurus
HUE-3237	Titanosauria_indet	74.46	Neuquensaurus	15.55	cf_Lirainosaurus
HUE-1183	Titanosauria_indet	45.43	LoHueco1	30.53	Antarctosaurus
HUE-1187	Titanosauria_indet	26.92	LoHueco1	24.41	Haplocanthosaurus
HUE-930	Titanosauria_indet	60.28	Saltasaurus	30.06	Antarctosaurus

Suppl.IV.I.J.1.2. DFA allocation results over the ORGDB testing group.

Specimen	OTU	1st Prob	1st Class	2nd Prob	2nd Class
C3-287	Ampelosaurus	47.45	Camarasaurus	18.4	Dicraeosaurus
MHN.Aix.PV.2008.1.7	Ampelosaurus	52.01	Saltasaurus	20.67	Antarctosaurus
MACN-6804-49	Antarctosaurus	50.33	Diplodocus	6.41	Europasaurus
CM-7163	Apatosaurus	36.42	Camarasaurus	15.9	Saltasaurus
BS-157	Apatosaurus	51.65	Camarasaurus	21.64	LoHueco1
CM-10039	Apatosaurus	53.07	Camarasaurus	25.44	Magyarosaurus
BYU601-17103	Apatosaurus	33.2	Camarasaurus	18.36	Saltasaurus
YPM-5862	Apatosaurus	30.65	Camarasaurus	12.28	Antarctosaurus
OMNH-01991	Apatosaurus	35.2	Camarasaurus	17.79	Dicraeosaurus
YPM-1908_1	Camarasaurus	19.59	Diplodocus	14.1	Phuwiangosaurus
YPM-1901	Camarasaurus	20.1	Camarasaurus	19.28	Saltasaurus
GMNH-PV-101	Camarasaurus	23.25	Titanosauria_indet	16.09	Saltasaurus
CM-11338_2	Camarasaurus	22.23	Apatosaurus	20.14	LoHueco1
WDC-B-BS-13	Camarasaurus	50.16	Camarasaurus	23.48	LoHueco1
DNM-2941	Camarasaurus	31.81	Camarasaurus	21.61	Phuwiangosaurus
CM-36663	Camarasaurus	36.81	Camarasaurus	27.95	Lirainosaurus
AMNH-945	Camarasaurus	29.22	Camarasaurus	14.16	Antarctosaurus
OMNH-1794	Camarasaurus	44.6	Camarasaurus	13.34	Antarctosaurus
AMHN-5764	Camarasaurus	38.21	Camarasaurus	20.09	LoHueco1
DNM-3735	Camarasaurus	14.94	Titanosauria_indet	13.74	Antarctosaurus
MHN.Aix.PV.2001.124	cf_Lirainosaurus	46.81	Diplodocus	13.26	Haplocanthosaurus
MB.R.4886.92	Dicraeosaurus	24.39	Diplodocus	18.75	Saltasaurus
MB.R.2697	Dicraeosaurus	25.43	Camarasaurus	19.51	Magyarosaurus
USNM-10865	Diplodocus	28.31	Diplodocus	16.04	Neuquensaurus
CM-21788	Diplodocus	44.97	Diplodocus	9.95	Haplocanthosaurus
BYU725-4889	Diplodocus	54.21	Diplodocus	7.19	Europasaurus
SDSM-25340	Diplodocus	35.1	Diplodocus	12.28	Saltasaurus
BYU725-13670	Diplodocus	54.18	Camarasaurus	35.36	Lirainosaurus
BYU725-16569	Diplodocus	24.3	Diplodocus	12.28	Haplocanthosaurus
BYU725-13643	Diplodocus	38.88	Diplodocus	10.52	Saltasaurus
BYU725-fe5dm-72	Diplodocus	27.43	Diplodocus	17.46	Saltasaurus
MOR592-35	Diplodocus	35.84	Diplodocus	10.68	Neuquensaurus
UMNH-VP-82	Diplodocus	57.05	Diplodocus	11.77	Neuquensaurus
MFN-II-27e	Giraffatitan	31.75	Camarasaurus	24.13	LoHueco1
MFN-Ng21	Giraffatitan	30.85	Camarasaurus	23.56	cf_Lirainosaurus
MCNA-14465	Lirainosaurus	26.14	Diplodocus	15.82	Saltasaurus
MGUV-17235	Lirainosaurus	31.16	Camarasaurus	21.57	Magyarosaurus
HUE-2636	LoHueco1	48.22	Diplodocus	6.59	Saltasaurus
HUE-1590	LoHueco1	41.94	Diplodocus	6.85	Europasaurus
HUE-2420	LoHueco2	50.96	Diplodocus	17.82	Europasaurus
HUE-594	LoHueco2	44.43	Camarasaurus	20.46	LoHueco1
NHM-R3856	Magyarosaurus	62.08	Diplodocus	7.17	Haplocanthosaurus
NHM-R3859_2	Magyarosaurus	26.05	Camarasaurus	21.8	LoHueco1
MLP-CS-1480	Neuquensaurus	42.48	Camarasaurus	16.84	Saltasaurus
MLP-CS-1122	Neuquensaurus	21.17	Magyarosaurus	18.16	Saltasaurus
MCS-5/28	Neuquensaurus	25.02	Diplodocus	16.21	Haplocanthosaurus
PC.DMR-K11-1_2	Phuwiangosaurus	28.21	Diplodocus	8.75	Saltasaurus
MCD-5031	Titanosauria_indet	48.06	Camarasaurus	22.14	cf_Lirainosaurus
HUE-1440	Titanosauria_indet	27.21	Magyarosaurus	25.88	Antarctosaurus
HUE-902	Titanosauria_indet	33.33	LoHueco2	21.83	Antarctosaurus
HUE-1508	Titanosauria_indet	23.59	Apatosaurus	20.01	Magyarosaurus
HUE-3237	Titanosauria_indet	25.42	Magyarosaurus	24.7	Dicraeosaurus
HUE-1183	Titanosauria_indet	31.1	Diplodocus	16.95	Neuquensaurus
HUE-1187	Titanosauria_indet	34.78	Camarasaurus	20.25	Dicraeosaurus
HUE-930	Titanosauria_indet	26.43	LoHueco2	15.19	Antarctosaurus

Suppl.IV.I.J.1.3. DFA allocation results over the RDB testing group.

SUPPL.IV.I.K. SUPPORT VECTOR MACHINE RESULTS

SUPPL.IV.I.K.1. PREDICTED ALLOCATION REPORT

Specimen	OTU	1st Prob	1st Class	2nd Prob	2nd Class
C3-287	Ampelosaurus	12.38	Neuquensaurus	8.62	Europasaurus
MHN.Aix.PV.2008	Ampelosaurus	12.41	Ampelosaurus	8.86	Bonatitan
MACN-6804-49	Antarctosaurus	10.15	Ampelosaurus	9.21	Saltasaurus
CM-7163	Apatosaurus	29.35	Camarasaurus	22.85	Europasaurus
BS-157	Apatosaurus	29.67	Camarasaurus	20.39	Saltasaurus
CM-10039	Apatosaurus	28.76	Camarasaurus	21.2	LoHueco2
BYU601-17103	Apatosaurus	29.53	Camarasaurus	23.69	LoHueco2
YPM-5862	Apatosaurus	31.2	Camarasaurus	24.55	LoHueco2
OMNH-01991	Apatosaurus	30.08	Camarasaurus	20.23	Saltasaurus
YPM-1908_1	Camarasaurus	11.19	Camarasaurus	9.31	Bonatitan
YPM-1901	Camarasaurus	9.52	Lirainosaurus	8.95	Europasaurus
GMNH-PV-101	Camarasaurus	29.74	Camarasaurus	27.48	Saltasaurus
CM-11338_2	Camarasaurus	25.22	Camarasaurus	10.93	Europasaurus
WDC-B-BS-13	Camarasaurus	33.24	Camarasaurus	23.23	LoHueco2
DNM-2941	Camarasaurus	30.44	Camarasaurus	20.92	LoHueco2
CM-36663	Camarasaurus	31.21	Camarasaurus	18.72	Europasaurus
AMNH-945	Camarasaurus	31.92	Camarasaurus	24.08	Saltasaurus
OMNH-1794	Camarasaurus	34.76	Diplodocus	21.4	Europasaurus
AMHN-5764	Camarasaurus	13.91	Neuquensaurus	8.6	LoHueco1
DNM-3735	Camarasaurus	30.01	Camarasaurus	22.25	LoHueco1
MHN.Aix.PV.200	cf_Lirainosaurus	10.09	Apatosaurus	9.51	Saltasaurus
MB.R.4886.92	Dicraeosaurus	32.27	Diplodocus	25.15	Saltasaurus
MB.R.2697	Dicraeosaurus	10.2	Neuquensaurus	8.94	Antarctosaurus
USNM-10865	Diplodocus	34.42	Diplodocus	26.3	Saltasaurus
CM-21788	Diplodocus	33.58	Diplodocus	19.73	Saltasaurus
BYU725-4889	Diplodocus	40.56	Diplodocus	18.51	Saltasaurus
SDSM-25340	Diplodocus	27.87	Camarasaurus	27.33	Saltasaurus
BYU725-13670	Diplodocus	32.21	Diplodocus	20.42	Bonatitan
BYU725-16569	Diplodocus	37.65	Diplodocus	22	LoHueco2
BYU725-13643	Diplodocus	29.03	Diplodocus	26.95	Saltasaurus
BYU725-fe5dm-7	Diplodocus	25.25	Camarasaurus	18.53	Saltasaurus
MOR592-35	Diplodocus	34.23	Diplodocus	19.86	Saltasaurus
UMNH-VP-82	Diplodocus	35.45	Diplodocus	19.18	Europasaurus
MFN-II-27e	Giraffatitan	37.3	Camarasaurus	20.8	Saltasaurus
MFN-Ng21	Giraffatitan	14.04	Camarasaurus	11.56	LoHueco1
MCNA-14465	Lirainosaurus	10.85	Camarasaurus	8.21	Diplodocus
MGUV-17235	Lirainosaurus	15.95	Neuquensaurus	9.67	Antarctosaurus
HUE-2636	LoHueco1	10.83	Neuquensaurus	8.9	Antarctosaurus
HUE-1590	LoHueco2	13.75	Ampelosaurus	11.82	Bonatitan
HUE-2420	LoHueco1	11.06	Neuquensaurus	9.61	Antarctosaurus
HUE-594	LoHueco2	14.02	Ampelosaurus	10.77	Bonatitan
NHM-R3856	Magyarosaurus	12.19	Ampelosaurus	10.49	Bonatitan
NHM-R3859_2	Magyarosaurus	13.24	Magyarosaurus	11.81	Antarctosaurus
MLP-CS-1480	Neuquensaurus	13.4	Neuquensaurus	9.17	Antarctosaurus
MLP-CS-1122	Neuquensaurus	15.46	Neuquensaurus	8.06	Antarctosaurus
MCS-5/28	Neuquensaurus	18.19	Neuquensaurus	11.99	Europasaurus
PC.DMR-K11-1_2	Phuwiangosaurus	11.97	Ampelosaurus	10.38	Europasaurus
MCD-5031	Titanosauria_indet	28.82	Camarasaurus	23.42	Saltasaurus
HUE-1440	Titanosauria_indet	12.61	Ampelosaurus	9.33	Bonatitan
HUE-902	Titanosauria_indet	14.14	Ampelosaurus	12.17	Bonatitan
HUE-1508	Titanosauria_indet	10.37	Magyarosaurus	9.54	Apatosaurus
HUE-3237	Titanosauria_indet	11.35	Neuquensaurus	10.41	Antarctosaurus
HUE-1183	Titanosauria_indet	12.68	LoHueco1	8.96	Antarctosaurus
HUE-1187	Titanosauria_indet	9	Neuquensaurus	8.79	Apatosaurus
HUE-930	Titanosauria_indet	11.21	LoHueco1	10.91	Antarctosaurus

Suppl.IV.I.K.1.1. SVM allocation results over the EXPDB testing group.

Specimen	OTU	1st Prob	1st Class	2nd Prob	2nd Class
C3-287	Ampelosaurus	17.8	Camarasaurus	8.61	Bonatitan
MHN.Aix.PV.200	Ampelosaurus	27.94	Camarasaurus	10.41	LoHueco1
MACN-6804-49	Antarctosaurus	21.68	Diplodocus	15.73	Bonatitan
CM-7163	Apatosaurus	25.52	Camarasaurus	13.86	Bonatitan
BS-157	Apatosaurus	24.55	Diplodocus	16.81	Bonatitan
CM-10039	Apatosaurus	27.44	Camarasaurus	15.34	Bonatitan
BYU601-17103	Apatosaurus	17.42	Camarasaurus	17.01	LoHueco1
YPM-5862	Apatosaurus	23.35	Diplodocus	12.8	cf_Lirainosaurus
OMNH-01991	Apatosaurus	41.14	Diplodocus	8.69	Ampelosaurus
YPM-1908_1	Camarasaurus	16.98	Camarasaurus	14.29	Neuquensaurus
YPM-1901	Camarasaurus	18.98	Camarasaurus	15.77	Bonatitan
GMNH-PV-101	Camarasaurus	16.83	Diplodocus	15.39	cf_Lirainosaurus
CM-11338_2	Camarasaurus	20.45	Diplodocus	14.06	Lirainosaurus
WDC-B-BS-13	Camarasaurus	24.63	Diplodocus	14.69	Saltasaurus
DNM-2941	Camarasaurus	20.08	Diplodocus	9.46	Haplocanthosaurus
CM-36663	Camarasaurus	35.55	Diplodocus	11.7	Bonatitan
AMNH-945	Camarasaurus	31.82	Camarasaurus	13.98	Magyarosaurus
OMNH-1794	Camarasaurus	28.32	Camarasaurus	13.68	LoHueco1
AMHN-5764	Camarasaurus	34.85	Camarasaurus	14.79	Bonatitan
DNM-3735	Camarasaurus	23.52	Camarasaurus	13.55	Lirainosaurus
MHN.Aix.PV.200	cf_Lirainosaurus	19.66	Diplodocus	8.61	Europasaurus
MB.R.4886.92	Dicraeosaurus	18.7	Diplodocus	16.58	cf_Lirainosaurus
MB.R.2697	Dicraeosaurus	28.72	Diplodocus	15.71	Bonatitan
USNM-10865	Diplodocus	39.74	Diplodocus	9.55	Bonatitan
CM-21788	Diplodocus	29.1	Diplodocus	15.79	Bonatitan
BYU725-4889	Diplodocus	31.4	Diplodocus	8.3	cf_Lirainosaurus
SDSM-25340	Diplodocus	11.51	Camarasaurus	11.39	Haplocanthosaurus
BYU725-13670	Diplodocus	21.15	Diplodocus	14.53	Bonatitan
BYU725-16569	Diplodocus	37.13	Diplodocus	19.45	Lirainosaurus
BYU725-13643	Diplodocus	37.69	Diplodocus	8.77	Bonatitan
BYU725-fe5dm-7	Diplodocus	23.01	Diplodocus	18.57	Bonatitan
MOR592-35	Diplodocus	40.79	Camarasaurus	12.69	Europasaurus
UMNH-VP-82	Diplodocus	20.76	Diplodocus	11.21	cf_Lirainosaurus
MFN-II-27e	Giraffatitan	33.68	Camarasaurus	12.38	Magyarosaurus
MFN-Ng21	Giraffatitan	21.91	Diplodocus	8.51	Ampelosaurus
MCNA-14465	Lirainosaurus	17.08	Camarasaurus	15.3	Bonatitan
MGUV-17235	Lirainosaurus	16.3	Diplodocus	9.88	Saltasaurus
HUE-2636	LoHueco1	25.37	Diplodocus	10.15	Lirainosaurus
HUE-1590	LoHueco1	14.53	Lirainosaurus	9.26	Haplocanthosaurus
HUE-2420	LoHueco2	10.11	LoHueco1	9.66	Haplocanthosaurus
HUE-594	LoHueco2	26.07	Camarasaurus	9.08	cf_Lirainosaurus
NHM-R3856	Magyarosaurus	26.59	Camarasaurus	8.6	cf_Lirainosaurus
NHM-R3859_2	Magyarosaurus	9.69	Magyarosaurus	9.39	Giraffatitan
MLP-CS-1480	Neuquensaurus	25.11	Diplodocus	13.43	Bonatitan
MLP-CS-1122	Neuquensaurus	27.79	Camarasaurus	17.03	Bonatitan
MCS-5/28	Neuquensaurus	18.47	Diplodocus	10.73	LoHueco1
PC.DMR-K11-1_2	Phuwiangosaurus	32.95	Camarasaurus	10.01	Diplodocus
MCD-5031	Titanosauria_indet	25.54	Camarasaurus	18.94	Bonatitan
HUE-1440	Titanosauria_indet	18.94	Diplodocus	14	Bonatitan
HUE-902	Titanosauria_indet	13.93	Camarasaurus	9.84	Bonatitan
HUE-1508	Titanosauria_indet	13.15	Camarasaurus	12.91	Giraffatitan
HUE-3237	Titanosauria_indet	12.97	Diplodocus	11.06	cf_Lirainosaurus
HUE-1183	Titanosauria_indet	10.66	LoHueco1	10.58	Saltasaurus
HUE-1187	Titanosauria_indet	19.78	Camarasaurus	9.25	cf_Lirainosaurus
HUE-930	Titanosauria_indet	15.93	Camarasaurus	11.05	Haplocanthosaurus

Suppl.IV.I.K.1.2. SVM allocation results over the ORGDB testing group.

Specimen	OTU	1st Prob	1st Class	2nd Prob	2nd Class
C3-287	Ampelosaurus	36.71	Camarasaurus	12.93	Antarctosaurus
MHN.Aix.PV.2008	Ampelosaurus	36.9	Camarasaurus	15.61	LoHueco2
MACN-6804-49	Antarctosaurus	30.14	Diplodocus	7.5	Haplocanthosaurus
CM-7163	Apatosaurus	29.59	Camarasaurus	12.57	LoHueco2
BS-157	Apatosaurus	34.34	Camarasaurus	16.73	LoHueco1
CM-10039	Apatosaurus	35.27	Camarasaurus	17.97	LoHueco1
BYU601-17103	Apatosaurus	24.74	Camarasaurus	14.35	cf_Lirainosaurus
YPM-5862	Apatosaurus	25.29	Camarasaurus	14.94	Europasaurus
OMNH-01991	Apatosaurus	30.85	Camarasaurus	12.34	LoHueco2
YPM-1908_1	Camarasaurus	18.09	Diplodocus	9.16	Europasaurus
YPM-1901	Camarasaurus	28.82	Camarasaurus	22.73	Magyarosaurus
GMNH-PV-101	Camarasaurus	12.15	Diplodocus	10.71	Saltasaurus
CM-11338_2	Camarasaurus	24.05	Camarasaurus	16.2	cf_Lirainosaurus
WDC-B-BS-13	Camarasaurus	34.27	Camarasaurus	18.47	LoHueco1
DNM-2941	Camarasaurus	29.16	Camarasaurus	16.26	cf_Lirainosaurus
CM-36663	Camarasaurus	32.47	Camarasaurus	16.23	LoHueco1
AMNH-945	Camarasaurus	23.77	Camarasaurus	12.47	Saltasaurus
OMNH-1794	Camarasaurus	30.16	Camarasaurus	14.22	cf_Lirainosaurus
AMHN-5764	Camarasaurus	28.79	Camarasaurus	14.5	LoHueco2
DNM-3735	Camarasaurus	13	Diplodocus	8.75	Europasaurus
MHN.Aix.PV.200	cf_Lirainosaurus	35.34	Diplodocus	6.16	Phuwiangosaurus
MB.R.4886.92	Dicraeosaurus	20.44	Camarasaurus	19.78	cf_Lirainosaurus
MB.R.2697	Dicraeosaurus	20.67	Camarasaurus	14.84	cf_Lirainosaurus
USNM-10865	Diplodocus	22.74	Diplodocus	12.79	Haplocanthosaurus
CM-21788	Diplodocus	33.05	Diplodocus	6.78	Saltasaurus
BYU725-4889	Diplodocus	34.41	Diplodocus	6.22	Camarasaurus
SDSM-25340	Diplodocus	22.71	Diplodocus	10.72	cf_Lirainosaurus
BYU725-13670	Diplodocus	37.1	Camarasaurus	12.11	Europasaurus
BYU725-16569	Diplodocus	16.48	Diplodocus	11.67	Saltasaurus
BYU725-13643	Diplodocus	25.12	Diplodocus	10.04	Haplocanthosaurus
BYU725-fe5dm-7	Diplodocus	31.28	Diplodocus	7.87	Neuquensaurus
MOR592-35	Diplodocus	25.99	Diplodocus	10.9	Haplocanthosaurus
UMNH-VP-82	Diplodocus	42.08	Diplodocus	6.13	Neuquensaurus
MFN-II-27e	Giraffatitan	27.2	Camarasaurus	15.75	cf_Lirainosaurus
MFN-Ng21	Giraffatitan	28.09	Camarasaurus	15.1	cf_Lirainosaurus
MCNA-14465	Lirainosaurus	19.94	Diplodocus	8.22	Ampelosaurus
MGUV-17235	Lirainosaurus	26.17	Camarasaurus	15.03	cf_Lirainosaurus
HUE-2636	LoHueco1	31.83	Diplodocus	6.94	Neuquensaurus
HUE-1590	LoHueco1	26.42	Diplodocus	8.2	cf_Lirainosaurus
HUE-2420	LoHueco2	41.07	Diplodocus	5.61	Saltasaurus
HUE-594	LoHueco2	30.91	Camarasaurus	16.04	LoHueco2
NHM-R3856	Magyarosaurus	40.75	Diplodocus	6.28	Camarasaurus
NHM-R3859_2	Magyarosaurus	24.18	Camarasaurus	14.13	LoHueco2
MLP-CS-1480	Neuquensaurus	32.75	Camarasaurus	11.28	LoHueco2
MLP-CS-1122	Neuquensaurus	12.98	Diplodocus	10.01	Ampelosaurus
MCS-5/28	Neuquensaurus	17.8	Diplodocus	12.68	Saltasaurus
PC.DMR-K11-1_2	Phuwiangosaurus	18.54	Diplodocus	9.87	cf_Lirainosaurus
MCD-5031	Titanosauria_indet	33.6	Camarasaurus	16.06	LoHueco1
HUE-1440	Titanosauria_indet	20.77	Diplodocus	6.77	Ampelosaurus
HUE-902	Titanosauria_indet	16.39	Diplodocus	12.7	Camarasaurus
HUE-1508	Titanosauria_indet	21.32	Camarasaurus	15.47	Haplocanthosaurus
HUE-3237	Titanosauria_indet	10.67	Apatosaurus	10.47	Ampelosaurus
HUE-1183	Titanosauria_indet	29.87	Diplodocus	7.49	Saltasaurus
HUE-1187	Titanosauria_indet	29.11	Camarasaurus	15.79	cf_Lirainosaurus
HUE-930	Titanosauria_indet	13.21	Diplodocus	10.92	Antarctosaurus

Suppl.IV.I.K.1.3. SVM allocation results over the RDB testing group.

SUPPL.IV.I.L. MULTIPLE IMPUTATIONS REPORT

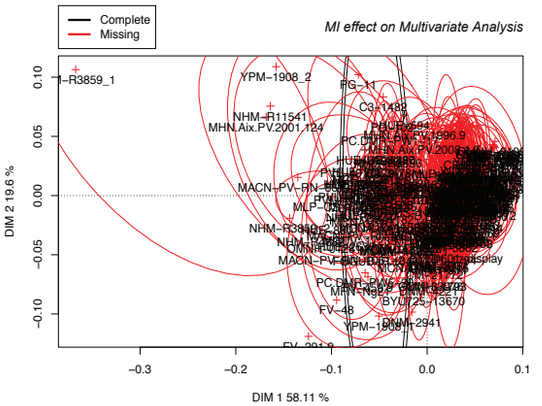

Suppl.IV.I.L.1. Multiple Imputatiuons effect over the complete dataset PCA results.

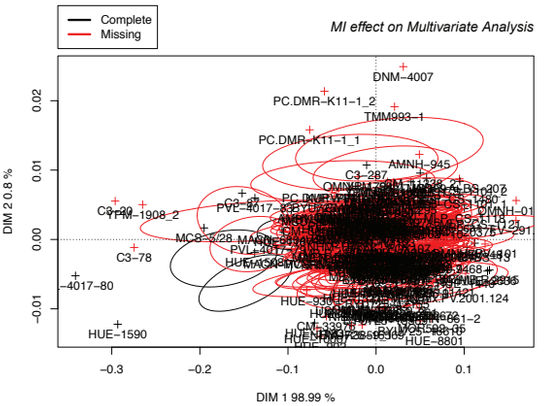

Suppl.IV.I.L.2. Multiple Imputatiuons effect over the RDB PCA results.

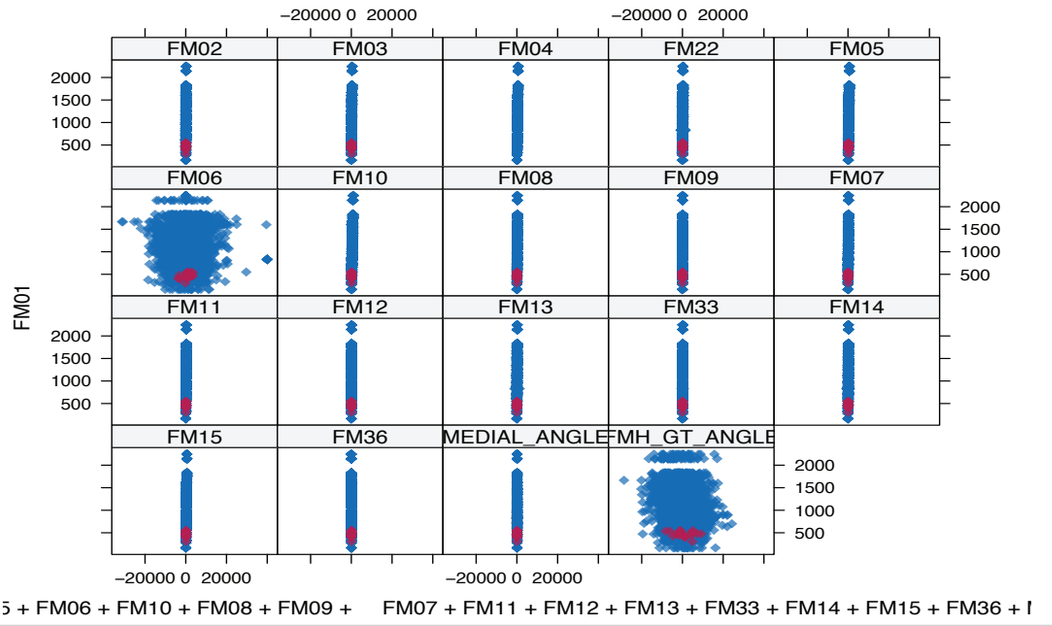

Suppl.IV.I.K.1.3. Distribution of the variables of the sample (blue) and the estimated data (red).

SUPP. MATERIAL IV.II:

3D Geometric morphometrics of the hindlimb in the titanosaur sauropods from Lo Hueco (Cuenca, Spain)

Supp.IV.II.A 3D meshes reconstruction precision report - electronic material

Supp.IV.II.B Complete PCAs of the reduced dataset

Suppl.IV.II.C K-means results of the reduced dataset

Suppl.IV.II.D Measurements and Proportions comparisons - electronic material

Suppl.IV.II.E Meaningful PCs for description - electronic material

Suppl.IV.II.F Landmark estimation precision - electronic material

Suppl.IV.II.G. Code - electronic material

SUPP.IV.II.B COMPLETE PCAS OF THE REDUCED DATASET

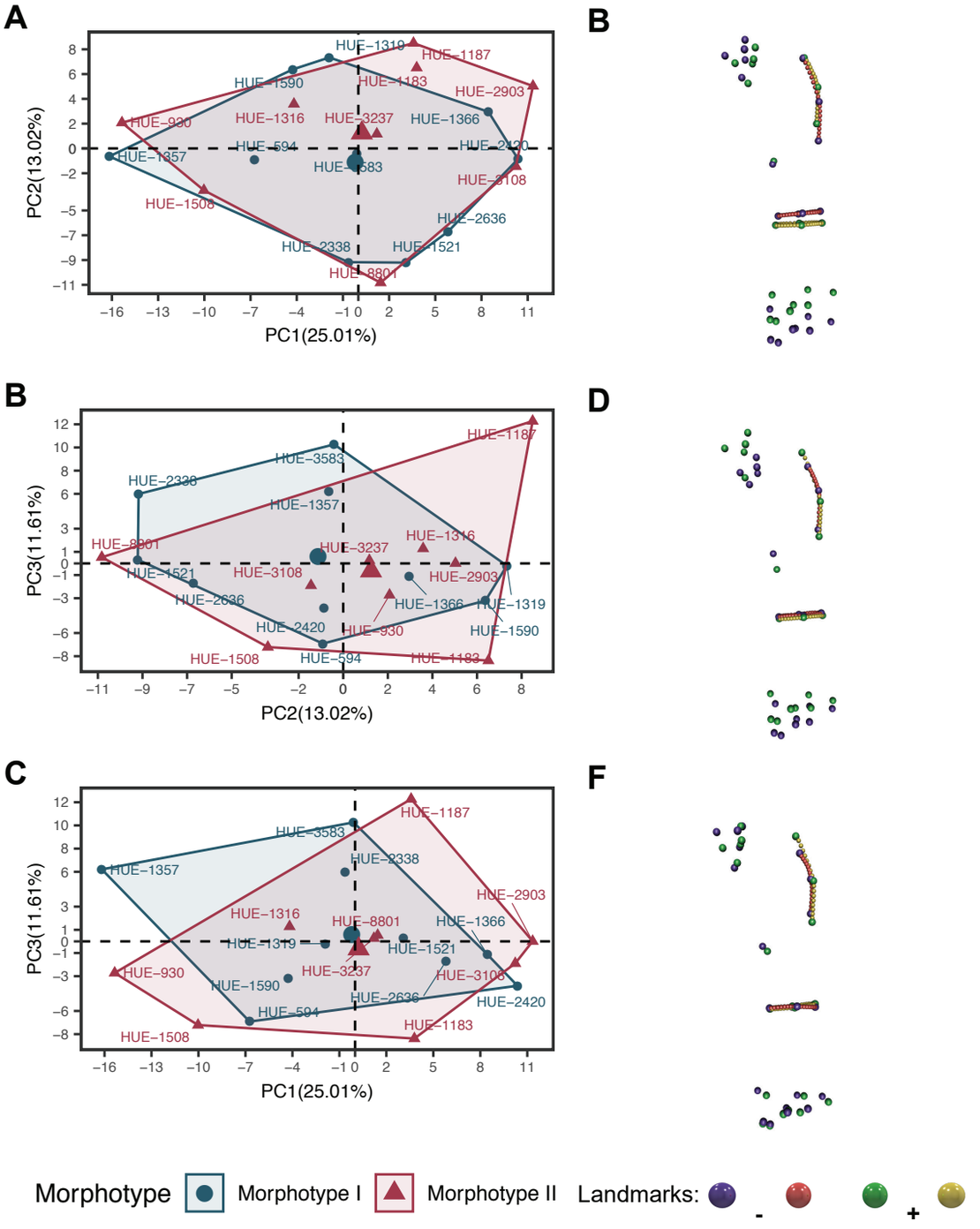

Suppl.IV.II.B.1. Femur shape PCA results over tps dataset with highlighted taphomorphospaces. (A) PC1-PC2. (B) PC2-PC3. (C) PC1-PC3. (D) Landmark configuration at the extremes of PC1 axis. (C) at the extremes of PC2 axis. (F) at the extremes of PC3 axis.

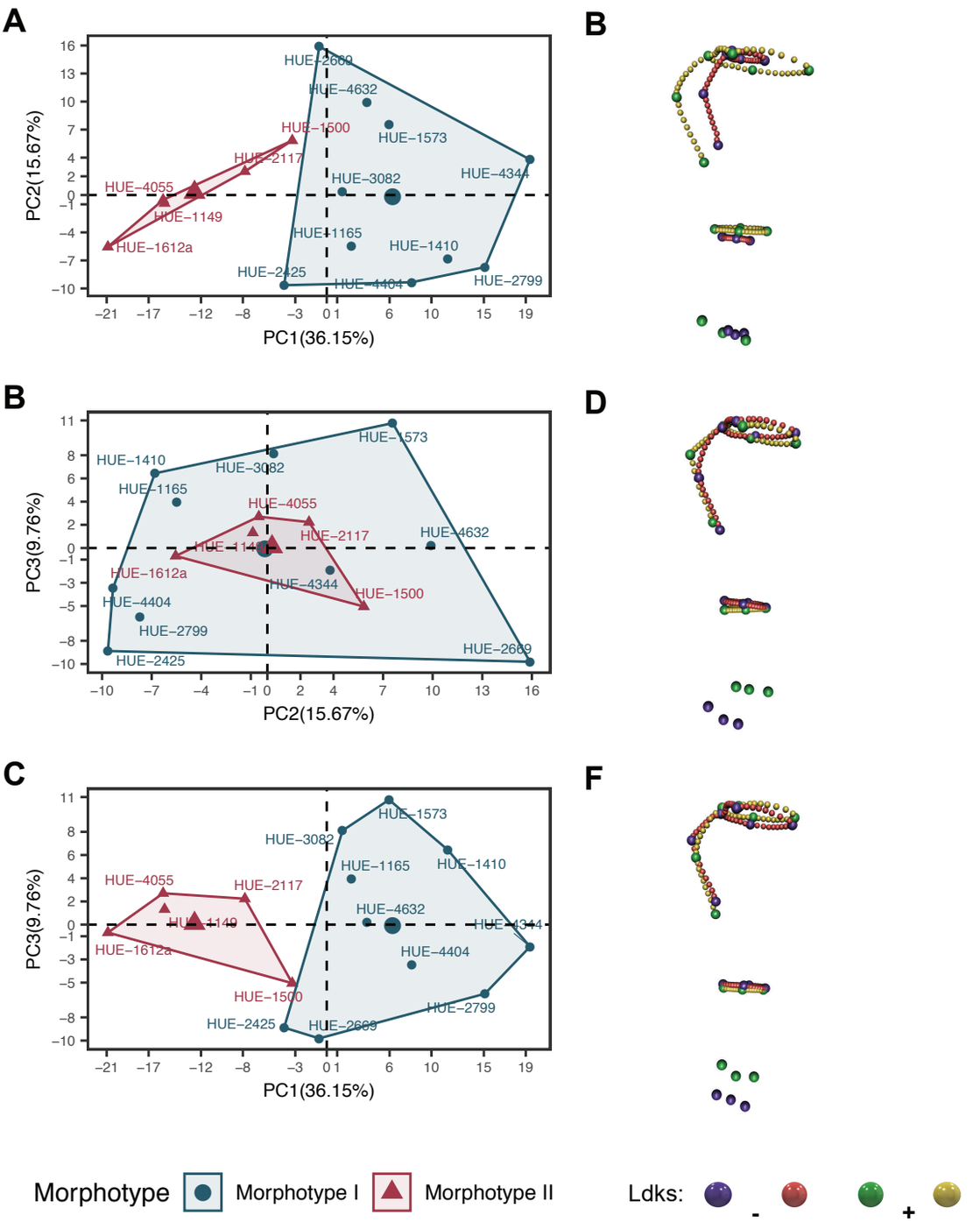

Suppl.IV.II.B.2. Tibia shape PCA results over tps dataset with highlighted taphomorphospaces. (A) PC1-PC2. (B) PC2-PC3. (C) PC1-PC3. (D) Landmark configuration at the extremes of PC1 axis. (C) at the extremes of PC2 axis. (F) at the extremes of PC3 axis.

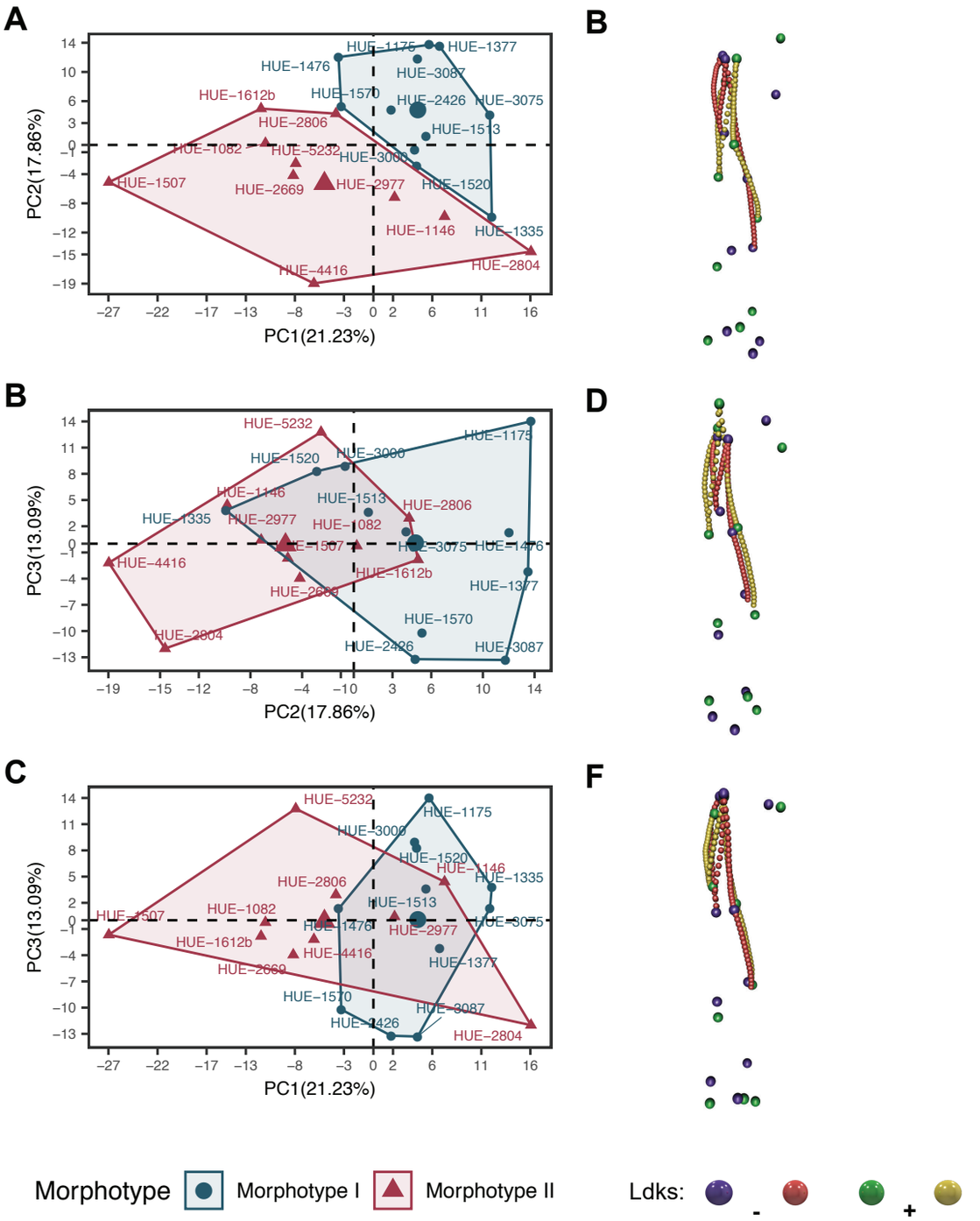

Suppl.IV.II.B.3. Fibula shape PCA results over tps dataset with highlighted taphomorphospaces. (A) PC1-PC2. (B) PC2-PC3. (C) PC1-PC3. (D) Landmark configuration at the extremes of PC1 axis. (C) at the extremes of PC2 axis. (F) at the extremes of PC3 axis.

SUPPL.IV.II.C K-MEANS RESULTS OF THE REDUCED DATASET

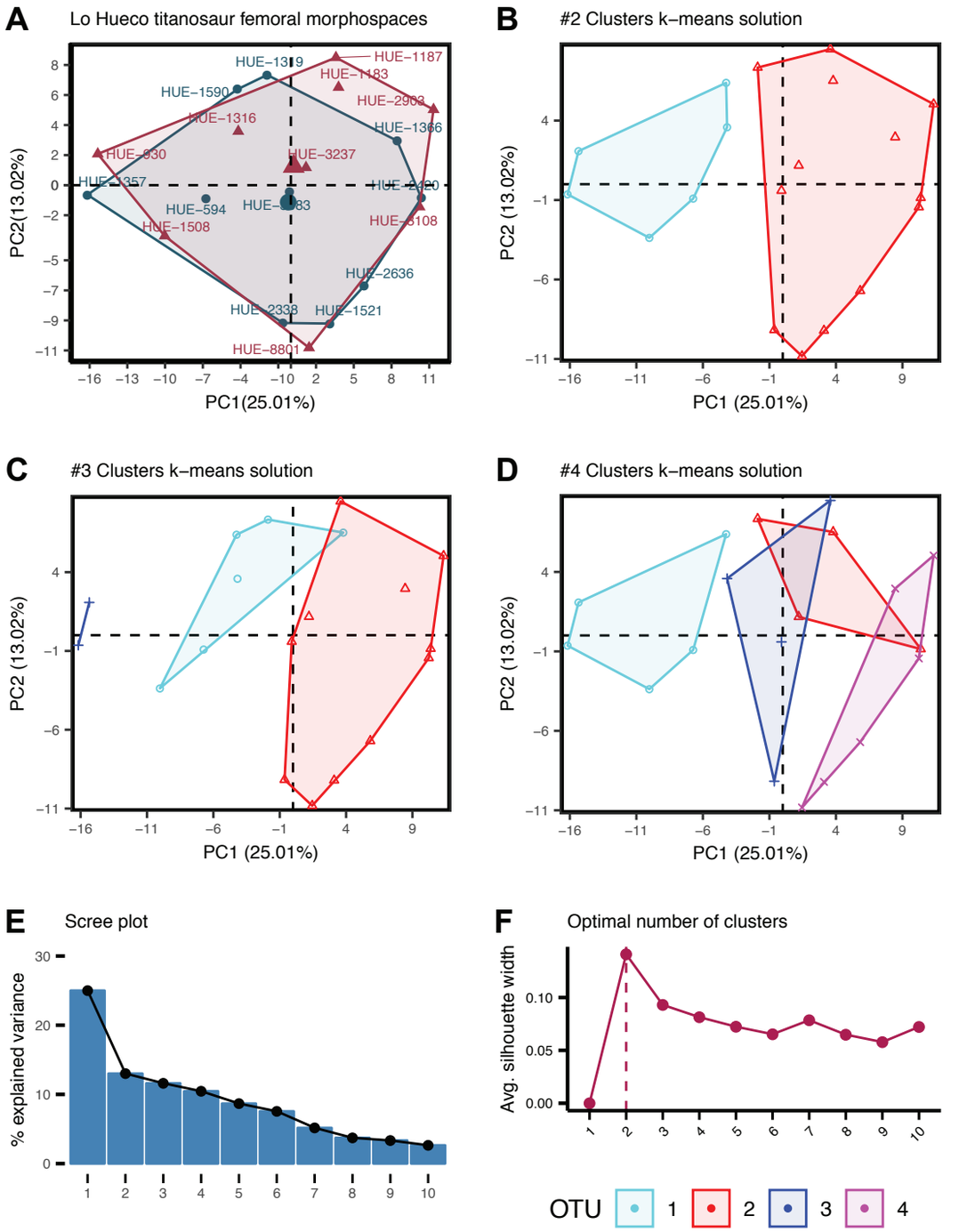

Suppl.IV.II.C.1. Femora group assessment via k-means algorithm. (A) Shape PCA PC1-PC2 with a priori morphotypes. (B) Classification for k= 2 groups. (C) k= 3 groups. (D) k = 4 groups (E) Variance explained by each PC. (F) Average silhouette width after partition of the morphospace into k groups.

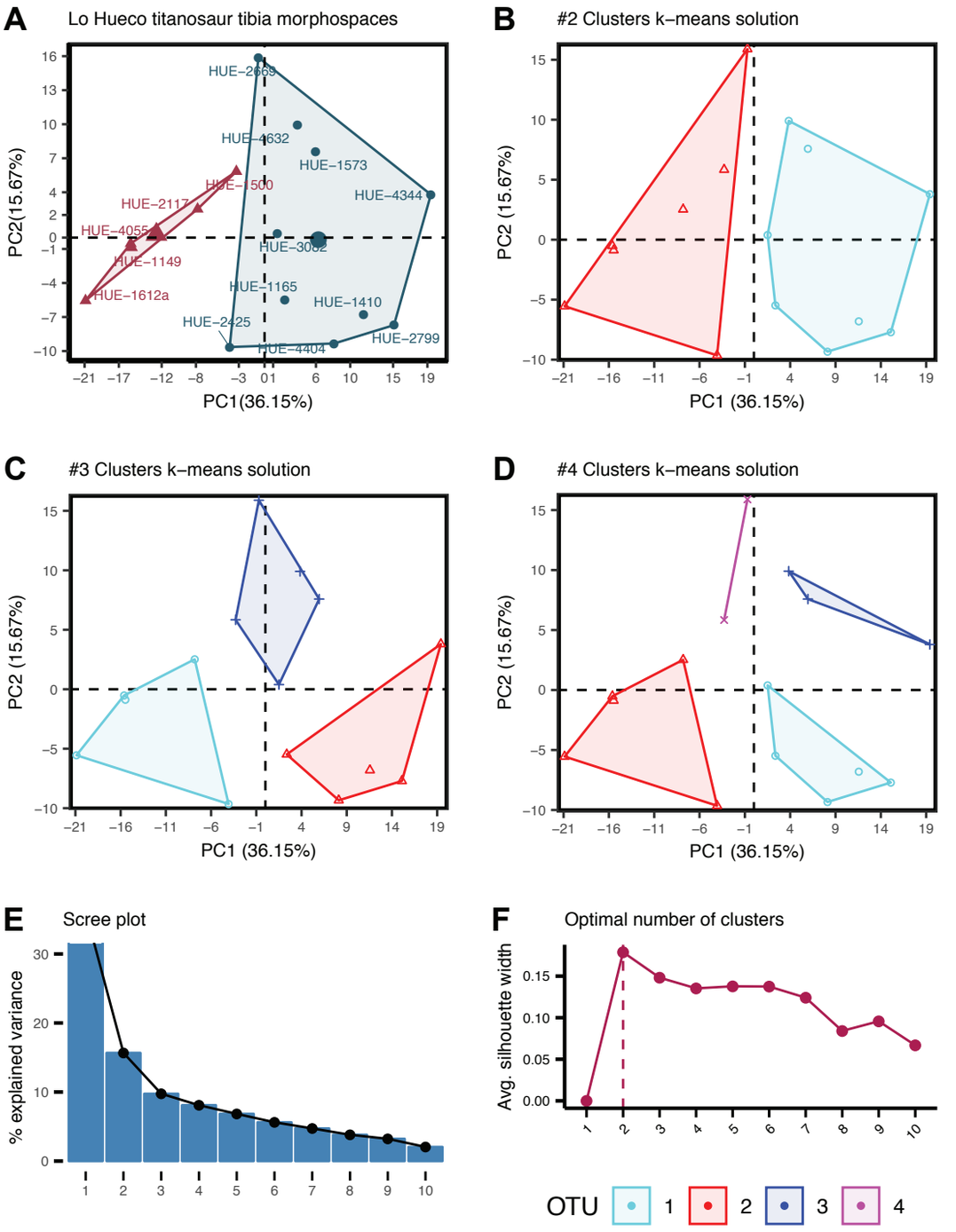

Suppl.IV.II.C.2.Tibiae group assessment via k-means algorithm. (A) Shape PCA PC1-PC2 with a priori morphotypes. (B) Classification for k= 2 groups. (C) k= 3 groups. (D) k = 4 groups (E) Variance explained by each PC. (F) Average silhouette width after partition of the morphospace into k groups.

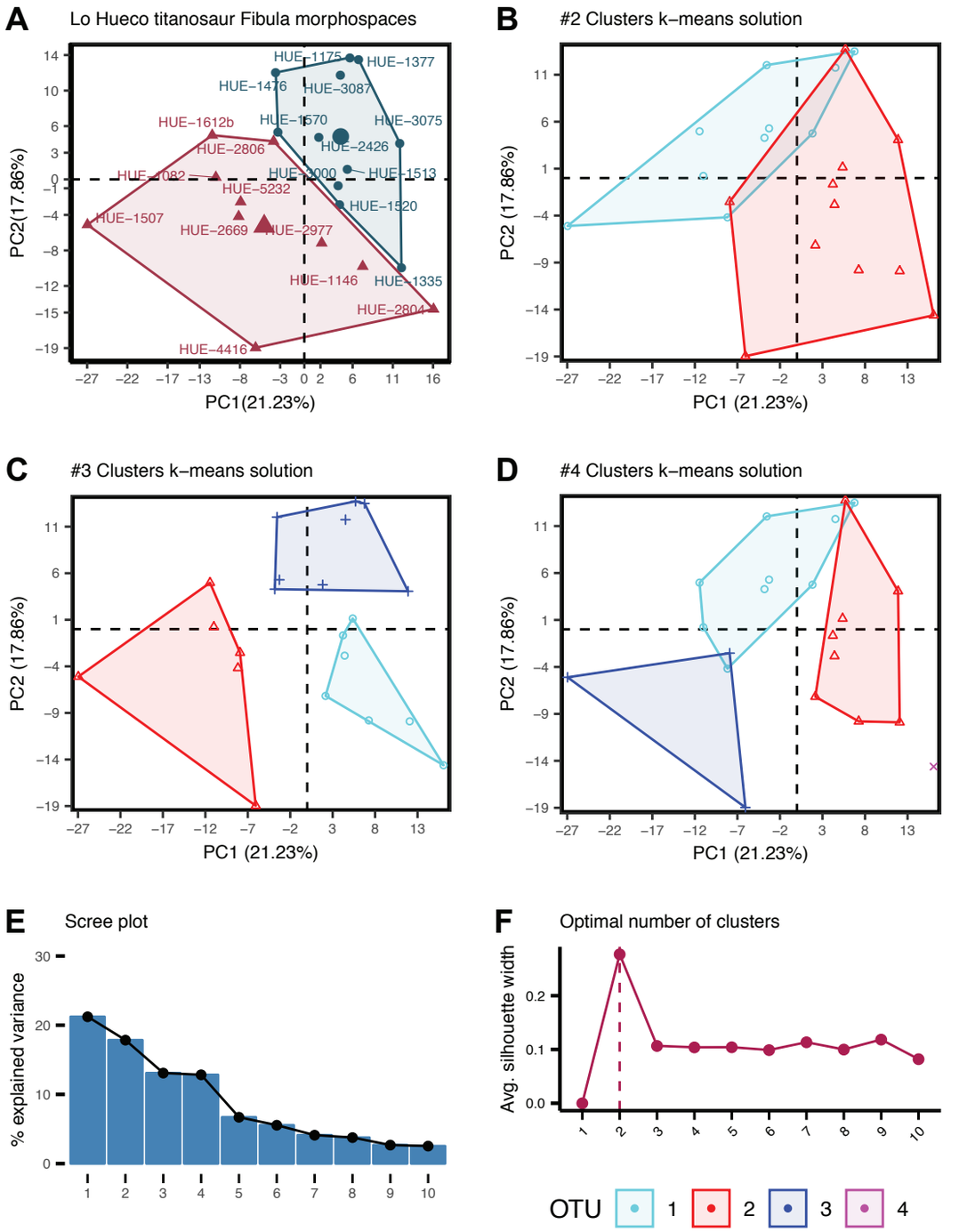

Suppl.IV.II.C.3. Fibulae group assessment via k-means algorithm. (A) Shape PCA PC1-PC2 with a priori morphotypes. (B) Classification for k= 2 groups. (C) k= 3 groups. (D) k = 4 groups (E) Variance explained by each PC. (F) Average silhouette width after partition of the morphospace into k groups.

SUPP. MATERIAL V.

Geometric Morphometric Analysis of the Intraspecifc Variability in the Appendicular Skeleton of the Titanosaur Sauropods from Lo Hueco (Cuenca, Spain): Functional Implications

SUPPL.V.A. LANDMARK DEFINITIONS

	ID	N	Definition	Missing %
Ladnmarks	s1		Humeral medial edge of proximal end	39.29%
	s2		Anteromedial edge of humeral head	46.43%
	s3		Anterolateral edge of humeral head	42.86%
	s4		Humeral lateral edge of proximal end	28.57%
	s5		Deltopectoral crest Mm. Supracoracoideus attachment	7.14%
	s6		Distal end of the deltopectoral crest	3.57%
	s7		Posterior edge of the humeral head	39.29%
	s8		Minimum midshaft width medial	0.00%
	s9		Minimum midshaft width anterior	0.00%
	s10		Minimum midshaft width lateral	3.57%
	s11		Minimum midshaft width posterior	3.57%
	s12		Anterior ectepicondyle - Medial edge of the distal end	17.86%
	s13		Middle anterodistal process / radial component	25.00%
	s14		Lateral anterodistal process / lateral component	21.43%
	s15		Lateral edge of the distal end	39.29%
	s16		Lateral edge of the anconeal fossa	32.14%
	s17		Middle anconeal fossa	10.71%
	s18		Medial edge of the anconeal fossa	10.71%
Curves	c1	30	Proximal end outline	60.71%
	c2	20	Humeral head - posterior outline	64.29%
	c3	20	Deltopectoral crest	42.86%
	c4	40	Midshaft outline	3.57%
	c5	70	Distal end outline	50.00%

Suppl.V.A.1. Humerus landmark definitions.

	ID	N	Definition	Missing %
Landmarks	s1		Anteromedial process	10.00%
	s2		Proximal of the radial articulation fossa	20.00%
	s3		Anterolateral process	50.00%
	s4		Lateral proximal end concavity	40.00%
	s5		Proximal of the posterior arm	60.00%
	s6		Posteromedial proximal end concavity	40.00%
	s7		Olecranon process	50.00%
	s8		Minimum midshaft width anteromedial	0.00%
	s9		Minimum midshaft width anterolateral	0.00%
	s10		Minimum midshaft width posterior	0.00%
	s11		Posterior edge of the distal end	20.00%
	s12		Anteromedial edge of the distal end	20.00%
	s13		Anterior distal process	40.00%
Curves	c1	60	Tibial proximal end outline	50.00%
	c2	30	Cnemial crest	0.00%
	c3	30	Midshaft outline	43.33%

Suppl.V.A.2. Ulna landmark definitions.

	ID	N	Definition	Missing %
Landmarks	s1		Proximal anteromedial process	0.00%
	s2		Proximal posterolateral edge	0.00%
	s3		Proximal interosseous ridge	0.00%
	s4		Ridge muscle insertion of M. biceps and M. brach. inferior	0.00%
	s5		Distal anteromedial edge	0.00%
	s6		Posteromedial distal condyle	0.00%
	s7		Posterolateral distal condyle	25.00%
	s8	supp	Top proximal end	0.00%
	s9	supp	Bottom distal end	0.00%
Curves	c1	28	Proximal end outline	0.00%
	c2	28	Radial interosseous ridge	0.00%
	c3	46	Radial medial interosseous distal ridge	0.00%
	c4	41	Distal end outline	25.00%

Suppl.V.A.3. Radius landmark definitions.

	ID	N	Definition	Missing %
Ladnmarks	s1		Medial point Femoral Head	28.00%
	s2		Roof of Femoral Head	32.00%
	s3		Lateral border of Femoral Head	64.00%
	s4		Proximolateral border of the Greater Trochanter	20.00%
	s5		Anterior Femoral Head	32.00%
	s6		Anterior Greater Trochanter	52.00%
	s7		Greater Trochanter top Trochanteric Shelf	64.00%
	s8		Posterior Femoral Head	36.00%
	s9		Lateral bulge	4.00%
	s10		Distal end lateral bulge	4.00%
	s11		Deflection femoral head	0.00%
	s12		Fourth trochanter	0.00%
	s13		Minimum midshaft width medial	0.00%
	s14		Minimium midshaft width anterior	0.00%
	s15		Minimum midshaft width lateral	0.00%
	s16		Minimum midshaft width posterior	0.00%
	s17		Tibial condyle medial margin	32.00%
	s18		Tibial condyle anteroproximal	48.00%
	s19		Anterior intercondylar fossa	32.00%
	s20		Fibular condyle anteroproximal	56.00%
	s21		Lateral epicondyle	44.00%
	s22		Fibular condyle posteroproximal	36.00%
	s23		Posterior intercondylar fossa	20.00%
	s24		Tibial condyle posteroproximal	4.00%
	s25	supp	Distalmost bottom of tibial condyle	44.00%
	s26	supp	Intercondylar fossa	40.00%
	s27	supp	Distalmost bottom of fibular condyle	56.00%
Curves	c1	50	Proximal end outline	68.00%
	c2	20	Lateral bulge	20.00%
	c3	40	Midshaft outline	0.00%
	c4	60	Distal articular condyles outline	60.00%

	ID	N	Definition	Missing %
Landmarks	s1		Top of cnemial crest	15.79%
	s2		Top of medial crest of the articular fossa	47.37%
	s3		Posterior tibial head	26.32%
	s4		Medial of tibial head	36.84%
	s5		Cnemial crest	5.26%
	s6		Distal end of cnemial crest	0.00%
	s7		Anterior midshaft	0.00%
	s8		Lateral midshaft	0.00%
	s9		Posterior midshaft	0.00%
	s10		Medial midshaft	0.00%
	s11		Anterior ascending process of distal	42.11%
	s12		Intercondylar sulcus	42.11%
	s13		Posterior ventral process of distal	47.37%
	s14		Distal condyle medial process	57.89%
	s15	supp	Top proximal end	36.84%
	s16	supp	Bottom distal end	36.84%
Curves	c1	40	Tibial proximal end outline	47.37%
	c2	20	Cnemial crest	52.63%
	c3	40	Midshaft outline	0.00%
	c4	50	Tibial distal end outline	73.68%

Suppl.V.A.5. Tibia landmark definitions.

	ID	N	Definition	Missing %
Landmarks	s1		Top anterior crest	18.52%
	s2		Top border anterior crest sulcus	3.70%
	s3		Posterior proximal end	29.63%
	s4		Bottom border anterior crest	0.00%
	s5		Lateral trochanter	0.00%
	s6		Bottom of the tibial scar	0.00%
	s7		Top of the anterolateral crest	0.00%
	s8		Anterior distal ending	37.04%
	s9		Lateral distal ending	37.04%
	s10		Posterior distal ending	37.04%
	s11	supp	Top proximal end	33.33%
	s12	supp	Bottom distal end	37.04%
Curves	c1	40	Proximal end outline	37.04%
	c2	40	Anterior fossa	25.93%
	c3	44	Lateral trochanter ridge	3.70%
	c4	10	Anterolateral crest	37.04%
	c5	40	Distal end outline	48.15%

Suppl.V.A.6. Fibula landmark definitions.

← **Suppl.V.A.2. Femur landmark definitions.**

SUPPL.V.D. COMPLETE PCA REPORTS

SUPPL.V.D.1. EIGENVALUES OF THE BPCA-ESTIMATED DATASET

	Eigenvalue	Variance (%)	Cumulative variance (%)	Chi.sq	p.value	Signif. (p<0.05)
PC1	132.800	22.357	22.357	2.401	0.301	
PC2	98.938	16.656	39.013	11.280	**0.004**	*
PC3	63.519	10.693	49.707	0.852	0.653	
PC4	48.234	8.120	57.827	3.410	0.182	
PC5	37.064	6.240	64.067	1.679	0.432	
PC6	31.577	5.316	69.382	0.574	0.751	
PC7	30.889	5.200	74.583	0.018	0.991	
PC8	23.311	3.924	78.507	6.748	**0.034**	*
PC9	20.002	3.367	81.874	2.882	0.237	
PC10	18.078	3.043	84.918	3.633	0.163	

Suppl.V.D.1.1. Humerus PCA eigenvalues and Kruskal-Wallis results

	Eigenvalue	Variance (%)	Cumulative variance (%)	Chi.sq	p.value	Signif. (p<0.05)
PC1	137.469	34.453	34.453	4.545	**0.033**	*
PC2	97.554	24.450	58.903	0.409	0.522	
PC3	65.693	16.464	75.367	0.045	0.831	
PC4	36.425	9.129	84.496	0.182	0.670	
PC5	25.265	6.332	90.828	0.409	0.522	
PC6	15.331	3.842	94.671	0.045	0.831	
PC7	12.603	3.159	97.829	0.045	0.831	
PC8	5.911	1.481	99.311	1.136	0.286	
PC9	2.750	0.689	100.000	0.182	0.670	

Suppl.V.D.1.2. Ulna PCA eigenvalues and Kruskal-Wallis results

	Eigenvalue	Variance (%)	Cumulative variance (%)	Chi.sq	p.value	Signif. (p<0.05)
PC1	212.598	47.244	47.244	1.800	0.180	
PC2	132.947	29.544	76.788	1.800	0.180	
PC3	104.455	23.212	100.000	1.800	0.180	

Suppl.V.D.1.3. Radius PCA eigenvalues and Kruskal-Wallis results

	Eigenvalue	Variance (%)	Cumulative variance (%)	Chi.sq	p.value	Signif. (p<0.05)
PC1	115.263	19.805	19.805	4.990	0.082	
PC2	82.778	14.223	34.028	4.025	0.134	
PC3	69.243	11.897	45.925	0.262	0.877	
PC4	46.981	8.072	53.997	4.904	0.086	
PC5	39.918	6.859	60.856	0.825	0.662	
PC6	33.971	5.837	66.693	3.431	0.180	
PC7	27.714	4.762	71.455	3.601	0.165	
PC8	25.369	4.359	75.814	2.777	0.249	
PC9	20.014	3.439	79.253	0.200	0.905	
PC10	17.674	3.037	82.289	4.415	0.110	

Suppl.V.D.1.4 Femur PCA eigenvalues and Kruskal-Wallis results

	Eigenvalue	Variance (%)	Cumulative variance (%)	Chi.sq	p.value	Signif. (p<0.05)
PC1	115.655	23.507	23.507	3.927	0.140	
PC2	95.726	19.457	42.964	6.076	**0.048**	*
PC3	54.544	11.086	54.050	3.366	0.186	
PC4	44.470	9.039	63.089	0.325	0.850	
PC5	35.954	7.308	70.396	2.507	0.286	
PC6	29.406	5.977	76.373	1.201	0.549	
PC7	27.054	5.499	81.872	0.144	0.930	
PC8	19.832	4.031	85.902	2.139	0.343	
PC9	15.339	3.118	89.020	0.419	0.811	
PC10	13.888	2.823	91.843	2.195	0.334	

Suppl.V.D.1.5 Tibia PCA eigenvalues and Kruskal-Wallis results

	Eigenvalue	Variance (%)	Cumulative variance (%)	Chi.sq	p.value	Signif. (p<0.05)
PC1	99.725	18.066	18.066	7.833	**0.020**	*
PC2	72.839	13.195	31.262	1.404	0.496	
PC3	67.510	12.230	43.492	0.704	0.703	
PC4	52.253	9.466	52.958	0.356	0.837	
PC5	42.527	7.704	60.662	4.626	0.099	
PC6	37.058	6.714	67.376	2.069	0.355	
PC7	32.596	5.905	73.281	3.049	0.218	
PC8	23.878	4.326	77.606	0.494	0.781	
PC9	21.025	3.809	81.415	4.593	0.101	
PC10	16.417	2.974	84.389	0.236	0.889	

Suppl.V.D.1.6 Fibula PCA eigenvalues and Kruskal-Wallis results

SUPPL.V.D.2.TPS-ESTIMATED DATASET PCA RESULTST

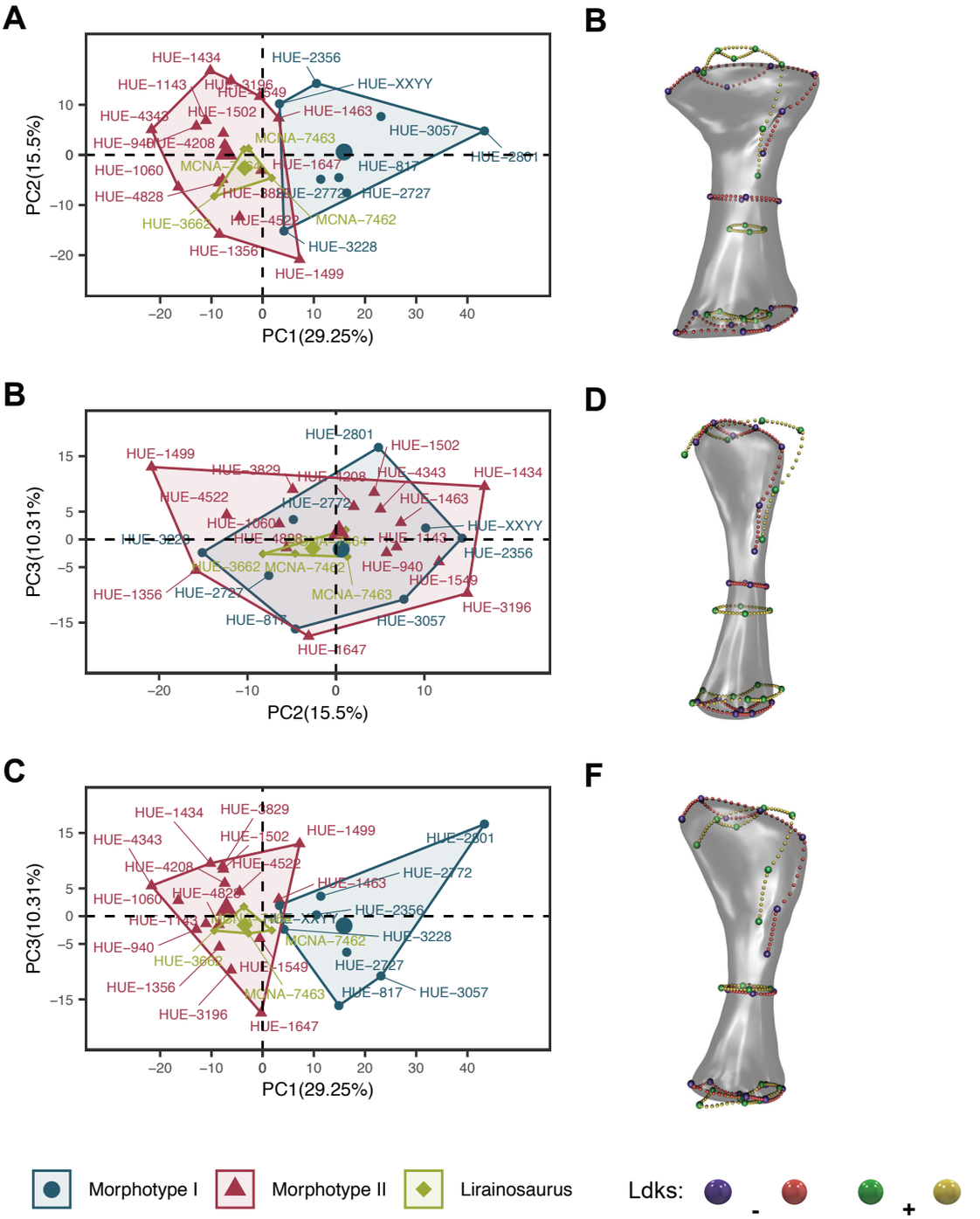

Suppl.V.D.2.1. Humerus shape PCA results over tps dataset with highlighted taphomorphospaces. (A) PC1-PC2. (B) PC2-PC3. (C) PC1-PC3. (D) Landmark configuration at the extremes of PC1 axis. (C) at the extremes of PC2 axis. (F) at the extremes of PC3 axis.

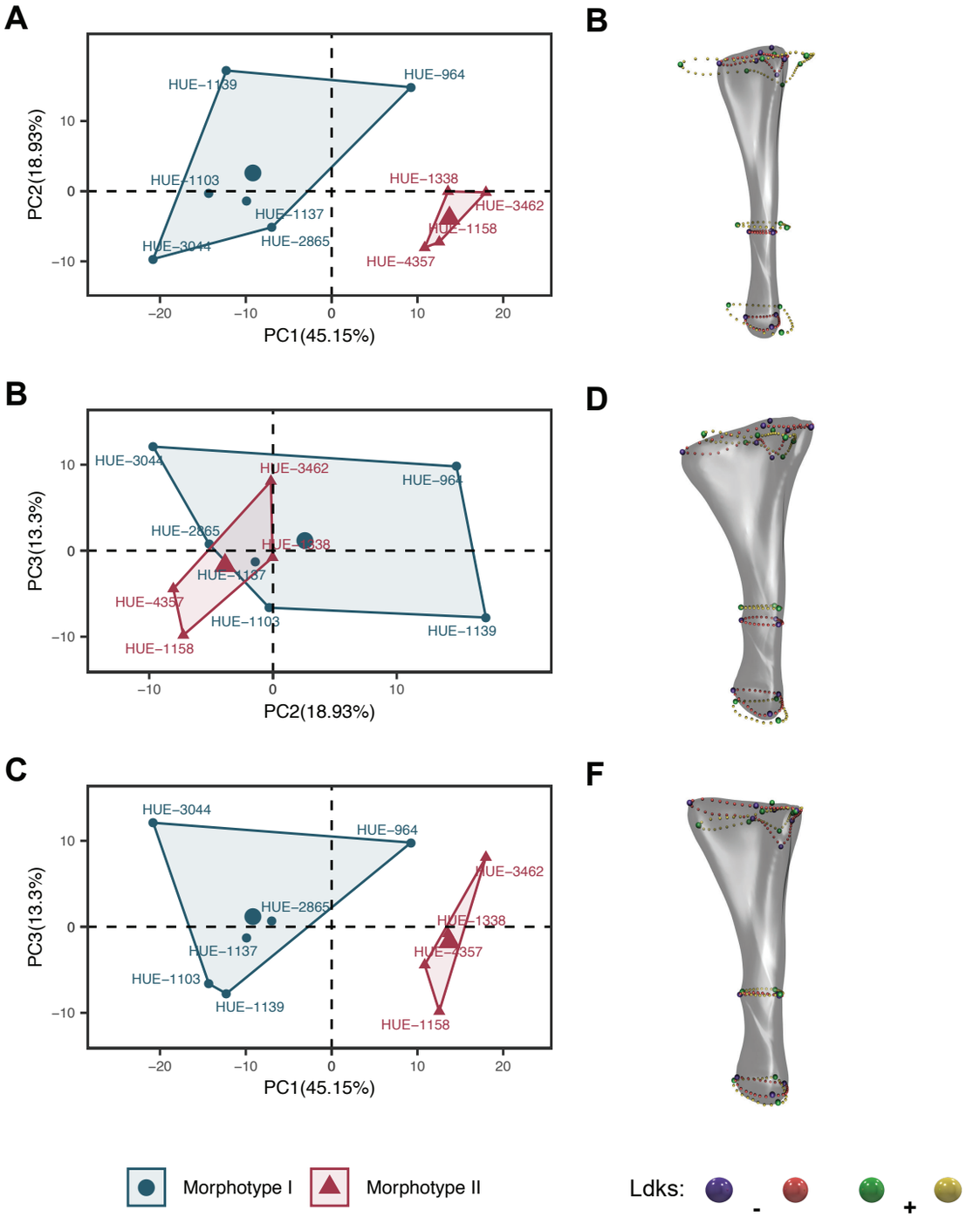

Suppl.V.D.2.2. Ulna shape PCA results over tps dataset with highlighted taphomorphospaces. (A) PC1-PC2. (B) PC2-PC3. (C) PC1-PC3. (D) Landmark configuration at the extremes of PC1 axis. (C) at the extremes of PC2 axis. (F) at the extremes of PC3 axis.

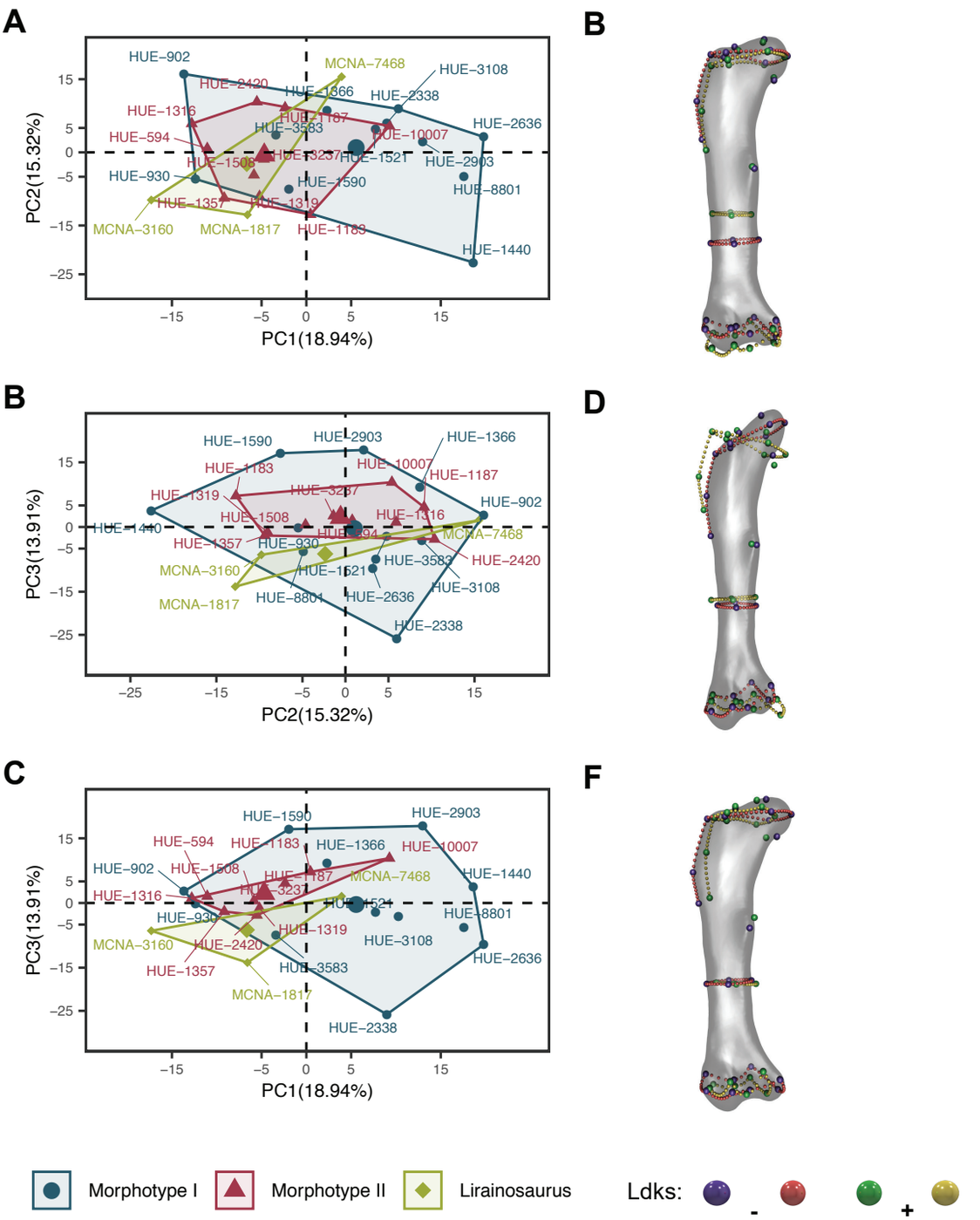

Suppl.V.D.2.3. Femur shape PCA results over tps dataset with highlighted taphomorphospaces. (A) PC1-PC2. (B) PC2-PC3. (C) PC1-PC3. (D) Landmark configuration at the extremes of PC1 axis. (C) at the extremes of PC2 axis. (F) at the extremes of PC3 axis.

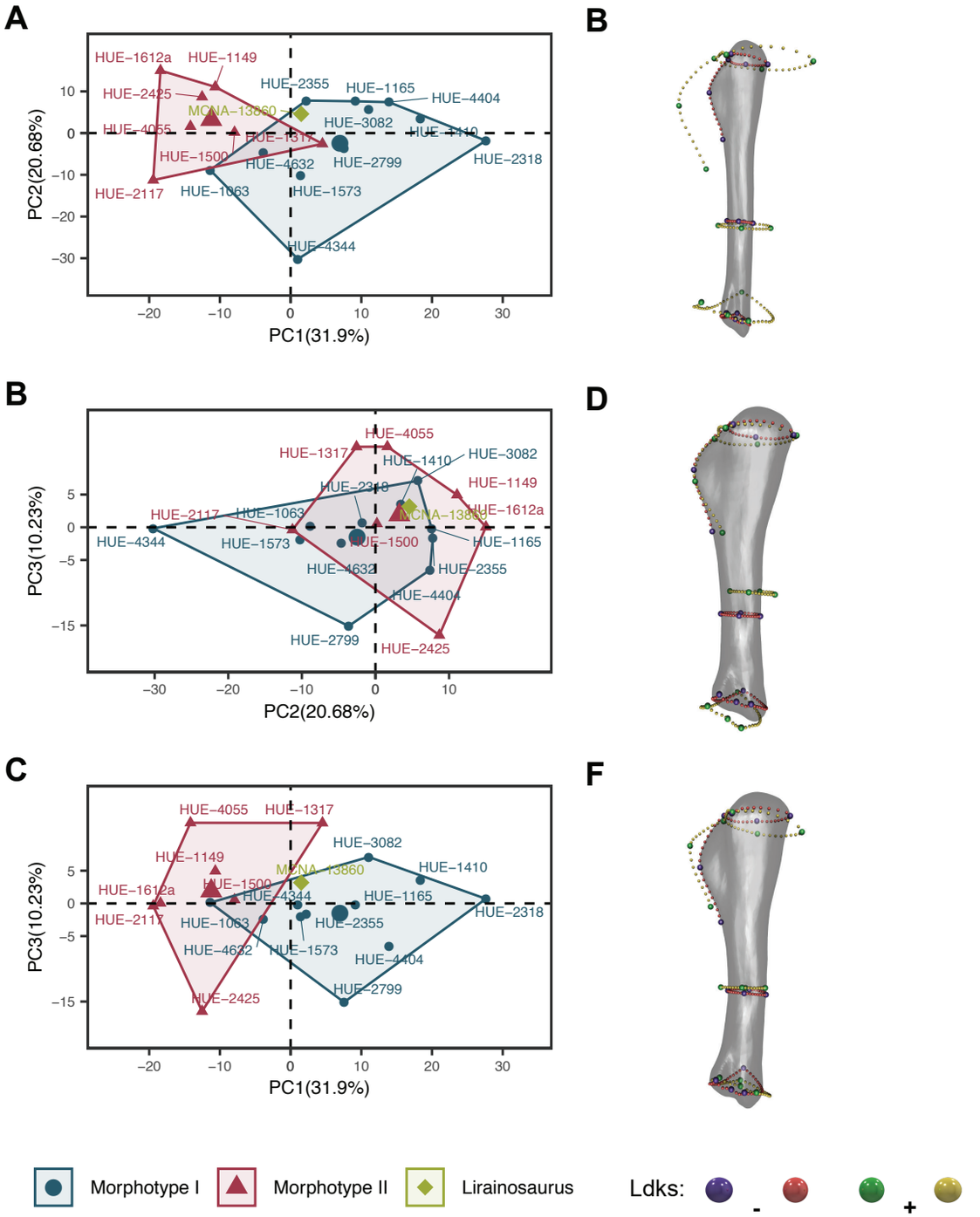

Suppl.V.D.2.4. Tibia shape PCA results over tps dataset with highlighted taphomorphospaces. (A) PC1-PC2. (B) PC2-PC3. (C) PC1-PC3. (D) Landmark configuration at the extremes of PC1 axis. (C) at the extremes of PC2 axis. (F) at the extremes of PC3 axis.

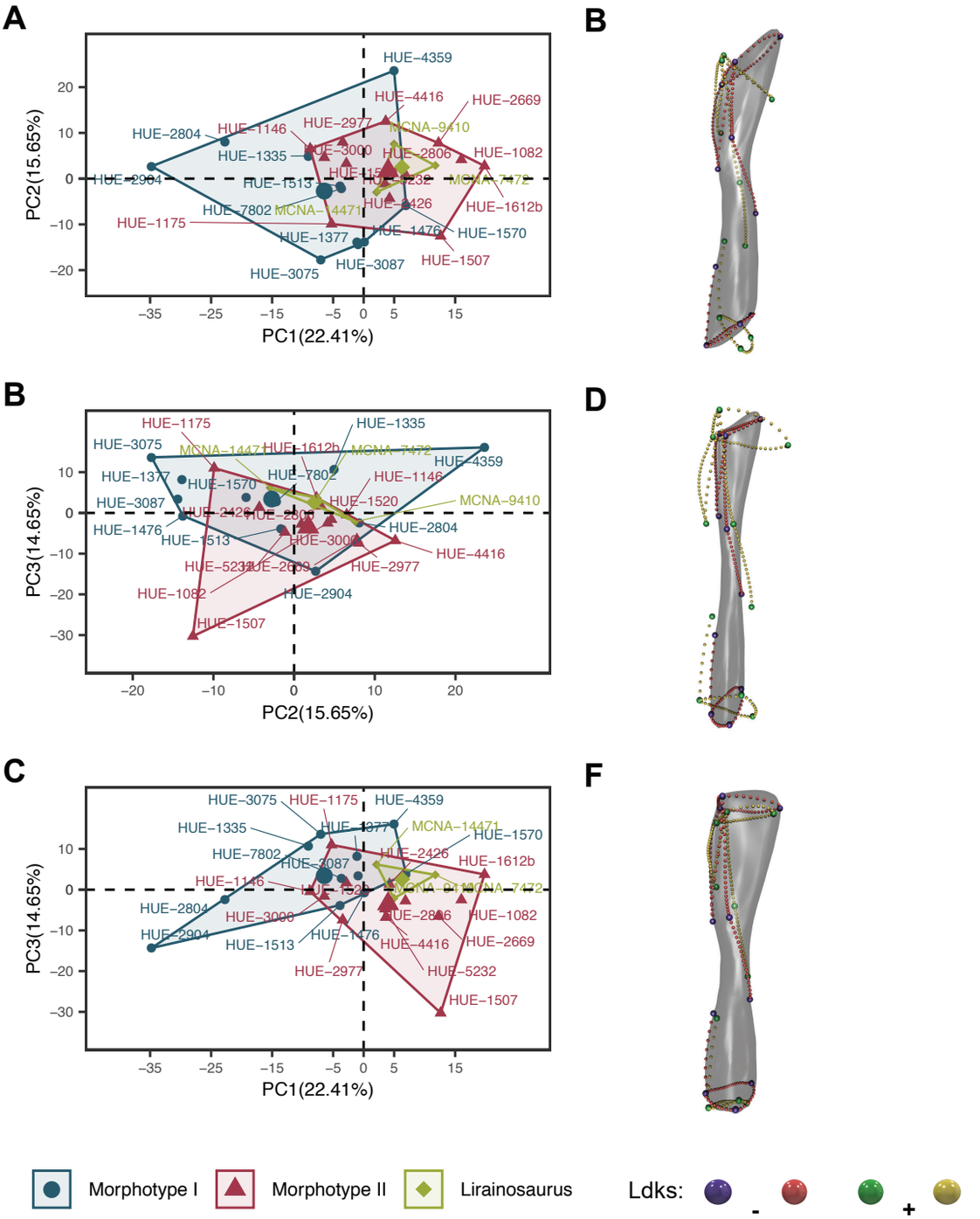

Suppl.V.D.2.5. Fibula shape PCA results over tps dataset with highlighted taphomorphospaces. (A) PC1-PC2. (B) PC2-PC3. (C) PC1-PC3. (D) Landmark configuration at the extremes of PC1 axis. (C) at the extremes of PC2 axis. (F) at the extremes of PC3 axis.

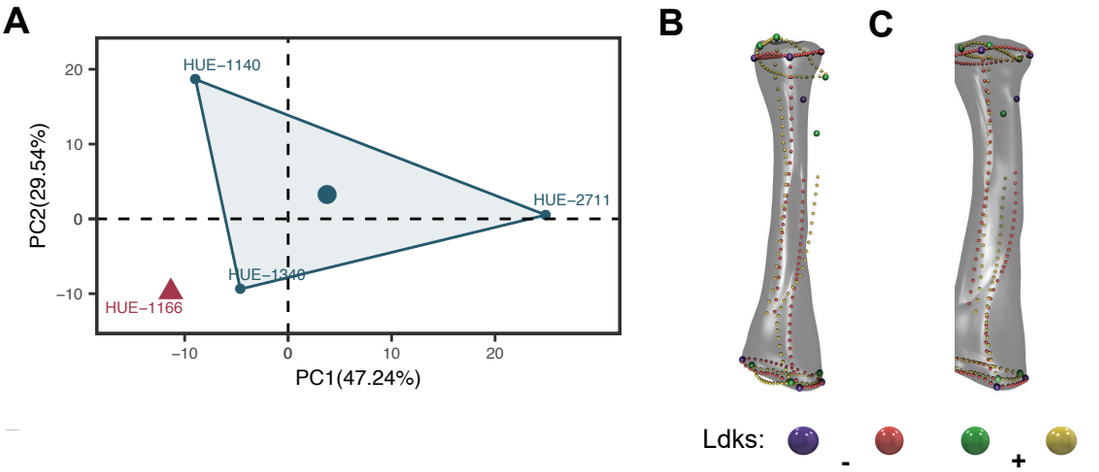

Suppl.V.D.2.6. Radius shape PCA results over tps dataset with highlighted taphomorphospaces. (A) PC1-PC2. (B) PC2-PC3. (C) PC1-PC3. (D) Landmark configuration at the extremes of PC1 axis. (C) at the extremes of PC2 axis. (F) at the extremes of PC3 axis.

SUPPL.V.E. K-MEANS CLUSTERING

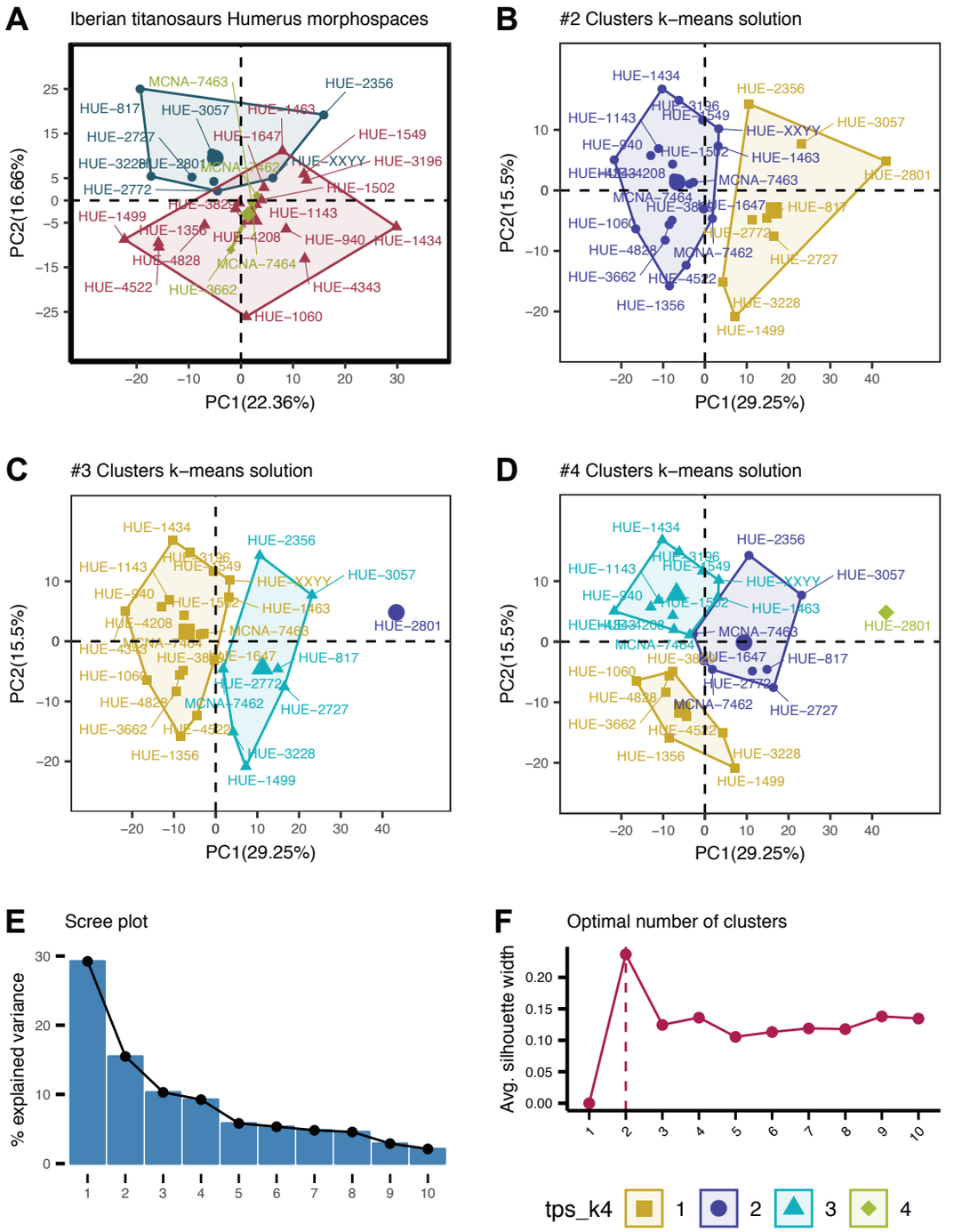

Suppl.V.E.1. Humeri group assessment via k-means algorithm. (A) Shape PCA PC1-PC2 with a priori morphotypes. (B) Classification for k= 2 groups. (C) k= 3 groups. (D) k = 4 groups (E) Variance explained by each PC. (F) Average silhouette width after partition of the morphospace into k groups.

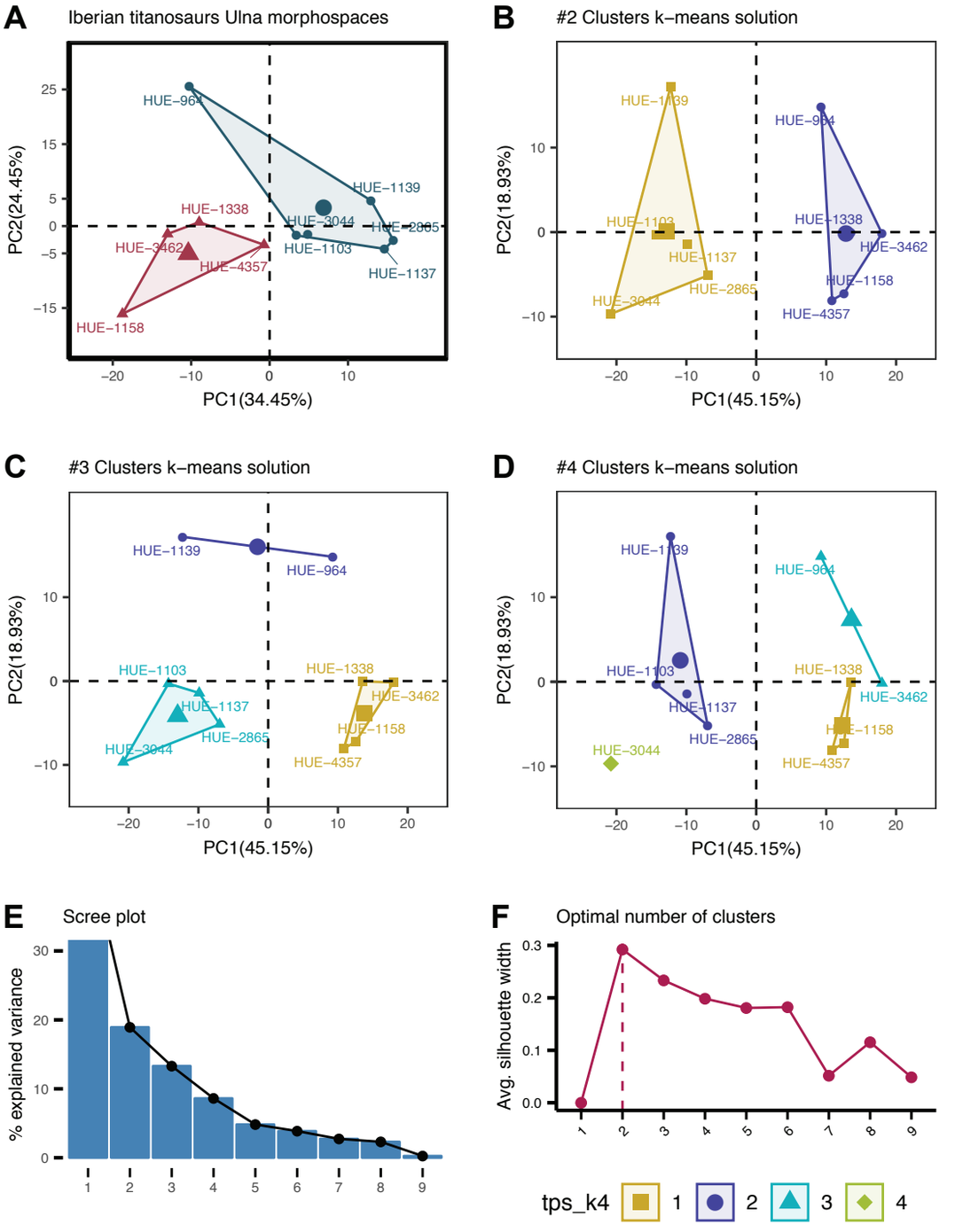

Suppl.V.E.2. Ulnae group assessment via k-means algorithm. (A) Shape PCA PC1-PC2 with a priori morphotypes. (B) Classification for k= 2 groups. (C) k= 3 groups. (D) k = 4 groups (E) Variance explained by each PC. (F) Average silhouette width after partition of the morphospace into k groups.

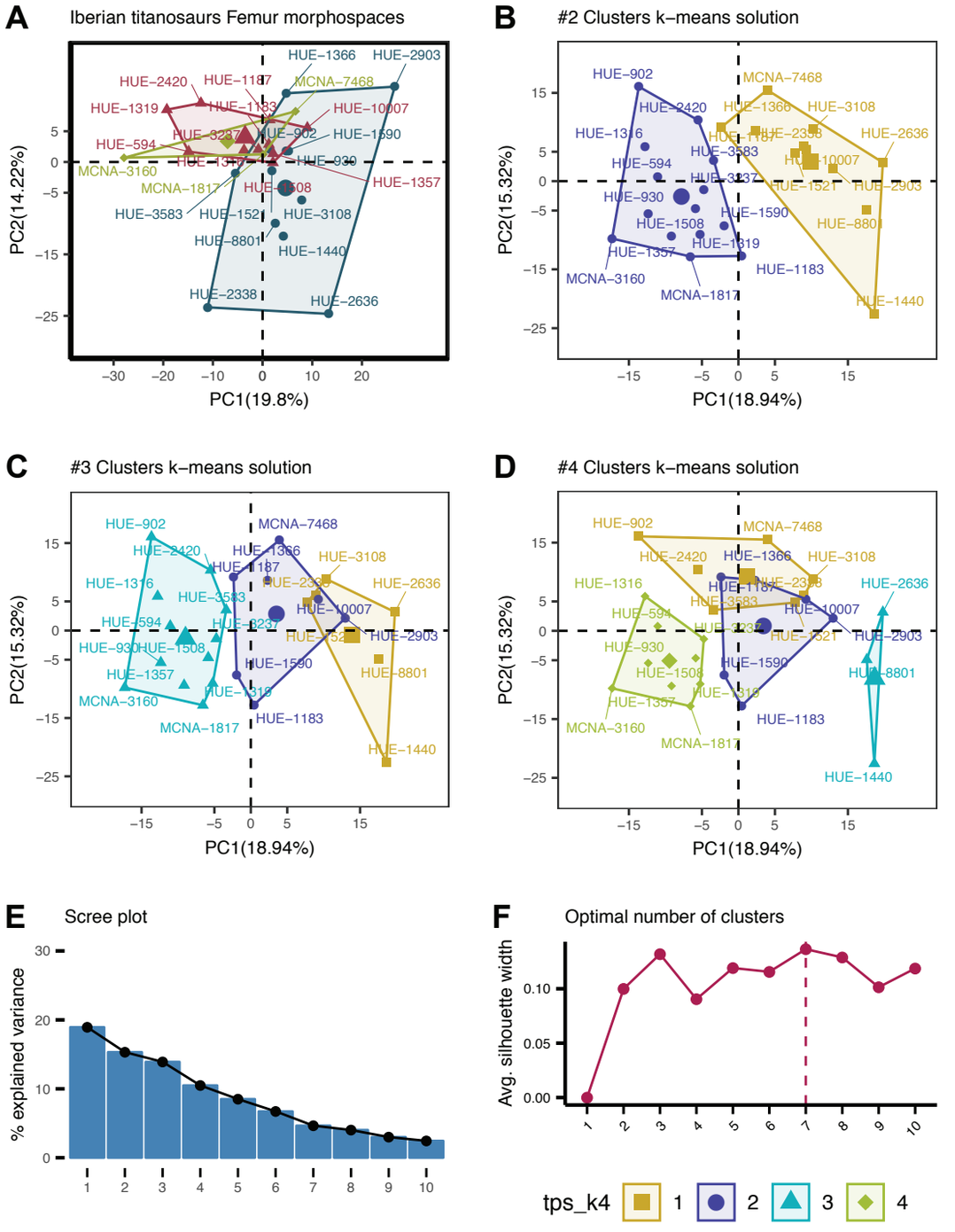

Suppl.V.E.3. Femora group assessment via k-means algorithm. (A) Shape PCA PC1-PC2 with a priori morphotypes. (B) Classification for k= 2 groups. (C) k= 3 groups. (D) k = 4 groups (E) Variance explained by each PC. (F) Average silhouette width after partition of the morphospace into k groups.

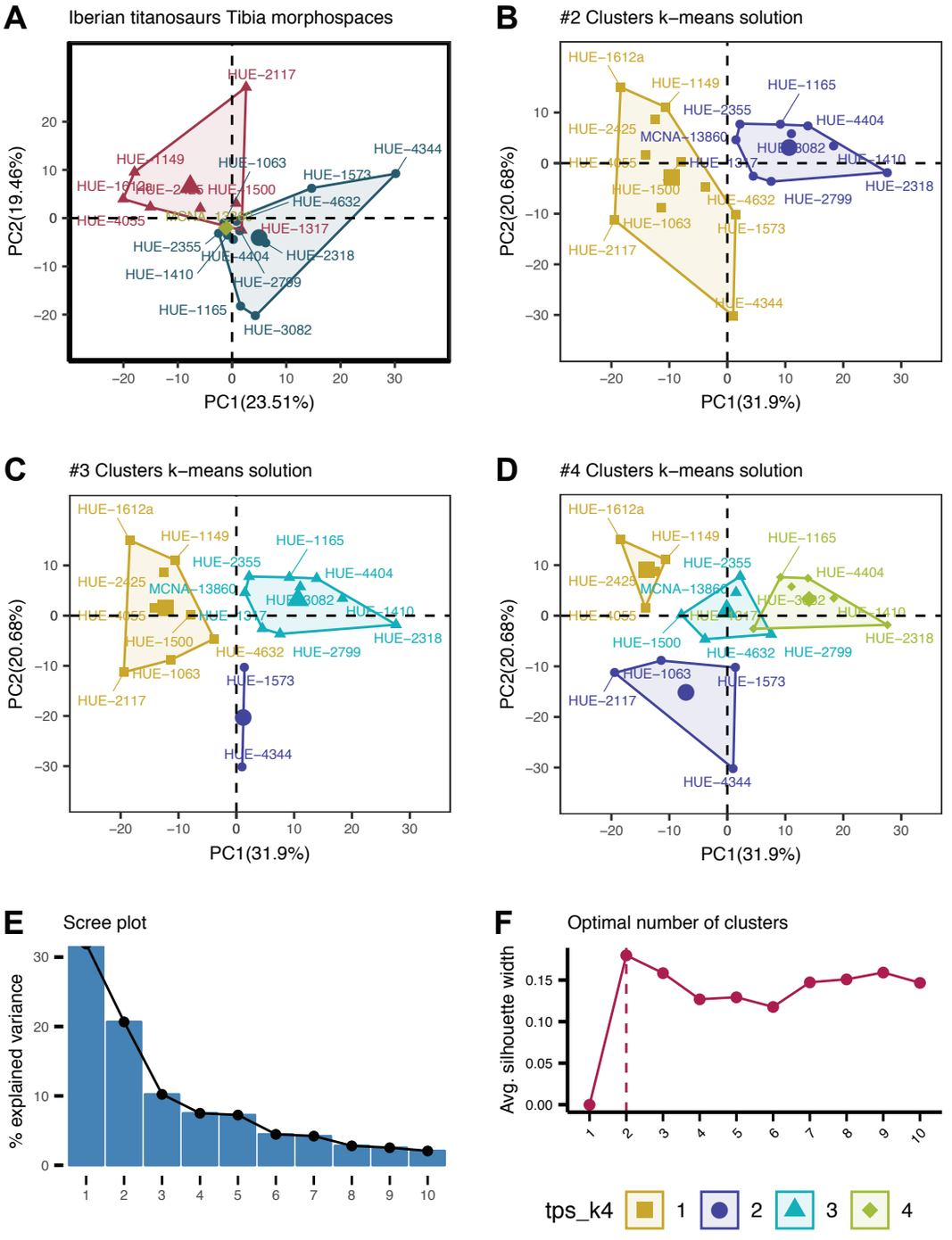

Suppl.V.E.4. Tibiae group assessment via k-means algorithm. (A) Shape PCA PC1-PC2 with a priori morphotypes. (B) Classification for k= 2 groups. (C) k= 3 groups. (D) k = 4 groups (E) Variance explained by each PC. (F) Average silhouette width after partition of the morphospace into k groups.

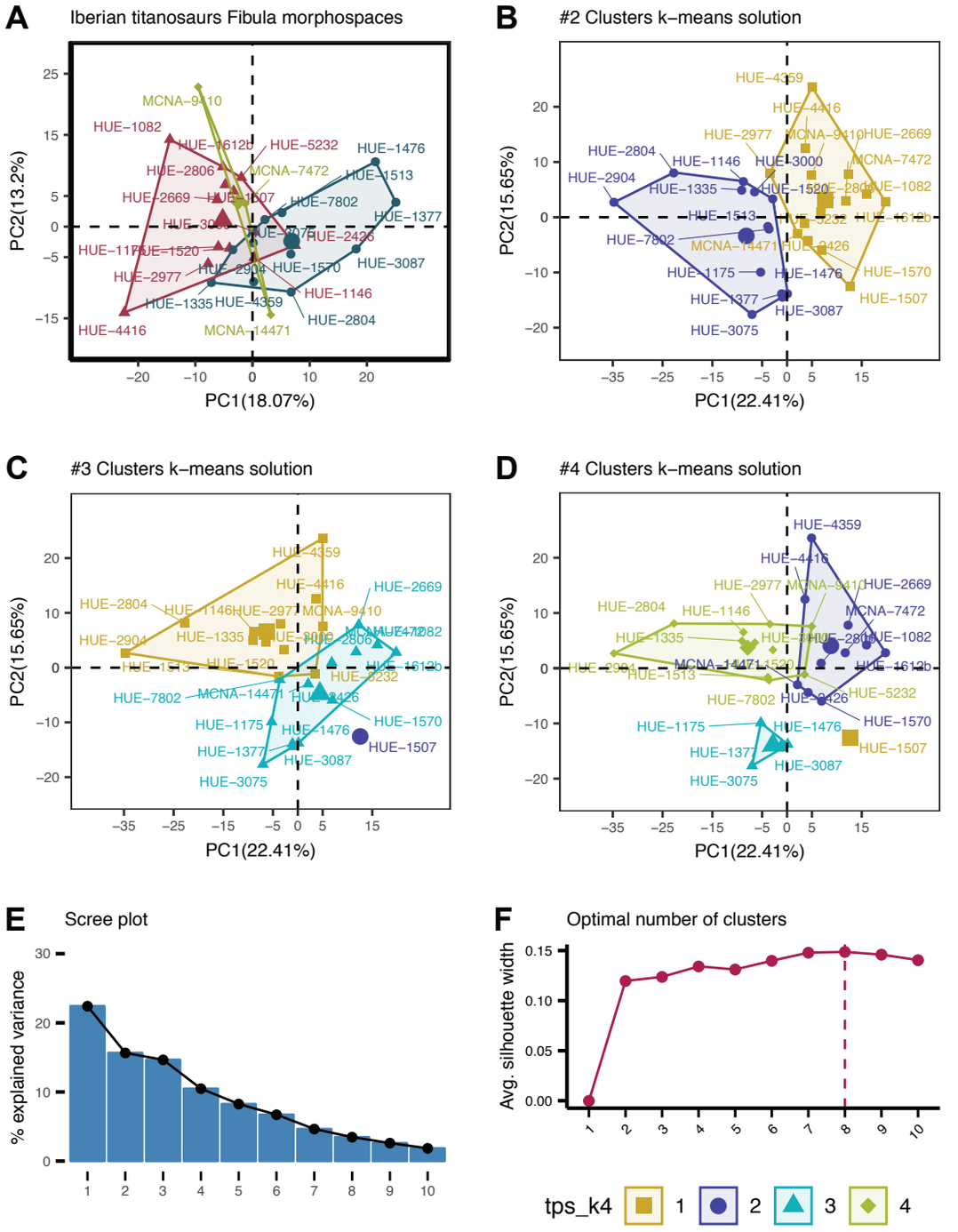

Suppl.V.E.5. Fibulae group assessment via k-means algorithm. (A) Shape PCA PC1-PC2 with a priori morphotypes. (B) Classification for k= 2 groups. (C) k= 3 groups. (D) k = 4 groups (E) Variance explained by each PC. (F) Average silhouette width after partition of the morphospace into k groups.

SUPPL. V.F. MORHOTYPE ALLOCATION

SUPPL. V.F.2. COMPARISON TESTS BETWEEN CAP IV AND CAP V GROUPS

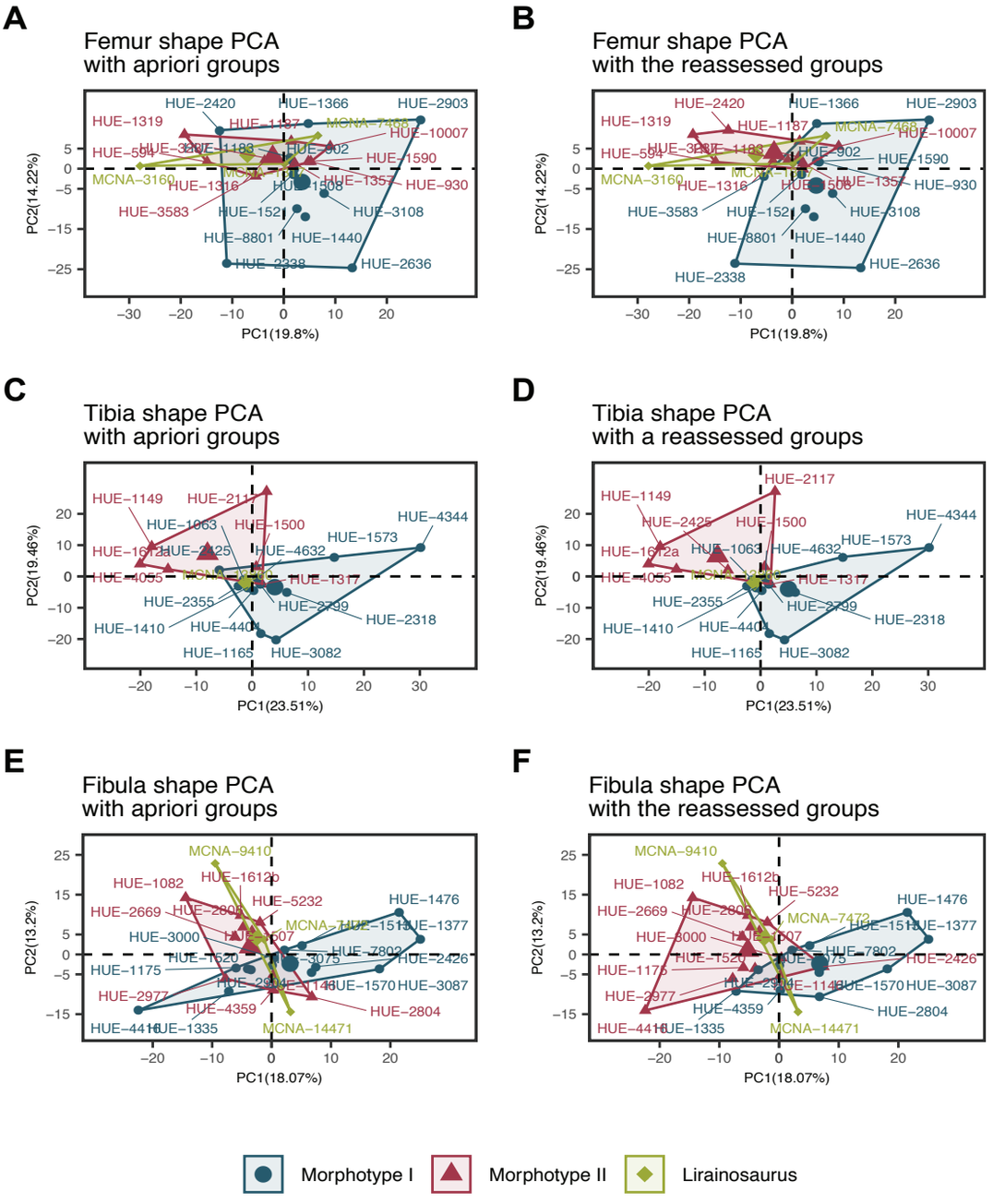

Suppl.V.F.1. Comparison between the reassessed specimens of the hindlimb. (A) Femur shape PCA PC1-PC2 with a Chap.IV morphotypes. (B) Femur shape PCA reassessement (C) Tibia shape PCA PC1-PC2 with a Chap.IV morphotypes. (D) Tibia shape PCA reassessement (E) Fibula shape PCA PC1-PC2 with Chap.IV morphotypes. (F) Femur shape PCA reassessement

SUPPL. V.H. MORPHOLOGICAL CHARACTERS

H1 - Deltopectoral crest of humerus developed and medially twisted (Sanz *et al.* 1999)

H2 - Posterior supracondylar ridged on the humerus: Anconeal fossa (Sanz *et al.* 1999)

H3 - Prominent process on the lateral portion of the proximal end of the humerus (Upchurch *et al.* 1998)

H4 - Position of the deltopectoral crest muscle insertion (Upchurch 1998; Upchurch *et al.*, 2004)

H5 - Lateral and proximal surfaces of the humerus (Upchurch 1998; Upchurch *et al.*, 2004)

H6 - Humeral head morphology (Gorcack *et al.* 2017 after González Riga 2003)

H7 - Deltopectoral crest lateromedial projection (Upchurch *et al.*1998)

H8 - Distal articular surface of the humerus (Upchurch (1998) & Upchurch *et al.*, 2004)

H9 - Humerus shaft twist (Tschopp *et al.* 2015)

H10 - Humerus proximal expansion (Tschopp *et al.* 2015)

H11 - Humerus shallow rugose tubercle at center of the concave proximal portion of anterior surface (Tschopp *et al.* 2015)

H12 - Humeral deltopectoral crest shape (Wilson 2002)

H13 - Humeral midshaft cross-section shape (Mannion *et al.* 2013 after Wilson 2002)

H14 - Humeral distal condyle shape (Wilson 2002)

H15 - Humeral diaphysis, shape of lateral margin (Curry Rogers 2005)

H16 - Humeral head position (proximodistal) (Curry Rogers 2005)

H17 - Distal condyles relative sizes (Curry Rogers 2005)

H18 - Humerus robustness index (sensu Wilson et Upchurch 2003) (Carballido & Sander 2014)

H19 - Humerus posterolateral bulge on around level of deltopectoral crest (D'Emic 2012)

U1 - Olecranon or craniomedial process development of the proximal end (Upchurch 1995)

U2 - Proximal end of the ulna (Upchurch 1998; Upchurch *et al.*, 2004)

U3 - Ulna proximal arms (D'Emic 2012)

U4 - Ulna distal end expansion (D'Emic 2012)

U5 - Ulnar articular surface angle between anterior and lateral branch (Tschopp *et al.* 2015)

U6 - Distal transverse expansion (Tschopp *et al.* 2015)

U7 - Distal end articular surface (Curry Rogers 2005)

U8 - Ulna robusticity (midshaft width to length ratio) (Curry Rogers 2005)

U9 - Length-to-proximal breadth ratio (Wilson 2002)

U10 - Vertical groove and ridge structure on posterolateral surface of distal shaft (Mannion *et*

al. 2017 after Royo-Torres *et al.* 2006)

U11 - Orientation of anteromedial process (González Riga *et al.* 2018 after Mannion *et al.* 2013)

R1 - Radius robustness of the proximal end (maximum width / length) (Mannion *et al.* 2013 after McIntosh 1990, Upchurch (1995)

R2 - Radius distal breadth (Tschopp *et al.* 2015)

R3 - Radius distal condyle orientation (Curry Rogers 2005)

R4 - Radial distal condyle shape (Gorscak *et al.* 2014; Carballido & Sanders 2014)

R5 - Well defined interosseous ridge (Curry Rogers (005)

R6 - Type of ends (Curry Rogers 2005)

FM1 - Lateromedial morphology (Royo-Torres 2009)

FM2 - Position of femoral head (Royo-Torres 2009) after Upchurch *et al.* 2004)

FM3 - Displacement of the proximal end (Royo-Torres 2009); Gorscak *et al.* 2017)

FM4 - Femoral head aligment with the condyles (Royo-Torres 2009)

FM5 - Form and Contourn of articulation Femoral head (Royo-Torres 2009)

FM6 - Canal between head and greater trochanter (Royo-Torres 2009)

FM7 - Lesser trochanter in femur (Royo-Torres 2009 after McIntosh 1990; Upchurch 1998)

FM8 - Lateral bulge under greater trochanter (Royo-Torres 2009 after McIntosh 1990; Calvo & Salgado 1995)

FM9 - Femur proximolateral margin development (Gorscak *et al.* 2017)

FM10 - Dorsoventral development lateral bulge (Royo-Torres 2009) after Salgado *et al.*1997)

FM11 - Ventromedial morphology femoral head (Royo-Torres 2009)

FM12 - Anteroposterior midshaft section (Royo-Torres 2009)

FM13 - Anteroposterior midshaft section - compression (Royo-Torres 2009)

FM14 - Sulcus joining intercondylar canal and proximal (Royo-Torres (2009) after Wilson (2002)

FM15 - Linea intermuscularis cranialis (D'Emic (2012)

FM16 - Least midshaft position (Royo-Torres (2009)

FM17 - 4th trochanter position (Royo-Torres (2009) after Upchurch *et al.* 2004)

FM18 - 4th trochanter morphology (Royo-Torres 2009 after Upchurch *et al.* 2004)

FM19 - Distal condyle orientation respective to axis (Royo-Torres 2009)

FM20 - Relative orientation of tibial condyle respective to the shaft (Royo-Torres 2009)

FM21 - Fibular-tibial condyle ratio in lateromedial (Royo-Torres 2009 after Wilson 2002)

FM22 - Fibular-tibial condyle ratio in anteroposterior (Royo-Torres 2009)

FM23 - Femoral head position of highest point in anterior view (Tschopp *et al.* 2015)

FM24 - Anteroposterior development distal condyles (Wilson 2002)

T1 - Contourn proximal end, anteroposterior and lateromedial expansion (Royo-Torres 2009) after Wilson 2002)

T2 - Proximal surface of the tibia (Wilson 2002)

T3 - Cnemial crest projection (Wilson 2002)

T4 - Dorsoventral development of the cnemial crest (Royo-Torres 2009 after Wilson 2002)

T5 - Anterolateral development of the cnemial crest / minimum anteroposterior width (Royo-Torres 2009)

T6 - Morphology of the cnemial crest (Royo-Torres 2009)

T7 - Dorsal contour of the articular surface with the fibula (Harris 2006; Royo-Torres 2009); Tschopp *et al.* 2015; Mannion *et al.* 2017)

T8 - Eccentricity of the midhsaft (Royo-Torres 2009)

T9 - Torsion of the distal end (Royo-Torres 2009 after Sanz *et al.* 1999)

T10 - Anteroposterior and lateromedial distal end (Salgado *et al.* 1997)

T11 - Contour of the distal end (Royo-Torres 2009 after Wilson 2002)

T12 - Maximal lateromedial length of the distal end (Royo-Torres 2009 after Salgado *et al.*1997; Upchurch *et al.* 2004)

T13 - Short ridge on anteromedial surface of distal end (Tschopp *et al.* 2015)

T14 - Posterior surface of cnemial crest (Tschopp *et al.* 2015)

FB1 - Fibular shaft in lateral or medial view (Royo-Torres 2009; D'Emic 2012)

FB2 - Proximal end shape (Royo-Torres 2009)

FB3 - Anterior trochanter/crest development (Royo-Torres 2009; D'Emic 2012)

FB4 - Presence of a anterolateral sulcus in the anterior crest (Royo-Torres 2009)

FB5 - Anterior proximal crest extending into a notch behind cnemial crest (Tschopp *et al.* 2015)

FB6 - Lateral trochanter development (Royo-Torres 2009)

FB7 - Lateral trochanter muscular scar (Curry Rogers 2005)

FB8 - Proximal tibial scar in medial (Wilson 2002)

FB9 - Fibula midshaft morphologoy (Royo-Torres 2009)

FB10 - Complexity of the lateral trochanter (Royo-Torres 2009)

FB11 - Position of the lateral trochanter (Royo-Torres 2009)

FB12 - Distal condyle expansion relative to midshaft (Curry Rogers 2005)

SUPPL. V.H.1. BIBLIOGRAPHY

Carballido JL, Sander PM. 2014. Postcranial axial skeleton of *Europasaurus holgeri* (Dinosauria, Sauropoda) from the Upper Jurassic of Germany: implications for sauropod ontogeny and phylogenetic relationships of basal Macronaria. *Journal of Systematic Palaeontology* 12: 335–387.

Curry Rogers K. 2005. Titanosauria: A phylogenetic overview. In: Curry Rogers K, Wilson JA, eds. *The Sauropods: Evolution and Paleobiology*. Berkeley: University of California Press, 50–103.

González Riga BJ. 2003. A New Titanosaur (Dinosauria, Sauropoda) from the Upper Cretaceous of Mendoza Province, Argentina. *Ameghiniana* 40: 155–172.

González Riga BJ, Lamanna MC, Otero A, Ortiz David LD, Kellner AWA, Ibiricu LM. 2019. An overview of the appendicular skeletal anatomy of South American titanosaurian sauropods, with definition of a newly recognized clade. *Anais da Academia Brasileira de Ciências* 91: e20180374.

Gorscak E, O'Connor PM. 2016. Time-calibrated models support congruency between Cretaceous continental rifting and titanosaurian evolutionary history. *Biology Letters* 12: 20151047.

Harris JD. 2006. The axial skeleton of the dinosaur *Suuwassea emiliae* (Sauropoda: Flagellicaudata) from the Upper Jurassic Morrison Formation of Montana, USA. *Journal of Systematic Palaeontology* 4: 185–198.

Mannion PD, Upchurch P, Barnes RN, Mateus O. 2013. Osteology of the Late Jurassic Portuguese sauropod dinosaur *Lusotitan atalaiensis* (Macronaria) and the evolutionary history of basal titanosauriforms. *Zoological Journal of the Linnean Society* 168: 98–206.

Mannion PD, Allain R, Moine O. 2017. The earliest known titanosauriform sauropod dinosaur and the evolution of Brachiosauridae. *PeerJ* 5: e3217.

Royo-Torres R, Cobos A, Alcalá L. 2006. A Giant European Dinosaur and a New Sauropod Clade. *Science* 314: 1925–1927.

Royo-Torres R. 2009. *El saurópodo de Peñarroya de Tastavins*. Teruel: Instituo de Estudios Turolenses y Fundación Conjunto Paleontológico de Teruel-Dinópolis.

Sanz JL, Powell JE, Le Loeuff J, Martínez RN, Pereda Suberbiola X. 1999. Sauropod remains from the Upper Cretaceous of Laño (north central Spain). Titanosaur phylogenetic relationships. *Estudios del Museo de Ciencias Naturales de Alava* 14: 235–255.

Tschopp E, Mateus O, Benson RBJ. 2015. A specimen-level phylogenetic analysis and taxonomic revision of Diplodocidae (Dinosauria, Sauropoda). *PeerJ* 3: e857.

Upchurch P. 1998. The phylogenetic relationships of sauropod dinosaurs. *Zoological Journal of the Linnean Society* 124: 43–103.

Upchurch P, Barrett PM, Dodson P. 2004. Sauropoda. In: Weishampel DB, Dodson P, Osmólska H, eds. *The Dinosauria*. Berkeley: University of California Press, 259–322.

Wilson JA. 2002. Sauropod dinosaur phylogeny: critique and cladistic analysis. *Zoological Journal of the Linnean Society* 136: 215–275.

SUPP. MATERIAL VI:

Ontogenetic Sequences on the Appendicular Skeleton of the titanosaur of Lo Hueco (Cuenca, Spain)

Suppl. VI.A. Ontogenetic Character Data Matrices - electronic material

Suppl. VI.B. Phylogenetic Character Data Matrices - electronic material

Suppl. VI.C. OCSA method MPT or Majority Rule tree - electronic material

Suppl. VI.D. OSA reticulate diagrams

Suppl. VI.E. Phenotype clusters and radius (ontogenetic characters and phylogenetic characters)

Suppl. VI.F. All MPTs - electronic material

Suppl. VI.FG. Code - electronic material

SUPPL. VI.D. OSA RETICULATE DIAGRAMS

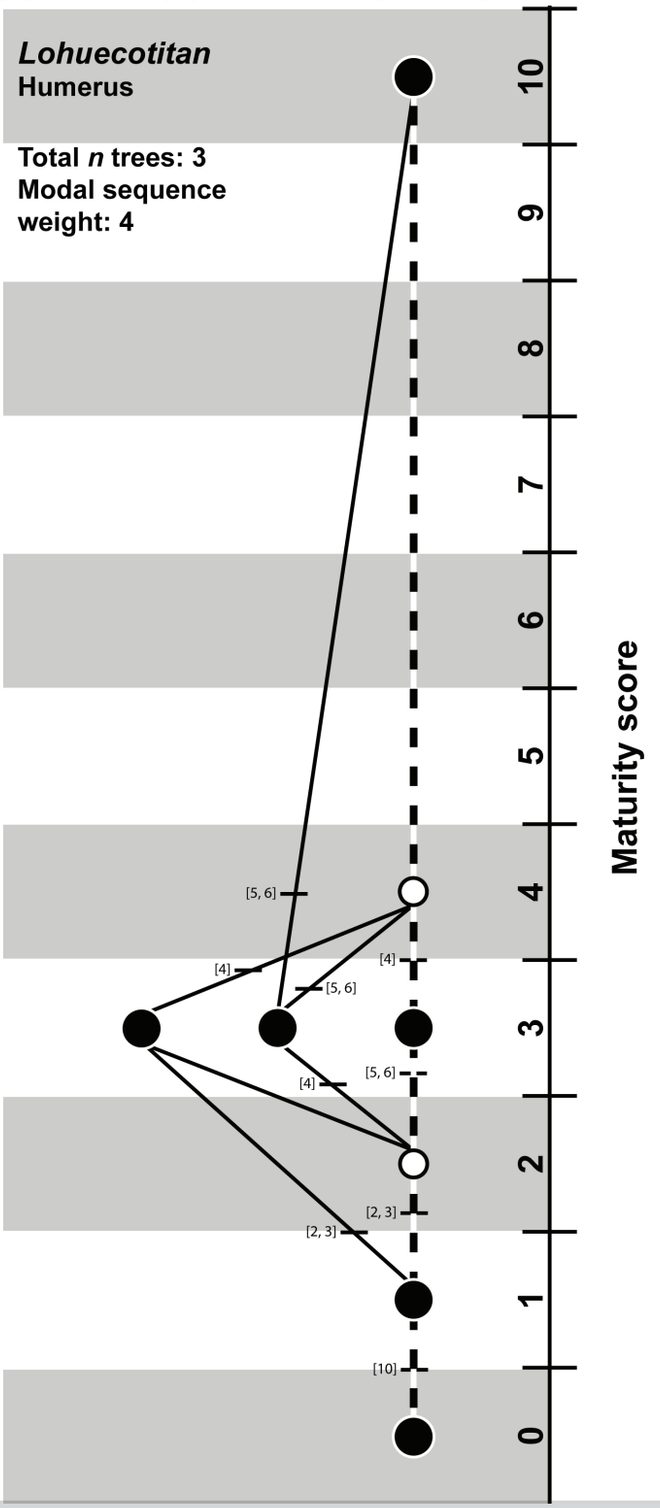

Suppl.VI.D.1 Morphotype I humeri OSA. Connection numbers indicate character change.

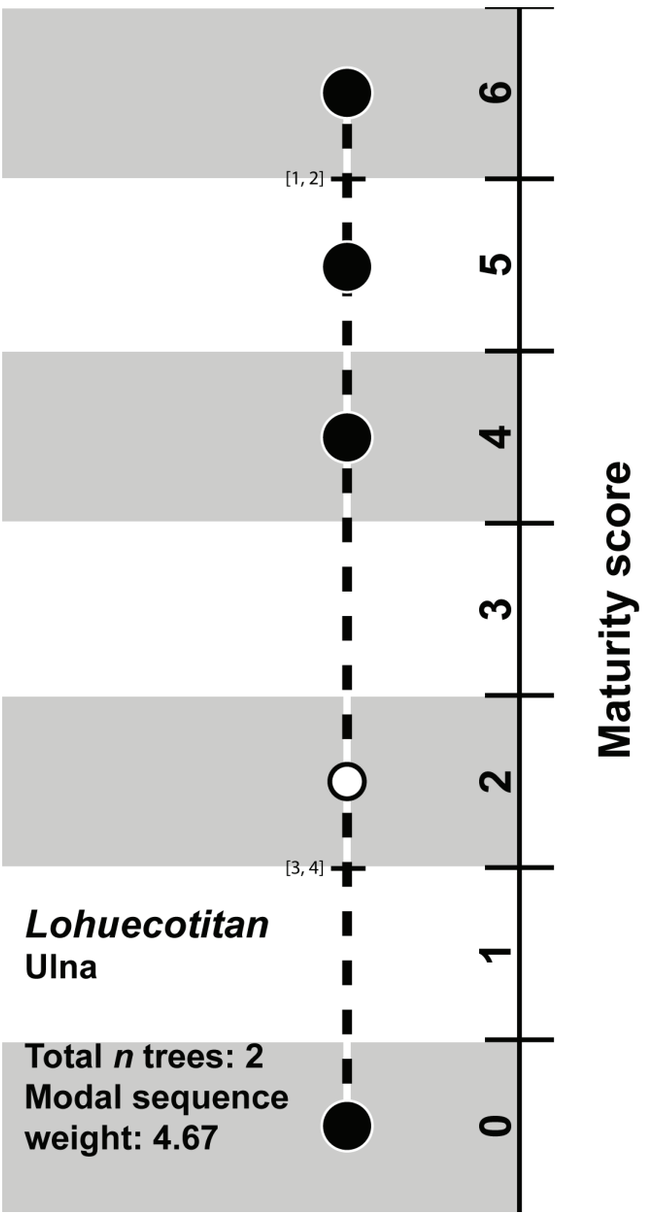

Suppl.VI.D.2 Morphotype I ulnae OSA. Connection numbers indicate character change.

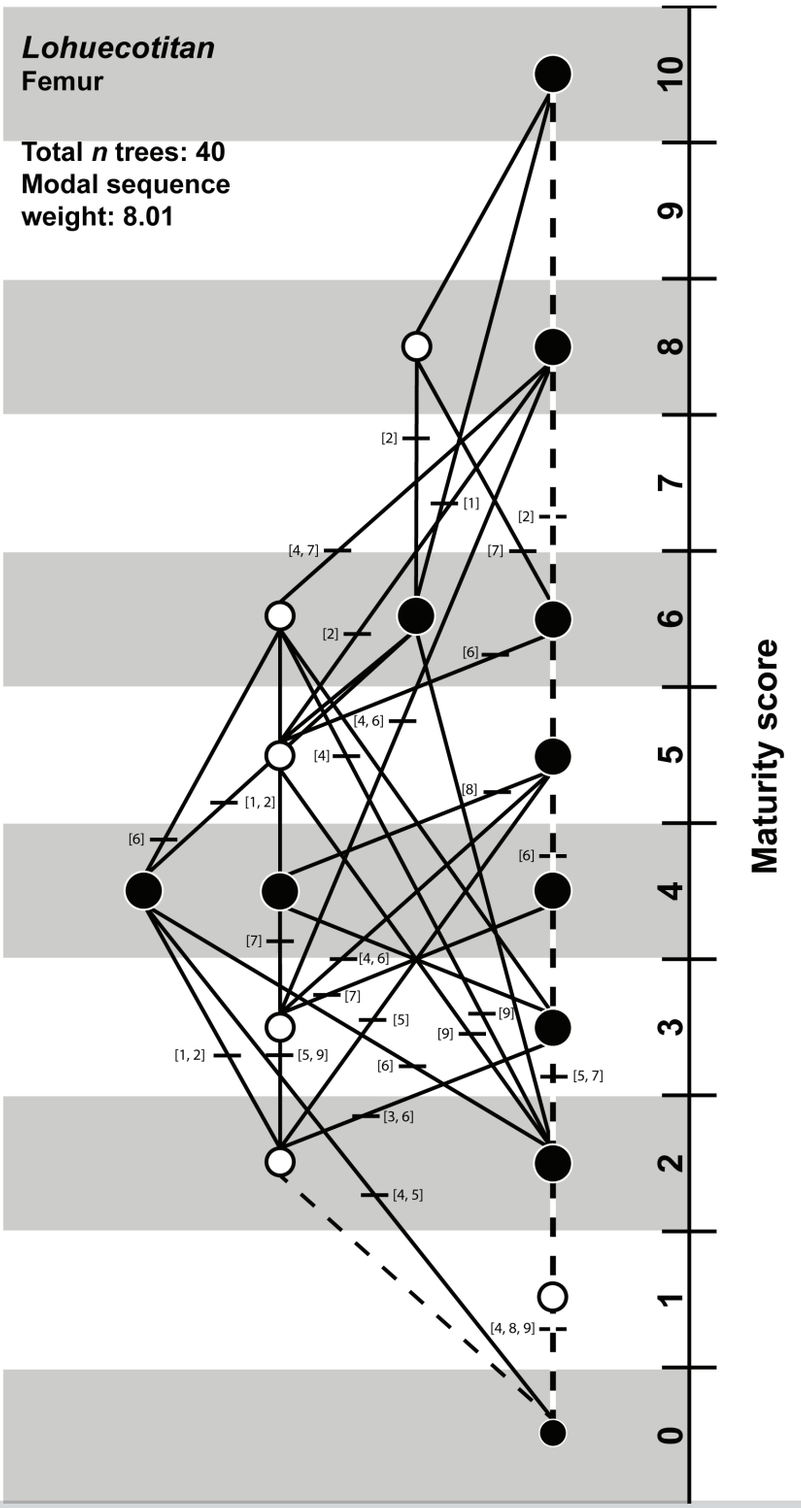

Suppl.VI.D.3 Morphotype I femora OSA. Connection numbers indicate character change.

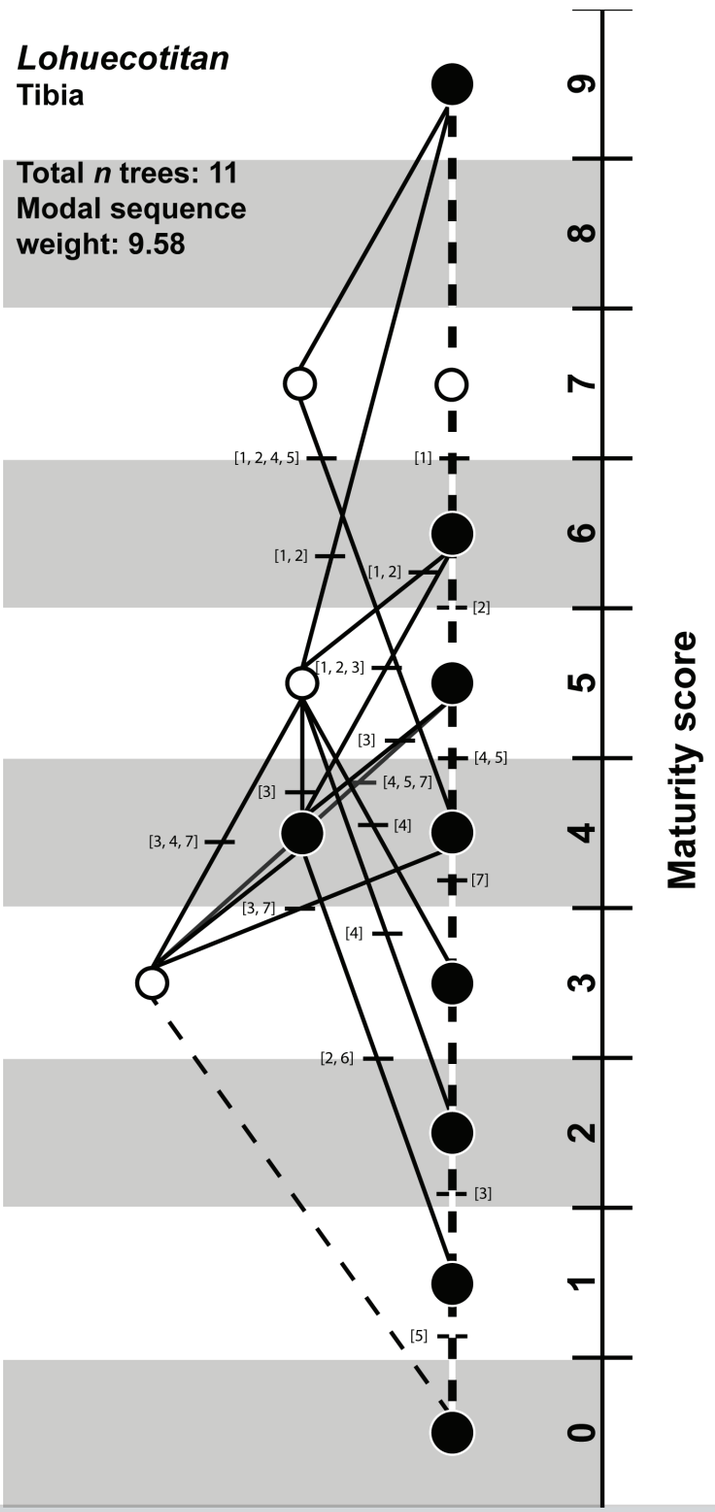

Suppl.VI.D.4 Morphotype I tibiae OSA. Connection numbers indicate character change.

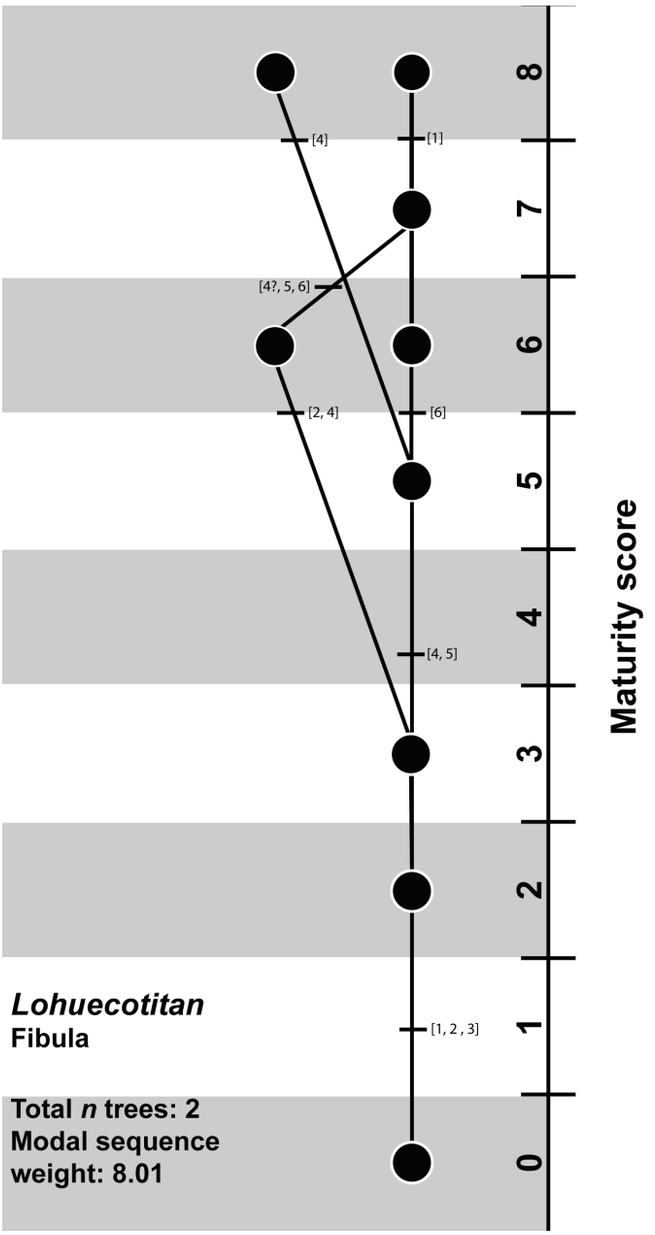

Suppl.VI.D.5 Morphotype I fibulae OSA. Connection numbers indicate character change.

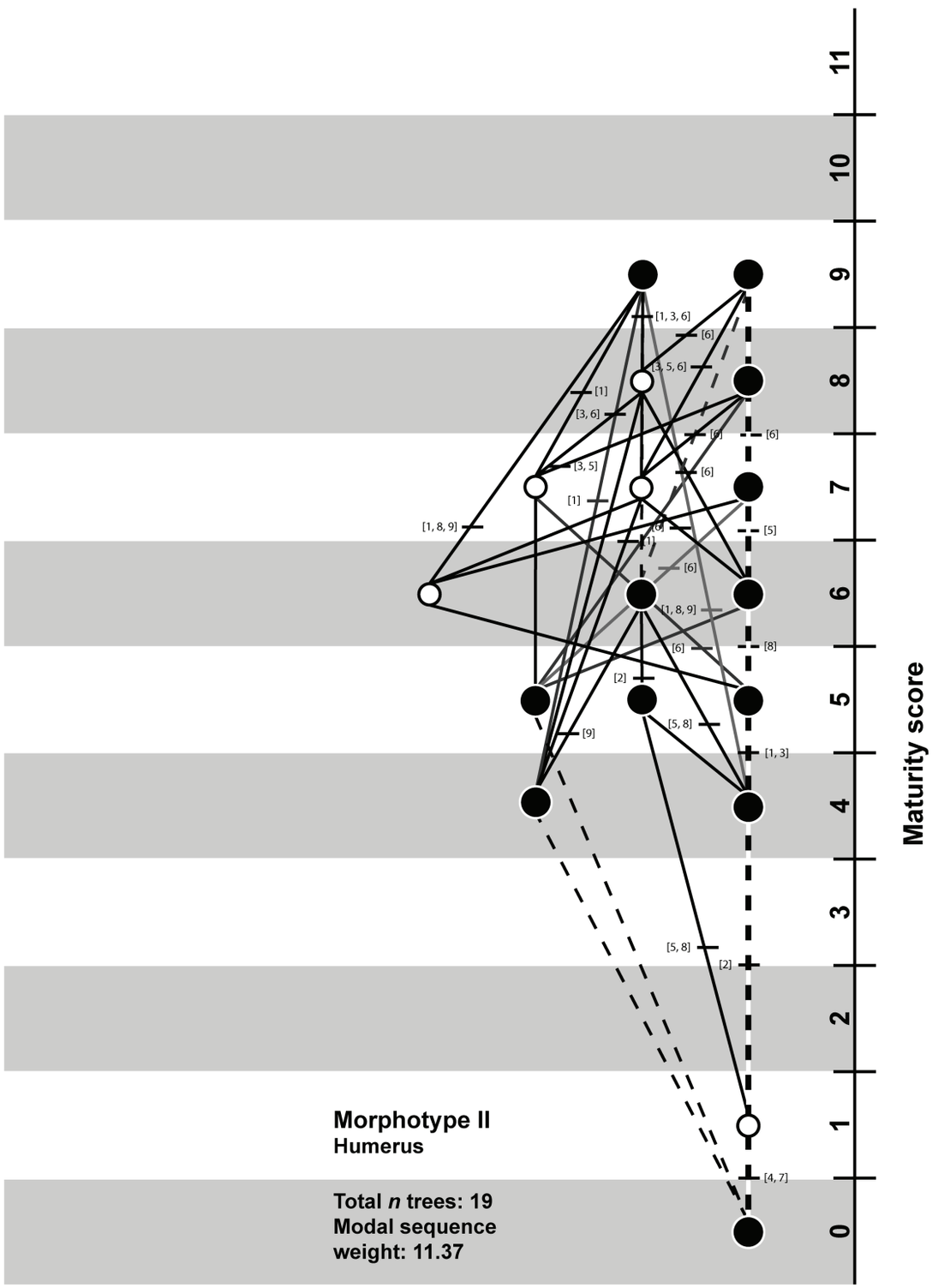

Suppl.VI.D.6 Morphotype II humeri OSA. Connection numbers indicate character change.

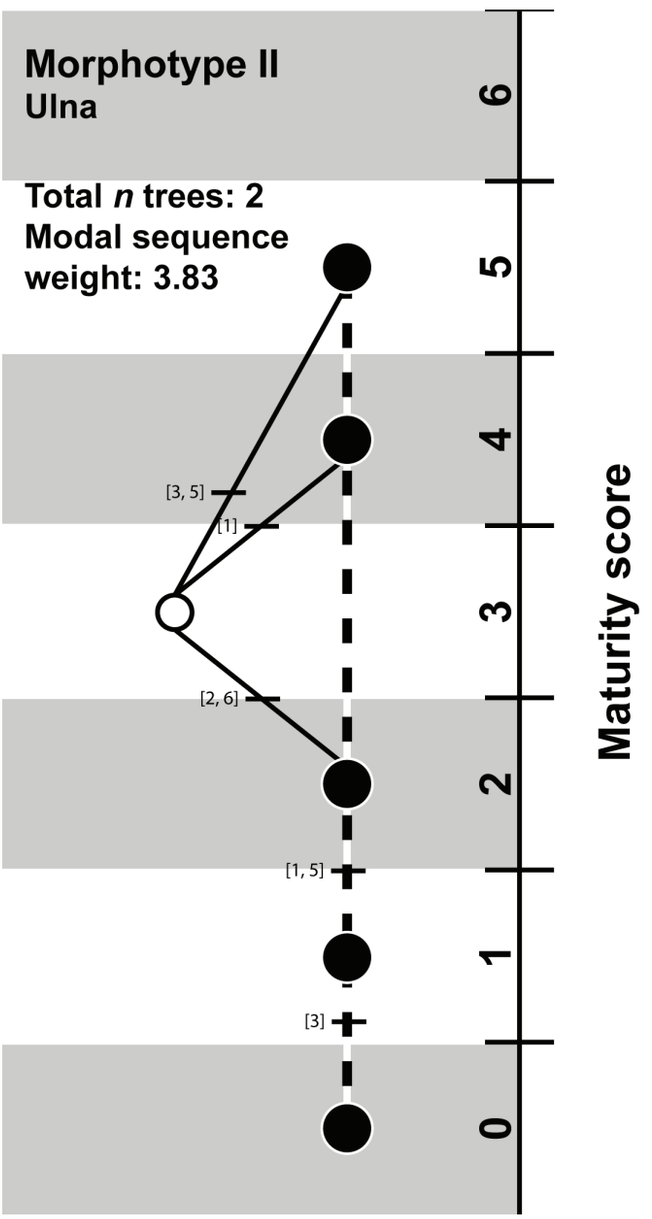

Suppl.VI.D.7 Morphotype II ulnae OSA. Connection numbers indicate character change.

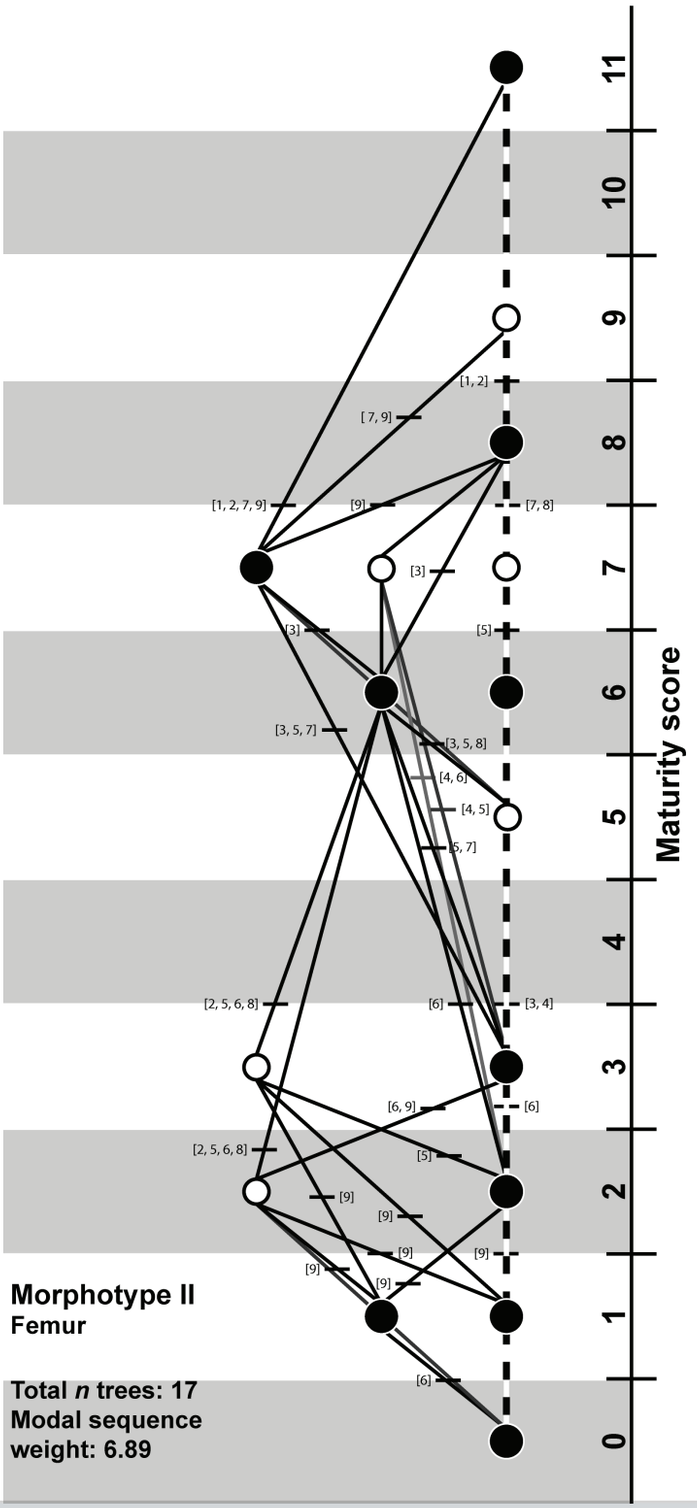

Suppl.VI.D.8 Morphotype II femora OSA. Connection numbers indicate character change.

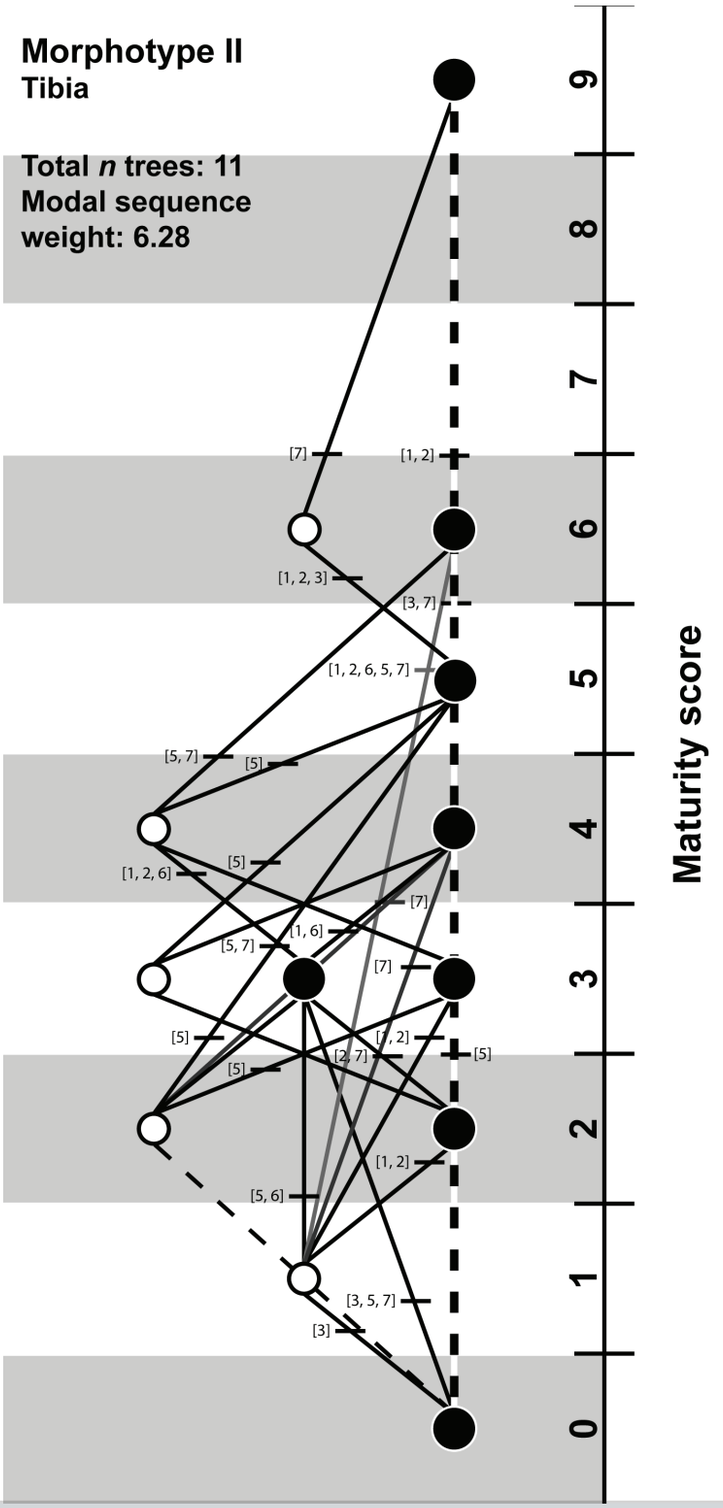

Suppl.VI.D.9 Morphotype II tibiae OSA. Connection numbers indicate character change.

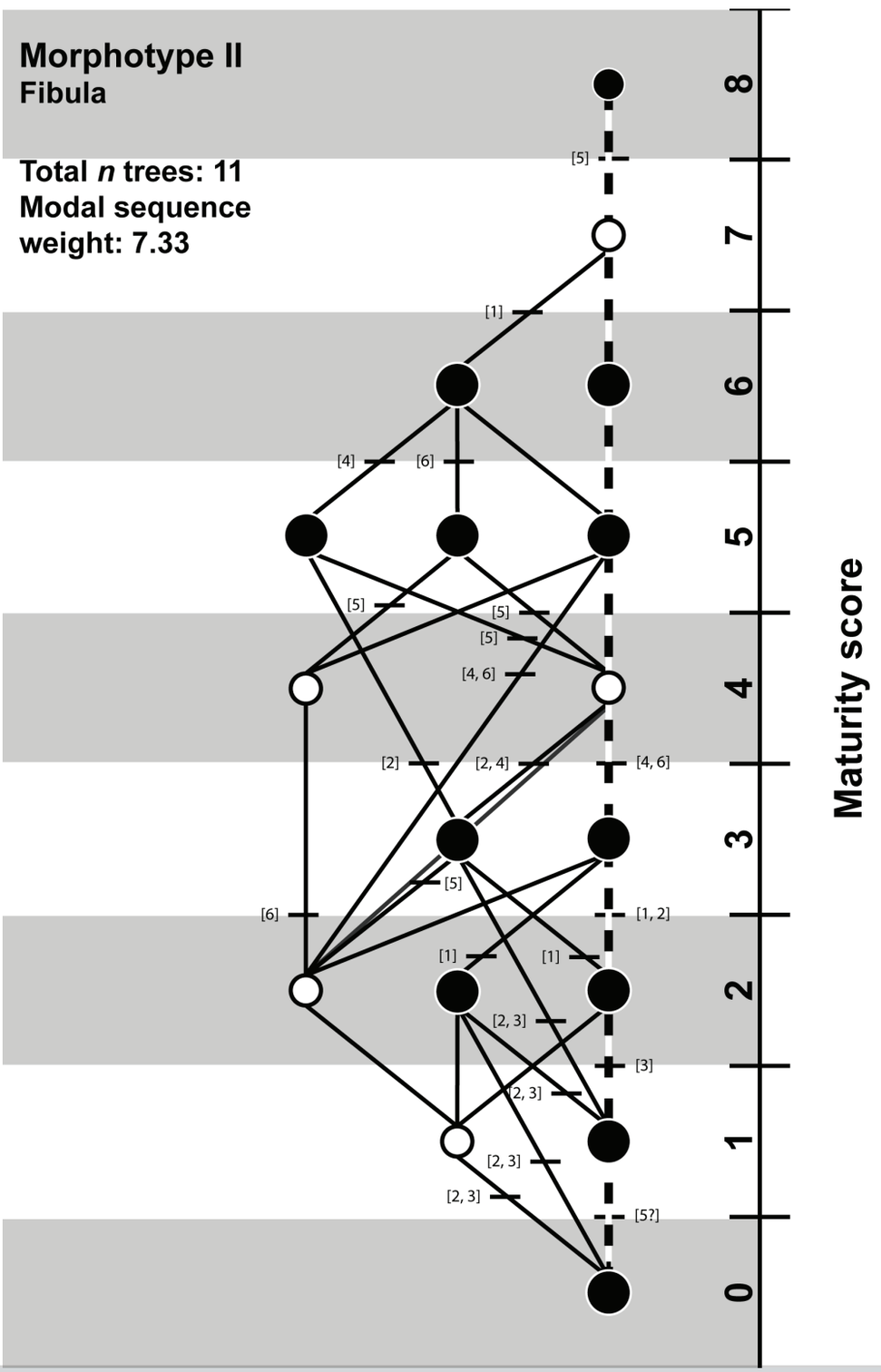

Suppl.VI.D.10 Morphotype II fibulae OSA. Connection numbers indicate character change.